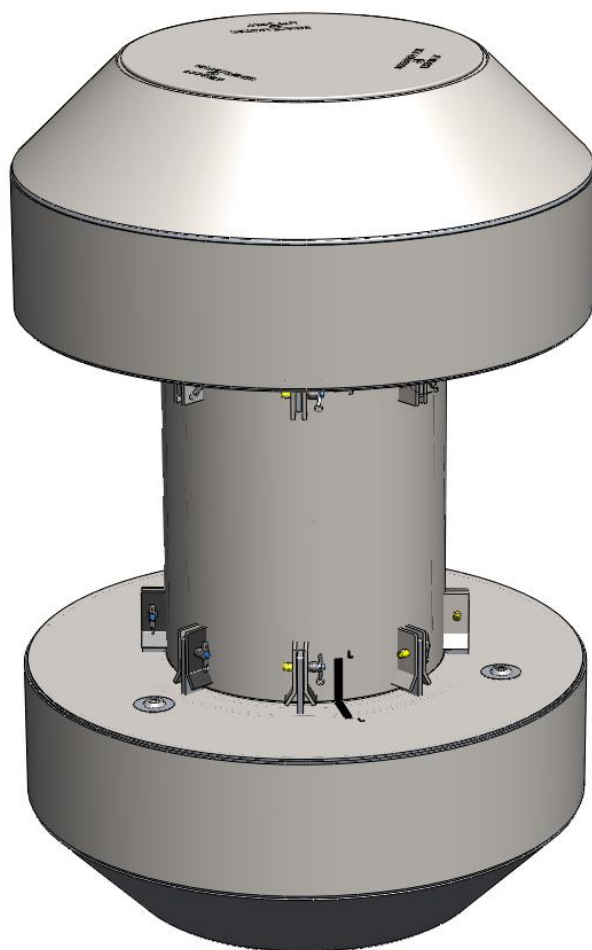




DOCKET 71-9341

# **BEA Research Reactor Package**



## ***Safety Analysis Report***

Revision 10  
May 2016

AREVA Federal Services LLC

**TABLE OF CONTENTS**

1.0	GENERAL INFORMATION.....	1.1-1
1.1	Introduction.....	1.1-1
1.2	Package Description.....	1.2-1
1.2.1	Packaging .....	1.2-1
1.2.2	Contents.....	1.2-5
1.2.3	Special Requirements for Plutonium.....	1.2-9
1.2.4	Operational Features .....	1.2-9
1.3	Appendices.....	1.3-1
1.3.1	References .....	1.3-1
1.3.2	Glossary of Terms and Acronyms.....	1.3-2
1.3.3	Packaging General Arrangement Drawings.....	1.3-4
2.0	STRUCTURAL EVALUATION .....	2.1-1
2.1	Structural Design .....	2.1-1
2.1.1	Discussion .....	2.1-1
2.1.2	Design Criteria .....	2.1-2
2.1.3	Weights and Centers of Gravity .....	2.1-6
2.1.4	Identification of Codes and Standards for Package Design .....	2.1-6
2.2	Materials .....	2.2-1
2.2.1	Material Properties and Specifications.....	2.2-1
2.2.2	Chemical, Galvanic, or Other Reactions .....	2.2-1
2.2.3	Effects of Radiation on Materials.....	2.2-2
2.3	Fabrication and Examination .....	2.3-1
2.3.1	Fabrication.....	2.3-1
2.3.2	Examination .....	2.3-1
2.4	General Standards for All Packages .....	2.4-1
2.4.1	Minimum Package Size.....	2.4-1
2.4.2	Tamper-Indicating Feature .....	2.4-1
2.4.3	Positive Closure.....	2.4-1
2.4.4	Valves.....	2.4-1
2.4.5	Package Design .....	2.4-1
2.4.6	External Temperatures .....	2.4-1
2.4.7	Venting .....	2.4-1
2.5	Lifting and Tie-down Standards for All Packages .....	2.5-1
2.5.1	Lifting Devices .....	2.5-1
2.5.2	Tie-down Devices.....	2.5-1
2.6	Normal Conditions of Transport.....	2.6-1
2.6.1	Heat .....	2.6-1
2.6.2	Cold .....	2.6-7
2.6.3	Reduced External Pressure.....	2.6-9
2.6.4	Increased External Pressure .....	2.6-10
2.6.5	Vibration.....	2.6-11
2.6.6	Water Spray.....	2.6-12
2.6.7	Free Drop.....	2.6-12

2.6.8	Corner Drop.....	2.6-15
2.6.9	Compression.....	2.6-16
2.6.10	Penetration.....	2.6-16
2.7	Hypothetical Accident Conditions.....	2.7-1
2.7.1	Free Drop.....	2.7-1
2.7.2	Crush .....	2.7-21
2.7.3	Puncture.....	2.7-21
2.7.4	Thermal .....	2.7-23
2.7.5	Immersion – Fissile .....	2.7-25
2.7.6	Immersion – All Packages.....	2.7-25
2.7.7	Deep Water Immersion Test.....	2.7-25
2.7.8	Summary of Damage.....	2.7-26
2.8	Accident Conditions for Air Transport of Plutonium .....	2.8-1
2.9	Accident Conditions for Fissile Material Packages for Air Transport .....	2.9-1
2.10	Special Form .....	2.10-1
2.11	Fuel Rods .....	2.11-1
2.12	Appendices.....	2.12-1
2.12.1	References .....	2.12.1-1
2.12.2	Certification Test Plan.....	2.12.2-1
2.12.3	Certification Test Results .....	2.12.3-1
2.12.4	Stress Analysis Finite Element Models.....	2.12.4-1
2.12.5	Impact Limiter Performance Evaluation .....	2.12.5-1
2.12.6	Analysis Software Descriptions .....	2.12.6-1
2.12.7	Seal Performance Tests .....	2.12.7-1
2.12.8	Fuel Basket Stress Analysis .....	2.12.8-1
3.0	THERMAL EVALUATION .....	3.1-1
3.1	Description of Thermal Design.....	3.1-1
3.1.1	Design Features .....	3.1-1
3.1.2	Content's Decay Heat.....	3.1-3
3.1.3	Summary Tables of Temperatures .....	3.1-4
3.1.4	Summary Tables of Maximum Pressures.....	3.1-4
3.2	Material Properties and Component Specifications.....	3.2-1
3.2.1	Material Properties .....	3.2-1
3.2.2	Technical Specifications of Components.....	3.2-3
3.3	Thermal Evaluation for Normal Conditions of Transport .....	3.3-1
3.3.1	Heat and Cold.....	3.3-1
3.3.2	Maximum Normal Operating Pressure .....	3.3-6
3.3.3	Cask Draining and Vacuum Drying Operations .....	3.3-8
3.3.4	Cask Cavity Backfill with Helium Gas .....	3.3-10
3.4	Thermal Evaluation for Hypothetical Accident Conditions .....	3.4-1
3.4.1	Initial Conditions.....	3.4-1
3.4.2	Fire Test Conditions .....	3.4-2
3.4.3	Maximum Temperatures and Pressure.....	3.4-2
3.4.4	Maximum Thermal Stresses.....	3.4-3
3.5	Appendices.....	3.5-1
3.5.1	References .....	3.5-2

3.5.2	Computer Analysis Results .....	3.5-5
3.5.3	Analytical Thermal Model .....	3.5-5
3.5.4	'Last-A-Foam' Response under HAC Conditions .....	3.5-36
4.0	CONTAINMENT .....	4.1-1
4.1	Description of the Containment System .....	4.1-1
4.1.1	Containment Boundary .....	4.1-1
4.1.2	Containment Penetrations .....	4.1-1
4.1.3	Seals .....	4.1-1
4.1.4	Welds.....	4.1-2
4.1.5	Closure .....	4.1-2
4.2	Containment Under Normal Conditions of Transport .....	4.2-1
4.3	Containment Under Hypothetical Accident Conditions .....	4.3-1
4.4	Leakage Rate Tests for Type B Packages.....	4.4-1
4.4.1	Fabrication Leakage Rate Tests .....	4.4-1
4.4.2	Maintenance/Periodic Leakage Rate Tests .....	4.4-1
4.4.3	Preshipment Leakage Rate Tests.....	4.4-1
4.5	Appendix.....	4.5-1
4.5.1	References .....	4.5-1
5.0	SHIELDING EVALUATION .....	5.1-1
5.1	Description of Shielding Design.....	5.1-1
5.1.1	Design Features .....	5.1-1
5.1.2	Summary Table of Maximum Radiation Levels .....	5.1-1
5.2	Source Specification .....	5.2-1
5.2.1	Gamma Source .....	5.2-1
5.2.2	Neutron Source.....	5.2-9
5.2.3	Irradiation Gas Generation .....	5.2-10
5.3	Shielding Model.....	5.3-1
5.3.1	Configuration of Source and Shielding.....	5.3-1
5.3.2	Material Properties .....	5.3-3
5.4	Shielding Evaluation.....	5.4-1
5.4.1	Methods.....	5.4-1
5.4.2	Input and Output Data .....	5.4-1
5.4.3	Flux-to-Dose Rate Conversion.....	5.4-2
5.4.4	External Radiation Levels .....	5.4-2
5.5	Appendices.....	5.5-1
5.5.1	References .....	5.5-1
5.5.2	Detailed TRIGA Results .....	5.5-1
5.5.3	Sample Input Files.....	5.5-8
6.0	CRITICALITY EVALUATION .....	6.1-1
6.1	Description of Criticality Design.....	6.1-1
6.1.1	Design Features .....	6.1-1
6.1.2	Summary Table of Criticality Evaluation .....	6.1-1
6.1.3	Criticality Safety Index .....	6.1-2
6.2	Fissile Material Contents .....	6.2-1
6.2.1	MURR Fuel Element.....	6.2-1
6.2.2	MITR-II Fuel Element .....	6.2-2



6.2.3	ATR Fuel Element .....	6.2-3
6.2.4	TRIGA Fuel Element .....	6.2-5
6.2.5	PULSTAR Fuel Element.....	6.2-6
6.2.6	Square Plate Fuels .....	6.2-6
6.3	General Considerations .....	6.3-1
6.3.1	Model Configuration .....	6.3-1
6.3.2	Material Properties .....	6.3-2
6.3.3	Computer Codes and Cross-Section Libraries .....	6.3-2
6.3.4	Demonstration of Maximum Reactivity.....	6.3-3
6.4	Single Package Evaluation.....	6.4-1
6.4.1	Configuration .....	6.4-1
6.4.2	Results .....	6.4-10
6.5	Evaluation of Package Arrays under Normal Conditions of Transport.....	6.5-1
6.5.1	Configuration .....	6.5-1
6.5.2	Results .....	6.5-1
6.6	Package Arrays under Hypothetical Accident Conditions.....	6.6-1
6.6.1	Configuration .....	6.6-1
6.6.2	Results .....	6.6-3
6.7	Fissile Material Packages for Air Transport .....	6.7-1
6.8	Benchmark Evaluations .....	6.8-1
6.8.1	Applicability of Benchmark Experiments.....	6.8-1
6.8.2	Bias Determination.....	6.8-3
6.9	Appendices.....	6.9-1
6.9.1	References .....	6.9-1
6.9.2	Parametric Evaluations to Determine the Most Reactive Fuel Geometries .....	6.9-1
6.9.3	Sample Input Files.....	6.9-12
7.0	PACKAGE OPERATIONS.....	7.1-1
7.1	Procedures for Loading the Package.....	7.1-1
7.1.1	Preparation for Loading .....	7.1-1
7.1.2	Loading of Contents .....	7.1-1
7.1.3	Preparation for Transport .....	7.1-7
7.2	Procedures for Unloading the Package.....	7.2-1
7.2.1	Receipt of Package from Carrier.....	7.2-1
7.2.2	Removal of Contents.....	7.2-1
7.3	Preparation of an Empty Package for Transport.....	7.3-1
7.4	Appendix.....	7.4-1
7.4.1	References .....	7.4-1
8.0	ACCEPTANCE TESTS AND MAINTENANCE PROGRAM.....	8.1-1
8.1	Acceptance Tests .....	8.1-1
8.1.1	Visual Inspection and Measurements.....	8.1-1
8.1.2	Weld Examinations .....	8.1-1
8.1.3	Structural and Pressure Tests .....	8.1-1
8.1.4	Fabrication Leakage Rate Tests .....	8.1-2
8.1.5	Component and Material Tests .....	8.1-5
8.1.6	Shielding Integrity Tests .....	8.1-12

8.1.7	Thermal Tests .....	8.1-13
8.2	Maintenance Program .....	8.2-1
8.2.1	Structural and Pressure Tests .....	8.2-1
8.2.2	Maintenance/Periodic Leakage Rate Tests .....	8.2-1
8.2.3	Component and Material Tests .....	8.2-3
8.2.4	Thermal Tests .....	8.2-4
8.3	Appendix .....	8.3-1
8.3.1	References .....	8.3-1

## 1.0 GENERAL INFORMATION

This section presents a general introduction and description of the BEA Research Reactor (BRR) package. The BRR package is used to transport fuel elements that have been irradiated in various test and research reactors. A full list of the fuel types included for transport in the package is given in Section 1.2.2, *Contents*. This application seeks authorization of the BRR package as a Type B(U)F-96 shipping container in accordance with the provisions of Title 10, Part 71 of the Code of Federal Regulations [1].

The major components comprising the package are discussed in Section 1.2.1, *Packaging*, and illustrated in Figure 1.2-1 through Figure 1.2-8. A glossary of terms is presented in Appendix 1.3.2, *Glossary of Terms and Acronyms*. Detailed drawings of the package design are presented in Appendix 1.3.3, *Packaging General Arrangement Drawings*.

### 1.1 Introduction

The BRR package has been developed to transport irradiated research reactor fuel. The fuel consists of the following types: high enriched and low enriched aluminum clad plate fuel, loose fuel plates, PULSTAR reactor fuel, and TRIGA fuel of varying enrichments. Within the package, the fuel is contained in basket structures that provide for optimum heat rejection and criticality control.

The packaging consists of a payload basket, a lead-shielded cask body, an upper shield plug, a closure lid, and upper and lower impact limiters. The package is of conventional design and utilizes ASTM Type 304 stainless steel as its primary structural material. The package is designed to provide leaktight containment of the radioactive contents under all NCT and HAC.<sup>1</sup>

The BRR package may be used in a pool or hot cell environment. The cask body is provided with a drain port, and is intended for use with a drying system to ensure that water is not present during transport. The package is designed to be transported singly, with its longitudinal axis vertical, by highway truck or by rail in exclusive use. When loaded and prepared for transport, the BRR package is 119.5 inches long, 78 inches in diameter (over the impact limiters), and weighs 32,000 lb.

Based on the criticality assessment provided in Chapter 6, *Criticality Evaluation*, the criticality safety index for the BRR package is zero.

---

<sup>1</sup> Leaktight is defined as a maximum of  $1 \times 10^{-7}$  reference-cm<sup>3</sup>/sec, air leakage per ANSI N14.5-1997 [2].

## 1.2 Package Description

This section presents a basic description of the BRR package components and construction. General arrangement drawings are provided in Appendix 1.3.3, *Packaging General Arrangement Drawings*.

### 1.2.1 Packaging

The BRR package consists of a payload basket, a lead-shielded cask body, a separate, removable upper shield plug, a closure lid, twelve closure bolts, and upper and lower impact limiters containing polyurethane foam. Except for the closure bolts and impact limiter attachments, the package is of primarily welded construction, using Type 304 austenitic stainless steel. These components will now be discussed in detail.

#### 1.2.1.1 Cask Body

The BRR cask body is a right circular cylinder 77.1 inches long and 38 inches in diameter (not including the impact limiter attachments and the thermal shield). It is composed of upper and lower massive end structures connected by inner and outer shells. Thick lead shielding is located between the two circular shells, in the lower end structure, and in the shield plug. The payload cavity has a diameter of 16 inches and a length of 54 inches.

The massive end structures may be cast from ASTM A351, Grade CF8A, or forged from ASTM A182, Type F304. The lower end structure contains a drain to allow removal of water from the payload cavity. The inner shell may be cast from ASTM A451, Grade CPF8A, or forged from ASTM A182, Type F304. The outer shell may be made from ASTM A240, Type 304 plate, or optionally cast from ASTM A451, Grade CPF8A or forged from ASTM A182, Type F304. The outer shell may have up to two, full penetration longitudinal seam welds. The inner shell is one inch thick, and is welded to each end structure using a full penetration weld. The outer shell is two inches thick, and is connected to each end structure using a full penetration weld. The weld of the outer shell to the upper end structure is made after lead pour.

The cask is lifted using four, 1-8 UNC threaded holes in the upper end structure, which may be optionally fitted with heavy duty thread inserts. See Zone D2 of sheet 3 of drawing 1910-01-01-SAR.

On the outside of the outer shell, in the region not covered by the impact limiters, is a thermal shield composed of an outer sheet of 12 gauge (0.105-inch thick) Type 304 stainless steel, separated from the outer shell by small strips of the same 12 gauge material.

A set of eight receptacles are attached to the outer shell at each end of the exposed region of the cask (total of 16 receptacles), that serve as impact limiter attachments (see Zone A4 of sheet 2 of drawing 1910-01-01-SAR). The receptacles consist of two closely spaced plates, 1/2-inches thick, that pass through the thermal shield and attach directly to the outer shell using a full penetration groove weld with a 1/2-inch fillet reinforcement on one side. Each impact limiter features eight, 3/4-inch thick blades that pass between the receptacle plates on the cask body. The attachment is completed by passing a one inch diameter, stainless steel ball lock pin through the three plates. The ball lock pins therefore act in double shear. Each impact limiter is retained by eight such attachments.

All lead shielding is made from ASTM B29, chemical lead, or optionally, from lead per Federal Specification QQ-L-171E, Grade A or C. The lead shield on the side of the cask body is cast-in-place through the upper end structure, and is nominally 8 inches thick. The shield at the

bottom is made from lead sheet material that is packed firmly into place, and is 7.7 inches thick. The bottom lead cavity is closed using a one inch thick plate secured with a full penetration groove weld, see Zone A6/7 of sheet 3 of drawing 1910-01-01-SAR.

The removable shield plug is located at the top of the payload cavity. The outer shell is made from Type 304 plate material of 1/2-inch, 3/8-inch, 1-inch, and 1½-inch thickness. See Zone D2 of sheet 4 of drawing 1910-01-01-SAR. The cavity is filled with lead sheet material that is packed firmly into place. The total thickness of the plug is 11.2 inches, and the lead thickness is 9.7 inches. The plug rests on a shoulder located approximately half way along the length of the plug. A corresponding shoulder is located in the upper end structure of the cask body to support the shield plug. A 3/4-inch diameter pipe passes through the plug to ensure proper draining and drying of the cask. The pipe is oriented approximately diagonally to prevent a deleterious shine path. The shield plug is lifted using a central, 1/2-13 UNC threaded hole.

The closure lid is made from 2-inch thick, ASTM A240, Type 304 stainless steel plate. It is attached to the cask using 12, 1-8 UNC bolts made of ASTM A320, Grade L43 material, with hardened steel washers. The bolts are plated with electroless nickel per MIL-DTL-26074 Rev. F Class 1 Grade B, and tightened to a torque of  $220 \pm 20$  ft-lb. The mating holes in the cask body may be optionally fitted with heavy duty thread inserts. The mating surface of the lid features a step relief located at the bolt circle. This relief prevents any contact from occurring between the lid and the body outside of the bolt circle, thus preventing prying loads from being applied to the closure bolts. The closure lid includes two O-ring seals made from butyl rubber of 3/8-inch cross sectional diameter. The inner O-ring is the containment seal, and the outer is the test seal. The seals are retained in dovetail grooves in the lid. The O-ring material (including the sealing washers, see below) is made from Rainier Rubber R-0405-70, and subject to the tests given in Section 8.1.5.2.

The BRR package provides a single level of leaktight containment. The containment boundary of the BRR package consists of the following elements. Unless noted, all elements are made of ASTM Type 304 stainless steel in various product forms.

- The lower massive end structure (including the passage to the drain port)
- The inner cylindrical shell
- The upper massive end structure
- The containment elastomer O-ring seal (the inner seal in the closure lid)
- The closure lid
- The vent port in the closure lid including elastomer sealing washer
- The drain port in the lower end structure including elastomer sealing washer

The containment boundary is shown in Figure 1.2-16.

As noted above, the BRR package features two ports that are part of the containment boundary: a vent port in the closure lid, and a drain port in the lower end structure. Both ports are closed with threaded plugs made of ASTM B16 brass and sealed with butyl rubber sealing washers. A threaded brass cover is used to protect the port plugs. A seal test port is located between the containment O-ring seal and test O-ring seals, and is not part of containment.

### 1.2.1.2 Impact Limiters

Impact limiters are attached to each end of the BRR package, having essentially identical design, and are shown in drawing 1910-01-02-SAR. Each limiter is 78 inches in diameter and 34.6 inches long overall, with a conical section 15 inches long towards the outer end. The impact limiter design consists of Type 304 stainless steel shells and approximately 9 lb/ft<sup>3</sup> polyurethane foam. The external shells (except for the end plate) are 1/4 inches thick, and the internal shells (that interface with the cask body) are 1/2 inches thick. The outer end plate is 1/2 inches thick. The closure end impact limiter features three reinforced, 1/2-13UNC holes for lifting of the impact limiter only. An optional drain tube, aligned along the long axis of the cask, may be included in the lower impact limiter. The polyurethane foam is rigid, closed-cell, and is poured in place. On the side that mates with the cask, the annular sheet features three plastic melt-out plugs designed to relieve pressure in the HAC fire event. The attachment of the impact limiters to the cask body is described in Section 1.2.1.1, *Cask Body*.

### 1.2.1.3 Baskets

There are five baskets used with the BRR package, one for MURR, MITR-II, ATR, and TRIGA fuel types, and one for several fuel types each having a square or rectangular cross section and loose plates. The baskets are shown in drawing 1910-01-03-SAR. The baskets are made from welded construction using Type 304 stainless steel in plate, bar, pipe, and tubular forms. Each basket has a diameter of 15.63 inches and a length of 53.45 inches, and features a number of cavities that fit the size and shape of the fuel. The cavities are sized to minimize free play between the fuel and the basket, while ensuring free insertion and removal of the elements. The baskets are open on the top, and the fuel is located at the top end, nearest the shield plug. The baskets are designed to freely drain water when the cask is lifted out of the spent fuel pool.

#### 1.2.1.3.1 MURR

The MURR basket consists of an outer rolled shell, an inner pipe, and thick radial plates that form eight pie-shaped cavities for the fuel in a circular array. The bottom of the fuel cavities is formed by a 3/8-inch thick plate that is welded to the inside of the shell. The lifting bar divides the interior of the inner tube in half and prevents loading any fuel within the inner tube. The MURR basket is shown in Figure 1.2-4.

#### 1.2.1.3.2 MITR-II

The MITR-II basket consists of a cylindrical weldment supported by a 14 inch diameter pedestal. Twenty-nine (29) flat plates of variable thicknesses are machined and stacked to create eight (8) diamond shaped fuel cavities. Fuel cavities are arranged symmetrically about the center axis of the basket. The top plate of the weldment is machined to prevent the loading of fuel into the central cavity of the basket. The bottom plate of the weldment provides support for the fuel and allows for drainage of water from the fuel cavities. The MITR-II basket is shown in Figure 1.2-5.

#### 1.2.1.3.3 ATR

The ATR basket consists of a rolled outer shell, an inner pipe, and radial plates that form eight pie-shaped cavities for the fuel in a circular array. Since the outer shell is somewhat smaller than the cask cavity, the ATR basket features four circular ribs having an outer diameter of 15.63 inches.

The bottom support plate is 1/2-inches thick. The lifting bar divides the interior of the inner tube in half and prevents loading any fuel within the inner tube. The ATR basket is shown in Figure 1.2-6.

#### **1.2.1.3.4 TRIGA**

The TRIGA basket consists of an array of 19 tubes having a 2-inch outer diameter and an 11-gauge wall thickness. The tubes are held in place by a top plate, a bottom support plate, and a central support plate. A 13-inch diameter, 1/4-inch thick circular shell forms the lower portion of the basket. The short spacer pedestal and the adjustable spacer pedestal are used to customize the fuel cavity for various TRIGA fuel lengths. The TRIGA basket is shown in Figure 1.2-7.

#### **1.2.1.3.5 Square Fuel**

The Square fuel basket is designed to house all of the fuel types listed in Section 1.2.2.5, *Square Fuel and Loose Plates*, which have a square or rectangular cross section, and three types of loose plates taken from those fuels. It consists of an array of eight square tubes having a wall thickness of 0.105 inches, held in position by three, 1/2-inch thick spacer plates. A 14-inch diameter, 1/4-inch thick circular shell forms the lower portion of the basket. The tubes are arranged with six around the outer circumference and two in the middle. Loose plates are contained in a loose plate box. Spacer pedestals are used in each cavity, as required, to support the fuel elements at the top of the basket. The Square fuel basket is shown in Figure 1.2-8.

#### **1.2.1.4 Gross Weight**

The gross weight of the BRR package, including the cask, impact limiters, and maximum payload, is 32,000 lb. A summary of overall component weights is shown in Table 2.1-2 and discussed in Section 2.1.3, *Weights and Centers of Gravity*.

#### **1.2.1.5 Neutron Moderation and Absorption**

The BRR package maintains criticality control by means of limitation of the quantity of fissile material present and by maintaining a safe configuration of the material under all NCT and HAC. The design of the BRR package does not include any components whose principal purpose is the absorption of neutrons. A more detailed description of the package criticality control functions is given in Chapter 6, *Criticality Evaluation*.

#### **1.2.1.6 Receptacles, Valves, Testing and Sampling Ports**

The BRR package closure lid contains a vent port and a containment seal test port. A body drain port is located on the side of the lower end of the cask. There are no valves or receptacles used in the BRR package.

#### **1.2.1.7 Heat Dissipation**

The dissipation of heat from the BRR package is entirely passive. The impact limiters are painted white to reduce the absorption of solar heat. A thermal shield is used on the cask body to limit the temperature of the lead gamma shield in the HAC fire event. A more detailed description of the package thermal design is given in Chapter 3, *Thermal Evaluation*.

### 1.2.1.8 Lifting and Tie-down Devices

Other than the threaded holes in the top of the cask body, there are no lifting or tie-down devices that are a structural part of the BRR package. The package is secured to the transport vehicle using structures that interface with the surfaces of the upper and lower impact limiters. The package rests on a lower frame that is attached to the vehicle. An upper frame contacts the upper impact limiter and is attached to the vehicle using cables or the equivalent. There are no provisions to lift the package with the impact limiters installed.

### 1.2.1.9 Pressure Relief System

There is no pressure relief system in the BRR package.

### 1.2.1.10 Shielding

Biological shielding of gamma radiation is provided by a combination of lead and the thick steel shells of the BRR package. Hydrogenous neutron shielding is not necessary and none is included in the package design. Details of the gamma shielding are provided in Section 1.2.1.1, *Cask Body*. A full assessment of the shielding design is provided in Chapter 5, *Shielding Evaluation*.

## 1.2.2 Contents

The BRR package may contain up to 8 irradiated MURR, MITR-II, ATR, and Square fuel elements or loose plate boxes, and up to 19 irradiated TRIGA fuel elements. Only one fuel element is allowed per basket location. Loose plate boxes may be loaded in the same basket as fuel elements. Details for each fuel type are provided in the following paragraphs.

### 1.2.2.1 MURR

The MURR fuel element may be irradiated to a maximum burnup of 180 MWD (218,196 MWD/MTU, or a U-235 depletion of 30.9%). The minimum cooling time is 180 days after discharge from the core.

Each fresh MURR element contains  $775.0 \pm 7.8$  g U-235, with an enrichment of  $93 \pm 1$  wt.%. The weight percents of the remaining uranium isotopes are 1.2 wt.% U-234, 0.7 wt.% U-236, and 5.0 – 7.0 wt.% U-238. The MURR fuel element fissile material is uranium aluminide (UAl<sub>x</sub>).

Each MURR fuel element contains 24 curved fuel plates. Fuel plate 1 has the smallest radius, while fuel plate 24 has the largest radius, as shown in Figure 1.2-9. The fuel “meat” is a mixture of uranium metal and aluminum, while the cladding and structural materials are an aluminum alloy. The fuel plates are rolled to shape and swaged into the two fuel element side plates. The fissile material (uranium aluminide) is nominally 0.02-in thick for all 24 plates. The minimum cladding thickness is 0.008-in. Fuel element side plates are fabricated of ASTM B 209, aluminum alloy 6061-T6 or 6061-T651 and are approximately 0.15-in thick. The averaged measured channel spacing between fuel plates, over the entire fuel element, is less than or equal to 0.088-in at the time of fabrication. The maximum local channel spacing at the time of fabrication is 0.090-in.

The MURR element overall length, including irradiation growth, is 32.75 inches. The bounding weight of one assembly is 15 lb. The maximum decay heat per fuel element is 158 W.



### 1.2.2.2 MITR-II

The MITR-II fuel element may be irradiated to a maximum burnup of 165 MWD (306,900 MWD/MTU, or a U-235 depletion of 43.9%). The minimum cooling time is 120 days after discharge from the core.

Each fresh MITR-II element contains  $510.0 \pm 3.0/-10.0$  g U-235, with an enrichment of  $93 \pm 1$  wt.%. The weight percents of the remaining uranium isotopes are 1.2 wt.% U-234, 0.7 wt.% U-236, and  $5.0 - 7.0$  wt.% U-238. Like the MURR fuel element, the MITR-II fuel element fissile material is uranium aluminide ( $UAl_x$ ).

Each MITR-II fuel element contains 15 flat fuel plates, as shown in Figure 1.2-10. The fuel plates are fabricated and swaged into the two fuel element side plates. The fuel “meat” is a mixture of uranium metal and aluminum, while the cladding and structural materials are an aluminum alloy. The fissile material (uranium aluminide) is nominally 0.03-in thick and the cladding is nominally 0.025-in thick. The minimum cladding thickness, including the thermal groove, is 0.008-in. Fuel element side plates are fabricated of ASTM B 209, aluminum alloy 6061-T6 and are approximately 0.19-in thick. The averaged measured channel spacing between fuel plates, over the entire fuel element, is less than or equal to 0.082-in at the time of fabrication (excluding the thermal grooves). The maximum local channel spacing at the time of fabrication is 0.090-in (excluding the thermal grooves).

The MITR-II element overall length, including irradiation growth, is 26.52 inches. The bounding weight of one assembly is 10 lb. The maximum decay heat per assembly is 150 W.

### 1.2.2.3 ATR

The ATR fuel element may be irradiated to a maximum burnup of 480 MWD<sup>1</sup> (491,155 MWD/MTU, or a U-235 depletion of 58.6%). The minimum cooling time is 1,670 days (4.6 years) after discharge from the core.

There are two general classes of ATR fuel element, XA and YA. The XA fuel element has a fresh fuel loading of  $1,075 \pm 10$  g U-235, with an enrichment of  $93 \pm 1$  wt.%. The weight percents of the remaining uranium isotopes are 1.2 wt.% U-234 (max), 0.7 wt.% U-236 (max), and  $5.0 - 7.0$  wt.% U-238. Like the MURR and MITR-II fuel elements, the fuel element fissile material is uranium aluminide ( $UAl_x$ ).

The XA fuel element is further subdivided into fuel element types 7F, 7NB, 7NBH. In the 7F fuel element, all 19 fuel plates are loaded with enriched uranium in an aluminum matrix with the eight outer plates (1 through 4 and 16 through 19) containing boron as a burnable poison. The fuel element with the greatest reactivity is the 7NB that contains no burnable poison. The 7NBH fuel element is similar to the 7NB fuel element except that it contains one or two borated plates. The YA fuel element is identical to the 7F fuel element except that plate 19 of the YA fuel element is an aluminum alloy plate containing neither uranium fuel nor boron burnable poison. The YA fuel element has a fresh fuel loading of  $1,022.4 \pm 10$  g U-235. A second YA fuel element design (YA-M) has the side plate width reduced by 15 mils.

<sup>1</sup> The element burnup of 480 MWD should not be a limit for licensing purposes because the element burnup is typically not known in units of MWD. The final U-235 mass within an element is computed and recorded by ATR staff.

The ATR fuel elements contain 19 curved fuel plates. A section view of an ATR fuel element is given in Figure 1.2-11. Note that an intact ATR fuel element has end boxes (as shown on Figure 1.2-11), although these end boxes are removed prior to insertion in the BRR package. The fuel plates are rolled to shape and swaged into the two fuel element side plates. Fuel plate 1 has the smallest radius, while fuel plate 19 has the largest radius. The fissile material (uranium aluminide) is nominally 0.02-in thick for all 19 plates. The minimum cladding thickness is 0.018-in for plates 1 and 19, and 0.008-in for plates 2 through 18. Fuel element side plates are fabricated of ASTM B 209, aluminum alloy 6061-T6 or 6061-T651 and are approximately 0.19-in thick. The averaged measured channel spacing between fuel plates, over the entire fuel element, is less than or equal to 0.085-in at the time of fabrication. The maximum local channel spacing is 0.087-in at the time of fabrication.

The ATR element overall length, after removal of the end box structures, 51.0 inches max. The bounding weight of one assembly is 25 lb. The maximum decay heat per assembly is 30 W.

#### 1.2.2.4 TRIGA

Many different types of TRIGA fuel elements have been fabricated over the past several decades. TRIGA fuel elements utilize a zirconium hydride fuel matrix. Twenty-six (26) different TRIGA element types are evaluated. These element types are identified by their General Atomics catalog number. TRIGA elements fall into five general categories:

- Standard (100 series)
- Instrumented (200 series). Instrumented rods contain thermocouples used to measure temperature during reactor operation. The fueled region is essentially the same as a standard rod, although instrumented rods may be longer.
- Fueled Follower Control Rods (FFCR) (300 series). FFCR rods contain boron carbide neutron absorber outside the active fuel region.
- Cluster rods (400 series). Typically three or four cluster rods are used to build a cluster assembly. For transportation in the BRR package, the cluster rods are disassembled from the cluster assembly.
- Instrumented cluster rods (500 series). Instrumented rods contain thermocouples used to measure temperature during reactor operation. The fueled region is essentially the same as a standard cluster rod, although instrumented cluster rods may be longer.

Basic fresh fuel data used to describe the various TRIGA fuel elements are summarized in Table 1.2-1. A basic TRIGA fuel element is depicted in Figure 1.2-12. The maximum length of an element, including irradiation growth, is 45.50 inches. Non-instrumented fuel elements are somewhat shorter. For all fuel elements, spacers are utilized within the TRIGA baskets.

The maximum burnup and minimum required cooling time after reactor discharge for the various element types is summarized in Table 1.2-2. The burnup and cooling time combinations are selected to limit the decay heat to 20 W. When using this table to qualify fuel for shipment, the actual burnup value shall be rounded up to the next higher burnup value shown in the table.

Table 1.2-2 is developed based on an in-core residence time of 4 years. It is expected that such a short residence time would result in bounding cooling times in most situations, as TRIGA fuel typically has an in-core residence time of at least 10 years. However, for fuel with an in-core residence time less than 4 years, the decay heat shall be independently confirmed to be  $\leq 20$  W.

The bounding weight of any TRIGA fuel element is 10 lb.

#### 1.2.2.5 Square Fuel and Loose Plates

The Square fuel basket is used to transport fuel that has a nominal square or rectangular geometry, including plate fuel, the loose plate box, and PULSTAR fuel. The heat load of the Square fuel basket is limited to 30 watts per compartment.

The Square plate fuels (i.e., all square fuels except PULSTAR) include Rhode Island Nuclear Science Center (RINSC), University of Massachusetts at Lowell (U-Mass), Ohio State University (Ohio State), Missouri University of Science and Technology (Missouri S&T), University of Florida (U-Florida), and Purdue University (Purdue). The plate fuels are 20% enriched. Fuel data for the square plate fuels is summarized in Table 1.2-3.

With the exception of U-Mass, the plate fuels have a uranium silicide ( $U_3O_2$ ) fuel matrix mixed with aluminum. U-Mass has two fuel element types currently in use, uranium silicide and uranium aluminide ( $UAl_x$ ). The U-Mass (aluminide) fuel originally was manufactured for the Worcester Polytechnic Institute (WPI) reactor.

Each RINSC fuel element contains 22 flat fuel plates fitted within aluminum side plates, and the maximum allowable channel spacing between fuel plates is less than or equal to 0.099 inches at the time of fabrication. The maximum burnup is limited to 52.5 MWD, and the minimum cooling time is 120 days after discharge from the core. RINSC fuel is illustrated in Figure 1.2-13, and is illustrative of the other square fuels that have swaged plate designs using side combs.

Each U-Mass (aluminide) fuel element contains 18 flat fuel plates fitted within aluminum side plates, and the maximum allowable channel spacing between fuel plates is less than or equal to 0.119 inches at the time of fabrication. The maximum burnup is limited to 9.7 MWD, and the minimum cooling time is 1,000 days after discharge from the core. This fuel was partially burned in the WPI reactor before being transferred to U-Mass for further irradiation. The burnup limit for this fuel element is the total combined burnup for the WPI and U-Mass reactors.

Each U-Mass (silicide) fuel element contains 16 flat fuel plates fitted within aluminum side plates, and the maximum allowable channel spacing between fuel plates is less than or equal to 0.122 inches at the time of fabrication. The maximum burnup is limited to 9.7 MWD, and the minimum cooling time is 1,000 days after discharge from the core.

Each Ohio State fuel element contains 16 flat fuel plates fitted within aluminum side plates, and the maximum allowable channel spacing between fuel plates is less than or equal to 0.127 inches at the time of fabrication. The maximum burnup is limited to 64 MWD, and the minimum cooling time is 120 days after discharge from the core.

Each Missouri S&T fuel element contains 18 curved fuel plates fitted within parallel aluminum side plates, and the maximum allowable channel spacing between fuel plates is less than or equal to 0.139 inches at the time of fabrication. The maximum burnup is limited to 74 MWD, and the minimum cooling time is 365 days after discharge from the core.

Each U-Florida fuel element contains 14 flat fuel plates that include spacers and combs and are screwed together at 4 corners (no side plates), and the maximum allowable channel spacing between fuel plates is less than or equal to 0.117 inches at the time of fabrication. The maximum burnup is limited to 87 MWD, and the minimum cooling time is 120 days after discharge from the core. The U-Florida screw-assembly design is illustrated in Figure 1.2-14.

Each Purdue fuel element contains a maximum of 14 flat fuel plates loaded into a grooved fuel box and contained with a screwed on lifting bar at top, and the maximum allowable channel spacing between fuel plates is less than or equal to 0.175 inches at the time of fabrication. The maximum burnup is limited to 0.57 MWD, and the minimum cooling time is 120 days after discharge from the core.

A loose plate box is used to transport up to 31 loose plates per box. Loose plates are limited to U-Mass (aluminide), U-Florida, and Purdue fuel plates. A depiction of the Square fuel basket, loose plate box, and loose plates inside a BRR package is shown in Figure 1.2-17.

The PULSTAR fuel element may be irradiated to a maximum burnup of 20,000 MWD/MTU. The minimum cooling time is 1.5 years after discharge from the core. PULSTAR fuel is similar to light water reactor fuel, as it has a  $\text{UO}_2$  fuel matrix, zirconium alloy cladding, cylindrical fuel rods, and a nominal enrichment between 4 and 6%. PULSTAR fuel data is summarized in Table 1.2-4. The fuel is arranged in a  $5 \times 5$  rectangular lattice, as shown in Figure 1.2-15. The active fuel region is contained within a zirconium alloy box, although the end fittings are aluminum alloy. Including a spacer pedestal, the weight of a PULSTAR element is 48 lb, which bounds the weight of all other fuels used in the Square fuel basket.

### 1.2.3 Special Requirements for Plutonium

The BRR package may contain plutonium in excess of 20 Ci as a consequence of irradiation of the reactor fuel. As such, the plutonium is in solid form within the fuel matrix. Table 1.2-5 summarizes the plutonium activity for each of the five basket types, both on a per-element and per-cask basis. The plutonium activities are extracted from the SCALE6/TRITON output files used to generate the gamma and neutron source terms. The source term development is described in detail in Section 5.2, *Source Specification*. The maximum quantity of plutonium for the BRR package is 6,500 Ci, which occurs for 4% enriched PULSTAR fuel. PULSTAR fuel has an approximately square outer dimension and is transported in the Square fuel basket.

### 1.2.4 Operational Features

The BRR package is of conventional design and is not complex to operate. Operational features are depicted on the drawings provided in Appendix 1.3.3, *Packaging General Arrangement Drawings*. Operating procedures and instructions for loading, unloading, and preparing an empty package for transport are provided in Chapter 7, *Package Operations*.

**Table 1.2-1 – TRIGA Fresh Fuel Characteristics**

ID	Type	Cladding	U (wt.% fuel)	Fuel Length (in)	U-235 (wt.% U)	U (g)	U-235 (g)	Fuel OD (in)	Rod OD (in)	Cladding Thickness (in)	H/Zr	Overall Length (in)	Er (wt.%)
101	Std.	Al	8.0	14	20	166	32	1.41	1.48	0.03	1.0	28.62	0
	Std.	Al	8.5	15	20	189	37	1.41	1.48	0.03	1.6	28.62	0
103	Std.	SS	8.5	15	20	197	39	1.44	1.48	0.02	1.6	29.15	0
105	Std.	SS	12	15	20	285	56	1.44	1.48	0.02	1.6	29.15	0
107	Std.	SS	12	15	20	271	53	1.40	1.48	0.02	1.6	30.14	0
109	Std.	SS	8.5	15	70	194	136	1.44	1.48	0.02	1.6	29.15	1.2
117	Std.	SS	20	15	20	503	99	1.44	1.48	0.02	1.6	29.93	0.5
119	Std.	SS	30	15	20	825	163	1.44	1.48	0.02	1.6	29.93	0.9
201	Ins.	Al	8.5	15	20	189	37	1.41	1.48	0.03	1.6	28.78	0
203	Ins.	SS	8.5	15	20	197	39	1.44	1.48	0.02	1.6	45.50	0
205	Ins.	SS	12	15	20	285	56	1.44	1.48	0.02	1.6	45.50	0
207	Ins.	SS	12	15	20	271	53	1.40	1.48	0.02	1.6	45.50	0
217	Ins.	SS	20	15	20	503	99	1.44	1.48	0.02	1.6	40.35	0.5
219	Ins.	SS	30	15	20	825	163	1.44	1.48	0.02	1.6	40.35	0.9
303	FFCR	SS	8.5	15	20	163	32	1.31	1.35	0.02	1.6	44.00	0
305	FFCR	SS	12	15	20	237	47	1.31	1.35	0.02	1.6	44.00	0
317	FFCR	SS	20	15	20	418	82	1.31	1.35	0.02	1.6	44.00	0.5
319	FFCR	SS	30	15	20	685	135	1.31	1.35	0.02	1.6	44.00	0.9

(continued)

**Table 1.2-1 – TRIGA Fresh Fuel Characteristics (concluded)**

ID	Type	Cladding	U (wt.% fuel)	Fuel Length (in)	U-235 (wt.% U)	U (g)	U-235 (g)	Fuel OD (in)	Rod OD (in)	Cladding Thickness (in)	H/Zr	Overall Length (in)	Er (wt.%)
403	Cluster	SS	8.5	15	20	166	33	1.37	1.41	0.02	1.6	30.38	0
405	Cluster	SS	12	15	20	243	48	1.37	1.41	0.02	1.6	30.38	0
417	Cluster	SS	20	15	20	427	85	1.37	1.41	0.02	1.6	30.38	0.5
419	Cluster	SS	30	15	20	710	141	1.37	1.41	0.02	1.6	30.38	0.9
503	Ins. cluster	SS	8.5	15	20	166	33	1.34	1.41	0.02	1.6	45.50	0
505	Ins. cluster	SS	12	15	20	243	48	1.34	1.41	0.02	1.6	45.50	0
517	Ins. cluster	SS	20	15	20	427	85	1.34	1.41	0.02	1.6	45.50	0.5
519	Ins. cluster	SS	30	15	20	710	141	1.34	1.41	0.02	1.6	45.50	0.9

Note: General Atomics catalog numbers are not necessarily unique. TRIGA elements with the same ID could have different fuel parameters. In this table, two variants of the Type 101 element are listed. Overall length includes 0.25 inches for irradiation growth.

**Table 1.2-2 – TRIGA Fuel Qualification Table**

Type	Maximum Burnup (MWD)	Minimum Cooling (days)	Type	Maximum Burnup (MWD)	Minimum Cooling (days)
101 (8.0%)	23	90	303	22	90
201/101 (8.5%)	26	90	305	32	90
109	88	350	317	58	210
	70	250		46	150
	52	170		34	90
	34	90	319	97	420
203/103	27	90		76	290
205/105	39	120		55	180
	33	90		34	90
207/107	38	120	503/403	23	90
	33	90	505/405	33	90
217/117	71	280	517/417	60	220
	52	180		47	150
	34	90		34	90
219/119	122	600	519/419	101	430
	91	370		79	290
	63	220		56	180
	34	90		34	90

Note: This table is developed based on an in-core residence time of 4 years to result in a decay heat  $\leq 20$  W. For fuel with an in-core residence time less than 4 years, the decay heat shall be independently confirmed to be  $\leq 20$  W.

**Table 1.2-3 –Square Plate Fuel Characteristics**

Parameter	RINSC	U-Mass (Al)	U-Mass (Si)	Ohio St	Miss. S&T	U-Florida	Purdue
U-235 loading (g)	275±7.7	167±3.3	200±5.6	200±5.6	225±6.3	175±4.9	129.92±2.52
Nominal U-235 Enrichment (%)	19.75	19.75	19.75	19.75	19.75	19.75	19.75
Fuel matrix	U <sub>3</sub> Si <sub>2</sub> +Al	UAl <sub>x</sub>	U <sub>3</sub> Si <sub>2</sub> +Al	U <sub>3</sub> Si <sub>2</sub> +Al	U <sub>3</sub> Si <sub>2</sub> +Al	U <sub>3</sub> Si <sub>2</sub> +Al	U <sub>3</sub> Si <sub>2</sub> +Al
Maximum burnup (MWD)	52.5	9.7	9.7	64.0	74.0	87.0	0.57
Minimum decay time (D)	120	1,000	1,000	120	365	120	120
Nominal fuel meat width (in.)	2.395	2.320	2.395	2.395	2.395	2.395	2.395
Nominal fuel meat thickness (in.)	0.02	0.03	0.02	0.02	0.02	0.02	0.02
Nominal fuel plate thickness (in.)	0.05	0.06	0.05	0.05	0.05	0.05	0.05
Nominal active fuel length (in.)	23.25	23.25	23.25	23.25	23.25	23.25	23.25
Number of fuel plates	22	18	16	16	18	14	14
Maximum channel spacing (in.)	0.099	0.119	0.122	0.127	0.139	0.117	0.175
Weight (lb)	14	12	12	12	14	10	10
Maximum cross section (in.)	3.097×3.097	3.097×3.097	3.097×3.097	3.05×3.05	3.036×3.212	2.9×2.424	3.011×3.011
Maximum overall length (in.) <sup>④</sup>	39.75	39.75	39.75	35.25	34.50	27.38	32.49
Loose plate <sup>④</sup>	no	①	no	no	no	②	③

Notes:

1. U-Mass (Al) loose plates have a U-235 loading of  $9.28 \pm 0.18\text{g}$  and dimensions of 2.78 inches wide by 24.88 inches long.
2. U-Florida loose plates have a U-235 loading of  $12.5 \pm 0.35\text{g}$  and dimensions of 2.85 inches wide by 25.88 inches long.
3. Purdue loose plates have a U-235 loading of  $9.28 \pm 0.18\text{g}$  and dimensions of 2.85 inches wide by 25.88 inches long.
4. Maximum length includes 0.25 inches for irradiation growth.



**Table 1.2-4 –PULSTAR Fuel Characteristics**

<b>Parameter</b>	<b>Value</b>
Nominal U-235 Enrichment (%)	4.0/6.0
Fuel matrix	UO <sub>2</sub>
Maximum burnup (MWD/MTU)	20,000
Decay time (years)	1.5
Maximum fuel pellet diameter (in.)	0.423
Minimum cladding thickness (in.)	0.0185
Cladding material	Zirconium alloy
Maximum cladding OD (in.)	0.474
Maximum active fuel length (in.)	24.1
Fuel rod pitch X (in.)	0.607
Fuel rod pitch Y (in.)	0.525
Box outer dimensions (in.)	3.15 x 2.74
Box thickness (in.)	0.06
Box material	Zirconium alloy
Maximum overall length (in.) <sup>①</sup>	38.23

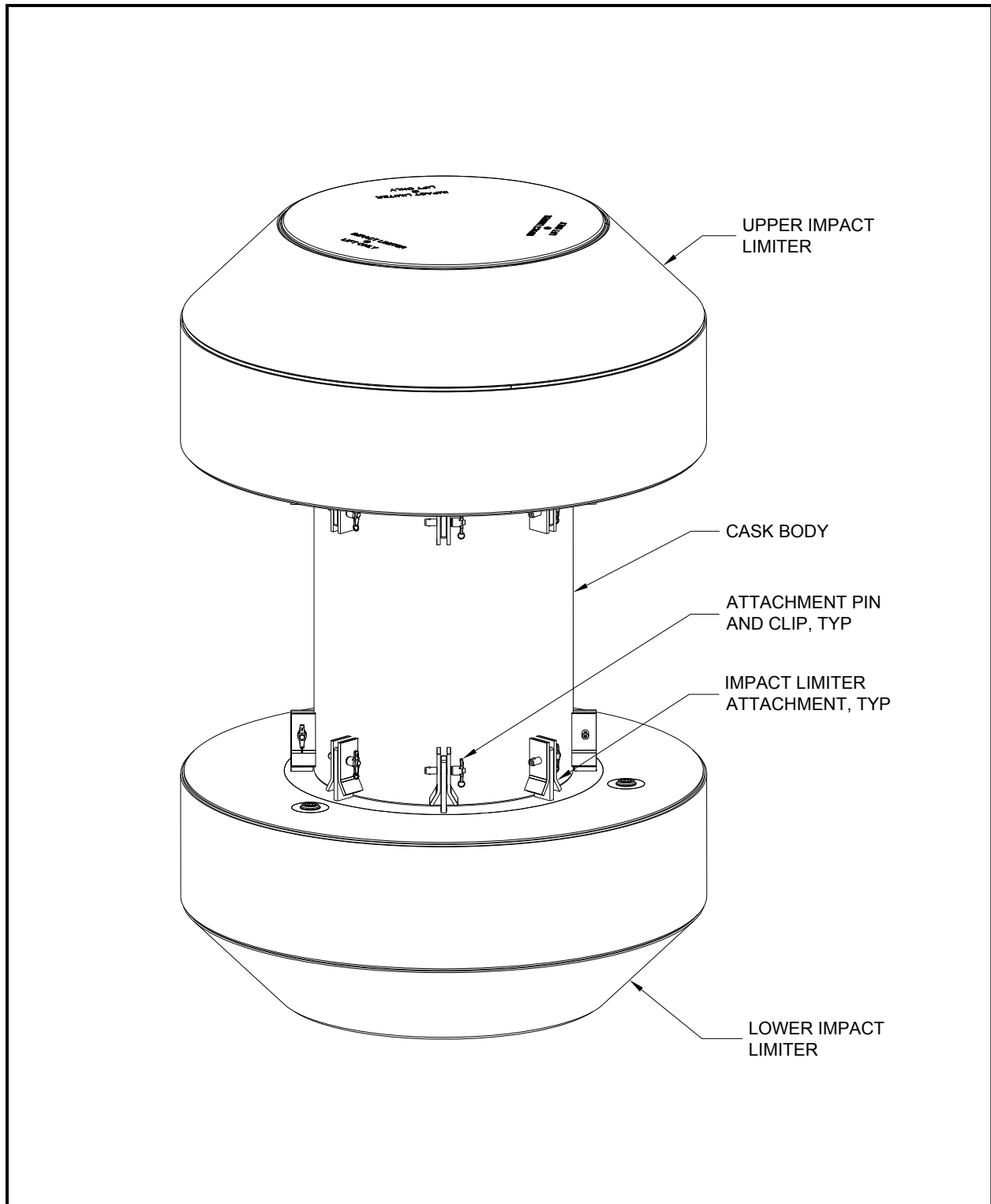
Notes:

1. Maximum length includes 0.25 inches for irradiation growth.

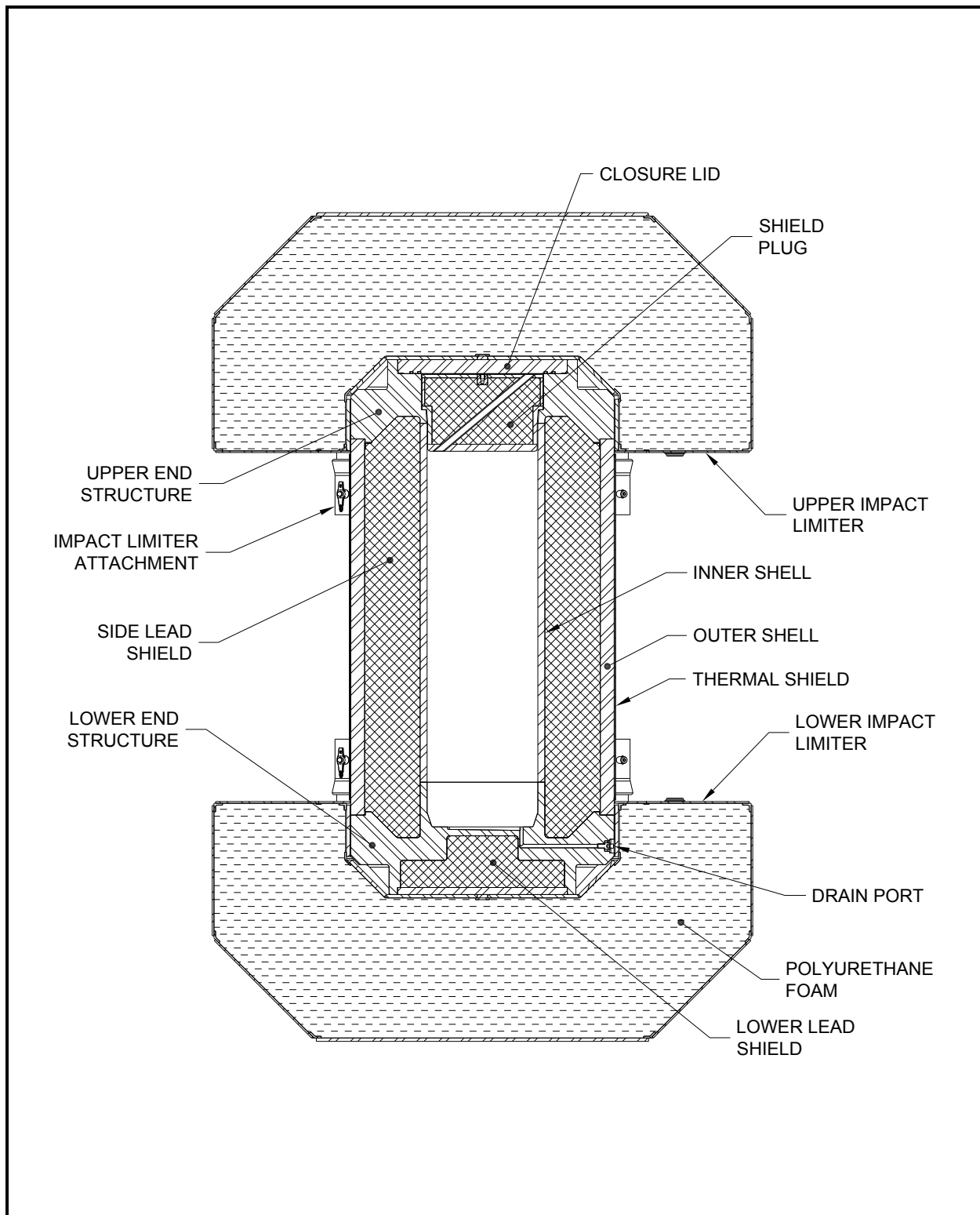
**Table 1.2-5 – Plutonium Activity**

<b>Plutonium Activity per Fuel Element (Ci)</b>					
<b>Isotope</b>	<b>MURR</b>	<b>MITR-II</b>	<b>ATR</b>	<b>TRIGA</b>	<b>Square<sup>①</sup></b>
Pu-238	1.63E+00	5.16E+00	8.38E+00	1.35E+01	1.32E+01
Pu-239	1.03E-01	9.80E-02	1.90E-01	4.91E-01	5.16E+00
Pu-240	4.91E-02	5.81E-02	1.38E-01	5.36E-01	3.46E+00
Pu-241	1.19E+01	2.61E+01	4.60E+01	2.27E+02	7.90E+02
Pu-242	3.66E-05	1.35E-04	4.93E-04	4.15E-03	4.48E-03
Total	1.37E+01	3.14E+01	5.48E+01	2.42E+02	8.12E+02
<b>Plutonium Activity per BRR Package (Ci)</b>					
<b>Isotope</b>	<b>MURR</b>	<b>MITR-II</b>	<b>ATR</b>	<b>TRIGA</b>	<b>Square<sup>①</sup></b>
Pu-238	1.30E+01	4.13E+01	6.70E+01	2.57E+02	1.06E+02
Pu-239	8.26E-01	7.84E-01	1.52E+00	9.32E+00	4.13E+01
Pu-240	3.93E-01	4.65E-01	1.10E+00	1.02E+01	2.77E+01
Pu-241	9.56E+01	2.09E+02	3.68E+02	4.32E+03	6.32E+03
Pu-242	2.93E-04	1.08E-03	3.95E-03	7.88E-02	3.59E-02
Total	1.10E+02	2.51E+02	4.38E+02	4.60E+03	6.50E+03

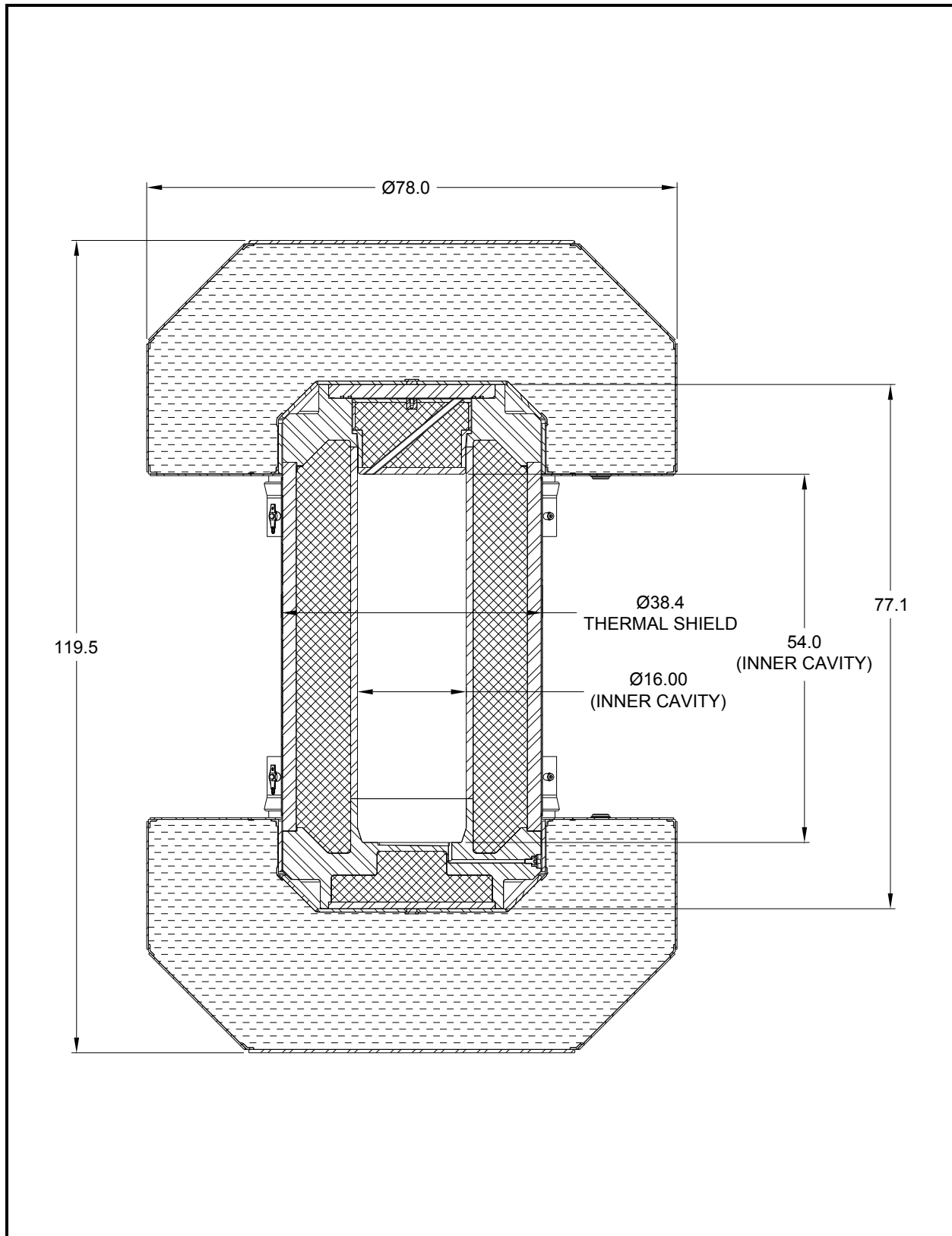
① Fuels transported in the Square fuel basket include RINSC, U-Mass, Ohio State, Missouri S&T, U-Florida, Purdue, and PULSTAR. The limiting plutonium activity occurs for PULSTAR.

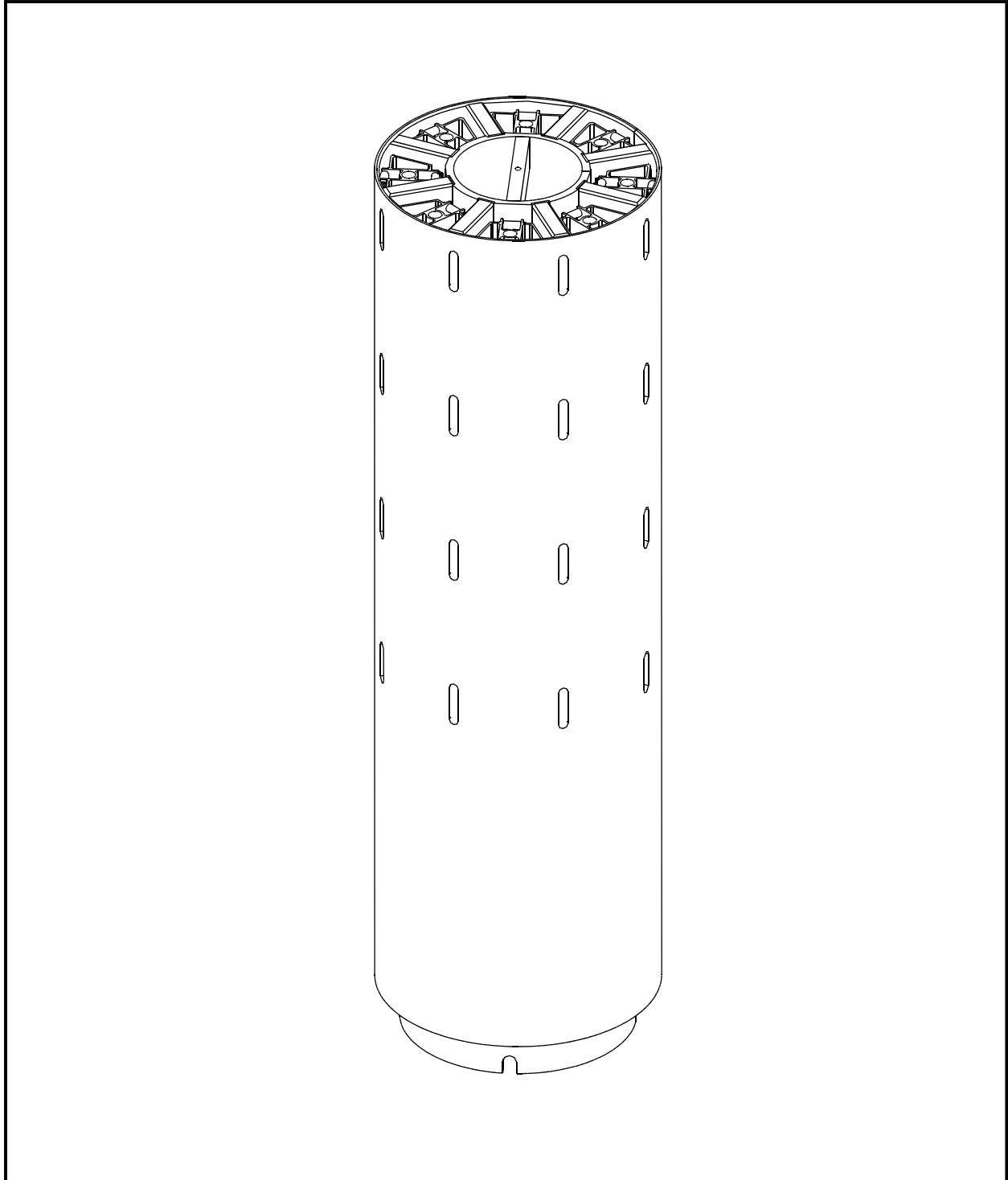


**Figure 1.2-1 – BRR Packaging Components**

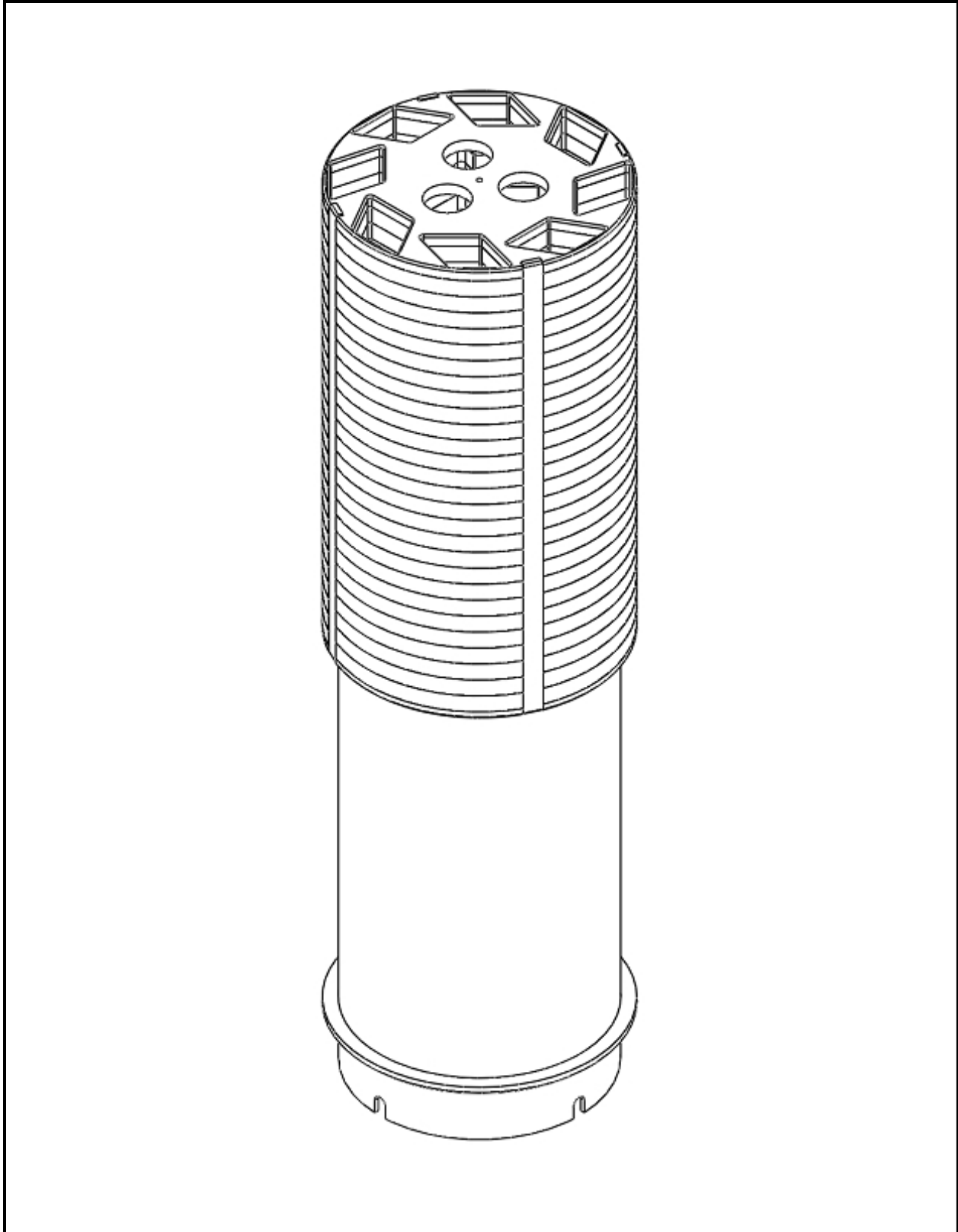


**Figure 1.2-2 – BRR Package Cross Section**

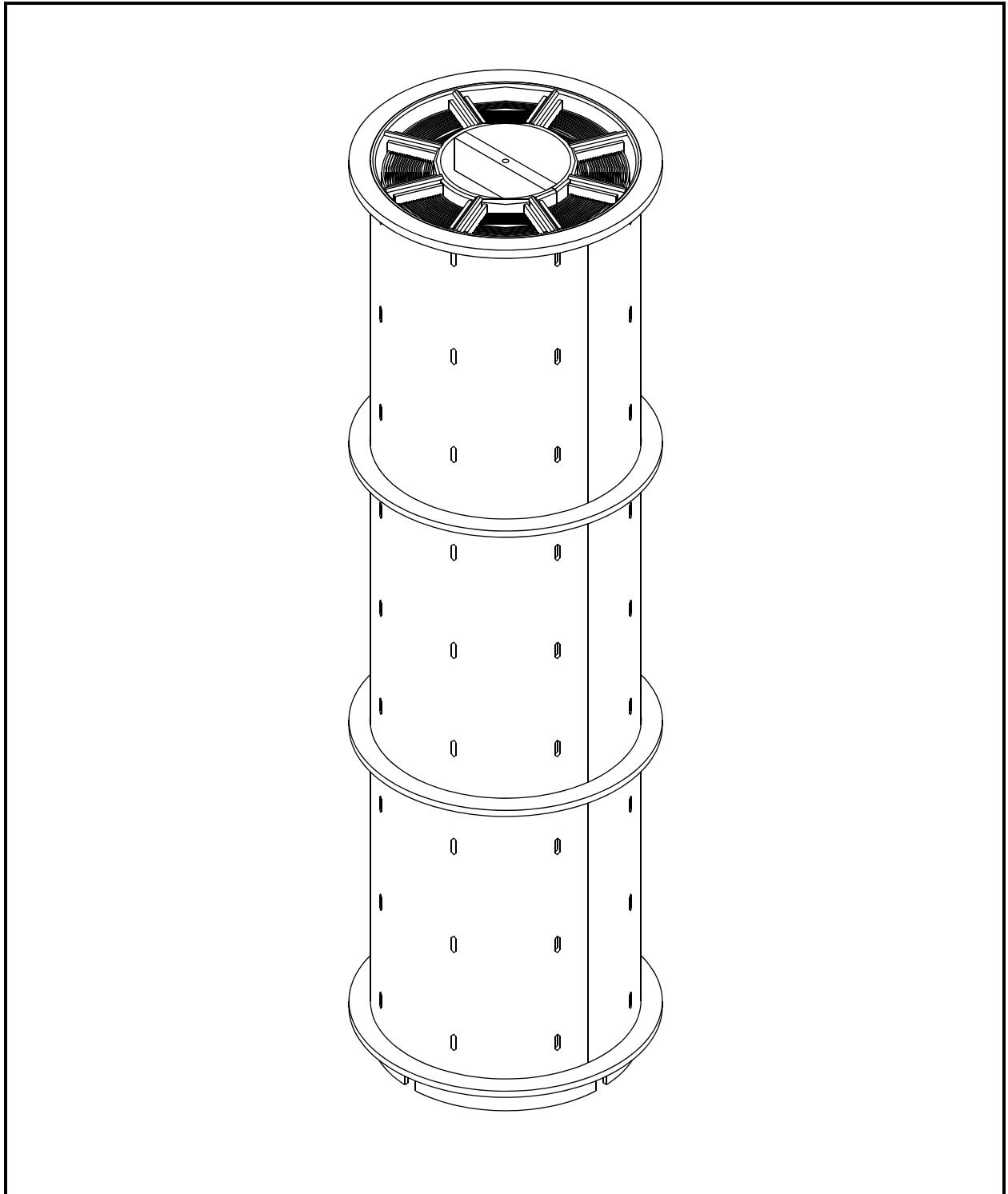
**Figure 1.2-3 – BRR Package Dimensions**



**Figure 1.2-4 – MURR Fuel Basket**

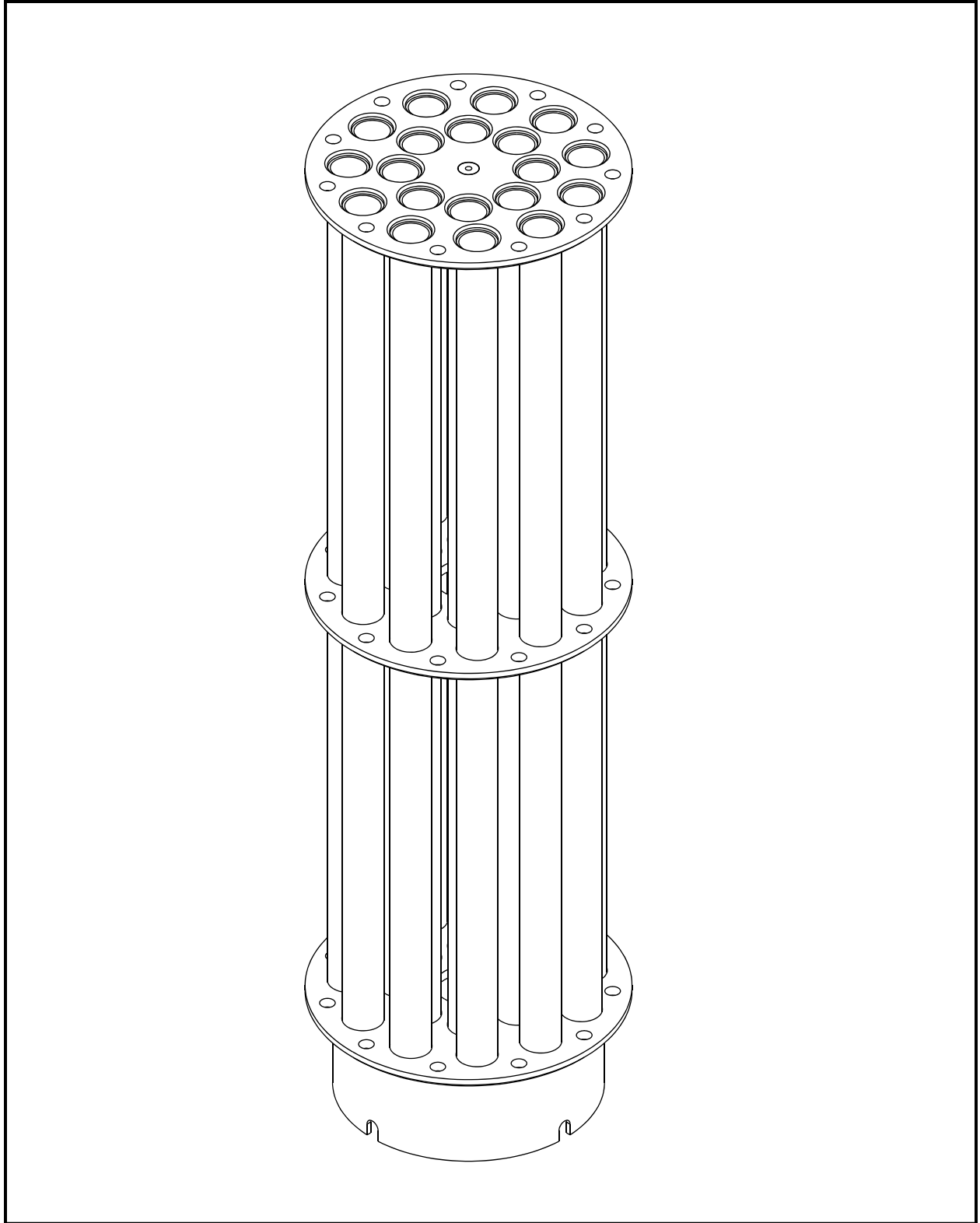


**Figure 1.2-5 – MITR-II Fuel Basket**

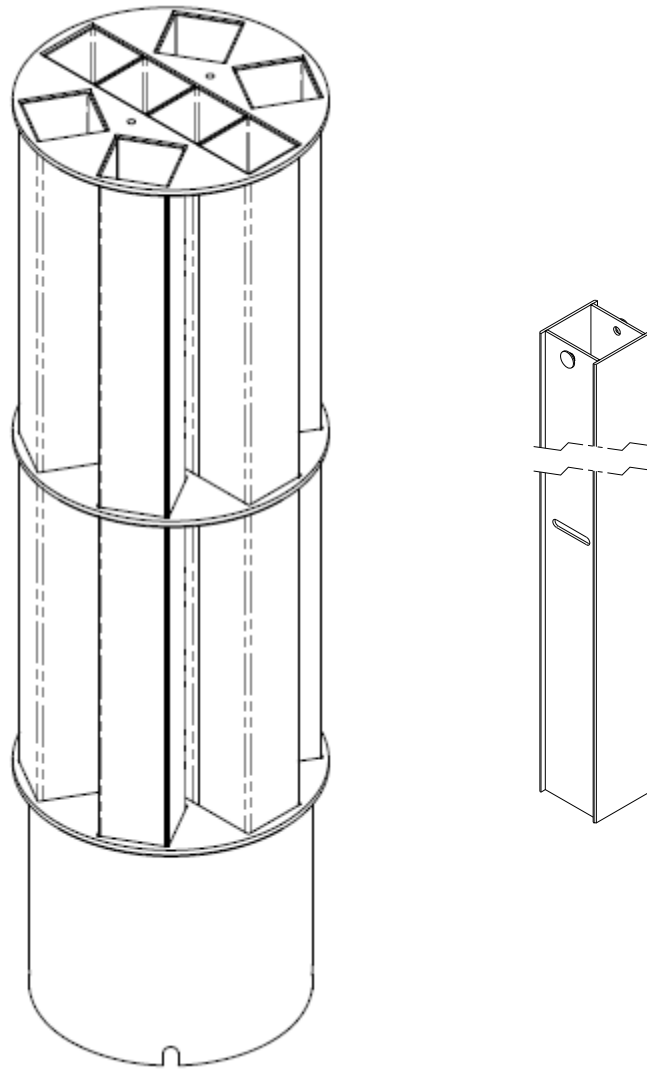


**Figure 1.2-6 –ATR Fuel Basket**

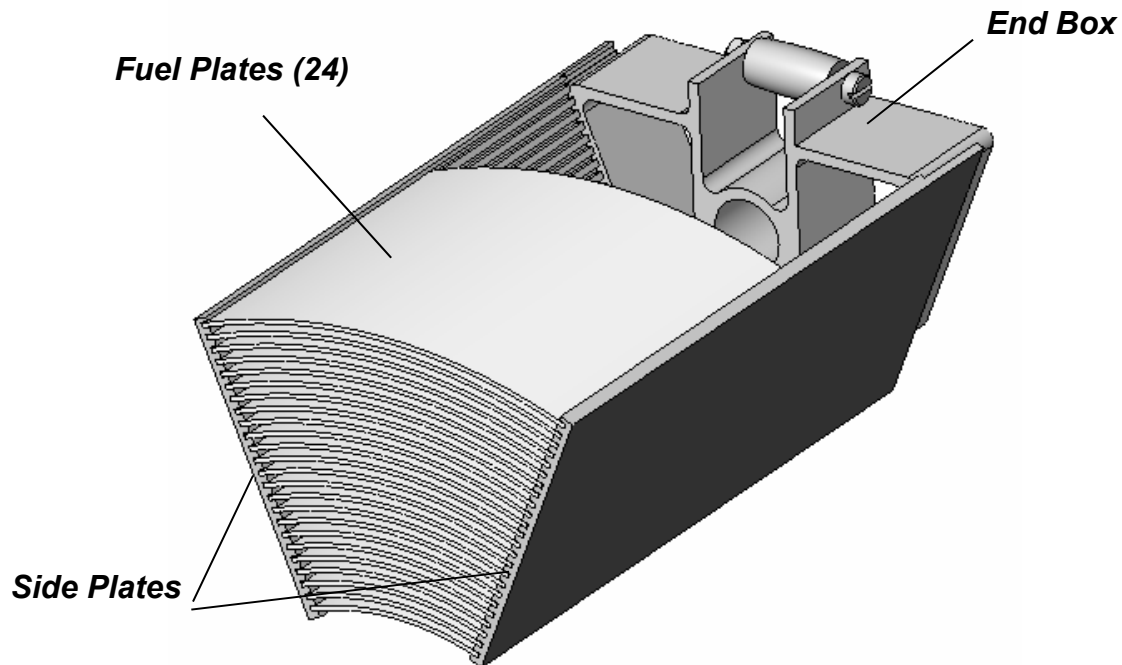




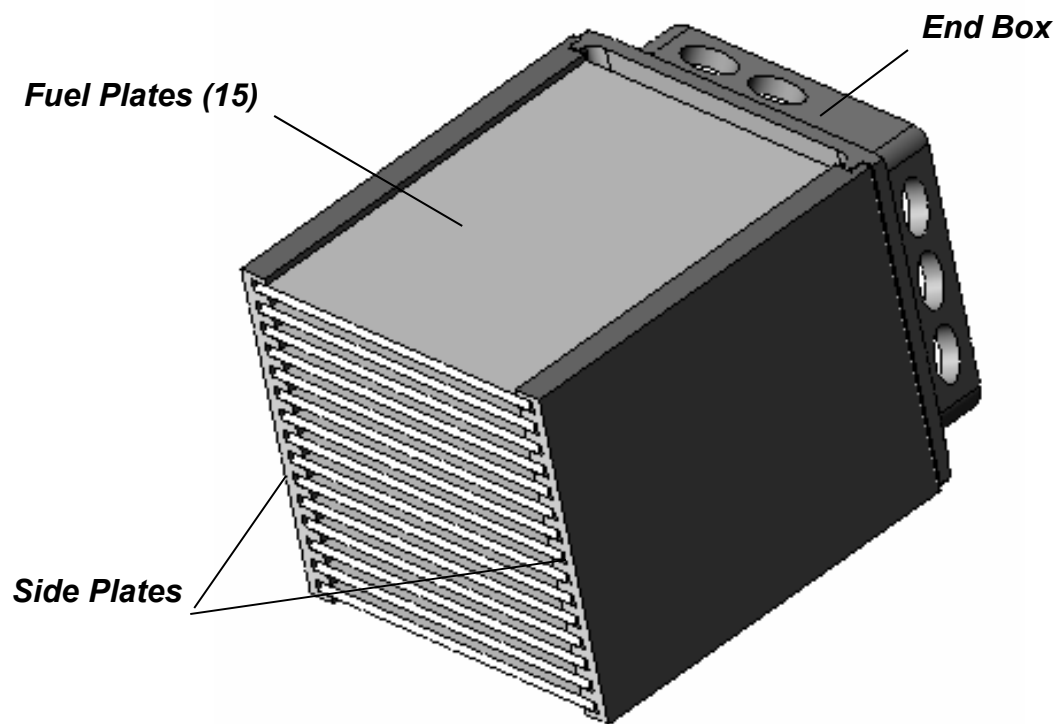
**Figure 1.2-7 – TRIGA Fuel Basket**



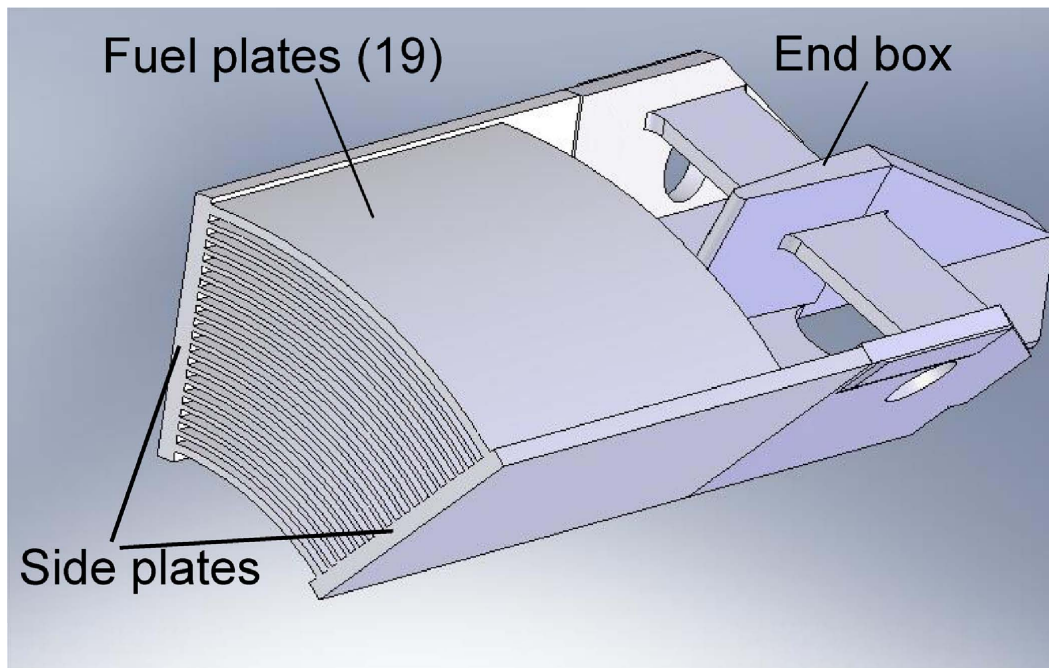
**Figure 1.2-8 – Square Fuel Basket and Loose Plate Box**



**Figure 1.2-9 – MURR Fuel Element – Section View**

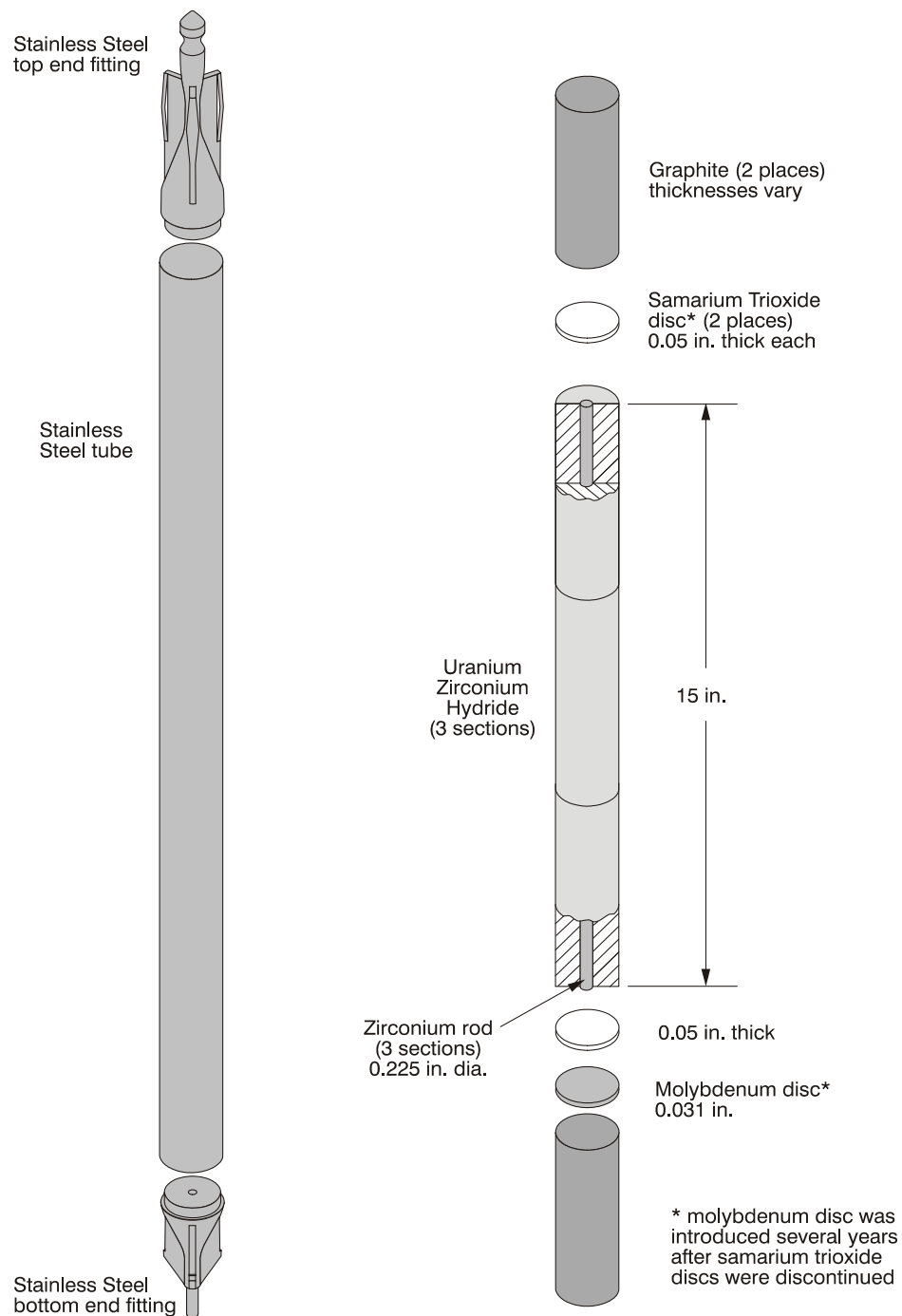


**Figure 1.2-10 – MITR-II Fuel Element – Section View**

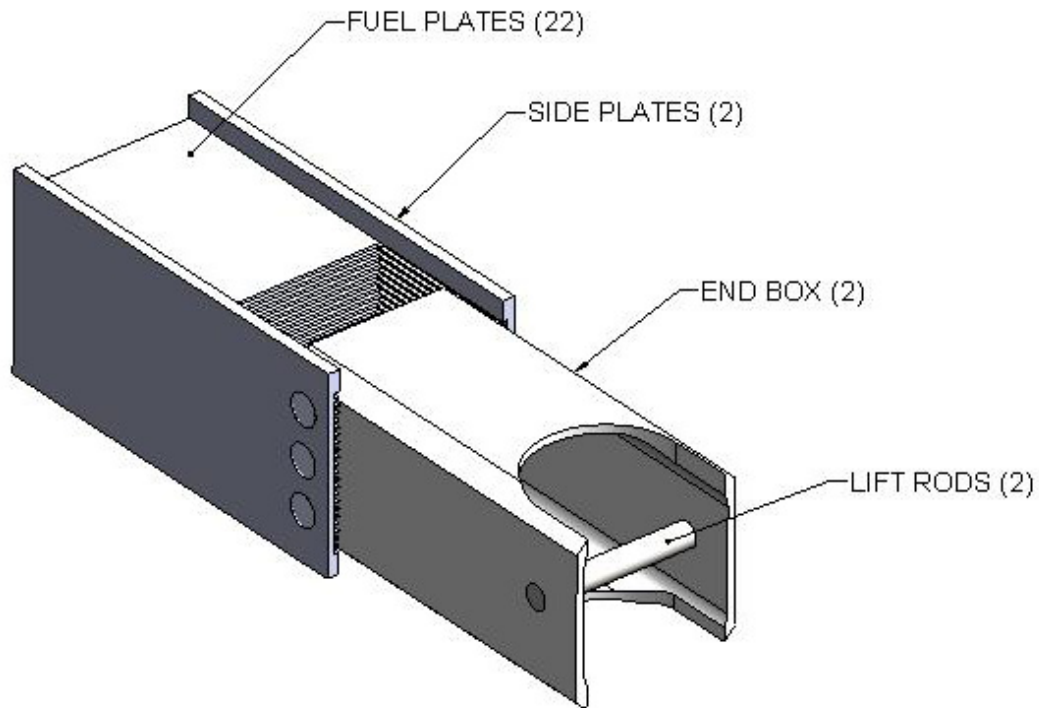


Note: The end box shown in this figure will be removed prior to insertion in the BRR package.

**Figure 1.2-11 – ATR Fuel Element – Section View**

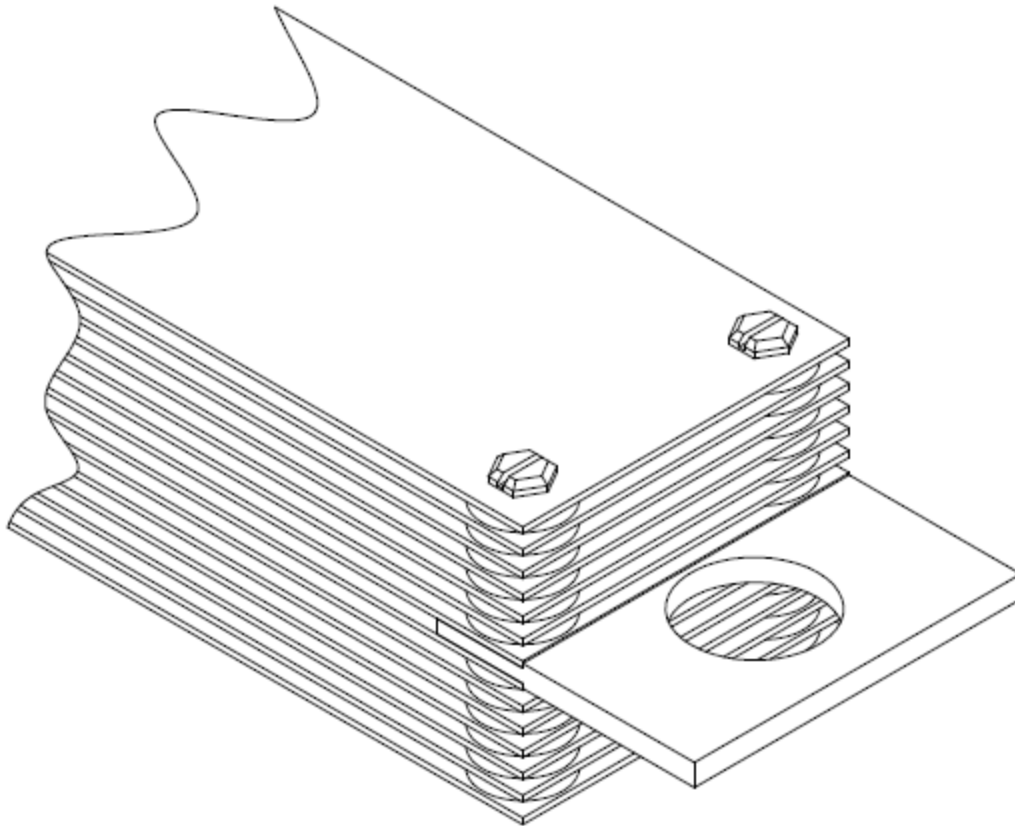


**Figure 1.2-12 – TRIGA Fuel Element (Stainless Steel Clad)**



(Representative of Square or Rectangular, Swaged Plate Designs)

**Figure 1.2-13 – Rhode Island Nuclear Science Center Fuel Element**

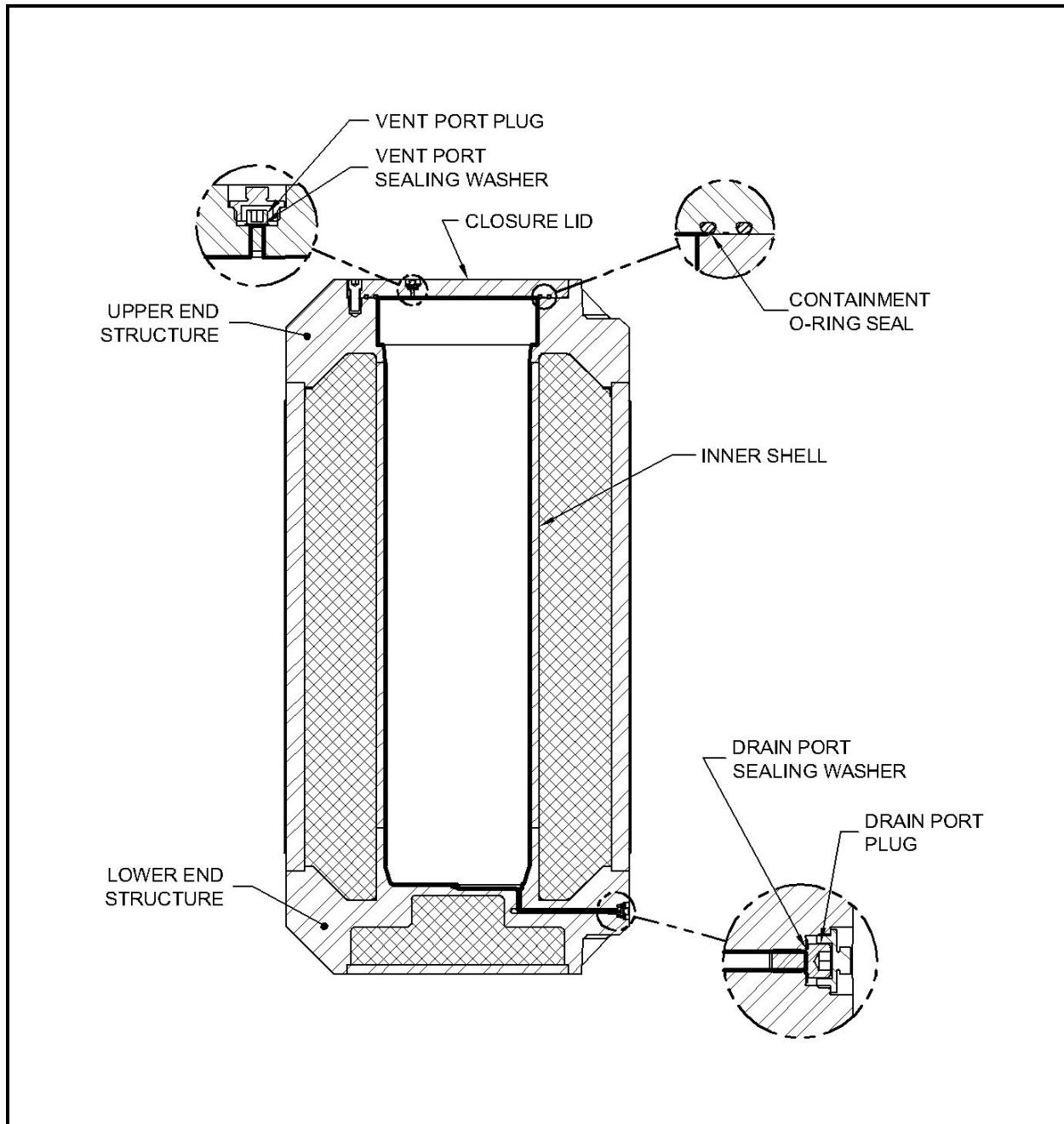


**Figure 1.2-14 – University of Florida Fuel Element**

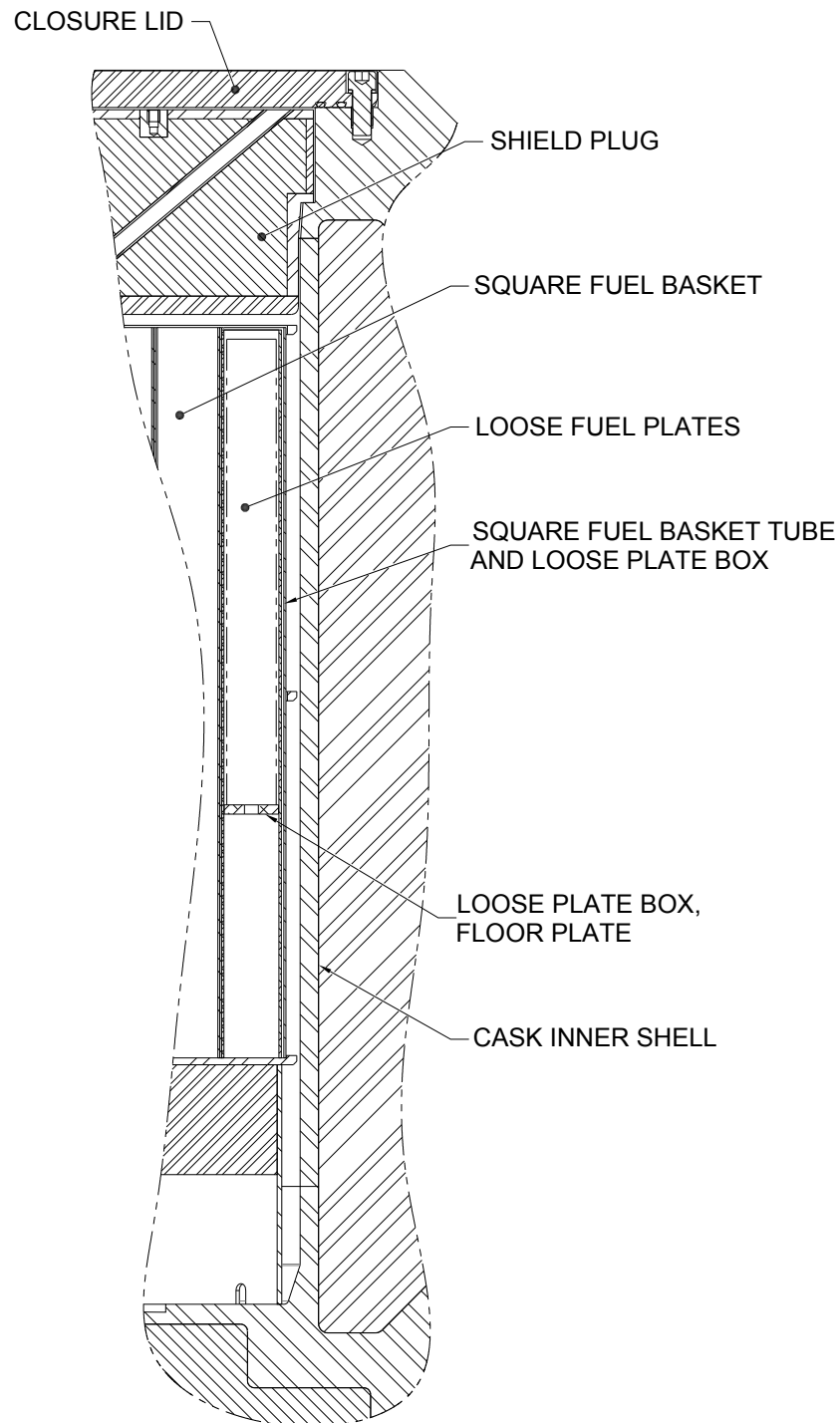
## Security-Related Information Figure Withheld Under 10 CFR 2.390.

**Figure 1.2-15 – PULSTAR Fuel Element**





**Figure 1.2-16 – BRR Package Containment Boundary**



**Figure 1.2-17 – Cross Section View of BRR Package Showing Basket, Loose Plate Box, and Loose Plates**

## **1.3 Appendices**

### **1.3.1 References**

1. Title 10, Code of Federal Regulations, Part 71 (10 CFR 71), Packaging and Transportation of Radioactive Material, 01–01–08 Edition.
2. ANSI N14.5–1997, *American National Standard for Radioactive Materials – Leakage Tests on Packages for Shipment*, American National Standards Institute (ANSI), Inc.

### 1.3.2 Glossary of Terms and Acronyms

ANSI –	American National Standards Institute.
ASME B&PV Code –	American Society of Mechanical Engineers Boiler and Pressure Vessel Code.
ASTM –	American Society for Testing and Materials.
ATR –	Advanced Test Reactor.
AWS –	American Welding Society.
Basket –	Structure that supports the fuel within the payload cavity.
Blade –	Part of impact limiter attachment, integral with the impact limiter. See <i>Receptacle</i> , below.
Cask Body –	BRR package component consisting of the inner shell, outer shell, upper and lower end structures, side and lower lead shielding.
Closure Lid –	Plate that completes the containment boundary. It contains the vent port, the test port, the containment O-ring seal, and the test O-ring seal.
Closure Bolts –	Fasteners that secure the closure lid to the body.
Containment O-ring Seal –	Inner elastomeric seal, retained in the closure lid, which forms part of the containment boundary.
Drain port –	Containment penetration at the lower end of the cask body through which water is drained from the cask during operations. Closed with the drain port plug, that is protected by a dust cover.
GA –	General Atomics.
HAC –	Hypothetical Accident Conditions.
HEU –	High Enriched Uranium.
LEU –	Low Enriched Uranium.
Lower End Structure –	Part of the cask body. Massive structural element made of casting or forging that connects to both inner and outer cask body shells, and that contains the lower lead shielding and drain port. Interfaces with the lower impact limiter.
Loose Plates –	Intact plates which have been removed from an irradiated plate fuel element.
MITR-II –	Massachusetts Institute of Technology Nuclear Research Reactor.
MNOP –	Maximum Normal Operating Pressure.
MURR –	University of Missouri Research Reactor.

NCT –	Normal Conditions of Transport.
OD –	Outer Diameter.
Sealing Washers –	Integrated metal and elastomer seals that are used with the vent, test, and drain ports.
Shield Plug –	A removable plug that serves as the upper shielding.
Square Fuel –	Fuel types that have a square, or nearly square rectangular cross section.
Receptacle –	The pair of plates, attached to the cask, that accepts the impact limiter blade and create the impact limiter attachment.
Test O-ring Seal –	Outer elastomeric seal, retained in the closure lid, used to allow leakage rate testing of the containment seal.
Test port –	Opening located between the containment O-ring seal and the test O-ring seal in the closure lid, used to test the leakage rate of the containment O-ring seal. Closed with the test port plug, which is protected by a dust cover.
Thermal Shield –	Thin sheet attached to the outside of the outer shell, forming a thin air gap that inhibits heat transfer into the package during the HAC fire event.
TRIGA –	Training, Research, Isotopes, General Atomics.
Upper End Structure –	Part of the cask body. Massive structural element made of casting or forging that connects to both inner and outer cask body shells, and interfaces with the closure lid, shield plug, and upper impact limiter.
Vent port –	Containment penetration located in the closure lid which is used to vent the cavity and to introduce helium for leakage rate testing during operations. Closed with the vent port plug, that is protected by a dust cover.

### **1.3.3 Packaging General Arrangement Drawings**

The packaging general arrangement drawings consist of:

- 1910–01–01–SAR, BRR Package Assembly SAR Drawing, 4 sheets
- 1910–01–02–SAR, BRR Package Impact Limiter SAR Drawing, 2 sheets
- 1910–01–03–SAR, BRR Package Fuel Baskets SAR Drawing, 4 sheets

# Security-Related Information Figure Withheld Under 10 CFR 2.390.


UNCONTROLLED

AREVA

NOV 23 2010

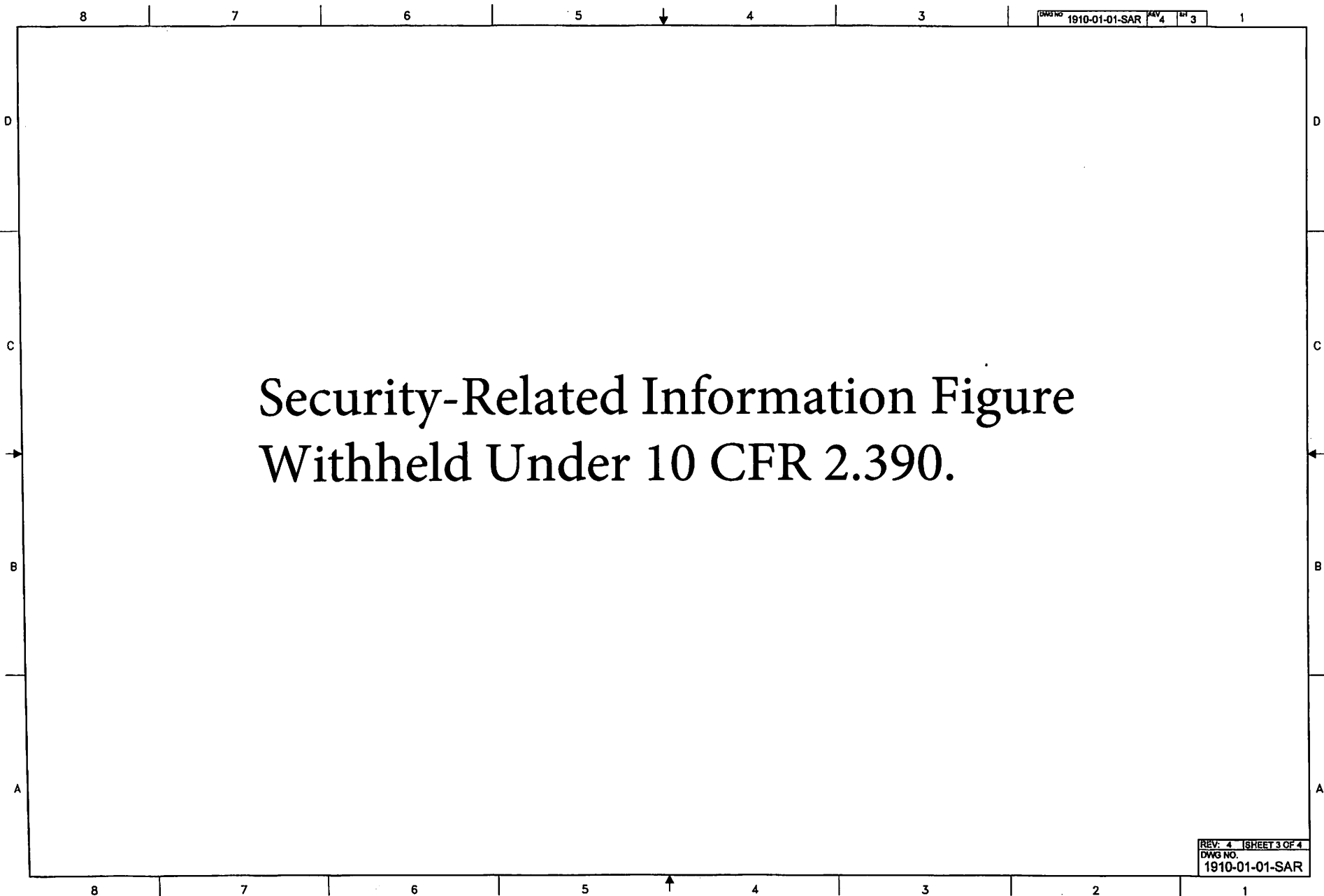
Records Management

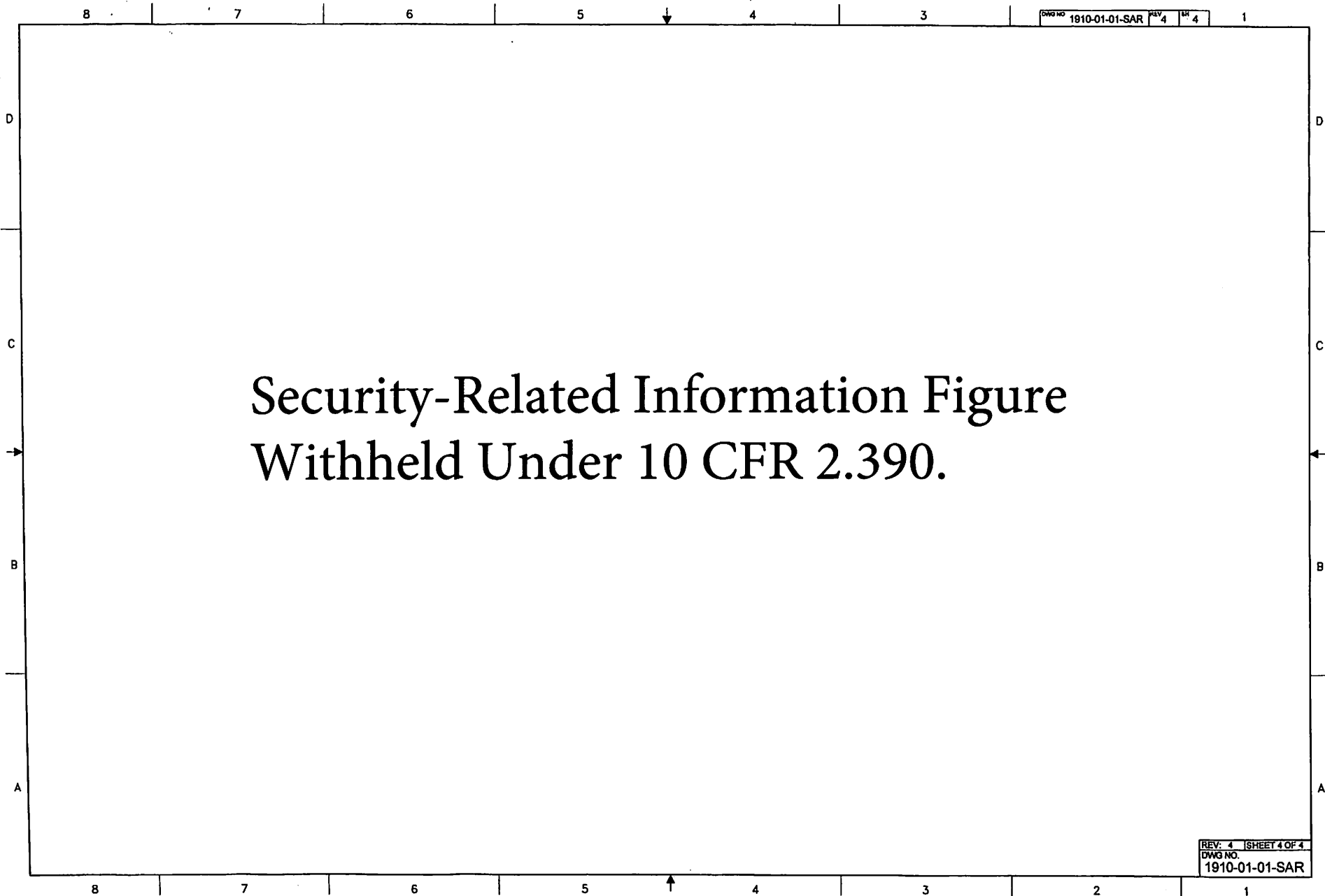
Released By *B. Hays*

NAME/SIGNATURE		DATE	 <p>AREVA Federal Services LLC Packaging Projects Tacoma, WA 98402</p>
APPD			
APPD	C. TEMUS	3/15/09	
ENGR	P. NOSS	3/15/09	
QA	K. KING	3/15/09	
CHECK	D. STEVENSON	3/15/09	<p>DWG TITLE</p> <p><b>BRR PACKAGE ASSEMBLY SAR DRAWING</b></p>
DRAWN	R. LE	3/15/09	
<p><b>TOLERANCES:</b> FRACTIONS ± 1/16 ANGLES ± 1° WELD A FORMED TOLERANCE: FRACTIONS ± 1/16 ANGLES ± 1°</p>			
<p>1 PLACE DECIMALS ± .01 1 PLACE DECIMALS ± .2 1 PLACE DECIMALS ± .12 1 PLACE DECIMALS ± .3</p>			<p>SCALE: SHOWN</p> <p>REV. 4</p> <p>DWG NO. 1910-01-01-SAR</p> <p>CADFILE: 19100101BARR.MCDRW</p>

Security-Related Information Figure  
Withheld Under 10 CFR 2.390.








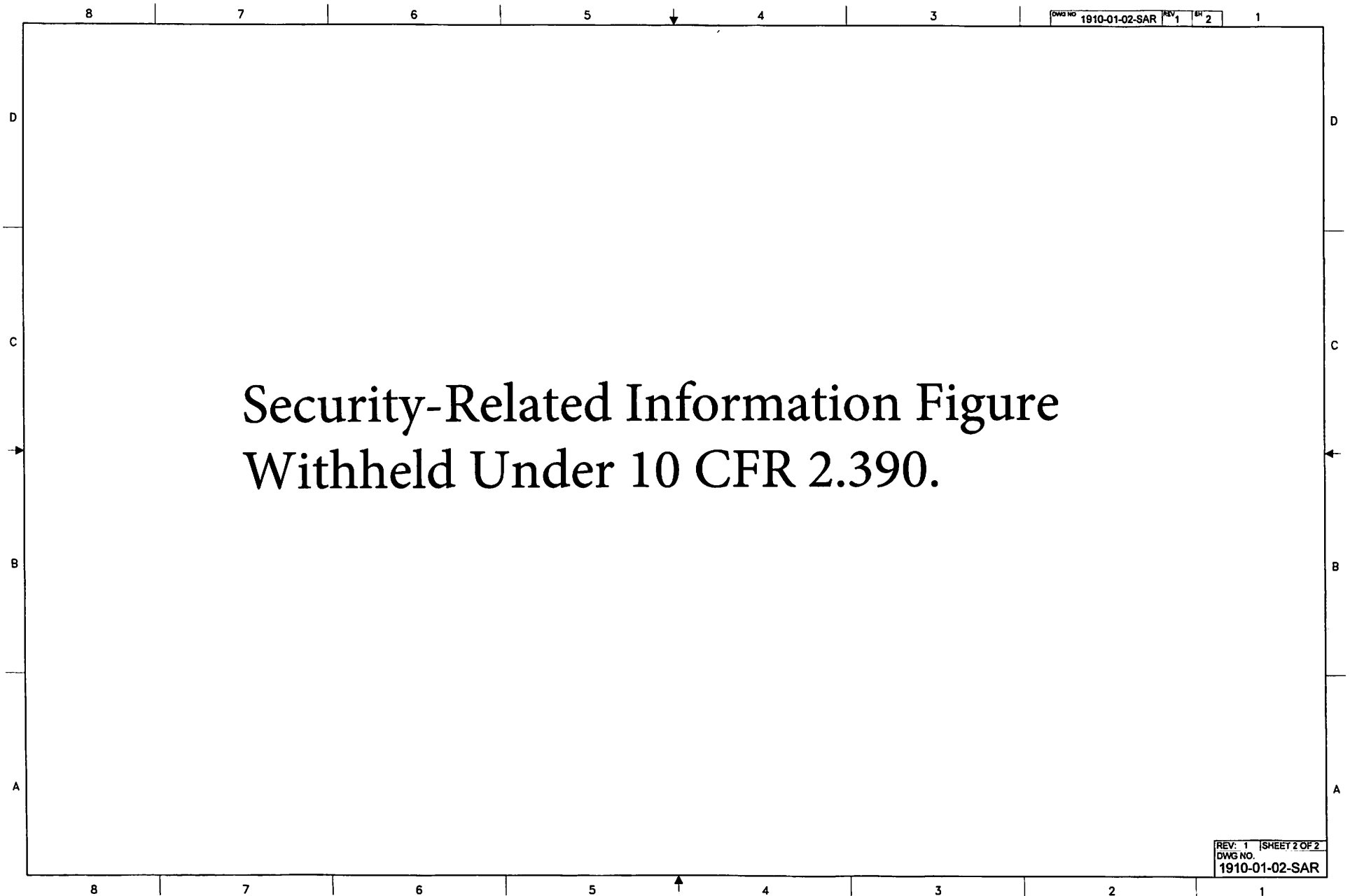
# Security-Related Information Figure Withheld Under 10 CFR 2.390.

AREVA  
DEC 09 2010  
Records Management  
Released By *R. Henrich*

NAME/SIGNATURE		DATE
APPD		
APPD	C. TEMUS	3/18/10
ENGR	P. NOSS	3/18/10
QA	K. KING	3/18/09
CHECK	D. STEVENSON	3/18/09
DRAWN	R. LE	3/18/09

		AREVA Federal Services LLC Packaging Projects Tacoma, WA 98402	
DWG TITLE: BRR PACKAGE IMPACT LIMITER SAR DRAWING			
MACHINE TOLERANCES: FRACTIONS : 1/4 ANGLES : 1/2°		2 PLACE DECIMALS : .00 1 PLACE DECIMALS : .2	
UNLESS OTHERWISE SPECIFIED: FRACTIONS : 1/4 ANGLES : 1/2°		2 PLACE DECIMALS : .00 1 PLACE DECIMALS : .2	
SCALE: NOTED REV: 1 DWG NO: 1910-01-02-SAR SIZE: D CAD FILE: 191002SAR1.XLDRW		WGT: ~ 2252 LBS SHEET 1 OF 2	



DWG NO 1910-01-03-SAR REV 6 SHEET 1

# Security-Related Information Figure Withheld Under 10 CFR 2.390.


**AREVA**  
JAN 14 2016  
Records Management

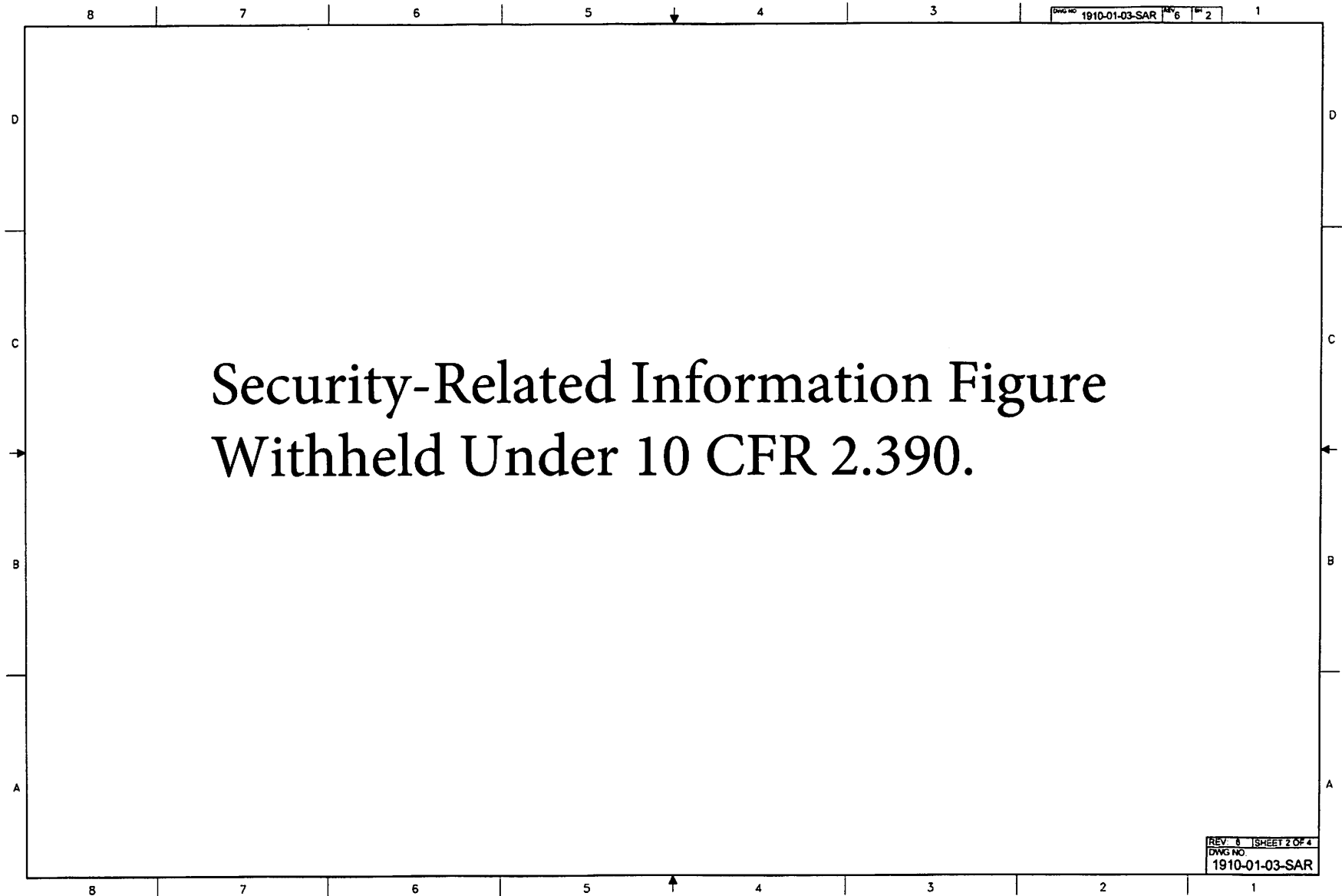
NAME/SIGNATURE		DATE
APPRO		
APPRO	C. TEMUS	3/18/09
ENGR	P. NOSS	3/18/09
QA	K. KING	3/18/09
CHECK	D. STEVENSON	3/18/09
DRAWN	R. LE	3/18/09

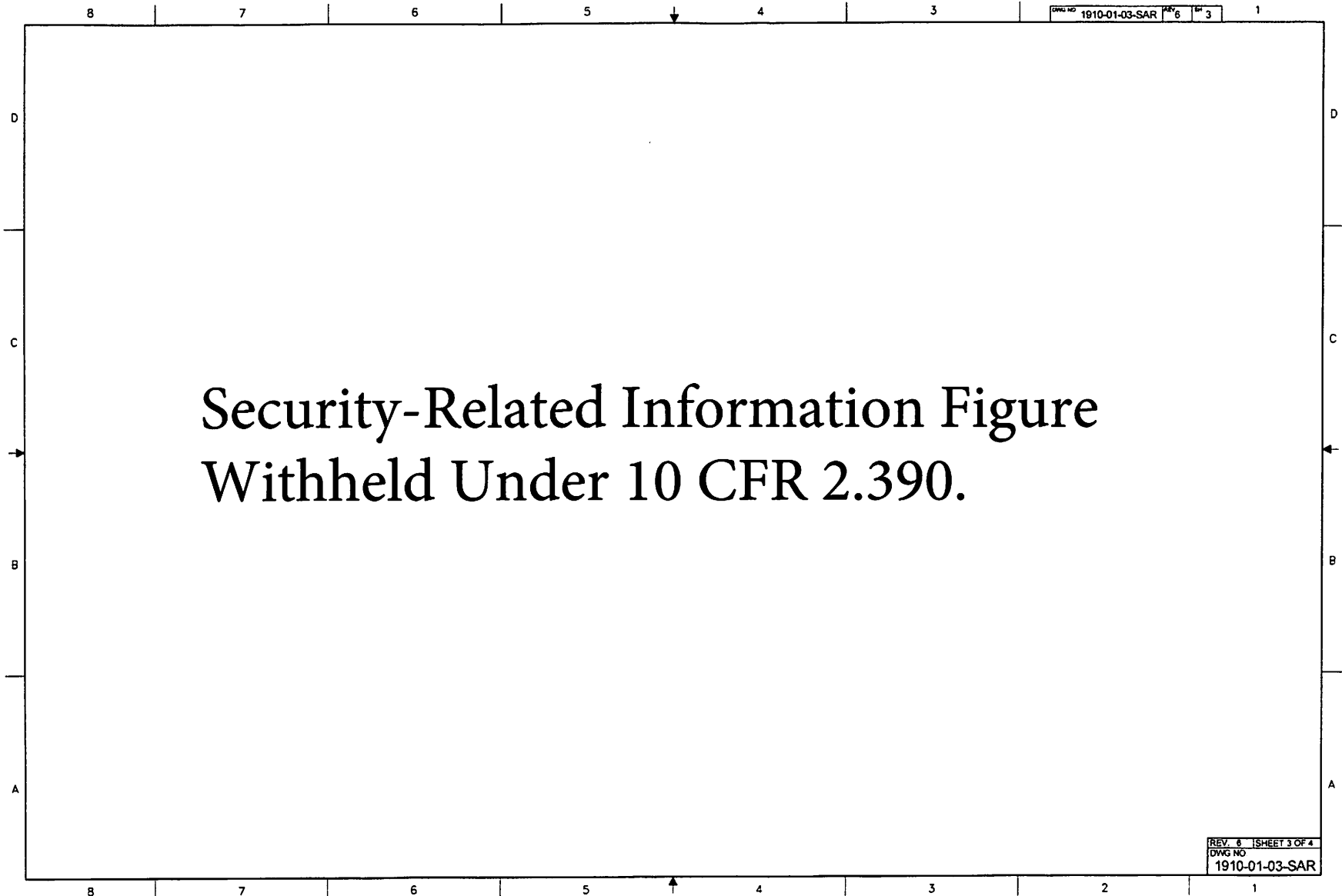
  

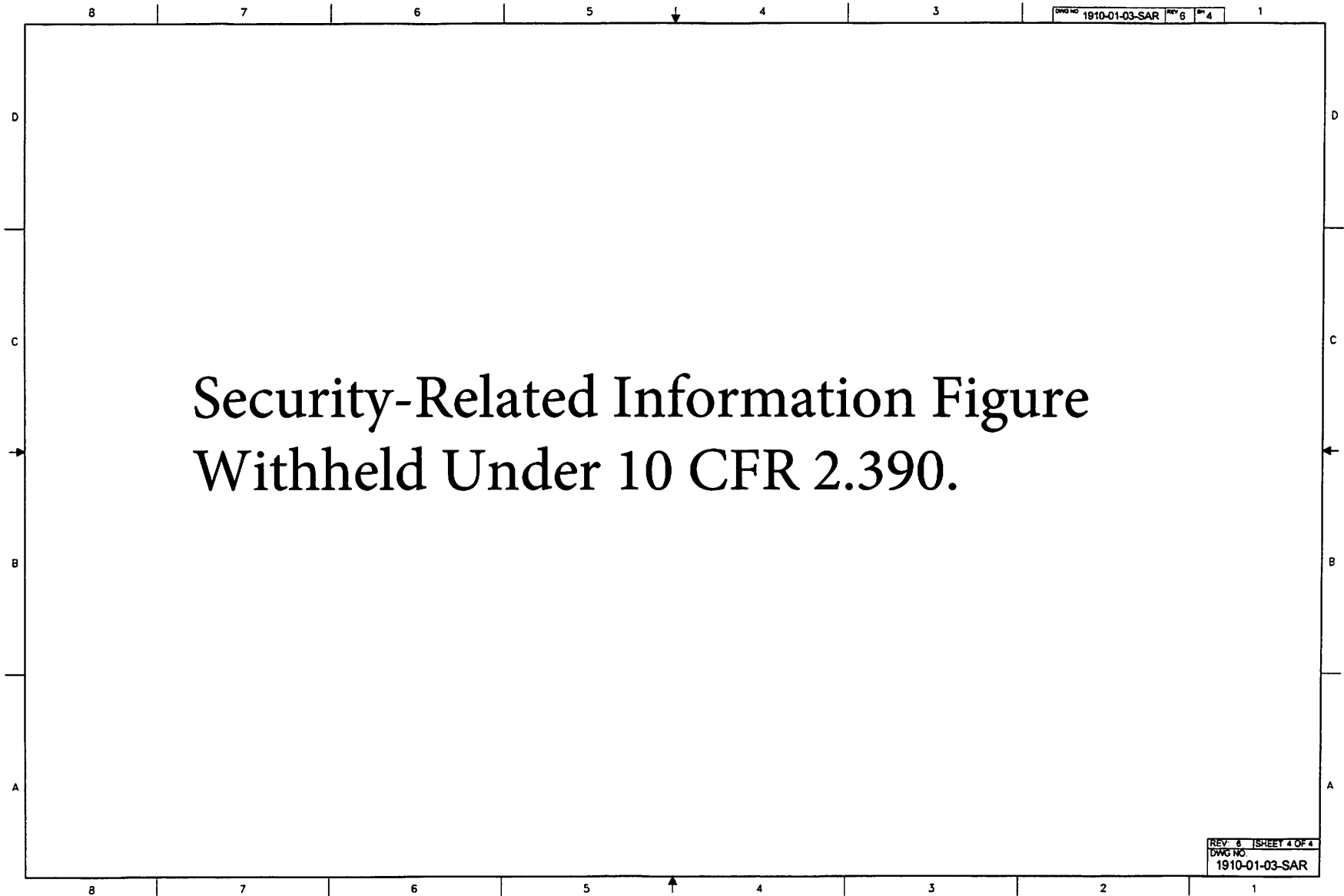
<b>MACHINE TOLERANCES:</b> FRACTION 1/16 ANGLES 1/2°		2 PLACE DECIMAL 1/16 1 PLACE DECIMAL 1/2
<b>WELD &amp; FORMED TOLERANCES:</b> FRACTION 1/16 ANGLES 1/2°		2 PLACE DECIMAL 1/16 1 PLACE DECIMAL 1/2

 AREVA Federal Services LLC Packaging Projects Tacoma, WA 98402	
DWG TITLE <b>BRR PACKAGE FUEL BASKETS            SAR DRAWING</b>	
SCALE SHOWN	WT. - LBS
REV 6	SHEET 1 OF 4
DWG NO	1910-01-03-SAR
SIZE	D
CAD FILE	19100103SAR.DWG
DWG - 3001277-006	









## 2.0 STRUCTURAL EVALUATION

This section presents evaluations demonstrating that the BRR package meets all applicable structural criteria. The BRR package, consisting of a fuel basket, cask assembly, and impact limiters, is evaluated and shown to provide adequate protection for the payload. Normal conditions of transport (NCT) and hypothetical accident condition (HAC) evaluations are performed to address 10 CFR 71 [1] performance requirements. The primary method of performance demonstration is by analysis. Analytic demonstration techniques comply with the methodology presented in NRC Regulatory Guides 7.6 [2] and 7.8 [3]. Impact limiter performance in the free drop and puncture drop events is demonstrated by certification testing utilizing a half-scale certification test unit (CTU). A discussion of the tests performed is given in Appendix 2.12.2, *Certification Test Plan*, and results of the certification tests are provided in Appendix 2.12.3, *Certification Test Results*.

### 2.1 Structural Design

#### 2.1.1 Discussion

The BRR package is designed to transport irradiated research reactor fuel. An isometric view of the cask is shown in Figure 1.2-1, a cross section view is shown Figure 1.2-2, and basic dimensions in Figure 1.2-3. The five types of fuel basket are shown in Figure 1.2-4 through Figure 1.2-8. The BRR package consists of a fuel basket, a cask body (which includes the gamma shielding), a shield plug, a closure lid, and two impact limiters. The payload cavity is 16 inches in diameter and 54 inches long. A lead shield plug of 11.2 inches in thickness is located at the top of the cavity. The inner (containment) shell is 1 inch thick, and the outer structural shell is 2 inches thick. The shells are welded to massive cast or forged end structures. The radial lead thickness is 8 inches, and the bottom lead thickness is 7.7 inches. A 12-gauge thermal shield is attached to the outside of the structural shell.

The closure lid is 2 inches thick and is attached with 12, 1-8 UNC socket head cap screws. Containment is afforded by a 3/8-inch cross-sectional diameter butyl O-ring seal. A test O-ring seal is used to provide a cavity for helium leak testing of the containment seal. The closure lid features vent and test ports and the bottom of the cask features a drain port. Impact limiters are located at each end of the cask to mitigate free drop and puncture drop impact. Each impact limiter has a 1/4-inch thick outer stainless steel shell which envelops a nominally 9 lb/ft<sup>3</sup> polyurethane foam impact absorbing material. Each impact limiter is attached using eight, 1-inch diameter ball-lock pins.

There are five different kinds of payload basket, one each for MURR, MITR-II, ATR, TRIGA, and square or rectangular fuel elements. Each fuel element cavity conforms to the overall geometric shape of the fuel, to ensure a nominally uniform support for the fuel elements under impact conditions. Loose plates are carried in a loose plate box.

All important structures are made from ASTM Type 304 stainless steel. The closure bolts are made from ASTM A320, Grade L43 alloy steel. Gamma shielding is made from ASTM B29, Chemical Lead, or equivalent lead. A comprehensive discussion of the BRR package design and configuration is provided in Section 1.2, *Package Description*.

## 2.1.2 Design Criteria

Proof of performance for the BRR package is achieved primarily by analysis. Impact limiter performance is demonstrated by half-scale certification testing. The acceptance criteria for analytic assessments are in accordance with Regulatory Guide 7.6. These design criteria meet the following safety requirements of 10 CFR §71.51:

1. For normal conditions of transport, there shall be no loss or dispersal of radioactive contents, as demonstrated to a sensitivity of  $10^{-6}$  A<sub>2</sub> per hour, no significant increase in external radiation levels, and no substantial reduction in the effectiveness of the packaging.
2. For hypothetical accident conditions, there shall be no escape of radioactive material exceeding a total amount A<sub>2</sub> in one week, and no external radiation dose rate exceeding one rem per hour at one meter from the external surface of the package.

The BRR package is conservatively designated a Category I container, which is the highest and most stringent category [4]. Per NUREG/CR-3019 [5] and NUREG/CR-3854 [6], the cask components are classified as follows:

- Containment components are classified as ASME Code, Section III, Subsection NB [7].
- Fuel basket components are classified as ASME Code, Section III, Subsection NG [8].
- The outer shell, thermal shield, and impact limiter attachments are classified as ASME Code, Section III, Subsection NF [9]. However, the outer shell is conservatively analyzed to the requirements of Subsection NB.

The remainder of this section presents the detailed acceptance criteria used for analytic structural assessments of the BRR package.

### 2.1.2.1 Containment and Criticality Control Structures

A summary of allowable stresses used for containment and criticality control structures is presented in Table 2.1-1. Containment structures include the inner shell, massive end structures, and the closure lid. Criticality control structures include the fuel baskets, loose plate boxes, and spacer pedestals. The allowable stresses shown in Table 2.1-1 are consistent with Regulatory Guide 7.6, and the ASME Code, Section III, Subsections NB and NG, and Appendix F. Peak stresses are further discussed in Section 2.1.2.3.2, *Fatigue Assessment*, and buckling in Section 2.1.2.3.3, *Buckling Assessment*. Closure bolts are evaluated utilizing NUREG/CR-6007 [10]. Furthermore, stress intensity in the cask closure region which could affect compression of the containment O-ring seal is limited to the lesser of the value shown in Table 2.1-1, or the yield strength.

### 2.1.2.2 Other Structures

Impact limiter structures, including the steel shells, energy-absorbing foam, and attachment structures, are expected to permanently deform under NCT and HAC. The impact limiter performance criteria are:

- Limit impact magnitude such that cask component stress and deflection criteria are met.
- Prevent "hard" contact of a rigid part of the cask with the ground due to excessive deformation of the foam.

- Maintain attachment to the cask and sufficient structural integrity subsequent to the HAC free drop and puncture drop events that the containment O-ring seal is protected from excessive temperature in the subsequent HAC fire event.

The performance of the impact limiters is discussed in Sections 2.7.1, *Free Drop*, and 2.7.3, *Puncture*. The thermal performance of the undamaged and damaged limiters is evaluated in Chapter 3, *Thermal Evaluation*.

The allowable stress for lifting components of the BRR package is limited to a maximum of one-third of the minimum yield strength of the material in the lifting load path, per the requirements of 10 CFR §71.45(a).

Since the BRR package is not attached to the conveyance using any structural part of the package, tiedown structural criteria are not required.

### 2.1.2.3 Miscellaneous Structural Failure Modes

#### 2.1.2.3.1 Brittle Fracture

With the exception of the closure lid bolts, all structural components of the BRR package are fabricated of austenitic stainless steel. Austenitic stainless steels do not undergo a ductile-to-brittle transition in the temperature range of interest (i.e., down to -40 °F), and thus do not need to be evaluated for brittle fracture. The closure lid bolts are fabricated from ASTM A320, Grade L43 alloy steel bolting material. This material is specifically intended for low temperature service. In addition, per Section 5 of NUREG/CR-1815 [11], bolts are not considered as fracture-critical components because multiple load paths exist and bolting systems are generally redundant, as is the case with the BRR package. Therefore, brittle fracture is not a failure mode of concern.

#### 2.1.2.3.2 Fatigue Assessment

##### 2.1.2.3.2.1 Normal Operating Cycles

Normal operating cycles do not present a fatigue concern for the BRR package components over its service life. The basis for this conclusion is reached using the six criteria of Article NB-3222.4(d) of the ASME Boiler and Pressure Vessel Code. A summary of the six criteria and their application are discussed below. The service life of the package is 25 years with up to 20 shipments per year for a maximum of 500 shipments in the service life.

**(1) Atmospheric to Service Pressure Cycle:** The total number of atmospheric-to-operating pressure cycles during normal operations does not exceed the number of cycles on the fatigue curve corresponding to a value of  $S_a = 3S_m$  for Type 304 stainless steel. From Section 2.2.1, *Material Properties and Specifications* at a bounding temperature of 250 °F per Section 2.6.1.1, *Summary of Pressures and Temperatures*, the  $S_m$  value for Type 304 stainless steel is 20 ksi, which corresponds to an alternating stress value of  $S_a = 3S_m = 60$  ksi. The corresponding number of cycles for a value of  $S_a = 60$  ksi is greater than 10,000 from Figure I-9.2.1 and Table I-9.1 of the ASME Code [12]. The package undergoes one atmospheric-to-operating pressure cycle per shipment, therefore the package will experience 500 atmospheric-to-operating pressure cycles in its life. Since the allowable number of cycles is greater than the maximum expected number of cycles, the first criterion is satisfied.

**(2) Normal Service Pressure Fluctuation:** The specified full range of pressure fluctuations during normal service does not exceed the quantity  $1/3 \times \text{Design Pressure} \times (S_a/S_m)$ , where the Design Pressure is 25 psi,  $S_a$  is the value obtained from the Type 304 stainless steel design fatigue curve for the total specified number of significant pressure fluctuations (SPF), and  $S_m$  is the allowable stress intensity for the material at the service temperature. The total number of service cycles is based on the fill gas extreme temperature range as stated below. Conservatively, two complete temperature cycles are assumed to occur for each of the 500 lifetime shipments for a total quantity of 1,000 pressure fluctuation cycles. From Table I-9.1,  $S_a = 119,000$  psi for 1,000 cycles. The value of  $S_m$  was defined above as 20 ksi at service temperature. The limiting full range of pressure fluctuations (FRF) becomes:

$$\text{FRF}_{\text{LIMIT}} = 1/3 \times \text{Design Pressure} \times (S_a/S_m) = 49.6 \text{ psi}$$

Next, the maximum pressure fluctuations in the package will be determined. Of note, the maximum pressure fluctuations will be conservatively assumed to be above the significance level, and therefore the value SPF does not need to be computed. The bulk average fill gas temperature varies between the extremes of  $T_1 = -40$  °F and a conservative bounding temperature of  $T_2 = 400$  °F. The maximum pressure (conservatively assuming that atmospheric pressure corresponds to -40 °F) is:

$$\frac{P_2}{P_1} = \frac{T_2}{T_1} \Rightarrow P_2 = P_1 \left( \frac{T_2}{T_1} \right) = 14.7 \left( \frac{400 + 460}{-40 + 460} \right) = 30.1 \text{ psia}$$

The resulting pressure fluctuation is  $\text{FRF} = 30.1 - 14.7 = 15.4$  psi, which is less than  $\text{FRF}_{\text{LIMIT}} = 49.6$  psi presented above and therefore, the second criterion is satisfied.

**(3) Temperature Difference — Startup and Shutdown:** The temperature between adjacent points of a package component during normal service does not exceed  $1/2(S_a/E\alpha)$ , where  $S_a$  is the design fatigue curve value taken from Table I-9.1 for Figure I-9.2.1 of the ASME Code for Type 304 stainless steel for the total specified number of temperature difference fluctuations,  $E$  is the modulus of elasticity, and  $\alpha$  is the mean coefficient of thermal expansion, all evaluated at temperature. The total number of temperature fluctuations will not exceed the number of uses of the package, which is 500 as calculated above. It will be conservative to use the value of  $S_a$  from Table I-9.1 of the ASME Code for 1,000 cycles, which is 119,000 psi. From Section 2.2.1, *Material Properties and Specifications* at a bounding temperature of 250 °F, the value of the mean thermal expansion coefficient is  $\alpha = 9.1(10^{-6})/\text{°F}$  and the modulus of elasticity,  $E = 27.3(10^6)$  psi. Therefore, the value of  $1/2(S_a/E\alpha) = 1/2(119,000/[27.3(10^6)9.1(10^{-6})]) = 240$  °F. Since the package design temperature is 250 °F under ambient conditions of 100 °F, the temperature difference between any two adjacent points cannot approach the 240 °F value. Thus, the third criterion is satisfied.

**(4) Temperature Difference — Normal Service:** The temperature difference between any two adjacent points does not change during normal service by more than the quantity  $1/2(S_a/E\alpha)$ , where  $S_a$ ,  $E$ , and  $\alpha$  are as defined above. However, normal operating temperatures of the containment boundary are largely determined by the steady heat load, and any changes in temperature due to changes in ambient conditions, warm-up, or cool-down will be relatively slow and even due to the large thermal mass of the package. Therefore, the fourth criterion is satisfied.

**(5) Temperature Difference — Dissimilar Materials:** The fifth criterion is concerned with dissimilar materials. Since the containment boundary is constructed entirely of Type 304 stainless steel, dissimilar materials are not of concern. Therefore the fifth criterion is satisfied.

**(6) Mechanical Loads:** The specified full range of mechanical loads does not result in load stresses whose range exceeds the  $S_a$  design fatigue curve for the total specified number of load fluctuations. The only repeating mechanical loads will be those associated with lifting the package and tightening of the closure bolts.

Lifting. As the containment boundary is handled twice for each transport cycle (load and unload), the maximum number of cycles is  $2 \times 500 = 1,000$ . From Table I-9.1,  $S_a = 119,000$  psi for 1,000 cycles. Of note, each load stress excursion will be conservatively assumed to be above the significance level, and therefore the actual significance level does not need to be computed. Lifting stress is limited by 10 CFR §71.45(a) to a value of one-third of the material's minimum yield strength. For a design temperature of 250 °F, the minimum yield strength of Type 304 stainless steel is 23,700 psi. Thus, one-third of the minimum yield strength is  $23,700/3 = 7,900$  psi. As  $119,000 \text{ psi} \gg 7,900 \text{ psi}$ , the sixth criterion is satisfied for lifting.

Closure bolts. The maximum stress intensity developed in the closure bolts during normal operations, given in Section 2.6.1.5, *Closure Bolts*, is bounded by a value of  $S_{\max} = 55,000$  psi. This stress includes preload stress, thermal stress, and a conservative inclusion of 50% of the applied preload torque as a residual torsion stress. From Table 2.2-3, the ASME allowable stress for the bolting material,  $S_m$ , at 250 °F is 32,450 psi. As defined by Table I-9.1 of the ASME B&PV Code, the Maximum Nominal Stress (MNS) of 55,000 psi is less than  $2.7S_m$  (i.e.,  $2.7(32,450) = 87,615$  psi). Per NB-3232.3(c), a stress concentration factor of four shall be applied to one-half the value of  $S_{\max}$ , i.e.,  $4(0.5S_{\max}) = 4 \times 0.5 \times 55,000 = 110,000$  psi. Per NB-3232.3(d), the alternating stress must be adjusted for the elastic modulus used in the fatigue curves. The modulus at a temperature of 250 °F is  $26.9(10^6)$  psi and the modulus used for the fatigue curve, per Table I-9.1 is  $30(10^6)$  psi. The adjusted alternating stress is:

$$S_{\text{ALT}} = \frac{30}{26.9} 110 = 123 \text{ ksi}$$

From Table I-9.1 for figure I-9.4, the service cycles allowed for a stress of 123 ksi is 670. Since closure bolts are tightened twice per package service cycle, the allowable number of package service cycles is half of this value. Therefore the closure bolts should be replaced every  $670/2 = 335$  service cycles for the package, and the sixth criterion is satisfied for closure bolts.

**Summary:** The previous discussion verifies that fatigue failure of the packaging containment boundary due to normal operating cycles is not a concern, per Section III, Subsection NB, Article NB-3222.4(d) of the ASME Code. Therefore the resistance of the BRR package to fatigue is adequate to ensure a minimum 25 year service life of up to 20 shipments per year.

#### 2.1.2.3.2 Normal Vibration Over the Road

Fatigue associated with normal vibration over the road is addressed in Section 2.6.5, *Vibration*.

#### 2.1.2.3.3 Buckling Assessment

Buckling, per Regulatory Guide 7.6, is an unacceptable failure mode for the containment vessel. The intent of this provision is to preclude large deformations that would compromise the validity

of linear analysis assumptions and quasi-linear stress allowable limits, as given in Paragraph C.6 of Regulatory Guide 7.6.

Buckling investigations contained herein consider the outer shell of the BRR package. The outer and inner shells of the cask are closely connected through the massive end structures, thus, the two shells act to strengthen each other. One shell cannot buckle independently of the other. However, the strength of the inner shell for buckling considerations is conservatively ignored.

The shell buckling analysis is performed using the methodology of ASME B&PV Code Case N-284-2 [13]. Consistent with Regulatory Guide 7.6 philosophy, factors of safety corresponding to ASME Boiler and Pressure Vessel Code, Level A and Level D service conditions are employed. For NCT (Service Level A), the factor of safety is 2.0, and for HAC (Service Level D), the factor of safety is 1.34. Buckling analysis details are provided in Section 2.6.4, *Increased External Pressure*, Section 2.7.1, *Free Drop*, and Section 2.7.6, *Immersion – All Packages*.

### **2.1.3 Weights and Centers of Gravity**

The maximum gross weight of the BRR package is 32,000 lb. The packaging component weights are summarized in Table 2.1-2, and the fuel basket and fuel weights in Table 2.1-3. The center of gravity (CG) of the package is located 38.7 inches from the bottom outside surface of the cask body. Note that this is directly on the geometric center of the package. The mass moment of inertia of the cask about a transverse axis through the center of gravity (including impact limiters, as prepared for transport) is 63,246 in-lb-s<sup>2</sup>.

### **2.1.4 Identification of Codes and Standards for Package Design**

The BRR package, without regard to content, is conservatively designated a Category I package. Per the guidance of NUREG/CR-3854, the appropriate design criteria for the containment is Section III, Subsection NB of the ASME B&PV Code. Consequently, the design of the containment boundary is based on the methodology of Regulatory Guide 7.6, and load cases are applied and combined according to Regulatory Guide 7.8. The outer shell is conservatively included under the NB criteria. The closure bolts are designed using the guidance of NUREG/CR-6007.

For the design of the baskets as criticality control components, the criteria is taken from Section III, Subsection NG of the ASME B&PV Code. For other structures such as the thermal shield, impact limiter shells, and impact limiter attachments, the criteria is taken from Section III, Subsection NF of the ASME B&PV Code.

**Table 2.1-1 – Containment and Criticality Control Structure Allowable Stress Limits**

<b>Stress Category</b>	<b>NCT</b>	<b>HAC</b>
General Primary Membrane Stress Intensity	$S_m$	Lesser of: $2.4S_m$ $0.7S_u$
Local Primary Membrane Stress Intensity <sup>①</sup>	$1.5S_m$	Lesser of: $3.6S_m$ $S_u$
Primary Membrane + Bending Stress Intensity	$1.5S_m$	Lesser of: $3.6S_m$ $S_u$
Range of Primary + Secondary Stress Intensity	$3.0S_m$	Not Applicable
Pure Shear Stress	$0.6S_m$	$0.42S_u$ <sup>②</sup>
Peak	Per Section 2.1.2.3.2, <i>Fatigue Assessment</i>	
Buckling	Per Section 2.1.2.3.3, <i>Buckling Assessment</i>	
<i>Containment Fasteners:</i> <sup>③</sup>		
Average Tensile Stress Intensity	$S_m$ <sup>④</sup>	Lesser of: $S_y$ $0.7S_u$
Average Tensile + Average Shear + Bending + Residual Torsion Stress Intensity	$1.35S_m$ for $S_u > 100$ ksi	Not Applicable

Notes:

1. This stress category does not apply to criticality control structures (Subsection NG).
2. For criticality control structures, the limit is the lesser of twice the NCT limit ( $2 \times 0.6S_m = 1.2S_m$ ) or  $0.42S_u$ , per NG-3225.
3. Containment fastener stress limits are in accordance with NUREG/CR-6007.
4.  $S_m$  is defined as  $(2/3)S_y$  as recommended by NUREG/CR-6007.

**Table 2.1-2 – BRR Package Component Weights**

Item	Weight, lb	CG, inches
Cask body <sup>①</sup>	25,400	---
Removable shield plug	950	---
Closure lid	280	---
Upper impact limiter	2,300	---
Lower impact limiter	2,300	---
<b>Total empty package</b>	<b>31,230</b>	<b>38.6<sup>④</sup></b>
MURR Fuel basket <sup>②</sup> (loaded)	770	32.7 <sup>③</sup>
MITR-II Fuel basket <sup>②</sup> (loaded)	640	35.5 <sup>③</sup>
ATR Fuel basket <sup>②</sup> (loaded)	650	27.1 <sup>③</sup>
TRIGA Fuel basket <sup>②</sup> (loaded)	480	28.1 <sup>③</sup>
Square fuel basket <sup>②</sup> (loaded)	634	30.9 <sup>③</sup>
<b>Total package, including MURR fuel (maximum)</b>	<b>32,000</b>	<b>38.7<sup>④</sup></b>
Total package, including MITR-II fuel	31,870	38.7 <sup>④</sup>
Total package, including ATR fuel	31,880	38.6 <sup>④</sup>
Total package, including TRIGA fuel	31,710	38.6 <sup>④</sup>
Total package, including Square fuel	31,864	38.6 <sup>④</sup>

Notes:

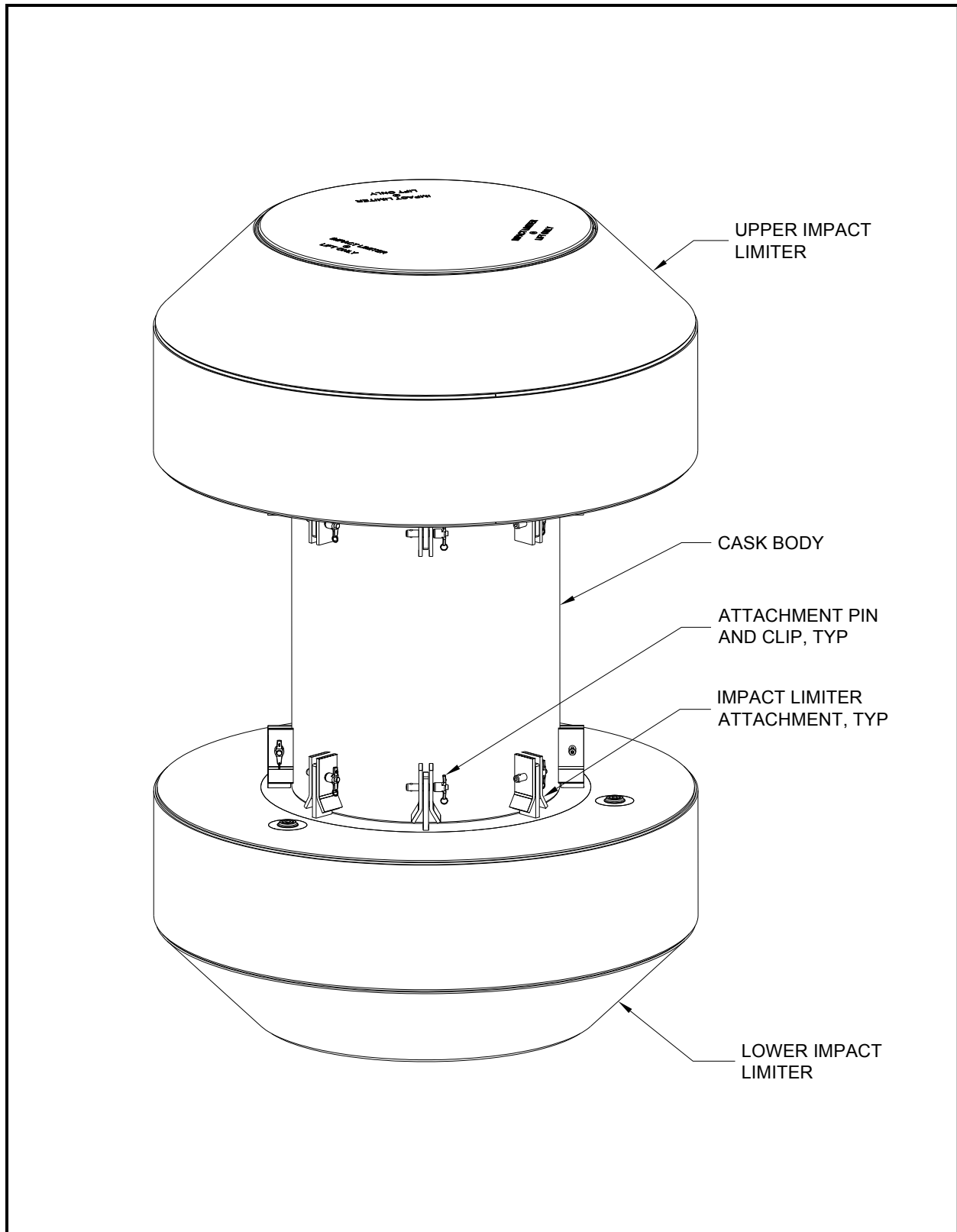
1. Includes all shells, end structures, and lead.
2. Individual basket and fuel weights are given in Table 2.1-3. Although Square fuel is the heaviest at 384 lb, the MURR basket plus fuel weight is greatest overall.
3. Measured from the bottom surface of the basket.
4. Measured from the bottom outside surface of the cask body.

**Table 2.1-3 – BRR Package Basket and Fuel Weights**

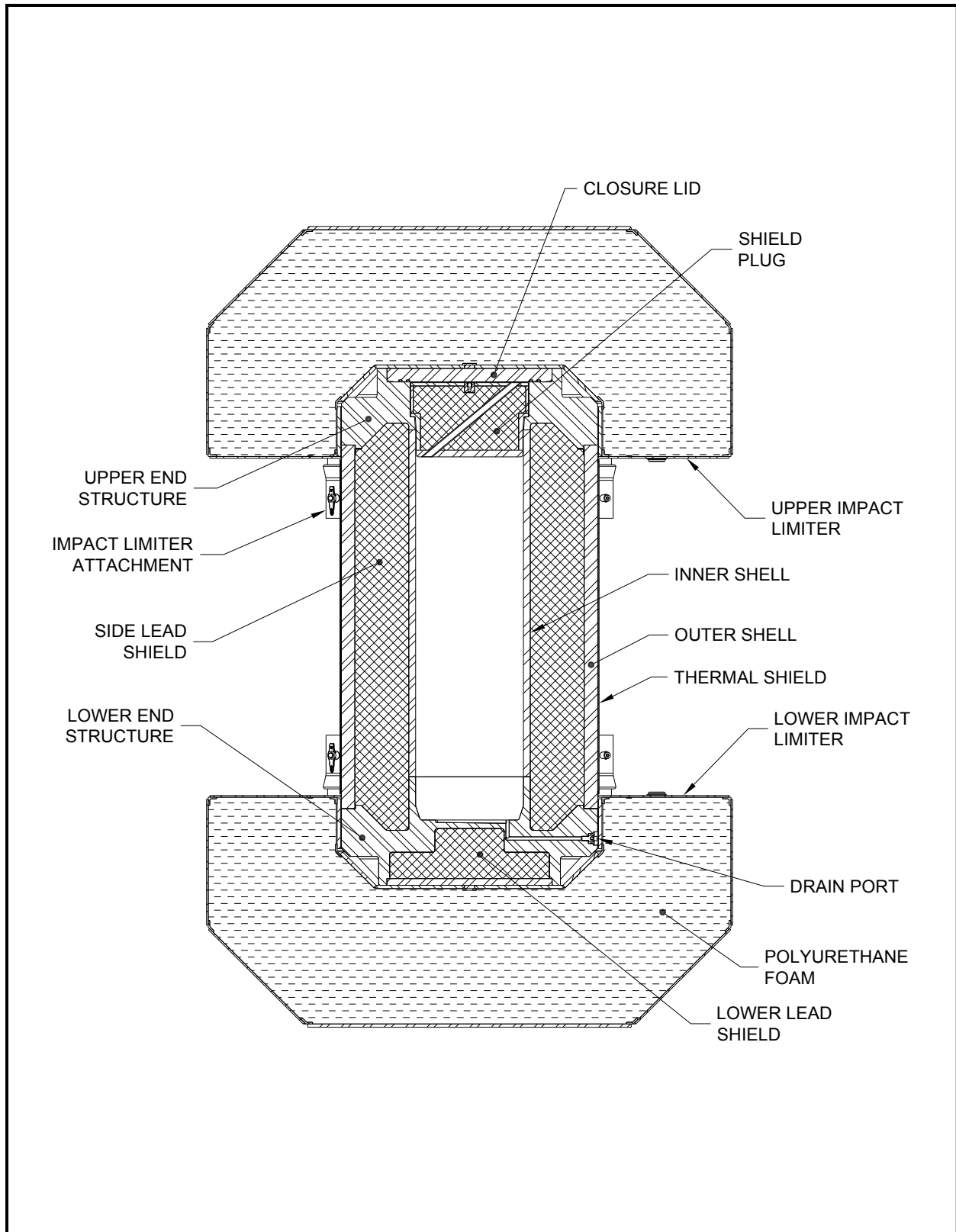
Design	Weight (lb)			
	Empty Basket	Fuel Element × Quan.	Combined Fuel	Total
MURR	650	15 × 8	120	770
MITR-II	560	10 × 8	80	640
ATR	450	25 × 8	200	650
TRIGA	290	10 × 19	190	480
Square fuel	250	48 <sup>①</sup> × 8	384	634

Note ①: PULSTAR represents the bounding fuel weight.

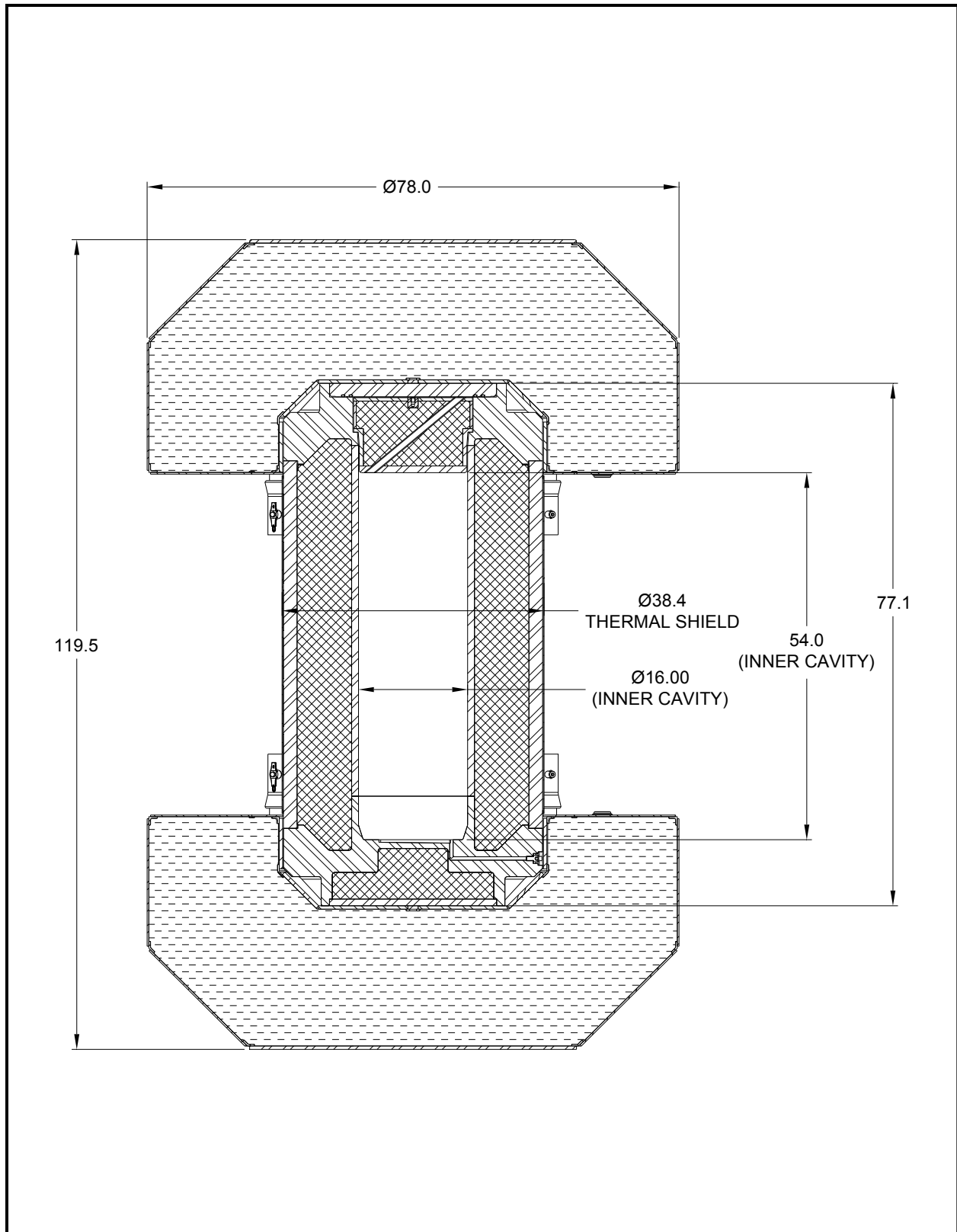




**Figure 2.1-1 – BRR Packaging Components**



**Figure 2.1-2 – BRR Package Cross Section**

**Figure 2.1-3 – BRR Package Dimensions**

## 2.2 Materials

The BRR package structural components, including the impact limiter shells, are fabricated primarily from Type 304 stainless steel in various product forms. The gamma shielding is made from ASTM B29, Chemical Lead, or equivalent lead. Polyurethane foam is used for impact energy absorption. Other materials performing a structural function are ASTM B16 UNS C36000 brass alloy (for the test, vent, and drain port plugs), and ASTM A320, L43, alloy steel for the closure lid bolts. Austenitic stainless steel is used for the heavy duty thread inserts used for the closure bolt holes and lifting holes in the upper end structure. The ball lock pins that attach the impact limiters to the cask are made from 17-4PH stainless steel. The containment O-ring seal is made from butyl rubber. Plastic is used for the fire-consumable vent plugs in the foam cavities. The loose plate box and fuel pedestals used with the square fuel basket or with the TRIGA fuel basket are made of stainless steel. The drawings presented in Appendix 1.3.3, *Packaging General Arrangement Drawings*, delineate the specific materials used for each BRR package component.

### 2.2.1 Material Properties and Specifications

Table 2.2-1 through Table 2.2-6 present the mechanical properties for the structural materials used in the BRR package. The density of stainless steel is  $0.29 \text{ lb/in}^3$ , and Poisson's ratio is 0.3. The density of lead is  $0.41 \text{ lb/in}^3$  and Poisson's ratio is 0.45. Data is interpolated or extrapolated from the available data, as necessary, as noted in the tables.

The performance of the BRR package in free drop and puncture events is partially dependent on the energy-absorbing performance of polyurethane foam. The foam is poured in place within the impact limiter steel shells. Nominally  $9 \text{ lb/ft}^3$  polyurethane foam is used. Section 8.1.5.1, *Polyurethane Foam* presents the details of acceptance tests for this material. The nominal, room-temperature crush properties of the polyurethane foam component are given in Table 2.2-6. Properties for both "parallel to rise" and "perpendicular to rise" are given. The "rise" direction is parallel to the force of gravity during solidification, and is oriented to be parallel to the cylindrical axis of the impact limiters.

### 2.2.2 Chemical, Galvanic, or Other Reactions

The materials of construction of the BRR package will not have significant chemical, galvanic or other reactions in air or water environments. These materials have been previously used, without incident, in radioactive material packages for transport of similar payload materials such as the RH-TRU 72-B (NRC Docket 9212) and the NAC LWT (NRC Docket 9225). The polyurethane foam is fully enveloped by sheets of stainless steel and welded closed. The foam is a rigid, closed-cell (non-water absorbent) material that is free of halogens and chlorides, as discussed in Section 8.1.5.1, *Polyurethane Foam*. The lead gamma shielding is fully encased in a stainless steel weldment and cannot be affected by water or atmospheric moisture.

The brass alloy vent port plug used in the closure lid is very corrosion resistant. Any damage that could occur to the material is easily detectable since the fitting is handled each time the BRR package is loaded and unloaded. Similarly, the alloy steel closure bolts, which are plated with corrosion-resistant nickel plating, can be readily inspected at each use for the presence of corrosion.

The butyl elastomer that is used for the containment O-ring seals contains no corrosives that would react with or adversely affect the BRR package. This material is organic in nature and noncorrosive to the stainless steel containment boundary of the BRR package.

A successful RAM packaging history combined with successful use of these fabrication materials in similar industrial environments ensures that the integrity of the BRR package will not be compromised by any chemical, galvanic or other reactions.

### **2.2.3 Effects of Radiation on Materials**

The radiation associated with the decay of spent fuel will have no effect on the austenitic stainless steel comprising the structural components of the BRR package. Since the payload of the BRR package is heavily shielded, the radiation exposure of the overpack materials (including the polyurethane foam) is negligible. The butyl rubber containment seal, which is also located outside of the gamma shielding, likewise receives a negligible exposure. For these reasons, there will be no deleterious radiation effects on the packaging, and the requirements of 10 CFR §71.43(d) are met.

**Table 2.2-1 – Mechanical Properties of Wrought Type 304 Stainless Steel**

Material Specification	Temperature (°F)	① Yield Strength, $S_y$ (psi)	② Ultimate Strength, $S_u$ (psi)	③ Allowable Strength, $S_m$ (psi)	④ Elastic Modulus, $E$ ( $\times 10^6$ psi)	⑤ Thermal Expansion Coefficient, $\alpha$ ( $\times 10^{-6}$ /°F)
ASTM A240 ASTM A249 ASTM A276 ASTM A479 Type 304	-40	30,000	75,000	20,000	28.9	8.2
	-20	30,000	75,000	20,000	28.8	8.2
	70	30,000	75,000	20,000	28.3	8.5
	100	30,000	75,000	20,000	28.1	8.6
	200	25,000	71,000	20,000	27.5	8.9
	300	22,400	66,200	20,000	27.0	9.2
	400	20,700	64,000	18,600	26.4	9.5
	500	19,400	63,400	17,500	25.9	9.7
	600	18,400	63,400	16,600	25.3	9.8
	700	17,600	63,400	15,800	24.8	10.0
	800	16,900	62,800	15,200	24.1	10.1

Notes: ① ASME Code, Section II, Part D, Table Y-1.

② ASME Code, Section II, Part D, Table U.

③ ASME Code, Section II, Part D, Table 2A.

④ ASME Code, Section II, Part D, Table TM-1, Material Group G. Values for -40 °F and -20 °F interpolated from 70 °F and -100 °F.

⑤ ASME Code, Section II, Part D, Table TE-1, Material Group 3, Mean Coefficient. Values for -40 °F and -20 °F extrapolated from 70 °F and 100 °F.

**Table 2.2-2 – Mechanical Properties of Forged and Cast Type 304 Stainless Steel**

<b>Material Specification</b>	<b>Temperature (°F)</b>	<b>① Yield Strength, <math>S_y</math> (psi)</b>	<b>② Ultimate Strength, <math>S_u</math> (psi)</b>	<b>③ Allowable Strength, <math>S_m</math> (psi)</b>	<b>④ Elastic Modulus, <math>E</math> (<math>\times 10^6</math> psi)</b>	<b>⑤ Thermal Expansion Coefficient, <math>\alpha</math> (<math>\times 10^{-6}</math> /°F)</b>
ASTM A182 Type F304, ASTM A351 Type CF8, and ASTM A451, Type CPF8 ⑥	-40	30,000	70,000	20,000	28.9	8.2
	-20	30,000	70,000	20,000	28.8	8.2
	70	30,000	70,000	20,000	28.3	8.5
	100	30,000	70,000	20,000	28.1	8.6
	200	25,000	66,300	20,000	27.5	8.9
	300	22,400	61,800	20,000	27.0	9.2
	400	20,700	59,700	18,600	26.4	9.5
	500	19,400	59,200	17,500	25.9	9.7
	600	18,400	59,200	16,600	25.3	9.8
	700	17,600	59,200	15,800	24.8	10.0
	800	16,900	58,600	15,200	24.1	10.1

Notes: ① ASME Code, Section II, Part D, Table Y-1.

② ASME Code, Section II, Part D, Table U.

③ ASME Code, Section II, Part D, Table 2A.

④ ASME Code, Section II, Part D, Table TM-1, Material Group G. Values for -40 °F and -20 °F interpolated from 70 °F and -100 °F.

⑤ ASME Code, Section II, Part D, Table TE-1, Material Group 3, Mean Coefficient. Values for -40 °F and -20 °F extrapolated from 70 °F and 100 °F.

⑥ Optional cast materials are ASTM A351 Type CF8A and ASTM A451 Type CPF8A. The yield, ultimate, and allowable strengths of these materials are higher than the values in this table at all temperatures with one exception: the allowable strength,  $S_m$ , is not given for a temperature of 800 °F. However, since the BRR package temperatures never exceed 700 °F, this limitation does not apply.

**Table 2.2-3 – Mechanical Properties of ASTM A320, Grade L43 Alloy Bolting Material**

Material Specification	Temperature (°F)	① Yield Strength, $S_y$ (psi)	② Ultimate Strength, $S_u$ (psi)	③ Allowable Strength, $S_m$ (psi)	④ Elastic Modulus, $E$ ( $\times 10^6$ psi)	⑤ Thermal Expansion Coefficient, $\alpha$ ( $\times 10^{-6}$ /°F)
ASTM A320 Grade L43	-40	105,000	125,000	35,000	28.3	6.2
	-20	105,000	125,000	35,000	28.2	6.3
	70	105,000	125,000	35,000	27.8	6.4
	100	105,000	125,000	35,000	27.6	6.5
	200	99,000	125,000	33,000	27.1	6.7
	300	95,700	125,000	31,900	26.7	6.9
	400	91,800	125,000	30,600	26.2	7.1
	500	88,500	125,000	29,500	25.7	7.3
	600	84,300	125,000	28,100	25.1	7.4
	700	79,200	125,000	26,400	24.6	7.6

Notes: ① ASME Code, Section II, Part D, Table Y-1.

② ASME Code, Section II, Part D, Table Y-1.

③ ASME Code, Section II, Part D, Table 4.

④ ASME Code, Section II, Part D, Table TM-1, Material Group B. Values for -40 °F and -20 °F interpolated from 70 °F and -100 °F.

⑤ ASME Code, Section II, Part D, Table TE-1, Material Group 1, Mean Coefficient. Values for -40 °F and -20 °F extrapolated from 70 °F and 100 °F.



**Table 2.2-4 – Mechanical Properties of Lead Shielding**

<b>Material Specification</b>	<b>Temperature (°F)</b>	<b>① Tensile Yield Strength, <math>S_y</math> (psi)</b>	<b>① Tensile Ultimate Strength, <math>S_u</math> (psi)</b>	<b>① Tensile Proportional Limit (psi)</b>	<b>② Elastic Modulus, <math>E</math> (<math>\times 10^6</math> psi)</b>	<b>② Thermal Expansion Coefficient, <math>\alpha</math> (<math>\times 10^{-6}</math> /°F)</b>
ASTM B29 Chemical Lead or Fed Spec QQ-L-121E, Gr. A or C	-99	---	---	---	2.50	15.3
	70	---	---	---	2.34	16.1
	100	584	1,585	276	2.30	16.2
	175	509	1,158	293	2.20	16.6
	250	498	839	277	2.09	17.0
	325	311	639	189	1.96	17.5
	440	---	---	---	1.74	18.5
	620	---	---	---	1.36	20.4

Notes: ① WADC Technical Report 57-695, ASTIA Document No. 151165, "Determination of the Mechanical Properties of a High Purity Lead and a 0.05% Copper-Lead Alloy," April 1958, by Thomas Tietz, Stanford Research Center, pp. 14, 21, for copperized lead.

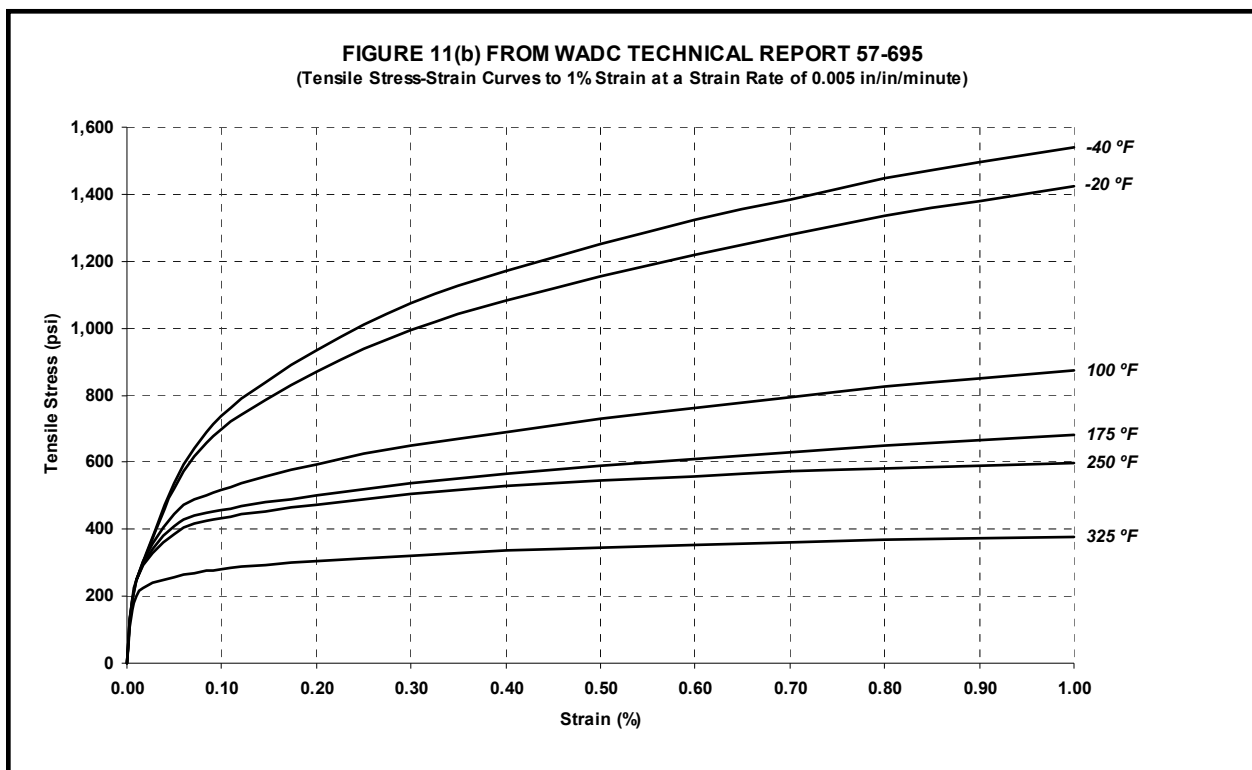
② NUREG/CR-0481, SAND77-1872, "An Assessment of Stress-Strain Data Suitable for Finite Element Elastic-Plastic Analysis of Shipping Containers," H. J. Rack and G. A. Knorovsky, Sept. 1978, p. 66.

**Table 2.2-5 – Mechanical Properties of Brass Material**

Material	Minimum Mechanical Properties
ASTM B16, UNS C36000, Temper H02	Yield Strength, $\sigma_y = 25,000$ psi Ultimate Strength, $\sigma_u = 55,000$ psi

**Table 2.2-6 – Nominal Material Properties of 9 lb/ft<sup>3</sup> Polyurethane Foam**

Property	Direction	Room Temperature Value
Compressive Strength, S	Axial (Parallel-to-Rise)	280 psi @ 10% Strain 306 psi @ 40% Strain 758 psi @ 70% Strain
	Radial (Perpendicular-to-Rise)	278 psi @ 10% Strain 303 psi @ 40% Strain 767 psi @ 70% Strain

**Figure 2.2-1 – Tensile Stress-Strain Curves for Lead Shielding** (Source: see note 1 of Table 2.2-4)

## 2.3 Fabrication and Examination

### 2.3.1 Fabrication

The BRR package is fabricated using conventional metal forming and joining techniques. All welding procedures and welding personnel must be qualified in accordance with Section IX of the ASME Boiler and Pressure Vessel Code [14]. Containment boundary welds, as well as the welds at each end of the outer shell, are full penetration joints. All non-containment joints are fabricated in accordance with the requirements delineated on the drawings in Appendix 1.3.3, *Packaging General Arrangement Drawings*. The containment shell and outer shell fabrications shall comply with the tolerance requirements of the ASME Code, Subsection NE, Article NE-4220 [15]. Article NE-4220 is selected because the package cylindrical shells are verified for buckling performance using the ASME Code Case N-284-2. This Code Case is for Section III, Division 1, Class MC construction, and is based on the fabrication requirements of NE-4222, as stated in Section 1120 of the Code Case. Therefore, it is appropriate to fabricate the BRR package using shell tolerances from NE-4220, rather than NB-4220.

The polyurethane foam and butyl rubber O-rings are procured using written procedures. See Section 8.1.5, *Component Tests*, for details of the fabrication and performance requirements of these components.

### 2.3.2 Examination

Each of the materials performing a significant safety function must meet the ASTM specifications delineated on the drawings in Appendix 1.3.3, *Packaging General Arrangement Drawings*. Safety-significant materials not having an ASTM designation are controlled by means of written procedures whose requirements are summarized in Section 8.1.5, *Component Tests*.

Forgings are subject to ultrasonic and liquid penetrant inspection per the ASME Code, Subsection NB, Article NB-2540 [16]. Castings are subject to radiographic and liquid penetrant inspection per the ASME Code, Subsection NB, Article NB-2570 [17].

All welds are subject to visual examination per AWS D1.6 [18]. The welds between the inner containment shell and either end structure, the welds between the outer shell and either end structure, and the longitudinal weld(s) in the outer shell, if any, are examined by ultrasonic inspection in accordance with the ASME Code, Subsection NB, Article NB-5000, and Section V, Article 4 [20]. Optionally, the weld between the inner containment shell and the lower end structure may be examined by radiographic inspection in accordance with the ASME Code, Subsection NB, Article NB-5000, and Section V, Article 2 [19]. All welds on the BRR package, except seal welds, are liquid penetrant inspected on the final pass in accordance with the ASME Code, Subsection Nx, Article Nx-5000, and Section V, Article 6 [21]. The appropriate Subsection for the containment welds and outer shell welds is NB; for other cask body welds and the impact limiter shells, NF; and for the fuel baskets, NG.

Each BRR package will also be subjected to the following tests:

- An internal pressure test, in which the containment boundary is pressurized to 125% of the design pressure per the ASME Code [22], or 150% of the MNOP, per 10 CFR §71.85(b),

whichever is greater. The pressure test requirements are described in Section 8.1.3.2, *Containment Boundary Pressure Testing*.

- Containment boundary leakage rate test, which includes helium leakage rate tests of the containment boundary, the closure lid containment O-ring seal, the vent port containment O-ring seal, and the drain port containment O-ring seal. The leakage rate test requirements are described in Section 8.1.4, *Fabrication Leakage Rate Tests*.
- A test to ensure the integrity of the lead gamma shielding. The gamma test requirements are described in Section 8.1.6, *Shielding Integrity Test*.

## 2.4 General Standards for All Packages

This section defines the general standards for all packages. The BRR package meets all requirements delineated for this section.

### 2.4.1 Minimum Package Size

The minimum dimension of the BRR package is approximately 38.5 inches (the package diameter). Thus, the 4-in. minimum requirement of 10 CFR §71.43(a) is satisfied.

### 2.4.2 Tamper-Indicating Feature

A tamper-indicating seal is made by passing a lock wire through a hole in one of the upper impact limiter attachments. The wire passes through both the blade (impact limiter) and receptacle (cask body) components comprising the attachment. The upper impact limiter covers the closure lid and vent port. The wire must be destroyed in order to remove the impact limiter, thus providing evidence of possible tampering. Thus, the requirement of 10 CFR §71.43(b) is satisfied.

### 2.4.3 Positive Closure

The BRR package cannot be opened unintentionally. The impact limiters, which are each secured with eight, 1-inch diameter ball lock pins, fully conceal all cask openings. Thus, the requirements of 10 CFR §71.43(c) are satisfied.

### 2.4.4 Valves

The containment boundary of the BRR package does not contain any valves. The closure lid contains one vent port, and the lower end structure contains one drain port, which penetrate the containment boundary and which are closed with brass port plugs. Both ports are closed and tested during pre-shipment leak testing of the BRR package. The ports are protected from inadvertent use or from tampering by the impact limiters as described above. Thus, the requirements of 10 CFR §71.43(e) are satisfied.

### 2.4.5 Package Design

As shown in Chapter 2.0, *Structural Evaluation*, Chapter 3.0, *Thermal Evaluation*, and Chapter 5.0, *Shielding Evaluation*, the structural, thermal, and shielding requirements, respectively, of 10 CFR §71.43(f) are satisfied for the BRR package.

### 2.4.6 External Temperatures

As shown in Table 3.3-1 from Section 3.3, *Thermal Evaluation for Normal Conditions of Transport*, the maximum accessible surface temperature with maximum internal decay heat load and no insulation is bounded by 185 °F. This satisfies the limit of 10 CFR §71.43(g) for exclusive use shipments.

### 2.4.7 Venting

The BRR package does not include any features intended to allow continuous venting of the containment boundary during transport. Thus, the requirements of 10 CFR §71.43(h) are satisfied.

## 2.5 Lifting and Tie-down Standards for All Packages

### 2.5.1 Lifting Devices

The BRR package is lifted from four lift points located in the upper massive end structure. Lifting devices are installed in threaded holes containing optional alloy steel inserts. The failure mode of the lifting device is via shear tearout of the threads. Since the parent material is Type 304 stainless steel, it is conservative to consider the case in which the alloy steel inserts are not used.

The cask will be lifted using two cables, each attached to two lifting devices on the same side of the cask to preclude any crossing of the cables. In this way, both cables will have the same seating in the crane hook, and carry the same load. Consequently, all four lift points will experience the same lifting load. Although normal operating procedures call for the cask to be lifted without the lower impact limiter, it is conservatively assumed for the purpose of this analysis that it is in place during lifting. Since the upper impact limiter must be removed prior to installation of the lifting devices, lifting the cask with the upper limiter in place is impossible. The weight of the loaded cask with bottom impact limiter is:

$$W = 32,000 - 2,300 = 29,700 \text{ lb}$$

where the maximum package weight is 32,000 lb, and the upper impact limiter weight is 2,300 lb, from Table 2.1-2. For this calculation, a bounding weight of 30,000 lb is used. Since the weight will be evenly distributed among the four lifting devices, the load on each cask lift point is  $F = 30,000/4 = 7,500 \text{ lb}$ .

The governing shear area is based on the hole thread specification, which is 1-8 UNC-2B. From [23],  $A_i = 2.3256 \text{ in}^2/\text{in}$ . The shear stress in the inner threads is

$$\tau_i = \frac{F}{A_i L} = 2,150 \text{ psi}$$

where the minimum thread length,  $L = 1.5 \text{ inches}$ . At the NCT hot bounding temperature of 250 °F, the yield strength of the Type 304 parent material from Table 2.6-1 is 23,700 psi. The margin of safety is

$$MS = \frac{23,700(0.6)}{2,150(3)} - 1 = +1.20$$

where the factor of 0.6 in the numerator accounts for the shear failure mode and the factor of 3 in the denominator ensures that a minimum factor of safety of 3 is present. In the case of lifting overload, the device will strip out of the parent material without damage to the cask. Therefore, the requirements of 10 CFR §71.45(a) are met.

### 2.5.2 Tie-down Devices

During transport, the BRR package rests on a steel pallet, and is held down to the pallet by means of a steel frame which rests on top of the upper impact limiter. The upper impact limiter covers the lifting holes described in the section just above, and the steel tiedown frame covers the threaded holes in the upper impact limiter, thus these holes could not be erroneously used for tiedown. The steel tiedown frame is attached by wire ropes or equivalent to the conveyance, so

that a nominal downward load is applied to keep the BRR package in place. In this configuration, the package contacts only the pallet on the bottom and the steel frame on the top, and therefore has no integral tie-down devices which are a structural part of the package. Therefore, per 10 CFR §71.45(b)(1), no evaluation of tie-down devices is required.

## 2.6 Normal Conditions of Transport

When subjected to normal conditions of transport (NCT) as specified in 10 CFR §71.71, the BRR package meets the performance requirements specified in Subpart E of 10 CFR 71. This is demonstrated in the following subsections where each NCT condition is addressed and shown to meet the applicable design criteria. Load combinations used in this section are consistent with Regulatory Guide 7.8.

### 2.6.1 Heat

The normal heat condition, as defined in 10 CFR §71.71(c)(1), is evaluated in Section 3.0, *Thermal Evaluation*. The bounding temperatures and pressures for use in structural analyses are summarized in the following section. Material properties and stress limits, consistent with the design criteria shown in Table 2.1-1, are summarized for the relevant bounding temperatures in Table 2.6-1.

#### 2.6.1.1 Summary of Pressures and Temperatures

The bounding maximum temperatures for the 100 °F ambient NCT condition of the BRR package are presented in Table 3.1-1 of Chapter 3, *Thermal Evaluation*. For purposes of structural evaluation, the bounding fuel basket temperature is 400 °F. All components of the cask body, including the end structures, shells, shield plug, lead, closure lid and bolts, and elastomer seals, are bounded by a temperature of 250 °F. The bulk average polyurethane foam in both limiters is bounded by a temperature of 150 °F.

The initial pressure in the package at assembly is ambient, i.e., 14.7 psia. As determined in Section 3.3.2, *Maximum Normal Operating Pressure*, the maximum normal operating pressure (MNOP) can be conservatively defined to be 10 psig. The design pressure of the BRR package is 25 psig, which is significantly higher than the MNOP.

#### 2.6.1.2 Differential Thermal Expansion

Acceptable minimum clearances are maintained, including consideration of worst-case tolerances, between the cask, the fuel baskets, and the fuel.

##### 2.6.1.2.1 Baskets

The baskets for each fuel type have a nominal length of 53.45 inches with a tolerance of  $\pm 0.12$  inches, giving a maximum length of 53.57 inches. The cask cavity, with the shield plug installed, has a nominal length of 54.0 inches, with a tolerance of  $\pm 0.1$  inches, for a minimum length of  $L_{\text{Cask-min}} = 53.9$  inches. The length of the basket at a bounding temperature of 400 °F is:

$$L_{\text{Bsk}} = 53.57[1 + \alpha(400 - 70)] = 53.74 \text{ inches}$$

where the coefficient of thermal expansion,  $\alpha$ , is taken from Table 2.6-1 for Type 304 stainless steel at 400 °F as  $9.5(10^{-6})$  in/in/°F, and the reference temperature is 70 °F. The cask cavity thermal expansion is conservatively ignored. The minimum axial clearance at the NCT hot temperature is:

$$\text{CLR}_{\text{Bsk-Axi}} = L_{\text{Cask-min}} - L_{\text{Bsk}} = 0.16 \text{ inches}$$



All baskets have a nominal outer diameter of 15.63 inches with a tolerance of  $\pm 0.12$  inches, giving a maximum diameter of 15.75 inches. The cask cavity has a diameter of 16.0 inches, with a tolerance of  $\pm 0.1$  inches, for a minimum diameter of  $D_{\text{Cask-min}} = 15.9$  inches. The diameter of the basket at a bounding temperature of 400 °F is:

$$D_{\text{Bsk}} = 15.75[1 + \alpha(400 - 70)] = 15.80 \text{ inches}$$

where the coefficient of thermal expansion is the same as above. Again, the cask cavity thermal expansion is ignored. The minimum diametral clearance at the NCT hot temperature is:

$$\text{CLR}_{\text{Bsk-Dia}} = D_{\text{Cask-min}} - D_{\text{Bsk}} = 0.10 \text{ inches}$$

Therefore, the thermal expansion of the baskets is not of concern.

### 2.6.1.2.2 Fuel

Under NCT, each fuel element is shorter than the basket cavity, including tolerances and thermal expansion. Thus, the fuel elements do not experience an axial load if the basket should come in contact with the shield plug. It is shown that the maximum fuel length, including the bounding irradiation growth of 0.25 inches and a thermal expansion based on aluminum at 400 °F, is shorter than the basket cavity, minus the length tolerance and including thermal expansion of stainless steel at 400 °F. The evaluation is performed in three groups: 1) ATR, MURR, and MITR-II fuel elements, 2) TRIGA fuel elements, and 3) Square fuel elements. The minimum axial clearances of each fuel type are shown in Table 2.6-2.

#### *Group 1: ATR, MURR, and MITR-II Elements*

These fuel types are made primarily of aluminum. At the bounding fuel temperature of 400 °F, the thermal expansion coefficient of 6061 aluminum alloy,  $\alpha_{\text{Al-400}} = 13.6(10^{-6})$  in/in/°F, per Table TE-3 of the ASME Code, Section II, Part D. As an example of the minimum clearance calculation, the MITR-II fuel type case is shown in detail.

From Section 1.2.2.2, MITR-II, the maximum length of the MITR-II fuel element (including variation, irradiation growth, and margin) is 26.52 inches. At 400 °F, the fuel length is:

$$L_{\text{Fuel-Hot-Max}} = 26.52[1 + \alpha_{\text{Al-400}}(400 - 70)] = 26.64 \text{ inches}$$

The basket fuel cavity length is 26.88 inches, with a tolerance of  $\pm 0.12$ , giving a minimum length of 26.76 inches at 70 °F. At a bounding temperature of 400 °F, the cavity length is:

$$L_{\text{Cav-Hot-Min}} = 26.76[1 + \alpha(400 - 70)] = 26.84 \text{ inches}$$

where the thermal expansion coefficient for Type 304 stainless steel is the same as used above. The minimum axial clearance between the MITR-II fuel assembly and the basket cavity at the NCT hot temperature is:

$$\text{Gap}(1) = L_{\text{Cav-Hot-Min}} - L_{\text{Fuel-Hot-Max}} = 0.20 \text{ inches}$$

#### *Group 2: TRIGA Elements*

TRIGA fuel elements include some aluminum clad versions, which will govern their thermal expansion behavior. All elements use a pedestal spacer of some length as shown in Table 2.6-2a. The maximum fuel length at 400 °F is found in the same manner as for the MITR-II case above, using the expansion coefficient for aluminum. The minimum basket cavity length is equal to the

nominal cavity length of 48.0 inches, minus the tolerance of 0.12 inches, minus the maximum pedestal spacer length (nominal pedestal length plus tolerance of 0.06 inches). The basket cavity length at 400 °F is found in the same manner as for the MITR-II case above, using the expansion coefficient for stainless steel. The minimum gap is:

$$\text{Gap}(2) = L_{Cav-Hot-Min} - L_{Fuel-Hot-Max} = 0.13 \text{ inches}$$

### Group 3: Square Fuel Elements

Square fuel elements are made of aluminum, except for the PULSTAR element, which is made of both aluminum and zircalloy. To obtain a bounding thermal expansion of the PULSTAR fuel, it is conservative to treat it as all aluminum. The spacer pedestals used with the square fuel are made of stainless steel, but they will be conservatively treated as aluminum for purposes of thermal expansion, including a tolerance of 0.06 inches. The loose plates are held in a loose plate box that serves both to keep the plates together and as a pedestal spacer. The loose plate box will also be conservatively treated as aluminum for purposes of thermal expansion. Thus, as shown in Table 2.6-2b, the length of any square fuel plus pedestal is equal to 39.75 inches. (The only exception is for the U-Mass (aluminide) loose plates which are an inch shorter than the rest.) The maximum fuel length at 400 °F is found in the same manner as for the MITR-II case above, using the expansion coefficient for aluminum. The minimum basket cavity length is equal to the nominal cavity length of 40.0 inches, minus the tolerance of 0.12 inches, and adjusted for a temperature of 400 °F in the same manner as for the MITR-II case above, using the expansion coefficient for stainless steel. The minimum gap for the square fuel elements is:

$$\text{Gap}(3) = L_{Cav-Hot-Min} - L_{Fuel-Hot-Max} = 0.08 \text{ inches}$$

Therefore, thermal expansion of the fuel is not of concern.

#### 2.6.1.2.3 Lead

Due to different thermal expansion coefficients, the lead gamma shielding creates a stress in the inner shell under NCT hot conditions. An upper bound interface pressure between the lead and the inner shell is now determined, and applied as a pressure load to the finite element model and to the buckling analysis. First, note that the lead and the cask inner and outer shells are all in contact, and are stress-free, at the point of solidification of the lead at 620 °F. As the cask and lead cool, the lead contracts more than the stainless steel, and an interface pressure develops between the lead and the inner shell. This interface pressure is a function of the amount of interference between the lead and inner shell, and of the yield point of the lead at the NCT temperature. Due to the effects of material creep, the interface pressure will diminish over a relatively short period of time, thus reducing the resulting inner shell stresses. However, the effects of lead creep are conservatively neglected. The amount of interference between the lead and the inner shell depends upon the free state radii of these components, both at their respective NCT temperatures. The free state outer radius of the inner shell at the NCT hot temperature is

$$r_{ioh} = r_{io} [1 + \alpha_{s200}(T_{sh} - 70)] = 9.010 \text{ inches}$$

where the outer free state radius of the inner shell at room temperature,  $r_{io} = 9$  inches, the lower bound NCT hot case temperature of the shell,  $T_{sh} = 200$  °F, and the coefficient of thermal expansion of the inner shell material at 200 °F is  $\alpha_{s200} = 8.9(10^{-6})$  /°F from Table 2.2-1. Note that

**BRR Package Safety Analysis Report**

the interface pressure calculation is conservative for lower bound temperatures, since the lead will contract more and apply a larger pressure.

To determine the free state radii of the lead under NCT temperatures, it is necessary to start with the radii of the steel shells at the lead solidification point at 620 °F, at which point all of the components are in stress free contact. The radii of the lead/steel interfaces at 620 °F are

$$r_{Li620} = r_{io620} = r_{io} [1 + \alpha_{s620} (620 - 70)] = 9.049 \text{ inches}$$

$$r_{Lo620} = r_{oi620} = r_{oi} [1 + \alpha_{s620} (620 - 70)] = 17.092 \text{ inches}$$

where  $r_{Li620}/r_{io620}$  represent the inner lead/steel interface radius, and  $r_{Lo620}/r_{oi620}$  represents the outer lead/steel interface radius at 620 °F. In these equations, the room temperature outer radius of the inner shell,  $r_{io} = 9$  inches, the inner radius of the outer shell,  $r_{oi} = 17$  inches, and the thermal expansion coefficient of the shells at 620 °F,  $\alpha_{s620} = 9.84(10^{-6})/^{\circ}\text{F}$ . These values are then used to find the free state lead dimensions at the NCT temperature of lead as follows. Note that two thermal expansion terms are used (first contracting the lead from 620 °F to 70 °F, then expanding it from 70 °F to the hot lead temperature), since the thermal expansion coefficients given in Table 2.2-4 are based on 70 °F. The NCT hot case temperature of the lead is given a conservative lower bound of  $T_{Lh} = 200$  °F as discussed above.

$$r_{Lih} = r_{Li620} [1 - \alpha_{L620} (620 - 70) + \alpha_{L200} (T_{Lh} - 70)] = 8.967 \text{ inches}$$

$$r_{Loh} = r_{Lo620} [1 - \alpha_{L620} (620 - 70) + \alpha_{L200} (T_{Lh} - 70)] = 16.937 \text{ inches}$$

where  $r_{Lih}$  is the free state inner radius of the lead, and  $r_{Loh}$  is the outer radius, at NCT. From Table 2.2-4, the thermal expansion coefficient of the lead from 620 °F to 70 °F,  $\alpha_{L620} = 20.4(10^{-6})/^{\circ}\text{F}$ , and from 70 °F to  $T_{Lh}$ , the corresponding coefficient is  $\alpha_{L200} = 16.7(10^{-6})/^{\circ}\text{F}$ . Next, the interference between the inner shell and the lead will be found. Since the lead has a relatively low yield stress, the interface pressure between the inner shell and the lead will be governed by the lead yield stress, which in turn depends on the location of the lead stress state on the lead stress-strain curve. The hoop strain in the lead is equal to  $u/r$ , where  $u$  represents the radial displacement of the inner surface, and  $r$  is the inner radius, of the lead. The interface pressure can be conservatively maximized by assuming that the cask inner shell is rigid, and that therefore all of the radial interference is taken by the lead. The radial interference is

$$u = r_{ioh} - r_{Lih} = 0.043 \text{ inches}$$

The maximum lead strain is then

$$\varepsilon_{Lh} = \frac{u}{r_{Lih}} (100) = 0.480 \%$$

Stress-strain curves for lead at various temperatures are reproduced in Figure 2.2-1. The hoop stress at a temperature of 200 °F, corresponding to a maximum strain of 0.480% may be conservatively bounded by a value of  $\sigma_{Lh} = 600$  psi. It may be observed from the figure that the actual stress would be somewhat lower. The maximum sustainable interface pressure can be backed out of the equation for hoop stress in a thick walled cylinder, Table 32, Case 1a [25], as

$$p_h = \frac{\sigma_{Lh}}{\frac{r_{Loh}^2 + r_{Lih}^2}{r_{Loh}^2 - r_{Lih}^2}} = 337 \text{ psi}$$

In the finite element thermal stress analysis discussed in Section 2.6.1.3.2, a conservative upper bound external pressure of 350 psi is applied to the inner shell to represent the worst case lead contraction loading.

### 2.6.1.3 Stress Calculations

#### 2.6.1.3.1 Stresses Due to Pressure Loading

The finite element model described in Appendix 2.12.4, *Stress Analysis Finite Element Models*, is loaded with the internal maximum design pressure of 25 psi, without thermal loading, and gives the result discussed in Section 2.12.4.4.1, *Case No. 1, Design Pressure Only*, and shown in Figure 2.12.4-5. The maximum overall stress intensity which results from the model, which bounds both the primary membrane and membrane plus bending stress, is 281 psi, located at the midpoint of the cavity bottom. Since this value is less than the lowest (primary membrane) stress allowable, as shown in Section 2.6.1.4, *Comparison with Allowable Stresses*, it is not necessary to identify the individual stress components.

Since the FEA model does not include the closure lid, the stress due to pressure on the lid is computed manually. From [25], Table 24, Case 10a for a simply supported, uniformly loaded plate, the bending moment is:

$$M = \frac{qa^2(3+\nu)}{16} = 668 \text{ in} - \text{lb/in}$$

where the radius,  $a = 22.75/2 = 11.38$  inches, the design pressure,  $q = 25$  psig, conservatively applied over the entire area within the bolt circle, and  $\nu = 0.3$ . The stress in the closure lid is:

$$\sigma = \frac{6M}{t^2} = 1,002 \text{ psi}$$

where the lid thickness,  $t = 2.0$  inches. As shown, the stress in the closure lid is bounding over the stress in the cavity bottom.

#### 2.6.1.3.2 Stresses Due to Thermal Loading

The same finite element model is loaded with 25 psi internal pressure, as well as with the structural temperatures shown in Figure 2.12.4-3 and the lead contraction pressure determined in Section 2.6.1.2.3, *Lead*, and gives the result discussed in Section 2.12.4.4.2, *Case No. 2, Lead Shrinkage Pressure With Thermal*, and shown in Figure 2.12.4-6. The structural temperatures are originally obtained from the SINDA® thermal model described in Chapter 3, *Thermal Evaluation*, and are imported into the stress analysis as described in Appendix 2.12.4.2.1, *Thermal Loads*. The maximum overall stress intensity due to pressure and thermal gradient loading is 6,933 psi and occurs at the top of the inner shell cross section. Since this value is less than the lowest (primary membrane) stress allowable, as shown in Section 2.6.1.4, *Comparison with Allowable Stresses*, it is not necessary to identify the individual stress components.

**BRR Package Safety Analysis Report****2.6.1.4 Comparison with Allowable Stresses**

From Table 2.1-1, the limit on primary membrane plus bending stress is  $1.5S_m$ . At the bounding temperature of 250 °F given in Section 2.6.1.1, *Summary of Pressures and Temperatures*, the value of  $1.5S_m$  for Type 304 is 30,000 psi from Table 2.6-1. Applying this limit to the bounding stress intensity of 1,002 psi given in Section 2.6.1.3.1, *Stresses Due to Pressure Loading*, the margin of safety is:

$$MS = \frac{30,000}{1,002} - 1 = +28.9$$

From Table 2.1-1, the limit on the range of primary plus secondary stress intensity is  $3S_m$ . For the range of stress intensity of 6,933 psi given in Section 2.6.1.3.2, *Stresses Due to Thermal Loading*, the margin of safety is:

$$MS = \frac{(3.0)20,000}{6,933} - 1 = +7.65$$

As shown, all margins of safety for the NCT warm condition are positive.

**2.6.1.5 Closure Bolts**

Twelve closure bolts attach the closure lid to the cask opening. The closure lid is sized such that support against lateral loads (in the plane of the lid) is obtained from the fit between the lid and the cask opening, thus preventing any shear loading of the closure bolts. In addition, the lid is prepared with a 1/16-inch deep step located on the bolt circle which extends to the outer edge of the lid. The step prevents any bolt prying or significant bolt bending from occurring as a result of lid deformation.

The closure bolts are tightened to  $220 \pm 20$  ft-lb of torque, or a maximum of 240 ft-lb. From Section 4.2 of [10], the maximum non-prying tensile force per bolt due to the preload,  $F_{a\_max}$ , is found from:

$$F_{a\_max} = \frac{Q_{max}}{(K)(D_b)} = 19,200 \text{ lb}$$

where  $Q_{max} = 240 \times 12 = 2,880$  in-lb is the maximum bolt torque,  $K = 0.15$  is the nut factor for a lubricated bolt (approximately equal to the average of the values for lubricated surfaces in Table 4.1 of [10]), and  $D_b = 1.0$  inches is the nominal diameter of the closure bolt. The maximum residual torsion is 50% of the applied torsion, or:

$$M_{tr} = 0.5(Q_{max}) = 1,440 \text{ in-lb}$$

From Section 4.4 of [10], the maximum non-prying tensile force per bolt,  $F_{a\_max}$ , due to pressure loads are:

$$F_{a\_max} = \frac{\pi D_l g^2 (P_{li} - P_{lo})}{4 N_b} = 789 \text{ lb}$$

where  $D_l g = 18.25$  inches is the diameter of the pressure boundary, i.e., the inner (containment) O-ring seal,  $P_{li} = 25 \text{ psig} + 14.7 \text{ psia} = 39.7 \text{ psia}$  is the internal pressure,  $P_{lo} = 3.5 \text{ psia}$  is the NCT cold external reduced pressure from Section 2.6.3, *Reduced External Pressure*, and  $N_b = 12$  is the quantity of closure bolts. From this it is clear that the preload force is governing over the pressure force.

**BRR Package Safety Analysis Report**

Even though the temperatures of the closure lid and bolts are the same, a thermally induced loading is applied to the closure bolts due to the difference in thermal expansion coefficient between the ASTM A320 L43 alloy steel closure bolts and the Type 304 stainless steel closure lid. From Section 4.5 of [10], the maximum non-prying tensile force due to thermal expansion effects is:

$$F_a = \frac{\pi}{4} D_b^2 (E_b) [a_l(T_l) - a_b(T_b)] = 8,747 \text{ lb}$$

where the modulus of elasticity of the bolt,  $E_b = 26.9(10^6)$  psi, the thermal expansion coefficient of the closure lid,  $a_l = 9.1(10^{-6})$  in/in/°F, and the thermal expansion coefficient of the bolt,  $a_b = 6.8(10^{-6})$  in/in/°F, all from Table 2.6-1. The change in temperature of both components,  $T_l = T_b = (250 - 70) = 180$  °F, where the bounding temperature of the components is 250 °F, and the ambient temperature is 70 °F.

The average axial bolt stress corresponding to these loadings is:

$$S_{ba} = 1.2732 \frac{(19,200 + 8,747)}{D_{ba}^2} = 46,158 \text{ psi}$$

where the load term in the numerator is the sum of the preload and thermal loads, and the stress diameter,  $D_{ba} = D_b - 0.9743(p) = 0.878$  inches, where  $D_b$  is 1.0 inches and the pitch,  $p$ , is 0.125 for the 1-8 UNC bolt. The residual torsional stress is:

$$S_{bt} = \frac{5.093(M_{tr})}{D_{ba}^3} = 10,836 \text{ psi}$$

From Table 2.1-1, for NCT the allowable average tensile stress is  $S_m = (2/3)S_y$ , which from Table 2.6-1 is equal to 64,900 psi at the NCT hot temperature of 250 °F. The margin of safety is:

$$MS_{S_{ba}} = \frac{64,900}{S_{ba}} - 1 = +0.41$$

Combining the axial and residual torsional shear stresses, the maximum closure bolt stress intensity is:

$$S_{bi} = \sqrt{S_{ba}^2 + 4S_{bt}^2} = 50,993 \text{ psi}$$

As noted at the beginning of this section, bolt shear or prying loads are precluded by the design of the closure lid. From Table 2.1-1, the allowable stress intensity is  $1.35S_m$  for cases where  $S_y$  is greater than 100 ksi. The margin of safety is:

$$MS_{S_{bi}} = \frac{1.35(64,900)}{50,993} - 1 = +0.72$$

Thus the closure bolts are not of concern for the NCT hot condition, including the reduced external pressure load case.

## 2.6.2 Cold

For the cold condition, a -40 °F steady state ambient temperature is utilized per Regulatory Guide 7.8 [3], with zero insolation and zero decay heat. This results in a uniform temperature of -40 °F throughout the cask. The materials of construction are not adversely affected by the -40 °F condition, including brittle fracture, which is evaluated in Section 2.1.2.3.1, *Brittle Fracture*.

In Section 2.6.1.2, *Differential Thermal Expansion*, the interface pressure between the cask inner shell and the lead gamma shielding was evaluated at the NCT maximum temperature. Since the lead will contract further at lower temperatures, that analysis is now repeated for the NCT cold condition. As discussed in Section 2.6.1.2, the lead and the cask inner and outer shells are all in contact, and stress free, at the point of solidification of the lead at 620 °F. As the cask and lead cool, the lead contracts more than the stainless steel, and an interface pressure develops between the lead and the inner shell. This interface pressure is a function of the amount of interference between the lead and inner shell, and of the yield point of the lead at the cold temperature. As stated in Section 2.6.1.2, material creep in the lead will reduce the interface pressure over time, but the effect is conservatively neglected. In addition, the entire strain history of the lead is assumed to occur at a temperature of -40 °F, which further maximizes the lead interface pressure. The amount of interference between the lead and the inner shell depends upon the free state radii of these components, both at -40 °F. The free state outer radius of the inner shell at -40 °F is:

$$r_{ioc} = r_{io} [1 + \alpha_{s-40}(-40 - 70)] = 8.992 \text{ inches}$$

where the outer free state radius of the inner shell at room temperature,  $r_{io} = 9$  inches, and the coefficient of thermal expansion of the shell at -40 °F,  $\alpha_{s-40} = 8.2(10^{-6})/^{\circ}\text{F}$  from Table 2.6-1.

To determine the free state radii of the lead at -40 °F, it is necessary to start with the radii of the steel shells at the lead solidification point at 620 °F, at which point all of the components are in stress free contact. The radii of the lead/steel interfaces at 620 °F were found in Section 2.6.1.2. The value  $r_{Li620} = 9.049$  inches represents the inner radius of the lead and  $r_{Lo620} = 17.092$  inches represents the outer lead radius. These values are then used to find the free state lead dimensions at the cold temperature of -40 °F as follows. Note that two thermal expansion terms are used (first contracting the lead from 620 °F to 70 °F, then contracting it further from 70 °F to -40 °F), since the thermal expansion coefficients given in Table 2.2-4 are based on 70 °F.

$$r_{Lic} = r_{Li620} [1 - \alpha_{L620}(620 - 70) + \alpha_{L-40}(-40 - 70)] = 8.932 \text{ inches}$$

$$r_{Loc} = r_{Lo620} [1 - \alpha_{L620}(620 - 70) + \alpha_{L-40}(-40 - 70)] = 16.871 \text{ inches}$$

where  $r_{Lic}$  is the free state inner radius of the lead, and  $r_{Loc}$  is the outer radius, at -40 °F. From Table 2.2-4, the thermal expansion coefficient of the lead from 620 °F to 70 °F,  $\alpha_{L620} = 20.4(10^{-6})/^{\circ}\text{F}$ , and from 70 °F to -40 °F,  $\alpha_{L-40} = 15.6(10^{-6})/^{\circ}\text{F}$ . Since the lead has a relatively low yield stress, the interface pressure between the inner shell and the lead will be governed by the lead yield stress, which in turn depends on the location of the lead stress state on the lead stress-strain curve. The hoop strain in the lead is equal to  $u/r$ , where  $u$  represents the radial displacement of the inner surface, and  $r$  is the inner radius of the lead. The interface pressure can be conservatively maximized by assuming that the inner shell is rigid, and therefore all of the radial interference is taken by the lead. The radial interference is

$$u = r_{ioc} - r_{Lic} = 0.060 \text{ inches}$$

The maximum lead strain is then

$$\epsilon_{Lh} = \frac{u}{r_{Lic}} (100) = 0.671 \%$$

**BRR Package Safety Analysis Report**

Stress-strain curves for lead at various temperatures are reproduced in Figure 2.2-1. From the curve representing a lead temperature of -40 °F, the maximum lead stress corresponding to a strain of 0.671% is bounded by  $\sigma_{Lc} = 1,400$  psi. The maximum sustainable interface pressure can be backed out of the equation for hoop stress in a thick walled cylinder, Table 32, Case 1a [25], as

$$p_c = \frac{\sigma_{Lc}}{\frac{r_{Loc}^2 + r_{Lic}^2}{r_{Loc}^2 - r_{Lic}^2}} = 787 \text{ psi}$$

Using this external pressure, the inner shell membrane stress is

$$\sigma_i = \frac{p_c r_{avg}}{t} = 6,690 \text{ psi}$$

where  $r_{avg}$  is the minimum average inner shell radius, 8.5 inches, and  $t$  is the wall thickness of 1 inch. From Table 2.6-1, the allowable primary membrane stress intensity ( $S_m$ ) is 20,000 psi. The margin of safety is

$$MS = \frac{20,000}{6,690} - 1 = +1.99$$

Therefore, the NCT cold condition is not of concern.

Since the coefficient of thermal expansion of the closure lid material is slightly larger than that of the bolting material, a reduction in closure bolt preload will occur at the NCT cold condition. Using the terminology of [10], the reduction in preload is:

$$F_a = \frac{\pi}{4} Db^2 (E_b) [a_l(T_l) - a_b(T_b)] = -4,890 \text{ lb}$$

where the bolt nominal diameter,  $Db = 1.0$  inches, the bolt modulus of elasticity,  $E_b = 28.3(10^6)$  psi, the coefficient of thermal expansion of the lid material,  $a_l = 8.2(10^{-6})$  in/in/°F for Type 304 stainless steel, the coefficient of thermal expansion of the bolt material,  $a_b = 6.2(10^{-6})$  in/in/°F for A320 L43 alloy steel, and  $T_l = T_b = -40 - 70 = -110$  °F. The material properties are taken from Table 2.6-1. The minimum bolt preload torque is 220 ft-lb minus 20 ft-lb, or  $Q_{min} = 2,400$  in-lb. The minimum bolt preload force is:

$$F_{a\_min} = \frac{Q_{min}}{K(Db)} = 16,000 \text{ lb}$$

where  $Db$  is defined above and  $K = 0.15$ , consistent with the definition in Section 2.6.1.5, *Closure Bolts*. Thus, the reduction in preload due to differential thermal expansion is only  $4,890/16,000 \times 100 = 31\%$ , and a large positive preload force remains at the NCT minimum temperature of -40 °F.

### 2.6.3 Reduced External Pressure

The effect of reduced external pressure of 3.5 psia, per 10 CFR §71.71(c)(3), is considered negligible for the BRR package compared to other design loadings. This conclusion is based on the NCT structural analyses presented in Section 2.6.1, *Heat*, demonstrating the structural integrity for a 25 psig internal design pressure. Based on the Maximum Normal Operating Pressure (MNOP) of 10 psig, the reduced external pressure conditions would cause a pressure of



**BRR Package Safety Analysis Report**

21.2 psig. Therefore, the 25 psig internal design pressure analysis is conservatively bounding for the reduced external pressure case.

### 2.6.4 Increased External Pressure

The effect of an increased external pressure of 20 psia, per 10 CFR §71.71(c)(4), is acceptable for the BRR package. Consistent with Regulatory Guide 7.8, this loading corresponds to an ambient temperature of -20 °F, no insolation, no decay heat, and minimum internal pressure. Additionally, the fabrication stress resulting from the shrinking of the radial lead shield of  $p_c = 787$  psi (see Section 2.6. 2, *Cold*) is included as a radial pressure on the outside of the inner shell. Note that the lead shrinkage stress corresponds to a temperature of -40 °F, which results in a conservatively higher shrinkage stress than would occur at the required ambient temperature of -20 °F. Conservatively, the inner shell is evaluated neglecting the outer shell, even though the external pressure would be applied to the much stronger outer shell rather than the inner shell.

Since the cask is closed under ambient conditions, the internal pressure in the cask at a temperature of -20 °F is

$$p_i = p_{amb} \frac{(-20 + 460)}{(70 + 460)} = 12.2 \text{ psia}$$

where  $p_{amb}$  is 14.7 psia. Therefore the net external differential gas pressure  $p_o = 20 - 12.2 = 7.8$  psi. The combined external pressure on the inner shell is  $p_{ext} = p_c + p_o = 794.8$  psi. An upper bound value of  $p_{ext} = 800$  psi is used. The compressive hoop stress is:

$$\sigma_\theta = p_{ext} \frac{r_{avg}}{t} = 6,800 \text{ psi}$$

where the mean inner shell radius,  $r_{avg} = 8.5$  inches, and the thickness,  $t =$  one inch. The compressive axial stress, obtained by supporting the pressure load from the entire cask cross section over the inner shell cross section, is:

$$\sigma_\phi = \frac{p_o \pi r_{cask}^2}{2 \pi r_{avg} t} = 169 \text{ psi}$$

where  $r_{cask} = 38.4/2 = 19.2$  inches. Using Mohr's circle, the maximum shear stress is:

$$\sigma_{\phi\theta} = \frac{1}{2}(\sigma_\theta - \sigma_\phi) = 3,316 \text{ psi}$$

The maximum stress intensity is twice this value, or  $SI = 6,632$  psi. From Table 2.6-1, the allowable membrane stress intensity for the inner shell is 20,000 psi. The margin of safety is:

$$MS = \frac{20,000}{6,632} - 1 = +2.02$$

The possibility of buckling of the inner shell is evaluated using [13]. Consistent with Regulatory Guide 7.6, a factor of safety corresponding to ASME Code, Service Level A is employed. In this case, the applicable factor of safety is 2.00 for normal conditions, as specified in [13]. The analysis used a modulus of elasticity of  $28.8(10^6)$  psi, corresponding to -20 °F. Buckling analysis geometry and loading parameters are listed in Table 2.6-3 and results of the analysis in Table 2.6-4. As shown,

all interaction check values, including the maximum value of 0.5974, are less than unity, as required. Thus, the increased external pressure load case is not of concern for the BRR package.

### 2.6.5 Vibration

The effects of vibration normally incident to transport are shown to be insignificant. Draft ANSI Standard N14.23 [24] identifies peak truck trailer vibration inputs. Table 2 of [24] shows peak vibration accelerations of a trailer bed as a function of package and tiedown system natural frequency. For the frequency range 0 to 5 Hz, and conservatively assuming a light package, Table 2 gives peak accelerations (99% level) of 2g in the vertical direction, and 0.1g in both the lateral and longitudinal directions. All other frequency ranges give significantly lower acceleration levels. Due to cask symmetry, the vertical load of  $\pm 2g$  governs the  $\pm 0.1g$  in the lateral and longitudinal directions.

Design fatigue curves are taken from Figure I-9.2.1 and Table I-9.2.2 of [12] for the Type 304 stainless steel cask material, from which the allowable amplitude,  $S_a$ , of the alternating stress component (1/2 of the alternating stress range) as a function of number of loading cycles may be obtained. Table I-9.2.2 extends the fatigue allowable data to the endurance limit, which is used in the fatigue assessment of transportation vibration. The allowable amplitude,  $S_a$ , from Table I-9.2.2 for Type 304 stainless steel cask material at  $10^{11}$  cycles is 13,600 psi. This value is adjusted based on the ratio of room temperature elastic modulus of  $28.3(10)^6$  psi, which is the basis for Table I-9.2.2, and the elastic modulus at NCT maximum temperature, as follows:

$$S_a = 13,600 \left[ \frac{27.3(10^6)}{28.3(10^6)} \right] = 13,119 \text{ psi}$$

where  $27.3(10^6)$  psi is the elastic modulus at the bounding temperature of all cask components of 250 °F from Table 2.2-1.

The BRR package is transported vertically. In this orientation, the closure lid experiences the  $\pm 2g$  loading transverse to the plane of the lid. The weight of the shield plug is conservatively assumed to act with the weight of the lid in responding to the vibratory input. From Table 2.1-2, the weight of the shield plug is 950 lb, and the weight of the lid is 280 lb, for a total of  $W = 1,230$  lb. The lid is modeled as a simply supported plate with an effective outer radius equal to the bolt circle of 22.75 inches. Under a load of 2g, the maximum bending moment in the plate (at the center) is found from Table 24, Case 10a of [25], and is:

$$M = 2K_M q a^2 = 161.7 \text{ in} - \text{lb/in}$$

where the factor 2 is the vibrational load,  $K_M = 0.20625$  for  $r_o = 0$  from [25], the bolt circle radius,  $a = 22.75/2 = 11.375$  inches, and  $q$  is the 1-g plate loading, equivalent to a pressure, found from:

$$q = \frac{W}{A} = 3.03 \text{ psi}$$

where  $W$  is defined above and  $A$  is the area defined by the bolt circle, equal to  $406.5 \text{ in}^2$ . The stress in the closure lid is:

$$\sigma = \frac{6M}{t^2} = 242.6 \text{ psi}$$

where the thickness of the closure lid,  $t = 2$  inches. For the allowable amplitude,  $S_a$ , found above, equal to 13,119 psi, the margin of safety against fatigue of the closure lid due to vibration is:

$$MS = \frac{13,119}{242.6} - 1 = +53.1$$

Therefore, fatigue of the BRR package due to transportation vibration is not of concern.

### **2.6.6 Water Spray**

The materials of construction used in the BRR package are not affected by the water spray test identified in 10 CFR §71.71(c)(6).

### **2.6.7 Free Drop**

Section 10 CFR §71.71(c)(7) specifies a free drop from a height of 2 ft for a package weight between 22,000 and 33,100 lb. The governing orientations of end and side are evaluated for the NCT free drop event. The choice of governing orientations is discussed in further detail in Appendix 2.12.2, *Certification Test Plan*. NCT free drop impacts are developed in Appendix 2.12.5, *Impact Limiter Performance Evaluation*. A value of 40g is chosen to bound the calculated impact magnitude for all NCT drop orientations.

Cask body stresses are analyzed for the NCT free drop using the same finite element model identified in Section 2.6.1.3, *Stress Calculations*, and which is also used for evaluation of the HAC free drop event. The model is loaded by a global, quasi-static acceleration field consistent with an impact of 40g. The cask stress analysis for NCT is identical with the analysis for HAC, with the following exceptions:

- Thermal stresses are included in the NCT stress analyses
- The applied quasi-static acceleration field corresponds to the NCT free drop impact of 40g
- Allowable stresses are lower, in accordance with Regulatory Guide 7.6 recommendations.

As discussed in Section 2.7.1.4, *Oblique Drop*, cask stresses are governed by those resulting from the end and side drop orientations. The stress analyses for NCT free drop are given in Sections 2.6.7.1, *NCT End Free Drop*, and 2.6.7.2, *NCT Side Free Drop*.

#### **2.6.7.1 NCT End Free Drop**

The construction of the finite element model is discussed in Appendix 2.12.4, *Stress Analysis Finite Element Models*. Temperature loading is applied as discussed in that appendix. The end drop case is evaluated for both top down and bottom down orientations by applying a quasi-static acceleration of 40g. Five analyses are performed:

- Cask body stress
- Closure bolt stress
- Closure lid stress
- Lower closure plate weld stress

- End drop buckling evaluation

**Cask Body Stress.** From Section 2.12.4.4.3, *Case No. 3, NCT Bottom-down End Drop*, the maximum stress intensity resulting from the bottom-down impact of 40g is 15,202 psi, located at the outside surface of the bottom end structure, as shown in Figure 2.12.4-8. From Table 2.1-1, the limit on primary membrane stress is  $S_m$ . At the bounding temperature of 250 °F, the value of  $S_m$  for Type 304 is 20,000 psi from Table 2.6-1. Conservatively applying the membrane stress limit to the maximum stress intensity of 15,202 psi, the margin of safety is:

$$MS = \frac{20,000}{15,202} - 1 = +0.32$$

From Section 2.12.4.4.4, *Case No. 4, NCT Bottom-down End Drop With Thermal*, the maximum stress intensity resulting from the bottom-down impact of 40g with thermal loads included is 14,586 psi, located at the top of the inner shell cross section, as shown in Figure 2.12.4-9. From Table 2.1-1, the limit on the range of primary plus secondary stress intensity is  $3S_m$ . The margin of safety is:

$$MS = \frac{(3.0)20,000}{14,586} - 1 = +3.11$$

From Section 2.12.4.4.6, *Case No. 6, NCT Top-down End Drop*, the maximum stress intensity resulting from the top-down impact of 40g is 13,248 psi, located at the top of the inner shell, as shown in Figure 2.12.4-13. From Table 2.1-1, the limit on primary membrane stress is  $S_m$ . Conservatively applying the membrane stress limit to the maximum stress intensity of 13,248 psi, the margin of safety is:

$$MS = \frac{20,000}{13,248} - 1 = +0.51$$

From Section 2.12.4.4.7, *Case No. 7, NCT Top-down End Drop With Thermal*, the maximum stress intensity resulting from the top-down impact of 40g with thermal loads included is 13,258 psi, located at the top of the inner shell, as shown in Figure 2.12.4-14. From Table 2.1-1, the limit on the range of primary plus secondary stress intensity is  $3S_m$ . The margin of safety is:

$$MS = \frac{(3.0)20,000}{13,258} - 1 = +3.53$$

As shown, all cask body margins of safety for the NCT end free drop condition are positive.

**Closure bolt stress.** In the top-down orientation, the non-prying closure bolt load is calculated according to Section 4.6 of [10] using:

$$F_a = \frac{1.34 \sin(\xi)(DLF)(a_i)(W_l + W_c)}{N_b} = 9,380 \text{ lb}$$

where the impact angle,  $\xi = 90^\circ$  for the end drop impact, the dynamic load factor,  $DLF = 1.05$  as discussed in Section 2.7.1.2, *End Drop*, the impact magnitude,  $a_i = 40g$  as discussed above, the weight of the lid,  $W_l = 280 \text{ lb}$ , and the weight of the contents,  $W_c = 1,720 \text{ lb}^1$  from Table 2.1-2,

<sup>1</sup> This weight consists of the shield plug plus the heaviest basket/fuel combination.

**BRR Package Safety Analysis Report**

and the quantity of bolts,  $N_b = 12$ . Note that no support for the lid is assumed from the inner surface of the impact limiter.

The sum of all applied loads (the NCT free drop load plus the load due to the design pressure, equal to 789 lb as determined in Section 2.6.1.5, *Closure Bolts*) is equal to  $9,380 + 789 = 10,169$  lb. This value is however much less than the sum of preload (19,200 lb) and thermal expansion load (8,747 lb). Therefore, the bolt load in the NCT free drop event is governed by the preload plus thermal load, and the margins of safety calculated in Section 2.6.1.5, *Closure Bolts*, are not affected by the free drop event.

**Closure lid stress.** In Section 2.7.1.2, *Free Drop*, the bending stress in the closure lid is calculated for the top-down HAC free drop under an impact load of 120g. The only difference in the case of the NCT free drop is that the impact is one-third as large, i.e., 40g. The following calculations rely on data given in Section 2.7.1.2. Since the total weight in the end drop is 2,000 lb, the applied load is  $2,000 \times 40 = 80,000$  lb. Since the area of the lid is  $A_{\text{lid}} = 406.9 \text{ in}^2$ , the uniform load on the lid is:

$$q = \frac{80,000}{A_{\text{lid}}} + 25 = 221.6 \text{ psi}$$

where the second term accounts for the design pressure of 25 psig. The uniform load in the HAC case is 614.8 psi, and the resulting stress is 25,865 psi. Using a ratio, the stress under the NCT free end drop is

$$\sigma_{\text{NCT}} = \frac{221.6}{614.8} 25,865 = 9,323 \text{ psi}$$

From Table 2.1-1, the allowable membrane plus bending stress is equal to  $1.5S_m$ . From Table 2.6-1,  $1.5S_m$  is equal to 30,000 psi at the NCT hot temperature of 250 °F. The margin of safety on the closure lid is:

$$MS = \frac{30,000}{9,323} - 1 = +2.22$$

Thus, the allowable stress is satisfied for the closure lid in the NCT end drop.

**Lower closure plate weld stress.** In Section 2.7.1.2, *Free Drop*, the combined stress in the lower closure plate weld is calculated for the top-down HAC free drop under an impact load of 120g. The resulting stress is 49,165 psi. This stress includes both fixed-edge bending effects as well as shear loading. Since the NCT impact is 40g and the HAC impact is 120g, the stress corresponding to the NCT free drop is:

$$\sigma_{\text{NCT}} = \sigma_{\text{HAC}} \frac{40}{120} = 16,388 \text{ psi}$$

From Table 2.1-1, the membrane plus bending stress allowable is  $1.5S_m$ , which from Table 2.6-1 is equal to 30,000 psi for Type 304 at 250 °F. The margin of safety is:

$$MS = \frac{30,000}{16,388} - 1 = +0.83$$

Thus, the allowable stress is satisfied for the lower closure plate weld stress in the NCT end drop.

**End drop buckling evaluation.** The cask shells are subject to buckling loads in the end drop orientation. Due to its much greater stiffness compared to the inner shell, the cask outer shell will carry most of the axial loading. The NCT case is essentially the same as the HAC case evaluated in Section 2.7.1.2, *End Drop*, except for the different impact load and factor of safety required by Code Case N-284-2 [13]. Since the HAC end drop is evaluated for an impact of 120g and the NCT for 40g, the axial stress in the NCT buckling evaluation is:

$$\sigma_{\phi-NCT} = \sigma_{\phi-HAC} \times \frac{40}{120} = 2,372 \text{ psi}$$

where  $\sigma_{\phi-HAC} = 7,117$  psi from Section 2.7.1.2, *End Drop*. No other stresses are applied for the end drop buckling evaluation. The outer shell is conservatively assumed to carry the entire axial load without assistance from the inner shell. Thermal stress, which is tensile in the outer shell, is conservatively ignored. Shell dimensions are taken from Table 2.6-5. The factor of safety is equal to 2.00, consistent with Code Case N-284-2 for NCT. The results are shown in Table 2.6-6. As shown, all interaction parameters are less than unity, as required. Therefore, buckling of the cask shells in the NCT free drop will not occur.

### 2.6.7.2 NCT Side Free Drop

The NCT side free drop is evaluated using the same finite element model which was used for the end drop case. The quasi-static acceleration of 40g also applies to the side drop, since it bounds the calculated side drop impact as discussed in Appendix 2.12.5, *Impact Limiter Performance Evaluation*. The side drop orientation is governing over the slapdown orientation as discussed in Section 2.7.1.4, *Oblique Drop*.

From Section 2.12.4.4.9, *Case No. 9, NCT Side Drop*, the maximum stress intensity resulting from the side drop impact of 40g is 18,935 psi, located at the bottom outside edge of the lower lead cavity, as shown in Figure 2.12.4-19. From Table 2.1-1, the limit on primary membrane stress is  $S_m$ . At the bounding temperature of 250 °F, the value of  $S_m$  for Type 304 is 20,000 psi from Table 2.6-1. Conservatively applying the membrane stress limit to the maximum stress intensity of 18,935 psi, the margin of safety is:

$$MS = \frac{20,000}{18,935} - 1 = +0.06$$

From Section 2.12.4.4.10, *Case No. 10, NCT Side Drop With Thermal*, the maximum stress intensity resulting from the side drop impact of 40g with thermal loads included is 22,704 psi, located at the shield plug shelf, as shown in Figure 2.12.4-20. From Table 2.1-1, the limit on the range of primary plus secondary stress intensity is  $3S_m$ . Conservatively applying the membrane stress limit to the maximum stress intensity of 22,704 psi, the margin of safety is:

$$MS = \frac{(3.0)20,000}{22,704} - 1 = +1.64$$

As shown, all cask body margins of safety for the NCT side free drop condition are positive.

### 2.6.8 Corner Drop

The BRR package is not required to be evaluated for the corner drop condition, since 10 CFR §71.71(c)(8) applies only to rectangular fiberboard or wood packages weighing less than 110 lb or

to cylindrical fiberboard or wood packages weighing less than 220 lb. The weight of the BRR package exceeds these limits and therefore does not need to be evaluated for the NCT corner drop.

### 2.6.9 Compression

The BRR package is not required to be evaluated for the compression condition, since 10 CFR §71.71(c)(9) applies only to packages weighing less than 11,000 lb. The weight of the BRR package exceeds this limit, and therefore does not need to be evaluated for compression.

### 2.6.10 Penetration

The impact of a 1.25-inch diameter, hemispherically ended, 13-lb steel bar, per 10 CFR §71.71(c)(10), dropped vertically from a height of 40 inches, has no significant effect on the BRR package. Slight denting of the thermal shield on the outside of the cask can occur, but the bar cannot penetrate or rip into the shield, and cannot harm the impact limiters or impact limiter attachments. Therefore, this test has no significant effect on the package.

**Table 2.6-1 – Summary of NCT Design Parameters**

Parameter	Body, Closure Lid (Type 304)	Closure Bolts (A320, Grade L43)	Baskets (all Type 304)
NCT Hot Bounding Temperature, °F	250	250	400
Coefficient of Thermal Expansion, $\alpha$ , (in/in/°F)	$9.1 \times 10^{-6}$	$6.8 \times 10^{-6}$	$9.5 \times 10^{-6}$
Elastic Modulus, psi	$27.3 \times 10^6$	$26.9 \times 10^6$	$26.4 \times 10^6$
Design Stress, $S_m$ , psi	20,000	64,900	18,600
Yield Stress, $S_y$ , psi	23,700	97,350	20,700
Primary Membrane Stress Intensity ( $P_m$ ), psi	$S_m = 20,000$	n/a*	$S_m = 18,600$
Primary Membrane + Bending Stress Intensity ( $P_m + P_b$ ), psi	$1.5S_m = 30,000$	n/a*	$1.5S_m = 27,900$
Primary Membrane + Bending + Secondary Stress Intensity ( $P_m + P_b + Q$ ), psi	$3.0S_m = 60,000$	n/a*	$3.0S_m = 55,800$
NCT Cold Bounding Temperature, °F	-40	-40	-40
Coefficient of Thermal Expansion, $\alpha$ , (in/in/°F)	$8.2 \times 10^{-6}$	$6.2 \times 10^{-6}$	$8.2 \times 10^{-6}$
Elastic Modulus, psi	$28.9 \times 10^6$	$28.3 \times 10^6$	$28.9 \times 10^6$

\* Bolting allowable stresses are discussed in the sections where they are used.

**Table 2.6-2 – Axial Clearance of Fuel Summary**

Type	Max. fuel len., 70°F, in.	Max. fuel len., 400 °F, in.	Basket cavity len., 70 °F, in.	Basket cavity, less 0.12 in. tol.	Min basket cavity len., 400 °F, in.	Axial clearance, min, in.
		$L_{Fuel-Hot-Max}$			$L_{Cav-Hot-Min}$	Gap(x)
MURR	32.75	32.90	33.13	33.01	33.11	0.21
MITR-II	26.52	26.64	26.88	26.76	26.84	0.20
ATR	51.00	51.23	51.38	51.26	51.42	0.19
TRIGA	See Table 2.6-2a					0.13
Square fuel	See Table 2.6-2b					0.08

**Table 2.6-2a –TRIGA Fuel Axial Clearance**

Catalog No.	Fuel Maximum Length, in. <sup>①</sup>	Max. Fuel Length at 400 °F, in.	Max. Pedestal Spacer Length, in.	Min. Basket Cavity length, in.	Min. Cavity Length at 400 °F, in.	Min Gap, in.
		$L_{Fuel-Hot-Max}$			$L_{Cav-Hot-Min}$	Gap(2)
101	28.62	28.75	19.07	28.81	28.90	0.15
201	28.78	28.91	18.54	29.34	29.43	0.52
103, 105, 109	29.15	29.28	18.54	29.34	29.43	0.15
117, 119	29.93	30.06	17.76	30.12	30.21	0.15
107	30.14	30.28	17.31	30.57	30.67	0.39
403, 405, 417, 419	30.38	30.52	17.31	30.57	30.67	0.15
217, 219	40.35	40.53	7.34	40.54	40.67	0.14
303, 305, 317, 319	44.00	44.20	3.69	44.19	44.33	0.13
203, 205, 207, 503, 505, 517, 519	45.50	45.70	2.19	45.69	45.83	0.13

Notes:

1. Lengths include 0.25 inches for irradiation growth.



**Table 2.6-2b – Square Fuel Axial Clearance**

Fuel Type	Fuel Maximum Length, in.	Max. Pedestal Spacer Length, in.	Total Length, Fuel + Ped., in	Max. Fuel Length at 400 °F, in.	Min. Cavity Length at 400 °F, in.	Min Gap, in.
				$L_{Fuel-Hot-Max}$	$L_{Cav-Hot-Min}$	Gap(3)
RINSC	39.75	0.00	39.75	39.93	40.01	0.08
U-Mass (aluminide)	39.75	0.00	39.75	39.93	40.01	0.08
U-Mass (silicide)	39.75	0.00	39.75	39.93	40.01	0.08
Ohio State	35.25	4.50	39.75	39.93	40.01	0.08
Missouri S&T	34.50	5.25	39.75	39.93	40.01	0.08
U-Florida	27.38	12.37	39.75	39.93	40.01	0.08
Purdue	32.49	7.26	39.75	39.93	40.01	0.08
PULSTAR	38.23	1.52	39.75	39.93	40.01	0.08
U-Mass (aluminide) Loose Plates	24.88	13.87	38.75	38.92	40.01	1.08
U-Florida & Purdue Loose Plates	25.88	13.87	39.75	39.93	40.01	0.08

**Table 2.6-3 – Increased External Pressure Buckling Evaluation: Geometry and Loads**

	Inner shell dimensions, inches	Applied stress, psi	
Inner Dia.	16.0	$\sigma_{\varphi}$	169
Outer Dia.	18.0	$\sigma_{\theta}$	6,800
Length*	62.0	$\sigma_{\varphi\theta}$	3,316

\* Bounding length used.

**Table 2.6-4 – Increased External Pressure: N-284-2 Results**

Parameter	Value	Remarks
<b>Capacity Reduction Factors (-1511)</b>		
$\alpha_{\phi L} =$	0.2795	
$\alpha_{\theta L} =$	0.8000	
$\alpha_{\phi\theta L} =$	0.8000	
<b>Plasticity Reduction Factors (-1610)</b>		
$\eta_{\phi} =$	0.0524	
$\eta_{\theta} =$	0.2811	
$\eta_{\phi\theta} =$	0.0410	
<b>Theoretical Buckling Values (-1712.1.1)</b>		
$C_{\phi} =$	0.6050	
$\sigma_{\phi eL} =$	2,049,882 psi	
$C_{\theta r} =$	0.0387	
$\sigma_{\theta eL} = \sigma_{reL} =$	133,985 psi	
$C_{\theta h} =$	0.0387	
$\sigma_{\theta eL} = \sigma_{heL} =$	133,985 psi	
$C_{\phi\theta} =$	0.1619	
$\sigma_{\phi\theta eL} =$	548,683 psi	
<b>Elastic Interaction Equations (-1713.1.1)</b>		
$\sigma_{xa} =$	286,471 psi	
$\sigma_{ha} =$	52,394 psi	
$\sigma_{ra} =$	52,394 psi	
$\sigma_{ta} =$	219,473 psi	
Axial + Shear $\Rightarrow$ Check (c):	0.0008	<1 $\therefore$ OK (see note*)
Hoop + Shear $\Rightarrow$ Check (d):	0.1300	<1 $\therefore$ OK
<b>Inelastic Interaction Equations (-1714.2.1)</b>		
$\sigma_{xc} =$	15,000 psi	
$\sigma_{rc} =$	14,730 psi	
$\sigma_{tc} =$	9,000 psi	
Max(Axial,Hoop) $\Rightarrow$ Check (a):	0.4616	<1 $\therefore$ OK
Axial + Shear $\Rightarrow$ Check (b):	0.1470	<1 $\therefore$ OK
Hoop + Shear $\Rightarrow$ Check (c):	0.5974	<1 $\therefore$ OK

\*Note: Elastic interaction checks (a), (b), (e), and (f) are not applicable.

**Table 2.6-5 – NCT Free Drop Buckling Evaluation: Geometry and Loads**

	Outer shell dimensions, inches	Applied stress, psi	
Inner Dia.	34.0	$\sigma_{\varphi}$	2,372
Outer Dia.	38.0	$\sigma_{\theta}$	0
Length*	55.0	$\sigma_{\varphi\theta}$	0

\* Bounding length used.

Table 2.6-6 – NCT Free Drop: N-284-2 Results

Parameter	Value	Remarks
<b>Capacity Reduction Factors (-1511)</b>		
$\alpha_{\phi L} =$	0.2279	
$\alpha_{\theta L} =$	0.8000	
$\alpha_{\phi\theta L} =$	0.8000	
<b>Plasticity Reduction Factors (-1610)</b>		
$\eta_{\phi} =$	0.0568	
$\eta_{\theta} =$	0.0850	
$\eta_{\phi\theta} =$	0.0232	
<b>Theoretical Buckling Values (-1712.1.1)</b>		
$C_{\phi} =$	0.6050	
$\sigma_{\phi eL} =$	1,831,806 psi	
$C_{\theta r} =$	0.1150	
$\sigma_{\theta eL} = \sigma_{reL} =$	348,340 psi	
$C_{\theta h} =$	0.1078	
$\sigma_{\theta eL} = \sigma_{heL} =$	326,534 psi	
$C_{\phi\theta} =$	0.2527	
$\sigma_{\phi\theta eL} =$	765,157 psi	
<b>Elastic Interaction Equations (-1713.1.1)</b>		
$\sigma_{xa} =$	208,750 psi	
$\sigma_{ha} =$	130,614 psi	
$\sigma_{ra} =$	139,336 psi	
$\sigma_{ta} =$	306,063 psi	
Axial + Shear $\Rightarrow$ Check (c):	0.0114	<1 $\therefore$ OK (see note*)
Hoop + Shear $\Rightarrow$ Check (d):	0.0000	<1 $\therefore$ OK
<b>Inelastic Interaction Equations (-1714.2.1)</b>		
$\sigma_{xc} =$	11,850 psi	
$\sigma_{rc} =$	11,850 psi	
$\sigma_{tc} =$	7,110 psi	
Max(Axial,Hoop) $\Rightarrow$ Check (a):	0.2002	<1 $\therefore$ OK
Axial + Shear $\Rightarrow$ Check (b):	0.2002	<1 $\therefore$ OK
Hoop + Shear $\Rightarrow$ Check (c):	0.0000	<1 $\therefore$ OK

\*Note: Elastic interaction checks (a), (b), (e), and (f) are not applicable.

## 2.7 Hypothetical Accident Conditions

When subjected to the hypothetical accident conditions (HAC) as specified in 10 CFR §71.73 [1], the BRR package meets the performance requirements specified in Subpart E of 10 CFR 71. This is demonstrated in the following subsections, where each accident condition is addressed and the cask shown to meet the applicable design criteria. The method of demonstration is primarily by analysis. The loads specified in 10 CFR §71.73 are applied sequentially, per Regulatory Guide 7.8 [3]. Resulting stresses are maintained below the limits established by Regulatory Guide 7.6 [2]. Dynamic testing of impact limiter performance is discussed in Section 2.12.3, *Certification Test Results*. A summary of cumulative damage is provided in Section 2.7.8, *Summary of Damage*.

### 2.7.1 Free Drop

Subpart F of 10 CFR 71 requires that a 30 ft free drop be considered. The free drop is to occur onto a flat, essentially unyielding, horizontal surface, and the cask is to strike the surface in an orientation for which maximum damage is expected. Several impact orientations and bounding ambient environments are considered. In order to minimize the number of specific analyses that must be performed, the worst case maximum cold drop impact loads are conservatively applied to the cask using material properties and allowables corresponding to maximum (warm) Normal Conditions of Transport (NCT) temperatures.

#### 2.7.1.1 Impact Forces and Deformations

In Section 2.1.2.2, *Other Structures*, the design criteria of the impact limiters of the BRR Package includes the requirement to limit the free drop impact such that cask component stress and deflection criteria are met. The impact and deformation response of the impact limiters is evaluated and discussed in Appendix 2.12.5, *Impact Limiter Performance Evaluation*. This appendix also includes a comparison of the analysis results to the results obtained from the half-scale certification testing of the impact limiters. The tests are described in Appendix 2.12.2, *Certification Test Plan*, and in Appendix 2.12.3, *Certification Test Results*. The analysis results contributed to informing the choice of physical test orientations. The half-scale test impacts (tests D1, D2R, and D3) were all lower than predicted. The maximum predicted impact in full-scale is 86.8g for the secondary impact in the 15° oblique slapdown orientation. All of the calculations in this section utilize a bounding HAC impact of 120g, which is nearly 40% higher than the maximum result obtained from either test or analysis. Although no NCT tests were performed, the same conservative prediction techniques were used to set the bounding NCT impact at 40g, as described in Appendix 2.12.5, *Impact Limiter Performance Evaluation*.

The second design criterion of the impact limiters is to prevent "hard" contact of a rigid part of the cask with the ground due to excessive deformation of the foam. Since all of the certification testing was performed at the cold condition in order to obtain the maximum impact, the maximum crush deformation, which occurs at the maximum NCT hot temperature, could not be obtained directly from the testing. However, as the crush distances obtained from the half-scale test were found to be below the predicted cold case values, it is conservative not to adjust the predicted hot case crush distances downward. The maximum predicted hot case crush distance occurs in the 15° oblique secondary impact event, and amounts to 15.9 inches, or 83.2% of the available crush distance. Not only is the majority of the foam in the limiter at a lower value of

strain than this maximum value, the value is well within the range in which strain energy absorption is effective. The bounding bulk average foam temperature used for the analysis of 150 °F conservatively bounds the temperature predicted in the thermal analysis.

The final requirement is that the impact limiter structures and attachments to the cask maintain sufficient integrity subsequent to the HAC free drop and puncture drop events so that the containment O-ring seal is protected from excessive temperature in the subsequent HAC fire event. As documented in Appendix 2.12.3, *Certification Test Results*, while the original design did not meet this requirement, the final design of the attachment structures did meet it, as demonstrated by half-scale test. Section 2.7.1.7, *Impact Limiter Attachments*, shows that the final design is stronger than the successfully tested design. In addition, the worst-case damage to the impact limiter shells as a result of the puncture tests is fully accounted for in the thermal model, as discussed in Chapter 3, *Thermal Evaluation*.

For these reasons, the performance of the impact limiters is considered acceptable.

### 2.7.1.2 End Drop

The HAC end orientation free drop is evaluated using a combination of computer and manual calculations using an acceleration of 120g as discussed in Section 2.7.1.1, *Impact Forces and Deformations*. Stresses in the cask body are evaluated using the finite element model described in Appendix 2.12.4, *Stress Analysis Finite Element Models*. Both bottom down and top down impact orientations are considered. Including manual calculations, eight analyses of the HAC end drop are performed:

- Cask body stress
- Closure bolt stress
- Closure lid stress
- Lower closure plate weld stress
- Shield plug shell stress
- Buckling evaluation
- Lead slump evaluation
- Fuel basket stress is discussed in Section 2.7.1.5, *Basket Stress Analysis*.

**Cask body stress.** From Section 2.12.4.4.5, *Case No. 5, HAC Bottom-down End Drop*, the maximum stress intensity resulting from the bottom-down impact of 120g is 45,681 psi, located at the outside surface of the bottom end structure, as shown in Figure 2.12.4-10. The stress is linearized through the lower massive end structure cross section, Figure 2.12.4-11, and the maximum primary membrane stress is 22,680 psi. From Table 2.1-1, the limit on primary membrane stress is the lesser of  $2.4S_m$  and  $0.7S_u$ , which for Type 304 cast or forged material (see Table 2.2-2) is  $0.7S_u = 44,835$  psi at 250 °F. The margin of safety is:

$$MS = \frac{44,835}{22,680} - 1 = +0.98$$

The maximum membrane plus bending stress through the lower massive end structure cross section is 43,080 psi. The allowable membrane plus bending stress, from Table 2.1-1, is the

lesser of  $3.6S_m$  or  $S_u$ , which for Type 304 cast or forged material is  $S_u = 64,050$  psi at 250 °F. The margin of safety is:

$$MS = \frac{64,050}{43,080} - 1 = +0.49$$

From Section 2.12.4.4.8, *Case No. 8, HAC Top-down End Drop*, the maximum stress intensity resulting from the bottom-down impact of 120g is 40,140 psi, located at the top of the inner shell, as shown in Figure 2.12.4-15. The stress is linearized through the inner shell cross section, Figure 2.12.4-16, and the maximum primary membrane stress is 22,720 psi. From Table 2.1-1, the limit on primary membrane stress is the lesser of  $2.4S_m$  and  $0.7S_u$ , which for Type 304 cast or forged material (see Table 2.2-2) is  $0.7S_u = 44,835$  psi at 250 °F. The margin of safety is:

$$MS = \frac{44,835}{22,720} - 1 = +0.97$$

The maximum membrane plus bending stress through the inner shell cross section is 33,400 psi. The allowable membrane plus bending stress, from Table 2.1-1, is the lesser of  $3.6S_m$  or  $S_u$ , which for Type 304 cast or forged material is  $S_u = 64,050$  psi at 250 °F. The margin of safety is:

$$MS = \frac{64,050}{33,400} - 1 = +0.92$$

As shown, all cask body margins of safety for the HAC end free drop condition are positive.

**Closure bolt stress.** In the top-down orientation, the non-prying closure bolt load is calculated according to Section 4.6 of [10] using:

$$F_a = \frac{1.34 \sin(\xi) (DLF)(a_i)(W_l + W_c)}{N_b} = 28,140 \text{ lb}$$

where the impact angle,  $\xi = 90^\circ$  for the end drop impact, the dynamic load factor,  $DLF = 1.05$  as discussed below, the impact magnitude,  $a_i = 120g$  for the HAC impact, the weight of the lid,  $W_l = 280$  lb, and the weight of the contents,  $W_c = 1,720$  lb<sup>1</sup> from Table 2.1-2, and the quantity of bolts,  $N_b = 12$ . Note that no support for the lid is assumed from the inner surface of the impact limiter.

The sum of all applied loads (the HAC free drop load of 28,140 lb plus the load due to the design pressure, equal to 789 lb as determined in Section 2.6.1.5, *Closure Bolts*) is equal to  $28,140 + 789 = 28,929$  lb. This value exceeds the preload of 19,200 lb. The average tensile stress is:

$$S_{ba} = 1.2732 \frac{F_a}{D_{ba}^2} = 47,779 \text{ psi}$$

where the value of  $D_{ba}$  was computed as 0.878 inches in Section 2.6.1.5, *Closure Bolts*. From Table 2.1-1, the allowable average tensile stress intensity for HAC is the lesser of  $0.7S_u$  or  $S_y$ , which for the ASTM A320 L43 bolting material is  $0.7S_u = 87,500$  psi at 250 °F. The margin of safety is:

$$MS = \frac{87,500}{47,779} - 1 = +0.83$$

<sup>1</sup> This weight consists of the shield plug plus the heaviest basket/fuel combination.

The dynamic load factor (DLF) used in this section and in Section 2.6.7.1, *NCT End Free Drop*, is calculated using NUREG/CR-3966 [26] (this quantity is called the DAF in that document). In Section 2.2.3 of [26], an estimated impact pulse duration is developed assuming a constant impact acceleration:

$$t_1 = \frac{Mv_o}{F_{\max}}$$

This equation, however, underestimates the duration of a varying pulse such as a sinusoidal pulse, which is the closest shape to an actual, measured pulse. For a sinusoidal pulse, from Newton's Second Law:

$$F = Ma = MA \sin \omega t$$

The area under the pulse is the total change in velocity. Since the impact velocity is  $v_o$ , and the package comes to a complete stop during impact, the change in velocity is simply  $v_o$ . This can be written:

$$v_o = A \int_0^{\pi/\omega} \sin \omega t dt = -\frac{A}{\omega} \cos \omega t \Big|_0^{\pi/\omega} = \frac{2A}{\omega}$$

From this,

$$\omega = \frac{2A}{v_o}$$

Since the pseudo-frequency of the pulse is a full sine wave (two pulse lengths), the pulse length is equal to:

$$t_1 = \frac{T_1}{2} = \frac{1/f}{2} = \frac{2\pi/\omega}{2} = \frac{\pi}{\omega}$$

Substituting from above,

$$t_{1-HAC} = \frac{\pi v_o}{2A} = \frac{828.6}{A}$$

where  $v_o$  is the impact speed for a 30-foot free drop of 527.5 in/s. Parameter A is the acceleration, in/s<sup>2</sup>. For the bounding impact acceleration of 120g, equivalent to  $A = 46,368$  in/s<sup>2</sup>, the pulse length of the sinusoidal impact time history is  $t_{1-HAC} = 0.018$  s, which compares well with the duration of the end drop impact pulse accelerometer traces shown in Section 2.12.3.7, *Accelerometer Plots*.

For the NCT impact, the impact velocity for the two foot free drop is 136.2 in/s, and the bounding impact is 40g. The corresponding impact pulse length is:

$$t_{1-NCT} = \frac{\pi v_o}{2A} = 0.014 \text{ s}$$

The frequency of the closure lid is found using [25], Table 36, Case 11a. The lowest mode frequency for a flat circular plate, assuming a simply supported edge, is found from:

$$f = \frac{K_n}{2\pi} \sqrt{\frac{Dg}{wr^4}} = 650 \text{ Hz}$$



where  $K_1 = 4.99$ ,  $g = 386.4 \text{ in/s}^2$ , and the lid bolt radius,  $r = 11.38 \text{ inches}$ . Since from Table 2.1-2, the weight of the lid,  $W = 280 \text{ lb}$  and the area,  $A_{\text{lid}} = \pi r^2 = 406.9 \text{ in}^2$ , the weight per unit area,  $w = W/A_{\text{lid}} = 0.688 \text{ psi}$ . Parameter  $D$  is found from:

$$D = \frac{Et^3}{12(1-\nu^2)} = 20.0(10^6) \text{ in-lb}$$

where  $E = 27.3(10^6) \text{ psi}$  for Type 304 steel at  $250^\circ\text{F}$ ,  $\nu = 0.3$ , and the thickness,  $t = 2.0 \text{ inches}$ . The period of the lid is equal to  $1/f$ , or  $T = 1/650 = 0.00154 \text{ s}$ . The amplification factor for a half sine wave is given in Figure 2-15 of [26]. The abscissa of the figure is the ratio  $t_1/T$ . The smallest value of the ratio occurs in the NCT impact, where  $t_{1\text{-NCT}} = 0.014 \text{ s}$ :

$$\frac{t_{1\text{-NCT}}}{T} = 9.09$$

This value exceeds the range shown in the figure. The corresponding ratio for HAC, where  $t_1$  equals  $0.018 \text{ s}$ , is even larger. As the curve is clearly tending toward unity, it is concluded that the DLF may be conservatively bounded by a value of 1.05 for both NCT and HAC.

**Closure lid stress.** In the top-down drop orientation, the closure lid supports both the contents weight and its self-weight against the impact load of  $120g$ . The lid is a solid, 2-inch thick plate made of Type 304 stainless steel. The outer diameter of the lid will be taken as the bolt circle, since that is the location of the step (see Section 2.6.1.5, *Closure Bolts*, for a discussion of the lid step). The bolt circle diameter is 22.75 inches. The self-weight of the lid is  $280 \text{ lb}$ , and the maximum contents weight is  $1,720 \text{ lb}$  (including the shield plug and the maximum basket/fuel weight), from Table 2.1-2. The total weight is  $1,720 + 280 = 2,000 \text{ lb}$ . For an impact of  $120g$ , the total force applied to the lid is  $2,000 \times 120 = 240,000 \text{ lb}$ . From above, the area of the lid,  $A_{\text{lid}} = 406.9 \text{ in}^2$ .

The lid will be considered as uniformly loaded. This is somewhat conservative, since the shield plug is very stiff, and will consequently shift some of the load toward the edges of the lid, lessening the bending stress. In addition, the internal design pressure is  $25 \text{ psig}$ . The uniform load is:

$$q = \frac{240,000}{A_{\text{lid}}} + 25 = 614.8 \text{ psi}$$

From [25], Table 24, Case 10a for a simply supported, uniformly loaded plate, the bending moment is:

$$M = \frac{qa^2(3+\nu)}{16} \text{ DLF} = 17,243 \text{ in-lb/in}$$

where the radius,  $a = 22.75/2 = 11.38 \text{ inches}$ ,  $\nu = 0.3$ , and the dynamic load factor,  $\text{DLF} = 1.05$  as discussed above. The stress is:

$$\sigma = \frac{6M}{t^2} = 25,865 \text{ psi}$$

where the plate thickness,  $t = 2.0 \text{ inches}$ . The allowable membrane plus bending stress, from Table 2.1-1, is the lesser of  $3.6S_m$  or  $S_u$ , which, from Table 2.2-1, is equal to  $68,600 \text{ psi}$  for ASTM A240, Type 304 at  $250^\circ\text{F}$ . The margin of safety is:

$$MS = \frac{68,600}{25,865} - 1 = +1.65$$

Thus, the allowable stress is satisfied for the closure lid in the HAC end drop.

As noted in Section 2.1.2.1, *Containment and Criticality Control Structures*, a stress intensity in the cask closure region (such as the closure lid) which could affect compression of the containment O-ring seal is limited to the lesser of the Table 2.1-1 allowable, or the yield strength. For ASTM A240, Type 304 at 250 °F, the yield strength from Table 2.6-1 is 23,700 psi. The calculated value of stress exceeds the yield stress by approximately 5%. However, as noted above, the calculation is conservative, and the impact magnitude of 120g is very conservative. As found in Table 2.12.5-11, the actual calculated end drop impact is 74.4g, which bounds an even lower actual impact recorded in the certification testing. Therefore it is evident that the actual stress in the closure lid is well below the yield stress of the lid material.

**Lower closure plate weld stress.** In the bottom-down drop orientation, the lower closure plate supports both the lower lead shield hydrostatic pressure and its self-weight against the impact load of 120g. The closure plate is a solid, 1-inch thick plate made of Type 304 stainless steel. The outer diameter of the plate is  $d = 24.5$  inches and connected by a full penetration weld to the adjacent massive end structure. The area of the closure plate is:

$$A_{cp} = \frac{\pi}{4} d^2 = 471.4 \text{ in}^2$$

The self-weight of the closure plate is:

$$W_{cp} = A_{cp} \rho_{ss} = 136.7 \text{ lb}$$

where the density of steel is  $\rho_{ss} = 0.29 \text{ lb/in}^3$ . The weight of the lower lead is modeled as two separate hydrostatic loads based the inner and outer lead depths above the upper surface of the closure plate (see Section 2.12.4.2.2, *Free Drop Impact Loads*). The maximum hydrostatic pressure will be conservatively applied to the entire plate. The hydrostatic force is:

$$F = \rho \cdot h \cdot A_{cp} = 1,488.2 \text{ lb}$$

where the maximum depth of the lead column,  $h = 7.7$  inches and the density of lead is 0.41. The total weight is  $1,488.2 \text{ lb} + 136.7 \text{ lb} = 1,624.9 \text{ lb}$ . For an impact of 120g, the total force applied to the closure plate is  $1,624.9 \times 120 = 194,988 \text{ lb}$ .

Conservatively the closure plate will be considered as uniformly loaded. The uniform load is:

$$q = \frac{194,988}{A_{cp}} = 413.6 \text{ psi}$$

From [25], Table 24, Case 10b for a fixed edge, uniformly loaded plate, the maximum bending moment at the edge of the plate is:

$$M = \frac{qa^2}{8} \text{DLF} = 8,146 \text{ in} - \text{lb} / \text{in}$$

where the radius,  $a = 24.5/2 = 12.25$  inches and the dynamic load factor,  $\text{DLF} = 1.05$  as discussed above. The stress is:

$$\sigma = \frac{6M}{t^2} = 48,876 \text{ psi}$$

where the plate thickness,  $t = 1.0$  inches. The shear stress at the fixed end of the closure plate is:

$$\tau = \frac{194,988}{24.5\pi t} \text{DLF} = 2,660 \text{ psi}$$

The maximum stress intensity is determined by combining the component stresses using Mohr's circle as follows:

$$SI = \sqrt{\sigma^2 + 4\tau^2} = 49,165 \text{ psi}$$

The allowable membrane plus bending stress found above is equal to 68,600 psi for ASTM A240, Type 304 at 250 °F. The margin of safety is:

$$MS = \frac{68,600}{49,165} - 1 = +0.40$$

Thus, the allowable stress is satisfied for the closure plate in the HAC end drop.

**Shield plug shell stress.** In a bottom-down end drop, the shield plug lead will be supported by the lower plate of the shield plug shell. The one-inch thick plate is 15.8 inches in diameter and connected by a complete joint penetration weld to the adjacent cylindrical shell. The weight of the lead in the shield plug, plus the self-weight of the lower steel plate, will be conservatively bounded by utilizing the weight of the full shield plug, from Table 2.1-2, of 950 lb. To simplify the calculation, the lead will be treated very conservatively as a liquid. The entire weight of 950 lb will therefore be applied as a pressure to the plate inner surface.

The area of the plate is:

$$A_p = \frac{\pi}{4} 15.8^2 = 196.1 \text{ in}^2$$

For the end drop impact of 120g, the total loading per unit area of the plate is:

$$q = \frac{950 \times 120}{A_p} = 581.3 \text{ psi}$$

It will be further conservatively assumed that the plate has a simply supported edge. From [25], Table 24, Case 10a, the maximum moment at the center of the plate is:

$$M_c = \frac{qa^2(3+\nu)}{16} \text{DLF} = 7,856.7 \text{ in-lb/in}$$

where the plate radius,  $a = 15.8/2 = 7.9$  inches and the DLF is defined as equal to 1.05 above. The maximum stress is:

$$\sigma_c = \frac{6M_c}{t^2} = 47,140 \text{ psi}$$

where the thickness,  $t = 1$  inch. The allowable membrane plus bending stress found above is equal to 68,600 psi for ASTM A240, Type 304 at 250 °F. The margin of safety is:

$$MS = \frac{68,600}{47,140} - 1 = +0.46$$

The side wall and weld are checked by establishing moment equilibrium between the bottom plate and cylindrical shell, solving for the common moment, and calculating the stress. The direct tension stress is also added.

The slope at the outer edge of the bottom plate is the sum of the slope of a simply supported plate with a pressure load  $q$ , and the slope from a restoring moment,  $M_o$ , applied in the opposite direction by the cylindrical shell. The pressure load causes the plate to deflect downward, and the moment causes it to deflect upward. The slope due to the pressure load,  $\theta_d$  (see [25], Table 24, Case 10a) is:

$$\theta_d = \frac{qa^3}{8D_p(1+\nu)}$$

The slope due to the moment load (see [25], Table 24, Case 13a, for  $r_o = a$ ) is:

$$\theta_m = K_\theta \frac{M_o a}{D_p}$$

The parameter  $D_p$  is:

$$D_p = \frac{Et_p^3}{12(1-\nu^2)} = 2.5(10^6) \text{ in-lb}$$

where  $E = 27.3(10^6)$  psi,  $\nu = 0.3$ , and the plate thickness,  $t_p = 1.0$  inches. The sum of these two slopes is:

$$\theta_d + \theta_m = 0.0098 - 2.338(10^{-6})M_o$$

where the lead hydrostatic pressure,  $q = 581.3$  psi, the radius to the meridian of the cylindrical shell,  $a = 7.6$  inches, and  $K_\theta = -0.76923$ .

The corresponding slope of a cylindrical shell under the action of an end moment is found from [25], Table 29, Case 3, as:

$$\theta_w = \frac{M_o}{D_w \lambda} \frac{C_{12}}{C_{11}}$$

Note that the notation for the slope has substituted  $\theta$  for  $\psi$  for consistency. In addition, the sign value of the slope has been redefined to be opposite to that given in the introduction to Table 29 [25], thus, the negative sign has been omitted from the equation. The parameter  $\lambda$  is:

$$\lambda = \left[ \frac{3(1-\nu^2)}{R^2 t_w^2} \right]^{1/4} = 0.602$$

where  $R = a = 7.6$  inches, and the thickness of the cylindrical wall,  $t_w = 0.6$  inches. The parameter  $D_w$  is:

$$D_w = \frac{Et_w^3}{12(1-\nu^2)} = 5.4(10^5) \text{ in-lb}$$

Since the length of the lower cylindrical shell is  $L = 5$  inches, the parameter  $\lambda L$  is 3.01 inches. Parameters  $C_{12}$  and  $C_{11}$  are essentially identical, so their ratio is unity. The slope of the shell can now be evaluated as:

$$\theta_w = \frac{M_o}{D_w \lambda} \frac{C_{12}}{C_{11}} = 3.076(10^{-6}) M_o$$

Setting  $\theta_w = \theta_d + \theta_m$ ,

$$3.076(10^{-6}) M_o = 0.0098 - 2.338(10^{-6}) M_o$$

Solving,  $M_o = 1,810.1$  in-lb/in. The stress in the cylindrical shell is:

$$\sigma_m = \frac{6M_o}{t_w^2} \text{DLF} = 31,677 \text{ psi}$$

To this stress, the direct tension stress is added. The area of the weld to the cylindrical shell is:

$$A_s = \frac{\pi}{4} (OD^2 - ID^2) = 28.65 \text{ in}^2$$

where the shell outer diameter,  $OD = 15.8$  inches and the inner diameter,  $ID = 14.6$  inches. The direct stress is therefore:

$$\sigma_D = \frac{950 \times 120}{A_s} \text{DLF} = 4,178 \text{ psi}$$

The stress sum in the weld is:

$$\sigma_{\text{Sum}} = \sigma_m + \sigma_D = 35,855 \text{ psi}$$

For a full penetration weld, the allowable stress is the same as determined above. The margin of safety is:

$$MS = \frac{68,600}{35,855} - 1 = +0.91$$

Thus, the allowable stress is satisfied for the shield plug lower plate stress and lower plate weld stress in the HAC end drop.

**Buckling evaluation.** In the end drop orientation, the outer shell will carry most of the axial loads due to its much greater stiffness compared to the inner shell. Therefore, end drop buckling analysis may be conservatively performed by considering only the outer shell. The outer shell, which is cooler than the inner shell, is subject to tensile thermal stress, but for the buckling evaluation, the thermal stress on the outer shell is conservatively neglected. Since the inner shell is neglected, lead shrinkage pressure, which only affects the inner shell, is not considered. The maximum cold HAC impact of 120g is conservatively applied along with the bounding hot temperature case of 250 °F.

The only applied stress is axial, and assumes a bottom-down end drop configuration, for which the weight supported by the outer shell is larger than for the top-down case. The total weight supported by the outer shell is the sum of the total cask body (25,400 lb), less the side lead and bottom lead (see below), the closure lid (280 lb), the shield plug (950 lb), and the upper impact limiter (2,300 lb). Weight values are taken from Table 2.1-2.

The weights for the side and bottom lead are calculated using a lead density of 0.41 lb/in<sup>3</sup>. The side lead has an outer diameter of 34.0 inches (outer shell ID), an inner diameter of 18.0 inches

(inner shell OD), and a lower-bound length (cylindrical length only) of 55.0 inches. The conservatively underestimated weight of the side lead is:

$$W_{\text{pBS}} = \frac{\pi}{4} (34.0^2 - 18.0^2) (55.0) (0.41) = 14,735 \text{ lb}$$

The bottom lead has a large diameter of 23.7 inches and a length of 4.2 inches, and a small diameter of 10.3 inches and a length of 3.5 inches. The weight of the bottom lead is:

$$W_{\text{pBB}} = \frac{\pi}{4} [(23.7^2) (4.2) + (10.3^2) (3.5)] (0.41) = 879 \text{ lb}$$

Conservatively, the bottom lead weight will be underestimated by 100 lb, so that  $W_{\text{pBB}} = 779 \text{ lb}$ . The total weight supported by the outer shell is therefore:

$$W_{\text{tot}} = 25,400 - 14,735 - 779 + 280 + 950 + 2,300 = 13,416 \text{ lb}$$

The weight used is conservative, since it underestimates the removed weight of the side lead and bottom lead, and includes the lower end structure as part of the cask body weight, even though it is not supported by the outer shell. The cross sectional area of the outer shell is:

$$A_{\text{OS}} = \frac{\pi}{4} (38.0^2 - 34.0^2) = 226.2 \text{ in}^2$$

The axial stress is:

$$\sigma_{\phi} = \frac{W_{\text{tot}}}{A_{\text{OS}}} (120) = 7,117 \text{ psi}$$

No other stresses are applied in the end drop. Shell dimensions are taken from Table 2.7-1. The factor of safety is equal to 1.34, consistent with Code Case N-284-2 for HAC. The results are shown in Table 2.7-2. As shown, all interaction parameters, including the maximum value of 0.4024 are less than unity, as required. Therefore, buckling of the cask shells in the HAC free drop will not occur.

**Lead Slump.** In the end drop, impact forces act on the lead gamma shield which could cause a reconfiguration of the lead in the direction of impact. As shown in the evaluation of the cask body stress above, the steel shells which enclose the lead will not significantly deform, but the lead could experience flow strains causing a gap to appear at the upper surface of the lead. In the following analysis, the lead is conservatively treated as a fluid, having no resistance to flow from impact forces. The lead will therefore occupy the lower portion of the volume available within the lead cavity. The difference between the cavity volume and the lead volume defines the maximum possible gap at the top of the lead. Of note, since the shield plug and bottom lead shield are installed manually, using small scraps and lead wool hammered into place to fill all cavities, lead slump cannot occur. The following analysis applies only to the side cavity in which lead is poured in the molten state.

The amount of lead installed in the side cavity of the BRR cask body is assumed to correspond to the volume of the cavity at the point of solidification of the lead of 620 °F. At this point, there is no difference between the volume of the cavity and the volume of the lead. As the cask cools to the minimum HAC temperature of -20 °F, the lead will shrink more than the cavity due to the greater thermal expansion coefficient of lead than steel, generating a volume difference. Assuming the lead behaves as a fluid in the end drop concentrates this volume difference at one

end or the other of the cask cavity, which constitutes the lead slump gap. This gap is further evaluated in Chapter 5, *Shielding Evaluation*.

To simplify calculations, the side lead shield is assumed to have a fully rectangular cross section, i.e., the lead cavity is assumed to have square corners at the full length. This simplification does not have a significant affect on the calculation. The lead cavity at the assumed fabrication temperature of 70 °F has an inner diameter of 18 inches (the inner shell OD), an outer diameter of 34 inches (the outer shell ID), and a length of 60.9 inches. The volume therefore is:

$$V_{\text{CAV-RT}} = \frac{\pi}{4} (34^2 - 18^2) 60.9 = 39,795 \text{ in}^3$$

It will be convenient to define a volumetric expansion relation. Note that, for a general case:

$$V_C = L_C^3$$

$$L_H = L_C (1 + \alpha \Delta T)$$

where  $V_C$  and  $L_C$  are the original (cold state) volume and length, respectively,  $L_H$  is the expanded (hot) length, and  $\alpha$  and  $\Delta T$  are the thermal expansion coefficient and the change in temperature, respectively. Since the expanded (hot) volume is:

$$V_H = L_H^3 = L_C^3 (1 + \alpha \Delta T)^3,$$

Then:

$$V_H = V_C (1 + \alpha \Delta T)^3$$

From Table 2.2-4, the thermal expansion coefficient of steel between 70 °F and 620 °F is  $\alpha_{s620} = 9.84(10^{-6}) \text{ in/in/}^\circ\text{F}$ . The lead cavity and lead volumes at the lead solidification temperature are then:

$$V_{\text{CAV620}} = V_{\text{L620}} = V_{\text{CAV-RT}} (1 + \alpha_{s620} \Delta T_{70-620})^3 = 40,445 \text{ in}^3$$

Next, calculate the volume of the lead at 70 °F and at -20 °F. This must be done in two steps because the thermal expansion coefficients are referenced to 70 °F. The thermal expansion of lead between 620 °F and 70 °F is  $\alpha_{L620} = 20.4(10^{-6}) \text{ in/in/}^\circ\text{F}$ , and between 70 °F and -20 °F is  $\alpha_{L-20} = 15.7(10^{-6}) \text{ in/in/}^\circ\text{F}$ , as shown in Table 2.2-4.

$$V_{\text{L-RT}} = V_{\text{L620}} (1 - \alpha_{L620} \Delta T_{620-70})^3 = 39,099 \text{ in}^3$$

$$V_{\text{L-20}} = V_{\text{L-RT}} (1 - \alpha_{L-20} \Delta T_{70--20})^3 = 38,933 \text{ in}^3$$

The volume of the cavity at -20 °F, utilizing the thermal expansion coefficient between 70 °F and -20 °F of  $\alpha_{s-20} = 8.2(10^{-6}) \text{ in/in/}^\circ\text{F}$ , is:

$$V_{\text{CAV-20}} = V_{\text{CAV-RT}} (1 - \alpha_{s-20} \Delta T_{70--20})^3 = 39,707 \text{ in}^3$$

The difference in volume between the cavity and the lead at the HAC free drop temperature of -20 °F is:

$$\Delta V_{-20} = V_{\text{CAV-20}} - V_{\text{L-20}} = 774 \text{ in}^3$$

The volume of the cavity per inch of length is:

$$\Delta V_{/in} = \frac{\pi}{4}(34^2 - 18^2) = 653 \text{ in}^3 / \text{in}$$

The lead slump dimension (the gap between the top of the lead cavity and the top of the lead) therefore has a bounding value of:

$$x_{\text{slump}} = \frac{\Delta V_{-20}}{\Delta V_{/in}} = 1.185 \text{ in}$$

This value is conservative since it takes no credit for any resistance to flow of the lead material. The effect of this gap is evaluated in Chapter 5, *Shielding Evaluation*.

### 2.7.1.3 Side Drop

The HAC side orientation free drop is evaluated using the finite element model described in Appendix 2.12.4, *Stress Analysis Finite Element Models*, and an acceleration of 120g as discussed in Section 2.7.1.1, *Impact Forces and Deformations*.

From Section 2.12.4.4.11, *Case No. 11, HAC Side Drop*, the maximum stress intensity resulting from the side drop impact of 120g is located at the bottom outside edge of the lower lead cavity as shown in Figure 2.12.4-21. The stress is linearized through the lower closure plate cross section, Figure 2.12.4-22, and the maximum primary membrane stress is 16,330 psi. From Table 2.1-1, the limit on primary membrane stress is the lesser of  $2.4S_m$  and  $0.7S_u$ , which for Type 304 cast or forged material is  $0.7S_u = 44,835$  psi at 250 °F. The margin of safety is:

$$MS = \frac{44,835}{16,330} - 1 = +1.75$$

The maximum membrane plus bending stress resulting through the lower closure plate cross section is 51,990 psi. The allowable membrane plus bending stress, from Table 2.1-1, is the lesser of  $3.6S_m$  or  $S_u$ , which for Type 304 cast or forged material is  $S_u = 64,050$  psi at 250 °F. The margin of safety is:

$$MS = \frac{64,050}{51,990} - 1 = +0.23$$

As shown, all cask body margins of safety for the HAC side drop condition are positive.

### 2.7.1.4 Oblique Drop

For the HAC free drop, the BRR package can strike the ground in any primary orientation. As shown in the following discussion, the cask stresses for all oblique drop orientations are conservatively bounded by the side drop (horizontal) orientation when performed using an impact of 120g. This evaluation is based on the axial, shear, and moment forces in the cask shells as derived in NUREG/CR-3966 [26]. It is shown that, for the specific impact forces developed in the HAC oblique free drops, the cask shell stress intensity is governed by the side drop case.

In Section 2.2 of [26], the maximum axial force,  $R$ , shear force,  $V$ , and bending moment,  $M$ , in the cask shells are given for the primary oblique impact as:

$$R_p = F_p \sin(\theta)$$

$$V_p = F_p \cos(\theta)$$



$$M_p = (4/27) F_p L \cos(\theta)$$

where the subscript p indicates the primary impact event, L is the overall length of the cask,  $\theta$  is the primary impact angle with respect to the horizontal, and  $F_p$  is the maximum primary impact limiter force. For the subsequent secondary (slapdown) impact, the maximum values of the above parameters are:

$$R_s = 0$$

$$V_s = F_s$$

$$M_s = (4/27) F_s L$$

where the subscript s indicates the secondary impact event, and  $F_s$  is the maximum secondary impact limiter force. In the horizontal side drop impact, the maximum values of the above parameters are:

$$R_h = 0$$

$$V_h = F_h$$

$$M_h = (1/4) F_h L$$

where the subscript h indicates the horizontal case, and  $F_h$  is the maximum impact limiter force in the side drop. The cask shell stresses resulting from these applied forces and moments can be calculated as follows:

$$\sigma_a = \frac{R_i}{A}$$

$$\tau = \frac{V_i}{A}$$

$$\sigma_b = \frac{M_i c}{I}$$

where  $\sigma_a$  is the axial stress,  $\tau$  the shear stress, and  $\sigma_b$  the bending stress in the cask shells, and where A is the cross sectional area of the cask shells, and I is the moment of inertia. The maximum stress intensity in the cask shells is determined by combining the component stresses using Mohr's circle as follows:

$$SI = \frac{\sigma_a + \sigma_b}{2} \pm \sqrt{\left(\frac{\sigma_a - \sigma_b}{2}\right)^2 + \tau^2}$$

For purposes of comparison, it is only necessary to consider one shell, for example, the inner shell. The cross sectional area of the inner shell is

$$A = (\pi/4)(d_o^2 - d_i^2) = 53.4 \text{ in}^2$$

and the moment of inertia is

$$I = (\pi/64)(d_o^4 - d_i^4) = 1,936 \text{ in}^4$$

where  $d_o = 18.0$  inches and  $d_i = 16.0$  inches. The parameter  $c = 18.0/2 = 9.0$  inches, and the length between the center of the cylindrical portion of each impact limiter is  $L = 70$  inches.

The maximum force on each impact limiter in the HAC 30 ft, horizontal side drop for the bounding impact value of  $g_h = 120g$  and an overall cask weight of  $W = 32,000$  lb is:

$$F_h = \frac{Wg_h}{2} = 1.920(10^6) \text{ lb}$$

The worst case oblique free drop is the shallow-angle side slapdown orientation at a primary impact angle of 15°, as discussed in Appendix 2.12.5, *Impact Limiter Performance Evaluation*. The primary and secondary impact limiter forces are found using the calculated maximum deformation at cold conditions and the force-deflection curves corresponding to the impact orientation. From Table 2.12.5-11, the maximum primary deformation for the 15° impact case is 10.7 inches, and from Table 2.12.5-12, the maximum secondary deformation is 12.1 inches. From Figure 2.12.5-4 (primary impact at 15°), the maximum crush force at the primary deformation of 10.7 inches is bounded by a value of 1,049,000 lb, and from Figure 2.12.5-3 (secondary impact, taken at 0°), the maximum crush force at the secondary deformation of 12.1 inches is bounded by a value of 1,220,000 lb.

The resulting cask shell forces and maximum combined stress intensities are shown in Table 2.7-3. Since only the inner shell properties are used, the stress intensity is relative, and is used for comparison between the different cases only. The stress values in the table therefore do not represent actual inner shell stress intensity. As shown, the stress intensity is greatest in the horizontal side drop case at the bounding value of 120g. Since, according to Section 2.7.1.1, *Impact Forces and Deformations*, the actual impacts are lower than the calculated values, the difference between the actual loading in the oblique impacts and the bounding side drop is even greater. Therefore, the side drop stress analyses, detailed in Section 2.7.1.3, *Side Drop*, are enveloping for all oblique drop orientations.

### 2.7.1.5 Fuel Basket Stress Analysis

Each of the five fuel baskets and the loose plate box is evaluated for structural integrity in the governing free drop orientations of end and side. The maximum cold impact acceleration of 120g is used, but conservatively the material allowable stresses are evaluated at the maximum NCT temperature of 400 °F. Allowable stresses are taken from Table 2.1-1. Each basket is analyzed for several modes of failure which are applicable to its design, including bending, weld shear, and buckling. Bounding weights for the baskets and fuel are given in Table 2.1-3.

The smallest margin of safety of any of these evaluations is +0.12, for the shear load on the TRIGA basket spacer pedestal screw. All of the evaluations and corresponding margins of safety are summarized in Table 2.7-4. The analysis details are provided in Appendix 2.12.8, *Fuel Basket Stress Analysis*. Therefore, the BRR package fuel baskets are adequate to support the fuel in all HAC free drops.

In the HAC side drop impact orientation, the fuel baskets apply a load to the inside of the inner shell. The heaviest basket is for MURR fuel, but this basket has no ribs and the load is well distributed. The next-heaviest basket, for ATR fuel (650 lb), has four ribs. The top rib is a 0.5-inch thick plate with a 0.19-inch chamfer, for a land width of 0.31 inches. The middle two ribs are made from 0.38-inch thick plate with 0.19-inch chamfers, for a land width of 0.19 inches each. The lowest rib is made from 0.50-inch thick plate with a 0.13-inch step and a 0.19-inch chamfer, for a land width of 0.18 inches. The diameter of each rib is 15.63 inches. The projected bearing area of the ribs against the inner shell is:

$$A = 15.63(0.31 + 0.19 + 0.19 + 0.18) = 13.60 \text{ in}^2$$

The side load, using the bounding side drop impact of 120g, is:

$$P = 650(120) = 78,000 \text{ lb}$$

The bearing stress is:

$$\sigma = \frac{P}{A} = 5,735 \text{ psi}$$

The MITR-II basket, with a loaded weight of 640 lb, is nearly the same weight as the ATR. But, as in the case of the MURR basket, the weight of the basket is well distributed to the interior wall of the cask; primarily over the area of the massive weldment with the minor addition of the pedestal support ring.

The TRIGA and Square fuel baskets are lighter than the other three baskets and not bounding. At the bounding fuel basket temperature of 400 °F, the minimum yield strength of the inner shell material, from Table 2.2-2, is 20,700 psi. Since this stress is over three times larger than the bearing stress, bearing yield of the basket ribs or of the inner shell will not occur.

### 2.7.1.6 Fuel Impact Deformation

During the end drop, the fuel elements may experience a separate, internal impact with the cask or basket structures. This impact could occur if, during the period of package free fall, the fuel was in contact with the upper end of its cavity, which would be possible due to the zero-g environment of free fall. When the package strikes the ground, the velocity of the cask would begin to decrease, but the fuel would continue to fall freely until impact with the lower end occurred. When the gap between the fuel and the cask was traversed, the fuel would hit the cavity end. The fuel would have the full free drop velocity,  $v_o$ , but the cask cavity would be traveling in the same direction with a lower velocity. See Figure 2.7-1.

To simplify calculations, it will be conservatively assumed that, at the moment of impact with the fuel, the cask inner contact surface is motionless and unyielding. Further, it will be assumed that the deceleration of the package during the period of fuel traversing the gap is constant and equal to the maximum bounding deceleration of 120g. The fuel will therefore experience an equivalent free drop. This analysis will determine the magnitude of the free drop impact and determine the effect on the fuel elements.

At the moment of impact with the ground, both the cask and fuel have a velocity of  $v_o$ . The cask immediately begins to decelerate according to:

$$v(t) = at + v_o$$

The distance the cask travels until the moment of impact with the fuel is:

$$x_c = a \int_0^T t dt = \frac{1}{2} at^2 + v_o t \Big|_0^T = \frac{1}{2} aT^2 + v_o T$$

where  $T$  is the time of fuel impact, and  $x_c = 0$  at  $t = 0$  (the time of package impact). Note that during time  $T$ , the fuel has traveled the distance the cask has traveled, plus the initial gap between the fuel and cask. Alternately, it can be stated that the fuel has traveled  $v_o T$ , since its velocity is unchanged during this interval. Therefore:

$$x_c + \text{GAP} = v_o T, \quad \text{or}$$

$$x_c = v_o T - \text{GAP}$$

Substituting this into the formula for  $x_c$  above,

$$x_c = \frac{1}{2} a T^2 + v_o T = v_o T - \text{GAP}$$

Simplifying,

$$T = \left( \frac{-2\text{GAP}}{a} \right)^{1/2}$$

Since the difference in velocity between the fuel and the cask at time  $T$  is equal to the decay in velocity over the interval, equal to  $(aT)$ , the difference can be written as:

$$\Delta v = aT = a \left( \frac{-2\text{GAP}}{a} \right)^{1/2} = (-2a\text{GAP})^{1/2}$$

(Note that since the acceleration is negative (deceleration), the quantity under the square root will be positive.) The energy associated with a change in velocity,  $\Delta v$ , is equivalent to the energy of a free drop height,  $h$ . Since:

$$h = \frac{\Delta v^2}{2g_g}$$

then the equivalent free drop height of the fuel element in the BRR package impact is:

$$h = \bar{g}\text{GAP}$$

where  $g_g$  is the acceleration due to gravity, and the deceleration in  $g$ -units,  $\bar{g} = a/g_g = 120g$ . The energy to be dissipated during the impact of the fuel is equal to  $Wh$ , or:

$$E = W\bar{g}\text{GAP}$$

where  $W$  is the weight of a fuel element. If this energy is absorbed in the fuel structure by volumetric plastic flow, the energy absorbed is related to the volume of flow according to:

$$E = V\sigma_f$$

where  $\sigma_f$  is the flow stress of the material, equal to the average of the yield and ultimate tensile strengths. Solving this for the volume,

$$V = \frac{W\bar{g}\text{GAP}}{\sigma_f}$$

Since the material flow is assumed to occur on the fuel cross section, the deformation length is equal to the volume divided by the cross-sectional area of the fuel element,  $L = V/A_{xc}$ , or:

$$L = \frac{W\bar{g}\text{GAP}}{\sigma_f A_{xc}}$$

This formula will be evaluated for the bounding fuel case. The fuel is made from 6061-T6 aluminum material. From the ASME B&PV Code, Section II, Part D, Table Y-1, the yield strength at a temperature of 400 °F is equal to 13.3 ksi. Since this material does not appear in

Table U, an ultimate tensile strength at temperature is not readily available. Conservatively, the yield strength will be used for the flow strength as defined above. Therefore,  $\sigma_f = 13,300$  psi.

The total gap value, GAP, consists of a) the free space between the fuel element and the basket cavity length, plus b) the difference between the cask cavity and the basket length. Parameter a), denoted as  $L_{FB}$ , is calculated by subtracting the fuel length from the basket cavity length, and is listed in Table 2.7-5. Parameter b) is found by subtracting the basket length (equal to 53.45 inches in all cases) from the cask cavity length of 54.0 inches, and is equal to 0.55 inches. The total fuel gap is therefore:

$$GAP = L_{FB} + 0.55$$

Due primarily to its larger gap and weight, the ATR fuel is the governing case. The maximum deformation length of any fuel element is therefore:

$$L = \left( \frac{W}{A_{xc}} \right) \frac{\bar{g}GAP}{\sigma_f} = 0.096 \text{ inches}$$

The fuel bounding weights, cross-sectional areas, and  $W/A_{xc}$  ratios are presented in Table 2.7-5. The bounding fuel weights are taken from Section 1.2.2, *Contents*. The areas are calculated from CAD drawings of the fuel active region cross section, and do not consider the end structures. The end structures are considered sacrificial since a) they do not contain any fissile material and b) the criticality analysis discussed in Section 6.3.1 does not model the end structures, and determines the most reactive axial position of the active length of the fuel as if the end structures were absent. Since the fuel end structures do not serve a safety function, they are ignored in the axial deformation analysis.

This maximum deformation length, which is just below  $1/10^{\text{th}}$  of an inch, is negligible from a structural, shielding, or criticality perspective. Therefore fuel behavior in the HAC end drop is acceptable.

### 2.7.1.7 Impact Limiter Attachments

As reported in Appendix 2.12.3, *Certification Test Results*, the initial design of the impact limiter attachments was not adequate, since they did not securely retain the primary impact limiter in the  $15^\circ$  oblique slapdown free drop impact. The redesigned attachments are shown in the drawings in Appendix 1.3.3, *Packaging General Arrangement Drawings*. One half-scale certification test limiter was refurbished, as far as possible, to incorporate the revised design and retested to confirm its adequacy. The attachment load path of the refurbished test article, when converted to full-scale, was conservatively less strong than the revised design, as shown by the comparison shown in Table 2.7-6. Note: in the table, the blade is the attachment component integral to the impact limiter, and the receptacle is the pair of plates, attached to the cask, that accept the blade.

As detailed in Section 2.12.3.6, *Confirmatory Test of Attachments*, the  $15^\circ$  oblique slapdown free drop was repeated, followed by a puncture test. The attachments that experienced the greatest loads from the puncture test were the same ones that experienced the greatest loads in the free drop test. The result was that the impact limiter was securely retained on the test cask. The only measurable change to the refurbished attachment hardware was a negligible elongation of one of the blade holes by 0.07 inches (full-scale). Other than that slight deformation, there were no signs of distress or impending failure in any other feature located in the attachment load path. Of note, no other free drop or puncture drop test orientation caused any significant damage to the

original, smaller design of the attachments. Therefore the impact limiter attachments are adequate to securely retain the impact limiter in the worst-case series of free drop and puncture events.

### 2.7.1.8 Fuel Impact Integrity

During the HAC impact, the fuel will experience forces which could affect their structural integrity. The following demonstration shows that all fuel, with the exception of U-Florida, retains its integrity following the governing impacts.

#### *Plate Fuel*

Plate fuels transported in the BRR package consist of MURR, MITR-II, ATR, RINSC, U-Mass, Ohio State, Missouri S&T, and Purdue. U-Florida plate fuel will be discussed separately. These fuel elements are represented in Figure 1.2-9, Figure 1.2-10, Figure 1.2-11, and Figure 1.2-13. As shown, the fuel elements include side plates (or “combs”) which support the fuel plates along their long sides. The side plates extend for the full length of the fuel plates and are incorporated into end structures (at one or both ends), providing a rigid structure. The ATR fuel element was physically tested in the certification test of the ATR-FFSC package (NRC Docket 71-9329) without loss of structural integrity and with damage only to the element’s end structures. The ATR-FFSC is a relatively light, rigid package without impact limiters, and thus the HAC free drop impact magnitude is much higher than that of the BRR package. For this reason, it may be concluded that the plate fuel elements will not lose structural integrity (i.e., remain a structural unit) in the governing HAC free drop. As discussed in [35], the corrosion sometimes found to be present on plate fuel elements after many years in storage is not structurally significant.

While the overall structural integrity of the plate fuels will not be affected by the HAC free drop, it is noted that in a side drop of the BRR package, the fuel plates could be loaded perpendicular to their plane. The stress generated in this scenario is well below the yield strength of the fuel plate cladding material, shown as follows. The discussion focuses on the governing flat plate.

To bound the behavior of all plates, the thickest plate from Table 5.2-10 (0.06 inches) will be loaded with the thickest and most dense meat (0.03 inches from Table 6.2-11 and 5.5 g/cm<sup>3</sup> from Table 6.2-12). The section properties, however, will be taken assuming the thinner plates from Table 5.2-10 (0.05 inches). The meat density is 5.5 g/cm<sup>3</sup> = 0.20 lb/in<sup>3</sup>, and with a thickness of 0.03 inches, the mass of the meat in one square inch of plate is  $m_m = 0.20 \times 0.03 = 0.006 \text{ lb/in}^2$ . The aluminum cladding (for mass purposes) is a total of 0.06 – 0.03 = 0.03 inches, having a mass per square inch of  $m_c = 0.099 \times .03 = 0.003 \text{ lb/in}^2$ , where the density of aluminum is taken as 0.099 lb/in<sup>3</sup>. The total weight per square inch is  $w = 0.009 \text{ lb/in}^2$ . Since the fuel plates are supported along their long sides, their behavior can be modeled using a unit width beam, where the width dimension is parallel to the axis of the fuel element, and the length of the beam is the plate width, upper-bounded by the basket opening dimension of 3.4 inches. The uniform loading on the beam is the value of  $w = 0.009 \text{ lb/in}$ , found above for one square inch of plate. Even though the fuel plates are typically swaged into the side plates, simple support at the comb side plate will be conservatively assumed. The section properties are based on the thinner fuel plates which are 0.05 inches thick, and conservatively neglecting the meat thickness of the thinner plates of 0.02 inches thick. The moment of inertia and the c-distance are:

$$I = \frac{1}{12} (0.05^3 - 0.02^3) = 9.75(10^{-6}) \text{ in}^3, c = \frac{0.05}{2} = 0.025 \text{ in}$$

## BRR Package Safety Analysis Report

For a bounding impact in the horizontal cask orientation of 120g, with a flat, horizontal fuel plate orientation, modeled as a simply supported beam  $L = 3.4$  inches long, the moment and stress in the fuel plate are:

$$M = \frac{w(L^2)}{8} 120 = 1.56 \text{ in} - \text{lb},$$

$$\sigma = \frac{Mc}{I} = 4,000 \text{ psi}$$

From the ASME B&PV Code, Section II, Part D, Table Y-1, the yield strength of 6061 aluminum alloy at a temperature of 400 °F is 13,300 psi. The margin of safety on the permanent deformation of the plate fuel in the side drop is:

$$MS = \frac{13,300}{4,000} - 1 = +2.33$$

Thus, the fuel plates will not deform out-of-plane. Since the plates are restrained all along their length, they will furthermore not buckle from axial impact forces.

Loose plates in the loose plate box are not joined together, but the clearance between the loose plates and the box in a direction normal to the plane of the plates is limited to a maximum of  $\frac{1}{4}$  inches per the procedure in Section 7.1.2.1, *Wet Loading*, and Section 7.1.2.1, *Dry Loading*. Since the loose fuel plates are closely confined in this way, any reconfiguration of the loose plates in the HAC impact event will be prevented. Note also that the axial stress in the aluminum cladding material is very low in the end drop impact. As shown above, the plates weigh no more than  $0.009 \text{ lb/in}^2$ . For bounding loose plate dimensions of 26 inches long and 3 inches wide, the weight of one plate is  $26 \times 3 \times 0.009 = 0.7 \text{ lb}$ , or a maximum of one pound. In a 120g end drop impact, the weight on the lower end of the plate is therefore bounded by 120 lb. As noted above, the non-fueled cladding thickness is  $0.05 - 0.02 = 0.03$  inches. The cross-sectional area, conservatively taking a plate width of only 2.5 inches is thus  $0.03 \times 2.5 = 0.075 \text{ in}^2$ . The stress in the aluminum cladding in the end drop (where the impact load is parallel to the plane of the plates) is:

$$\sigma = \frac{120}{0.075} = 1,600 \text{ psi}$$

Since the same allowable applies from the previous stress analysis, the margin against yield of the loose plates is:

$$MS = \frac{13,300}{1,600} - 1 = +7.31$$

Since the loose plates are confined by the sides and bottom plate of the loose plate box and by the shield plug over the top of the box, the plates cannot come out of the box. Nor can the plates reconfigure within the box as just shown. A depiction of a partial cross section of the cask with the loose plate box and loose plate fuel is shown in Figure 1.2-17.

The U-Florida fuel element is different in that it does not have full length side plates, instead having a small number of discrete side combs. There are also small spacers made of aluminum, welded to the fuel plates near their center. Because the U-Florida fuel element lacks full side plates, both buckling and bending of the plates are possible in the HAC free drop impact. However, the four screws located at the four corners of the fuel element will not be subjected to

critical levels of tension or shear loading. This is because the U-Florida fuel element is confined by the square fuel basket tube and supported by a pedestal spacer on the bottom and the shield plug on the top. Thus, the fuel element will remain an integral unit. In addition, a solid spacer of 0.8-inch thickness will be used alongside the U-Florida element to reduce free space in the basket tube. But because the U-Florida fuel plates may not remain planar or equally spaced over their entire extent, the criticality safety evaluation of the U-Florida fuel assumes a worst-case plate spacing, as discussed in Section 6.4.1.2, *HAC Single Package Configuration*.

#### *TRIGA Fuel*

TRIGA fuel elements are loaded into the tubes of the TRIGA fuel basket, which are 1.76 inches inner diameter. As such, the maximum clearance to the minimum diameter TRIGA fuel element of 1.35 inches is 0.41 inches. Thus, the TRIGA fuel basket prevents buckling or lateral deformation in TRIGA fuel during the HAC free drop impact.

#### *PULSTAR Fuel*

PULSTAR fuel elements consist of an array of 25 fuel rods having a configuration very similar to commercial nuclear fuel, but only approximately 26 inches long. The fuel element is supported along its entire length in the square fuel basket. The rods are held in position at each end by thick aluminum spacer plates, and at three locations along their length, the rods are separated by orthogonally located tabs, attached to the cladding OD. The array is surrounded by a 0.06-inch thick, Zr-2 alloy outer box. All of the rods are in nominal contact with each other and with the outer box by means of the tabs. The tabs support the rods in all directions and thus, the maximum free length of any rod is equal to the maximum axial distance between the tabs, equal to  $L = 6.37$  inches. Both bending and buckling in this span will be checked.

The cladding OD is 0.474 inches and the ID is 0.430 inches. Thus the moment of inertia of the cladding is:

$$I = \frac{\pi}{64} (0.474^4 - 0.430^4) = 8.0(10^{-4}) \text{ in}^4$$

The weight of one rod is 1.45 lb, or  $w = 0.0604$  lb/in, using the active fuel length of 24 inches. A fixed-end, uniformly loaded beam is used to model a governing intermediate length of rod. For a 120g side drop impact, the maximum moment is:

$$M = \frac{w(L^2)}{12} 120 = 24.51 \text{ in} - \text{lb}$$

The bending stress is:

$$\sigma = \frac{Mc}{I} = 7,261 \text{ psi}$$

where  $c = 0.474/2 = 0.237$  inches. From [36], the yield strength of Zr-2 at 400 °F is bounded by a value of 25,000 psi. The margin of safety on yield in bending is:

$$MS = \frac{25,000}{7,261} - 1 = +2.44$$

Consequently the rods will not permanently deform due to lateral bending. The buckling of the fuel rods will be evaluated using [37], equation 18. The modulus of elasticity of the cladding,  $E_c = 12.0(10^6)$  psi from [36],  $I_c = 8.0(10^{-4}) \text{ in}^4$  as found above,  $(W_c + W_f)$  = the total weight of the



fuel rod of 1.45 lb, and the maximum unbraced length of the rods is  $l_c = 6.37$  inches. The critical inertia magnitude,  $\alpha_{cr}$ , is:

$$\alpha_{cr} = \frac{\pi^2}{l_c^2} \frac{E_c I_c}{(W_c + W_f)} = 1,610 \text{ g}$$

Since this value is much greater than 120g, the rods will not buckle. The margin of safety against buckling is:

$$MS = \frac{1,610}{120} - 1 = +12.4$$

Thus the PULSTAR fuel element will remain intact and undeformed in the bounding HAC free drop impact.

As stated in Section 7.1.2.1, *Wet Loading* and Section 7.1.2.2, *Dry Loading*, all fuel elements must be intact and undamaged prior to loading into the BRR package (note that ATR fuel elements may be trimmed per Section 1.2.2.3, *ATR*).

## 2.7.2 Crush

Since the weight of the BRR package exceeds 1,100 lb, the crush test specified in 10 CFR §71.73(c)(2) does not apply.

## 2.7.3 Puncture

The BRR package is evaluated for puncture resistance under HAC as defined in 10 CFR §71.73(c)(3). The puncture event is defined as a free drop from a height of 40 inches onto a vertical, cylindrical mild steel bar, 6 inches in diameter, in an orientation and in a location for which maximum damage is expected. Puncture performance of the BRR package is divided into two categories: puncture on the impact limiters, which was evaluated by half-scale certification test, and puncture of the package body, which is evaluated by analysis.

### 2.7.3.1 Puncture on the Impact Limiters

Appendix 2.12.2, *Certification Test Plan*, discusses the strategy used to evaluate the puncture performance of the impact limiters under the worst-case conditions, including the test objectives and success criteria. Section 2.12.2.4.1, *Test Sequence and Damage Accumulation*, identifies the five puncture tests that were performed on the half-scale certification test unit. The results of these tests is summarized below. Details are to be found in Appendix 2.12.3, *Certification Test Results*. The configuration of each test is shown schematically in Figure 2.12.3-2.

**Test P1.** This test was designed to show that the puncture bar would not penetrate beyond the impact limiter shell located on the flat bottom. This protects the closure lid from direct puncture bar loading, and prevents possible excessive loss of foam for protection in the HAC fire event. This test was performed subsequent to the end free drop test. The bar impacted the shell at an oblique angle through the cask c.g., which would enhance its ability to perforate the plate. The result shown in Figure 2.12.3-12 demonstrates that the impact limiter shell prevents perforation by the bar.

**Test P2.** This test was designed to show that the puncture bar would not create a significant exposure of foam adjacent to the cask (and containment seal) or dislodge the impact limiter from

the end of the cask. Although Figure 2.12.3-2 shows the impact occurring on the same side as the slapdown free drop primary damage, it was found that it would be much more challenging to impact the side opposite to this damage, since that is the azimuth location where the attachments experienced the greatest loading in the free drop. This test was successfully repeated (test P2C) after the redesign of the impact limiter attachments, and subsequent to the repeated 15° oblique slapdown free drop (test D2C). As shown in Figure 2.12.3-40, the impact with the bar did not perforate the shell or expose any foam, and the discussion in Section 2.12.3.6.4, *Examination of Attachments*, documents that the impact limiter was not dislodged by the impact.

**Test P3.** This test was designed to show that the puncture bar would not enter the impact limiter through a side impact on the limiter shell (in this case, the secondary slapdown damage area caused by the 15° oblique slapdown free drop) and rip open a large area that could compromise the performance in the subsequent HAC fire event. As shown in Figure 2.12.3-34, no perforation of the shell occurred.

**Test P4.** This test was designed to show that the puncture bar damage from impact on the c.g.-over-corner free drop damage would be acceptable. The bar impacted the thinner shell material (formerly the conical portion of the limiter shell, before the free drop deformation occurred), adjacent to the thicker bottom plate material. As shown in Figure 2.12.3-29, the exposure of foam from this test was modest, and is bounded by a large margin by the exposure of foam from test P5.

**Test P5.** This test was originally designed to apply an oblique impact on a damaged portion of the shell to determine that the exposure of foam would be acceptable. When it was determined that the limiter shell corner joint between the top flat annular portion and the cylindrical side had developed a crack in the secondary 15° oblique slapdown free drop, this test was used to accumulate the maximum amount of damage in that area. The orientation of the test is shown in Figure 2.12.3-30. The impact with the bar opened up the cracked region and peeled back part of the annular plate, exposing the underlying foam. The final configuration is shown in Figure 2.12.3-31 and Figure 2.12.3-32. Since this test is clearly governing above the other puncture tests regarding the HAC fire event, it is used in modeling the fire event as discussed in Section 3.4, *Thermal Evaluation for Hypothetical Accident Conditions*. It is worth noting that a design change was made subsequent to this test, aimed at preventing this breach of the joint from recurring. The design shown in Appendix 1.3.3, *Packaging General Arrangement Drawings*, includes the stronger joint. The details of the change are discussed in Section 2.12.3.3, *Test Unit Configuration*. However, as just noted, in spite of the design change, the result from the half-scale puncture test P5 was conservatively used for the HAC fire event analysis.

### 2.7.3.2 Puncture on the Cask Body

The puncture resistance of the outer surface of the cask body is evaluated using Nelms' Equation [27], which is used to determine the resistance to puncture of lead-backed stainless steel shells. For the NCT hot case temperature of 250 °F, the ultimate strength of the Type 304 outer shell (assuming the lower strength cast or forged option) is  $S_u = 64,050$  psi from Table 2.2-2. The bounding weight of the BRR package, including impact limiters, is  $W = 32,000$  lb. The required thickness of the outer shell to resist puncture is:

$$t = \left( \frac{W}{S_u} \right)^{0.71} = 0.61 \text{ inches}$$

The thickness of the outer shell is 2 inches. The margin of safety on the cask outer shell thickness is:

$$MS = \frac{2.0}{0.61} - 1 = +2.28$$

Therefore, puncture of the BRR package is not of concern.

## 2.7.4 Thermal

The BRR package is designed to withstand the HAC 30 minute fire specified in 10 CFR §71.73(c)(4). The thermal evaluation is presented in Section 3.4, *Thermal Evaluation under Hypothetical Accident Conditions*.

### 2.7.4.1 Summary of Pressures and Temperatures

As shown in Table 3.1-2, the maximum internal cask pressure as a result of the HAC fire event is 11.7 psig. This is significantly lower than the design pressure of 25 psig stated in Section 2.6.1.1, *Summary of Temperatures and Pressures*. Package component stresses were calculated for an internal pressure of 25 psig in Section 2.6.1.3, *Stress Calculations*, and are compared to allowable stress at the higher HAC temperature in Section 2.7.4.3, *Stress Calculations*.

From Table 3.1-1, as a result of the HAC fire event, the maximum temperature of any part of the cask (except closure bolts) may be bounded by a temperature of 710 °F. The maximum temperature of the closure bolts is considered to be the same as that of the closure lid, bounded by a temperature of 350 °F. Conservatively, all stainless steel components will be assumed to be made from cast or forged Type 304 material, which has a lower ultimate strength than plate material. From Table 2.2-2,  $S_u = 59,140$  psi at 710 °F. The value of  $S_u$  for the closure bolts at 350 °F is equal to 125,000 psi, from Table 2.2-3.

### 2.7.4.2 Differential Thermal Expansion

Differential expansion under NCT is evaluated in Section 2.6.1.2.1, *Baskets*. In that case, the basket was given a uniform bounding temperature of 400 °F, and the thermal expansion of the cask was conservatively neglected. The resulting minimum axial clearance is shown as 0.16 inches, and the minimum diametral clearance is 0.10 inches. In the HAC fire event, from Table 3.1-1, the peak basket temperature is given as 437 °F. Since the basket temperature is locally only 37 °F hotter than the uniform NCT assumption, and in consideration of the significant thermal expansion of the cask cavity dimensions (for example, the inner shell peak temperature is 393 °F), the clearance between the basket and the cask will not be significantly affected by the cask temperatures resulting from the fire event.

Similarly, the fuel axial clearance was evaluated using a uniform bounding temperature of 400 °F in Section 2.6.1.2.2, *Fuel*, and found to have a minimum value of 0.08 inches. Given that the local peak fuel temperature, from Table 3.1-1 is only 451 °F, and that the NCT evaluation again neglected the thermal expansion of the cask components, the clearance between the fuel and the basket will not be significantly affected by the cask temperatures resulting from the fire event.

### 2.7.4.3 Stress Calculations

Cask stress due to the internal design pressure of 25 psig is presented in Section 2.6.1.3.1, *Stresses Due to Pressure Loading*, as equal to 1,002 psi. This corresponds to the stress in the

outer fiber of the closure lid, and is classified as a membrane plus bending stress. This stress clearly bounds the stress generated under an internal pressure in the HAC fire event of 8.8 psig, and the margin of safety may be conservatively calculated using this stress along with the lower fire case allowable stress determined in Section 2.7.4.1, *Summary of Temperatures and Pressures*. The margin of safety is:

$$MS = \frac{59,140}{1,002} - 1 = +58.0$$

The primary load on the closure bolts is governed by the preload force, calculated in Section 2.6.1.5, *Closure Bolts*, as equal to 19,200 lb. The stress is:

$$S_{bs} = 1.2732 \frac{19,200}{D_{ba}^2} = 31,711 \text{ psi}$$

where the stress diameter,  $D_{ba} = 0.878$  inches from Section 2.6.1.5. From Table 2.1-1, the allowable average tensile stress intensity for HAC is the lesser of  $0.7S_u$  or  $S_y$ , which for the ASTM A320 L43 bolting material is  $0.7S_u = 87,500$  psi at 350 °F. The margin of safety is:

$$MS = \frac{87,500}{31,711} - 1 = +1.76$$

Per Regulatory Guide 7.6, paragraph C.7, the extreme range of stress must be considered. Of all the various allowable stresses corresponding to the different conditions evaluated (including fabrication stresses and normal conditions of transport), the largest allowable stress is equal to the material ultimate strength,  $S_u$ . It is therefore conservative to assume that  $S_u$  bounds all stresses actually developed in the structure. For Type 304 stainless steel,  $S_u = 75,000$  psi at 70 °F. The maximum possible stress intensity range is twice this value, or 150,000 psi. Applying a factor of four to account for possible stress concentrations at structural discontinuities gives a total elastic stress range of 600,000 psi. The alternating component is one-half of this value, or 300,000 psi. To account for temperature effects, this value of alternating stress is factored by the ratio of modulus of elasticity. This ratio is formed between the modulus of elasticity at room temperature (at which the test data applies directly) and the modulus of elasticity at the maximum temperature, conservatively bounded by a temperature of 710 °F for any structural part of the package. The adjusted stress is

$$S_{alt} = 300,000 \frac{E_{70^\circ F}}{E_{710^\circ F}} = 343,725 \text{ psi}$$

where  $E_{70^\circ F} = 28.3(10^6)$  psi and  $E_{710^\circ F} = 24.7(10^6)$  psi. Per Figure I-9.2.1 and Table I-9.1 of the ASME Code [9], the allowable value for  $S_{alt}$  at 10 cycles is 708,000 psi. The margin of safety is

$$MS = \frac{708,000}{343,725} - 1 = +1.06$$

Considering the significant conservatism used in the underlying assumptions (e.g., use of allowable stress rather than smaller actual stresses, assuming worst case stresses are fully reversing, use of the maximum factor of stress concentration), it is apparent that the actual margin of safety is larger than 1.06. Thus, the requirement of paragraph C.7 of Regulatory Guide 7.6 is met.

### 2.7.5 Immersion – Fissile

An immersion test for fissile material packages is required by 10 CFR §71.73(c)(5). The criticality evaluation presented in Chapter 6, *Criticality Evaluation*, assumes optimum hydrogenous moderation of the contents, thereby conservatively addressing the effects and consequences of water in-leakage.

### 2.7.6 Immersion – All Packages

An immersion test for all packages is required by 10 CFR §71.73(c)(6), in which a separate, undamaged specimen must be subjected an equivalent pressure of 21.7 psig. Since the BRR package is evaluated to the much greater hydrostatic pressure of the deep immersion test (see the next section), this test does not need to be evaluated.

### 2.7.7 Deep Water Immersion Test (for Type B Packages Containing More than $10^5 A_2$ )

For Type B packages containing an activity of more than  $10^5 A_2$ , 10 CFR §71.61 requires that an undamaged containment system withstand an external pressure of  $p_o = 290$  psig for a period of not less than one hour without collapse, buckling, or inleakage of water. This test will not have a significant effect on the BRR package. Although a temperature is not specified for this test, a lead shrinkage (fabrication) stress corresponding to a temperature of  $-40^\circ\text{F}$ , taken from Section 2.6.2, *Cold*, will be conservatively applied in addition to the specified hydrostatic pressure. The lead shrinkage pressure is  $p_c = 787$  psi. Conservatively, the inner shell is evaluated neglecting the outer shell, even though the external pressure would be applied to the much stronger outer shell.

The internal pressure in the cask is assumed to be ambient, thus the net external pressure across the inner shell on its outer cylindrical surface is equal to a sum of the applied hydrostatic pressure of 290 psig and the lead shrinkage pressure of 787 psi, or a total of:

$$p_{\text{cyl}} = 290 + 787 = 1,077 \text{ psi}$$

The compressive hoop stress is:

$$\sigma_\theta = p_{\text{cyl}} \frac{r_{\text{avg}}}{t} = 9,155 \text{ psi}$$

where the mean inner shell radius,  $r_{\text{avg}} = 8.5$  inches, and the thickness,  $t =$  one inch. The compressive axial stress, obtained by supporting the hydrostatic pressure load,  $p_o$ , from the entire cask end cross section over the inner shell cross section, is:

$$\sigma_\phi = \frac{p_o \pi r_{\text{cask}}^2}{2 \pi r_{\text{avg}} t} = 6,289 \text{ psi}$$

where  $r_{\text{cask}} = 38.4/2 = 19.2$  inches. Using Mohr's circle, the maximum shear stress is:

$$\sigma_{\phi\theta} = \frac{1}{2}(\sigma_\theta - \sigma_\phi) = 1,433 \text{ psi}$$

The possibility of buckling of the inner shell is evaluated using [13]. Consistent with Regulatory Guide 7.6, a factor of safety corresponding to ASME Code, Service Level D is employed. In this case, the applicable factor of safety is 1.34 for hypothetical accident conditions, as specified in [13].

The analysis used a modulus of elasticity of  $28.3(10^6)$  psi, corresponding to 70 °F. Buckling analysis geometry and loading parameters are listed in Table 2.7-7 and results of the analysis in Table 2.7-8. As shown, all interaction parameters, including the maximum value of 0.4286, are less than unity, as required. Thus, the deep water immersion test is not of concern for the BRR package.

### 2.7.8 Summary of Damage

From the analyses presented, it is shown that the HAC sequence does not result in significant damage to the BRR package, and that all stress criteria established for HAC in Section 2.1.2, *Design Criteria*, are satisfied. The margins of safety resulting from the analyses performed in this section are shown in Table 2.7-9.

The BRR cask body and internal components were evaluated primarily by analysis, and the impact limiters and attachments were evaluated by test. The test results confirmed that the impact acceleration of 120g used in the analyses was bounding for all free drop orientations. The tests are summarized below.

The analysis of the cask body and internal components under free drop impact included the cask body structure, the closure lid, the closure bolts, and the shield plug shell. Bounding orientations of end and side drop were evaluated. A demonstration that the side drop governs over the worst-case slapdown is provided in Section 2.7.1.4, *Oblique Drop*. The cask body was analyzed using finite element analysis, in which the cask was loaded by self-weight and contents weight, and supported by the impact limiters. Conservatively, the lead shielding was considered to act as a fluid, having no structural strength. The minimum margin of safety from the finite element analysis, which corresponded to the side drop impact case, was +0.23. All of the manual evaluations resulted in larger margins of safety, as shown in Table 2.7-9. The end drop buckling analysis of the package shells, performed using ASME Code Case N-284-2, resulted in a maximum check value of 0.4024, which is well below the limit of unity, as required by the Code Case. An evaluation of lead slump in the end drop orientation was performed, and resulted in a bounding value of 1.185 inches. This value was used in the shielding evaluation documented in Chapter 5.0, *Shielding Evaluation*. An analysis of the fuel baskets, loose plate box, and spacer pedestals was performed as documented in Appendix 2.12.8, *Fuel Basket Stress Analysis*. Each basket was evaluated for governing modes of failure, with a minimum margin of safety of +0.12. A summary of the margins of safety for the fuel baskets is provided in Table 2.7-4. An analysis of fuel impact integrity is summarized in Table 2.7-4. An analysis of the puncture test on the cask body was performed using Nelms' equation, and resulted in a margin of safety of +2.28. Therefore, since all margins of safety are positive, the criteria of Section 2.1.2, *Design Criteria*, are satisfied for the BRR package.

The impact limiter design was tested using half-scale, prototypic certification test units and a dummy cask body. The impact limiters successfully performed their role in limiting the impact acceleration to a value considerably lower than the value of 120g used for stress analysis. In addition, the test showed that the calculated maximum strain in the energy-absorbing polyurethane foam of 83.2% was conservative. Some exposure of the foam was produced by the worst-case sequence of free drop and puncture tests. The final configuration of the impact limiter shell and of the exposed foam was included in the HAC fire event thermal model as described in Section 3.5.3.7, *Description of Thermal Model for HAC Conditions*. The impact limiter attachments, subsequent to a redesign and retest under the worst-case free drop and

puncture conditions, successfully retained the impact limiters on the cask. Therefore the impact limiters satisfy their design criteria established in Section 2.1.2.2, *Other Structures*.

**Table 2.7-1 – HAC Free Drop Buckling Evaluation: Geometry and Loads**

	Outer shell dimensions, inches	Applied stress, psi	
Inner Dia.	34.0	$\sigma_{\varphi}$	7,117
Outer Dia.	38.0	$\sigma_{\theta}$	0
Length (bounding)	55.0	$\sigma_{\varphi\theta}$	0

Table 2.7-2 – HAC Free Drop: N-284-2 Results

Parameter	Value	Remarks
<b>Capacity Reduction Factors (-1511)</b>		
$\alpha_{\phi L} =$	0.2279	
$\alpha_{\theta L} =$	0.8000	
$\alpha_{\phi\theta L} =$	0.8000	
<b>Plasticity Reduction Factors (-1610)</b>		
$\eta_{\phi} =$	0.0568	
$\eta_{\theta} =$	0.0850	
$\eta_{\phi\theta} =$	0.0232	
<b>Theoretical Buckling Values (-1712.1.1)</b>		
$C_{\phi} =$	0.6050	
$\sigma_{\phi eL} =$	1,831,806 psi	
$C_{\theta r} =$	0.1150	
$\sigma_{\theta eL} = \sigma_{reL} =$	348,340 psi	
$C_{\theta h} =$	0.1078	
$\sigma_{\theta eL} = \sigma_{heL} =$	326,534 psi	
$C_{\phi\theta} =$	0.2527	
$\sigma_{\phi\theta eL} =$	765,157 psi	
<b>Elastic Interaction Equations (-1713.1.1)</b>		
$\sigma_{xa} =$	311,567 psi	
$\sigma_{ha} =$	194,946 psi	
$\sigma_{ra} =$	207,964 psi	
$\sigma_{\tau a} =$	456,810 psi	
Axial + Shear $\Rightarrow$ Check (c):	0.0228	<1 $\therefore$ OK (see note*)
Hoop + Shear $\Rightarrow$ Check (d):	0.0000	<1 $\therefore$ OK
<b>Inelastic Interaction Equations (-1714.2.1)</b>		
$\sigma_{xc} =$	17,687 psi	
$\sigma_{rc} =$	17,687 psi	
$\sigma_{\tau c} =$	10,612 psi	
Max(Axial,Hoop) $\Rightarrow$ Check (a):	0.4024	<1 $\therefore$ OK
Axial + Shear $\Rightarrow$ Check (b):	0.4024	<1 $\therefore$ OK
Hoop + Shear $\Rightarrow$ Check (c):	0.0000	<1 $\therefore$ OK

\*Note: Elastic interaction checks (a), (b), (e), and (f) are not applicable.



**Table 2.7-3 – Cask Shell Force and Stress Comparison**

<b>Case</b>	<b>Impact Limiter Force, lb</b>	<b>Axial Force, R, lb</b>	<b>Shear Force, V, lb</b>	<b>Bending Moment, M, in-lb</b>	<b>Relative Stress Intensity, psi</b>
Side Drop	1.920(10 <sup>6</sup> )	0	1.920(10 <sup>6</sup> )	33.600(10 <sup>6</sup> )	164,077*
15°, Primary	1.049(10 <sup>6</sup> )	271,501	1.013(10 <sup>6</sup> )	10.508(10 <sup>6</sup> )	59,940*
15°, Secondary	1.220(10 <sup>6</sup> )	0	1.220(10 <sup>6</sup> )	12.652(10 <sup>6</sup> )	66,647*

\*Stress for comparison purposes only; not actual inner shell stress.

**Table 2.7-4 – Fuel Basket Stress Analysis Results**

<b>Analysis Description</b>	<b>Reference Section<sup>①</sup></b>	<b>Margin of Safety</b>
<b>MURR Basket</b>		
Fuel Support Plate Bending		+8.32
Outer Shell Slot Welds		+3.00
Buckling of Lower Shell		Pass <sup>②</sup>
<b>MITR-II Basket</b>		
Buckling of Lower Shell		Pass <sup>②</sup>
<b>ATR Basket</b>		
Fuel Support Plate Bending		+10.2
Outer Shell Slot Welds		+1.02
Side Drop Bending		+4.16
<b>TRIGA Basket</b>		
Fuel Support Plate Bending		+0.65
Shear Load on Spacer Screw		+0.12
Buckling of Fuel Tubes		Pass <sup>②</sup>
Side Drop Bending		+1.81
<b>Square Fuel Basket</b>		
Fuel Support Plate Bending		+0.23
Lower Shell Buckling		Pass <sup>②</sup>
Side Drop Bending		+9.82
<b>Loose Plate Box and Pedestals</b>		
Floor Plate Slot Weld		+1.08
Pedestal Tube		+18.3
<b>Fuel Impact Integrity</b>		
Plate Fuel Lateral Bending Deformation		+2.33
PULSTAR Fuel Lateral Bending		+2.44
PULSTAR Fuel Buckling		+12.4

Notes:

1. Calculational details are presented in Appendix 2.12.8, *Fuel Basket Stress Analysis*.
2. Interaction equation checks are less than unity, as required by [13].

**Table 2.7-5 – Fuel Impact Deformation Results**

Fuel Type	W, lb	L <sub>FB</sub> <sup>①</sup>	A <sub>xc</sub> , in <sup>2</sup>	W/A <sub>xc</sub> , lb/in <sup>2</sup>	GAP	L, in
MURR	15	0.63	4.584	3.27	1.18	0.035
MITR-II	10	0.61	3.814	2.62	1.17	0.028
ATR	25	1.13	3.961	6.31	1.68	0.096
TRIGA	10	0.99	1.720 <sup>②</sup>	5.81	1.54	0.081
Square <sup>③</sup>	14	0.50	2.520	5.56	1.05	0.053

Notes:

1. L<sub>FB</sub> is equal to the basket cavity length minus the minimum fuel length. Minimum fuel length is equal to the maximum length stated in Section 1.2.2, *Contents*, less the irradiation growth of 0.25 inches (0.75 inches for ATR).
2. TRIGA fuel has 0.03-inch thick cladding for aluminum clad and 0.02-inch thick cladding for stainless steel clad fuel. Since the entire fuel cross-section is made of a strong material (fuel pellet of UZrH), the area used is that of the entire pellet cross-section of 1.48 inches.
3. Missouri S&T represents bounding Square fuel case.

**Table 2.7-6 – Impact Limiter Attachment Comparisons**

Feature Description	Refurbished Test article (Full-scale Equiv.)	Final Production Design (per Appendix 1.3.3)	Remarks
Blade and receptacle material	ASTM Type 304	ASTM Type 304	Same
Blade thickness, in.	3/4	3/4	Same
Blade width, in.	3.0	3.3	Improved
Hole diameter in blade, in.	1.13	1.13	Same
Hole-to-blade edge, in.	0.94	1.06	Improved
Blade weld to limiter inner shell structure	3/8-in. fillet on both sides	3/8-in. fillet on both sides	Same
Receptacle plate thickness, in.	3/8	1/2	Improved
Ball lock pin diameter, in.	1.0	1.0	Same
Pin material	Carbon steel	Stainless steel	Improved
Pin rated double shear strength, lb	65,600	73,500	Improved
Attachment quantity per limiter	6	8	Improved

**Table 2.7-7 – Deep Immersion Test: Geometry and Loads**

	Inner shell dimensions, inches	Applied stress, psi	
Inner Dia.	16.0	$\sigma_{\varphi}$	6,289
Outer Dia.	18.0	$\sigma_{\theta}$	9,155
Length (bounding)	62.0	$\sigma_{\varphi\theta}$	1,433

Table 2.7-8 – Deep Immersion Test: N-284-2 Results

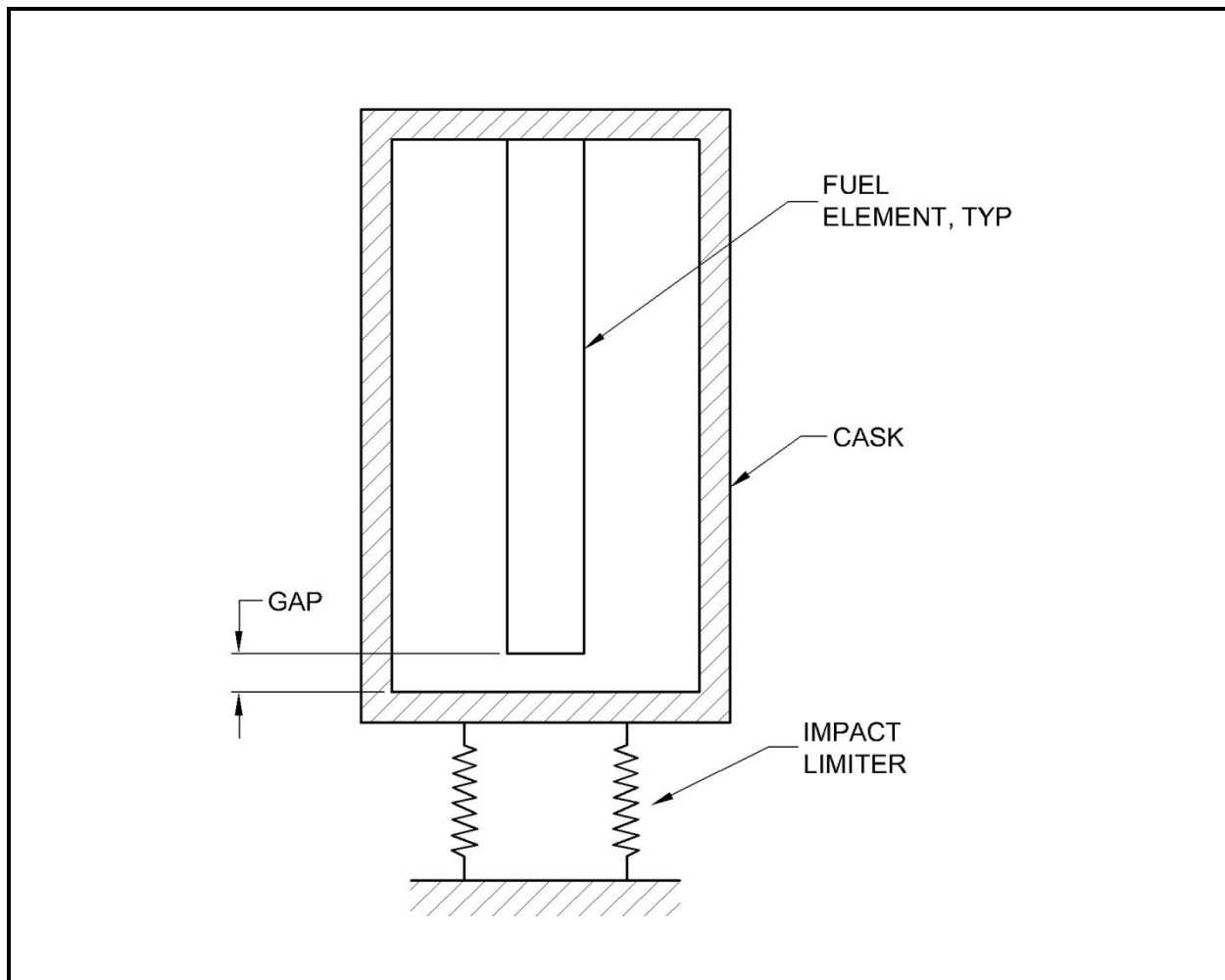
Parameter	Value	Remarks
<b>Capacity Reduction Factors (-1511)</b>		
$\alpha_{\phi L} =$	0.2850	
$\alpha_{\theta L} =$	0.8000	
$\alpha_{\phi\theta L} =$	0.8000	
<b>Plasticity Reduction Factors (-1610)</b>		
$\eta_{\phi} =$	0.0523	
$\eta_{\theta} =$	0.2856	
$\eta_{\phi\theta} =$	0.0417	
<b>Theoretical Buckling Values (-1712.1.1)</b>		
$C_{\phi} =$	0.6050	
$\sigma_{\phi eL} =$	2,014,294 psi	
$C_{\theta r} =$	0.0387	
$\sigma_{\theta eL} = \sigma_{reL} =$	128,711 psi	
$C_{\theta h} =$	0.0387	
$\sigma_{\theta eL} = \sigma_{heL} =$	128,711 psi	
$C_{\phi\theta} =$	0.1619	
$\sigma_{\phi\theta eL} =$	539,157 psi	
<b>Elastic Interaction Equations (-1713.1.1)</b>		
$\sigma_{xa} =$	428,445 psi	
$\sigma_{ha} =$	76,843 psi	
$\sigma_{ra} =$	76,843 psi	
$\sigma_{\tau a} =$	321,885 psi	
Axial + Shear $\Rightarrow$ Check (c):	0.0147	<1 $\therefore$ OK (see note*)
Hoop + Shear $\Rightarrow$ Check (d):	0.1192	<1 $\therefore$ OK
<b>Inelastic Interaction Equations (-1714.2.1)</b>		
$\sigma_{xc} =$	22,388 psi	
$\sigma_{rc} =$	21,943 psi	
$\sigma_{\tau c} =$	13,433 psi	
Max(Axial,Hoop) $\Rightarrow$ Check (a):	0.4172	<1 $\therefore$ OK
Axial + Shear $\Rightarrow$ Check (b):	0.2923	<1 $\therefore$ OK
Hoop + Shear $\Rightarrow$ Check (c):	0.4286	<1 $\therefore$ OK

\*Note: Elastic interaction checks (a), (b), (e), and (f) are not applicable.

**Table 2.7-9 – Minimum Margins of Safety from HAC Evaluations**

Component	Loading Condition	Minimum Margin of Safety
<i>Free Drop</i>		
Cask body (FEA)	End drop, bottom down, membrane stress	+0.98
	End drop, bottom down, membrane + bending	+0.49
	End drop, top down, membrane stress	+0.97
	End drop, top down, membrane + bending stress	+0.92
	Side drop, membrane stress	+1.75
	Side drop, membrane + bending stress	+0.23
Lower closure plate	End drop, bottom down, membrane + bending	+0.40
Closure bolts	End drop, top down	+0.83
Closure lid	End drop, top down	+1.65
Shield plug shell lower plate	End drop, bottom down, assuming simple support, stress at center	+0.46
	End drop, bottom down, assuming fixed edge support, stress at edge (weld)	+0.91
Cask outer shell	End drop, buckling (Code Case N-284-2)	0.4024*
<i>Puncture</i>		
Cask outer shell	Nelms' Equation	+2.28
<i>Thermal</i>		
Containment boundary	Internal pressure, fire conditions	+58.0
Closure bolts	Internal pressure, fire conditions	+1.76
Cask	Range of stress	+1.06

\*Maximum check value must be less than unity.



**Figure 2.7-1 – Cask Cavity and Fuel During Free End Drop**

## **2.8 Accident Conditions for Air Transport of Plutonium**

This section does not apply, since air transport is not used for the BRR package.



## **2.9 Accident Conditions for Fissile Material Packages for Air Transport**

This section does not apply, since air transport is not used for the BRR package.

## **2.10 Special Form**

This section does not apply, since special form is not claimed for the BRR package.

## **2.11 Fuel Rods**

This section does not apply, since fuel rod cladding is not credited with containment in the BRR package.

## **2.12 Appendices**

- 2.12.1 References
- 2.12.2 Certification Test Plan
- 2.12.3 Certification Test Results
- 2.12.4 Stress Analysis Finite Element Models
- 2.12.5 Impact Limiter Performance Evaluation
- 2.12.6 Impact Analysis Software Descriptions
- 2.12.7 Seal Performance Tests
- 2.12.8 Fuel Basket Stress Analysis

## 2.12.1 References

1. Title 10, Code of Federal Regulations, Part 71 (10 CFR 71), *Packaging and Transportation of Radioactive Material*, 01-01-08 Edition.
2. U. S. Nuclear Regulatory Commission, Regulatory Guide 7.6, *Design Criteria for the Structural Analysis of Shipping Cask Containment Vessels*, Revision 1, March 1978.
3. U. S. Nuclear Regulatory Commission, Regulatory Guide 7.8, *Load Combinations for the Structural Analysis of Shipping Casks for Radioactive Material*, Revision 1, March 1989.
4. U. S. Nuclear Regulatory Commission, Regulatory Guide 7.11, *Fracture Toughness Criteria of Base Material for Ferritic Steel Shipping Cask Containment Vessels with a Maximum Wall Thickness of 4 Inches (0.1 m)*, June 1991.
5. R. E. Monroe, H. H. Woo, and R. G. Sears, *Recommended Welding Criteria for Use in the Fabrication of Shipping Containers for Radioactive Materials*, NUREG/CR-3019, UCRL-53044, March 1985.
6. L. E. Fischer, W. Lai, *Fabrication Criteria for Shipping Containers*, NUREG/CR-3854, UCRL-53544, U.S. Nuclear Regulatory Commission, March 1985.
7. American Society of Mechanical Engineers (ASME) Boiler and Pressure Vessel Code, Section III, *Rules for Construction of Nuclear Facility Components*, Division 1 – Subsection NB, *Class 1 Components*, 2007 Edition.
8. American Society of Mechanical Engineers (ASME) Boiler and Pressure Vessel Code, Section III, *Rules for Construction of Nuclear Facility Components*, Division 1 – Subsection NG, *Core Support Structures*, 2007 Edition.
9. American Society of Mechanical Engineers (ASME) Boiler and Pressure Vessel Code, Section III, *Rules for Construction of Nuclear Facility Components*, Division 1 – Subsection NF, *Supports*, 2007 Edition.
10. G.C. Mok, L.E. Fischer, S.T. Hsu, *Stress Analysis of Closure Bolts for Shipping Casks*, NUREG/CR-6007, UCRL-ID-110637, U.S. Nuclear Regulatory Commission, April 1992.
11. W.R. Holman, R. T. Langland, *Recommendations for Protecting Against Failure by Brittle Fracture in Ferritic Steel Shipping Containers Up to Four Inch Thick*, NUREG/CR-1815, UCRL-53013, August 1981.
12. American Society of Mechanical Engineers (ASME) Boiler and Pressure Vessel Code, Section III, *Rules for Construction of Nuclear Facility Components*, Appendix I, *Design Stress Intensity Values, Allowable Stresses, Material Properties, and Design Fatigue Curves*, 2007 Edition.
13. American Society of Mechanical Engineers (ASME) Boiler and Pressure Vessel Code, Section III, *Rules for Construction of Nuclear Power Plant Components*, Division 1, Class MC, Code Case N-284-2, *Metal Containment Shell Buckling Design Methods*, 2007 Edition.
14. American Society of Mechanical Engineers (ASME) Boiler and Pressure Vessel Code, Section IX, *Qualification Standard for Welding and Brazing Procedures, Welders, Brazers, and Welding and Brazing Operators*, 2007 Edition.

15. American Society of Mechanical Engineers (ASME) Boiler and Pressure Vessel Code, Section III, *Rules for Construction of Nuclear Facility Components*, Division 1 – Subsection NE, *Class MC Components*, Article NE-4220, 2007 Edition.
16. American Society of Mechanical Engineers (ASME) Boiler and Pressure Vessel Code, Section III, *Rules for Construction of Nuclear Facility Components*, Division 1 – Subsection NB, *Class 1 Components*, Article NB-2540, 2007 Edition.
17. American Society of Mechanical Engineers (ASME) Boiler and Pressure Vessel Code, Section III, *Rules for Construction of Nuclear Facility Components*, Division 1 – Subsection NB, *Class 1 Components*, Article NB-2570, 2007 Edition.
18. ANSI/AWS D1.6:2007, *Structural Welding Code–Stainless Steel*, American Welding Society (AWS).
19. American Society of Mechanical Engineers (ASME) Boiler and Pressure Vessel Code, Section III, *Rules for Construction of Nuclear Facility Components*, Division 1 – Subsection NB, *Class 1 Components*, and Section V, *Nondestructive Examination*, Article 2, *Radiographic Examination*, 2007 Edition.
20. American Society of Mechanical Engineers (ASME) Boiler and Pressure Vessel Code, Section III, *Rules for Construction of Nuclear Facility Components*, Division 1 – Subsection NB, *Class 1 Components*, and Section V, *Nondestructive Examination*, Article 4, *Ultrasonic Examination Methods for Welds*, 2007 Edition.
21. American Society of Mechanical Engineers (ASME) Boiler and Pressure Vessel Code, Section III, *Rules for Construction of Nuclear Facility Components*, Division 1 – Subsection NB, *Class 1 Components*, and Section V, *Nondestructive Examination*, Article 6, *Liquid Penetrant Examination*, 2007 Edition.
22. American Society of Mechanical Engineers (ASME) Boiler and Pressure Vessel Code, Section III, *Rules for Construction of Nuclear Facility Components*, Division 1 – Subsection NB, *Class 1 Components*, Article NB-6220, 2007 Edition.
23. Boucher, R. C., *Strength of Threads*, Product Engineering, November 27, 1961.
24. ANSI N14.23, *Design Basis for Resistance to Shock and Vibration of Radioactive Material Packages Greater Than One Ton in Truck Transport (DRAFT)*, 1980, American National Standards Institute, Inc, New York.
25. Roark's Formulas for Stress and Strain, Sixth Edition, McGraw-Hill, New York, 1989.
26. T.A. Nelson and R. C. Chun, *Methods for Impact Analysis of Shipping Casks*, NUREG/CR-3966, UCID-20639, U.S. Nuclear Regulatory Commission, November 1987.
27. A. Nelms, *Structural Analysis of Shipping Casks, Effect of Jacket Physical Properties and Curvature on Puncture Resistance*, ORNL-TM-1312, Vol. 3, Oak Ridge National Laboratory, 1968.
28. General Plastics Manufacturing Company, *Design Guide for Use of Last-A-Foam® FR-3700 For Crash & Fire Protection of Radioactive Material Shipping Containers*, Issue 004.
29. NRC Docket No. 71-9295, Mixed Oxide Fresh fuel Package Safety Analysis Report, Revision 7, July 2008.

30. G. D. Sjaardema and G. W. Wellman, *Numerical and Analytical Methods for Approximating the Eccentric Impact Response (Slapdown) of Deformable Bodies*, SAND88-0616 (UC-71), Sandia National Laboratories.
31. **SCANS** (*Shipping Cask ANalysis System*), *A Microcomputer Based Analysis System for Shipping Cask Design Review*, NUREG/CR-4554 (UCID-20674), Lawrence Livermore National Laboratory.
32. American Society of Mechanical Engineers (ASME) Boiler and Pressure Vessel Code, Section III, *Rules for Construction of Nuclear Facility Components*, Division 1 – Subsection NG, *Core Support Structures*, Article NG-3350, 2007 Edition.
33. American Society of Mechanical Engineers (ASME) Boiler and Pressure Vessel Code, Section III, *Rules for Construction of Nuclear Facility Components*, Appendix F, *Rules for Evaluation of Service Loadings with Level D Service Limits*, 2007 Edition.
34. General Plastics Manufacturing Company, *General Plastics Last-A-Foam® FR-3700 For Crash & Fire Protection of Radioactive Material Shipping Containers*, June 1997.
35. Vinson, D., Sindelar, R., and Iyer, N., *Containment Evaluation of Breached AL-SNF For Cask Transport*, Savannah River National Laboratory - Materials Science & Technology, Aiken, SC.
36. Whitmarsh, C. L., *Review of Zircaloy-2 and Zircaloy-4 Properties Relevant to N. S. Savannah Reactor Design*, ORNL-3281, Oak Ridge National Laboratory, Oak Ridge, TN.
37. Bjorkman, Gordon S., *The Buckling of Fuel Rods in Transportation Casks Under Hypothetical Accident Conditions*, 14<sup>th</sup> International Symposium on the Packaging and Transportation of Radioactive Materials (PATRAM 2004), Berlin, Germany, September 20-24, 2004.

## 2.12.2 Certification Test Plan

This appendix describes the certification tests that were performed on the BEA Research Reactor package impact limiters. The justification for choosing the specific tests is presented and discussed. Since this material served for test planning purposes, the future tense is used. The results of the tests is provided in Appendix 2.12.3, *Certification Test Results*.

Because the BRR package includes a conventional, austenitic stainless steel cask shielded by lead and closed by a bolted lid, testing of the cask body is not necessary. The licensing basis for the cask body is by analysis. Physical testing will focus only on the impact limiters and attachments. The licensing basis for the impact limiters will be a combination of half-scale physical test and analysis. Free drop and puncture drop damage of steel-shell, polyurethane foam-filled impact limiters can be adequately modeled using scaled test specimens with appropriate scaling factors.

The test unit configuration will therefore consist of a half-scale dummy cask and half-scale prototypic impact limiters and attachments. Testing will consist of free drops and puncture drops. Test data will consist of measured accelerations and measurements of the damaged configuration.

### 2.12.2.1 Certification Objective

The objective of the certification test program is to demonstrate the adequacy of the BRR package impact limiter design. The impact limiters were designed using computer software to predict the impact (maximum at cold temperature) and the crush deformation (maximum at hot temperature). Refer to Appendix 2.12.5, *Impact Limiter Performance Evaluation*. The certification tests will demonstrate the performance of the limiters in both the hypothetical accident condition (HAC) free drop and puncture drop events. Free drop impact and crush deformation results will be used to benchmark the computer program for use in non-tested orientations or conditions. Puncture drop deformation results will be used to demonstrate impact limiter structural integrity and in the HAC thermal analysis as discussed below.

Several orientations will be tested to ensure that the worst-case series of free and puncture drop events has been considered. The maximum combination of free and puncture drop deformation will be used in the thermal analysis to show that under these worst-case conditions, the elastomer containment O-ring seal temperatures do not exceed safe limits during the HAC fire event.

Since a half-scale test unit will be used, a scaling of the various test parameters is necessary. All of the dimensions of the test unit will be one half of the full-scale design. Dimensional results from the half-scale model (e.g., crush distance) must be multiplied by a factor of two to obtain the full-scale equivalent result. Similarly, the measured accelerations must be divided by two to convert to full-scale. The test unit weight will be 1/8 the weight of the full-scale design, and the rotational moment of inertia will be 1/32 of the full-scale package.

### 2.12.2.2 Initial Test Conditions

#### 2.12.2.2.1 Temperature

To confirm the maximum free drop impact accelerations that have been obtained from computer analysis, the free drops must occur at or near the minimum temperature of -20 °F, due to the increase in crush strength of the energy absorbing materials (polyurethane foam) with decreasing temperature. The maximum crush, which occurs at the maximum NCT temperature, will be



**BRR Package Safety Analysis Report**

obtained by first benchmarking the computer code using the cold case impacts and deformations, and then performing runs with material properties at maximum temperature. Consequently, free drop impacts will occur with the foam material at a bulk average temperature at or near -20 °F. A temperature somewhat below -20 °F is desirable. However, to facilitate testing, a small deviation of as much as 10 °F (to -10 °F) is permissible, since the difference can be accounted for analytically.

Puncture damage depends on the perforation resistance of the shell and the compressive/shearing behavior of the foam subsequent to perforation. Perforation resistance is least at cold temperature, since the underlying foam is stronger and supports a greater shearing action of the edge of the puncture bar. Subsequent to perforation, if that occurs, the 9 lb/ft<sup>3</sup> (pcf) foam used for the BRR package impact limiters will not present a significant resistance to the puncture bar, regardless of strength. Therefore, the cold condition is worst-case when perforation resistance is of primary interest. However, since most puncture drop tests are expected to perforate the thinner shells regardless of temperature, only the puncture drop tests on the thicker shell (the flat, circular shell located at the end of the impact limiter, which is expected to resist perforation) needs to be performed at the cold, -20 °F temperature. As for the free drop, a small deviation up to a bulk foam temperature of -10 °F is acceptable.

**2.12.2.2.2 Test Facilities and Instrumentation**

The certification drop and puncture testing will be conducted using a drop pad having a mass of at least 10 times the weight of the certification test unit (CTU), or at least 40,000 lb. The top of the pad will be covered by an embedded steel plate of adequate thickness such that the drop pad will represent an essentially unyielding surface. The half-scale puncture bar will be a 3-in diameter bar of mild steel, mounted perpendicular to the drop pad, and having an edge radius not exceeding 1/8-inch. The bar will be reinforced by gussets at its base and fastened securely to the pad. The length of the bar will permit the bar to do maximum damage before the package becomes supported by the drop pad, and it will be at least 8 inches long. More than one length of bar may be used. Puncture bars will not be reinforced beyond what is necessary to provide rigidity at the baseplate joint.

CTU temperature will be measured by means of thermocouples embedded in the foam. As a minimum, the region of foam expected to undergo crush deformation will be monitored.

The primary means of recording the results of the certification testing will be physical measurements and observations of the CTU before and after testing. In addition, each free drop impact will be recorded using active accelerometers.

**2.12.2.2.3 Certification Test Unit Configuration**

The certification tests will be performed using a test unit consisting of a dummy cask assembled with prototypic, half-scale impact limiters. The impact limiter attachments, including the welds of the mating attachments to the dummy cask, will be prototypic. The dummy cask will be made of steel and lead, and possess a weight of 1/8 of the weight of the full-scale cask (consistent with half-scale). The dummy cask's impact limiter interface dimensions and features, and its overall length, will be in prototypic half-scale.

The impact limiters will be constructed using the same materials and details as the full-scale limiters, using half-scale dimensions. The polyurethane foam will use the same procurement specification, including crush properties, as the full-scale components. Lifting features will be omitted from the half-

scale components. Prior to testing, the impact limiters will receive a certificate of compliance with all fabrication drawing and specification requirements.

### **2.12.2.3 Identification of Worst-Case Test Orientations**

The objectives of the certification test program are:

1. To confirm maximum free drop impact accelerations obtained from computer calculations.
2. To calibrate or benchmark the computer program, in order to validate calculations for orientations not tested.
3. To demonstrate the general structural integrity of the impact limiter during impact.
4. To demonstrate the effectiveness of the impact limiter attachments in both free drop and puncture drop events.
5. To demonstrate that the puncture bar will not penetrate the circular end plate of the upper impact limiter shell.
6. To quantify the worst-case puncture damage for the HAC fire event thermal analysis.

These objectives will now be discussed under the headings of free drop impact and puncture damage.

#### **2.12.2.3.1 Free Drop Impact Objectives**

The computer analysis documented in Appendix 2.12.5, *Impact Limiter Performance Evaluation*, shows that the governing free drop orientation for impact is the 15° slapdown secondary impact in the cold case, at 87g (full scale). Similarly, the governing crush damage occurs for the primary impact in the 15° slapdown orientation in the hot case, at a strain of 81%. The c.g.-over-corner impact is next closest in damage severity, having a maximum strain of 76% in the hot case. Therefore, the 15° slapdown and c.g.-over-corner orientations should be considered for the certification test. In addition, since the end drop orientation is of critical importance to the analysis of the cask body shells, the closure lid bolts, and lead slump, the end drop orientation should also be considered.

The 15° slapdown test in the cold condition will directly result in the worst-case impact occurring in the 30-foot free drop. The primary impact crush deformation will not be the worst-case, since the worst-case occurs at maximum temperature. However, the impact analysis will be benchmarked for the cold case, and by subsequently adjusting the foam and steel properties for hot temperatures, the maximum crush can be demonstrated using a computer calculation.

The end drop test will directly result in the maximum impact occurring in the 30-foot end drop. This data can be used to ensure that the impact used in the quasi-static finite element analysis for the end drop is adequately bounding.

The c.g.-over-corner free drop will not result in the worst-case deformation that could occur in that orientation, which occurs at hot temperature. However, using the same benchmarking technique as for the slapdown test, the maximum crush deformation for this orientation can be readily calculated. Of note, this test could be performed using hot temperature, but it is more convenient to use the naturally occurring temperature, so long as it is adequately characterized to support the benchmarking procedure.

**BRR Package Safety Analysis Report**

The finite element analysis which is documented in Chapter 2.0, *Structural Evaluation*, will include both the end drop orientation and the side drop orientation. From the data collected in other drop tests, the impact analysis software can adequately predict a bounding impact acceleration for the side drop. Therefore, a side drop orientation does not need to be performed.

The licensing strategy for demonstrating the adequacy of the impact limiter attachments depends upon test. The multiplicity of the free drops considered above (along with puncture drops, see below) ensures that this can be done solely by means of the test results. Furthermore, the general integrity of the impact limiter shells and joints, and the energy absorbing efficiency of the foam at cold temperatures, can also be clearly demonstrated with the proposed tests.

**2.12.2.3.2 Puncture Drop Objectives**

The circular plate on the end of the upper impact limiter is designed to prevent perforation by the puncture bar. This prevents concentrated puncture loads from occurring directly on the closure lid. Perforation of the conical or side cylindrical impact limiter shells is expected, however the possible orientation of the bar with respect to the closure lid would either be too oblique to be damaging to the lid, or would impact the relatively strong end structure. To demonstrate the puncture resistance of the plate, an end puncture should be considered. The angle should be somewhat oblique to enhance perforation. Per Section 10 CFR §71.73(a), the puncture should follow the free drops, and should occur on the surface impacted in the end drop, if determined to be the worst orientation.

As a part of achieving the worst-case damage to bound the fire event thermal analysis, a puncture on the c.g.-over-corner free drop damage should be considered. The bar should be oriented so that the potential penetration depth is not hindered by the resistance of the cask end structure. This would also examine the possibility that significant damage could occur from the cask rolling off of the bar, if the impact limiter becomes impaled on it. The resulting puncture damage measurements can be added to the hot case bounding free drop damage calculation to obtain the worst-case from this sequence of events.

Another possibility is that the puncture bar could penetrate the conical region from a side, or near-side orientation, and rip deeply into the limiter in a direction more or less parallel to the cask end surface, and either cause a chimney to occur, or rip out a large section of the limiter as the cask is rolling off of the bar, if the impact limiter becomes impaled on it. This action might be somewhat limited by the fact that the bar orientation would not be toward the c.g., allowing the package to rotate away from the damage site. This test could be located on the slapdown primary or secondary free drop damage.

The cask drain port, located in the cask lower end structure, is closed using an elastomer O-ring seal that may be damaged in the HAC fire event. Therefore, exposure of the end structure side could allow excessive temperatures in the drain port area. An attack from a puncture bar more or less parallel to the package axis, contacting the edge of the damaged area from the secondary slapdown event, could either cause a local exposure of the top end structure of the cask, or possibly substantially dislodge the upper impact limiter due to partial or complete failure of the attachments.

Significant puncture damage could also occur from an attack on the slapdown damage if the puncture bar is aimed at the massive cask end structure. The angle of the bar to the damaged surface will need to be a compromise between an angle that aims through the package c.g., without being so steep that it just bounces off. This test will also explore the maximum damage at the drain port.

**BRR Package Safety Analysis Report****2.12.2.3.3 NCT Free Drop**

For the BRR package, which weighs just over 30,000 lb, the normal conditions of transport (NCT) free drop height required by 10 CFR §71.71(c)(7) is 2 feet. This represents only 6.7% of the energy of the HAC free drop height of 30 feet. The effect of the NCT free drop on the maximum impact and crush deformation can be found by increasing the free drop height from 30 feet to 32 feet. The governing impact (cold, 15° slapdown, secondary impact) increases by less than 4%, and the governing crush deformations (c.g.-over-corner, hot, and 15° slapdown, secondary, hot) increase by only 2%. These differences may be neglected, particularly considering that the bounding impact used in the finite element analysis is approximately 35% greater than that predicted by Appendix 2.12.5, *Impact Limiter Performance Evaluation*. Therefore, the NCT free drop does not need to be included in the certification test program.

**2.12.2.4 Summary of Certification Tests**

Based on the discussions in Section 2.12.2.3, *Identification of Worst-Case Test Orientations*, the planned certification tests for the BRR package are summarized below and in Table 2.12.2-1. Free drops are depicted in Figure 2.12.2-1 and puncture drops in Figure 2.12.2-2.

**2.12.2.4.1 Test Sequence and Damage Accumulation**

The order of free drops and punctures is given below. The order and sequence of free drop and puncture damage may be altered as long as the test objectives, as outlined above, are satisfied. If stated to be cold, the bulk average temperature of the foam must be per the discussion given in Section 2.12.2.2.1, *Temperature*. Interference of damage is expected to be negligible.

The test sequence envisions three separate prototypic impact limiter test articles. Package No. 1 consists of impact limiter nos. 1 and 2, and Package No. 2 consists of Impact Limiter nos. 2 and 3, each using the same dummy cask. The test series consists of three, 30-foot free drops, and five, 40-inch puncture drops.

Note that since all test articles are identical and include the thicker end plate, each end of the test package qualifies as the package "top", as necessary. No tests need to be performed on the package "bottom".

**Test D1.** Package No. 1, Limiter No. 1 will be tested in the end drop orientation at cold temperature. The purpose of this test is to quantify the maximum end drop impact acceleration, and to prepare a surface for the subsequent puncture on the thicker end plate (test P1).

**Test P1.** Package No. 1, Limiter No. 1 will be dropped on the puncture bar through the package c.g., onto the thicker end plate at cold temperature. The axis of the bar should pass approximately one bar diameter in from the plate edge. The axis of the bar should be oblique in order to enhance its ability to cut into the plate. The purpose of this test is to demonstrate that the thicker end plate does not perforate.

**Test D2.** Package No. 2, Limiter Nos. 2 (primary) and 3 (secondary) will be tested in the 15° slapdown orientation at cold temperature. The purpose of this test is to quantify the maximum impact acceleration (secondary impact) and, using analysis, to quantify the maximum crush strain (secondary impact). An additional purpose is to prepare a surface for subsequent puncture testing.

**BRR Package Safety Analysis Report**

**Test D3.** Package No. 2, Limiter No. 3 will be tested in the c.g.-over-corner orientation. The temperature does not need to be controlled, but it must be well characterized for later analysis. The purpose of this test is to quantify the maximum crush strain in the c.g.-over-corner orientation (analytically using properties at maximum temperature); also to ensure the thicker end plate does not cause unexpected results or failure of the weld joints; and to prepare a surface for the subsequent puncture test (test P4). The impact point should be opposite from the slapdown damage.

**Test P2.** Package No. 2, Limiter No. 2 will be dropped such that the puncture bar strikes the inside edge of the slapdown primary-end damage from test D2. The cask axis will be as vertical as possible, given that the secondary impact limiter must clear the puncture bar. The purpose of this puncture test is to either expose a region next to the cask top end structure which could soak in heat in the HAC fire, or possibly dislodge the limiter by failing some or all attachments. The puncture bar will need to have adequate length; bending of the bar would not be an unexpected outcome of this test.

**Test P3.** Package No. 2, Limiter No. 2 will be dropped onto the puncture bar with an impact point on the primary-end impact damage from test D2. The exact impact point and orientation of the package axis may be chosen by the Test Engineer in light of the damage which occurs in test D2, but the package axis should be nearly horizontal ( $0^{\circ}$  to  $15^{\circ}$  from the horizontal), and the impact point approximately halfway between the cask end surface and the limiter outside end surface. Therefore, the bar axis is not through the package c.g., but could do significant damage before the package has time to rotate.

**Test P4.** Package No. 2, Limiter No. 3 will be dropped on the damage from the c.g.-over-corner free drop, with impact on the thinner conical shell material. The puncture bar edge will align with the joint between the thick end plate and the thinner conical plate, and be aimed to miss significant support from the cask end structure, i.e., with the package axis inclined approximately  $75^{\circ}$  from the horizontal. This will miss the package c.g. by only a few inches, and the energy loss will be insignificant. The purpose of this test is to quantify a possible worst-case configuration for the HAC fire thermal analysis.

**Test P5.** Package No. 2, Limiter No. 3 will be dropped such that the puncture bar strikes the approximate center of the slapdown secondary damage, in order to create the smallest remaining foam thickness adjacent to the cask end structure (location of the drain port). The cask axis should be approximately  $30^{\circ}$  to the horizontal. The bar axis should be aimed directly at the cask end structure, but it will not be directly through the c.g. To aim through the c.g. would mean that impact with the damaged limiter would be too oblique, and the cask would be expected to only bounce off of the bar.

#### **2.12.2.4.2 Measurements**

Measurements of the certification test results will be made in explicit support of the test objectives identified in Section 2.12.2.3, *Identification of Worst-Case Test Orientations*, and will consist of configuration (dimensional) measurements of the damage, and acceleration measurements of the free drops. Temperature measurements will be made on an ongoing basis to fully characterize the bulk average temperature of the foam.

Measurements of the free drop deformation damage will take springback of the limiter into account, and by use of crush gages or other techniques, attempt to obtain the maximum crush at the moment of impact. Puncture measurements should be made from the prevailing damage surface

and record the depth and diameter, or other relevant information, of the puncture test damage. A conventional speed video and still photographic record of each drop and puncture should also be made.

Accelerometers should be redundant, and placed to adequately characterize the primary and secondary slapdown impacts. The data should be filtered to obtain the rigid body impact, using the guidance of a fast Fourier transform (FFT), or equivalent, of the time history data.

#### **2.12.2.5 Acceptance Criteria**

The following are the acceptance criteria for certification testing of the BRR package:

1. The impact limiter shells must retain their general integrity for all impacts and deformations. Ripped welds or other tears or fissures are acceptable as long as they are limited in extent and compatible with the HAC fire thermal analysis. Full puncture perforation of the impact limiter shells in regions of standard thickness is expected.
2. The impact limiter attachments must retain the limiters on the cask. A limited degree of distortion or dislodging of the limiters is acceptable, but must be compatible with the HAC fire thermal analysis.
3. The impact limiters must maintain package deceleration to acceptable levels. The safety analyses will utilize as inputs values which bound the results of the certification test.
4. The thicker end plate must not perforate in the puncture drop test.
5. The maximum damage to the limiter from the single worst-case free drop and puncture test sequence must fall within the bounding assumptions used in the HAC fire thermal analysis.

**BRR Package Safety Analysis Report****Table 2.12.2-1 - Summary of Certification Tests**

<b>No.</b>	<b>Test Description</b>	<b>Test Limiter</b>	<b>Temperature</b>	<b>Purpose of Test &amp; Expected Damage</b>
D1	End drop	#1	Cold (see note 2)	Maximum end impact
D2	Slapdown oblique drop, 15°	#2 & #3	Cold (see note 2)	Maximum slapdown secondary impact, obtain data to permit calculation of maximum strain
D3	C.G. over corner drop	#3	Not controlled	Obtain data to permit calculation of maximum strain
P1	Oblique through c.g. on thicker end plate on test D1 damage	#1	Cold (see note 2)	Demonstrate perforation resistance of thicker end plate
P2	Approx. parallel to package axis, on test D2 primary-end damage	#2	Not controlled	Quantifies possible maximum accumulation of free drop and puncture damage – local severe damage or dislodge limiter
P3	Approx. perpendicular to package axis, on test D2 primary-end damage	#2	Not controlled	Quantifies possible maximum accumulation of free drop and puncture damage – chimney or other severe damage
P4	On test D3 damage, on thick/thin joint, near c.g.	#3	Not controlled	Quantifies possible maximum accumulation of free drop and puncture damage – minimum foam thickness at cask corner
P5	Oblique to package axis, on test D3 secondary-end damage	#3	Not controlled	Quantifies possible maximum accumulation of free drop and puncture damage – minimum foam thickness at cask side

Notes:

1. All free drops (Dx) are from 30 feet, and all punctures (Px) are from 40 inches.
2. See Section 2.12.2.2.1, *Temperature*.

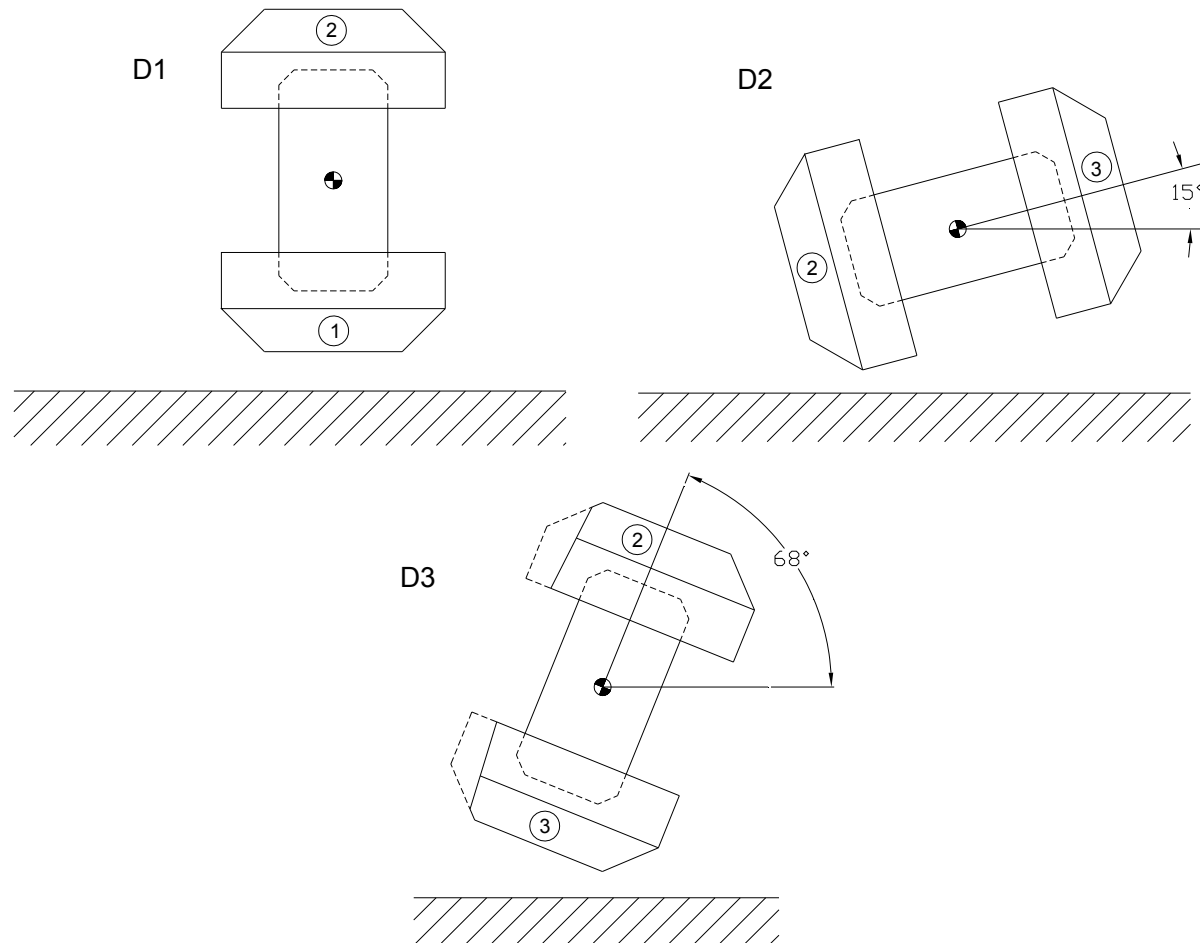


Figure 2.12.2-1 - BRR Package Free Drop Orientations



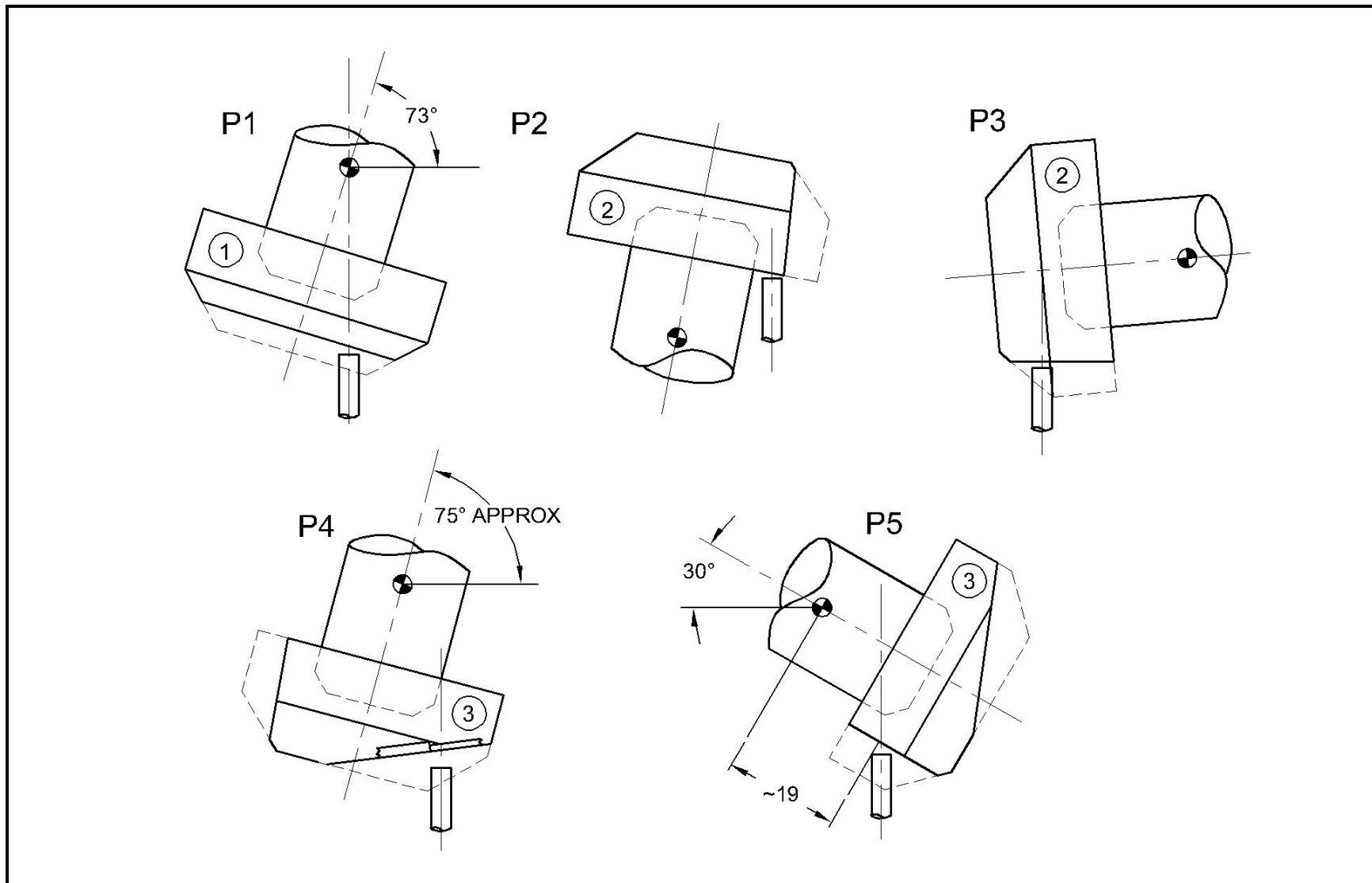


Figure 2.12.2-2 - BRR Package Puncture Drop Orientations

### **2.12.3 Certification Test Results**

This appendix presents results of the certification tests that were performed on the BEA Research Reactor package impact limiters. The information contained in the certification test report is summarized.

#### **2.12.3.1 Introduction**

Demonstration of the compliance of the BRR package design with the requirements of 10 CFR §71.73 is achieved primarily by analysis. Certification testing is used to demonstrate the performance of the polyurethane foam-filled impact limiters. The tests reported in this appendix were performed using prototypic, half-scale test impact limiters and a dummy cask which had prototypically scaled weight. Both the impact limiters and the attachments (including the limiter attachment components and the cask attachment components) were of prototypic materials and construction. The impact limiter test specimens were in full compliance with the drawings in Section 1.3.3, *Packaging General Arrangement Drawings*, except for the scale factor of 1/2, and with the exceptions discussed below in Section 2.12.3.3, *Test Unit Configuration*.

The objectives of these tests were to demonstrate the general structural integrity of the impact limiters and attachments in free drop and puncture events, to confirm the maximum impact magnitudes, and to verify that the maximum damage to the impact limiters was bounded by the assumptions used in the thermal and criticality analyses. Further discussion of the tests, including a justification of the tests chosen, is provided in Appendix 2.12.2, *Certification Test Plan*. A comparison of the test results to the impact limiter calculations is given in Section 2.12.5.3, *Reconciliation with Certification Test Results*.

#### **2.12.3.2 Test Facilities**

Free drop and puncture testing was performed at Hiline Engineering in Richland, Washington. The drop pad had a total weight of approximately 50,000 lb. The embedded steel plate target had a thickness of 2½ inches. The pad therefore constituted an essentially unyielding surface for the test package, which weighed somewhat less than 4,000 lb.

In accordance with the requirements of 10 CFR §71.73(c)(3), the half-scale puncture bars were fabricated from solid, 3-inch diameter mild steel bars. Puncture bars of two lengths were used: 25 inches and 50 inches long, measured from the top of the baseplate. The length of each bar was designed to allow the puncture event to proceed to completion before the test package gained any support from the unyielding surface, but without excessive length. Each puncture bar was welded with gussets perpendicularly to a thick, mild steel plate. The top edge of each puncture bar was finished to a 1/8-inch maximum radius. Each puncture bar assembly was securely welded to the impact surface.

#### **2.12.3.3 Test Unit Configuration**

The certification test articles were essentially prototypic, half-scale models of the BRR package impact limiters. Three test articles were fabricated using drawings which were in compliance with the drawings in Section 1.3.3, *Packaging General Arrangement Drawings*, except for the differences enumerated and justified below.

The dummy cask was a steel cylinder which represented the BRR cask in half-scale. It consisted of a thick-walled carbon steel outer cylinder, having an outer diameter of 19 inches and an inner diameter of 12.3 inches. The inner cavity was occupied by a lead-filled pipe. The cask impact limiter attachments were prototypic and made of Type 304 stainless steel. The cask attachments were welded to stainless steel plates which were embedded in the surface of the dummy cask, thus ensuring that the entire impact limiter attachment load path was fully prototypic. The weights of the dummy cask and impact limiters are given in Table 2.12.3-1.

The following list summarizes the differences between the test articles and the full-scale production impact limiters:

1. The half-scale impact limiters had no lifting features, which consist of threaded lifting bosses located in the end sheet of the upper limiter. This omission had no effect on the test results.
2. The half-scale impact limiters had no paint. This omission had no effect on the test results.
3. The dummy cask, which modeled the cask, shield plug, closure lid, and maximum contents, weighed 3,181 lb. In full-scale, that weight would be eight times larger, or 25,448 lb. This is approximately 7% less than the estimated upper bound weight of the full-scale cask body, less impact limiters, of 27,400 lb. This difference is not significant.
4. Subsequent to testing, the impact limiter corner joint between the top surface and the cylindrical outer shell has been revised. This change came about as a result of the tests documented in Section 2.12.3.5.4, *Repeated Oblique Slapdown Free Drop Test D2R* and Section 2.12.3.5.8, *Puncture Drop Test P5*. In the secondary slapdown impact of free drop D2R, and exacerbated in the subsequent puncture drop P5, the outer shell seam split open, exposing the polyurethane foam. To prevent this seam failure from recurring, the outer shell joint has been redesigned to include two lap joints on the corner angle. The 'from' and 'to' configuration of the outer shell joint is shown in Figure 2.12.3-3. Since the outer joint can no longer be used as a final closure joint of the impact limiter shell during fabrication, a new seam has been introduced near the inner shell, as shown in Figure 2.12.3-4. Since the redesigned corner joint is stronger than the tested design, the change is conservative.
5. Subsequent to testing, the full-scale inner diameter of the impact limiter was reduced from 38.5 inches to 38.25 inches, which reduces the diametral clearance between the impact limiter and the cask OD from 0.5 inches to 0.25 inches. This change has the effect of reducing the attachment loads, since it will more closely couple the impact limiter to the cask. Thus the change is conservative.
6. The impact limiter attachment ball-lock pins used in testing were made of carbon steel. The full-scale production pins will be made of stainless steel. Since the stainless steel pins have a higher rated load than the carbon steel pins, this difference is conservative.
7. Subsequent to testing, the impact limiter attachment to the cask has been increased in size. This change came about as a result of the tests documented in Section 2.12.3.5.3, *Oblique Slapdown Free Drop Test D2* and Section 2.12.3.5.4, *Repeated Oblique Slapdown Free Drop Test D2R*. In the oblique slapdown drops D2 and D2R, a majority of the attachments of the primary impact limiter failed. To prevent this failure from recurring, the attachments have been increased in size and in quantity. The detail of the change, and the result of a confirmatory retest, are documented in Section 2.12.3.6, *Confirmatory Test of Attachments*.

## 2.12.3.4 Instrumentation

### 2.12.3.4.1 Accelerometers

Accelerometers were used to record the impact of each free drop, except drop D2C, which was a confirmatory test for the revised impact limiter attachments. Accelerations of the puncture drops were not recorded. For axial or near-axial drop orientations (D1 – end drop, and D3 – c.g.-over-corner drop), the measurement axis of the accelerometers was axial. For the near-horizontal, 15° slapdown drops (D2 and D2R), the measurement axis was transverse to the cask axis.

Four axial and four transverse mounting positions were provided at each end of the cask. The measurement axes were as close to the cask surface as possible, and the mounting blocks were rigidly welded to the cask. The transverse measurement axis was located 8.68 inches from the flat end of the cask. The mounting location and orientation of each accelerometer is shown in Figure 2.12.3-5 and Figure 2.12.3-6. The transverse accelerometers at each end were all mounted on the same axial plane with their axes parallel.

The raw data was conditioned and low-pass filtered at a level of 1019 Hz. As shown in Section 2.12.3.7, *Accelerometer Plots*, the filtered accelerometer time histories retain a significant vibrational component, indicating that a lower filter cutoff frequency could have been used, which would have lowered the peak values. The rigid body peak accelerations (i.e., without a vibrational component) are estimated by observation of the accelerometer time histories and are shown in Table 2.12.3-6 in Section 2.12.3.7, *Accelerometer Plots*.

The (1019 Hz) filtered peak acceleration values are adjusted using the accelerometer calibration constants listed in Table 2.12.3-5 below. The calibration constants were not entered into the signal conditioner, and therefore are applied manually only to the peak value of the accelerometer output, as shown in Section 2.12.3.5, and not to the entire output. Thus, the filtered accelerometer plots, in Section 2.12.3.7, do not show the effect of this adjustment. Since the calibration constants are all between 0.89 and 0.97 mV/g, the adjusted peak acceleration value is approximately 10% higher than the peak value shown on the plots in Section 2.12.3.7. Individual results are discussed in Section 2.12.3.5.

### 2.12.3.4.2 Thermocouples

A refrigerated trailer was present onsite to chill the certification test articles prior to assembly onto the dummy cask for testing. Thermocouples were inserted in 1/8-inch diameter holes in each test article, five inches deep, and approximately 6.75 inches from the flat annulus side of the test article. Two thermocouples were used for each test article, located 180° apart. Since the minimum temperature which could be set on the chiller unit was -20 °F, the test articles were generally between -10 °F and -20 °F at the time of test. The temperature of the foam in tests D3, P2, P2C, P3, P4, and P5 was not required to be cold. Temperature of the foam was recorded just prior to the test for the impact limiter(s) experiencing impact or puncture.

## 2.12.3.5 Test Results

Results for the initial series of four, 30-ft free drop tests and five puncture drop tests are given in the sections below. (Results for the confirmatory test of the attachments (tests D2C and P2C) are given in Section 2.12.3.6, *Confirmatory Test of Attachments*.) The tests were performed in the order D1, P1, D2, D2R, P2, D3, P4, P5, P3. A description of the tests is given in Table 2.12.3-2. Figures of the tests are shown in Figure 2.12.3-1 and Figure 2.12.3-2. Peak accelerations given

in tables below are taken from column B, 'From Plots, Calibration Adjusted' of Table 2.12.3-6, in Section 2.12.3.7, *Accelerometer Plots*. The average of the peak values is then resolved to a value which is perpendicular to the ground, when necessary. Since the data was collected orthogonal to the cask axes, the resolution of the data in the oblique impact cases is as follows.

For test D1, which was a vertical end drop, the accelerometers were mounted with their measurement axes parallel to the dummy cask axis. Therefore, the accelerometer readings require no adjustment.

For tests D2 and D2R, which were identical, 15° slapdown free drops, the accelerometers were mounted with their measurement axes transverse to the dummy cask axis. For the secondary impact, in which the cask axis is essentially parallel to the ground, the accelerometer readings require no adjustment. For the primary impact at 15°, the average accelerometer reading is divided by the cosine of the recorded impact angle to obtain the impact which occurred perpendicular to the ground.

For test D3, which was the c.g.-over-corner free drop, the accelerometers were mounted with their measurement axes parallel to the dummy cask axis. The average accelerometer reading is divided by the cosine of 23°, which corresponds to the recorded angle between the cask axis in the c.g.-over-corner drop and the ground, to obtain the impact perpendicular to the ground.

All puncture drop tests were performed from a height of 40 inches above the top of the puncture bar. All puncture tests except P2 and P2C were performed using a 25-inch long puncture bar. Tests P2 and P2C utilized the 50-inch long bar. The puncture bars remained securely attached to the steel drop pad in all cases.

For each test, the recorded temperature of the polyurethane foam was taken as described in Section 2.12.3.4.2, *Thermocouples*. Note that all data reported in this appendix applies to the half-scale test unless stated otherwise. According to the laws of scaling, the full-scale linear measurements are twice those recorded here, and the full-scale accelerations are half of those recorded here. The tests are documented in the order in which they were performed.

#### 2.12.3.5.1 Free Drop, Vertical (D1)

Test D1 was performed using a drop height of 30 feet, oriented with the cask axis vertical, as shown in Figure 2.12.3-1 and Figure 2.12.3-7. The lower impact limiter was serial number 1. The two polyurethane foam temperature readings were -16.4 °F and -15.6 °F. Four accelerometers were used. Results are shown in the table below.

Free Drop Test D1 (End)					
Channel	12	13	14	15	Avg.
Peak Value	110g	121g	113g	118g	116g

The impact deformation was a combination of outside-in and inside-out. The outside-in crush depth is calculated from the diameter of the scuff mark (contact area) on the bottom of the limiter. Two orthogonal diameter measurements showed a scuff diameter of 27-1/2 and 27-5/8 inches, or an average of 27.6 inches. Since the original diameter of the bottom of the impact limiter was 24.0 inches, and the tapered portion had an angle of 45°, the outside-in crush distance is:

$$(D_{\text{suff}} - D_{\text{orig}}) / 2 = 1.8 \text{ inches}$$

The inside-out crush distance is calculated from the dimension from the top of the dummy cask (with the upper impact limiter removed) to the outside rim of the lower impact limiter. Since the outside rim of the limiter is undeformed, this measurement will reveal how far the dummy cask has "sunk" into the lower impact limiter. Measurements of this distance, taken in four quadrants, were 29-7/8, 29-7/8, 30-1/2, and 30-7/16 inches. The average value is 30.2 inches. In an undeformed limiter, the top surface of the cask would stand  $(38.6 - 6.8) = 31.8$  inches above the outer rim of the lower limiter, given that the cask is 38.6 inches long, and the center pocket of the limiter is 6.8 inches deep. The inside-out crush is therefore  $(31.8 - 30.2) = 1.6$  inches. The sum of the outside-in and inside-out crush distances is therefore  $1.8 + 1.6 = 3.4$  inches.

The impact limiter was securely attached following the test. Of the six impact limiter attachment pins, one failed by bending and shear, and others showed signs of bending without failure. At least two had no noticeable damage. The shells of the limiter deformed without any tearing or exposure of foam. The post-test configuration is depicted in Figure 2.12.3-8 and Figure 2.12.3-9.

#### **2.12.3.5.2 Puncture Drop Test P1**

Puncture test P1 was performed immediately after drop test D1. The test was a c.g.-over-corner impact on the thicker bottom plate of the impact limiter, near the outer edge of the thicker plate, as shown in Figure 2.12.3-2 and Figure 2.12.3-10. The impact took place on the crush damage from free drop test D1, on serial number 1. The angle of the cask axis was  $73^\circ \pm 3^\circ$  to the horizontal. The two polyurethane foam temperature readings were  $-3.8^\circ\text{F}$  and  $-5.0^\circ\text{F}$ .

The bar impact was located approximately one inch from the outer edge of the thicker bottom plate (i.e., the center of the 3-inch bar was approximately 2-1/2 inches in from the edge). The impact created a dent approximately 1-3/4 inches deep. One or two rebound impacts having negligible deformation also occurred. There were no signs of cracking in the dent or in the nearby weld seam. The post-test configuration is depicted in Figure 2.12.3-11 and Figure 2.12.3-12.

#### **2.12.3.5.3 Oblique Slapdown Free Drop Test D2**

Test D2 was performed using a drop height of 30 feet, oriented with the cask axis at  $16^\circ$  to the horizontal, as shown in Figure 2.12.3-1 and Figure 2.12.3-13. The primary (lower) impact limiter was serial number 2, and the secondary (upper) impact limiter was serial number 3. The polyurethane foam temperature reading in the primary limiter was  $-15.6^\circ\text{F}$  (only one thermocouple was functioning), and in the secondary limiter, the readings were  $-13.8^\circ\text{F}$  and  $-16.4^\circ\text{F}$ . Four accelerometers were used at each end. Results are shown in the table below.

The general post-test configuration is shown in Figure 2.12.3-14. Comparing the measurements of the undeformed and deformed impact limiters, as shown in Figure 2.12.3-15, the crush distance, perpendicular to the ground, was 3.9 inches for the primary impact limiter and 4.0 inches for the secondary impact limiter.

Free Drop Test D2 (15° Oblique)					
Channel	16	17	18	19	Avg., Primary End
Peak Value, g	Severed wire	133g	137g	135g	140g $\perp$ to ground*
Channel	12	13	14	15	Avg., Secondary End
Peak Value, g	102g	108g	110g	108g	107g

\*Equal to  $(133 + 137 + 135)/3/\cos(16^\circ)$ .

In the test, all of the attachment pins on the primary impact limiter sheared off. The limiter remained attached to the cask, although after coming to rest, it was displaced approximately 1-1/2 inches at the top, as shown in Figure 2.12.3-16. None of the pins failed on the secondary impact limiter. There was some incipient cracking of the weld seam on the secondary limiter, but the cracks were of insignificant size and no foam was exposed. The impact surfaces of the impact limiters are shown in Figure 2.12.3-17.

#### 2.12.3.5.4 Repeated Oblique Slapdown Free Drop Test D2R

Test D2R was designed as a repeat of test D2, made after increasing the size of the attachment pins from the original diameter of 1/4 inches to 1/2 inches. To accommodate this increase, the hole through the cask attachment lugs was increased to 1/2 inches and the hole in the impact limiter blade was increased to 5/8 inches. The effect of increasing the blade hole size was to reduce the ligament width on both sides of the hole, but especially on the inner side (toward the cask body). These changes were made to all three impact limiter test articles. Due to the small size of these ligaments, the inner ligament width on serial numbers 1 and 3 were enhanced after drilling by application of a Type 308 weld overlay. Serial number 2 ligaments were not enhanced after drilling. The average ligament widths of the three impact limiters are as follows:

- S/N 001: 0.306 inches (weld overlay enhanced)
- S/N 002: 0.243 inches (not welded)
- S/N 003: 0.320 inches (weld overlay enhanced)

The attachment pins were Carr-Lane part no. CL-8-BLPT-2.00, 1/2-inch diameter carbon steel ball lock pins, having a rated load of 16,000 lb, or four times that of the 1/4-inch pins.

Test D2R was performed using a drop height of 30 feet, oriented with the cask axis at 17° to the horizontal, as shown in Figure 2.12.3-1 and Figure 2.12.3-18. The primary (lower) impact limiter was serial number 2, rotated 180° from its orientation in test D2. The secondary (upper) impact limiter was serial number 1. The polyurethane foam temperature readings in the primary limiter were -13.4 °F and -12.8 °F, and in the secondary limiter, the readings were -13.0 °F and -13.4 °F. Four accelerometers were used at each end. Results are shown in the table below.

Free Drop Test D2R (15° Oblique)					
Channel	16	17	18	19	Avg., Primary End
Peak Value, g	111g	116g	106g	106g	115g $\perp$ to ground*
Channel	12	13	14	15	Avg., Secondary End
Peak Value, g	113g	111g	106g	124g	114g

\*Equal to  $(111 + 116 + 106 + 106)/4/\cos(17^\circ)$ .

**BRR Package Safety Analysis Report**

The general post-test configuration is shown in Figure 2.12.3-19. Comparing the measurements of the undeformed and deformed impact limiters, as shown in Figure 2.12.3-20, the crush distance, perpendicular to the ground, was 4.0 inches for the primary impact limiter and 3.9 inches for the secondary impact limiter. Note that the measurements of the crush in test D2 are very similar to these (3.9 inches primary and 4.0 inches secondary). This is to be expected since the tests are essentially identical. However, since test D2 showed the apparent anomaly of the primary impact being significantly higher than the secondary impact (the opposite would be expected), then test D2R will be taken as the official crush results for this orientation.

In the test, none of the attachment pins failed, but four out of six of the blades of the primary limiter failed by tensile failure of the inner ligaments, as shown in Figure 2.12.3-21. The limiter remained attached to the cask, although after coming to rest, it was displaced approximately 2 inches at the top, as shown in Figure 2.12.3-19. None of the pins or ligaments failed on the secondary impact limiter, although the holes were elongated up to 0.854 inches.

In addition, the corner joint between the top annular plate and the outer cylindrical shell of the secondary impact limiter (serial number 1) failed in the impact region, as shown in Figure 2.12.3-22. This limiter had been tested in the 30-foot end drop (D1) and the subsequent puncture (P1), and the torn joint may have been the result of over-testing. The tear had a maximum opening of 1/2 inches. It appeared to start at the outer edges of the impact zone and travel inward. The length of the torn joint on one side was 7-1/2 inches, and on the other side 10-1/4 inches, with approximately 4-3/4 inches of sound material in the center. The tear appeared in both the weld as well as in the leg of the corner angle located on the top surface. However, the tear did not occur in the outer cylindrical shell side of the joint, where the thickness is double by virtue of the lap joint used in that position.

**2.12.3.5.5 Puncture Drop Test P2**

Puncture test P2 was performed immediately after drop test D2R. The longer puncture bar was used to impact the top annular surface of the damaged primary impact limiter (serial number 2), as shown in Figure 2.12.3-2 and Figure 2.12.3-23. The orientation could not be over the center of gravity due to the desired impact location. The impact occurred just to the inside of the bulge, in approximately the radial center of the annular plate. The two polyurethane foam temperature readings were -0.2 °F and -3.0 °F.

The impact dent on the annular plate was negligible, but the impact limiter became significantly dislodged from the cask end due to the failure of the impact limiter attachment blades, as shown in Figure 2.12.3-24. By inspection of the conventional-speed video record, the impact limiter was displaced by a greater amount than is shown in the figure, before it was driven partially back on by a secondary impact with the safety wall.

**2.12.3.5.6 CG-Over-Corner Free Drop Test D3**

Test D3 was performed from a drop height of 30 feet, with the cask axis oriented at 67° to the horizontal, or essentially center of gravity over corner, as shown in Figure 2.12.3-1 and Figure 2.12.3-25. The lower impact limiter was serial number 3, rotated 180° from its orientation in test D2. The polyurethane foam temperature reading in the lower limiter was -2.2 °F (the other thermocouple was not functioning). Four accelerometers were used at each end, oriented parallel to the cask axis. Results are shown in the table below. Note, since channels 16 – 17 exhibited excess noise, only channels 12 – 15 are used.



Free Drop Test D3 (CG Over Corner)					
Channel	12	13	14	15	Avg.
Peak Value, g	106g	111g	110g	103g	117g $\pm$ to ground*

\*Equal to  $(106 + 111 + 110 + 103)/4/\cos(23^\circ)$ .

The general post-test configuration is shown in Figure 2.12.3-26. Comparing the measurements of the undeformed and deformed impact limiters, as shown in Figure 2.12.3-27, the crush distance perpendicular to the ground was 5.5 inches.

None of the pins or ligaments failed the test, although the holes were elongated up to 0.725 inches. There were no shell failures and no exposure of foam.

#### 2.12.3.5.7 Puncture Drop Test P4

Puncture test P4 was performed on the damage incurred in free drop test D3, on serial number 3. The bar impacted just outside the thicker bottom plate, on the 0.12-inch thick material which once constituted the tapered region of the shell. The orientation is shown in Figure 2.12.3-2 and Figure 2.12.3-28. The cask axis was oriented at  $74^\circ$  to the horizontal. The line of action was nearly, but not completely, c.g.-over-corner. The polyurethane foam temperature readings in the lower limiter were  $17.6^\circ\text{F}$  and  $5.0^\circ\text{F}$ .

As expected, the puncture bar penetrated the shell, and entered the foam to a depth of 2-1/4 inches. The width of the hole was 4 inches, and the length of the hole/torn flap was 5 inches. The impact limiter attachments were not affected. A close-up view of the damage is shown in Figure 2.12.3-29.

#### 2.12.3.5.8 Puncture Drop Test P5

Puncture test P5 was performed on the damaged corner joint created in free drop test D2R on serial number 1 (the secondary impact end). The orientation is shown in Figure 2.12.3-2 and Figure 2.12.3-30. The puncture bar was oriented at approximately  $45^\circ$  to the package axis, and contacted a fold which was adjacent to the damaged corner joint. Since the test was carried out shortly after puncture test P4, the polyurethane foam temperature is considered to be essentially the same as that recorded for test P4.

The bar caught the fold and tore the damaged joint open as shown in Figure 2.12.3-31 and Figure 2.12.3-32. The total length of the damage, measured as a chord, was approximately 26 inches. At the location of the bar (i.e., the center of the damage), the width was 5 inches. On either side the width of the opening was approximately 2-1/2 inches, tapering to zero at the ends. Only negligible amounts of foam were lost from the shells as shown in Figure 2.12.3-32.

#### 2.12.3.5.9 Puncture Drop Test P3

Puncture test P3 was performed on the secondary slapdown damage incurred by serial number 3 in free drop test D2. The orientation is shown in Figure 2.12.3-2 and Figure 2.12.3-33. The bar struck the damaged area approximately in the center. The cask axis was at a small angle to the horizontal. Since the test was carried out shortly after puncture tests P4 and P5, the polyurethane foam temperature is considered to be essentially the same as that recorded for test P4.

The depth of the impact dent was approximately one inch. There was no sign of cracking or tearing of the impact limiter shell, as shown in Figure 2.12.3-34.

### 2.12.3.6 Confirmatory Test of Attachments

The confirmatory tests were performed on February 17, 2009 at Hilina, in order to demonstrate the adequacy of the redesigned impact limiter attachments. The test used the existing dummy cask and impact limiters, which had been altered to enhance the strength of the attachments. The revisions made to the test articles resulted in attachments which, in full-scale, were not stronger than the attachment design used on the production hardware.

None of the other tests will be invalidated by the increase in the strength of the attachments. In all of the other tests, the attachments did not fail, therefore, making the attachments stronger had no effect on the prior tests.

The tests that were selected to demonstrate the attachments were the D2 free drop and P2 puncture drop configurations. The D2 drop was chosen since that is the orientation in which the primary impact limiter attachments consistently failed. Attachment failures did not occur in any other impacts. The P2 puncture was chosen since a) a puncture subsequent to free drop is required by 10 CFR 71, and b) it is the puncture test that places the greatest load on the attachments. The test article having the greatest remaining capacity for an additional impact was serial no. 2, which was the primary limiter in tests D2 and D2R. The secondary limiter in the confirmatory tests was serial no. 3, which was less damaged than serial no. 1. The confirmatory tests were designated D2C and P2C.

Prior damage required that the CTU be rotated 90° about its axis. Since the attachment pattern has only one plane of symmetry, this meant that instead of one worst-case loaded attachment at 12 o'clock (relative to the impact at 6 o'clock), there were two attachments at approximately 11 and 1 o'clock, which were loaded somewhat less than in the prior drops. However, since the production redesign now features eight attachments, the load developed in each of the two maximum-loaded attachments in this test was greater than the maximum load which would develop in the production design.

#### 2.12.3.6.1 Description of Design Changes

The configuration of the attachments was increased in capacity as much as possible given the limitations of the existing hardware. In no case did the revised test hardware have a greater strength than the revised full-scale design. A detailed comparison of the test configuration and the full-scale design is given in Section 2.7.1.7, *Impact Limiter Attachments*. The revised CTU attachment is depicted in Figure 2.12.3-35. The nominal thickness of the blades, made of ASTM Type 304 material, was 3/8 inches. The width of the blades was increased to 1.5 inches, and their inner edge was set at 1/8 inches from the inner diameter of the impact limiter. The new blades were attached to the original blade roots using a full penetration weld, and the region between the top surface of the limiter and the new blade (approximately 1/2-inches) was buttered with weld metal to approximately the dimensions of the new blade. The hole in the blade was match-drilled from the existing hole in the cask attachments, and drilled out to 9/16 inches in diameter. The thickness, width, hole diameter, and hole-to-inner edge dimension for each blade before testing are given in Table 2.12.3-3. Serial no. 2 was mated with end A of the dummy cask, at the existing orientation marks.

Since the secondary impact limiter attachments did not fail in either prior slapdown drop, the refurbishment to serial no. 3 was minimal. The existing 3/16-inch thick blade was cut off and replaced with the same thickness material by a full penetration weld, match drilled to the existing

**BRR Package Safety Analysis Report**

holes on cask end B, and drilled out to 9/16-inch diameter. Both limiters were attached using 1/2 inch diameter carbon steel ball lock pins (the same specification as used in test D2R).

Since the test articles had both received two prior 30-ft drop impacts, and since good data was collected in the same orientation in tests D2 and D2R, test D2C was not instrumented with accelerometers. Both impact limiters were cold for the free drop test. Foam temperature was not recorded for the secondary limiter since the purpose of this test was not related to the secondary impact event.

**2.12.3.6.2 Oblique Slapdown Free Drop Test D2C Results**

Test D2C was performed using a drop height of 30 feet, oriented with the cask axis at 17° to the horizontal, as shown in Figure 2.12.3-1 and Figure 2.12.3-36. The primary (lower) impact limiter was serial no. 2, and the secondary (upper) impact limiter was serial no. 3. The polyurethane foam temperature readings in the primary limiter were -8.8 °F and -5.6 °F. The primary limiter was oriented so that blade nos. 5 and 6 were directly opposite the impact, where experience showed that the attachment loads are the highest.

The crush deformations were very similar to those obtained in tests D2 and D2R on the same limiter. All of the attachments, both primary and secondary, remained completely intact. Figure 2.12.3-37 and Figure 2.12.3-38 show the post-test configuration of the two most highly loaded attachments, at locations #5 and #6, respectively. All welds attaching the blades to the impact limiter appeared in good condition without failure. The attachments were examined in further detail following the puncture test.

**2.12.3.6.3 Puncture Drop P2C Results**

Puncture test P2C was performed immediately after drop test D2C. The longer puncture bar was used to impact the top annular surface of the damaged primary impact limiter (serial no. 2), as shown in Figure 2.12.3-2 and Figure 2.12.3-39. The orientation could not be over the center of gravity due to the desired impact location. The impact occurred adjacent to the outside edge of the limiter, halfway between attachment locations #5 and #6, thus maximizing the moment arm and loading of those attachments. The polyurethane foam temperature reading closest to the impact was lower than -3.0 °F.

The impact caused the long puncture bar to bend somewhat, but the attachment to the steel drop pad plate remained intact. The impact dent on the annular plate was negligible, without any cracking or tearing of the steel shell, and no exposure of foam. The attachments all appeared to be in good shape following the test. Figure 2.12.3-40 shows the impact dent and the attachment at location #5.

**2.12.3.6.4 Examination of Attachments**

After removal of the impact limiters from the dummy cask, the attachments were examined in detail. There was very little evidence of plastic deformation in the attachments, except that the holes of the most highly loaded blades were very slightly elongated. There was no evidence of bearing yielding in the hole, and no evidence of bending or cracking in the attachment pins. There was no evidence of weld cracking or deformation, except in one case, part of the weld between the blade and the annular sheet showed some shear. This was due to deformation of the annular plate in the puncture test, and this weld has no role in the impact limiter attachment load path. Table 2.12.3-4 shows the measurements of the blade after test. Comparing Table 2.12.3-3

**BRR Package Safety Analysis Report**

---

and Table 2.12.3-4, the largest increase in the hole dimension (measured in-line with the attachment loading direction, parallel to the cask axis) was 0.034 inches for blade no. 5, which is negligible. A comparison of the hole-to-edge dimension indicates that this distance appeared to increase slightly in several cases (ranging between a 0.016-inch decrease in width to a 0.010-inch increase), but as this goes against reason, it is assumed to be caused by measuring error on the rough surfaces. Figure 2.12.3-41 shows the blade configuration at location #5, and Figure 2.12.3-42 shows location #6, after all testing. Figure 2.12.3-43 shows a view of all of the pins used to retain the primary impact limiter. These photographs demonstrate that the attachments were essentially unchanged by the test loads.

The cask receptacle plate holes were somewhat elongated from prior testing (they were not refurbished). After the tests, the holes did not appear to have deteriorated any further.

**Table 2.12.3-1 - CTU Weights**

Component	Weight, lb
Dummy Cask	3,181
Impact Limiter Serial No. 1	278
Impact Limiter Serial No. 2	276
Impact Limiter Serial No. 3	276

**Table 2.12.3-2 - Summary of Certification Tests**

No.	Test Description	Test Limiter	Temperature
D1	End drop	#1	Cold per Section 4.3
D2	Slapdown oblique drop, 15°	#2 & #3	Cold per Section 4.3
D2R	Slapdown oblique drop, 15°	#2 & #1	Cold per Section 4.3
D2C	Slapdown oblique drop, 15°	#2 & #3	Cold per Section 4.3
D3	C.G.-over-corner drop	#3	Not controlled
P1	Oblique through c.g. on thicker end plate on test D1 damage	#1	Cold per Section 4.3
P2	Approx. parallel to package axis, on test D2 primary-end damage	#2	Not controlled
P2C	Approx. parallel to package axis, on test D2C primary-end damage	#2	Not controlled
P3	Approx. perpendicular to package axis, on test D2 primary-end damage	#2	Not controlled
P4	On test D3 damage, on thick/thin joint, near c.g.	#3	Not controlled
P5	Oblique to package axis, on test D3 secondary-end damage	#3	Not controlled

Notes:

1. All free drops (Dx) are from 30 feet, and all punctures (Px) are from 40 inches.
2. Figures of each orientation are provided in Figure 2.12.3-1 and Figure 2.12.3-2.
3. See Section 2.12.3.6, *Confirmatory Test of Attachments*, for a description of tests D2C and P2C.

**Table 2.12.3-3 - Attachment Pretest Data (Serial No. 2 Before D2C), inches**

No.	Blade Thick	Blade Width	Hole Dia.	Hole-to-Edge
1	0.376	1.515	0.565	0.376
2	0.375	1.517	0.565	0.353
3	0.375	1.520	0.563	0.375
4	0.377	1.519	0.565	0.471
5	0.376	1.519	0.565	0.420
6	0.377	1.519	0.565	0.396

**Table 2.12.3-4 - Attachment Post-test Data (Serial No. 2 After D2C), inches**

No.	Hole Axial* Diameter	Hole Lateral** Diameter	Hole-to-Edge
1	0.573	0.567	0.360
2	0.569	0.565	0.354
3	0.568	0.565	0.375
4	0.567	0.566	0.472
5	0.599	0.566	0.430
6	0.585	0.569	0.400

Note: Blade thickness and width were unchanged from the pre-test measurements.

\*Parallel to cask axis

\*\*Taken at right angle to axial diameter

**Table 2.12.3-5 - Accelerometer Calibration Constants**

Accelerometer Channel	Calibration Constant (mV/g)
12	0.935
13	0.926
14	0.930
15	0.941
16	0.916
17	0.889
18	0.905
19	0.973

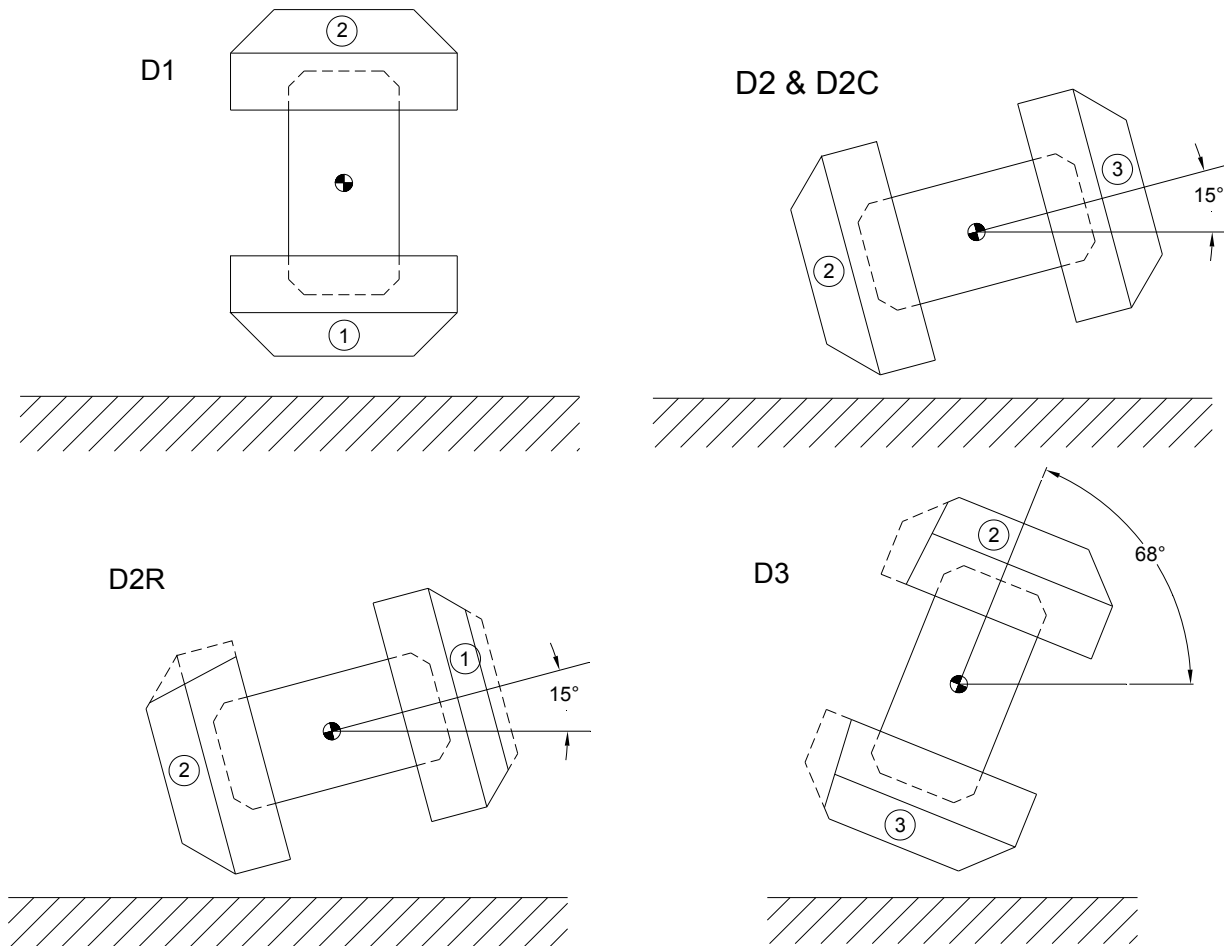


Figure 2.12.3-1 - BRR Package Free Drop Orientations

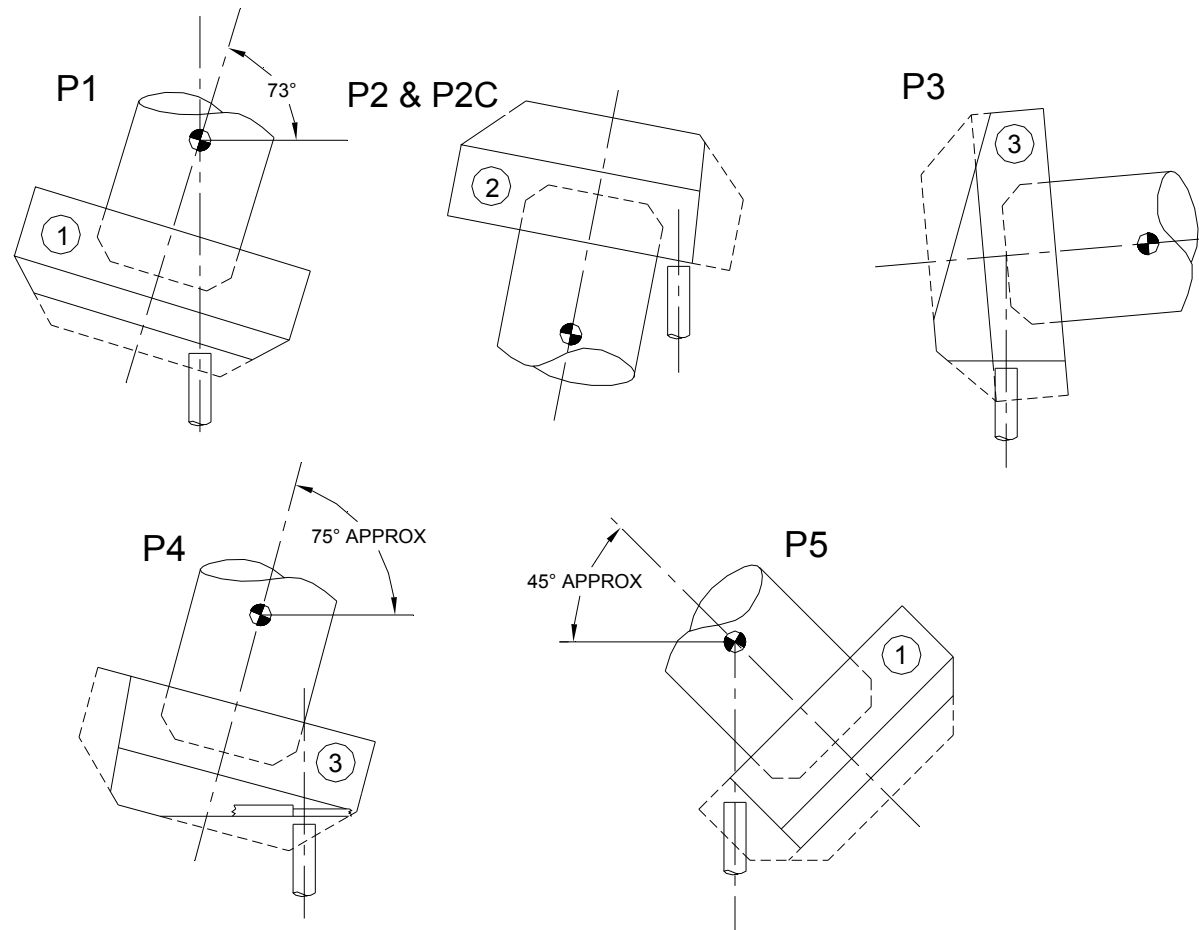
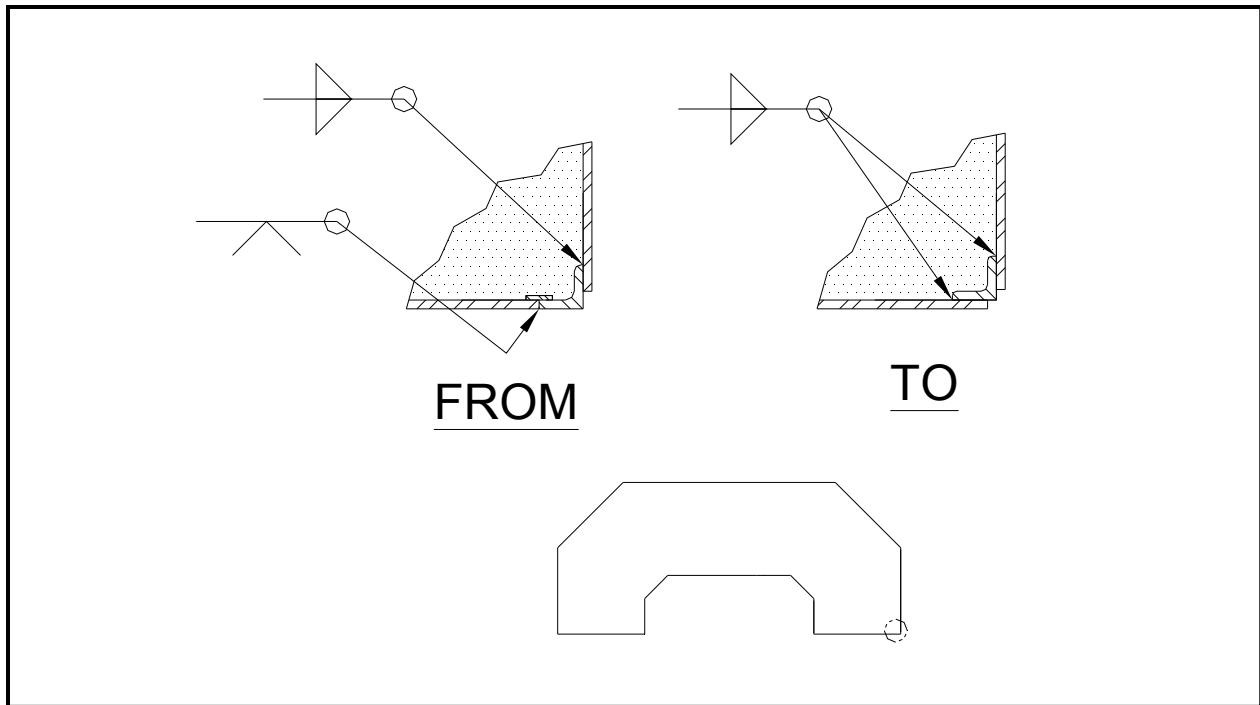
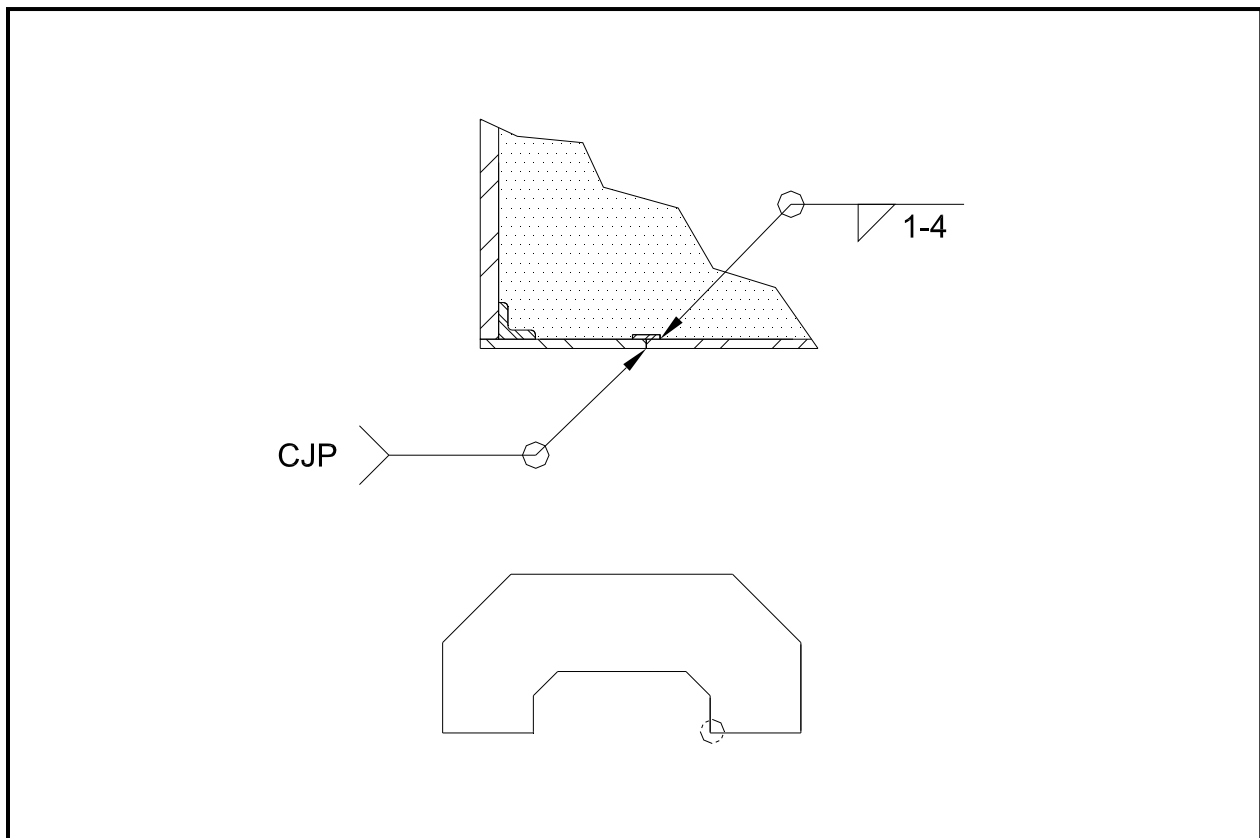


Figure 2.12.3-2 - BRR Package Puncture Drop Orientations

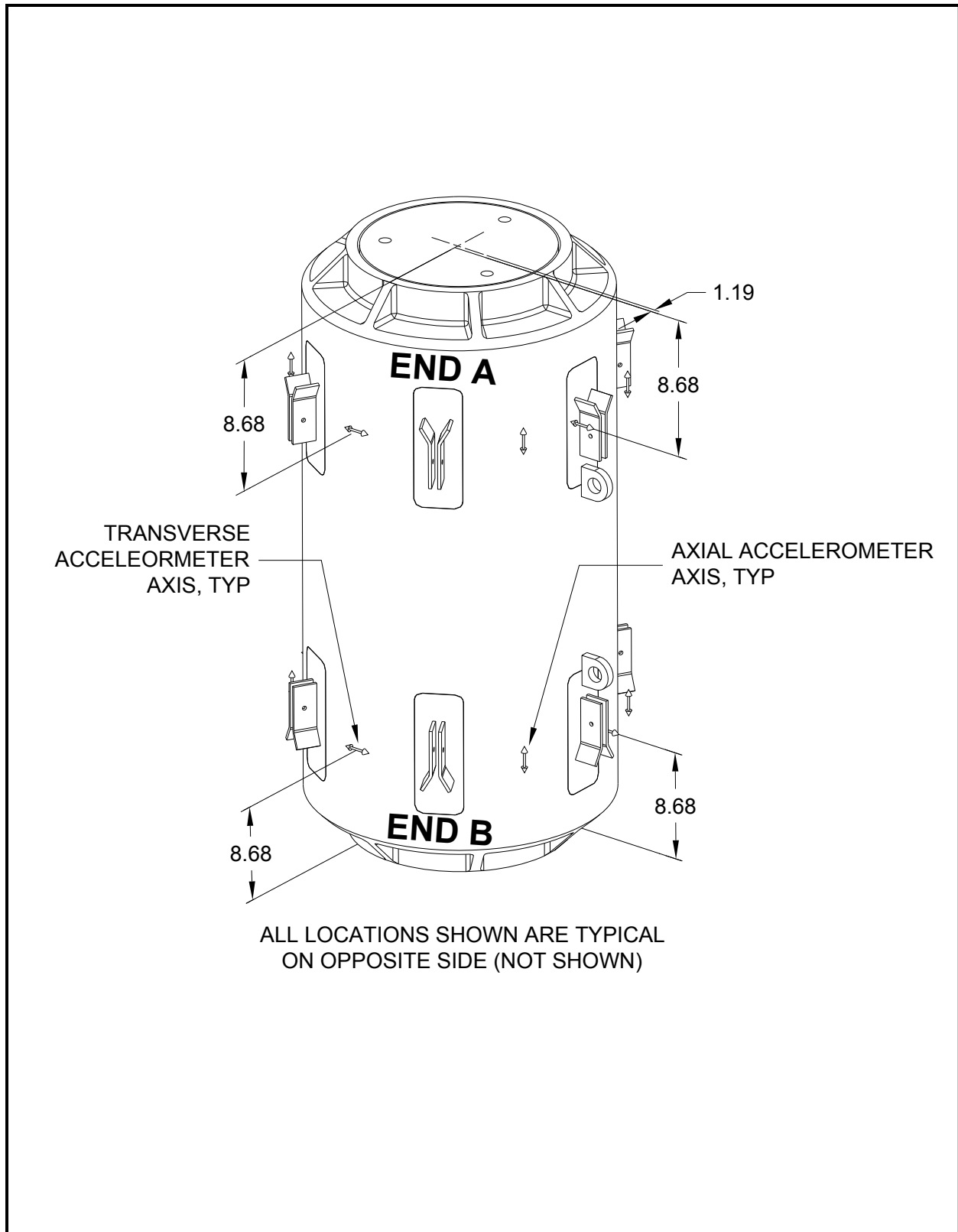




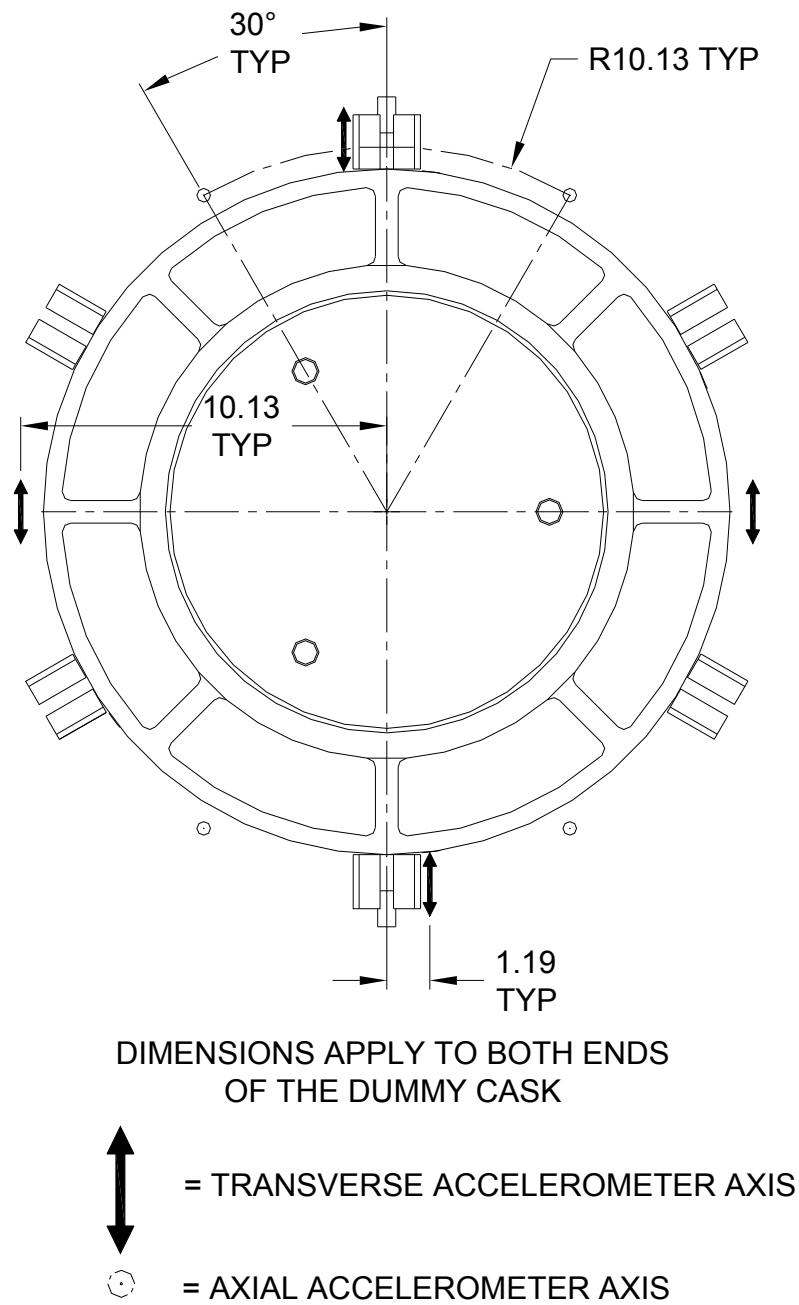
**Figure 2.12.3-3 - Change to Outer Impact Limiter Joint**



**Figure 2.12.3-4 - Added Weld Seam Near Impact Limiter Inner Diameter**



**Figure 2.12.3-5 - Accelerometer Mounting**



**Figure 2.12.3-6 - Accelerometer Mounting, Top View**



**Figure 2.12.3-7 - Free Drop Test D1 Orientation**



**Figure 2.12.3-8 - Free Drop Test D1 Inside-Out Deformation**





**Figure 2.12.3-9 - Free Drop Test D1 Outside-In Deformation**



**Figure 2.12.3-10 - Puncture Test P1 Orientation**



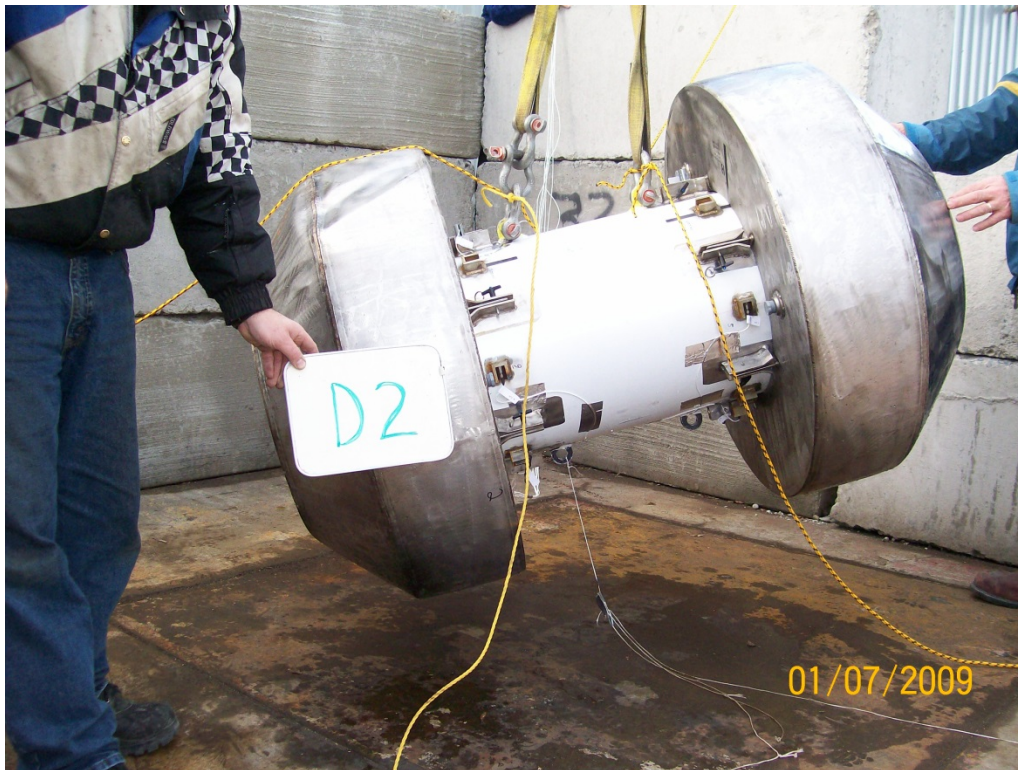


**Figure 2.12.3-11 - Puncture Test P1 Deformation**



**Figure 2.12.3-12 - Puncture Test P1 Deformation – Close-up View**

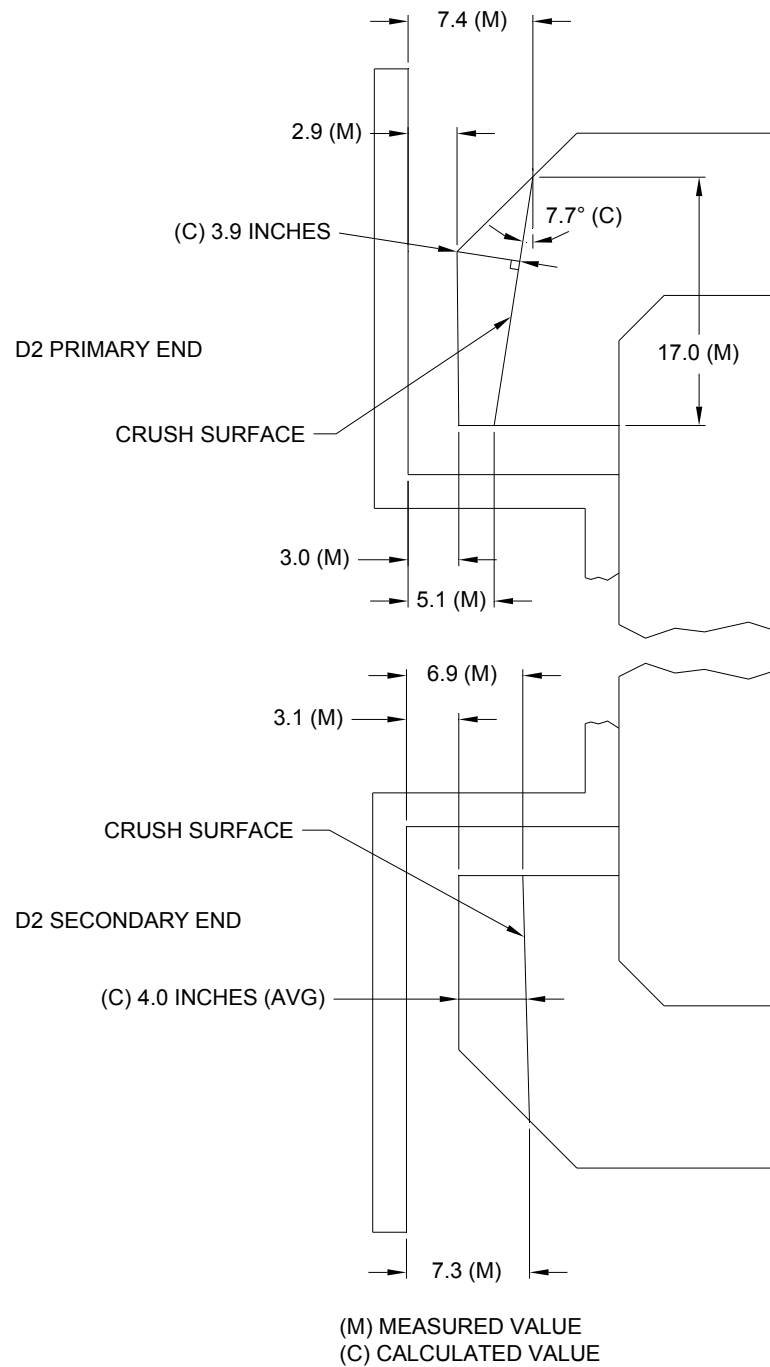




**Figure 2.12.3-13 - Free Drop Test D2 Orientation**



**Figure 2.12.3-14 - Free Drop Test D2 Post-test Configuration**



**Figure 2.12.3-15 - Free Drop Test D2 Crush Measurements**



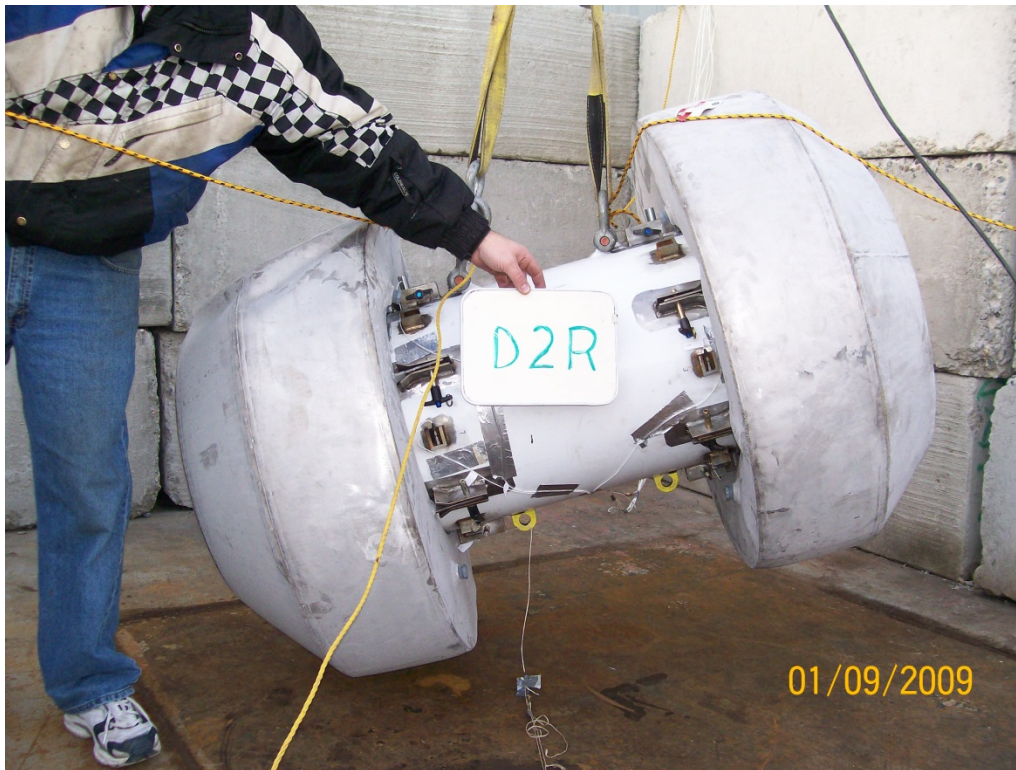


**Figure 2.12.3-16 - Free Drop Test D2, Close-up View of Failed Attachments**



**Figure 2.12.3-17 - Free Drop Test D2 Impact Deformation Surfaces**

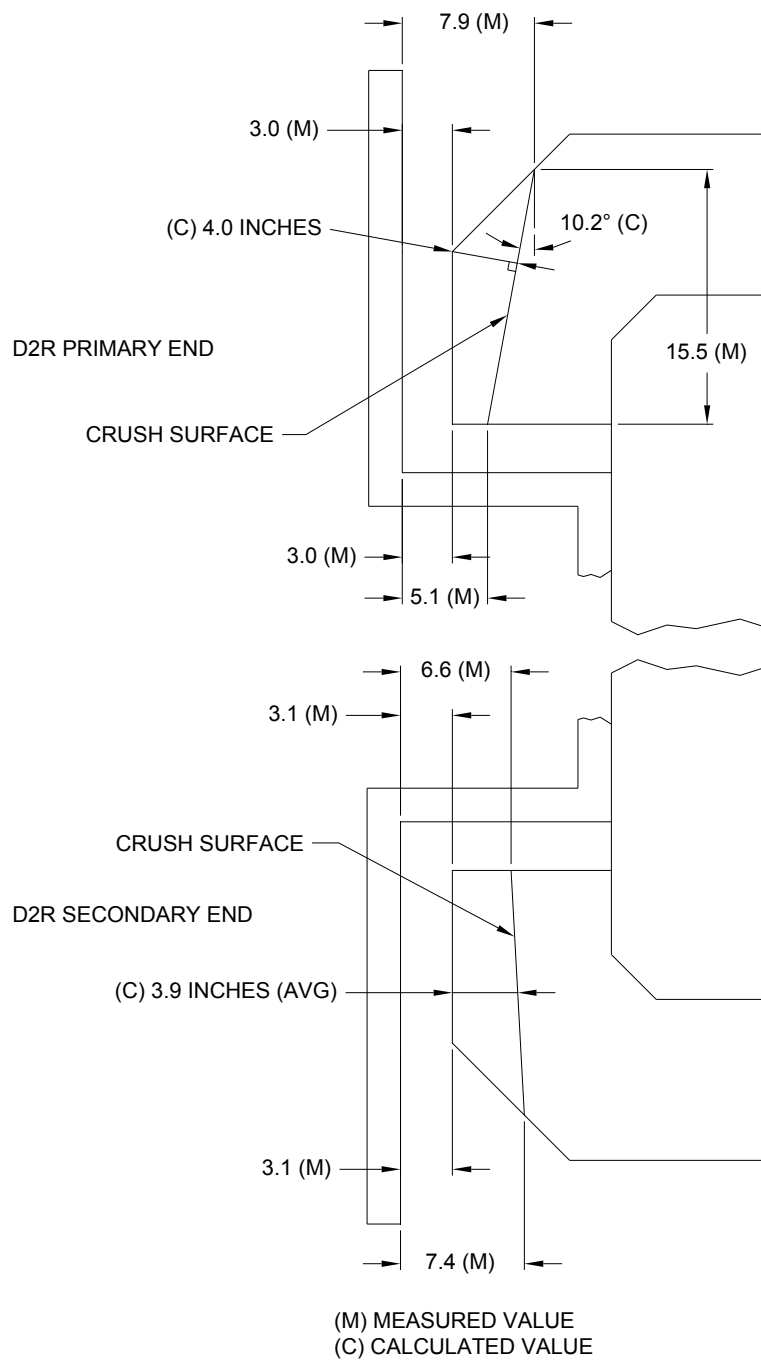




**Figure 2.12.3-18 - Free Drop Test D2R Orientation**



**Figure 2.12.3-19 - Free Drop Test D2R Post-test Configuration**



**Figure 2.12.3-20 - Free Drop Test D2R Crush Measurements**





**Figure 2.12.3-21** - Free Drop Test D2R, Close-up View of Failed Attachments



**Figure 2.12.3-22** - Free Drop Test D2R, View of Torn Corner Joint





**Figure 2.12.3-23 - Puncture Test P2 Orientation**



**Figure 2.12.3-24 - Puncture Test P2 Result**

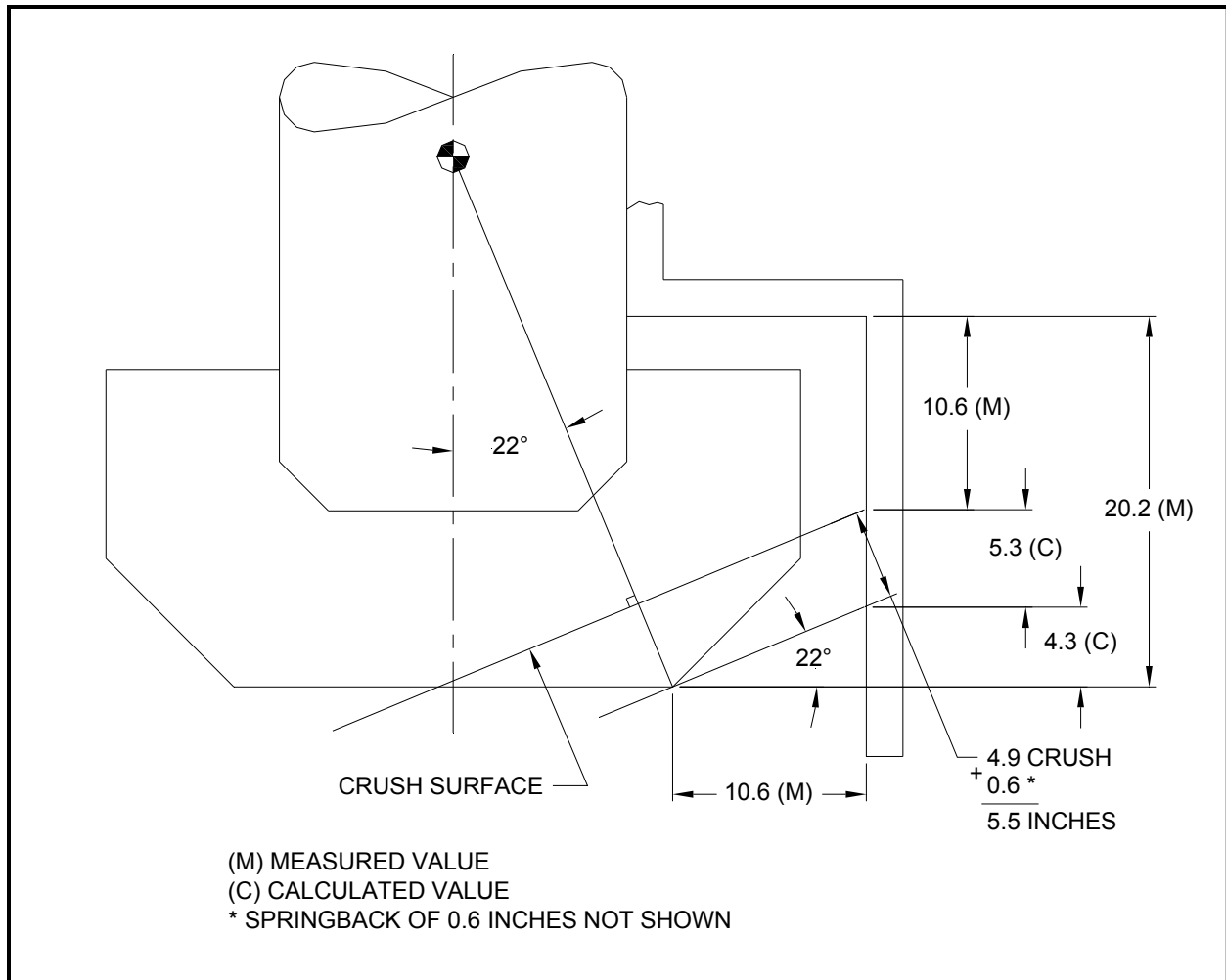




**Figure 2.12.3-25 - Free Drop Test D3 Orientation**



**Figure 2.12.3-26 - Free Drop Test D3 Deformation**



**Figure 2.12.3-27 - Free Drop Test D3 Crush Measurements**





**Figure 2.12.3-28 - Puncture Test P4 Orientation**



**Figure 2.12.3-29 - Puncture Test P4 Damage**





**Figure 2.12.3-30 - Puncture Test P5 Orientation**



**Figure 2.12.3-31 - Puncture Test P5 Damage**





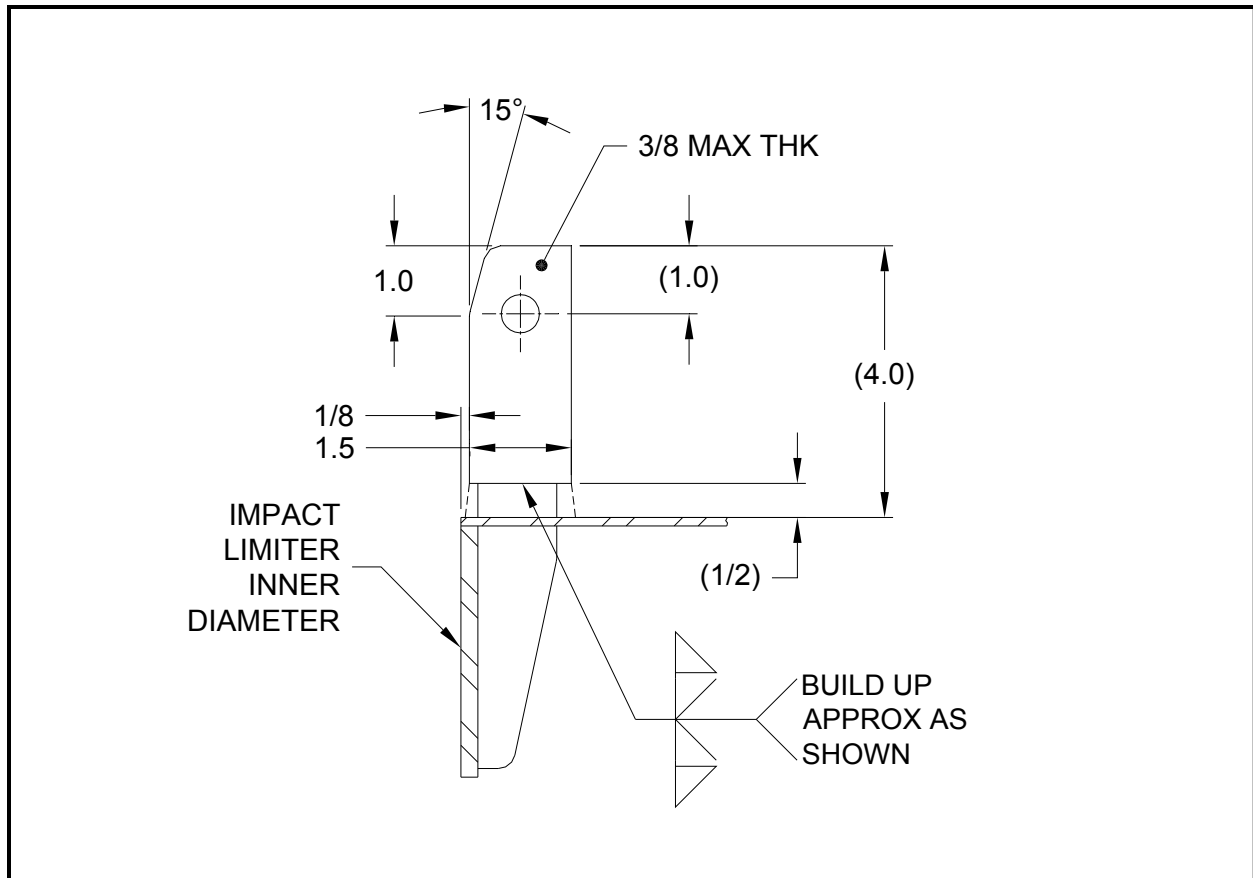
**Figure 2.12.3-32 - Puncture Test P5 Damage**



**Figure 2.12.3-33 - Puncture Test P3 Orientation**



**Figure 2.12.3-34 - Puncture Test P3 Damage**



**Figure 2.12.3-35 - Revised Half-Scale Attachment Configuration**





**Figure 2.12.3-36 - Free Drop Test D2C Orientation**



**Figure 2.12.3-37 - Attachment Location #5 After Free Drop D2C**





**Figure 2.12.3-38 - Attachment Location #6 After Free Drop D2C**



**Figure 2.12.3-39 - Puncture Test P2C Orientation**





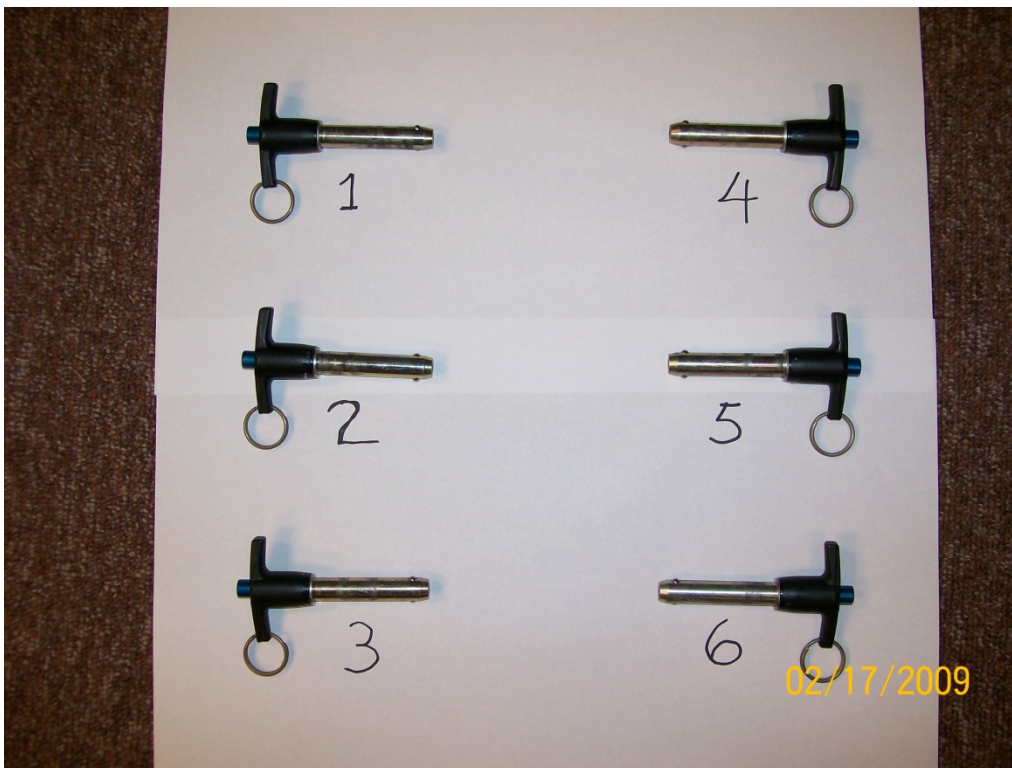
**Figure 2.12.3-40 - Puncture Test P2C Result**



**Figure 2.12.3-41 - Blade Location #5 Post-test Configuration**



**Figure 2.12.3-42** - Blade Location #6 Post-test Configuration



**Figure 2.12.3-43** - Primary Impact Limiter Attachment Ball Lock Pins, Post-test



### 2.12.3.7 Accelerometer Plots

The following figures show the filtered time history accelerometer responses by channel number. Results for all instrumented tests (D1, D2, D2R, and D3) are given. Test D1 used two accelerometers at each end; all other tests used four at each end. For the slapdown cases (D2 and D2R), channels 12 – 15 were located at the secondary end, and channels 16 – 19 were located at the primary end. The time histories in these plots are the result of filtering the accelerometer outputs at 1019Hz. They are not adjusted for the accelerometer calibration constants.

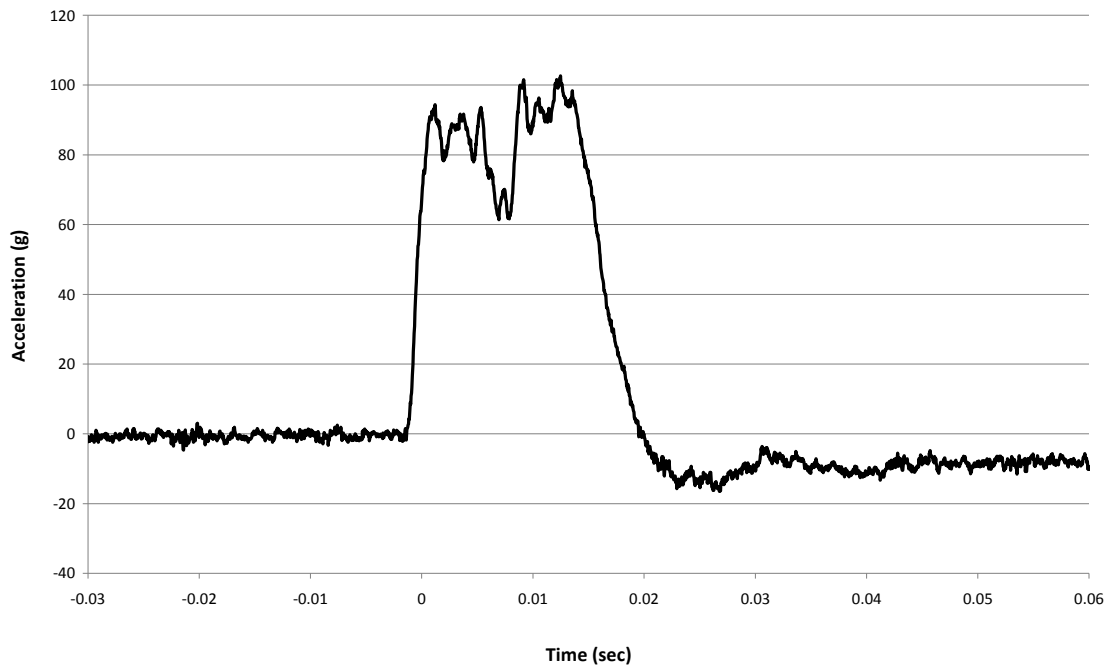
Table 2.12.3-6 (on the following page) lists the estimated rigid body peak accelerations obtained from the plots. Notes for Table 2.12.3-6:

1. The 'Peak From Plots' (column A) is the peak value taken directly off of the following acceleration time histories. For example, for test D1, channel 12, the peak value is 103g.
2. The 'From Plots, Calibration Adjusted' (column B) is found by dividing the 'Peak From Plots' data by the accelerometer calibration constant found in Table 2.12.3-5. For channel 12, the constant is 0.935. Therefore the adjusted peak value of the example is  $103/0.935 = 110\text{g}$ .
3. The 'Estimated Rigid Body Peak' (column C) is made by inspection of the corresponding accelerometer output plot. For the example case, the estimated rigid body peak is 95g.
4. The 'Rigid Body, Calibration Adjusted' (column D) is found by dividing the 'Estimated Rigid Body Peak' by the accelerometer calibration adjustment constant as described above. Following the example,  $95/0.935 = 102\text{g}$ .
5. The 'Reduction, ½ Scale' (column E) is the reduction in peak impact which could be credited if the estimated rigid body peak is used instead of the peak from the plot. For the example case, the reduction is 110 (column B) minus 102 (column D) = 8g in half-scale. The average reduction for each set of four accelerometers corresponding to each impact is also given in column E.

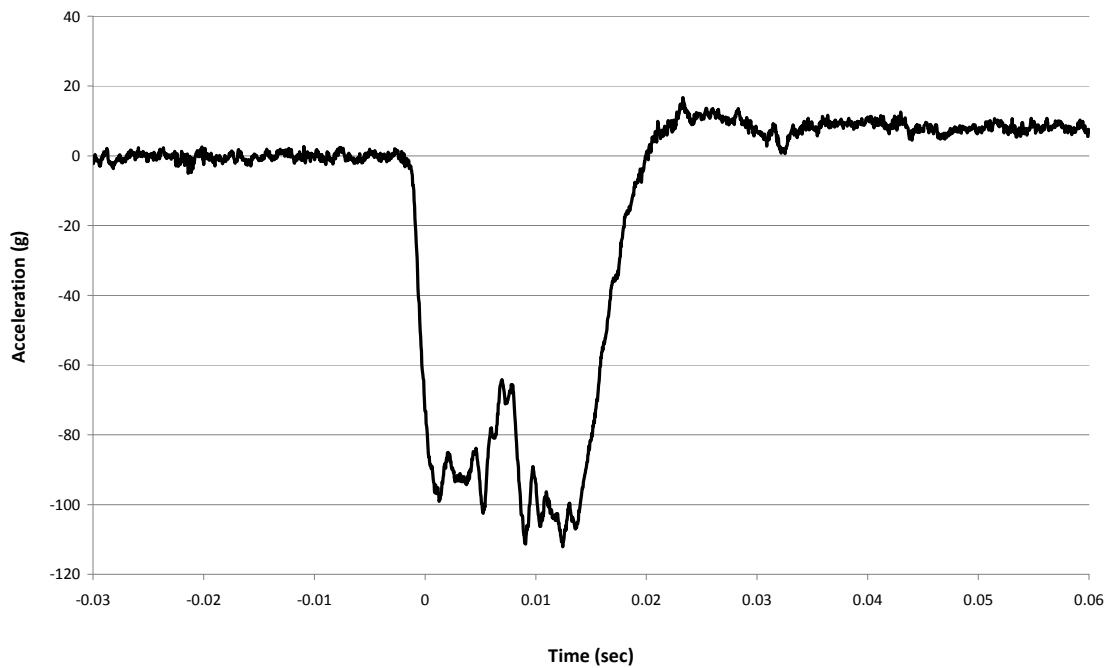
Table 2.12.3-6 – Rigid Body Results Estimates (see notes on previous page)

Test No.	Channel	Peak from Plots, g	From Plots, Calibration Adjusted, g	Estimated Rigid Body Peak, g	Rigid Body, Calibration Adjusted, g	Reduction, ½ Scale, g
		<b>A</b>	<b>B</b>	<b>C</b>	<b>D</b>	<b>E</b>
D1	12	103	110	95	102	8
(Primary)	13	112	121	104	112	9
	14	105	113	101	109	4
	15	111	118	105	112	6
Avg.						<b>7</b>
D2	12	95	102	91	97	5
(Secondary)	13	100	108	97	105	3
	14	102	110	100	108	2
	15	102	108	97	103	5
Avg.						<b>4</b>
D2	16	Severed wire	---	---	---	---
(Primary)	17	118	133	106	119	14
	18	124	137	110	122	15
	19	131	135	116	119	16
Avg.						<b>15</b>
D2R	12	105	113	96	103	10
(Secondary)	13	103	111	97	105	6
	14	99	106	93	100	6
	15	117	124	95	101	23
Avg.						<b>11</b>
D2R	16	102	111	92	100	11
(Primary)	17	103	116	97	109	7
	18	96	106	85	94	12
	19	103	106	90	92	14
Avg.						<b>11</b>
D3	12	99	106	85	91	15
(Primary)	13	103	111	87	94	17
	14	102	110	84	90	20
	15	97	103	85	90	13
Avg.						<b>16</b>

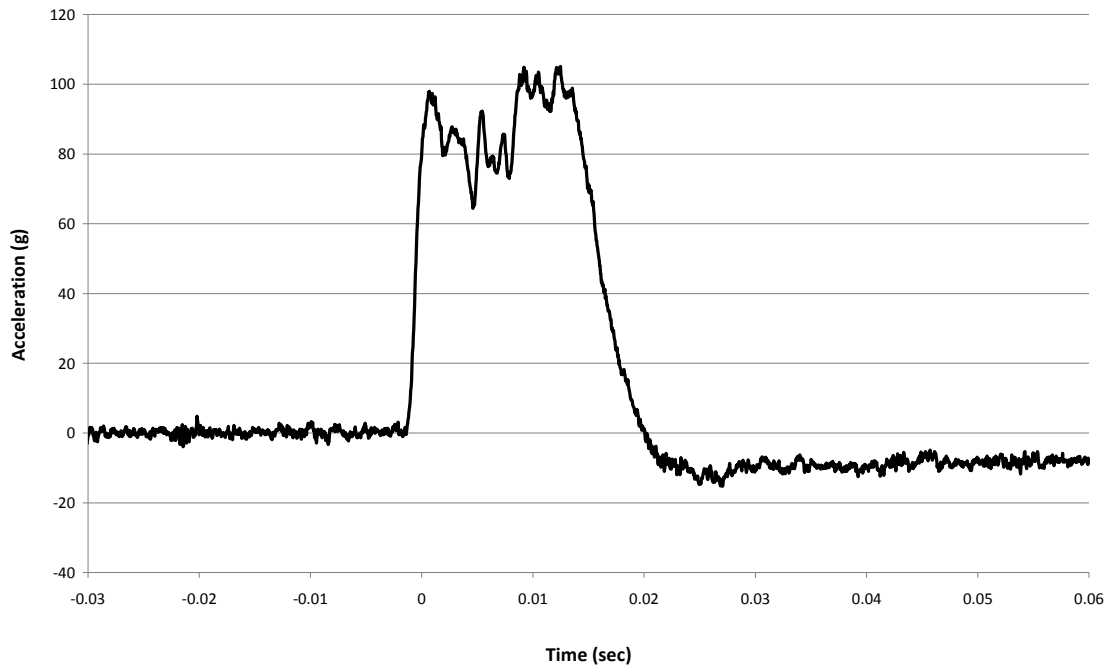
**BEA Research Reactor Package Half-Scale Free Drop Test  
Test D1 (End), Channel 12**



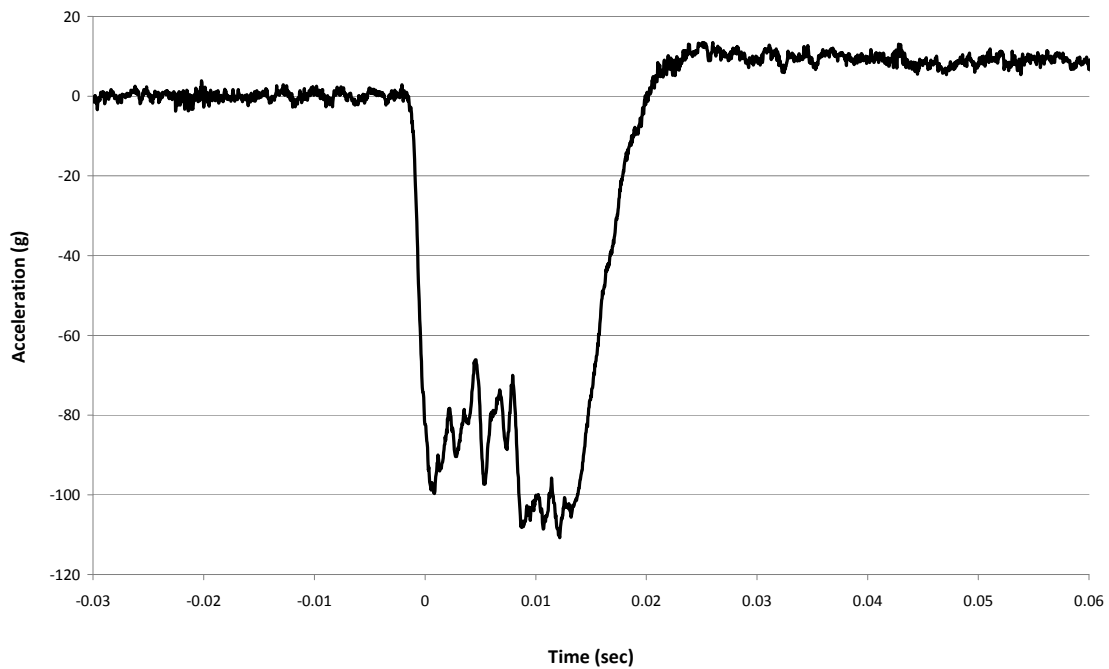
**BEA Research Reactor Package Half-Scale Free Drop Test  
Test D1 (End), Channel 13**



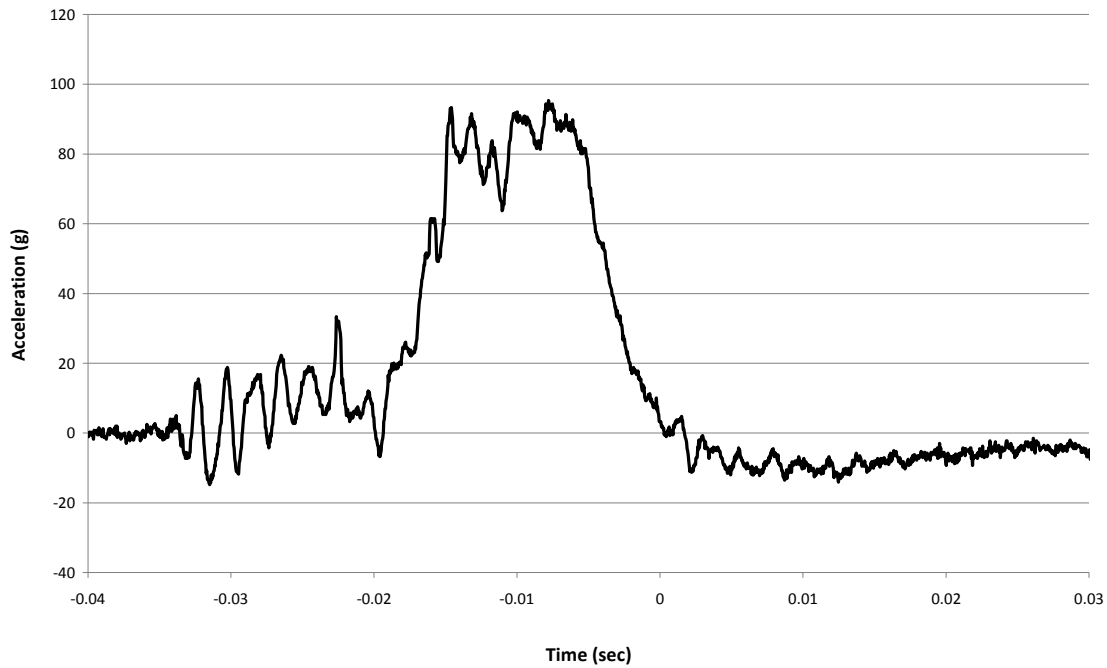
**BEA Research Reactor Package Half-Scale Free Drop Test  
Test D1 (End), Channel 14**



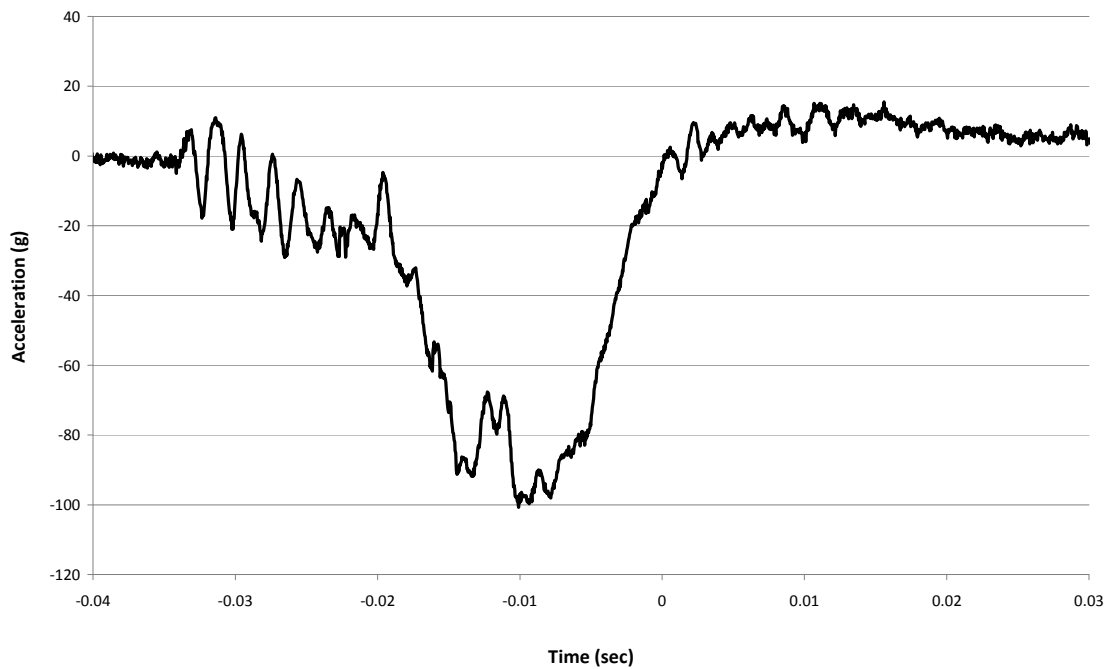
**BEA Research Reactor Package Half-Scale Free Drop Test  
Test D1 (End), Channel 15**



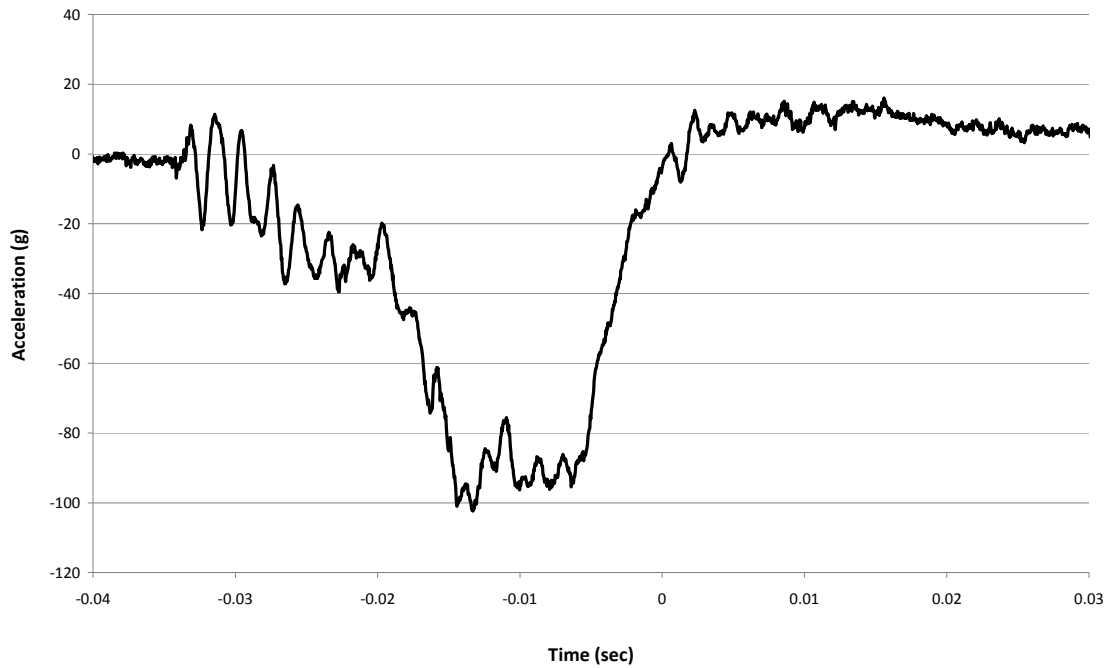
**BEA Research Reactor Package Half-Scale Free Drop Test  
Test D2 (15° Oblique), Channel 12 (Secondary Impact)**



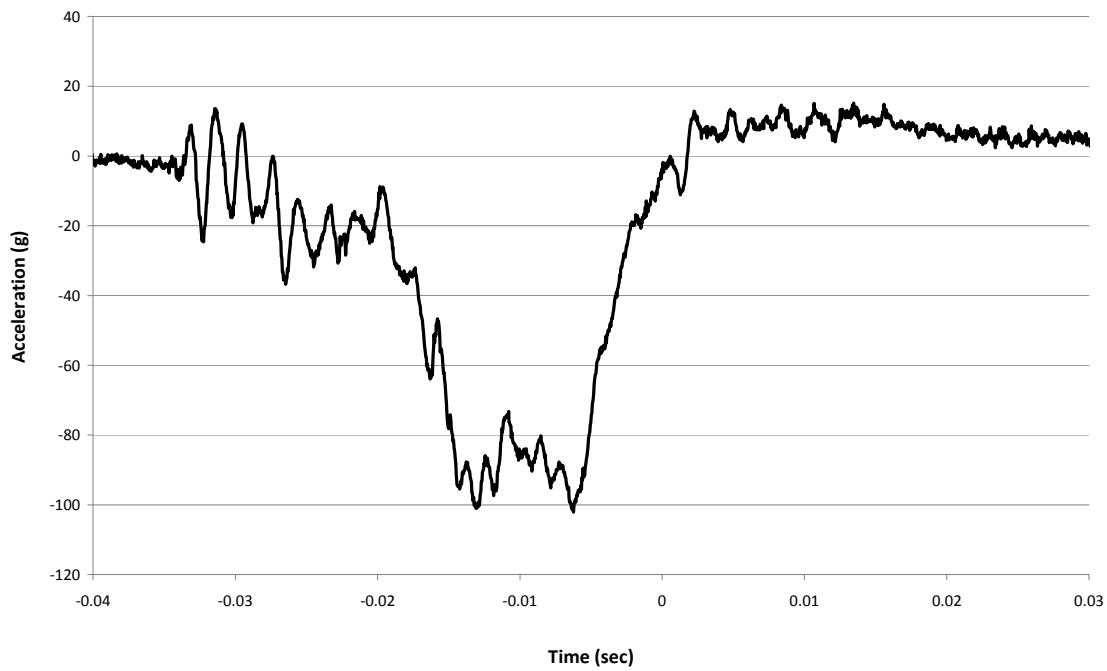
**BEA Research Reactor Package Half-Scale Free Drop Test  
Test D2 (15° Oblique), Channel 13 (Secondary Impact)**



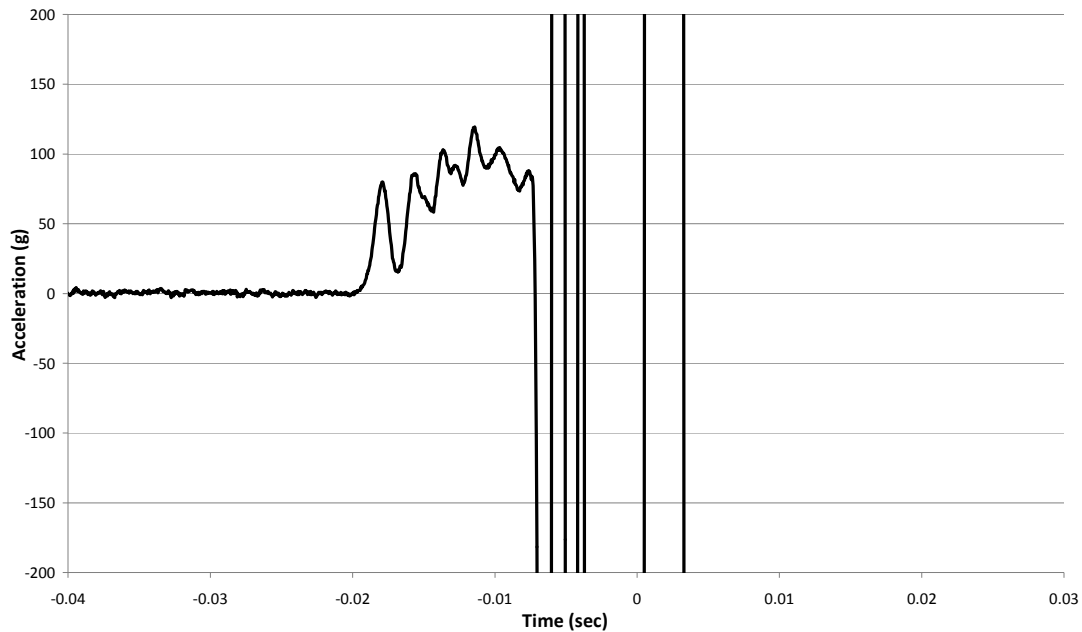
**BEA Research Reactor Package Half-Scale Free Drop Test  
Test D2 (15° Oblique), Channel 14 (Secondary Impact)**



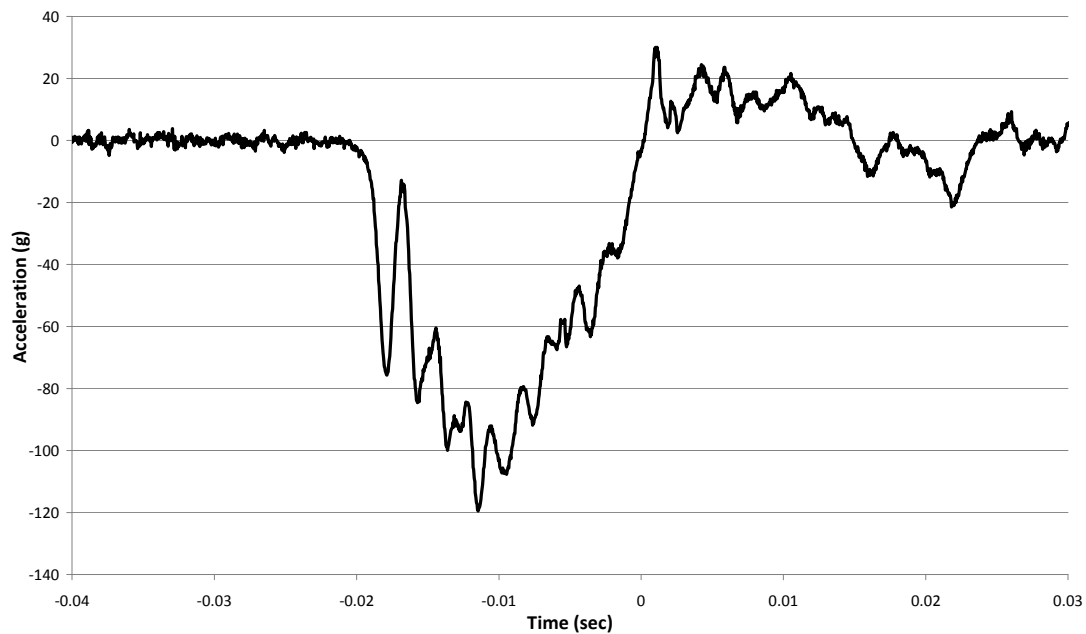
**BEA Research Reactor Package Half-Scale Free Drop Test  
Test D2 (15° Oblique), Channel 15 (Secondary Impact)**



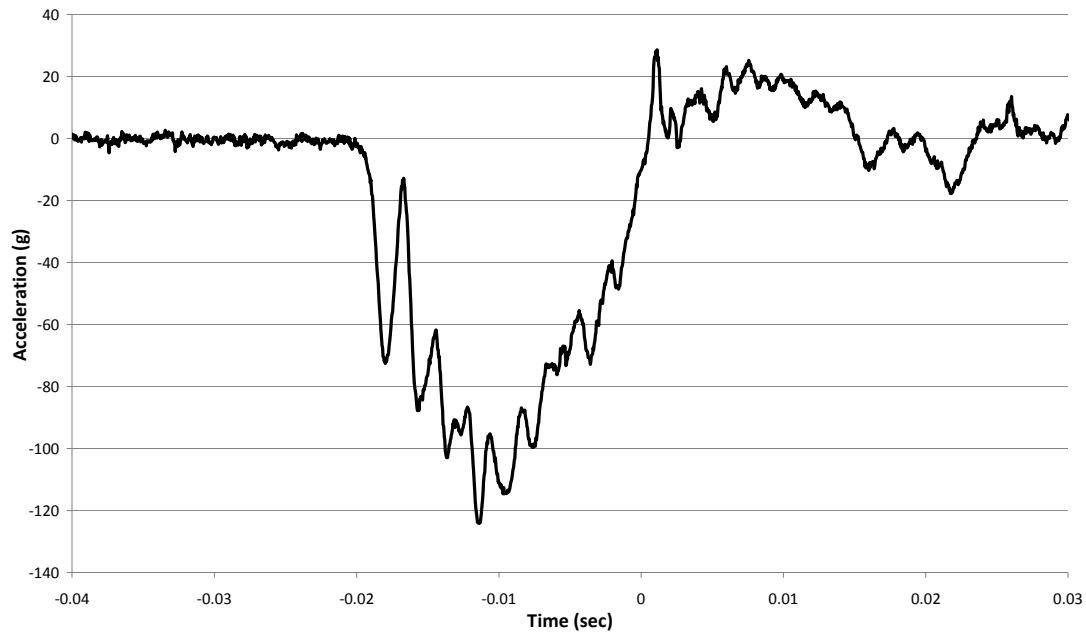
**BEA Research Reactor Package Half-Scale Free Drop Test  
Test D2 (15° Oblique), Channel 16 (Primary Impact)**



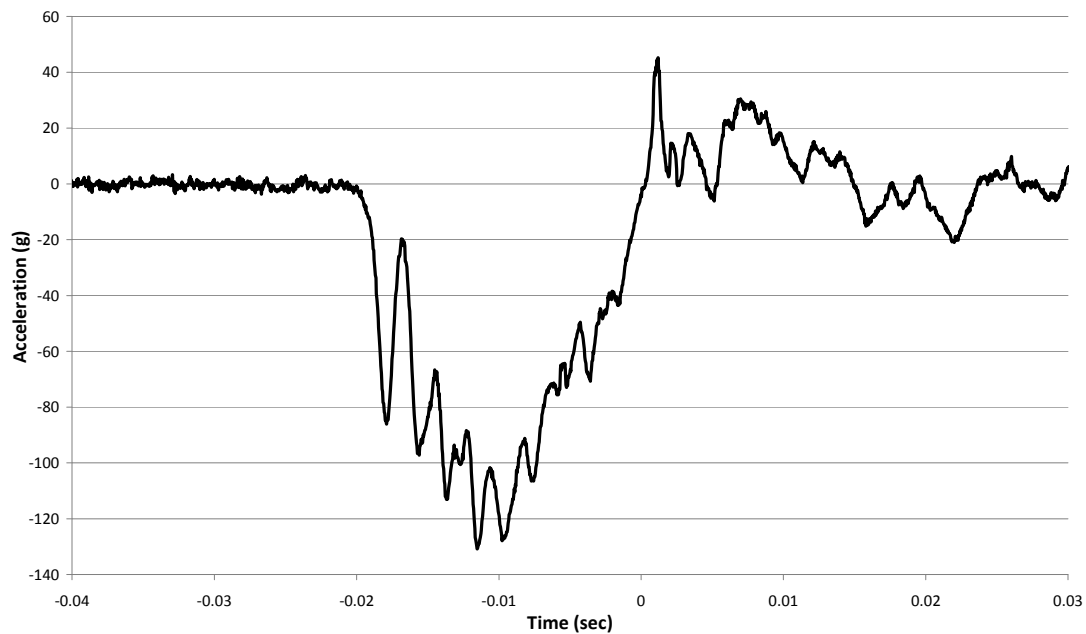
**BEA Research Reactor Package Half-Scale Free Drop Test  
Test D2 (15° Oblique), Channel 17 (Primary Impact)**



**BEA Research Reactor Package Half-Scale Free Drop Test  
Test D2 (15° Oblique), Channel 18 (Primary Impact)**

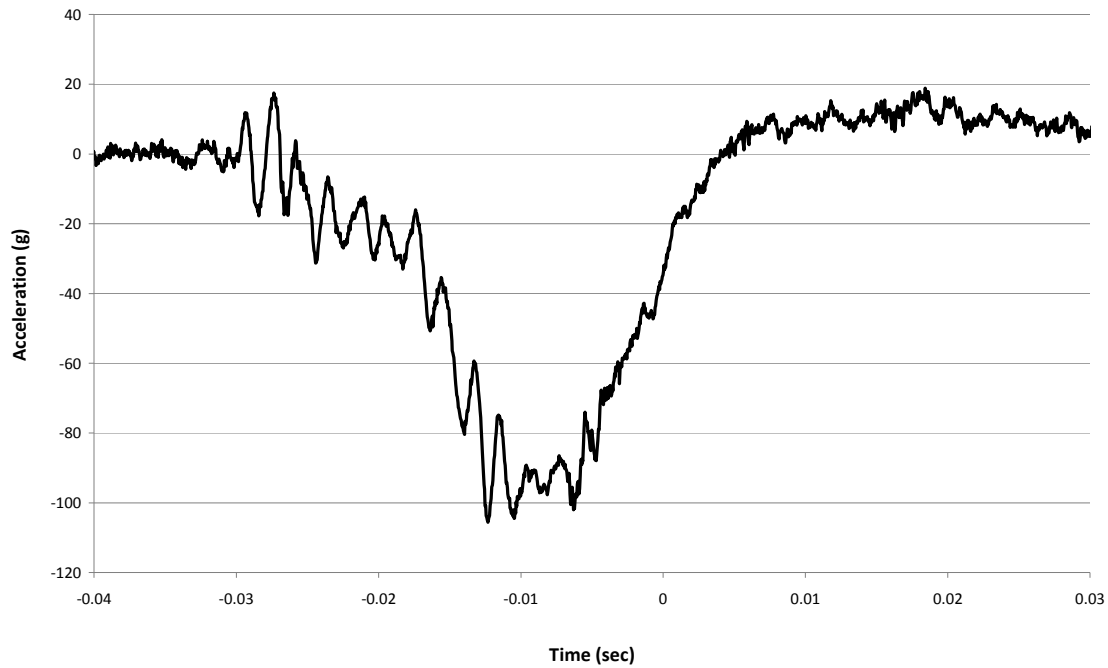


**BEA Research Reactor Package Half-Scale Free Drop Test  
Test D2 (15° Oblique), Channel 19 (Primary Impact)**

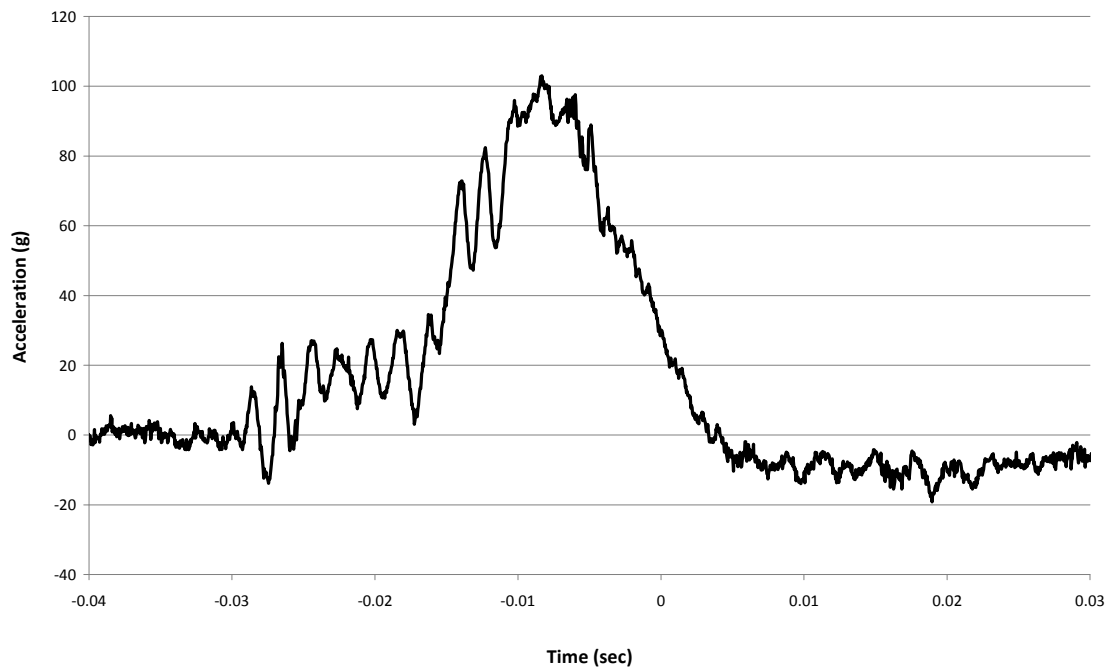




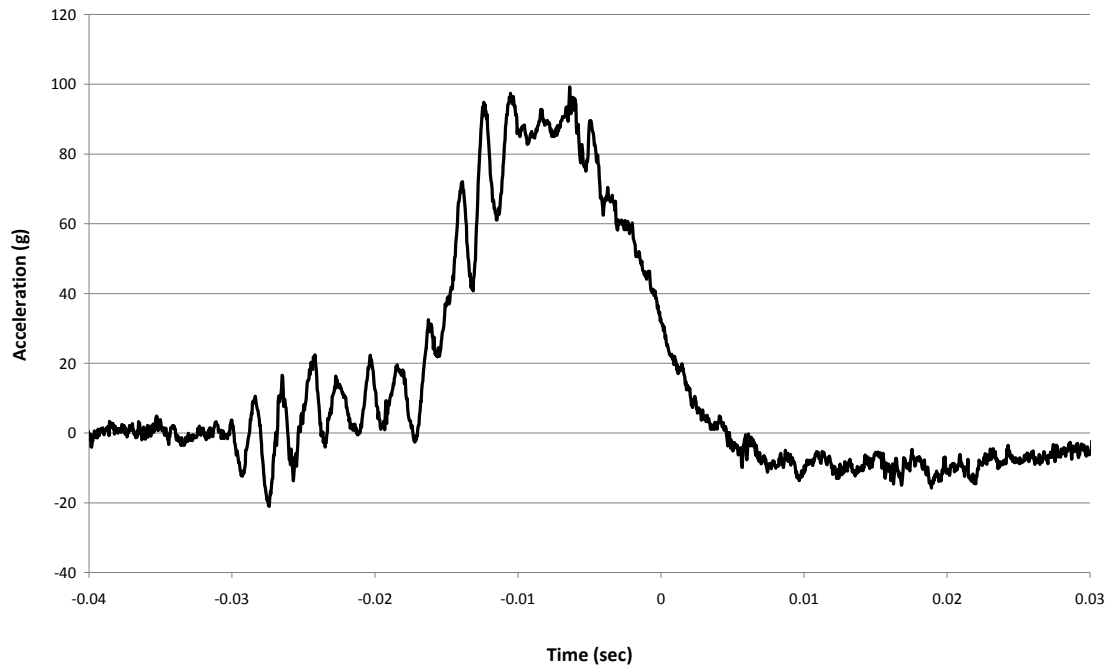
**BEA Research Reactor Package Half-Scale Free Drop Test  
Test D2R (15° Oblique), Channel 12 (Secondary Impact)**



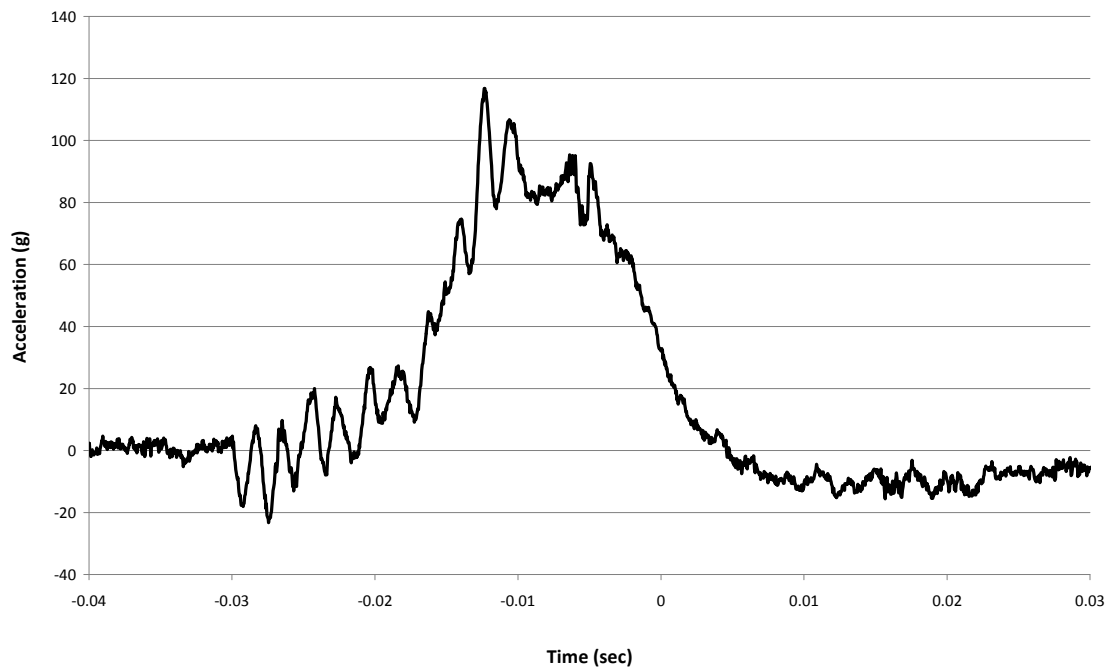
**BEA Research Reactor Package Half-Scale Free Drop Test  
Test D2R (15° Oblique), Channel 13 (Secondary Impact)**



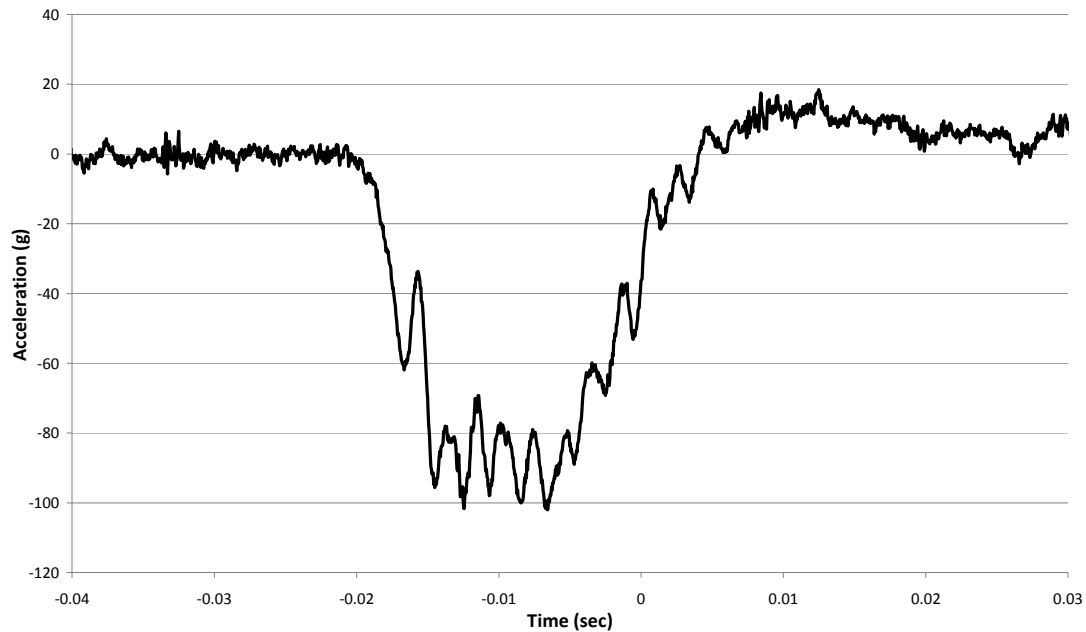
**BEA Research Reactor Package Half-Scale Free Drop Test  
Test D2R (15° Oblique), Channel 14 (Secondary Impact)**



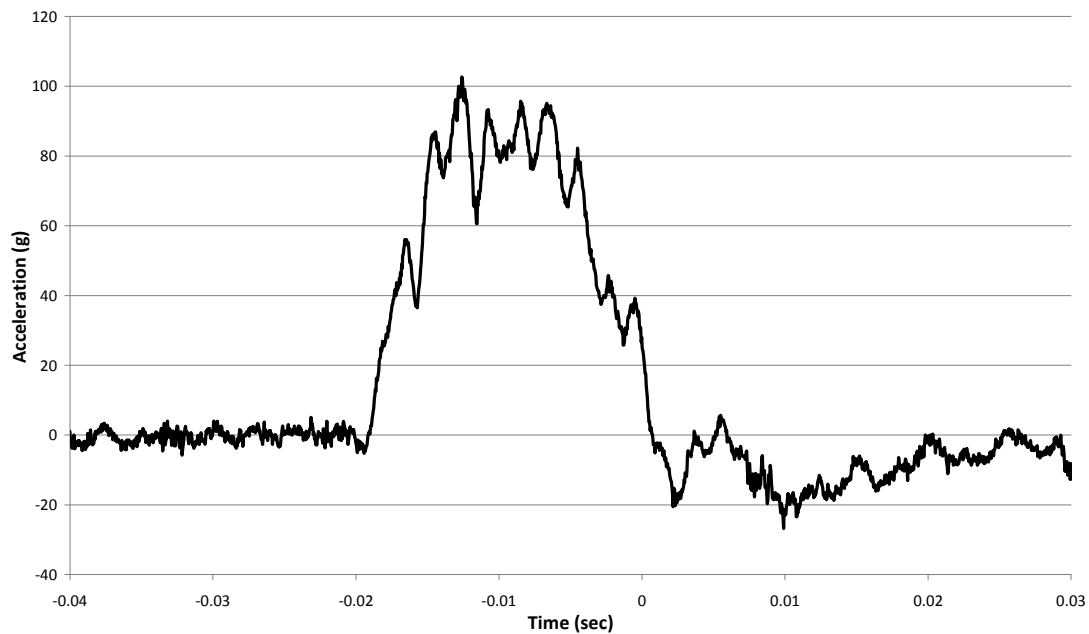
**BEA Research Reactor Package Half-Scale Free Drop Test  
Test D2R (15° Oblique), Channel 15 (Secondary Impact)**



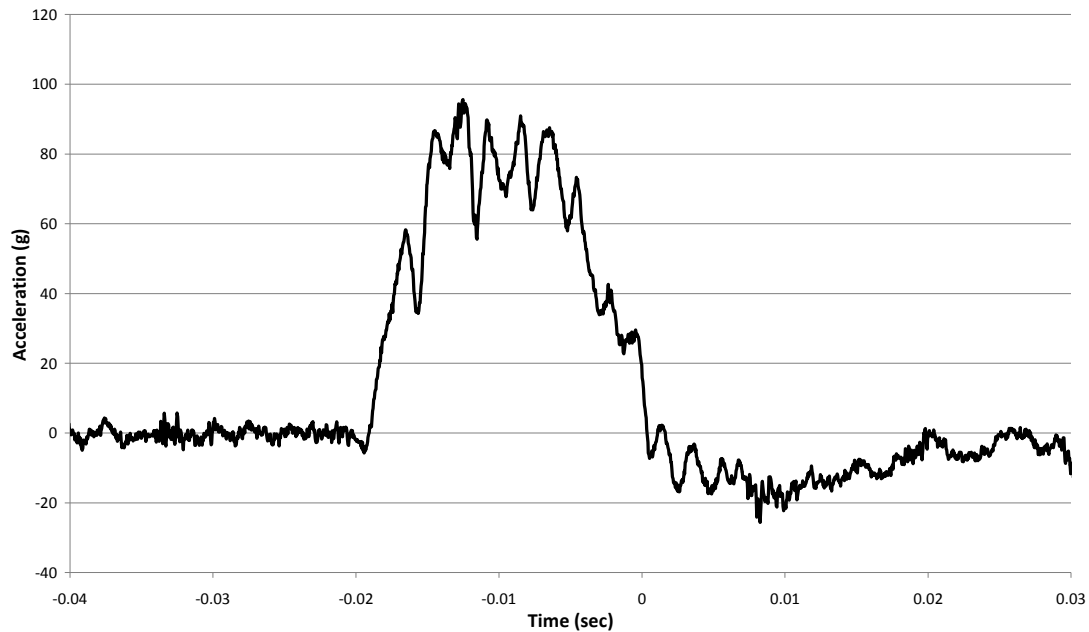
**BEA Research Reactor Package Half-Scale Free Drop Test  
Test D2R (15° Oblique), Channel 16 (Primary Impact)**



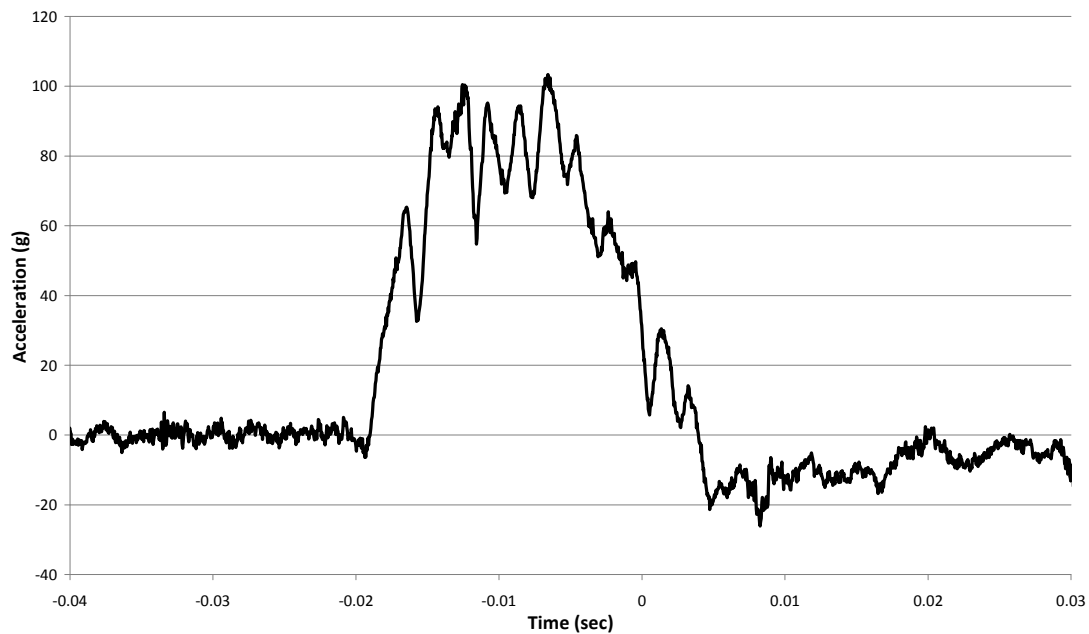
**BEA Research Reactor Package Half-Scale Free Drop Test  
Test D2R (15° Oblique), Channel 17 (Primary Impact)**



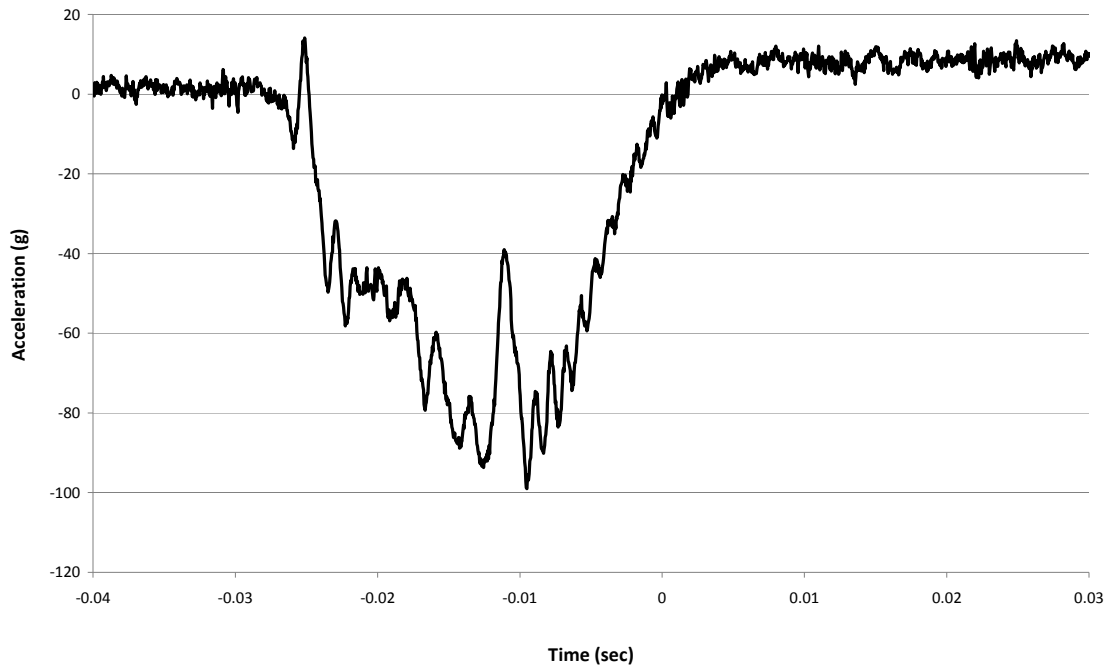
**BEA Research Reactor Package Half-Scale Free Drop Test  
Test D2R (15° Oblique), Channel 18 (Primary Impact)**



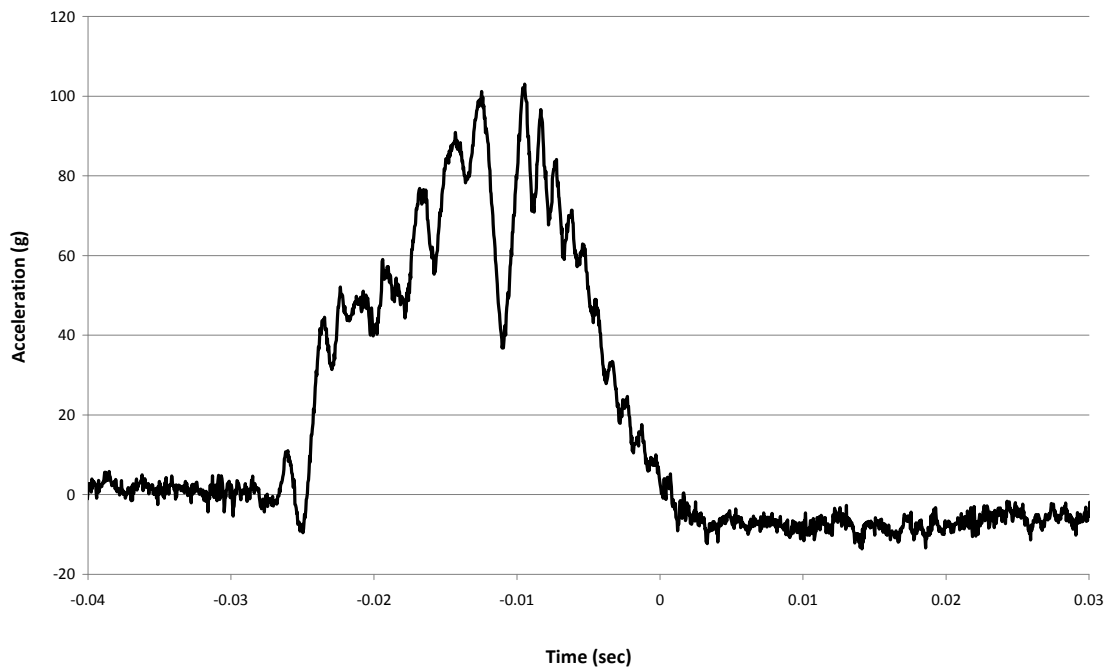
**BEA Research Reactor Package Half-Scale Free Drop Test  
Test D2R (15° Oblique), Channel 19 (Primary Impact)**



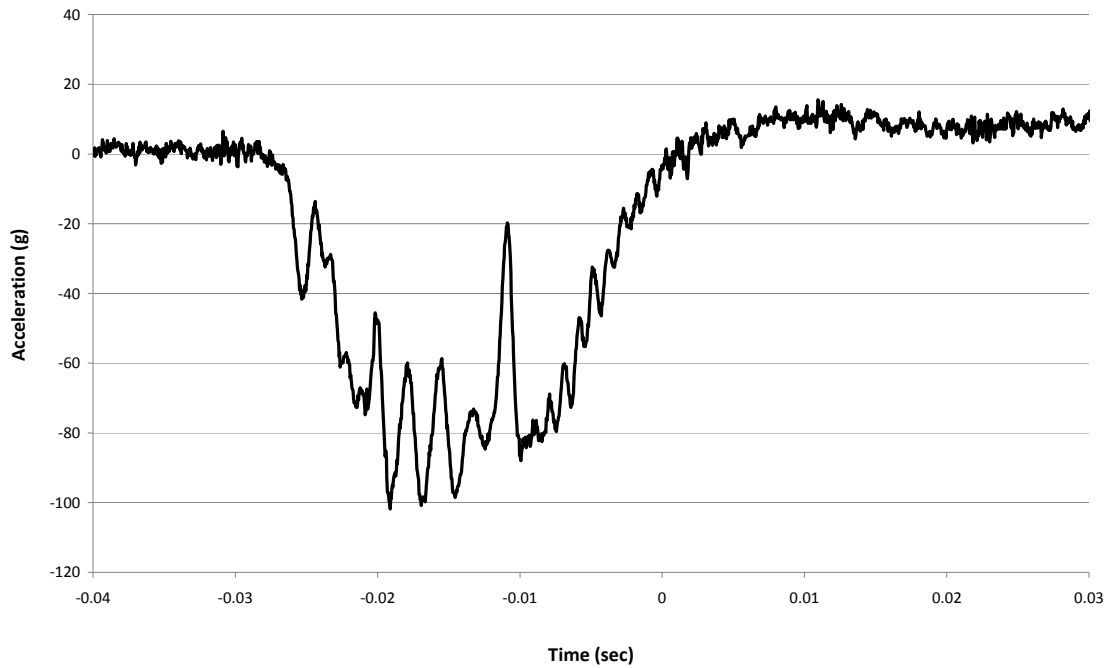
**BEA Research Reactor Package Half-Scale Free Drop Test  
Test D3 (CG Over Corner), Channel 12**



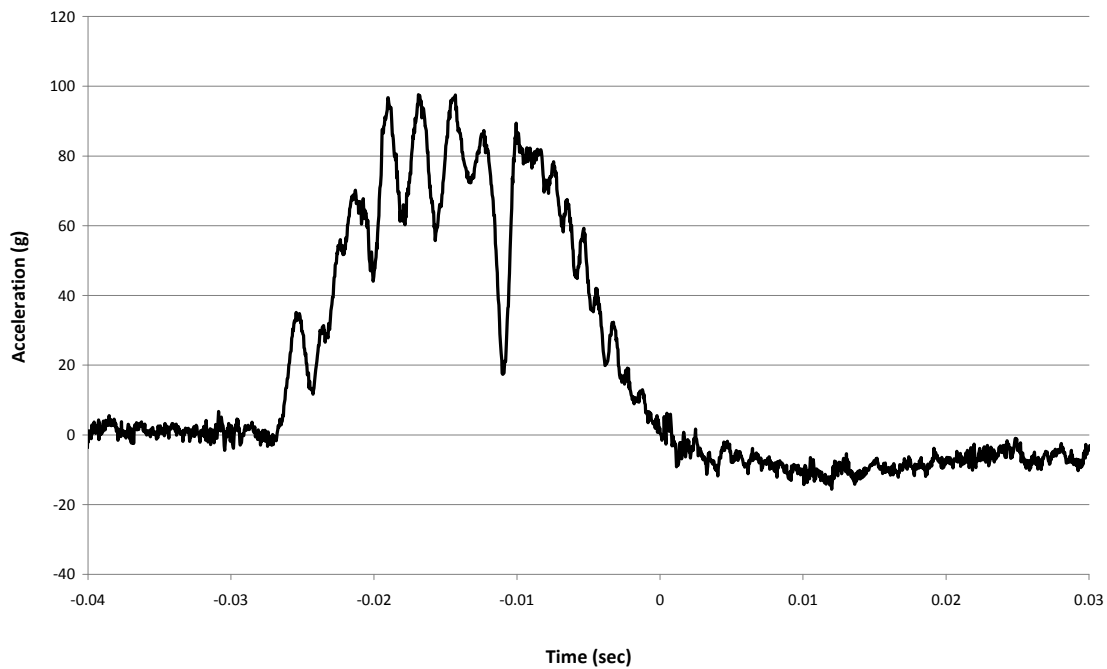
**BEA Research Reactor Package Half-Scale Free Drop Test  
Test D3 (CG Over Corner), Channel 13**



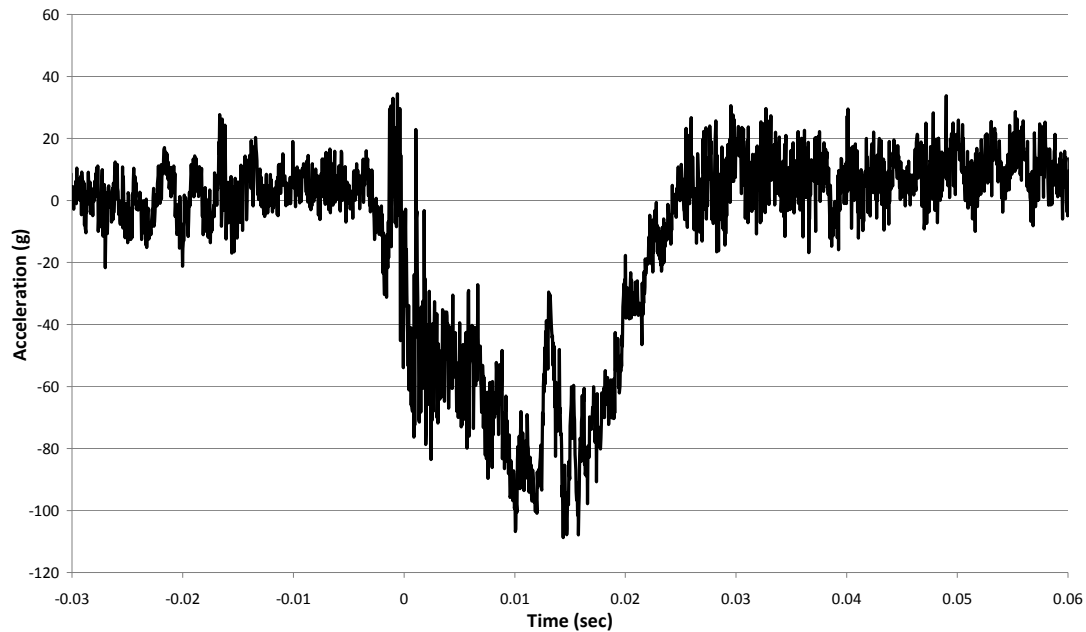
**BEA Research Reactor Package Half-Scale Free Drop Test  
Test D3 (CG Over Corner), Channel 14**



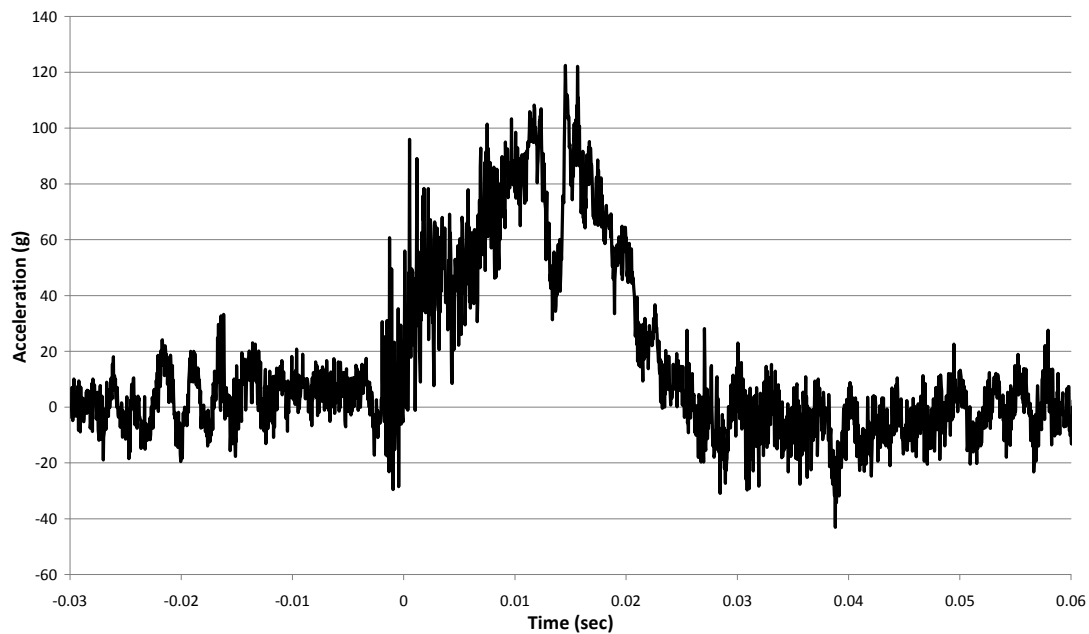
**BEA Research Reactor Package Half-Scale Free Drop Test  
Test D3 (CG Over Corner), Channel 15**

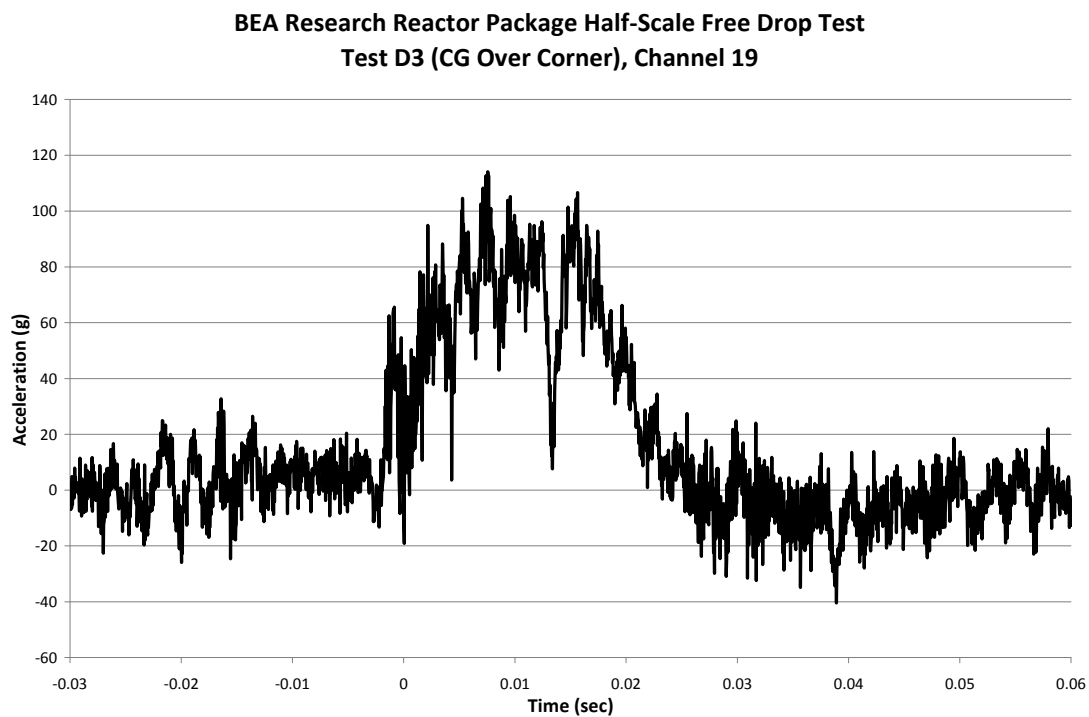
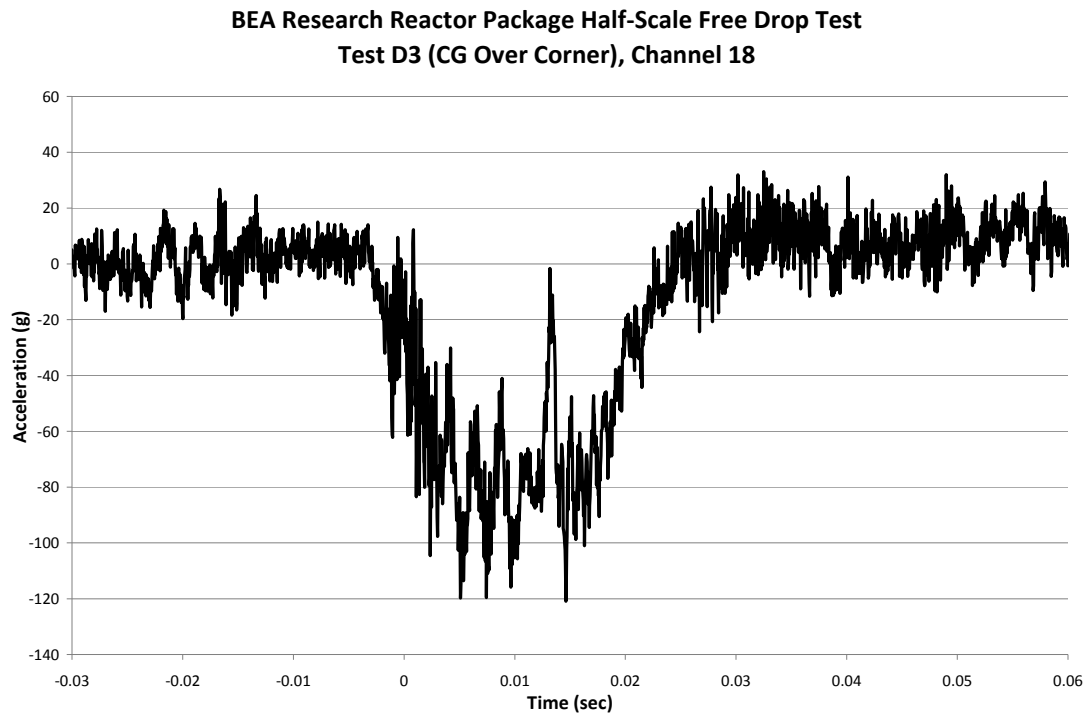


**BEA Research Reactor Package Half-Scale Free Drop Test  
Test D3 (CG Over Corner), Channel 16**



**BEA Research Reactor Package Half-Scale Free Drop Test  
Test D3 (CG Over Corner), Channel 17**







## 2.12.4 Stress Analysis Finite Element Models

This appendix describes the finite element analysis of the BRR package body. The structural components considered are the upper and lower end structures, the inner shell, and the outer shell. The shield plug, closure lid, and fuel baskets are analyzed separately. Both Normal Conditions of Transport (NCT) and Hypothetical Accident Conditions (HAC) are considered. Loading types include design pressure, thermal, and free drop impact.

### 2.12.4.1 Analysis Model Description

The finite element model of the BRR package body is used to calculate stress under NCT and HAC in the structural members of the cask, which consist of the upper and lower massive end structures, the inner shell, and the outer shell. The impact limiters, the fuel baskets, the shield plug, the thermal shield, the impact limiter attachments, and the closure lid are not modeled structurally, but their mass is accounted for as discussed below. The lead shielding material in the sides and bottom of the cask body is also not explicitly modeled, and is further discussed below. The model is built in ANSYS Revision 11.0 using half symmetry along a vertical plane through the cask center. The structural elements are SOLID95, 20-node bricks, and the thermal elements are SOLID90, 20-noded bricks. A pressure of 25 psi, corresponding to the design pressure identified in Section 2.6.1.1, *Summary of Pressures and Temperatures*, is applied to the interior surface of the model in each case. The pressure is applied to all element interior surfaces which fall within the location of the inner (containment) O-ring. The pressure creates a small net force which is reacted by forces in the opposite direction applied at the bolt circle of the closure lid. For load cases which do not include inertia forces, the model is constrained by the symmetry plane and by fixed nodes at the edge of the cask outer bottom surface. When inertia loads are applied, the model constraint is individually discussed in the following sections. The finite element mesh is shown in Figure 2.12.4-1.

### 2.12.4.2 Loading of the Model

Besides the design pressure discussed above, the model is loaded by thermal loads and by free drop impact loads.

#### 2.12.4.2.1 Thermal Loads

A detailed thermal analysis is performed in Chapter 3, *Thermal Evaluation*. The thermal analysis performed using the model described in this section is done only to transform the thermal results obtained in Chapter 3 into the form required by the stress analysis model. This is done by assigning selected key nodal temperatures taken from the Chapter 3 analysis, and running the thermal/stress model described in this section using thermal elements (SOLID90) to obtain temperatures at each node of the model. The location of the key nodes at which the Chapter 3 NCT temperatures were transferred directly to the thermal/stress model are shown in Figure 2.12.4-2. Convection and radiation are set to zero. Thermal conductivity is a required SOLID90 input but does not affect the result and is therefore set to an arbitrary value of 1. The resulting temperature distribution is essentially the same as that obtained in Chapter 3, and is shown in Figure 2.12.4-3. The nodal temperatures are used in the stress analysis along with temperature-dependent coefficients of thermal expansion taken from Table 2.2-1 and Table 2.2-2 to obtain thermal stress.

Another source of thermal loading is the lead gamma shield used in the annulus between the inner and outer shells. Due to different thermal expansion coefficients, the lead gamma shielding applies a radial pressure to the outer surface of the inner shell under NCT hot conditions. As shown in Section 2.6.1.2.3, *Lead*, this pressure can be assigned an upper bound value of 350 psi. For the NCT hot case, this pressure is applied to the inner shell outer surface over the entire length of the side lead cavity. The treatment of lead in load cases which include free drop impact loads is discussed below.

#### 2.12.4.2.2 Free Drop Impact Loads

Stress is generated in the BRR cask body in a free drop impact through self weight of the components and the applied loads of components not modeled. The resulting forces are reacted over the interface areas of the impact limiter(s). A bounding impact deceleration field of 40g is applied for the NCT cases as discussed in Section 2.6.7, *Free Drop*, and 120g is applied for the HAC cases as discussed in Section 2.7.1, *Free Drop*. As shown in Section 2.7.1, the governing orientations for stress analysis are the end drop (top end down and bottom end down), and the side drop.

The weight of the shield plug, fuel basket, closure lid, and the impact limiter not in contact with the ground (e.g., the one on top in an end drop) are accounted for by applying pressure to the region of contact. The applied load is equal to the weight of the component multiplied by the appropriate impact g-load, divided by the contact area. Component weights are taken from Table 2.1-2, (half of these values are used for half symmetry) and the contact areas are calculated using the drawings in Appendix 1.3.3, *Packaging General Arrangement Drawings*. The density of stainless steel is 0.29 lb/in<sup>3</sup>. The weight of the thermal shield and impact limiter attachments is included in the cask body model by a slight adjustment of the material density.

The lead gamma shielding is not explicitly modeled. Instead, for simplicity and conservatism, it is treated as a liquid material, thus applying a hydrostatic pressure within the side and lower lead cavities. The magnitude of the pressure is:

$$p = \gamma gh$$

where the pressure at any point,  $p$ , is applied on the side and lower surfaces of the lead cavity,  $g$  is the acceleration of gravity,  $h$  is the depth of the lead, and  $\gamma$  is the density of lead, equal to 0.41 lb/in<sup>3</sup>. Due to the conservatism of this assumption, it is not necessary to additionally apply the lead thermal load of 350 psi (see Section 2.12.4.2.1, *Thermal Loads*) to any free drop load cases.

Once all of the impact loads have been applied, the model is constrained at a minimum number of nodes for stability. The impact limiter support loads are then adjusted until near-perfect balance is achieved between the applied loads (inertia loads of the cask structure, lead, and separate components) and the impact reaction (the impact limiter). In each case, the total reaction force is essentially equal to the total decelerated weight (i.e., total weight of the BRR package, less the weight of the limiter(s) contacting the ground) times 40 (NCT) or 120 (HAC). Greater detail on the application of the inertia loads, the lead hydrostatic pressure loads, and the displacement constraints is provided in the sections discussing each load case.

These analyses do not include a dynamic load factor (DLF), since the impact acceleration used is nearly 50 % higher than the maximum test result (see Section 2.12.5.3, *Reconciliation with Certification Test Results*), and because the cask structures are relatively stiff, which would result in a DLF not significantly different from unity.

#### 2.12.4.3 Material Properties

For load cases that do not evaluate thermal stress, the modulus of elasticity is evaluated at the bounding NCT hot temperature of 250 °F, or  $E = 27.3 \times 10^6$  psi from Table 2.6-1. Poisson's ratio is equal to 0.3. For load cases in which thermal stress is included, both the modulus of elasticity and the thermal expansion coefficient are evaluated at the nodal temperatures determined in the thermal run, using data from Table 2.2-1 and Table 2.2-2. All allowable stresses are evaluated at the NCT hot temperature of 250 °F.

#### 2.12.4.4 Load Cases and Allowable Stress

Load cases are identified which allow the evaluation of the model stresses using the allowable stresses defined in Table 2.1-1. For NCT, numerical values of allowable stress are taken from Table 2.6-1 for a temperature of 250 °F. The primary membrane ( $P_m$ ) allowable stress is  $S_m$ , which is equal to 20,000 psi. The primary membrane plus bending ( $P_m + P_b$ ) stress allowable is  $1.5S_m$ , or 30,000 psi, and the primary plus bending plus secondary ( $P_m + P_b + Q$ ) stress allowable is  $3.0S_m$ , or 60,000 psi.

For HAC, the numerical values depend on the value of  $S_u$ , which is smaller for the forged or cast materials used for the upper and lower end structures and the inner shell (see Table 2.2-2). At a temperature of 250 °F, the minimum value of  $S_u = 64,050$  psi. The primary membrane ( $P_m$ ) allowable stress is the lesser of  $2.4S_m$  or  $0.7S_u$ , or a minimum of 44,835 psi. The primary membrane plus bending ( $P_m + P_b$ ) stress allowable is the lesser of  $3.6S_m$  or  $S_u$ , or a minimum of 64,050 psi.

Because, in the NCT cases, the resulting stresses are relatively low and it is not necessary to separately identify the membrane stress. Therefore the margin of safety may be conservatively determined by applying the maximum stress intensity to the primary membrane stress allowable.

For the HAC cases, the maximum stress resulting from the model is evaluated by decoupling the primary stress from bending and secondary stress. Thus, in each HAC case, the stresses are linearized to distinguish between the decoupled stresses and separate allowables are applied.

The load cases and allowable stresses are listed in the following table. Note: the design pressure of 25 psig is present in all load cases.

Case No.	Section No.	Description	Stress Evaluated
1	2.12.4.4.1	Design pressure only	Primary
2	2.12.4.4.2	Lead shrinkage pressure with thermal	Secondary
3	2.12.4.4.3	NCT bottom-down end drop	Primary
4	2.12.4.4.4	NCT bottom-down end drop with thermal	Secondary
5	2.12.4.4.5	HAC bottom-down end drop	Primary
6	2.12.4.4.6	NCT top-down end drop	Primary
7	2.12.4.4.7	NCT top-down end drop with thermal	Secondary
8	2.12.4.4.8	HAC top-down end drop	Primary
9	2.12.4.4.9	NCT side drop	Primary
10	2.12.4.4.10	NCT side drop with thermal	Secondary
11	2.12.4.4.11	HAC side drop	Primary

#### 2.12.4.4.1 Case No. 1, Design Pressure Only

In this case, the only applied load is the design pressure of 25 psig, applied to the interior of the cask body at a radius less than or equal to that of the inner (containment) O-ring. The design pressure loading is shown in Figure 2.12.4-4. The model is constrained by the symmetry plane and by nodes at the outer edge of the cask bottom surface.

Results are shown in Figure 2.12.4-5. The maximum stress intensity is 281 psi at the midpoint of the payload cavity bottom. Conservatively using the NCT membrane stress allowable of 20,000 psi, the margin of safety is:

$$MS = \frac{20,000}{281} - 1 = +70.2$$

#### 2.12.4.4.2 Case No. 2, Lead Shrinkage Pressure With Thermal

Case No. 2 starts with the 25 psig pressure of Case No. 1 and adds the lead shrinkage pressure to the outside surface of the inner shell, all along the side lead cavity. In addition, thermal stress is calculated using the NCT hot case temperatures and temperature dependent coefficients of thermal expansion. Both of these loads are described in Section 2.12.4.2.1, *Thermal Loads*. The model is constrained by the symmetry plane and by nodes at the outer edge of the cask bottom surface.

Results are shown in Figure 2.12.4-6. The maximum stress intensity is 6,933 psi at the top of the inner shell cross section. Since this result includes secondary stress, the allowable is 60,000 psi. The margin of safety is:

$$MS = \frac{60,000}{6,933} - 1 = +7.65$$

**BRR Package Safety Analysis Report****2.12.4.4.3 Case No. 3, NCT Bottom-Down End Drop**

In this case, the applied loads are the design pressure from Case No. 1 and the free drop weight of the shield plug, fuel basket, closure lid, and impact limiter. The free drop loads are described in Section 2.12.4.2.2, *Free Drop Impact Loads*. The cask body orientation is vertical, with the bottom end down. The weight of the side lead applies a hydrostatic pressure based on depth as described in Section 2.12.4.2.2. The weight of the lower lead is modeled as two separate hydrostatic loads based the inner and outer lead columns above the upper surface of the lower closure plate. The bottom-down end drop loading is shown in Figure 2.12.4-7. The model is constrained by the symmetry plane and by nodes at the outer edge of the cask bottom surface.

Results are shown in Figure 2.12.4-8. The maximum stress intensity is 15,202 psi at the outside surface of the bottom end structure. Conservatively using the NCT membrane stress allowable of 20,000 psi, the margin of safety is:

$$MS = \frac{20,000}{15,202} - 1 = +0.32$$

**2.12.4.4.4 Case No. 4, NCT Bottom-Down End Drop With Thermal**

Case No. 4 adds the thermal loading described in Section 2.12.4.2.1, *Thermal Loads*, to Case No. 3.

Results are shown in Figure 2.12.4-9. The maximum stress intensity is 14,586 psi at the top of the inner shell cross section. Since this result includes secondary stress, the allowable is 60,000 psi. The margin of safety is:

$$MS = \frac{60,000}{14,586} - 1 = +3.11$$

**2.12.4.4.5 Case No. 5, HAC Bottom-Down End Drop**

Case No. 5 is the same as Case No. 3, except with an HAC inertia field of 120g.

Results are shown in Figure 2.12.4-10. The maximum stress intensity is 45,681 psi at the outside surface of the bottom end structure. In the prior NCT load cases, the membrane allowable has been conservatively applied to the maximum stress intensity, which makes it unnecessary to differentiate the actual membrane stress from the membrane plus bending stress. Since this is an HAC case, the less conservative approach is applied; the stress is linearized through the lower massive end structure cross section. Results are shown in Figure 2.12.4-11. The maximum primary membrane stress is 22,680 psi. The HAC membrane stress allowable is 44,835 psi. The margin of safety is:

$$MS = \frac{44,835}{22,680} - 1 = +0.98$$

The maximum membrane plus bending stress is 43,080 psi. The HAC membrane plus bending stress allowable is 64,050. The margin of safety is:

$$MS = \frac{64,050}{43,080} - 1 = +0.49$$

**2.12.4.4.6 Case No. 6, NCT Top-Down End Drop**

In this case, the weight of the shield plug, fuel basket and closure lid are modeled as forces located at the lid bolt circle. The shield plug is modeled as a pressure distributed on the impact limiter contact area. Design pressure is applied as in Case No. 1. The cask body orientation is vertical, with the top end down. The weight of the side lead applies a hydrostatic pressure based on depth as described in Section 2.12.4.2.2, *Free Drop Impact Loads*. The weight of the lower lead is modeled as two separate hydrostatic loads based the inner and outer lead columns above the upper and lower shelves of the lower lead cavity. The top-down end drop loading is shown in Figure 2.12.4-12. The model is constrained by the symmetry plane and by nodes at the outer edge of the cask top surface.

Results are shown in Figure 2.12.4-13. The maximum stress intensity is 13,248 psi at the top of the inner shell. Conservatively using the NCT membrane stress allowable of 20,000 psi, the margin of safety is:

$$MS = \frac{20,000}{13,248} - 1 = +0.51$$

**2.12.4.4.7 Case No. 7, NCT Top-Down End Drop With Thermal**

Case No. 7 adds the thermal loading described in Section 2.12.4.2.1, *Thermal Loads*, to Case No. 6.

Results are shown in Figure 2.12.4-14. The maximum stress intensity is 13,258 psi at the top of the inner shell. Since this result includes secondary stress, the allowable is 60,000 psi. The margin of safety is:

$$MS = \frac{60,000}{13,258} - 1 = +3.53$$

**2.12.4.4.8 Case No. 8, HAC Top-Down End Drop**

Case No. 8 is the same as Case No. 6, except with an HAC inertia field of 120g.

Results are shown in Figure 2.12.4-15. The maximum stress intensity is 40,140 psi at the top of the inner shell. In this HAC case, the stress is linearized, through the line of highest stress intensity in the top inner shell cross section. The linearized results are shown in Figure 2.12.4-16. The maximum primary membrane stress is 22,720 psi. The HAC membrane stress allowable is 44,835 psi. The margin of safety is:

$$MS = \frac{44,835}{22,720} - 1 = +0.97$$

The maximum membrane plus bending stress is 33,400 psi. The HAC membrane plus bending stress allowable is 64,050. The margin of safety is:

$$MS = \frac{64,050}{33,400} - 1 = +0.92$$

**BRR Package Safety Analysis Report****2.12.4.4.9 Case No. 9, NCT Side Drop**

In this case, the applied loads are the design pressure from Case No. 1 and the free drop weight of the shield plug, fuel basket, and closure lid. The applied loads and supporting pressures are applied as pressures over an included angle of 30°, which represents the circumferential extent of contact. The cask body orientation is horizontal. The weight of the side and bottom lead shields are modeled as a hydrostatic pressures as described in Section 2.12.4.2.2, *Free Drop Impact Loads*. The side drop loading is shown in Figure 2.12.4-17 and Figure 2.12.4-18. The model is constrained by the symmetry plane and by two nodes at the top and bottom of the cask and one node at the top to constrain radial and axial motion respectively.

Results are shown in Figure 2.12.4-19. The maximum stress intensity is 18,935 psi at the bottom outside edge of the lower lead cavity. Conservatively using the NCT membrane stress allowable of 20,000 psi, the margin of safety is:

$$MS = \frac{20,000}{18,935} - 1 = +0.06$$

**2.12.4.4.10 Case No. 10, NCT Side Drop With Thermal**

Case No. 10 adds the thermal loading described in Section 2.12.4.2.1, *Thermal Loads*, to Case No. 9.

Results are shown in Figure 2.12.4-20. The maximum stress intensity is 22,704 psi at the shield plug shelf. Since this result includes secondary stress, the allowable is 60,000 psi. The margin of safety is:

$$MS = \frac{60,000}{22,704} - 1 = +1.64$$

**2.12.4.4.11 Case No. 11, HAC Side Drop**

Case No. 11 is the same as Case No. 9, except with an HAC inertia field of 120g.

Results are shown in Figure 2.12.4-21. The maximum stress intensity is 56,810 psi at the bottom outside edge of the lower lead cavity. The stress, as in prior HAC cases, is linearized through the lower closure plate cross section. Results are shown in Figure 2.12.4-22. The maximum primary membrane stress is 16,330 psi. The HAC membrane stress allowable is 44,835 psi. The margin of safety is:

$$MS = \frac{44,835}{16,330} - 1 = +1.75$$

The maximum membrane plus bending stress is 51,990 psi. The HAC membrane plus bending stress allowable is 64,050. The margin of safety is:

$$MS = \frac{64,050}{51,990} - 1 = +0.23$$

**2.12.4.5 Summary**

Table 2.12.4-1 summarizes the margins of safety of the BRR package finite element analysis, as established in the sections above. Since all margins of safety are positive, the structural

components considered (the upper and lower end structures, the inner shell, and the outer shell) are not of concern.



**Table 2.12.2-1 – Finite Element Analysis Results**

<b>Analysis Description</b>	<b>Reference Section</b>	<b>Margin of Safety</b>
Case No. 1, Design Pressure Only	2.12.4.4.1	+ 70.2
Case No. 2, Lead Shrinkage Pressure With Thermal	2.12.4.4.2	+ 7.65
Case No. 3, NCT Bottom-Down End Drop	2.12.4.4.3	+ 0.32
Case No. 4, NCT Bottom-Down End Drop With Thermal	2.12.4.4.4	+ 3.11
Case No. 5, HAC Bottom-Down End Drop	2.12.4.4.5	+ 0.49 <sup>①</sup>
Case No. 6, NCT Top-Down End Drop	2.12.4.4.6	+ 0.51
Case No. 7, NCT Top-Down End Drop With Thermal	2.12.4.4.7	+ 3.53
Case No. 8, HAC Top-Down End Drop	2.12.4.4.8	+ 0.92 <sup>①</sup>
Case No. 9, NCT Side Drop	2.12.4.4.9	+ 0.06
Case No. 10, NCT Side Drop With Thermal	2.12.4.4.10	+ 1.64
Case No. 11, HAC Side Drop	2.12.4.4.11	+ 0.23 <sup>①</sup>

Notes:

1. Minimum value shown.

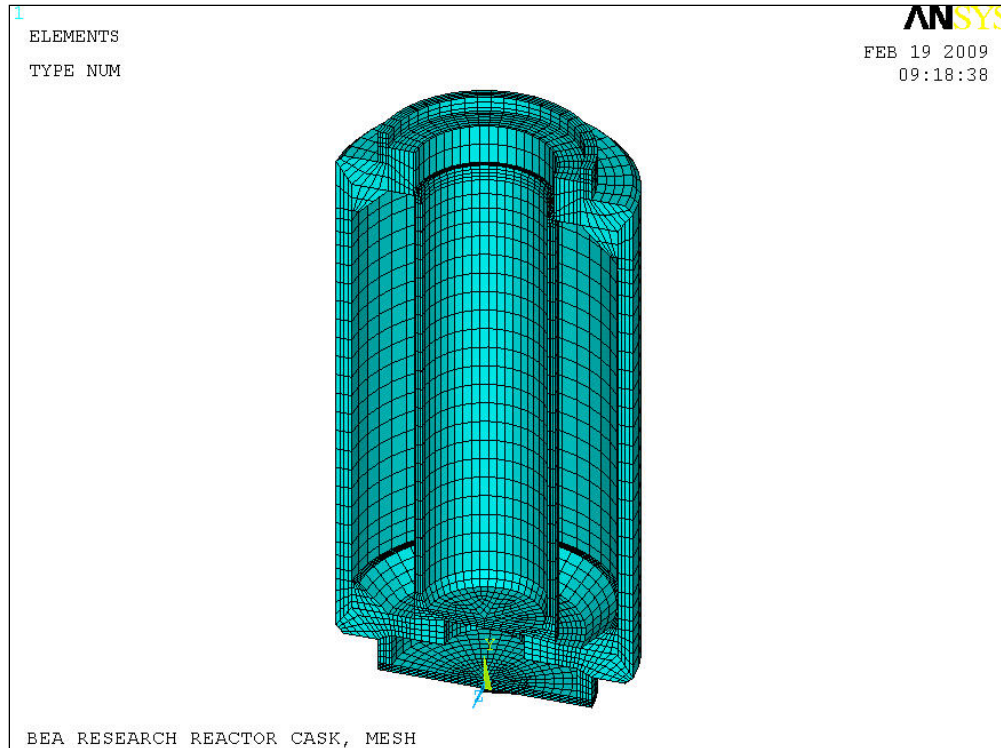


Figure 2.12.4-1 – Finite Element Mesh

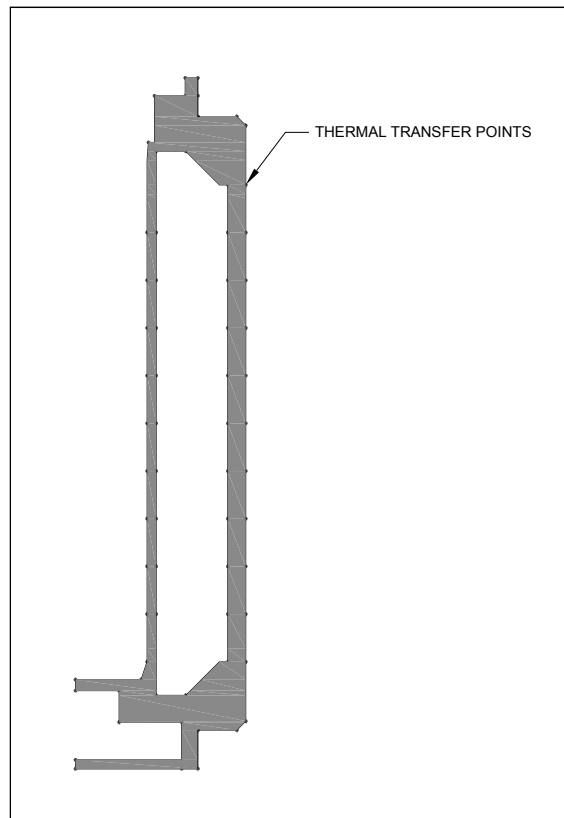


Figure 2.12.4-2 – Thermal Transfer Points

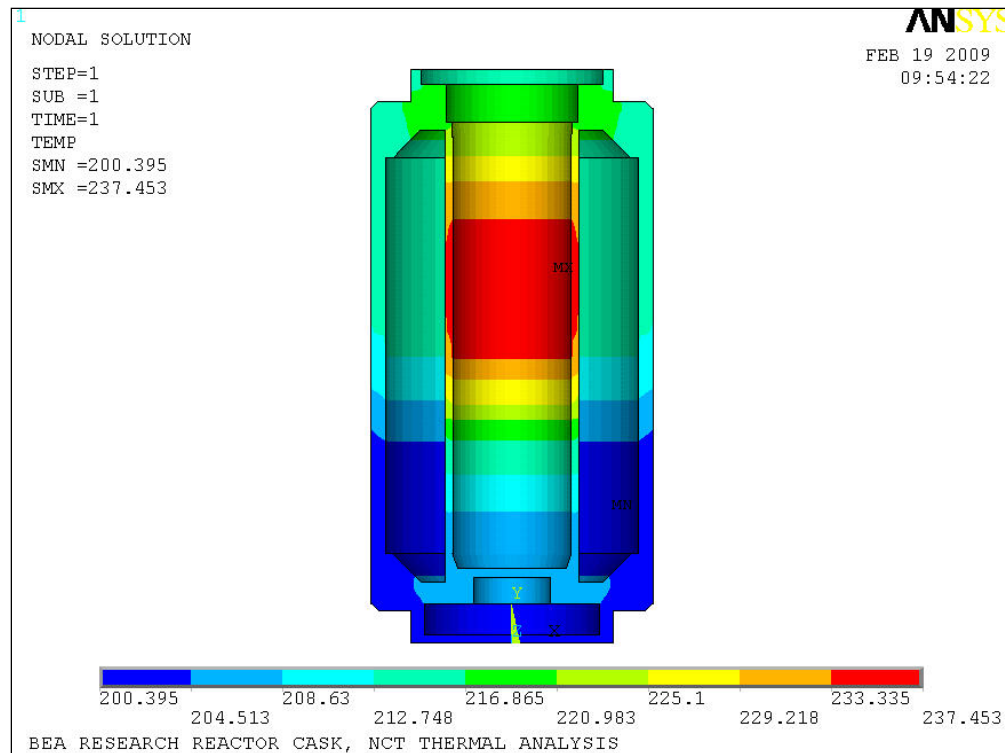


Figure 2.12.4-3 – Temperature Distribution

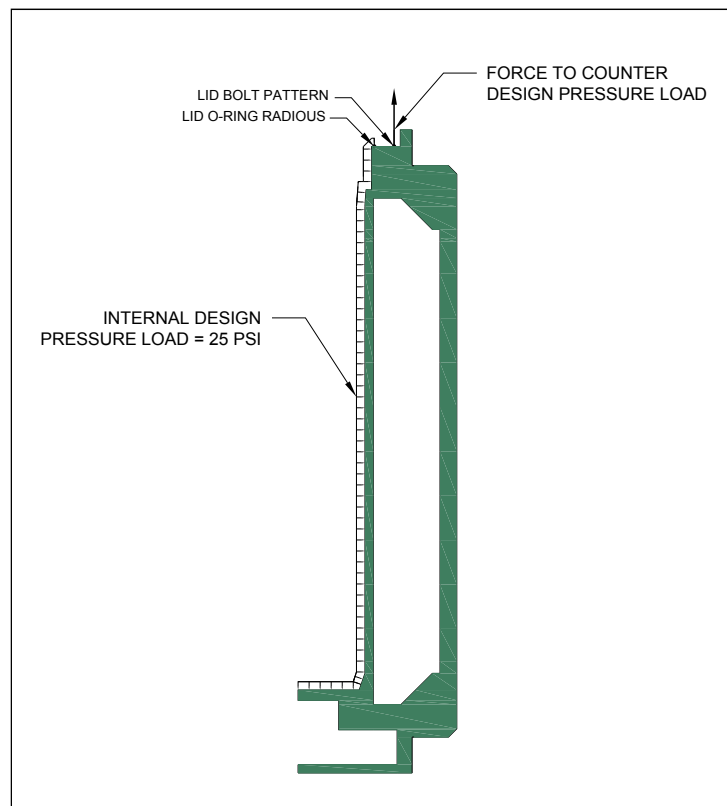


Figure 2.12.4-4 – Design Pressure Loading

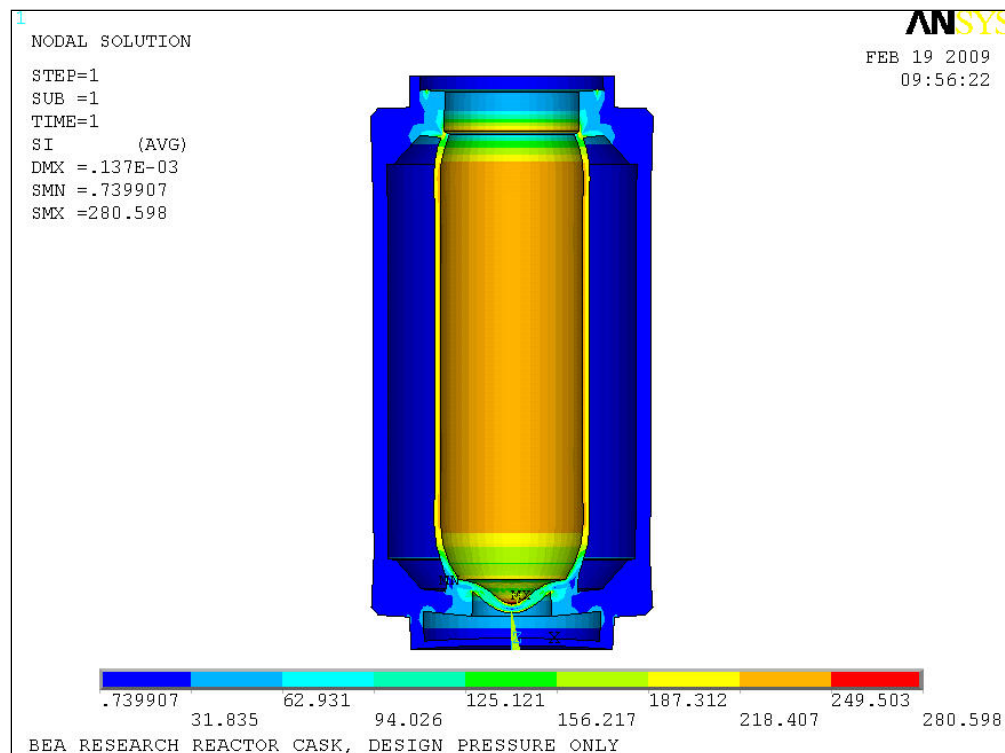


Figure 2.12.4-5 – Internal Pressure Only

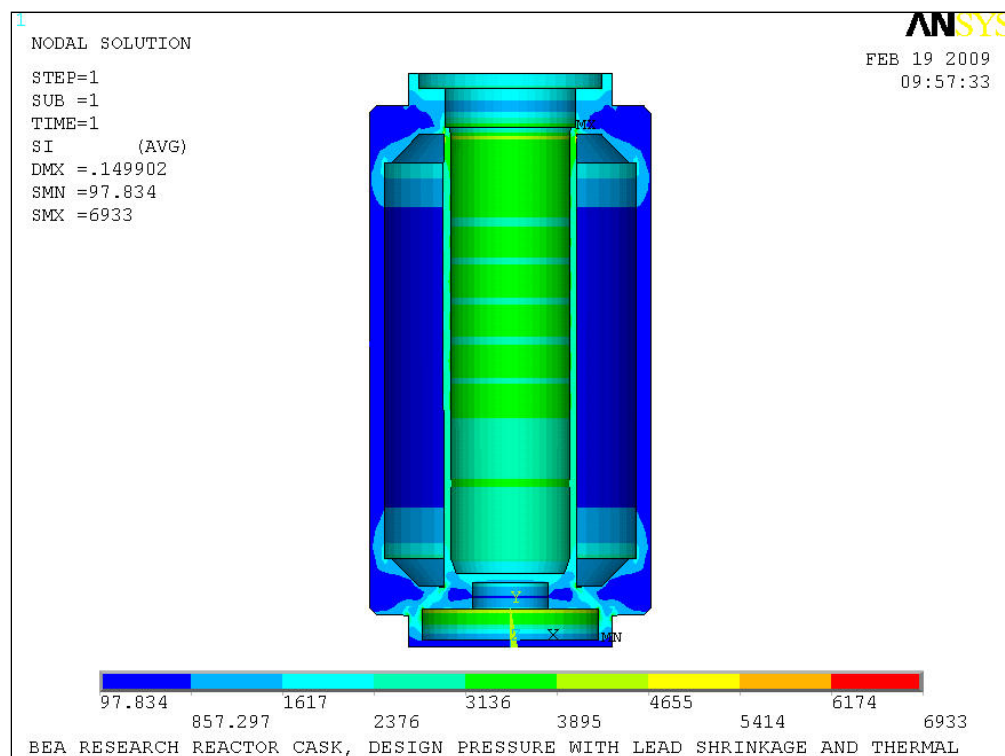


Figure 2.12.4-6 – Lead Shrinkage Pressure With Thermal

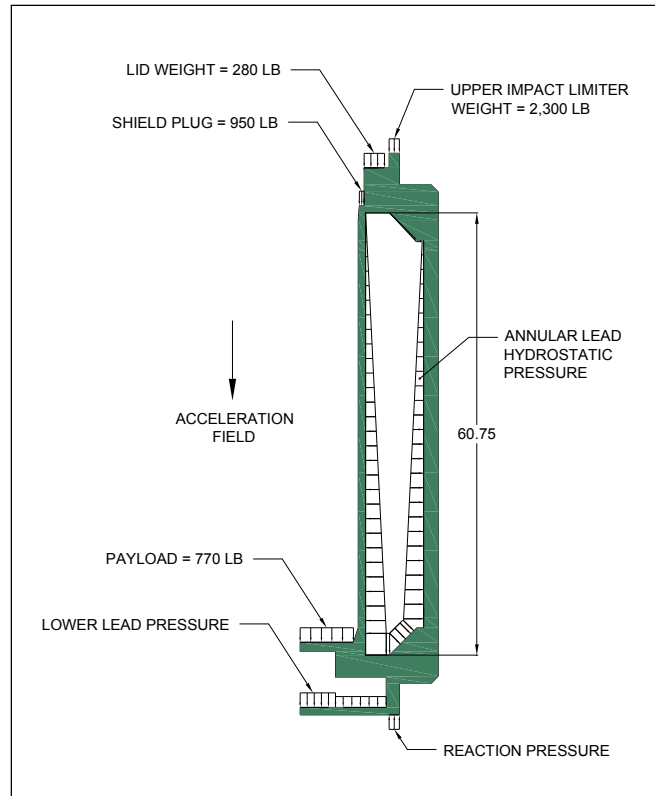


Figure 2.12.4-7 –Bottom-Down End Drop Loading

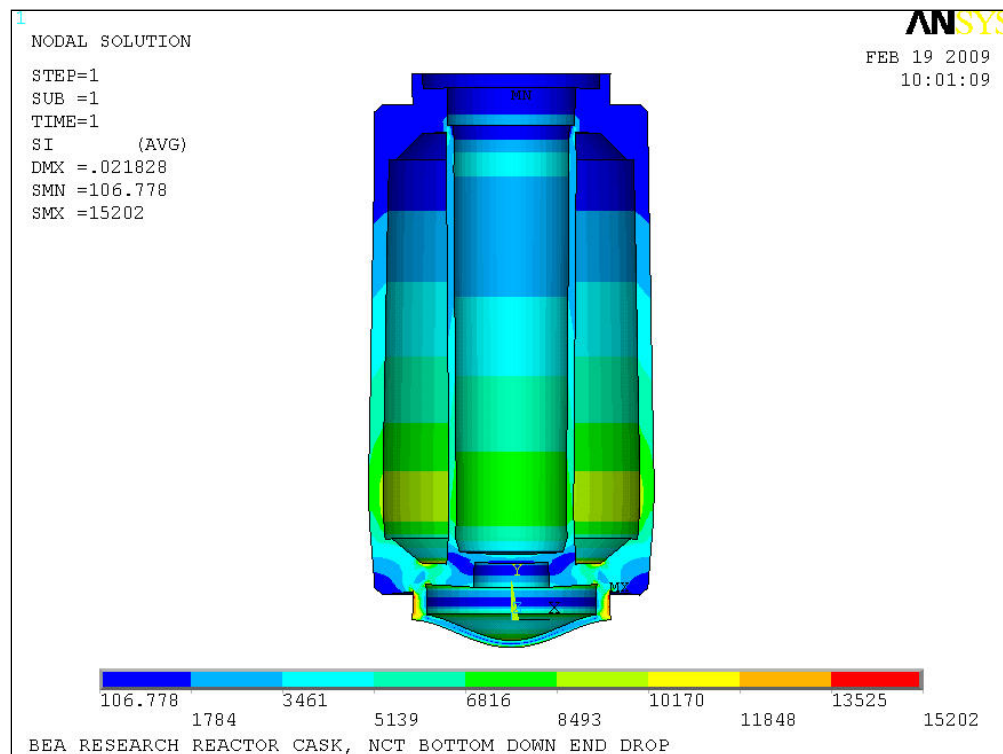


Figure 2.12.4-8 – NCT Bottom-Down End Drop

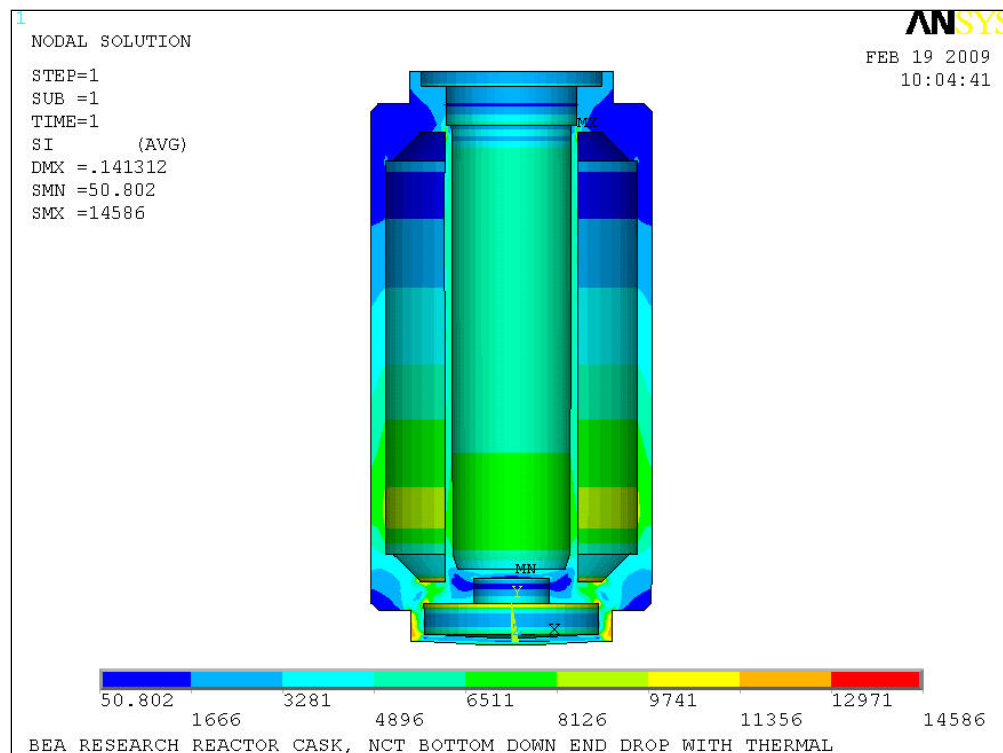


Figure 2.12.4-9 – NCT Bottom-Down End Drop With Thermal

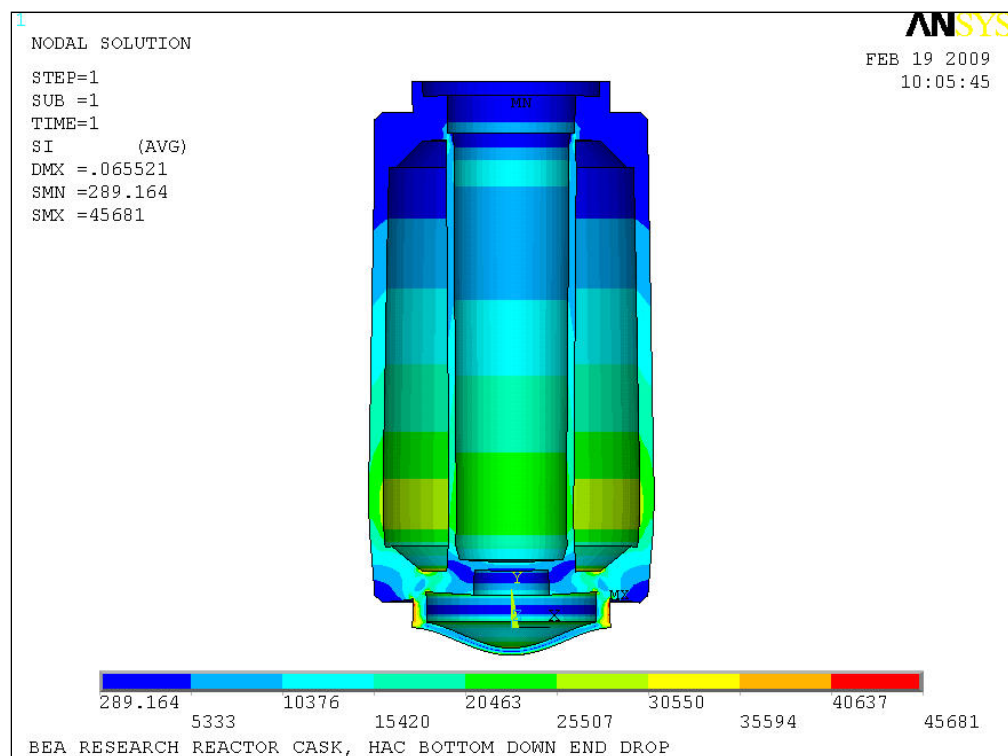


Figure 2.12.4-10 – HAC Bottom-Down End Drop

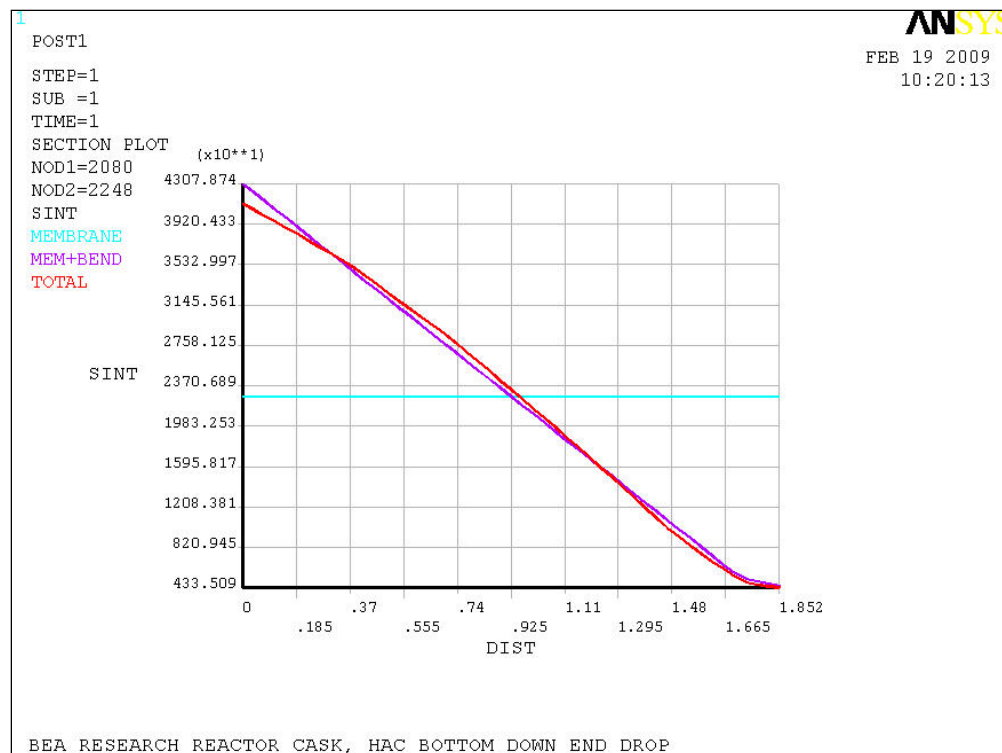


Figure 2.12.4-11 – HAC Bottom-Down End Drop Linearized Stress

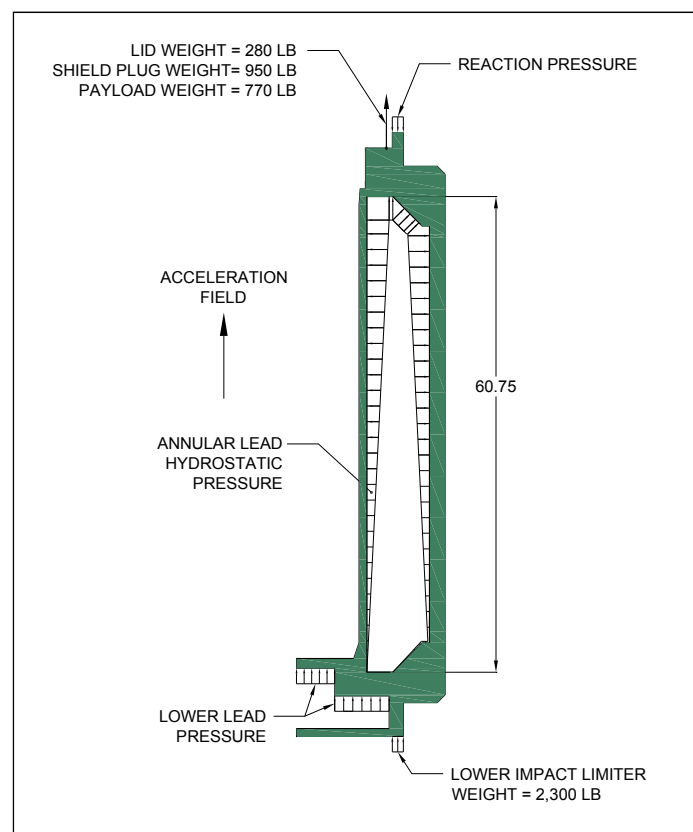


Figure 2.12.4-12 –Top-Down End Drop Loading

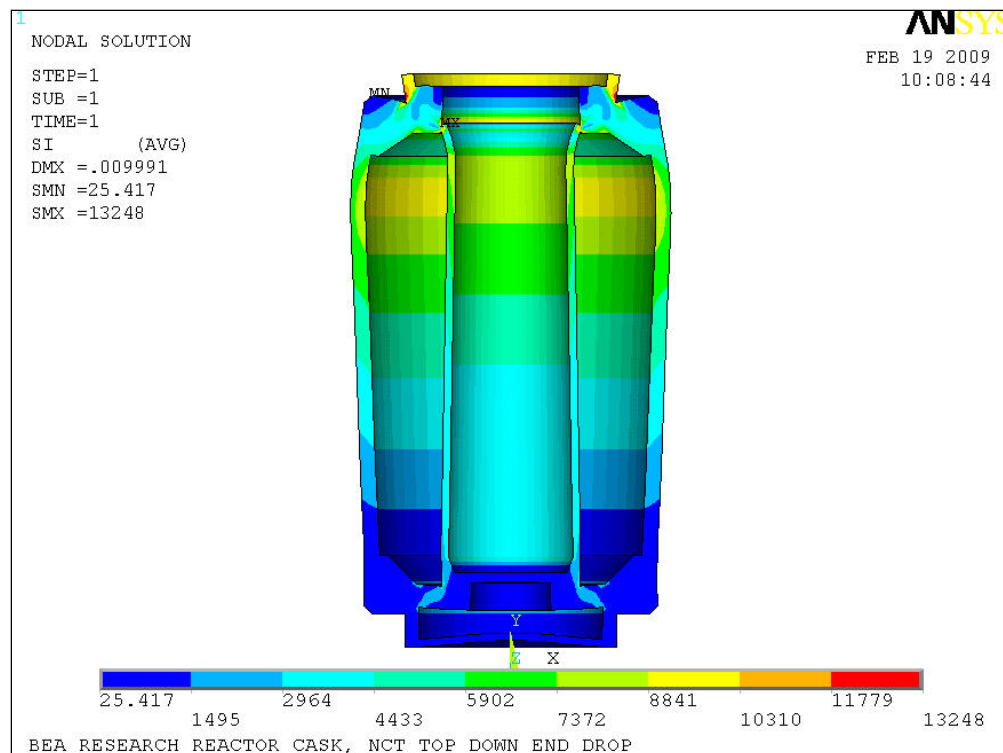


Figure 2.12.4-13 – NCT Top-Down End Drop

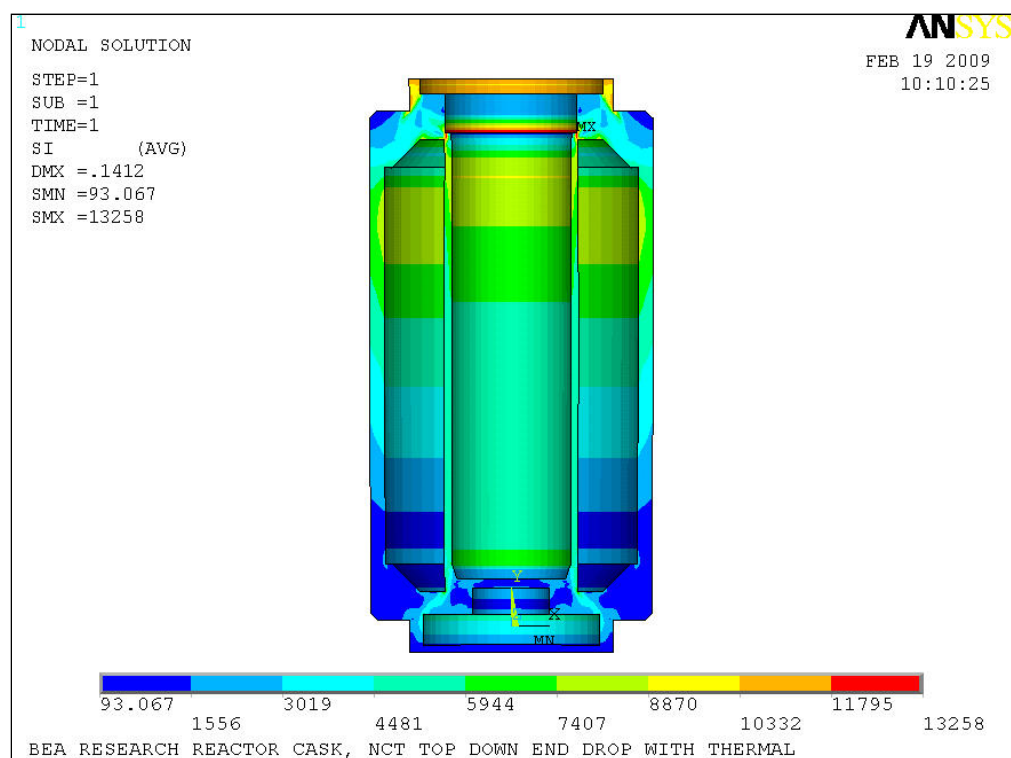


Figure 2.12.4-14 – NCT Top-Down End Drop With Thermal



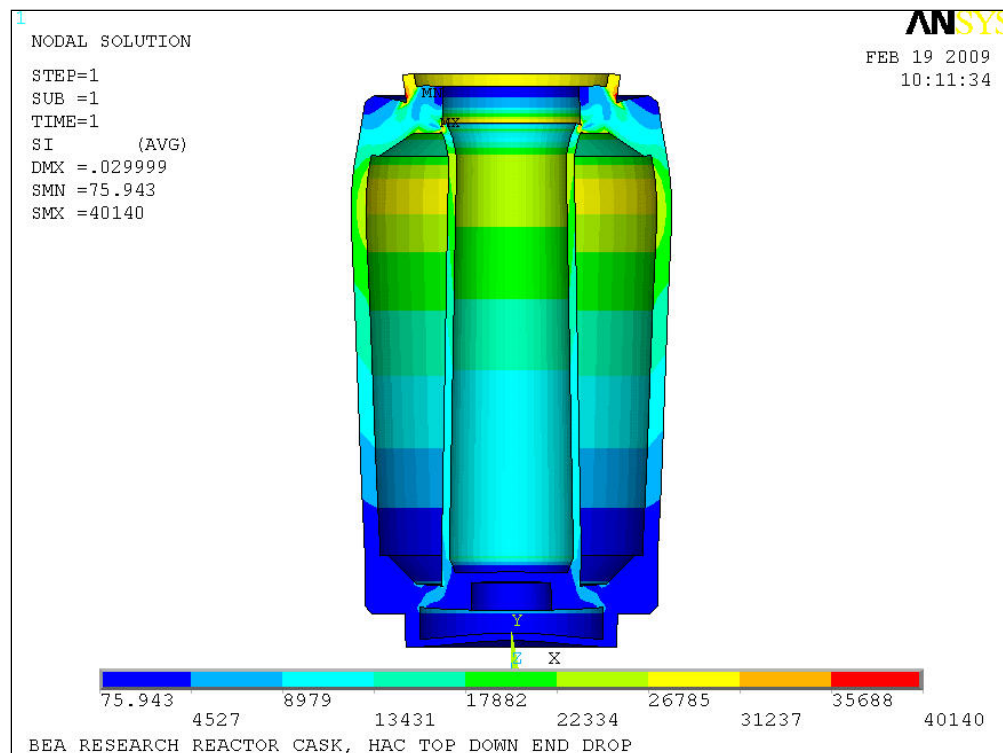


Figure 2.12.4-15 – HAC Top-Down End Drop

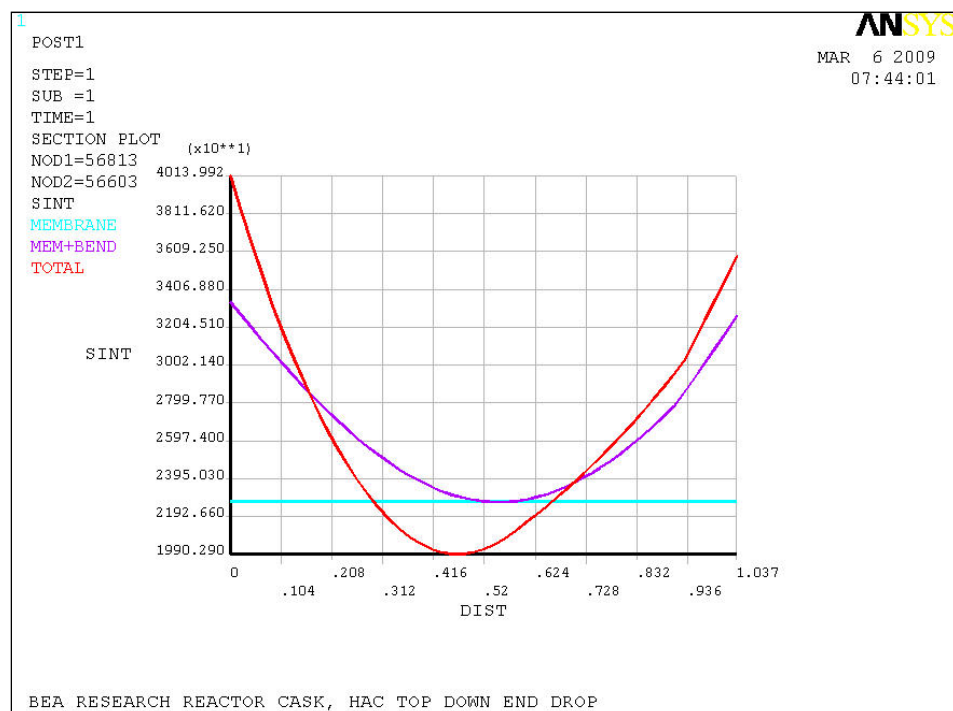


Figure 2.12.4-16 – HAC Top-Down End Drop Linearized Stress

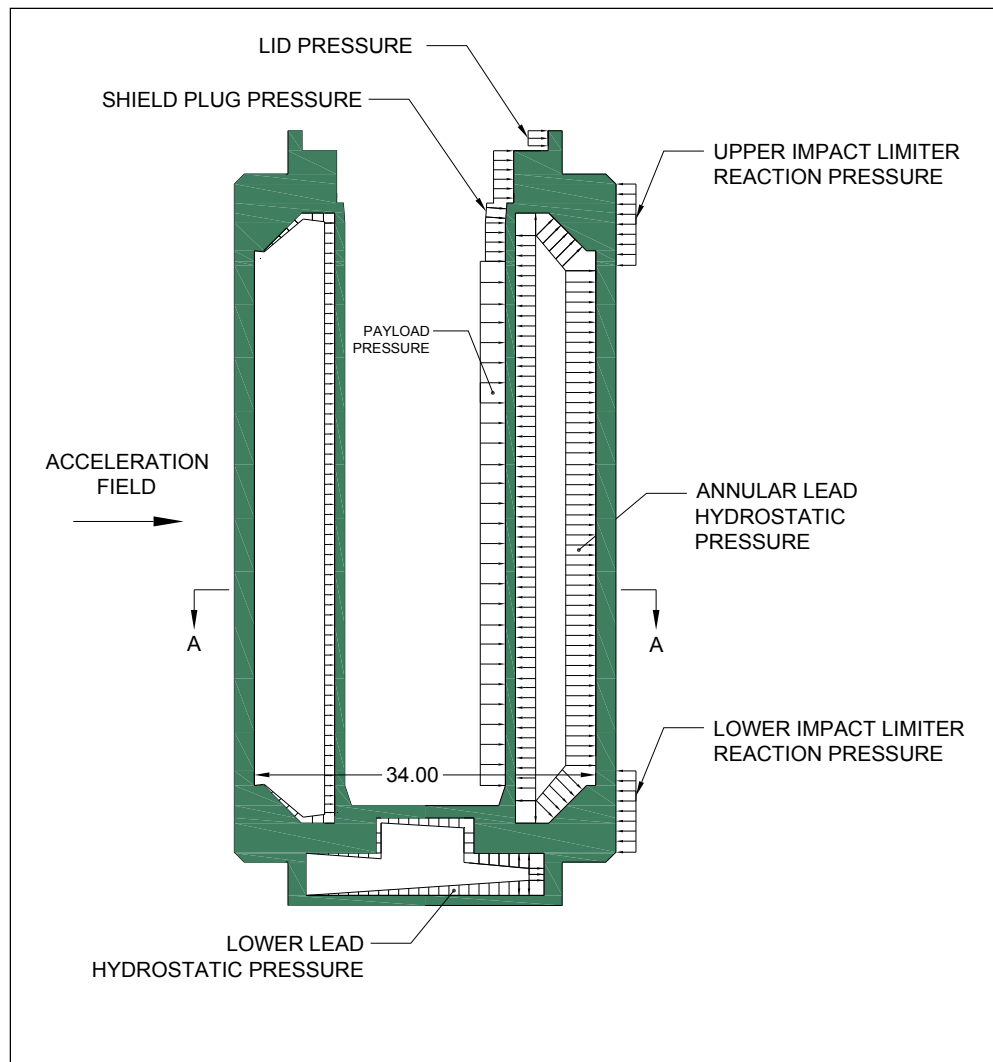


Figure 2.12.4-17 – NCT Side Drop Loading

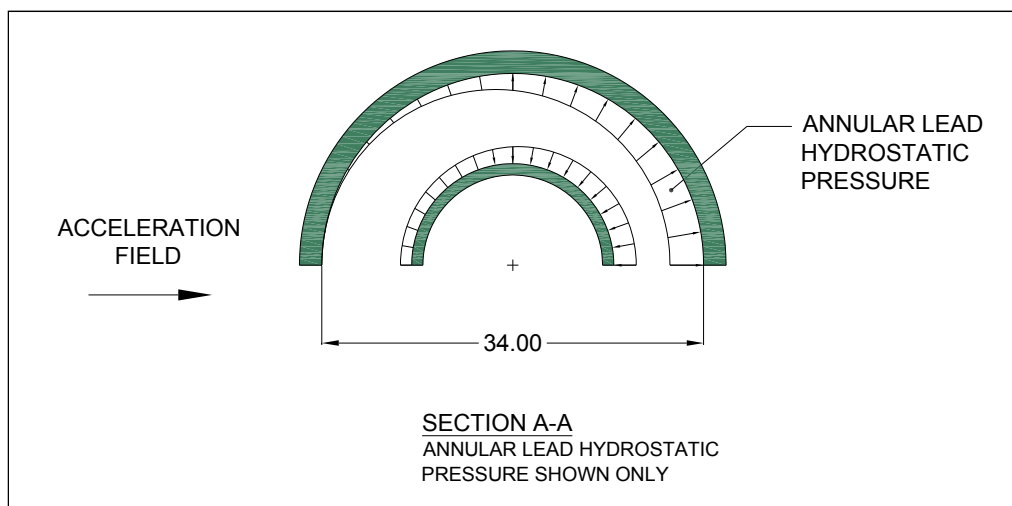


Figure 2.12.4-18 – NCT Side Drop Loading

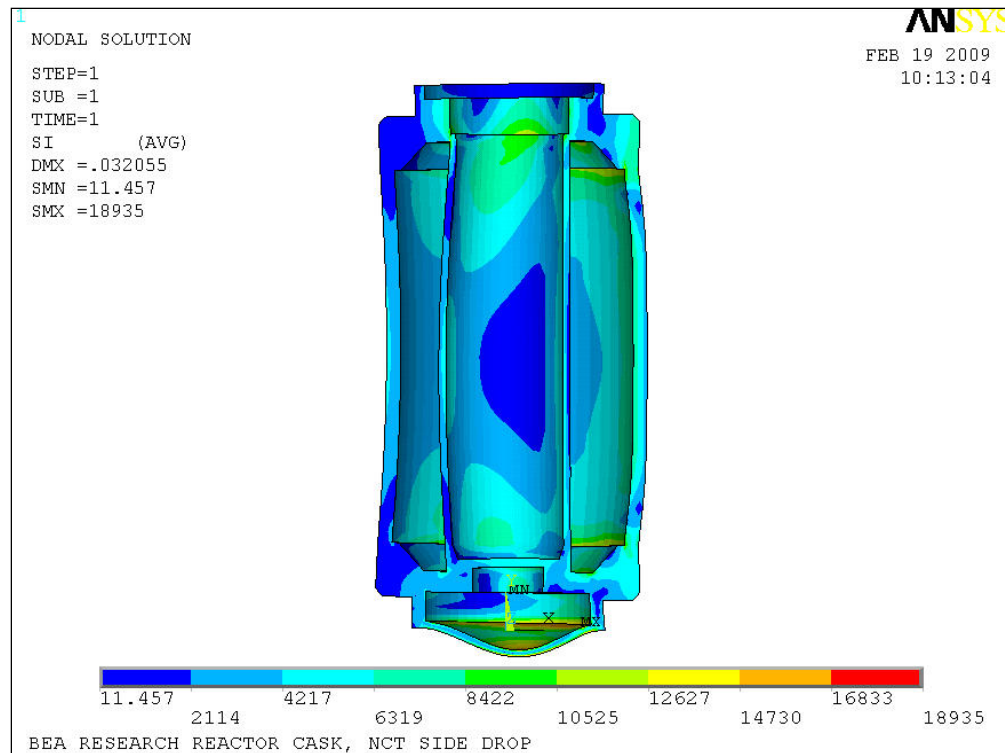


Figure 2.12.4-19 – NCT Side Drop

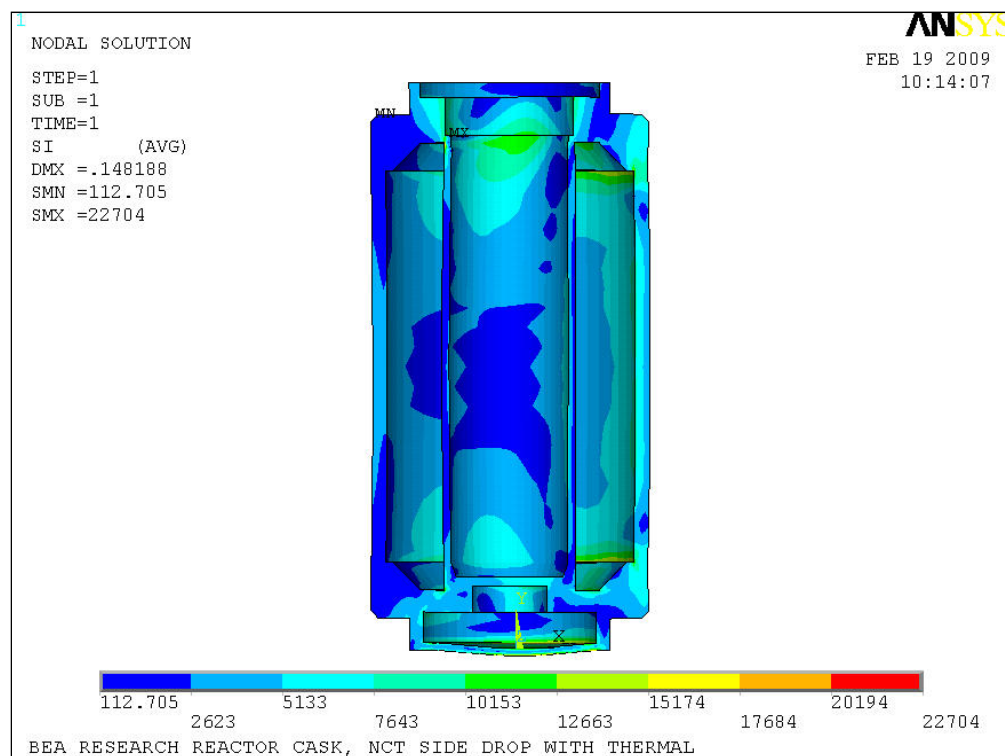


Figure 2.12.4-20 – NCT Side Drop With Thermal

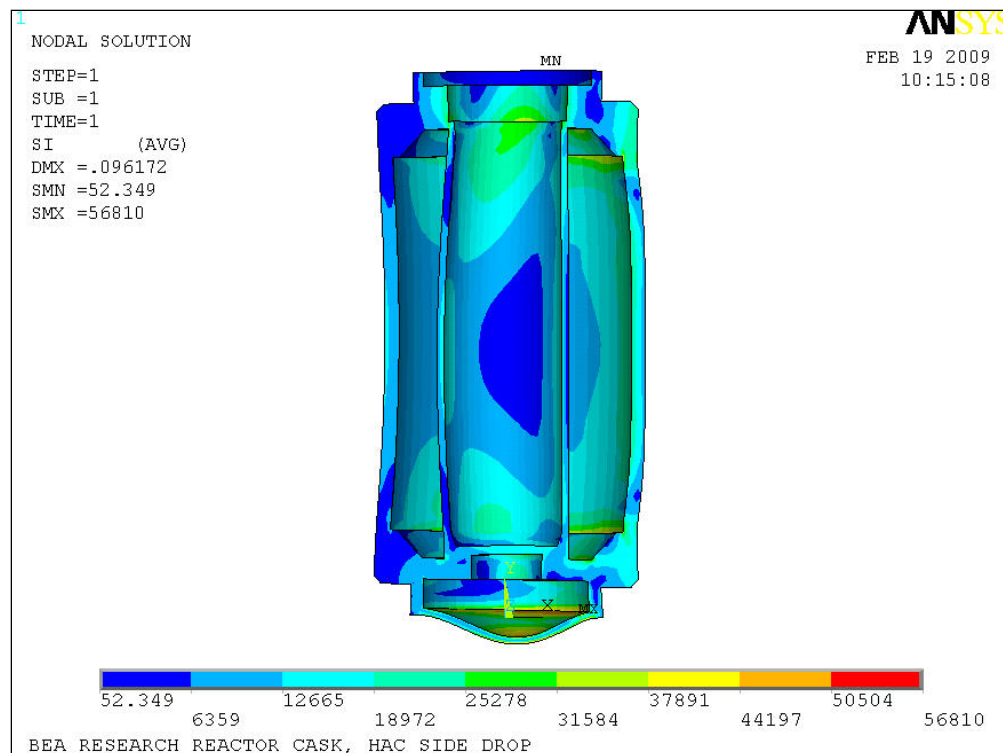


Figure 2.12.4-21 – HAC Side Drop

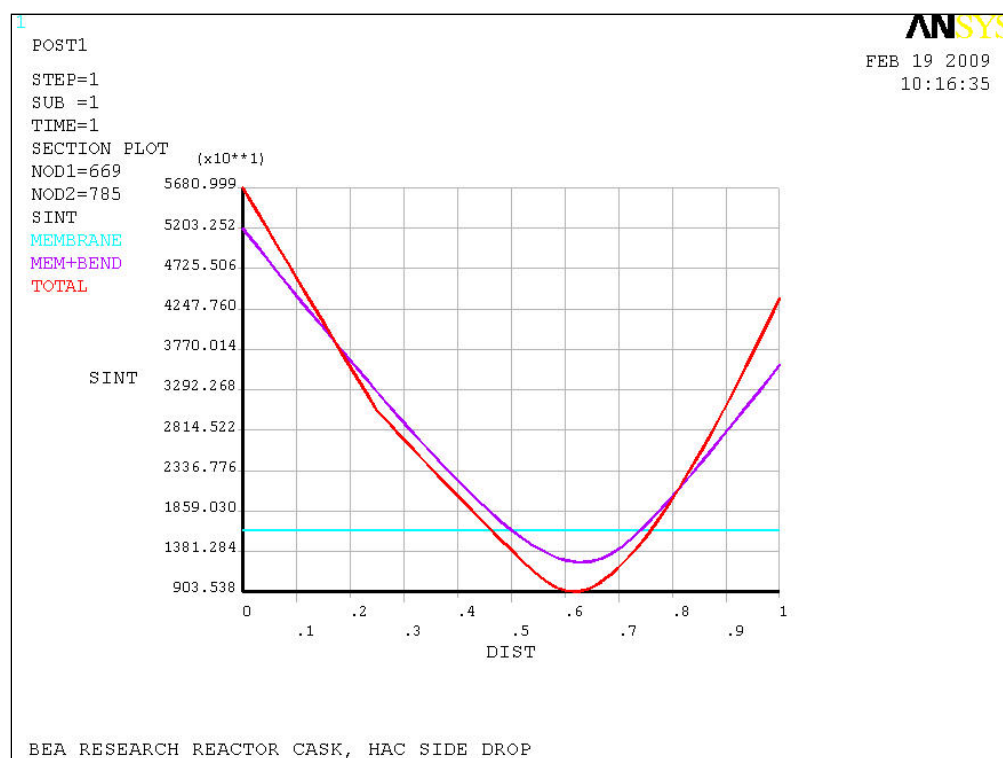


Figure 2.12.4-22 – HAC Side Drop Linearized Stress

## 2.12.5 Impact Limiter Performance Evaluation

This appendix presents the analytical evaluation of the impact and crush performance of the BRR package impact limiters. The impact magnitude and crush deformation of the limiters in several impact orientations, and at hot and cold bounding temperatures, is presented. Each step of the analysis is presented in detail, including the establishment of the crush properties of the polyurethane energy-absorbing foam, the calculation of the impact limiter force-deflection curves using the CASKDROP computer program, and the calculation of the impact response of the package using the SLAPDOWN computer program. A description of CASKDROP and SLAPDOWN are given in Appendix 2.12.6, *Analysis Software Descriptions*.

This appendix concludes with a reconciliation between the analysis results and test results, which shows that the analysis results are generally bounding. Of note, the impact magnitude used for stress analysis of 120g is nearly 50% greater than the highest test or analysis result.

### 2.12.5.1 Introduction

The analysis procedure of the impact limiter performance proceeds in three steps:

1. Calculate the effective stress-strain properties of the 9 lb/ft<sup>3</sup> polyurethane foam used within the limiter to absorb energy. The analysis begins with the room temperature, quasi-static stress-strain curves obtained from the foam manufacturer, and then adjusts the curves for minimum (-20 °F) and maximum (150 °F) temperature, for manufacturing tolerance ( $\pm 10\%$  on the bulk average strength property), for a dynamic (strain rate) effect, for the difference between the crush axis and the axes of material orthotropy, and for the effect of the outer steel shell.
2. Calculate the overall force-deflection relation for the limiter in each orientation, using the fully adjusted stress-strain curve established above and the geometry of the limiter. The result is a force-deflection curve for each orientation at each extreme temperature.
3. Calculate the overall response of the cask and impact limiters, modeling the cask as a rigid rod and the impact limiters as non-linear springs. The result is the impact magnitude and crush deformation of each impact limiter. If the impact orientation is not stable (i.e., a "slapdown"), calculate the acceleration at the end of the payload cavity farthest from the c.g. of the package.

These steps will now be presented in detail. The impact limiter geometry is found on drawing 1910-01-02-SAR in Appendix 1.3.3, *Packaging General Arrangement Drawings*. The basic, room temperature, quasi-static polyurethane foam stress-strain properties are taken from the database provided by the foam manufacturer, General Plastics Manufacturing Co. of Tacoma, WA. Pertinent pages from their web site are shown in Figure 2.12.5-1. Both limiters are taken to be identical, since the only actual difference is the presence of lifting bosses in the upper limiter. The maximum foam temperature of 150 °F is established in Section 2.6.1.1, *Summary of Pressures and Temperatures*. The minimum temperature is -20 °F as defined in [1].

The polyurethane foam is introduced into the impact limiter steel shells as a liquid, which then solidifies. During solidification, orthotropy of properties is established along an axis perpendicular to the ground ("parallel-to-rise") and on the orthogonal axis ("perpendicular-to-rise"). The parallel-to-rise direction is the same as the axis of the package.

### 2.12.5.1.1 Foam Stress-Strain Determination

The foam stress-strain curves are a function of the given strain, temperature, manufacturing tolerance, dynamic crush factor, drop orientation, and a steel shell adjustment. This procedure is illustrated by means of example calculations for 10% strain and a drop orientation of 15° from the horizontal. The static crush strength at ambient temperature (75 °F) for both perpendicular and parallel-to-foam rise are calculated using the method and formulas given in Tables 7 and 8 of the manufacturer's data sheet shown in Figure 2.12.5-1. The resulting static, room temperature crush strengths are shown in the left-hand columns of Table 2.12.5-1 (parallel-to-rise) and Table 2.12.5-2 (perpendicular-to-rise). The basic equation for static crush strength is:

$$\sigma = Y\rho^S$$

where  $\sigma$  is the crush strength in psi,  $\rho$  is the foam density in lb/ft<sup>3</sup>, and Y and S are constants which depend on the strain level. As an example, for 10% strain,

$$\sigma_{\text{Para}}(\varepsilon = 10\%) = Y\rho^S = (7.3058)(9)^{1.6590} = 280 \text{ psi}$$

$$\sigma_{\text{Perp}}(\varepsilon = 10\%) = Y\rho^S = (6.3841)(9)^{1.7182} = 278 \text{ psi}$$

The static crush strength is modified by a temperature coefficient and a manufacturing tolerance for both the hot (150 °F) and cold (-20 °F) conditions. The manufacturing tolerance is included by entering a  $\pm 10\%$  variation in the crush strength. These two effects are conservatively combined such that the -10% manufacturing tolerance is applied to the hot temperature case (both tend to reduce crush strength) and the +10% manufacturing tolerance is applied to the cold temperature case (both tend to increase crush strength).

Static crush strength using the  $C_T$  values found in Tables 7 and 8 of Figure 2.12.5-1 combining the cold (-20 °F) temperature with the plus manufacturing tolerance is illustrated by the following example for 10% strain:

$$\sigma_{\text{Para}}(\varepsilon = 10\%) = C_T(\sigma_{\text{Para}})(1 + \text{Bias}) = 1.29(280)(1 + 0.1) = 397 \text{ psi}$$

$$\sigma_{\text{Perp}}(\varepsilon = 10\%) = C_T(\sigma_{\text{Perp}})(1 + \text{Bias}) = 1.32(278)(1 + 0.1) = 404 \text{ psi}$$

Similarly, static crush strength at the hot (150 °F) temperature with the minus manufacturing tolerance gives:

$$\sigma_{\text{Para}}(\varepsilon = 10\%) = C_T(\sigma_{\text{Para}})(1 - \text{Bias}) = 0.71(280)(1 - 0.1) = 179 \text{ psi}$$

$$\sigma_{\text{Perp}}(\varepsilon = 10\%) = C_T(\sigma_{\text{Perp}})(1 - \text{Bias}) = 0.72(278)(1 - 0.1) = 180 \text{ psi}$$

The manufacturer's data extends as far as a strain of 70%. In some drop orientations at the hot temperature, local strains are expected to exceed this value. In order to account for this, the manufacturer's data was extrapolated between 70% and 80% strain. To demonstrate the validity of this approach, the extrapolated curve is compared to data up to 80% strain that has been previously published [34] by the same manufacturer, in Figure 2.12.5-18<sup>1</sup>. The curves shown in Figure 2.12.5-18 are for a temperature of 150 °F and parallel to rise. Note that between zero and

<sup>1</sup> Note from Figure 2.12.5-18 that polyurethane foam does not have a discrete "lock up" point. While the foam becomes much stiffer at high strains, this occurs relatively gradually compared to other materials such as aluminum honeycomb.

70% strain, the two curves are quite similar, which demonstrates that foam behavior has not changed significantly since the previous data was published. As shown in the figure, the lower curve (current data, extrapolated above 70%) has a slower rise in stress with increasing strain than the upper (previously published) data curve. Use of the extrapolated curve (according to the procedure used in this appendix) will result in a conservatively greater crush deformation prediction than the upper curve. Since the actual foam behavior may tend to be more in line with the upper stress-strain curve, a calculation of package impact acceleration was made using the upper curve, according to the procedure described in Section 2.12.5.1, *Introduction*. This calculation results in the largest impact acceleration that would be expected from the hot case utilizing foam stress-strain behavior like that previously published in the region beyond 70% strain. Since the largest impact was desired, the stress-strain curve was conservatively increased by 10% for manufacturing variability. The results are given in Table 2.12.5-25, which compare the results of the two curves utilizing the governing 15° slapdown orientation. The results, as expected, show less strain and higher impact for the previously published stress-strain data. Although the maximum impact of 89.6g is slightly higher than the cold case maximum value of 86.8g, it is still far below the bounding value used in stress calculations of 120g. Therefore, the method of extrapolating the hot case foam stress-strain values is acceptable. Note that in the one case where a strain of up to 83.2% is needed (see Table 2.12.5-14), the stress for 80% is used, adding further conservatism to the maximum impact limiter deformation strain result.

The resulting static crush strengths at the temperature extremes are shown in the right-hand columns of Table 2.12.5-1 (parallel-to-rise) and Table 2.12.5-2 (perpendicular-to-rise).

The static crush strength is further modified to account for the dynamic loading of the impact limiter. Table 9 in the manufacture's datasheet (reproduced in Figure 2.12.5-1) provides the method used to calculate the dynamic crush strength. The formula used is:

$$\sigma_{\text{Dynamic}} = Y_{\text{int}} (\sigma_{\text{Static}})^S$$

where  $Y_{\text{int}}$  and  $S$  are different values than those defined above, and  $\sigma_{\text{Static}}$  is the static crush strength given on the right-hand side of Table 2.12.5-1 and Table 2.12.5-2. Examples for 10% strain at room temperature and the two temperature extremes are given as follows:

Dynamic crush strength at room temperature:

$$\sigma_{\text{Para}}(\epsilon = 10\%) = Y \sigma_{\text{Para}}^S = (1.2971)(280)^{1.0330} = 437 \text{ psi}$$

$$\sigma_{\text{Perp}}(\epsilon = 10\%) = Y \sigma_{\text{Perp}}^S = (1.2971)(278)^{1.0330} = 434 \text{ psi}$$

Dynamic crush strength at the cold temperature:

$$\sigma_{\text{Para}}(\epsilon = 10\%) = Y \sigma_{\text{Para}}^S = (1.2971)(397)^{1.0330} = 627 \text{ psi}$$

$$\sigma_{\text{Perp}}(\epsilon = 10\%) = Y \sigma_{\text{Perp}}^S = (1.2971)(404)^{1.0330} = 639 \text{ psi}$$

Dynamic crush strength at the hot temperature:

$$\sigma_{\text{Para}}(\epsilon = 10\%) = Y \sigma_{\text{Para}}^S = (1.2971)(179)^{1.0330} = 276 \text{ psi}$$

$$\sigma_{\text{Perp}}(\epsilon = 10\%) = Y \sigma_{\text{Perp}}^S = (1.2971)(180)^{1.0330} = 277 \text{ psi}$$

Table 9 does not provide values for the dynamic crush strength for strains above 70%. The values for S and Y for 70% strain are used to extend the curve up to 80% for the hot case (the room temperature case must also be extended in order to perform the adjustment for the steel shell as shown below). This keeps the dynamic crush strength dependence on the static crush strength similar to that of the highest strain in Table 9. If the value of either variable (S or Y) is modeled too high, the dynamic crush strength will be greatly increased resulting in much lower deformation. Since much of the energy from the crush will be dissipated in the initial 70% strain, small variations of the dynamic crush strength at the highest strains are negligible. The effect of this assumption will be compared against the test data. Table 2.12.5-3 and Table 2.12.5-4 show the result of the dynamic crush adjustment.

The variation in crush strength due to drop orientation is calculated based on the angle of the drop test with respect to the horizontal plane and the axis of the cask. The rise direction of the polyurethane foam is assumed to be parallel to the axis of the cask. An ellipse function is used to combine the parallel and perpendicular crush strength curves to obtain the crush curve for a particular drop orientation. The example for 10% strain and an impact orientation of 15° is carried out below.

Room temperature crush strength adjusted for orientation:

$$\sigma_{\text{Ambient}} = \frac{1}{\sqrt{\left(\frac{\sin \theta}{\sigma_{\text{Para}}}\right)^2 + \left(\frac{\cos \theta}{\sigma_{\text{Perp}}}\right)^2}} = \frac{1}{\sqrt{\left(\frac{\sin(15^\circ)}{437}\right)^2 + \left(\frac{\cos(15^\circ)}{434}\right)^2}} = 434 \text{ psi}$$

Cold crush strength adjusted for orientation:

$$\sigma_{\text{Cold}} = \frac{1}{\sqrt{\left(\frac{\sin \theta}{\sigma_{\text{Para}}}\right)^2 + \left(\frac{\cos \theta}{\sigma_{\text{Perp}}}\right)^2}} = \frac{1}{\sqrt{\left(\frac{\sin(15^\circ)}{627}\right)^2 + \left(\frac{\cos(15^\circ)}{639}\right)^2}} = 638 \text{ psi}$$

Hot crush strength adjusted for orientation:

$$\sigma_{\text{Hot}} = \frac{1}{\sqrt{\left(\frac{\sin \theta}{\sigma_{\text{Para}}}\right)^2 + \left(\frac{\cos \theta}{\sigma_{\text{Perp}}}\right)^2}} = \frac{1}{\sqrt{\left(\frac{\sin(15^\circ)}{276}\right)^2 + \left(\frac{\cos(15^\circ)}{277}\right)^2}} = 277 \text{ psi}$$

Table 2.12.5-5, Table 2.12.5-6, and Table 2.12.5-7 show the stress-strain values adjusted for dynamic loading.

Finally, the stress-strain curves generated by this method were biased upward to account for the steel shell of the impact limiter. A bias equivalent to a 47 percent strength increase was applied to the foam crush strength at ambient (75 °F) temperature. This bias is based on results obtained in engineering tests of the MOX Fresh Fuel Package (MFFP, NRC Docket 71-9295, Appendix 2.12.1). The bias was applied by adding 47% of the room temperature adjusted crush strength (see Table 2.12.5-5) to either the cold or hot adjusted crush strengths (Table 2.12.5-6 and Table 2.12.5-7, respectively). Following the example,

Crush strength biased for steel shell, cold (10% strain, 15° orientation):



**BRR Package Safety Analysis Report**

$$\sigma(\varepsilon) = 0.47(\sigma_{\text{Ambient}}) + \sigma_{\text{Cold}} = .47(434) + 638 = 842 \text{ psi}$$

Crush strength biased for steel shell, hot (10% strain, 15° orientation):

$$\sigma(\varepsilon) = 0.47(\sigma_{\text{Ambient}}) + \sigma_{\text{Hot}} = .47(434) + 277 = 481 \text{ psi}$$

Table 2.12.5-8 presents the complete set of stress-strain data that supports the calculation of impact limiter force-deflection curves. These values represent a summary of the adjustments to the static, room temperature data for temperature extremes, manufacturing tolerance, dynamic effect, impact orientation, and steel shell bias.

### 2.12.5.1.2 Force-Deflection Curves

The force-deflection curves are calculated using the computer program CASKDROP. Given an impact limiter external geometry, orientation to the impacting surface, and crush strength corresponding to that orientation, CASKDROP calculates the total crush force for each increment of deflection. The calculational technique is described in detail in Appendix 2.12.6, *Analysis Software Descriptions*. In summary, CASKDROP divides the crush area into small regions, and for each differential element, calculates the strain and, by means of the stress-strain table, the corresponding stress. Multiplying the stress times the differential area and summing all of the individual forces results in the total force at a given level of crush deformation. Repeating this process at a range of crush deformations results in the complete force-deflection curve.

The geometry shown in Figure 2.12.5-2 is utilized with CASKDROP. There are very small differences between the geometry shown and the drawings given in Appendix 1.3.3, *Packaging General Arrangement Drawings*, but the effect on the force-deflection curves is negligible.

The drop angle formed when the package center of gravity is directly over the conical diameter corner of the impact limiter is of particular interest. This angle is known as the center of gravity over corner, or cg-over-corner. At this angle, the impact limiter will absorb all of the drop kinetic energy on the primary impact. This angle is calculated as:

$$\theta_{\text{cg}} = \tan^{-1} \frac{L}{d_c} = \tan^{-1} \left[ \frac{119.5}{48.1} \right] = 68^\circ$$

where L is the total height of the cask, and  $d_c$  is the conical diameter.

CASKDROP was used to generate force-deflection curves for drop orientations of 0°, 15°, 30°, 45°, 60°, 68° and 90° from a horizontal cask orientation. Since the cg-over-corner drop orientation is considered critical for the calculation, that angle was selected instead of 75° in the sequence. Table 2.12.5-9 summarizes the input data used with the CASKDROP program for this solution. Note: because CASKDROP actually solves for the total crush in stable orientations using an energy approach, the program requires inputs of package weight and drop height. However, since only the force-deflection output is relevant here, the weight and drop height are not listed in the table.

Force-deflection curves are taken directly from the CASKDROP output files, except for the case of the horizontal side drop. Since CASKDROP outputs a single force-deflection curve, the result must be divided by 2 in this case, since two limiters are in contact with the ground. The force-deflection curves for the stated orientations, for hot and cold conditions, are shown in Figure 2.12.5-3 through Figure 2.12.5-9.

**BRR Package Safety Analysis Report****2.12.5.1.3 Impact Acceleration and Crush Deformation**

The SLAPDOWN program, as described in Appendix 2.12.6, *Analysis Software Descriptions*, was used to analyze the impact response of the BRR package with the unyielding surface. It is particularly useful when the center of gravity is not directly over the impact point. Under these circumstances, the package will generally hit, begin to rotate, and strike the ground a second time as a “slapdown” impact. SLAPDOWN conducts a time-integration analysis using a model of the package as a rigid rod, and of the impact limiters as non-linear springs. Given a drop height, the package has an initial velocity at impact. The energy is absorbed first by the primary spring/impact limiter ('nose'), which imparts a rotational force to the model, until the secondary spring/impact limiter ('tail') comes in contact. Most of the energy absorbed by the springs is lost, except the portion that is restored by springback. The position, angle, velocity, and acceleration in both linear and rotational modes are calculated for each time step.

The force-deflection curves calculated by CASKDROP were input into SLAPDOWN to produce the results listed in this analysis. The primary impact limiter non-linear spring data was equal to the force-deflection curve created for the corresponding impact orientation. The secondary impact limiter non-linear spring was equal to the force-deflection curve for the zero degree orientation (i.e., horizontal) in each case. Additional input variables used in SLAPDOWN are summarized in Table 2.12.5-10, and briefly described below.

**Length, Nose-to-CG** – the distance along the cask axis from the location of impact to the CG of the cask. The impact location is dependent on the drop angle and ranges from one-half the total span between impact limiter springs of  $77.13/2 = 38.565$  inches for the side drop, to zero for the cg-over-corner drop ( $68^\circ$ ) and end drop ( $90^\circ$ ). Note that the discrete location of the impact limiter springs has been taken as coincident with the flat ends of the cask body.

**Length, Tail-to-CG** – the distance from the location of the secondary impact to the CG. This value remains the same as the secondary impact is considered to be a horizontal impact in all cases.

**Radius, Nose Limiter** – the radius of the primary impact limiter.

**Radius, Tail Limiter** – the radius of the secondary impact limiter.

**Body Mass** – the total mass of the cask and impact limiters expressed in  $\text{lb}_m\text{-s}^2/\text{in}$ , equivalent to the bounding package weight of 32,000 lb from Table 2.1-2.

**Rotational Moment of Inertia** – the rotational moment of inertia of the cask and assembly, calculated using the weight and geometry of the package.

**Drop Height** – the initial height of the cask prior to free drop measured in feet.

**Impact Angle** – the orientation of the primary impact, measured to the horizontal.

**2.12.5.2 Results**

The results of the analysis include the maximum crush and acceleration values for the given orientations. For unstable, i.e., slapdown orientations, the acceleration output is taken at a distance of 29.565 inches from the c.g. of the cask, which is conservatively further from the c.g. than either end of the payload cavity, and it is the maximum acceleration that the payload will experience.

**BRR Package Safety Analysis Report**

The calculated impact limiter strain is determined as a percentage of the maximum allowable crush. The allowable crush is the distance between the point of impact on the limiter and the closest point of the internal shell of the limiter, and is calculated from the drawings for each orientation of primary impact. The allowable crush for secondary impact is the same for all cases, since the orientation is assumed to be horizontal in each case. The actual crush distance is the value provided as part of the SLAPDOWN output. The impact limiter strain is:

$$\varepsilon_{IL} = \frac{\text{Actual Crush}}{\text{Allowable Crush}}(100\%)$$

**2.12.5.2.1 HAC Free Drop Results**

Table 2.12.5-11 through Table 2.12.5-14 summarize the HAC free drop results. Note that maximum accelerations are governed by the cold case, and maximum impact limiter strain by the hot case. Figure 2.12.5-10 and Figure 2.12.5-11 show the maximum impact limiter strain developed for the primary and secondary impacts for the specified impact orientations. From a comparison of the two plots, the overall maximum impact limiter strain occurs in the secondary impact, hot case, for a primary impact orientation of 15°. Figure 2.12.5-12 and Figure 2.12.5-13 show the maximum acceleration of the cask for the specified drop orientations. The overall maximum impact acceleration occurs in the secondary impact, cold case, for a primary impact orientation of 15°.

**2.12.5.2.2 NCT Free Drop Results**

The NCT test requires the cask to be dropped from a height of two feet, per 10 CFR §71.71(c)(7). Table 2.12.5-15 through Table 2.12.5-18 summarize the NCT free drop results, using the same orientations and force-deflection curves as for the HAC cases.

Figure 2.12.5-14 and Figure 2.12.5-15 show the maximum impact limiter strain developed for the NCT primary and secondary impacts for the specified impact orientations. The maximum strain for the primary impact occurs at 68°, while the maximum strain for the secondary impact is seen to occur at a primary impact orientation of 15°. In both cases, the maximum strain is bounded by all the HAC strains for both primary and secondary impacts.

Figure 2.12.5-16 and Figure 2.12.5-17 show the maximum acceleration of the cask for the specified drop orientations. The maximum impact acceleration occurs in the 90° orientation. As expected, all NCT impact cases are bounded by the HAC cases. The NCT governing cases are different than the HAC governing cases, but this is to be expected due to the difference in impact velocity and energy absorbed.

**2.12.5.2.3 Combined HAC and NCT Free Drop Results**

Since 10 CFR 71 requires that the NCT free drop precede the HAC free drop, the effect of the combination of both drops is next considered. Since the impact acceleration is a function of the crush of the limiter, and the crush of the limiter is a function of the energy absorbed, a 2-foot free drop followed by a 30-foot free drop (taken in the same orientation on the same spot) may be modeled as a single 32-foot free drop. This is a conservative assumption, which neglects the effect of material springback which will occur after the initial NCT impact.

A sample of selected cold impact cases, where the acceleration was shown to be the highest, as shown in Table 2.12.5-19 and Table 2.12.5-20 demonstrates that the maximum increase in

**BRR Package Safety Analysis Report**

acceleration is less than 5 percent. A sample of selected hot impact cases, where the strain was shown to be greater than the cold impact cases, is shown in Table 2.12.5-21 and Table 2.12.5-22. From the results of the combined NCT and HAC drop, it is clear that the effect of the NCT free drop on the HAC free drop is negligible.

**2.12.5.3 Reconciliation with Certification Test Results**

To verify the BRR Package functions as intended, a half-scale CTU was tested in three drop orientations as described in Appendix 2.12.3, *Certification Test Results*. The results of the test indicate that the results predicted in this calculation are conservative. The test results for the HAC end, slapdown, and c.g.-over-corner orientations are shown in Table 2.12.5-23. To convert the half-scale results to full-scale, the acceleration is divided by 2, and the crush distance is multiplied by 2.

The transverse accelerometers were located 8.68 inches from the end of the cask, or 17.36 inches in the equivalent full-scale, whereas the SLAPDOWN calculations correspond to the end of the cask cavity at the bottom, bounded by a distance of 29.565 inches from the cask c.g. This difference does not affect the stable impact orientations such as the end (D1) and c.g. over corner (D3), but for the slapdown impact (D2R), an adjustment of the test results must be made before comparison to the SLAPDOWN calculations.

The acceleration at any point along the axis in an oblique impact can be found from:

$$a_i = a_{c.g.} + \alpha L$$

where  $a_{c.g.}$  is the acceleration of the center of gravity ( $\text{in/s}^2$ ),  $\alpha$  is the rotational acceleration in  $\text{rad/s}^2$ , and  $L$  is the distance of the point  $i$  from the c.g. in inches. Since  $a_{c.g.}$  was not measured in the test, it must be calculated using the known location of the transverse accelerometers and the rotational acceleration calculated using SLAPDOWN. At the moment of maximum primary impact, the rotational acceleration is calculated by SLAPDOWN to be  $\alpha_p = 534 \text{ rad/s}^2$ . The full scale equivalent location of the accelerometers from the cask c.g. was:

$$L_{\text{accel}} = \frac{L_{\text{cask}}}{2} - 17.36 = 21.21 \text{ in}$$

where  $L_{\text{cask}} = 77.13$  inches, and the full scale equivalent location of the accelerometers from the cask end was 17.36 inches. The full-scale acceleration of the cask c.g. for the primary event in the test therefore can be computed as:

$$a_{\text{test c.g.-p}} = a_{\text{accel-p}} - \alpha_p L_{\text{accel}} = 10,892 \text{ in/s}^2$$

where the full-scale measured acceleration from Table 2.12.5-23 for the primary impact of test D2R,  $a_{\text{accel-p}} = 57.5g$  (i.e.,  $22,218 \text{ in/s}^2$ ), and the location of the accelerometers,  $L_{\text{accel}} = 21.21$  inches from the cask c.g. The acceleration of the test cask at the location of used for the SLAPDOWN runs (i.e., the bottom end of the payload cavity) is therefore:

$$a_{\text{adj-p}} = a_{\text{test c.g.-p}} + \alpha_p L_{\text{adj}} = 26,680 \text{ in/s}^2 = 69.0g$$

where the distance from the cask c.g. to the location of the SLAPDOWN output is  $L_{\text{adj}} = 29.565$  inches. The corresponding SLAPDOWN calculated output acceleration for the primary impact is equal to 71.0g from Table 2.12.5-11.

Similarly, at the moment of maximum secondary impact, the rotational acceleration is calculated by SLAPDOWN to be  $\alpha_S = 687 \text{ rad/s}^2$ . The full-scale acceleration of the cask c.g. for the secondary event in the test can be computed as:

$$a_{\text{test c.g.-S}} = a_{\text{accel-S}} - \alpha_S L_{\text{accel}} = 7,454 \text{ in/s}^2$$

where the full-scale measured acceleration from Table 2.12.5-23 for the secondary impact of test D2R,  $a_{\text{accel-S}} = 57.0g$  (i.e.,  $20,025 \text{ in/s}^2$ ), and  $L_{\text{accel}}$  is the same as above. The acceleration of the test cask at the location used for the SLAPDOWN runs (i.e., the bottom end of the payload cavity) is therefore:

$$a_{\text{adj-S}} = a_{\text{test c.g.-S}} + \alpha_S L_{\text{adj}} = 27,765 \text{ in/s}^2 = 71.8g$$

The corresponding SLAPDOWN calculated output acceleration for the secondary impact is equal to 86.8g from Table 2.12.5-12.

The results show that the corrected test accelerations are still below the maximum acceleration used in stress analysis of 120g. The maximum secondary acceleration of 71.8g is lower than the calculated value of 86.8g. The corrected primary acceleration of 69.0g is also below the calculated value of 71.0g. This indicates that the calculation is essentially bounding for all cases. The principal conclusion, however, is that the actual accelerations of the BRR package are well below the bounding value of 120g used in the stress calculations.

As stated in Section 2.12.3.3, *Test Unit Configuration*, the weight of the test cask was 3,181 lb, or when properly adjusted for scale, approximately 7% below the maximum equivalent full-scale weight of 32,000 lb. This had the effect of conservatively increasing the recorded accelerations of the CTU. Correspondingly, the crush deformations were slightly underestimated in the test, since there was less kinetic energy in the drop.

The force-deflection curves discussed in Section 2.12.5.1.2, *Force-Deflection Curves*, show that the strain increases nonlinearly with an increase in applied load. Therefore, although an increase in weight will result in an increased deformation, each succeeding crush strain increment becomes smaller as a greater force is applied, particularly as the end of crush is neared. Thus the percent change in the crush distance will be smaller in magnitude than the percent change in weight. Since the increase in the crush distance will be less than the weight increase, and since the weight increase is small in magnitude, the crush distance is bounded by the values in the calculation. This holds true for both the cold and hot temperature conditions developed in this calculation. The bounding crush strain corresponds to the 15° secondary impact in the hot case. As shown in Table 2.12.5-14, the predicted crush is 15.9 inches. Since, as shown in Table 2.12.5-24, the cold secondary crush was measured to be 36% lower than the prediction, then the small increase in weight of 7% will not invalidate the hot case maximum predicted crush. Thus the predictions are conservative.

A comparison of the calculated ('Calc') and full-scale equivalent test ('Actual') impact limiter performance is given in Table 2.12.5-24. A negative sign in the '% Less' columns indicates that the test result was lower than the calculated value.

#### 2.12.5.4 Analysis of Optional Drain Tube

An optional drain tube may be included in the lower impact limiter. The drain tube is made from Type 304 stainless steel tube with an outer diameter of 5/8" and a wall thickness of  $0.05 \pm 0.02$  inches.

The lower end of the drain tube is welded to the penetration in the impact limiter shell with a weld nominally equal to the thickness of the tube wall thickness.

The upper end of the tube is inserted over a transitional fitting which is welded to the inner shell of the impact limiter. This fitting is sized to allow for free axial movement between the tube and fitting. This arrangement prevents any axial load from being applied to the tube from the weight of the cask during normal use.

Under free end drop conditions, the tube is intended to crush along with the impact limiter foam. With an ultimate tensile stress of  $\sigma_U = 75$  ksi, the maximum force applied by the tube may be calculated with the maximum cross-sectional area.

$$A = \frac{\pi}{4} [d_o^2 - d_i^2] = 0.123 \text{ in}^2$$

where the outer diameter of the tube is  $d_o = 0.63$  inches, and the minimum inner diameter is  $d_i = 0.49$  inches for a maximum wall thickness of 0.07 inches. A conservative upper bound compressive load will therefore be:

$$F = \sigma_U A = 9,225 \text{ lb}$$

For a package weight of 32,000 lbs, this applies an insignificant acceleration of 0.3g. This result is rather conservative as it ignores buckling of the tube and assumes uniform flow of the material at a value equal to the ultimate stress.

A bounding value for the HAC end drop impact of 120g (See Section 2.7.1.1, *Impact Forces and Deformation*) was used to bound the full-scale equivalent end drop test result of 58g (from Table 2.12.5-23.) Therefore the loading due to the drain tube on the package is of negligible concern.

#### 2.12.5.5 Conclusion

The impact limiter evaluation is used to establish a bounding impact magnitude for stress analysis in other sections of this SAR. The maximum impact occurs in the cold temperature case. For NCT, the maximum overall impact is equal to 32.9g in the 90° orientation, from which a bounding impact for all orientations of 40g is taken. For HAC, the maximum overall impact is 86.8g in the 15° secondary slapdown impact, and a very conservative value of 120g is used as a bounding impact for all orientations.

The maximum strain occurs under HAC in the hot temperature case, and equals 83.2% in the 15° secondary slapdown case.

**Table 2.12.5-1 - Parallel-to-Rise Static Compressive Strength (psi)**

Strain	Room Temperature (75 °F)				-20 °F		150 °F	
	Y, int	density	S	Crush Str	C <sub>T</sub>	Crush Str	C <sub>T</sub>	Crush Str
10%	7.3058	9	1.6590	280	1.29	397	0.71	179
20%	6.7276	9	1.7021	283	1.36	423	0.73	186
30%	6.4961	9	1.7350	294	1.32	427	0.74	196
40%	6.9137	9	1.7255	306	1.29	434	0.75	207
50%	5.6711	9	1.8877	359	1.26	498	0.76	246
60%	5.3279	9	2.0431	474	1.28	667	0.76	324
65%	5.9871	9	2.0870	587	1.29	833	0.76	402
70%	6.2085	9	2.1868	758	1.37	1142	0.81	553
75%				952				710
80%				1,204				928

**Table 2.12.5-2 - Perpendicular-to-Rise Static Compressive Strength (psi)**

Strain	Room Temperature (75 °F)				-20 °F		150 °F	
	Y, int	density	S	Crush Str	C <sub>T</sub>	Crush Str	C <sub>T</sub>	Crush Str
10%	6.3841	9	1.7182	278	1.32	404	0.72	180
20%	6.5943	9	1.6946	273	1.35	405	0.74	182
30%	6.1154	9	1.7403	280	1.34	413	0.79	199
40%	5.7722	9	1.8023	303	1.32	440	0.77	210
50%	5.3041	9	1.9054	349	1.32	507	0.77	242
60%	5.3181	9	2.0392	470	1.33	688	0.77	326
65%	5.7864	9	2.1002	584	1.34	861	0.77	405
70%	5.7701	9	2.2255	767	1.36	1,147	0.78	538
75%				971				683
80%				1,240				878

**Table 2.12.5-3 - Parallel-to-Rise Dynamic Crush Strength**

Strain	Dynamic Crush Strength Coefficients		Dynamic Crush Strength (psi)		
	Y, int	S	75 °F	-20 °F	150 °F
10%	1.2971	1.0330	437	627	276
20%	1.4397	1.0069	424	635	278
30%	1.5181	0.9941	432	625	288
40%	1.3887	1.0028	432	613	292
50%	1.4419	0.9912	492	680	338
60%	1.4275	0.9831	610	853	419
65%	1.3871	0.9910	769	1088	528
70%	1.4660	0.9586	844	1251	624
75%	1.4660	0.9586	1,051		793
80%	1.4660	0.9586	1,316		1,025

**Table 2.12.5-4 - Perpendicular-to-Rise Dynamic Crush Strength**

Strain	Dynamic Crush Strength Coefficients		Dynamic Crush Strength (psi)		
	Y, int	S	75 °F	-20 °F	150 °F
10%	1.2971	1.0330	434	639	277
20%	1.4397	1.0069	409	608	272
30%	1.5181	0.9941	411	605	293
40%	1.3887	1.0028	428	622	296
50%	1.4419	0.9912	478	692	332
60%	1.4275	0.9831	605	879	422
65%	1.3871	0.9910	765	1124	532
70%	1.4660	0.9586	854	1256	608
75%	1.4660	0.9586	1,071		764
80%	1.4660	0.9586	1,354		972



**Table 2.12.5-5 - Dynamic Strength Adjusted for Impact Angle (75 °F)**

Strain	Angle of Impact (degrees)						
	0	15	30	45	60	68	90
	Compressive Stress (psi)						
10%	434	434	435	435	436	437	437
20%	409	410	413	416	420	422	424
30%	411	412	416	421	426	429	432
40%	428	428	429	430	431	431	432
50%	478	479	481	485	488	490	492
60%	605	605	606	607	609	609	610
65%	765	765	766	767	768	768	769
70%	854	853	851	849	846	845	844
75%	1,071	1,070	1,066	1,061	1,056	1,054	1,051
80%	1,354	1,351	1,344	1,335	1,325	1,321	1,316

**Table 2.12.5-6 - Dynamic Strength Adjusted for Impact Angle (-20 °F)**

Strain	Angle of Impact (degrees)						
	0	15	30	45	60	68	90
	Compressive Stress (psi)						
10%	639	638	636	633	630	629	627
20%	608	610	614	621	628	631	635
30%	605	606	610	615	620	622	625
40%	622	621	620	617	615	614	613
50%	692	691	689	686	683	682	680
60%	879	877	872	866	859	857	853
65%	1,124	1,121	1,115	1,106	1,097	1,093	1,088
70%	1,256	1,256	1,255	1,253	1,252	1,252	1,251

**Table 2.12.5-7 - Dynamic Strength Adjusted for Impact Angle (150 °F)**

Strain	Angle of Impact (degrees)						
	0	15	30	45	60	68	90
	Compressive Stress (psi)						
10%	277	277	277	276	276	276	276
20%	272	272	273	275	276	277	278
30%	293	293	292	290	289	289	288
40%	296	296	295	294	293	293	292
50%	332	332	333	335	336	337	338
60%	422	422	421	420	420	419	419
65%	532	532	531	530	529	529	528
70%	608	609	612	616	620	622	624
75%	764	766	771	778	785	789	793
80%	972	975	984	997	1,011	1,017	1,025

**Table 2.12.5-8 - Fully Adjusted Polyurethane Foam Stress-Strain Data**

Strain	Angle of Impact (degrees)						
	0	15	30	45	60	68	90
<b>-20 °F Stress (psi)</b>							
10%	843	842	840	837	835	834	832
20%	800	803	808	817	825	829	834
30%	798	800	806	813	820	824	828
40%	823	822	822	819	818	817	816
50%	917	916	915	914	912	912	911
60%	1,163	1,161	1,157	1,151	1,145	1,143	1,140
65%	1,484	1,481	1,475	1,466	1,458	1,454	1,449
70%	1,657	1,657	1,655	1,652	1,650	1,649	1,648
<b>150 °F Stress (psi)</b>							
10%	481	481	481	480	481	481	481
20%	464	465	467	471	473	475	477
30%	486	487	488	488	489	491	491
40%	497	497	497	496	496	496	495
50%	557	557	559	563	565	567	569
60%	706	706	706	705	706	705	706
65%	892	892	891	890	890	890	889
70%	1,009	1,010	1,012	1,015	1,018	1,019	1,021
75%	1,267	1,269	1,272	1,277	1,281	1,284	1,287
80%	1,608	1,610	1,616	1,624	1,634	1,638	1,644

**Table 2.12.5-9 - CASKDROP Input Data**

<b>Input Data</b>	<b>Value</b>
Impact Limiter Outside Diameter, in.	78.0
Impact Limiter Overall Length, in.	34.6
Impact Limiter Conical Diameter, in.	48.1
Impact Limiter Conical length, in.	15.0
Impact Limiter End Thickness, in.	21.2
Impact Limiter Hole Diameter, in.	0
Impact Limiter Hole Length, in.	0
Body Outside Diameter, in.	38.0
Body Overall Length, in.	77.13
Frictional Coefficient	0

**Table 2.12.5-10 - SLAPDOWN Input Data**

<b>Input data</b>	<b>Value</b>
Length, Nose-to-C.G., in.	Variable
Length, Tail-to-C.G., in.	38.565
Radius, Nose Limiter, in.	39.0
Radius, Tail Limiter, in.	39.0
Body Mass, lb <sub>m</sub> -s <sup>2</sup> /in.	82.816
Rotational Moment of inertia, in-lb <sub>m</sub> -s <sup>2</sup>	63,246
HAC Drop Height, ft.	30
NCT Drop Height, ft	2
HAC + NCT Drop Height, ft	32
Impact Angle (with Horizontal)	Variable
Force Deflection Curves	Variable
Friction Coefficient	0

**Table 2.12.5-11 - Cold Primary Impact Results, HAC**

<b>Primary Impact Angle</b>	<b>Acceleration</b>	<b>Crush</b>	<b>Allowable Crush</b>	<b>Crush Margin</b>	<b>Limiter Strain</b>
<b>(deg)</b>	<b>(g)</b>	<b>(in)</b>	<b>(in)</b>	<b>(in)</b>	<b>%</b>
0	63.3	11.0	19.1	8.1	57.6
15	71.0	10.7	21.4	10.7	50.0
30	79.7	12.3	22.1	9.8	55.7
45	80.4	11.0	21.4	10.4	51.4
60	82.6	13.1	22.6	9.5	58.0
68	69.6	13.3	22.5	9.2	59.1
90	72.4	7.3	20.2	12.9	36.1

**Table 2.12.5-12 - Cold Secondary Impact Results, HAC**

<b>Primary Impact Angle</b>	<b>Acceleration</b>	<b>Crush</b>	<b>Allowable Crush</b>	<b>Crush Margin</b>	<b>Limiter Strain</b>
<b>(deg)</b>	<b>(g)</b>	<b>(in)</b>	<b>(in)</b>	<b>(in)</b>	<b>%</b>
0	63.3	11.0	19.1	8.1	57.6
<b>15</b>	<b>86.8</b>	12.1	19.1	7.0	63.4
30	66.2	9.3	19.1	9.8	48.7
45	56.0	7.7	19.1	11.4	40.3
60	40.1	5.1	19.1	14.0	26.7

**Table 2.12.5-13 - Hot Primary Impact Results, HAC**

<b>Primary Impact Angle</b>	<b>Acceleration</b>	<b>Crush</b>	<b>Allowable Crush</b>	<b>Crush Margin</b>	<b>Limiter Strain</b>
<b>(deg)</b>	<b>(g)</b>	<b>(in)</b>	<b>(in)</b>	<b>(in)</b>	<b>%</b>
0	55.1	14.5	19.1	4.6	75.9
15	53.4	13.6	21.4	7.8	63.6
30	60.8	15.8	22.1	6.3	71.5
45	66.6	14.4	21.4	7.0	67.3
60	67.9	16.5	22.6	6.1	73.0
68	55.4	16.6	22.5	5.9	73.8
90	54.8	10.5	20.2	9.7	52.0

**Table 2.12.5-14 - Hot Secondary Impact Results, HAC**

<b>Primary Impact Angle</b>	<b>Acceleration</b>	<b>Crush</b>	<b>Allowable Crush</b>	<b>Crush Margin</b>	<b>Limiter Strain</b>
<b>(deg)</b>	<b>(g)</b>	<b>(in)</b>	<b>(in)</b>	<b>(in)</b>	<b>%</b>
0	55.1	14.5	19.1	4.6	75.9
<b>15</b>	83.2	15.9	19.1	3.2	<b>83.2</b>
30	54.2	12.5	19.1	6.6	65.4
45	43.4	10.5	19.1	8.6	55.0
60	29.9	7.1	19.1	12.0	37.2

**Table 2.12.5-15 - Cold Primary Impact Results, NCT**

<b>Primary Impact Angle</b>	<b>Acceleration</b>	<b>Crush</b>	<b>Allowable Crush</b>	<b>Crush Margin</b>	<b>Limiter Strain</b>
<b>(deg)</b>	<b>(g)</b>	<b>(in)</b>	<b>(in)</b>	<b>(in)</b>	<b>%</b>
0	19.7	2.8	19.1	16.3	14.7
15	19.1	4.1	21.4	17.3	19.2
30	21.2	4.7	22.1	17.4	21.3
45	25.9	3.0	21.4	18.4	14.0
60	24.2	5.0	22.6	17.6	22.1
68	15.2	5.2	22.5	17.3	23.1
<b>90</b>	<b>32.9</b>	1.5	20.2	18.7	7.4

**Table 2.12.5-16 - Cold Secondary Impact Results, NCT**

<b>Primary Impact Angle</b>	<b>Acceleration</b>	<b>Crush</b>	<b>Allowable Crush</b>	<b>Crush Margin</b>	<b>Limiter Strain</b>
<b>(deg)</b>	<b>(g)</b>	<b>(in)</b>	<b>(in)</b>	<b>(in)</b>	<b>%</b>
0	19.7	2.8	19.1	16.3	14.7
15	29.6	3.7	19.1	15.4	19.4
30	29.5	3.4	19.1	15.7	17.8
45	30.1	3.5	19.1	15.6	18.3
60	28.2	3.2	19.1	15.9	16.8

**Table 2.12.5-17 - Hot Primary Impact Results, NCT**

<b>Primary Impact Angle</b>	<b>Acceleration</b>	<b>Crush</b>	<b>Allowable Crush</b>	<b>Crush Margin</b>	<b>Limiter Strain</b>
<b>(deg)</b>	<b>(g)</b>	<b>(in)</b>	<b>(in)</b>	<b>(in)</b>	<b>%</b>
0	13.9	3.7	19.1	15.4	19.4
15	15.7	4.9	21.4	16.5	22.9
30	16.8	5.8	22.1	16.3	26.2
45	20.0	3.9	21.4	17.5	18.2
60	19.0	6.1	22.6	16.5	27.0
<b>68</b>	12.4	6.4	22.5	16.1	<b>28.4</b>
90	23.9	2.0	20.2	18.2	9.9

**Table 2.12.5-18 - Hot Secondary Impact Results, NCT**

<b>Primary Impact Angle</b>	<b>Acceleration</b>	<b>Crush</b>	<b>Allowable Crush</b>	<b>Crush Margin</b>	<b>Limiter Strain</b>
<b>(deg)</b>	<b>(g)</b>	<b>(in)</b>	<b>(in)</b>	<b>(in)</b>	<b>%</b>
0	13.9	3.7	19.1	15.4	19.4
15	22.5	5.1	19.1	14.0	26.7
30	21.8	4.5	19.1	14.6	23.6
45	20.8	4.6	19.1	14.5	24.1
60	21.1	4.3	19.1	14.8	22.5

**Table 2.12.5-19 - Cold Primary Impact Results, HAC + NCT**

<b>Primary Impact Angle</b>	<b>HAC Acceleration</b>	<b>HAC+NCT Acceleration</b>	<b>Acceleration Increase</b>	<b>Percent Increase</b>
<b>(deg)</b>	<b>(g)</b>	<b>(g)</b>	<b>(g)</b>	<b>%</b>
15	71.0	73.2	2.2	3.1
68	69.6	71.9	2.3	3.3
90	72.4	73.9	1.5	2.1

**Table 2.12.5-20 - Cold Secondary Impact Results, HAC + NCT**

Primary Impact Angle	HAC Acceleration	HAC+NCT Acceleration	Acceleration Increase	Percent Increase
(deg)	(g)	(g)	(g)	%
15	86.8	90.1	3.3	3.8

**Table 2.12.5-21 - Hot Primary Impact Results, HAC + NCT**

Primary Impact Angle	HAC Crush	HAC+NCT Crush	Crush Increase	Percent Increase
(deg)	(in)	(in)	(in)	%
15	13.6	14.0	0.4	2.9
68	16.6	17.0	0.4	2.4
90	10.5	10.9	0.4	3.8

**Table 2.12.5-22 - Hot Secondary Impact Results, HAC + NCT**

Primary Impact Angle	HAC Crush	HAC+NCT Crush	Crush increase	Percent Increase
(deg)	(in)	(in)	(in)	%
15	15.9	16.3	0.4	2.5

**Table 2.12.5-23 - CTU Test Results**

Test #	Type	Location	Half-Scale*			Full-Scale**			
			Measured Accel. (g)		Crush Distance (in)	Measured Accel. (g)			Crush Distance (in)
			1019 Hz Cutoff	Rigid Body Estimate		1019 Hz Cutoff	Rigid Body Estimate	Δ	
D1	End Drop	Primary	116	109	3.4	58.0	54.5	3.5	6.8
D2R	Oblique Slapdown	Primary	115	104	4.0	57.5	52.0	5.5	8.0
		Secondary	114	103	3.9	57.0	51.5	5.5	7.8
D3	CG Over Corner	Primary	117	101	5.5	58.5	50.5	8.0	11.0

\*Values in the '1019Hz Cutoff' and 'Crush Distance' columns are obtained from Section 2.12.3.5. The 'Rigid Body Estimate' in half-scale is formed by subtracting the average reduction value for the impact event (found in column 'E' of Table 2.12.3-6) from the 1019Hz cutoff accelerometer response. For example, for test D1, the average reduction value is 7g, and therefore the rigid body estimate is  $116 - 7 = 109$ g.

\*\*Full-scale accelerations are one-half of the half-scale results. The column labeled 'Δ' is equal to the difference between the 1019Hz cutoff result and the rigid body estimate in full scale. For example, for test D1, the rigid body estimate is  $58.0 - 54.5 = 3.5$ g lower than the 1019Hz cutoff result. From this it can be seen that the 1019Hz cutoff results are reasonable, and moderately conservative.



**Table 2.12.5-24 - CTU Percentage of Predicted Results (Full-Scale)**

Test #	Location	Acceleration (g)*			Crush Distance (in)		
		Calc	Actual	% Less	Calc	Actual	% Less
D1	Primary	72.4	58.0/54.5	-19.9/-24.7	7.3	6.8	-6.8
D2R	Primary	71.0	69.0/63.5	-2.8/-10.6	10.7	8.0	-25
	Secondary	86.8	71.8/66.3	-17.3/-23.6	12.1	7.8	-36
D3	Primary	69.6	58.5/50.5	-15.9/-27.4	13.3	11.0	-17

\* Calculated accelerations are taken from Table 2.12.5-11 and Table 2.12.5-12. Actual acceleration values are given as A/B, where A is the value derived from the 1019 Hz cutoff data, and B is the value for the rigid body estimate. The actual acceleration values for tests D1 and D3 are taken directly from Table 2.12.5-23. The actual acceleration values for test D2R are taken from the results of the adjustment procedure described in Section 2.12.5.3. The rigid body estimates for D2R are formed by subtracting the 'Δ' value (see Table 2.12.5-23) from the adjusted values. For example, for the D2R primary case, the adjusted value derived from the 1019Hz cutoff data in Section 2.12.5.3 is 69.0g, and the 'Δ' value from Table 2.12.5-23 is 5.5g, thus the rigid body estimate for D2R primary is  $69.0 - 5.5 = 63.5$ g. The two values in the '% Less' column correspond to the two values in the 'Actual' column, and show the amount that the actual values are less than the calculated values.

**Table 2.12.5-25 - Comparison of Results Using Previously Published Stress-Strain Data\***

Dataset	Primary Impact		Secondary Impact	
	Deflection, in	Acceleration, g	Deflection, in	Acceleration, g
Current Data	13.6	53.4	15.9	83.2
Previous Data	13.0	57.3	15.2	89.6

\* HAC, 15° slapdown, 150 °F. "Current Data" results correspond to Table 2.12.5-13 and Table 2.12.5-14.

**Design Guide for use of LAST-A-FOAM FR-3700 for Crash and Fire Protection of Radioactive Material Shipping Containers**

**Table 7: Static Nominal Crush Strength, Parallel to Direction of Rise (see Table 8 for Perpendicular to Rise)**

For 4 to 10 lb <sub>m</sub> /ft <sup>3</sup>									
Temp	Correlation Factors	Crush Strength, psi, Parallel to Direction of Rise							
		10%	20%	30%	40%	50%	60%	65%	70%
-20°F	C <sub>T</sub>	1.29	1.36	1.32	1.29	1.26	1.28	1.29	1.37
75°F	Y <sub>int</sub>	7.3058	6.7276	6.4961	6.9137	5.6711	5.3279	5.9871	6.2085
	S	1.6590	1.7021	1.7350	1.7255	1.8877	2.0431	2.0870	2.1868
100°F	C <sub>T</sub>	0.87	0.88	0.89	0.89	0.90	0.91	0.91	0.96
140°F	C <sub>T</sub>	0.73	0.75	0.76	0.77	0.78	0.78	0.79	0.84
180°F	C <sub>T</sub>	0.65	0.66	0.67	0.68	0.69	0.68	0.68	0.71
220°F	C <sub>T</sub>	0.61	0.60	0.60	0.61	0.61	0.59	0.59	0.61
260°F	C <sub>T</sub>	0.45	0.44	0.46	0.47	0.48	0.49	0.49	0.52
For 11 to 40 lb <sub>m</sub> /ft <sup>3</sup>									
Temp	Correlation Factor	Crush Strength, psi, Parallel to Direction of Rise							
		10%	20%	30%	40%	50%	60%	65%	70%
-20°F	C <sub>T</sub>	1.35	1.33	1.32	1.31	1.31	1.30	1.28	1.26
75°F	Y <sub>int</sub>	4.3422	3.8755	3.5241	3.0307	3.0402	3.4889	5.8935	5.6055
	S	1.8809	1.9321	1.9872	2.0755	2.1451	2.2143	2.1041	2.2368
100°F	C <sub>T</sub>	0.86	0.87	0.88	0.88	0.89	0.90	0.90	0.97
140°F	C <sub>T</sub>	0.72	0.74	0.75	0.75	0.75	0.76	0.76	0.81
180°F	C <sub>T</sub>	0.62	0.63	0.65	0.65	0.65	0.65	0.64	0.68
220°F	C <sub>T</sub>	0.56	0.56	0.57	0.57	0.56	0.54	0.54	0.57
260°F	C <sub>T</sub>	0.40	0.40	0.41	0.42	0.41	0.43	0.43	0.47

The room temperature (75°F) foam crush strength is calculated at each %-Crush and is a function of density;  $\sigma = Y_{int}(\rho)^S$ , where  $Y_{int}$  and  $S$  are defined above,  $\rho$  is the nominal foam density in lb/ft<sup>3</sup>, and  $\sigma$  is the resulting crush stress in psi at the indicated strain. The foam crush strength at temperatures other than 75°F is calculated at each %-Crush and is a function of the strength at 75°F;  $\sigma = \sigma_{75°F} C_T$ . General Plastics Mfg. Co. is re-investigating the correlations factors at temperatures above and below 75°F. Please contact us for more specific and detailed data, as needed.

**GENERAL PLASTICS MANUFACTURING COMPANY**



10 Iss004

**Figure 2.12.5-1 - General Plastics Data (Page 1 of 3)**

**Design Guide for use of LAST-A-FOAM FR-3700 for Crash and Fire Protection of Radioactive Material Shipping Containers**
**Table 8: Static Nominal Crush Strength, Perpendicular to Direction of Rise (see Table 7 for Parallel to Rise)**

For 4 to 10 lb <sub>m</sub> /ft <sup>3</sup>									
Temp	Correlation Factors (see below)	Crush Strength, psi, Perpendicular to Direction of Rise							
		10%	20%	30%	40%	50%	60%	65%	70%
-20°F	C <sub>T</sub>	1.32	1.35	1.34	1.32	1.32	1.33	1.34	1.36
75°F	Y <sub>int</sub>	6.3841	6.5943	6.1154	5.7722	5.3041	5.3181	5.7864	5.7701
	S	1.7182	1.6946	1.7403	1.8023	1.9054	2.0392	2.1002	2.2255
100°F	C <sub>T</sub>	0.85	0.87	0.88	0.89	0.90	0.91	0.91	0.92
140°F	C <sub>T</sub>	0.75	0.77	0.78	0.79	0.79	0.79	0.79	0.80
180°F	C <sub>T</sub>	0.63	0.66	0.68	0.69	0.69	0.70	0.69	0.70
220°F	C <sub>T</sub>	0.59	0.59	0.60	0.61	0.60	0.60	0.59	0.60
260°F	C <sub>T</sub>	0.45	0.45	0.47	0.48	0.48	0.48	0.48	0.48
For 11 to 40 lb <sub>m</sub> /ft <sup>3</sup>									
Temp	Correlation Factors (see below)	Crush Strength, psi, Perpendicular to Direction of Rise							
		10%	20%	30%	40%	50%	60%	65%	70%
-20°F	C <sub>T</sub>	1.34	1.33	1.32	1.33	1.30	1.28	1.24	1.17
75°F	Y <sub>int</sub>	4.1342	3.5581	3.2664	2.8352	2.8988	3.3972	6.5439	5.6464
	S	1.8957	1.9593	2.0109	2.0955	2.1602	2.2242	2.0660	2.2321
100°F	C <sub>T</sub>	0.84	0.85	0.86	0.88	0.87	0.88	0.88	0.90
140°F	C <sub>T</sub>	0.72	0.73	0.74	0.76	0.75	0.76	0.76	0.79
180°F	C <sub>T</sub>	0.62	0.63	0.64	0.65	0.65	0.65	0.65	0.67
220°F	C <sub>T</sub>	0.53	0.53	0.54	0.55	0.54	0.54	0.54	0.56
260°F	C <sub>T</sub>	0.39	0.39	0.40	0.41	0.41	0.40	0.40	0.42

The room temperature (75°F) foam crush strength is calculated at each %-Crush and is a function of density;  $\sigma = Y_{int}(\rho)^S$ , where  $Y_{int}$  and  $S$  are defined above,  $\rho$  is the nominal foam density in lb/ft<sup>3</sup>, and  $\sigma$  is the resulting crush stress in psi at the indicated strain. The foam crush strength at temperatures other than 75°F is calculated at each %-Crush and is a function of the strength at 75°F;  $\sigma = \sigma_{75°F} C_T$ . General Plastics Mfg. Co. is re-investigating the correlations factors at temperatures above and below 75°F. Please contact us for more specific and detailed data, as needed.

**GENERAL PLASTICS MANUFACTURING COMPANY**


11 Iss004

**Figure 2.12.5-1 - General Plastics Data, continued (Page 2 of 3)**

**Design Guide for use of LAST-A-FOAM FR-3700 for Crash and Fire Protection of Radioactive Material Shipping Containers**

**Dynamic Crush Strength**

The crush strength of LAST-A-FOAM<sup>®</sup>, like many materials, is modestly sensitive to strain rate. The static to dynamic adjustment shown in Table 9 is based on a significant testing program and included strain rates in the range of 30 sec<sup>-1</sup> to 100 sec<sup>-1</sup>. It is expected that the adjustment will provide good predictions of dynamic impact strength of FR-3700 for most Packaging design conditions. This information is intended to be a guide for designers of impact mitigating devices. The constitutive material models may be useful in targeting a foam density or range for a particular application. However, each design should be thoroughly analyzed or tested to understand the implications of the complete design.

**Table 9: Static to Dynamic Crush Strength Adjustment**

Strain	10%	20%	30%	40%	50%	60%	65%	70%
Y <sub>int</sub>	1.2971	1.4397	1.5181	1.3887	1.4419	1.4275	1.3871	1.4660
S	1.0330	1.0069	0.9941	1.0028	0.9912	0.9831	0.9910	0.9586

The dynamic crush strength is calculated at each %-strain and a function of the static crush strength at the same %-strain;

$$\sigma_{\text{Dynamic}} = Y_{\text{int}} (\sigma_{\text{Static}})^S$$

CAUTION: Use only units of PSI for input  $\sigma_{\text{Static}}$  value.



**General Plastics Manufacturing Company**

4910 Burlington Way • P.O. box 9097  
Tacoma, WA 98409

Telephone: (800) 806-6051 or (253) 473-5000

Facsimile: (253) 473-5104

See our World Wide Web Site at:

[www.generalplastics.com](http://www.generalplastics.com)

E-mail address: [sales@generalplastics.com](mailto:sales@generalplastics.com)

**GENERAL PLASTICS MANUFACTURING COMPANY**



12

ISS004

**Figure 2.12.5-1 - General Plastics Data, continued (Page 3 of 3)**

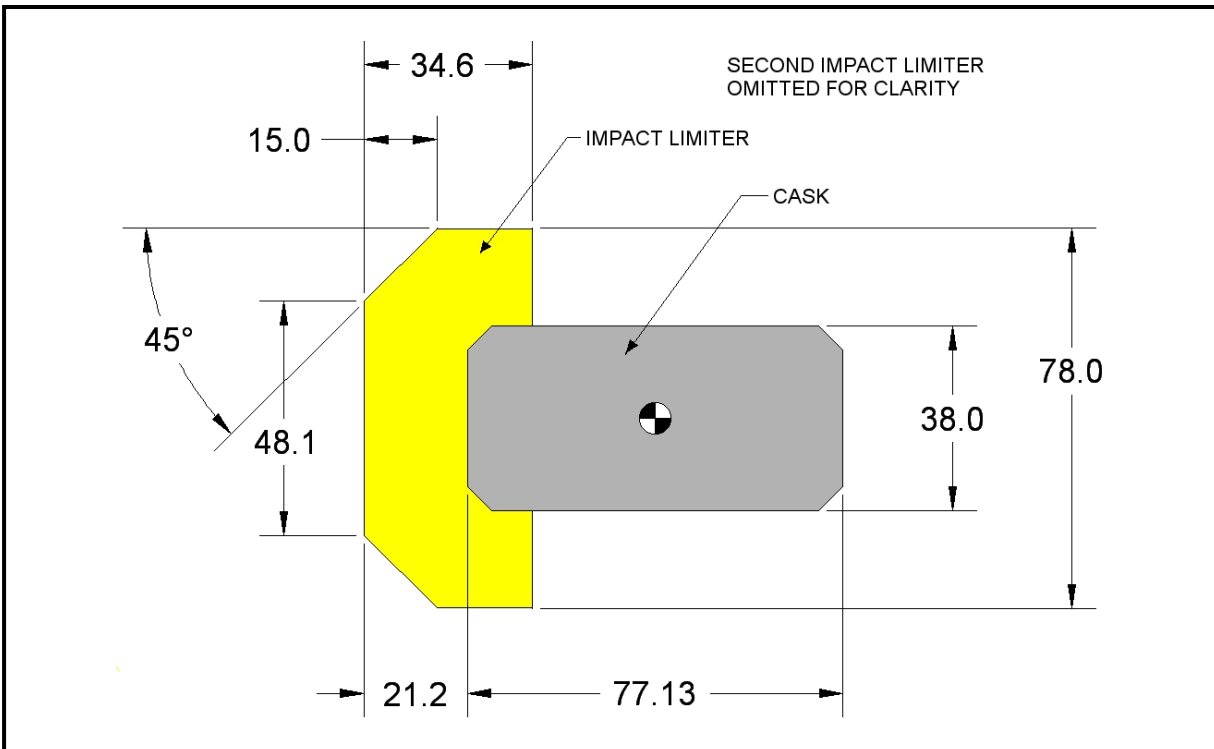


Figure 2.12.5-2 - Dimensions Used in CASKDROP

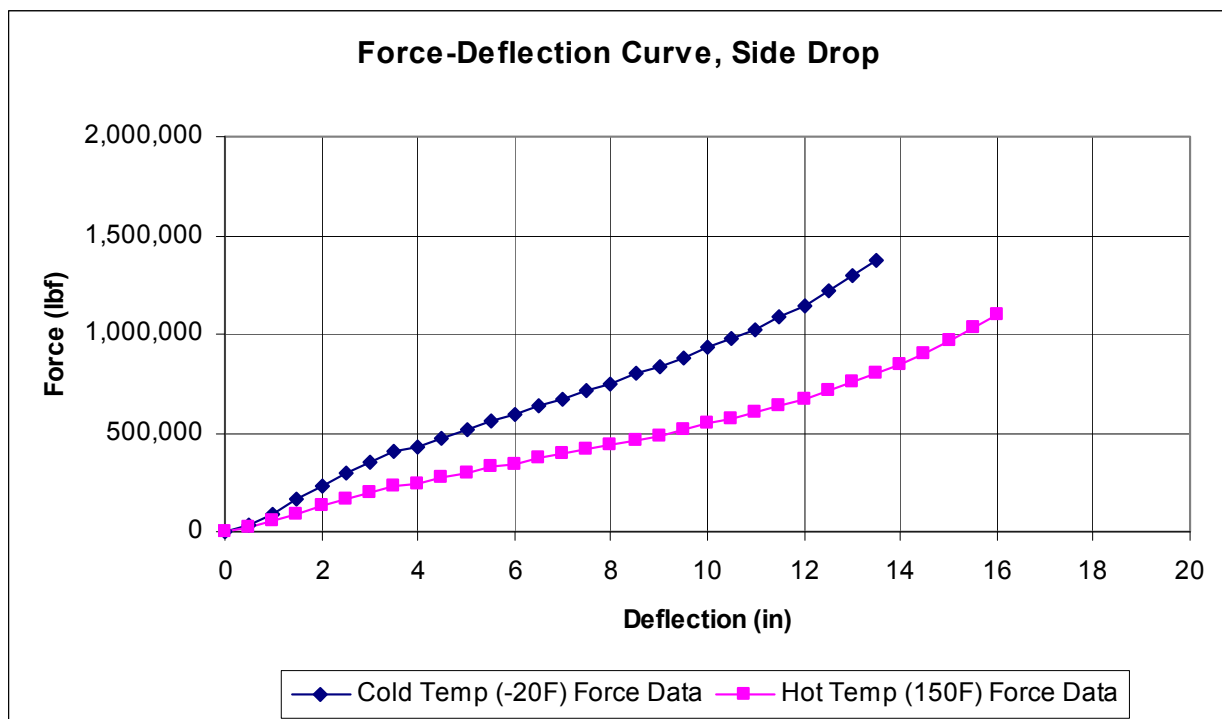
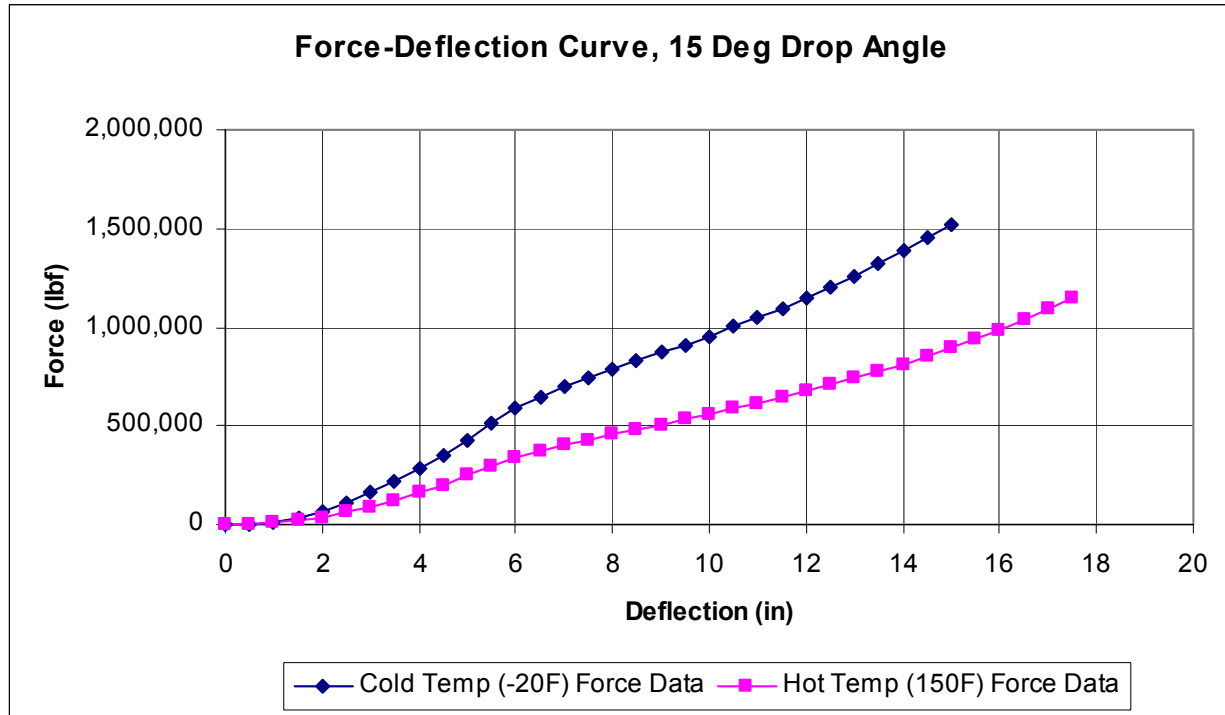
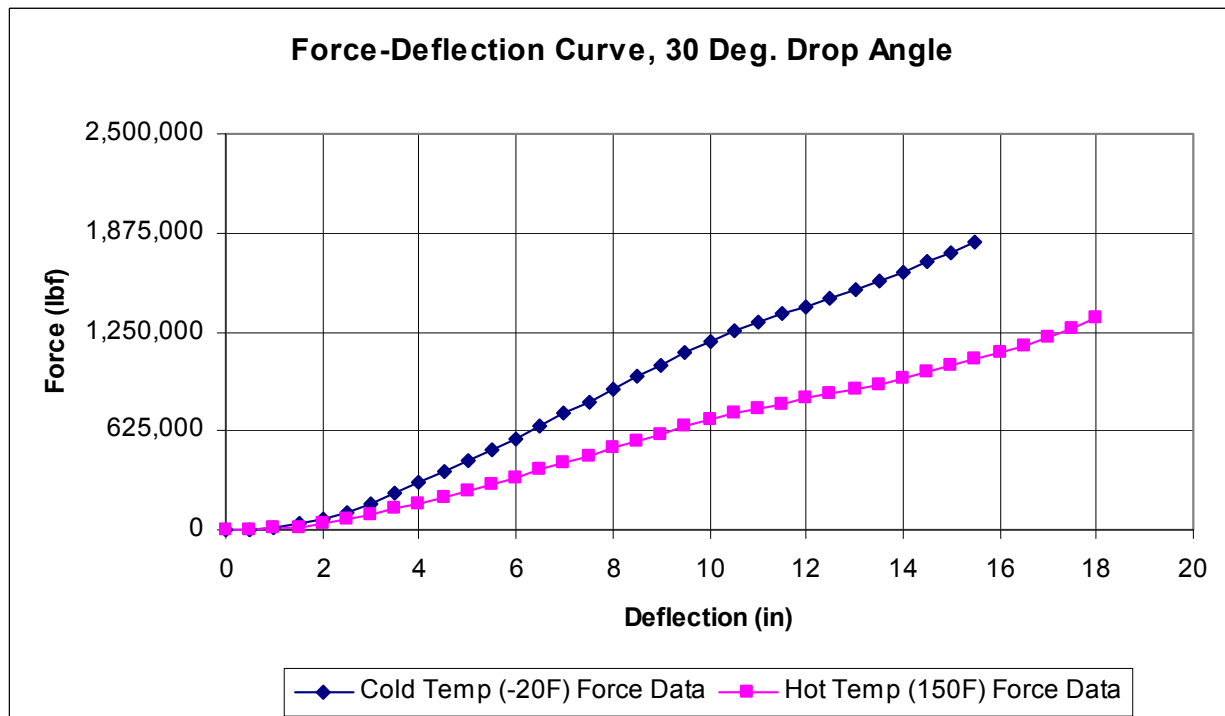
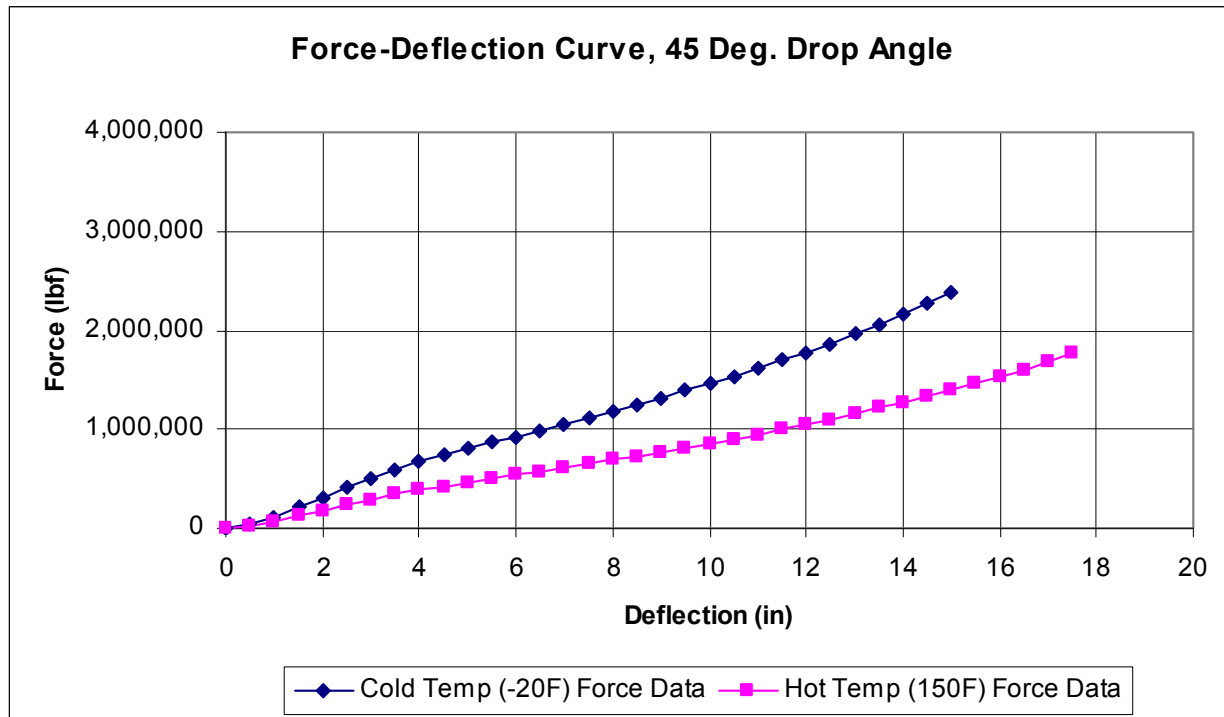
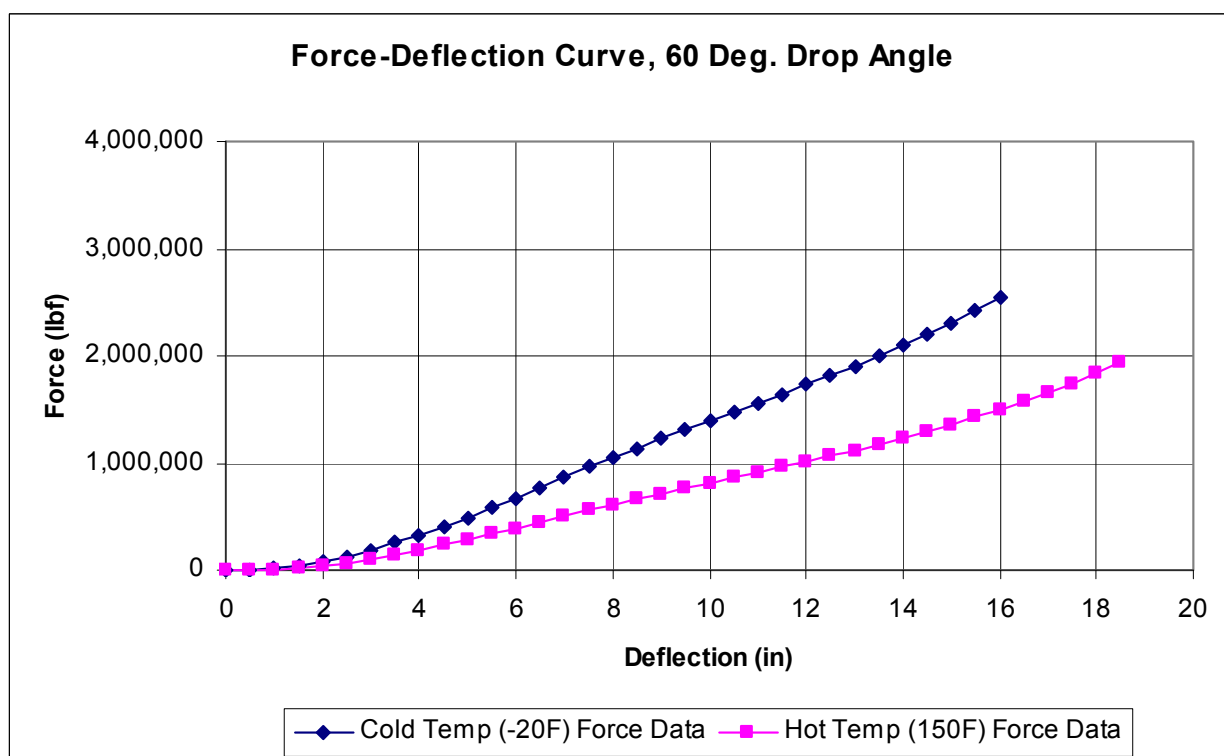


Figure 2.12.5-3 - Force-Deflection Curve, Side Orientation

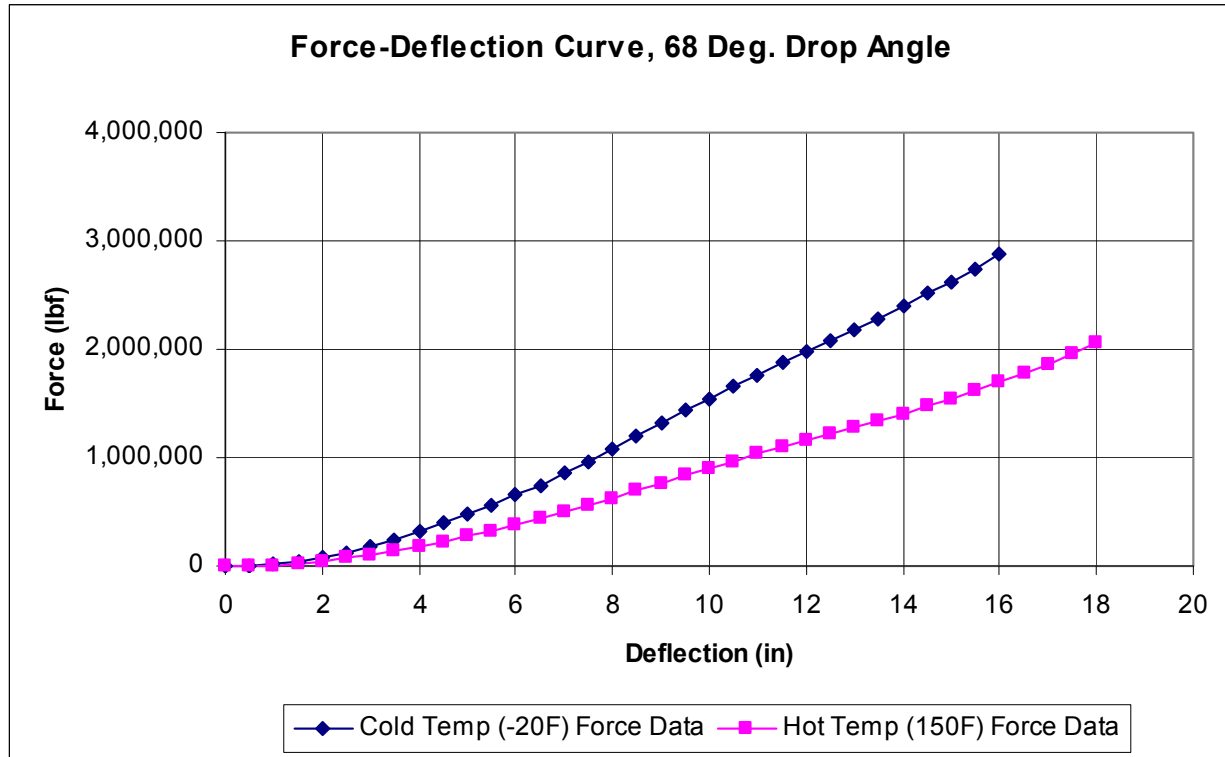
**Figure 2.12.5-4 - Force-Deflection Curve, 15° Orientation****Figure 2.12.5-5 - Force-Deflection Curve, 30° Orientation**



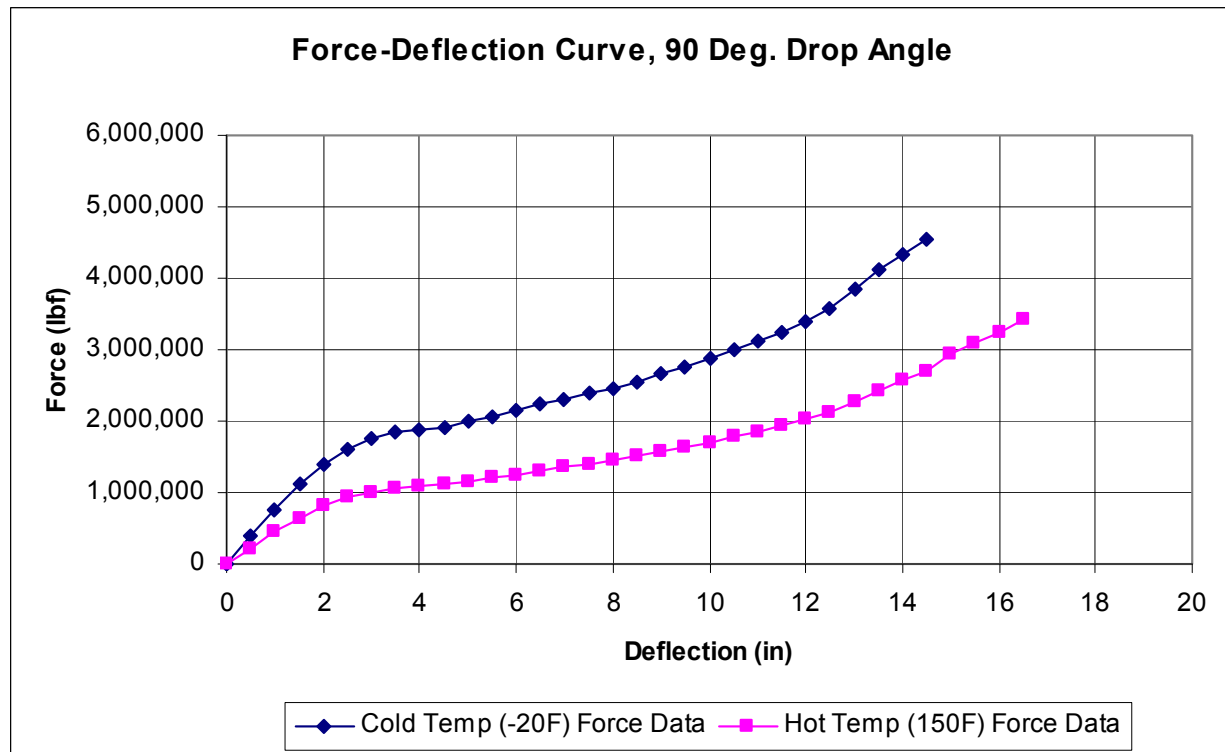
**Figure 2.12.5-6 - Force-Deflection Curve, 45° Orientation**



**Figure 2.12.5-7 - Force-Deflection Curve, 60° Orientation**



**Figure 2.12.5-8 - Force-Deflection Curve, 68° Orientation**



**Figure 2.12.5-9 - Force-Deflection Curve, 90° Orientation**



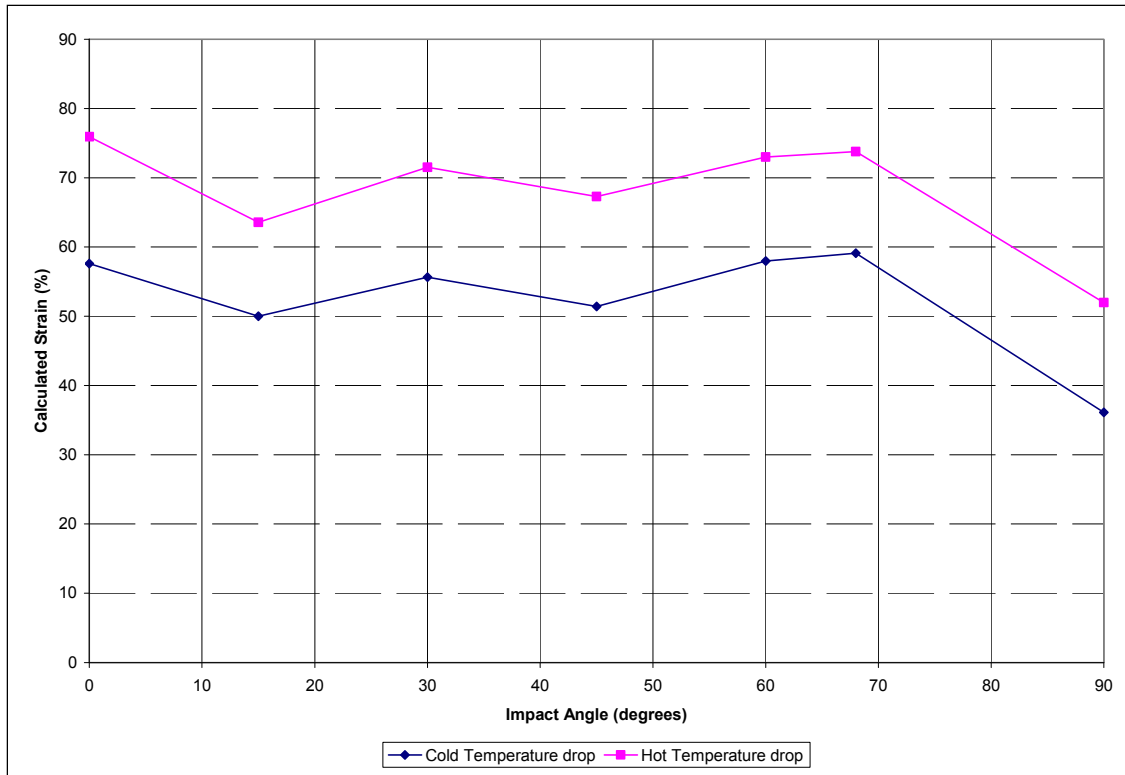


Figure 2.12.5-10 - Primary Impact Limiter Strain, HAC

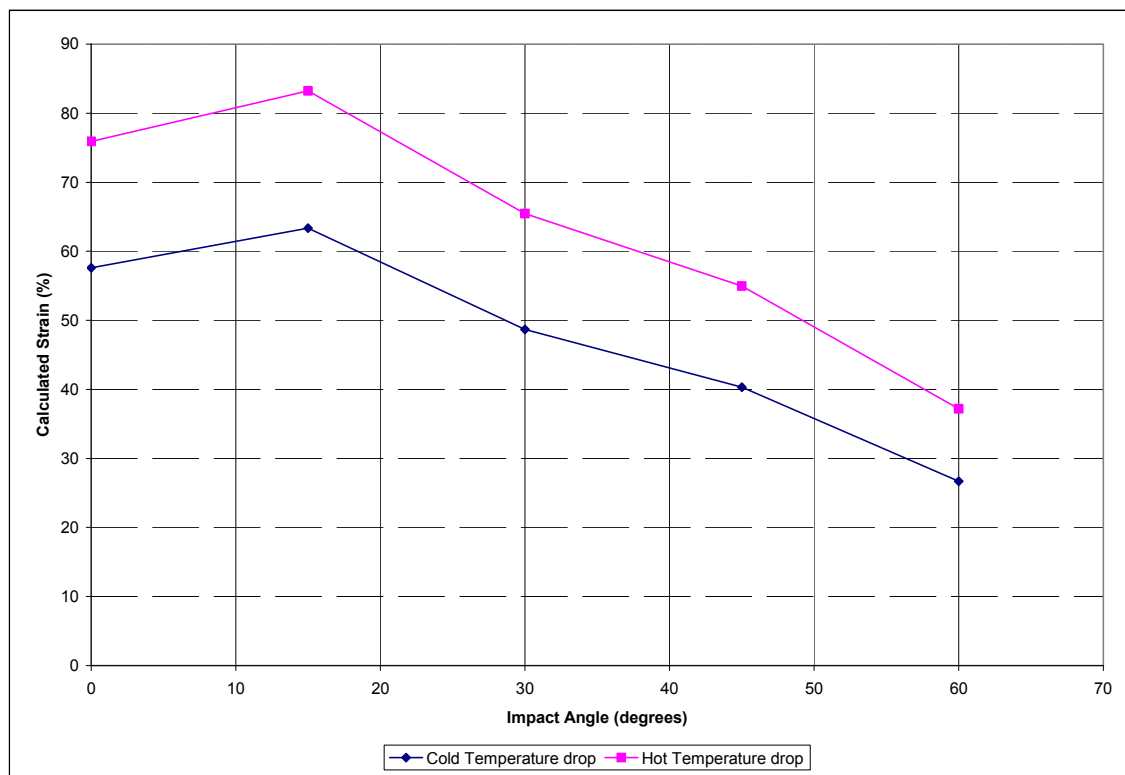


Figure 2.12.5-11 - Secondary Impact Limiter Strain, HAC

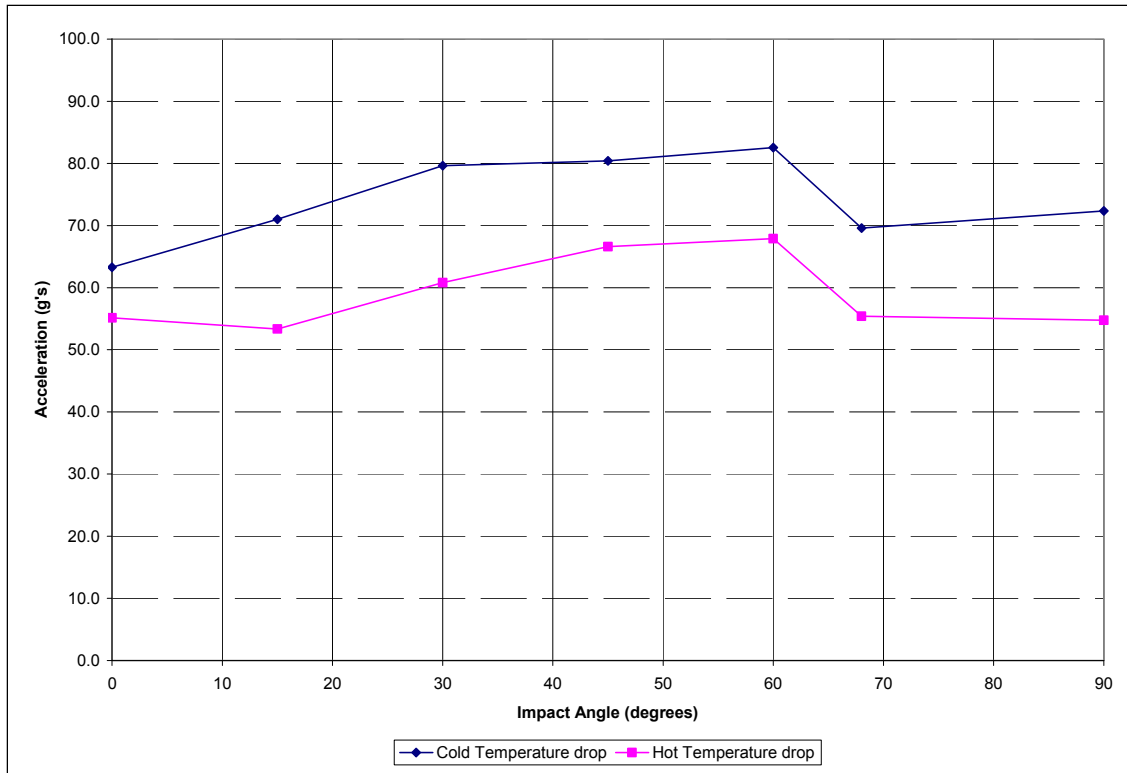


Figure 2.12.5-12 - Primary Impact Acceleration, HAC

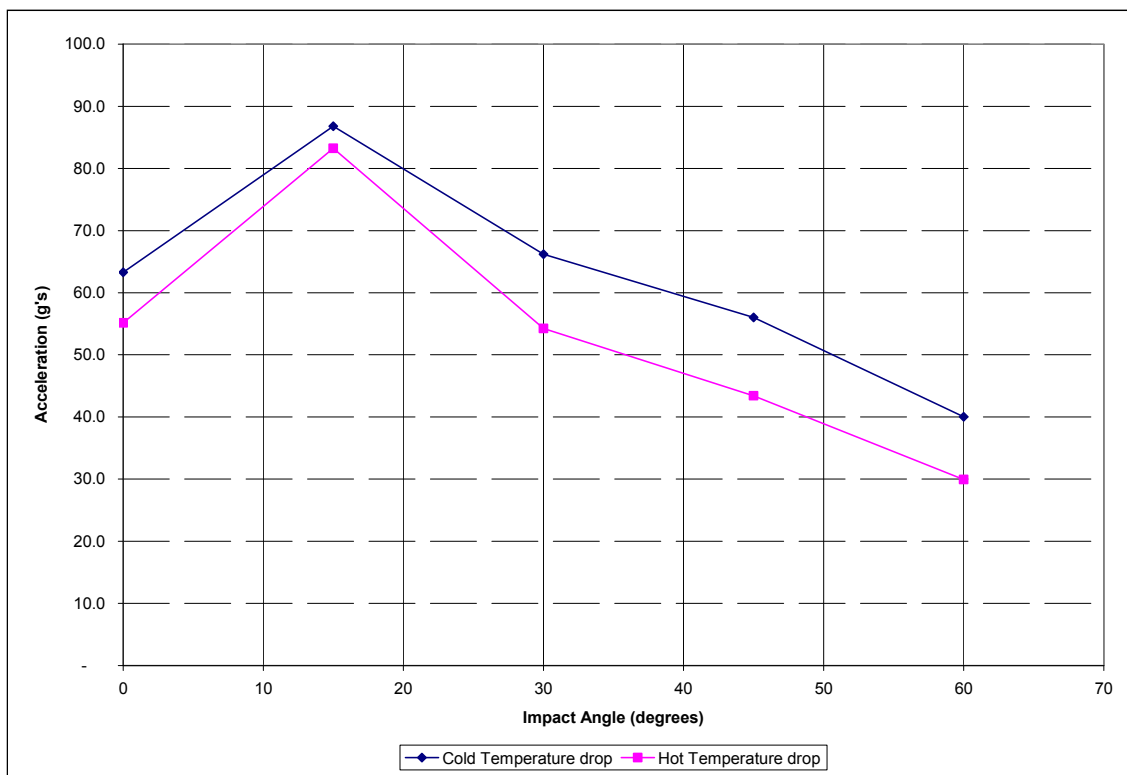


Figure 2.12.5-13 - Secondary Impact Acceleration, HAC

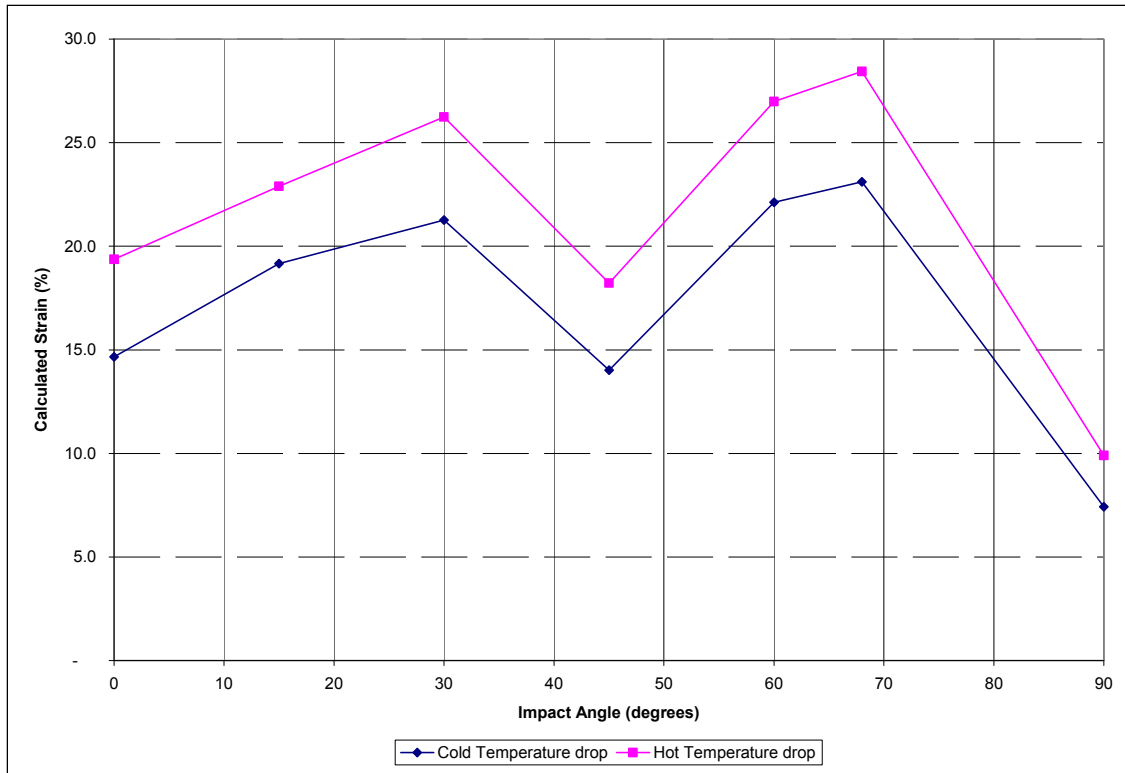


Figure 2.12.5-14 - Primary Impact Limiter Strain, NCT

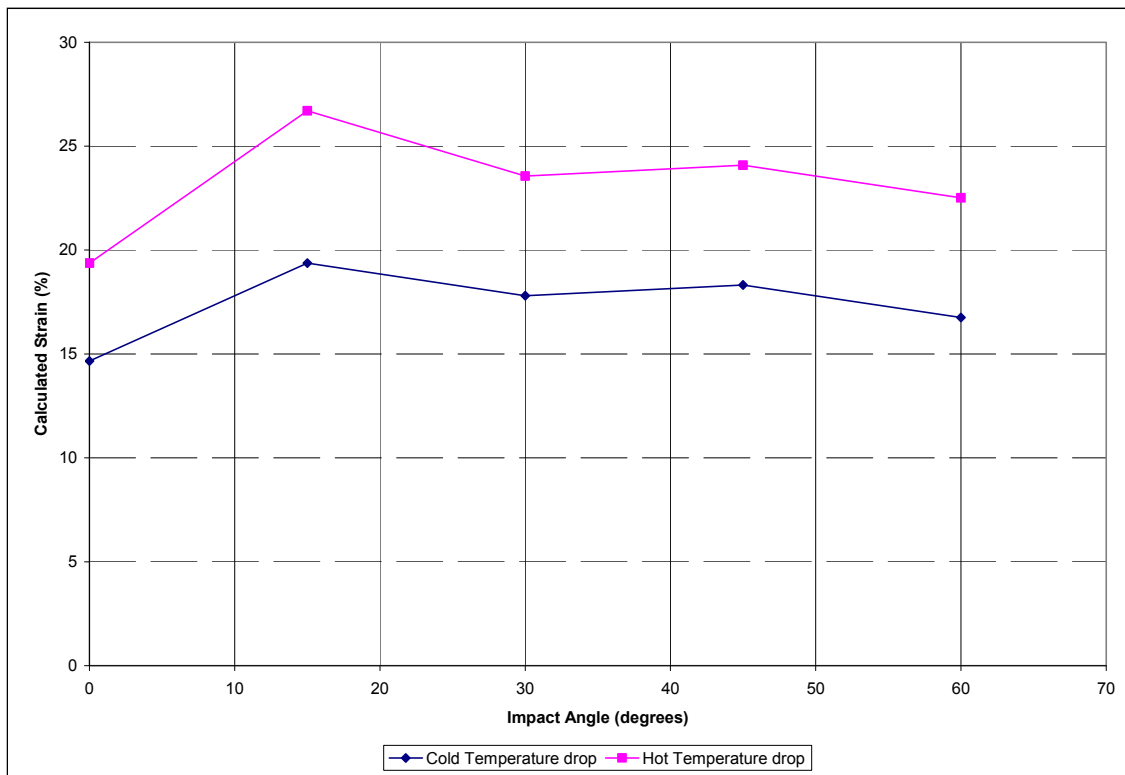


Figure 2.12.5-15 - Secondary Impact Limiter Strain, NCT

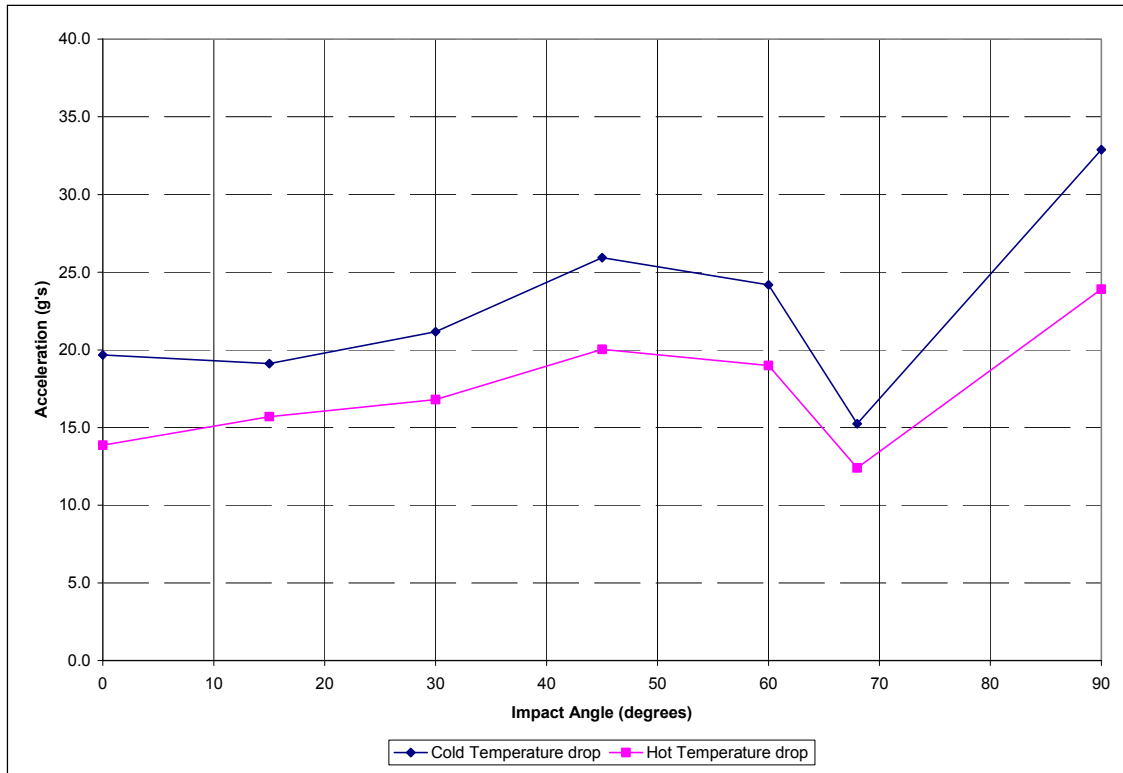


Figure 2.12.5-16 - Primary Impact Acceleration, NCT

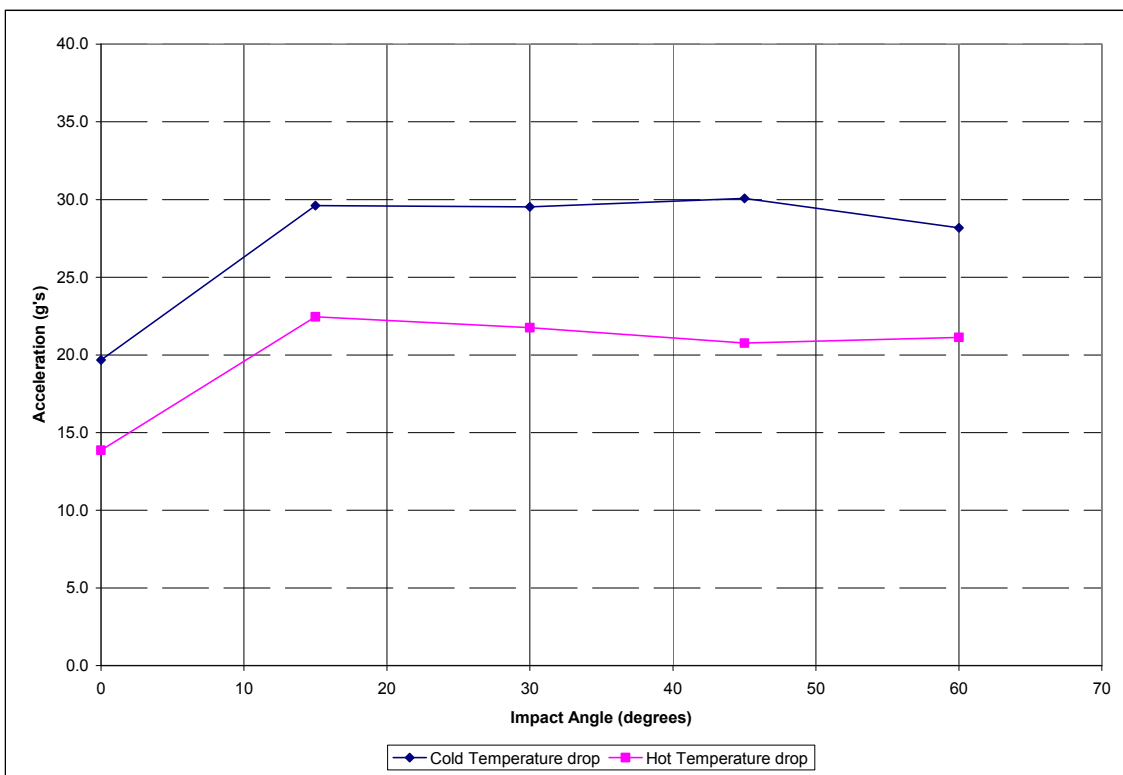
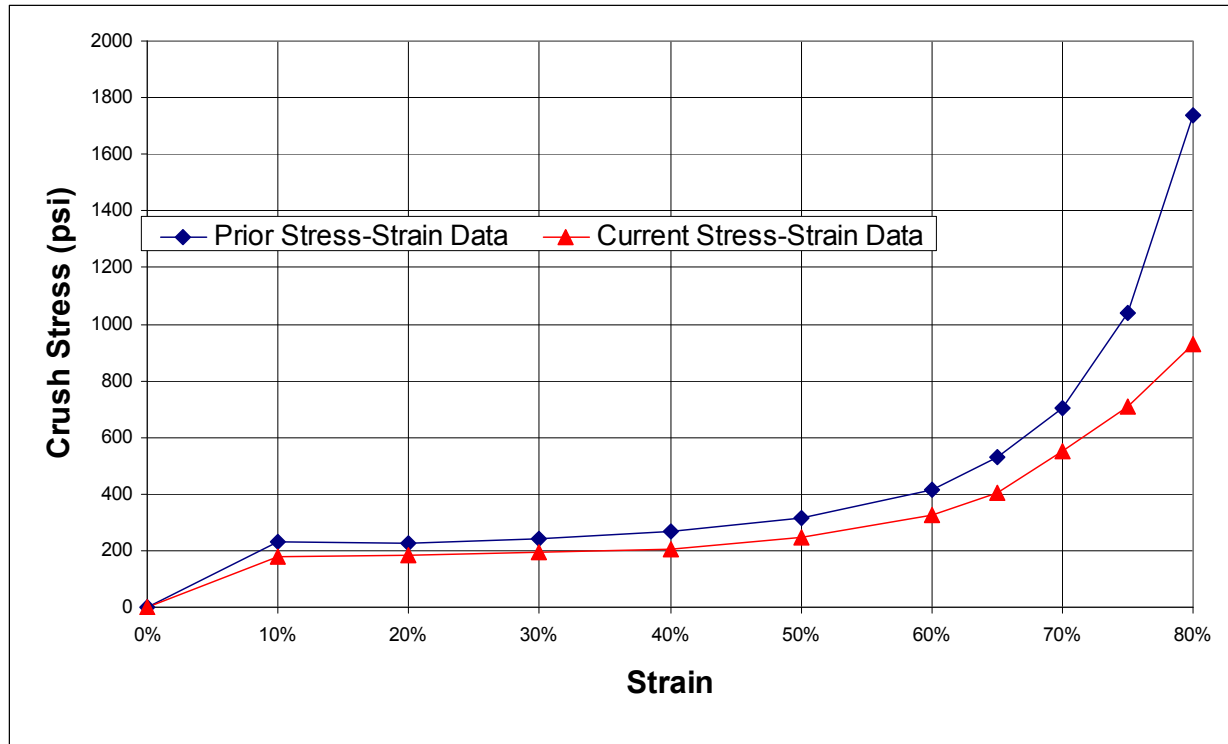


Figure 2.12.5-17 - Secondary Impact Acceleration, NCT



**Figure 2.12.5-18** - Previously Published vs. Current Stress-Strain Data (150 °F)

## 2.12.6 Analysis Software Descriptions

This appendix contains descriptions of the computer codes CASKDROP and SLAPDOWN. Both of these programs are used in Appendix 2.12.5, *Impact Limiter Performance Evaluation*.

### 2.12.6.1 CASKDROP

This appendix briefly documents the methodology employed by the AREVA Federal Services proprietary computer program CASKDROP. Used in conjunction with an appropriate packaging dynamic analysis computer code (see Section 2.12.6.2, *SLAPDOWN*), the computer program CASKDROP is used to demonstrate compliance of the package with 10 CFR §71.71(c)(7) and 10 CFR §71.73(c)(1) for normal conditions of transport (NCT) and hypothetical accident conditions (HAC) of transport free drop analyses, respectively.

#### 2.12.6.1.1 Using CASKDROP to Determine Impact Limiter Deformation Behavior

CASKDROP evaluates all angles of drop from 0° (horizontal) to 90° (vertical) by performing a quasi-static analysis that ignores rotational effects. At orientations where rotational effects are important, use of a dynamic analysis computer program such as SLAPDOWN is required utilizing the force-deflection data developed by CASKDROP. Note that although CASKDROP is capable of completely solving the impact analysis for orientations where rotation effects are not important (e.g., end, side, and c.g.-over-corner), the only program output which is utilized in the evaluation of the BRR Package free drop events is the formulation of the force-deflection relation for the impact limiters. The program SLAPDOWN, using the force-deflection input from CASKDROP, is utilized for the final evaluation of all orientations. The following material is a general documentation of CASKDROP, and is not limited to the features utilized for the BRR package.

CASKDROP assumes the package is protected by polyurethane foam-filled, energy absorbing impact limiters. Since the impact surface is unyielding, the impact limiters are assumed to absorb all of the potential energy of the drop event.

For all orientations of impact, the prediction of impact limiter deformation behavior can be approached from straightforward energy balance principles:

$$E = W(h + \delta) = \int_0^{\delta} F_x dx$$

where  $W$  is the package gross weight,  $h$  is the drop height,  $\delta$  is the maximum impact limiter deformation, and  $F_x$  is the force imposed on the target at an impact limiter deformation of  $x$ . The left-hand term represents the potential energy of the free drop. The right-hand term represents the strain energy of the deformed impact limiter(s).

Given a specific drop angle,  $\theta$ , and impact limiter deformation,  $\delta$ , as illustrated in Figure 2.12.6-1, the result is an impact limiter crush plane “footprint.” Integration of the impact limiter crush plane yields a total crush force and centroidal distance of:

$$F = \iint \sigma\{\varepsilon\} dA \quad \text{and} \quad \bar{X} = \left(\frac{1}{F}\right) \iint \bar{x} \sigma\{\varepsilon\} dA$$

**BRR Package Safety Analysis Report**

respectively, where  $F$  is the total integrated force,  $\sigma\{\epsilon\}$  is the differential stress as a function of strain,  $dA$  is the differential area (i.e.,  $dA$  is a function of the “x” and “y” directions, or  $dx$  and  $dy$ ),  $\bar{X}$  is the total integrated centroidal distance from the package center of gravity, and  $\bar{x}$  is the differential centroidal distance from the package center of gravity.

With reference to Figure 2.12.6-1, the geometric calculations for the impact surface (crush plane) and the associated strains are carried out using a translating X'-Y'-Z' coordinate system, with the X'-Y' plane corresponding to the crush plane. Due to the cylindrical nature of the problem, the overall crush plane is comprised of a segment of an ellipse corresponding to the outside surface of the impact limiter. The optional end hole requires removal of its associated elliptical segment. Similarly, the optional conical surface is an elliptical, parabolic, or hyperbolic segment depending on both the drop angle,  $\theta$ , and angle of the cone.

Calculation of the differential strain is somewhat more complex. As illustrated in Figure 2.12.6-2, the differential strain,  $\epsilon\{x,y\}$ , is calculated at the center of the differential area,  $dA$ . The differential strain is determined by calculating the amount of vertical deformation at the  $(x, y)$  location on the crush plane. The vertical distance from point  $(x, y)$  on the impact surface to the package or upper impact limiter surface is found and denoted  $z_{TOP}$ . Similarly, the vertical distance from point  $(x, y)$  on the impact surface to the undeformed lower impact limiter surface is found and denoted  $z_{BOT}$ . In equation format the differential strain at location  $(x, y)$  is simply:

$$\epsilon = \frac{z_{BOT}}{z_{BOT} + z_{TOP}}$$

This strain is used to determine the corresponding crush stress from an implicit tabular definition of the crushable media stress-strain characteristics. For each differential area,  $dA$ , the differential force,  $dF$ , is found. The total force,  $F$ , is therefore the summation of the differential forces. Similarly, the centroidal distance,  $\bar{X}$ , is the summation of the moments,  $\bar{x} \times dF$ , divided by the total force.

Unbacked regions are defined as having an  $(x, y)$  location where  $z_{TOP}$  is calculated to occur outside the package's “shadow” (i.e., or backing, occurring on the impact limiter surface). Unbacked regions usually utilize the nominal crush strength of the crushable media (typically 10% for polyurethane foam material) for integrated force purposes. The crush strength for unbacked regions is user-definable in the program CASKDROP.

For most drop angles,  $\theta$ , and impact limiter deformations,  $\delta$ , the impact limiter crush force,  $F$ , is transmitted to the package body in direct compression. Hence, the forces transmitted to the circumferential impact limiter attachments are essentially zero. However, for nearly vertical or horizontal orientations at small deformations where the crush force occurs beyond the edge of the package, the forces transmitted to the impact limiter attachments can be substantially large. It is important to note that only the nearly vertical or nearly horizontal orientations are required to produce the prying motion; all other orientations will always compress the impact limiter onto the package body. Figure 2.12.6-3 illustrates the near vertical and near horizontal orientations producing impact limiter separation forces.

For the near vertical orientation, the moment about point “a” determines whether a separation force exists at the impact limiter attachments. Assuming for this case that a counterclockwise moment is positive (i.e., will tend to “pry” the impact limiter off the package), the equation for the moment about point “a,”  $M_a$ , is:

$$M_a = Fx_F + F_{IL}x_{IL}$$

Similarly, for the near horizontal orientation, the moment about point “b” determines whether a separation force exists at the impact limiter attachments. Assuming for this case that a clockwise moment is positive (i.e., will tend to “pry” the impact limiter off the package), the equation for the moment about point “b,”  $M_b$ , is:

$$M_b = Fx_F - F_{IL}x_{IL}$$

If  $M_a$  or  $M_b$  are positive, a separation force will occur at the impact limiter attachments whereas if  $M_a$  or  $M_b$  are zero or negative, a separation force will not occur. Note that use of a conically shaped impact limiter typically eliminates the impact limiter separation force by causing the crush force,  $F$ , to almost always occur between points “a” and “b.”

#### 2.12.6.1.2 An Example Problem for the CASKDROP Program

An example problem is illustrated in Figure 2.12.6-4. The CASKDROP program utilizes a variety of physical input data to determine package and impact limiter geometry. In all cases, the package and impact limiter are assumed axisymmetric. The package is cylindrical, as is the impact limiter. Two fundamental variations in the basic cylindrical shape of the impact limiter are an optional end hole and optional conical end. The end hole may extend part or all of the way from the outside surface of the impact limiter to the package end. The conical end may be a truncated or fully developed cone, defined by a cone diameter and a cone length at the outside surface of the impact limiter. By varying the impact limiter dimensions the result is a wide variety of possible impact limiter shapes, from a totally enclosing “overpack” to pointed end-only buffers.

The CASKDROP program was primarily developed as an impact limiter design tool. Geometry and analysis control input to the CASKDROP program is fully interactive allowing changes “on the fly.” Figure 2.12.6-5 illustrates the CASKDROP screen for data entry into the *Input Window*.

The CASKDROP program allows for three types of crushable media definition:

1. **CONSTANT:** a constant crush stress independent of calculated strain.
2. **VARIABLE:** a variable, user-defined stress-strain definition. The BRR package analysis uses this option by inputting the adjusted stress-strain curves as discussed in Appendix 2.12.5.
3. **POLYFOAM:** a built-in polyurethane foam database providing accurate stress-strain definition for 5 to 25 pound per cubic foot (pcf) density and temperatures of -20 °F to +300 °F based on extensive sample testing.

The example problem assumes 20 pcf polyurethane foam at a temperature of -20 °F. A +60% bias is applied to the temperature-corrected stress-strain data to account for dynamic strain rate effects for the example problem. Figure 2.12.6-6 illustrates the CASKDROP input screen for the polyurethane foam crush media for the example problem.

For the example problem, the CASKDROP program utilizes polyurethane foam where “parallel to rise” foam curing occurs in the axial direction and “perpendicular to rise” foam curing occurs in the radial direction, although the difference between these two directions is small. The user may optionally select the “parallel-to-rise” or “perpendicular-to-rise” properties to be reversed or global for all drop orientations. For orientations other than axial (end drop) and radial (side drop), the CASKDROP program interpolates foam properties using an ellipse function. For the case where



crush stress “parallel-to-rise” is in the axial direction,  $\sigma_{PAR}$ , and crush stress “perpendicular-to-rise” is in the radial direction,  $\sigma_{PER}$ , the interpolation equation at drop angle,  $\theta$ , is:

$$\sigma_{\theta} = \sqrt{\frac{1}{\left(\frac{\sin \theta}{\sigma_{PAR}}\right)^2 + \left(\frac{\cos \theta}{\sigma_{PER}}\right)^2}}$$

Similarly, for the case where crush stress “perpendicular-to-rise” is in the axial direction,  $\sigma_{PER}$ , and crush stress “parallel-to-rise” is in the radial direction,  $\sigma_{PAR}$ , the interpolation equation is:

$$\sigma_{\theta} = \sqrt{\frac{1}{\left(\frac{\sin \theta}{\sigma_{PER}}\right)^2 + \left(\frac{\cos \theta}{\sigma_{PAR}}\right)^2}}$$

The *Control Window* allows the user to specify various analysis and output controls. The *Control Window* is separated into *Analysis*, *Crush*, *Angle*, *Static*, *Dynamic*, *Print*, and *File*.

Three *Analysis* options are available: *dXY* defines the number of integration elements in the crush plane, 25 for the example problem; *Sln* defines the analysis methodology (Global versus Local Strain Theory), *Global* for the example problem;  $\varepsilon/\sigma$  defines the strain (or crush stress) value to be utilized in unbacked regions (e.g., if a value is specified between 0 and 1, it is assumed a strain value and the corresponding crush stress at that strain is used; if a value is specified greater than 1, it is assumed to be a crush stress), 0.1 for the example problem corresponding to a crush stress at 10% strain from the polyurethane foam database.

The *Crush* options define the incremental deformations to be analyzed. The example problem specifies analyzing for crush deformations from 0.25 inch to 20 inch in 0.25 inch increments. Specifying a *Max* value greater than the actual maximum available crush depth (as determined geometrically) flags the CASKDROP program to not exceed the maximum available crush depth.

Similarly, the *Angle* options define the incremental angular orientations to be analyzed. The example problem specifies analyzing for drop angles from 0° to 90° in 15° increments.

The *Static* options allow the user to specify quasi-static analyses providing *Full* display output, *Smry* (summary) output, or *Both*. The example problem specifies *Full* output to the display only. Similarly, the *Dynamic* options allow the user to specify dynamic analyses providing *Full* display output, *Smry* (summary) output, or *Both*. The example problem does not specify a dynamic analysis as that module is not completed in the CASKDROP program.

The *Print* and *File* options allow the user to specify *Full* display output, *Smry* (summary) output, or *Both* to the printer or a file. The example problem specifies *Full* output to an output file only.

The *Output Window* provides the location for *Static* and *Dynamic* display output. A quasi-static solution is achieved when the strain energy of the crushable media (*SE*) is equal to the free-falling kinetic energy of the package (*KE*), or  $SE/KE = 1$ . The following tables provide a sample file output at 0° (side drop), at 45°, and at 90° (end drop).

# BRR Package Safety Analysis Report

Docket No. 71-9341

Rev. 8, July 2015

Side Drop  
05-16-1995, 15:38:39

\*\*\* PACKAGING TECHNOLOGY \*\*\*

CASKDROP, v2.21  
Jul 01, 1994

SAMPLE PROBLEM FOR QUALITY ASSURANCE CHECK (AREAS AND VOLUMES)			
Impact Limiter Weight (each) -	1,000 lbs	Cask and Payload Weight -	10,000 lbs
Impact Limiter Outside Diameter -	60.0000 in	Cask Outside Diameter -	40.0000 in
Impact Limiter Overall Length -	24.0000 in	Cask Overall Length -	48.0000 in
Impact Limiter Conical Diameter -	48.0000 in	Dynamic Unloading Modulus -	1.000E+07 lbs/in
Impact Limiter Conical Length -	10.0000 in	Rad Mass Moment of Inertia -	12,235 lb-in-s <sup>2</sup>
Impact Limiter End Thickness -	12.0000 in	Frictional Coefficient -	0.0000
Impact Limiter Hole Diameter -	20.0000 in	Drop Height -	30.0000 ft
Impact Limiter Hole Length -	8.0000 in	Drop Angle from Horizontal -	0.0000°
Unbacked Area Threshold Strain -	0.1000 in/in	Crush Analysis Theory -	Global
Unbacked Area Crush Stress -	2,675 psi	Number of Integration Incs -	25

POLYFOAM CRUSH STRESS (Axial: "  " to rise)	
Density = 20.000 pcf	
Temp = -20.000 F	
$\sigma$ -yield = 2,552.3 psi	
Bias = 60.000%	
$\epsilon$ (in/in)	$\sigma$ (psi)
0.000	0.0
0.100	2,552.3
0.200	2,687.0
0.300	2,868.8
0.400	3,302.9
0.500	4,115.1
0.600	6,074.3
0.650	7,942.0
0.700	10,925.0
0.750	15,001.8
0.800	26,829.5

POLYFOAM CRUSH STRESS (Radial: "⊥" to rise)	
Density = 20.000 pcf	
Temp = -20.000 F	
$\sigma$ -yield = 2,675.0 psi	
Bias = 60.000%	
$\epsilon$ (in/in)	$\sigma$ (psi)
0.000	0.0
0.100	2,675.0
0.200	2,785.4
0.300	2,959.9
0.400	3,345.9
0.500	4,147.7
0.600	6,062.8
0.650	7,868.8
0.700	10,180.0
0.750	15,554.4
0.800	29,704.8

POLYFOAM CRUSH STRESS (Actual Data @ 0.0°)	
Density = 20.000 pcf	
Temp = -20.000 F	
$\sigma$ -yield = 2,675.0 psi	
Bias = 60.000%	
$\epsilon$ (in/in)	$\sigma$ (psi)
0.000	0.0
0.100	2,675.0
0.200	2,785.4
0.300	2,959.9
0.400	3,345.9
0.500	4,147.7
0.600	6,062.8
0.650	7,868.8
0.700	10,180.0
0.750	15,554.4
0.800	29,704.8

DEFL (in)	MAX $\epsilon$ (%)	AREA (in <sup>2</sup> )	VOLUME (in <sup>3</sup> )	XBAR (in)	IMPACT FORCE (lbs)	ACCEL (g's)	I/L MOMENT (in-lbs)	STRAIN ENERGY (in-lbs)	KINETIC ENERGY (in-lbs)	SE/KE RATIO
0.250	2.50	221	37	0.00	106,881	8.9	0	13,360	4,323,000	0.00
0.500	5.00	318	105	0.00	289,508	24.1	0	62,909	4,326,000	0.01
0.750	7.50	396	194	0.00	518,875	43.2	0	163,957	4,329,000	0.04
1.000	10.00	465	302	0.00	733,200	61.1	0	320,466	4,332,000	0.07

# BRR Package Safety Analysis Report

Docket No. 71-9341

Rev. 8, July 2015

Side Drop  
05-16-1995, 15:38:39

\*\*\* PACKAGING TECHNOLOGY \*\*\*  
(continued...)

CASKDROP, v2.21  
Jul 01, 1994

DEFL (in)	MAX $\epsilon$ (%)	AREA (in <sup>2</sup> )	VOLUME (in <sup>3</sup> )	XBAR (in)	IMPACT FORCE (lbs)	ACCEL (g's)	I/L MOMENT (in-lbs)	STRAIN ENERGY (in-lbs)	KINETIC ENERGY (in-lbs)	SE/KE RATIO
1.250	12.49	528	425	0.00	955,009	79.6	0	531,492	4,335,000	0.12
1.500	14.99	587	565	0.00	1,107,366	92.3	0	789,289	4,338,000	0.18
1.750	17.49	644	719	0.00	1,270,225	105.9	0	1,086,488	4,341,000	0.25
2.000	19.99	699	886	0.00	1,371,441	114.3	0	1,416,697	4,344,000	0.33
2.250	22.49	752	1,068	0.00	1,509,207	125.8	0	1,776,778	4,347,000	0.41
2.500	24.99	804	1,262	0.00	1,668,937	139.1	0	2,174,046	4,350,000	0.50
2.750	27.49	855	1,469	0.00	1,761,221	146.8	0	2,602,815	4,353,000	0.60
3.000	29.99	906	1,690	0.00	1,946,101	162.2	0	3,066,230	4,356,000	0.70
3.250	32.49	955	1,921	0.00	2,044,813	170.4	0	3,565,095	4,359,000	0.82
3.500	34.98	1,005	2,167	0.00	2,249,052	187.4	0	4,101,828	4,362,000	0.94
3.614	36.13	1,027	2,285	0.00	2,326,676	193.9	0	4,363,372	4,363,372	1.00
3.750	37.48	1,053	2,424	0.00	2,419,003	201.6	0	4,956,582	4,365,000	1.14
4.000	39.98	1,101	2,692	0.00	2,640,297	220.0	0	5,588,994	4,368,000	1.28
4.250	42.48	1,149	2,975	0.00	2,759,520	230.0	0	6,263,971	4,371,000	1.43
4.500	44.98	1,197	3,267	0.00	2,956,003	246.3	0	6,978,412	4,374,000	1.60
4.750	47.48	1,244	3,571	0.00	3,208,534	267.4	0	7,748,979	4,377,000	1.77
5.000	49.98	1,292	3,889	0.00	3,357,376	279.8	0	8,569,718	4,380,000	1.96
5.250	52.48	1,339	4,219	0.00	3,603,141	300.3	0	9,439,782	4,383,000	2.15
5.500	54.97	1,385	4,556	0.00	3,906,997	325.6	0	10,378,550	4,386,000	2.37
5.750	57.47	1,432	4,909	0.00	4,215,273	351.3	0	11,393,833	4,389,000	2.60
6.000	59.97	1,479	5,275	0.00	4,573,066	381.1	0	12,492,376	4,392,000	2.84
6.250	62.47	1,520	5,650	0.00	4,961,100	413.4	0	13,684,147	4,395,000	3.11
6.500	64.97	1,559	6,035	0.00	5,404,072	450.3	0	14,979,793	4,398,000	3.41
6.750	67.47	1,597	6,430	0.00	5,893,283	491.1	0	16,391,963	4,401,000	3.72
7.000	69.97	1,632	6,834	0.00	6,440,254	536.7	0	17,933,655	4,404,000	4.07
7.250	72.47	1,666	7,246	0.00	7,087,717	590.6	0	19,624,651	4,407,000	4.45
7.500	74.96	1,698	7,667	0.00	8,001,352	666.8	0	21,510,785	4,410,000	4.88
7.750	77.46	1,730	8,095	0.00	9,446,226	787.2	0	23,691,732	4,413,000	5.37
8.000	79.96	1,760	8,532	0.00	11,484,412	957.0	0	26,308,062	4,416,000	5.96
8.250	82.46	1,790	8,976	0.00	13,964,555	1,163.7	0	29,489,183	4,419,000	6.67
8.500	84.96	1,818	9,427	0.00	16,801,077	1,400.1	0	33,334,887	4,422,000	7.54
8.750	87.46	1,846	9,885	0.00	19,931,256	1,660.9	0	37,926,428	4,425,000	8.57
9.000	89.96	1,873	10,350	0.00	23,276,639	1,939.7	0	43,327,415	4,428,000	9.78
9.250	92.45	1,899	10,822	0.00	26,896,391	2,241.4	0	49,599,044	4,431,000	11.19
9.500	94.95	1,925	11,300	0.00	30,724,250	2,560.4	0	56,801,624	4,434,000	12.81
9.750	97.45	1,950	11,784	0.00	34,740,688	2,895.1	0	64,984,741	4,437,000	14.65
10.000	99.95	1,974	12,275	0.00	38,887,797	3,240.6	0	74,188,302	4,440,000	16.71

# BRR Package Safety Analysis Report

Docket No. 71-9341

Rev. 8, July 2015

Corner Drop  
05-16-1995, 15:38:39

\*\*\* PACKAGING TECHNOLOGY \*\*\*

CASKDROP, v2.21  
Jul 01, 1994

SAMPLE PROBLEM FOR QUALITY ASSURANCE CHECK (AREAS AND VOLUMES)			
Impact Limiter Weight (each) -	1,000 lbs	Cask and Payload Weight -	10,000 lbs
Impact Limiter Outside Diameter -	60.0000 in	Cask Outside Diameter -	40.0000 in
Impact Limiter Overall Length -	24.0000 in	Cask Overall Length -	48.0000 in
Impact Limiter Conical Diameter -	48.0000 in	Dynamic Unloading Modulus -	1.000E+07 lbs/in
Impact Limiter Conical Length -	10.0000 in	Rad Mass Moment of Inertia -	12,235 lb-in-s <sup>2</sup>
Impact Limiter End Thickness -	12.0000 in	Frictional Coefficient -	0.0000
Impact Limiter Hole Diameter -	20.0000 in	Drop Height -	30.0000 ft
Impact Limiter Hole Length -	8.0000 in	Drop Angle from Horizontal -	45.0000°
Unbacked Area Threshold Strain -	0.1000 in/in	Crush Analysis Theory -	Global
Unbacked Area Crush Stress -	2,611 psi	Number of Integration Incs -	25

POLYFOAM CRUSH STRESS (Axial: "I" to rise)	
Density = 20.000 pcf	
Temp = -20.000 F	
$\sigma$ -yield = 2,552.3 psi	
Bias = 60.000%	
$\epsilon$ (in/in)	$\sigma$ (psi)
0.000	0.0
0.100	2,552.3
0.200	2,687.0
0.300	2,868.8
0.400	3,302.9
0.500	4,115.1
0.600	6,074.3
0.650	7,942.0
0.700	10,925.0
0.750	15,001.8
0.800	26,829.5

POLYFOAM CRUSH STRESS (Radial: "I" to rise)	
Density = 20.000 pcf	
Temp = -20.000 F	
$\sigma$ -yield = 2,675.0 psi	
Bias = 60.000%	
$\epsilon$ (in/in)	$\sigma$ (psi)
0.000	0.0
0.100	2,675.0
0.200	2,785.4
0.300	2,959.9
0.400	3,345.9
0.500	4,147.7
0.600	6,062.8
0.650	7,868.8
0.700	10,180.0
0.750	15,554.4
0.800	29,704.8

POLYFOAM CRUSH STRESS (Actual Data @ 45.0°)	
Density = 20.000 pcf	
Temp = -20.000 F	
$\sigma$ -yield = 2,611.5 psi	
Bias = 60.000%	
$\epsilon$ (in/in)	$\sigma$ (psi)
0.000	0.0
0.100	2,611.5
0.200	2,734.9
0.300	2,913.3
0.400	3,324.2
0.500	4,131.3
0.600	6,068.5
0.650	7,905.2
0.700	10,532.8
0.750	15,270.6
0.800	28,157.6

DEFL (in)	MAX $\epsilon$ (%)	AREA (in <sup>2</sup> )	VOLUME (in <sup>3</sup> )	XBAR (in)	IMPACT FORCE (lbs)	ACCEL (g's)	I/L MOMENT (in-lbs)	STRAIN ENERGY (in-lbs)	KINETIC ENERGY (in-lbs)	SE/KE RATIO
0.250	1.44	7	1	-8.30	1,351	0.1	0	169	4,323,000	0.00
0.500	2.88	20	4	-8.11	7,756	0.6	0	1,307	4,326,000	0.00
0.750	4.33	36	11	-7.90	21,631	1.8	0	4,981	4,329,000	0.00
1.000	5.79	55	22	-7.68	44,807	3.7	0	13,286	4,332,000	0.00
1.250	7.25	78	39	-7.44	78,737	6.6	0	28,729	4,335,000	0.01
1.500	8.71	102	61	-7.19	124,483	10.4	0	54,131	4,338,000	0.01
1.750	10.18	129	90	-6.92	182,320	15.2	0	92,481	4,341,000	0.02

# BRR Package Safety Analysis Report

Docket No. 71-9341

Rev. 8, July 2015

Corner Drop  
05-16-1995, 15:38:39

\*\*\* PACKAGING TECHNOLOGY \*\*\*  
(continued...)

CASKDROP, v2.21  
Jul 01, 1994

DEFL (in)	MAX $\epsilon$ (%)	AREA (in <sup>2</sup> )	VOLUME (in <sup>3</sup> )	XBAR (in)	IMPACT FORCE (lbs)	ACCEL (g's)	I/L MOMENT (in-lbs)	STRAIN ENERGY (in-lbs)	KINETIC ENERGY (in-lbs)	SE/KE RATIO
2.000	11.66	158	126	-6.65	250,919	20.9	0	146,636	4,344,000	0.03
2.250	13.14	189	169	-6.39	327,791	27.3	0	218,975	4,347,000	0.05
2.500	14.63	222	221	-6.15	409,985	34.2	0	311,197	4,350,000	0.07
2.750	16.12	256	280	-5.92	495,229	41.3	0	424,349	4,353,000	0.10
3.000	17.64	290	349	-5.70	581,988	48.5	0	559,001	4,356,000	0.13
3.250	19.14	321	425	-5.53	666,955	55.6	0	715,119	4,359,000	0.16
3.500	21.04	350	509	-5.39	750,161	62.5	0	892,258	4,362,000	0.20
3.750	23.53	379	600	-5.30	832,241	69.4	0	1,090,058	4,365,000	0.25
4.000	26.04	407	698	-5.24	913,114	76.1	0	1,308,228	4,368,000	0.30
4.250	28.58	435	804	-5.21	993,967	82.8	0	1,546,613	4,371,000	0.35
4.500	31.14	462	916	-5.20	1,075,026	89.6	0	1,805,237	4,374,000	0.41
4.750	33.55	490	1,035	-5.22	1,157,389	96.4	0	2,084,289	4,377,000	0.48
5.000	35.86	517	1,161	-5.24	1,240,678	103.4	0	2,384,048	4,380,000	0.54
5.250	38.16	545	1,293	-5.27	1,325,202	110.4	0	2,704,783	4,383,000	0.62
5.500	40.44	573	1,433	-5.30	1,413,119	117.8	0	3,047,073	4,386,000	0.69
5.750	42.71	600	1,579	-5.33	1,503,231	125.3	0	3,411,616	4,389,000	0.78
6.000	44.96	628	1,733	-5.37	1,596,230	133.0	0	3,799,049	4,392,000	0.86
6.250	47.21	656	1,894	-5.40	1,692,397	141.0	0	4,210,127	4,395,000	0.96
6.359	48.17	668	1,966	-5.41	1,735,814	144.7	0	4,396,303	4,396,303	1.00
6.500	49.43	684	2,061	-5.42	1,792,981	149.4	0	4,837,403	4,398,000	1.10
6.750	51.75	711	2,236	-5.44	1,897,584	158.1	0	5,298,723	4,401,000	1.20
7.000	54.19	739	2,417	-5.46	2,009,560	167.5	0	5,787,116	4,404,000	1.31
7.250	56.65	767	2,605	-5.47	2,128,316	177.4	0	6,304,351	4,407,000	1.43
7.500	59.12	795	2,800	-5.48	2,255,709	188.0	0	6,852,354	4,410,000	1.55
7.750	61.60	824	3,002	-5.48	2,392,365	199.4	0	7,433,363	4,413,000	1.68
8.000	64.10	852	3,212	-5.47	2,538,941	211.6	0	8,049,776	4,416,000	1.82
8.250	66.60	881	3,429	-5.47	2,701,943	225.2	0	8,704,887	4,419,000	1.97
8.500	69.12	909	3,652	-5.45	2,882,629	240.2	0	9,402,959	4,422,000	2.13
8.750	71.65	938	3,883	-5.43	3,079,002	256.6	0	10,148,162	4,425,000	2.29
9.000	74.19	967	4,121	-5.38	3,300,885	275.1	0	10,945,648	4,428,000	2.47
9.250	76.75	995	4,367	-5.32	3,573,055	297.8	0	11,804,891	4,431,000	2.66
9.500	79.31	1,024	4,619	-5.26	3,901,592	325.1	0	12,739,222	4,434,000	2.87
9.750	81.89	1,053	4,879	-5.17	4,292,510	357.7	0	13,763,484	4,437,000	3.10
10.000	84.49	1,082	5,146	-5.06	4,763,070	396.9	0	14,895,432	4,440,000	3.35
10.250	87.09	1,109	5,419	-4.95	5,316,128	443.0	0	16,155,332	4,443,000	3.64
10.500	89.71	1,134	5,698	-4.83	5,947,562	495.6	0	17,563,293	4,446,000	3.95
10.750	92.34	1,161	5,985	-4.74	6,665,548	555.5	0	19,139,932	4,449,000	4.30
11.000	94.98	1,184	6,270	-4.63	7,465,195	622.1	0	20,906,275	4,452,000	4.70
11.250	97.64	1,206	6,563	-4.54	8,360,345	696.7	0	22,884,467	4,455,000	5.14

# BRR Package Safety Analysis Report

Docket No. 71-9341

Rev. 8, July 2015

End Drop  
05-16-1995, 15:38:39

\*\*\* PACKAGING TECHNOLOGY \*\*\*

CASKDROP, v2.21  
Jul 01, 1994

SAMPLE PROBLEM FOR QUALITY ASSURANCE CHECK (AREAS AND VOLUMES)			
Impact Limiter Weight (each) -	1,000 lbs	Cask and Payload Weight -	10,000 lbs
Impact Limiter Outside Diameter -	60.0000 in	Cask Outside Diameter -	40.0000 in
Impact Limiter Overall Length -	24.0000 in	Cask Overall Length -	48.0000 in
Impact Limiter Conical Diameter -	48.0000 in	Dynamic Unloading Modulus -	1.000E+07 lbs/in
Impact Limiter Conical Length -	10.0000 in	Rad Mass Moment of Inertia -	12,235 lb-in-s <sup>2</sup>
Impact Limiter End Thickness -	12.0000 in	Frictional Coefficient -	0.0000
Impact Limiter Hole Diameter -	20.0000 in	Drop Height -	30.0000 ft
Impact Limiter Hole Length -	8.0000 in	Drop Angle from Horizontal -	90.0000°
Unbacked Area Threshold Strain -	0.1000 in/in	Crush Analysis Theory -	Global
Unbacked Area Crush Stress -	2,552 psi	Number of Integration Incs -	25

POLYFOAM CRUSH STRESS (Axial: "  " to rise)	
Density = 20.000 pcf	
Temp = -20.000 F	
σ-yield = 2,552.3 psi	
Bias = 60.000%	
ε (in/in)	σ (psi)
0.000	0.0
0.100	2,552.3
0.200	2,687.0
0.300	2,868.8
0.400	3,302.9
0.500	4,115.1
0.600	6,074.3
0.650	7,942.0
0.700	10,925.0
0.750	15,001.8
0.800	26,829.5

POLYFOAM CRUSH STRESS (Radial: "⊥" to rise)	
Density = 20.000 pcf	
Temp = -20.000 F	
σ-yield = 2,675.0 psi	
Bias = 60.000%	
ε (in/in)	σ (psi)
0.000	0.0
0.100	2,675.0
0.200	2,785.4
0.300	2,959.9
0.400	3,345.9
0.500	4,147.7
0.600	6,062.8
0.650	7,868.8
0.700	10,180.0
0.750	15,554.4
0.800	29,704.8

POLYFOAM CRUSH STRESS (Actual Data @ 90.0°)	
Density = 20.000 pcf	
Temp = -20.000 F	
σ-yield = 2,552.3 psi	
Bias = 60.000%	
ε (in/in)	σ (psi)
0.000	0.0
0.100	2,552.3
0.200	2,687.0
0.300	2,868.8
0.400	3,302.9
0.500	4,115.1
0.600	6,074.3
0.650	7,942.0
0.700	10,925.0
0.750	15,001.8
0.800	26,829.5

DEFL (in)	MAX ε (%)	AREA (in <sup>2</sup> )	VOLUME (in <sup>3</sup> )	XBAR (in)	IMPACT FORCE (lbs)	ACCEL (g's)	I/L MOMENT (in-lbs)	STRAIN ENERGY (in-lbs)	KINETIC ENERGY (in-lbs)	SE/KE RATIO
0.250	2.08	1,518	377	0.00	810,360	67.5	0	101,295	4,323,000	0.02
0.500	4.17	1,541	759	0.00	1,592,808	132.7	0	401,691	4,326,000	0.09
0.750	6.25	1,564	1,147	0.00	2,311,804	192.7	0	889,768	4,329,000	0.21
1.000	8.33	1,587	1,541	0.00	2,931,701	244.3	0	1,545,206	4,332,000	0.36
1.250	10.42	1,610	1,941	0.00	3,416,844	284.7	0	2,338,774	4,335,000	0.54
1.500	12.50	1,634	2,346	0.00	3,752,646	312.7	0	3,234,960	4,338,000	0.75
1.750	14.58	1,657	2,758	0.00	3,971,661	331.0	0	4,200,498	4,341,000	0.97

# BRR Package Safety Analysis Report

Docket No. 71-9341

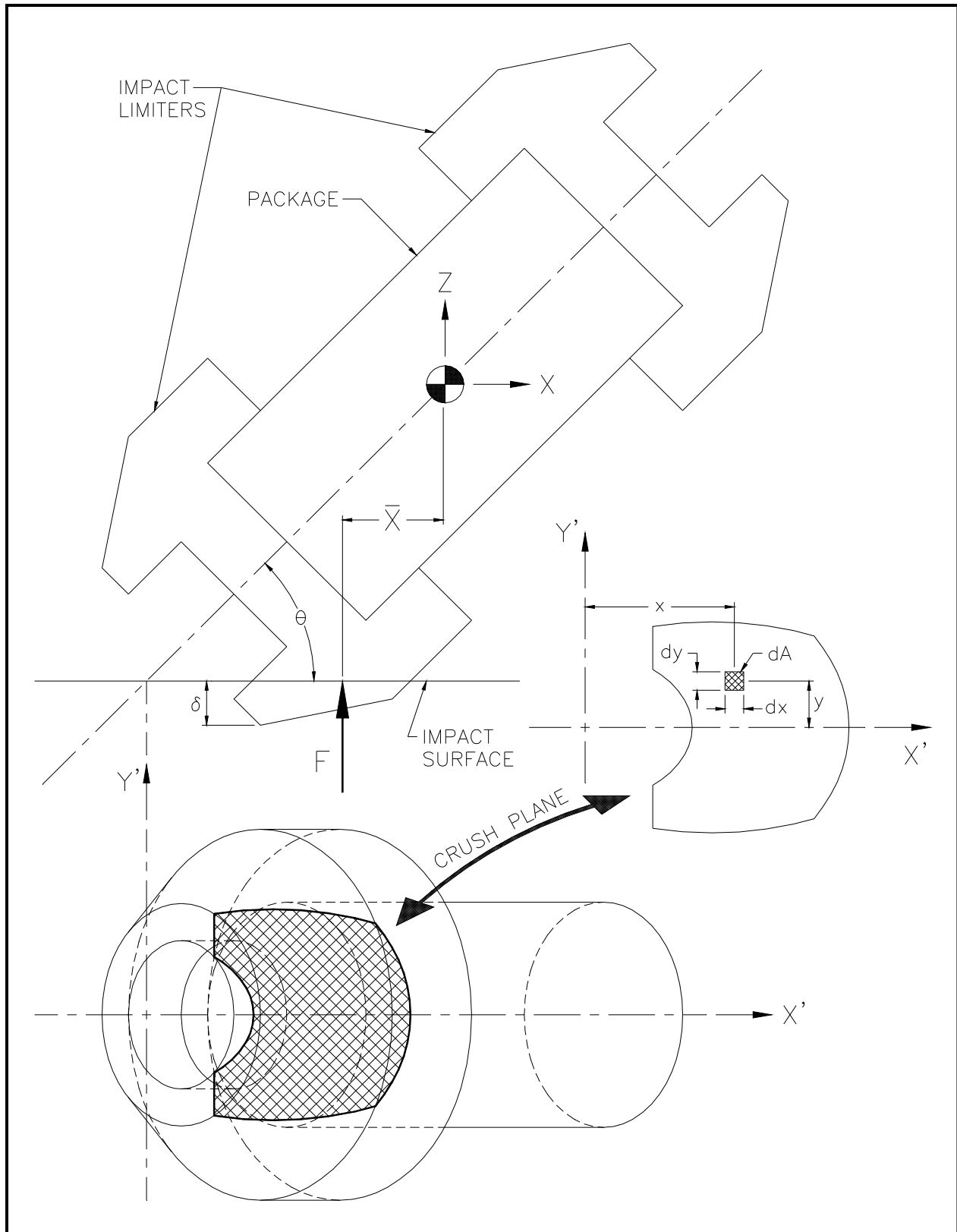
Rev. 8, July 2015

End Drop  
05-16-1995, 15:38:39

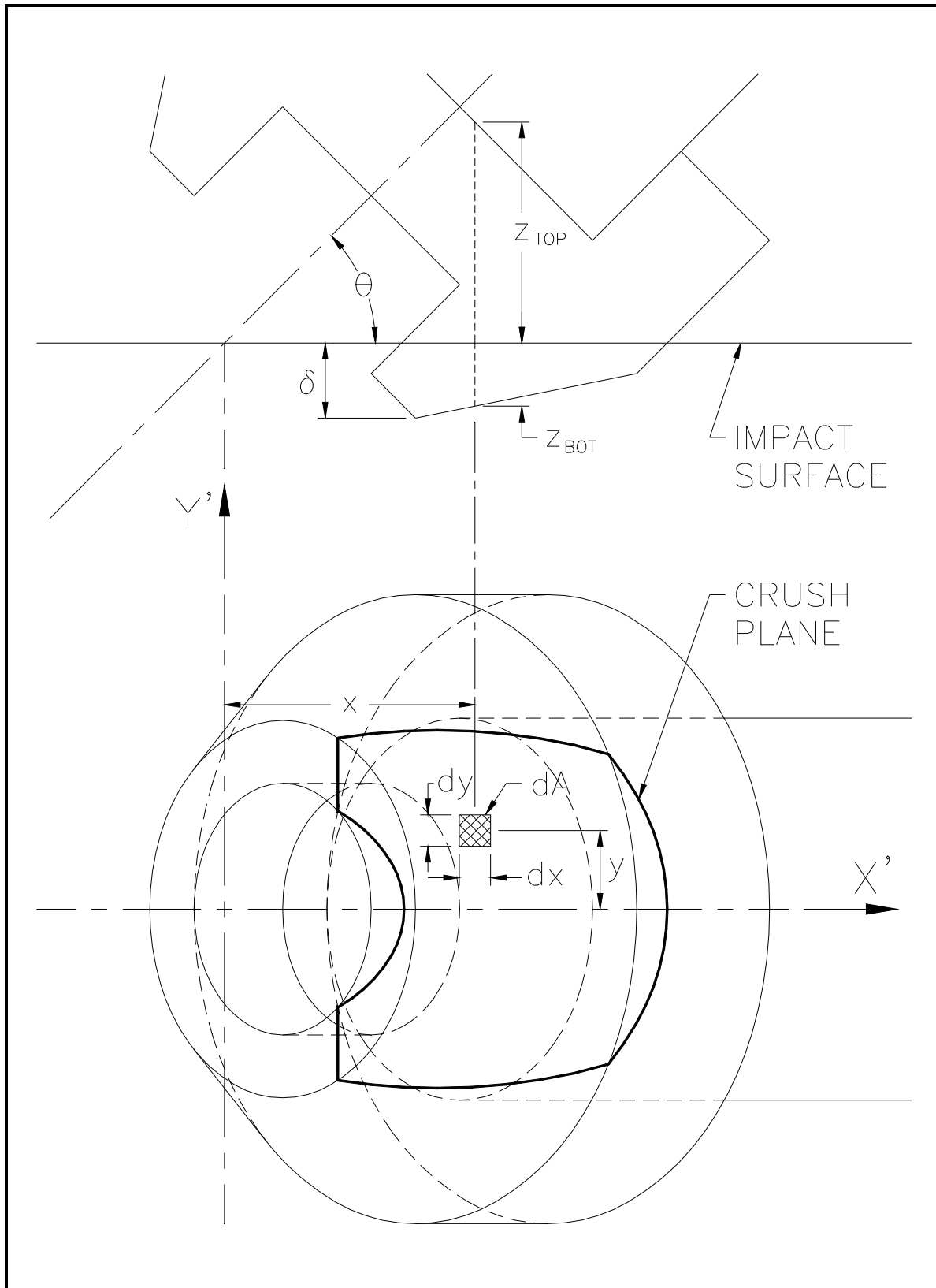
\*\*\* PACKAGING TECHNOLOGY \*\*\*  
(continued...)

CASKDROP, v2.21  
Jul 01, 1994

DEFL (in)	MAX $\epsilon$ (%)	AREA (in <sup>2</sup> )	VOLUME (in <sup>3</sup> )	XBAR (in)	IMPACT FORCE (lbs)	ACCEL (g's)	I/L MOMENT (in-lbs)	STRAIN ENERGY (in-lbs)	KINETIC ENERGY (in-lbs)	SE/KE RATIO
1.785	14.88	1,661	2,816	0.00	3,995,461	333.0	0	4,341,425	4,341,425	1.00
2.000	16.67	1,681	3,175	0.00	4,112,712	342.7	0	5,354,946	4,344,000	1.23
2.250	18.75	1,705	3,598	0.00	4,214,497	351.2	0	6,395,847	4,347,000	1.47
2.500	20.83	1,729	4,027	0.00	4,287,704	357.3	0	7,458,622	4,350,000	1.71
2.750	22.92	1,753	4,462	0.00	4,351,294	362.6	0	8,538,497	4,353,000	1.96
3.000	25.00	1,777	4,904	0.00	4,445,683	370.5	0	9,638,119	4,356,000	2.21
3.250	27.08	1,801	5,351	0.00	4,562,636	380.2	0	10,764,159	4,359,000	2.47
3.500	29.17	1,826	5,804	0.00	4,693,990	391.2	0	11,921,237	4,362,000	2.73
3.750	31.25	1,851	6,264	0.00	4,831,784	402.6	0	13,111,959	4,365,000	3.00
4.000	33.33	1,875	6,730	0.00	4,973,522	414.5	0	14,337,622	4,368,000	3.28
4.250	35.42	1,900	7,202	0.00	5,120,673	426.7	0	15,599,396	4,371,000	3.57
4.500	37.50	1,925	7,680	0.00	5,274,868	439.6	0	16,898,839	4,374,000	3.86
4.750	39.58	1,951	8,164	0.00	5,437,800	453.2	0	18,237,922	4,377,000	4.17
5.000	41.67	1,976	8,655	0.00	5,611,685	467.6	0	19,619,108	4,380,000	4.48
5.250	43.75	2,002	9,152	0.00	5,802,397	483.5	0	21,045,868	4,383,000	4.80
5.500	45.83	2,027	9,656	0.00	6,018,789	501.6	0	22,523,516	4,386,000	5.14
5.750	47.92	2,053	10,166	0.00	6,268,472	522.4	0	24,059,424	4,389,000	5.48
6.000	50.00	2,079	10,682	0.00	6,560,063	546.7	0	25,662,991	4,392,000	5.84
6.250	52.08	2,105	11,205	0.00	6,900,740	575.1	0	27,345,591	4,395,000	6.22
6.500	54.17	2,131	11,735	0.00	7,296,837	608.1	0	29,120,288	4,398,000	6.62
6.750	56.25	2,158	12,271	0.00	7,751,903	646.0	0	31,001,381	4,401,000	7.04
7.000	58.33	2,184	12,814	0.00	8,272,373	689.4	0	33,004,415	4,404,000	7.49
7.250	60.42	2,211	13,363	0.00	8,862,880	738.6	0	35,146,322	4,407,000	7.98
7.500	62.50	2,238	13,919	0.00	9,556,877	796.4	0	37,448,792	4,410,000	8.49
7.750	64.58	2,265	14,482	0.00	10,454,871	871.2	0	39,950,260	4,413,000	9.05
8.000	66.67	2,606	15,051	0.00	11,632,851	969.4	0	42,711,226	4,416,000	9.67
8.250	68.75	2,633	15,706	0.00	13,506,993	1,125.6	0	45,853,706	4,419,000	10.38
8.500	70.83	2,660	16,368	0.00	14,954,954	1,246.2	0	49,411,449	4,422,000	11.17
8.750	72.92	2,688	17,037	0.00	16,218,008	1,351.5	0	53,308,070	4,425,000	12.05
9.000	75.00	2,715	17,712	0.00	18,519,890	1,543.3	0	57,650,307	4,428,000	13.02
9.250	77.08	2,743	18,394	0.00	22,571,268	1,880.9	0	62,786,702	4,431,000	14.17
9.500	79.17	2,771	19,084	0.00	27,794,818	2,316.2	0	69,082,462	4,434,000	15.58
9.750	81.25	2,799	19,780	0.00	33,405,583	2,783.8	0	76,732,513	4,437,000	17.29
10.000	83.33	2,827	20,483	0.00	39,286,171	3,273.8	0	85,818,982	4,440,000	19.33
10.250	85.42	2,827	21,190	0.00	45,050,964	3,754.2	0	96,361,124	4,443,000	21.69
10.500	87.50	2,827	21,897	0.00	51,018,884	4,251.6	0	108,369,855	4,446,000	24.37
10.750	89.58	2,827	22,604	0.00	57,507,705	4,792.3	0	121,935,678	4,449,000	27.41
11.000	91.67	2,827	23,311	0.00	64,451,479	5,371.0	0	137,180,576	4,452,000	30.81
11.250	93.75	2,827	24,017	0.00	74,690,773	6,224.2	0	154,573,358	4,455,000	34.70
11.500	95.83	2,827	24,724	0.00	85,563,336	7,130.3	0	174,605,121	4,458,000	39.17
11.750	97.92	2,827	25,431	0.00	96,435,898	8,036.3	0	197,355,026	4,461,000	44.24
12.000	100.00	2,827	26,138	0.00	107,308,461	8,942.4	0	222,823,071	4,464,000	49.92

**Figure 2.12.6-1 – Impact Limiter Force and Centroid Development**



**Figure 2.12.6-2 – Strain Determination**

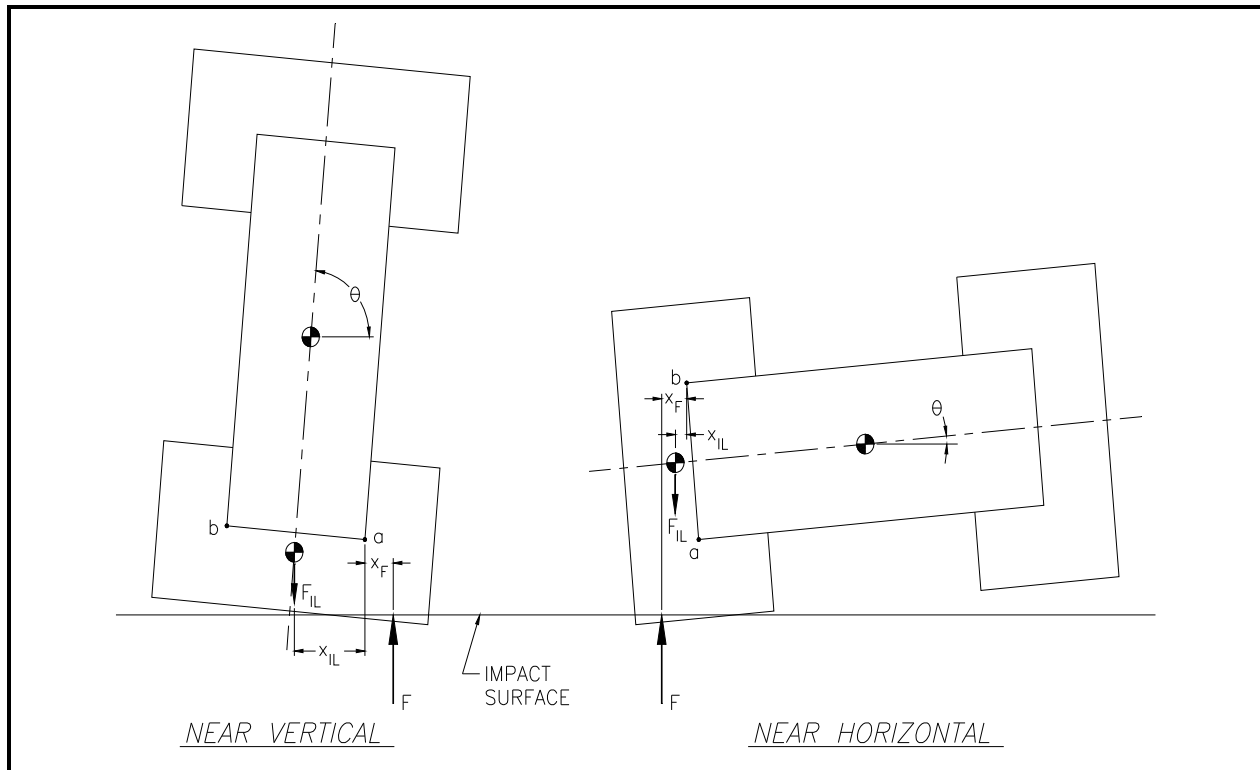


Figure 2.12.6-3 – Determination of Impact Limiter Separation Moments

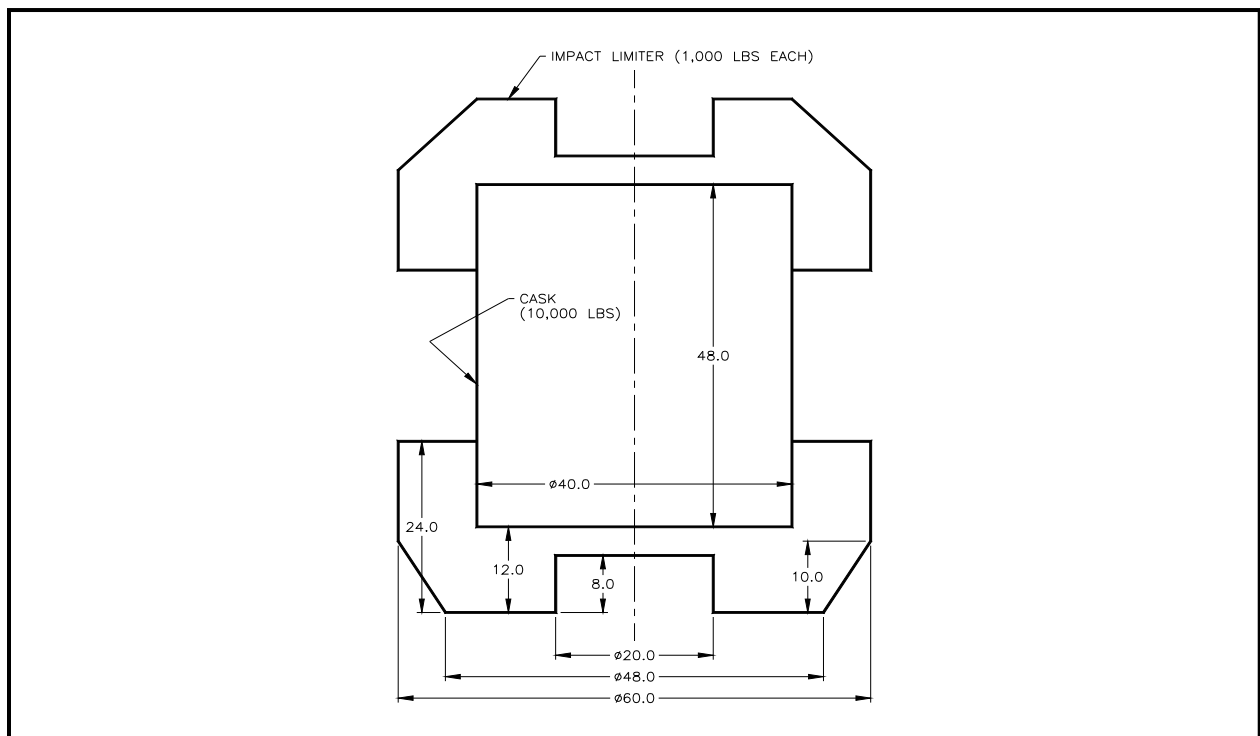


Figure 2.12.6-4 – Example Problem for CASKDROP

Packaging Technology's Cask Drop Analysis Program, v2.21						
Tuesday, May 16, 1995				3:38:19 pm		
[Input Window]						
Title: <b>SAMPLE PROBLEM FOR QUALITY ASSURANCE CHECK (AREAS AND VOLUMES)</b>						
IL Weight (each, lbs): 1000			Cask/Payload Weight (lbs): 10000			
IL Outside Diameter (in): 60			Cask Outside Diameter (in): 40			
IL Overall Length (in): 24			Cask Overall Length (in): 48			
IL Conical Diameter (in): 48			Free Drop Height (ft): 30			
IL Conical Length (in): 10			Radial Mass MI (lb-in-s <sup>2</sup> ): 12235.16			
IL End Thickness (in): 12			Frictional Coefficient ( $\mu$ ): 0			
IL End Hole Diameter (in): 20			Unloading Modulus (lbs/in): 10000000			
IL End Hole Length (in): 8			Crush Media Specification: PolyFoam			
[Control Window]						
Analysis	Crush (in)	Angle (°)	Static	Dynamic	Print	File
dXY: 25	Min: 0.25	Min: 0	Full <input checked="" type="checkbox"/>	Full <input type="checkbox"/>	Full <input type="checkbox"/>	Full <input checked="" type="checkbox"/>
Sln: Global	Max: 20	Max: 90	Smry <input type="checkbox"/>	Smry <input type="checkbox"/>	Smry <input type="checkbox"/>	Smry <input type="checkbox"/>
$\epsilon/\sigma$ : 0.1	Inc: 0.25	Inc: 45	Both <input type="checkbox"/>	Both <input type="checkbox"/>	Both <input type="checkbox"/>	Both <input type="checkbox"/>
[Output Window]						
[PgUp]/[PgDn] keys toggle active window; [F10] exits program						

Figure 2.12.6-5 – The CASKDROP Program *Input Window*

Packaging Technology's Cask Drop Analysis Program, v2.21						
Tuesday, May 16, 1995				3:38:29 pm		
[Input Window]						
Title: <b>SAMPLE PROBLEM FOR QUALITY ASSURANCE CHECK (AREAS AND VOLUMES)</b>						
IL Weight (each, lbs): 1000			Cask/Payload Weight (lbs): 10000			
IL Outside Diameter (in): 60			Cask Outside Diameter (in): 40			
IL Overall Length (in): 24			Cask Overall Length (in): 48			
IL Conical Diameter (in): 48			Free Drop Height (ft): 30			
IL Conical Length (in): 10			Radial Mass MI (lb-in-s <sup>2</sup> ): 12235.16			
IL End Thickness (in): 12			Frictional Coefficient ( $\mu$ ): 0			
IL End Hole Diameter (in): 20			Unloading Modulus (lbs/in): 10000000			
IL End Hole Length (in): 8			Crush Media Specification: <b>PolyFoam</b>			
[Polyurethane Foam Database]						
D (pcf): 20.0000			T (°F): -20.00			
$\sigma$ (psi): 2552.3			Bias (%): 60			
"  " to rise		"I" to rise				
$\epsilon$ (in/in)	$\sigma$ (psi)	$\epsilon$ (in/in)	$\sigma$ (psi)			
0.00	0.0	0.00	0.0			
0.10	2,552.3	0.10	2,675.0			
0.20	2,687.0	0.20	2,785.4			
0.30	2,868.8	0.30	2,959.9			
0.40	3,302.9	0.40	3,345.9			
0.50	4,115.1	0.50	4,147.7			
0.60	6,074.3	0.60	6,062.8			
0.65	7,942.0	0.65	7,868.8			
0.70	10,925.0	0.70	10,180.0			
0.75	15,001.8	0.75	15,554.4			
0.80	26,829.5	0.80	29,704.8			
Orientation: Axial		Orientation: Radial				
[Control Window]						
Analysis	Crush (in)	Angle (°)	Static	Dynamic	Print	File
dXY: 25	Min: 0.25	Min: 0	Full <input checked="" type="checkbox"/>	Full <input type="checkbox"/>	Full <input type="checkbox"/>	Full <input checked="" type="checkbox"/>
Sln: Global	Max: 20	Max: 90	Smry <input type="checkbox"/>	Smry <input type="checkbox"/>	Smry <input type="checkbox"/>	Smry <input type="checkbox"/>
$\epsilon/\sigma$ : 0.1	Inc: 0.25	Inc: 45	Both <input type="checkbox"/>	Both <input type="checkbox"/>	Both <input type="checkbox"/>	Both <input type="checkbox"/>
[Output Window]						
[F2] calculates stress data and [F3] toggles orientation; [F10] exits...						

Figure 2.12.6-6 – The CASKDROP Program *Polyurethane Foam Window*

### 2.12.6.2 SLAPDOWN

Impact limiter deflections and package accelerations are calculated using the Sandia National Laboratories-developed computer code SLAPDOWN [30]. This program solves the rigid-body equations of motion for a transportation package, given parameters such as weight, rotational moment of inertia, geometric relationships, and impact limiter force-deflection curves. The output consists of maximum impact limiter deformations and a time history of the parameters of motion (of principal interest, the acceleration at the center of gravity and angular acceleration). From these outputs, accelerations at any point on the package are found. Figure 2.12.6-7 shows the geometric parameters used, and Table 2.12.6-1 lists the required input parameters.

With respect to Figure 2.12.6-7, the line connecting points 1, 2, and 3 is the centerline axis of the cask. Points 4 and 5 represent the points of contact of the impact limiter with the impact surface. It is shown with the cask axis at an angle  $\theta$  to the horizontal, but may impact the ground at any angle, up to and including vertical. The primary end is the end of the cask which strikes the ground first, and the secondary end (the slapdown end) is the end which strikes the ground second. The distances  $R_1$  and  $R_2$  are the outer radii, respectively, of each impact limiter. The impact limiter forces (which act along the lines of  $R_1$  and  $R_2$ ) are assumed to be always perpendicular to the impact surface, which is consistent with the assumption for each orientation that the force-deflection curve is defined perpendicular to the surface. The impact limiters are modeled as nonlinear, inelastic springs, and consist of the force-deflection relations developed in Section 2.12.6.1, *CASKDROP*. The elastic rebound stiffness determines how much of the energy absorbed by the limiter (the area under the force-deflection curve) is elastically recovered. Elastic rebound stiffness has a small effect on SLAPDOWN response, and is normally set at a value of  $10^7$  lb/in. The equations of motion are solved for all five nodes. The center of gravity (C.G.) is taken as the geometric center of the cask. Friction is assigned a value of zero, since this maximizes the impact forces and deflections for the secondary (slapdown) impact limiter.

Table 2.12.6-1 shows a listing of sample input for the SLAPDOWN program. Table 2.12.6-2 shows a listing of sample force-deflection data for the SLAPDOWN program. The force-deflection data for the primary impact limiter are obtained from *CASKDROP* for the stated primary impact orientation. The secondary impact limiter data is for a horizontal orientation. Table 2.12.6-3 shows a sample output of the SLAPDOWN program from the general output file. This is performed for a  $15^\circ$  primary oblique orientation. The angle of secondary contact with the ground surface is displayed at the end of the output list ("Tail Impact Angle"), and is nearly equal to zero, thus the horizontal orientation force-deflection data for the secondary impact is justified.

Table 2.12.6-4 shows a portion of the corresponding time history output file, showing the results only through the end of the primary impact. The time variable is given in the first column. In the second, third and fourth columns are given the results at the cask center of gravity (SLAPDOWN node 2): the vertical position is in the column headed POSY(2) (inches), the velocity is in the column headed VELY(2) (in/s), and the acceleration is in the column headed ACCY(2) (in/s<sup>2</sup>). The last three columns give the rotational parameters of angular position: the angle THETA (radians, horizontal is zero), the angular velocity OMEGA (r/s) and the angular acceleration ALPHA (r/s<sup>2</sup>).

As verification of the SLAPDOWN code analysis methodology, the sample problem described above was compared to output from the public domain program SCANS [31]. The results

compare well, as demonstrated in Table 2.12.6-5. Input data for the comparison is taken from Table 2.12.6-1.

**Table 2.12.6-1 – Sample Inputs to the SLAPDOWN Program**

<b>Input Parameter</b>	<b>Description</b>	<b>Sample Value</b>
Z1, Z2	Length from primary end to C.G., and from C.G. to secondary end, respectively (inch)*	90.38 (both sides)
R1, R2	Length from cask axis to impact limiter contact point, primary and secondary ends, respectively (inch)	63.0 (both ends)
$\mu 1, \mu 2$	Coefficient of friction, primary and secondary ends, respectively	0.0 (both ends)
m	Overall package mass (lb-s <sup>2</sup> /inch)	611.0
I <sub>cg</sub>	Radial mass moment of inertia about the package C.G. (in-lb-s <sup>2</sup> )	3.1(10) <sup>6</sup>
h	Drop height (ft)	30
$\theta$	Angle with respect to horizontal of primary impact	Variable (15° used for example)
k	Elastic rebound stiffness of the impact limiter material (lb/inch)	10 <sup>7</sup>

\*This dimension is measured from the cask C.G. to the center of the cylindrical portion of the impact limiter, which is the location of the line of action of side drop impact force.

**Table 2.12.6-2 – Sample Force-Deflection to the SLAPDOWN Program**

Primary Impact Limiter		Secondary Impact Limiter	
Deflection (in)	Force (lb)	Deflection (in)	Force (lb)
0	0	0	0
1	207,100	1	2,383,000
2	583,900	2	3,363,000
3	1,069,000	3	3,963,000
4	1,640,000	4	4,450,000
5	2,285,000	5	4,885,000
6	2,998,000	6	5,289,000
7	3,767,000	7	5,671,000
8	4,444,000	8	6,041,000
9	5,146,000	9	6,310,000
10	5,756,000	10	6,513,000
11	6,304,000	11	6,721,000
12	6,818,000	12	6,936,000
13	7,223,000	13	7,157,000
14	7,573,000	14	7,384,000
15	7,926,000	15	7,614,000

**Table 2.12.6-3 – Sample of SLAPDOWN General Output**

Sample Cask, 15 Degree Oblique

\*\*\*\*\* SEQUENCE OF EVENTS \*\*\*\*\*

```

** NOSE HIT      AT TIME 0.000E+0 VELOCITY = -5.275E+2  RATIO =  1.00E+0
** NOSE REBOUND AT TIME 3.311E-2 VELOCITY =  1.506E+1  RATIO = -2.86E-2
** NOSE UNLOAD  AT TIME 4.008E-2 VELOCITY =  1.346E+2  RATIO = -2.55E-1
** TAIL HIT      AT TIME 7.318E-2 VELOCITY = -7.061E+2  RATIO =  1.34E+0
** TAIL REBOUND AT TIME 1.037E-1 VELOCITY =  2.410E+1  RATIO = -4.57E-2
** TAIL UNLOAD  AT TIME 1.106E-1 VELOCITY =  1.422E+2  RATIO = -2.70E-1

```

```

Event over at time      0.11152      Time step size  0.00087
Time step multiplier    0.10         128 Plot times written to database

```

	DISPLACEMENT	VELOCITY	ACCELERATION	
NOSE	1.159E+1	1.346E+2	2.7317E+4	(MAX)
		-5.275E+2	-7.2971E+3	(MIN)
TAIL	1.206E+1	1.422E+2	2.9272E+4	(MAX)
		-7.061E+2	-6.4780E+3	(MIN)
CG		2.781E+1	1.0987E+4	(MAX)
		-5.277E+2	-3.8600E+2	(MIN)
ANGULAR		1.267E+0	2.0245E+2	(MAX)
		-4.623E+0	-1.8804E+2	(MIN)

```

MAXIMUM ENERGY:          3.4879E+7 (NOSE)
MAXIMUM ENERGY:          5.9471E+7 (TAIL)
IMPACT AT 80 IN FROM C.G. (x-n)      65.93 (g)
IMPACT AT 80 IN FROM C.G. (x-t)      70.35 (g)
TAIL IMPACT ANGLE =          1.91 DEG.

```



**BRR Package Safety Analysis Report****Rev. 8, July 2015****Table 2.12.6-4 – Sample of SLAPDOWN Time History Output**

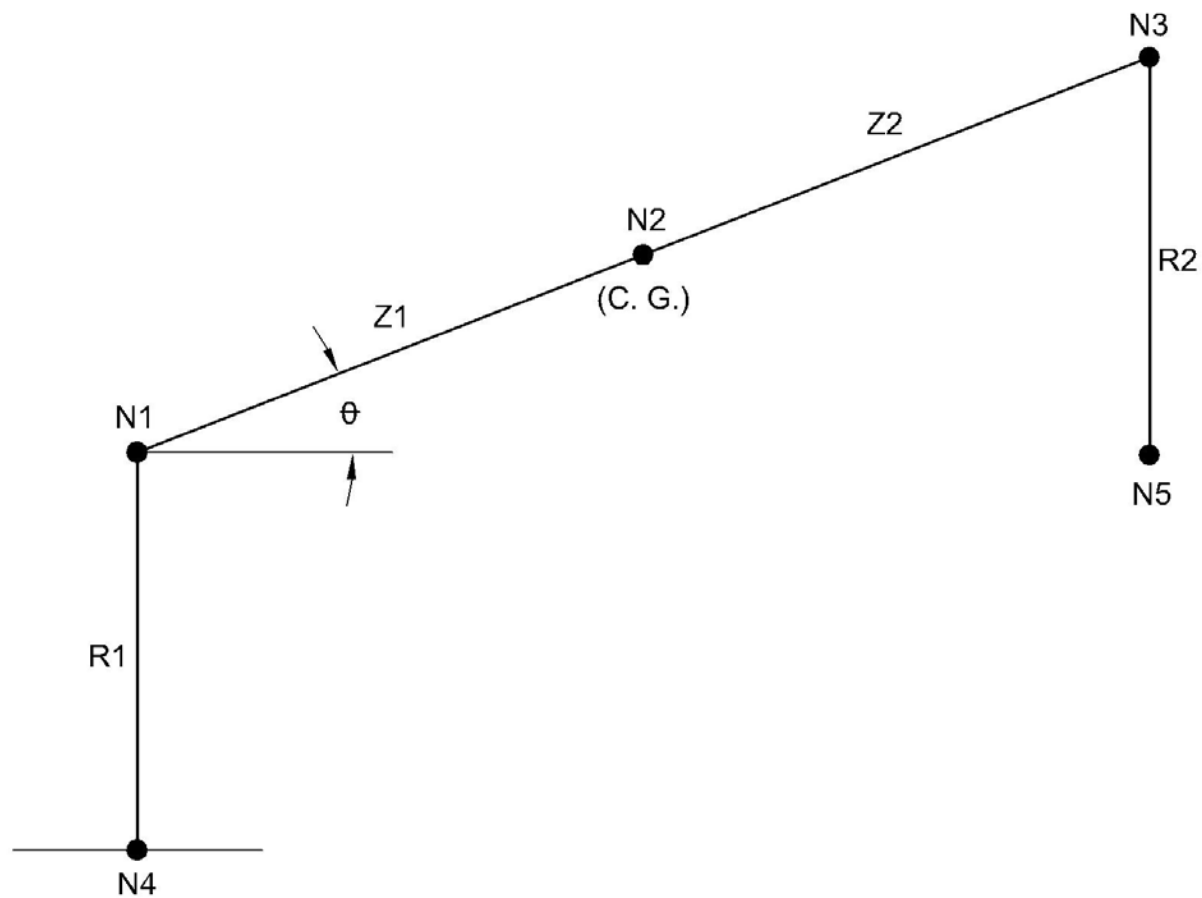
Title: Sample Cask, 15 Degree Oblique

9/29/2008 10:39:46 AM

Time,S	POSY(2)	VELY(2)	ACCY(2)	THETA	OMEGA	ALPHA
.0000E+0	.8639E+2	-.5275E+3	-.3860E+3	.2618E+0	.0000E+0	.0000E+0
.8712E-3	.8593E+2	-.5277E+3	-.2302E+3	.2618E+0	-.2335E-2	-.2680E+1
.1742E-2	.8547E+2	-.5277E+3	-.7449E+2	.2618E+0	-.7005E-2	-.5360E+1
.2614E-2	.8501E+2	-.5276E+3	.1862E+3	.2618E+0	-.1558E-1	-.9846E+1
.3485E-2	.8455E+2	-.5271E+3	.4689E+3	.2618E+0	-.2840E-1	-.1471E+2
.4356E-2	.8409E+2	-.5264E+3	.8029E+3	.2618E+0	-.4622E-1	-.2046E+2
.5227E-2	.8364E+2	-.5254E+3	.1164E+4	.2617E+0	-.6946E-1	-.2668E+2
.6098E-2	.8318E+2	-.5241E+3	.1552E+4	.2617E+0	-.9851E-1	-.3334E+2
.6970E-2	.8272E+2	-.5224E+3	.1972E+4	.2616E+0	-.1339E+0	-.4057E+2
.7841E-2	.8227E+2	-.5203E+3	.2399E+4	.2614E+0	-.1756E+0	-.4792E+2
.8712E-2	.8181E+2	-.5178E+3	.2863E+4	.2613E+0	-.2243E+0	-.5592E+2
.9583E-2	.8136E+2	-.5149E+3	.3321E+4	.2611E+0	-.2799E+0	-.6380E+2
.1045E-1	.8091E+2	-.5116E+3	.3817E+4	.2609E+0	-.3429E+0	-.7233E+2
.1133E-1	.8047E+2	-.5078E+3	.4306E+4	.2606E+0	-.4133E+0	-.8076E+2
.1220E-1	.8003E+2	-.5036E+3	.4807E+4	.2602E+0	-.4912E+0	-.8939E+2
.1307E-1	.7959E+2	-.4990E+3	.5312E+4	.2598E+0	-.5766E+0	-.9809E+2
.1394E-1	.7915E+2	-.4939E+3	.5801E+4	.2593E+0	-.6694E+0	-.1065E+3
.1481E-1	.7872E+2	-.4885E+3	.6221E+4	.2587E+0	-.7686E+0	-.1138E+3
.1568E-1	.7830E+2	-.4827E+3	.6628E+4	.2580E+0	-.8738E+0	-.1208E+3
.1655E-1	.7788E+2	-.4766E+3	.7025E+4	.2573E+0	-.9850E+0	-.1277E+3
.1742E-1	.7746E+2	-.4702E+3	.7416E+4	.2564E+0	-.1102E+1	-.1344E+3
.1830E-1	.7705E+2	-.4634E+3	.7790E+4	.2554E+0	-.1225E+1	-.1409E+3
.1917E-1	.7665E+2	-.4563E+3	.8132E+4	.2544E+0	-.1353E+1	-.1469E+3
.2004E-1	.7625E+2	-.4490E+3	.8426E+4	.2532E+0	-.1485E+1	-.1520E+3
.2091E-1	.7586E+2	-.4414E+3	.8704E+4	.2519E+0	-.1622E+1	-.1568E+3
.2178E-1	.7547E+2	-.4336E+3	.8964E+4	.2505E+0	-.1762E+1	-.1614E+3
.2265E-1	.7510E+2	-.4256E+3	.9189E+4	.2489E+0	-.1906E+1	-.1653E+3
.2352E-1	.7472E+2	-.4174E+3	.9391E+4	.2473E+0	-.2054E+1	-.1689E+3
.2439E-1	.7436E+2	-.4090E+3	.9577E+4	.2455E+0	-.2204E+1	-.1722E+3
.2527E-1	.7400E+2	-.4005E+3	.9746E+4	.2436E+0	-.2356E+1	-.1752E+3
.2614E-1	.7366E+2	-.3919E+3	.9897E+4	.2415E+0	-.2511E+1	-.1779E+3
.2701E-1	.7331E+2	-.3832E+3	.1002E+5	.2393E+0	-.2668E+1	-.1802E+3
.2788E-1	.7298E+2	-.3744E+3	.1013E+5	.2370E+0	-.2827E+1	-.1822E+3
.2875E-1	.7265E+2	-.3654E+3	.1023E+5	.2345E+0	-.2987E+1	-.1839E+3
.2962E-1	.7234E+2	-.3565E+3	.1030E+5	.2319E+0	-.3148E+1	-.1853E+3
.3049E-1	.7203E+2	-.3474E+3	.1036E+5	.2292E+0	-.3311E+1	-.1864E+3
.3136E-1	.7172E+2	-.3384E+3	.1040E+5	.2263E+0	-.3474E+1	-.1873E+3
.3223E-1	.7143E+2	-.3293E+3	.1042E+5	.2233E+0	-.3638E+1	-.1878E+3
.3311E-1	.7114E+2	-.3202E+3	.1043E+5	.2201E+0	-.3801E+1	-.1880E+3
.3398E-1	.7086E+2	-.3111E+3	.1042E+5	.2168E+0	-.3965E+1	-.1880E+3
.3485E-1	.7059E+2	-.3027E+3	.9658E+4	.2134E+0	-.4118E+1	-.1749E+3
.3572E-1	.7033E+2	-.2951E+3	.8787E+4	.2098E+0	-.4257E+1	-.1598E+3
.3659E-1	.7007E+2	-.2884E+3	.7627E+4	.2061E+0	-.4378E+1	-.1397E+3
.3746E-1	.6982E+2	-.2830E+3	.6214E+4	.2022E+0	-.4479E+1	-.1152E+3
.3833E-1	.6957E+2	-.2790E+3	.4593E+4	.1983E+0	-.4555E+1	-.8695E+2
.3920E-1	.6933E+2	-.2766E+3	.2814E+4	.1944E+0	-.4603E+1	-.5594E+2
.4008E-1	.6909E+2	-.2757E+3	.9348E+3	.1904E+0	-.4623E+1	-.2310E+2
.4095E-1	.6885E+2	-.2761E+3	-.3860E+3	.1863E+0	-.4623E+1	.0000E+0

**Table 2.12.6-5 – Comparison of SLAPDOWN and SCANS Results**

Parameter	SLAPDOWN Result	SCANS Result
Primary impact limiter deflection, inch	11.6	11.6
Secondary impact limiter deflection, inch	12.1	12.1
Primary vertical acceleration (e.g.), g	26.9	26.8
Secondary vertical acceleration (e.g.), g	28.5	28.5
Primary angular acceleration, radians/s <sup>2</sup>	-188	-186
Secondary angular acceleration, radians/s <sup>2</sup>	202	218

**Figure 2.12.6-7 – SLAPDOWN Analytical Model**

## 2.12.7 Seal Performance Tests

This appendix contains descriptions of the performance tests which have been run on the butyl rubber compound used for the containment O-ring seal and sealing washers used in the BRR package. The material is designated as Rainier Rubber R-0405-70. The performance tests which will be discussed have demonstrated the ability of this material to maintain a leaktight<sup>1</sup> containment boundary under minimum compression, minimum temperature, and maximum temperature conditions which are beyond those experienced in the BRR package.

### 2.12.7.1 Performance Tests Associated with the TRUPACT-II Package

Two sets of butyl rubber performance tests have been done in support of the TRUPACT-II package certification (NRC Docket 71-9218). All relevant tests have used a bore-type fixture which is consistent with the configuration of the O-ring seals in the TRUPACT-II.

The test configuration and procedure was similar between the two tests and will now be briefly described. More details are available in Section 2.10.7.4 and Section 2.10.7.4A of [2]. Only the small test fixture is considered, since it was used in both sets of tests. The test fixture consists of an inner ring containing two O-ring grooves on its outer diameter and an outer ring which fits over the inner ring and provides compression of the two test O-rings. The cross-sectional diameter of the test O-rings was nominally 0.400 inches, which is essentially equivalent to the 0.375 nominal dimension of the BRR package containment O-ring seal. To vary the O-ring compression in the test fixture, the radial position of the inner ring was controlled by jacking screws. When the inner ring was shifted to one side within the outer ring, a maximum compression was obtained on the side toward which the inner ring was shifted, and a minimum compression was obtained on the opposite side. The entire fixture could be placed in an environmental chamber and either cooled or heated for a set time. A helium leakage rate test was performed at various stages by testing the leakage rate between the outside of the fixture and the space between the two test O-rings.

The first set of tests was performed in 1989 and is documented in Section 2.10.7.4 of [2]. A typical test sequence consisted of the following steps:

1. Assemble the test fixture at ambient conditions.
2. Perform a leakage rate test with the inner ring centered in the outer ring.
3. Chill the fixture to -40 °F and perform a helium leakage rate test.
4. Allow the fixture to warm to -20 °F.
5. Shift the inner ring laterally within the outer ring to achieve maximum compression on one side and minimum compression on the other side.
6. Perform a helium leakage rate test with the fixture still at -20 °F.
7. Heat to an elevated temperature, maintaining the inner ring in the shifted position.

---

<sup>1</sup> Leaktight is defined as a maximum leakage rate of  $1 \times 10^{-7}$  ref-cc/sec, air, per [1].

**BRR Package Safety Analysis Report**

8. Hold at temperature for 8 hours. Create a hard vacuum between the two test O-rings to confirm their integrity. A helium leakage rate test was not performed due to the tendency toward rapid saturation of the O-rings with helium at elevated temperature.
9. Chill the fixture to -20 °F, maintaining the inner ring in the shifted position.
10. Perform a final helium leakage rate test with the fixture still at -20 °F.

For each test, the maximum and minimum compressions were calculated using the dimensions of the fixture and of the test O-rings. The principal result of these tests was a demonstration that the subject rubber compound is capable of maintaining a leaktight condition at -20 °F with a minimum compression of 14.9% subsequent to an 8 hour soak at 400 °F. Details of the five small fixture tests are given in Table 2.12.7-1, adapted from Table 2.10.7-1 of [2]. Note that the term 'disk' in the table corresponds to the term 'inner ring' used in this description.

The second set of tests was performed in 1999, and are documented in Section 2.10.7.4A of [2]. These tests served to lower the minimum compression value at which a leaktight condition was demonstrated to be maintained. The tests used the same small test fixture, modified to allow it to achieve a lower minimum compression. The same test procedure was followed, except that all tests were run at a temperature of 400 °F. The principal result of these tests was a demonstration that the subject rubber compound is capable of maintaining a leaktight condition at -20 °F with a minimum compression of 12.9% subsequent to an 8 hour soak at 400 °F. Details of the three tests are given in Table 2.12.7-2, adapted from Table 2.10.7.4A-2 of [2].

### **2.12.7.2 Performance Tests Associated with the RTG Package**

#### **2.12.7.2.1 Face Seal Tests**

O-ring tests were also performed in support of the Radioisotope Thermoelectric Generator (RTG) package certification (DOE Docket 94-6-9904). The results are reported in Section 2.10.6 of [3]. In these tests, a face-type fixture was used which permitted four different compressions to be tested at once. Unlike the TRUPACT-II testing, and consistent with the conditions in a face-type configuration, the O-rings were not mechanically moved or disturbed throughout the test. The fixture consisted of an inner plate having three concentric grooves on each side. Each groove had a different depth and contained an O-ring made from butyl compound R-0405-70 as described above. The inner and outer O-rings on each side were the test specimens; the center O-rings were used only to support leakage rate testing of the test specimens. The O-rings were compressed by outer plates which were set off from the inner plate by shims which, along with the groove depths, controlled the amount of compression of each test O-ring. The nominal test O-ring cross-sectional diameter was 0.275 inches. The minimum compression created by the fixture was 10%, which was uniform around the entire circumference of the fixture. Compressions of 12%, 14%, and 15.5% were tested at the same time. The dimensions of the fixture and of the test specimens, and the resulting compression values, are shown in Table 2.12.7-3.

The time/temperature sequence was as follows:

1. Assemble the test fixture at ambient conditions and perform a helium leakage rate test.
2. Chill the fixture to -40 °F and perform a helium leakage rate test.

**BRR Package Safety Analysis Report**

3. Heat the fixture to 380 °F, and hold for 24 hours. Confirm integrity of the test O-rings by placing a hard vacuum on the test cavity (less than 0.2 mbar).
4. Allow the fixture to cool to 350 °F, and hold for 144 hours. The total time at elevated temperature is 168 hours, or one full week. Confirm integrity of the test O-rings by placing a hard vacuum on the test cavity (less than 0.2 mbar).
5. Cool the fixture to -20 °F and perform a final helium leakage rate test.

Each of the helium leakage rate tests demonstrated a leakage rate below the leaktight criterion of  $1 \times 10^{-7}$  ref-cc/sec, air, as defined by [1]. Of note, only the results from the outer O-ring tests (10% and 14% compression) were available at the time of publication of [3]. The successful completion of the inner O-ring tests (12% and 15.5% compression) was confirmed in [4].

**2.12.7.2.2 Bore Seal Tests**

Further O-ring tests were performed by Westinghouse Hanford Company in association with the RTG package, and documented in [5] and [6]<sup>2</sup>. In these tests, the same bore-type fixture was used as that used for the TRUPACT-II tests described in Section 2.12.7.1, *Performance Tests Associated with the TRUPACT-II Package*. The procedure differed slightly in that a cold shift (step no. 5 from Section 2.12.7.1) was not performed. The test sequence was as follows:

1. Assemble the fixture at ambient conditions, and shift the inner ring fully to one side, generating minimum compression on one side and maximum on the other. Perform a helium leakage rate test.
2. Chill the fixture to -40 °F and perform a helium leakage rate test.
3. Heat to the specified elevated temperature and hold for the specified time. At the end of the hold time, perform a helium leakage rate test (saturation with helium at the high temperature was not reported to have had an effect on the helium leakage rate test).
4. Chill the fixture to -20 °F and perform the final helium leakage rate test.

For each test, the maximum and minimum compressions were calculated using the dimensions of the fixture and of the test O-rings. A number of different time/temperature tests were run, showing leaktight performance of the butyl material for 430 °F for one hour [6], 375 °F for 25 hours [6], and 350 °F for 168 hours [5]. Data is summarized in Table 2.12.7-4.

**2.12.7.3 Long Term Performance of Butyl Rubber Seals**

The tests of the Rainier Rubber R-0405-70 compound described in this appendix were performed at relatively high temperatures for relatively short times, consistent with the HAC fire event. Demonstration of the performance of the material at the lower temperature and longer duration associated with the NCT hot environment is made by extrapolation of this data.

Reference 7 uses thermogravimetric analysis to predict the relative lifetimes of some elastomers. One of the results of this study is to show that elastomer lifetime is linear when plotted on a log-lifetime (ordinate) vs. 1000/Temp (K) (abscissa) scales. This is shown in figure 3 of [7], which

---

<sup>2</sup> Note that some of the test reports refer to the material as 'RR-0405-70' while in some instances, 'R-0405-70' is used. Both refer to the same compound, where 'RR' is used for uncured material, and 'R' for a cured product form. All testing was performed on cured material.

is reproduced as Figure 2.12.7-1. The curve for butyl will not necessarily have the same slope or be placed in the same position relative to the scales as is shown in the figure. The position and slope for butyl will need to be established using the test data. Then, using linear extrapolation, its performance at longer lifetimes can be found. Note, since the abscissa is based on the inverse of temperature, temperature is actually decreasing along the abscissa towards the right, even though the values of  $1000/\text{Temp (K)}$  are increasing. Consequently, the longest lifetimes correlate to the lowest temperature, as expected.

Figure 2.12.7-2 shows several time/temperature data points from the tests discussed above, along with the best-fit line through the data. For consistency, only data from the bore-type test fixture are considered. Note that this is not a locus of exact failure points (points defining the border between pass/fail), but of tests that passed (i.e., met the leaktight requirements of [1]). The possibility exists that some or all of these tests were "undertests", i.e., were not tested to the extreme limit of the material. Because the margin to failure may be different for each test, the actual locus of borderline results (zero-margin pass) may have a shallower slope than the best-fit curve to the data. If that curve were used to extrapolate upward to longer lifetimes, it might over predict the acceptable temperature (recall that temperature is decreasing to the right).

For the BRR package, it is desired to determine the acceptable temperature for leaktight performance for a duration of one year (8,760 hours). The most conservative extrapolation (the lowest acceptable temperature) will be generated from the data curve fit having the shallowest (conservative) slope. To find the shallowest slope, a data point for a test failure (450 °F for 8 hours) is introduced, as shown in Figure 2.12.7-3. This is taken from the TRUPACT-II test results shown in Table 2.12.7-1. The straight line between this failure point and the longest-term successful data point (350 °F for 168 hours) has the shallowest slope which is consistent with the known data points. This can be concluded from the following observations:

1. The 450 °F/8 hour data point cannot be an undertest, since it is a known failure. Therefore, the actual zero-margin pass temperature must lie to the right of, but not to the left of, the test data point.
2. The 350 °F/168 hour data point is likely somewhat undertested. Therefore, the actual zero-margin pass temperature must lie to the left of, but not to the right of, the test data point.
3. Consequently, the actual locus of zero-margin performance could be steeper than, but could not be shallower than, the line formed by joining the 450 °F/8 hour and 350 °F/168 hour data points.

The equation of the line connecting these two data points is:

$$\text{Log}_{10}(\text{hrs}) = 5.396(1000/T(\text{K})) - 9.775$$

Using this expression, the maximum leak tight temperature for 8,760 hours (one year) is 249 °F. Therefore, the R-0405-70 butyl material can be held at at least 249 °F for one full year (constant temperature night/day) and is expected to be leak tight per ANSI N14.5. This is the most conservative extrapolation that can be made from the known data and is essentially equal to the long term limit for the butyl material of 250 °F which is stated in Section 3.2.2, *Technical Specification of Components*.

#### 2.12.7.4 Summary

The butyl rubber compound used for the BRR package containment seals was tested in both a bore-type and a face-type test fixture at low compression and elevated temperature. In the bore-type testing, the O-rings were demonstrated to be helium leaktight at a temperature of -20 °F after a soak at 400 °F for 8 hours at a minimum compression of 11.9%. In the face-type testing, the O-rings were demonstrated to be helium leaktight at a temperature of -20 °F after a soak at 380 °F for 24 hours followed by a soak at 350 °F for 144 hours at a minimum compression of 10%. These compression and temperature/time conditions exceed the severity of those experienced in the BRR package. In addition, the seals are expected to be leaktight after one full year at a constant temperature of at least 249 °F. Because this value was conservatively obtained, the value of 250 °F used in Section 3.2.2, *Technical Specification of Components* is acceptable. The minimum compression of the BRR package containment seal O-ring is calculated in Section 4.1.3, *Seals*, and the maximum temperature under NCT and HAC is discussed in Chapter 3, *Thermal Evaluation*.

**Table 2.12.7-1 – TRUPACT–II O-ring Seal Performance Test Results (1989)⑦**

Test Number	O-ring Seal Cross-Sectional Diameter (inches)				Stretch (%)		Maximum Gap (inches)		Minimum Compression (%)				Soak Temperature and Helium Leakage Rate Test Results ④				
	O-ring Seal No. 1		O-ring Seal No. 2		Min	Max	Disk Center	Disk Offset	Disk Centered		Disk Offset		Disk Centered		Disk Offset		
	Min	Max	Min	Max					Min	Max	Min	Max	Ambient	-40 °F	-20 °F	8 hrs⑤	-20 °F
1	0.387	0.397	0.387	0.396	2.0	4.1	0.026	③	22.1	25.6	14.9	20.0	Yes	Yes	Yes	350 °F	Yes
2	0.388	0.398	0.387	0.398	2.0	4.1	0.029	0.050	21.3	25.1	15.7	19.7	Yes	Yes	⑥	450 °F	No
3	0.387	0.397	0.387	0.399	2.0	4.1	0.027	0.052	21.9	25.8	15.2	19.4	Yes	Yes	Yes	400 °F	Yes
4	②	②	②	②	2.0	4.1	0.027	0.053	21.9	25.8	<b>14.9</b>	19.1	Yes	Yes	Yes	<b>400 °F</b>	<b>Yes</b>
5	②	②	②	②	2.0	4.1	0.026	0.050	22.1	26.0	15.7	19.9	Yes	Yes	Yes	400 °F	Yes

Notes:

- ① Material for all O-ring seal test specimens was butyl rubber compound R-0405-70, Rainier Rubber Co., Seattle, WA.
- ② Not measured; calculations assume the worst case range as taken from Tests Numbers 1 - 3 (i.e., Ø0.387 minimum to Ø0.399 maximum).
- ③ Range of values is 0.048 in. minimum to 0.053 in. maximum due to an indirect method of gap measurement (used for this test only).
- ④ A “Yes” response indicates that helium leakage rate testing demonstrated a leaktight condition as defined in [1], i.e., the leakage rate was less than or equal to  $1 \times 10^{-7}$  ref-cc/sec, air. In all cases, measured leak rates were less than or equal to  $2.0 \times 10^{-8}$  ref cc/s, helium, for tests with a “Yes” response.
- ⑤ No helium leakage rate tests were performed at elevated temperatures due to O-ring seal permeation and saturation by helium gas. The ability of the test fixture to establish a rapid, hard vacuum between the O-ring seals was used as the basis for leakage rate test acceptance at elevated temperatures. All tests rapidly developed a hard vacuum, with the exception of Test Number 2 at an elevated temperature of 450 °F, which slowly developed a vacuum.
- ⑥ Initial leakage rate of  $1.0 \times 10^{-5}$  ref cc/s, helium; became leaktight approximately one minute later.
- ⑦ Adapted from Table 2.10.7-1 of [2].



**Table 2.12.7-2 – Supplementary TRUPACT–II O-ring Seal Performance Test Results (1999)④**

Test No.	Disk Centered % Comp.		Disk Offset % Comp.		Helium Leak Tight②				
	O-ring #1	O-ring #2	O-ring #1	O-ring #2	Ambient Temp.	-40 °F	-20 °F (Disk Offset)	Hot Soak (Disk Offset)③	-20 °F (Disk Offset)
1	18.5	17.9	12.7	12.0	Yes	Yes	Yes	Held Vacuum	Yes
2	20.8	20.0	12.9	<b>11.9</b>	Yes	Yes	Yes	Held Vacuum	<b>Yes</b>
3	19.2	19.2	12.1	12.1	Yes	Yes	Yes	Held Vacuum	Yes

Notes:

- ① Material for all O-ring seal test specimens was butyl rubber compound R-0405-70, Rainier Rubber Co., Seattle, WA.
- ② Seal is considered to be leaktight if the actual leakage rate is less than or equal to  $8 \times 10^{-8}$  atm-cc/sec.
- ③ Hot soak was 8 hours at a uniform temperature of 400 °F.
- ④ Adapted from Table 2.10.7.4A-2 of [2].

**Table 2.12.7-3 – RTG O-ring Face Seal Performance Test Parameters<sup>③</sup>**

Fixture Side	Outer groove depth, in.	Inner groove depth, in.	Shim Thickness, in.	Outer O-ring X- section, in.	Inner O-ring X- section, in.	Outer O-ring compression, %	Inner O-ring compression, %
Side A	0.2053	0.2000	0.044	0.2770	0.2773	10	12
Side B	0.2075	0.2033	0.031	0.2776	0.2774	14	15.5

Notes:

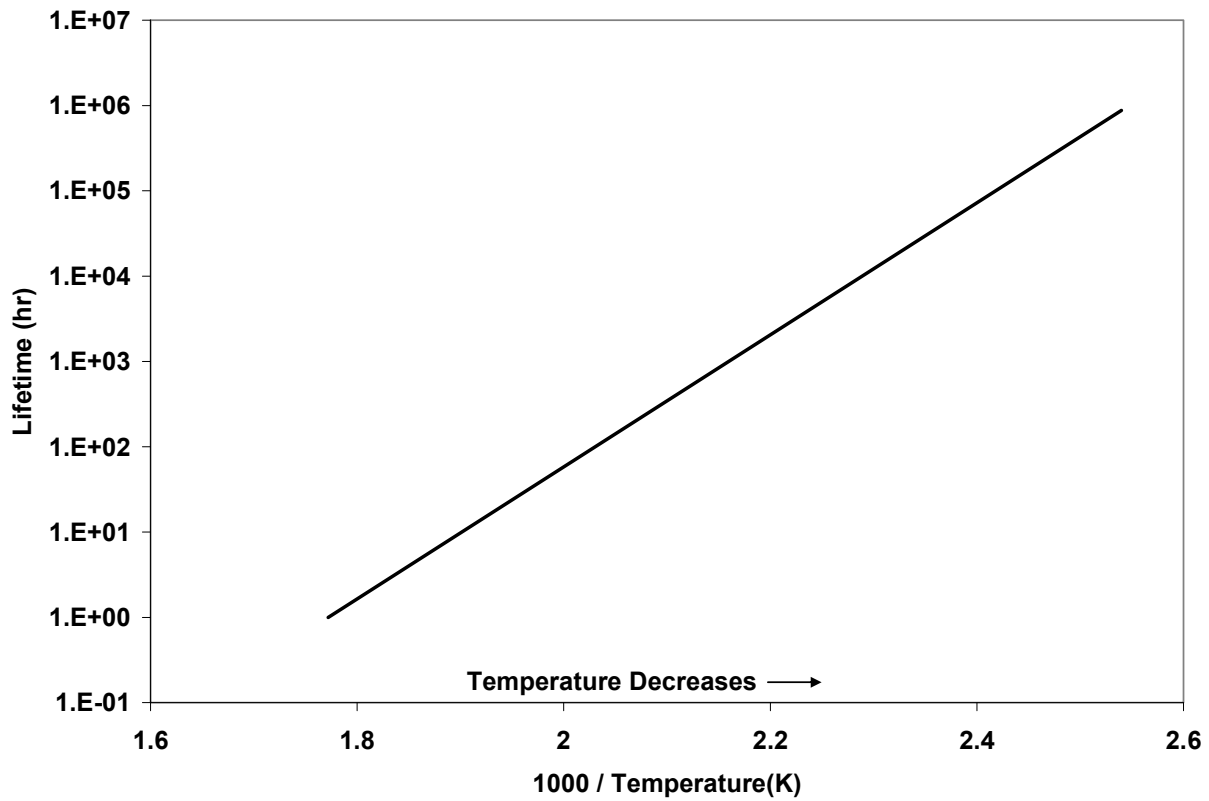
- ① Material for all O-ring seal test specimens was butyl rubber compound R-0405-70, Rainier Rubber Co., Seattle, WA.
- ② Each of the four test O-ring seals were leaktight per [1] when tested at a temperature of -20 °F following the time/temperature sequence of 380 °F for 24 hours followed by 350 °F for 144 hours.
- ③ Adapted from Table 4.1-1 and Table 4.1-2 of [3].

**Table 2.12.7-4 – RTG O-ring Bore Seal Performance Test Parameters**

Test No.	Min Compression, %	Max Compression, %	Max Temperature, °F	Hold Time, hours	Data Source
4	17.5	30.5	350	168	Table 3 of [5]
4B	17.8	31.3	375	25	Table 3 of [6]
3	19.2	32.3	430	1	Table 3 of [6]

Notes:

- ① Material for all O-ring seal test specimens was butyl rubber compound R-0405-70, Rainier Rubber Co., Seattle, WA.
- ② O-ring seals were leaktight per [1] when tested initially at room temperature, at a temperature of -40 °F, again at the stated maximum temperature at the end of the hold time, and finally when chilled to -20 °F.



**Figure 2.12.7-1** – Elastomer Time-Temperature Behavior (adapted from Figure 3 of [7])

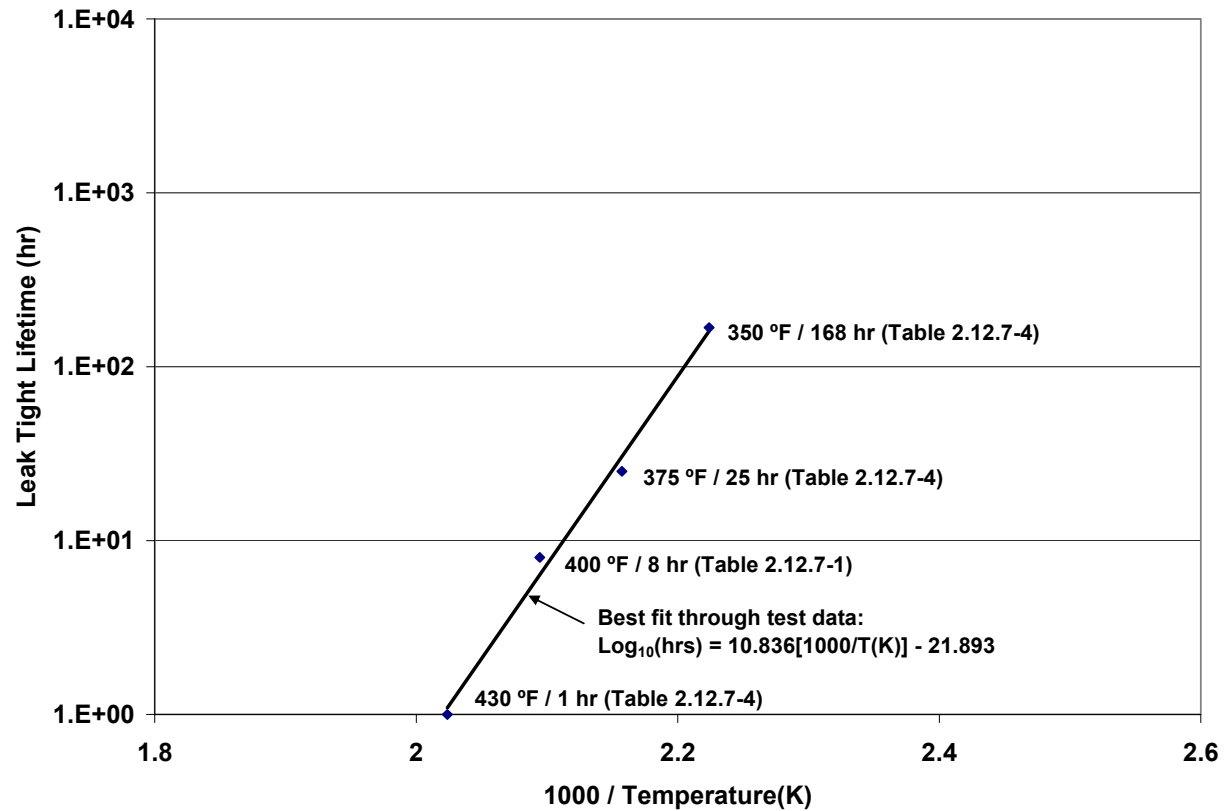


Figure 2.12.7-2 – R-0405-70 Test Data and Best Fit Curve

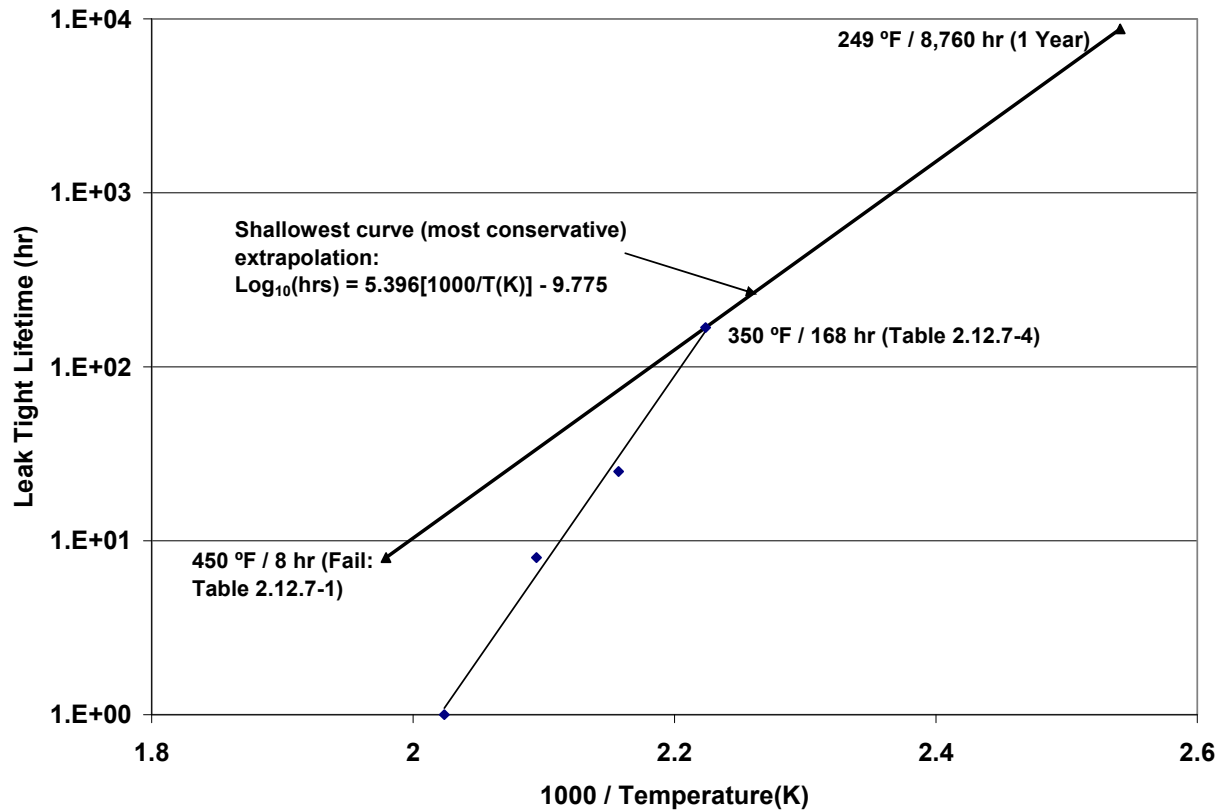


Figure 2.12.7-3 – Conservative Extrapolation to One Year

**2.12.7.5 References**

1. ANSI N14.5-1997, *American National Standard for Radioactive Materials – Leakage Tests on Packages for Shipment*, American National Standards Institute (ANSI), Inc.
2. *Safety Analysis Report for the TRUPACT-II Shipping Package*, USNRC Docket 71-9218, Revision 18, U.S. Department of Energy, Carlsbad Field Office, Carlsbad, New Mexico.
3. DOE Docket No. 94-6-9904, *Radioisotope Thermoelectric Generator Transportation System Safety Analysis Report for Packaging*, WHC-SD-RTG-SARP-001, prepared for the U.S. Department of Energy Office of Nuclear Energy under Contract No. DE-AC06-87RL10930 by Westinghouse Hanford Company, Richland, WA.
4. Westinghouse Hanford Company, *RTG Transportation System Packaging O-ring Material Thermal Validation Test Report for Face Seal Test Fixture*, WHC-SD-RTG-TRP-010, Rev 0.
5. Westinghouse Hanford Company, *Radioisotope Thermoelectric Generator (RTG) Transportation System Packaging O-ring Material Thermal Validation Test Report*, WHC-SD-RTG-TRP-001, Rev. 1.
6. Westinghouse Hanford Company, *Radioisotope Thermoelectric Generator (RTG) Transportation System Packaging O-ring Material Elevated Temperature Test Report*, WHC-SD-RTG-TRP-002, Rev. 0.
7. Nigrey, P. J., *Prediction of Packaging Seal Life Using Thermoanalytical Techniques*, Proceedings of the 12<sup>th</sup> International Conference on the Packaging and Transportation of Radioactive Materials, PATRAM 98, Vol. 4, p. 1730.

### 2.12.8 Fuel Basket Stress Analysis

This appendix provides details of the stress analysis evaluations of the five fuel baskets used in the BRR package under HAC free drop conditions. One basket corresponds to each type of fuel, which includes the University of Missouri Research Reactor (MURR), the Massachusetts Institute of Technology Nuclear Research Reactor (MITR-II), Advanced Test Reactor (ATR), Square fuels, and Training, Research, Isotopes, General Atomics (TRIGA) reactors.

The evaluations consist of manual calculations and buckling evaluations using ASME B&PV Code Case N-284-2 [13]. All buckling evaluations use a minimum factor of safety of 1.34, consistent with [13]. The bounding HAC impact acceleration of 120g is used for all analyses, which include free drops on the package end and on the package side. Basket and fuel weight is taken from Table 2.1-3. All of the material used in the fuel baskets is ASTM Type 304 stainless steel in various product forms including A240 (plate), A249 (tube), A269 (tube), A511 (tube), and A312 (pipe). Material properties are evaluated at the NCT maximum temperature of 400 °F, and taken from Table 2.2-1. Allowable stresses are taken from Table 2.1-1. The numeric values of allowable stress are given in Table 2.12.8-1. The analyses described in this appendix are based on the most critical load paths and demonstrate the structural integrity of the basket. Since each basket has a different design, the analyses which are most critical for each basket will be somewhat different.

Basket analyses do not include a dynamic load factor (DLF), since the impact acceleration used is nearly 50% higher than the maximum test result (see Section 2.12.5.3, *Reconciliation with Certification Test Results*), and because the basket structures are relatively stiff, which would result in a DLF not significantly different from unity.

#### 2.12.8.1 MURR Basket

The MURR basket provides positioning and support for up to eight MURR fuel elements. The structure consists of an outer shell, an inner shell, eight radial separation plates, a support plate, and other stiffening components. From Table 2.1-3, the empty basket has a weight of 650 lb, and with eight fuel elements, the bounding weight is 770 lb. A cross sectional view of the basket is shown in Figure 2.12.8-1 and a view of the support plate is shown in Figure 2.12.8-2.

##### 2.12.8.1.1 Fuel Support Plate Bending

The fuel support plate provides lower end support of the fuel elements. In the bottom-down vertical impact, the support plate is loaded by a maximum of eight fuel elements. Since each fuel element slot is supported by welds along three sides as shown in Figure 2.12.8-2, the loading of the plate can be analyzed for a single segment of the plate.

Stresses loading the plate can be modeled using [25], Table 24, Case 27. This is a conservative approach using the simply supported case. This method will ignore the in-plane moment reducing effects of the welds. The effective area of plate for the applied load is:

$$A_p = \frac{\pi}{4}(d_o^2 - d_i^2) - 8 \cdot \frac{\pi}{4}d_H^2 - 8 \cdot A_s = 106.3 \text{ in}^2$$

## **BRR Package Safety Analysis Report**

where  $d_o = 15.1$  inches is the outer diameter of the plate,  $d_i = 7.0$  inches is the center hole diameter of the plate,  $d_H = 0.8$  inches is the diameter of the eight drain holes, and  $A_S = 3.781 \text{ in}^2$  is the area of the separator plates. For a density  $\rho = 0.29 \text{ lb/in}^3$  and a plate thickness  $t = 0.375$  inches, the weight of the plate is:

$$W_p = A_p t \rho = 11.6 \text{ lb}$$

For a single sector of the plate, the plate load is:

$$P_p = (nW_{FE} + W_p) \cdot a = 15,792 \text{ lb}$$

where the number of fuel elements,  $n = 8$ , the weight of individual MURR element,  $W_{FE} = 15 \text{ lb}$ , and the bounding acceleration is  $a = 120g$ . The distributed pressure load over each sector of the plate is equivalent to the total fuel load over the effective area of the plate.

$$q = \frac{P_p}{A_p} = 148.6 \text{ psi}$$

From Case 27 the maximum plate stress for each segment is:

$$\sigma_t = \beta_1 \frac{qa^2}{t^2} = 6,867 \text{ psi}$$

where  $a = \frac{1}{2}d_o$  is the radius of the segment of plate,  $t = 0.375$  inches is the thickness of the plate, and  $\beta_1 = 0.114$  is a constant. The allowable combined membrane and bending stress is  $S = 64,000 \text{ psi}$  from Table 2.12.8-1. The margin of safety is:

$$MS = \frac{S}{\sigma_t} - 1 = +8.32$$

Therefore the plate has sufficient capacity to support the applied load.

### **2.12.8.1.2 Outer Shell Slot Welds**

The slot welds connect the outer shell to the inner components of the basket. In a bottom-down drop, the slot welds will take the full weight of the fuel, center shell, spacer plates, and fuel support plate. The  $\frac{1}{4}$  inch fillet weld between the fuel support plate and the outer shell will be conservatively excluded from this calculation.

The combined slot weld area for the 32, 2.0 inch x 0.6 inch long slots with full radii is:

$$A_{SW} = 32 \left[ \frac{\pi}{4} (0.6)^2 + 2.0(0.6) \right] = 47.4 \text{ in}^2$$

For this load case, the applied load is conservatively taken as the full weight of the loaded basket at an acceleration,  $a = 120g$ :

$$P_{SW} = (nW_{FE} + W_b) a = 92,400 \text{ lb}$$

where the weight of the fuel basket is  $W_b = 650 \text{ lb}$ . The shear stress due to the direct load is:

$$\tau_{SW} = \frac{P_{SW}}{A_{SW}} = 1,949 \text{ psi}$$



From Table NG-3352-1 of [32] the allowable stress of the weld is multiplied by a weld quality factor of 0.35, which applies to an intermittent or plug weld with surface PT examination. From Table 2.12.8-1, the allowable stress for pure shear is  $S = 22,320$  psi. The margin of safety is:

$$MS = \frac{(0.35)S}{\tau_{sw}} - 1 = +3.00$$

Therefore the slot welds have sufficient capacity to support the applied load.

### 2.12.8.1.3 Lower Shell Buckling

The lower section of shell is an unsupported column for a length of about 17.50 inches. The buckling load is analyzed using the method of ASME Code Case N284-2 [13]. Using the full weight of the basket as before will yield a conservative result. The loading on the lower shell from Section 2.12.8.1.2, *Outer Shell Slot Welds*, is  $P_{sw} = 92,400$  lb. The cross sectional area of the shell is based on the inner diameter,  $d_i$ , of 15.1 inches and the wall thickness,  $t$ , of 0.25 inches.

$$A_{LS} = \pi(d_i + t)t = 12.1 \text{ in}^2$$

The axial stress is then:

$$\sigma_{\phi} = \frac{P_{sw}}{A_{LS}} = 7,636 \text{ psi}$$

An inner diameter of 15.1 inches, an outer diameter of 15.6 inches, and a length of 18.0 inches are used in the buckling analysis. A factor of safety of 1.34 is used, consistent with the requirements of [13]. The results, shown in Table 2.12.8-2, show that all the interaction parameters are less than unity, as required. Therefore, buckling of the lower shell of the MURR basket under the HAC end drop will not occur.

### 2.12.8.2 MITR-II Basket

The MITR-II basket provides support and positioning for up to eight MITR-II fuel elements. The structure consists of a basket weldment fabricated from a stack of 28 plates that are machined to accept the fuel elements. The basket weldment sets upon a base support shell, and a fuel support plate. From Table 2.1-3, the empty basket has a weight of 560 lb, and with eight fuel elements, the bounding weight is 640 lb. A cross sectional view of the basket is shown in Figure 2.12.8-3.

#### 2.12.8.2.1 Lower Shell Buckling

The lower section of shell is an unsupported column for a significant portion of its length. The buckling will be checked for an unbraced length of 26.3 inches which bounds the unbraced length. The buckling load is analyzed using the method of ASME Code Case N284-2 [13]. Using the full weight of the basket as before will yield a conservative result. The basket weight is  $W = 640$  lb, the acceleration is  $a = 120g$ .

$$P = Wa = 76,800 \text{ lb}$$

The cross sectional area of the shell is based on the inner diameter,  $d_i$ , of 13.5 inches and the wall thickness,  $t$ , of 0.25 inches.

$$A_{LS} = \pi(d_i + t)t = 10.8 \text{ in}^2$$

The axial stress is then:

$$\sigma_\phi = \frac{P}{A_{LS}} = 7,111 \text{ psi}$$

An inner diameter of 13.5 inches, an outer diameter of 14.0 inches, and a length of 26.3 inches are used in the buckling analysis. A factor of safety of 1.34 is used, consistent with the requirements of [13]. The results, shown in Table 2.12.8-2, show that all the interaction parameters are less than unity, as required. Therefore, buckling of the lower shell of the MITR-II basket under the HAC end drop will not occur.

### 2.12.8.3 ATR Basket

The ATR basket provides support and positioning for up to eight ATR fuel elements. The structure consists of an outer shell, an inner shell, eight radial separation plates, a support plate, and other stiffening components. From Table 2.1-3, the empty basket has a weight of 450 lb, and with eight fuel elements, the bounding weight is 650 lb. A cross sectional view of the basket is shown in Figure 2.12.8-4 and a view of the support plate is shown in Figure 2.12.8-5.

#### 2.12.8.3.1 Fuel Support Plate Bending

The fuel support plate provides lower end positioning of the fuel elements. In a bottom-down end drop, the support plate is loaded by a maximum of eight fuel elements. Each fuel element section of the plate is supported by welds along three sides as shown in Figure 2.12.8-4.

The plate is modeled using [25] Table 24, Case 27. This is the same conservative approach used in Section 2.12.8.1.1, *Fuel Support Plate Bending*. The load applied by eight fuel elements is averaged over the entire plate. The effective area of plate for the applied load is:

$$A_p = \frac{\pi}{4}(d_o^2 - d_i^2) - 8\frac{\pi}{4}d_H^2 - 8A_s = 86.3 \text{ in}^2$$

where  $d_o = 13.0$  inches is the outer diameter of the plate,  $d_i = 6.5$  inches is the center hole diameter of the plate,  $d_H = 0.8$  inches is the diameter of the eight drain holes, and  $A_s = 1.15 \text{ in}^2$  is the area of the separator plates. For a density  $\rho = 0.29 \text{ lb/in}^3$ , and a plate thickness  $t = 0.5$  inches, the weight of the plate is:

$$W_p = A_p t \rho = 12.5 \text{ lb}$$

For a single sector of the plate, the plate load is:

$$P_p = (nW_{FE} + W_p)a = 25,512 \text{ lb}$$

where the number of fuel elements,  $n = 8$ , the weight of an individual element,  $W_{FE} = 25 \text{ lb}$ , and the acceleration,  $a = 120g$ . The distributed pressure load of the plate is:

$$q = \frac{P_p}{A_p} = 296 \text{ psi}$$

From [25] Table 24, Case 27, the maximum plate stress for each plate is:

## BRR Package Safety Analysis Report

$$\sigma_p = \beta_1 \frac{qa^2}{t^2} = 5,703 \text{ psi}$$

Where  $a = \frac{1}{2}d_o$  is the radius of the segment of plate,  $t = 0.5$  inches is the thickness of the plate, and  $\beta_1 = 0.114$  is a constant. The allowable combined membrane and bending stress is  $S = 64,000$  psi from Table 2.12.8-1. The margin of safety is:

$$MS = \frac{S}{\sigma_p} - 1 = +10.2$$

Therefore the plate has sufficient capacity to support the applied load.

### 2.12.8.3.2 Outer Shell Slot Welds

The slot welds connect the outer shell to the inner components of the basket. In a bottom-down drop, the slot welds are assumed to take the full load of the fuel, center shell, spacer plates, and fuel support plate. Conservatively, the full basket weight  $W = 650$  lb will be applied. The combined slot weld area for the 72, 0.8 inch x 0.3 inch long slots with full radii is:

$$A_{sw} = 72 \left[ \frac{\pi}{4} (0.3)^2 + 0.8(0.3) \right] = 20.2 \text{ in}^2$$

The applied load is the full weight at an acceleration of  $a = 120g$ .

$$P_{sw} = Wa = 78,000 \text{ lb}$$

The shear stress due to the direct load is:

$$\tau_{sw} = \frac{P}{A_{sw}} = 3,861 \text{ psi}$$

From Table NG-3352-1 of [32], the allowable stress of the weld is multiplied by a weld quality factor of 0.35, which applies to an intermittent or plug weld with surface PT examination. From Table 2.12.8-1, the allowable stress for pure shear is  $S = 22,320$  psi. The margin of safety is:

$$MS = \frac{(0.35)S}{\tau_{sw}} - 1 = +1.02$$

Therefore the slot welds have sufficient capacity to support the applied load.

### 2.12.8.3.3 Side Drop Bending

For the side drop impact, the ATR basket can be modeled as a simply supported beam, supported on the end plates. Conservatively, the support plates at intermediate spacings will be neglected. The applied load, assumed to be distributed along the beam, is equal to the bounding weight of 650 lb and the acceleration of  $a = 120g$ . The full basket load from Section 2.12.8.3.2, *Outer Shell Slot Welds*, is  $P_{sw} = 78,000$  lb. The bending moment is:

$$M = \frac{wL_s^2}{8} = \frac{P_{sw}L_s}{8} = 500,955 \text{ in} \cdot \text{lb}$$

where  $L_s = 51.38$  inches, which is the full length of the inner shell. The moment of inertia from the combination of the two shells, (neglecting the contribution of any other components) is:

$$I = \frac{\pi}{64} [d_{1o}^4 - d_{1i}^4] + \frac{\pi}{64} [d_{2o}^4 - d_{2i}^4] = 272.7 \text{ in}^4$$

Where  $d_{1o} = 13.5$  inches and  $d_{1i} = 13.0$  inches are the inner and outer diameters of the outer shell, and  $d_{2o} = 7.2$  inches and  $d_{2i} = 6.5$  inches are the inner and outer diameters of the inner shell after machining. The highest bending stress is located at the outer radius of the outer shell,  $c = 6.75$  inches. The bending stress is:

$$\sigma_b = \frac{Mc}{I} = 12,400 \text{ psi}$$

The allowable combined membrane and bending stress is  $S = 64,000$  psi from Table 2.12.8-1. The margin of safety is:

$$MS = \frac{S}{\sigma_b} - 1 = +4.16$$

Therefore bending of the ATR basket in the side drop will not occur.

#### 2.12.8.4 TRIGA Basket

The TRIGA basket provides support and positioning for up to nineteen TRIGA fuel elements. The structure consists of nineteen support tubes arranged in two concentric circles, a base plate, a center stiffener, and a top plate. The base plate is supported by two concentric circular shells. Fuel spacers are used with shorter versions of TRIGA fuel. From Table 2.1-3, the empty basket has a weight of 290 lb, and with nineteen fuel elements, the bounding weight is 480 lb. A cross sectional view of the basket is shown in Figure 2.12.8-6 and a view of the support plate is shown in Figure 2.12.8-7.

##### 2.12.8.4.1 Fuel Support Plate Bending

The fuel support plate provides lower end support of the fuel elements. In the bottom-down vertical impact, the support plate is loaded by a maximum of nineteen fuel elements, the top plate, center plate, and the fuel tubes and fuel spacers. Conservatively, the full weight of the basket will be taken as a distributed load across the plate. This load is distributed evenly over the plate and is reacted by the outer and inner shells which support the plate.

The loaded surface area of the plate consists of the basic plate surface between the outer support shell outer diameter,  $d_p = 13.0$  inches, and the inner support shell inner diameter of  $d_i = 3.5$  inches. This area is further reduced by the 19 drain holes with a diameter of  $d_h = 0.8$  inches.

$$A_p = \frac{\pi}{4} (d_p^2 - d_i^2 - 19d_h^2) = 113.6 \text{ in}^2$$

The load per unit area on the plate is:

$$q = \frac{Wa}{A_p} = 507 \text{ psi}$$

where the weight on the plate is  $W = 480$  lb, and the acceleration,  $a = 120g$ .

The maximum plate stress can be calculated from [25] Table 24, Case 2c. The distributed load is applied over the area between the outer edge (radius  $a = d_p/2$ ) of the outer base shell to the inner

## BRR Package Safety Analysis Report

edge (radius  $b = d_i/2$ ) of the schedule 40 pipe inner base shell. The interpolated values from case 2c of  $K_{Mrmax} = 0.0575$  and  $K_{Mtb} = -0.0754$  are based on the ratio of the outer and inner plate radii  $b/a = 0.27$ . The maximum moment in the plate is based on the maximum absolute value of these to factors,  $K_{Max} = 0.0754$ . The maximum bending moments is:

$$M_{Max} = K_{Max} qa^2 = 1,615 \text{ lb}$$

The maximum bending stress using the material thickness of the plate,  $t = 0.5$  in, is:

$$\sigma_b = -\frac{6M_{Max}}{t^2} = 38,760 \text{ psi}$$

The allowable combined membrane and bending stress is  $S = 64,000$  psi from Table 2.12.8-1. The margin of safety is:

$$MS = \frac{S}{\sigma_b} - 1 = +0.65$$

Therefore the plate has sufficient capacity to support the applied load.

### 2.12.8.4.2 Shear Load on Pedestal Spacer Screw

Once adjusted, the length of the pedestal assembly is held in one of three positions by a single 1/4-20 UNC screw (minimum diameter,  $d_n = 0.196$  inches). The load on this screw will be in double shear and consist of the weight of one fuel element plus the weight of the spacer cap.

The weight of a single maximum length TRIGA fuel element is  $W_L = 10$  lbs. Conservatively using the weight of the heaviest element, even though the pedestals are only used with short fuel elements, the maximum shear load on the screw is:

$$P_{SS} = W_L(120) = 1,200 \text{ lb}$$

The shear area of the screw (double shear) is:

$$A_s = 2\frac{\pi}{4}(d_n^2) = 0.0603 \text{ in}^2$$

The shear stress is:

$$\tau_s = \frac{P_{SS}}{A_s} = 19,900 \text{ psi}$$

From Table 2.12.8-1, the allowable for pure shear is  $S = 22,320$  psi. The margin of safety for HAC is:

$$MS_{HAC} = \frac{S}{\tau_s} - 1 = +0.12$$

Therefore the screw has sufficient capacity to sustain the applied load.

### 2.12.8.4.3 Buckling of Fuel Tubes (Top Down Drop)

The TRIGA assembly may be supported by the 19 fuel tubes during a top down drop orientation. For consistency, this buckling case will be evaluated using the full weight of the assembly,  $W = 290$  lb distributed over the 19 tubes. The buckling load is analyzed using the method of

ASME Code Case N284-2 [13]. The complete length of the tube will be used as if it was not braced at the middle of its span. The applied load for each tube is:

$$P_{ft} = \frac{W_a}{19} = 1,832 \text{ lb}$$

The area of each tube is:

$$A_{ft} = \pi(d_i + t)t = 0.71 \text{ in}^2$$

where the inner diameter of each tube is  $d_i = 1.76$  inches and the wall thickness is 0.12 inches. Based on this area the axial stress is:

$$\sigma_{ft} = \frac{P_{ft}}{A_{ft}} = 2,580 \text{ psi}$$

An inner diameter of 1.76 inches, an outer diameter of 2.0 inches, and a length of 48.00 inches are used. A factor of safety of 1.34 is used, consistent with the requirements of [13]. The results, shown in Table 2.12.8-2, show that all the interaction parameters are less than unity, as required. Therefore, buckling of the TRIGA basket fuel tubes under the HAC end drop will not occur.

#### 2.12.8.4.4 Side Drop Bending

For the side drop impact, each fuel tube in the TRIGA basket is modeled as a simply supported beam. For an inner and outer diameter of the tube  $d_i = 1.76$  inches,  $d_o = 2.0$  inches, a length  $L_t = 48.00$  inches, and a density  $\rho = 0.29 \text{ lb/in}^3$ , the weight of the tube is:

$$V_b = \frac{\pi}{4}(d_o^2 - d_i^2)L_t = 34.0 \text{ in}^3$$

$$W_T = V_b \rho = 9.86 \text{ lb}$$

The applied load, assumed to be distributed along the beam, will be equal to the bounding weight of the largest fuel element  $W_F = 10$  lbs. For the combined weight the load is:

$$P = 120(W_F + W_T) = 2,383 \text{ lb}$$

The bending moment is:

$$M = \frac{wL_t^2}{8} = \frac{PL_t}{8} = 7,149 \text{ in} - \text{lb}$$

where the reaction point separation is the unbraced length of the tube,  $L_t = 24.0$  inches. The moment of inertia and area of a single tube is:

$$I = \frac{\pi}{64}[d_o^4 - d_i^4] = 0.314 \text{ in}^4$$

The bending stress is

$$\sigma_b = \frac{Mc}{I} = 22,767 \text{ psi}$$

## BRR Package Safety Analysis Report

where  $c = \frac{1}{2}d_o$ . From Table 2.12.8-1, the allowable stress is  $S = 64,000$  psi for the combined membrane and bending stress. The margin of safety is:

$$MS = \frac{S}{\sigma_b} - 1 = +1.81$$

Therefore bending of the TRIGA fuel tubes will not occur.

### 2.12.8.5 Square Fuel Basket

The square fuel basket is designed to transport a quantity of up to eight of a variety of square or nearly square cross section fuels. The structure consists of two support disks, a lower support plate, eight square tubes, a lower skirt, and a skirt reinforcing plate which provides reinforcement across a diagonal of the lower support plate. From Table 2.1-3, the empty basket has a weight of 250 lb, and with eight maximum weight fuel elements, the bounding weight is 634 lb. The maximum weight of an individual fuel element (including spacer pedestal) is 48 lb. A partial cross sectional view of the basket is shown in Figure 2.12.8-8.

#### 2.12.8.5.1 Fuel Support Plate Bending

In the bottom-down HAC free drop, the lower support plate is loaded by the eight fuel elements, the eight square tubes, and the upper two support plates. The lower support plate is supported on its lower side by the skirt at a diameter of 14.0 inches. Note that the outer six tubes are located such that their load path is directly into the lower skirt, through the lower support plate. Since the upper two support plates and the two center tubes are attached to the outer six tubes, then the inertia loading from all of the tubes and the upper two support plates is carried directly by the skirt, and does not produce stress in the lower support plate. The lower support plate is therefore loaded only by the eight fuel elements and from the self-weight of the plate. The weight of the lower support plate is 27.8 lb. Thus the pressure applied to the lower support plate in a bottom-down HAC free drop is:

$$p = \frac{27.8 + 384}{A_p}(a) = 321 \text{ psi}$$

where the value of 384 lb represents the bounding weight of all eight fuel elements,  $a = 120g$ , and the area of the plate inside the support diameter is:

$$A_p = \frac{\pi}{4}(14.0)^2 = 153.9 \text{ in}^2$$

The stress in the plate is found using [25], Table 24, Case 28, for a semi-circular plate, since the center reinforcement plate supports the center of the plate. The drain holes in the plate have a negligible effect on the stress. The maximum stress is:

$$\sigma = \beta \frac{qa^2}{t^2} = 52,116 \text{ psi}$$

Where  $q = p$  as found above,  $\beta$  is found from the reference as 0.4536 for  $\theta = 180^\circ$ ,  $a = 7.0$  inches (the supported radius at the skirt OD), and the thickness  $t = 0.37$  inches (since the 0.5-inch thick plate is countersunk by 0.13 inches over the tube mounting areas, which conservatively neglects the large area of full thickness plate in between the tubes).

The allowable combined membrane and bending stress is  $S = 64,000$  psi from Table 2.12.8-1. The margin of safety is:

$$MS = \frac{S}{\sigma_b} - 1 = +0.23$$

The support plate has sufficient capacity to support the applied load.

### 2.12.8.5.2 Lower Shell Buckling

The lower shell (i.e., the skirt) supports the upper body of the basket. The total weight of the loaded basket is bounded by a value of 634 lb. The skirt is 14.0 inches in outer diameter and is 0.25 inches thick. Of note, the MITR-II basket has a total loaded weight of 640 lb and an identical skirt, except the unbraced length is greater. As shown in Section 2.12.8.2, *MITR-II Basket*, the MITR-II support skirt has a positive margin of safety against buckling failure in the bottom-down HAC free drop. Thus, the square fuel basket is bounded by the MITR-II results and will not buckle in the bottom-down free drop.

### 2.12.8.5.3 Side Drop Bending

For the side drop impact, each square fuel basket tube is modeled as a simply supported beam with a span equal to the unsupported length. This conservatively neglects the moment restraint due to the welded ends and the zero-slope condition at the center support. The span length is  $L = 20.0$  inches. The tubes are 3.61 inches square on the outside and 3.4 inches square on the inside. The bending moment of inertia is:

$$I = \frac{1}{12} (3.61^4 - 3.4^4) = 3.0 \text{ in}^4$$

and the area of the tube cross section is:

$$A = (3.61^2 - 3.4^2) = 1.47 \text{ in}^2$$

The c-distance is  $3.61/2 = 1.81$  inches. From Table 1.2-4, the length of the maximum weight fuel (the PULSTAR) is 38.23 inches and the maximum length of the pedestal that is used with it is 1.52, for a total length of 39.75 inches. In addition, the total weight of the fuel element and pedestal is bounded by 48 lb. Thus the distributed weight of the fuel, conservatively assuming no bending strength, is  $48/39.75 = 1.208$  lb/in. The weight of one tube is 17.0 lb, or  $17.0/40 = 0.425$  lb/in. The distributed load is therefore:

$$w = (1.208 + 0.425)a = 196.0 \text{ lb/in}$$

where  $a = 120g$  is the bounding side drop impact. The maximum moment in the tube is:

$$M = \frac{wL^2}{8} = 9,800 \text{ in} - \text{lb}$$

The bending stress is:

$$\sigma_b = \frac{Mc}{I} = 5,913 \text{ psi}$$

From Table 2.12.8-1, the allowable stress is  $S = 64,000$  psi. The margin of safety is:

$$MS = \frac{S}{\sigma_b} - 1 = +9.82$$

The design has sufficient capacity to support the developed load.

The Square Fuel basket can also be used with loose plate boxes for transport of loose plates, or with spacer pedestals, whose purpose is to keep the shorter fuel types near the top of the basket.



## BRR Package Safety Analysis Report

### 2.12.8.6 Loose Plate Box

The loose plate box, shown on sheet 4 of drawing 1910-01-03-SAR, is constructed of 1/8-inch thick stainless steel plates which forms a cavity for loose square fuel plates. The plates are maintained at the top of the cask cavity by means of a 1/2-inch thick floor plate welded into the box walls. Since the box is nominally filled with either loose fuel plates or aluminum dunnage plates, and since it fits closely within the basket cavity, there is no credible failure mode in a lateral (side drop) direction. In an end drop, the weight of the plates is applied to the welds holding the floor plate.

The floor plate is connected to two opposite side plates by two slot welds, 1.75 inches long. Each slot is welded all around, so that each slot weld consists in two, 1.75-inch long, 1/8-inch fillet welds, for a total of four fillet welds (conservatively neglecting the weld around the radius at each end of each slot). The total length of weld is therefore  $L = 4 \times 1.75 = 7.0$  inches. The throat of the weld is  $t = 0.707 \times 0.13 = 0.092$  inches, for a total weld shear area of:

$$A = Lt = 0.644 \text{ in}^2$$

The weight of the floor plate is approximately one pound, and the weight of the loose plates, taken as a solid block of aluminum filling the box cavity, is 19.2 lb, for a total weight on the welds of  $w = 20.2$  lb. For an end drop impact of  $a = 120g$ , the weld stress is:

$$\tau = \frac{wa}{A} = 3,764 \text{ psi}$$

From Table 2.12.8-1, the allowable stress in pure shear is 22,320 psi. From Table NG-3352-1 of [32], the allowable stress of the weld is multiplied by a weld quality factor of 0.35, which applies to an intermittent or plug weld with surface PT examination. The margin of safety is:

$$MS = \frac{22,320(0.35)}{\tau} - 1 = +1.08$$

Thus, the loose plate box is adequate for the applied loads.

### 2.12.8.7 Square Fuel Pedestals

Since square fuel pedestals are located within basket tubes, the only credible failure mode is in compression or buckling. As shown on sheet 4 of drawing 1910-01-03-SAR, the OD of the support tube is 2.5 inches, and the wall section is 1/8 inches. The cross-sectional area of the pedestal is:

$$A = \frac{\pi}{4} (2.5^2 - 2.25^2) = 0.933 \text{ in}^2$$

From Table 1.2-3, the maximum weight of a fuel element plus a bounding, 4-lb pedestal is 18 lb. Of note, the PULSTAR fuel is not included since its short pedestal is solid material without a credible failure mode. For an end drop impact of 120g, the stress in the support tube is:

$$\sigma = \frac{wa}{A} = 2,315 \text{ psi}$$

From Table 2.12.8-1, the allowable stress for primary membrane stress intensity under HAC is 44,640 psi. The margin of safety is:

$$MS = \frac{44,640}{\sigma} - 1 = +18.3$$

Of note, the stress in the tube is only 11% of the yield stress of 20,700 psi. Consequently, buckling is not of concern.

### 2.12.8.8 Summary

Table 2.12.8-3 summarizes the margins of safety of the BRR package fuel baskets, as established in the sections above. Since all margins of safety are positive, and all Code Case N-284-2 interaction checks are less than unity, the BRR package fuel baskets are not of concern.

**Table 2.12.8-1 – Material Properties and Allowable Stress**

Parameter	(ASTM, Type 304) <sup>①④</sup>
NCT Hot Bounding Temperature, °F	400
Elastic Modulus, psi	$26.4 \times 10^6$
Design Stress, $S_m$ , psi	18,600
Yield Stress, $S_y$ , psi	20,700
Ultimate Stress, $S_u$ , psi	64,000
<b>HAC Allowable Stresses</b>	
Primary Membrane Stress Intensity ( $P_m$ ), psi	Lesser of: <b><math>2.4S_m = 44,640</math></b> $0.7S_u = 44,800$
Primary Membrane + Bending Stress Intensity ( $P_m + P_b$ ), psi	Lesser of: <b><math>S_u = 64,000</math></b> $3.6S_m = 66,960$
Pure Shear Stress Intensity, psi	Lesser of: $0.42S_u = 26,880$ <sup>②</sup> <b><math>1.2S_m = 22,320</math></b> <sup>③</sup>

Notes:

1. ASTM A240, A249, A269, A276, A511, and A312.
2. ASME Code, Section III, Appendix F, Paragraph F-1334.2.
3. ASME Code, Section III, Subsection NG, Article NG-3225.
4. Governing values of allowable stress are in bold type.

Table 2.12.8-2 - Code Case N-284-2 Results Summary

Parameter	MURR	MITR-II	TRIGA	Remarks
<b>Capacity Reduction Factors (-1511)</b>				
$\alpha_{\phi L} =$	0.2070	0.2070	0.2070	
$\alpha_{\theta L} =$	0.8000	0.8000	0.8000	
$\alpha_{\phi\theta L} =$	0.8000	0.8000	0.8000	
<b>Plasticity Reduction Factors (-1610)</b>				
$\eta_{\phi} =$	0.1876	0.1706	0.0490	
$\eta_{\theta} =$	0.3655	0.4924	0.2187	
$\eta_{\phi\theta} =$	0.0865	0.0970	0.0510	
<b>Theoretical Buckling Values (-1712.1.1)</b>				
$C_{\phi} =$	0.6050	0.6050	0.6050	
$\sigma_{\phi eL} =$	520,261 psi	580,800 psi	2,038,979 psi	
$C_{\theta r} =$	0.0778	0.0487	0.0351	
$\sigma_{\theta eL} = \sigma_{reL} =$	66,906 psi	46,753 psi	118,324 psi	
$C_h =$	0.0744	0.0474	0.0351	
$\sigma_{\theta eL} = \sigma_{heL} =$	64,015 psi	45,468 psi	118,324 psi	
$C_{\phi\theta} =$	0.2087	0.1668	0.0904	
$\sigma_{\phi\theta eL} =$	179,445 psi	160,127 psi	304,652 psi	
<b>Elastic Interaction Equations (-1713.1.1)</b>				
$\sigma_{xa} =$	80,369 psi	89,721 psi	314,977 psi	
$\sigma_{ha} =$	38,218 psi	27,145 psi	70,641 psi	
$\sigma_{ra} =$	39,944 psi	27,912 psi	70,641 psi	
$\sigma_{ta} =$	107,131 psi	95,598 psi	181,882 psi	
Axial + Hoop $\Rightarrow$ Check (a):	N/A	N/A	N/A	<1 $\therefore$ OK
Axial + Hoop $\Rightarrow$ Check (b):	N/A	N/A	N/A	<1 $\therefore$ OK
Axial + Shear $\Rightarrow$ Check (c):	0.0950	0.0793	0.0082	<1 $\therefore$ OK
Hoop + Shear $\Rightarrow$ Check (d):	0.0000	0.0000	0.0000	<1 $\therefore$ OK
Axial + Hoop + Shear $\Rightarrow$ Check (e,a):	N/A	N/A	N/A	<1 $\therefore$ OK
Axial + Hoop + Shear $\Rightarrow$ Check (e,b):	N/A	N/A	N/A	<1 $\therefore$ OK
<b>Inelastic Interaction Equations (-1714.2.1)</b>				
$\sigma_{xc} =$	15,077 psi	15,305 psi	15,448 psi	
$\sigma_{rc} =$	14,601 psi	13,745 psi	15,448 psi	
$\sigma_{tc} =$	9,269 psi	9,269 psi	9,269 psi	
Max(Axial, Hoop) $\Rightarrow$ Check (a):	0.5065	0.4646	0.1670	<1 $\therefore$ OK
Axial + Shear $\Rightarrow$ Check (b):	0.5065	0.4646	0.1670	<1 $\therefore$ OK
Hoop + Shear $\Rightarrow$ Check (c):	0.0000	0.0000	0.0000	<1 $\therefore$ OK

**Table 2.12.8-3 – Fuel Basket Stress Analysis Results**

<b>Analysis Description</b>	<b>Reference Section</b>	<b>Margin of Safety</b>
<b>MURR Basket</b>		
Fuel Support Plate Bending	2.12.8.1.1	+8.32
Outer Shell Slot Welds	2.12.8.1.2	+3.00
Lower Shell Buckling	2.12.8.1.3	Pass*
<b>MITR-II Basket</b>		
Lower Shell Buckling	2.12.8.2.1	Pass*
<b>ATR Basket</b>		
Fuel Support Plate Bending	2.12.8.3.1	+10.2
Outer Shell Slot Welds	2.12.8.3.2	+1.02
Side Drop Bending	2.12.8.3.3	+4.16
<b>TRIGA Basket</b>		
Fuel Support Plate Bending	2.12.8.4.1	+0.65
Spacer Screw Shear Load	2.12.8.4.2	+0.12
Fuel Tube Buckling	2.12.8.4.3	Pass*
Side Drop Bending	2.12.8.4.4	+1.81
<b>Square Fuel Basket</b>		
Fuel Support Plate Bending	2.12.8.5.1	+0.23
Lower Shell Buckling	2.12.8.5.2	Pass*
Side Drop Bending	2.12.8.5.3	+9.82
<b>Loose Plate Box and Pedestals</b>		
Floor Plate Slot Weld	2.12.8.6	+1.08
Pedestal Tube	2.12.8.7	+18.3

\*Interaction equation checks are less than unity, as required by [13].

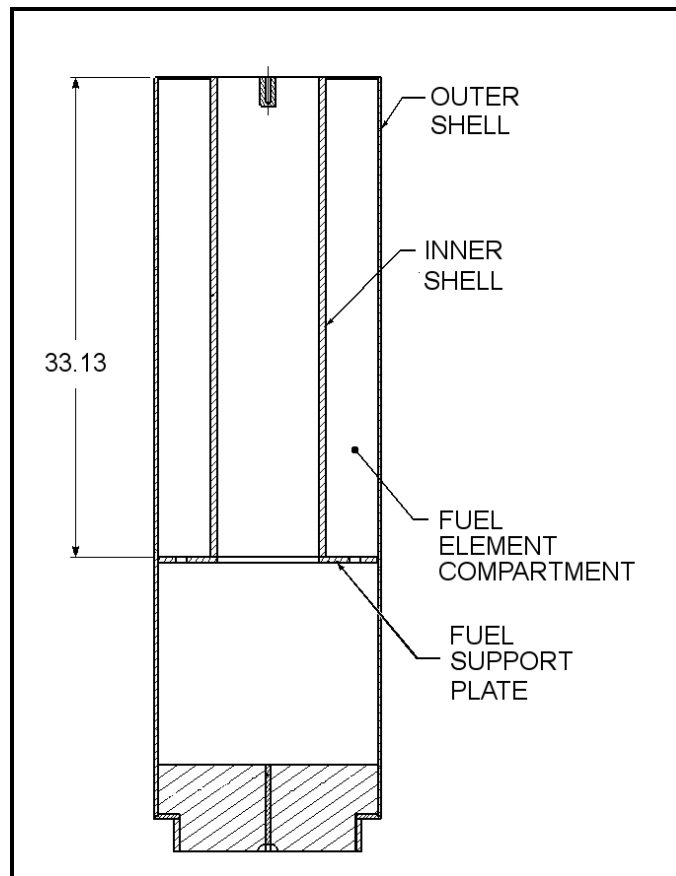


Figure 2.12.8-1 - MURR Fuel Basket Cross Section

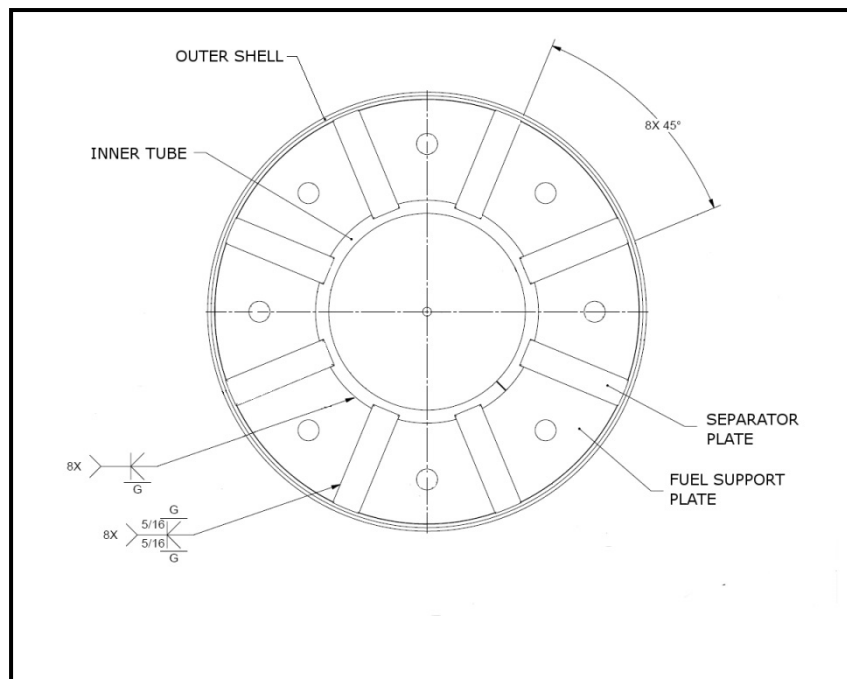
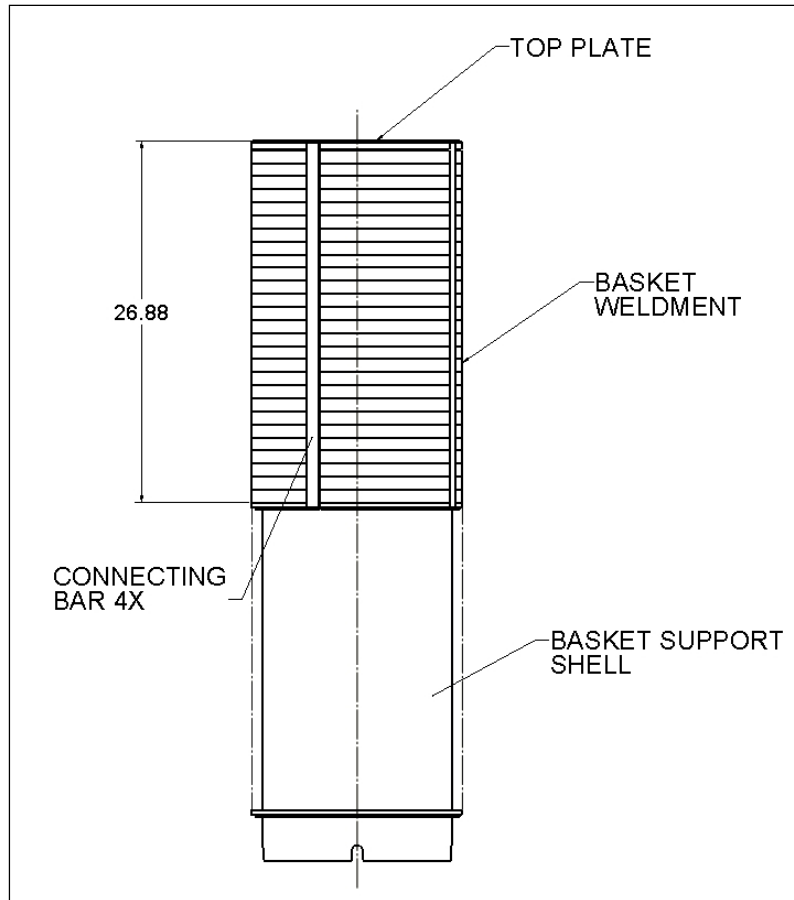
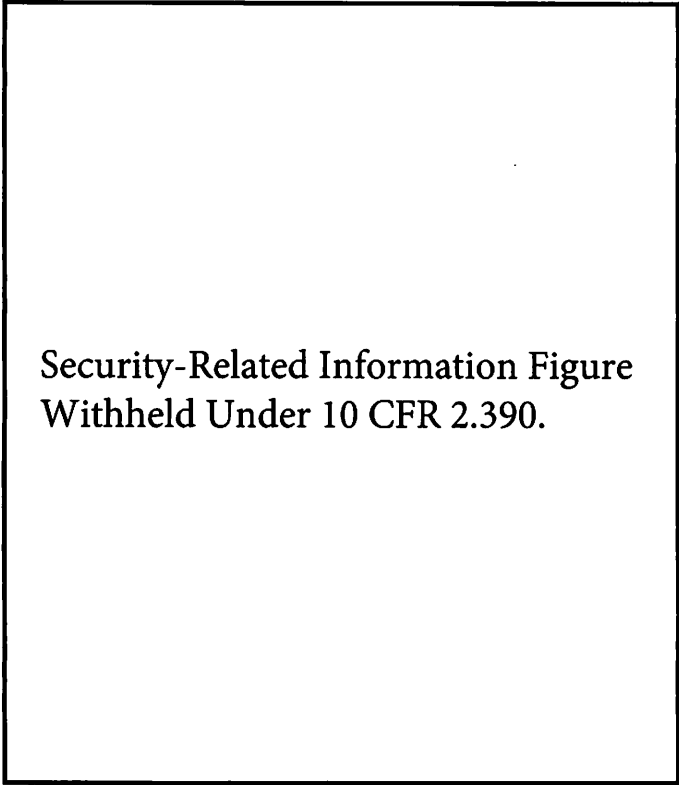


Figure 2.12.8-2 - MURR Fuel Basket View of Support Plate

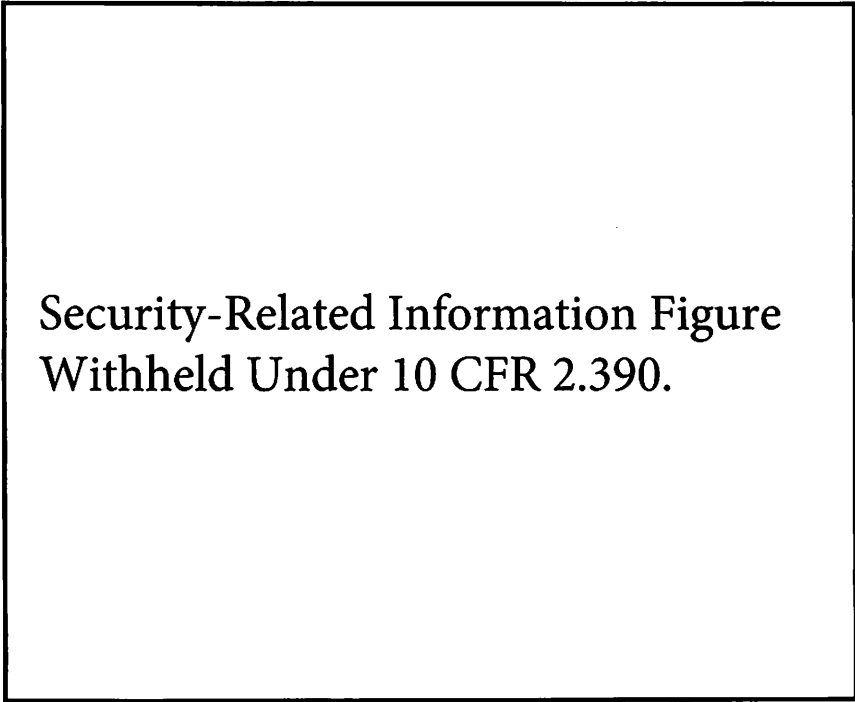


**Figure 2.12.8-3 - MITR-II Fuel Basket Cross Section**



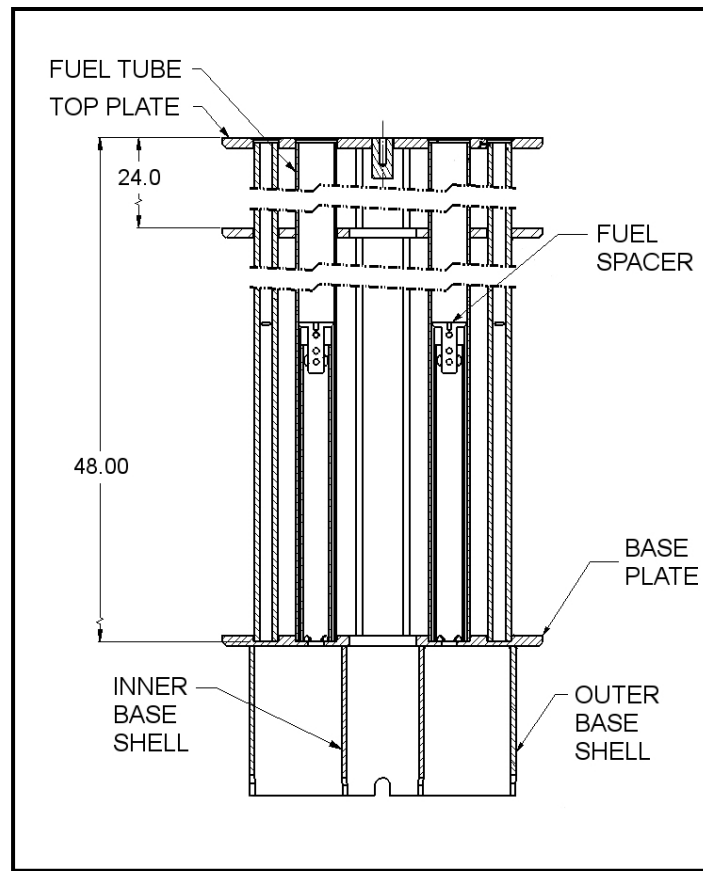
Security-Related Information Figure  
Withheld Under 10 CFR 2.390.

**Figure 2.12.8-4 - ATR Fuel Basket Cross Section**

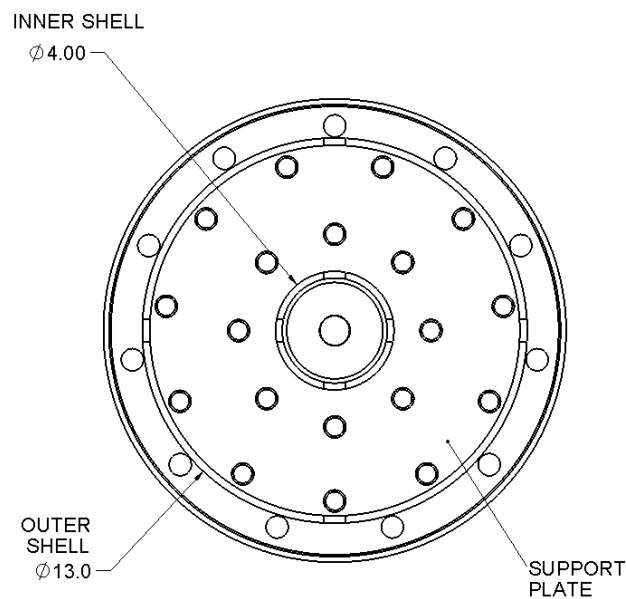


Security-Related Information Figure  
Withheld Under 10 CFR 2.390.

**Figure 2.12.8-5 - ATR Fuel Basket View of Support Plate**



**Figure 2.12.8-6 - TRIGA Fuel Basket Cross Section**



**Figure 2.12.8-7 - TRIGA Fuel Basket View of Support Plate**



## Security-Related Information Figure Withheld Under 10 CFR 2.390.

**Figure 2.12.8-8 - Square Fuel Basket Partial Cross Section**

### 3.0 THERMAL EVALUATION

This chapter identifies and describes the principal thermal design aspects of the BEA Research Reactor (BRR) package. The evaluations presented in this chapter demonstrate the compliance of the BRR package<sup>1</sup> as a Type B(U)F-96 shipping container with the thermal requirements of Title 10, Part 71 of the Code of Federal Regulations [1] when transporting a payload of irradiated fuel assemblies from various test and research reactors. A full list of the fuel types included for transport in the package is given in Section 1.2.2, *Contents*.

Specifically, all package components are shown to remain within their respective temperature limits under the normal conditions of transport (NCT). Further, per 10 CFR §71.43(g), the maximum temperature of the accessible package surfaces is demonstrated to be less than 185 °F for the maximum decay heat loading, an ambient temperature of 100 °F, and no insolation. Finally, the BRR package is shown to retain sufficient thermal protection following the HAC free and puncture drop scenarios to maintain all package component temperatures within their respective short term limits during the regulatory fire event and subsequent package cool-down.

### 3.1 Description of Thermal Design

The principal components of the BRR package are illustrated in Figure 1.2-1 through Figure 1.2-3 of Section 1.0, *General Information*. The principal components are: 1) a lead-shielded cask body, 2) a separate, removable upper shield plug, 3) a bolted closure lid, 4) upper and lower impact limiters containing polyurethane foam, and 5) a payload basket specific to the type of fuel being transported. Except for the closure bolts, the lead shielding, and the impact limiter attachment pins, the package is primarily of welded construction, using Type 304 austenitic stainless steel.

#### 3.1.1 Design Features

The primary heat transfer mechanisms within the BRR packaging are conduction and radiation. The principal heat transfer from the exterior of the packaging is via convection and radiation to the ambient environment. The upper and lower impact limiter assemblies serve as the primary impact protection for the BRR package and its enclosed payload. The impact limiters also provide the principal thermal protection to the ends of the packaging, while a thermal shield is used to protect the portion of the packaging between the limiters from the high heat flux generated during the transient HAC fire event.

There is no pressure relief system included in the BRR packaging design. The thermal design features of the principal package components are described in the following paragraphs. See Section 1.0, *General Information*, for more detail.

##### 3.1.1.1 BRR Cask Body

The BRR cask body is a right circular cylinder approximately 77.1 inches long and 38 inches in diameter (not including the impact limiter attachments and the thermal shield). It is composed of

---

<sup>1</sup> In the remainder of this chapter, the term ‘packaging’ refers to the assembly of components necessary to ensure compliance with the regulatory requirements, but does not include the payload. The term ‘package’ includes both the packaging components and the payload.

upper and lower end structures that connect circular inner and outer shells. Lead located between the two circular shells, in the lower end closure structure, and in the shield plug provides radiological shielding for the package. This design results in a large thermal mass to surface area ratio capable of absorbing the high heat flux generated during the HAC fire event and limiting the temperature rise within the interior of the package. The payload cavity has a diameter of 16 inches and a length of 54 inches. Figure 1.2-3 provides an overview of the packaging dimensions.

The inner and outer shells and the end structures may be cast or forged from Type F304 stainless steel. Since the BRR package is designed to permit loading and unloading under water, the lower end structure contains a drain to allow removal of water from the payload cavity. The drain is sealed using a brass plug, butyl rubber seal, and a dust cap.

A thermal shield, composed of an outer sheet of 12 gauge (0.105-inch thick) Type 304 stainless steel and offset from the outer shell by small strips of the same 12 gauge material, covers the region of the outer shell not covered by the impact limiters. The shield serves to protect the outer shell from direct exposure to the high heat fluxes associated with the HAC fire accident event.

The lead shielding is made from ASTM B29, chemical lead, or optionally, from lead per Federal Specification QQ-L-171E, Grade A or C. The 8 inches thick lead shield in the side of the cask body is cast-in-place through openings in the upper end structure, thus eliminating/minimizing gaps between the lead and the steel shells. The shield at the bottom is made from lead sheet material which is packed firmly into place to yield a nominal thickness of 7.7 inches.

### **3.1.1.2 Removable Shield Plug**

The removable shield plug rests on a shoulder located approximately half way along the length of the plug. The plug has a total thickness of 11.2 inches and a lead thickness of 9.7 inches. The outer shell is made from Type 304 plate material of various thicknesses and the cavity is filled with lead sheet material packed firmly into place. A 3/4-inch diameter tube passes diagonally through the plug to ensure proper draining and drying of the cask while preventing a harmful shine path. Besides providing radiological shielding, the shield plug ensures a thermally significant separation distance between the basket's decay heat and the temperature sensitive closure seals.

### **3.1.1.3 BRR Cask Closure**

The closure lid is made from 2-inch thick Type 304 stainless steel plate. It is attached to the cask using 12, 1-8 UNC electroless nickel plated bolts made of ASTM A320, Grade L43 material. The closure lid includes two O-ring seals made from butyl rubber of 3/8-inch cross sectional diameter. The inner O-ring is the containment seal, and the outer is the test seal. The seals are retained in dovetail grooves in the lid.

The BRR package features two ports which are also part of the containment boundary: a vent port in the closure lid, and a drain port in the lower end structure. Both ports are closed with threaded brass plugs and sealed with butyl rubber washers. A brass dust cover protects the port plugs. The seal test port is not part of the containment boundary.

#### 3.1.1.4 Impact Limiters

The impact limiters attached to ends of the BRR packaging, each with essentially identical designs, provide a significant level of thermal protection to the package. Each limiter is 78 inches in diameter and 34.6 inches long overall, with a conical section 15 inches long towards the outer end. The impact limiters are filled with rigid, closed-cell polyurethane foam with a nominal 9 lb/ft<sup>3</sup> density that is poured in place. As described in Appendix 3.5.4, *'Last-A-Foam' Response under HAC Conditions*, the thermal decomposition of the closed-cell polyurethane foam during the HAC event absorbs a majority of the heat energy entering the impact limiters.

The foam is encased in a stainless steel shell for structural protection. The external shells (except for the outer end plates) are ¼ inches thick, while the internal shells which interface with the cask body are ½ inches thick. The outer end plates of the impact limiters are ½-inches thick. Plastic melt-out plugs are incorporated into the exterior shells of the limiters. The plugs are designed to soften and be expelled during the HAC fire event, thus relieving any pressure buildup in the limiters due to foam decomposition under elevated temperatures. The external surfaces of the impact limiter shell are covered with a white acrylic polyurethane coating to control solar absorptivity and raise thermal emissivity.

Each impact limiter is attached to the cask body via a set of eight (8) bayonet type connectors. The connectors consist of eight sets of two closely spaced plates, 1/2 inch thick, which go through the thermal shield and are welded to the outer shell of the cask. Mating with these plates are eight 3/4 inch thick plates attached to each limiter and which pass between the receptacle plates on the cask body. Each connection is completed by a stainless steel ball lock pin that passes through the three plates (two receptacle plates and one impact limiter plate).

#### 3.1.1.5 Fuel Baskets

Five fuel baskets will be used with the BRR packaging, one for each type of fuel to be transported. Section 1.0, *General Information*, presents a description and illustration of each basket and fuel type to be loaded in the package. The baskets are made from welded construction using Type 304 stainless steel in plate, bar, pipe, and tubular forms. Each basket has a maximum diameter of 15.63 inches and a maximum length of 53.45 inches. The fuel cavities incorporated into each basket are sized and shaped to minimize free play between each fuel type and the basket, while ensuring the free insertion and removal of the elements. The baskets are open on the top with the basket designed to hold the fuel elements within approximately 3/8-inches of the basket's top end, nearest the shield plug. The baskets are designed to freely drain water when the cask is lifted out of the spent fuel pool.

### 3.1.2 Content's Decay Heat

The design basis decay heat loading for the irradiated fuel to be transported within the BRR packaging is a function of the irradiation history and the cooling time since discharge. Section 1.2.2, *Contents*, provides details of the fuel elements to be transported. For the purposes of this evaluation, the design basis decay heat loadings are as follows:

- MURR fuel: 158 W maximum per element, 1,264 W per basket
- MITR-II fuel: 150 W maximum per element, 1,200 W per basket
- ATR fuel: 30 W maximum per element, 240 W per basket

- TRIGA fuel: 20 W maximum per element, 380 W per basket
- Square fuel: 30 W maximum per element, 240 W per basket

### 3.1.3 Summary Tables of Temperatures

Table 3.1-1 provides a summary of the package component temperatures under normal and accident conditions. The temperatures for normal conditions are based on an analytical model of the BRR package for steady-state operation with an ambient temperature of 100 °F and the 10 CFR §71.71(c)(1) prescribed insolation averaged over 24 hours. The temperatures for accident conditions are based on a transient simulation using an analytical model of a damaged BRR package. The damage conditions represent the worst-case hypothetical pre-fire damage predicted from a combination of physical drop testing using a half-scale certification test unit (CTU) and analytical structural evaluations.

The results for NCT conditions demonstrate that significant thermal margin exists for all package components. Further, the NCT evaluations demonstrate that the accessible surface temperatures will be below the maximum temperature of 185 °F permitted by 10 CFR §71.43(g) in an exclusive use shipment when transported in a 100 °F environment with no insolation. The results for HAC conditions also demonstrate that the design of the BRR package provides sufficient thermal protection to yield component temperatures that are significantly below the acceptable limits defined for each component. See Sections 3.2.2, *Technical Specifications of Components*, Section 3.3.1.1, *Maximum Temperatures*, and Section 3.4.3, *Maximum Temperatures and Pressure*, for more discussion.

Table 3.1-3 summarizes the permitted fuel basket loadings determined by this safety evaluation.

### 3.1.4 Summary Tables of Maximum Pressures

Table 3.1-2 presents a summary of the maximum pressures predicted under NCT and HAC conditions. The BRR package has a design maximum pressure of 25 psig (39.7 psia). As discussed in Section 3.3.2, *Maximum Normal Operating Pressure*, the contribution to cask pressure from the release of fission gases is negligible under NCT. Based on an assumed fill gas temperature of 70 °F, the maximum pressure under NCT will be 5.2 psig. The maximum normal operating pressure (MNOP) is thus set at a bounding level of 10 psig. Under HAC, including a small contribution from the potential release of fission gases from PULSTAR fuel, the maximum pressure is 11.7 psig as determined in Section 3.4.3.2, *Maximum HAC Pressures*.

**Table 3.1-1 – Maximum Temperatures for NCT and HAC Conditions**

Location / Component <sup>①</sup>	NCT Hot Conditions, °F	Accident Conditions, °F	Maximum Allowable	
			Normal	Accident
Fuel Element Plate	350	451	400	1,100
Fuel Element Side Plate	348	449	400	1,100
Fuel Basket	334	437	800	800
Inner Shell	237	393	800	800
Lead	234	482	620	620
Outer Shell	216	704	800	2,700
Thermal Shield	185	1,256	800	2,700
Lower End Structure	205	335	800	800
Upper End Structure	222	485	800	800
Shield Plug	230	317	620 <sup>②</sup>	620 <sup>②</sup>
Cask Lid	218	306	800	800
Closure/Vent Port Elastomeric Seals	217	306	250	400
Drain Port Elastomeric Seal	202	373	250	400
Upper Impact Limiter				
- Max. Foam	217	-	300	N/A
- Avg. Foam	147	-	300	N/A
- Shell	217	1,475	250 <sup>③</sup>	2,700 <sup>④</sup>
Lower Impact Limiter				
- Max. Foam	200	-	300	N/A
- Avg. Foam	142	-	300	N/A
- Shell	200	1,475	250 <sup>③</sup>	2,700 <sup>④</sup>
Max. Accessible Surface without Insolation	185 <sup>⑤</sup>	-	185	N/A
Cask Cavity Bulk Gas	259	388	N/A	N/A

Notes: ① Results based on either a payload of eight (8) MURR fuel elements dissipating 158 W each or a payload of eight (8) MITR-II fuel elements dissipating 150 W each and helium as the backfill gas.

② Temperature criterion based on melting point of the enclosed lead shielding.

③ Temperature criterion based on long term temperature limit for shell coating.

④ Temperature criterion based on melting point for the shell. No criteria for the polyurethane foam since its thermal decomposition serves as its principal means of providing thermal protection during the HAC event.

⑤ Maximum temperature occurs at the root of the upper cask impact limiter attachment lugs.

**Table 3.1-2 – Summary of Maximum Pressures**

Condition	Cask Cavity Pressure
NCT Hot	5.2 psi gauge
HAC Hot	11.7 psi gauge

**Table 3.1-3 – Summary of Permissible BRR Package Fuel Basket Loadings**

Payload	Backfill Gas for Transport	Max. Decay Heat Per Element	Max. Package Decay Heat
MURR Fuel	Helium	158	1,264
MITR-II Fuel	Helium	150	1,200
ATR Fuel	Helium	30	240
TRIGA Fuel	Helium	20	380
Square Fuels	Helium	30	240

## 3.2 Material Properties and Component Specifications

The BRR packaging is fabricated primarily of a variety of Type 304 stainless steel product forms, lead, and polyurethane foam. The payload materials include 6061-T6 and/or 6061-0 aluminum, uranium-aluminide (UAlx), uranium-silicide ( $U_3Si_2$ ),  $UO_2$ , and uranium-zirconium hydride (UZrH).

### 3.2.1 Material Properties

While a variety of Type 304 stainless steel specifications apply to the various components of the BRR packaging, each type exhibits the same thermal properties. Table 3.2-1 presents the thermal properties used to simulate the various Type 304 stainless steels used in the packaging. The thermal properties are taken from the ASME material properties database [2] and the density is taken from an on-line database [6]. Properties for temperatures between the tabulated values are calculated via linear interpolation within the heat transfer code.

Table 3.2-1 also presents the thermal properties for ASTM B29 chemical lead, as taken from reference [4]. The density value is taken from an on-line database [6].

The 9 lb<sub>m</sub>/ft<sup>3</sup> (pcf) polyurethane foam used in the package impact limiters is based on a proprietary formulation that provides predictable impact-absorption performance under dynamic loading, while also providing an intumescent char layer that insulates and protects the underlying materials when exposed to HAC fire conditions. The thermal properties under NCT conditions are obtained from the manufacturer's on-line website [18]. Since the thermal conductivity of the material is tied to its density and the manufacturing process can yield densities that are  $\pm 15\%$  of the targeted value, this safety evaluation addresses the properties associated with both the low and high tolerance density foam (see Table 3.2-1). Since the low tolerance foam yields a lower thermal conductivity, it is assumed for NCT operations, while the higher thermal conductivity of the high tolerance density foam is used for HAC evaluation to conservatively bound the heat flow into the package.

Table 3.2-2 presents the thermal properties for the reactor fuel element material. The MURR, MITR-II, and ATR fuel elements are uranium-aluminide (UAlx) based fuels, while the TRIGA fuel element is a uranium-zirconium hydride (UZrH) based fuel. The thermophysical properties for the MURR, MITR-II, and ATR fuel elements are based on information provided in reference [5]. While the reference was developed specifically for the ATR fuel element, the thermal properties are also applicable to the MURR and MITR-II fuel elements (after adjustment for fuel plate geometry and composition) for the purposes of this safety evaluation given the similarity in the base materials for all three fuel elements. For analysis purposes, the material used for the side plates, covers, and fuel cladding are assumed to be 6061-0 aluminum. The thermal properties for the fuel plates are determined as a composite of the cladding and the fuel core materials based on the fuel design drawings [12, 13, and 14] and the thermal properties for the materials of fabrication [5]. The material properties of the Uranium-silicide ( $U_3Si_2$ ) plate fuels and PULSTAR fuel are discussed in Section 3.3.1.1, *Maximum Temperatures*.

The details of the computed values for the MURR, MITR-II, and ATR fuel elements are presented in Appendix 3.5.3.9, *Determination of Composite Thermal Properties for Fuel Plates*. For simplicity, the thermal properties are assumed to be constant with temperature based on the use of conservatively high thermal conductivity and conservatively low specific heat values.



This approach maximizes the heat transfer into the fuel components during the HAC event, while under estimating the ability of the components to store the heat.

The TRIGA fuel element uses uranium-zirconium hydride metal (UZrH) as its active fuel component, graphite as a spacer material, and aluminum or stainless steel for the end fixtures and for the fuel cladding. While a variety of TRIGA fuel designs exist, the active fuel length is either 14 or 15 inches. Table 3.2-2 presents representative thermal properties for the simulated TRIGA fuel element. The properties for graphite are based on representative values for KK-8 graphite [16], while the thermal properties for UZrH are based on [17]. The properties for the end fixtures and fuel cladding are assumed to be stainless steel (Type 304) for the purposes of this safety evaluation since this conservatively limits the axial heat spreading within the fuel element given its lower conductivity versus that of aluminum.

The thermal properties for air and helium, presented in Table 3.2-3 and Table 3.2-4, respectively, are derived from curve fits provided in [19]. Because the gas thermal conductivity varies significantly with temperature, the computer model calculates the thermal conductivity across the gas filled spaces and between the package and the ambient as a function of the mean film temperature. All void spaces within the BRR cask cavity are assumed to be filled with helium at a pressure of one atmosphere following draining and drying.

The emissivity of 'as-received' Type 304 stainless steel has been measured as 0.25 to 0.28 [7], while the emissivity of weathered Type 304 stainless steel has been measured as being between 0.46 to 0.50 [8]. For the purpose of this analysis, an emissivity of 0.25 is assumed for the emittance from all radiating stainless steel surfaces of the cask cavity to account for the surface finish required for decontamination considerations. The exterior surfaces of the upper and lower end structures of the cask body assume a slightly higher emissivity of 0.30 assuming a lower level of surface finish and greater wear and tear.

The exterior surface of the outer shell covered by the thermal shield is assumed to have an emissivity of 0.587 [9] to account for its elevated surface oxidation following the lead pour procedure. Since this surface will not be directly exposed to the pool, it will receive only limited surface finishing following fabrication. The emissivity for the exterior surfaces of the package thermal shield is assumed to be 0.45 to account for weathering, while an emissivity of 0.40 is used for the inner surface of the thermal shield to account for its lower level of weathering. The solar absorptivity of Type 304 stainless steel is approximately 0.52 [9].

The surfaces of the fuel baskets are assumed to have an emissivity of 0.30 to account for the degree of polishing, etc. required for these surfaces due to decontamination considerations. This is slightly higher than the 0.25 value assumed for the cask cavity interior surfaces due to the greater wear and tear on these surfaces and the higher operating temperatures.

Exposed surfaces of lead are expected to oxidize rapidly and exhibit an emissivity of 0.6 [9].

The 6061-0 aluminum used for the MURR, MITR-II, and ATR fuel cladding, end fittings, and side plates is assumed to have a surface coating of boehmite ( $\text{Al}_2\text{O}_3\cdot\text{H}_2\text{O}$ ). Per [10], a 25  $\mu\text{m}$  boehmite film will exhibit a surface emissivity of approximately 0.92.

The exterior surfaces of the impact limiters will be finished with a white color coating system [11]. This coating system is expected to yield an emissivity in excess of 0.9 and a solar absorptivity of approximately 0.20. For conservatism, an emissivity of 0.9 and a solar absorptivity of 0.30 are assumed by this evaluation.

The char layer associated with the decomposed polyurethane foam has a conservative surface emissivity of approximately 0.95 based on a combination of the material type, color, and surface roughness. No free surfaces will exist for the 'poured in place' foam under NCT conditions.

Under HAC conditions, all exterior surfaces of the package are assumed to attain an emissivity of 0.9. This assumption exceeds the minimum requirements of 10 CFR §71.73(c)(4) [1].

### **3.2.2 Technical Specifications of Components**

The materials used in the BRR packaging that are considered temperature sensitive are the lead used for the radiological shielding, the polyurethane foam used in the impact limiters, the epoxy coating used on the impact limiter exterior surfaces, the butyl rubber compound used for the containment boundary seals, and the aluminum cladding and UAl<sub>x</sub> fuel matrix used for the enclosed fuel assemblies. The other materials either have temperature limits above the maximum expected temperatures or are not considered essential to the function of the package.

Type 304 stainless steel has a melting point above 2,700 °F [6], but in compliance with the ASME B&PV Code [3], its allowable temperature is limited to 800 °F if the component serves a structural purpose (e.g., the material's structural properties are relied on for loads postulated to occur in the respective operating mode or accidental free drop condition). As such, the appropriate upper temperature limit under normal conditions is 800 °F for stainless steel components that form the containment boundary or are used in the fuel baskets. The upper limit for all other stainless steel components is 2,700 °F for both normal and accident conditions.

The applicable temperature criterion for the ASTM B29 lead is its melting point of approximately 620 °F [6].

Below 250 °F the variation in the thermal properties of the proprietary polyurethane foam with temperature are slight and reversible. While small variations in the foam properties will occur between 250 and 500 °F as water vapor and non-condensable gases are driven out of the foam, the observed changes are very slight. For conservatism, a long-term limit of 300 °F is assumed for the foam. There is no short term temperature limit for the foam as its decomposition under exposure to high temperatures is part of its mechanism for providing thermal protection during the HAC fire event. A detailed description of the foam's behavior under elevated temperatures is presented in Appendix 3.5.4, *'Last-A-Foam' Response under HAC Conditions*.

The exterior surfaces of the impact limiter shells are to be coated in a two step process consisting of a primer coat of polyamide epoxy, followed by an acrylic polyurethane top coat [11]. The color is white. The coating system is resistant to long term temperature exposure up to 250 °F and for intermittent exposure up to 275 °F.

The butyl rubber compound used for the containment seals is fabricated from Rainier Rubber compound R0405-70 [20]. Butyl rubber has a long term temperature range of -75 °F to 250 °F [21]. Per Appendix 2.12.7, *Seal Performance Tests*, an acceptable short duration limit for this compound is 400 °F for 8 hours, 380 °F for 24 hours, and 350 °F for 144 hours. For conservatism, a long-term limit of 250 °F, a short-term limit of 400 °F for 8 hours, and a low temperature limit of -40 °F are assumed for this analysis.

Aluminum has a melting point of approximately 1,100 °F [6]; however for strength purposes the normal operational temperature is limited to 400°F based on structural strength considerations for aluminum [3]. The limit under HAC conditions is 1,100°F.

The allowable temperatures for the irradiated test and research reactor fuel elements under any condition of operation within the reactor facility are established by the NRC [34, 35] as follows (see Section 2.1 of Appendix 14.1 of [34]):

- 1) for stainless steel clad TRIGA fuel
  - for a cladding temperature at or less than 500 °C (932 °F), the peak fuel temperature shall be at or less than 1150 °C (2102 °F),
  - for a cladding temperature greater than 500 °C (932 °F), the peak fuel temperature shall be at or less than 950 °C (1742 °F),
- 2) for aluminum-clad TRIGA fuel, a peak fuel temperature should not exceed 500 °C (932 °F),
- 3) for highly enriched uranium (HEU) and uranium-silicide low-enriched uranium (LEU) aluminum clad fuel, a peak cladding and fuel temperature shall be at or less than 530 °C (986 °F).

Of the potential fuel payloads, only the TRIGA fuel uses both stainless steel and aluminum cladding. For simplicity, this evaluation conservatively uses the lower bounding permissible cladding temperature limit of 932 °F (500 °C) to cover both stainless steel and aluminum clad fuel. This temperature limit is applicable to cask draining and vacuum drying operations only. All other operations and transport conditions assume a permissible peak cladding and fuel temperature at or less than 400 °F.

The minimum allowable service temperature for all BRR package components is below -40 °F.

**Table 3.2-1 – Thermal Properties of Packaging Materials**

<b>Material</b>	<b>Temperature (°F)</b>	<b>Thermal Conductivity (Btu/hr-ft-°F)</b>	<b>Specific Heat (Btu/lb<sub>m</sub>-°F)</b>	<b>Density (lb<sub>m</sub>/in<sup>3</sup>)</b>
Stainless Steel <sup>①</sup> Type 304	-40	8.2	0.112	0.289
	70	8.6	0.114	
	100	8.7	0.115	
	200	9.3	0.119	
	300	9.8	0.123	
	400	10.4	0.126	
	500	10.9	0.129	
	600	11.3	0.130	
	700	11.8	0.132	
	800	12.3	0.134	
	1000	13.1	0.135	
	1200	14.0	0.138	
	1400	14.9	0.141	
	1500	15.3	0.142	
Lead <sup>②</sup> ASTM B29, chemical lead	-58	21.67	0.030	0.4097
	32	20.4	0.030	
	80.6	19.99	0.030	
	158	19.88	0.031	
	260.6	19.36	0.032	
	428	18.43	0.033	
	608	16.49	0.033	
	620.6	16.35	0.036	
Polyurethane Foam	-	0.01872 <sup>③</sup>	0.353	0.00599 <sup>③</sup>
	-	0.01728 <sup>④</sup>	0.353	0.00443 <sup>④</sup>

Notes:

① Reference [2], Material Group J. Properties valid for ASTM A351, Grade CF8A, ASTM A182, Type F304, ASTM A451, Grade CPF8A, and ASTM A240, Type 304 stainless steels.

② Reference [4].

③ Based on FR3709 ‘Last-a-Foam’ high tolerance foam density (i.e., 9 pcf + 15%) properties [18].

④ Based on FR3709 ‘Last-a-Foam’ low tolerance foam density (i.e., 9 pcf - 15%) properties [18].

**Table 3.2-2 – Thermal Properties of Fuel Element Materials**

<b>Material</b>	<b>Temperature (°F)</b>	<b>Thermal Conductivity (Btu/hr-ft-°F)</b>	<b>Specific Heat (Btu/lb<sub>m</sub>-°F)</b>	<b>Density (lb<sub>m</sub>/in<sup>3</sup>)</b>
Aluminum <sup>①</sup> Type 6061-0	32	102.3	-	0.0976
	62	-	0.214	
	80	104.0	-	
	170	107.5	-	
	260	109.2	0.225	
	350	109.8	-	
	440	110.4	0.236	
	530	110.4	-	
	620	109.8	0.247	
	710	108.6	-	
	800	106.9	0.258	
	890	105.2	-	
	980	103.4	0.269	
	1080	101.1	0.275	
MURR Fuel Plate <sup>②</sup>	-	49.2	0.195	0.119
MITR-II Fuel Plate <sup>②</sup>	-	66.6	0.208	0.113
ATR Fuel Plate 1 <sup>②</sup>	-	46.6	0.193	0.120
ATR Fuel Plates 2 to 18 <sup>②</sup>	-	69.6	0.210	0.112
ATR Fuel Plate 19 <sup>②</sup>	-	38.9	0.188	0.122
TRIGA Graphite <sup>③</sup>	-	46.2	0.250	0.060
TRIGA Fuel <sup>④</sup>	-	10.40	0.191	0.134

Notes:

- ① Reference [5]
- ② Values determined based on composite value of aluminum cladding and fuel core material (see Appendix 3.5.3.9, *Determination of Composite Thermal Properties for Fuel Plates*). Thermal conductivity value valid for axial and circumferential heat transfer within fuel plates.
- ③ Representative value, based on Reference [16].
- ④ Representative value, based on Reference [17].

**Table 3.2-3 – Thermal Properties of Air**

Temperature (°F)	Density lb <sub>m</sub> /in <sup>3</sup> <sup>①</sup>	Specific Heat (Btu/lb <sub>m</sub> -°F)	Dynamic Viscosity (lb <sub>m</sub> /ft-hr)	Thermal Conductivity (Btu/hr-ft-°F)	Prandtl Number <sup>②</sup>	Coef. Of Thermal Exp. (°R <sup>-1</sup> ) <sup>③</sup>
-40	Use Ideal Gas Law w/ Molecular wt = 28.966	0.240	0.03673	0.0121	Compute as Pr = c <sub>p</sub> μ / k	Compute as β = 1/(°F+459.67)
0		0.240	0.03953	0.0131		
50		0.240	0.04288	0.0143		
100		0.241	0.04607	0.0155		
200		0.242	0.05207	0.0178		
300		0.243	0.05764	0.0199		
400		0.245	0.06286	0.0220		
500		0.248	0.06778	0.0240		
600		0.251	0.07242	0.0259		
700		0.253	0.07680	0.0278		
800		0.256	0.08098	0.0297		
900		0.259	0.08500	0.0315		
1000		0.262	0.08887	0.0333		
1200		0.269	0.09620	0.0366		
1400		0.274	0.10306	0.0398		
1500		0.277	0.10633	0.0412		

## Table Notes:

- ① Density computed from ideal gas law as  $\rho = PM/RT$ , where R= 1545.35 ft-lbf/lb-mole-R, T= temperature in °R, P= pressure in lbf/ft<sup>2</sup>, and M= molecular weight of air. For example, at 100 °F and atmospheric pressure of 14.69lbf/in<sup>2</sup>,  $\rho = (14.69 \times 144 \text{ in}^2/\text{ft}^2 \times 28.966 \text{ lbm/lb-mole}) / (1545.35 \times (100 + 459.67)) = 0.071 \text{ lbm/ft}^3 = 4.099 \times 10^{-5} \text{ lbm/in}^3$ .
- ② Prandtl number computed as  $Pr = c_p \mu / k$ , where c<sub>p</sub>= specific heat, μ = dynamic viscosity, and k = thermal conductivity. For example, at 100 °F,  $Pr = 0.241 \times 0.04607 / 0.0155 = 0.72$ .
- ③ Coefficient of thermal expansion is computed as the inverse of the absolute temperature. For example, at 100 °F,  $\beta = 1/(100 + 459.67) = 0.00179$ .

**Table 3.2-4 – Thermal Properties of Helium**

Temperature (°F)	Density lb <sub>m</sub> /in <sup>3</sup> ) <sup>①</sup>	Specific Heat (Btu/lb <sub>m</sub> -°F)	Dynamic Viscosity (lb <sub>m</sub> /ft-hr)	Thermal Conductivity (Btu/hr-ft-°F)	Prandtl Number <sup>②</sup>	Coef. Of Thermal Exp. (°R <sup>-1</sup> ) <sup>③</sup>
-40	Use Ideal Gas Law w/ Molecular wt = 4.0026 g/mole	1.240	0.04032	0.0738	Compute as Pr = c <sub>p</sub> μ / k	Compute as β = 1/(°F+459.67)
0		1.240	0.04306	0.0784		
50		1.240	0.04634	0.0837		
100		1.240	0.04944	0.0886		
200		1.240	0.05520	0.0981		
300		1.240	0.06088	0.1075		
400		1.240	0.06643	0.1177		
500		1.240	0.07153	0.1291		
600		1.240	0.07640	0.1403		
700		1.240	0.08116	0.1508		
800		1.240	0.08580	0.1607		
900		1.240	0.09033	0.1702		
1000		1.240	0.09475	0.1793		
1200		1.240	0.10327	0.1971		
1400		1.240	0.11139	0.2144		
1500		1.240	0.11531	0.2231		

Table Notes:

- ① Density computed from ideal gas law as  $\rho = PM/RT$ , where R= 1545.35 ft-lbf/lb-mole-R, T= temperature in °R, P= pressure in lbf/ft<sup>2</sup>, and M= molecular weight of helium.
- ② Prandtl number computed as  $Pr = c_p\mu / k$ , where c<sub>p</sub>= specific heat, μ = dynamic viscosity, and k = thermal conductivity.
- ③ Coefficient of thermal expansion is computed as the inverse of the absolute temperature.

### 3.3 Thermal Evaluation for Normal Conditions of Transport

This section presents the thermal evaluation of the BRR for normal conditions of transport (NCT). Under NCT, the package will be transported in a vertical orientation. This establishes the orientation of the exterior surfaces of the package for determining the free convection heat transfer coefficients and insolation loading. The package support system is configured to mate with the lower impact limiter such that the conical and base surfaces of the limiter are fully enclosed. As such, the NCT evaluations conservatively assume an adiabatic condition for these surfaces (i.e. there is no heat transfer to or from the ambient).

#### 3.3.1 Heat and Cold

The NCT thermal performance is determined using a three-dimensional thermal model of the BRR packaging and its enclosed payloads. The models provide a full height, half symmetry representation of the packaging and payload components. The modeling approach permits simulation of the varying insolation loads along the length of the package, captures the various degrees of symmetry within the fuel baskets, and allows the non-symmetry conditions of the HAC free drop damage to be simulated. A separate thermal model is used to evaluate the NCT thermal performance for each of the four potential fuel payloads. The details of the NCT thermal modeling are provided in Appendix 3.5.3, *Analytical Thermal Model*.

The safety evaluation for the BRR packaging components is based on a payload of eight (8) MURR fuel elements and a payload of eight (8) MITR-II fuel elements since their maximum decay heat loadings of 1,264 W and 1,200 W, respectively, exceeds by a factor of over 3 the maximum package decay heat loading of 380 W for the TRIGA fuel payload and the 240 W for the ATR and Square fuel payloads. As such, the peak temperatures achieved by the packaging components for the transport of the ATR, Square fuel, and TRIGA payloads are bounded by those predicted for either the MURR or MITR-II fuel payloads. The peak packaging component temperatures for the MITR-II payload are similar to those achieved with the MURR payload given their similar decay heat loadings.

##### 3.3.1.1 Maximum Temperatures

###### MURR Fuel Basket

Table 3.3-1 presents the predicted BRR package temperatures under NCT conditions for the transportation of a fully loaded MURR fuel basket dissipating 1,264 W of decay heat. The analysis assumes a helium gas backfill in order to limit the peak temperature of the MURR fuel plates to 400 °F or less, based on structural considerations.

The results demonstrate that large thermal margins exist for essentially all of the packaging and payload components. The minimum thermal margin of 34 °F (i.e., 250 - 216 °F), occurs for the cask closure seals. A similar thermal margin of 35 °F occurs for the coating used on the external surfaces of the impact limiters. These margins are adequate given the conservative assumptions used in the modeling, including neglecting the beneficial contribution of the stand-off strips when computing the temperature rise between the thermal shield and the outer shell and the assumption of a small, but uniform gap between the lead and the outer shell. Removing these



conservatisms will decrease the cask body surface temperatures and increase the thermal margins for the seals and the impact limiter coating by an estimated 9 °F.

Figure 3.3-1 to Figure 3.3-4 present the predicted temperature distribution within the BRR package for the NCT Hot condition. The elevation of the MURR fuel payload within the cask cavity is clearly evident from the temperature distribution seen in Figure 3.3-1 and Figure 3.3-3. The temperature distribution within the impact limiters illustrated in Figure 3.3-2 also reflects the elevation of the payload, plus the upright orientation of the package for NCT conditions in that the inside face of the lower impact limiter experiences the solar loading for a flat horizontal surface, while the same face for the upper impact limiter has a zero solar loading because of its downward orientation.

Figure 3.3-3 illustrates the temperature distribution in the structural shell of the cask. The presence of the impact limiter attachment lugs can be seen by the localized ‘cool’ spots in the temperature distribution of the outer shell. As noted in the description of the NCT thermal model provided in Appendix 3.5.3, *Analytical Thermal Model*, the NCT Hot results are based on an earlier cask design that used 6 instead of the current 8 attachment lugs per limiter, cask lug plates that are 0.38-inches thick by 2.75-inches wide vs. the current 0.5-inches thick by 3.63-inches wide, and a 0.25-inch vs. 0.125-inch radial gap between the limiter and the cask shell. Since the earlier design version provides slightly conservative results for NCT due to its lower surface area for heat dissipation to the ambient, it is appropriate for predicting the peak NCT temperatures.

Figure 3.3-4 presents the predicted temperature distribution within the MURR fuel basket under the NCT Hot condition.

Evaluation of the package for an ambient air temperature of 100 °F without insolation loads demonstrates that the temperatures of all exterior surfaces of the packaging are below the maximum temperature of 185 °F permitted by 10 CFR §71.43(g) for accessible surface temperature in an exclusive use shipment. The peak accessible surface temperature occurs at the root of the upper impact limiter attachment lugs. A sensitivity analysis, based on the revised lug design, as described in Appendix 3.5.3, *Analytical Thermal Model*, confirms that the peak accessible surface temperature in the vicinity of the upper impact limiter attachment lugs (see temperature distribution in Figure 3.3-5) is 185 °F or less.

### **MITR-II Fuel Basket**

Table 3.3-2 presents the predicted maximum temperature achieved within the MITR-II fuel basket and the BRR package under the NCT Hot condition with a helium gas backfill. A design basis maximum decay heat loading of 150 W per element, or 1,200 W for a payload of eight (8) fuel elements, is assumed for the transportation of the MITR-II payload. As expected, given their similar total decay heat loads, the peak temperatures achieved within the BRR packaging components are similar to those presented in Table 3.3-1. The MITR-II fuel element is shorter than the MURR fuel element. As a result, the MITR-II payload decay heat source resides a little higher in the cask cavity which, in turn, leads to reduced heat flow into the lower components of the BRRC packaging (i.e., the lower end structure, the drain port, etc.), and lower temperatures versus those seen with the MURR payload.

The results in Table 3.3-2 demonstrate that the design criterion of a maximum fuel plate temperature of 400 °F is met if helium is used as the backfill gas. Figure 3.3-6 presents the predicted temperature distribution within the MITR-II fuel basket under the NCT Hot condition.

### **ATR Fuel Basket**

Table 3.3-3 presents the predicted maximum temperature achieved within the ATR fuel basket under the NCT Hot condition with a helium gas backfill. The peak temperatures for the BRR packaging are again bounded by those presented in Table 3.3-1. The design basis maximum decay heat loading for the ATR fuel elements to be transported is 30 W per element, or 240 W for a payload of eight (8) fuel elements. Although this level of decay heat loading could be accommodated using air as the backfill gas, a helium gas backfill is to be used to maintain consistency with the loading procedures for the other payloads. Figure 3.3-7 presents the predicted bounding temperature distribution within the ATR fuel basket under the NCT Hot condition.

### **TRIGA Fuel Basket**

Table 3.3-4 presents the predicted maximum temperature achieved within the TRIGA fuel basket under the NCT Hot condition with a helium backfill. The design basis maximum decay heat loading for the TRIGA fuel elements to be transported is 20 W per element, or 380 W for a payload of nineteen (19) fuel elements. As seen from Table 3.3-4, the results demonstrate that the design criterion of a maximum fuel element temperature of 400 °F is met. Figure 3.3-8 presents the predicted bounding temperature distribution within the TRIGA fuel basket under the NCT Hot condition for TRIGA catalog types 101, 103, 203, 109, and 117.

Additional catalog types of TRIGA fuel are included in the allowable fuel type listed in Table 1.2-1. These include catalog numbers 105, 107, 119, 201, 205, 207, 217, 219, 303, 305, 317, 319, 403, 405, 417, 419, 503, 505, 517, and 519. These additional fuels each share all key aspects of the initially licensed fuel but some have a slightly reduced outer diameter. The smaller diameter increases the originally analyzed small nominal gap by approximately 20 percent. This will introduce a very small temperature increase to the fuel cladding temperature due to the increase in the conductive heat transfer path length.

This case can be conservatively explored using a purely conductive, 1-dimensional model, i.e. all heat transfer from the fuel to the basket is radial and in the form of conduction. Furthermore, radiative heat transfer is not directly affected by the increase in the gap thickness and therefore need not be included in the comparison. The increase in fuel temperature is the difference between the conductive temperature change for the new ( $\Delta T_N$ ) and the original ( $\Delta T_O$ ) fuel types. All fuel catalog types are analyzed using the TRIGA bounding heat load of 20W. From Fourier's law the fuel cladding temperature will increase by:

$$T_{\text{increase}} = \Delta T_N - \Delta T_O = Q \left( \frac{\ln \left( \frac{d_T}{d_2} \right)}{2\pi Lk} - \frac{\ln \left( \frac{d_T}{d_1} \right)}{2\pi Lk} \right) = 7.1^\circ\text{F}$$

where the basket tube inner diameter is  $d_T = 1.76$  inches, and the original and new smaller fuel outer diameters are  $d_1 = 1.48$  inches and  $d_2 = 1.35$  inches, respectively. The decay heat bounding value of  $Q = 20\text{W}$  is distributed over the nominal active fuel length of  $L = 15$  inches, and the

conductivity of helium at the peak TRIGA fuel element temperature of 355 °F is  $k = 0.1177$  Btu/hr-ft-°F (interpolated from Table 3.2-4). The maximum TRIGA element temperature is thus  $355 + 7 = 362$  °F.

The increase is relatively small in comparison to the existing margin of 45°F that can be calculated from Table 3.3-4. With the addition of the new TRIGA fuel catalog types there is no significant increase in temperature; therefore additional analysis is not required.

### **Square Fuel Basket Cases**

The square fuel basket allows for the transportation of eight types of fuel assembly and three types of loose fuel plates. The characteristics and low decay heat of the new fuel types permits a qualitative analysis of the basket and its payload; therefore explicit modeling need not be included.

The square basket is a single weldment fabricated from Type 304 stainless steel. The basket has a maximum diameter of 15.63 inches and a maximum length of 53.45 inches. The eight fuel cavities are sized to fit the nominally square cross section of the eight fuel types. A loose fuel plate holder may be used to transport the three specified loose fuel plate types in up to eight of the fuel cavities. Spacers are placed in the bottom of each fuel cavity in the case of shorter fuels to ensure that the top ends of each of the fuel assemblies are held near the top of the basket's top end. The basket is designed to freely drain water when the cask is lifted out of a spent fuel pool.

### ***The Effect of Basket Design and Fuel Decay Heat on Basket and Cask Temperature***

The maximum decay heat of the eight new fuel types ranges from 0.1 for the Purdue University fuel to 25 Watts for the PULSTAR Fuel as shown in Tables 5.2-11 and 5.2-15. However, a maximum allowable decay heat limit of 30 Watts per fuel element or 240 W per basket is used for the square fuel basket. The following paragraphs justify why the temperatures of the square fuel elements and of the BRR cask when transporting the square fuel elements or loose plates are bounded by the temperatures associated with the MURR and MITR-II fuel elements.

As discussed in Section 3.3.1, *Heat and Cold*, the safety evaluation of the BRR packaging components is based on two NCT thermal models: the first with a payload of eight MURR, and the second with a payload of eight MITR-II fuel elements. The maximum allowable decay heat for the square fuel basket package configuration is 240W. This decay heat is bounded by the 1,264W MURR and the 1,200W MITR-II payload configurations by at least a factor of five. Figure 3.3-9 shows a representation of the axial heat load (W per inch) of the BRR package fuel baskets. The maximum decay heat load for each basket is averaged over the active lengths of its particular fuel. This figure demonstrates that the square fuel basket distributed heat load, applied over the active length of the fuel, is bounded by the distributed heat load of the MURR and MITR-II payloads by a significant margin. The lower decay heat load and active region positioning are selected to ensure that the temperature profile throughout the packaging will be bounded by the peak temperature profile of the MURR (Table 3.3-1) and MITR-II payloads (Table 3.3-2).

It should be noted that the square fuel basket design is somewhat different than that of the MURR and MITR-II fuel baskets. The MURR and MITR-II basket designs consist of a single layer of eight fuel openings equally spaced around the axis of the basket. The square fuel basket has an outer layer of six fuel cell tubes with two fuel cell tubes positioned in the center of the basket. The square fuel basket design is akin to the TRIGA basket which has eleven fuel cell

tubes in an outer row and eight fuel cell tubes in an inner row closer to the center axis of the basket. This configuration will produce a more complex radial temperature gradient in the fuel basket due to the increased radial dispersion of the heat load. In the TRIGA basket the multi-layer arrangement results in a peak fuel temperature that is similar to that of the MURR and MITR-II basket peak fuel temperatures.

However, the TRIGA basket maximum decay heat load of 380 W is 1.6 times that of the 240 W heat load of the square fuel basket. In addition, the TRIGA basket places 160 W of its decay heat load (42% of the total heat load) in the inner ring-layer while the square fuel basket only places 60 W of its heat load (25% of the total heat load) in the inner layer. In addition, the heat load of the TRIGA fuel is dispersed over a much smaller area than that of the square fuel basket fuel types due to the smaller cross sectional area of the TRIGA fuel. This drives a steeper temperature gradient through each fuel cell tube layer in the TRIGA basket. Therefore due to the lower heat load and radial dispersion of the heat load, the square fuel basket and square fuel temperatures are predicted to remain bounded by that of the MURR, MITR-II, and TRIGA baskets. Of note, since the heat flow is primarily radial (due to the restriction posed by the impact limiters at each end of the cask), the presence of the pedestals with the shorter fuels will not have a significant effect on temperatures in the square fuel cases.

Since the position of the active region of the square fuel is essentially the same as that of the MITR-II fuel, and the magnitude of the heat load is one-fifth that of the MITR-II fuel, the temperature profile of the BRR Package with the square fuel basket and payload will be bounded by the temperature profile of the MITR-II fuel basket. Also, the temperature of the packaging components will not exceed those found in Table 3.3-2, all which have significant margin to meet their performance requirements. The temperatures of the closure and vent port seals are less than 217°F; that of the drain port seal less than 194°F; and the average bulk foam temperature of the impact limiters will be less than 147°F. The accessible surface temperatures will be less than 185°F.

### ***The Effect of Fuel Design on Fuel Temperature***

There are two particular styles of fuel assembly for transport within the square fuel basket. Details of the fuel assemblies are presented in Table 3.3-5. The first style is flat plate fuels—either with a uranium-oxide dispersion or uranium-silicide dispersion meat in an aluminum matrix, bonded with an aluminum alloy cladding. (The Missouri S&T fuel, with a slight curve to the fuel plate profile, is included in this style of fuel assembly.) This style of assembly shares the characteristics of the MURR, MITR-II, and ATR fuel assemblies discussed in detail in Section 3.5.3.9, *Determination of Composite Thermal Properties for Fuel Plates*. It has been shown that silicide dispersion fuels have better thermal conductivity than  $UAl_x$  dispersion fuels [37]. In addition, based on a comparison of the mass and materials of the various fuel assemblies, the heat capacity of the fuel assembly will not significantly affect the transient analyses. Therefore, given the similar construction and materials, the flat plate fuels are bounded by the MITR-II ( $UAl_x$ ) fuel properties.

The second style of fuel assembly is the PULSTAR fuel assembly, which consists of a 5x5 array of fuel rods enclosed within a rectangular can. Each fuel rod is filled with cylindrical uranium oxide fuel pellets. At room temperature, uranium oxide ( $UO_2$ ) has a conductivity of 2.29 Btu/hr-ft-°F and a specific heat of 0.05 Btu/lb<sub>m</sub>-°F [38]. In comparison, from Table 3.2-2, uranium-zirconium hydride (i.e., TRIGA fuel) has a conductivity of 10.40 Btu/hr-ft-°F and a

specific heat of 0.191 Btu/lb<sub>m</sub>-°F. In a solid cylinder, centerline temperature is a function of the square of the radius, and thus the fuel rod radius has a significant effect on peak temperature. For radial heat flow in a solid cylinder with a uniform heat generation  $\dot{q}$ , conductivity  $k$ , and outer radius  $r_o$ ,

$$\Delta T = \frac{\dot{q} r_o^2}{4k}$$

Thus, since the pellet diameter of the PULSTAR fuel is less than one-third that of the smallest TRIGA fuel (0.423/1.31 = 0.32), and the pellet conductivity of the PULSTAR fuel is approximately one-fifth (2.29/10.4 = 0.22) that of the TRIGA fuel, the  $\Delta T$  from centerline to edge of the PULSTAR fuel is approximately  $(0.32)^2/0.22 = 0.47$ , or just under half as much as for the TRIGA fuel, assuming the same heat generation. Including the effect of lower heat generation, the PULSTAR fuel cladding temperatures will remain significantly lower than those of the current analysis, remaining well below the 400°F limit for NCT.

In addition, PULSTAR fuel has a much higher allowable temperature than the TRIGA fuel. The NRC has accepted that the UO<sub>2</sub> temperature should not exceed 2400°C (4,352°F) and the Zircalloy-2 cladding temperature should not exceed 1500°C (2,732°F) [34]. Given the characteristics of the PULSTAR fuel and these temperature limits, the fuel is well protected for both steady state and all short term transients such as the HAC fire, cask draining operations, and vacuum drying operations.

The lower decay heat load and decay heat location in the square fuel basket ensures that the temperature profile throughout the packaging will be bounded by the peak temperature profile of the MURR and MITR-II payloads. This will also result in a lower thermal gradient and a lower peak basket temperature than that of the original four basket designs. With a lower basket temperature and with similar fuel material thermal properties the peak fuel temperature will then remain bounded by the existing analyses. Therefore, the square fuel basket is bounded by the existing analysis and meets the thermal requirements of 10 CFR 71.

### 3.3.1.2 Minimum Temperatures

The minimum temperature achieved within each of the fuel baskets would be achieved with a zero decay heat load and an ambient air temperature of -40 °F per 10 CFR §71.71(c)(2). The evaluation of this thermal condition requires no thermal calculation. Instead, all package components will eventually achieve the -40 °F temperature under steady-state conditions. As discussed in Section 3.2.2, *Technical Specifications of Components*, the -40 °F temperature is within the allowable operating temperature range for all package components.

### 3.3.2 Maximum Normal Operating Pressure

The cask cavity is to be filled with helium at atmospheric pressure following the draining and drying process. Since the release of fission generated gases from uranium-aluminide and uranium-zirconium hydride based fuel is diffusion-limited as opposed to the direct release mechanism for commercial spent nuclear fuel, the pressurization of the cask cavity due to gaseous release from breached plate-type or TRIGA fuel elements will be insignificant [30, 31] and is ignored for this safety evaluation.

The peak pressure developed within the cask cavity under NCT conditions can be conservatively estimated by assuming that the cavity gas reaches a bulk average temperature that is equal to the mean of the average inner shell temperature and the average fuel basket temperature. Under the NCT Hot condition with the MURR fuel payload the average temperature of the inner shell is 225 °F. Combining this temperature with the average fuel basket temperature of 293 °F yields a predicted bulk average backfill gas temperature of 259 °F.

Assuming the backfill gas has an initial temperature of 70 °F at the time of filling and that a fill pressure of one atmosphere is used, the predicted maximum operating pressure within the cask cavity for the transport of the MURR payload can be estimated via:

$$\text{Cavity Pressure} = 14.7 \text{ psia} \frac{(259^\circ \text{F} + 460^\circ \text{F})}{(70^\circ \text{F} + 460^\circ \text{F})} - 14.7 \text{ psia}$$

$$\text{Cavity Pressure} = 5.2 \text{ psig}$$

The equivalent peak bulk average fill gas temperatures for the MITR-II, ATR, and TRIGA baskets are 254, 164, and 174 °F, respectively. As such, the associated peak cask cavity pressures under NCT conditions are 5.1, 2.6, and 2.9 psig, respectively. Based on these NCT pressures, the maximum normal operating pressure (MNOP) within the cask cavity is set at a bounding level of 10 psig.

#### ***Fission Gas Release from PULSTAR Fuel***

Unlike the other fuels transported in the BRR package, the PULSTAR fuel assembly resembles commercial fuels and may contribute fission gases to the cavity volume of the BRR package. As noted above in this section, fission gases are not released in significant quantities from either the plate-type fuels or TRIGA fuels. Similarly, the release of fission gases from the PULSTAR fuel will not be significant as calculated below.

The cylindrical cask payload cavity has a volume of 10,857 in<sup>3</sup> based on its nominal diameter of 16.0 inches and length of 54.0 inches. The displaced volume of the square fuel basket is 862 in<sup>3</sup> based on its upper bounding weight of 250 lb and a density for stainless steel of 0.29 lb/in<sup>3</sup>.

Neglecting the small displaced volume of the fuel, the volume of fill gas is:

$$V = 10,857 - 862 = 9,995 \text{ in}^3$$

Fission gas produced is shown to be less than 0.35 g-moles per fuel assembly in Section 5.2.3, *Irradiation Gas Generation*. As stated in Table 4-1 of [39], 100% of the fuel rods are assumed to release 30% of the fission gases available in the rods under HAC. With eight fuel assemblies per basket load, the amount of fission gases under HAC will increase by  $n_{FG} = 0.35 \times 8 \times 0.3 = 0.84$  g-moles of gas. The addition of the fission gases during HAC will increase the cavity pressure by:

$$\Delta P_{HAC} = \frac{n_{FG} R T_{HAC}}{V(454)} = 2.9 \text{ psi}$$

where the ideal gas constant,  $R = 1,545 \text{ ft}\cdot\text{lb}/(\text{lb}\cdot\text{mol}\cdot^\circ\text{R})$ , the cask cavity volume  $V = 9,995 \text{ in}^3$  as found above, and the average cavity gas temperature is conservatively taken from the MURR basket case of  $T_{HAC} = 388^\circ\text{F}$  from Table 3.4-1. The factor of 454 is used to convert lb-moles to g-moles. As stated in Table 4-1 of [39], only 3 percent of the fuel cladding is considered to be in the breached condition under NCT. Given that the NCT gas temperature remains much lower

than the HAC gas temperature, and less than 1% of the fission gas is assumed released during NCT (i.e.,  $0.03 \times 0.3 = 0.009$ ), the increase in NCT pressure is negligible.

### 3.3.3 Cask Draining and Vacuum Drying Operations

An evaluation of the vacuum drying operation was conducted to ensure that the component temperatures will remain within their acceptable temperature limits. The vacuum drying operations consist of the following general steps:

- 1) the cask body with the appropriate fuel basket, but without the impact limiters, bottom drain plug, cask lid, and cask shield plug is lowered into the reactor pool and secured in the facility fuel loading station,
- 2) the fuel elements to be transported are placed in the fuel basket within the cask,
- 3) the shield plug is placed into the cask,
- 4) the loaded cask is lifted above the pool while spraying the exposed portions with clean demineralized water,
- 5) the enclosed water is drained from the cask's cavity and the cask is placed in the facility work area. Optionally, the cavity may be drained after securing the cask body in the facility work area. Following draining, the cask cavity is prepared for vacuum drying by flowing pressurized air (or nitrogen) through the cask cavity,
- 6) following the draining and decon operations, the drain port plug and the cask lid are installed. The vent port tool is installed and vacuum drying is initiated.
- 7) the minimum pressure achieved under vacuum drying is 1 to 3 torr.

The transient evaluation of these operations used a modified version of the NCT thermal model described in Appendix 3.5.3, *Analytical Thermal Model*. The modifications made for this evaluation consisted of assuming air as the backfill gas during draining and vacuum drying operations and disconnecting the thermal connections between the cask end surfaces and the impact limiters to simulate a bare cask within the reactor facility. The effect of being submerged in the reactor pool is addressed by assuming all cask components are at equilibrium with a maximum assumed pool water temperature of 80 °F at the start of the cask draining operation.

At time = 0, the loaded cask is assumed to be lifted from the pool, the water drained and the cask cavity filled with air or nitrogen. The transient draining and vacuum drying simulation incorporates several conservative assumptions, including:

- while cask draining will require several hours to complete, this safety evaluation conservatively assumes it is completed instantaneously in order to bound the minimum time required to reach steady-state conditions.
- the analysis conservatively ignores the latent heat cooling associated with the evaporation of the residual water on the surfaces of the fuel, basket, and cask,
- the increased thermal conductivity provided by moist air over the dry air conductivity assumed by the thermal modeling is conservatively ignored,
- the cooling effect created by the optional use of a continuous air or nitrogen gas purge during the draining process is conservatively ignored.

- the ambient conditions in the facility work area are conservatively assumed to be 100 °F without insolation.

The transient analysis is conducted for a period of 8 hours followed by a steady-state evaluation to illustrate the heat up rate and establish the peak temperatures that would occur if the helium backfill is not established. The MURR fuel element payload is selected as a basis for the vacuum drying evaluation since its decay heat loading bounds the other authorized payloads.

The thermal analysis of vacuum drying assumes that the thermal conductivity of the gas filling the voids of the packaging and the payload remain unchanged from its base value at atmospheric pressure conditions for vacuum pressures of 1 torr or greater. There are two states that define the process by which heat is transferred by a gas [32]:

**viscous state**, in which the totality of molecules is responsible for the heat transfer. The viscous state occurs as long as the pressure is higher than the range in which the molecular state occurs. Within the viscous state the thermal conductivity of a gas is independent of pressure.

**molecular state**, heat conductivity in the molecular state is when the gas pressure is so low that the molecular mean free path is about equal or greater than the distance between the plates. The thermal conductivity of the gas is no longer characterized by the viscous state for conductivity and therefore the conductivity is dependent on pressure. The heat transfer process under these conditions is called free molecular conduction.

The pressure at which the molecular mean free path is equal to the minimum distance between the surfaces within the packaging is determined below for air as the fill gas. Per [33], the mean free path of the fill gas molecules is computed via:

$$L = \frac{k \times T}{\pi \times \sqrt{2} \times P \times d^2}$$

where:

$k = 1.380658 \times 10^{-23}$  J/K, the Boltzmann constant

$P$  = pressure in Pa

$T$  = temperature in K

$d$  = molecule diameter, in m

At the lowest practical vacuum pressure of 1 torr (133 Pa) used for vacuum drying and a conservatively high gas temperature of 480 °F (522K) based on the hottest fuel element (as determined from the steady-state analysis), the mean free path for air with a molecule diameter of about  $3 \times 10^{-10}$  m (based on oxygen, [33]) is:

$$L = \frac{1.380658 \times 10^{-23} \times 522}{\pi \times \sqrt{2} \times 133 \times (3 \times 10^{-10})^2}$$

$$L = 1.36 \times 10^{-4} \text{ m} = 0.005 \text{ inches}$$

Since this mean free path is much smaller than the smallest significant gap in the model (i.e., the gap between fuel plates), the gas heat transfer everywhere within the model can be characterized as being in the viscous state and independent of the gas pressure.



Figure 3.3-10 illustrates the predicted package heat up following removal from the fuel pool. The illustrated thermal transient shows that approximately 10 hours is required (based on extrapolation of the transient trend) before the peak fuel plate temperature reaches 400°F. The computed peak fuel plate temperature under steady-state conditions of 480°F will require a total of approximately 17 hours to achieve. Table 3.3-6 provides a listing of the peak temperatures achieved by the cask and payload components for steady-state conditions. Since the peak fuel plate temperature of 480°F is well below the 932°F limit established in Section 3.2.2, *Technical Specifications of Components*, for this condition, indefinite operation under either air (or nitrogen gas) filled conditions or vacuum drying is permissible for in-facility operations.

### 3.3.4 Cask Cavity Backfill with Helium Gas

Once fuel drying is complete, the cask cavity is backfilled with helium to a pressure of slightly greater than atmospheric pressure, i.e., +1, -0 psig. An evaluation of the cool down transient following the helium gas backfill operation was conducted to establish the time required to lower the component temperatures from the peak level under vacuum drying conditions to at or below their associated temperature limits for transport conditions. The transient evaluation uses the same thermal model described above for the cask draining and vacuum drying evaluation. The only exception is that helium gas at one atmosphere is assumed for the gas filling the cask cavity. The initial component temperatures assumed for the start of the helium gas backfill transient are taken from those calculated for steady-state conditions with an air backfill (see Table 3.3-6). The ambient conditions in the facility work area remain the same at 100 °F without insolation. The transient analysis is conducted for a period of 4 hours to illustrate the cool down rate following the introduction of helium gas to the cask cavity.

Figure 3.3-11 illustrates the cool down transient after helium backfill assuming an initial temperature distribution of steady-state operations with an air or nitrogen atmosphere in the cask cavity. As seen from the figure, less than one hour is required to lower the peak fuel plate temperature to below 400°F. Approximately three hours are required to lower the fuel and cask component temperatures to those reported in Section 3.3.1.1, *Maximum Temperatures*, for the *NCT Hot* condition. Given that final leak testing and cask closure will take much longer than three hours, the temperature of the package and payload will be at or near those computed for the *NCT Hot without Solar* condition well before transport begins. Thus, no changes to the thermal or structural analyses for transport are necessary as a result of the elevated fuel cladding temperature potentially achieved under vacuum drying operations.

In conclusion, the results presented above demonstrate that steady-state operations under cask draining and vacuum drying conditions are permissible without exceeding the maximum allowable component temperature limits. The one hour time period following helium gas backfill required to reduce the peak fuel plate temperature below 400°F is so short compared with the time to complete preparation of the cask for transport that no specific tracking of the elapsed time will be required. Once filled with the helium gas, the package temperatures are bounded by those presented in Section 3.3.1.1, *Maximum Temperatures*, for NCT conditions.

**Table 3.3-1 – NCT Temperatures for BRR Packaging with MURR Fuel**

Component	Temperature (°F) <sup>①</sup>		
	NCT Hot <sup>②</sup>	NCT Hot without Solar	Max. Allowable
MURR Fuel Plate	350	331	400
MURR Side Plate	348	329	400
MURR Fuel Basket	334	315	800
Inner Shell	237	216	800
Lead	233	213	620
Outer Shell	216	195	800
Thermal Shield	185	182	800
Lower End Structure	205	184	800
Upper End Structure	220	200	800
Shield Plug	225	205	620 <sup>②</sup>
Cask Lid	216	197	800
Closure/Vent Port Elastomeric Seals	216	197	250
Drain Port Elastomeric Seal	202	181	250
Upper Impact Limiter			
- Max. Foam	215	196	300
- Avg. Foam	146	132	300
- Shell	215	196	250 <sup>③</sup>
Lower Impact Limiter			
- Max. Foam	200	179	300
- Avg. Foam	142	127	300
- Shell	200	179	250 <sup>③</sup>
Max. Accessible Surface	-	185 <sup>④</sup>	185
Cask Cavity Bulk Gas	259	239	N/A

Notes: ① Results assume a payload of eight (8) MURR fuel elements dissipating 158 W each and helium as the backfill gas.

② Temperature criterion based on melting point of the enclosed lead shielding.

③ Temperature criterion based on long term temperature limit for shell coating.

④ Results conservatively based on an earlier design for the cask and impact limiter attachment lugs. See Appendix 3.5.3 for a description of the design change and the conservative impact of ignoring the design change for NCT Hot modeling.

⑤ Maximum temperature occurs at the root of the upper cask impact limiter attachment lugs.

**Table 3.3-2 – NCT Hot Temperatures for BRR Packaging with MITR-II Fuel**

Component <sup>①</sup>	Temperature (°F)	
	8 Elements @ 150 W Each <sup>④</sup>	Max. Allowable
MITR-II Fuel Plate	348	400
MITR-II Side Plate	347	400
MITR-II Fuel Basket	331	800
Inner Shell	237	800
Lead	234	620
Outer Shell	216	800
Thermal Shield	185	800
Lower End Structure	197	800
Upper End Structure	222	800
Shield Plug	230	620 <sup>②</sup>
Cask Lid	218	800
Closure/Vent Port Elastomeric Seals	217	250
Drain Port Elastomeric Seal	194	250
Upper Impact Limiter		
- Max. Foam	217	300
- Avg. Foam	147	300
- Shell	217	250 <sup>③</sup>
Lower Impact Limiter		
- Max. Foam	192	300
- Avg. Foam	140	300
- Shell	192	250 <sup>③</sup>
Cask Cavity Bulk Gas	254	N/A

Notes: ① Results assume a payload of eight (8) MITR-II fuel elements dissipating 150 W each and helium as the backfill gas.

② Temperature criterion based on melting point of the enclosed lead shielding.

③ Temperature criterion based on long term temperature limit for shell coating.

④ Results conservatively based on an earlier design for the cask and impact limiter attachment lugs. See Appendix 3.5.3 for a description of the design change and the conservative impact of ignoring the design change for NCT Hot modeling.

**Table 3.3-3 – NCT Hot Temperatures for BRR Packaging with ATR Fuel**

Component <sup>①</sup>	Temperature (°F)	
	8 Elements @ 30 W Each	Max. Allowable
ATR Fuel Plate	197	400
ATR Side Plate	197	400
ATR Fuel Basket	195	800
Cask Cavity Bulk Gas	164	NA

Note: ① Temperatures for packaging components bounded by values in Table 3.3-1.

**Table 3.3-4 – NCT Hot Temperatures for BRR Packaging with TRIGA Fuel**

Component <sup>①</sup>	Temperature (°F)	
	19 Elements @ 20 W Each	Max. Allowable
TRIGA Fuel Element	355 <sup>②</sup>	400
TRIGA End Fitting	308	400
TRIGA Fuel Basket	287	800
Cask Cavity Bulk Gas	174	NA

Note: ① Temperatures for packaging components bounded by values in Table 3.3-1.

② Maximum TRIGA fuel element temperature bounded by 362 °F as discussed in Section 3.3.1.1, *Maximum Temperature*.

**Table 3.3-5 – Square Fuel Characteristics**

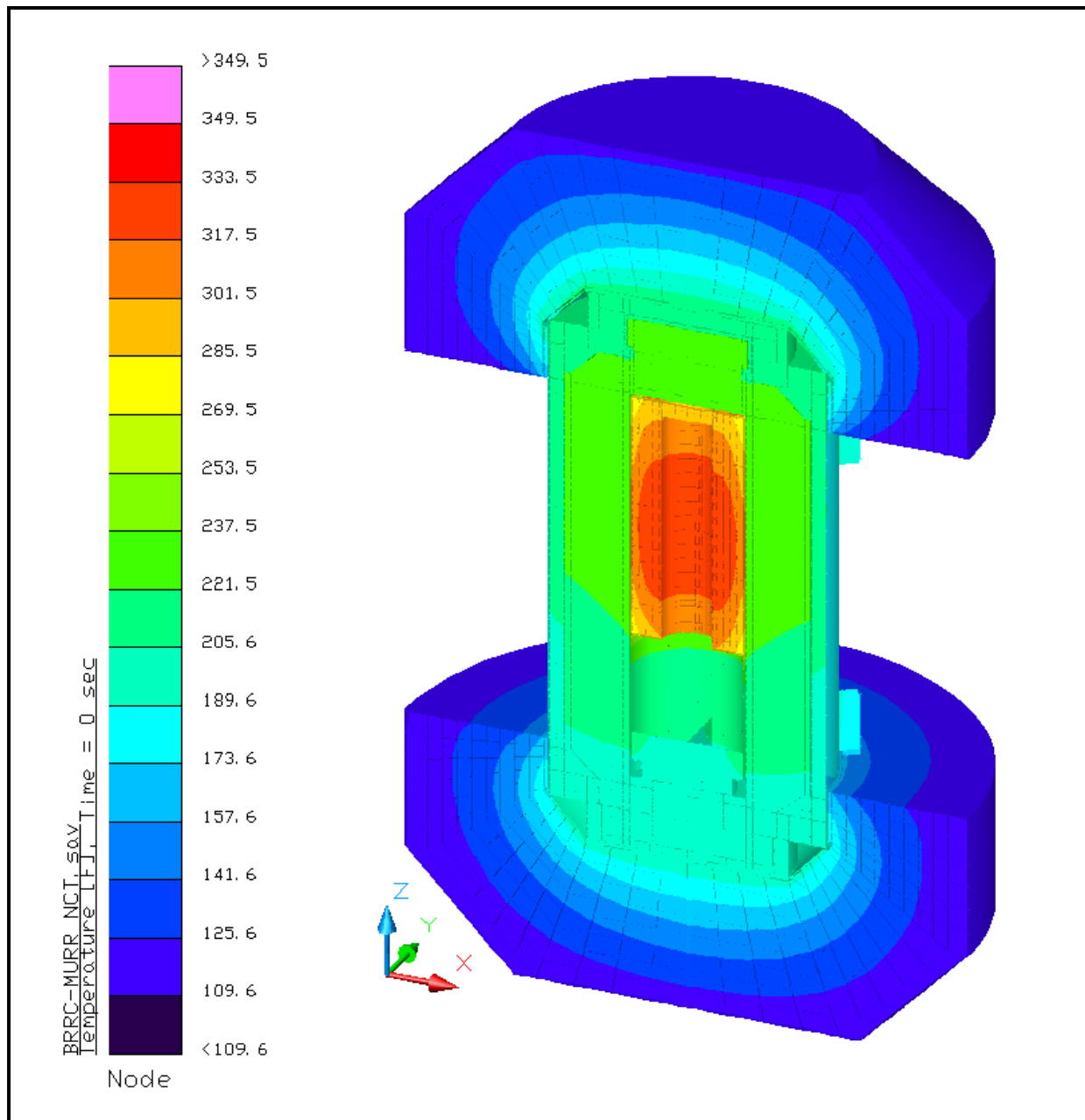
Fuel	Core Material	Cladding Material	Geometry
U-Mass (aluminide)	UAl <sub>x</sub>	Aluminum	18 flat aluminum clad fuel plates, 2 aluminum side plates
Rhode Island	U <sub>3</sub> Si <sub>2</sub>		22 flat aluminum clad fuel plates, 2 aluminum side plates
U-Mass (silicide)			16 flat aluminum clad fuel plates, 2 aluminum side plates
Ohio State			16 flat aluminum clad fuel plates, 2 aluminum side plates
Missouri S&T			18 curved aluminum clad fuel plates, 2 aluminum side plates
U-Florida			14 flat aluminum clad fuel plates with spacer and combs
Purdue	14 flat aluminum clad fuel plates within a grooved aluminum fuel box		
PULSTAR	UO <sub>2</sub>	Zirconium Alloy	Cylindrical fuel pellets contained in 25 fuel rods in a 5 × 5 matrix within a rectangular can

**Table 3.3-6 – Peak Temperatures for Vacuum Drying Operations**

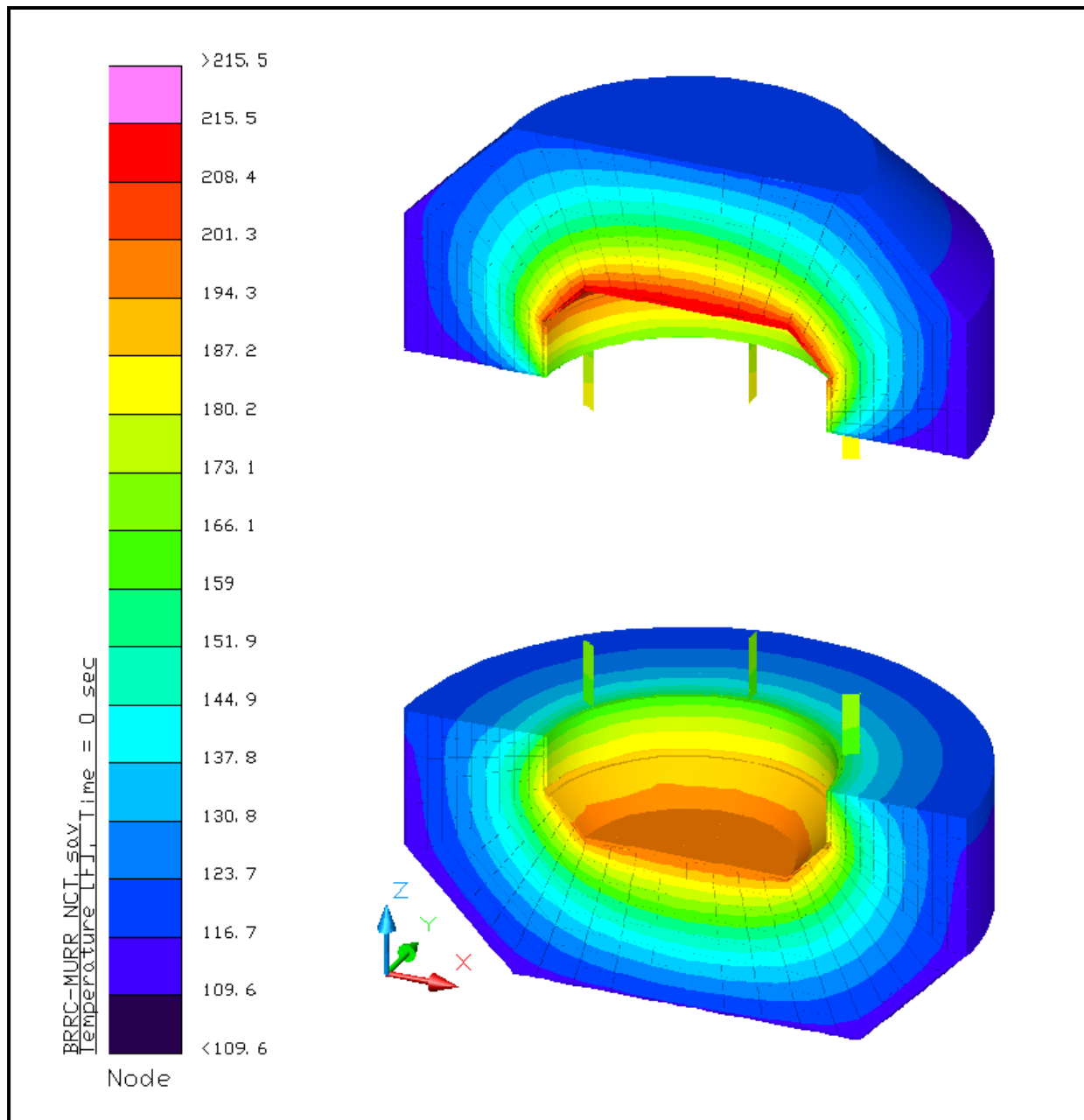
Component	Temperature (°F)	
	Steady-state with Air Filled or Evacuated Cask Cavity <sup>①</sup>	Max. Allowable
MURR Fuel Plate	480	932
MURR Side Plate	477	932
MURR Fuel Basket	431	800
Inner Shell	197	800
Lead	194	620
Outer Shell	178	800
Thermal Shield	167	800
Lower End Structure	177	800
Upper End Structure	174	800
Shield Plug	188	620 <sup>②</sup>
Cask Lid	162	800
Closure/Vent Port Seals	162	250
Drain Port Seal	170	250
Cask Cavity Bulk Gas	326	N/A

Notes: ① Results assume a payload of eight (8) MURR fuel elements dissipating 158 W each and air as the backfill gas.

② Temperature criterion based on melting point of the enclosed lead shielding.



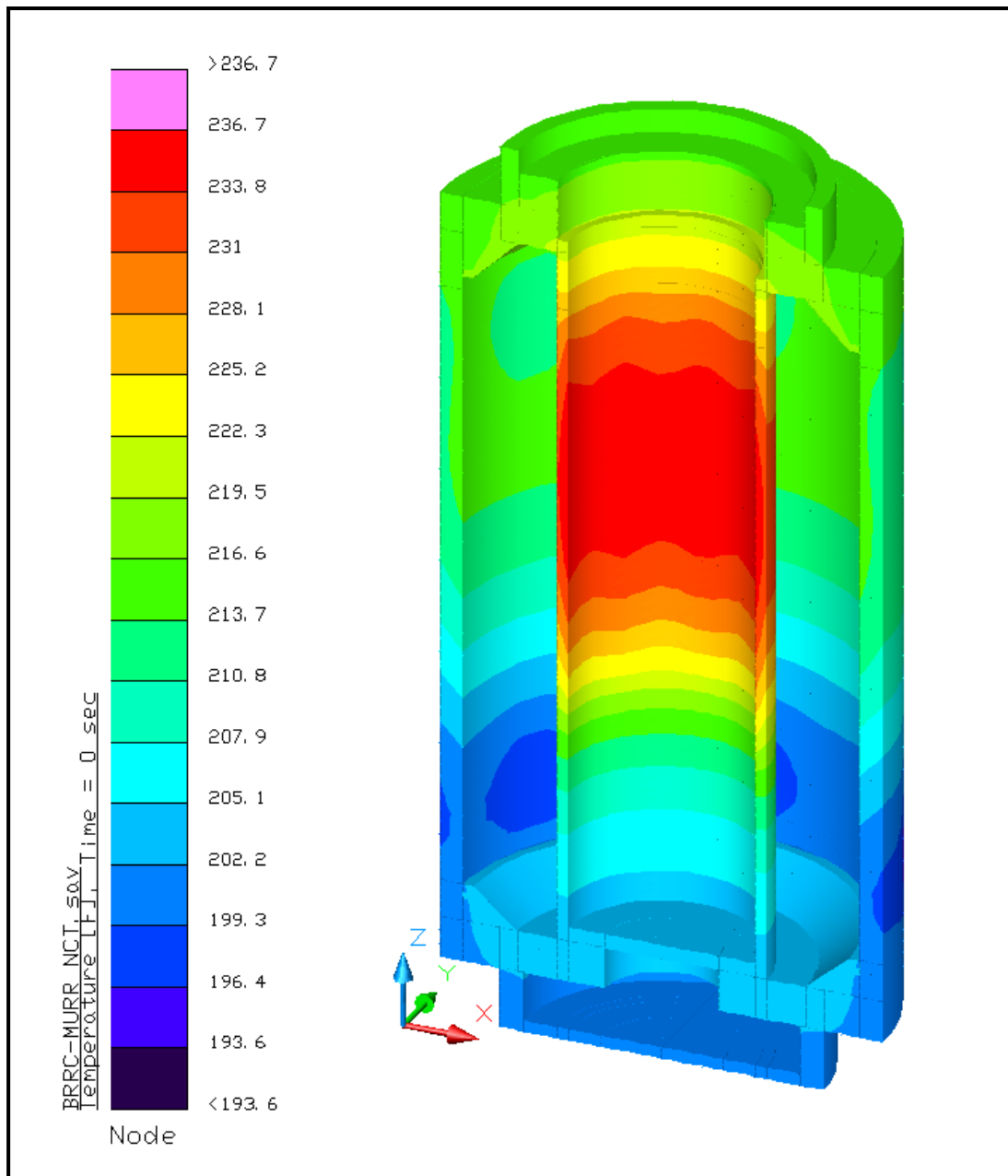
**Figure 3.3-1** – BRR Package Temperature Distribution for NCT Hot Condition with MURR Fuel Basket



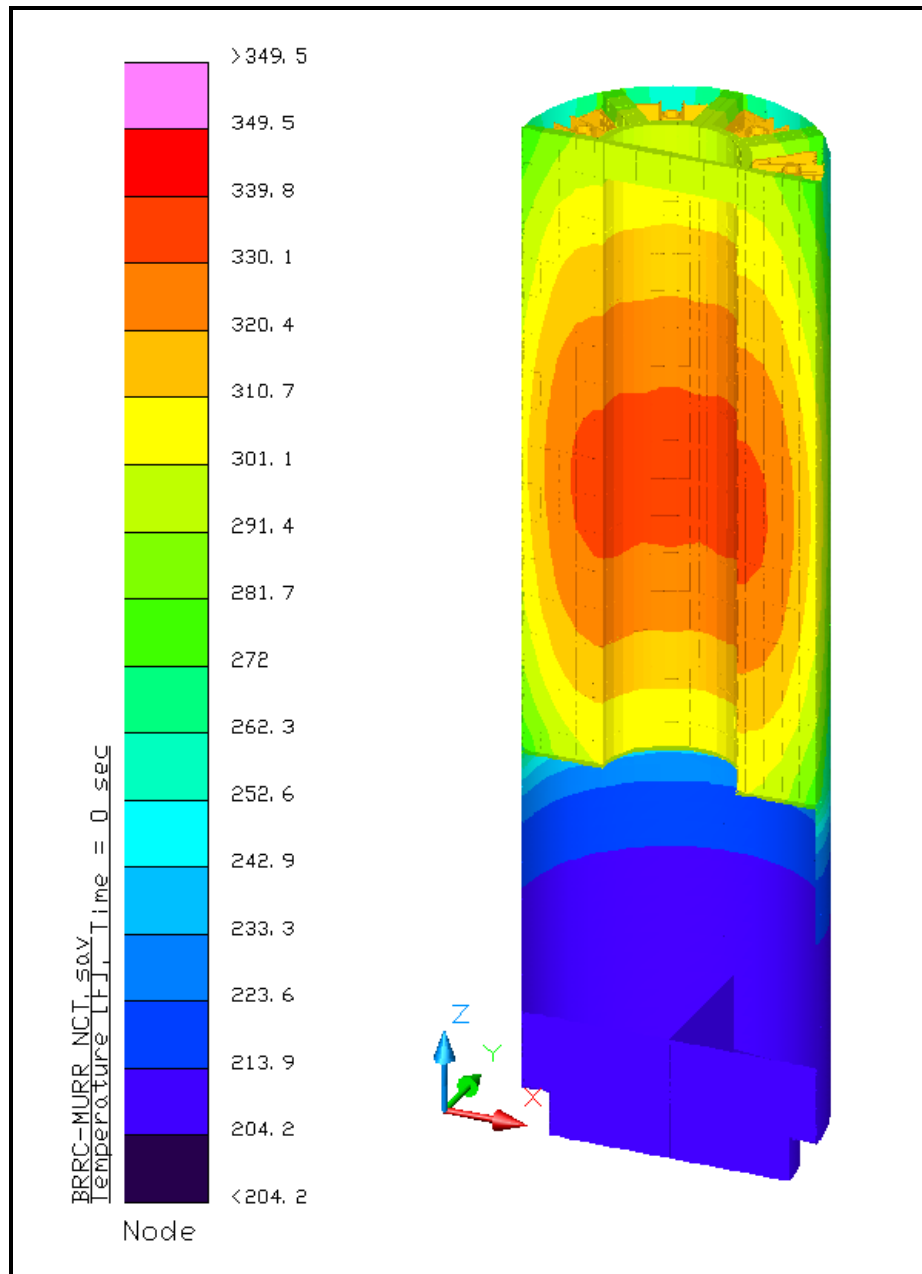
Note: Earlier design of 6 vs. 8 attachment lugs per limiter depicted. Results bound the revised design under NCT

**Figure 3.3-2 – Impact Limiter Temperature Distribution for NCT Hot Condition with MURR Fuel Basket**

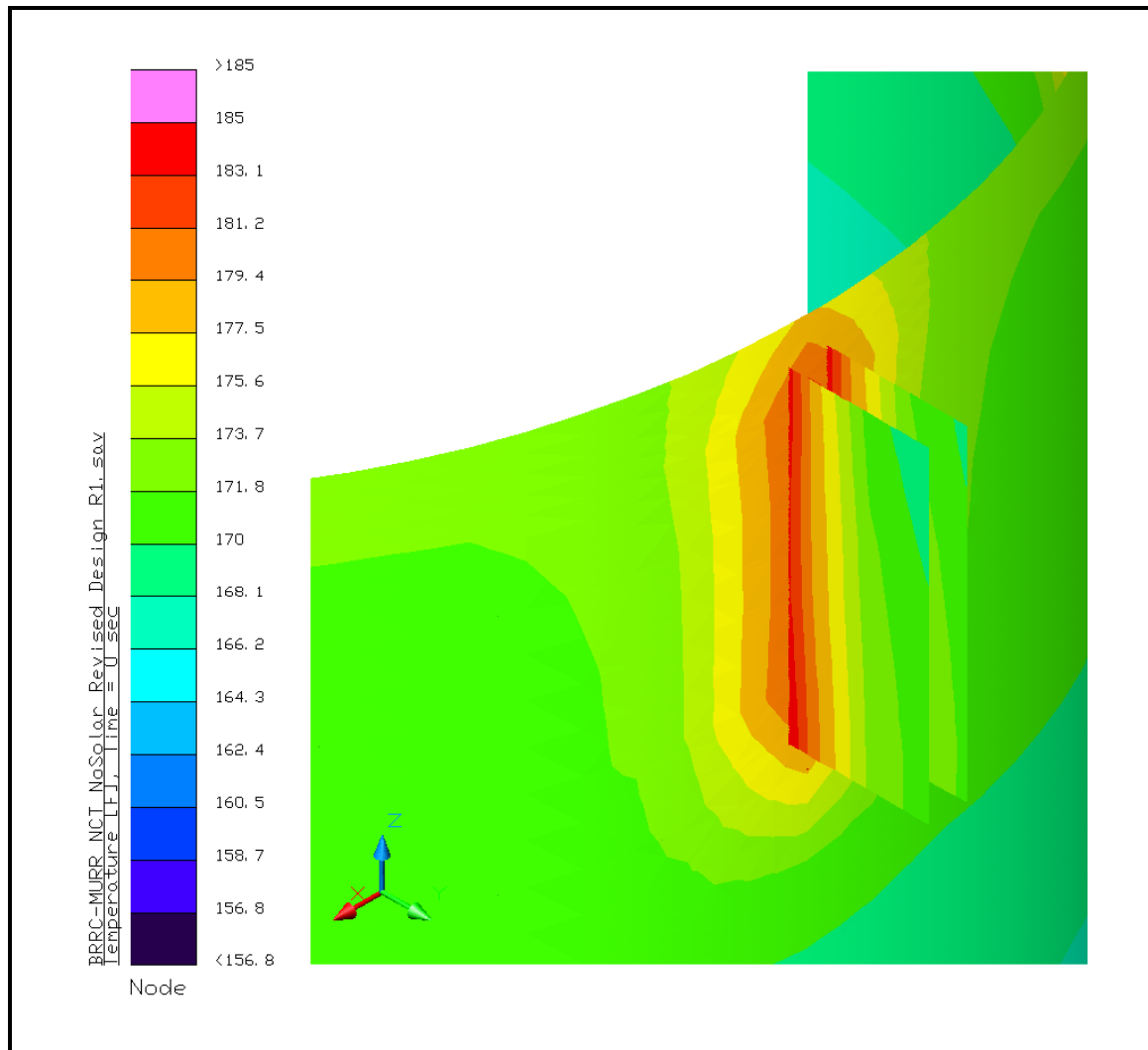




**Figure 3.3-3** – Structural Shell Temperature Distribution for NCT Hot Condition with MURR Fuel Basket

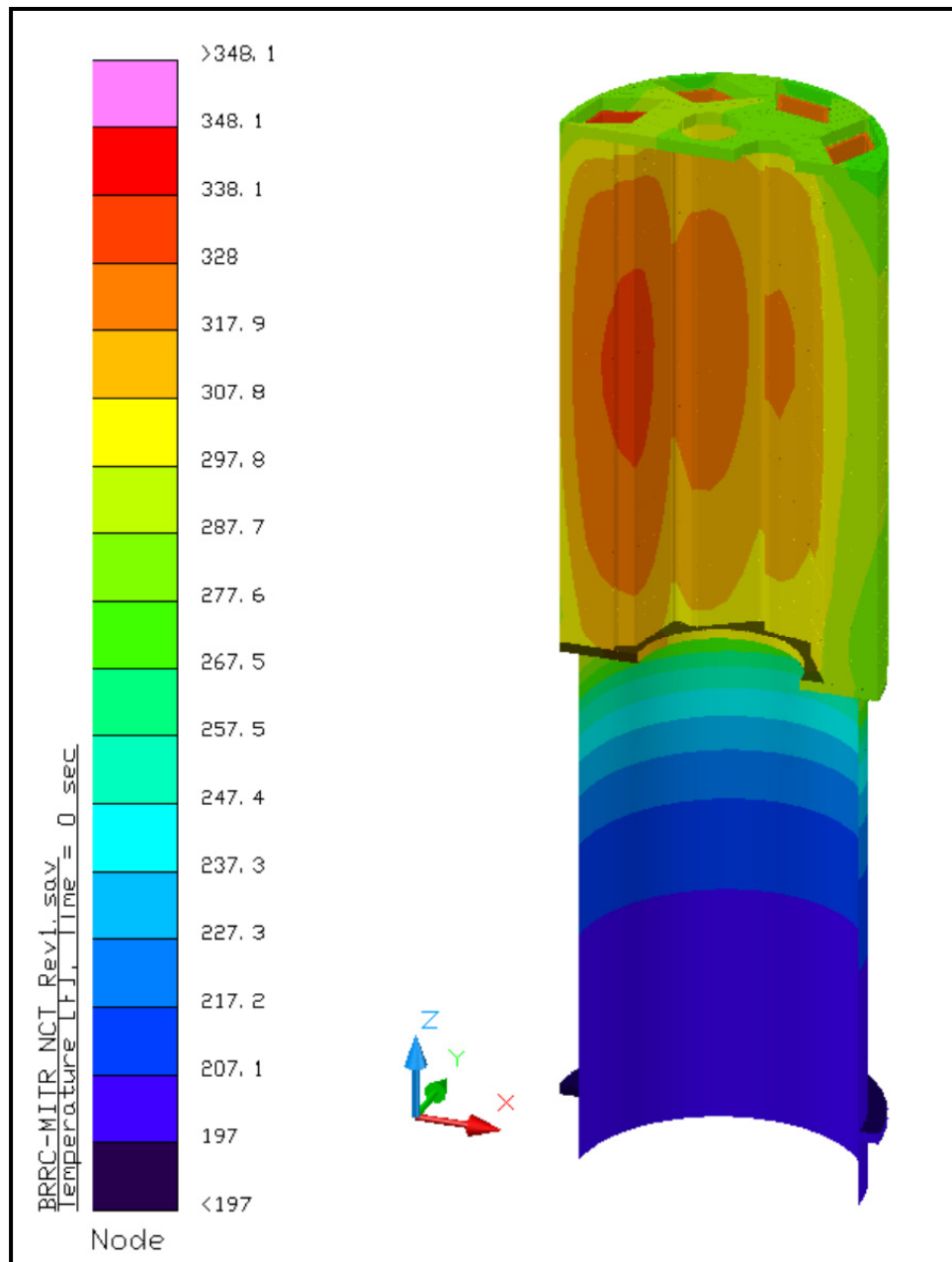


**Figure 3.3-4 – MURR Fuel Basket Temperature Distribution for NCT Hot Condition**



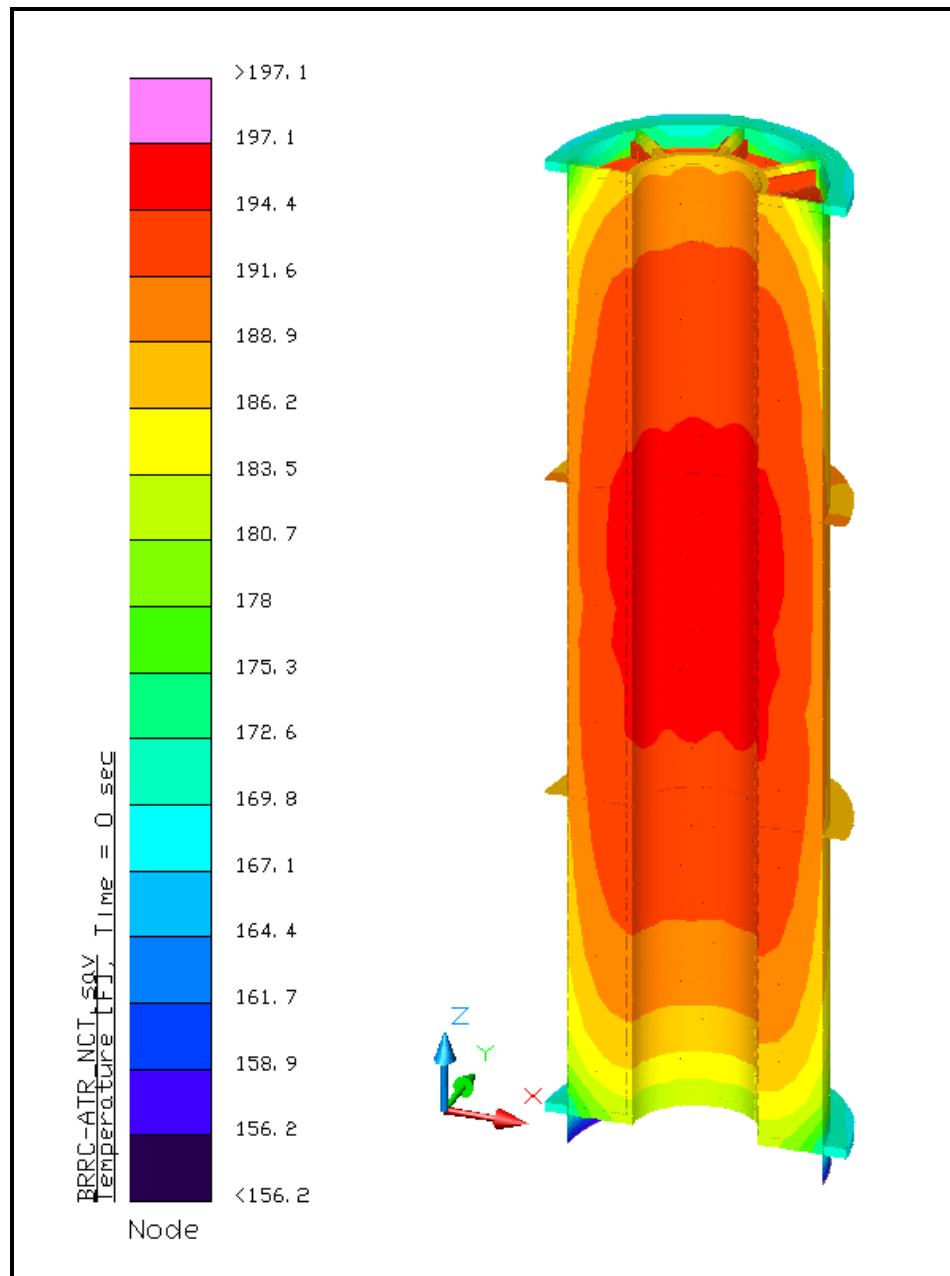
Surface Temperature Distribution in Vicinity of Impact Limiter Attachment Lugs

**Figure 3.3-5** – Peak Accessible Surface Temperature for NCT No Solar



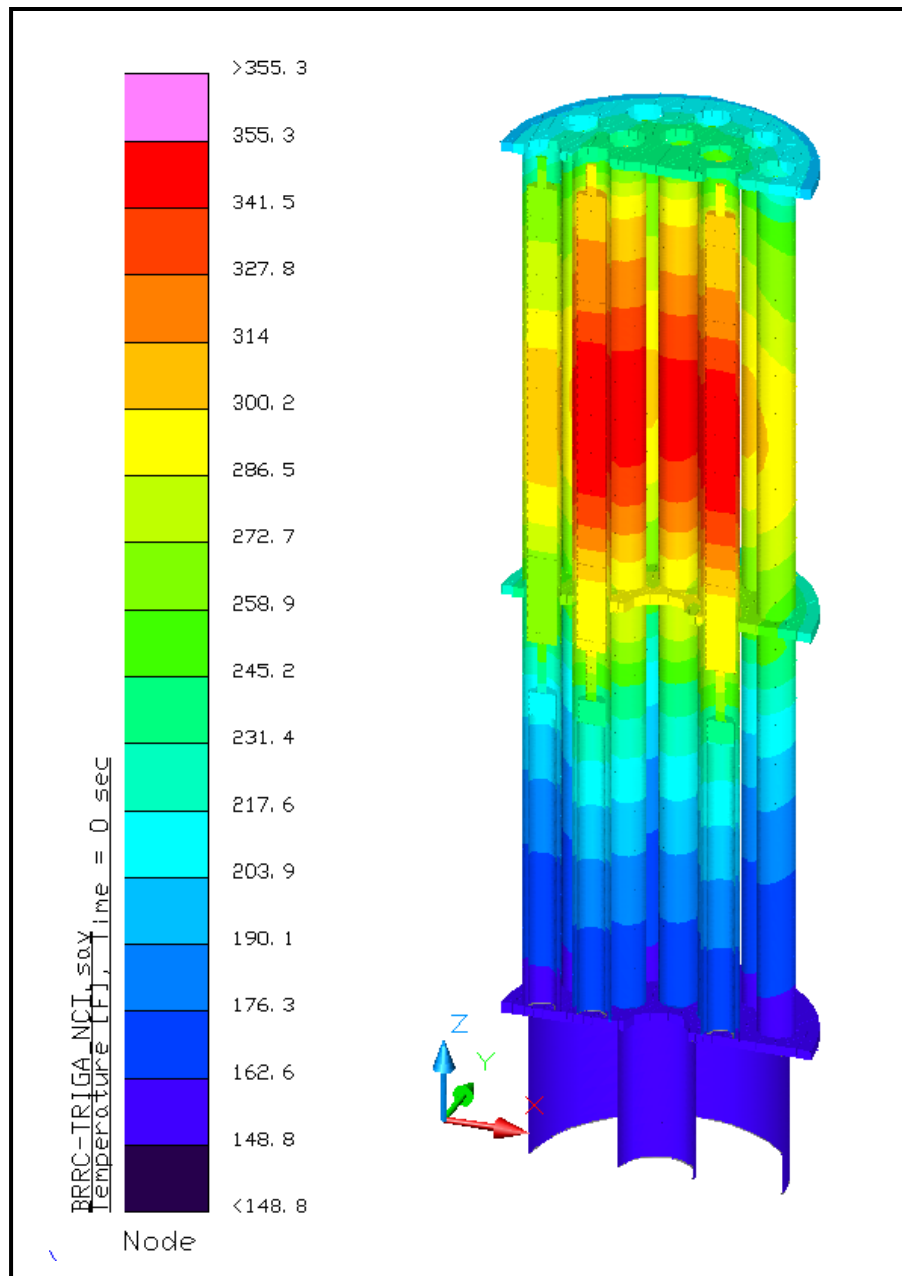
Note: Results are for basket decay heat loading of 1,200 W

**Figure 3.3-6 – MITR-II Fuel Basket Temperature Distribution for NCT Hot Condition**



Note: Results are for basket decay heat loading of 240 W

**Figure 3.3-7 – ATR Fuel Basket Temperature Distribution for NCT Hot Condition**



Note: Results are for basket decay heat loading of 380 W

**Figure 3.3-8 – TRIGA Fuel Basket Temperature Distribution for NCT Hot Condition**

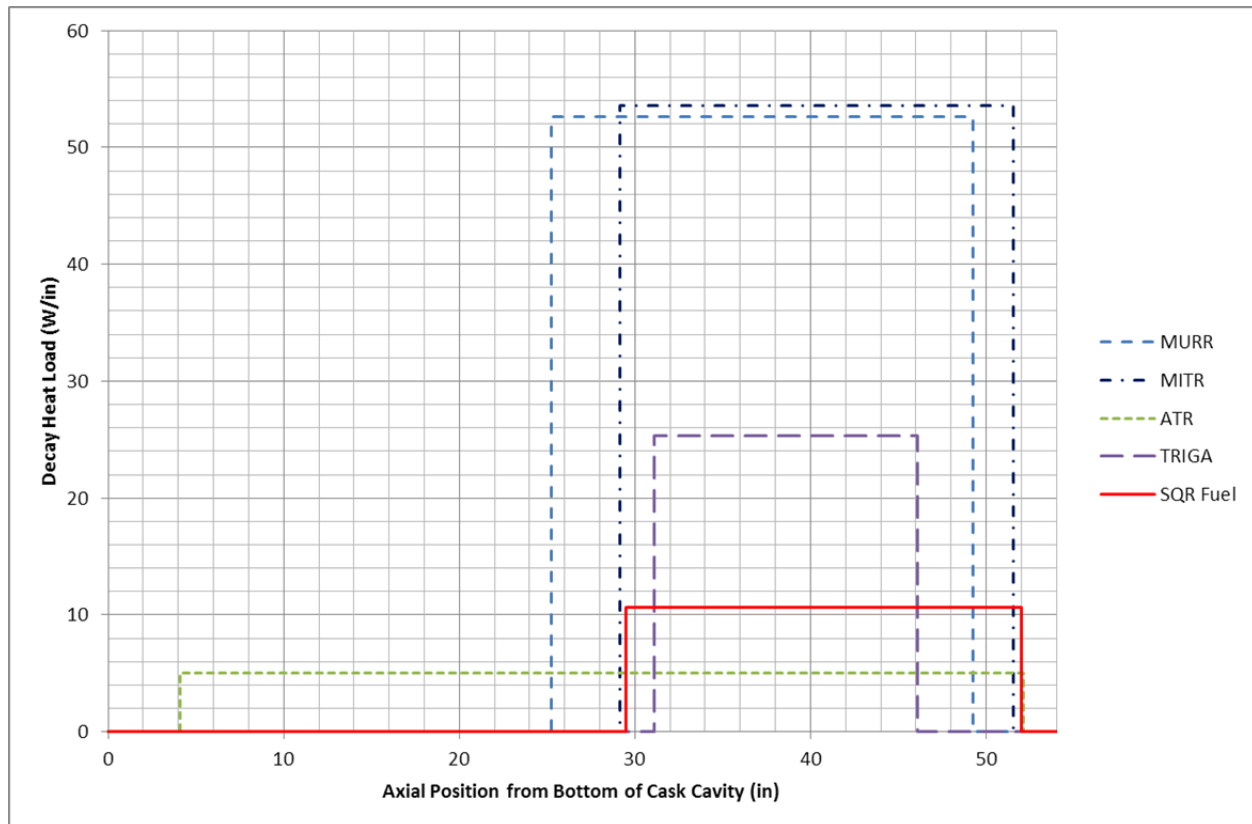


Figure 3.3-9 – Average Heat Load Zone Along Active Fuel Length

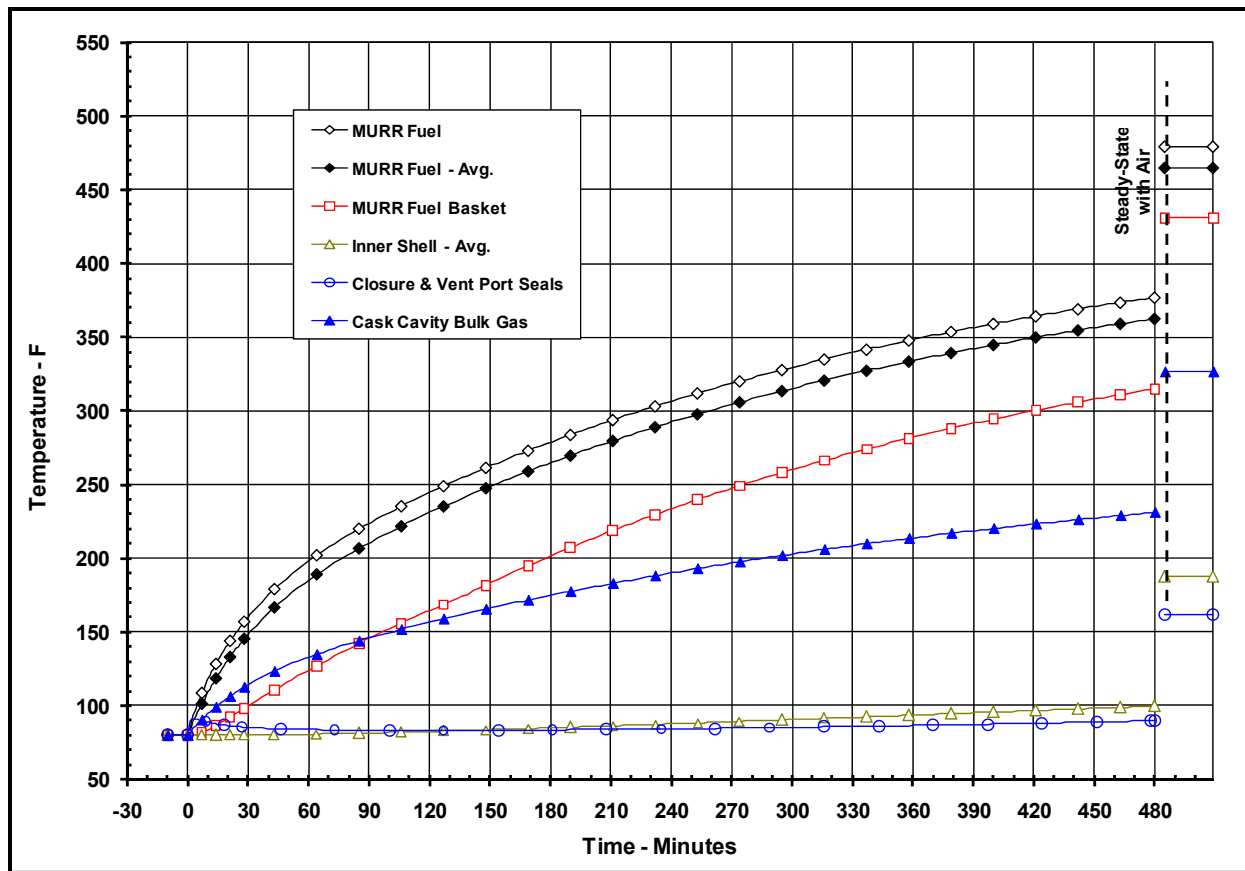
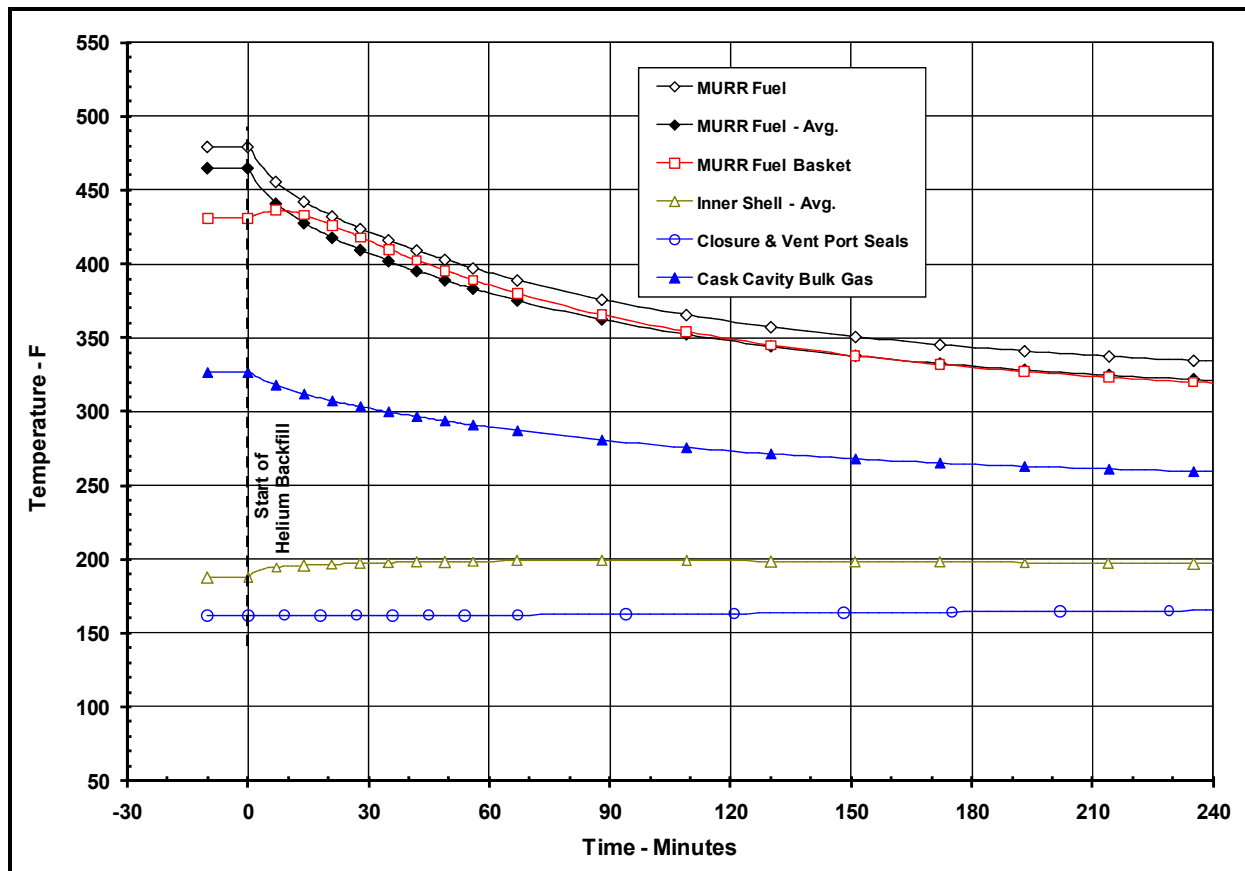


Figure 3.3-10 – Bounding Transient Heat Up During Vacuum Drying





**Figure 3.3-11 – Bounding Transient Cool Down Following Helium Backfill**

### 3.4 Thermal Evaluation for Hypothetical Accident Conditions

This section presents the thermal evaluation of the BRR package under the hypothetical accident condition (HAC) specified in 10 CFR §71.73(c)(4) based on an analytical thermal model of the BRR. The analytical model for HAC is a modified version of the half symmetry NCT model described in Appendix 3.5.3.1, *Description of BRR Packaging Thermal Model for NCT Conditions*, with the MURR fuel element payload. The MURR payload is selected as a basis for the HAC evaluation since its decay heat loading is more than 3 times greater than either the TRIGA, ATR, or Square fuel payloads and since its decay heat loading of 1,264 W exceeds the 1,200 W for the MITR-II fuel payload. As such, the peak HAC temperatures for the TRIGA, ATR, and Square fuel payloads will be bounded by those achieved for the MURR payload, while those for the MITR-II payload will be essentially the same given the similar decay heat loading and the similar initial package temperatures.

The principal model modifications made to convert the NCT thermal model to the HAC model consists of modifying the impact limiter attachment thermal model to reflect the design modifications following the drop testing, simulating the expected package damage resulting from the HAC defined drop events, capturing the thermal decomposition of the polyurethane foam under HAC conditions, changing the package surface emissivities to reflect the assumed presence of soot and/or surface oxidization, assumed contact between the thermal shield and the outer shell and zero lead gap to maximize the heat flow into the package, and changing the package orientation from upright to horizontal to reflect its probable orientation following the HAC drop event.

Physical testing using a half scale certified test unit (CTU) is used to establish the expected level of damage sustained by the BRR package from the 10 CFR 71.73 prescribed free and puncture drops that are assumed to precede the HAC fire event. Appendix 2.12.3, *Certification Test Results*, provides the configuration and initial conditions of the test articles, the test facilities and instrumentation used, and the test results. Appendix 3.5.3.7, *Description of Thermal Model for HAC Conditions*, provides an overview of the test results, the rationale for selecting the worst-case damage scenario, and the details of the thermal modeling used to simulate the package conditions during the HAC fire event.

#### 3.4.1 Initial Conditions

The initial conditions assumed for the package prior to the HAC event are described below in terms of the modifications made to the NCT thermal model to simulate the assumed package conditions prior to and during the HAC event. These modifications are:

- Simulated the worst-case damage arising from the postulated HAC free and puncture drops as described in Appendix 3.5.3.7, *Description of Thermal Model for HAC Conditions*,
- Changed the package orientation from upright to horizontal to reflect the assumed position of the package following an HAC accident event,
- Increased the emissivity of all external surfaces to 0.9 and the solar absorptivity to 0.9 to account for possible oxidation and/or soot accumulation on the surfaces,
- Increased the emissivity of the interior surface of the thermal shield from 0.4 to 0.6 to account for oxidization during the HAC event,

- Added heat transfer via radiation within the impact limiter enclosures with an emissivity of 0.95 to account for the potential loss of polyurethane foam from thermal decomposition,
- Assumed an initial temperature distribution equivalent to the package at steady-state conditions with a 100 °F ambient and no insolation. This assumption complies with the requirement of 10 CFR §71.73(b).

Following the free and puncture bar drop events, the BRR package is assumed come to rest in a horizontal position prior to the initiation of the fire event. The MURR basket and the fuel element are predicted to remain intact and experience no significant re-positioning as a result of the drop events. Since the package geometry is essentially axi-symmetrical, the thermal performance under HAC conditions is independent of the rotational orientation of the package.

### 3.4.2 Fire Test Conditions

The fire test conditions analyzed to address the 10 CFR §71.73(c) requirements are as follows:

- The initial ambient conditions are assumed to be 100 °F ambient with no insolation,
- At time = 0, a fully engulfing fire environment consisting of a 1,475 °F ambient with an effective emissivity of 1.0 is used to simulate the average flame temperature of the hydrocarbon fuel/air fire event. The assumption of an average flame emissivity coefficient of 1.0 conservatively bounds the minimum 0.9 flame emissivity specified by 10 CFR Part §71.73(c)(4).
- The convection heat transfer coefficients between the package and the ambient during the 30-minute fire event are based on an average gas velocity of 10 m/sec [29]. Following the 30-minute fire event the convection coefficients are based on still air.
- The ambient condition of 100 °F with insolation is assumed following the 30-minute fire event. A solar absorptivity of 0.9 is assumed for the exterior surfaces to account for potential soot accumulation on the package surfaces.

The transient analysis is continued for 4.5 hours after the end of the 30-minute fire to capture the peak package temperatures.

### 3.4.3 Maximum Temperatures and Pressure

#### 3.4.3.1 Maximum HAC Temperatures

Table 3.4-1 presents the predicted peak temperature for the BRR package with the MURR fuel payload under HAC conditions. As seen from the table, significant thermal margins exist for all components. The closure and vent/drain port seals remain below their maximum allowable temperature due to a combination of their location, the amount of foam remaining, even after the conservative damage assumptions, and the surrounding thermal mass of the upper and lower end structures. For example, the peak temperature predicted for the vent/drain port seals arises for the improbable condition of the worst case damage described in Appendix 3.5.3.7, *Description of Thermal Model for HAC Conditions*, for the impact limiter aligning directly opposite of the drain port location. Without that conservative assumption, the peak vent/drain port temperature would be approximately 300 °F.

Figure 3.4-1 illustrates the temperature profile within the BRR package at the end of the 30-minute hypothetical fire. The illustrated profile demonstrates the thermal protection afforded to the package by the thermal shield and the polyurethane filled impact limiters since the high temperatures are limited to narrow regions on the exterior of the packaging. This thermal protection occurs despite the conservative level of damage assumed for the impact limiters.

Figure 3.4-2 and Figure 3.4-3 illustrate the temperature response profiles for selected package components. The relatively low temperature rise seen for the fuel elements and the fuel basket over the HAC event further demonstrates the thermal protection afforded by the BRR package design.

### 3.4.3.2 Maximum HAC Pressures

The peak cask cavity pressure under HAC conditions is conservatively estimated in the same manner as for NCT conditions (i.e., the bulk average cavity gas temperature is assumed to be equal to the mean of the average inner shell temperature and the average fuel basket temperature). The potential pressurization of the cask cavity due to failed cladding on the uranium-aluminide and uranium-zirconium hydride based fuel elements is ignored for this safety evaluation since the release of fission generated gases from these fuel types is diffusion-limited as opposed to the direct release mechanism for commercial spent nuclear fuel. At the conditions seen within the BRR package, the pressurization of the cask cavity due to gaseous release from breached fuel elements will be insignificant [30, 31] and is ignored for this safety evaluation.

Under the HAC condition with the MURR fuel payload, the peak bulk average gas temperature achieved during the HAC transient is 388 °F. Based on an assumed backfill gas temperature of 70 °F, the predicted maximum pressure within the cask cavity is computed via:

$$\text{Cavity Pressure} = 14.7 \text{ psia} \frac{(388^\circ \text{F} + 460^\circ \text{F})}{(70^\circ \text{F} + 460^\circ \text{F})} - 14.7 \text{ psia}$$

$$\text{Cavity Pressure} = 8.8 \text{ psig}$$

Given the significantly greater decay heat of the MURR fuel element payload, the computed peak HAC pressure will bound those achieved for the ATR and TRIGA baskets. The peak HAC pressure reached with the MITR-II payload will be slightly lower given the slightly lower decay heat loading and the similar pre-fire package starting temperatures. As calculated in Section 3.3.2, *Maximum Normal Operating Pressure*, the maximum potential pressure increase under HAC due the release of fission gases from the PULSTAR fuel is 2.9 psig. Thus, the maximum HAC pressure is  $8.8 + 2.9 = 11.7$  psig.

### 3.4.4 Maximum Thermal Stresses

The maximum thermal stresses under the HAC condition are addressed in Section 2.7.4, *Thermal*.

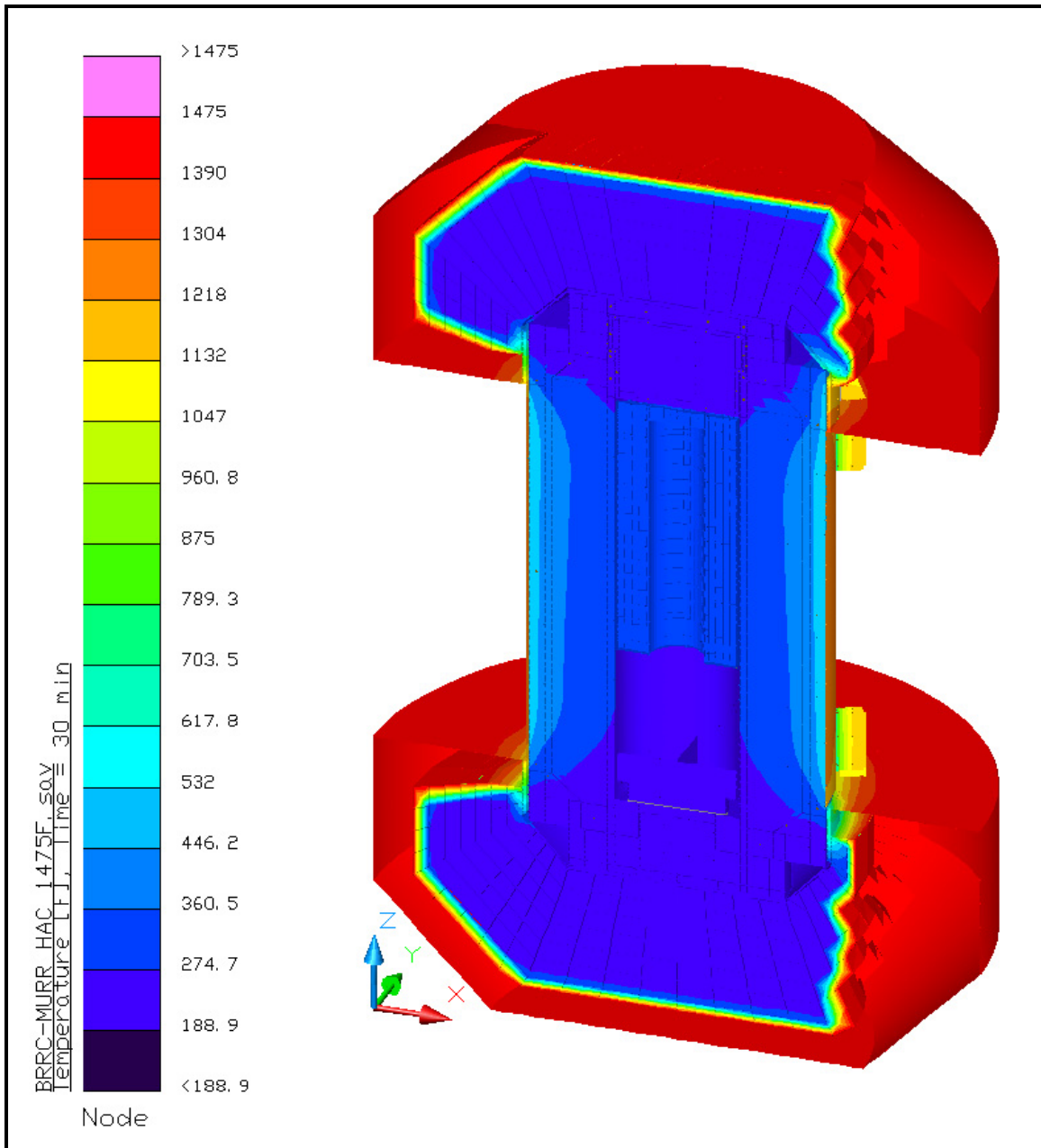
**Table 3.4-1 – HAC Temperatures**

Component	Temperature (°F) <sup>①</sup>			
	End of Fire	Peak	Post-fire Steady State	Max. Allowable
MURR Fuel Plate	344	451	326	1,100
MURR Side Plate	341	449	324	1,100
MURR Fuel Basket	326	437	310	800
Inner Shell	301	393	211	800
Lead	471	482	207	620
Outer Shell	704	704	200	2,700
Thermal Shield	1,256	1,256	180	2,700
Lower End Structure	318	335	182	800
Upper End Structure	485	485	198	800
Shield Plug	234	317	201	620 <sup>②</sup>
Cask Lid	215	306	196	800
Closure/Vent Port Elastomeric Seals	212	306	196	400
Drain Port Elastomeric Seal	365	373	195	400
Upper Impact Limiter				
- Max. Foam	-	-	-	N/A <sup>③</sup>
- Avg. Foam	-	-	-	N/A <sup>③</sup>
- Shell	1,475	1,475	195	2,700 <sup>③</sup>
Lower Impact Limiter				
- Max. Foam	-	-	-	N/A <sup>③</sup>
- Avg. Foam	-	-	-	N/A <sup>③</sup>
- Shell	1,475	1,475	190	2,700 <sup>③</sup>
Cask Cavity Bulk Gas	305	388	257	N/A

Notes: ① Results assume a payload of eight (8) MURR fuel elements dissipating 158 W each and helium as the backfill gas.

② Temperature criterion based on melting point of the enclosed lead shielding.

③ Temperature criterion based on melting point for the shell. No criteria for the polyurethane foam since its thermal decomposition serves as its principal means of providing thermal protection during the HAC event.



**Figure 3.4-1** – BRR Package HAC Temperature Distribution at End of 30 Minute Fire

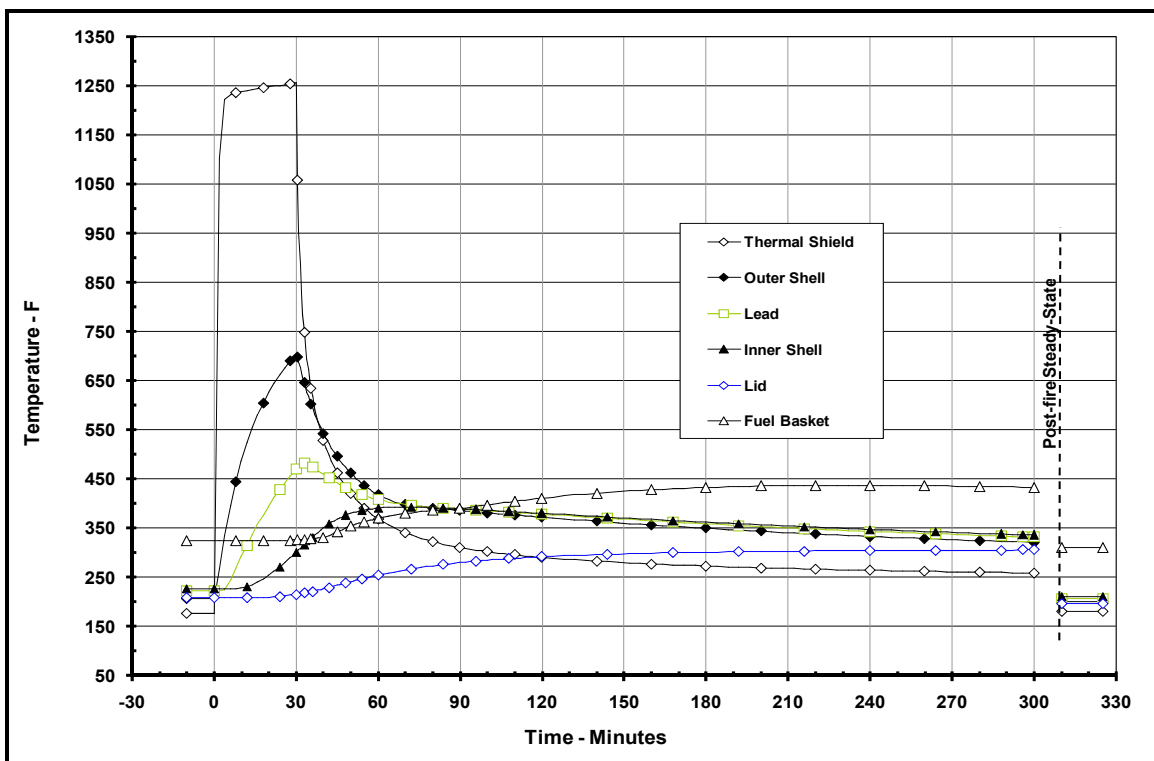


Figure 3.4-2 –Thermal Response to HAC Event, Package Components

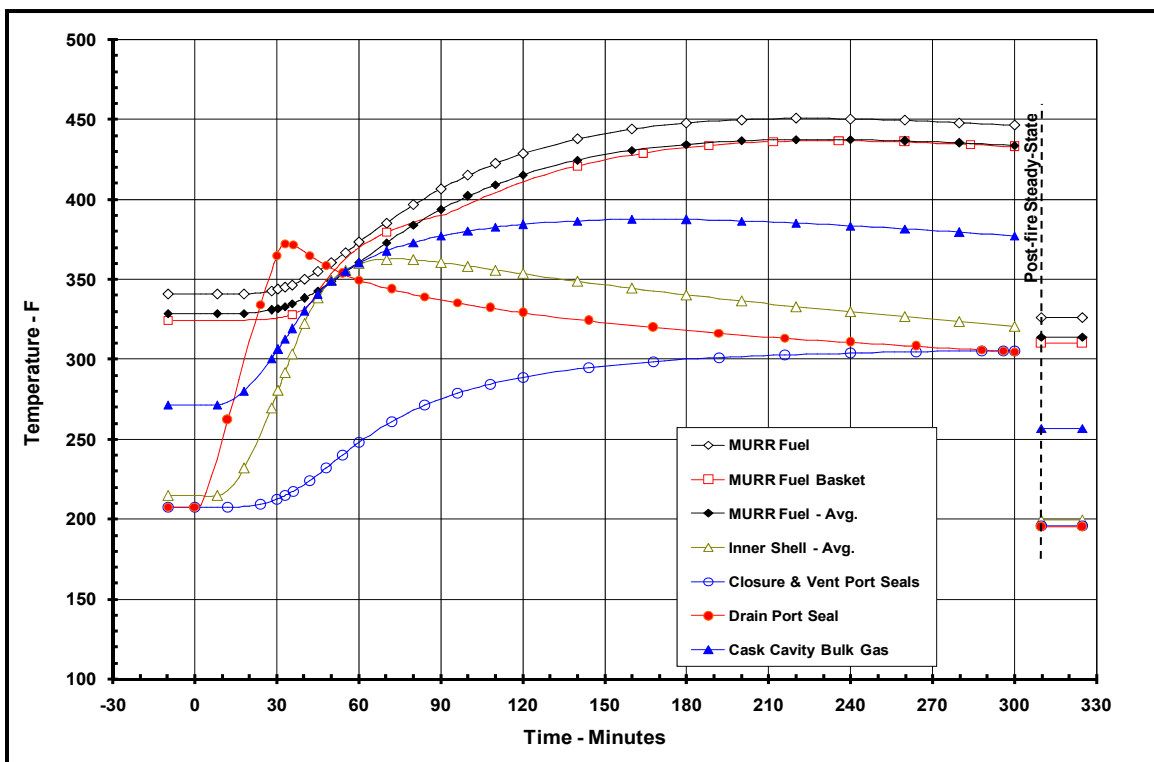


Figure 3.4-3 – Thermal Response to HAC Event, Payload, Seals, and Bulk Gas

## **3.5 Appendices**

- 3.5.1 References
- 3.5.2 Computer Analysis Results
- 3.5.3 Analytical Thermal Model
- 3.5.4 ‘Last-A-Foam’ Response under HAC Conditions



### 3.5.1 References

1. Title 10, Code of Federal Regulations, Part 71 (10 CFR 71), *Packaging and Transportation of Radioactive Materials*, United States Nuclear Regulatory Commission (USNRC), 01-01-08 Edition.
2. American Society of Mechanical Engineers (ASME) Boiler and Pressure Vessel (B&PV) Code, Section II, Part D, 2007.
3. American Society of Mechanical Engineers (ASME) Boiler & Pressure Vessel Code, Section III, Rules for Construction of Nuclear Facility Components, Division 1, Subsection NB, Class 1 Components, & Subsection NG, Core Support Structures, 2007 Edition.
4. Y.S. Touloukian, *Thermophysical Properties of Matter*, the TPRC Data Series, Plenum Publishing Corp., New York, NY, 1970.
5. Polkinghorne, S. and Lacy, J., *Thermophysical And Mechanical Properties Of ATR Core Materials*, Report No. PG-T-91-031, August 1991, EG&G Idaho, Inc.
6. Matweb, Online Material Data Sheets, [www.matweb.com](http://www.matweb.com).
7. Frank, R., and Plagemann, W., *Emissivity Testing of Metal Specimens*, Boeing Analytical Engineering coordination sheet No. 2-3623-2-RF-C86-349, August 21, 1986. Testing accomplished in support of the TRUPACT-II design program.
8. Azzazy, M., *Emissivity Measurements of 304 Stainless Steel*, prepared for Southern California Edison, September 6, 2000, Transnuclear File No. SCE-01.0100.
9. Gubareff, G., Janssen, J., and Torborg, R., *Thermal Radiation Properties Survey*, 2nd Edition, Honeywell Research Center, 1960.
10. Gustavsen, Arild, *Heat Transfer in Window Frames with Internal Cavities*, PhD Thesis, Norwegian University of Science and Technology, Trondheim, Norway, September 2001.
11. Series 66 and 73 Product Data Sheets, Tnemec Company, Inc. 6800 Corporate Drive Kansas City, MO, [www.tnemec.com](http://www.tnemec.com).
12. MURR Fuel Drawings, EG&G Drawings No. 409406 and 409407.
13. MITR-II Fuel Drawings, EG&G Drawings No. 410368, 410369, and 419486.
14. ATR Mark VII Fuel Element Assembly, INEEL Drawing No. DWG-405400.
15. TRIGA Fuel Element Description, University of Utah Class Notes, Nuclear Engineering, CVEEN 5700/6700.
16. *KK-8 Graphite High Temperature Thermal Characteristics with Supporting Data*, letter from Harold E. Cook (Carbon/Graphite Group, Inc.) to Corwin Robinson (EG&G Mound Applied Technologies), dated March 13, 1992.
17. Greenspan, E., *Hydride Fuel for Improving the Design and Performance of LWRs*, Presentation to 233<sup>rd</sup> ACS National Meeting, Chicago, IL, 2007.
18. Last-A-Foam™ On-line Data Sheet, [www.generalplastics.com](http://www.generalplastics.com).
19. Rohsenow, Hartnett, and Choi, *Handbook of Heat Transfer*, 3rd edition, McGraw-Hill, 1998.

20. Rainier Rubber Company, Seattle, WA, [www.rainierrubber.com](http://www.rainierrubber.com).
21. *Parker O-Ring Material Offering Guide*, ORD 5712, August 2002, [www.parkerorings.com](http://www.parkerorings.com).
22. Thermal Desktop<sup>®</sup>, Version 5.1 and 5.3, Cullimore & Ring Technologies, Inc., Littleton, CO, 2007 and 2010.
23. SINDA/FLUINT, *Systems Improved Numerical Differencing Analyzer and Fluid Integrator*, Version 5.1 and 5.3, Cullimore & Ring Technologies, Inc., Littleton, CO, 2007 and 2010.
24. AFS Report TR-VV-06-001, Rev. 0, *Thermal Desktop<sup>®</sup> and SINDA/FLUINT Testing and Acceptance Report*, Version 5.1, AREVA Federal Services, LLC, 2008.
25. Kreith, Frank, *Principles of Heat Transfer*, 3rd edition, Harper & Row, 1973.
26. Guyer, Eric, *Handbook of Applied Thermal Design*, McGraw-Hill, Inc., 1989.
27. Williamson, C., and Iams, Z., *Thermal Assault and Polyurethane Foam - Evaluating Protective Mechanisms for Transport Containers*, General Plastics Manufacturing Company, Tacoma, WA, Waste Management '05 Symposium, Tucson, AZ, 2005.
28. Williamson, C., and Iams, Z., *Thermal Assault and Polyurethane Foam - Evaluating Protective Mechanisms*, General Plastics Manufacturing Company, Tacoma, WA, presented at PATRAM International Symposium, Berlin, Germany, 2004.
29. Schneider, M.E and Kent, L.A., *Measurements of Gas Velocities and Temperatures in a Large Open Pool Fire*, Heat and Mass Transfer in Fire - HTD Vol. 73, 1987, ASME, New York, NY.
30. Vinson, D., Sindelar, R., and Iyer, N., *Containment Evaluation of Breached AL-SNF For Cask Transport*, Savannah River National Laboratory - Materials Science & Technology, Aiken, SC 29808.
31. Whittemore, W. L., *Higher Power Density TRIGA<sup>®</sup> Research Reactors*, General Atomics, Sand Diego, CA.
32. Roth A, *Vacuum Technology*, 2nd Edition, Elsevier Science, 1982.
33. Lide, D., *Handbook of Chemistry and Physics*, 83rd Edition, The Chemical Rubber Co., 2002-2003.
34. NUREG-1537, Part 1, *Guidelines for Preparing and Reviewing Applications for the Licensing of Non-Power Reactors*, Office of Nuclear Reactor Regulation, U.S. Nuclear Regulatory Commission, Washington, DC 20555-0001, February 1996.
35. NUREG-1313, *Safety Evaluation Report related to the Evaluation of Low-Enriched Uranium Silicide-Aluminum Dispersion Fuel for Use in Non-Power Reactors*, Office of Nuclear Reactor Regulation, U.S. Nuclear Regulatory Commission, Washington, DC 20555-0001, July 1988.
36. AFS Report AFS-TR-VV-013, Rev. 0, *Thermal Desktop<sup>®</sup> and SINDA/FLUINT Testing and Acceptance Report*, Version 5.3, AREVA Federal Services, LLC, 2010.
37. Williams, R.K. et al, *Thermal Conductivities of U<sub>3</sub>Si and U<sub>3</sub>Si<sub>2</sub>-Al Dispersion Fuels*, U.S. Department of Energy, December 1986.

38. NUREG/CR-0497, *MATPRO-Version 11: A Handbook of Materials Properties for Use in the Analysis of Light Water Reactor Fuel Rod Behavior*, EG&G, Inc. February, 1979.
39. U.S. Nuclear Regulatory Commission, NUREG-1617, *Standard Review Plan for Transportation Packages for Spent Nuclear Fuel*, Final Report, January 2000.

### **3.5.2 Computer Analysis Results**

Due to the size and number of the output files associated with each analyzed condition, results from the computer analysis are provided on a CD-ROM.

### **3.5.3 Analytical Thermal Model**

The analytical thermal model of the BRR package was developed for use with the Thermal Desktop<sup>®</sup> [22] and SINDA/FLUINT [23] computer programs. These programs are designed to function together to build, exercise, and post-process a thermal model. The Thermal Desktop<sup>®</sup> computer program is used to provide graphical input and output display function, as well as computing the radiation exchange conductors for the defined geometry and optical properties. Thermal Desktop<sup>®</sup> is designed to run as an AutoCAD<sup>®</sup> application. As such, all of the CAD tools available for generating geometry within AutoCAD<sup>®</sup> can be used for generating a thermal model. In addition, the use of the AutoCAD<sup>®</sup> layers tool presents a convenient means of segregating the thermal model into its various elements.

The SINDA/FLUINT computer program is a general purpose code that handles problems defined in finite difference (i.e., lumped parameter) and/or finite element terms and can be used to compute the steady-state and transient behavior of the modeled system. Although the code can be used to solve any physical problem governed by diffusion-type equations, specialized functions used to address the physics of heat transfer and fluid flow make the code primarily a thermal code.

The SINDA/FLUINT and Thermal Desktop<sup>®</sup> computer programs have been validated for safety basis evaluations for nuclear related projects [24, 36].

Together, the Thermal Desktop<sup>®</sup> and SINDA/FLUINT codes provide the capability to simulate steady-state and transient temperatures using temperature dependent material properties and heat transfer via conduction, convection, and radiation. Complex algorithms may be programmed into the solution process for the purposes of computing heat transfer coefficients as a function of the local geometry, gas thermal properties as a function of species content, temperature, and pressure, or, for example, to estimate the effects of buoyancy driven heat transfer as a function of density differences and flow geometry.

#### **3.5.3.1 Description of BRR Packaging Thermal Model for NCT Conditions**

The BRR packaging is represented by a 3-dimensional, half symmetry thermal model for the NCT evaluations. This modeling choice captures the full height of the packaging components and allows the incorporation of the varying insolation loads that will occur along the length of the package, the various degrees of symmetry within the fuel baskets, and the non-symmetry of the HAC free drop damage. The various packaging components are defined using a combination of planar and solid elements. Program features within the Thermal Desktop<sup>®</sup> computer program automatically compute the various areas, lengths, thermal conductors, and view factors involved in determining the individual elements that make up the thermal model of the complete assembly.

It should be noted that the NCT thermal model described below is based on an earlier design that used 6 instead of the current 8 attachment lugs per limiter, lug plates that are 0.38-inches thick

by 2.75-inches wide vs. the current 0.5-inches thick by 3.63-inches wide, and a 0.25-inch vs. 0.125-inch radial gap between the limiter and the cask shell. Since these variations from the current design result in a lower surface area for heat dissipation to the ambient, the predicted NCT temperatures will be slightly higher than those expected for the current design. Because of this conservatism, the results are valid for the safety evaluations under NCT conditions. The design variations are incorporated for the HAC evaluations.

Figure 3.5-1 to Figure 3.5-5 illustrates ‘solid’ views of the BRR packaging thermal model. The model is composed of solid and plate type elements representing the various packaging components. Thermal communication between the various components is via conduction, radiation, and surface-to-surface contact. A total of approximately 20,500 nodes, 110 planar elements, and 4,900 solid elements are used to simulate the modeled components. Nearly 80 of the solid elements are finite difference solids (i.e., FD solids), a Thermal Desktop<sup>®</sup> computer program feature that permits a group of solid elements to be represented by a single entity. As such, the number of individual solid ‘bricks’ utilized in the modeling is actually significantly larger than the 4,900 value indicated above. In addition, one boundary node is used to represent the ambient environment for convection purposes and two boundary nodes is used to represent the ambient temperature for the purpose of radiation heat transfer. The use of separate boundary nodes for radiation heat transfer allows the model to capture the effective emissivity of the ambient environment.

As seen from Figure 3.5-1, the modeling accurately captures the geometry of the various components of the packaging, including the impact limiters, the inner and outer shells, the upper and lower end structures, the closure lid and shield plug, and lead sections. Also captured, but not easily seen in the figure due to the scale of the figures, is the thermal shield and the impact limiter attachment lugs. The minimal spatial resolution provided by the thermal modeling for the cask body components is approximately 1.75 inches in the radial direction, 2 inches in the axial direction, and every 10° in the circumferential direction. Greater spatial resolution (i.e., smaller radial and axial distances) is provided near the cask ends where larger thermal gradients are expected. A slightly lower spatial resolution is provided for the exterior portions of the impact limiters since the relatively low thermal conductivity of the polyurethane foam will yield correspondingly low heat flows.

Figure 3.5-2 illustrates the thermal modeling used for the various stainless steel components of the BRR cask body, while Figure 3.5-3 illustrates the thermal modeling of the lead structures within the cask body. The figures demonstrate that the geometry of the cask components is accurately captured by the thermal modeling.

Figure 3.5-4 illustrates the modeling used for the shell of the shield plug. While the height, radius, and shell thickness of the shield plug are accurately captured, the diagonal pipe and 4° taper are not included for modeling simplicity and because these details have no significant effect on the thermal performance of the packaging. Although the lead sheets used to fill the shield plug cavity are to be oversized and then hammered into place, the thermal modeling conservatively assumes a small (i.e., 0.0625-inch) uniform gap exists between the lead sheets and the shield plug shell.

The thermal modeling of the impact limiters, as illustrated in Figure 3.5-5, accurately captures the compound shape of the limiter’s inner shell and the placement of the attachment lugs. Since the fabrication tolerance of the polyurethane foam used to fill the impact limiters can yield foam

densities that are  $\pm 15\%$  of the targeted  $9 \text{ lb}_m/\text{ft}^3$  (pcf) foam density and since the foam's conductivity is a function of its density, the thermal modeling conservatively assumes a low tolerance foam density (i.e., 9 pcf less  $15\% \approx 7.65 \text{ pcf}$ ) for NCT evaluations and a high tolerance foam density (i.e., 9 pcf plus  $15\% \approx 10.35 \text{ pcf}$ ) for HAC evaluations.

### 3.5.3.2 Description of MURR Fuel and Basket Thermal Model

Figure 3.5-6 illustrates the thermal modeling of the MURR fuel basket and fuel element used for this evaluation. Approximately 2,600 nodes, 160 planar elements, and 1,000 solid elements are used to simulate the modeled components of the fuel basket, while approximately 3,300 nodes, 340 planar elements, and 550 solid elements are used to simulate the modeled components of each MURR fuel element.

The fuel basket modeling captures the inner and outer shells, the plates used to section off or divide the basket into compartments to house the individual fuel elements, and the base. While the inner shell and the divider plates are simulated using solid elements, the 0.25-inch thick outer shell and the base plates are represented by planar elements since the temperature difference though their thickness will be small. All of the basket components are assumed to be Type 304 stainless steel. The fuel elements are assumed to be essentially centered within in each compartment with the heat transfer between the fuel elements and the basket assumed to be via conduction and radiation across the separation gap and via contact with the plate supporting the fuel elements.

The fuel element simulation includes separate representation of the twenty-four (24) curved composite fuel plates, the side plates, and the upper and lower end box castings. Heat transfer between the individual fuel plates is simulated via conduction and radiation, while the heat transfer between the fuel plates and the side plates is via radiation and conduction through the crimped edges. The size, curvature, distance between the fuel plates, and the composite thermal properties of the plates are based on the information presented in Appendix 3.5.3.9, *Determination of Composite Thermal Properties for Fuel Plates*. The decay heat loading for the fuel elements is applied as a surface heat flux over the active fuel length of the plates.

Heat transfer between the fuel basket and the BRR packaging is assumed to be via conduction and radiation across the assumed uniform gap between the basket and the inner shell of the packaging. Direct contact is assumed between the base of the fuel basket and the base of the cask cavity. Because of the combination of decay heat and the criterion to limit the maximum fuel plate temperature to  $400^\circ\text{F}$  or less (see Section 3.2.2), the BRR cask cavity is to be filled with helium gas at a pressure of one atmosphere following the draining and drying process.

### 3.5.3.3 Description of MITR-II Fuel and Basket Thermal Model

Figure 3.5-7 illustrates the thermal modeling of the MITR-II fuel basket and fuel element used for this evaluation, while Figure 3.5-8 illustrates the layout of the solids modeling for the basket internal geometry. Approximately 4,500 nodes, 2 planar elements, and 2,200 solid elements are used to simulate the modeled components of the fuel basket, while approximately 1,480 nodes, 75 planar elements, and 230 solid elements are used to simulate the modeled components of each MITR-II fuel element.

The fuel basket modeling captures the geometry of the machined stainless steel plates used to house the fuel elements, the top plate, the individual tie bars used to hold the basket together, and the pedestal base. All of the basket components are assumed to be Type 304 stainless steel. The fuel elements are assumed to be essentially centered within in each compartment with the heat transfer between the fuel elements and the basket assumed to be via conduction and radiation across the separation gap and via contact with the plate supporting the fuel elements.

The fuel element simulation includes separate representation of the fifteen (15) composite fuel plates, the side plates, and the upper and lower end box castings. Heat transfer between the individual fuel plates is simulated via conduction and radiation, while the heat transfer between the fuel plates and the side plates is via radiation and conduction through the crimped edges. The size, distance between the fuel plates, and the composite thermal properties of the plates are based on the information presented in Appendix 3.5.3.9, *Determination of Composite Thermal Properties for Fuel Plates*. The decay heat loading for the fuel elements is applied as a uniform surface heat flux over the active fuel length of the plates.

Heat transfer between the fuel basket and the BRR packaging is assumed to be via a combination of conduction and radiation across the gaps between the various basket surfaces and the inner shell of the packaging. The cask cavity is to be filled with helium gas to limit the maximum fuel plate temperature to 400 °F or less (see Section 3.2.2).

#### 3.5.3.4 Description of ATR Fuel and Basket Thermal Model

Figure 3.5-9 illustrates the thermal modeling of the ATR fuel basket and fuel element used for this evaluation. Approximately 3,000 nodes, 50 planar elements, and 90 FD solid elements are used to simulate the modeled components of the fuel basket, while approximately 3,300 nodes, 95 planar elements, and 325 solid elements are used to simulate the modeled components of each ATR fuel element. As previously explained, an FD solid is a Thermal Desktop<sup>®</sup> computer program feature that permits a group of solid elements to be represented by a single entity. As such, the number of individual solid ‘bricks’ utilized in the modeling of the ATR fuel basket is actually significantly larger than 90.

The fuel basket modeling captures the inner and outer shells, the plates used to section off or divide the basket into compartments to house the individual fuel elements, the stiffening ribs, and the base. All of the basket components are assumed to be Type 304 stainless steel. The fuel elements are assumed to be essentially centered within in each compartment with the heat transfer between the fuel elements and the basket assumed to be via conduction and radiation across the separation gap.

The fuel element simulation includes separate representation of the nineteen (19) curved composite fuel plates and the side plates (including the cutouts). The upper and lower end boxes are to be removed prior to loading of the fuel assemblies within the basket. Heat transfer between the individual fuel plates is simulated via conduction and radiation, while the heat transfer between the fuel plates and the side plates is via radiation and conduction through the crimped edges. The size, curvature, distance between the fuel plates, and the composite thermal properties of the plates are based on the information presented in Appendix 3.5.3.9, *Determination of Composite Thermal Properties for Fuel Plates*. The decay heat loading for the fuel elements is applied as a uniform surface heat flux over the active fuel length of the plates.

Heat transfer between the fuel basket and the BRR packaging is assumed to be via a combination of conduction and radiation across the gaps between the various basket surfaces and the inner shell of the packaging. The thermal evaluations assume the cask cavity is filled with helium gas.

#### **3.5.3.5 Description of TRIGA Fuel and Basket Thermal Model**

Figure 3.5-10 illustrates the thermal modeling of the TRIGA fuel basket and fuel element used for this evaluation, while Figure 3.5-11 illustrates the solids modeling used to represent the void spaces between the fuel tubes. Approximately 7,500 nodes, 60 planar elements, and 1,000 solid elements are used to simulate the modeled components of the fuel basket, while approximately 1,030 nodes and 7 FD solid elements are used to simulate the modeled components of each TRIGA fuel element. As previously explained, an FD solid is a Thermal Desktop<sup>®</sup> computer program feature that permits a group of solid elements to be represented by a single entity. As such, the number of individual solid ‘bricks’ utilized in the modeling of each TRIGA fuel element is actually significantly larger than 7.

The fuel basket modeling captures the individual tubes used to house each fuel element, stiffening ribs, and the spacers used to position the shorter length fuel elements within the basket. All of the basket components are assumed to be fabricated of Type 304 stainless steel. The fuel elements are assumed to be essentially centered within in each compartment with the heat transfer between the fuel elements and the basket assumed to be via conduction and radiation across the separation gap and via contact with the plate supporting the fuel elements.

The fuel element simulation includes separate representation of the uranium zirconium hydride metal section, the graphite section, and the upper and lower end fittings. Since the temperature difference across the fuel cladding is small for the decay heats involved, the cladding is not modeled separately. The TRIGA fuel has two design active fuel lengths; 14 and 15 inches. The decay heat loading for the fuel elements is applied as a uniform volumetric heat flux over the active fuel length. The modeling assumes the shorter length to conservatively bound the maximum volumetric heat generation.

Heat transfer between the fuel basket and the BRR packaging is assumed to be via a combination of conduction and radiation across the gaps between the various basket surfaces and the inner shell of the packaging. The thermal evaluations assume the cask cavity is filled with helium.

#### **3.5.3.6 Insolation Loads**

The insolation loading on the BRR package is based on the 10CFR71.71(c)(1) specified insolation values over a 24-hour period. Since the BRR packaging is characterized by thermally massive shells and large foam filled impact limiters, the interior temperatures of the packaging will be effectively ‘decoupled’ from the diurnal changes in insolation loading. As such, a steady-state thermal model based on the application of the 10CFR71.71(c)(1) specified insolation values averaged over 24 hours is used to evaluate the design basis package temperatures under NCT conditions.

#### **3.5.3.7 Description of Thermal Model for HAC Conditions**

The thermal evaluations for the hypothetical accident condition (HAC) are conducted using an analytical thermal model of the BRR package. The HAC thermal model is a modified version of



the half symmetry NCT model described above. The principal model modifications consist of simulating the expected package damage resulting from the drop events that are assumed to precede the HAC fire, changing the package surface emissivities to reflect the assumed presence of soot and/or surface oxidization, and simulating the thermal performance of the polyurethane foam used in the impact limiters.

Physical testing using a half scale certification test unit (CTU) is used to establish the expected level of damage sustained by the BRR packaging as a result of the 10 CFR 71.73 prescribed free and puncture drops that are assumed to precede the HAC fire event. The configuration and initial conditions of the test article, a description of the test facility, test article instrumentation, and the test results are documented Section 2.12.3, *Certification Test Results*. The drop tests covered a range of hypothetical free drop orientations and puncture bar drops. An overview of the results of the drop tests is provided below. For full details, including photographs and figures, see Section 2.12.3, *Certification Test Results*. It should be noted that all of the noted dimensions in this discussion are for the half scale model and need to be doubled to yield the equivalent full scale results.

- 1) The worst case physical damage to the exterior of the package occurs from an oblique slap down free drop. Overall, the resulting damage is thermally insignificant: an inward crush of approximately 4 inches and two small breaches in the joint along the outer diameter of the limiter. However, a subsequent drop on a puncture bar caught the fold in the limiter shell created by the oblique slap down drop and tore the damaged joint open. The total chord length of the damaged area measured approximately 26 inches. The width of the opening at the center was 5 inches and tapering to nearly zero at the ends. The chord length of the flap opening is approximately 22.6 inches. Negligible amounts of foam were lost from the limiter from the opening.
- 2) The CG over corner drop resulted in a crush distance of 5.5 inches. A subsequent puncture bar drop on the damage area resulted in the partial penetration of the shell. The puncture bar penetrated the underlying foam to a depth of 2-1/4 inches. The width of the breach/torn flap in the limiter shell was 4 inches and its length was 5 inches.
- 3) The vertical end drop resulted in impact limiter deformation that was a combination of outside-in and inside-out. The drop resulted in no tearing of the limiter shell and no exposure of the underlying foam. The crush distance was 3.4 inches. A subsequent puncture bar drop on the damaged area created a dent approximately 1-3/4 inches deep. One or two rebound impacts also occurred with negligible deformation. There were no signs of cracking in the dent or in the nearby weld seam.
- 4) The drop testing showed the original impact limiter attachment design was not adequate to fully retain the impact limiters on the package for the slapdown free drop event. The attachments were redesigned and retested to ensure complete attachment of the limiters. See Section 2.12.3, *Certification Test Results*, for further discussion.
- 5) No deformation of the impact limiter inner shell was noted.

Subsequent to the drop test, the impact limiter design was modified to improve its performance. These modifications increased the number of attachment lugs from 6 to 8 per limiter, increased the size and thickness of each lug from 0.38-inches thick by 2.75-inches wide to 0.5-inches thick by 3.63-inches wide, increased the size of the attachment pins, reduced the gap between the cask and the impact limiter inner shell from 0.25 to 0.125 inches, and a re-design of the limiter joint that cracked under the side/slap down drop (see Item 1 above).

Besides scaling the noted crush dimensions to the full scale design, the projected damage also needs to reflect the effect of temperature on the polyurethane foam's structural properties since the drop test was conducted under cold conditions and the worst case crush will arise under warm conditions. Figure 3.5-12 depicts the predicted crush depths under hot conditions for the vertical end, C.G. over corner, and side/slap down drop orientations based on an evaluation presented in Section 2.12.5, *Impact Limiter Performance Evaluation*. As seen from the figure, the side/slap down drop orientation is predicted to result in both the greatest crush depth and the closest approach to the inner shell of the limiter. Per Appendix 3.5.4, '*Last-A-Foam*' *Response under HAC Conditions*, approximately 3.5 to 3.8 inches of the nominally 9 pcf polyurethane foam will decompose during a 30 minute HAC fire event. This foam loss (or recession depth) will be even less for foam in the vicinity of crush damage since its effective density will have increased as a result of the crush damage. Any foam depths greater than 4 inches remaining after the HAC drop events will result in the underlying temperatures rising only marginally during the HAC fire event. Examination of Figure 3.5-12 demonstrates that the vertical end drop and C.G. over corner drops will leave more than 4 inches of foam everywhere, even without credit for increased foam density due to crush. As such, the side/slap down drop event is selected as the controlling scenario for impact limiter damage for the HAC evaluations.

The controlling puncture bar damage is determined from the half-scale drop results described in Section 2.12.3, *Certification Test Results*. Since the polyurethane foam forms an intumescent char that swells and tends to fill voids or gaps created by the puncture bar damage, the level of damage incurred by direct attack to the impact limiter's exterior shell would be thermally insignificant. An untested puncture bar scenario consisting of an impact to the thermal shield of the cask is also considered. This type of impact can be expected to cause a local depression in the thermal shield and potentially a small tear. However, overall, the thermal shield would retain its functionality with the region of elevated temperatures being localized to the size of the puncture bar and similar in temperature level to that seen at the impact limiter attachment lug locations. Therefore, the controlling puncture bar damage is assumed to be an attack on the impact limiter skin joint that tears a flap type opening in the limiter skin (see Item 1 above). While the re-design of the impact limiters following the drop tests is expected to eliminate this type of damage, it is assumed for the HAC evaluation to conservatively bound all other potential puncture bar damage scenarios.

Based on the above observations and the general assumptions for the package condition for the HAC evaluations, the NCT thermal model described above was modified for the HAC evaluations via the following steps:

- 1) Assume the package has been ejected from its support stand and is lying on its side. As such, the convective heat transfer from the package's exterior surfaces is based on a horizontal orientation. In addition, the adiabatic boundary condition assumed for selected surfaces of the lower impact limiter under NCT conditions are switched to active heat transfer surfaces.
- 2) The surface emissivity for all exterior surfaces is assumed to be 0.9 to account for potential oxidation and/or soot accumulation. The emissivity of all inside surfaces of the impact limiter exposed as the result of foam decomposition is assumed to be 0.95 to account for adherence of foam char.
- 3) The small, uniform gap conservatively assumed between the lead and the outer shell under NCT conditions is eliminated to maximize the heat flow into package.

- 4) Thermal conductance via the stand-off strips under the thermal shield is assumed for the HAC condition. Thermal credit for the stand-off strips was conservatively ignored for the NCT evaluations.
- 5) The number and size of the impact limiter attachments are increased for the HAC evaluation to reflect the re-design of the impact limiter following the drop testing. The NCT evaluations ignored this change since neglecting the added surface area yields conservative results.
- 6) A minimum of 3.8 inches of foam is removed from around the perimeter of the impact limiters at the start of the HAC evaluation. This change conservatively bounds the impact of the gradual decomposition of the foam over the 30 minute fire event. The conductivity of the remaining foam is set to that associated with foam fabricated at the high end of the density tolerance range (i.e., 9 pcf + 15%) in order to conservatively bound the heat transfer into the package.
- 7) Simulate the sideways crushing of the upper and lower impact limiters under hot drop conditions. This consisted of removing approximately 15.8 inches from one side of the impact limiters.
- 8) Simulate the conservative assumption that a puncture bar attack tears a flap in the upper impact limiter. This consisted of removing a total of 6.1 inches of foam over a 60° segment of the impact limiter to conservatively capture the additional recession depth over 3.8 inches that may occur due to the direct exposure of the foam surfaces to the flame (see Appendix 3.5.4, *'Last-A-Foam' Response under HAC Conditions*). Added radiation and convection conductors to the exposed region of the impact limiter's inner shell to reflect the conservative assumption that a flap opening has occurred in the upper impact limiter.
- 9) Simulated the possible shifting of the impact limiter by replacing the 0.125 inch nominal gap between the inner shell of the limiters and the cask shell with a direct contact conductance over an approximate 1 inch x 7.2 inch area (i.e., the modeled height of the cylindrical portion of the limiter's inner shell). The contact is placed in the center of the side drop foam crush damage and conservatively bounds the line-contact expected between two cylindrical bodies with no deformation.

Figure 3.5-13 illustrates the revised thermal model of the impact limiters used for the HAC evaluations. All other aspects of the BRR packaging remain the same as used for the NCT thermal evaluations.

#### 3.5.3.8 Convection Coefficient Calculation

The BRR package thermal model uses semi-empirical relationships to determine the level of convection heat transfer from the exterior package surfaces under both the regulatory NCT and HAC conditions. The convective heat transfer coefficient,  $h_c$ , has a form of:

$$h_c = \text{Nu} \frac{k}{L}$$

where  $k$  is the thermal conductivity of the gas at the mean film temperature and  $L$  is the characteristic length of the vertical or horizontal surface. The convection coefficient is

correlated via semi-empirical relationships against the local Rayleigh number and the characteristic length. The Rayleigh number is defined as:

where

$$Ra_L = \frac{\rho^2 g_c \beta L^3 \Delta T}{\mu^2} \times Pr$$

$g_c$  = gravitational acceleration, 32.174 ft/s<sup>2</sup>     $\beta$  = coefficient of thermal expansion, °R<sup>-1</sup>  
 $\Delta T$  = temperature difference, °F     $\rho$  = density of air at the film temperature, lb<sub>m</sub>/ft<sup>3</sup>  
 $\mu$  = dynamic viscosity, lb<sub>m</sub>/ft-s     $Pr$  = Prandtl number =  $(c_p \mu) / k$   
 $L$  = characteristic length, ft     $k$  = thermal conductivity at film temp., Btu/ft-hr-°F  
 $c_p$  = specific heat, Btu/ lb<sub>m</sub> -°F     $Ra_L$  = Rayleigh #, based on length 'L'

Note that  $k$ ,  $c_p$ , and  $\mu$  are each a function of air temperature as taken from Table 3.2-3. Values for  $\rho$  are computed using the ideal gas law,  $\beta$  for an ideal gas is simply the inverse of the absolute temperature of the gas, and  $Pr$  is computed using the values for  $k$ ,  $c_p$ , and  $\mu$  from Table 3.2-3. Unit conversion factors are used as required to reconcile the units for the various properties used.

The natural convection from a discrete vertical surface is computed using Equations 4-13, 4-24, 4-31, and 4-33 of reference [19], which is applicable over the range  $1 < \text{Rayleigh number } (Ra) < 10^{12}$ :

$$\begin{aligned}
 Nu^T &= \bar{C}_L Ra^{1/4} \\
 \bar{C}_L &= \frac{0.671}{\left(1 + (0.492/Pr)^{9/16}\right)^{4/9}} \\
 Nu_L &= \frac{2.0}{\ln(1 + 2.0/Nu^T)} \\
 Nu_t &= C_t^V Ra^{1/3} / (1 + 1.4 \times 10^9 Pr/Ra) \\
 C_t^V &= \frac{0.13 Pr^{0.22}}{(1 + 0.61 Pr^{0.81})^{0.42}} \\
 Nu &= \frac{h_c L}{k} = \left[ (Nu_L)^6 + (Nu_t)^6 \right]^{1/6}
 \end{aligned}$$

The natural convection from a vertical cylindrical surface is computed by applying a correction factor to the laminar Nusselt number ( $Nu_L$ ) determined using the same methodology and  $Nu_t$  for a vertical plate (see above). The characteristic dimension,  $L$ , is the height of the vertical cylinder and  $D$  is the cylinder's diameter. The correction factor as defined by Equations 4-44 of reference [19] is:

$$\begin{aligned}
 Nu_{L-Cylinder} &= \frac{\delta}{\ln(1 + \delta)} Nu_{L-Plate} \\
 \delta &= \frac{1.8 \times L/D}{Nu_{Plate}^T}
 \end{aligned}$$

$$Nu_{\text{Vert. Cylinder}} = \frac{h_c L}{k} = \left[ (Nu_{L-\text{Cylinder}})^6 + (Nu_{t-\text{Plate}})^6 \right]^{1/6}$$

Natural convection from horizontal surfaces is computed from Equations 4-13, 4-25, 4-39, and 4-40 of reference [19], where the characteristic dimension (L) is equal to the plate surface area divided by the plate perimeter. For a heated surface facing upwards or a cooled surface facing downwards and  $Ra > 1$ :

$$Nu = \frac{h_c L}{k} = \left[ (Nu_L)^{10} + (Nu_t)^{10} \right]^{1/10}$$

$$Nu_L = \frac{1.4}{\ln \left( 1 + 1.4 / \left( 0.835 \times \bar{C}_L Ra^{1/4} \right) \right)}$$

$$\bar{C}_L = \frac{0.671}{\left( 1 + (0.492/Pr)^{9/16} \right)^{4/9}}$$

$$Nu_t = 0.14 \times \left( \frac{1 + 0.0107 \times Pr}{1 + 0.01 \times Pr} \right) \times Ra^{1/3}$$

For a heated surface facing downwards or a cooled surface facing upwards and  $10^3 < Ra < 10^{10}$ , the correlation is as follows:

$$Nu = Nu_L = \frac{2.5}{\ln \left( 1 + 2.5 / Nu^T \right)}$$

$$Nu^T = \frac{0.527}{\left( 1 + (1.9/Pr)^{9/10} \right)^{2/9}} Ra^{1/5}$$

Calculation of the convection coefficient from a horizontal cylindrical surface is computed using Equation 3-43, Chapter 1, from [26], where the characteristic length, D, is the outer diameter of the cylinder. This equation, applicable for  $10^{-5} < Ra < 10^{12}$ , is as follows:

$$Nu = \frac{h_c D}{k} = \left\{ 0.60 + \frac{0.387 Ra_D^{1/6}}{\left[ 1 + (0.559/Pr)^{9/16} \right]^{8/27}} \right\}^2$$

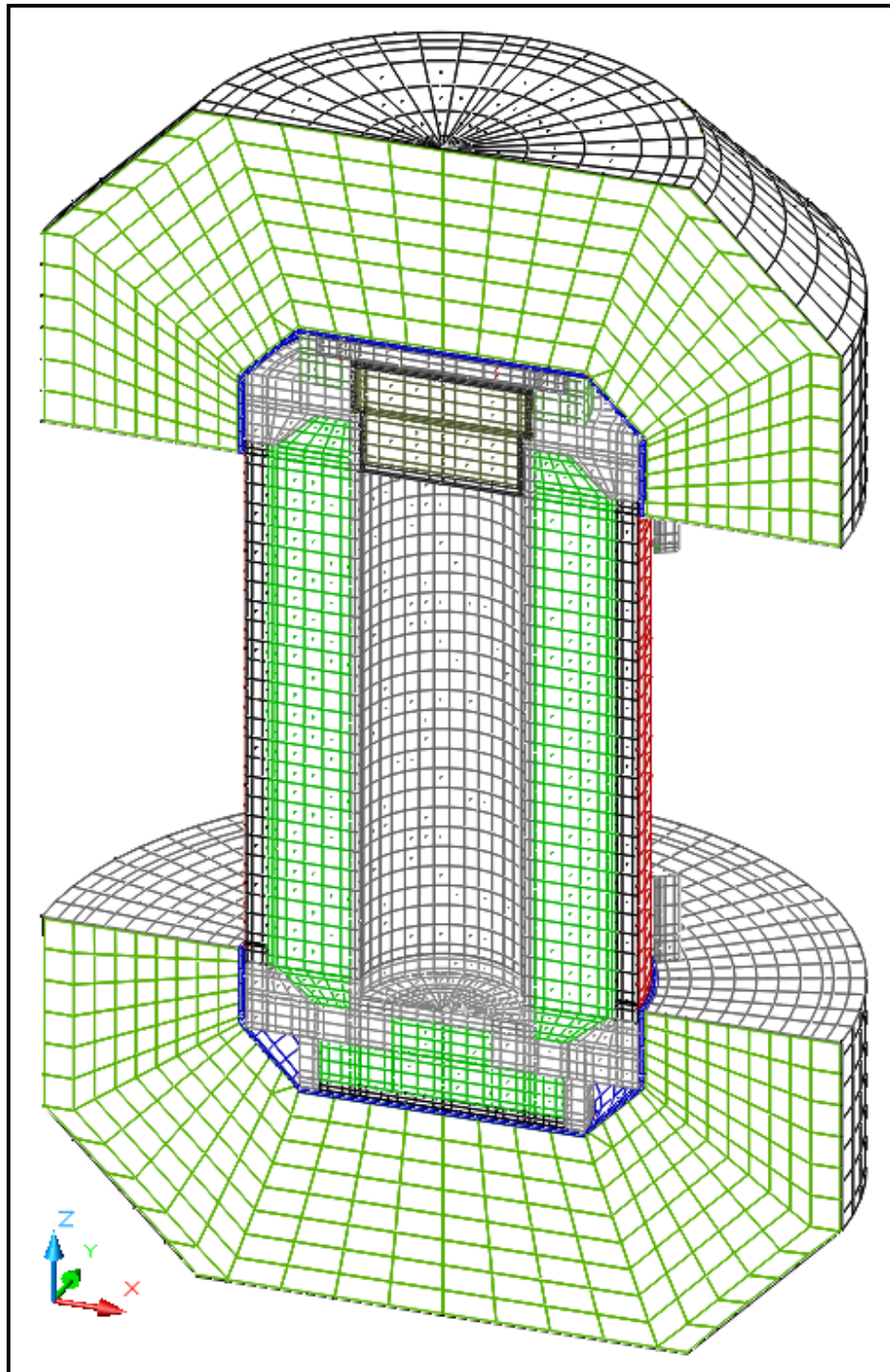
The forced convection coefficients applied during the HAC fire event are computed using the relationships in Table 6-5 of reference [25] for a flat surface, where the characteristic dimension (L) is equal to the length along the surface and the free stream flow velocity is V. The heat transfer coefficient is computed based on the local Reynolds number, where the Reynolds number is defined as:

$$Re_L = \frac{V \times \rho \times L}{\mu}$$

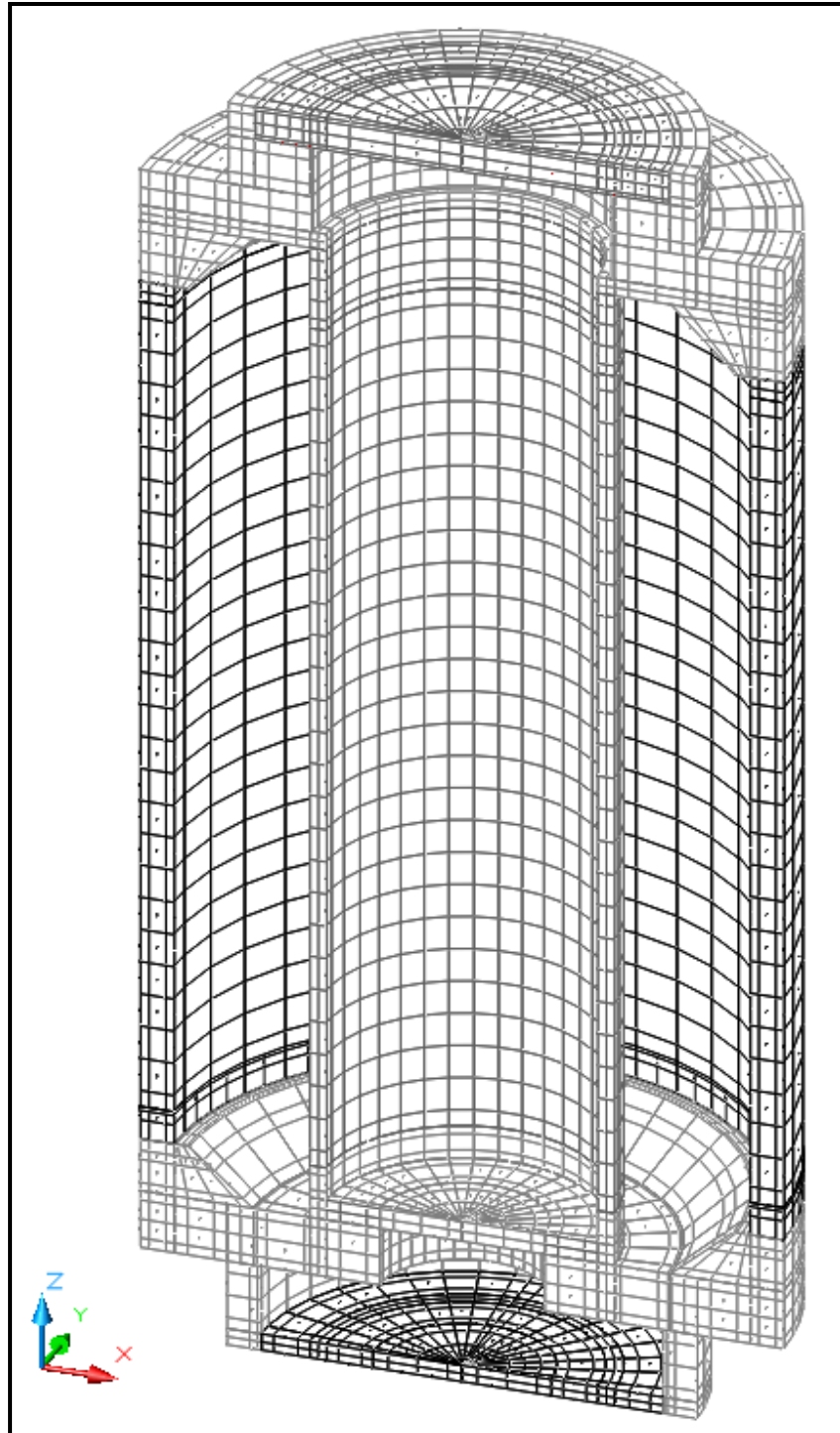
$$\text{For } Re < 5 \times 10^5 \text{ and } Pr > 0.1: Nu = 0.664 \times Re_L^{0.5} \times Pr^{0.33}$$

$$\text{For } Re > 5 \times 10^5 \text{ and } Pr > 0.5: Nu = 0.036 \times Pr^{0.33} \times \left[ Re_L^{0.8} - 23,200 \right]$$

Given the turbulent nature of the 30-minute fire event, a characteristic length of 0.25 feet is used for all surfaces to define the probable limited distance for boundary growth. Figure 3.5-14 presents an illustration of the level of convective heat transfer coefficient predicted by the above equation during the HAC transient.

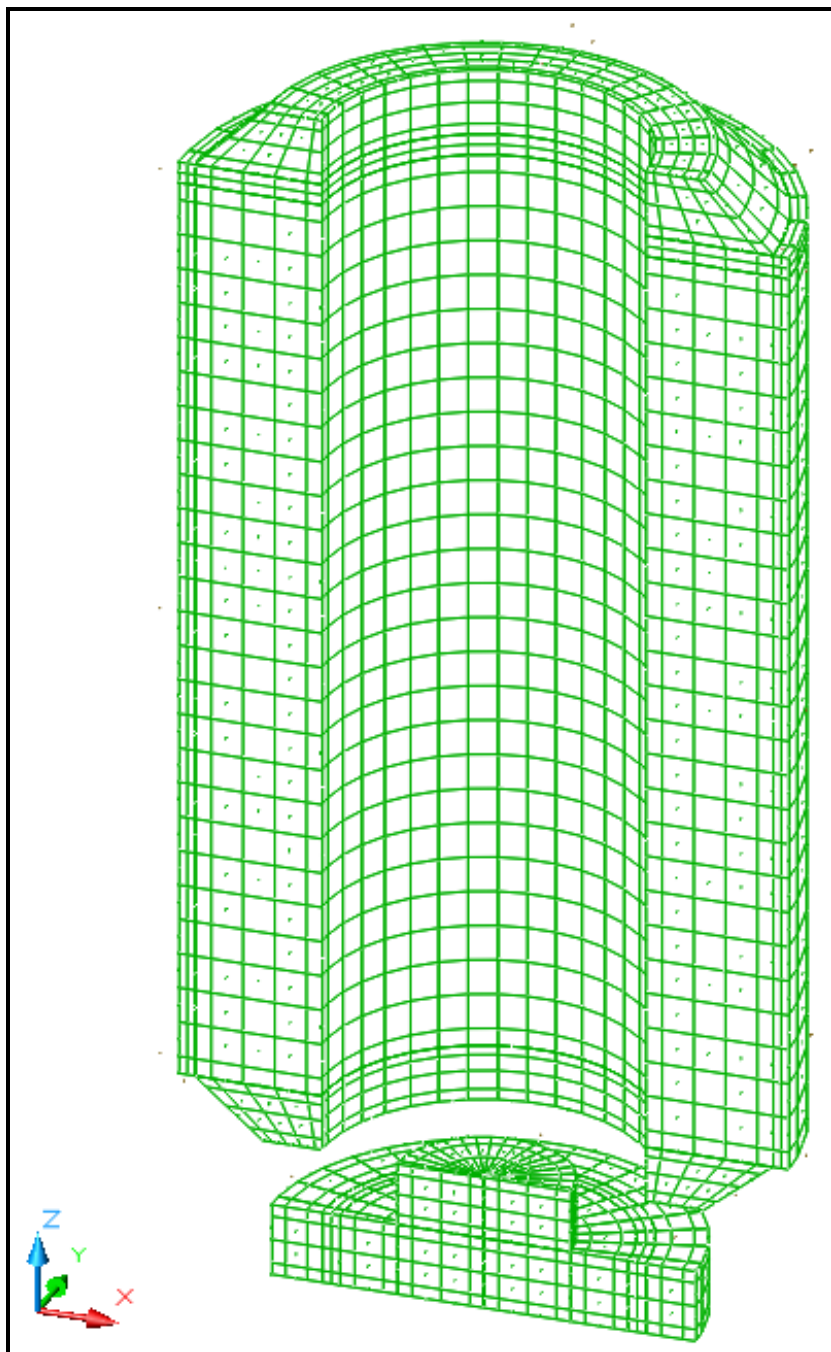


**Figure 3.5-1 – Isometric View of ‘Solids’ Thermal Model for BRR Packaging**

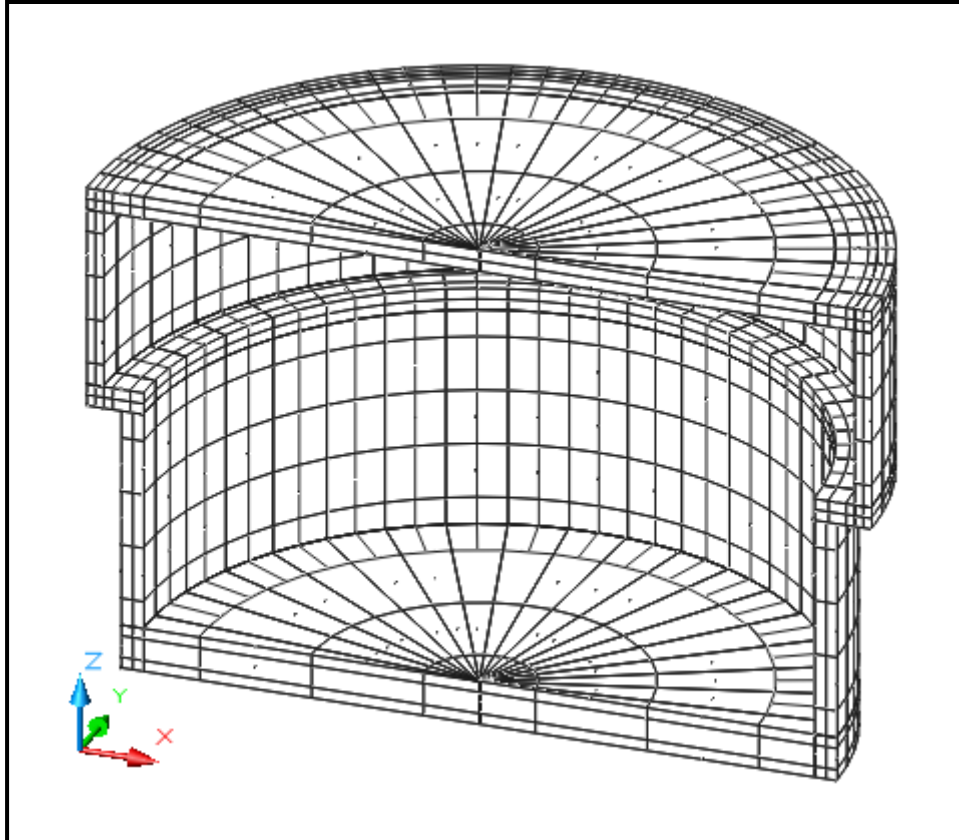


**Figure 3.5-2 – Isometric View of ‘Solids’ Thermal Model for Inner/Outer Shells and Upper/Lower Structures**

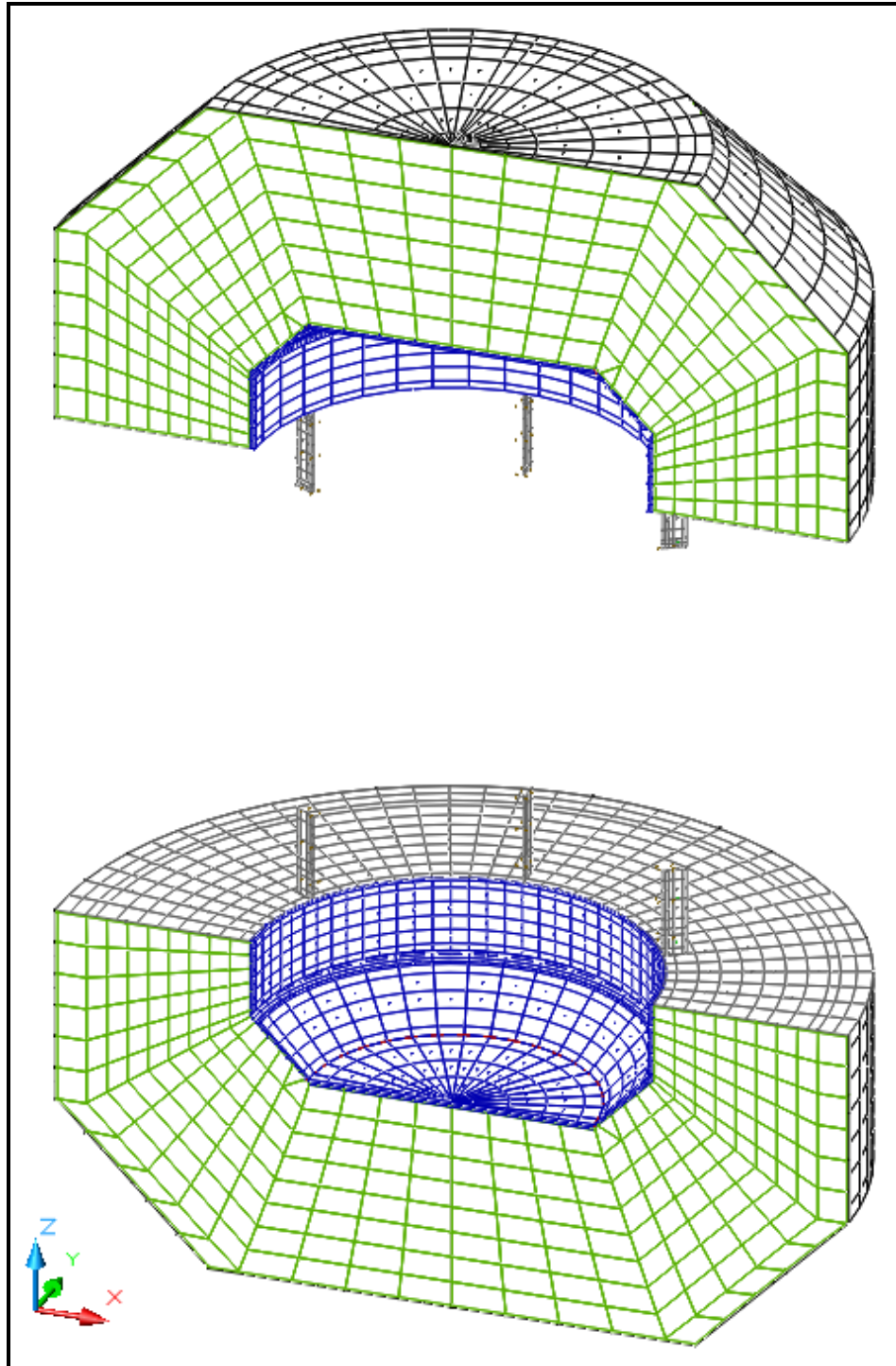




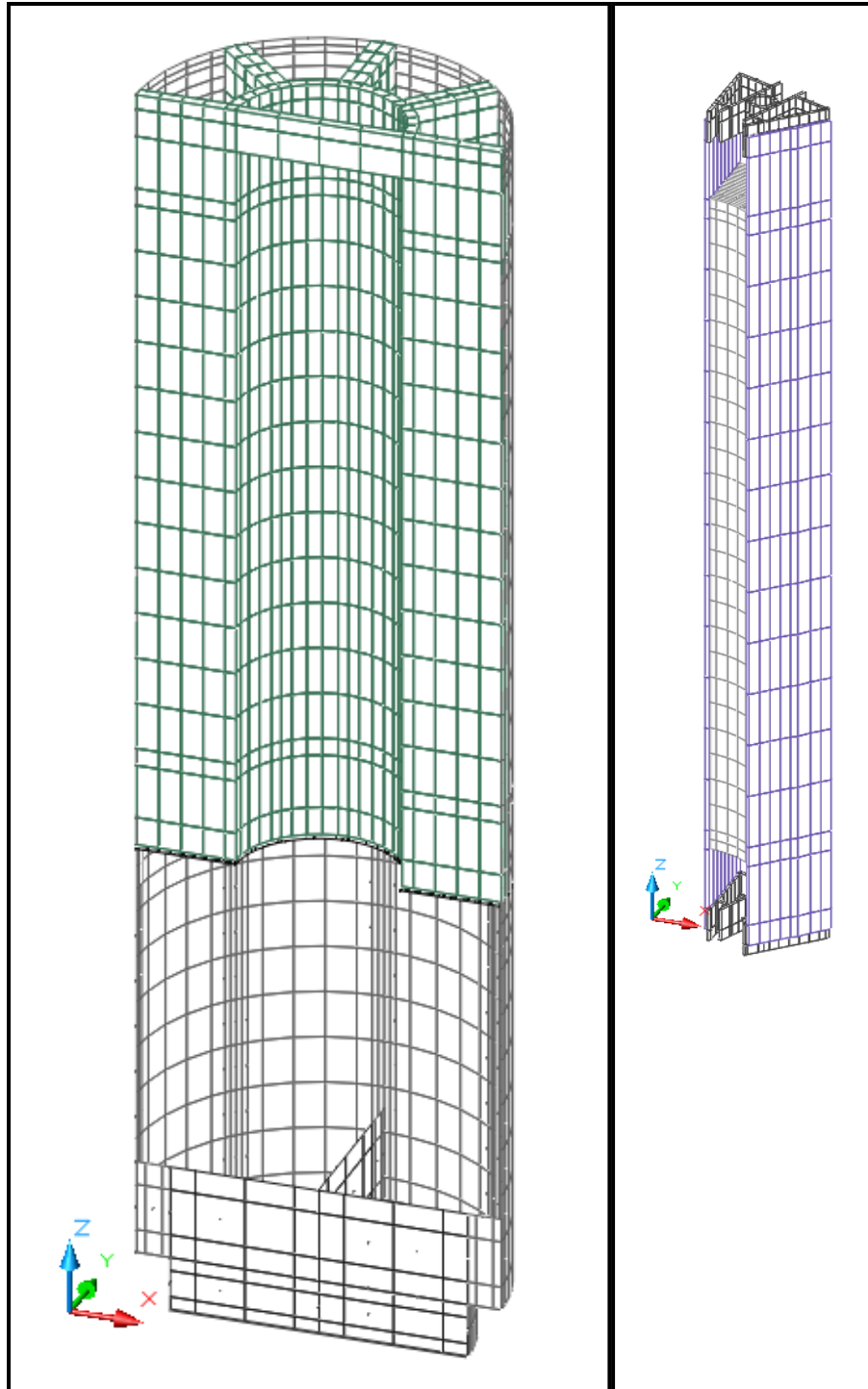
**Figure 3.5-3** – Isometric View of ‘Solids’ Thermal Model for Cask Lead Sections



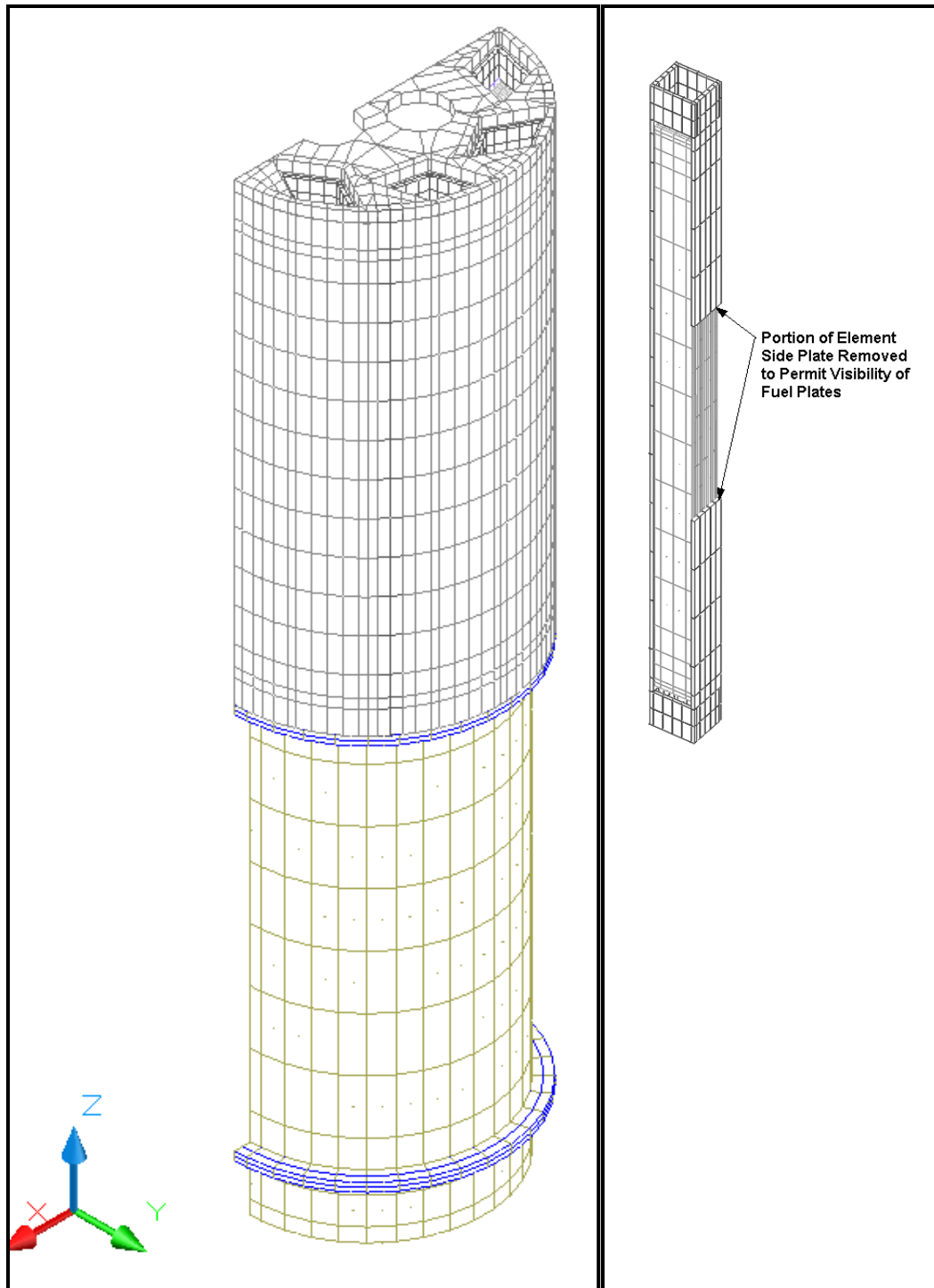
**Figure 3.5-4** – Isometric View of ‘Solids’ Thermal Model for Shield Plug Shell



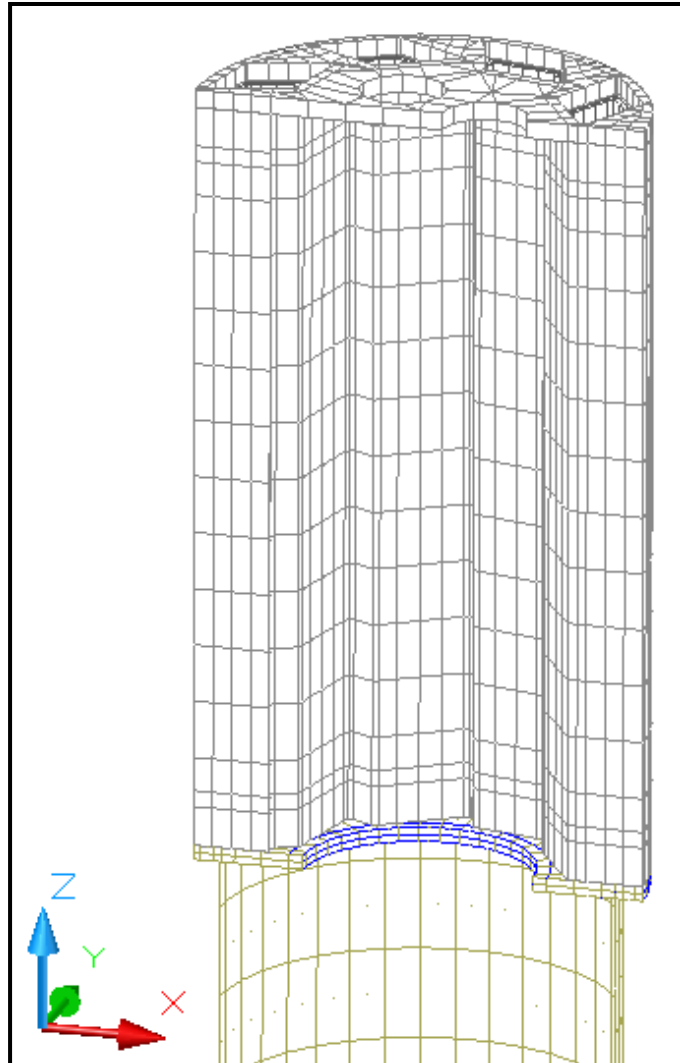
**Figure 3.5-5** – Isometric View of ‘Solids’ Thermal Model for Impact Limiters



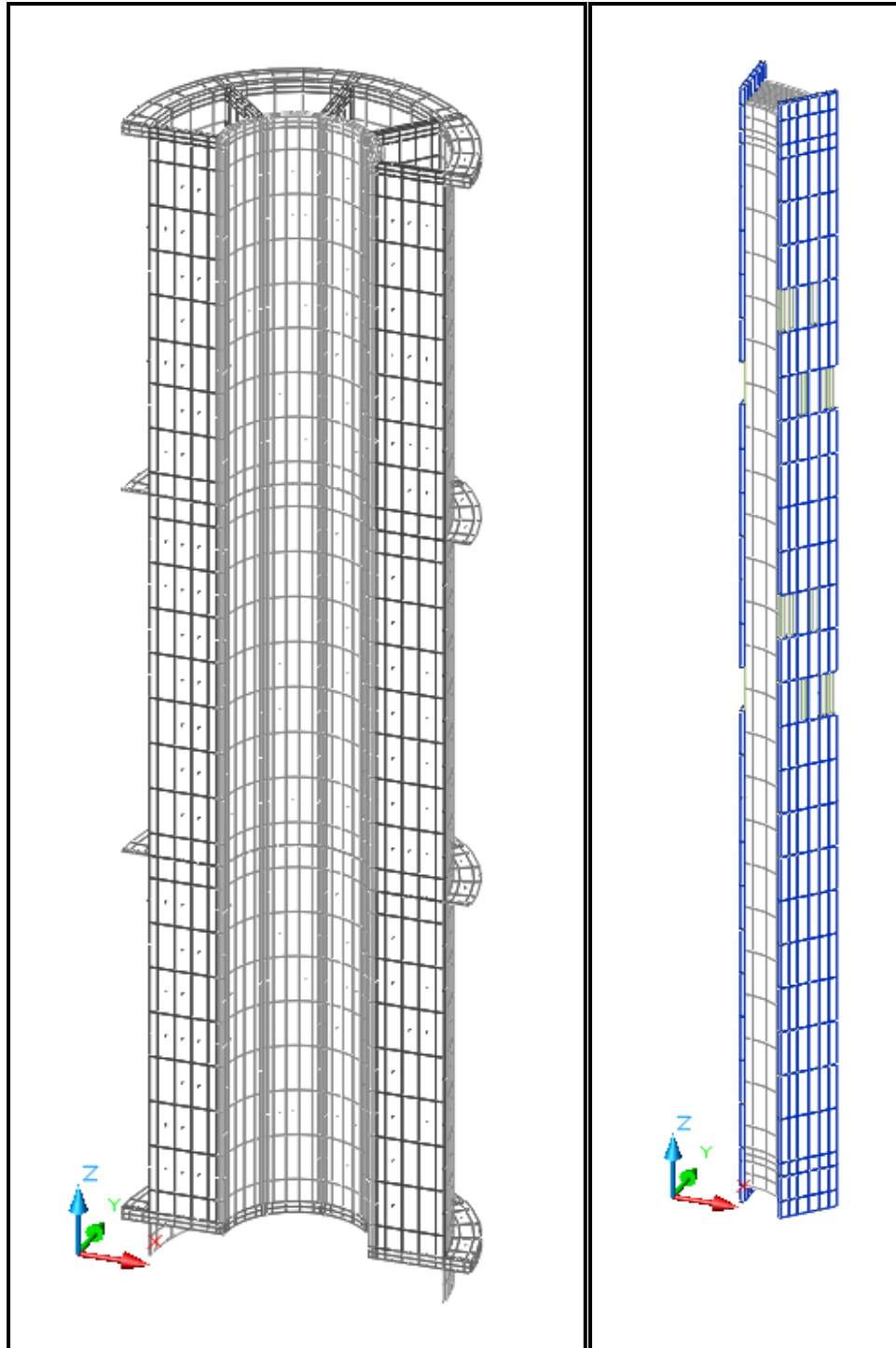
**Figure 3.5-6** – Isometric View of ‘Solids’ Thermal Model for MURR Fuel Basket and Element



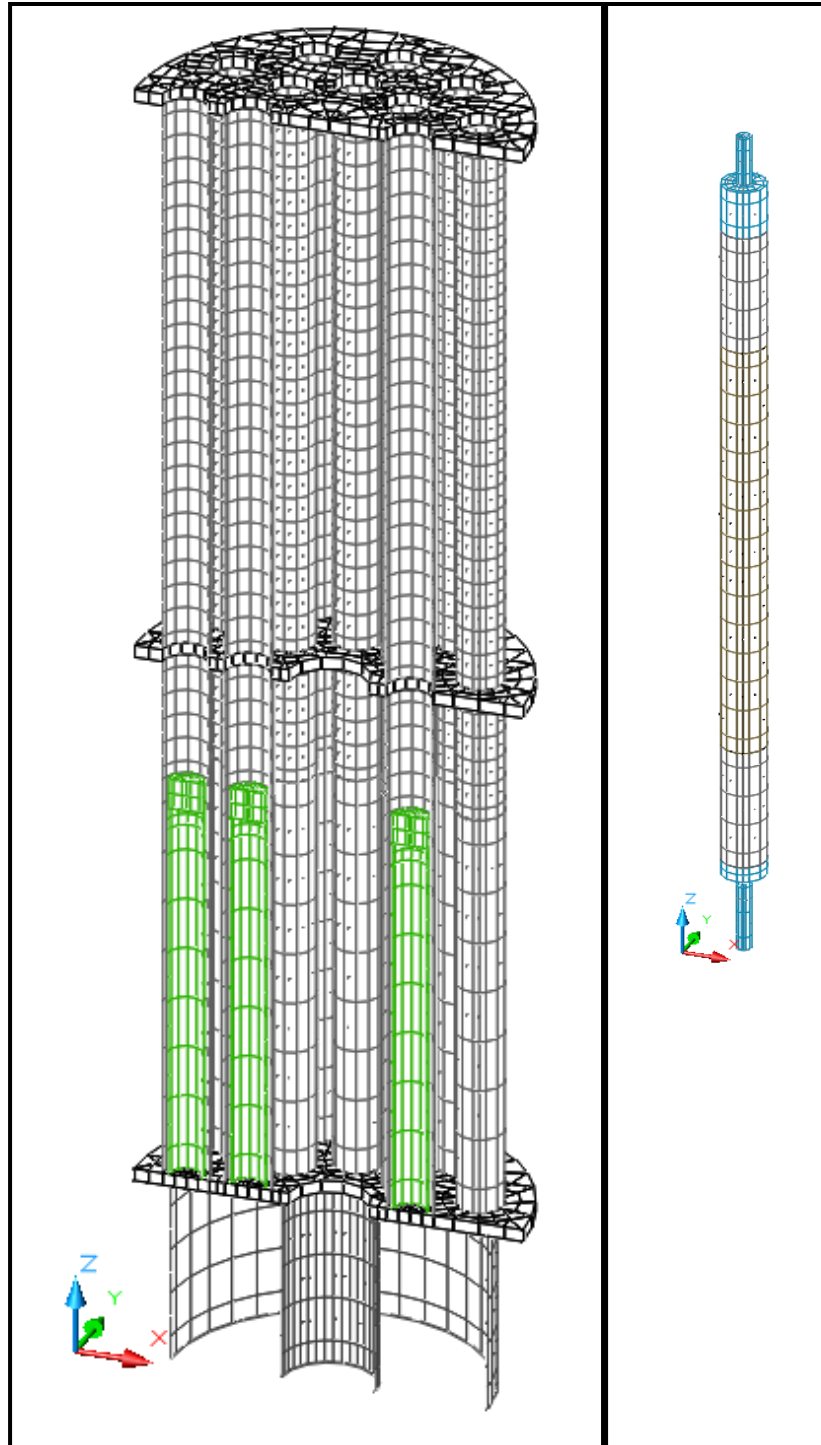
**Figure 3.5-7 – Isometric View of ‘Solids’ Thermal Model for MITR-II Fuel Basket and Element**



**Figure 3.5-8 – Isometric View of Internal MITR-II Basket Model**

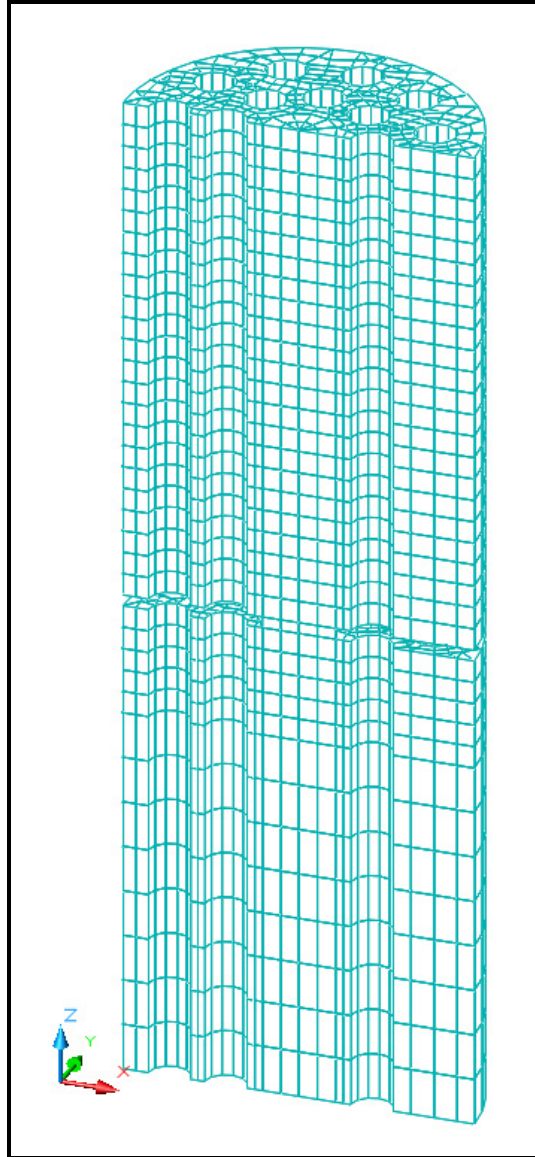


**Figure 3.5-9** – Isometric View of ‘Solids’ Thermal Model for ATR Fuel Basket and Element

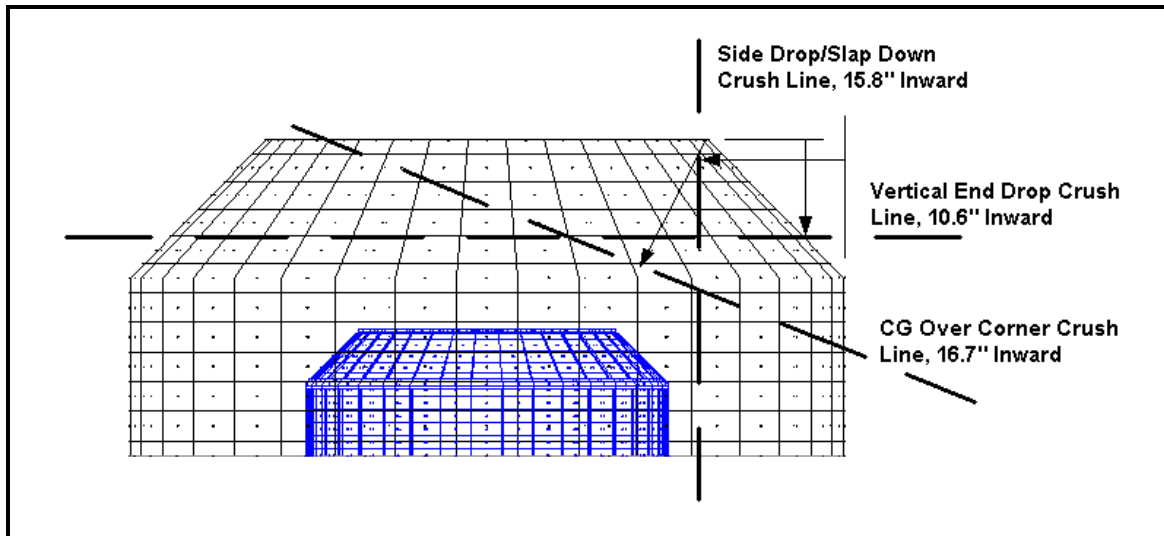


**Figure 3.5-10** – Isometric View of ‘Solids’ Thermal Model for TRIGA Fuel Basket and Element

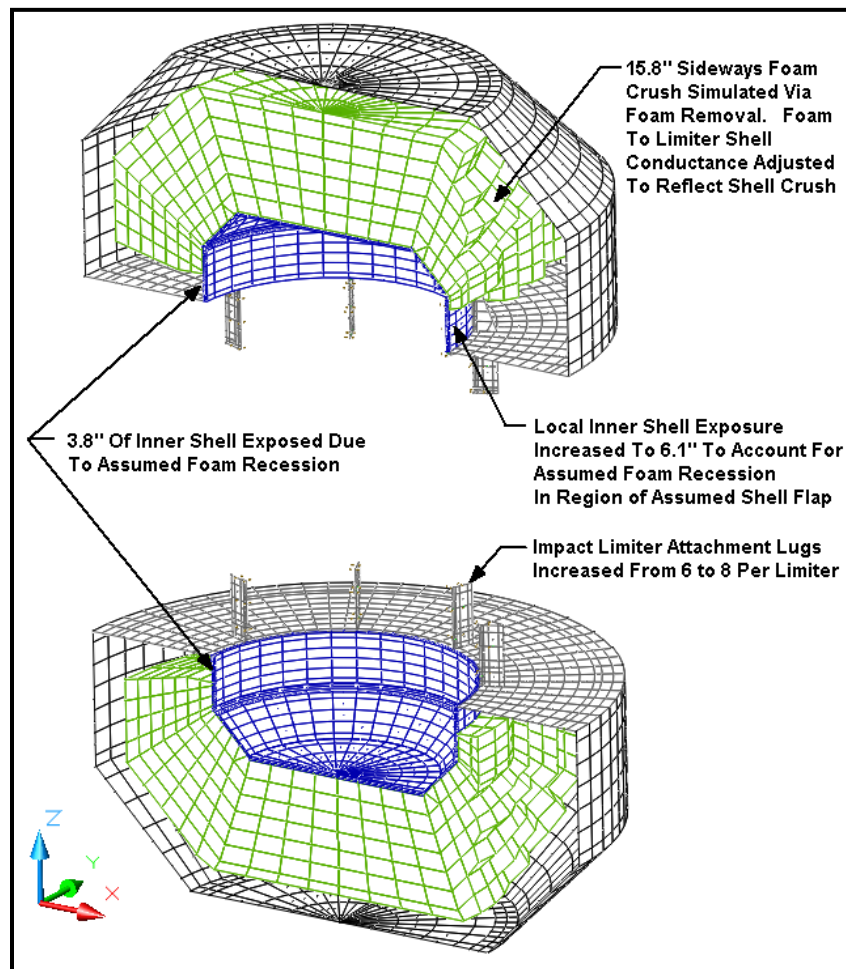




**Figure 3.5-11** – Isometric View of ‘Void Space’ Modeling for TRIGA Basket



**Figure 3.5-12 – Impact Limiter HAC Drop Crush Distances**



**Figure 3.5-13 – Simulated HAC Damage to Impact Limiters**

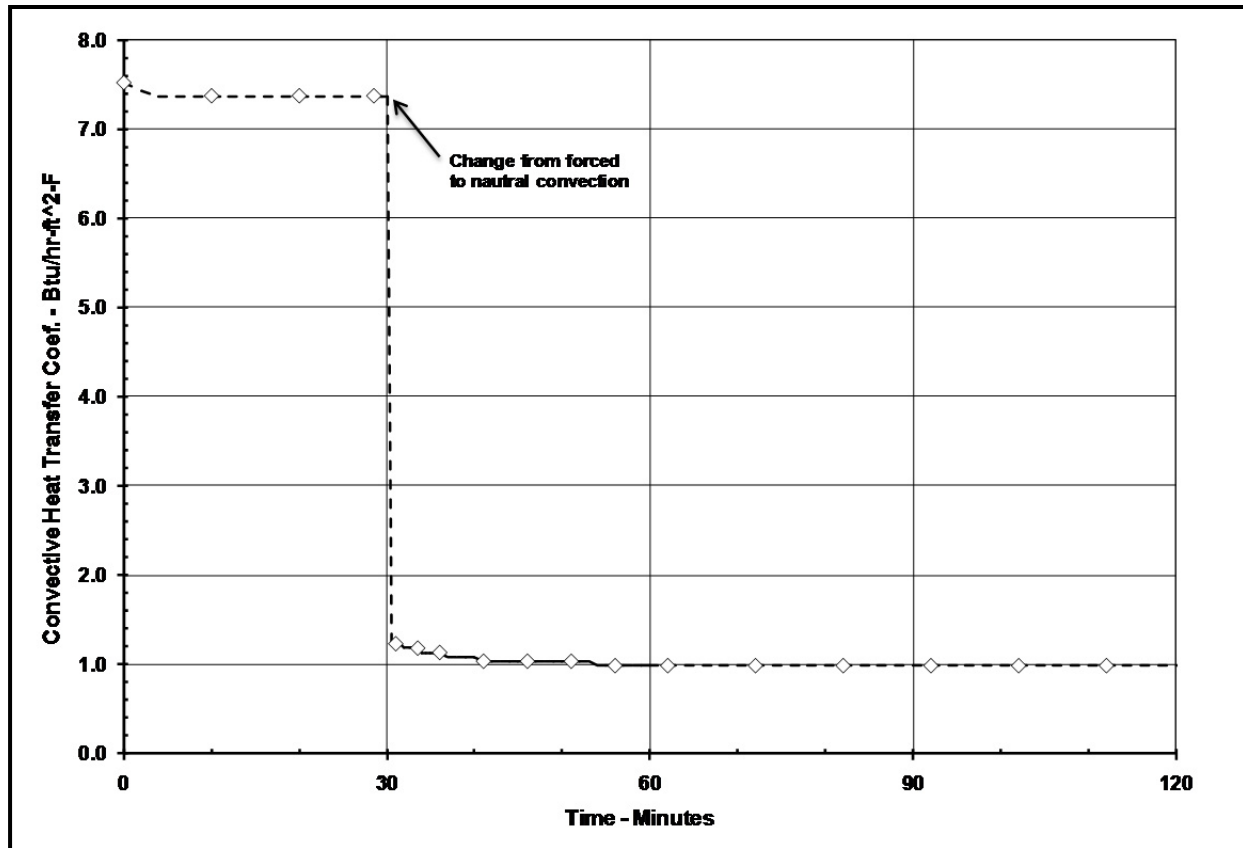
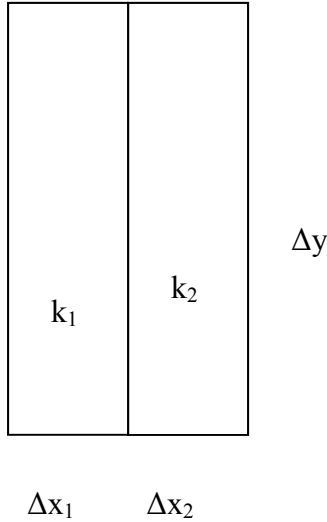


Figure 3.5-14 – Convection Coefficient Variation During HAC Transient

### 3.5.3.9 Determination of Composite Thermal Properties for Fuel Plates

#### Thermal Properties for ATR Fuel Plates

The ATR fuel plates are a composite material consisting of a fissile fuel matrix sandwiched within aluminum cladding. For the purposes of this calculation, the fuel composite is treated as a homogenous material with lumped thermal properties as defined below. This modeling approach is justified since the thermal gradient within the fuel element will be very low given that the un-irradiated fuel has essentially no decay heat.



Because of the thinness of the plates, the average conductivity is required only for the axial and circumferential direction. Conductivity through the plates is not required as this analysis assumes a zero temperature gradient in that direction. Mean density and specific heat values are also defined below.

#### Circumferential and Axial Conductivity

Ignoring the affect of curvature, the heat flow can be written as,

$$q = -\Delta x \Delta z \bar{k} \frac{\Delta T}{\Delta y} = -\Delta x_1 \Delta z k_1 \frac{\Delta T}{\Delta y} - \Delta x_2 \Delta z k_2 \frac{\Delta T}{\Delta y}$$

$$\text{where } \Delta x = \sum_i \Delta x_i$$

$$\text{From which, } \bar{k} = \frac{\Delta x_1 k_1 + \Delta x_2 k_2}{\Delta x}$$

#### Mean Density

The mean density of the fuel plates is computed from:

$$\text{Mass} = \Delta x \Delta y \Delta z \bar{\rho} = \Delta x_1 \Delta y \Delta z \rho_1 + \Delta x_2 \Delta y \Delta z \rho_2, \text{ from which } \bar{\rho} = \frac{\Delta x_1 \rho_1 + \Delta x_2 \rho_2}{\Delta x}$$

#### Mean Specific Heat

In the same manner used to define the mean density, the mean specific heat for the fuel plates is computed as;

$$\bar{\rho} \bar{c}_p \Delta x \Delta y \Delta z = \rho_1 c_{p_1} \Delta x_1 \Delta y \Delta z + \rho_2 c_{p_2} \Delta x_2 \Delta y \Delta z, \text{ from which, } \bar{c}_p = \frac{\rho_1 c_{p_1} \Delta x_1 + \rho_2 c_{p_2} \Delta x_2}{\bar{\rho} \Delta x}$$

The thermal properties for the individual plates making up the ATR fuel element are computed using the above approach and thermophysical [5] and geometric data [14] for the ATR fuel element.

Based on these data sources, the radius of the inner plate is 3.015 inches, while the radius of the outer plate is 5.44 inches. The gap between the plates is 0.078 inches. The thickness of the aluminum cladding is 0.015 inches.

While the thermal properties for the aluminum cladding and the fissile fuel matrix material will vary with temperature, for the purposes of this evaluation, fixed material properties are assumed in order to simplify the calculation. To provide conservatism for this modeling approach, conservatively low value is assumed for the specific heat for each component, while a conservatively high thermal conductivity value is used. This methodology will result in over-predicting the temperature rise within the composite material during the HAC fire event.

The thermal properties used in this calculation are:

- 1) Aluminum cladding thermal conductivity = 191 W/m-K, conservatively high value from [5], page 18
- 2) Fissile fuel matrix ( $UAl_x$ ) = 14.47 W/m-K, conservatively high based on equation 2.3 from [5], at 300K
- 3) Aluminum cladding density = 2702 kg/m<sup>3</sup>, from [5], page 16
- 4) Fissile fuel matrix ( $UAl_x$ ) density = 3680 kg/m<sup>3</sup>, from [5], Table 2.5, average density
- 5) Aluminum cladding specific heat = 1034 J/kg-K, from [5], Table 3.2, mean value at 600K
- 6) Fissile fuel matrix ( $UAl_x$ ) specific heat = 708 J/kg-K, from [5], Table 2.4, average value at 600K

Table 3.5-1 presents the composite thermal conductivity, specific heat, and density values for each of the nineteen (19) fuel plates making up the ATR fuel element. These composite values are based on the thermal property values given above and the geometry depicted in Figure 3.5-15.

### **Thermal Properties for MIT Fuel Plates**

Like the ATR fuel, the MIT fuel plates are a composite material consisting of a fissile fuel matrix sandwiched within an aluminum cladding. The thermal properties for the plates making up the MIT fuel element are computed using the same approach described above for the ATR fuel and the data contained in [5] and [13]. The plates have a thickness of 0.08 inches and a width of 2.526 inches. The nominal gap between the plates is 0.078 inches. Since the aluminum cladding contains 110 grooves on each side of the plate, the effective thickness of the cladding is reduced from 0.025 inches to 0.02 inches.

Table 3.5-2 presents the composite thermal conductivity, specific heat, and density values for the fifteen (15) fuel plates making up the MIT fuel element. These composite values are based on the thermal property values provided above for the ATR fuel element and the geometry described in Table 3.5-2 and depicted in Figure 3.5-16.

### **Thermal Properties for MURR Fuel Plates**

The MURR fuel plates are also a composite of a fissile fuel matrix sandwiched within an aluminum cladding. The thermal properties for the MURR fuel element are computed using the same approach described above for the ATR fuel and the data contained in [5] and [12]. The inner plate has an inner radius of 2.77 inches and an arc length of 1.993 inches, while the outer

plate has an inner radius of 5.76 inches and an arc length of 4.342 inches. The nominal gap between the plates is 0.08 inches. The thickness of the aluminum cladding is 0.01 inches.

Table 3.5-3 presents the composite thermal conductivity, specific heat, and density values for the twenty four (24) fuel plates making up the MURR fuel element. These composite values are based on the thermal property values provided above for the ATR fuel element and the geometry described in Table 3.5-3 and depicted in Figure 3.5-17.

### **Thermal Properties for TRIGA Fuel Element**

The cladding thickness for the TRIGA fuel is relatively thin and the fuel's thermal properties are dominated by the homogenous properties for the uranium-zirconium hydride fuel and the graphite materials. As such, composite properties are not required. Instead, the thermal properties listed in Table 3.2-2 for the uranium-zirconium hydride fuel and the graphite are used directly in the thermal model.

**Table 3.5-1 – Composite ATR Fuel Plate Thermal Properties**

Plate	Plate Thickness, in	UALx Thickness, in	Axial & Circumferential Conductivity (W/m-K)	Inner radius, in	Outer radius, in	Mean radius, in	Mean density, kg/m <sup>3</sup>	Mean specific heat, J/(kg K)
1	0.08	0.05	80.7	3.015	3.095	3.055	3313.3	807.7
2	0.05	0.02	120.4	3.173	3.223	3.198	3093.2	878.9
3	0.05	0.02	120.4	3.301	3.351	3.326	3093.2	878.9
4	0.05	0.02	120.4	3.429	3.479	3.454	3093.2	878.9
5	0.05	0.02	120.4	3.557	3.607	3.582	3093.2	878.9
6	0.05	0.02	120.4	3.685	3.735	3.710	3093.2	878.9
7	0.05	0.02	120.4	3.813	3.863	3.838	3093.2	878.9
8	0.05	0.02	120.4	3.941	3.991	3.966	3093.2	878.9
9	0.05	0.02	120.4	4.069	4.119	4.094	3093.2	878.9
10	0.05	0.02	120.4	4.197	4.247	4.222	3093.2	878.9
11	0.05	0.02	120.4	4.325	4.375	4.350	3093.2	878.9
12	0.05	0.02	120.4	4.453	4.503	4.478	3093.2	878.9
13	0.05	0.02	120.4	4.581	4.631	4.606	3093.2	878.9
14	0.05	0.02	120.4	4.709	4.759	4.734	3093.2	878.9
15	0.05	0.02	120.4	4.837	4.887	4.862	3093.2	878.9
16	0.05	0.02	120.4	4.965	5.015	4.990	3093.2	878.9
17	0.05	0.02	120.4	5.093	5.143	5.118	3093.2	878.9
18	0.05	0.02	120.4	5.221	5.271	5.246	3093.2	878.9
19	0.1	0.07	67.4	5.349	5.449	5.399	3386.6	786.0

**Table 3.5-2 – Composite MIT Fuel Plate Thermal Properties**

Plate	Plate Thickness, in	UALx Thickness, in	Axial and Circumferential Conductivity (W/m-K)	Plate Width, in	Mean density, kg/m <sup>3</sup>	Mean specific heat, J/(kg K)
1 to 15	0.08*	0.03	115.3	2.314	3121.1	869.3

\* - mean plate thickness estimated at 0.07 inches after allowance for ribbing

**Table 3.5-3 – Composite MURR Fuel Plate Thermal Properties**

Plate	Plate Thickness, in	UAlx Thickness, in	Axial and Circumferential Conductivity (W/m-K)	Inner radius, in	Outer radius, in	Plate Arc Length, in	Mean density, kg/m <sup>3</sup>	Mean specific heat, J/(kg K)
1	0.05	0.03	85.1	2.77	2.82	1.993	3288.8	815.1
2	0.05	0.03	85.1	2.9	2.95	2.095	3288.8	815.1
3	0.05	0.03	85.1	3.03	3.08	2.197	3288.8	815.1
4	0.05	0.03	85.1	3.16	3.21	2.300	3288.8	815.1
5	0.05	0.03	85.1	3.29	3.34	2.402	3288.8	815.1
6	0.05	0.03	85.1	3.42	3.47	2.504	3288.8	815.1
7	0.05	0.03	85.1	3.55	3.6	2.606	3288.8	815.1
8	0.05	0.03	85.1	3.68	3.73	2.708	3288.8	815.1
9	0.05	0.03	85.1	3.81	3.86	2.810	3288.8	815.1
10	0.05	0.03	85.1	3.94	3.99	2.912	3288.8	815.1
11	0.05	0.03	85.1	4.07	4.12	3.014	3288.8	815.1
12	0.05	0.03	85.1	4.2	4.25	3.116	3288.8	815.1
13	0.05	0.03	85.1	4.33	4.38	3.218	3288.8	815.1
14	0.05	0.03	85.1	4.46	4.51	3.321	3288.8	815.1
15	0.05	0.03	85.1	4.59	4.64	3.423	3288.8	815.1
16	0.05	0.03	85.1	4.72	4.77	3.525	3288.8	815.1
17	0.05	0.03	85.1	4.85	4.9	3.627	3288.8	815.1
18	0.05	0.03	85.1	4.98	5.03	3.729	3288.8	815.1
19	0.05	0.03	85.1	5.11	5.16	3.831	3288.8	815.1
20	0.05	0.03	85.1	5.24	5.29	3.933	3288.8	815.1
21	0.05	0.03	85.1	5.37	5.42	4.035	3288.8	815.1
22	0.05	0.03	85.1	5.5	5.55	4.137	3288.8	815.1
23	0.05	0.03	85.1	5.63	5.68	4.239	3288.8	815.1
24	0.05	0.03	85.1	5.76	5.81	4.342	3288.8	815.1



Security-Related Information Figure  
Withheld Under 10 CFR 2.390.

**Figure 3.5-15 – ATR Fuel Element Cross Section**

Security-Related Information Figure  
Withheld Under 10 CFR 2.390.

**Figure 3.5-16 – MIT Fuel Element Cross Section**

Security-Related Information Figure  
Withheld Under 10 CFR 2.390.

**Figure 3.5-17 – MURR Fuel Element Cross Section**

### 3.5.4 'Last-A-Foam' Response under HAC Conditions

The General Plastics LAST-A-FOAM® FR-3700 rigid polyurethane foam [18] used in the impact limiters has been used for numerous transportation packages. The FR-3700 formulation is specially designed to allow predictable impact-absorption performance under dynamic loading, while also providing a significant level of thermal protection under the HAC conditions. Upon exposure to fire temperatures, this proprietary foam decomposes into an intumescent char that swells and tends to fill voids or gaps created by free drop or puncture bar damage. This thermal decomposition absorbs a significant amount of the heat transferred into the foam, which is then expelled from the impact limiters as a high temperature gas. Because the char has no appreciable structural capacity and will not develop unless there is space available, the char will not generate stresses within the adjacent package components. Without available space the pyrolysis gases developed as a result of the charring process will move excess char mass out through the vent ports and prevent its buildup. Only as the charring process continues and space becomes available will the char be retained, filling the available space and plugging holes at the surface of the impact limiters. The thermal decomposition process does not alter or cause a chemical reaction within the adjacent materials.

The mechanisms behind the observed variations in the thermal properties and behavior of the FR-3700 foam at elevated temperatures are varied and complex. A series of fire tests [27 and 28] conducted on 5-gallon cans filled with FR-3700 foam at densities from 6.7 to 25.8 lb/ft<sup>3</sup> helped define the expected performance of the foam under fire accident conditions. Under the referenced fire tests, one end of the test article was subjected to an open diesel fueled burner flame at temperatures of 980 to 1,200°C (1,800 to 2,200 °F) for more than 30 minutes. A thermal shield prevented direct exposure to the burner flame on any surface of the test article other than the hot face. Each test article was instrumented with thermocouples located at various depths in the foam. In addition, samples of the foam were subjected to thermogravimetric analysis (TGA) to determine the thermal decomposition vs. temperature. The exposure temperatures for the TGA tests varied from 70 to 1,500 °F, and were conducted in both air and nitrogen atmospheres. The result for the nitrogen environment (see Figure 3.5-18) is more representative of the low oxygen environment existing within the impact limiter shells encasing the foam. These test results indicate that the following steps occur in the thermal breakdown of the foam under the level of elevated temperatures reached during the HAC fire event:

- Below 250 °F, the variation in foam thermal properties with temperature is slight and reversible. As such, fixed values for specific heat and thermal conductivity are appropriate.
- Between 250 and 500 °F, small variations in foam thermal properties occur as water vapor and non-condensable gases are driven out of the foam. As such, fixed values for specific heat and thermal conductivity are also appropriate for this temperature range. Further, the observed changes are so slight that the same thermal properties used for temperatures below 250 °F may also be used to characterize the thermal performance of the foam between 250 and 500 °F.
- Irreversible thermal decomposition of the foam begins as the temperature rises above 500 °F and increases non-linearly with temperature. Based on the TGA testing (see Figure 3.5-18), approximately 2/3's of this decomposition occurs over a narrow temperature range centered about 670 °F.

- The decomposition is accompanied by vigorous out-gassing from the foam and an indeterminate amount of internal heat generation. The internal heat generation arises from the gases generated by the decomposition process that are combustible under piloted conditions. However, since the decomposition process is endothermic, the foam will not support combustion indefinitely. Further, the out-gassing process removes a significant amount of heat from the package via mass transport.
- The weight loss due to out-gassing not only has direct affect on the heat flux into the remaining virgin foam, but changes the composition of the resulting foam char since the foam constituents are lost at different rates. This change in composition affects both the specific heat and the thermal conductivity of the foam char layer.
- As temperature continues to rise, the developing char layer begins to take on the characteristics of a gas-filled cellular structure where radiative interchange from one cell surface to another becomes the dominant portion of the overall heat transfer mechanism. This change in heat transfer mechanisms causes the apparent heat conductivity to take on a highly non-linear relationship with temperature.
- Finally, at temperatures above 1,250 °F, the thermal breakdown of the foam is essentially completed and only about 5 to 10% of the original mass is left. In the absence of direct exposure to a flame or erosion by the channeling of the outgas products through the foam, the char layer will be the same or slightly thicker than the original foam depth. This char layer will continue to provide radiative shielding to the underlying foam material.

Since the thermal decomposition of the foam is an endothermic process, the foam is self-extinguishing and will not support a flame once the external flame source is removed. However, the gases generated by the decomposition process are combustible and will burn under piloted conditions. A portion of these generated gases can remain trapped within the charred layer of the foam after the cessation of the HAC fire event and continue to support further combustion, although at a much reduced level, until a sufficient time has passed for their depletion from the cell structure. This extended time period is typically from 15 to 45 minutes.

The sharp transition in the state of the foam noted in Figure 3.5-18 at or about 670 °F can be used to correlate the observed depth of the foam char following a burn test with the occurrence of this temperature level within the foam. The correlation between the foam recession depth and the foam density, as compiled from a series of tests, is expressed by the relation:

$$y = -0.94581 - 11.64 \times \log_{10}(x)$$

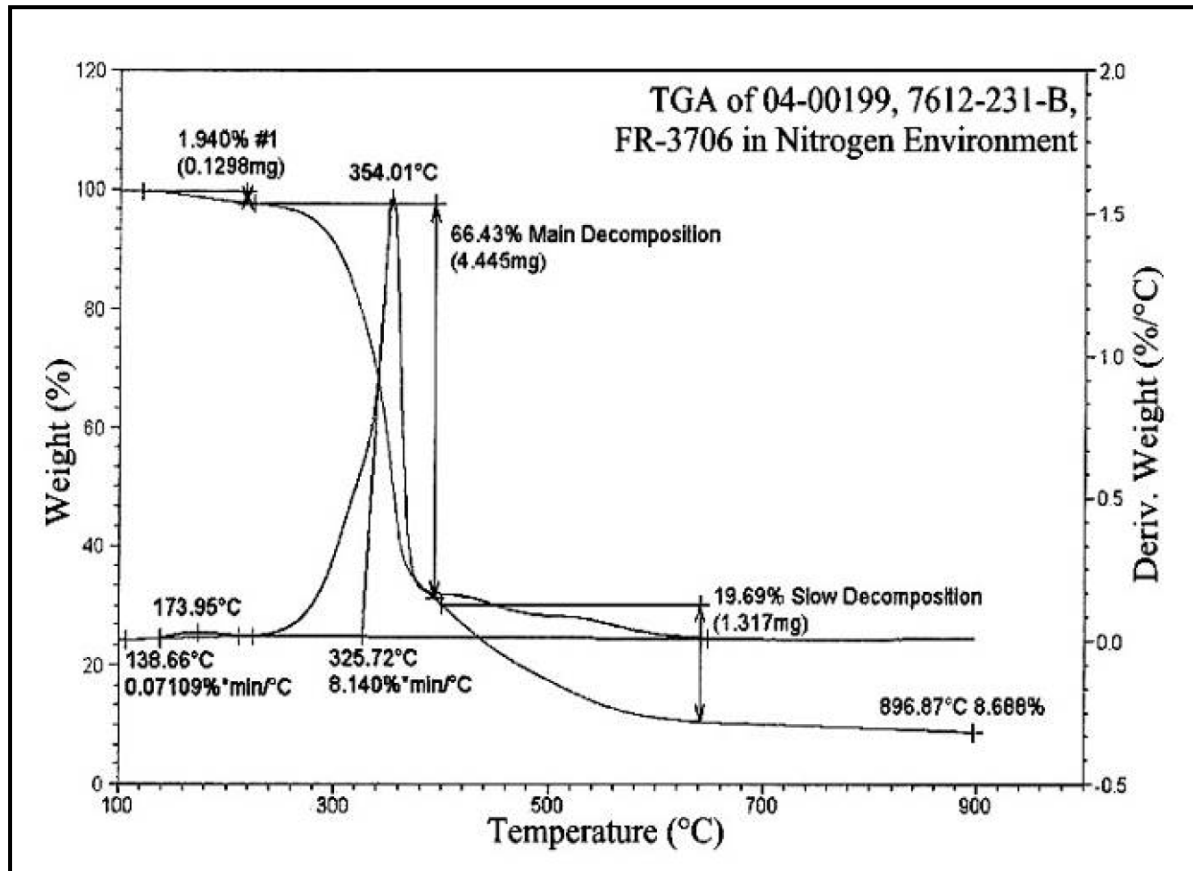
where,  $y$  = the recession depth, cm

$x$  = foam density ( $\text{g}/\text{cm}^3$ )

Based on this correlation, the recession depth expected for the nominal 9 pcf density foam used in the packaging is estimated to be 3.5 inches. The loss of foam could increase to a depth of approximately 3.8 inches for foam fabricated at the low end of the density tolerance (i.e., 7.65 pcf).

It should be noted that these results assume that the foam is enclosed within a steel shell with surface openings that are approximately 0.3 ft<sup>2</sup> or smaller. The presence of the steel enclosure helps shield the foam from the heat flux of a HAC fire event and helps contain the foam char that

is generated. Test results with and without a steel interface between the foam and the heat source indicates that the foam loss could be an additional 1.5 inches for the 7.65 pcf foam if larger face areas are exposed directly to the fire.



**Figure 3.5-18 – TGA Analysis of Foam Decomposition in Nitrogen Environment**

## 4.0 CONTAINMENT

### 4.1 Description of the Containment System

#### 4.1.1 Containment Boundary

The BRR package provides a single level of leaktight containment, defined as a leakage rate of less than  $1 \times 10^{-7}$  reference cubic centimeters per second (ref-cm<sup>3</sup>/s), air, per ANSI N14.5 [1]. The containment boundary of the BRR package consists of the following elements. Unless noted, all elements are made of ASTM Type 304 stainless steel in various product forms. A full description of the packaging is given in Section 1.2.1, *Packaging*.

- The lower massive end structure (including the passage to the drain port)
- The inner cylindrical shell
- The upper massive end structure
- The containment O-ring seal (the inner seal in the closure lid; face-type seal made of butyl elastomer)
- The closure lid
- The vent port in the closure lid (closed using a brass port plug, sealed with a butyl sealing washer)
- The drain port in the lower end structure (closed using a brass port plug, sealed with a butyl sealing washer)

The containment boundary is shown in Figure 4.1-1.

#### 4.1.2 Containment Penetrations

Besides the bolted closure lid, there are two containment penetrations: the vent port, located in the closure lid, and the drain port, located in the lower end structure, as described above. Each penetration is designed and tested to ensure leaktight sealing integrity, i.e., a leakage rate not exceeding  $1 \times 10^{-7}$  ref-cm<sup>3</sup>/s, per ANSI N14.5.

#### 4.1.3 Seals

The elastomeric portion of the containment boundary is comprised of a nominally 3/8-inch diameter, O-ring face seal located in the inner groove in the closure lid, and seal washer sealing elements (an O-ring integrated with a stainless steel washer) for the vent and drain ports. The seals are made using a butyl elastomer compound suitable for continuous use between the temperatures of -65 °F and 225 °F [2], and capable of much higher temperatures during the HAC fire case transient. Further discussion of the thermal performance capabilities of the butyl rubber seals is provided in Appendix 2.12.7, *Containment Seal Performance Tests*.

Two O-ring seals are provided in the closure lid: the inner seal is containment, and the outer forms an annular space for leakage rate testing of the containment seal. The leakage rate tests

used for various purposes are summarized in Section 4.4, *Leakage Rate Tests for Type B Packages*, and described in detail in Chapter 8, *Acceptance Tests and Maintenance Program*.

The O-ring containment seal is retained in the closure lid using a dovetail groove having a depth of  $0.284 \pm 0.003$  inches, or  $0.281 - 0.287$  inches. The O-ring has a cross sectional diameter of  $0.375 \pm 0.007$  inches, or  $0.368 - 0.382$  inches. The minimum compression corresponds to the maximum groove depth and the minimum O-ring cross-sectional diameter:

$$C_{\text{Min}} = 100 \times \left( 1 - \frac{G_{\text{Max}}}{D_{\text{Min}}} \right) = 22\%$$

where  $G_{\text{Max}} = 0.287$  inches and  $D_{\text{Min}} = 0.368$  inches. The maximum compression corresponds to the minimum groove depth and the maximum O-ring cross-sectional diameter:

$$C_{\text{Max}} = 100 \times \left( 1 - \frac{G_{\text{Min}}}{D_{\text{Max}}} \right) = 26\%$$

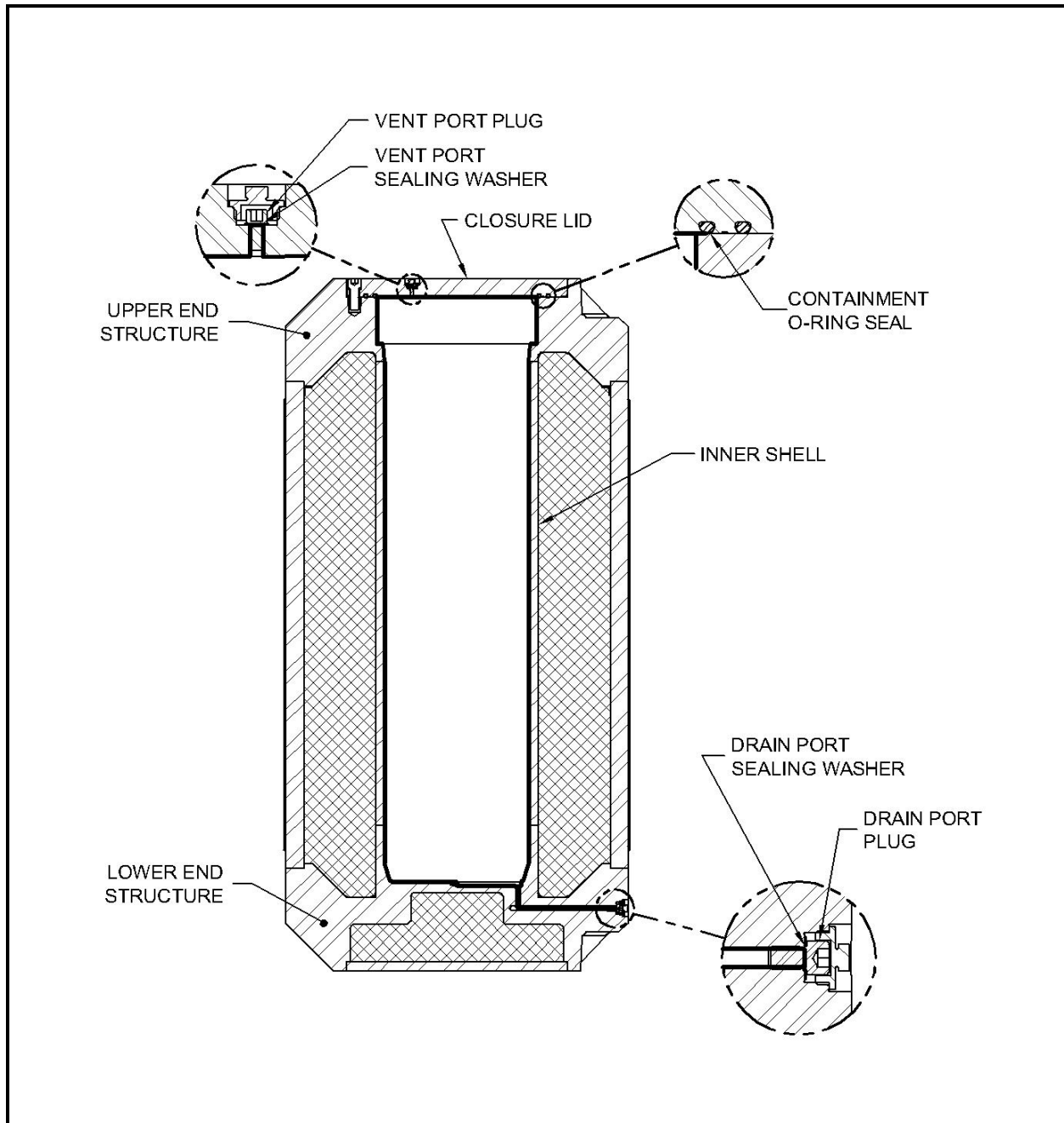
where  $G_{\text{Min}} = 0.281$  inches and  $D_{\text{Max}} = 0.382$  inches. The Parker O-ring Handbook [7] recommends a minimum compression of 16%. The limit for maximum compression is when the O-ring cross-section, adjusted for maximum temperature, fills the cross sectional area of the dovetail groove. This condition occurs for the BRR package closure O-ring at a compression of 31.2%. The compression range of 22% to 26% will therefore provide satisfactory performance of the O-ring during all NCT and HAC.

#### 4.1.4 Welds

All welds used in the containment boundary are full penetration and volumetrically inspected to ensure structural and containment integrity. The welds joining the inner shell to either end structure are ultrasonically inspected in accordance with the ASME Code, Subsection NB, Article NB-5000, and Section V, Article 4 [4]. The weld joining the inner shell and the lower end structure may be optionally radiograph inspected in accordance with the ASME Code, Subsection NB, Article NB-5000, and Section V, Article 2 [3]. All containment boundary welds are inspected by liquid penetrant inspection on the final pass in accordance with the ASME Code, Subsection NB, Article NB-5000, and Section V, Article 6 [5]. All containment boundary welds are confirmed to be leaktight as discussed in Section 8.1.4, *Fabrication Leakage Rate Tests*.

#### 4.1.5 Closure

The closure lid completes the containment boundary, and is attached to the cask body using (12) 1-8 UNC socket head cap screws tightened to  $220 \pm 20$  ft-lb. As shown in Chapter 2, *Structural Evaluation*, the closure lid cannot become detached by any internal pressure, NCT, or HAC events. The closure lid, including the vent port, is completely covered by the upper impact limiter, which is attached to the cask using eight (8) 1-inch diameter ball lock pins. Similarly, the drain port is covered by the lower impact limiter. Thus, the containment openings cannot be inadvertently opened.



**Figure 4.1-1 – BRR Package Containment Boundary**



## **4.2 Containment Under Normal Conditions of Transport**

The results of the NCT structural and thermal evaluations presented in Sections 2.6, *Normal Conditions of Transport*, and 3.3, *Thermal Evaluation Under Normal Conditions of Transport*, respectively, demonstrate that there is no release of radioactive materials per the “leaktight” definition of ANSI N14.5 under any of the NCT tests described in 10 CFR §71.71 [6].

### **4.3 Containment Under Hypothetical Accident Conditions**

The results of the HAC structural and thermal evaluations performed in Sections 2.7, *Hypothetical Accident Conditions*, and 3.4, *Thermal Evaluation Under Hypothetical Accident Conditions*, respectively, demonstrate that there is no release of radioactive materials per the “leaktight” definition of ANSI N14.5 under any of the hypothetical accident condition tests described in 10 CFR §71.73.

## 4.4 Leakage Rate Tests for Type B Packages

### 4.4.1 Fabrication Leakage Rate Tests

During fabrication, the containment boundary is leakage rate tested as described in Section 8.1.4, *Fabrication Leakage Rate Tests*. The fabrication leakage rate tests are consistent with the guidelines of Section 7.3 of ANSI N14.5. This leakage rate test verifies the containment integrity of the BRR packaging to a leakage rate not to exceed  $1 \times 10^{-7}$  ref-cm<sup>3</sup>/s, air.

### 4.4.2 Maintenance/Periodic Leakage Rate Tests

Annually, or at the time of damaged containment seal replacement or sealing surface repair, the containment O-ring seal and the vent port and drain port sealing washers are leakage rate tested as described in Section 8.2.2, *Maintenance/Periodic Leakage Rate Tests*. The maintenance/periodic leakage rate tests are consistent with the guidelines of Section 7.4 of ANSI N14.5. This test verifies the sealing integrity of the containment seals to a leakage rate not to exceed  $1 \times 10^{-7}$  ref-cm<sup>3</sup>/s, air.

### 4.4.3 Preshipment Leakage Rate Tests

Prior to shipment of the loaded BRR package, the containment O-ring seal and the vent port and drain port sealing washers are leakage rate tested per Section 8.2.2, *Maintenance/Periodic Leakage Rate Tests*. The preshipment leakage rate tests are consistent with the guidelines of Section 7.6 of ANSI N14.5. This test verifies the sealing integrity of the containment seals to a leakage rate not to exceed  $1 \times 10^{-7}$  ref-cm<sup>3</sup>/s, air.

## 4.5 Appendix

### 4.5.1 References

1. ANSI N14.5–1997, *American National Standard for Radioactive Materials – Leakage Tests on Packages for Shipment*, American National Standards Institute (ANSI), Inc.
2. Rainier Rubber Company, Seattle, WA.
3. American Society of Mechanical Engineers (ASME) Boiler and Pressure Vessel Code, Section III, *Rules for Construction of Nuclear Facility Components*, Division 1 – Subsection NB, *Class 1 Components*, and Section V, *Nondestructive Examination*, Article 2, *Radiographic Examination*, 2007 Edition.
4. American Society of Mechanical Engineers (ASME) Boiler and Pressure Vessel Code, Section III, *Rules for Construction of Nuclear Facility Components*, Division 1 – Subsection NB, *Class 1 Components*, and Section V, *Nondestructive Examination*, Article 4, *Ultrasonic Examination Methods for Welds*, 2007 Edition.
5. American Society of Mechanical Engineers (ASME) Boiler and Pressure Vessel Code, Section III, *Rules for Construction of Nuclear Facility Components*, Division 1 – Subsection NB, *Class 1 Components*, and Section V, *Nondestructive Examination*, Article 6, *Liquid Penetrant Examination*, 2007 Edition.
6. Title 10, Code of Federal Regulations, Part 71 (10 CFR 71), *Packaging and Transportation of Radioactive Material*, 01–01–08 Edition.
7. Parker O–ring Handbook, ORD–5700, Parker-Hannifin Corporation, Cleveland, OH, © 2007.

## 5.0 SHIELDING EVALUATION

The Battelle Energy Alliance (BEA) Research Reactor (BRR) Package is used to transport spent fuel from a variety of research reactors, including the University of Missouri Research Reactor (MURR), Massachusetts Institute of Technology Research Reactor (MITR-II), Advanced Test Reactor (ATR), various types of Training, Research, Isotope General Atomics (TRIGA) reactors, Rhode Island Nuclear Science Center (RINSC), University of Massachusetts at Lowell (U-Mass), Ohio State University (Ohio State), Missouri University of Science and Technology (Missouri S&T), University of Florida (U-Florida), Purdue University (Purdue), and PULSTAR.

The following analyses demonstrate that the BRR Package complies with the external radiation requirements of 10 CFR §71.47 [1]. MCNP5 v1.30 [2] is used to compute the dose rates for MURR, MITR-II, and ATR, and MCNP5 v1.51 [2] is used to compute the dose rates for the remaining fuel types. MCNP5 v1.51 is used in the newer analyses to take advantage of parallel processing.

### 5.1 Description of Shielding Design

#### 5.1.1 Design Features

The principal design features are a lead-filled shield plug, lead-filled side wall, and lead-filled bottom. The top plug consists of approximately 9.5-in lead, with a 1-in stainless steel bottom plate, and 0.5-in stainless steel top plate. The lid is constructed of stainless steel 2-in thick. The lead in the side wall of the cask is 8-in thick. The inner steel shell is 1-in thick, and the outer stainless steel shell is 2-in thick. The cask bottom consists of 7.7-in of lead through the centerline, with a 1-in stainless steel bottom cover plate, and approximately 1.2-in stainless steel inner forging.

The fuel is positioned within one of five custom-designed baskets. The baskets maintain their geometry under normal conditions of transport (NCT) and hypothetical accident conditions (HAC), as demonstrated in Section 2.7.1.5, *Fuel Basket Stress Analysis*, thereby maintaining the location of the source.

#### 5.1.2 Summary Table of Maximum Radiation Levels

Because the cask is heavy and only one cask will be transported per vehicle, exclusive use dose rate limits are applied.

Maximum NCT and HAC dose rates are reported in Table 5.1-1. MURR, MITR-II, ATR, and TRIGA fuel are transported in baskets custom designed for each fuel type. The remaining “square” fuels are transported in the square fuel basket (SFB). The square fuels include RINSC, U-Mass (aluminide fuel matrix), U-Mass (silicide fuel matrix), Ohio State, Missouri S&T, U-Florida, Purdue, the loose plate box, and PULSTAR. The loose plate box contains up to 31 loose plates from U-Mass (aluminide), U-Florida, or Purdue.

The fuel type associated with each dose rate is provided in the table. Because the geometry of the source, basket design, and source strength vary widely between the fuel types, no one fuel type may be considered bounding at all dose rate locations. MITR-II is bounding at the top, while TRIGA is bounding at the remaining locations.

**BRR Package Safety Analysis Report**

---

The cask is transported in a vertical orientation in an open vehicle. Because the transport vehicle is open, the dose rate limit is 200 mrem/hr at both the package and vehicle surfaces. The vehicle is assumed to be 8 feet wide, and the vehicle side surface is the projection at this distance. The top and bottom vehicle surfaces are assumed to correspond to the top and bottom of the impact limiters, although the vehicle does not have a top because it is open. The 2 m dose rate is computed 2 m from the vehicle side, while the occupied location (i.e., the driver) is computed 25 feet (7.6 m) from the centerline of the cask.

Dose rates are relatively low. Under NCT, the maximum package surface dose rate is 68.1 mrem/hr, the maximum vehicle surface dose rate is 9.9 mrem/hr, the maximum dose rate 2 m from the vehicle surface is 1.2 mrem/hr, and the dose rate in the occupied location is 0.2 mrem/hr. Under HAC, the maximum dose rate at 1 m from the package is 6.1 mrem/hr.

**Table 5.1-1 – Summary of Maximum Total Dose Rates (Exclusive Use)**

<b>NCT</b>	<b>Package Surface (mrem/hr)</b>			<b>Vehicle Surface (mrem/hr)</b>		
<b>Fuel→</b>	<b>MITR-II</b>	<b>TRIGA</b>	<b>TRIGA</b>	<b>MITR-II</b>	<b>TRIGA</b>	<b>TRIGA</b>
<b>Radiation</b>	<b>Top</b>	<b>Side</b>	<b>Bottom</b>	<b>Top</b>	<b>Side</b>	<b>Bottom</b>
Gamma	9.7	4.9	2.3	9.7	0.8	2.3
Neutron	0.2	63.1	4.1	0.2	8.4	4.1
Total	9.9	68.1	6.5	9.9	9.2	6.5
Limit	200	200	200	200	200	200

<b>NCT</b>	<b>2 m from Vehicle Surface (mrem/hr)</b>			<b>Occupied Location (mrem/hr)</b>
<b>Fuel→</b>	<b>NA</b>	<b>TRIGA</b>	<b>NA</b>	<b>TRIGA</b>
<b>Radiation</b>	<b>Top</b>	<b>Side</b>	<b>Bottom</b>	<b>Side</b>
Gamma	NA	0.1	NA	0.02
Neutron	NA	1.1	NA	0.2
Total	NA	1.2	NA	0.2
Limit	10	10	10	2

<b>HAC</b>	<b>1 m from Package Surface (mrem/hr)</b>		
<b>Fuel→</b>	<b>MITR-II</b>	<b>TRIGA</b>	<b>TRIGA</b>
<b>Radiation</b>	<b>Top</b>	<b>Side</b>	<b>Bottom</b>
Gamma	2.7	0.5	0.9
Neutron	0.1	5.5	1.2
Total	2.8	6.1	2.1
Limit	1000	1000	1000

Note: The total dose rate is the sum of unrounded values.

## 5.2 Source Specification

A neutron and gamma source term is developed for each of the fuel types. All source terms are developed using the TRITON sequence of SCALE6 [3].

### 5.2.1 Gamma Source

#### 5.2.1.1 MURR Fuel

The MURR gamma source term is generated by the TRITON sequence of SCALE6. TRITON is a control module that coordinates program flow between the SCALE6 modules involved in the depletion sequence, primarily NEWT and ORIGEN-S.

The TRITON sequence uses a predictor-corrector approach. The two-dimensional discrete ordinates module NEWT calculates the burnup-dependent flux distribution across the fuel element, which is collapsed to three groups for input to the ORIGEN-S depletion module. The first NEWT calculation is performed using the 238-group ENDF/B-VII cross-section library. This flux distribution is then used to collapse the 238-group cross-section library to 49 groups to accelerate subsequent NEWT calculations. Therefore, the 49-group library is problem-dependent. The fuel is depleted over a specified time interval, and the depleted mixture is then used as input to the subsequent NEWT flux calculation. The number of time steps is determined by the user-defined input. One library generation per fuel cycle is the default, although more steps may be requested to improve accuracy. A more detailed discussion of the predictor-corrector approach of the TRITON sequence may be found in Section T.1.2.3 of the TRITON user's manual [3]. An annotated TRITON input file is included in Section 5.5.3.1, *TRITON Input File*. A discussion of this input file follows.

The two-dimensional NEWT model of the MURR fuel element has been simplified compared to the actual fuel element geometry. The MURR fuel element has 24 curved plates, although these plates are modeled as flat in NEWT. Only half of the fuel element is modeled, taking credit for symmetry. In the actual fuel element, the arc length of the fuel meat is different for each plate. To simplify the NEWT model, one-half the average fuel meat arc length is modeled for all 24 plates. Therefore, it is necessary to define only one fuel plate, and then repeat this fuel plate in a 1x24 array. All relevant data used to develop the TRITON model is shown in Table 5.2-1. The NEWT model geometry is shown in Figure 5.2-1.

The nominal fuel meat arc length for each plate is provided in Table 6.9-3 of Chapter 6, *Criticality Evaluation*. Based on these nominal arc lengths, the average fuel meat arc length is 2.882-in. The nominal fuel meat thickness is 0.02-in, and the nominal plate thickness is 0.05-in. The nominal channel thickness between plates is 0.08-in, so the nominal pitch is  $0.05 + 0.08 = 0.13$ -in. These parameters are used as input both in the NEWT model and the LATTICECELL card.

Three materials are modeled; fuel, cladding, and moderator. The number densities of the fuel are computed based on the fuel loading and fuel meat volume. The density of the fuel meat is estimated using the equation listed in Table 6.2-5 of Chapter 6, *Criticality Evaluation*, using the known density of U-235. Aluminum and water are modeled as pure. Temperatures for the fuel, cladding, and water during reactor operation are typical values for this reactor.



The MURR fuel element has a fuel loading of  $775.0 \pm 7.8$  g U-235. Two TRITON models are developed, one for the minimum fuel loading (767.2 g U-235), and a second for the maximum fuel loading (782.8 g U-235). The U-235 nominal enrichment is 93%. The balance of uranium is modeled as U-238. The fuel is burned in 21 cycles. The first 20 cycles are 7 days in duration, and the final cycle is 4 days in duration, giving a total irradiation time of 144 days. The total core power is 10.0 MW, with 8 fuel elements, so the average element power is 1.25 MW. A peak fuel element could have a power greater than 1.25 MW for any particular cycle, but because no fuel element is ever maintained at the peak power throughout its entire life, modeling an average value of 1.25 MW is conservative. For an element power of 1.25 MW, the total burnup is 180 MWD. Power is input to TRITON in units of MW/MTU. Two weeks of cooling is assumed between each cycle. The source is allowed to cool 180 days after reactor shutdown.

The fuel cycle is modeled as an extreme case of the MURR fuel cycle. Unlike many other research reactors, MURR does not use a once-through fuel cycle. Each fuel element is cycled in and out of the core several times before reaching the final discharge burnup. Typically, a given fuel element is irradiated in several 6.2 to 6.5-day periods with varying cooling (non-irradiation) times in between the irradiation periods. For this calculation, the fuel assembly is irradiated in 7.0-day periods in a one-week-in and two-week-out pattern until the fuel is discharged. This overestimates the source term since MURR fuel elements generally remain outside the core for several weeks at a time during their active life and are never cycled in and out of the core continuously until discharge. Therefore, the irradiation parameters utilized result in a source term that bounds any expected MURR fuel element.

The OPUS module of SCALE6 is used to extract key data from the output, including decay heat, U-235 mass, plutonium activity, and the source term. Note that all TRITON output uses a basis of 1 MTU because the specific power must be input in units of MW/MTU. Therefore, the results must be multiplied by the fuel loading (in MTU) of the fuel element to obtain the desired results for a single fuel element.

The gamma source term for both the maximum and minimum fuel loadings are nearly identical (within 0.02%), although the source term computed for the minimum fuel loading is slightly higher. The MURR gamma source computed with the minimum fuel loading is summarized in Table 5.2-3. Note that the MURR basket may transport up to eight fuel elements.

A representative axial burnup distribution is provided in Table 5.2-4. This distribution is the ratio of the burnup in each segment to the average burnup.

Key output data are summarized in Table 5.2-2. The fuel depletion may be computed based on the initial and final U-235 mass. The initial U-235 mass is 767.2 g, and the final U-235 mass is 530.4 g, or a depletion of 30.9%. The decay heat at a decay time of 180 days is 147.6 W.

### **5.2.1.2 MITR-II Fuel**

The MITR-II gamma source term is generated by the TRITON sequence in the same manner as MURR fuel. Data used to develop the TRITON model is summarized in Table 5.2-1, and the NEWT model for MITR-II is shown in Figure 5.2-2. An actual MITR-II fuel element has a trapezoidal design, although the fuel is modeled in NEWT as a simple rectangle for simplicity. The MITR-II fuel element has a loading of  $510.0 +3/-10$  g U-235. Two TRITON models are developed, one for the minimum fuel loading (500.0 g U-235), and a second for the maximum

fuel loading (513.0 g U-235). The U-235 nominal enrichment is 93%. The balance of uranium is modeled as U-238.

The fuel is burned in six cycles, with 7 days between cycles. The first 5 cycles have an irradiation time of 120 days, and the last cycle has an irradiation time of 60 days, for a total irradiation time of 660 days. The average fuel element power is 0.25 MW for a 6.0 MW reactor with 24 fuel elements. A peak fuel element could have a power greater than 0.25 MW for any particular cycle, but because no fuel element is ever maintained at the peak power throughout its entire life, modeling an average value of 0.25 MW is conservative. Therefore, for an element power of 0.25 MW, the burnup is 165 MWD. The irradiation time is highly conservative because the MITR-II reactor typically operates on a monthly cycle, and operates only 300 days per year. The source is allowed to cool 120 days after reactor shutdown.

The MITR-II gamma source is summarized in Table 5.2-3. Consistent with the MURR gamma source, the source is slightly larger using the minimum fuel loading. Note that the MITR-II basket may transport up to 8 fuel elements.

The axial burnup distribution is provided in Table 5.2-5. This distribution is the ratio of the burnup in each segment to the average burnup. A symmetric distribution is utilized. Because the widths of the distribution are not constant (the end segments are half the width of the remaining segments), the distribution input to MCNP must be divided by 2 for the end regions, as indicated in the last column in the table.

Key output data are summarized in Table 5.2-2. The fuel depletion may be computed based on the initial and final U-235 mass. The initial U-235 mass is 500.0 g, and the final U-235 mass is 280.6 g, or a depletion of 43.9%. The decay heat at a decay time of 120 days is 142.5 W.

### 5.2.1.3 ATR Fuel

The ATR gamma source term is generated by the TRITON sequence in the same manner as MURR and MITR-II fuel. Data used to develop the TRITON model is summarized in Table 5.2-1, and the NEWT model for ATR is shown in Figure 5.2-3. An ATR fuel element is similar in geometry to a MURR fuel element, although an ATR fuel element has 19 fuel plates instead of 24. The NEWT model uses the same base assumption as the MURR model that the plates may be modeled as flat using the average half-width of the fuel meat. The average fuel meat arc length is 2.65-in (see Table 6.9-1 in Chapter 6, *Criticality Evaluation*).

There are two general classes of ATR fuel element, XA and YA. The XA fuel element has a fresh fuel loading of  $1,075 \pm 10$  g U-235. The XA fuel element is further subdivided into fuel element types 7F, 7NB, 7NBH. In the 7F fuel element, all 19 fuel plates are loaded with enriched uranium in an aluminum matrix with the eight outer plates (1 through 4 and 16 through 19) containing boron as a burnable poison. The fuel element 7NB contains no burnable poison. The 7NBH fuel element is similar to the 7NB fuel element except that it contains one or two borated plates. The YA fuel element is identical to the 7F fuel element except that plate 19 of the YA fuel element is an aluminum alloy plate containing neither uranium fuel nor boron burnable poison. The YA fuel element has a fresh fuel loading of  $1,022.4 \pm 10$  g U-235.

ATR fuel has an additional complexity that each fuel plate has different uranium number densities. The U-235 number densities in plates 5 through 15 are approximately constant, although the U-235 number densities in plates 1 through 4 and 16 through 19 are reduced. In the NEWT models, all 19 plates are assigned the same number densities for simplicity, although the

total fuel loading is preserved. This level of detail is sufficient to generate a source term for shielding applications, especially since that the ATR fuel element is homogenized in the MCNP shielding model.

Both the XA type 7NB and 7F fuel elements are modeled in TRITON. The B-10 loading of the type 7F element is 660 mg (which has been conservatively rounded up to 700 mg), and for simplicity is distributed evenly throughout all 19 plates rather than only on the eight outer plates. The 7NBH element is bounded by the 7F element. The XA element bounds the YA element because the fission density (fissions/cm<sup>3</sup>) limit is the same for both fuel types, and the type XA element has a larger fuel volume than the type YA element.

Fuel plate 1 is nominally 0.080-in thick, fuel plates 2 through 18 are nominally 0.050-in thick, and fuel plate 19 is nominally 0.100-in thick. In the TRITON models, 0.050-in is used for all plates for simplicity. The fuel meat is nominally 0.02-in thick for all 19 plates. Channels 2 through 10 have a nominal width of 0.078-in, while channels 11 through 19 have a nominal width of 0.077-in. The channel width is modeled at 0.078-in between all plates for simplicity. Therefore, the pitch is  $0.05+0.078 = 0.128$ -in.

Three TRITON models are developed:

- Type 7NB, minimum fuel loading (1065.0 g U-235),
- Type 7NB, maximum fuel loading (1085.0 g U-235),
- Type 7F, minimum fuel loading (1065.0 g U-235),

The U-235 nominal enrichment is 93%. The balance of uranium is modeled as U-238.

The burnup parameters are selected to bound the highest burned ATR fuel element ever generated. This element had a starting U-235 loading of 1075 g, and a final U-235 loading of 457 g, or a depletion of 57.5%. The fuel is burned in one continuous cycle for 48 days to achieve approximately the same level of depletion of the highest burned ATR element. A bounding element power of 10 MW is utilized, for a total burnup of 480 MWD<sup>1</sup>. The source is allowed to cool 1670 days after reactor shutdown.

The fuel cycle modeled is an extreme case of the ATR fuel cycle. The ATR reactor consists of 5 lobes of 8 fuel elements each, and the maximum lobe power is 60 MW (total reactor power is limited to 250 MW). Therefore, the average power in a maximum power lobe is 7.5 MW, although the maximum fuel element power may be in the range from 8 to 9 MW. A fuel element power of 10 MW is conservatively modeled. Likewise, a typical cycle length is in the range from 49 to 56 days, while 48 days is modeled. To completely burn a fuel element would typically require a minimum of three cycles, and any down time between cycles has been conservatively ignored in the calculation.

The ATR gamma source is summarized in Table 5.2-3. Note that the ATR basket may transport up to eight fuel elements.

The axial burnup distribution provided in Table 5.2-6 is simply assumed based upon a peak of 1.45 at the axial center. This distribution is the ratio of the burnup in each segment to the

---

<sup>1</sup> The element burnup of 480 MWD should not be a limit for licensing purposes because the element burnup is typically not known in units of MWD. ATR staff compute and report the final U-235 mass within an element.

**BRR Package Safety Analysis Report**

average burnup. The distribution is divided over 10 segments of equal width over the fuel length of 48-in (121.92 cm).

Key output data are summarized in Table 5.2-2. The fuel depletion may be computed based on the initial and final U-235 mass. The initial U-235 mass is 1065.0 g, and the final U-235 mass is 440.5 g, or a depletion of 58.6%. The decay heat at a decay time of 1670 days is 29.8 W.

**5.2.1.4 TRIGA Fuel**

Twenty-six (26) different TRIGA element types are evaluated. These element types are identified by their General Atomics catalog number. Key parameters for the TRIGA elements are summarized in Table 5.2-7. These TRIGA elements fall into five general categories:

- Standard (100 series)
- Instrumented (200 series). Instrumented rods contain thermocouples used to measure temperature during reactor operation. The fueled region is essentially the same as a standard rod, although instrumented rods may be longer.
- Fueled Follower Control Rods (FFCR) (300 series). FFCR rods contain boron carbide neutron absorber outside the active fuel region.
- Cluster rods (400 series). Typically three or four cluster rods are used to build a cluster assembly. For transportation in the BRR package, the cluster rods are disassembled from the cluster assembly.
- Instrumented cluster rods (500 series). Instrumented rods contain thermocouples used to measure temperature during reactor operation. The fueled region is essentially the same as a standard cluster rod, although instrumented cluster rods may be longer.

The data in Table 5.2-7 is used to build TRITON models for the various TRIGA elements. The objective is to determine a bounding source term to use in the TRIGA dose rate calculations. The maximum decay heat is limited to 20 watts per element by the thermal analysis in Chapter 3, *Thermal Evaluation*. Because the BRR package is highly shielded, the source term is limited by decay heat rather than dose rate.

It is desired to transport the fuel using the shortest possible cooling time. For each fuel type, the fuel is burned to a high value of ~80% U-235 depletion, and the fuel is cooled until the decay heat does not exceed 20 watts. The cooling time typically exceeds 90 days for ~80% depletion. The burnup is then incrementally reduced until a 90 day cooling time is achieved for the same decay heat.

To simplify the analysis, the set of 26 TRIGA elements is reduced to 16 elements. The 200 series instrumented elements bound the equivalent 100 series standard elements. Also, the 500 series instrumented cluster elements bound the equivalent 400 series cluster elements.

TRIGA reactors tend to run only sporadically rather than continuously, and TRIGA fuel elements often have residence times exceeding 10 years [4]. Following the guidance of [4], a short irradiation time of 4 years (1461 days) is used for all inputs. This irradiation time is expected to bound actual TRIGA elements encountered in the field. Because the irradiation time is treated as a fixed quantity, the specific power (MW/MTU) is input to give the desired burnup. TRIGA rods with a residence time of less than 4 years may produce decay heats that exceed the TRITON computed values.

**BRR Package Safety Analysis Report**

Most TRIGA elements have stainless steel cladding and end caps. Stainless steel results in a Co-60 source when irradiated, mostly due to activation of a Co-59 impurity. The Co-59 impurity in stainless steel is 800 ppm [7]. Co-60 is also generated by an (n,p) reaction with Ni-60, which is a basic component of stainless steel. The Co-60 activation source is accounted for in TRITON by adding Co-59 and Ni-60 to the TRACE block.

From [4], the mass of stainless steel in the stainless steel clad standard rod (Type 103) is 800 g. This rod is 29.15-in long. It is assumed that all TRIGA rods with a length < 30-in will have 800 g stainless steel. The longest rods have an overall length of 45.5-in. The difference in length is 45.5-in – 29.15-in = 16.35-in. If it is assumed that the end cap mass remains the same for a longer element, the increase of stainless steel mass is due to the increased cladding length, or 195 g based on a stainless steel density of 7.94 g/cm<sup>3</sup> and the cladding dimensions in Table 5.2-7. The total stainless steel mass for the 45.5-in long rod is then 800 g + 195 g = 995 g, or 1000 g. Due to the increased cladding length, it is assumed that all rods with a length > 30-in have 1000 g stainless steel.

When computing the source term from activated hardware (such as stainless steel), it is customary to take credit for the reduced neutron flux outside of the active fuel region. Outside of the 15-in active fuel, the flux will decrease. For commercial PWR and BWR fuel, this scaling factor ranges from 0.1 to 0.2 [8]. For TRIGA fuel, a scaling factor of 0.2 is applied for stainless steel outside the active fuel region. Much of the stainless steel mass outside the active fuel region is concentrated in the end caps, which are typically at least 7-in from the active fuel region for a standard rod and as much as 15-in from the active fuel for an instrumented rod. Therefore, an effective mass of stainless steel is used to compute the Co-59 and Ni-60 inputs. The effective mass is defined as  $M_{AF} + 0.2 \cdot M_O$ , where  $M_{AF}$  is the steel mass in the active fuel region and  $M_O$  is the steel mass outside the active fuel region.

TRIGA reactors are highly standardized and the elements may be arranged in either a circular or hexagonal lattice. The pitch for a circular lattice is variable, with an average pitch of 4.052 cm and a minimum pitch of 3.885 cm. The pitch for a hexagonal lattice is 4.354 cm. The minimum fuel element pitch of 3.885 cm is used in the TRITON models for the 100, 200, and 300 series elements and is modeled as a hexagonal lattice, see Figure 5.2-4. Minimizing the pitch is conservative for source term generation, as the harder neutron spectrum leads to more absorption in U-238, resulting in enhanced curium production. Curium is the primary contributor to the neutron source, which dominates the TRIGA dose rate for high-burnup elements.

Conversion reactors are reactors originally designed to use plate fuel but converted to use TRIGA fuel. Cluster assemblies used to replace plate fuel are typically comprised of four TRIGA elements arranged in a square lattice. The 400 and 500 series elements are part of a cluster assembly. The square pitch between fuel elements in a cluster assembly is 3.886 cm. This square pitch is used in the TRITON models for the 400 and 500 series cluster elements, see Figure 5.2-5.

The fuel, cladding, and water temperatures are representative. The temperatures for the fuel, cladding, and water are 333 K, 323 K, and 293 K, respectively.

Based on the above considerations, gamma (and neutron) sources are computed for each TRIGA element type for a variety of burnups and cooling times. For each element type, the maximum burnup (in MWD), minimum cooling time (in days), and decay heat are summarized in Table 5.2-8. This table may be used to qualify TRIGA fuel to be shipped. Because this table is

developed for a minimum in-core residence time of 4 years, for fuel with an in-core residence time less than 4 years, the decay heat should be independently confirmed to be  $\leq 20$  watts.

From the large number of sources used to generate Table 5.2-8, a single bounding TRIGA source is selected for detailed dose rate calculations. The bounding source is determined using the computed gamma and neutron sources, although neutron sources are summarized in a subsequent section (see Section 5.2.2, *Neutron Source*). To determine the bounding TRIGA source, a detailed MCNP model is developed to determine which source maximizes the dose rate on the surface of the BRR package. This MCNP model is described in detail in Section 5.3, *Shielding Model*. In the MCNP model, element Type 109 materials and geometry are modeled explicitly and the source is distributed evenly throughout the fuel matrix. Element Type 109 materials and geometry are modeled in MCNP because it has the highest U-235 enrichment (70%) of all TRIGA elements and the criticality analysis demonstrated it is the most reactive (see Chapter 6, *Criticality Evaluation*). Because the fuel matrix is conservatively modeled as fresh in MCNP, subcritical neutron multiplication is maximized using the most reactive element. The dose rate due to TRIGA fuel is dominated by neutron radiation for the high-burnup elements because the neutron source increases substantially at high burnups and the BRR package does not have a hydrogenous neutron shield. Although Type 109 materials and geometry are modeled in MCNP, the source term modeled represents the TRIGA element under consideration.

The dose rates computed at the side of the cask for each TRIGA source are provided in Table 5.2-8. The maximum package surface dose rate of 61.6 mrem/hr occurs for Type 219 with a burnup of 122 MWD and a cooling time of 600 days. This dose rate is dominated by neutron radiation due to the high burnup. TRIGA Type 219 has the largest uranium loading of all TRIGA elements considered (825 g U) and the largest burnup (in MWD).

The presence of erbium is ignored for simplicity when developing the source terms used to generate Table 5.2-8. However, as indicated in Table 5.2-7, elements with higher U-235 loadings contain erbium to hold down the reactivity. For the bounding TRIGA element Type 219, the fuel matrix contains 0.9 wt.% erbium. The presence of a thermal absorber hardens the neutron spectrum and enhances curium production, which is the primary contributor to the neutron source. Therefore, a TRITON model is developed for element Type 219 with 0.9 wt.% erbium in the fuel matrix. With erbium in the fuel matrix, the neutron source increases and the side dose rate increases slightly to 64.9 mrem/hr.

Note that the dose rates used to rank the candidate source terms are not the final licensing dose rates. The dose rates for licensing purposes are computed in Section 5.4.4, *External Radiation Levels*, with a more detailed tally structure and source definition.

The gamma source term for Type 219 (with erbium) contains 32 Ci of Co-60, which is concentrated in the fuel cladding. The cladding source term may be separated from the fuel matrix source term. The design basis TRIGA gamma source for the cladding and fuel matrix is summarized in Table 5.2-9.

No axial burnup profile is provided for TRIGA fuel. However, a U-235 depletion of ~80% is assumed along the entire active length of the fuel, and it is not expected a depletion of ~80% would be exceeded at any point along the active fuel length. Therefore, modeling the axial profile as flat is appropriate.

### 5.2.1.5 Square Fuel Basket Fuels

The Square Fuel Basket (SFB) is used to transport fuel that has a nominal square geometry, including plate fuel, the loose plate box, and PULSTAR fuel. The heat load of the SFB is limited to 30 watts per compartment. The flat plate fuels include RINSC, U-Mass (aluminide), U-Mass (silicide), Ohio State, Missouri S&T, U-Florida, and Purdue. The flat plate fuels are 20% enriched. A loose plate box is used to transport up to 31 loose plates per box. Loose plates are limited to U-Mass (aluminide), U-Florida, and Purdue fuel plates. PULSTAR fuel is similar to light water reactor fuel, as it has a  $\text{UO}_2$  fuel matrix, cylindrical fuel rods, and an enrichment between 4 and 6%.

U-Mass (aluminide) fuel originally was manufactured for the Worcester Polytechnic Institute (WPI) reactor, although the fuel has been transferred to U-Mass. This fuel may have been partially burned in the WPI reactor before being transferred to U-Mass for further irradiation. The burnup limit for this fuel element is the total combined burnup for the WPI and U-Mass reactors.

The source term for each of these fuels is computed using TRITON. It is confirmed that the decay heat is less than 30 watts for the irradiation history and minimum required cooling time of the host reactors. The maximum burnups and minimum cooling times are determined from consultations with the host reactor staff to meet their programmatic needs.

All of these research reactors are operated on an as-needed basis. Reactors are typically operated less than or equal to 8 hours per day and less than or equal to 40 hours per week. Therefore, the in-core residence time is long and the power history is sporadic. A conservative power history is modeled by assuming the reactor is operated continuously at the maximum power until the desired maximum burnup is achieved.

An exception is made for RINSC fuel because a continuous power history at maximum power leads to unrealistically high decay heat values. For RINSC fuel, it is assumed that the reactor is operated 40 hours per week at maximum power (0.14 MW per fuel element) until the maximum burnup is achieved (52.5 MWD), which results in an in-core residence time of 1575 days. For simplicity, the irradiation is modeled in TRITON as continuous but with a reduced power of 0.0333 MW to give the desired burnup. This power history conservatively bounds the true irradiation history, which would be longer.

Key TRITON input data for the seven flat-plate fuel elements is summarized in Table 5.2-10. The maximum burnup is defined in units of MWD. Based on the MURR, MITR-II, and ATR results summarized in Table 5.2-2, it is slightly more conservative to model the minimum U-235 loading rather than the maximum U-235 loading, although the effect is small. Therefore, the minimum U-235 loading is modeled in TRITON for the Square plate fuels.

Decay heat and depletion results for the seven flat plate elements are summarized in Table 5.2-11. The thermally hottest flat plate element is RINSC, with a decay heat of 22.5 watts. The fuel element with the largest burnup is U-Florida (87 MWD), with a U-235 depletion of 60.1%. However, because the power of the U-Florida reactor is low and the irradiation time is long, the decay heat of the U-Florida assembly is only 5.1 watts, which is relatively low. The gamma source terms for the flat plate elements are summarized in Table 5.2-12.

The only three loose plate types authorized for the loose plate box are U-Mass (aluminide), U-Florida, and Purdue, as indicated in Table 5.2-11. The loose plate box is limited to 31 plates per

box. Therefore, the maximum decay heat of a loose plate box is 11.4 watts, which is based on 31 U-Florida plates. This decay heat is significantly less than the limit of 30 watts. It may be observed from Table 5.2-11 that U-Florida is the bounding plate that may be transported in the loose plate box, as U-Mass (aluminide) and Purdue both have low burnups and low decay heats. Because the U-Florida fuel element has 14 plates and the loose plate box is limited to 31 plates, the loose plate box source magnitude is  $31/14 = 2.2$  times the strength of the U-Florida fuel element source.

All the flat plate fuels have an active fuel length of approximately 23-in and are expected to have similar axial burnup profiles. For simplicity, the U-Mass profile is assumed to be a reasonable representation for all of the flat plate fuels. This profile is provided in Table 5.2-13. The burnup profile is renormalized to 1.000, and this renormalized profile is the gamma axial source distribution because the gamma source is proportional to the burnup profile. For convenience, the neutron axial source distribution is included in Table 5.2-13, although the derivation of this profile is discussed in Section 5.2.2, *Neutron Source*.

Key TRITON input data for PULSTAR fuel is summarized in Table 5.2-14. A bounding fuel pellet density is utilized to maximize the source. Two PULSTAR designs are considered, which are identical except for the U-235 enrichment. The enrichments are 4% and 6%. PULSTAR fuel is similar in design to standard PWR fuel. The fuel matrix is  $\text{UO}_2$  fuel rods with zirconium alloy cladding. The fuel rods are arranged in a 5x5 lattice, with an x-pitch of 0.607-in and a y-pitch of 0.525-in. The fuel lattice is surrounded by a zirconium alloy box. The active fuel length is approximately 24-in, which is similar to the flat plate fuels. The maximum fuel element burnup is 20,000 MWD/MTU with a minimum cooling time of 1.5 years. Because the active fuel length is similar to the flat plate fuels, the same axial burnup profile may be applied. A sketch for PULSTAR fuel is provided in Figure 5.2-6, and the TRITON model is shown in Figure 5.2-7.

Decay heat and depletion results for the two PULSTAR element types are summarized in Table 5.2-15. The decay heat of the two PULSTAR fuel element types is similar, although the 4% enriched case has a slightly larger decay heat of 24.6 watts. This decay heat is less than the limit of 30 watts. While the burnups of the two fuel element types is the same, the 4% enriched fuel has a larger percent U-235 depletion because the initial U-235 mass is much smaller than the 6% enriched case. The gamma source terms for the two PULSTAR element types are summarized in Table 5.2-16.

## 5.2.2 Neutron Source

The neutron sources are extracted from the same output files that define the gamma sources, as described in Section 5.2.1, *Gamma Source*. The neutron source for MURR, MITR-II, ATR, and TRIGA are presented in Table 5.2-17. The neutron sources presented are the combined spontaneous fission and  $(\alpha, n)$  components. Aluminum in the fuel matrix is used as the target nucleus to generate the  $(\alpha, n)$  source for the MURR, MITR-II, and ATR fuels. For the TRIGA fuels, essentially no  $(\alpha, n)$  target nuclides are present in the fuel matrix, and the neutron source is primarily due to spontaneous fission. The TRIGA neutron source is based upon TRIGA element Type 219.

The neutron sources for MURR, MITR-II, and ATR are extracted from the minimum fuel loading models, consistent with the gamma sources. However, while the fuel loading had essentially no effect on the gamma source, the neutron source is noticeably larger when the



minimum fuel loading is utilized. For these fuels, the increase in neutron source strength when using the minimum fuel loading rather than maximum fuel loading is approximately 1 to 3%.

The neutron sources for MURR, MITR-II, ATR, and TRIGA fuel are input with the same axial distribution provided in Section 5.2.1, *Gamma Source*. These fuel types are high-enriched and have relatively small neutron sources, as the primary contributors to the neutron source are Cm-242 and Cm-244. Curium arises from the capture chain of U-238 and the subsequent plutonium cycle, and little U-238 is present in the high-enriched elements.

The U-235 enrichment for the Square plate fuels is 20%, and the minimum U-235 enrichment for the PULSTAR fuel is 4%. Therefore, these fuel types will have a much larger neutron source compared to the high-enriched fuels, and the axial source distribution of the neutron source is treated explicitly.

Curium production in a fuel element is non-linear with burnup and is approximately proportional to the 4<sup>th</sup> power of the burnup [9]. Therefore, low-burnup elements have small neutron sources while high-burnup elements have significantly larger neutron sources. In a fuel element, the burnup is higher in the middle and lower at the ends, and the neutron axial source distribution is significantly more peaked than the gamma axial source distribution. The neutron axial source distribution may be estimated by raising the gamma axial source distribution to the 4<sup>th</sup> power. The neutron axial source distribution is provided in Table 5.2-13 for the flat plate fuels.

When using a two-dimensional source generation program such as TRITON, the neutron source is generated for a flat axial burnup profile. However, due to the non-linear behavior of the neutron source with burnup, the neutron source for a fuel element with an axial burnup profile is larger than the source computed by TRITON because the burnup in the central portion is larger than the average burnup. The ratio of the true neutron source to the TRITON computed neutron source is estimated as the average value of the neutron source distribution, or 1.586 from Table 5.2-13. This neutron source peaking factor is applied to the Square plate element neutron source magnitudes computed by TRITON, as shown in Table 5.2-18.

It is observed that U-Florida has the largest neutron source of the flat plate fuels due to the high burnup value. For U-Florida, approximately 85% of the neutron source is due to ( $\alpha$ ,n) reactions in the aluminum and silicon in the fuel matrix, while only 15% is due to spontaneous fission. Eighty-five percent (85%) of the U-Florida neutron source is due to Cm-242.

The neutron source for the two PULSTAR fuel element types is summarized in Table 5.2-19. Because the active length of PULSTAR fuel is approximately the same as the flat plate fuels in the SFB, the same axial source distribution is used for PULSTAR, as well as the same neutron peaking factor of 1.586. This peaking factor is applied in Table 5.2-19. Note that the 4% enriched fuel element neutron source is more than twice as large as the 6% enriched fuel element, as neutron sources increase with decreasing U-235 enrichment. The PULSTAR neutron source is due to both spontaneous fission and ( $\alpha$ ,n) reactions with O-17 and O-18.

### 5.2.3 Irradiation Gas Generation

For the plate and TRIGA fuels, the irradiation gases are mostly trapped in the fuel matrix and will not be released in the event of a cladding breach, as discussed in Section 3.1.4, *Summary Tables of Maximum Pressures*. However, PULSTAR fuel uses a UO<sub>2</sub> ceramic pellet design

similar to commercial fuel, and some irradiation gases may be released to the cask cavity in an accident. Therefore, the quantity of irradiation gases is estimated for PULSTAR fuel.

During irradiation in a reactor, the fuel assembly will generate gases due to fission, alpha decay, and light element activation. The noble gases (He, Ne, Ar, Kr, Xe, and Rn) are of primary interest as these gases do not react with other elements. The elements H, N, F, and Cl are conservatively assumed to be present in a gaseous state, although these elements may have formed solid compounds and may not be present as a gas. Bromine and iodine are also assumed to be present as a gas because the boiling points of these elements are low. Oxygen is not treated as a gas because it is present primarily in the compound  $\text{UO}_2$ .

The results are summarized in Table 5.2-20 for a single PULSTAR fuel assembly enriched to 4% and burned to 20,000 MWD/MTU. The total quantity of gas is 0.337 moles and is mostly due to Kr and Xe.

**Table 5.2-1 – TRITON Input and Supporting Data (MURR, MITR-II, ATR)**

Parameter	MURR(-)	MURR(+)	MITR-II(-)	MITR-II(+)	ATR(-)①	ATR(+)
U-235 loading (g)	767.2	782.8	500.0	513.0	1065.0	1085.0
Fuel meat temperature (K)	358.0	358.0	341.0	341.0	378.0	378.0
Fuel cladding temp. (K)	355.2	355.2	338.0	338.0	372.4	372.4
Water temp. (K)	327.4	327.4	323.0	323.0	340.8	340.8
Water density (g/cm <sup>3</sup> )	0.983	0.983	0.9968	0.9968	0.9786	0.9786
Fuel meat width (in)	2.88	2.88	2.08	2.08	2.65	2.65
Fuel meat thickness (in)	0.02	0.02	0.03	0.03	0.02	0.02
Fuel plate thickness (in)	0.05	0.05	0.08②	0.08	0.05	0.05
Fuel plate pitch (in)	0.13	0.13	0.158	0.158	0.128	0.128
Active fuel length (in)	24.0	24.0	22.375	22.375	48.0	48.0
Number of fuel plates	24	24	15	15	19	19
Fuel Meat Volume (cm <sup>3</sup> )	544.1	544.1	342.5	342.5	792.6	792.6
U density (g/cm <sup>3</sup> )	1.52	1.55	1.57	1.61	1.44	1.47
U-235 density (g/cm <sup>3</sup> )	1.41	1.44	1.46	1.50	1.34	1.37
U-238 density (g/cm <sup>3</sup> )	0.1061	0.1083	0.1099	0.1127	0.1011	0.1030
Al density (g/cm <sup>3</sup> )	2.25	2.25	2.24	2.23	2.26	2.26
UAlx+Al density (g/cm <sup>3</sup> )	3.77	3.79	3.81	3.84	3.71	3.73
N U-235 (atom/b-cm)	3.6124E-03	3.6859E-03	3.7399E-03	3.8371E-03	3.4426E-03	3.5072E-03
N U-238 (atom/b-cm)	2.6847E-04	2.7393E-04	2.7794E-04	2.8517E-04	2.5584E-04	2.6065E-04
N Al (atom/b-cm)	5.0239E-02	5.0110E-02	5.0015E-02	4.9844E-02	5.0538E-02	5.0425E-02
U mass (g)	824.9	841.7	537.6	551.6	1145.2	1166.7
U mass (MTU)	8.2495E-04	8.4172E-04	5.3763E-04	5.5161E-04	1.1452E-03	1.1667E-03
Element power (MW)	1.25	1.25	0.25	0.25	10.0	10.0
Sp. Power (MW/MTU)	1515.3	1485.1	465.0	453.2	8732.4	8571.4
Irradiation time (D)	144.0	144.0	660.0	660.0	48.0	48.0
Cycles (#)	21	21	6	6	1	1
Decay time (D)	180	180	120	120	1670	1670
Burnup (MWD)	180.0	180.0	165.0	165.0	480.0	480.0
Burnup (MWD/MTU)	218,196	213,848	306,900	299,123	419,155	411,429

①Data in this column is for the model without B-10. For the model including B-10, the B-10 number density is 5.3115E-05 atoms/b-cm. The nominal B-10 loading in an ATR Type 7F assembly is 660 mg. This value has been conservatively rounded up to 700 mg.

②The grooves present in MITR-II cladding have been neglected.

**Table 5.2-2 – TRITON Output Data (MURR, MITR-II, ATR)**

<b>Parameter</b>	<b>MURR(-)①</b>	<b>MURR(+)</b>	<b>MITR-II(-)</b>	<b>MITR-II(+)</b>
Initial U-235 (g)	<b>767.2</b>	782.8	<b>500.0</b>	513.0
Final U-235 (g)	<b>530.4</b>	545.8	<b>280.6</b>	293.2
Depleted mass (g)	<b>236.8</b>	237.0	<b>219.4</b>	219.8
Depletion (%)	<b>30.9%</b>	30.3%	<b>43.9%</b>	42.8%
Element decay heat (W)	<b>147.6</b>	147.6	<b>142.5</b>	142.5
<b>Parameter</b>	<b>ATR(-)</b>	<b>ATR(+)</b>	<b>ATR(-) with B-10</b>	<b>--</b>
Initial U-235 (g)	1065.0	1085.0	<b>1065.0</b>	--
Final U-235 (g)	440.8	460.1	<b>440.5</b>	--
Depleted mass (g)	624.2	624.9	<b>624.5</b>	--
Depletion (%)	58.6%	57.6%	<b>58.6%</b>	--
Element decay heat (W)	29.8	29.8	<b>29.8</b>	--

①Bounding analysis values in boldface.

**Table 5.2-3 – Gamma Source Terms, MURR, MITR-II, ATR**

	<b>MURR</b>	<b>MITR-II</b>	<b>ATR</b>
<b>Upper Energy Bin (MeV)</b>	<b>Gamma Source (γ/s)</b>	<b>Gamma Source (γ/s)</b>	<b>Gamma Source (γ/s)</b>
4.50E-02 <sup>ⓐ</sup>	2.576E+14	2.343E+14	5.575E+13
1.00E-01	9.423E+13	8.380E+13	1.973E+13
2.00E-01	9.441E+13	9.049E+13	1.527E+13
3.00E-01	1.976E+13	1.756E+13	3.897E+12
4.00E-01	1.478E+13	1.304E+13	2.881E+12
6.00E-01	4.237E+13	5.917E+13	1.445E+13
8.00E-01	4.328E+14	4.460E+14	5.736E+13
1.00E+00	7.534E+12	1.117E+13	5.941E+12
1.33E+00	3.040E+12	3.308E+12	1.387E+12
1.66E+00	1.786E+12	2.576E+12	5.689E+11
2.00E+00	2.304E+11	2.013E+11	3.490E+10
2.50E+00	2.171E+12	1.795E+12	2.387E+11
3.00E+00	8.765E+09	3.290E+10	1.346E+09
4.00E+00	4.661E+08	6.118E+08	1.061E+08
5.00E+00	9.414E+01	7.015E+02	7.644E+02
6.50E+00	3.740E+01	2.802E+02	3.051E+02
8.00E+00	7.270E+00	5.473E+01	5.955E+01
1.00E+01	1.582E+00	1.195E+01	1.300E+01
Total	9.707E+14	9.634E+14	1.775E+14
Number of Fuel Elements in Basket	8	8	8
Basket Total	7.766E+15	7.707E+15	1.420E+15

<sup>ⓐ</sup>The lower energy bound for this group is 0.01 MeV.

**Table 5.2-4 – Axial Burnup Distribution, MURR**

Distance from Bottom of Fuel Element (cm)	Axial Burnup Distribution
5	0.872
10	0.939
15	1.132
20	1.233
25	1.367
30	1.358
35	1.308
40	1.233
45	1.023
50	0.679
55	0.486
60	0.369

**Table 5.2-5 – Axial Burnup Distribution, MITR-II**

Distance from Bottom of Fuel Element (cm)	Axial Burnup Distribution	MCNP Input
2.368	0.999	0.500
4.736	0.788	0.394
9.472	0.788	0.788
14.208	0.901	0.901
18.944	1.042	1.042
23.680	1.140	1.140
28.416	1.253	1.253
33.152	1.267	1.267
37.888	1.112	1.112
42.624	1.028	1.028
47.360	0.901	0.901
52.096	0.774	0.774
54.464	0.802	0.401
56.833	0.999	0.500

**Table 5.2-6 – Axial Burnup Distribution, ATR**

<b>Distance from Bottom of Fuel Element (cm)</b>	<b>Axial Burnup Distribution</b>
12.19	0.50
24.38	0.70
36.58	1.00
48.77	1.30
60.96	1.45
73.15	1.45
85.34	1.30
97.54	1.00
109.73	0.70
121.92	0.50

Table 5.2-7 – TRIGA Fuel Parameters

ID	Type	Cladding	U (wt.% fuel)	Fuel Length (in)	U-235 (wt.% U)	U (g)	U-235 (g)	Fuel OD (in)	Rod OD (in)	Cladding Thickness (in)	H/Zr	Overall Length (in)	Er (wt.%)
101	Std.	Al	8.0	14	20	166	32	1.41	1.48	0.03	1.0	28.62	0
	Std.	Al	8.5	15	20	189	37	1.41	1.48	0.03	1.6	28.62	0
103	Std.	SS	8.5	15	20	197	39	1.44	1.48	0.02	1.6	29.15	0
105	Std.	SS	12	15	20	285	56	1.44	1.48	0.02	1.6	29.15	0
107	Std.	SS	12	15	20	271	53	1.40	1.48	0.02	1.6	30.14	0
109	Std.	SS	8.5	15	70	194	136	1.44	1.48	0.02	1.6	29.15	1.2
117	Std.	SS	20	15	20	503	99	1.44	1.48	0.02	1.6	29.93	0.5
119	Std.	SS	30	15	20	825	163	1.44	1.48	0.02	1.6	29.93	0.9
201	Ins.	Al	8.5	15	20	189	37	1.41	1.48	0.03	1.6	28.78	0
203	Ins.	SS	8.5	15	20	197	39	1.44	1.48	0.02	1.6	45.50	0
205	Ins.	SS	12	15	20	285	56	1.44	1.48	0.02	1.6	45.50	0
207	Ins.	SS	12	15	20	271	53	1.40	1.48	0.02	1.6	45.50	0
217	Ins.	SS	20	15	20	503	99	1.44	1.48	0.02	1.6	40.35	0.5
219	Ins.	SS	30	15	20	825	163	1.44	1.48	0.02	1.6	40.35	0.9
303	FFCR	SS	8.5	15	20	163	32	1.31	1.35	0.02	1.6	44.00	0
305	FFCR	SS	12	15	20	237	47	1.31	1.35	0.02	1.6	44.00	0
317	FFCR	SS	20	15	20	418	82	1.31	1.35	0.02	1.6	44.00	0.5
319	FFCR	SS	30	15	20	685	135	1.31	1.35	0.02	1.6	44.00	0.9

(continued)



**Table 5.2-7 – TRIGA Fuel Parameters (concluded)**

ID	Type	Cladding	U (wt.% fuel)	Fuel Length (in)	U-235 (wt.% U)	U (g)	U-235 (g)	Fuel OD (in)	Rod OD (in)	Cladding Thickness (in)	H/Zr	Overall Length (in)	Er (wt.%)
403	Cluster	SS	8.5	15	20	166	33	1.37	1.41	0.02	1.6	30.38	0
405	Cluster	SS	12	15	20	243	48	1.37	1.41	0.02	1.6	30.38	0
417	Cluster	SS	20	15	20	427	85	1.37	1.41	0.02	1.6	30.38	0.5
419	Cluster	SS	30	15	20	710	141	1.37	1.41	0.02	1.6	30.38	0.9
503	Ins. cluster	SS	8.5	15	20	166	33	1.34	1.41	0.02	1.6	45.50	0
505	Ins. cluster	SS	12	15	20	243	48	1.34	1.41	0.02	1.6	45.50	0
517	Ins. cluster	SS	20	15	20	427	85	1.34	1.41	0.02	1.6	45.50	0.5
519	Ins. cluster	SS	30	15	20	710	141	1.34	1.41	0.02	1.6	45.50	0.9

Note: General Atomics catalog numbers are not necessarily unique. TRIGA elements with the same ID could have different fuel parameters. In this table, two variants of the Type 101 element are listed.

Table 5.2-8 – TRIGA Fuel Qualification Table

Type	Maximum Burnup (MWD)	Depletion (%)	Minimum Cooling (days)	Decay Heat (watts)	Surface Dose Rate (mrem/hr)①
101 (8.0%)	23	80.6%	90	14.0	5.5
201/101 (8.5%)	26	79.8%	90	15.6	5.2
109	88	80.4%	350	19.6	12.3
	70	65.0%	250	19.6	7.5
	52	49.0%	170	19.4	5.2
	34	32.4%	90	19.6	4.4
203/103	27	78.4%	90	16.6	6.3
205/105	39	78.2%	120	19.9	9.1
	33	67.9%	90	19.8	6.9
207/107	38	80.0%	120	19.5	9.3
	33	71.2%	90	19.9	7.4
217/117	71	78.6%	280	19.6	20.5
	52	60.7%	180	19.2	8.9
	34	41.4%	90	19.8	5.4
219/119	122	79.4%	600	19.8	<b>61.6</b>
	91	63.1%	370	19.8	20.2
	63	45.9%	220	19.5	8.8
	34	26.0%	90	19.5	4.8
303	22	78.7%	90	13.5	4.7
305	32	77.7%	90	19.4	7.4
317	58	79.1%	210	19.7	13.7
	46	65.1%	150	19.5	7.9
	34	49.6%	90	19.8	5.6
319	97	78.7%	420	19.9	31.6
	76	64.5%	290	19.5	14.2
	55	48.6%	180	19.9	7.5
	34	31.1%	90	19.5	4.9
503/403	23	80.0%	90	14.1	4.9
505/405	33	78.7%	90	20.0	7.3
517/417	60	79.6%	220	19.5	12.5
	47	64.6%	150	19.8	7.3
	34	48.1%	90	19.7	5.3
519/419	101	79.2%	430	19.9	27.6
	79	64.7%	290	20.0	12.9
	56	47.6%	180	20.0	7.0
	34	29.9%	90	19.4	4.7

① The surface dose rates reported in this column are used only to rank the source terms. The dose rates computed for licensing are reported in Section 5.4.4, *External Radiation Levels*.

**Table 5.2-9 – Gamma Source Terms, TRIGA**

	<b>Cladding</b>	<b>Fuel Matrix</b>
<b>Upper Energy Bin (MeV)</b>	<b>Gamma Source (γ/s)</b>	<b>Gamma Source (γ/s)</b>
4.50E-02 <sup>①</sup>	3.199E+10	3.317E+13
1.00E-01	7.759E+09	1.242E+13
2.00E-01	1.543E+09	1.068E+13
3.00E-01	7.662E+07	2.616E+12
4.00E-01	1.005E+08	1.993E+12
6.00E-01	6.354E+06	1.794E+13
8.00E-01	2.207E+06	2.961E+13
1.00E+00	8.320E+07	7.233E+12
1.33E+00	1.868E+12	1.336E+12
1.66E+00	5.274E+11	6.577E+11
2.00E+00	0.000E+00	4.656E+10
2.50E+00	1.262E+07	2.232E+11
3.00E+00	1.078E+04	2.757E+09
4.00E+00	0.000E+00	2.414E+08
5.00E+00	0.000E+00	3.636E+04
6.50E+00	0.000E+00	1.459E+04
8.00E+00	0.000E+00	2.862E+03
1.00E+01	0.000E+00	6.268E+02
Total	2.437E+12	1.179E+14
Number of Fuel Elements in Basket	19	19
Basket Total	4.630E+13	2.241E+15

<sup>①</sup>The lower energy bound for this group is 0.01 MeV.

**Table 5.2-10 – TRITON Input and Supporting Data, Square Plate Fuels**

Parameter	RINSC	U-Mass(Al)	U-Mass(Si)	Ohio State	Miss. S&T	U-Florida	Purdue
U-235 loading (g)	275±7.7	167±3.3	200±5.6	200±5.6	225±6.3	175±4.9	129.92±2.52
Uranium mass (MTU)	1.3534E-03	8.2886E-04	9.8430E-04	9.8430E-04	1.1073E-03	8.6127E-04	6.4506E-04
Burnup (MWD)	52.5	9.7	9.7	64.0	74.0	87.0	0.57
Irradiation time (D)	1575	203.7	203.7	2560	7048	20714	7808
Decay time (D)	120	1000	1000	120	365	120	120
Element power (MW)	0.033	0.048	0.048	0.025	0.011	0.0042	0.000073
Sp. Power (MW/MTU)	24.629	57.451	48.378	25.399	9.482	4.877	0.113
Fuel meat width (in)	2.395	2.320	2.395	2.395	2.395	2.395	2.395
Fuel meat thickness (in)	0.02	0.03	0.02	0.02	0.02	0.02	0.02
Fuel plate thickness (in)	0.05	0.06	0.05	0.05	0.05	0.05	0.05
Fuel plate pitch (in)	0.138	0.167	0.167	0.162	0.174	0.161	0.180
Active fuel length (in)	23.25	23.25	23.25	23.25	23.25	23.25	23.25
Number of fuel plates	22	18	16	16	18	14	14
Fuel meat volume (cm <sup>3</sup> )	401.5	477.3	292.0	292.0	328.5	255.5	255.5
U density (g/cm <sup>3</sup> )	3.37	1.74	3.37	3.37	3.37	3.37	2.52
Si density (g/cm <sup>3</sup> )	0.27	-	0.27	0.27	0.27	0.27	0.20
Al density (g/cm <sup>3</sup> )	1.90	1.10	1.90	1.90	1.90	1.90	2.10
N U-235 (atom/b-cm)	1.7057E-03	8.7869E-04	1.7057E-03	1.7057E-03	1.7057E-03	1.7057E-03	1.2775E-03
N U-238 (atom/b-cm)	6.8433E-03	3.5253E-03	6.8433E-03	6.8433E-03	6.8433E-03	6.8433E-03	5.1254E-03
N Si (atom/b-cm)	5.6850E-03	-	5.6850E-03	5.6850E-03	5.6850E-03	5.6850E-03	4.2579E-03
N Al (atom/b-cm)	4.2301E-02	2.4522E-02	4.2301E-02	4.2301E-02	4.2301E-02	4.2301E-02	4.6810E-02
Fuel meat temperature (K)	350	339	339	334	333	338	302
Fuel cladding temp. (K)	349	339	339	333	333	337	302
Water temp. (K)	325	323	323	308	300	333	300
Water density (g/cm <sup>3</sup> )	0.9880	0.9968	0.9968	0.9982	0.9900	0.9940	0.9989

**Table 5.2-11 – TRITON Output Data, Square Plate Fuels**

Parameter	RINSC	U-Mass (Al)	U-Mass (Si)	Ohio State	Miss. S&T	U-Florida	Purdue
Initial U-235 (g)	267.3	163.7	194.4	194.4	218.7	170.1	127.4
Final U-235 (g)	202.3	151.4	182.1	116.8	128.9	68.0	126.6
Depleted mass (g)	65.0	12.3	12.3	77.6	89.8	102.1	0.8
Depletion (%)	24.3%	7.5%	6.3%	39.9%	41.1%	60.1%	0.6%
Decay heat per element (W)	22.5	1.1	1.1	18.3	4.7	5.1	0.1
Parameter	Loose Plate Box						
Allowed in loose plate box	No	Yes	No	No	No	Yes	Yes
Plates per element	NA	18	NA	NA	NA	14	14
Heat per plate (W)	NA	0.061	NA	NA	NA	0.37	0.0045
Number of plates in box	NA	31	NA	NA	NA	31	31
Heat per loose plate box (W)	NA	1.88	NA	NA	NA	11.4	0.14

**Table 5.2-12 – Gamma Source Terms, Square Plate Fuels**

	RINSC	U-Mass (Al)	U-Mass (Si)	Ohio State	Miss. S&T	U-Florida	Purdue
Upper Energy Bin (MeV)	Gamma Source (γ/s)	Gamma Source (γ/s)	Gamma Source (γ/s)	Gamma Source (γ/s)	Gamma Source (γ/s)	Gamma Source (γ/s)	Gamma Source (γ/s)
4.50E-02①	3.971E+13	2.594E+12	2.593E+12	3.196E+13	9.413E+12	8.060E+12	1.122E+11
1.00E-01	1.431E+13	9.544E+11	9.545E+11	1.151E+13	3.414E+12	2.867E+12	4.010E+10
2.00E-01	1.486E+13	8.546E+11	8.545E+11	1.165E+13	2.784E+12	2.512E+12	3.792E+10
3.00E-01	2.988E+12	1.957E+11	1.956E+11	2.398E+12	6.873E+11	5.752E+11	8.045E+09
4.00E-01	2.247E+12	1.518E+11	1.517E+11	1.800E+12	5.193E+11	4.228E+11	6.018E+09
6.00E-01	7.910E+12	2.225E+11	2.199E+11	7.178E+12	1.495E+12	1.951E+12	1.419E+10
8.00E-01	6.361E+13	1.075E+12	1.072E+12	5.056E+13	8.537E+12	1.288E+13	1.731E+11
1.00E+00	9.965E+11	4.122E+10	4.004E+10	1.198E+12	4.978E+11	5.260E+11	1.082E+09
1.33E+00	4.789E+11	2.670E+10	2.646E+10	4.517E+11	1.617E+11	1.818E+11	8.895E+08
1.66E+00	3.501E+11	1.473E+10	1.464E+10	2.988E+11	6.911E+10	7.716E+10	7.045E+08
2.00E+00	3.624E+10	2.483E+09	2.480E+09	2.980E+10	7.672E+09	6.080E+09	7.633E+07
2.50E+00	2.999E+11	2.038E+10	2.038E+10	2.285E+11	5.298E+10	3.802E+10	6.796E+08
3.00E+00	4.949E+09	9.016E+07	8.989E+07	3.882E+09	3.210E+08	7.173E+08	1.037E+07
4.00E+00	1.279E+08	6.714E+06	6.687E+06	1.132E+08	2.565E+07	2.565E+07	2.223E+05
5.00E+00	1.616E+02	2.353E+00	2.311E+00	5.521E+02	2.818E+02	2.327E+03	3.559E-01
6.50E+00	6.460E+01	9.260E-01	9.085E-01	2.210E+02	1.127E+02	9.315E+02	1.418E-01
8.00E+00	1.263E+01	1.784E-01	1.749E-01	4.326E+01	2.203E+01	1.823E+02	2.763E-02
1.00E+01	2.760E+00	3.859E-02	3.779E-02	9.460E+00	4.814E+00	3.988E+01	6.025E-03
Total	1.478E+14	6.154E+12	6.146E+12	1.193E+14	2.764E+13	3.010E+13	3.949E+11
Number of Fuel Elements in Basket	8	8	8	8	8	8	8
Basket Total	1.182E+15	4.923E+13	4.917E+13	9.541E+14	2.211E+14	2.408E+14②	3.160E+12

①The lower energy bound for this group is 0.01 MeV.

②For the loose plate box, the total source magnitude is  $2.408\text{E}+14 \times 31/14 = 5.332\text{E}+14$  γ/s.

**Table 5.2-13 – Axial Source Distributions, Square Plate Fuels**

<b>Distance from Bottom of Fuel Element (cm)</b>	<b>Axial Power Distribution</b>	<b>Axial Source Distribution, Gamma</b>	<b>Axial Source Distribution, Neutron</b>
4.921	0.862	0.872	0.578
9.843	1.036	1.048	1.207
14.764	1.230	1.244	2.398
19.685	1.352	1.368	3.501
24.606	1.385	1.401	3.855
29.528	1.331	1.347	3.288
34.449	1.202	1.216	2.187
39.370	1.029	1.041	1.175
44.291	0.846	0.856	0.537
49.213	0.666	0.674	0.206
54.134	0.501	0.507	0.066
59.055	0.421	0.426	0.033
Average	0.988	1.000	1.586

**Table 5.2-14 – TRITON Input and Supporting Data, PULSTAR**

Parameter	4% U-235	6% U-235
U-235 Enrichment (%)	4.0	6.0
Burnup (MWD/MTU)	20,000	20,000
Fuel matrix	UO <sub>2</sub>	UO <sub>2</sub>
UO <sub>2</sub> density (g/cm <sup>3</sup> )	10.7408	10.7408
Fuel pellet diameter (in)	0.423	0.423
Cladding thickness (in)	0.0185	0.0185
Cladding material	Zirconium alloy	Zirconium alloy
Cladding OD (in)	0.474	0.474
Active fuel length (in)	24.1	24.1
Uranium mass (MTU)	1.3136E-02	1.3136E-02
Uranium mass (kg)	13.136	13.136
U-235 per rod (g)	21.018	31.528
Irradiation time (D)	3,284	3,284
Decay time (years)	1.5	1.5
Element power (MW)	0.08	0.08
Sp. Power (MW/MTU)	6.09	6.09
Fuel rod pitch X (in)	0.607	0.607
Fuel rod pitch Y (in)	0.525	0.525
Average rod pitch (in)	0.566	0.566
Box outer dimensions (in)	3.15 x 2.74	3.15 x 2.74
Box thickness (in)	0.06	0.06
Box material	Zirconium alloy	Zirconium alloy
Oxygen per element (g)	1766.25	1766.25
O-17 per element (g)	0.759	0.759
O-18 per element (g)	3.974	3.974
O-17 per element (g/MTU)	57.815	57.815
O-18 per element (g/MTU)	302.521	302.521
Fuel meat temperature (K)	633	633
Fuel cladding temp. (K)	433	433
Water temp. (K)	333	333
Water density (g/cm <sup>3</sup> )	0.9982	0.9982

**Table 5.2-15 – TRITON Output Data, PULSTAR**

Parameter	4% U-235	6% U-235
Initial U-235 (g)	525.5	788.2
Final U-235 (g)	279.7	510.2
Depleted mass (g)	245.8	278.0
Depletion (%)	46.8%	35.3%
Decay heat per element (W)	24.6	23.1



**Table 5.2-16 – Gamma Source Terms, PULSTAR**

	<b>4% U-235</b>	<b>6% U-235</b>
<b>Upper Energy Bin (MeV)</b>	<b>Gamma Source (γ/s)</b>	<b>Gamma Source (γ/s)</b>
4.50E-02 <sup>⓪</sup>	4.427E+13	4.339E+13
1.00E-01	1.641E+13	1.596E+13
2.00E-01	1.341E+13	1.316E+13
3.00E-01	3.430E+12	3.303E+12
4.00E-01	2.601E+12	2.506E+12
6.00E-01	1.571E+13	1.332E+13
8.00E-01	3.830E+13	3.632E+13
1.00E+00	5.613E+12	4.806E+12
1.33E+00	1.600E+12	1.333E+12
1.66E+00	5.919E+11	5.213E+11
2.00E+00	6.064E+10	5.185E+10
2.50E+00	2.469E+11	2.509E+11
3.00E+00	3.829E+09	2.990E+09
4.00E+00	3.409E+08	2.610E+08
5.00E+00	1.376E+04	5.897E+03
6.50E+00	5.513E+03	2.361E+03
8.00E+00	1.080E+03	4.622E+02
1.00E+01	2.364E+02	1.011E+02
Total	1.422E+14	1.349E+14
Number of Fuel Elements in Basket	8	8
Basket Total	1.138E+15	1.079E+15

<sup>⓪</sup>The lower energy bound for this group is 0.01 MeV

**Table 5.2-17 – Neutron Source Terms, MURR, MITR-II, ATR, TRIGA**

	<b>MURR</b>	<b>MITR-II</b>	<b>ATR</b>	<b>TRIGA</b>
<b>Upper Energy Bin (MeV)</b>	<b>Neutron Source (n/s)</b>	<b>Neutron Source (n/s)</b>	<b>Neutron Source (n/s)</b>	<b>Neutron Source (n/s)</b>
1.000E-08 <sup>ⓐ</sup>	6.449E-09	4.868E-08	1.201E-08	7.273E-07
3.000E-08	7.938E-09	6.084E-08	3.617E-08	1.889E-06
5.000E-08	8.240E-09	6.354E-08	4.933E-08	2.507E-06
1.000E-07	2.361E-08	1.828E-07	1.652E-07	8.289E-06
2.250E-07	7.635E-08	5.933E-07	5.993E-07	2.982E-05
3.250E-07	7.588E-08	5.906E-07	6.239E-07	3.095E-05
4.140E-07	7.688E-08	5.988E-07	6.430E-07	3.186E-05
8.000E-07	4.171E-07	3.250E-06	3.556E-06	1.759E-04
1.000E-06	2.611E-07	2.035E-06	2.254E-06	1.112E-04
1.125E-06	1.772E-07	1.381E-06	1.534E-06	7.571E-05
1.300E-06	2.632E-07	2.052E-06	2.284E-06	1.127E-04
1.855E-06	1.351E-05	1.000E-04	8.317E-06	4.081E-04
3.059E-06	3.703E-05	2.741E-04	2.319E-05	1.102E-03
1.068E-05	2.487E-04	1.837E-03	2.809E-04	1.152E-02
2.902E-05	2.430E-03	1.040E-02	1.047E-02	4.735E-02
1.013E-04	1.556E-02	6.678E-02	6.686E-02	3.364E-01
5.830E-04	1.850E-01	7.886E-01	8.143E-01	5.087E+00
3.035E-03	2.194E+00	9.182E+00	9.925E+00	5.964E+01
1.503E-02	2.700E+01	1.127E+02	1.204E+02	6.502E+02
1.111E-01	8.508E+02	3.446E+03	3.766E+03	1.325E+04
4.076E-01	5.625E+03	2.377E+04	2.328E+04	7.571E+04
9.072E-01	1.323E+04	5.727E+04	5.285E+04	1.646E+05
1.423E+00	1.235E+04	5.086E+04	5.203E+04	1.686E+05
1.827E+00	8.372E+03	3.444E+04	3.576E+04	1.171E+05
3.012E+00	7.363E+03	3.685E+04	2.753E+04	2.473E+05
6.376E+00	5.001E+02	4.004E+03	4.327E+03	2.165E+05
2.000E+01	4.587E+01	3.817E+02	4.356E+02	2.215E+04
Total	4.837E+04	2.111E+05	2.001E+05	1.026E+06
Number of Fuel Elements in Basket	8	8	8	19
Basket Total	3.869E+05	1.689E+06	1.601E+06	1.949E+07

<sup>ⓐ</sup>The lower energy bound for this group is 1.0E-11 MeV.

**Table 5.2-18 – Neutron Source Terms, Square Plate Fuels**

	<b>RINSC</b>	<b>U-Mass (Al)</b>	<b>U-Mass (Si)</b>	<b>Ohio State</b>
<b>Upper Energy Bin (MeV)</b>	<b>Neutron Source (n/s)</b>	<b>Neutron Source (n/s)</b>	<b>Neutron Source (n/s)</b>	<b>Neutron Source (n/s)</b>
1.000E-08 <sup>①</sup>	1.295E-08	1.329E-11	1.555E-11	5.065E-08
3.000E-08	1.512E-08	7.813E-11	7.867E-11	5.688E-08
5.000E-08	1.527E-08	1.184E-10	1.174E-10	5.597E-08
1.000E-07	4.289E-08	4.145E-10	4.088E-10	1.542E-07
2.250E-07	1.363E-07	1.546E-09	1.520E-09	4.816E-07
3.250E-07	1.345E-07	1.626E-09	1.596E-09	4.713E-07
4.140E-07	1.359E-07	1.682E-09	1.650E-09	4.747E-07
8.000E-07	7.345E-07	9.350E-09	9.171E-09	2.557E-06
1.000E-06	4.605E-07	5.930E-09	5.890E-09	1.597E-06
1.125E-06	3.132E-07	4.039E-09	4.054E-09	1.084E-06
1.300E-06	4.657E-07	6.017E-09	6.046E-09	1.610E-06
1.855E-06	2.087E-05	2.219E-08	2.212E-08	8.048E-05
3.059E-06	5.718E-05	5.996E-08	5.951E-08	2.205E-04
1.068E-05	3.864E-04	7.490E-07	7.214E-07	1.479E-03
2.902E-05	1.152E-03	6.317E-06	5.931E-06	4.198E-03
1.013E-04	7.348E-03	3.745E-05	3.532E-05	2.682E-02
5.830E-04	1.055E-01	3.292E-03	3.067E-03	3.417E-01
3.035E-03	1.159E+00	3.385E-02	3.180E-02	3.766E+00
1.503E-02	1.421E+01	4.231E-01	3.961E-01	4.614E+01
1.111E-01	4.186E+02	1.391E+01	1.326E+01	1.331E+03
4.076E-01	3.314E+03	1.222E+02	1.157E+02	1.046E+04
9.072E-01	8.047E+03	2.433E+02	2.344E+02	2.627E+04
1.423E+00	7.075E+03	2.907E+02	2.697E+02	2.188E+04
1.827E+00	4.547E+03	1.659E+02	1.544E+02	1.436E+04
3.012E+00	5.695E+03	6.562E+01	6.979E+01	2.040E+04
6.376E+00	9.266E+02	8.380E+00	8.851E+00	3.313E+03
2.000E+01	7.802E+01	5.659E-01	5.357E-01	2.860E+02
Total	3.012E+04	9.110E+02	8.670E+02	9.835E+04
Peaking Factor	1.586	1.586	1.586	1.586
Number of Fuel Elements in Basket	8	8	8	8
Basket Total	3.821E+05	1.156E+04	1.100E+04	1.248E+06

①The lower energy bound for this group is 1.0E-11 MeV.

(continued)

**Table 5.2-18 – Neutron Source Terms, Square Plate Fuels (concluded)**

	<b>Miss. S&amp;T</b>	<b>U-Florida</b>	<b>Purdue</b>
<b>Upper Energy Bin (MeV)</b>	<b>Neutron Source (n/s)</b>	<b>Neutron Source (n/s)</b>	<b>Neutron Source (n/s)</b>
1.000E-08①	2.155E-08	2.118E-07	9.831E-12
3.000E-08	2.564E-08	2.394E-07	1.925E-11
5.000E-08	2.617E-08	2.363E-07	2.390E-11
1.000E-07	7.406E-08	6.523E-07	7.650E-11
2.250E-07	2.370E-07	2.042E-06	2.695E-10
3.250E-07	2.345E-07	2.000E-06	2.773E-10
4.140E-07	2.371E-07	2.015E-06	2.857E-10
8.000E-07	1.284E-06	1.086E-05	1.582E-09
1.000E-06	8.052E-07	6.780E-06	9.989E-10
1.125E-06	5.476E-07	4.597E-06	6.790E-10
1.300E-06	8.187E-07	6.847E-06	1.011E-09
1.855E-06	3.424E-05	3.313E-04	3.673E-09
3.059E-06	9.377E-05	9.077E-04	9.886E-09
1.068E-05	6.492E-04	6.140E-03	1.063E-07
2.902E-05	2.266E-03	1.842E-02	5.231E-07
1.013E-04	1.404E-02	1.163E-01	3.447E-06
5.830E-04	1.925E-01	1.444E+00	2.084E-04
3.035E-03	2.154E+00	1.605E+01	2.175E-03
1.503E-02	2.632E+01	1.963E+02	2.665E-02
1.111E-01	7.790E+02	5.658E+03	8.426E-01
4.076E-01	5.894E+03	4.352E+04	7.255E+00
9.072E-01	1.436E+04	1.098E+05	1.466E+01
1.423E+00	1.261E+04	9.093E+04	1.688E+01
1.827E+00	8.237E+03	6.028E+04	9.570E+00
3.012E+00	1.009E+04	8.598E+04	4.807E+00
6.376E+00	1.626E+03	1.421E+04	1.001E+00
2.000E+01	1.380E+02	1.248E+03	3.792E-02
Total	5.377E+04	4.119E+05	5.508E+01
Peaking Factor	1.586	1.586	1.586
Number of Fuel Elements in Basket	8	8	8
Basket Total	6.822E+05	5.225E+06②	6.988E+02

①The lower energy bound for this group is 1.0E-11 MeV.

②For the loose plate box, the total source magnitude is  $5.225\text{E}+06 \times 31/14 = 1.157\text{E}+07$  n/s.

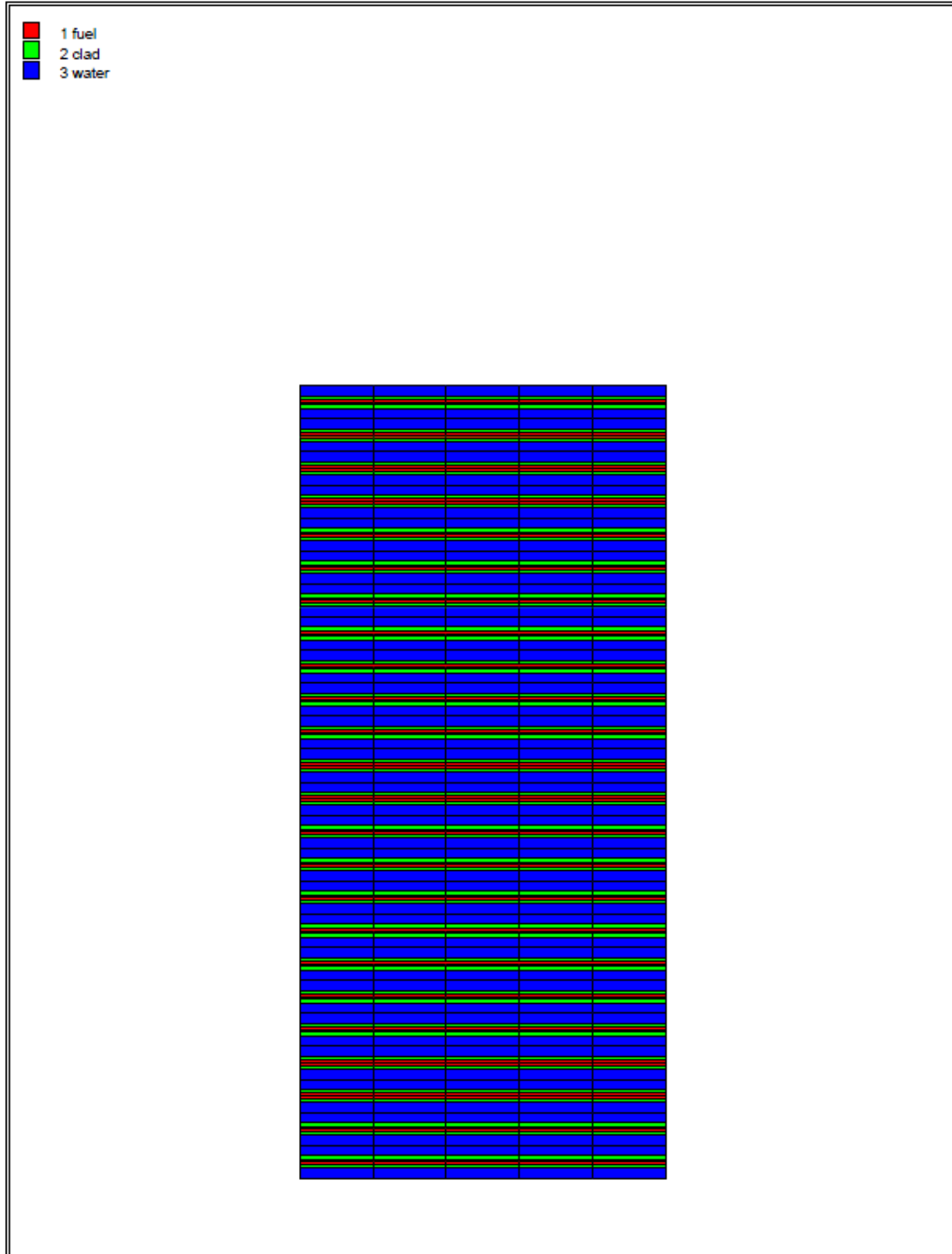
**Table 5.2-19 – Neutron Source Terms, PULSTAR**

	<b>4% U-235</b>	<b>6% U-235</b>
<b>Upper Energy Bin (MeV)</b>	<b>Neutron Source (n/s)</b>	<b>Neutron Source (n/s)</b>
1.000E-08 <sup>①</sup>	5.499E-07	2.785E-07
3.000E-08	9.052E-07	4.166E-07
5.000E-08	1.065E-06	4.732E-07
1.000E-07	3.305E-06	1.438E-06
2.250E-07	1.195E-05	5.446E-06
3.250E-07	1.241E-05	5.743E-06
4.140E-07	1.271E-05	5.824E-06
8.000E-07	6.941E-05	3.135E-05
1.000E-06	4.325E-05	1.930E-05
1.125E-06	2.928E-05	1.301E-05
1.300E-06	4.343E-05	1.924E-05
1.855E-06	1.562E-04	6.880E-05
3.059E-06	4.178E-04	1.825E-04
1.068E-05	4.306E-03	1.856E-03
2.902E-05	1.763E-02	7.536E-03
1.013E-04	1.281E-01	5.526E-02
5.830E-04	1.931E+00	8.316E-01
3.035E-03	2.258E+01	9.713E+00
1.503E-02	2.473E+02	1.067E+02
1.111E-01	5.053E+03	2.182E+03
4.076E-01	2.878E+04	1.239E+04
9.072E-01	6.241E+04	2.681E+04
1.423E+00	6.477E+04	2.802E+04
1.827E+00	4.672E+04	2.063E+04
3.012E+00	1.093E+05	5.073E+04
6.376E+00	9.058E+04	4.044E+04
2.000E+01	7.900E+03	3.262E+03
Total	4.158E+05	1.846E+05
Peaking Factor	1.586	1.586
Number of Fuel Elements in Basket	8	8
Basket Total	5.275E+06	2.342E+06

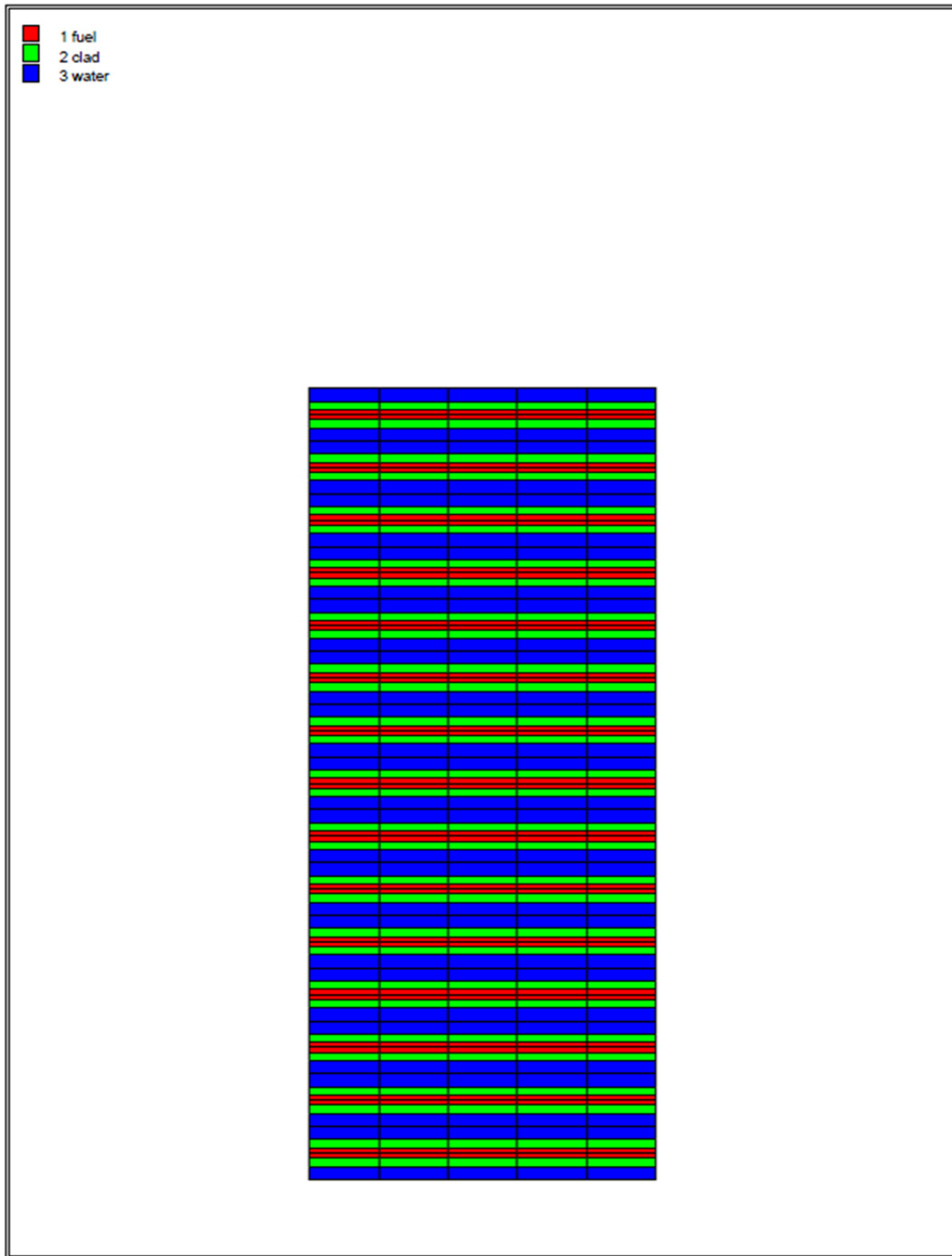
①The lower energy bound for this group is 1.0E-11 MeV.

**Table 5.2-20 – Irradiation Gases, PULSTAR**

<b>Element</b>	<b>Quantity (moles)</b>
H	2.02E-04
He	8.14E-03
N	3.00E-06
F	4.83E-08
Ne	1.99E-06
Cl	0.00E+00
Ar	0.00E+00
Br	2.18E-03
Kr	3.75E-02
I	1.11E-02
Xe	2.78E-01
Rn	2.94E-16
Total	3.37E-01

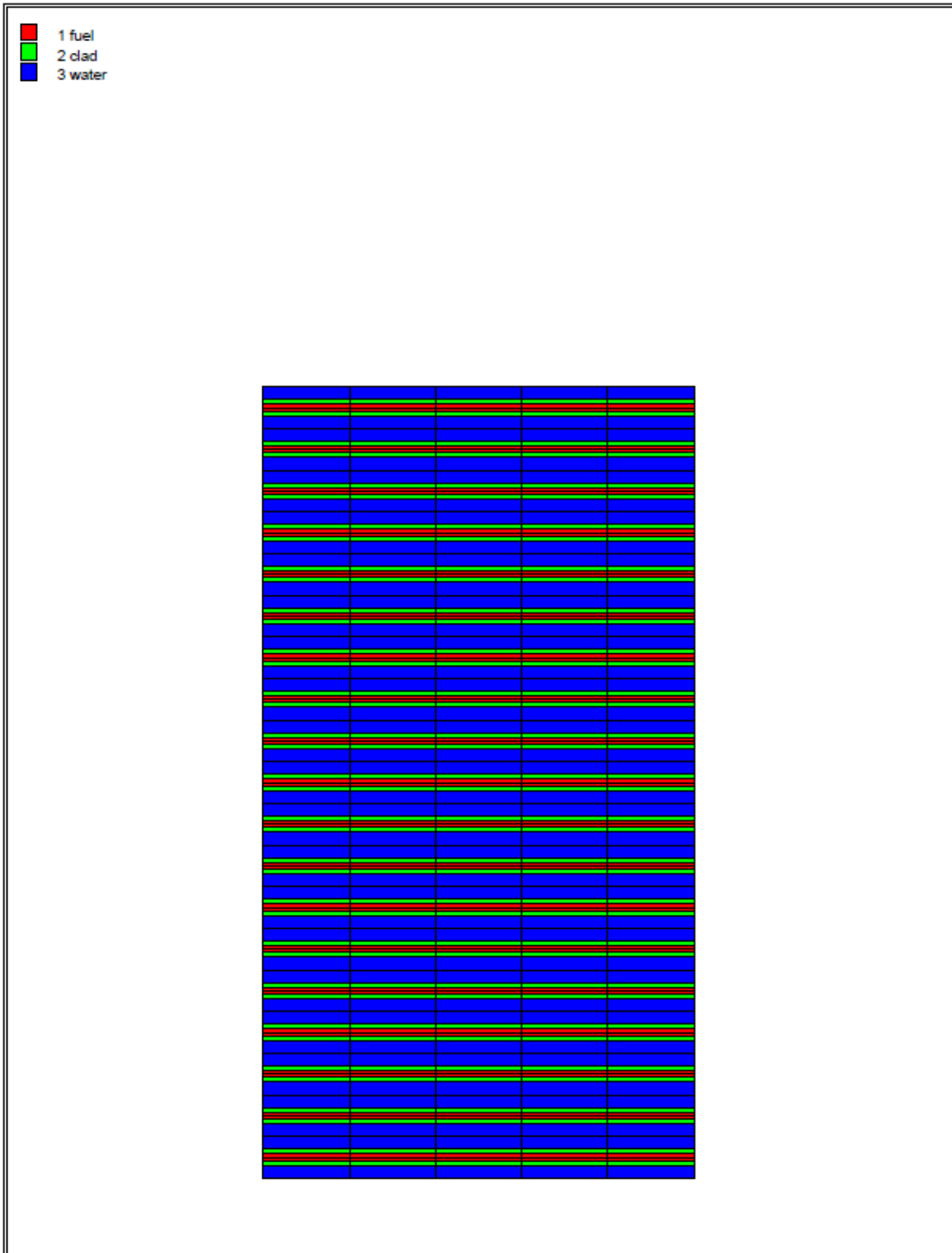


**Figure 5.2-1 – NEWT Model for MURR**

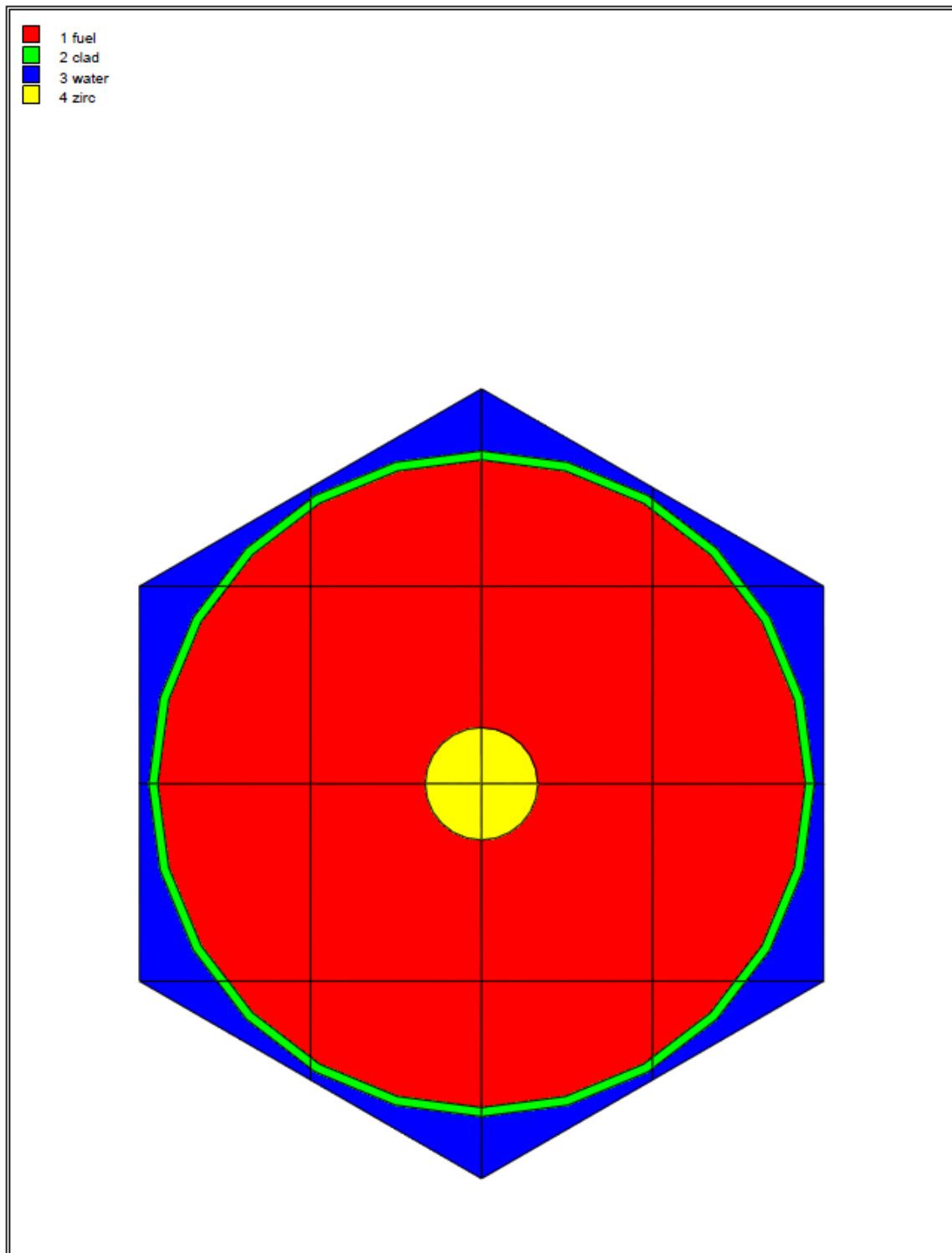


**Figure 5.2-2 – NEWT Model for MITR-II**

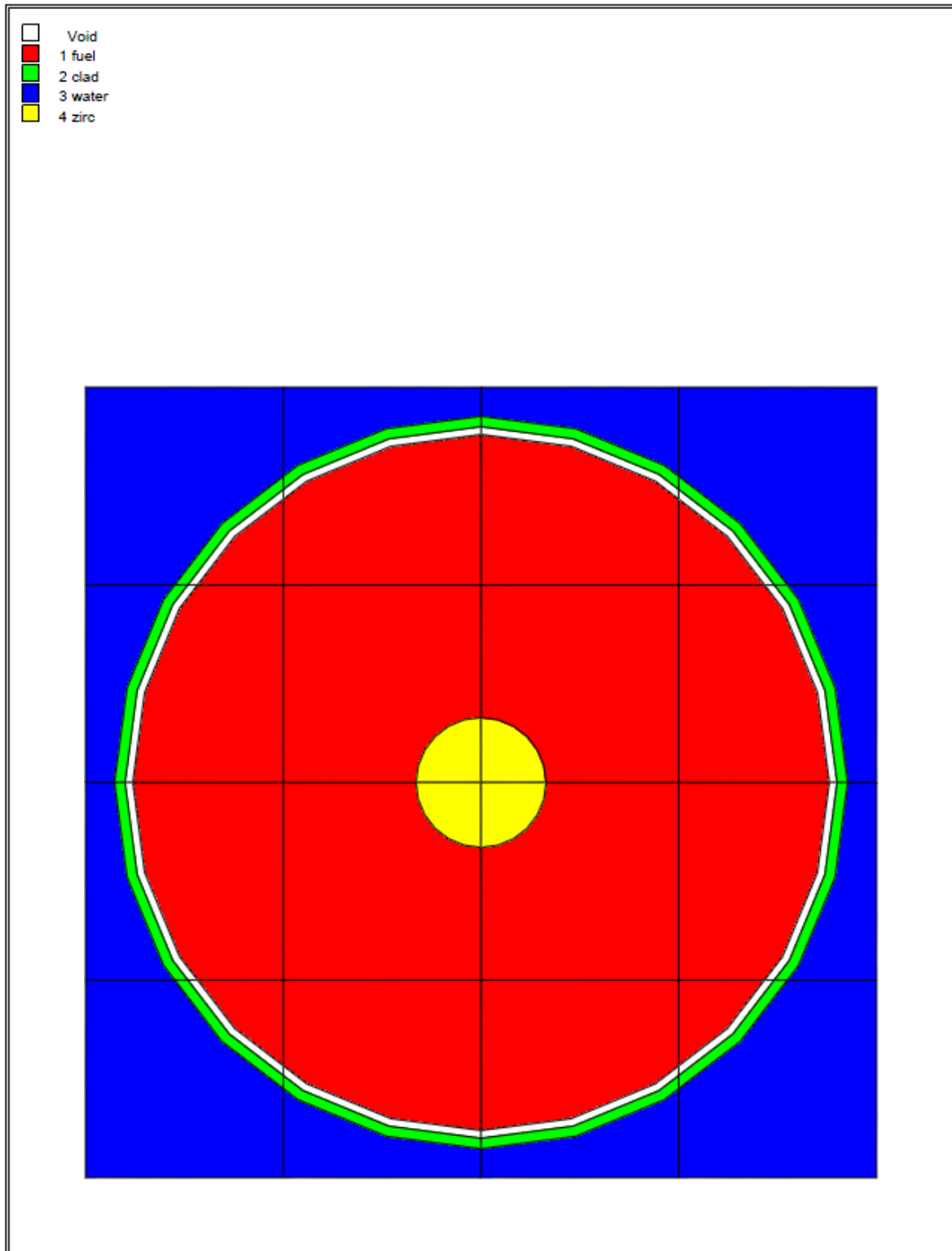




**Figure 5.2-3 – NEWT Model for ATR**



**Figure 5.2-4** – NEWT Model for TRIGA (Series 100, 200, 300)



**Figure 5.2-5** – NEWT Model for TRIGA (Series 400, 500)

**Security-Related Information Figure  
Withheld Under 10 CFR 2.390.**

**Figure 5.2-6 – PULSTAR Fuel Element**

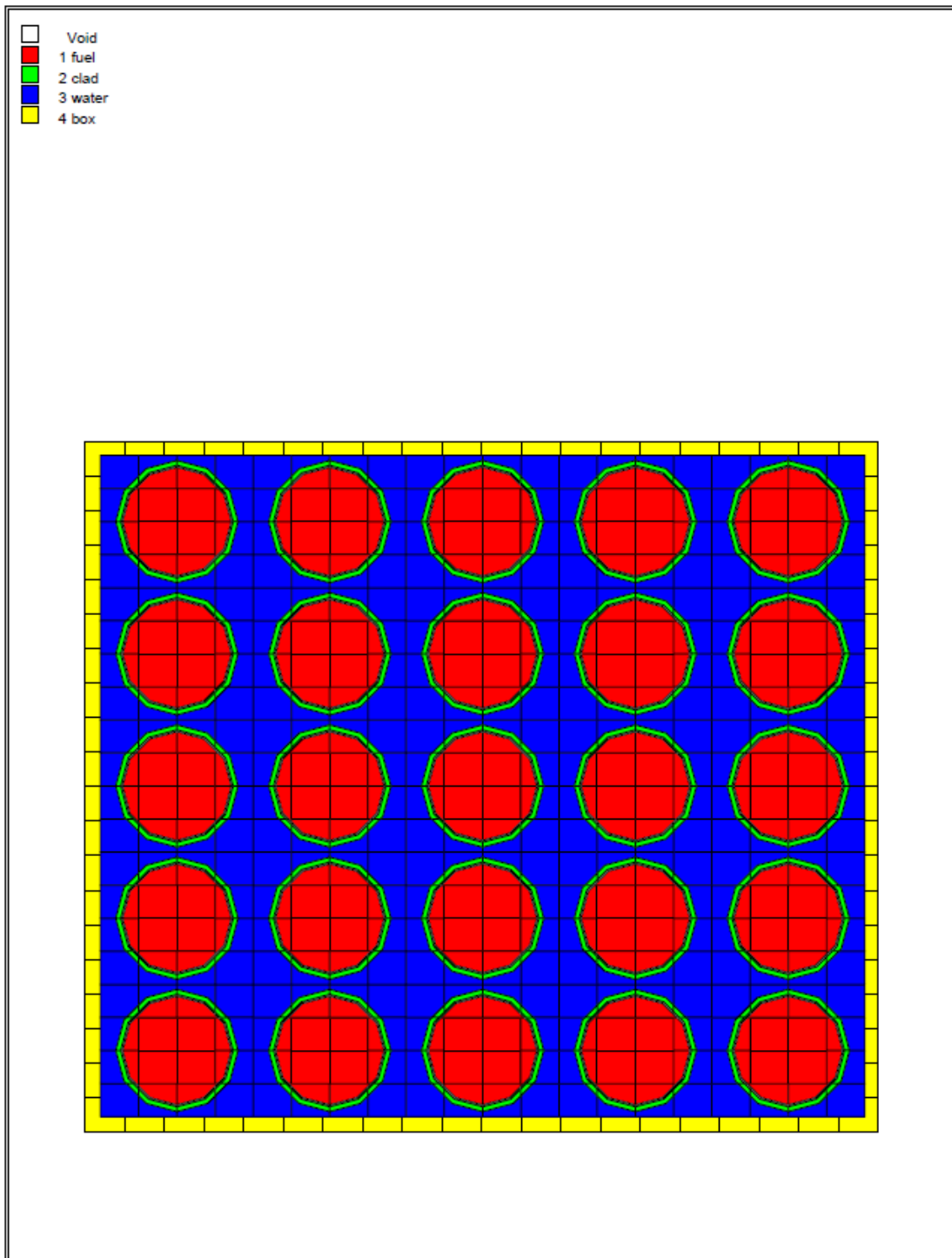


Figure 5.2-7 – NEWT Model for PULSTAR

## 5.3 Shielding Model

### 5.3.1 Configuration of Source and Shielding

All relevant design features of the BRR Package are modeled in three-dimensions in MCNP, as shown in Figure 5.3-1. The key dimensions relevant to the MCNP model are summarized in Table 5.3-1 and are obtained from Section 1.3.3, *Packaging General Arrangement Drawings*. Minor details are not included in this table but may be inferred from the drawings.

Some differences exist between the as-modeled and packaging general arrangement drawing dimensions, as shown in Table 5.3-1. Most differences are small and may be neglected. The only notable differences are the outer diameter of the impact limiters, and the diameter of lead at the bottom of the cask. The outer diameter of the impact limiters is modeled at a reduced diameter of 72.0-in, which is conservative because the dose rate tally location is brought closer to the source. Also, the lead diameter in the cask bottom is modeled at 9.75-in rather than 10.3-in, which is conservative for shielding.

To simplify model preparation and add conservatism, the impact limiters are modeled simply as air, neglecting the impact limiter foam and outer steel shell. The “impact limiter air” is modeled with a different material number than the other air regions to more clearly illustrate the location of the impact limiters (see Figure 5.3-1), although the composition is unchanged. Credit is taken for the distance provided by the impact limiters, although the impact limiters are modeled simply as cylinders without the conical regions.

An axial lead slump of 1.18-in (see Section 2.7.1.2, *End Drop*) is modeled at the top of the cask. This slump represents the maximum expected slump due to lead shrinkage and a drop event. Also, an additional 0.0625-in radial lead shrinkage is assumed.

Five different basket designs are used. MURR, MITR-II, ATR, and TRIGA each utilize a unique basket that is modeled explicitly in MCNP. The SFB is used to transport various “square” research reactor fuels and the loose plate box. The “square” fuels are RINSC, U-Mass (aluminide), U-Mass (silicide), Ohio State, Missouri S&T, U-Florida, Purdue, and PULSTAR. Key geometrical parameters for the five basket designs (and the loose plate box) are summarized in Table 5.3-2. The inner cavity region of the MITR-II basket is modeled as a cylinder with the largest possible diameter to minimize shielding, as the actual geometry is complex. The inner cutout is also conservatively neglected for the top plate of the MITR-II basket. These simplifications are expected to have a negligible impact on the results. As with the cask, this table shows both the actual and as-modeled dimensions. Most differences are within round-off and may be neglected. The baskets and payloads are also shown graphically in Figure 5.3-2 through Figure 5.3-7. In the SFB figures, the U-Florida element is shown, as the RINSC, Ohio State, and Missouri S&T fuel element models differ only in the number of fuel plates per element

Because the MURR, MITR-II, and ATR fuels are geometrically complex, the fuel elements are homogenized over the active length of the fuel and distributed across the width of each basket compartment. Fuel element homogenization is a standard practice utilized to simplify complex source geometry and has little effect on the final results. Basic fuel dimensions used in the homogenization calculation are summarized in Table 5.3-3. These fuel dimensions are not modeled explicitly in MCNP.

For the TRIGA fuel and “square” fuels, the fuel designs are sufficiently simple to allow explicit modeling of the fuel. The TRIGA and “square” fuel elements are modeled explicitly as fresh fuel. For TRIGA fuel, the active fuel source is distributed over the fuel pellets and the cladding source is distributed throughout the cladding to minimize self-shielding. Basic geometrical data for the modeled TRIGA fuel is summarized in Table 5.3-3. For the TRIGA fuel, the Type 109 fuel geometry and composition is modeled (with the larger Type 219 source) to maximize subcritical neutron multiplication.

For the square “plate” fuels and PULSTAR, the source is modeled in the fuel matrix because the cladding contains negligible source. The aluminum side plates for the flat plate fuels are conservatively ignored. The outer zircaloy box is explicitly modeled for the PULSTAR fuel.

For the SFB, the bounding fuel element type is determined. All SFB sources are provided in Section 5.2, *Source Specification*. It is observed that the U-Mass (aluminide), U-Mass (silicide), and Purdue fuel elements have low burnups and low decay heats compared to the other fuel types and will not result in bounding dose rates. Therefore, the bounding SFB payload is one of the following: RINSC, Ohio State, Missouri S&T, U-Florida, PULSTAR, or the loose plate box. The dose rate on the side of the BRR is explicitly computed for each of these payloads, and detailed dose rate calculations are performed for the bounding SFB payload.

The loose plate box may contain loose plates from either U-Mass (aluminide), U-Florida, or Purdue, although U-Florida is the bounding plate in the loose plate box because it has the highest burnup and largest neutron source of the loose plate fuels.

The top of the fuel element is always located near the bottom of the cask lid. When fuel types of multiple lengths are used in a basket (such as TRIGA or the SFB), pedestals are used to raise the fuel. These pedestals are not explicitly modeled in MCNP, although the fuel is modeled near the lid. Modeling the fuel near the lid places the source in the closest proximity to the interface between the lid and cask side, where the lead concentration is at a minimum. Generally, the active fuel is modeled closer to the lid than the actual configuration because the active fuel is offset from the top due to the fuel element support structures (end caps, nozzles, etc.), and the support structures are conservatively ignored in the models.

Table 5.3-3 provides both the active fuel length and total overall length of each fuel element. If it is assumed that the active fuel is centered within the fuel element, the minimum distance between the active fuel and cask lid may be estimated. In all models, the distance between the top of the active fuel and bottom of the cask lid is less than or equal to this minimum distance. The minimum estimated and modeled distances from the top of the active fuel to the bottom of the lid are listed below.

- MURR: 4.25-in estimated, 4.00-in modeled
- MITR-II: 1.945-in estimated, 0.54-in modeled
- ATR: 1.5-in estimated, 0.54-in modeled
- TRIGA: 6.5-in estimated, 6.5-in modeled (fuel shifted up)
- SFB with flat plate elements: 1.2-in estimated (U-Florida, other elements have larger end box lengths), 0.0-in modeled
- SFB with PULSTAR: 4.15-in estimated, 3.1-in modeled

- SFB with loose plate box: 1.2-in estimated (U-Florida), 0.0-in modeled

Because TRIGA fuel has a wide range of available lengths, long TRIGA fuel would be much closer to the bottom of the cavity than short TRIGA fuel, as all TRIGA fuel is supported by pedestals. To bound this effect, TRIGA models are also developed with the fuel shifted down. The geometry of the two axial models of TRIGA fuel are shown in Figure 5.3-6.

NCT dose rates are tallied at the package surface (i.e., surface of cask body and impact limiters), surface of the vehicle (the vehicle is assumed to be 8 feet wide), 2 m from the surface of the vehicle, and in the occupied location of the vehicle driver (assumed to be 25 feet from the cask centerline.) Details of the tally locations, with figures, are provided with the results in Section 5.4.4, *External Radiation Levels*.

Because the impact limiters are modeled as air, both NCT and HAC dose rates may be computed from a single MCNP model. Under HAC, tallies are measured 1 m from the surface of the package. In the radial direction, this distance is measured from the surface of the cask, so any radial impact limiter crush does not impact the dose rate location. In the axial direction, because an end drop results in a maximum crush of 10.5-in, as shown in Appendix 2.12.5, *Impact Limiter Performance Evaluation*, Table 2.12.5-13, a bounding crush of 12-in is applied at each end. The 1 m tally surface is measured from the hypothetical crushed end of the impact limiter, although the impact limiter crush is not modeled explicitly (since the impact limiter is modeled simply as air). It is demonstrated in Section 2.7.1.5, *Fuel Basket Stress Analysis* that the baskets remain intact after a drop event, and therefore the baskets may be modeled as undamaged for both NCT and HAC. The loose plate box also maintains its configuration in the hypothetical accident.

### 5.3.2 Material Properties

As indicated in Section 5.3.1, *Configuration of Source and Shielding*, homogenized fuel atom densities are utilized in the MURR, MITR-II, and ATR MCNP fuel models. For nominal fuel meat and cladding thicknesses, the total mass of U-235, U-238, and aluminum is estimated for each fuel element. For this computation, all structural aluminum is ignored, and the width of the plates is treated as equal to the width of the fuel matrix for simplicity. These assumptions result in a conservative underestimate of the aluminum mass. These masses are distributed over the volume of each basket over the active fuel length. The basket compartment volumes are computed based on the dimensions provided in Table 5.3-2. The homogenized data are summarized in Table 5.3-4, and homogenized atom densities are provided in Table 5.3-5. Note that the atom densities of all three fuel types are quite similar, as all three fuel types are aluminum plate fuel.

The remaining fuel types are modeled explicitly. The TRIGA fuel composition is provided in Table 5.3-6 and is based on Type 109 (70% enrichment). The composition is modeled as fresh, which conservatively maximizes subcritical neutron multiplication. The most reactive TRIGA element is conservatively modeled. The composition of stainless steel cladding utilized is taken from the SCALE material library [5] and is provided in Table 5.3-9. The zirconium rod in the center of the active fuel is modeled as pure with a density of  $6.5 \text{ g/cm}^3$  [6]. The graphite reflectors in the TRIGA fuel elements are modeled as air.

The square plate fuels are modeled in MCNP with a fuel meat of  $\text{U}_3\text{Si}_2$  mixed with aluminum. The fuel plates for RINSC, Ohio State, Missouri S&T, and U-Florida have an identical fuel meat composition, which is provided in Table 5.3-7. (Note that MCNP models are not developed for



## **BRR Package Safety Analysis Report**

---

U-Mass (aluminide), U-Mass (silicide), and Purdue.) The plates are clad in aluminum, which is modeled as pure with a density of  $2.7 \text{ g/cm}^3$ .

PULSTAR fuel has  $\text{UO}_2$  fuel pellets with an enrichment of either 4% or 6% U-235. The pellet density is modeled as  $10.4 \text{ g/cm}^3$ , which is on the lower end of PULSTAR fuel to minimize self-shielding. The fuel pellet composition is provided in Table 5.3-8. PULSTAR fuel is clad in zirconium alloy tubing, which is modeled as pure zirconium with a density of  $6.5 \text{ g/cm}^3$ . A box of zirconium alloy surrounds the 5x5 array of fuel rods.

The baskets and loose plate box are manufactured out of stainless steel, and the cask is constructed of stainless steel and lead. The stainless steel composition and density utilized in the MCNP models are provided in Table 5.3-9. Lead is modeled as pure with a density of  $11.35 \text{ g/cm}^3$  [6].

Void spaces are filled with dry air. The composition is obtained from SCALE material library [5] and is provided in Table 5.3-10.

**Table 5.3-1 – Key Cask Model Dimensions**

Item	Dimension (in)
<b>Cask Radial</b>	
Cask inner diameter	16.0
Cask inner steel thickness	1.0
Cask lead thickness	8.0, modeled as 7.9375
Cask lead radial shrinkage gap (assumed)	0.0625
Cask outer steel thickness	2.0
Cask outer diameter (w/o heat shield)	38.0
Cask to heat shield gap	0.105
Heat shield thickness	0.105
Upper and lower impact limiter diameter	78.0, modeled as 72.0
<b>Cask Axial Top</b>	
Shield plug bottom plate thickness	1.0
Shield plug lead thickness	9.7, modeled as 9.58
Shield plug top plate thickness	0.5
Shield plug overall height	11.2, modeled as 11.08
Shield plug vent pipe inner diameter (schedule 40S)	0.824
Lid thickness	2.0
Upper impact limiter thickness at centerline	21.2
Overall height (including impact limiters)	119.5
<b>Cask Axial Bottom</b>	
Bottom outer plate thickness	1.0
Bottom lead thickness at centerline	7.7, modeled as 7.72
Bottom casting inner thickness (after machining)	1.1, modeled as 1.22
Bottom lead major diameter	23.7
Bottom lead minor diameter	10.3, modeled as 9.75
Drain hole diameter	0.5
Lower impact limiter thickness at centerline	21.2

**Table 5.3-2 – Key Basket Model Dimensions**

Item	Dimension (in)
<b>MURR Basket</b>	
Overall height	53.45
Cavity length	33.13
Support plate thickness	0.375
Compartment separator width	1.0
Shell outer diameter	15.63
Shell thickness	0.25
Inner tube outer diameter	7.9, modeled as 7.938
Inner tube inner diameter	7.0
<b>MITR-II Basket</b>	
Overall height	53.45
Cavity length	26.88
Support plate thickness	0.5
Inner Diameter	Complex, modeled as 9.45
Outer Diameter	15.63
Compartment perpendicular width	2.7
Distance, cutout to center	4.8
<b>ATR Basket</b>	
Overall height	53.45
Cavity length	51.38, modeled as 51.37
Support plate thickness	0.5
Compartment separator width	0.375
Shell outer diameter	13.5
Shell thickness	0.25
Inner tube outer diameter	7.2
Inner tube inner diameter	6.5
<b>TRIGA Basket</b>	
Overall height	53.45
Cavity length	48.0
Support plate thickness (after machining)	0.3, modeled as 0.25
Tube outer diameter	2.0
Tube wall thickness	0.12, modeled as 0.11
Inner row position diameter	6.5
Outer row position diameter	11.5

(continued)

**Table 5.3-2 – Key Basket Model Dimensions (concluded)**

Item	Dimension (in)
<b>Square Fuel Basket</b>	
Overall height	53.45, modeled as 54.0
Cavity length	40.0
Inner lateral dimensions	3.4 x 3.4
Stainless steel compartment wall thickness	0.105
Support plate thickness	0.37, modeled as 0.36
Centerline radius, outer compartments	5.47, modeled as 5.42
<b>Loose Plate Box</b>	
Overall height	39.75, modeled as 40.0
Inner lateral dimensions	3.0 x 2.5
Stainless steel plate thickness	0.125

**Table 5.3-3 – Key Fuel Parameters**

Item	Parameter
<b>MURR<sup>①</sup></b>	
Nominal active fuel length (in)	24
Overall length (in)	32.5
Nominal cladding thickness (in)	0.015
Nominal fuel matrix thickness (in)	0.02
Nominal fuel matrix width (in)	variable
<b>MITR-II<sup>①</sup></b>	
Nominal active fuel length (in)	22.375
Overall length (in)	26.265
Nominal cladding thickness (in)	0.025
Nominal fuel matrix thickness (in)	0.03
Nominal fuel matrix width (in)	2.076
<b>ATR<sup>①</sup></b>	
Nominal active fuel length (in)	48
Overall length (in)	51
Nominal cladding thickness (plate 1 / plates 2 – 18, plate 19) (in)	0.03 / 0.015 / 0.04
Nominal fuel matrix thickness (in)	0.02
Nominal fuel matrix width (in)	variable
<b>TRIGA<sup>②</sup></b>	
Active fuel length (in)	15
Overall length (in)	28.0
Fuel pellet outer diameter (in)	1.44
Fuel pellet inner diameter (in)	0.25
Cladding outer diameter (in)	1.48
Cladding thickness (in)	0.02
Zirconium rod diameter (in)	0.225

①The fuel dimensions for MURR, MITR-II, and ATR are used in the homogenization calculations, but are not modeled explicitly.

②TRIGA Type 109 materials and geometry is conservatively modeled in MCNP to maximize subcritical neutron multiplication, although the bounding TRIGA Type 219 source is used.

(continued)

**Table 5.3-3 – Key Fuel Parameters (concluded)**

Item	Parameter
<b>RINSC, Ohio State, Missouri S&amp;T, U-Florida Elements</b>	
Number of plates, RINSC	22
Number of plates, Ohio State	16
Number of plates, Missouri S&T	18
Number of plates, U-Florida	14
Nominal active fuel length (in)	23.25
Overall length (U-Florida) (in)	27.38
Nominal plate thickness (in)	0.05
Nominal fuel matrix thickness (in)	0.02
Nominal fuel matrix width (in)	2.395
<b>U-Florida Fuel Plate (for Loose Plate Box)</b>	
Nominal active fuel length (in)	23.25
Overall length (in)	27.38
Nominal plate thickness (in)	0.05
Nominal fuel matrix thickness (in)	0.02
Nominal fuel matrix width (in)	2.395
<b>PULSTAR</b>	
Maximum active fuel length (in)	24.1
Overall length (region with zircaloy box) (in)	32.4
Minimum cladding thickness (in)	0.0185
Maximum pellet diameter (in)	0.423
Maximum rod diameter (in)	0.474
Nominal pitch (in)	0.607 x 0.525
Fuel layout (in)	5 x 5
Zircaloy box outer dimensions (in)	3.15 x 2.74
Zircaloy box wall thickness (in)	0.06

**Table 5.3-4 – Homogenized Fuel Data, MURR, MITR-II, ATR**

Parameter	MURR	MITR-II	ATR
U-235 (g)	785	515	1200
U-238 (g)	50.1	32.9	76.6
Al (g)	3353.1	2311.9	5414.5
Compartment volume (cm <sup>3</sup> )	4884.2	3018.3	8192.0

**Table 5.3-5 – Homogenized Fuel Atom Densities (atom/b-cm), MURR, MITR-II, ATR**

Isotope	MURR	MITR-II	ATR
U-235	4.1178E-04	4.3716E-04	3.7531E-04
U-238	2.5952E-05	2.7552E-05	2.3653E-05
Al	1.5322E-02	1.7095E-02	1.4752E-02
Total	1.5760E-02	1.7560E-02	1.5151E-02

**Table 5.3-6 – TRIGA Fuel Atom Densities (atom/b-cm)**

Isotope	TRIGA
U-235	8.9746E-04
U-238	3.7791E-04
H	5.5825E-02
Zr	3.4891E-02
Total	9.1991E-02

**Table 5.3-7 – Square Plate Fuel Atom Densities (atom/b-cm)**

Isotope	Plate Fuel <sup>①</sup>
U-235	1.7057E-03
U-238	6.8433E-03
Si	5.6850E-03
Al	4.2301E-02
Total	5.6535E-02

<sup>①</sup>Applies to RINSC, Ohio State, Missouri S&T, and U-Florida MCNP models. MCNP models are not developed for U-Mass (aluminide), U-Mass (silicide), or Purdue.

**Table 5.3-8 – PULSTAR Pellet Composition**

<b>Isotope</b>	<b>4% Enriched (Wt.%)</b>	<b>6% Enriched (Wt.%)</b>
U-235	3.5259	5.2889
U-238	84.6222	82.8593
O	11.8519	11.8519
Density (g/cm <sup>3</sup> )	10.4	10.4

**Table 5.3-9 – SS304 Composition**

<b>Component</b>	<b>Wt.%</b>
C	0.08
Si	1.0
P	0.045
Cr	19.0
Mn	2.0
Fe	68.375
Ni	9.5
Density (g/cm <sup>3</sup> )	7.94

**Table 5.3-10 – Air Composition**

<b>Component</b>	<b>Wt.%</b>
N	76.508
O	23.4793
C	0.0126
Density (g/cm <sup>3</sup> )	0.0012



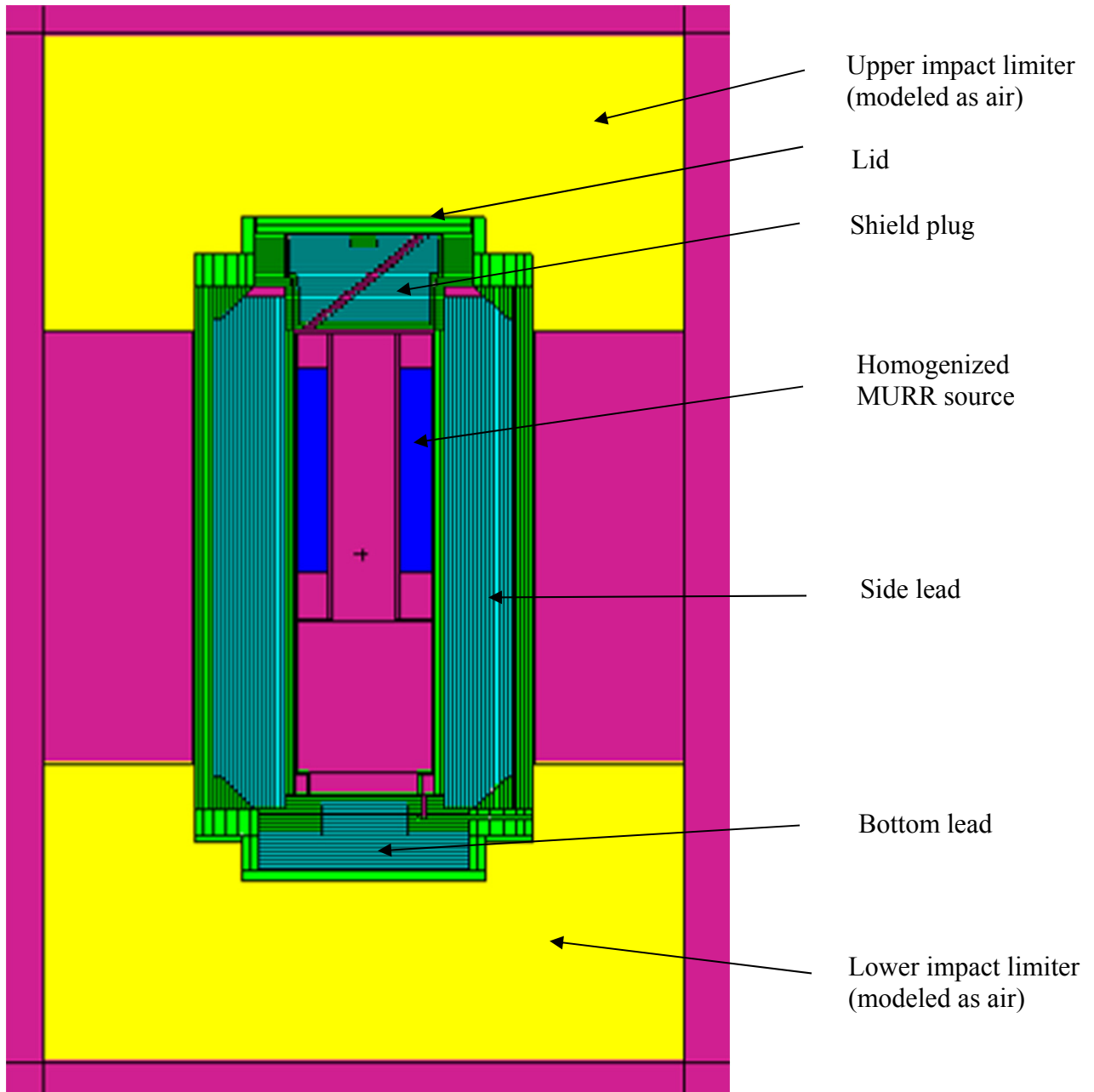
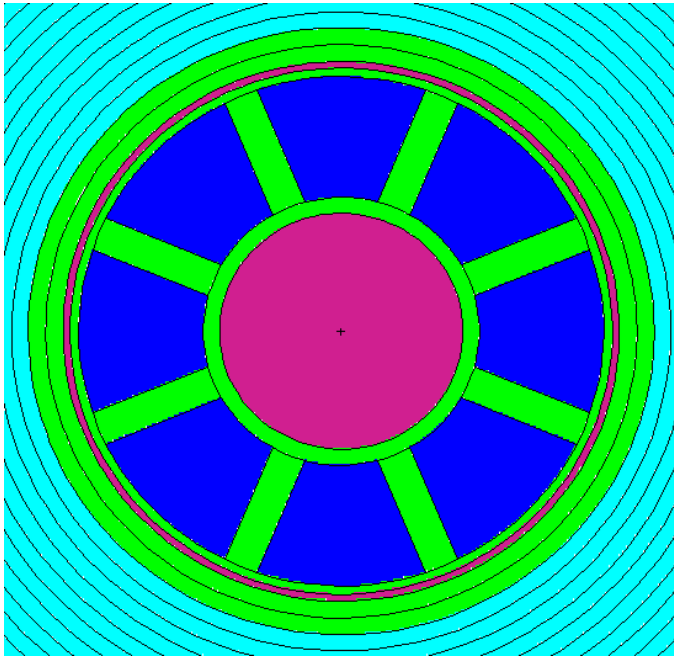
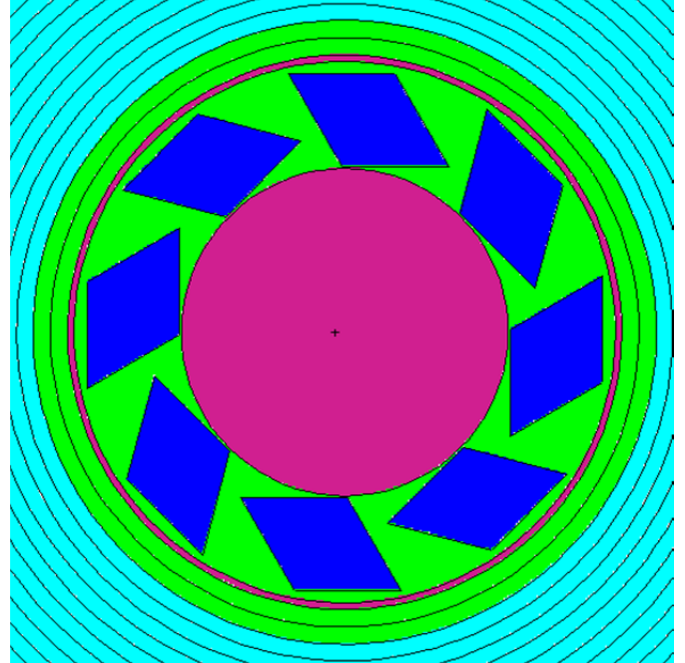


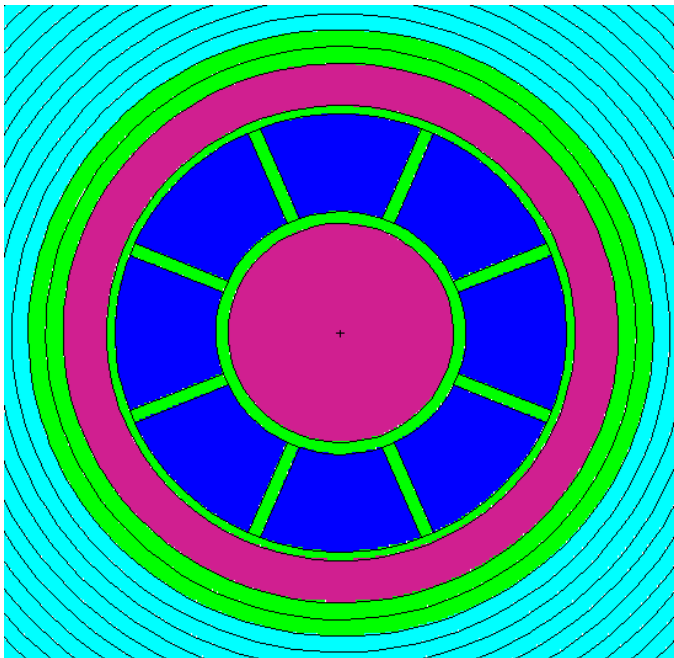
Figure 5.3-1 – Shielding Model



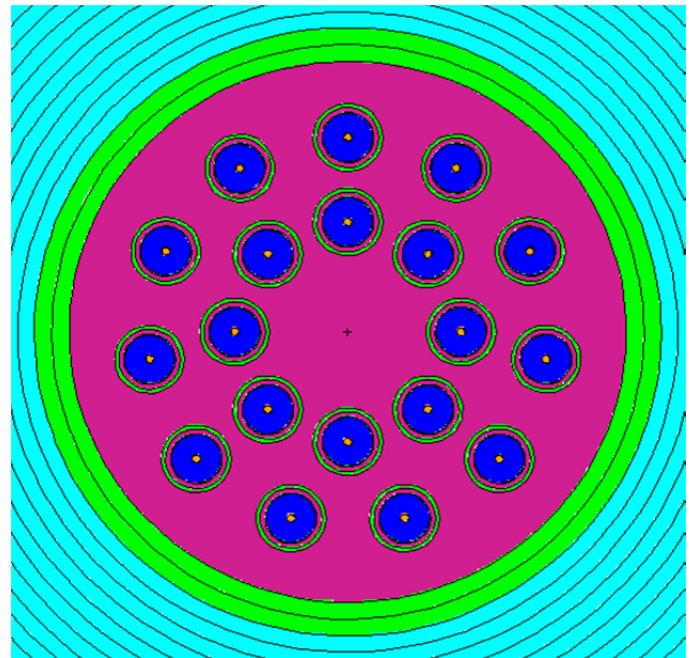
MURR



MITR-II

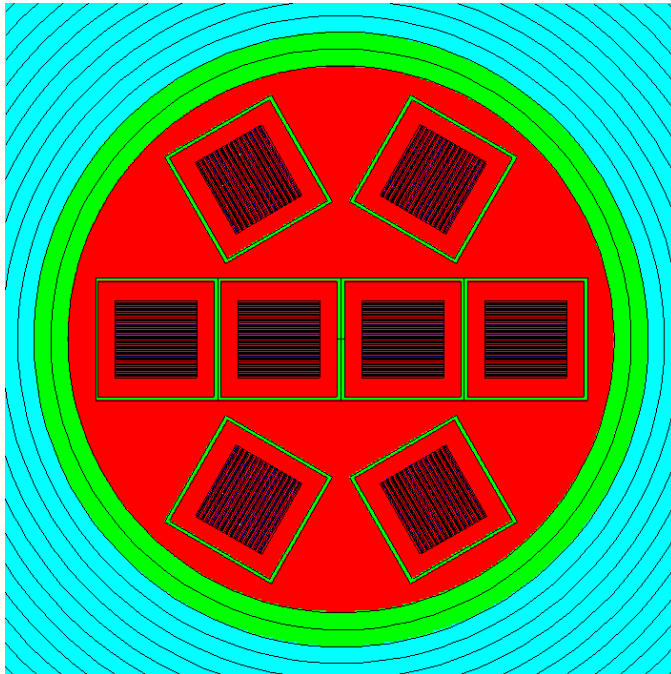


ATR

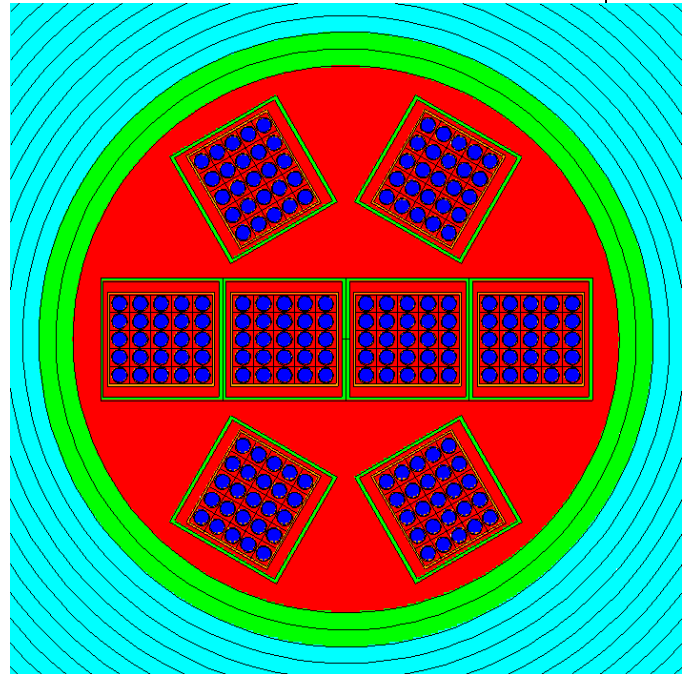


TRIGA

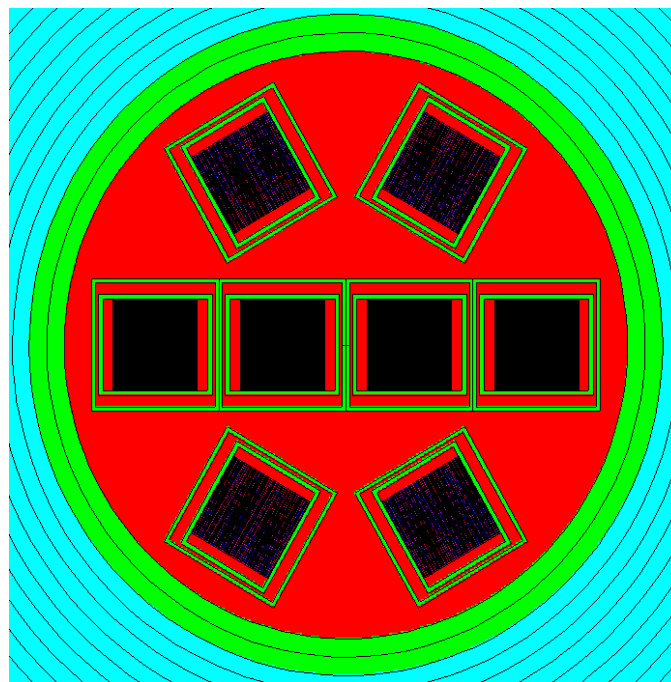
**Figure 5.3-2 – Basket Models (cross section), MURR, MITR-II, ATR, TRIGA**



U-Florida Element

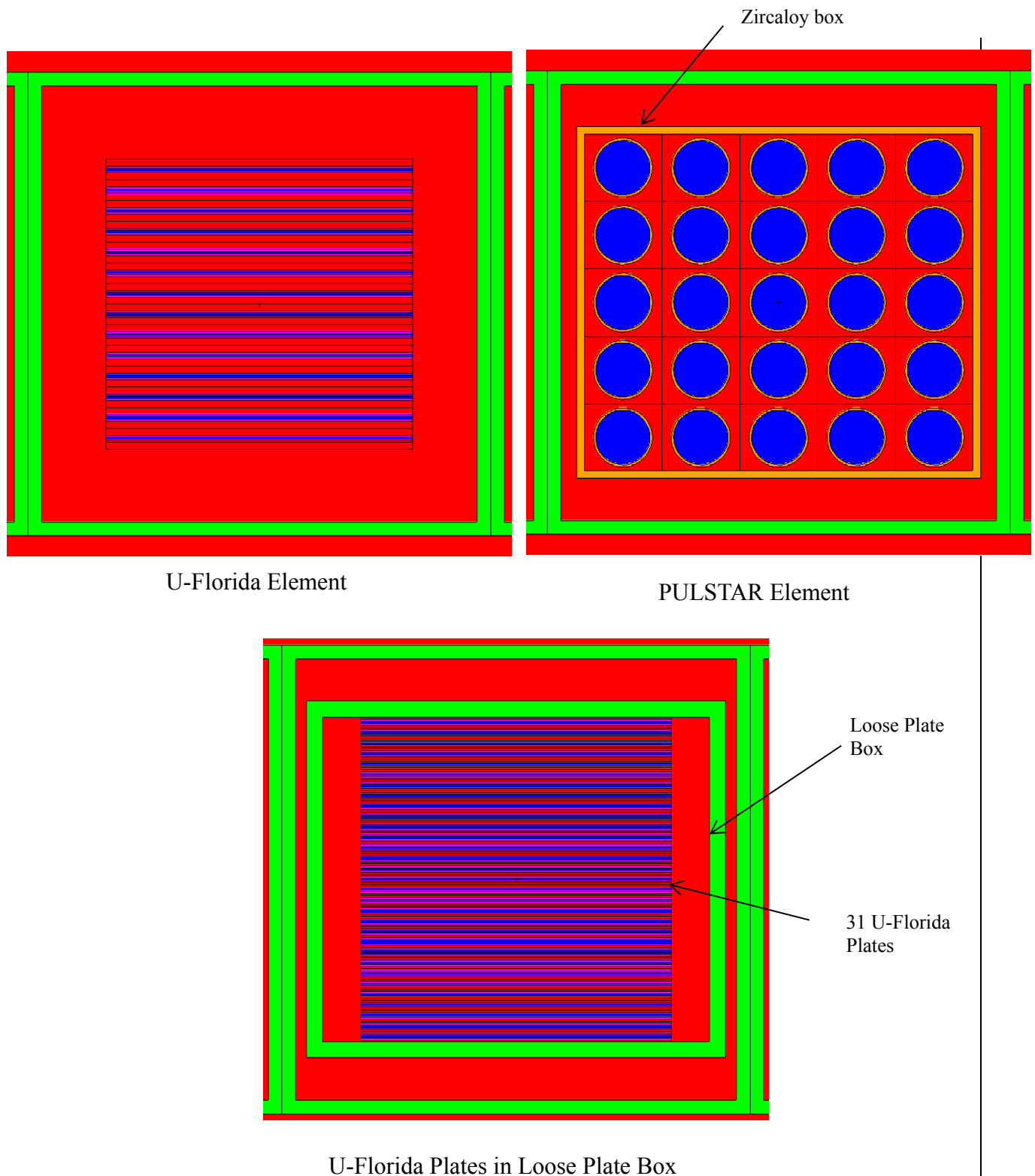


PULSTAR Element

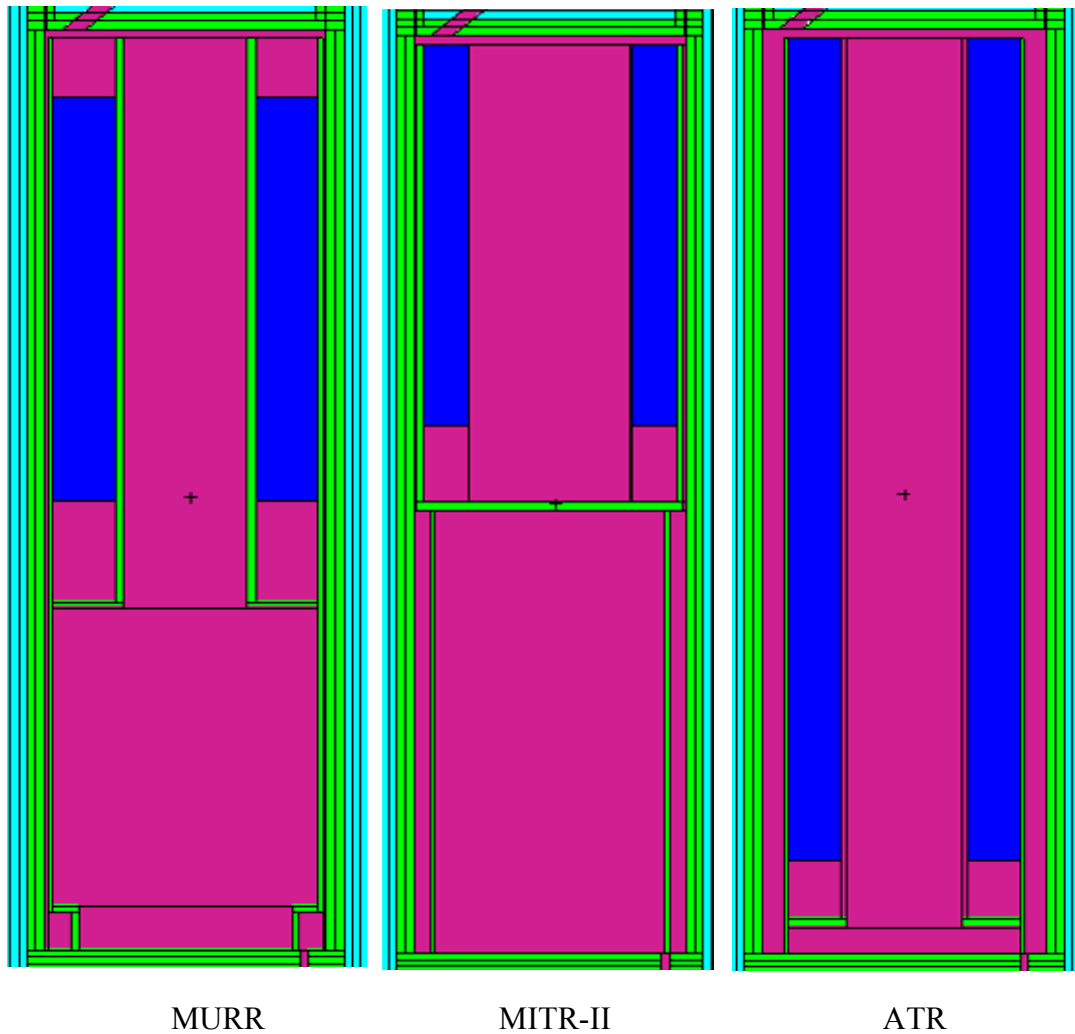


U-Florida Plates in Loose Plate Box

**Figure 5.3-3 – Basket Model (cross section), SFB**



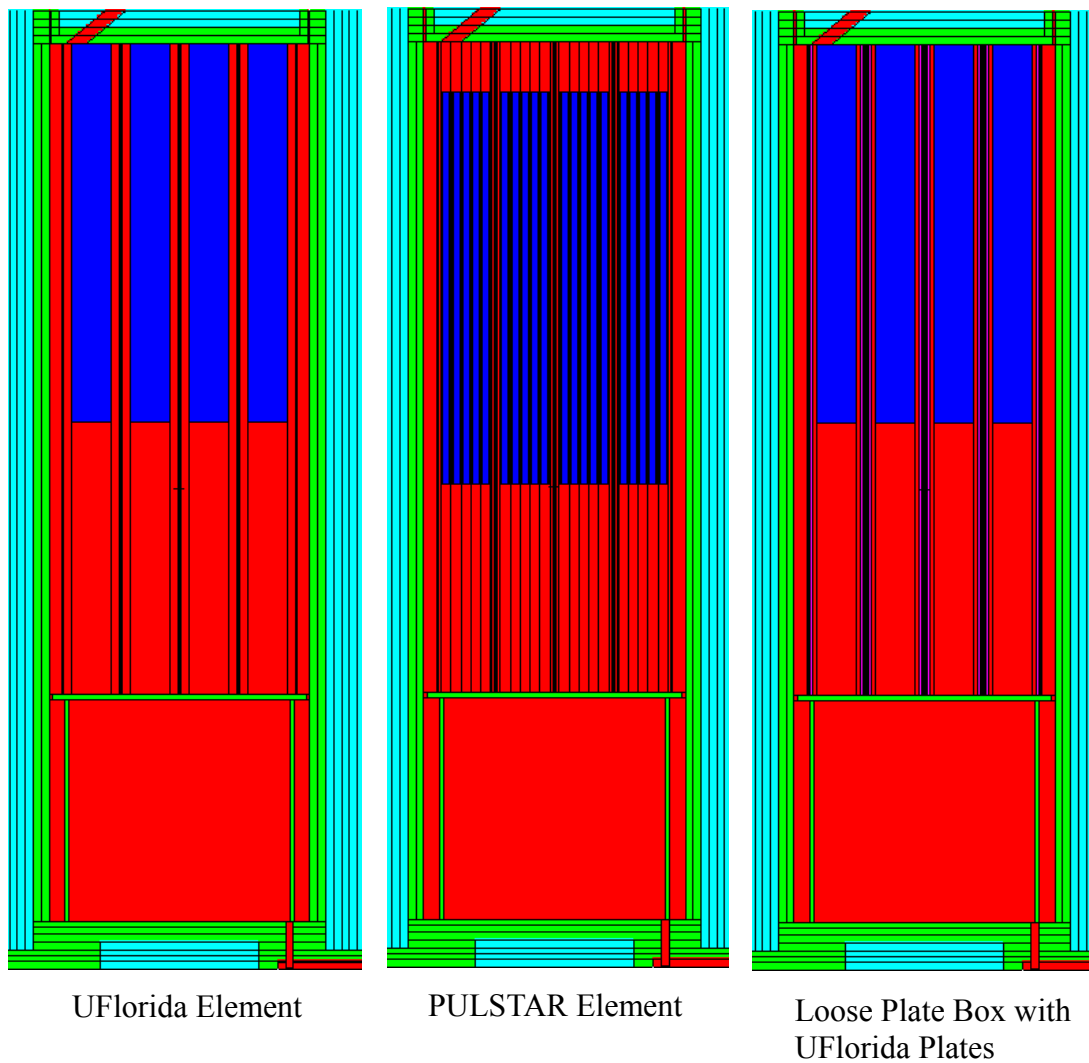
**Figure 5.3-4 – Basket Model (cross section), SFB, Close-Up View**



**Figure 5.3-5** – Basket Models (axial), MURR, MITR-II, ATR



**Figure 5.3-6** – Basket Models (axial), TRIGA



**Figure 5.3-7 – Basket Models (axial), Square Fuel Basket**

## 5.4 Shielding Evaluation

### 5.4.1 Methods

The dose rates for MURR, MITR-II, and ATR fuel are computed using the MCNP5 v1.30 computer program [2], while dose rates for the SFB and TRIGA fuel are computed using MCNP5 v1.51. All relevant package features are modeled in three-dimensions. For simplicity, the impact limiters are modeled simply as air, although the outer surfaces of the impact limiters are treated as the outer surfaces of the package when computing surface dose rates at the ends of the package. It is assumed that under HAC the impact limiters remain attached and suffer 12-in axial crush on each end, and the same MCNP model is used to compute both NCT and HAC dose rates. This approach is reasonable, because no shielding credit is taken for the impact limiters, other than distance.

Separate models are developed for neutron and gamma radiation. For MURR, MITR-II, and ATR fuel, the fuel plates are homogenized and fill the basket cavities. Homogenization is performed to simplify the source description. For the TRIGA fuel and “square” fuels, because the fuel geometry is simple, the fuel is modeled explicitly, and the source is distributed over the fuel matrix. The TRIGA stainless steel cladding source is also explicitly modeled in the cladding. Note that subcritical neutron multiplication is handled automatically by MCNP.

Little clearance is available in any of the designs for axial shifting of the fuel. Because the fuel is positioned by the baskets closer to the lid end, to maximize the dose rates at the impact limiter surface, the fuel is modeled as shifted to the top of the cavity. Distance credit is taken for non-fuel structural material, such as the cladding and end caps in the TRIGA fuel. Because TRIGA fuel has a wide range of lengths, TRIGA models are developed for the fuel at either the bottom or the top of the basket.

In general, secondary gammas generated by neutron capture are not computed, as there is no hydrogenous neutron shielding material. Secondary gamma dose rates are computed only for the TRIGA fuel because hydrogen is included in the fuel matrix. However, even for the TRIGA fuel, the secondary gamma dose rate is essentially zero, because the secondary gammas are generated inside the cask, and are then attenuated in the shield.

In all cases, dose rates are computed on segmented surfaces so that the maximum dose rates may be located. Neutron and gamma surface fluxes are computed by MCNP, and converted to dose rates using flux-to-dose rate conversion factors (see Section 5.4.3, *Flux-to-Dose Rate Conversion*). Side dose rates are averaged over the circumference of the cylindrical tallies.

### 5.4.2 Input and Output Data

A sample input file (gamma source, MITR-II fuel) is included in Section 5.5.3.2, *MCNP Input File*. The input file may be compared against the gamma sources in table Table 5.2-3 and gamma axial distribution in Table 5.2-5 to verify proper model setup. Model geometry and material descriptions may be verified by inspection of the supplied input file.

The results are highly converged for all dose rate locations of interest. In the models with a gamma source, the materials are split into thin layers, and the importance of each layer is increased away from the source. In the models with a neutron source, the importances are all set



to the same value, as there is no neutron shield. Statistical uncertainties are typically in the range of 2-3%.

### 5.4.3 Flux-to-Dose Rate Conversion

ANSI/ANS-6.1.1-1977 flux-to-dose rate conversion factors are used in this analysis. These are obtained from the MCNP User's Manual [2], Tables H.1 and H.2, although these values have been converted to provide results in mrem/hr rather than rem/hr. These conversion factors are provided in Table 5.4-1.

### 5.4.4 External Radiation Levels

The objective is to determine the dose rates for the bounding payload in each of the five unique baskets: MURR, MITR-II, ATR, TRIGA, and SFB. For MURR, MITR-II, and ATR, only one fuel type is allowed and the bounding payload is simply the fuel type. For TRIGA fuel, the bounding payload is TRIGA Type 219, which is demonstrated in Table 5.2-8.

For the SFB, due to the wide range of fuel types, the bounding payload is determined using explicit MCNP models. The approach is to determine the dose rate at the side of the cask using each of the candidate SFB payloads. The U-Mass (aluminide and silicide) and Purdue fuel elements have low burnups and low decay heat and it is determined by inspection that these fuel types are bounded by the other SFB payloads. Explicit MCNP models are developed for the SFB with the following payloads: RINSC, Ohio State, Missouri S&T, U-Florida, PULSTAR (4% and 6% enriched), and the loose plate box with 31 U-Florida fuel plates. The results of this study are reported in Table 5.4-2 with the SFB payloads ranked in order from high to low dose rate.

The bounding SFB payload is the loose plate box with 31 U-Florida plates per box. The maximum side dose rate with the loose plate box is approximately twice the dose rate of the PULSTAR fuel element, which is the bounding SFB fuel element. The dose rate is almost entirely due to neutron radiation because of the high burnup of the U-Florida fuel. Therefore, detailed dose rate results for the SFB are reported only for the loose plate box.

A gamma and neutron model is developed for each of the five baskets. For TRIGA fuel, separate gamma models are developed for source in the active fuel and cladding regions. Also, due to the wide range of lengths available for TRIGA fuel, the TRIGA models are run with the fuel shifted up or down. Top and side TRIGA results are reported for the fuel shifted up, and bottom TRIGA results are reported for the fuel shifted down. Side TRIGA results are reported for the maximum dose rates of the two axial source locations, although the magnitude of the side dose rate is largely insensitive to the axial location of the source. The other fuels have standard lengths and are modeled consistent with their location in the cask.

For exclusive use transport, the following 10 CFR 71.47 dose rates must be met:

- Maximum NCT cask surface dose rate of 200 mrem/hr. The higher 1000 mrem/hr limit is not claimed because the vehicle will be open. The dose rate limit applies at the outer surface of the heat shield, and the outer surface of the impact limiters. These results are summarized in Table 5.4-3 and Table 5.4-4. See also Figure 5.4-1 and Figure 5.4-2 for a graphical depiction of the tally locations.

- Maximum NCT vehicle surface dose rate of 200 mrem/hr. This limit is somewhat redundant because it is the same as the cask surface limit, and the cask surface dose rates are always higher than the vehicle surface dose rates. In this case, the vehicle surface is projected at the side because the actual vehicle will be open. It is assumed the vehicle is 8 ft wide, and the cask is laterally centered on the vehicle. The bottom surface of the vehicle may be considered the bottom surface of the lower impact limiter, and the top surface of the vehicle may be considered the top surface of the upper impact limiter. These side results are summarized in Table 5.4-5, and the top/bottom results are included in Table 5.4-4. See also Figure 5.4-2 through Figure 5.4-4 for a graphical depiction of the tally locations.
- Maximum NCT dose rate 2 m from the vehicle surface of 10 mrem/hr. These results are summarized in Table 5.4-6. See also Figure 5.4-3 and Figure 5.4-4 for a graphical depiction of the tally locations.
- Maximum NCT dose rate in any occupied location of 2 mrem/hr. The only occupied location is the driver of the vehicle, which is assumed to be 25 ft (7.6 m) from the centerline of the cask. These results are summarized in Table 5.4-7. See also Figure 5.4-3 and Figure 5.4-4 for a graphical depiction of the tally location.
- Maximum HAC dose rate of 1000 mrem/hr 1 m from the surface of the cask. As the impact limiters will remain attached under HAC, the end dose rates are computed 1 m from the ends of the impact limiters, assuming 12-in crush on each end. In the radial direction, the dose rates are computed 1 m from the heat shield. These results are summarized in Table 5.4-8 and Table 5.4-9. See also Figure 5.4-3, Figure 5.4-4, and Figure 5.4-5 for a graphical depiction of the tally locations.

Dose rates are not constant along the side of the cask. The dose rate is typically at a maximum next to the active fuel, and becomes lower away from this region. Therefore, it is customary to segment the tallies into small regions in order to capture the maximum dose rate. On the side surface of the cask, the tally is divided into 12 equal segments 10.7 cm wide (see Figure 5.4-1). On the cylindrical sides of the impact limiters, the tally is divided into 5 equal segments 17.6 cm wide (see Figure 5.4-2). On the upper and lower impact limiter surfaces, the tally is divided into 9 concentric rings of width 10.2 cm (see Figure 5.4-2).

For the four side tallies (vehicle surface, 2 m from vehicle surface, occupied location, and 1 m HAC), the tallies are segmented into 15 segments 20.3 cm wide (see Figure 5.4-3 and Figure 5.4-4). In addition, the side dose rates above and below the impact limiter surfaces are also reported, although these tallies are approximately 70 cm wide.

The HAC 1 m tallies from the top and bottom of the impact limiters are divided into 11 segments, up to 1 m radially from the surface of the thermal shield (see Figure 5.4-5).

The dose rates reported in the following tables are the summed gamma and neutron dose rates. Dose rates are presented for each of the five baskets. The maximum cask surface dose rate is 68.1 mrem/hr (limit = 200 mrem/hr). The maximum vehicle surface dose rate is 9.9 mrem/hr (limit = 200 mrem/hr) and occurs on the top of the package. The maximum dose rate 2 m from the surface of the vehicle is 1.2 mrem/hr (limit = 10 mrem/hr), and the maximum dose rate at the occupied location is 0.2 mrem/hr (limit = 2 mrem/hr). Therefore, all of the NCT dose rates are met with large margins.

The maximum HAC dose rate 1 m from the cask is 6.1 mrem/hr (limit = 1000 mrem/hr) and occurs at the side. Clearly, the HAC dose rate limit is met with a large margin.

The detailed results from the TRIGA basket, including statistical uncertainties, are reported in Section 5.5.2, *Detailed TRIGA Results*. The TRIGA basket is selected for this detailed presentation because it results in the largest cask surface dose rate.

**Table 5.4-1 – Flux-to-Dose Rate Conversion Factors**

<b>E (MeV)</b>	<b>Neutron Factors (mrem/hr)/(n/cm<sup>2</sup>/s)</b>	<b>E (MeV)</b>	<b>Neutron Factors (mrem/hr)/(n/cm<sup>2</sup>/s)</b>
2.50E-08	3.67E-03	0.5	9.26E-02
1.00E-07	3.67E-03	1.0	1.32E-01
1.00E-06	4.46E-03	2.5	1.25E-01
1.00E-05	4.54E-03	5.0	1.56E-01
1.00E-04	4.18E-03	7.0	1.47E-01
0.001	3.76E-03	10.0	1.47E-01
0.01	3.56E-03	14.0	2.08E-01
0.1	2.17E-02	20.0	2.27E-01
<b>E (MeV)</b>	<b>Gamma Factors (mrem/hr)/(γ/cm<sup>2</sup>/s)</b>	<b>E (MeV)</b>	<b>Gamma Factors (mrem/hr)/(γ/cm<sup>2</sup>/s)</b>
0.01	3.96E-03	1.4	2.51E-03
0.03	5.82E-04	1.8	2.99E-03
0.05	2.90E-04	2.2	3.42E-03
0.07	2.58E-04	2.6	3.82E-03
0.1	2.83E-04	2.8	4.01E-03
0.15	3.79E-04	3.25	4.41E-03
0.2	5.01E-04	3.75	4.83E-03
0.25	6.31E-04	4.25	5.23E-03
0.3	7.59E-04	4.75	5.60E-03
0.35	8.78E-04	5.0	5.80E-03
0.4	9.85E-04	5.25	6.01E-03
0.45	1.08E-03	5.75	6.37E-03
0.5	1.17E-03	6.25	6.74E-03
0.55	1.27E-03	6.75	7.11E-03
0.6	1.36E-03	7.5	7.66E-03
0.65	1.44E-03	9.0	8.77E-03
0.7	1.52E-03	11.0	1.03E-02
0.8	1.68E-03	13.0	1.18E-02
1.0	1.98E-03	15.0	1.33E-02

**Table 5.4-2 – SFB Payload Ranking, Cask Side Maximum Dose Rate (mrem/hr)**

<b>SFB Payload</b>	<b>Gamma</b>	<b>Neutron</b>	<b>Total</b>
Loose Plate Box	0.5	38.7	39.2
PULSTAR (4%)	1.0	18.0	19.0
U-Florida	0.4	17.8	18.2
PULSTAR (6%)	1.0	8.0	9.0
Ohio State	2.1	4.3	6.4
RINSC	2.5	1.3	3.8
Missouri S&T	0.5	2.3	2.8
U-Mass (aluminide)	NA	NA	< 2.8
U-Mass (silicide)	NA	NA	< 2.8
Purdue	NA	NA	< 2.8

**Table 5.4-3 – NCT Cask Side Total Dose Rates (mrem/hr)**

<b>Location</b>	<b>MURR</b>	<b>MITR-II</b>	<b>ATR</b>	<b>TRIGA</b>	<b>SFB</b>
1	2.2	8.2	2.1	40.0	21.6
2	5.0	11.3	2.9	54.8	30.2
3	8.5	12.9	3.6	65.8	37.1
4	10.9	12.4	4.2	68.1	39.2
5	11.1	10.0	4.7	61.0	35.6
6	9.0	6.4	4.9	48.5	28.4
7	5.2	3.4	4.8	34.9	20.5
8	2.1	1.9	4.5	24.5	14.1
9	0.7	1.2	4.0	16.9	9.5
10	0.3	0.8	3.3	11.9	6.4
11	0.2	0.6	2.5	8.3	4.4
12	0.1	0.4	1.8	5.8	3.0
Max	11.1	12.9	4.9	68.1	39.2
Limit = 200 mrem/hr					

**Table 5.4-4 – NCT Impact Limiter Total Dose Rates (mrem/hr)**

	Upper Impact Limiter Side					Lower Impact Limiter Side				
Location	MURR	MITR-II	ATR	TRIGA	SFB	MURR	MITR-II	ATR	TRIGA	SFB
1	2.0	8.0	0.5	5.4	1.6	0.2	0.3	0.6	9.2	1.8
2	1.4	5.5	0.5	5.2	1.9	0.1	0.2	0.4	6.7	1.2
3	0.9	3.2	0.4	5.6	2.6	0.2	0.2	0.5	5.9	0.8
4	0.7	2.3	0.5	7.2	3.7	0.3	0.3	0.6	6.5	0.6
5	1.0	2.3	0.6	10.2	5.6	0.3	0.2	0.6	6.2	0.4
Max	2.0	8.0	0.6	10.2	5.6	0.3	0.3	0.6	9.2	1.8
	Upper Impact Limiter Horizontal/Vehicle Top					Lower Impact Limiter Horizontal/Vehicle Bottom				
Location	MURR	MITR-II	ATR	TRIGA	SFB	MURR	MITR-II	ATR	TRIGA	SFB
1	1.4	4.3	0.3	5.0	2.1	3.5	2.7	0.7	6.5	0.5
2	1.5	4.5	0.3	4.9	2.0	3.7	3.0	0.7	6.3	0.5
3	2.0	5.4	0.4	5.0	1.9	2.8	2.2	0.6	5.9	0.5
4	2.1	5.7	0.4	4.7	1.7	1.8	1.6	0.5	5.3	0.4
5	1.7	5.5	0.4	4.5	1.6	1.1	0.9	0.4	4.6	0.3
6	1.6	5.6	0.4	4.4	1.4	0.6	0.5	0.4	4.1	0.3
7	1.8	6.5	0.5	4.7	1.4	0.4	0.3	0.4	4.1	0.3
8	2.3	8.5	0.6	5.5	1.5	0.3	0.3	0.5	4.5	0.3
9	2.3	9.9	0.6	5.6	1.5	0.3	0.2	0.5	5.2	0.4
Max	2.3	9.9	0.6	5.6	2.1	3.7	3.0	0.7	6.5	0.5
Limit = 200 mrem/hr										

**Table 5.4-5 – NCT Vehicle Side Total Dose Rates (mrem/hr)**

Location	MURR	MITR-II	ATR	TRIGA	SFB
1	1.0	3.8	0.3	0.6	0.9
2	0.7	2.6	0.3	1.1	1.4
3	0.6	1.9	0.3	1.5	1.8
4	0.6	1.5	0.3	2.0	2.5
5	0.7	1.5	0.4	2.9	3.4
6	1.2	1.8	0.6	4.1	4.2
7	1.7	2.1	0.7	5.6	4.9
8	1.9	2.0	0.9	7.2	5.0
9	1.6	1.6	0.9	8.6	4.6
10	1.1	1.1	0.8	9.2	3.8
11	0.6	0.7	0.7	8.7	3.0
12	0.3	0.4	0.6	7.4	2.1
13	0.2	0.3	0.4	5.8	1.5
14	0.1	0.2	0.3	4.6	1.1
15	0.2	0.2	0.3	4.0	0.8
16	0.2	0.2	0.4	3.9	0.6
17	0.2	0.1	0.3	2.9	0.3
Max	1.9	3.8	0.9	9.2	5.0
Limit = 200 mrem/hr					

**Table 5.4-6 – NCT 2 m Total Dose Rates (mrem/hr)**

Location	MURR	MITR-II	ATR	TRIGA	SFB
1	0.1	0.3	0.1	0.6	0.4
2	0.2	0.3	0.1	0.8	0.5
3	0.2	0.3	0.1	0.8	0.6
4	0.2	0.3	0.1	0.9	0.6
5	0.2	0.3	0.1	1.0	0.6
6	0.2	0.3	0.1	1.1	0.7
7	0.3	0.3	0.1	1.1	0.7
8	0.3	0.3	0.1	1.2	0.7
9	0.3	0.3	0.1	1.2	0.7
10	0.2	0.3	0.1	1.2	0.6
11	0.2	0.2	0.1	1.2	0.6
12	0.2	0.2	0.1	1.2	0.6
13	0.2	0.2	0.1	1.2	0.5
14	0.1	0.2	0.1	1.1	0.5
15	0.1	0.1	0.1	1.1	0.5
16	0.1	0.1	0.1	1.0	0.4
17	0.1	0.1	0.1	0.9	0.3
Max	0.3	0.3	0.1	1.2	0.7
Limit = 10 mrem/hr					

**Table 5.4-7 – NCT Occupied Location Total Dose Rates (mrem/hr)**

Location	MURR	MITR-II	ATR	TRIGA	SFB
1	0.04	0.06	0.02	0.2	0.1
2	0.04	0.06	0.02	0.2	0.1
3	0.04	0.06	0.02	0.2	0.1
4	0.04	0.06	0.02	0.2	0.1
5	0.04	0.06	0.02	0.2	0.1
6	0.05	0.06	0.02	0.2	0.1
7	0.05	0.05	0.02	0.2	0.1
8	0.04	0.05	0.02	0.2	0.1
9	0.04	0.05	0.02	0.2	0.1
10	0.04	0.05	0.02	0.2	0.1
11	0.04	0.05	0.02	0.2	0.1
12	0.04	0.05	0.02	0.2	0.1
13	0.04	0.05	0.02	0.2	0.1
14	0.04	0.05	0.02	0.2	0.1
15	0.04	0.04	0.02	0.2	0.1
16	0.04	0.04	0.02	0.2	0.1
17	0.03	0.04	0.02	0.2	0.1
Max	0.05	0.06	0.02	0.2	0.1
Limit = 2 mrem/hr					

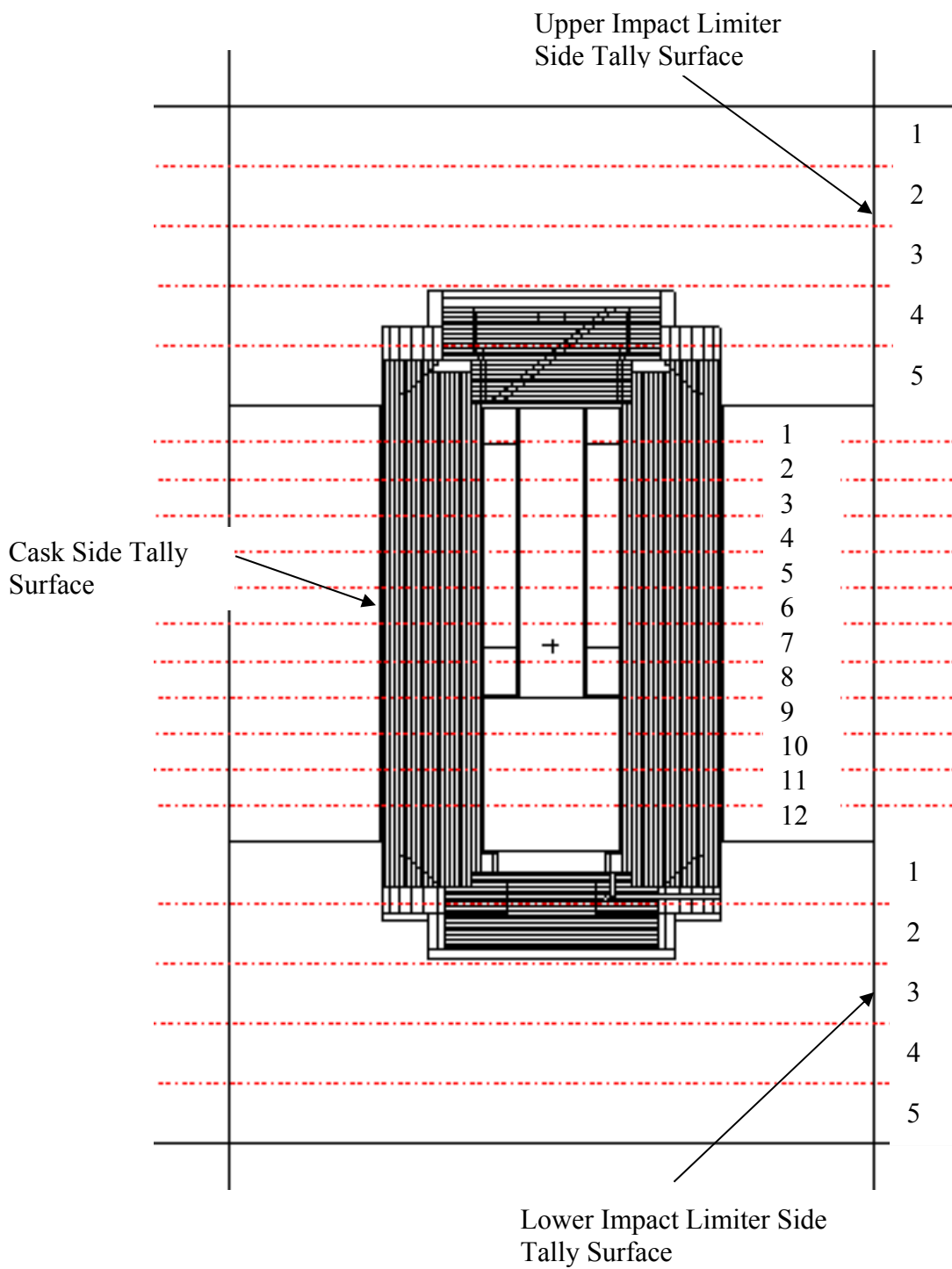


**Table 5.4-8 – HAC 1 m Side Total Dose Rates (mrem/hr)**

Location	MURR	MITR-II	ATR	TRIGA	SFB
1	0.6	2.4	0.2	0.7	0.8
2	0.4	1.4	0.2	1.2	1.3
3	0.4	1.2	0.2	1.5	1.6
4	0.5	1.1	0.3	2.0	2.0
5	0.6	1.2	0.4	2.6	2.5
6	0.9	1.3	0.4	3.4	2.9
7	1.2	1.4	0.5	4.3	3.2
8	1.3	1.4	0.6	5.1	3.3
9	1.1	1.1	0.6	5.8	3.1
10	0.9	0.9	0.6	6.1	2.7
11	0.6	0.6	0.5	5.8	2.3
12	0.4	0.4	0.4	5.2	1.8
13	0.2	0.3	0.3	4.4	1.4
14	0.2	0.2	0.3	3.7	1.1
15	0.1	0.2	0.2	3.2	0.8
16	0.1	0.2	0.2	2.8	0.6
17	0.1	0.1	0.2	2.5	0.4
Max	1.3	2.4	0.6	6.1	3.3
Limit = 1000 mrem/hr					

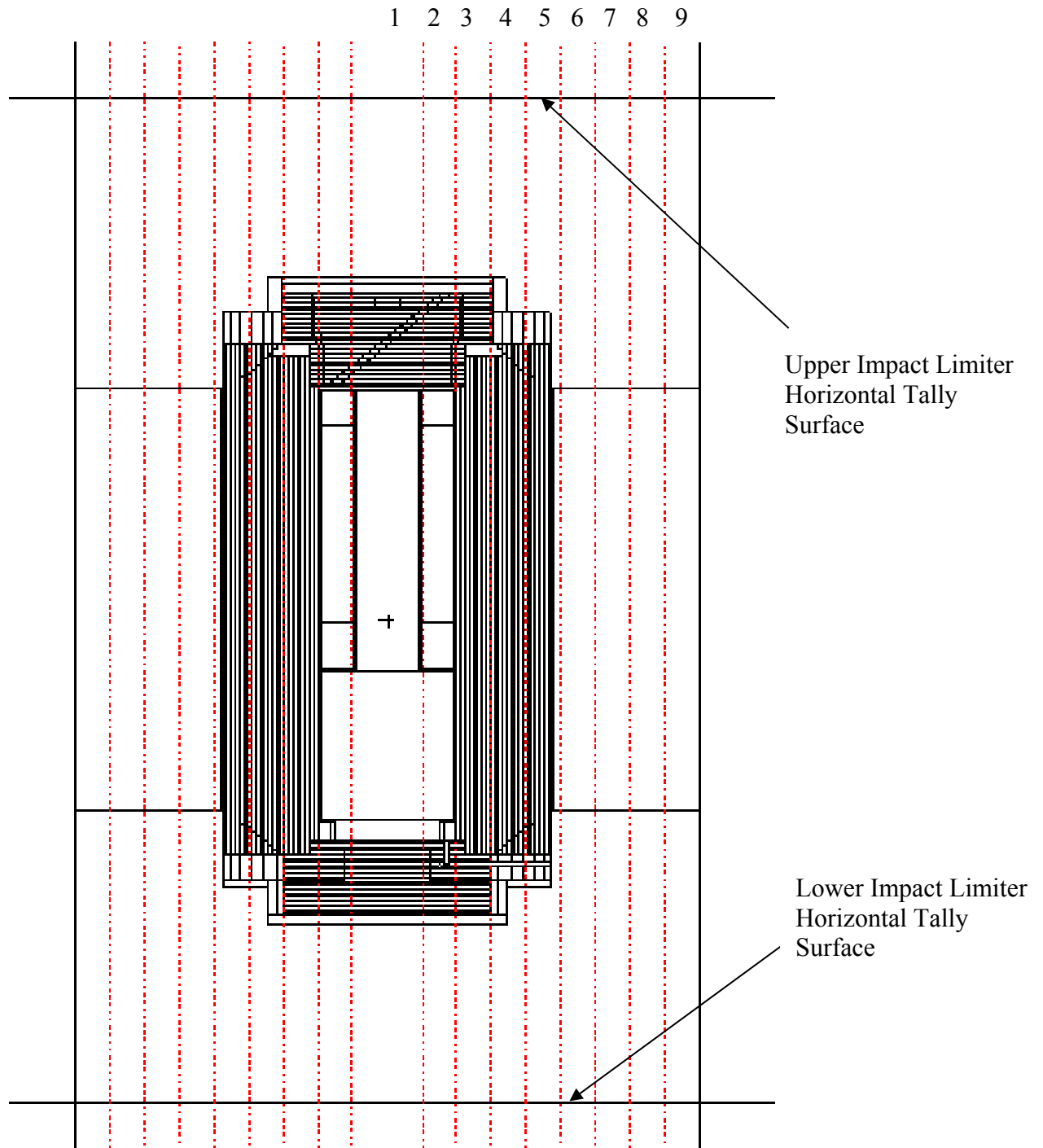
**Table 5.4-9 – HAC 1 m End Total Dose Rates (mrem/hr)**

Location	Upper Impact Limiter					Lower Impact Limiter				
	MURR	MITR-II	ATR	TRIGA	SFB	MURR	MITR-II	ATR	TRIGA	SFB
1	0.6	1.8	0.1	1.7	0.7	1.4	1.1	0.3	2.1	0.2
2	0.7	1.8	0.1	1.8	0.7	1.5	1.2	0.3	2.1	0.2
3	0.8	2.1	0.1	1.8	0.6	1.3	1.0	0.2	2.1	0.2
4	0.8	2.1	0.1	1.8	0.6	1.0	0.8	0.2	2.1	0.2
5	0.8	2.2	0.1	1.7	0.6	0.8	0.7	0.2	1.9	0.2
6	0.7	2.1	0.1	1.7	0.6	0.6	0.6	0.2	1.8	0.1
7	0.7	2.0	0.1	1.7	0.6	0.5	0.4	0.2	1.7	0.1
8	0.6	2.0	0.1	1.7	0.6	0.3	0.3	0.1	1.6	0.2
9	0.6	2.0	0.1	1.7	0.6	0.3	0.2	0.1	1.6	0.2
10	0.6	2.3	0.2	1.8	0.6	0.2	0.1	0.1	1.6	0.2
11	0.8	2.8	0.2	2.0	0.6	0.1	0.1	0.2	1.8	0.2
Max	0.8	2.8	0.2	2.0	0.7	1.5	1.2	0.3	2.1	0.2
Limit = 1000 mrem/hr										

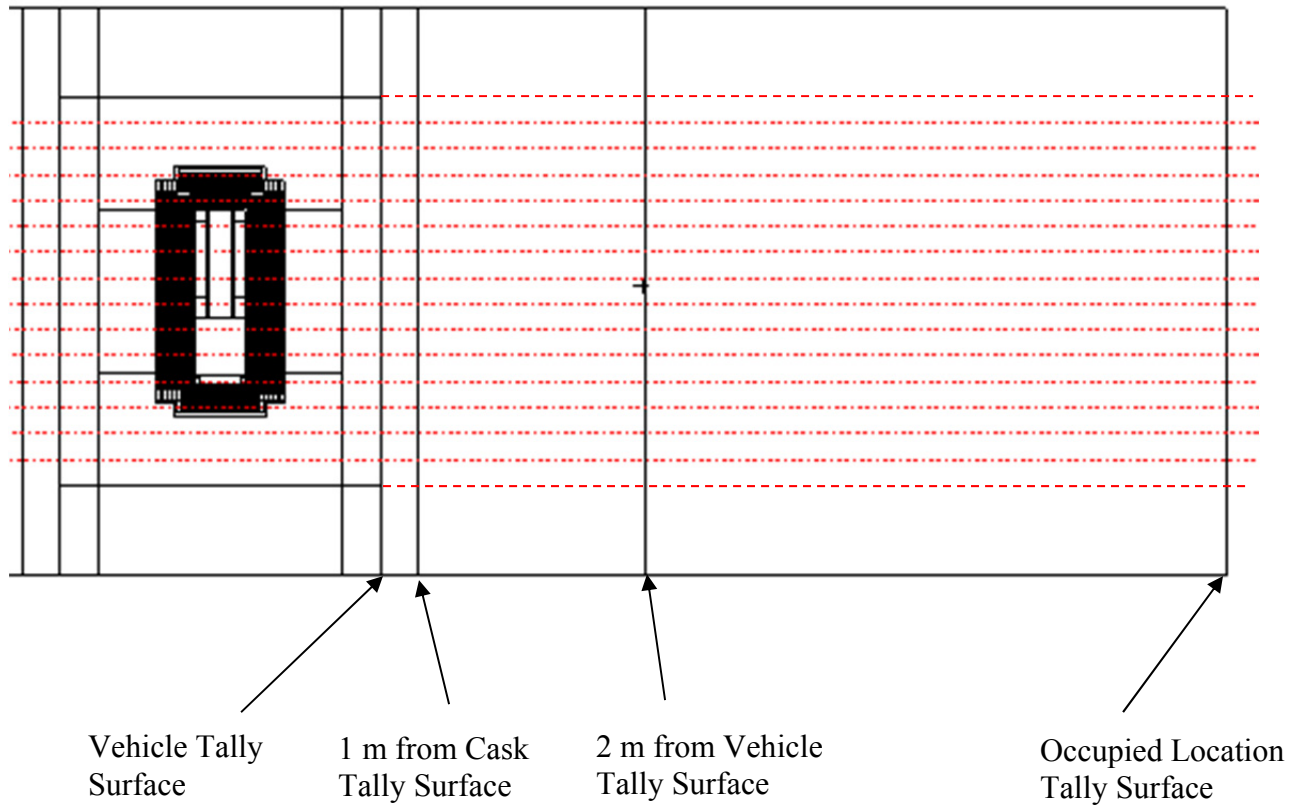


Note: All tallies are circumferential.

**Figure 5.4-1 – Cask/Impact Limiter Side Tally Segmentations**

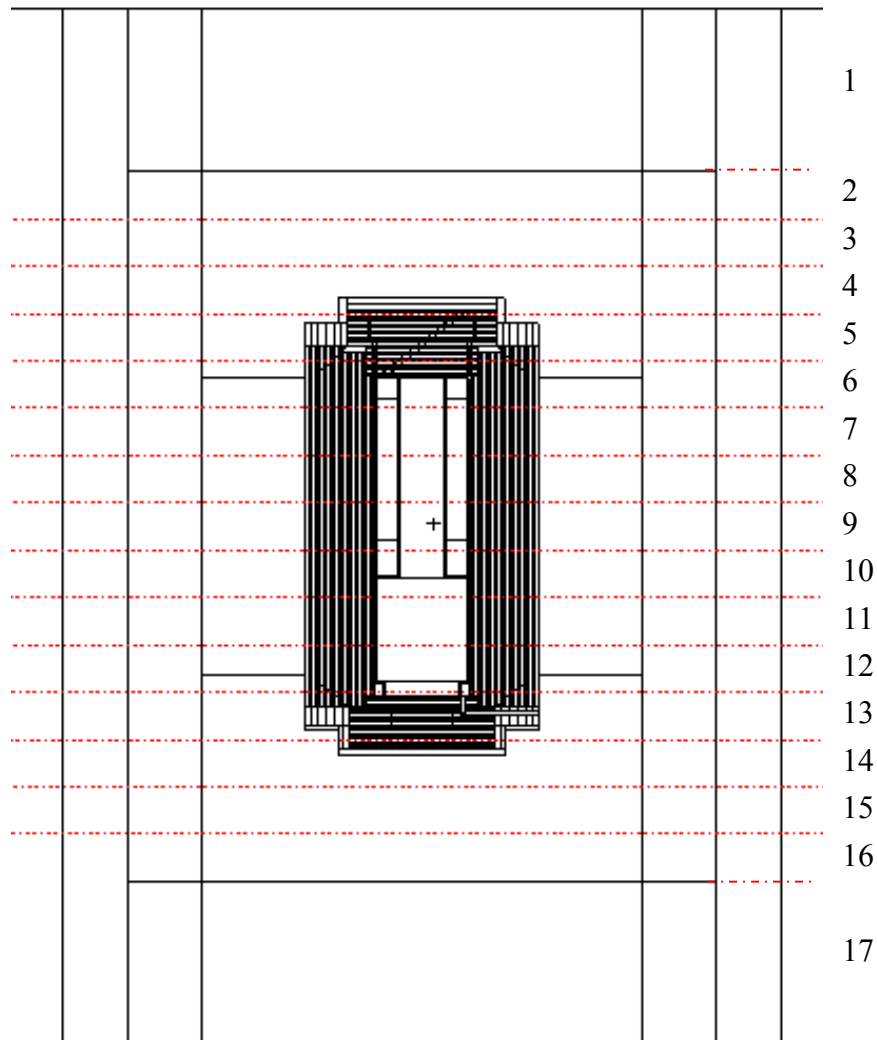


**Figure 5.4-2 – Impact Limiter Horizontal Tally Segmentations**



Note: All tallies are circumferential.

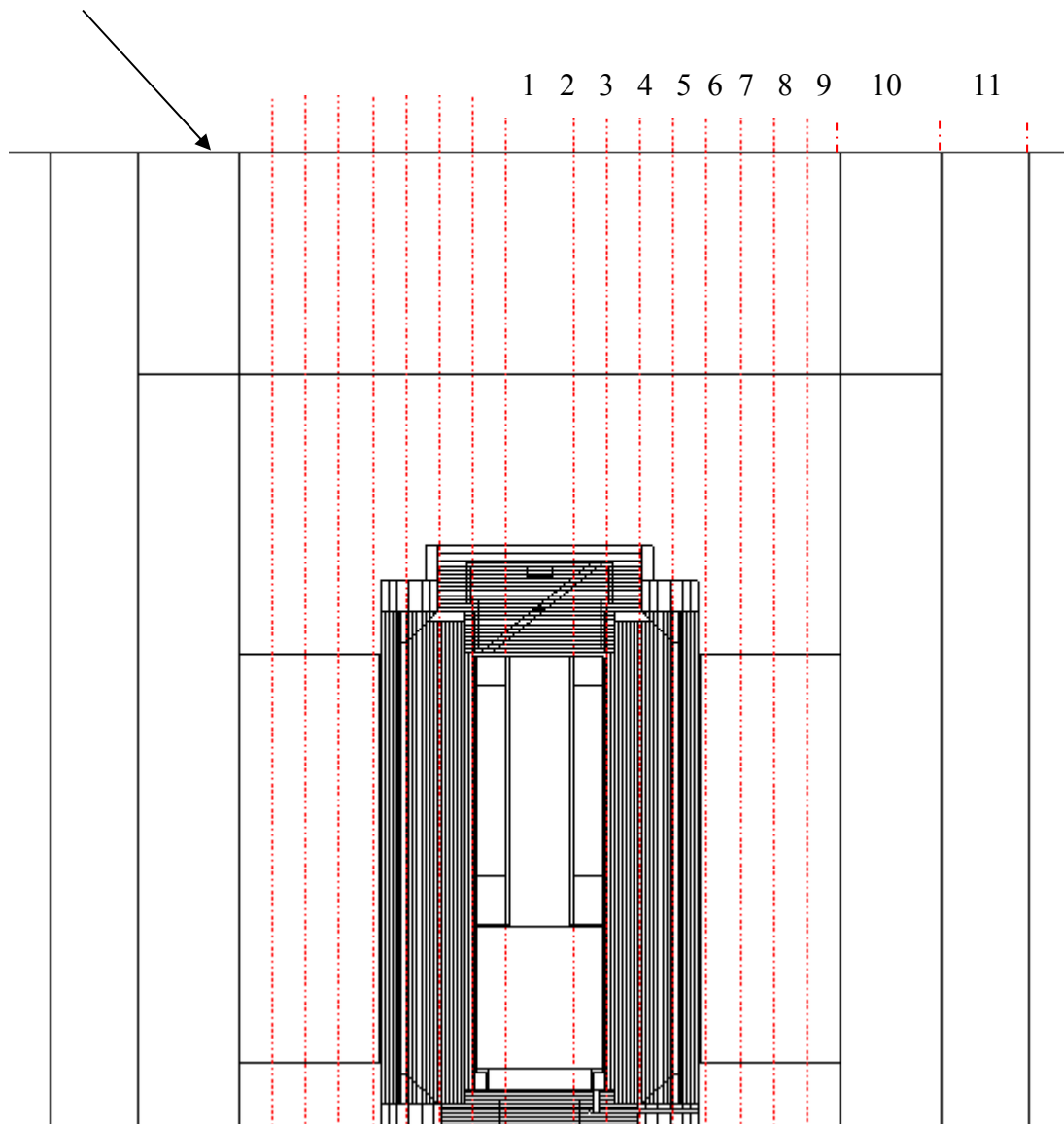
**Figure 5.4-3 – Side Tally Locations**



Note: All tallies are circumferential.

**Figure 5.4-4 – Side Tally Segmentations (excluding cask surface)**

1 m from Cask Impact  
Limiter Tally Surface



**Figure 5.4-5 – HAC 1 m End Tally Segmentations**

## 5.5 Appendices

### 5.5.1 References

1. Title 10, Code of Federal Regulations, Part 71 (10 CFR 71), Packaging and Transportation of Radioactive Material, 1-1-09 Edition.
2. MCNP5, “MCNP – A General Monte Carlo N-Particle Transport Code, Version 5; Volume II: User’s Guide,” LA-CP-03-0245, Los Alamos National Laboratory, April 2003 (Revised 10/3/2005, 2/1/2008).
3. *SCALE: A Modular Code System for Performing Standardized Computer Analyses for Licensing Evaluations*, ORNL/TM-2005/39, Version 6, Vols. I-III, January 2009.
4. JW Sterbentz, *Radionuclide Mass Inventory, Activity, Decay Heat, and Dose Rate Parametric Data for TRIGA Spent Nuclear Fuels*, INEL-96/0482, Idaho National Engineering Laboratory, March 1997.
5. *Standard Composition Library*, ORNL/TM-2005/39, Version 6, Vol. III, Section M8, January 2009.
6. *Nuclides and Isotopes, Chart of the Nuclides, Fifteenth Edition*, General Electric Co. and KAPL, Inc., 1996.
7. ORNL/TM-11018, *Standard- and Extended-Burnup PWR and BWR Reactor Models for the ORIGEN2 Computer Code*, Oak Ridge National Laboratory, December 1989.
8. PNL-6906, Vol. 1, *Spent Fuel Assembly Hardware: Characterization and 10 CFR 61 Classification for Waste Disposal, Volume 1 – Activation Measurements and Comparison with Calculations for Spent Fuel Assembly Hardware*, Pacific Northwest Laboratory, June 1989.
9. NUREG-1536, Rev. 1, *Standard Review Plan for Spent Fuel Dry Storage Systems at a General License Facility*, July 2010.

### 5.5.2 Detailed TRIGA Results

The following tables provide the detailed results for the TRIGA basket, because this fuel is limiting on the side of the cask.



**Table 5.5-1 – TRIGA NCT Cask Side Dose Rates (mrem/hr)**

Location	Gamma	$\sigma$	Neutron	$\sigma$	Total	$\sigma$
1	1.7	0.5%	38.3	0.3%	40.0	0.3%
2	3.2	0.5%	51.6	0.3%	54.8	0.3%
3	4.6	0.4%	61.2	0.3%	65.8	0.2%
4	4.9	0.4%	63.1	0.3%	68.1	0.2%
5	4.1	0.5%	56.9	0.3%	61.0	0.2%
6	2.5	0.5%	46.0	0.3%	48.5	0.3%
7	1.2	0.6%	33.7	0.3%	34.9	0.3%
8	0.4	0.8%	24.1	0.4%	24.5	0.4%
9	0.1	1.2%	16.7	0.5%	16.9	0.5%
10	0.1	1.7%	11.8	0.6%	11.9	0.5%
11	0.04	2.4%	8.3	0.7%	8.3	0.6%
12	0.03	3.1%	5.7	0.8%	5.8	0.8%

**Table 5.5-2 – TRIGA NCT Impact Limiter Dose Rates (mrem/hr)**

Location	Gamma	$\sigma$	Neutron	$\sigma$	Total	$\sigma$
<b>Upper Impact Limiter Side</b>						
1	2.9	1.3%	2.5	0.6%	5.4	0.8%
2	2.0	1.0%	3.2	0.5%	5.2	0.5%
3	1.2	0.8%	4.4	0.4%	5.6	0.4%
4	0.7	0.5%	6.5	0.3%	7.2	0.3%
5	0.6	0.3%	9.5	0.3%	10.2	0.2%
<b>Lower Impact Limiter Side</b>						
1	0.5	0.7%	8.7	0.2%	9.2	0.2%
2	0.8	0.5%	5.9	0.3%	6.7	0.3%
3	1.9	0.6%	4.1	0.4%	5.9	0.3%
4	3.5	0.7%	2.9	0.5%	6.5	0.4%
5	3.9	1.1%	2.3	0.5%	6.2	0.7%
<b>Upper Impact Limiter Horizontal</b>						
1	1.1	1.0%	4.0	1.9%	5.0	1.5%
2	1.1	1.0%	3.8	1.1%	4.9	0.9%
3	1.5	1.1%	3.5	0.9%	5.0	0.7%
4	1.6	1.0%	3.1	0.9%	4.7	0.7%
5	1.7	0.9%	2.7	0.8%	4.5	0.6%
6	1.9	0.9%	2.5	0.8%	4.4	0.6%
7	2.4	1.2%	2.3	0.8%	4.7	0.7%
8	3.3	1.6%	2.2	0.7%	5.5	1.0%
9	3.5	1.7%	2.2	0.7%	5.6	1.1%
<b>Lower Impact Limiter Horizontal</b>						
1	2.3	0.8%	4.1	1.7%	6.5	1.1%
2	2.4	0.8%	3.9	1.0%	6.3	0.7%
3	2.4	0.7%	3.6	0.8%	5.9	0.6%
4	2.1	0.6%	3.1	0.8%	5.3	0.5%
5	1.8	0.6%	2.7	0.7%	4.6	0.5%
6	1.7	0.6%	2.4	0.7%	4.1	0.5%
7	1.9	0.8%	2.2	0.7%	4.1	0.5%
8	2.4	1.1%	2.1	0.7%	4.5	0.7%
9	3.1	1.4%	2.0	0.7%	5.2	0.9%

**Table 5.5-3 – TRIGA NCT Vehicle Surface Dose Rates (mrem/hr)**

Location	Gamma	$\sigma$	Neutron	$\sigma$	Total	$\sigma$
1	0.1	2.8%	0.6	0.5%	0.6	0.5%
2	0.1	1.8%	1.0	0.7%	1.1	0.6%
3	0.1	1.3%	1.4	0.5%	1.5	0.5%
4	0.1	0.7%	2.0	0.4%	2.0	0.4%
5	0.1	0.4%	2.8	0.4%	2.9	0.3%
6	0.1	0.3%	4.0	0.3%	4.1	0.3%
7	0.3	0.3%	5.3	0.2%	5.6	0.2%
8	0.4	0.3%	6.7	0.2%	7.2	0.2%
9	0.7	0.3%	7.9	0.2%	8.6	0.2%
10	0.8	0.3%	8.4	0.2%	9.2	0.2%
11	0.7	0.3%	8.0	0.2%	8.7	0.2%
12	0.5	0.3%	6.8	0.2%	7.4	0.2%
13	0.5	0.6%	5.3	0.2%	5.8	0.2%
14	0.6	0.5%	4.0	0.3%	4.6	0.3%
15	1.0	0.6%	3.0	0.3%	4.0	0.3%
16	1.6	0.7%	2.2	0.4%	3.9	0.4%
17	1.6	0.9%	1.4	0.3%	2.9	0.5%

**Table 5.5-4 – TRIGA NCT 2 m Vehicle Surface Dose Rates (mrem/hr)**

Location	Gamma	$\sigma$	Neutron	$\sigma$	Total	$\sigma$
1	0.03	0.4%	0.6	0.3%	0.6	0.2%
2	0.04	0.3%	0.7	0.4%	0.8	0.4%
3	0.05	0.3%	0.8	0.4%	0.8	0.4%
4	0.1	0.3%	0.9	0.4%	0.9	0.3%
5	0.1	0.3%	0.9	0.3%	1.0	0.3%
6	0.1	0.3%	1.0	0.3%	1.1	0.3%
7	0.1	0.3%	1.0	0.3%	1.1	0.3%
8	0.1	0.3%	1.1	0.3%	1.2	0.3%
9	0.1	0.3%	1.1	0.3%	1.2	0.3%
10	0.1	0.3%	1.1	0.3%	1.2	0.3%
11	0.1	0.3%	1.1	0.3%	1.2	0.3%
12	0.1	0.4%	1.1	0.3%	1.2	0.3%
13	0.1	0.7%	1.0	0.3%	1.2	0.3%
14	0.1	0.3%	1.0	0.3%	1.1	0.3%
15	0.1	0.3%	0.9	0.3%	1.1	0.3%
16	0.1	0.3%	0.9	0.3%	1.0	0.3%
17	0.1	0.4%	0.7	0.2%	0.9	0.2%

**Table 5.5-5 – TRIGA NCT Occupied Location Dose Rates (mrem/hr)**

Location	Gamma	$\sigma$	Neutron	$\sigma$	Total	$\sigma$
1	0.01	0.3%	0.2	0.3%	0.2	0.3%
2	0.02	0.4%	0.2	0.5%	0.2	0.5%
3	0.02	0.4%	0.2	0.5%	0.2	0.4%
4	0.02	0.4%	0.2	0.5%	0.2	0.4%
5	0.02	0.4%	0.2	0.5%	0.2	0.4%
6	0.02	0.4%	0.2	0.5%	0.2	0.4%
7	0.02	0.4%	0.2	0.5%	0.2	0.4%
8	0.02	0.4%	0.2	0.5%	0.2	0.4%
9	0.02	0.4%	0.2	0.5%	0.2	0.4%
10	0.02	0.4%	0.2	0.5%	0.2	0.4%
11	0.02	0.6%	0.2	0.5%	0.2	0.4%
12	0.02	0.4%	0.2	0.5%	0.2	0.4%
13	0.02	1.3%	0.2	0.5%	0.2	0.4%
14	0.02	0.5%	0.2	0.5%	0.2	0.4%
15	0.02	0.3%	0.2	0.5%	0.2	0.4%
16	0.02	0.3%	0.2	0.5%	0.2	0.4%
17	0.02	0.3%	0.2	0.3%	0.2	0.2%

**Table 5.5-6 – TRIGA HAC 1 m Side Dose Rates (mrem/hr)**

Location	Gamma	$\sigma$	Neutron	$\sigma$	Total	$\sigma$
1	0.04	1.9%	0.7	0.4%	0.7	0.4%
2	0.04	1.2%	1.1	0.5%	1.2	0.5%
3	0.05	0.8%	1.5	0.5%	1.5	0.4%
4	0.1	0.4%	1.9	0.4%	2.0	0.4%
5	0.1	0.3%	2.5	0.3%	2.6	0.3%
6	0.1	0.3%	3.2	0.3%	3.4	0.3%
7	0.2	0.3%	4.0	0.2%	4.3	0.2%
8	0.4	0.3%	4.8	0.2%	5.1	0.2%
9	0.5	0.3%	5.3	0.2%	5.8	0.2%
10	0.5	0.3%	5.5	0.2%	6.1	0.2%
11	0.5	0.3%	5.3	0.2%	5.8	0.2%
12	0.4	0.3%	4.8	0.2%	5.2	0.2%
13	0.4	0.5%	4.0	0.2%	4.4	0.2%
14	0.4	0.4%	3.3	0.3%	3.7	0.3%
15	0.5	0.5%	2.6	0.3%	3.2	0.3%
16	0.8	0.6%	2.1	0.4%	2.8	0.3%
17	1.2	0.8%	1.3	0.3%	2.5	0.4%

**Table 5.5-7 – TRIGA HAC Impact Limiter 1m End Dose Rates (mrem/hr)**

Location	Gamma	$\sigma$	Neutron	$\sigma$	Total	$\sigma$
<b>1 m from Upper Impact Limiter</b>						
1	0.5	1.1%	1.2	3.4%	1.7	2.4%
2	0.5	0.9%	1.2	2.0%	1.8	1.4%
3	0.6	1.1%	1.2	1.5%	1.8	1.1%
4	0.6	1.0%	1.2	1.4%	1.8	1.0%
5	0.7	1.1%	1.1	1.2%	1.7	0.9%
6	0.7	1.0%	1.0	1.1%	1.7	0.8%
7	0.7	0.9%	1.0	1.1%	1.7	0.8%
8	0.7	1.0%	1.0	1.0%	1.7	0.7%
9	0.7	0.9%	1.0	1.0%	1.7	0.7%
10	0.9	1.2%	1.0	0.5%	1.8	0.6%
11	1.1	1.5%	1.0	0.5%	2.0	0.8%
<b>1 m from Lower Impact Limiter</b>						
1	0.9	1.1%	1.2	3.0%	2.1	1.7%
2	0.9	0.9%	1.2	1.8%	2.1	1.1%
3	0.9	0.9%	1.2	1.4%	2.1	0.9%
4	0.9	0.8%	1.1	1.2%	2.1	0.8%
5	0.9	0.7%	1.1	1.1%	1.9	0.7%
6	0.8	0.7%	1.0	1.1%	1.8	0.7%
7	0.7	0.6%	1.0	1.0%	1.7	0.6%
8	0.7	0.6%	1.0	0.9%	1.6	0.6%
9	0.6	0.6%	0.9	0.9%	1.6	0.6%
10	0.7	0.8%	0.9	0.5%	1.6	0.4%
11	0.9	1.3%	0.9	0.5%	1.8	0.7%

### 5.5.3 Sample Input Files

#### 5.5.3.1 TRITON Input File

A sample TRITON input file for MURR is included. The file is annotated to aid in understanding the input.

Adding parm=weight instructs TRITON to collapse the 238-group ENDF/B-VII data library to a 49-group library for use in the NEWT calculations. The first NEWT calculation is performed with 238 groups, but all subsequent NEWT calculations use the collapsed library to accelerate the run time.

```
=t-depl          parm=weight
MURR Fuel Model
v7-238
read comp
```

# BRR Package Safety Analysis Report

```
'Fuel
u-235  1  0  3.6124e-3      358.0 end
u-238  1  0  2.6847e-4      358.0 end
al      1  0  5.0239e-2      358.0 end
'Cladding
al      2              1.0  355.2 end
'Water
h2o     3  den=0.983      1.0  327.4 end
end comp
```

The pitch, fuel meat thickness, and cladding thickness are specified.

```
read celldata
latticecell symmslabcell  pitch=0.3302 3 fueld=0.0508 1 cladd=0.127  2  end
end celldata
```

Depletion is to be carried out only in material 1 (aluminum cladding has negligible depletion and is neglected). The negative sign means that the total power is to be normalized to the fuel mixture region only. If a positive sign were entered, the power would be normalized across the entire fuel element model (including cladding and water). Due to small amounts of power generated by the cladding and water as a result of (n,γ) reactions, normalizing the power over the entire assembly results in less than the specified power in the fuel itself.

The power is specified in units of MW/MTU. BURN is the number of days at power, while DOWN is the number of days between cycles. NLIB is the number of data libraries to be generated for each burnup specification. Increasing the value of NLIB increases the accuracy (and length) of the calculation, although in this case the days at power are relatively short and one library per cycle is sufficient.

```
read depletion -1 end depletion
read burndata
power=1515.3 burn=7  down=14      nlib=1 end
power=1515.3 burn=7  down=14      nlib=1 end
power=1515.3 burn=7  down=14      nlib=1 end
power=1515.3 burn=7  down=14      nlib=1 end
power=1515.3 burn=7  down=14      nlib=1 end
power=1515.3 burn=7  down=14      nlib=1 end
power=1515.3 burn=7  down=14      nlib=1 end
power=1515.3 burn=7  down=14      nlib=1 end
power=1515.3 burn=7  down=14      nlib=1 end
power=1515.3 burn=7  down=14      nlib=1 end
power=1515.3 burn=7  down=14      nlib=1 end
power=1515.3 burn=7  down=14      nlib=1 end
power=1515.3 burn=7  down=14      nlib=1 end
power=1515.3 burn=7  down=14      nlib=1 end
power=1515.3 burn=7  down=14      nlib=1 end
power=1515.3 burn=7  down=14      nlib=1 end
power=1515.3 burn=7  down=14      nlib=1 end
power=1515.3 burn=7  down=14      nlib=1 end
power=1515.3 burn=7  down=14      nlib=1 end
power=1515.3 burn=7  down=14      nlib=1 end
power=1515.3 burn=7  down=14      nlib=1 end
power=1515.3 burn=7  down=14      nlib=1 end
power=1515.3 burn=7  down=14      nlib=1 end
power=1515.3 burn=4  down=180     nlib=1 end
end burndata
```



```
read opus
  units=watts
  matl=0 end
new case
  units=gram symnuc=u-235 end
new case
  units=curie symnuc=pu-238 pu-239
  pu-240 pu-241 pu-242 end
new case
  units=particles/s typarams=nspectrum
new case
  units=particles/s typarams=gspectrum
end opus
```

[illegible]

```

end array
read bounds all=refl end bounds
end model
' End of NEWT model
end

```

### 5.5.3.2 MCNP Input File

A sample input file is provided for the MITR-II fuel with a gamma source (filename MIT\_G3).

```

BRRC
c
c lateral cask wall including Pb shield
c
10 4 -7.94 100 -157 1 -2 imp:p=1 $ SS inner shell split
11 4 -7.94 100 -157 2 -3 imp:p=2 $ SS inner shell split
12 8 -11.35 103 -133 3 -4 imp:p=4 $ Pb gamma shield split
13 8 -11.35 103 -133 4 -5 imp:p=8 $ Pb gamma shield split
14 8 -11.35 103 -133 5 -6 imp:p=16 $ Pb gamma shield split
15 8 -11.35 103 -133 6 -7 imp:p=32 $ Pb gamma shield split
16 8 -11.35 103 -133 7 -8 imp:p=64 $ Pb gamma shield split
17 8 -11.35 103 -133 8 -801 imp:p=128 $ Pb gamma shield split
18 8 -11.35 103 -133 801 -9 imp:p=200 $ Pb gamma shield split
19 4 -7.94 103 300 9 -10 imp:p=256 $ SS
20 4 -7.94 301 -132 9 -10 imp:p=256 $ SS
21 8 -11.35 -300 -301 -133 9 -10 imp:p=256 $ Pb gamma shield split
22 4 -7.94 103 300 10 -11 imp:p=512 $ SS
23 4 -7.94 301 -132 10 -11 imp:p=512 $ SS
24 8 -11.35 -300 -133 10 -11 imp:p=512 $ Pb gamma shield split
25 4 -7.94 103 300 11 -12 imp:p=1024 $ SS
26 4 -7.94 301 -132 11 -12 imp:p=1024 $ SS
27 8 -11.35 -300 -133 -301 11 -12 imp:p=1024 $ Pb gamma shield split
28 4 -7.94 103 300 12 -13 imp:p=2048 $ SS
29 4 -7.94 301 -132 12 -13 imp:p=2048 $ SS
30 8 -11.35 -300 -301 12 -13 imp:p=2048 $ Pb gamma shield split
31 4 -7.94 103 300 13 -14 imp:p=4096 $ SS
32 4 -7.94 301 -132 13 -14 imp:p=4096 $ SS
33 8 -11.35 -300 -301 13 -14 imp:p=4096 $ Pb gamma shield split
34 4 -7.94 103 300 14 -15 imp:p=8192 $ SS
35 4 -7.94 301 -132 14 -15 imp:p=8192 $ SS
36 8 -11.35 -300 -301 14 -15 imp:p=8192 $ Pb gamma shield split
37 4 -7.94 103 300 15 -16 imp:p=1.6e4 $ SS
38 4 -7.94 301 -132 15 -16 imp:p=1.6e4 $ SS
39 8 -11.35 -300 -301 15 -16 imp:p=1.6e4 $ Pb gamma shield split
40 4 -7.94 103 300 16 -17 imp:p=3.2e4 $ SS
41 4 -7.94 301 -132 16 -17 imp:p=3.2e4 $ SS
42 8 -11.35 -300 -301 16 -17 imp:p=3.2e4 $ Pb gamma shield split
43 4 -7.94 103 -101 17 -18 imp:p=6.4e4 $ SS
44 4 -7.94 102 -132 17 -18 imp:p=6.4e4 $ SS
45 8 -11.35 101 -102 17 -18 imp:p=6.4e4 $ Pb gamma shield split
46 4 -7.94 103 -101 18 -19 imp:p=1.3e5 $ SS
47 4 -7.94 102 -132 18 -19 imp:p=1.3e5 $ SS
48 8 -11.35 101 -102 18 -19 imp:p=1.3e5 $ Pb gamma shield split
49 4 -7.94 103 -101 19 -20 imp:p=2.6e5 $ SS
50 4 -7.94 102 -132 19 -20 imp:p=2.6e5 $ SS
51 1 -0.0012 101 -102 19 -20 imp:p=1.3e5 $ radial gap (Pb shrinkage
1/16")
52 1 -0.0012 133 -132 3 -301 imp:p=256 $ top axial gap (Pb shrinkage
1/4")
53 4 -7.94 3 -36 132 -152 imp:p=512
54 4 -7.94 103 -132 20 -21 imp:p=2.6e5 $ SS outer shell split
55 4 -7.94 103 -132 21 -22 imp:p=5.2e5 $ SS outer shell split

```

# BRR Package Safety Analysis Report

Docket No. 71-9341

Rev. 9, January 2016

56	4	-7.94	103	-132	22	-23	imp:p=1.0e6	\$ SS outer shell split
57	4	-7.94	103	-132	23	-24	imp:p=2.1e6	\$ SS outer shell split
58	1	-0.0012	201	-200	24	-25	imp:p=2.1e6	\$ air gap thermal shield
59	4	-7.94	201	-200	25	-26	imp:p=2.1e6	\$ SS shell over thermal gap
c								
c cask body bottom including Pb shield								
c								
100	4	-7.94	104	-100	-3	#174	imp:p=1	\$ SS axial split bottom cask
101	4	-7.94	-104	105	-3	#174	imp:p=2	\$ SS axial split bottom cask
102	4	-7.94	-105	106	-3	#174	imp:p=4	\$ SS axial split bottom cask
104	8	-11.35	-106	103	-27		imp:p=8	\$ Bottom cask Pb split
105	4	-7.94	-106	103	-3	27 #174	imp:p=8	\$ SS split bottom cask
106	8	-11.35	-103	108	-27		imp:p=16	\$ bottom cask Pb split
107	8	-11.35	-108	109	-27		imp:p=32	\$ bottom cask Pb split
108	8	-11.35	-109	110	-27		imp:p=64	\$ bottom cask Pb split
109	8	-11.35	-110	111	-27		imp:p=128	\$ bottom cask Pb split
110	8	-11.35	-111	112	-27		imp:p=256	\$ bottom cask Pb split
111	8	-11.35	-112	113	-27		imp:p=512	\$ bottom cask Pb split
112	8	-11.35	-113	115	-27		imp:p=1024	\$ bottom cask Pb split
113	8	-11.35	115	-114	27	-33	imp:p=1024	\$ radius of first gap (Pb shrinkage)
c								
120	4	-7.94	108	-103	27	-801 #174	imp:p=16	\$ SS split bottom cask
121	4	-7.94	109	-108	27	-801 #174	imp:p=32	\$ SS split bottom cask
122	4	-7.94	110	-109	27	-801 #174 #175	imp:p=64	\$ SS split bottom cask
123	4	-7.94	111	-110	27	-801 #175	imp:p=128	\$ SS split bottom cask
124	4	-7.94	112	-111	27	-801	imp:p=256	\$ SS split bottom cask
125	4	-7.94	113	-112	27	-801	imp:p=512	\$ SS split bottom cask
126	4	-7.94	114	-113	27	-801	imp:p=1024	\$ SS split bottom cask
128	4	-7.94	-103	114	801	-10 #175	imp:p=1024	\$ SS radial split bottom
cask								
129	4	-7.94	-103	114	10	-13 #175	imp:p=2048	\$ SS radial split bottom
cask								
130	4	-7.94	-103	114	13	-16 #175	imp:p=1.6e4	\$ SS radial split bottom
cask								
131	4	-7.94	-103	114	16	-20 #175	imp:p=1.3e4	\$ SS radial split bottom
cask								
132	4	-7.94	-103	114	20	-22 #175	imp:p=5.2e4	\$ SS radial split bottom
cask								
133	4	-7.94	-103	114	22	-24 #175	imp:p=2.1e6	\$ SS radial split bottom
cask								
c								
141	8	-11.35	-115	116	-33		imp:p=2048	\$ bottom cask Pb split
142	8	-11.35	-116	117	-33		imp:p=4096	\$ bottom cask Pb split
143	8	-11.35	-117	118	-33		imp:p=8192	\$ bottom cask Pb split
144	8	-11.35	-118	119	-33		imp:p=1.6e4	\$ bottom cask Pb split
145	8	-11.35	-119	120	-33		imp:p=3.3e4	\$ bottom cask Pb split
146	8	-11.35	-120	121	-33		imp:p=6.6e4	\$ bottom cask Pb split
147	8	-11.35	-121	122	-33		imp:p=1.3e5	\$ bottom cask Pb split
148	8	-11.35	-122	123	-33		imp:p=2.6e5	\$ bottom cask Pb split
149	8	-11.35	-123	125	-33		imp:p=5.2e5	\$ bottom cask Pb split
c								
170	4	-7.94	-114	125	33	-10	imp:p=5.2e5	\$ SS radial split bottom cask
171	4	-7.94	-114	125	10	-35	imp:p=1e6	\$ SS radial split bottom cask
172	4	-7.94	-114	126	35	-24	imp:p=2.1e6	\$ SS shoulder
173	4	-7.94	-125	127	-35		imp:p=1e6	\$ SS bottom plate (1")
174	1	-0.0012	309	-100	-306		imp:p=32	\$ vertical drain hole 95
175	1	-0.0012	-307	308	-24	#174	imp:p=1024	\$ horizontal drain hole 96
c								
c cask body top								
c								
201	4	-7.94	-134	145	41	-36	imp:p=1.3e5	\$ SS tapered interface with shield plug

**BRR Package Safety Analysis Report****Docket No. 71-9341**  
**Rev. 9, January 2016**

202	4	-7.94	-145 146	41 -36	imp:p=6.6e4	\$ SS tapered interface with shield plug
203	4	-7.94	-146 147	41 -36	imp:p=3.3e4	\$ SS tapered interface with shield plug
204	4	-7.94	-147 148	41 -36	imp:p=1.6e4	\$ SS tapered interface with shield plug
205	4	-7.94	-148 149	41 -36	imp:p=8192	\$ SS tapered interface with shield plug
206	4	-7.94	-149 150	41 -36	imp:p=4096	\$ SS tapered interface with shield plug
207	4	-7.94	-150 151	302 -36	imp:p=2048	\$ SS tapered interface with shield plug
208	4	-7.94	-151 152	302 -36	imp:p=1024	\$ SS tapered interface with shield plug
209	4	-7.94	-152 153	302 -3	imp:p=512	\$ SS tapered interface with shield plug
210	4	-7.94	-153 154	302 -3	imp:p=256	\$ SS tapered interface with shield plug
211	4	-7.94	155 -154	1 -3	imp:p=128	\$ SS interface with shield plug
212	4	-7.94	1551 -155	1 -3	imp:p=64	\$ SS interface with shield plug
213	4	-7.94	1552 -1551	1 -3	imp:p=32	\$ SS interface with shield plug
214	4	-7.94	1553 -1552	1 -3	imp:p=16	\$ SS interface with shield plug
215	4	-7.94	1554 -1553	1 -3	imp:p=8	\$ SS interface with shield plug
216	4	-7.94	1555 -1554	1 -3	imp:p=4	\$ SS interface with shield plug
217	4	-7.94	156 -1555	1 -3	imp:p=2	\$ SS interface with shield plug
218	4	-7.94	157 -156	1 -3	imp:p=1	\$ SS interface with shield plug
c						
223	4	-7.94	-138 132	36 -11	imp:p=2.6e5	\$ SS radial split
224	4	-7.94	-138 132	11 -13	imp:p=5.2e5	\$ SS radial split
225	4	-7.94	-138 132	13 -16	imp:p=1.04e6	\$ SS radial split
226	4	-7.94	-138 132	16 -20	imp:p=2.1e6	\$ SS radial split
227	4	-7.94	-138 132	20 -22	imp:p=4.2e6	\$ SS radial split
228	4	-7.94	-138 132	22 -24	imp:p=8.4e6	\$ SS radial split
c						
230	4	-7.94	137 -136	-37	imp:p=4.2e6	\$ SS top closure lid split
231	4	-7.94	-135 136	-37	imp:p=8.4e6	\$ SS top closure lid split
232	1	-0.0012	-135 137	37 -36	imp:p=8.4e6	\$ radial gap at lid
233	4	-7.94	138 -135	36 -35	imp:p=4.2e6	\$ cask body
c						
240	4	-7.94	134 -143	-36 41	imp:p=2.6e5	\$ cask body top
241	4	-7.94	143 -142	-36 41	imp:p=5.2e5	\$ cask body top
242	4	-7.94	142 -140	-36 41	imp:p=1e6	\$ cask body top
243	4	-7.94	140 -137	-36 41	imp:p=2.1e6	\$ cask body top
c						
c						
c shield plug						
c						
300	4	-7.94	140 -141 -40 161		imp:p=2.1e6	\$ SS top shield plug
301	1	-0.0012	-137 141 -41		imp:p=2.1e6	\$ axial gap at top of shield plug
302	1	-0.0012	140 -141 40 -41		imp:p=2.1e6	\$ radial gap at top of shield plug
303	8	-11.35	-140 142 -43 46 161		imp:p=1e6	\$ shield plug Pb split (no radial gap)
304	4	-7.94	-140 142 43 -40		imp:p=1e6	\$ SS top shield plug

305	1	-0.0012	-140 142 40 -41	imp:p=1e6	\$ gap split
306	4	-7.94	-140 142 -46	imp:p=1e6	\$ SS rod center
307	8	-11.35	-142 143 -43 46 161	imp:p=5.2e5	\$ shield plug Pb split
308	4	-7.94	-142 143 43 -40	imp:p=5.2e5	\$ SS top shield plug
309	1	-0.0012	-142 143 40 -41	imp:p=5.2e5	\$ gap split
310	4	-7.94	-142 143 -46	imp:p=5.2e5	\$ SS rod center
311	4	-7.94	-143 1431 -46	imp:p=2.6e5	\$ SS rod center
312	8	-11.35	-143 134 -43 #311 161	imp:p=2.6e5	\$ shield plug Pb split
313	4	-7.94	-143 134 43 -40	imp:p=2.6e5	\$ SS top shield plug
314	1	-0.0012	-143 134 40 -41	imp:p=2.6e5	\$ gap split
315	8	-11.35	-134 145 -43 161	imp:p=1.3e5	\$ shield plug Pb split
316	4	-7.94	-134 145 43 -40	imp:p=1.3e5	\$ SS top shield plug
317	1	-0.0012	-134 145 40 -41	imp:p=1.3e5	\$ gap split
318	8	-11.35	-145 146 -43 161	imp:p=6.6e4	\$ shield plug Pb split
319	4	-7.94	-145 146 43 -40	imp:p=6.6e4	\$ SS top shield plug
320	1	-0.0012	-145 146 40 -41	imp:p=6.6e4	\$ gap split
321	8	-11.35	-146 147 -43 161	imp:p=3.3e4	\$ shield plug Pb split
322	4	-7.94	-146 147 43 -40	imp:p=3.3e4	\$ SS top shield plug
323	1	-0.0012	-146 147 40 -41	imp:p=3.3e4	\$ gap split
324	8	-11.35	-147 148 -43 161	imp:p=1.6e4	\$ shield plug Pb split
325	4	-7.94	-147 148 43 -40	imp:p=1.6e4	\$ SS top shield plug
326	1	-0.0012	-147 148 40 -41	imp:p=1.6e4	\$ gap split
327	8	-11.35	-148 149 -43 161	imp:p=8192	\$ shield plug Pb split
328	4	-7.94	-148 149 43 -40	imp:p=8192	\$ SS top shield plug
329	1	-0.0012	-148 149 40 -41	imp:p=8192	\$ gap split
330	8	-11.35	(-149 150 -45 161):(160 -149 45 -43)	imp:p=4096	\$ shield plug Pb split
331	4	-7.94	-149 150 43 -40	imp:p=4096	\$ SS top shield plug
332	1	-0.0012	-149 150 40 -41	imp:p=4096	\$ gap split
333	4	-7.94	-160 150 45 -43	imp:p=4096	\$ SS ring at seating surface
334	8	-11.35	-150 151 -45 161	imp:p=2048	\$ shield plug Pb split
335	4	-7.94	-150 151 45 -303	imp:p=2048	\$ SS top shield plug
336	1	-0.0012	-150 151 303 -302	imp:p=2048	\$ gap split
337	8	-11.35	-151 152 -45 161	imp:p=1024	\$ shield plug Pb split
338	4	-7.94	-151 152 45 -303	imp:p=1024	\$ SS top shield plug
339	1	-0.0012	-151 152 303 -302	imp:p=1024	\$ gap split
340	8	-11.35	-152 153 -45 161	imp:p=512	\$ shield plug Pb split
341	4	-7.94	-152 153 45 -303	imp:p=512	\$ SS top shield plug
342	1	-0.0012	-152 153 303 -302	imp:p=512	\$ gap split
343	8	-11.35	-153 154 -45 161	imp:p=256	\$ shield plug Pb split
344	4	-7.94	-153 154 45 -303	imp:p=256	\$ SS top shield plug
345	1	-0.0012	-153 154 303 -302	imp:p=256	\$ gap split
346	8	-11.35	-154 155 -45 161	imp:p=128	\$ shield plug Pb split
347	4	-7.94	-154 155 45 -44	imp:p=128	\$ SS
348	1	-0.0012	-154 155 44 -1	imp:p=128	\$ gap split
350	8	-11.35	-155 1551 -45 161	imp:p=64	\$ shield plug Pb split
351	4	-7.94	-155 1551 45 -44	imp:p=64	\$ SS
352	1	-0.0012	-155 1551 44 -1	imp:p=64	\$ gap split
353	8	-11.35	-1551 1552 -45 161	imp:p=32	\$ shield plug Pb split
354	4	-7.94	-1551 1552 45 -44	imp:p=32	\$ SS
355	1	-0.0012	-1551 1552 44 -1	imp:p=32	\$ gap split
356	8	-11.35	-1552 1553 -45 161	imp:p=16	\$ shield plug Pb split
357	4	-7.94	-1552 1553 45 -44	imp:p=16	\$ SS
358	1	-0.0012	-1552 1553 44 -1	imp:p=16	\$ gap split
359	8	-11.35	-1553 1554 -45 161	imp:p=8	\$ shield plug Pb split
360	4	-7.94	-1553 1554 45 -44	imp:p=8	\$ SS
361	1	-0.0012	-1553 1554 44 -1	imp:p=8	\$ gap split
362	8	-11.35	-1554 1555 -45 161	imp:p=4	\$ shield plug Pb split
363	4	-7.94	-1554 1555 45 -44	imp:p=4	\$ SS
364	1	-0.0012	-1554 1555 44 -1	imp:p=4	\$ gap split
365	4	-7.94	-1555 156 -45 161	imp:p=2	\$ shield plug ss
366	4	-7.94	-1555 156 45 -44	imp:p=2	\$ SS
367	1	-0.0012	-1555 156 44 -1	imp:p=2	\$ gap split

```

368 4 -7.94 -156 157 -44 161 imp:p=1 $ SS bottom shield plug
369 1 -0.0012 -156 157 44 -1 imp:p=1 $ gap split
370 1 -0.0012 157 -156 -161 imp:p=1 $ plug drain
371 1 -0.0012 156 -1555 -161 imp:p=2 $ plug drain
372 1 -0.0012 1555 -1554 -161 imp:p=4 $ plug drain
373 1 -0.0012 1554 -1553 -161 imp:p=8 $ plug drain
374 1 -0.0012 1553 -1552 -161 imp:p=16 $ plug drain
375 1 -0.0012 1552 -1551 -161 imp:p=32 $ plug drain
376 1 -0.0012 1551 -155 -161 imp:p=64 $ plug drain
377 1 -0.0012 155 -154 -161 imp:p=128 $ plug drain
378 1 -0.0012 154 -153 -161 imp:p=256 $ plug drain
379 1 -0.0012 153 -152 -161 imp:p=512 $ plug drain
380 1 -0.0012 152 -151 -161 imp:p=1024 $ plug drain
381 1 -0.0012 151 -150 -161 imp:p=2048 $ plug drain
382 1 -0.0012 150 -149 -161 imp:p=4096 $ plug drain
383 1 -0.0012 149 -148 -161 imp:p=8192 $ plug drain
384 1 -0.0012 148 -147 -161 imp:p=1.6e4 $ plug drain
385 1 -0.0012 147 -146 -161 imp:p=3.3e4 $ plug drain
386 1 -0.0012 146 -145 -161 imp:p=6.6e4 $ plug drain
387 1 -0.0012 145 -134 -161 imp:p=1.3e5 $ plug drain
388 1 -0.0012 134 -143 -161 imp:p=2.6e5 $ plug drain
389 1 -0.0012 143 -142 -161 imp:p=5.2e5 $ plug drain
390 1 -0.0012 142 -140 -161 imp:p=1e6 $ plug drain
391 1 -0.0012 140 -141 -161 imp:p=2.1e6 $ plug drain
c
999 0 -1 100 -157 fill=1(22) imp:p=1 $ insert basket
c
c placeholders for IL and outside air volumes
c
400 3 -0.0012 (200 24 -50 -202):
(138 -202 -24 35) :(-202 135 -35) imp:p=8.4e6 $ placeholder for
upper IL
401 3 -0.0012 (-201 24 203 -50):
(-24 -126 203 35):(-127 203 -24) imp:p=4.2e6 $ placeholder for
lower IL
c
402 1 -0.0012 201 -200 -50 26 imp:p=4.2e6 $ lateral cask outer
air
403 1 -0.0012 50 -540 203 -202 imp:p=4.2e6 $ outer air
404 1 -0.0012 -203 211 -50 imp:p=4.2e6 $ bottom outer air
405 1 -0.0012 -203 211 50 -540 imp:p=4.2e6 $ bottom outer air
406 1 -0.0012 202 -210 -50 imp:p=8.4e6 $ outer air
407 1 -0.0012 202 -210 50 -540 imp:p=8.4e6 $ outer air
408 1 -0.0012 211 -210 540 -543 imp:p=4.2e6 $ outer air
409 1 -0.0012 211 -210 543 -541 imp:p=4.2e6 $ outer air
410 1 -0.0012 211 -210 541 -542 imp:p=4.2e6 $ outer air
c
1000 1 -0.0012 (542:-211:210) -999 imp:p=4.2e6
1001 0 999 imp:p=0
c
c Universe 1: Basket
c
600 0 630 -631 633 -632 680 -681 fill=5 u=1 imp:p=1 $ basket loc. 1
601 like 600 but trcl=2 u=1 imp:p=1 $ basket location
2
602 like 600 but trcl=3 u=1 imp:p=1 $ basket location
3
603 like 600 but trcl=4 u=1 imp:p=1 $ basket location
4
604 like 600 but trcl=5 u=1 imp:p=1 $ basket location
5
605 like 600 but trcl=6 u=1 imp:p=1 $ basket location
6

```

```

606      like 600 but trcl=7                      u=1 imp:p=1 $ basket location
7
607      like 600 but trcl=8                      u=1 imp:p=1 $ basket location
8
620      4 -7.94          680 -681 687 -683 #600 #601 #602 #603
                        #604 #605 #606 #607          u=1 imp:p=1 $ inside basket
630      1 -0.0012        681                      u=1 imp:p=1 $ above basket
631      4 -7.94          682 -680 -683            u=1 imp:p=1 $ support plate
632      4 -7.94          684 -685 -682            u=1 imp:p=1 $ basket bottom
633      1 -0.0012        -684 -682                u=1 imp:p=1
634      1 -0.0012        682 -680 683             u=1 imp:p=1
635      1 -0.0012        685 -682                u=1 imp:p=1
636      1 -0.0012        680 -681 -687            u=1 imp:p=1 $ inner air
637      1 -0.0012        680 -681 683             u=1 imp:p=1 $ annular air
c
c      Universe 2: Fuel
c
700      2  1.7560E-02    686          u=2      imp:p=1  $ fuel
701      1  -0.0012      -686          u=2      imp:p=1  $ air around fuel
c
c      Universe 5: Fuel Shifted (for source purposes)
c
500      0      991 -992 fill=2(1.7413 15.5236 0) u=5 imp:p=1

c
c ***** cylindrical cask surfaces
c
1      cz  20.32          $ cask inner surface cavity wall radius
2      cz  21.59          $ split of cavity wall (1/2")
3      cz  22.86          $ outside inner shell radius
4      cz  24.06          $ gamma shield split
5      cz  25.26          $ gamma shield split
6      cz  26.46          $ gamma shield split
7      cz  27.66          $ gamma shield split
8      cz  28.86          $ gamma shield split
801    cz  30.06          $ gamma shield split
9      cz  31.2801        $ gamma shield split ***
10     cz  32.4725        $ gamma shield split
11     cz  33.6725        $ gamma shield split
12     cz  34.8725        $ gamma shield split
13     cz  36.0725        $ gamma shield split
14     cz  37.2725        $ gamma shield split
15     cz  38.4725        $ gamma shield split
16     cz  39.6725        $ gamma shield split
17     cz  40.8051        $ gamma shield split ***
18     cz  41.9975        $ gamma shield split
19     cz  43.02125       $ outer gamma shield (Pb shrinkage surface - 1/16")
20     cz  43.18          $ cask inner surface outer wall
21     cz  44.45          $ split outer wall (1/2")
22     cz  45.72          $ split outer wall (1/2")
23     cz  46.99          $ split outer wall (1/2")
24     cz  48.26          $ cask outer surface outer wall
25     cz  48.5267        $ air gap ( 0.105 ")
26     cz  48.7934        $ thermal shield outer surface
27     cz  12.3825        $ bottom lead sheet cavity (small)
c 28    cz  12.1285       $ radial gap due to lead shrinkage (1/10")
c
c 29     cz  14.0825       $ SS split bottom cask
c 30     cz  15.7825       $ SS split bottom cask
c 31     cz  17.4825       $ SS split bottom cask
c
33     cz  30.099         $ bottom lead sheet cavity (large)

```

**BRR Package Safety Analysis Report**

```

c 34      cz      30.32125      $ bottom cask second radial gap surface due to lead
shrinkage
35      cz      34.6837      $ bottom and top cask SS outer surface
36      cz      31.115      $ top cask inner cavity for closure lid
37      cz      30.7975      $ closure lid radius
c
40      cz      22.1361      $ shield plug - SS outer radius(upper cylindrical region)
41      cz      22.3901      $ shield plug cavity
c 42      cz      19.15      $ shield plug SS inner radius at seating (item 7)
43      cz      21.1836      $ shield plug- SS inner radius (upper cylindrical region)
44      cz      20.066      $ shield plug - SS outer radius (lower cylindrical region)
45      cz      18.796      $ shield plug - SS inner radius (lower cylindrical region)
46      cz      3.81      $ SS bar at center of shield plug
c
50      cz      91.44      $ outer radius of impact limiter
c
c tally surfaces
c
c 51      cz      800      $ problem radial delimiter
c
c **** Horizontal planes
c
100     pz      -0.6426      $ bottom of cask inner cavity
101     pz      4.445      $ horizontal surface for lateral gamma shield
102     pz      139.7      $ horizontal surface at top of lateral gamma shield +3"
103     pz      -5.08      $ horizontal surface at bottom of lateral gamma shield
c
104     pz      -1.5      $ SS bottom cask split
105     pz      -2.54      $ SS bottom cask split
106     pz      -3.7338      $ bottom cask interface of SS - shrinkage gap
c 107     pz      -3.9878      $ bottom cask - lower horizontal surface of lead shrinkage
gap (1/10")
108     pz      -6      $ bottom cask - Pb split
109     pz      -6.845      $ bottom cask - Pb split
110     pz      -8.045      $ bottom cask - Pb split
111     pz      -9.245      $ bottom cask - Pb split
112     pz      -10.445      $ bottom cask - Pb split
113     pz      -11.645      $ bottom cask - Pb split
114     pz      -12.7      $ bottom cask - Pb split
115     pz      -12.954      $ bottom cask - lower horizontal surface of lead shrinkage gap
(1/10")
116     pz      -14.154      $ bottom cask - Pb split
117     pz      -15.354      $ bottom cask - Pb split
118     pz      -16.554      $ bottom cask - Pb split
119     pz      -17.754      $ bottom cask - Pb split
120     pz      -18.954      $ bottom cask - Pb split
121     pz      -20.154      $ bottom cask - Pb split
122     pz      -21.354      $ bottom cask - Pb split
123     pz      -22.554      $ bottom cask - Pb split
125     pz      -23.3426      $ bottom cask - lower Pb surface
126     pz      -14.9352      $ bottom cask - SS outer surface (shoulder)
127     pz      -25.8826      $ bottom cask - SS outer surface
c
c 131     pz      144.3736      $ horizontal surface at cask body top
132     pz      149.225      $ horizontal surface at top of lateral Pb shield cavity
133     pz      146.2278      $ top surface of lateral Pb shield after drop (1.12")
134     pz      159.7152      $ cask body top outer surface (shoulder)
135     pz      170.0276      $ top surface of closure lid
136     pz      167.4876      $ SS split in top lid
137     pz      164.9476      $ seating surface for top lid
138     pz      159.0802
c
140     pz      163.3728      $ shield plug Pb top surface

```



**BRR Package Safety Analysis Report**

```

141 pz 164.6428 $ shield plug top surface
142 pz 162.1536 $ shield plug Pb split surface
143 pz 160.8836 $ shield plug Pb split surface
1431 pz 160.6296 $ surface for SS rod (surface 141- 1.5")
c 144 pz 159.6136 $ shield plug Pb split surface
145 pz 158.3436 $ shield plug Pb split surface
146 pz 157.0736 $ shield plug Pb split surface
147 pz 155.8036 $ shield plug Pb split surface
148 pz 154.5336 $ shield plug Pb split surface
149 pz 153.2636 $ shield plug Pb split surface
150 pz 151.7396 $ shield plug Pb split surface - modified
151 pz 150.7236 $ shield plug Pb split surface
152 pz 149.4536 $ shield plug Pb split surface
153 pz 148.1836 $ shield plug Pb split surface
154 pz 146.7104 $ shield plug Pb split surface - modified
155 pz 145.3896 $ new Pb split
1551 pz 144.1196 $ new Pb split
1552 pz 142.8496 $ new Pb split
1553 pz 141.5796 $ new Pb split
1554 pz 140.3096 $ new Pb split
1555 pz 139.0396 $ bottom plug steel
156 pz 137.7696 $ SS surface at shield plug bottom -modified
157 pz 136.4996 $ bottom surface of shield plug -modified
160 pz 153.0096 $ upper SS surface at seating ring -new
161 20 cz 1.04648 $ pipe in shield plug
c
c surfaces for IL
c
200 pz 135.9916 $ upper interface IL with thermal shield
201 pz 8.1534 $ lower interface IL with thermal shield
202 pz 223.8756 $ upper surface of top impact limiter
203 pz -79.7306 $ bottom surface of bottom impact limiter
c
210 pz 293.3956 $ HAC upper surface
211 pz -149.2506 $ HAC lower surface
c
c various conical surfaces
c
300 kz -36.3601 1 1 $ tapered surface at bottom of lateral gamma shield
301 kz 180.5051 1 -1 $ tapered surface at top of lateral gamma shield
302 kz -143.9353 0.00489 1 $ tapered surface at cask top tapered cavity
303 kz -140.2468 0.00489 1 $ tapered surface at shield plug (SS)
c 304 kz -220.38 0.00275 1 $ tapered surface at shield plug (gap)
c 305 kz -122.0849 0.00489 1 $ tapered surface at shield plug (lead surface)
c
c bottom drain
c
306 c/z 17.145 0 0.635 $ vertical cylinder for bottom drain
307 c/x 0 -7.5184 0.635 $ horizontal cylinder for bottom drain
308 px 15.24 $ start of horizontal bottom drain
309 pz -7.94 $ depth of vertical drain
c
540 cz 121.92 $ surface of vehicle (4 ft=121.92 cm from BRRC centerline)
541 cz 321.92 $ 2 m from vehicle surface
542 cz 762.0 $ driver (25 ft=7.62m) from BRRC centerline)
543 cz 148.7934 $ 1m for HAC
c
c basket surfaces
c
630 1 py -3.3909
631 1 py 3.3909
632 1 p -1.7321 -1 0 6.7818 $ left basket inner bound
633 1 p -1.7321 -1 0 -6.7818 $ right basket inner bound

```

**BRR Package Safety Analysis Report**

c  
680 pz 67.4878 \$ top of plate  
681 pz 135.763 \$ top of fuel (22.375")  
682 pz 66.2178 \$ bottom of plate  
683 cz 19.8501 \$ OR of basket  
684 cz 17.145  
685 cz 17.78  
686 pz 78.9305  
687 cz 12 \$ IR of basket

c  
c horizontal surfaces for segmentation

c  
701 pz 18.8  
702 pz 29.5  
703 pz 40.1  
704 pz 50.8  
705 pz 61.4  
706 pz 72.1  
707 pz 82.7  
708 pz 93.4  
709 pz 104.0  
710 pz 114.7  
711 pz 125.3

c  
720 pz 153.6 \$ top IL  
721 pz 171.1  
722 pz 188.7  
723 pz 206.3

c  
740 pz -62.2 \$ bottom IL  
741 pz -44.6  
742 pz -27.0  
743 pz -9.4

c  
c cylindrical surfaces for segmentation

c  
760 cz 10.2  
761 cz 20.3  
762 cz 30.5  
763 cz 40.6  
764 cz 50.8  
765 cz 61.0  
766 cz 71.1  
767 cz 81.3

c  
770 pz -59.5  
771 pz -39.2  
772 pz -19.0  
773 pz 1.2  
774 pz 21.5  
775 pz 41.7  
776 pz 62.0  
777 pz 82.2  
778 pz 102.4  
779 pz 122.7  
780 pz 142.9  
781 pz 163.2  
782 pz 183.4  
783 pz 203.6

c  
991 pz -1000  
992 pz 1000  
999 sz 100 1000

```

c *****
c Dry air; density = 0.0012 g/cm^3
c *****
m1 7014 -76.508
    8016 -23.4793
    6000 -0.0126
c *****
c Homogenized fuel; atomic density = 1.7560E-02 atoms/(barn*cm)
c *****
m2 92235 4.3716E-04
    92238 2.7552E-05
    13027 1.7095E-02
c *****
c Dry air; density = 0.0012 g/cm^3
c *****
m3 7014 -76.508
    8016 -23.4793
    6000 -0.0126
c *****
c SS304; Density = 7.94 g/cm^3
c *****
m4 6012 -0.08
    14000 -1.0
    15000 -0.045
    24000 -19
    25000 -2
    26000 -68.375
    28000 -9.5
c *****
c Lead; Density = 11.35 g/cm^3
c *****
m8 82000 1.0 $ lead
c
mode p
sdef cel=d1 rad=d2 ext=d3 erg=d10 axs=0 0 1 pos=0 0 78.9305 wgt=7.707E+15
si1 L 999:600:500:700 999:601:500:700 999:602:500:700
    999:603:500:700 999:604:500:700 999:605:500:700
    999:606:500:700 999:607:500:700
sp1 1 1 1 1 1 1 1 1
si2 7.0
# si3 sp3 $ fuel axial dist
    0 0
    2.368 0.500
    4.736 0.394
    9.472 0.788
    14.208 0.901
    18.944 1.042
    23.680 1.140
    28.416 1.253
    33.152 1.267
    37.888 1.112
    42.624 1.028
    47.360 0.901
    52.096 0.774
    54.464 0.401
    56.833 0.500
# si10 sp10
    H D
    0 0

```

```

1.00E-02 0
4.50E-02 2.343E+14
1.00E-01 8.380E+13
2.00E-01 9.049E+13
3.00E-01 1.756E+13
4.00E-01 1.304E+13
6.00E-01 5.917E+13
8.00E-01 4.460E+14
1.00E+00 1.117E+13
1.33E+00 3.308E+12
1.66E+00 2.576E+12
2.00E+00 2.013E+11
2.50E+00 1.795E+12
3.00E+00 3.290E+10
4.00E+00 6.118E+08
5.00E+00 7.015E+02
6.50E+00 2.802E+02
8.00E+00 5.473E+01
1.00E+01 1.195E+01
c      Total 9.634E+14
c      Total*8 7.707E+15
c
c      ansi/ans-6.1.1-1977 flux-to-dose, photons (mrem/hr)/(p/cm**2/s)
de0    0.01 0.03 0.05 0.07 0.10 0.15 0.20 0.25 0.30
        0.35 0.40 0.45 0.50 0.55 0.60 0.65 0.70 0.80
        1.00 1.40 1.80 2.20 2.60 2.80 3.25 3.75 4.25
        4.75 5.00 5.25 5.75 6.25 6.75 7.50 9.00 11.0
        13.0 15.0
df0    3.96-3 5.82-4 2.90-4 2.58-4 2.83-4 3.79-4 5.01-4 6.31-4 7.59-4
        8.78-4 9.85-4 1.08-3 1.17-3 1.27-3 1.36-3 1.44-3 1.52-3 1.68-3
        1.98-3 2.51-3 2.99-3 3.42-3 3.82-3 4.01-3 4.41-3 4.83-3 5.23-3
        5.60-3 5.80-3 6.01-3 6.37-3 6.74-3 7.11-3 7.66-3 8.77-3 1.03-2
        1.18-2 1.33-2
c
c      Tallies
c
c      FC2      Radial doses at contact (between IL on heat shield)
F2:p    26
FS2     -701 -702 -703 -704 -705 -706 -707 -708 -709 -710 -711
c
c      FC12     Radial doses at top side IL surface
F12:p   50
FS12    -200 -720 -721 -722 -723 -202
c
c      FC22     Radial doses at bottom side IL surface
F22:p   50
FS22    -203 -740 -741 -742 -743 -201
c
c      FC32     Doses at top limiter horizontal surface
F32:p   202
FS32    -760 -761 -762 -763 -764 -765 -766 -767 -50
c
c      FC42     Doses at bottom limiter horizontal surface
F42:p   203
FS42    -760 -761 -762 -763 -764 -765 -766 -767 -50
c
c      FC52     Doses at vehicle surface (4 ft from BRR centerline)
F52:p   540
FS52    -203 -770 -771 -772 -773 -774 -775 -776 -777 -778
        -779 -780 -781 -782 -783 -202
c
c      FC62     Doses at 2m from vehicle surface
F62:p   541

```

# BRR Package Safety Analysis Report

```

FS62      -203 -770 -771 -772 -773 -774 -775 -776 -777 -778
          -779 -780 -781 -782 -783 -202
C
FC72      Doses at driver seat (25 ft from BRRC centerline)
F72:p     542
FS72      -203 -770 -771 -772 -773 -774 -775 -776 -777 -778
          -779 -780 -781 -782 -783 -202
C
FC82      HAC Doses at 1 m side
F82:p     543
FS82      -203 -770 -771 -772 -773 -774 -775 -776 -777 -778
          -779 -780 -781 -782 -783 -202
C
FC92      HAC Doses at 1m top
F92:p     210
FS92      -760 -761 -762 -763 -764 -765 -766 -767 -50 -540 -543
C
FC102     HAC Doses at 1m bottom
F102:p    211
FS102     -760 -761 -762 -763 -764 -765 -766 -767 -50 -540 -543
C
c   TRCL definitions
C
*tr1      1.7413 15.5236 0                      $ wedge 1
*tr2      0 0 0          45 135 90 45 45 90      $ wedge 2(8)
*tr3      0 0 0          90 180 90 0 90 90       $ wedge 3(7)
*tr4      0 0 0          135 225 90 45 135 90    $ wedge 4(6)
*tr5      0 0 0          180 90 90 90 180 90     $ wedge 5
*tr6      0 0 0          135 45 90 225 135 90    $ wedge 6
*tr7      0 0 0          90 0 90 180 90 90       $ wedge 7
*tr8      0 0 0          45 45 90 135 45 90      $ wedge 8
*tr20     0 0 150.022 50 90 140 90 0 90 40 90 50 $ pipe
*tr22     0 0 -0.6426
C
prdmp     j j 1 2
ctme      3600
phys:p    4j 1

```

## 6.0 CRITICALITY EVALUATION

The Battelle Energy Alliance (BEA) Research Reactor (BRR) package is used to transport spent fuel from a variety of research reactors, including the University of Missouri Research Reactor (MURR), Massachusetts Institute of Technology Research Reactor (MITR-II), Advanced Test Reactor (ATR), PULSTAR, and various types of Training, Research, Isotope General Atomics (TRIGA) reactors. Square plate fuel (plate-type fuel in assemblies that are approximately square in cross-section) used by the Rhode Island Nuclear Science Center (RINSC), University of Massachusetts at Lowell (U-Mass), Ohio State University (Ohio State), Missouri University of Science and Technology (Missouri S&T), University of Florida (U-Florida), and Purdue University (Purdue) may also be transported. The following analyses demonstrate that the BRR package complies with the requirements of 10 CFR §71.55 and §71.59. Based on the analysis, the Criticality Safety Index (CSI), per 10 CFR §71.59, is 0.

### 6.1 Description of Criticality Design

#### 6.1.1 Design Features

Five basket types are used to properly position the fuel within the cask cavity. These baskets limit the number of fuel elements that may be shipped at a given time, and also control the spacing between the fuel elements. No poisons are utilized in the package. The separation provided by the packaging is sufficient to maintain criticality safety.

#### 6.1.2 Summary Table of Criticality Evaluation

The upper subcritical limit (USL) for ensuring that the package is acceptably subcritical, as determined in Section 6.8, *Benchmark Evaluations*, is:

$$\text{USL} = 0.9209$$

The package is considered to be acceptably subcritical if the computed  $k_{\text{safe}}$  ( $k_s$ ), which is defined as  $k_{\text{effective}}$  ( $k_{\text{eff}}$ ) plus twice the statistical uncertainty ( $\sigma$ ), is less than or equal to the USL, or:

$$k_s = k_{\text{eff}} + 2\sigma \leq \text{USL}$$

The USL is determined on the basis of a benchmark analysis and incorporates the combined effects of code computational bias, the uncertainty in the bias based on both benchmark-model and computational uncertainties, and an administrative margin. The results of the benchmark analysis indicate that the USL is adequate to ensure subcriticality of the package.

The packaging design is shown to meet the requirements of 10 CFR 71.55(b). No credit is taken for fuel element burnup in any models. In the single package normal conditions of transport (NCT) models, credit is taken for the leaktight performance of the cask, while in the single package hypothetical accident condition (HAC) models, water is modeled in all cavities at the density in which reactivity is maximized. For the aluminum plate fuel elements, the most reactive credible configuration is utilized by maximizing the gap between the fuel plates. Maximizing this gap maximizes the moderation and hence the reactivity because the fuel elements are undermoderated. In all single package models, 12-in of water reflection is utilized.

Infinite reflection is utilized in both NCT and HAC array models. In the HAC array cases, internal and external water moderation is selected to maximize the reactivity.

The maximum results of the criticality calculations for each of the fuel element types are summarized in Table 6.1-1. The maximum calculated  $k_s$  is 0.827, which occurs for the HAC array case for the MURR payload. The maximum reactivity is less than the USL of 0.9209. The most reactive MITR-II, ATR, TRIGA, and Square fuel basket (SFB) cases are well below the USL.

Note that PULSTAR, the Loose Plate Box (LPB), and the Square plate-fuels are transported in the SFB. PULSTAR bounds the LPB and Square plate-fuels. The LPB is used to transport U-Florida, U-Mass(AI), or Purdue fuel plates. Up to eight LPBs may be loaded per package, and the limit on the number of plates per LPB is  $\leq 31$  for the three plate types authorized:

- Limit on U-Florida plates:  $\leq 31$  plates per LPB
- Limit on U-Mass(AI) plates:  $\leq 31$  plates per LPB
- Limit on Purdue plates:  $\leq 31$  plates per LPB

The LPB is most reactive when filled with the maximum allowed number of fuel plates, although the maximally loaded system is undermoderated. Reactivity is reduced when fewer than 31 fuel plates are loaded, and the analysis bounds loading/unloading operations. Transporting PULSTAR, Square plate fuels, and the LPB within the same basket is authorized, as this payload is bounded by a payload of eight PULSTAR fuel elements.

Note that the TRIGA fuel is significantly more reactive than the plate fuel types and PULSTAR under NCT. This is because hydrogen is included in the TRIGA fuel matrix, providing some moderation. However, the reactivity of the NCT TRIGA cases is still very low.

### **6.1.3 Criticality Safety Index**

An infinite number of packages is used in the array calculations for both NCT and HAC. Therefore, the criticality safety index per 10 CFR 71.59 is 0.

**Table 6.1-1 – Summary of Criticality Evaluation**

Normal Conditions of Transport (NCT)							
Basket	MURR	MITR-II	ATR	TRIGA	SFB		
Fuel	MURR	MITR-II	ATR	TRIGA	PULSTAR	LPB	Square Plate
Case	$k_s$	$k_s$	$k_s$	$k_s$	$k_s$	$k_s$	$k_s$
Single Unit Maximum	0.085	0.058	0.088	<b>0.417</b>	0.147	0.052	0.036
Infinite Array Maximum	0.197	0.144	0.234	<b>0.539</b>	0.229	0.121	0.094
Hypothetical Accident Conditions (HAC)							
Basket	MURR	MITR-II	ATR	TRIGA	SFB		
Fuel	MURR	MITR-II	ATR	TRIGA	PULSTAR	LPB	Square Plate
Case	$k_s$	$k_s$	$k_s$	$k_s$	$k_s$	$k_s$	$k_s$
Single Unit Maximum	0.784	0.574	0.704	0.709	<b>0.812</b>	0.641	0.741
Infinite Array Maximum	<b>0.827</b>	0.609	0.721	0.720	0.822	0.647	0.746
USL = 0.9209							



## 6.2 Fissile Material Contents

Allowed spent fuel contents are MURR, MITR-II, ATR, TRIGA, PULSTAR, and the Square plate-fuels RINSC, U-Mass (silicide or aluminide), Ohio State, Missouri S&T, U-Florida, and Purdue. Up to 31 U-Mass (aluminide), U-Florida, and Purdue plates may also be transported in a Loose Plate Box (LPB). For criticality control purposes, all fuel is modeled as fresh, and the information provided in this section pertains to fresh fuel.

### 6.2.1 MURR Fuel Element

The package can accommodate up to eight MURR fuel elements. Each MURR element contains up to 782.8 g U-235, with an enrichment of  $93 \pm 1$  wt.%. This fuel loading and enrichment is bounded by modeling 785 g U-235 and 94% enrichment. The weight percents of the remaining uranium isotopes are 1.2 wt.% U-234, 0.7 wt.% U-236, and 5.0-7.0 wt.% U-238. Each fuel element contains 24 curved fuel plates. Fuel plate 1 has the smallest radius, while fuel plate 24 has the largest radius, as shown in Figure 6.2-1. The fuel “meat” is a mixture of uranium metal and aluminum, while the cladding and structural materials are an aluminum alloy.

The relevant fuel element information is summarized in Figure 6.2-2. Each fuel plate is nominally 0.05-in thick, with a thickness tolerance of  $\pm 0.002$ -in. The fuel meat is nominally 0.02-in thick, and the cladding is nominally 0.015-in thick. The minimum cladding thickness is 0.008-in. The plate cladding material is aluminum. Fuel element side plates are fabricated of ASTM B 209, aluminum alloy 6061-T6 or 6061-T651. These fuel element side plates have a minimum thickness of 0.145-in. The average measured channel spacing between fuel plates, over the entire fuel element, is less than or equal to 0.088-in. The maximum local channel spacing is 0.090-in.

The midpoint radii of the fuel plates are treated as fixed quantities, and are computed based on nominal dimensions. Therefore, due to the modeling technique employed, the pitch is fixed at 0.130-in, and the cladding thickness and channel spacing are linked. If the fuel plates are modeled at the maximum average channel spacing of 0.088-in, the as-modeled cladding thickness is 0.011-in. However, if the cladding is modeled at the minimum value of 0.008-in, the as-modeled channel spacing is 0.094-in. Modeling a minimum cladding thickness of 0.008-in and channel spacing of 0.094-in between each fuel plate is conservative, although an actual fuel element would not be constructed in this manner. In the NCT models, a channel spacing of 0.088-in is modeled, and in the most reactive HAC models, the more conservative 0.094-in channel spacing is modeled. The relationship between cladding thickness and channel spacing for the various scenarios is illustrated in Figure 6.2-1.

The arc length of the fuel meat changes from plate to plate. Reference minimum fuel meat arc length and inner radius dimensions for each plate are provided on Figure 6.2-2. The active fuel length ranges from 23.25-in to 24.75-in.

It is necessary to determine the number densities of the fuel meat, which are the same for all fuel plates. To determine the number densities of the fuel meat, it is first necessary to compute the volume of the fuel meat. The volume of the fuel meat for each plate is the maximum arc length of the meat (nominal + 0.065-in) multiplied by the nominal active fuel length (24.0-in) and meat thickness (0.02-in). The active fuel length and meat thickness are modeled at nominal values in all final (i.e., non-parametric) fuel element models, and the use of these dimensions is justified in

Section 6.9.2, *Parametric Evaluations to Determine the Most Reactive Fuel Geometries*. It is demonstrated in Section 6.9.2.2, *MURR Fuel Parametric Evaluation*, that reactivity increases with increasing meat arc length. The results of the fuel meat volume computations for all 24 plates are provided in Table 6.2-1 for maximum fuel arc length.

The U-235 gram density for each fuel plate is computed by dividing the U-235 mass by the total volume, or  $785 \text{ g}/556.4 \text{ cm}^3 = 1.41 \text{ g/cm}^3$ . The fuel itself is a mixture of  $\text{UAl}_x$  and aluminum. An equation that relates the U-235 density to the overall fuel meat density for ATR fuel is presented in Table 6.2-5. Because ATR and MURR fuel are of the same type, the fuel density equation shown in Table 6.2-5 is also used to develop the MURR fuel matrix density. Using this equation, the total density of the fuel matrix is computed to be approximately  $3.77 \text{ g/cm}^3$ .

From the fuel volumes, U-235 gram densities, and total mixture densities provided, the number densities for the fuel region may be computed. These number densities are provided in Table 6.2-2. The U-235 weight percent is modeled at 94%. Representative weight percents of 0.6% and 0.35% are utilized for U-234 and U-236, respectively, and the balance (5.05%) is modeled as U-238.

## 6.2.2 MITR-II Fuel Element

The package can accommodate up to eight MITR-II fuel elements. Each MITR-II element contains up to 513 g U-235, with an enrichment of  $93 \pm 1 \text{ wt.}\%$ . This fuel loading and enrichment is bounded by modeling 515 g U-235 and 94% enrichment. The weight percents of the remaining uranium isotopes are 1.2 wt.% U-234, 0.7 wt.% U-236, and 5.0-7.0 wt.% U-238. Each fuel element contains 15 flat fuel plates, as shown in Figure 6.2-3. The fuel “meat” is a mixture of uranium metal and aluminum, while the cladding and structural materials are an aluminum alloy.

The relevant fuel element information is summarized in Figure 6.2-4. Each fuel plate is nominally 0.08-in thick, with a thickness tolerance of  $\pm 0.003$ -in. The fuel meat is nominally 0.03-in thick, and the cladding is nominally 0.025-in thick. The minimum cladding thickness, including the thermal groove, is 0.008-in. The plate cladding material is aluminum. Fuel element side plates are fabricated of ASTM B 209, aluminum alloy 6061-T6. These fuel element side plates have a nominal thickness of 0.188-in. The channel spacing between the plates is  $0.078 \pm 0.004$ -in (excluding the thermal grooves). These tolerances represent average and not localized channel spacing. For an actual fuel element, the channel spacing may exceed these tolerances in localized areas. The maximum local channel spacing is 0.090-in (excluding the thermal grooves).

The maximum and minimum active fuel lengths and maximum and minimum active fuel widths may be computed based the dimensions on Figure 6.2-4:

- Maximum active fuel length =  $(23.0+0.01)-2(0.125) = 22.76$ -in
- Minimum active fuel length =  $(23.0-0.01)-2(0.5) = 21.99$ -in
- Maximum active fuel width =  $2.531 - 2(0.18) = 2.171$ -in
- Minimum active fuel width =  $2.521 - 2(0.27) = 1.981$ -in.

The nominal active fuel length may be estimated as the average of the maximum and minimum values, or 22.375-in.

It is necessary to determine the number densities of the fuel meat, which are the same for all fuel plates. To determine the number densities of the fuel meat, it is first necessary to compute the volume of the fuel meat. The volume of the fuel meat for each plate is the maximum width of the meat (2.171-in) multiplied by the active fuel length (22.375-in) and meat thickness (0.03-in). The active fuel length and meat thickness are modeled at nominal values in all final (i.e., non-parametric) fuel element models, and the use of these dimensions is justified in Section 6.9.2, *Parametric Evaluations to Determine the Most Reactive Fuel Geometries*. It is demonstrated in Section 6.9.2.3, *MITR-II Fuel Parametric Evaluation*, that reactivity increases with increasing meat width. The total meat volume is therefore  $(15)(0.03)(22.375)(2.171)(2.54^3) = 358.2 \text{ cm}^3$ .

The centerlines of the fuel plates are treated as fixed quantities, and are computed based on nominal dimensions. Therefore, due to the modeling technique employed, the pitch is fixed at 0.158-in, and the cladding thickness and channel spacing are linked. The average measured channel spacing between fuel plates, over the entire fuel element, is less than or equal to 0.082-in (excluding the thermal grooves). The fuel plates also have grooves a maximum of 0.012-in deep cut into the surface of the fuel plates to increase heat transfer. Because the grooves cover approximately half the surface area of the cladding, half of the groove depth (i.e., 0.006-in) is removed from each cladding plate in the NCT models, increasing the effective channel spacing to 0.094-in. A channel spacing of 0.094-in is modeled in all NCT cases. To achieve this channel spacing between all fuel plates, the cladding is artificially reduced to a thickness of 0.017-in, or a total plate thickness of 0.064-in. However, if the as-modeled cladding thickness is 0.006-in for each plate, the as-modeled channel spacing is 0.116-in. This cladding thickness is conservatively lower than the 0.008-in minimum cladding thickness. The most reactive HAC models utilize a channel spacing of 0.116-in. The relationship between cladding thickness and channel spacing for the various scenarios is illustrated in Figure 6.2-3.

The U-235 gram density for each fuel plate is computed by dividing the U-235 mass by the total volume, or  $515 \text{ g}/358.2 \text{ cm}^3 = 1.44 \text{ g/cm}^3$ . The fuel itself is a mixture of  $\text{UAl}_x$  and aluminum. An equation that relates the U-235 density to the overall fuel meat density for ATR fuel is presented in Table 6.2-5. Because ATR and MITR-II fuel are of the same type, the fuel density equation shown in Table 6.2-5 is also used to develop the MITR-II fuel matrix density. Therefore, using this equation, the total density of the fuel matrix is computed to be approximately  $3.79 \text{ g/cm}^3$ .

From the fuel volumes, U-235 gram densities, and total mixture densities provided, the number densities for the fuel region may be computed. These number densities are provided in Table 6.2-3. The U-235 weight percent is modeled at 94%. Representative weight percents of 0.6% and 0.35% are utilized for U-234 and U-236, respectively, and the balance (5.05%) is modeled as U-238.

### 6.2.3 ATR Fuel Element

The package can accommodate up to eight ATR fuel elements. Each element contains up to 1085 g U-235, with an enrichment of  $93 \pm 1 \text{ wt.}\%$ . This fuel loading and enrichment is bounded by modeling 1200 g U-235 and 94% enrichment. The weight percents of the remaining uranium isotopes are 1.2 wt.% U-234 (max), 0.7 wt.% U-236 (max), and 5.0-7.0 wt.% U-238. Each fuel element contains 19 curved fuel plates. Fuel plate 1 has the smallest radius, while fuel plate 19 has the largest radius, as shown in Figure 6.2-5. The fuel “meat” is a mixture of uranium metal and aluminum, while the cladding and structural material are an aluminum alloy.

The relevant fuel element details are summarized on Figure 6.2-6. Fuel plate 1 is nominally 0.080-in thick, fuel plates 2 through 18 are nominally 0.050-in thick, and fuel plate 19 is nominally 0.100-in thick. The plate thickness tolerance is +0.000/-0.002-in for all plates. The fuel meat is nominally 0.02-in thick for all 19 plates. The minimum cladding thickness is 0.018-in for plates 1 and 19, and 0.008-in for plates 2 through 18. The plate cladding material is aluminum ASTM B 209, 6061-0. Fuel element side plates are fabricated of ASTM B 209, aluminum alloy 6061-T6 or 6061-T651. These fuel element side plates have a minimum thickness of 0.182-in. Channels 2 through 10 have an average spacing of  $0.078 \pm 0.007$ -in, while channels 11 through 19 have an average spacing of  $0.077 +0.008/-0.006$ -in. The average measured channel spacing between fuel plates, over the entire fuel element, is less than or equal to 0.085-in. The maximum local channel spacing is 0.087-in.

The midpoint radii of the fuel plates are treated as fixed quantities, and are computed based on nominal dimensions. Therefore, due to the modeling technique employed, the pitch is fixed at 0.128-in (plates 2 through 18), and the cladding thickness and channel spacing are linked. If the fuel plates are modeled at the maximum average channel spacing of 0.085-in, the as-modeled cladding thickness is 0.0265-in for plate 1, 0.0115-in for plates 2 through 18, and 0.0365-in for plate 19. However, if the cladding is modeled at the minimum values, the as-modeled channel spacing is 0.097-in between plates 1 and 2, 0.107-in between plates 18 and 19, and 0.092-in between the remaining plates. Modeling the minimum cladding thicknesses for each fuel plate is conservative, although an actual fuel element would not be constructed in this manner. In the NCT models, a channel spacing of 0.085-in is modeled between each plate, and in the most reactive HAC models, the more conservative channel spacing is modeled based on minimum cladding thicknesses, as provided above. The relationship between cladding thickness and channel spacing for the various scenarios is illustrated in Figure 6.2-5.

The arc length of the fuel meat changes from plate to plate. This arc length varies based on the distance from the edge of the fuel meat to the fuel element side plate, as defined for each plate on Figure 6.2-6. This dimension is 0.245-in (max)/0.145-in (min) for fuel plates 1 and 19, 0.145-in (max)/0.045-in (min) for fuel plates 2 through 17, and 0.165-in (max)/0.065-in (min) for fuel plate 18. The smaller this dimension, the larger the arc length of the fuel meat.

The active fuel length varies between a minimum of 47.245-in ( $= 49.485 - 2*1.12$ ) and a maximum of 48.775-in ( $= 49.515 - 2*0.37$ ) for all fuel plates.

It is demonstrated in Section 6.9.2.1, *ATR Fuel Parametric Evaluation*, that reactivity increases with increasing meat arc length. Therefore, the arc length is modeled at the maximum value. To determine the number densities of the fuel meat, it is first necessary to compute the volume of the fuel meat. The volume of the fuel meat for each plate is the maximum arc length of the meat multiplied by the fuel length (48-in) and meat thickness (0.02-in). The fuel length and meat thickness are treated as fixed quantities in all fuel element models, and the use of these dimensions is justified in Section 6.9.2.1.

The fuel meat volume for each of the 19 fuel plates is provided in Table 6.2-4. The mass of U-235 per plate utilized in the analysis is also provided in Table 6.2-4. The U-235 gram density for each fuel plate is also computed. Note that the U-235 gram density is higher in the inner plates compared to the outer plates.

The fuel itself is a mixture of  $UAl_x$  and aluminum. The density of this mixture is proportional to the U-235 gram density, as shown in Table 6.2-5. These data are perfectly linear, and a linear fit

of the data is  $\rho_2 = 0.8733\rho_1 + 2.5357$ , where  $\rho_2$  is the total gram density of the mixture, and  $\rho_1$  is the gram density of the U-235 in the mixture. This equation is used to compute the total mixture gram density provided as the last column in Table 6.2-4.

From the fuel volumes, U-235 gram densities, and total mixture densities provided, the number densities for the fuel region of each fuel plate may be computed. These number densities are provided in Table 6.2-6. The U-235 weight percent is modeled at 94%. Representative weight percents of 0.6% and 0.35% are utilized for U-234 and U-236, respectively, and the balance (5.05%) is modeled as U-238.

## 6.2.4 TRIGA Fuel Element

The package can accommodate up to 19 TRIGA fuel elements. While many different types of TRIGA fuel elements have been fabricated over the past 50 years, only 26 specific TRIGA fuel element types are considered in this analysis. Data for these element types are summarized in Table 6.2-7. Of these 26, two types that bound the other designs are selected for explicit analysis:

1. 8.5 wt.% uranium in the fuel matrix, 70 wt.% U-235 in uranium (136 g U-235), stainless steel clad (General Atomics catalog number 109)
2. 30 wt.% uranium in the fuel matrix, 20 wt.% U-235 in uranium (163 g U-235), stainless steel clad (General Atomics catalog number 119)

The two bounding rod types are selected based on enrichment and total U-235 loading. Rod Type 109 is enriched to 70 wt.% U-235 (U-235/U), which significantly bounds the enrichment of all the other rods, which are enriched to 20 wt.% U-235. Rod Type 119 has a total U-235 loading of 163 grams and bounds the U-235 loading of all the other rod types by a minimum of 22 grams per rod. Note that rod Type 219 is an instrumented version of rod Type 119 and has no differences that are significant to criticality.

The fuel matrix of a TRIGA fuel element consists of a mixture of uranium and zirconium hydride. Therefore, the TRIGA elements contain hydrogen moderator material. A schematic of a typical stainless steel clad fuel element is shown in Figure 6.2-8.

TRIGA fuel elements consist of a central active fuel region with graphite axial reflectors above and below the active fuel. Standard TRIGA fuel elements manufactured prior to 1964 utilize thin samarium trioxide discs between the active fuel and graphite reflectors. Later designs utilize a thin molybdenum disc between the active fuel and lower reflector rather than samarium trioxide. The samarium trioxide discs act as a burnable poison and are conservatively omitted from the models. The molybdenum disc is only 0.031-in thick and has essentially no effect on the reactivity. For this reason, the molybdenum disc is also omitted from the models.

For all TRIGA fuel elements with the exception of Type 101, a solid zirconium rod with an outer diameter of 0.225-in is placed along the active fuel length in the center of the fuel pellet. It is assumed that the inner diameter of the fuel pellet is 0.25-in to allow a small clearance between the rod and the fuel.

The fuel elements are modeled in detail from the bottom of the bottom reflector to the top of the top reflector. The end cap regions are neglected for simplicity. The graphite reflectors are modeled at the same diameter as the fuel pellets for simplicity, although the actual graphite

reflectors have a slightly smaller diameter, as shown in Table 6.2-7. Fuel elements with high U-235 loadings may contain erbium poison, although this poison is conservatively ignored in the criticality models.

The material densities within the evaluated TRIGA fuel elements are computed based upon the information in Table 6.2-7. Because the masses of U-235 and uranium are provided, the uranium densities in the fuel may be computed based on the known volumes. The uranium is treated as a mix of only U-235 and U-238 for simplicity. The fuel densities for the two evaluated fuel types are summarized in Table 6.2-8.

### **6.2.5 PULSTAR Fuel Element**

The PULSTAR fuel element comes in one of two subtypes that are differentiated by the U-235 enrichment of the uranium in their fuel material. Up to eight elements of either subtype are permitted for transport in the BRR package using the SFB. The nominal enrichments of fuel in the two element subtypes are 4 and 6 wt.% U-235. These enrichments correspond to element-total U-235 mass loadings of 504 and 770 grams (nominal), respectively. All other aspects of the element designs are shared by the two subtypes and are identical. Those features are described below. The bounding higher enrichment is used for all analysis.

Detailed design information for PULSTAR fuel is summarized in Table 6.2-9. Each element contains 25 fuel rods in a regular, rectangular arrangement with a pitch of 0.524-in x 0.606-in. The rod lattice is centered within a zirconium box that extends beyond the ends of the 26.2-in long fuel rods. The surrounding box has a nominal thickness of 0.06-in and outer dimensions of 2.740-in x 3.150-in. Each of the 25 fuel rods in the element contains a stack of  $\text{UO}_2$  pellets with a density range of 10.4 to 10.7 g/cm<sup>3</sup> and a height of 24.0-in (max 24.1-in). The maximum diameter of the fuel pellets is 0.423-in. A zirconium alloy is used as cladding for the pellets. The cladding has a minimum thickness of 0.0185-in and an outer diameter ranging from 0.471-in to 0.474-in. Solid zirconium alloy plugs cap each end of the fuel stack.

The modeled density is the density that yields the exact nominal U-235 loading (10.494 g/cm<sup>3</sup>). As discussed above, the enrichment of U-235 in the uranium component of the  $\text{UO}_2$  is 4 or 6 wt.% depending on the subtype, but all rods in a given element subtype have the same enrichment. An enrichment of 6 wt.% is modeled in all cases and uncertainty in the enrichment (less than 0.1 %) is safely ignored. Each dimension is modeled at its maximum except for cladding thickness, which is modeled at the minimum acceptable value.

The material composition used for PULSTAR fuel is given in Table 6.2-10. The general geometry is shown in Figure 6.2-9.

### **6.2.6 Square Plate Fuels**

#### Fuel Elements

The plate fuels include elements for RINSC, U-Mass with  $\text{UAl}_x$  fuel matrix (U-Mass (Al)), U-Mass with  $\text{U}_3\text{Si}_2$ -Al fuel matrix (U-Mass (Si)), Ohio State, Missouri S&T, U-Florida, and Purdue. The  $\text{UAl}_x$  fuel matrix is referred to as “aluminide” and the  $\text{U}_3\text{Si}_2$ -Al fuel matrix is referred to as “silicide”. With the exception of U-Mass (Al), all Square plate fuels have a silicide fuel matrix. U-Mass (Al) fuel originally was manufactured for the Worcester Polytechnic Institute (WPI) reactor; however, the fuel will be used at U-Mass Lowell.

Uranium in the flat plate fuels is  $19.75 \pm 0.2$  % enriched, by weight, in U-235. The design of the elements varies between facilities, but has the same general arrangement of 14 to 22 plates, flat or with mild curvature, arranged in a regular array with 0.099-in to 0.175-in channel spacing. Except for U-Mass (Al) and Purdue, which both contain 9.3 g U-235 per plate, plates of each element contain 12.5 g U-235 per plate. The uranium foils that constitute the meat in each plate are 0.020-in thick except in the aluminide fuel of the U-Mass (Al) element, which is slightly thicker at 0.030-in. The maximum width and length of the foils are 2.5-in and 24.0-in. Aluminum cladding encases the fuel foils. The aluminum cladding has a minimum thickness of 0.005-in.

A summary of the plate and element characteristics that are significant to criticality is given in Table 6.2-11. Plate pitch for each element is adjusted to maintain the channel spacing and plate dimensions. Mass densities for the fuel materials are provided in Table 6.2-12. Note that all silicide fuels have matching composition except Purdue. Material densities are determined assuming U-235 loadings at the maximum of reported ranges.

#### Loose Plate Box (LPB)

The LPB is used to transport loose plates from three of the elements discussed in the preceding paragraphs. Each LPB can carry up to 31 loose plates per box and occupies 1 of the 8 compartments of the SFB. A payload of 8 LPBs may be transported in the SFB. Loose plates are limited to those from U-Mass (Al), U-Florida, and Purdue fuel. A U-Florida plate with 12.5 grams U-235 per plate is used in the analysis to bound U-Mass (Al) and Purdue plates, which both carry 9.3 grams U-235 per plate.

**Table 6.2-1 – MURR Fuel Volume Computation (maximum arc length)**

Plate	Midpoint Radius (cm)	Fuel Arc (cm)	Volume <sup>①</sup> (cm <sup>3</sup> )
1	7.0993	4.5034	13.9460
2	7.4295	4.7625	14.7484
3	7.7597	5.0216	15.5507
4	8.0899	5.2832	16.3608
5	8.4201	5.5423	17.1632
6	8.7503	5.8014	17.9655
7	9.0805	6.0604	18.7678
8	9.4107	6.3195	19.5701
9	9.7409	6.5786	20.3724
10	10.0711	6.8377	21.1747
11	10.4013	7.0968	21.9770
12	10.7315	7.3558	22.7793
13	11.0617	7.6149	23.5816
14	11.3919	7.8765	24.3918
15	11.7221	8.1356	25.1941
16	12.0523	8.3947	25.9964
17	12.3825	8.6538	26.7987
18	12.7127	8.9129	27.6011
19	13.0429	9.1719	28.4034
20	13.3731	9.4310	29.2057
21	13.7033	9.6901	30.0080
22	14.0335	9.9492	30.8103
23	14.3637	10.2083	31.6126
24	14.6939	10.4699	32.4228
Total			556.4024

① Volume is computed as Fuel Arc\*Active Fuel Height\*Fuel Thickness, where Active Fuel Height = 24-in (60.96 cm) and Fuel Thickness = 0.02-in (0.0508 cm).

**Table 6.2-2 – MURR Fuel Number Densities (maximum arc length)**

Isotope	Number Density (atom/b-cm)
U-234	2.3171E-05
U-235	3.6147E-03
U-236	1.3402E-05
U-238	1.9174E-04
Al	5.0596E-02
Total	5.4439E-02



**Table 6.2-3 – MITR-II Fuel Number Densities (maximum meat width)**

<b>Isotope</b>	<b>Number Density (atom/b-cm)</b>
U-234	2.3613E-05
U-235	3.6835E-03
U-236	1.3657E-05
U-238	1.9539E-04
Al	5.0481E-02
Total	5.4398E-02

**Table 6.2-4 – ATR Fuel Element Volume and Gram Densities (maximum arc length)**

<b>Plate</b>	<b>Fuel Meat Arc Length (cm)</b>	<b>Fuel Meat Volume (cm<sup>3</sup>)</b>	<b>U-235 Mass Per Plate (g)</b>	<b>U-235 density, <math>\rho_1</math> (g/cm<sup>3</sup>)</b>	<b>Total UAl<sub>x</sub> + Al Density, <math>\rho_2</math> (g/cm<sup>3</sup>)</b>
1	4.2247	26.2	27.1	1.04	3.44
2	5.0209	31.1	32.5	1.04	3.45
3	5.2764	32.7	43.2	1.32	3.69
4	5.5319	34.3	45.1	1.32	3.69
5	5.7873	35.8	58.2	1.62	3.95
6	6.0427	37.4	60.9	1.63	3.96
7	6.2982	39.0	63.6	1.63	3.96
8	6.5536	40.6	66.3	1.63	3.96
9	6.8090	42.2	69.0	1.64	3.96
10	7.0644	43.8	71.7	1.64	3.97
11	7.3198	45.3	74.3	1.64	3.97
12	7.5752	46.9	77.0	1.64	3.97
13	7.8306	48.5	79.7	1.64	3.97
14	8.0860	50.1	82.4	1.64	3.97
15	8.3414	51.7	85.2	1.65	3.98
16	8.5968	53.2	71.4	1.34	3.71
17	8.8521	54.8	73.6	1.34	3.71
18	9.0058	55.8	60.1	1.08	3.48
19	8.9039	55.1	58.7	1.06	3.47
Total	--	824.5	1200.0	--	--

**Table 6.2-5 – ATR Fuel Density Equation**

U-235 Density (g/cm <sup>3</sup> ) $\rho_1$	Total Fuel Density (g/cm <sup>3</sup> ) $\rho_2$
1.00	3.409
1.30	3.671
1.60	3.933
Linear Fit: $\rho_2 = 0.8733\rho_1 + 2.5357$	

**Table 6.2-6 – ATR Fuel Number Densities (maximum arc length)**

Plate	U-234 (atom/b-cm)	U-235 (atom/b-cm)	U-236 (atom/b-cm)	U-238 (atom/b-cm)	Aluminum (atom/b-cm)	Total (atom/b-cm)
1	1.7026E-05	2.6560E-03	9.8475E-06	1.4089E-04	5.2187E-02	5.5010E-02
2	1.7156E-05	2.6763E-03	9.9226E-06	1.4196E-04	5.2153E-02	5.4998E-02
3	2.1711E-05	3.3869E-03	1.2557E-05	1.7966E-04	5.0974E-02	5.4574E-02
4	2.1618E-05	3.3724E-03	1.2503E-05	1.7889E-04	5.0998E-02	5.4583E-02
5	2.6648E-05	4.1571E-03	1.5413E-05	2.2051E-04	4.9696E-02	5.4115E-02
6	2.6746E-05	4.1724E-03	1.5470E-05	2.2132E-04	4.9670E-02	5.4106E-02
7	2.6790E-05	4.1791E-03	1.5495E-05	2.2168E-04	4.9659E-02	5.4102E-02
8	2.6830E-05	4.1854E-03	1.5518E-05	2.2201E-04	4.9649E-02	5.4098E-02
9	2.6867E-05	4.1911E-03	1.5539E-05	2.2232E-04	4.9639E-02	5.4095E-02
10	2.6901E-05	4.1965E-03	1.5559E-05	2.2260E-04	4.9630E-02	5.4092E-02
11	2.6933E-05	4.2015E-03	1.5577E-05	2.2287E-04	4.9622E-02	5.4089E-02
12	2.6963E-05	4.2061E-03	1.5595E-05	2.2311E-04	4.9614E-02	5.4086E-02
13	2.6990E-05	4.2105E-03	1.5611E-05	2.2334E-04	4.9607E-02	5.4083E-02
14	2.7017E-05	4.2145E-03	1.5626E-05	2.2356E-04	4.9600E-02	5.4081E-02
15	2.7077E-05	4.2239E-03	1.5661E-05	2.2406E-04	4.9585E-02	5.4075E-02
16	2.2037E-05	3.4377E-03	1.2746E-05	1.8235E-04	5.0889E-02	5.4544E-02
17	2.2037E-05	3.4377E-03	1.2745E-05	1.8235E-04	5.0889E-02	5.4544E-02
18	1.7683E-05	2.7586E-03	1.0228E-05	1.4633E-04	5.2016E-02	5.4949E-02
19	1.7487E-05	2.7279E-03	1.0114E-05	1.4470E-04	5.2067E-02	5.4967E-02

Table 6.2-7 – TRIGA Fuel Characteristics

Catalog Number	Element Type	Cladding Type	Fuel Length (in)	Fuel OD (in)	U (wt% fuel)	U (grams)	U-235 (wt% U)	U-235 (grams)	H/Zr Ratio	Zirconium Rod (in)	Reflector	
											Top / Bot. (in)	OD (in)
101	Standard	Al	14	1.41	8.0	166	20	32	1.0	N/A	4.0 / 4.0	1.4
	Standard	Al	15	1.41	8.5	189	20	37	1.6	15	3.53 / 3.53	1.4
103	Standard	SS	15	1.44	8.5	197	20	39	1.6	15	2.6 / 3.7	1.4
105	Standard	SS	15	1.44	12	285	20	56	1.6	15	2.6 / 3.7	1.4
107	Standard	SS	15	1.40	12	271	20	53	1.6	15	2.6 / 3.7	1.4
<b>109</b>	<b>Standard</b>	<b>SS</b>	<b>15</b>	<b>1.44</b>	<b>8.5</b>	<b>194</b>	<b>70</b>	<b>136</b>	<b>1.6</b>	<b>15</b>	<b>2.6 / 3.7</b>	<b>1.4</b>
117	Standard	SS	15	1.44	20	503	20	99	1.6	15	2.6 / 3.7	1.4
<b>119</b>	<b>Standard</b>	<b>SS</b>	<b>15</b>	<b>1.44</b>	<b>30</b>	<b>825</b>	<b>20</b>	<b>163</b>	<b>1.6</b>	<b>15</b>	<b>2.6 / 3.7</b>	<b>1.4</b>
201	Instrumented	Al	15	1.41	8.5	189	20	37	1.6	15	3.53 / 3.53	1.3
203	Instrumented	SS	15	1.44	8.5	197	20	39	1.6	15	3.1 / 3.4	1.4
205	Instrumented	SS	15	1.44	12	285	20	56	1.6	15	3.1 / 3.4	1.4
207	Instrumented	SS	15	1.40	12	271	20	53	1.6	15	3.1 / 3.4	1.4
217	Instrumented	SS	15	1.44	20	503	20	99	1.6	15	3.1 / 3.4	1.4
219	Instrumented	SS	15	1.44	30	825	20	163	1.6	15	3.1 / 3.4	1.4
303	FFCR	SS	15	1.31	8.5	163	20	32	1.6	15	n/a	n/a
305	FFCR	SS	15	1.31	12	237	20	47	1.6	15	n/a	n/a
317	FFCR	SS	15	1.31	20	418	20	82	1.6	15	n/a	n/a
319	FFCR	SS	15	1.31	30	685	20	135	1.6	15	n/a	n/a
403	Cluster	SS	15	1.37	8.5	166	20	33	1.6	15	3.42 / 3.42	1.3
405	Cluster	SS	15	1.37	12	243	20	48	1.6	15	3.42 / 3.42	1.3
417	Cluster	SS	15	1.37	20	427	20	85	1.6	15	2.6 / 3.4	1.3
419	Cluster	SS	15	1.37	30	710	20	141	1.6	15	2.6 / 3.4	1.3
503	Ins. Cluster	SS	15	1.34	8.5	166	20	33	1.6	15	3.42 / 3.42	1.3
505	Ins. Cluster	SS	15	1.34	12	243	20	48	1.6	15	3.42 / 3.42	1.3
517	Ins. Cluster	SS	15	1.34	20	427	20	85	1.6	15	2.6 / 3.4	1.3
519	Ins. Cluster	SS	15	1.34	30	710	20	141	1.6	15	2.6 / 3.4	1.3

Note: The “Catalog Numbers” do not necessarily uniquely identify fuel. See full specification for identification.

**Table 6.2-8 – TRIGA Fuel Pellet Mass Densities**

<b>Isotope</b>	<b>Type 109 (g/cm<sup>3</sup>)</b>	<b>Type 119 (g/cm<sup>3</sup>)</b>
H	0.094	0.086
Zr	5.306	4.872
U-235	0.353	0.420
U-238	0.152	1.705
Total	5.904	7.083

**Table 6.2-9 – PULSTAR Fuel Characteristics**

Parameter	4% U-235	6% U-235
Fuel Meat Material	Uranium Oxide (UO <sub>2</sub> )	Uranium Oxide (UO <sub>2</sub> )
Cladding Material	Zirconium Alloy	Zirconium Alloy
Shape	25 fuel rods loaded in a 5 by 5 matrix in a rectangular can	25 fuel rods loaded in a 5 by 5 matrix in a rectangular can
<b>Fuel Rod</b>		
Maximum fuel pellet diameter	0.423"	0.423"
Minimum cladding thickness	0.0185"	0.0185"
Outer diameter	0.474" – 0.471"	0.474" – 0.471"
Active fuel height	24.0" Nom, 24.1" Max	24.0" Nom, 24.1" Max
Length	26.2 ± 0.005"	26.2 ± 0.005"
Rod Pitch	0.524 x 0.606 ± 0.002"	0.524 x 0.606 ± 0.002"
<b>Fuel Assembly</b>		
Length	37.98" (Nom)	37.98" (Nom)
Outside Width	2.740" x 3.150" ± 0.020"	2.740" x 3.150" ± 0.020"
Box wall thickness	0.06" (Nom)	0.06" (Nom)
Fuel Rod Weight	1.45 pounds (Nom)	1.45 pounds (Nom)
Fuel Assembly Weight	44 pounds (Nom)	44 pounds (Nom)
Enrichment (wt% U <sub>235</sub> )	4% ± 0.056%	6% (Nom)
U <sub>235</sub> content per fuel rod	20.17 g ± 2%	30.8 g (Nom)
Percent theoretical density	10.4 – 10.7 g/cc	10.4 – 10.7 g/cc
U Weight (kg/fuel rod)	0.504 kg ± 2%	0.514 kg (Nom)
U Weight (kg/fuel assembly)	12.6 kg ± 2%	12.8 kg (Nom)
UO <sub>2</sub> Weight (kg/fuel assembly)	14.3 kg ± 2%	14.3 kg ± 2%

**Table 6.2-10 – PULSTAR Fuel Pellet Mass Densities**

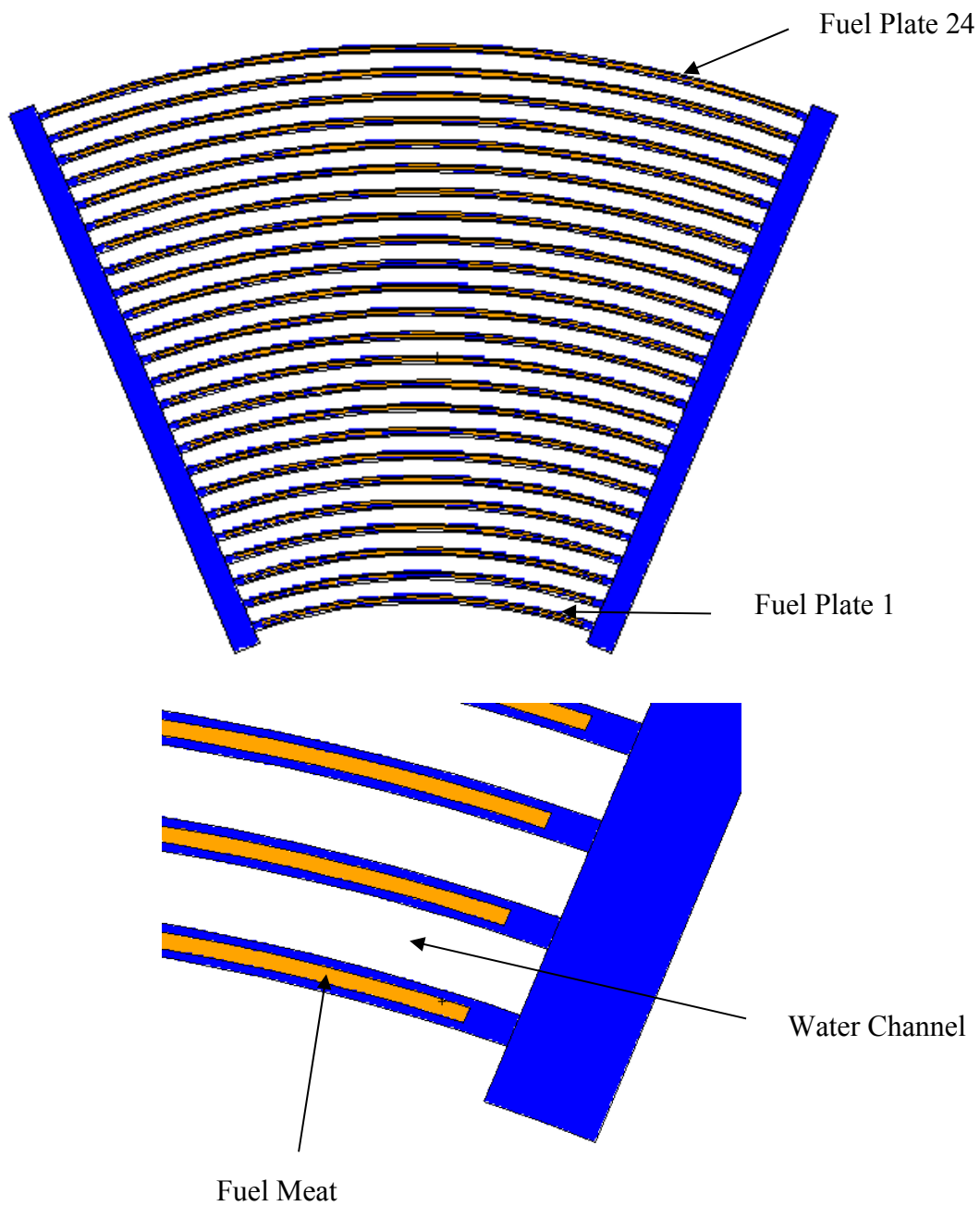
Isotope	Mass Density (g/cm <sup>3</sup> )
O	1.244
U-235	0.555
U-238	8.694
Total	10.494

**Table 6.2-11 – Square Plate Fuel Characteristics**

Element	Fuel Form	U-235 Mass per Element (g)	U-235 Mass Uncertainty ( $\pm$ g)	Plates per Element	U-235 Mass per Plate (nom.) (g)	Plate Geometry	Fuel Meat Thickness (nom.) (in)	Max Fuel Meat Width (in)	Max Fuel Meat Length (in)	Min Cladding Thickness (in)	Max Channel Spacing (in)
RINSC	U <sub>3</sub> Si <sub>2</sub> -Al	275.0	7.7	22	12.5	flat	0.020	2.47	24.0	0.005	0.099
Missouri S&T	U <sub>3</sub> Si <sub>2</sub> -Al	225.0	6.3	18	12.5	curved	0.020	2.47	24.0	0.005	0.139
U-Mass (Si)	U <sub>3</sub> Si <sub>2</sub> -Al	200.0	5.6	16	12.5	flat	0.020	2.47	24.0	0.005	0.122
U-Mass (Al)	UAl <sub>x</sub>	167.0	3.3	18	9.3	flat	0.030	2.50	24.0	0.005	0.119
Ohio State	U <sub>3</sub> Si <sub>2</sub> -Al	200.0	5.6	16	12.5	flat	0.020	2.47	24.0	0.005	0.127
U-Florida	U <sub>3</sub> Si <sub>2</sub> -Al	175.0	4.9	14	12.5	flat	0.020	2.47	24.0	0.005	0.117
Purdue	U <sub>3</sub> Si <sub>2</sub> -Al	129.92	2.52	14	9.3	flat	0.020	2.47	24.0	0.005	0.175

**Table 6.2-12 – Square Plate Fuel Meat Mass Densities**

Isotope	RINSC, Missouri S&T, U-Mass (Si), Ohio State, U-Florida (g/cm <sup>3</sup> )	Purdue (g/cm <sup>3</sup> )	U-Mass (Al) (g/cm <sup>3</sup> )
Al	1.908	2.117	2.472
Si	0.261	0.192	-
U-235	0.661	0.487	0.321
U-238	2.654	1.954	1.287
Total	5.485	4.750	4.079



**Figure 6.2-1 – MURR Fuel Element Model**  
(continued)

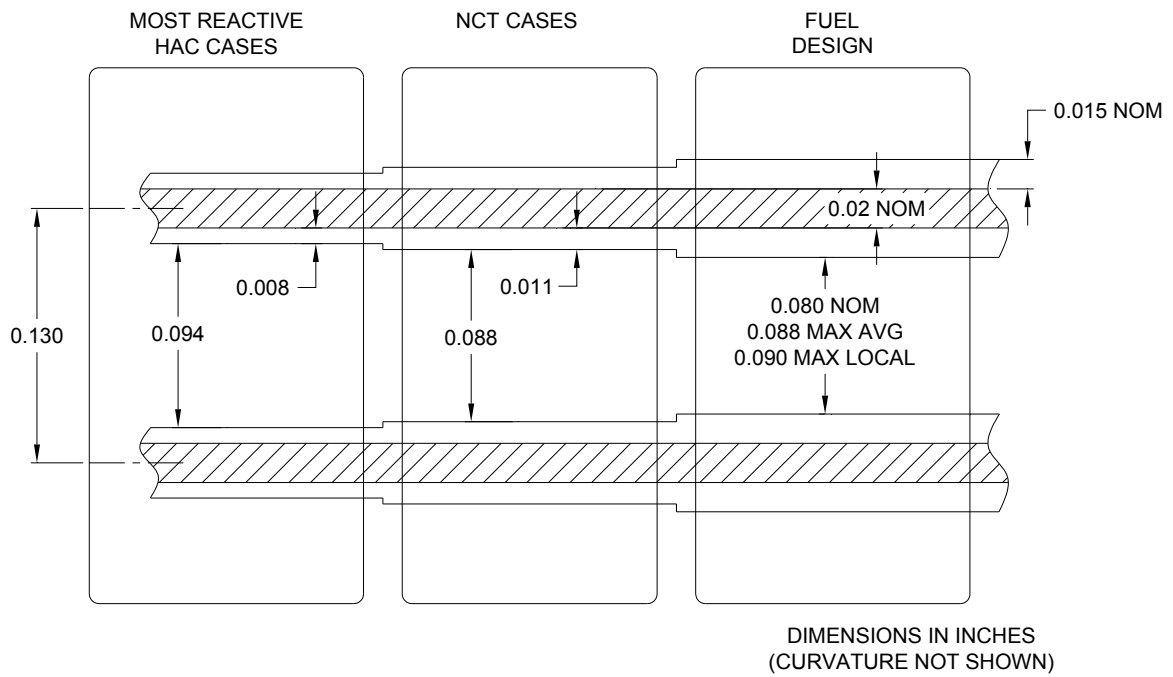
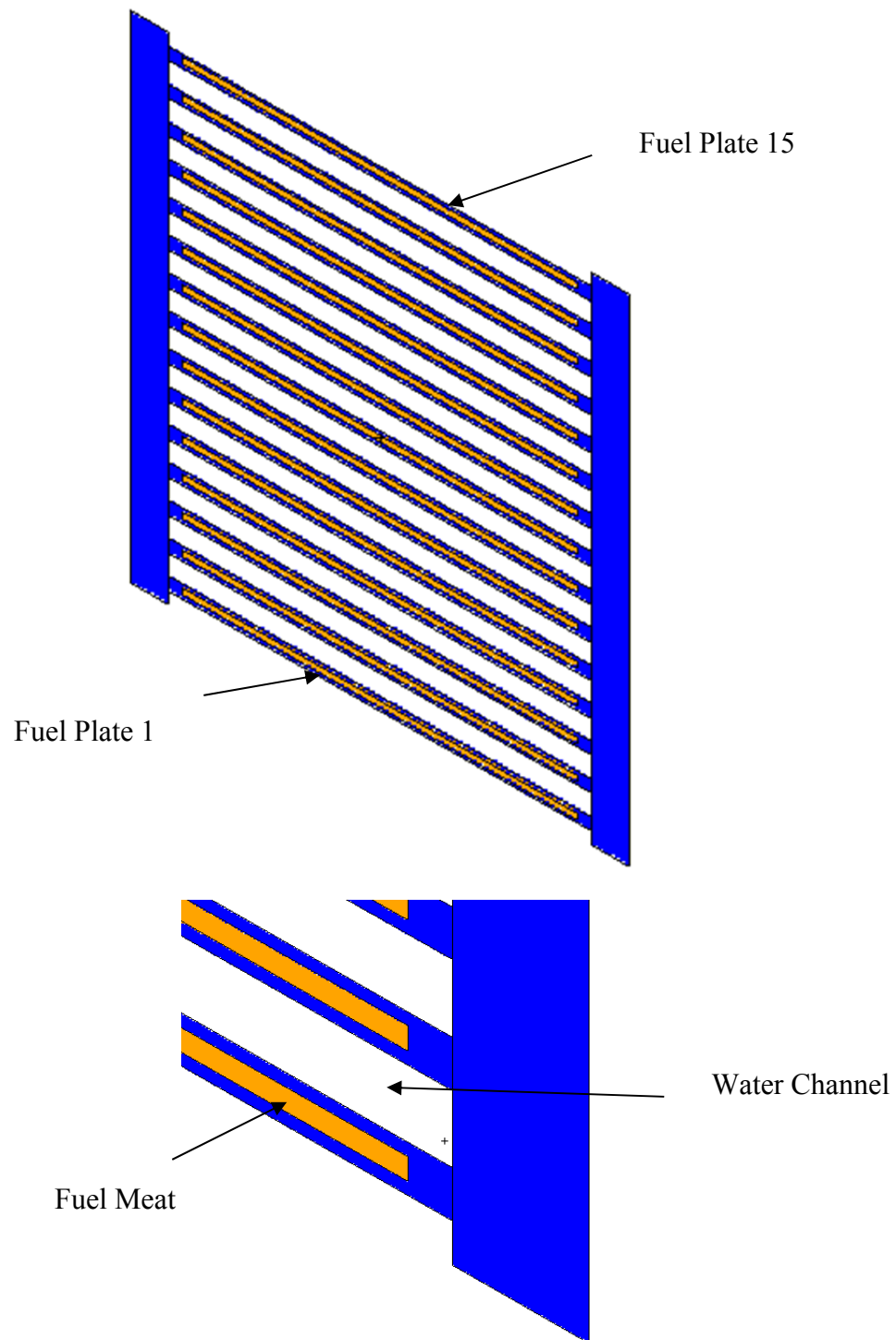


Figure 6.2-1 – MURR Fuel Element Model (concluded)



**Security-Related Information Figure  
Withheld Under 10 CFR 2.390.**

**Figure 6.2-2 – MURR Fuel Element Details**



**Figure 6.2-3 – MITR-II Fuel Element Model**  
(continued)

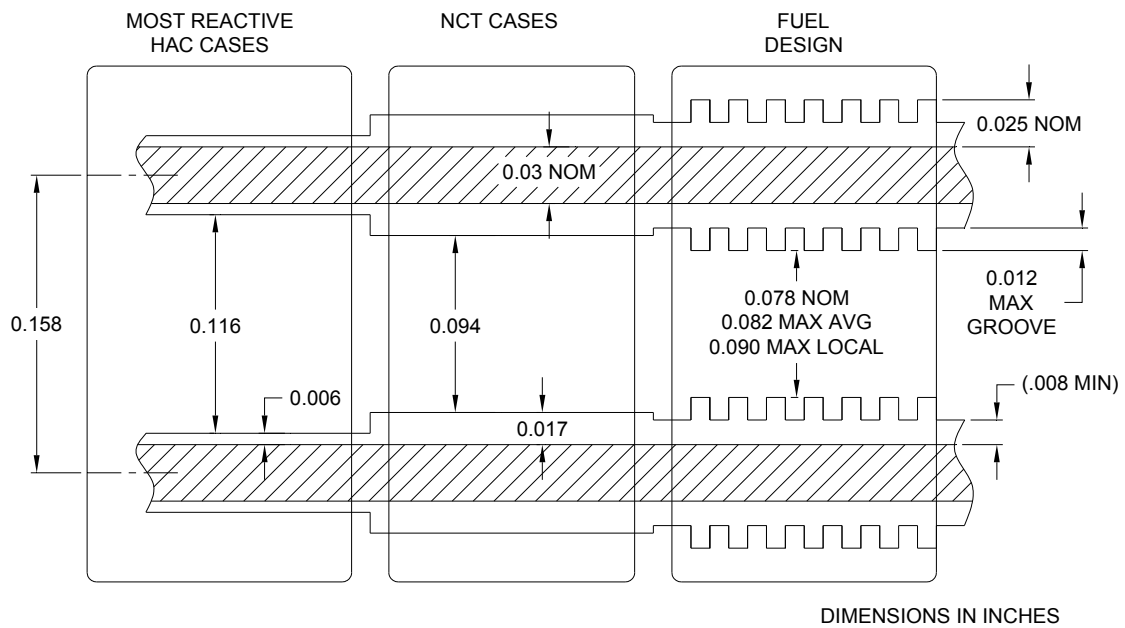
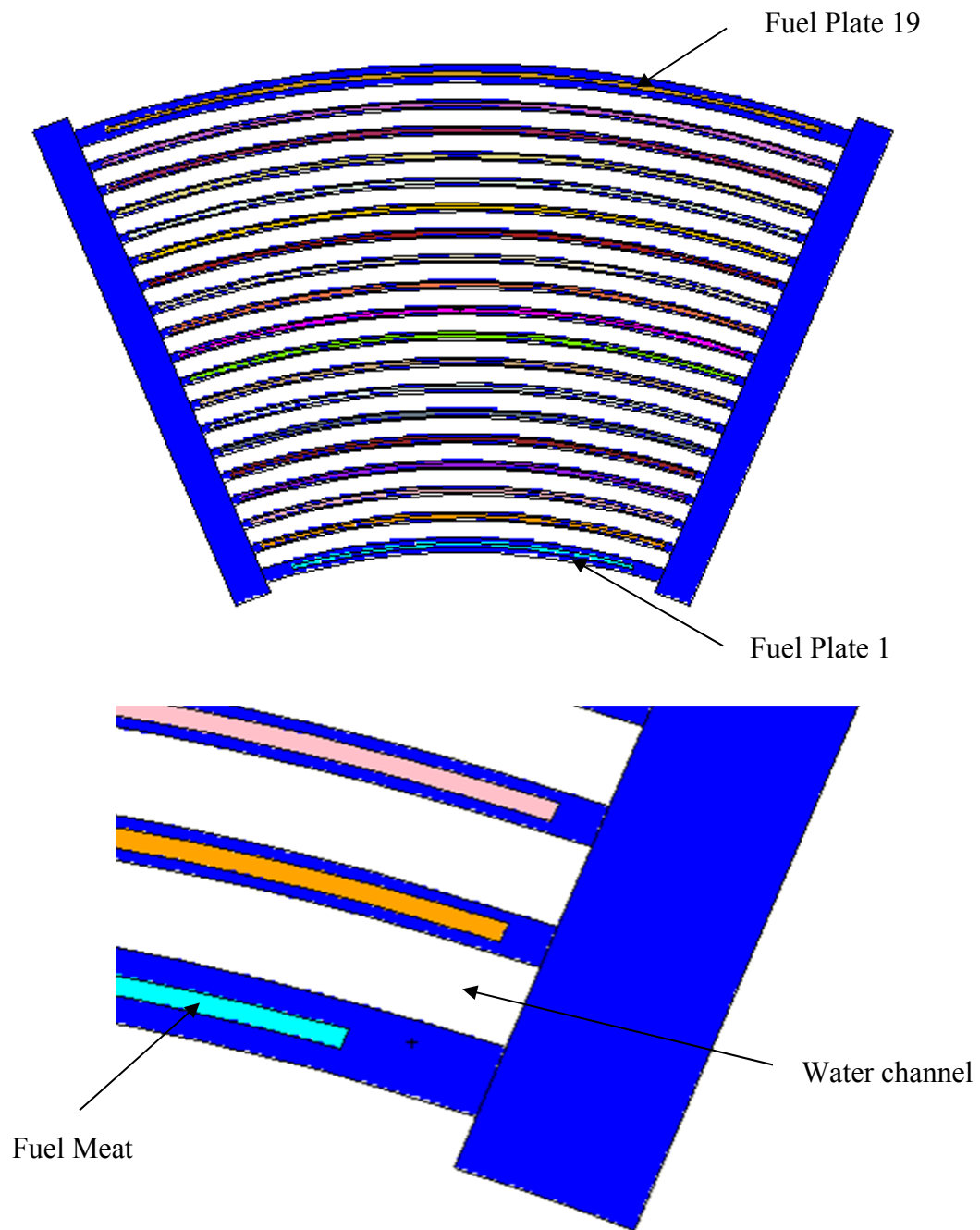


Figure 6.2-3 – MITR-II Fuel Element Model (concluded)

**Security-Related Information Figure  
Withheld Under 10 CFR 2.390.**

**Figure 6.2-4 – MITR-II Fuel Element Details**



**Figure 6.2-5 – ATR Fuel Element Model**  
(continued)

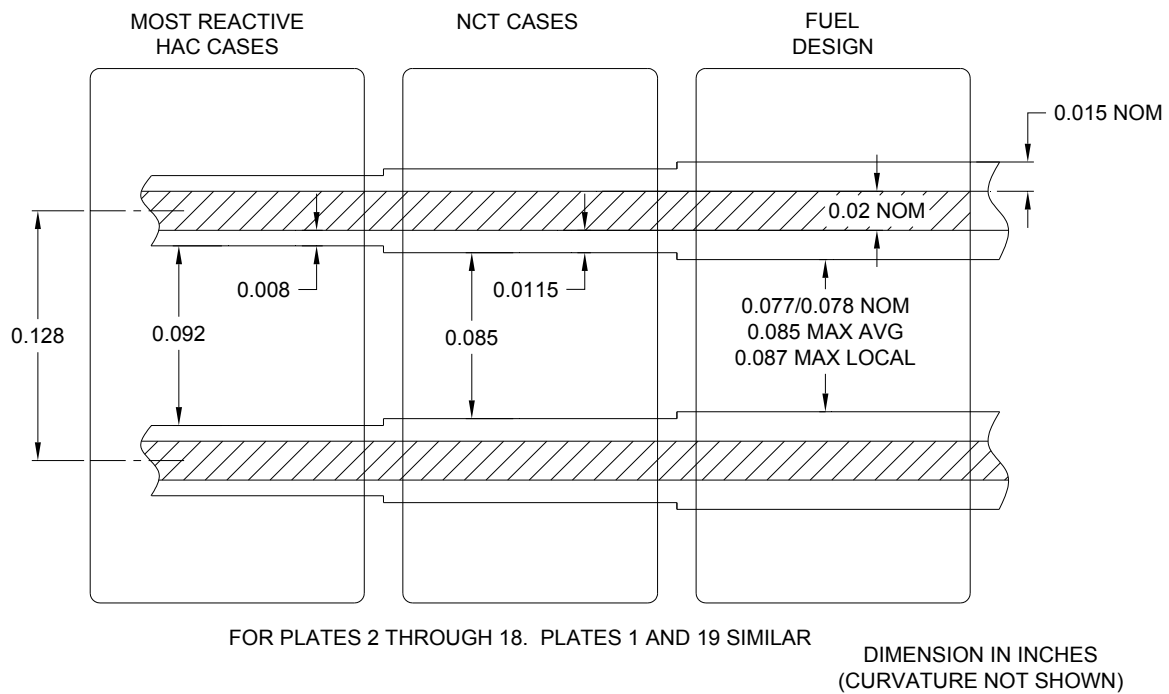
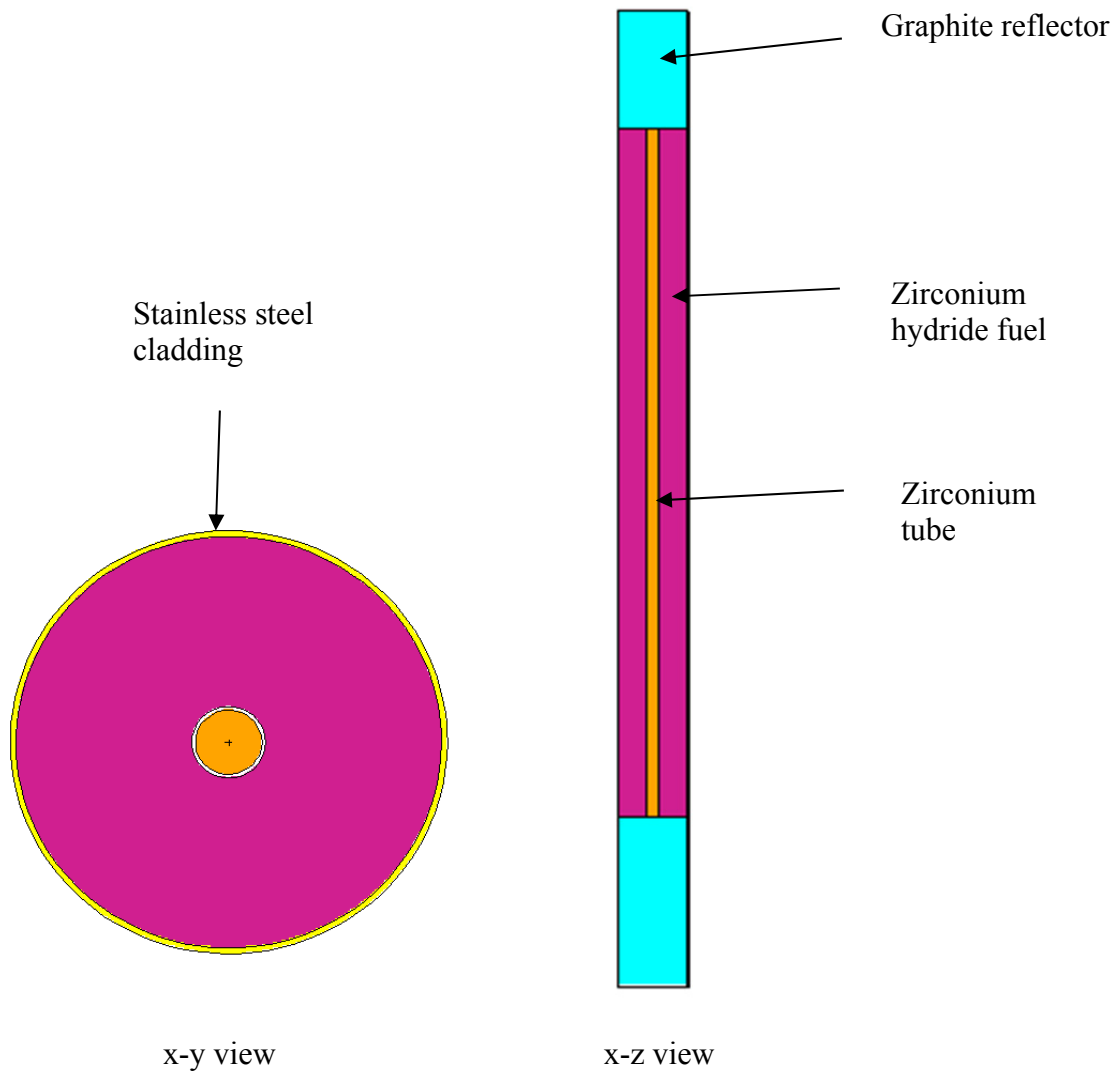


Figure 6.2-5 – ATR Fuel Element Model (concluded)

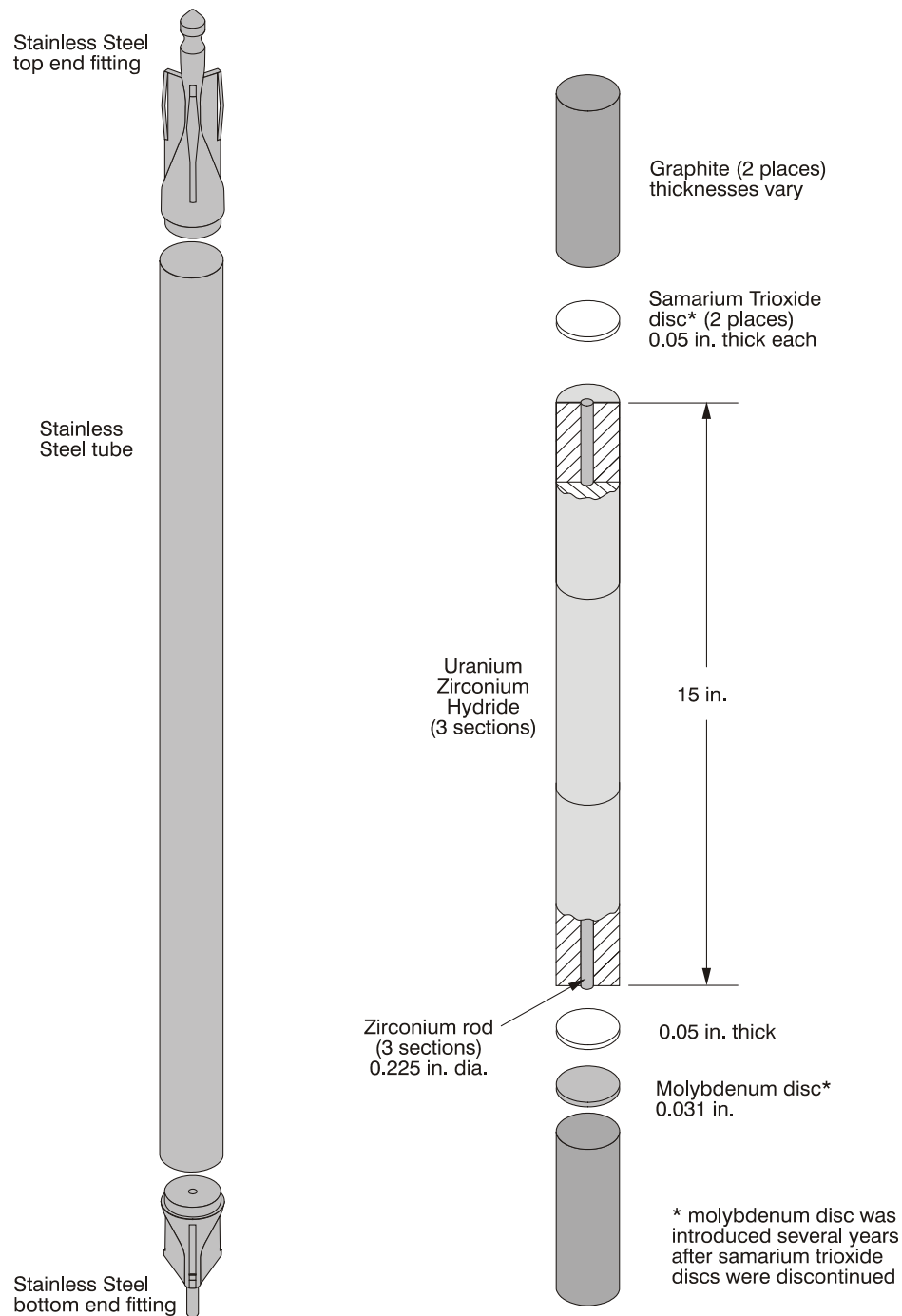
Security-Related Information Figure  
Withheld Under 10 CFR 2.390.

**Figure 6.2-6 – ATR Fuel Element Details**



**Figure 6.2-7 – Stainless Steel Clad TRIGA Fuel Element (Type 109)**





**Figure 6.2-8 – Typical Stainless Steel Clad TRIGA Fuel Element**

## Security-Related Information Figure Withheld Under 10 CFR 2.390.

Dimensions in inches

**Figure 6.2-9 – PULSTAR Fuel Element**

## 6.3 General Considerations

### 6.3.1 Model Configuration

The BRR cask is modeled using conservative simplifying assumptions. The impact limiters are not modeled, and in the single package cases the cask is reflected with 12-in of water. In the array cases, removing the impact limiters conservatively minimizes the separation between the packages and increases the reactivity. The cask body itself is simply modeled as cylinders of steel-lead-steel without modeling the minor cask details, as these minor details have a negligible effect on the system reactivity.

The modeled cask geometry is shown in Figure 6.3-1, and the key model dimensions are provided in Table 6.3-1. Cask dimensions are based on the drawings in Section 1.3.3, *Packaging General Arrangement Drawings*. Note that the cask model in the upper region is simply representative of the shield plug thicknesses and that the 2-in thick steel lid is not included in the model, thereby bringing the casks closer together in the array configuration.

Five baskets are available to accommodate the different fuel geometries. The baskets are modeled in sufficient detail to capture the relevant criticality effects, which are primarily of interest near the active fuel region. The key basket dimensions are included in Table 6.3-2, and x-y and x-z views of the five basket designs are provided in Figure 6.3-2 and Figure 6.3-3, respectively. Basket dimensions are based on the drawings in Section 1.3.3, *Packaging General Arrangement Drawings*. Note that the axial and radial fuel positions shown in these figures do not reflect the most reactive configurations, which is determined in Section 6.4, *Single Package Evaluation*.

Minor differences exist between the as-modeled and packaging general arrangement drawing dimensions, as shown in Table 6.3-1 and Table 6.3-2. These differences are small and are within the uncertainty of the Monte Carlo method and may therefore be neglected.

The baskets are modeled as undamaged in all NCT and HAC models. The baskets have been shown to be elastic in all accident scenarios and maintain their geometry (see Section 2.7.1.5, *Fuel Basket Stress Analysis*). The fuel is modeled in the most reactive axial location and the spacer pedestals are ignored. The LPB has also been shown to maintain its structural integrity in an accident and is credited in the analysis.

With the exception of U-Florida, all fuels transported in the BRR are shown to maintain their structural integrity in an accident (see Section 2.7.1.6, *Fuel Impact Deformation*). Because structural integrity under HAC for U-Florida has not been demonstrated, conservative fuel damage is modeled for U-Florida in which the plates reconfigure within the basket compartment at the most reactive uniform or non-uniform pitch. While PULSTAR fuel is shown to maintain its structural integrity in an accident, damage to PULSTAR fuel under HAC is conservatively modeled. Under HAC, PULSTAR rods are repositioned at the maximum pitch possible within the confines of the fuel element box.

In the NCT cases, credit is taken for the leaktight nature of the package, and the cask cavity is modeled as dry (void). Although the package has been shown to be leaktight under accident conditions, in the HAC cases, water is conservatively modeled in the cask cavity at the density that maximizes reactivity. If it is assumed that water is free to flow throughout the cask cavity and fuel elements (as the baskets are designed to drain freely), the moderator water density

between the fuel plates may be modeled at the same value as the water density between the fuel elements. This assumption is utilized in all MCNP criticality models. However, it has been shown that when an ATR fuel element is removed from a spent fuel pool and allowed to drip dry, a small volume of water remains between the fuel plates due to the surface tension in the thin channels between the fuel plates. Because the quantity of residual water is relatively small, any minor surface tension effects have been neglected in the MCNP modeling. In addition, no models are developed in which the cask is partially filled with water with some fuel elements uncovered (such as might be the case if the cask were on its side in an accident), because this scenario would be less reactive due to lack of moderation in the uncovered fuel elements.

In the array cases, a close-packed hexagonal array is modeled by adding a hexagonal reflective boundary condition. The water density between the casks in the array is adjusted to determine the most reactive condition.

### 6.3.2 Material Properties

The fuel meat compositions are provided in Table 6.2-2, Table 6.2-3, Table 6.2-6, and Table 6.2-8 for MURR, MITR-II, ATR, and TRIGA fuel, respectively. Fuel meat compositions for PULSTAR and Square plate fuels are provided in Table 6.2-10 and Table 6.2-12, respectively. For all fuels, aluminum structural material is modeled as pure aluminum with a density of  $2.7 \text{ g/cm}^3$ . Similarly, all zirconium alloy is modeled as pure zirconium with a density of  $6.5 \text{ g/cm}^3$ .

The TRIGA fuel contains materials not found in the aluminum plate fuels, such as stainless steel, graphite, and zirconium. For the stainless steel clad TRIGA fuel, the composition of stainless steel utilized is the standard composition provided in the SCALE material library [4] and is provided in Table 6.3-3. For the TRIGA fuels that contain a zirconium rod in the center of the fuel element, the zirconium is modeled as pure with a density of  $6.5 \text{ g/cm}^3$ . The graphite reflectors in the TRIGA fuel elements is modeled as pure graphite with a density of  $1.6 \text{ g/cm}^3$ . The density is obtained from the TRIGA benchmark experiments (IEU-COMP-THERM-003) listed in the *International Handbook of Evaluated Criticality Benchmark Experiments* [3]. The material properties of the remaining packaging and moderating materials are described as follows.

The inner and outer shells of the package are constructed from stainless steel 304. The baskets and LPB are also constructed of stainless steel 304. The standard compositions for stainless steel 304 are obtained from the SCALE material library [4], which is a standard set accepted for use in criticality analyses. The stainless steel composition and density utilized in the MCNP models are provided in Table 6.3-3. Lead is modeled as pure with a density of  $11.35 \text{ g/cm}^3$ .

Water is modeled with a density ranging up to  $1.0 \text{ g/cm}^3$  and the chemical formula  $\text{H}_2\text{O}$ .

### 6.3.3 Computer Codes and Cross-Section Libraries

MCNP5 v1.30 is used for the criticality analysis [1]. All cross sections utilized are at room temperature (293.6 K). The uranium isotopes utilize preliminary ENDF/B-VII cross section data that are considered by Los Alamos National Laboratory to be more accurate than ENDF/B-VI cross sections. ENDF/B-V cross sections are utilized for chromium, nickel, iron, and lead because natural composition ENDF/B-VI cross sections are not available for these elements. The remaining isotopes utilize ENDF/B-VI cross sections. Titles of the cross sections utilized in

the models have been extracted from the MCNP output (when available) and provided in Table 6.3-4. The S( $\alpha,\beta$ ) card LWTR.60T is used to simulate hydrogen bound to water in all models. For the TRIGA models only, the S( $\alpha,\beta$ ) cards H/ZR.60T and ZR/H.60T are used to simulate hydrogen and zirconium in zirconium hydride, respectively.

All moderated ATR, MITR-II, MURR, and TRIGA cases are run with at least 2500 neutrons per generation for 250 generations, skipping the first 50. All moderated PULSTAR and Square fuel basket intact fuel element cases are run with at least 5000 neutrons per generation for 250 generations, skipping the first 50 (some cases use 15,000 neutrons per generation for 200 generations, skipping the first 25, which is a larger number of total neutrons run). All moderated loose plate box and damaged U-Florida cases are run with 5000 neutrons per generation for 1050 generations, skipping the first 50. The 1-sigma uncertainty is approximately 0.001 or less for the HAC cases, and somewhat less for the NCT cases.

### 6.3.4 Demonstration of Maximum Reactivity

The reactivities of the NCT single package and array cases are small ( $<0.6$ ) because the package is leaktight and no water is present in the package cavity. The TRIGA fuel is the most reactive under NCT because hydrogen moderator is included in the zirconium hydride fuel matrix, although the reactivity is still relatively low.

Under HAC, water is allowed to enter the package cavity at the density that maximizes reactivity. For the intact plate fuels, the system is always the most reactive when full-density water is utilized because the system is undermoderated. Because the intact plate fuel is undermoderated, modeling the minimum cladding thickness and hence maximum channel spacing results in the most reactive condition. For the TRIGA fuel, optimum reactivity is achieved for a reduced water density (0.6 or 0.7 g/cm<sup>3</sup>).

It is demonstrated that reactivity increases when the fuel is axially shifted to the top of the cavity, as this configuration maximizes reflection from the lead in the shield plug. It is also demonstrated that reactivity increases when the fuel elements are moved to the radial center of the package. For the MITR-II fuel, which has an inner and outer row of fuel elements, reactivity is maximized by moving the inner row outward and the outer row inward, which decreases the distance between the fuel elements.

For the array cases, a hexagonal reflective boundary condition is placed around the cask, simulating a hexagonal lattice. The water density between the packages is varied between 0 and 1.0 g/cm<sup>3</sup>, and the array reactivities (both NCT and HAC) are maximized with no water between the packages.

It has been demonstrated in the structural analysis that the baskets and LPB maintain their structural integrity during an accident condition. With the exception of U-Florida, all fuels transported in the BRR are shown to maintain their structural integrity in an accident. Because structural integrity under HAC for U-Florida has not been demonstrated, conservative fuel damage is modeled for U-Florida in which the plates reconfigure within the basket compartment at the most reactive uniform or non-uniform pitch. While PULSTAR fuel is shown to maintain its structural integrity in an accident, damage to PULSTAR fuel under HAC is conservatively modeled. Under HAC, PULSTAR rods are repositioned at the maximum pitch possible within the confines of the fuel element box.

The MURR payload is the most reactive, with  $k_s = 0.827$  (Case D8), which is below the USL of 0.9209. This most reactive case occurs under HAC-array conditions, with full density water flooding the basket and no water between packages.

**Table 6.3-1 – Key Cask Model Dimensions**

Item	Dimension (in)
<b>Cask Radial</b>	
Cask inner diameter	16.0
Cask inner steel thickness	1.0
Cask lead thickness	8.0
Cask outer steel thickness	2.0
Cask outer diameter (w/o heat shield)	38.00
<b>Cask Axial Top</b>	
Shield plug bottom plate thickness	1.0
Shield plug lead thickness	9.7, modeled as 9.58
Shield plug top plate thickness	0.5
Shield plug overall height	11.2, modeled as 11.08
<b>Cask Axial Bottom</b>	
Bottom outer plate thickness	1.0
Bottom lead thickness at centerline	7.7, modeled as 7.72
Bottom casting inner thickness (after machining)	1.1, modeled as 1.22

**Table 6.3-2 – Key Basket Model Dimensions**

Item	Dimension (in)
<b>MURR Basket</b>	
Compartment separator width	1.0
Shell outer diameter	15.63
Shell thickness	0.25
Inner tube outer diameter	7.9, modeled as 7.938
Inner tube inner diameter	7.0
<b>MITR-II Basket</b>	
Compartment perpendicular width	2.7
Inner Diameter	Complex, modeled as 9.45
Outer Diameter	15.63
Distance, cutout to center	4.8
<b>ATR Basket</b>	
Compartment separator width	0.375
Shell outer diameter	13.5
Shell thickness	0.25
Inner tube outer diameter	7.2
Inner tube inner diameter	6.5
<b>TRIGA Basket</b>	
Tube outer diameter	2.0
Tube wall thickness	0.12, modeled as 0.11
Inner row position diameter	6.5
Outer row position diameter	11.5
<b>Square Fuel Basket</b>	
Compartment Width (Square)	3.40
Wall thickness	0.1054
Centerline radius, outer compartments	5.42
<b>Loose Plate Box</b>	
Inner lateral dimensions	3.0 x 2.5
Plate thickness	0.125

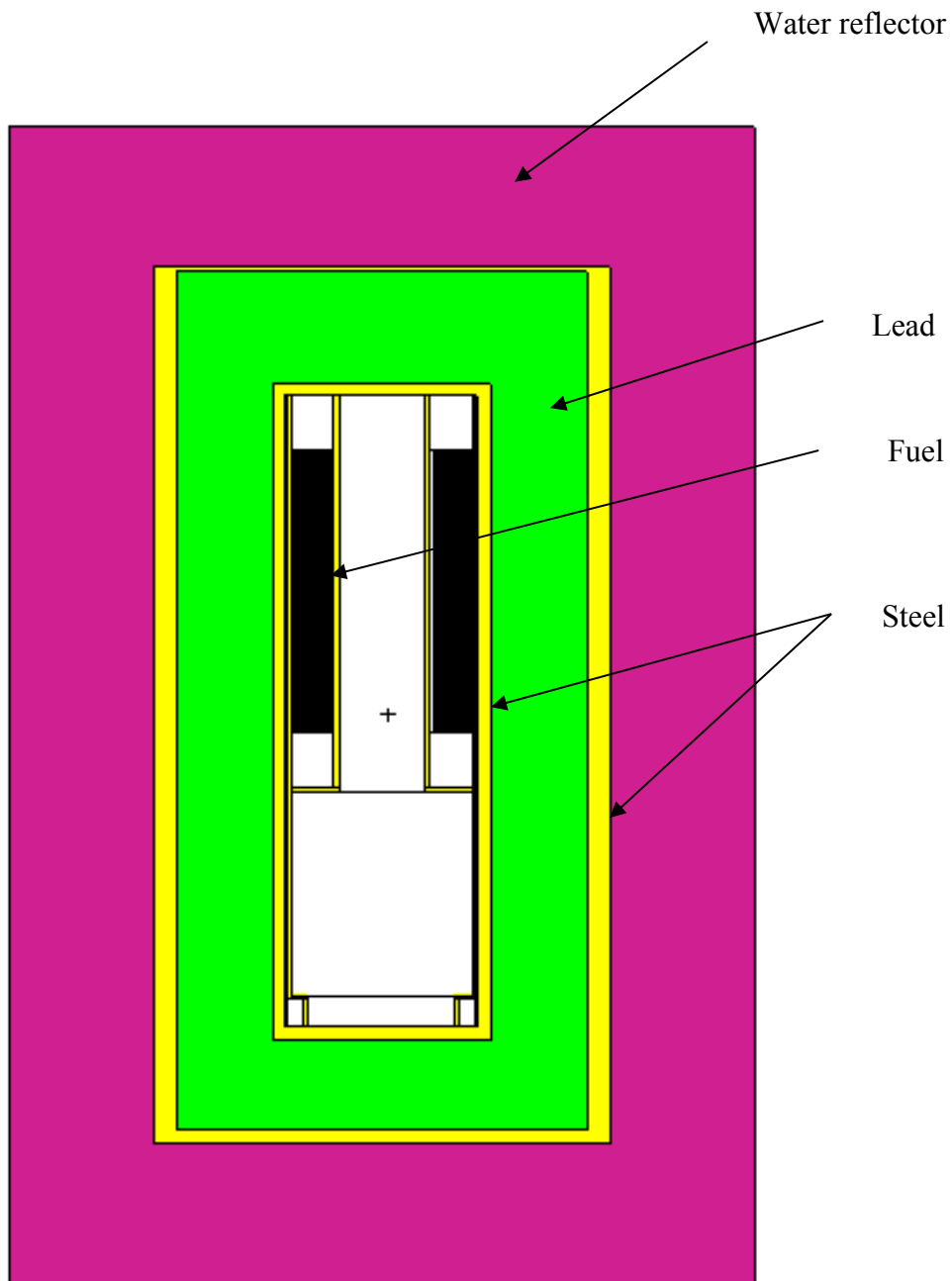
**Table 6.3-3 – SS304 Composition**

Component	Wt. %
C	0.08
Si	1.0
P	0.045
Cr	19.0
Mn	2.0
Fe	68.375
Ni	9.5
Density (g/cm <sup>3</sup> )	7.94

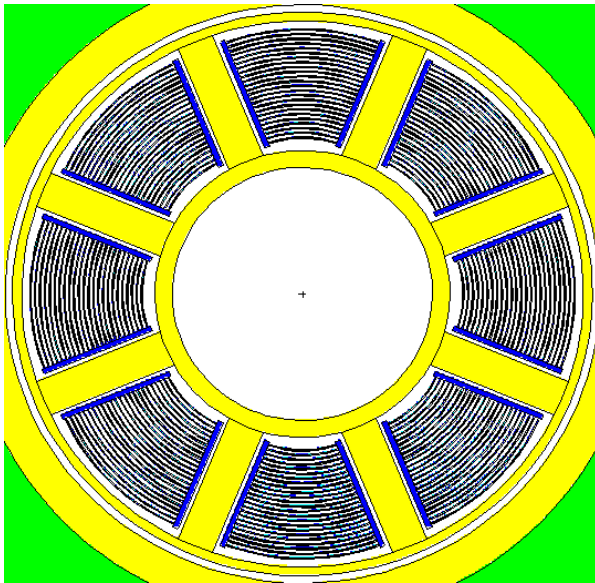
**Table 6.3-4 – Cross Section Libraries Utilized**

Isotope/Element	Cross Section Label (from MCNP output)
1001.62c	1-h-1 at 293.6K from endf-vi.8 njoy99.50
6000.66c	6-c-0 at 293.6K from endf-vi.6 njoy99.50
8016.62c	8-o-16 at 293.6K from endf-vi.8 njoy99.50
13027.62c	13-al-27 at 293.6K from endf-vi.8 njoy99.50
14000.60c	14-si-nat from endf/b-vi
15031.66c	15-p-31 at 293.6K from endf-vi.6 njoy99.50
17000.66c	17-cl-0 at 293.6K from endf-vi.0 njoy99.50
24000.50c	njoy
25055.62c	25-mn-55 at 293.6K from endf/b-vi.8 njoy99.50
26000.55c	njoy
28000.50c	njoy
40000.66c	40-zr-0 at 293.6K from endf-vi.1 njoy99.50
82000.50c	njoy
92234.69c	92-u-234 at 293.6K from t16 u234la4 njoy99.50
92235.69c	92-u-235 at 293.6K from t16 u235la9d njoy99.50
92236.69c	92-u-236 at 293.6K from t16 u236la2d njoy99.50
92238.69c	92-u-238 at 293.6K from t16 u238la8h njoy99.50

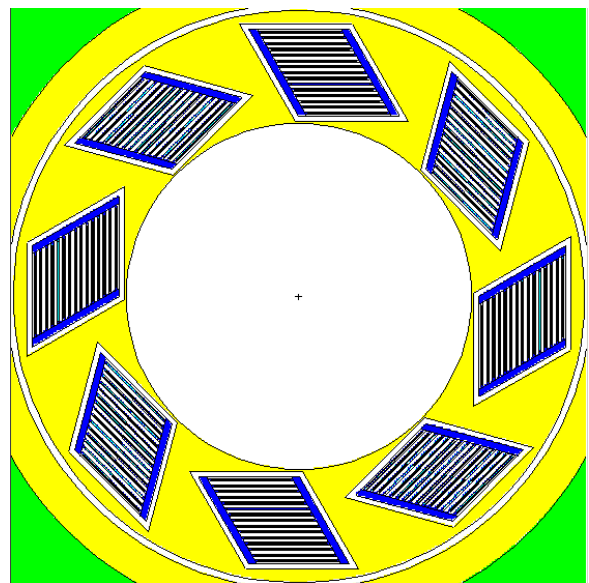




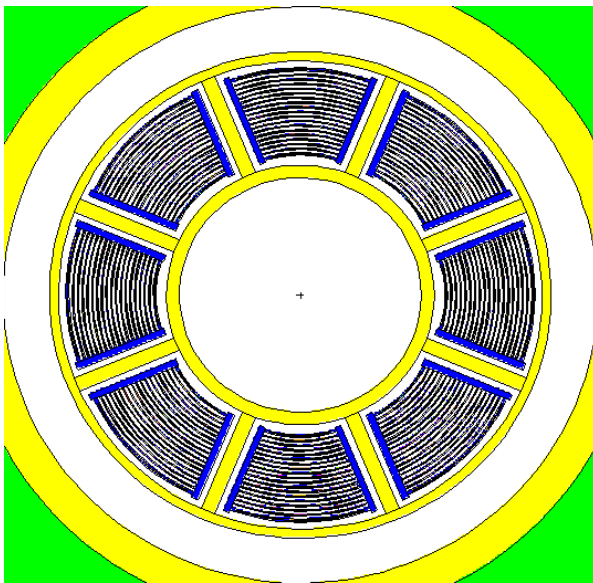
**Figure 6.3-1 – NCT Single Package Model (x-z view)**



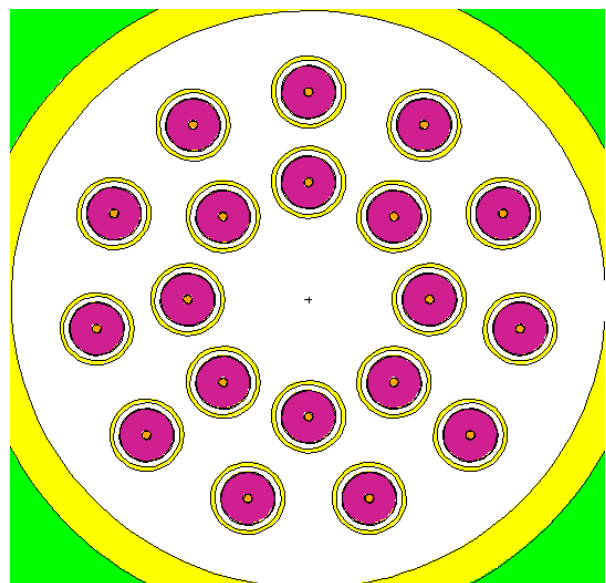
MURR



MITR-II

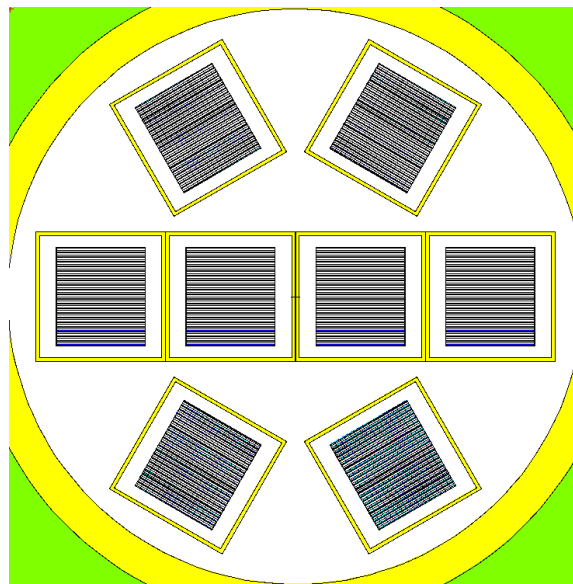


ATR



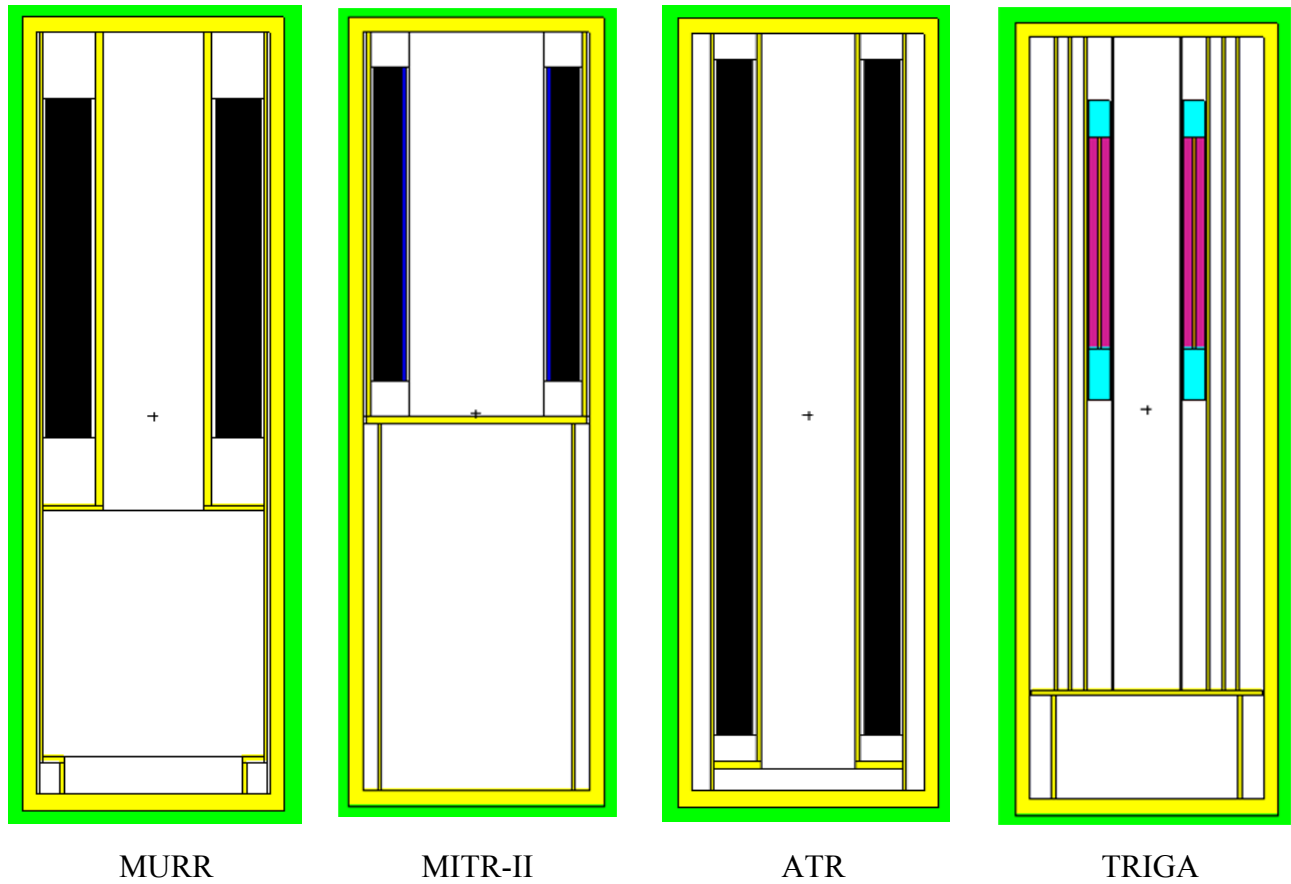
TRIGA

**Figure 6.3-2 – Basket Models (x-y view)**  
(continued)

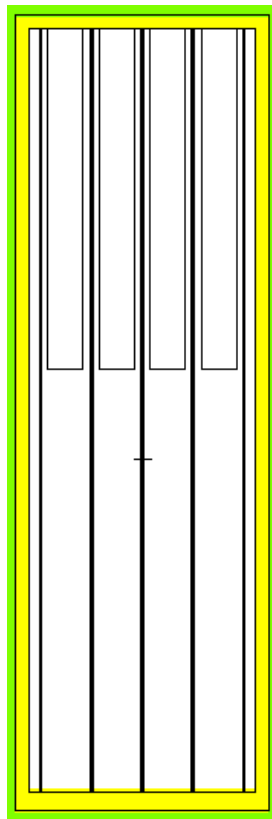


Square Fuel Basket

Figure 6.3-2 – Basket Models (x-y view) (concluded)



**Figure 6.3-3 – Basket Models (x-z view)**  
(continued)



Square Fuel Basket

Figure 6.3-3 – Basket Models (x-z view) (concluded)

## 6.4 Single Package Evaluation

### 6.4.1 Configuration

#### 6.4.1.1 NCT Single Package Configuration

The geometry of the NCT single package configuration is discussed in Section 6.3.1, *Model Configuration*. For MURR, MITR-II, and ATR, the fuel element geometry is consistent with the most reactive fuel element models, including tolerances, as determined in Section 6.9.2, *Parametric Evaluations to Determine the Most Reactive Fuel Geometries*.

TRIGA models are developed for a bounding subset of the allowable rod types. The bounding rods (catalog numbers 109 and 119) contain the highest enrichment fuel (136 g U-235 at 70 wt.%) and the highest U-235 loading (163 g U-235 at 20 wt. %), respectively. Other permissible rods are all enriched to 20 wt.% U-235. Given no other significant differences in the design of other permissible rods, Type 109 and 119 are justifiably treated as bounding. Molybdenum discs, a mild neutron absorber, are conservatively ignored.

PULSTAR fuel is modeled with the maximum U-235 enrichment of 6%. The Square plate-fuels are modeled with minimum cladding thickness and maximum possible channel spacing, as the analysis for MURR, MITR-II, and ATR indicated this is the most reactive configuration for plate-type fuel.

#### MURR

The MURR results are listed in Table 6.4-1 as Cases A1 through A3. In Case A1, the active fuel region is centered both axially and laterally within the basket compartments. In Case A2, all fuel elements are moved within the basket compartments towards the radial center. In Case A3, the fuel elements are moved radially inward (like Case A2) and shifted axially to the top of the package. In actual practice, it would not be possible to shift the active fuel all the way to the top due to the presence of the end fittings. This configuration is the most reactive, as reflection from the package shield plug is maximized. Therefore, Case A3 is the most reactive, with  $k_s = 0.08545$ . Clearly, the reactivity of unmoderated MURR fuel is very low.

#### MITR-II

The MITR-II results are listed in Table 6.4-1 as Cases A10 through A13. In Case A10, the active fuel region is centered both axially and laterally within the basket compartments. In Case A11, the fuel elements are moved within the basket compartments towards the radial center. In Case A12, the fuel elements are pushed to the radial center of the package and shifted axially to the top of the package. In actual practice, it would not be possible to shift the active fuel all the way to the top due to the presence of the end fittings. Case A13 is the same as Case A12 except the fuel elements are shifted radially outward rather than radially inward. The reactivity of all four cases is rather similar. Case A12 is the most reactive, with  $k_s = 0.05836$ . Clearly, the reactivity of unmoderated MITR-II fuel is very low.

#### ATR

The ATR results are listed in Table 6.4-1 as Cases A20 through A22. In Case A20, the active fuel region is centered both axially and laterally within the basket compartments. In Case A21, all fuel elements are moved within the basket compartments towards the radial center. In Case

A22, the fuel elements are moved radially inward (like Case A21) and shifted axially to the top of the package. All three configurations have similar reactivities, although Case A22 is the most reactive, with  $k_s = 0.08849$ . Clearly, the reactivity of unmoderated ATR fuel is very low.

### TRIGA

The TRIGA results for Type 109 rods are listed in Table 6.4-2 as Cases A30 through A33. In Case A30, the fuel elements are laterally centered in the basket compartments, and the fuel elements are offset from the package lid. In Case A31, the fuel elements are moved within the basket tubes towards the radial center. In Case A32, the outer row of elements are moved radially inward, and the inner row is moved radially outward. Comparing Cases A30 through A32, Case A31 is the most reactive. In Case A33, the fuel elements are moved radially inward (like Case A31) and shifted axially to the top of the package. In actual practice, it would not be possible to shift the active fuel all the way to the top due to the end fittings. This configuration is the most reactive, as reflection from the package shield plug is maximized. Therefore, Case A33 is the most reactive, with  $k_s = 0.41671$ . In Case TL1A1, the most reactive configuration for Type 109 is repeated for Type 119, and the reactivity decreases.

Clearly, the reactivity of unmoderated TRIGA fuel is very low and is significantly less than the USL, although the unmoderated TRIGA fuel results in the highest reactivity compared to the other fuel types.

### Square Fuel Basket Fuels

In the absence of internal moderation, the reactivity of SFB fuels is low. Therefore, the most reactive moderated cases from Section 6.4.1.2, *HAC Single Package Configuration*, are modeled with no water in the package cavity. A more detailed description of the model geometry for these cases may be found in Section 6.4.1.2. Other configurations are not investigated because the dry system has a remarkably low  $k_s$  value and is not significantly sensitive to changes anticipated under NCT conditions.

Results for SFB fuels are provided in Table 6.4-3. The reactivity of the LPB is maximized with the maximum fuel loading (31 plates), and the bounding plate fuel has the largest fissile mass (RINSC). The results are:

- $k_s = 0.14683$  for PULSTAR
- $k_s = 0.05214$  for the LPB, and
- $k_s = 0.03647$  for plate fuels (RINSC)

### **6.4.1.2 HAC Single Package Configuration**

The HAC single package configurations are similar to the NCT single package configurations except that water is allowed inside the package at the most reactive density. PULSTAR, U-Florida, and LPB payloads are further evaluated to account for changes to the geometric configuration of the fuel under HAC.

### MURR

The MURR results are summarized in Table 6.4-4 as Cases B1 through B6. In Cases B1 through B5, the cladding thickness and channel spacing are modeled consistent with the NCT analysis. In Cases B1 through B3, the package cavity is flooded with full-density water. In Case B1, the active fuel is centered both laterally and axially within the basket compartments. In Case B2, the

**BRR Package Safety Analysis Report**

active fuel is moved within the basket compartments towards the radial center. In Case B3, the radial configuration from Case B2 is maintained, and the fuel elements are shifted upward to the maximum possible extent, maximizing reflection from the shield plug. Case B3 is the most reactive of the three configurations examined.

In Cases B4 and B5, the configuration of Case B3 is modified so that the basket/fuel element water density is reduced to 0.8 and 0.9 g/cm<sup>3</sup>, respectively. Because the MURR fuel is undermoderated, reducing the water density will reduce the reactivity. As expected, the reactivity for Case B4 and B5 drops rapidly as the water density is reduced.

In Case B6, Case B3 is rerun using the minimum cladding thickness of 0.008-in and channel spacing of 0.094-in. Case B6 is the most reactive, with  $k_s = 0.78432$ .

### MITR-II

The MITR-II results are summarized in Table 6.4-4 as Cases B20 through B28. In Cases B20 through B27, the cladding thickness and channel spacing are modeled consistent with the NCT analysis. In Cases B20 through B25, the package cavity is flooded with full-density water. In Case B20, the active fuel is centered both laterally and axially within the basket compartments. In Case B21, the active fuel is pushed to the radial center of the package, and the reactivity increases. In Case B22, the radial configuration from Case B21 is maintained, and the fuel elements are pushed upward to the maximum possible extent, maximizing reflection from the lid. In Case B23, the fuel is pushed radially outward but shifted upward as in Case B22. Case B22 is the most reactive of the four configurations examined, although the reactivity effect of the axial shifting is small.

In Cases B25 and B26, the reactivity effect of the basket inner cavity radius is examined. The inner cavity of the basket has an irregular shape that is approximated as a cylinder with a radius of 12.0 cm, which is the largest radius that does not interfere with the fuel element cavity cell descriptions. Cases B25 and B26 are the same as Case B20 except this radius is modeled as 11.0 and 11.5 cm, respectively. Reactivity decreases as the radius decreases, indicating that modeling with the largest possible radius of 12.0 cm is conservative.

In Cases B26 and B27, the configuration of Case B22 is modified so that the basket water density is reduced to 0.8 and 0.9 g/cm<sup>3</sup>, respectively. Because the fuel elements and basket are free to drain, reducing the water density in the basket also reduces the water density between the fuel plates. Because the MITR-II fuel is undermoderated, reducing the water density will reduce the reactivity. As expected, the reactivity for Case B26 and B27 drops rapidly as the water density is reduced.

In Case B28, Case B22 is rerun using a cladding thickness of 0.006-in and channel spacing of 0.116-in. Case B28 is the most reactive, with  $k_s = 0.57382$ .

### ATR

The ATR results are summarized in Table 6.4-4 as Cases B40 through B45. In Cases B40 through B44, the cladding thickness and channel spacing are modeled consistent with the NCT analysis. In Cases B40 through B42, the package cavity is fully flooded with full-density water. In Case B40, the fuel elements are centered both axially and laterally within the basket compartments. In Case B41, the fuel elements are moved within the basket compartments towards the radial center. In Case B42, the fuel is also shifted axially to the top of the package in



addition to be moved toward the radial center. Comparing these three cases, Case B42 is the most reactive, although the reactivities are somewhat similar.

In Cases B43 and B44, the configuration of Case B42 is modified so that the basket/fuel element water density is reduced to 0.8 and 0.9 g/cm<sup>3</sup>, respectively. Because the ATR fuel is undermoderated, reducing the water density will reduce the reactivity. As expected, the reactivity for Case B43 and B44 drops rapidly as the water density is reduced.

In Case B45, Case B42 is rerun using a cladding thickness of 0.018-in for plates 1 and 19, and 0.008-in for plates 2 through 18. The resulting channel spacing is 0.097-in between plates 1 and 2, 0.107-in between plates 18 and 19, and 0.092-in between the remaining plates. Case B45 is the most reactive, with  $k_s = 0.70409$ .

### TRIGA

The TRIGA results for element Type 109 are summarized in Table 6.4-5 as Cases B60 through B70. In Cases B60 through B64, the package cavity is fully flooded with full-density water. In Case B60, the fuel elements are laterally centered within the basket tubes, at an arbitrary distance away from the package lid. In Case B61, the fuel elements are moved within the basket tubes towards the radial center, and the reactivity increases. In Case B62, the outer row is moved radially inward and the inner row is moved radially outward. Cases B63 and B64 are essentially repeats of Cases B60 and B61, respectively, except that the fuel elements are shifted upward until the top of the graphite reflector touches the bottom of the shield plug. Comparing these five cases, Case B64 is the most reactive. Therefore, the remaining HAC single package cases utilize this configuration (i.e., fuel elements moved to the radial center, shifted up to the maximum extent.)

In Cases B65 through B70, the configuration of Case B64 is modified so that the water density inside of the basket is allowed to vary between 0.4 and 0.9 g/cm<sup>3</sup>. The reactivity peaks at a density of 0.7 g/cm<sup>3</sup> and then decreases with decreasing density. The maximum reactivity occurs for Case B68, with  $k_s = 0.70869$ .

The TRIGA results for element Type 119 are summarized in Table 6.4-5 as Cases TL2A1 through TL2A6. Because of the difference in composition between rod Types 109 and 119, the effect of moderator density is re-evaluated for the payload. The highest  $k_s$  observed for the Type 119 payload is 0.70703 and occurs with a moderator density of 0.8 g/cm<sup>3</sup>. The Type 119 rods are therefore slightly less reactive than the HEU-bearing Type 109 rods. Peak reactivity for the Type 119 rod occurs at a somewhat higher moderator density (0.8 g/cm<sup>3</sup> vs. 0.7 g/cm<sup>3</sup>), which is attributable to the reduced enrichment and the corresponding increased role of U-238.

### PULSTAR

The results of the PULSTAR analysis are provided in Table 6.4-6. Three series are used to find maximum reactivity for this condition. The first series, P2A, shows the effect of varied moderator density and demonstrates that maximum reactivity is achieved when full density water floods the basket. The associated  $k_s$  value is 0.77926.

The next series, P2B, is based on the most reactive case from P2A (P2A06) and varies the horizontal placement of elements within the two outer SFB compartments in the central horizontal row (dimension R2 in Table 6.4-6 and Figure 6.4-1). The other four outer elements are held fixed at their inner-most position. Series P2B demonstrates that the most reactive placement of the two elements is at their inner-most position.

Next, series P2C, using the most reactive case in Series P2A and P2B (P2A06) as a basis, is used to show the most reactive position of fuel elements in the inner SFB compartments (dimension R1 in Table 6.4-6 and Figure 6.4-1). Series P2C starts with the two inner elements at their most inward position ( $R1 = 3.76$  cm). Nine cases are used to show the change in reactivity as the elements are moved to their most radially-outward position ( $R1 = 5.42$  cm). A peak in reactivity occurs for  $R1 = 4.17$  cm. The  $k_s$  value in that position is 0.78274.

It is demonstrated that PULSTAR fuel maintains its structural integrity during HAC. However, as an additional conservatism, it is postulated under HAC that the pitch expands until constrained by the Zircaloy fuel element box. The expanded pitch geometry is illustrated in Figure 6.4-2. A final case, P2D01, models the most reactive case from Series P2B and P2C with the maximum pitch. The maximum reactivity occurs for Case P2D01, with  $k_s = 0.81215$ .

### Loose Plate Box

The LPB may contain up to 31 loose plates and are limited to U-Florida, U-Mass(Al), and Purdue. Void volume within the LPB is filled with aluminum dunnage so that the void space is small. For U-Mass(Al) and Purdue fuel plates, the plates are in close contact due to the dunnage and the pitch will be small. For U-Florida fuel plates, spacers 0.112-in thick are welded to the fuel plates so that the channel spacing must be at least 0.112-in. The pitch is the sum of the channel spacing and plate thickness, and the minimum pitch for U-Florida plates is 0.112-in + 0.03-in = 0.142-in (0.3607 cm), where 0.03-in is the fuel plate thickness from Table 6.2-11. Because the LPB is 2.5-in wide, the maximum number of U-Florida plates that would fit in the LPB is  $2.5/0.142 \sim 17$ . However, it is demonstrated that loading  $\leq 31$  plates per LPB in each of the eight LPBs in a package is acceptable.

In the loose plate box analysis, no credit is taken for the aluminum dunnage, which reduces the plate pitch. The analysis is performed for both uniform and non-uniform plate pitches in order to determine the most reactive configuration. The U-Florida plate is modeled to bound the U-Mass(Al) and Purdue plates because the U-Florida plate has more U-235 per plate (12.5 g) than either U-Mass(Al) or Purdue (9.3 g), as shown in Table 6.2-11. Modeling all plates as U-Florida also bounds mixtures of the three different plate types.

Any number of plates, up to the maximum of 31 plates, may be present in each of the eight LPBs in a package. As each LPB is loaded, the LPB may be overmoderated for a small number of plates, optimally moderated for a medium number of plates, and undermoderated for a large number of plates. For a system in which the number of plates is fixed, a reactivity curve may be developed by plotting  $k_{eff}$  as a function of plate pitch. This is illustrated in a simple sensitivity study consisting of only fuel plates and water. In this sensitivity study, the LPB, basket, and package are not modeled because the intent is to allow the plate pitch to increase without restriction. The system of plates is reflected by at least 12-in of water in all directions.

Four representative plate systems are examined (31 plates, 19 plates, 15 plates, and 7 plates), and the pitch is adjusted between 0.1 and 1.2 cm to determine the optimum moderation for each system, as shown on Figure 6.4-3. Based on Figure 6.4-3, the optimum pitch for each of the systems examined is shown in following table.

Number of Plates in System	Optimum Pitch (cm)
31	0.7
19	0.8
15	0.9
7	1.2

Based on this study, it is observed that the optimum pitch increases as the number of plates decreases. It is also observed for all cases that the optimum pitch is relatively large in relation to the width of the LPB (6.35 cm). Therefore, optimum moderation is achieved in the LPB for approximately 7 plates (pitch ~1.1 cm). For more than approximately 7 plates, the system will be undermoderated.

It is also observed from Figure 6.4-3 that an undermoderated system with a large number of plates may be more reactive than an optimally moderated system with fewer plates. For 31 plates in the LPB, the pitch ~ 0.2 cm. From Figure 6.4-3, 31 undermoderated plates at a pitch of 0.2 cm ( $k \sim 0.4$ ) is significantly more reactive than an optimally moderated system with 7 plates ( $k \sim 0.3$ ).

In the subsequent cases, the LPB is modeled in the Square fuel basket within the BRR package. In the first series of cases (Series L2A), only uniform plate pitches are examined with the plates centered in the LPB. An example model geometry for 31 plates is shown in the upper half of Figure 6.4-4. Results for the LPB payload pitch studies are provided in Table 6.4-7. In the first four cases (Cases L2A01 through L2A04), 31 plates are modeled from a small pitch (0.12 cm) to the maximum pitch (0.2092 cm). Consistent with the plate pitch study, reactivity increases with increasing plate pitch, reaching a maximum value of  $k_s = 0.59880$  for Case L2A04. Because further pitch expansion is limited by the LPB, the system remains undermoderated.

In Cases L2A05 through L2A16, the number of plates in the LPB is varied from 29 to 7 plates. Based on Figure 6.4-3, the system will remain undermoderated if the number of plates per LPB is greater than approximately 7 plates. Because the system is undermoderated, the plates are modeled with the largest uniform pitch that fills the LPB. The pitch ranges from 0.2240 cm (29 plates, Case L2A05) to 1.0456 cm (7 plates, Case L2A16). However, while moderation is increased by removing plates and expanding the pitch, the reactivity steadily decreases as the plates are removed. It may be concluded that the reactivity of an undermoderated system with a large fissile mass is more reactive than a more moderated system with less fissile mass. The case with 7 plates, which is the closest to optimum moderation, has the lowest reactivity.

In Series L2A, uniform pitches are investigated. In Series L2B, the effect of a non-uniform pitch is investigated. While non-uniform pitches may form an infinite number of combinations, the approach is to model some plates in close-contact so that the pitch for the remaining plates may continue to expand. Based on Series L2A, it is expected that 31 plates with a non-uniform pitch would bound a fewer number of plates with a non-uniform pitch. A non-uniform pitch analysis is performed for 31 plates, 25 plates, and 19 plates to confirm the non-uniform pitch system is most reactive for 31 plates. This approach maximizes the fissile mass while allowing greater moderation for most of the plates. A non-uniform pitch configuration is illustrated in the lower half of Figure 6.4-4.

Results for the non-uniform pitch cases are provided in Table 6.4-8. Reactivity increases compared to the uniform pitch cases, but the increase is not significant. The maximum reactivity

occurs with 31 total plates (Case L2B06,  $k_s = 0.61048$ , 25 plates in an expanded pitch and the remaining plates in close-contact). The most reactive 31 plate non-uniform pitch case is ~12 milli-k larger than the corresponding 31 plate uniform pitch case.

Reactivity for the non-uniform pitch cases with 25 total plates and 19 total plates are bounded by the 31 plate model. Compared to the uniform pitch cases, a non-uniform pitch results in a ~9 milli-k increase for 25 total plates and ~6 milli-k increase for 19 total plates. It is observed that as the total number of plates decreases, the uniform and non-uniform pitch cases become closer in reactivity. Because 31 plates in a uniform pitch bounds a lesser number of plates in a uniform pitch (Series L2A), and 31 plates results in the largest reactivity gain when non-uniform pitches are considered (Series L2B), it is concluded that 31 plates in a non-uniform pitch bounds a lesser number of plates in a non-uniform pitch. Therefore, in subsequent cases, only 31 plates are modeled.

The 31 plate system is undermoderated and in fact has less moderation than the cases with fewer plates. However, for the LPB in the Square fuel basket, undermoderated cases with higher fissile mass are more reactive than higher moderated cases with lower fissile mass. Optimum moderation can be achieved for only a low number of plates (~7 plates per LPB), and the reactivity for an optimally moderated system is low due to the low fissile mass.

The results for the following three series are provided in Table 6.4-9. In Series L2C, the 31 plates are horizontally fanned (offset) in an alternating pattern. Non-uniform pitch Case L2B06 is used as the base case. The geometry for the fanned cases is shown in Figure 6.4-5. This horizontal fanning further increases moderation and increases the reactivity. Note that in the actual configuration the horizontal fanning would be much smaller because the aluminum cladding on the side is not modeled for simplicity. Vertical fanning is neglected because the amount of space for vertical fanning is negligible compared to the length of the fuel plates.

In Series L2D, the eight LPBs are radially shifted to the centerline of the package. This is a more compact configuration and causes the reactivity to increase. Two different configurations are considered, with and without plate fanning. The geometry for the two configurations cases is shown in Figure 6.4-6. Case L2D01 is based on plate geometry without fanning but with the plates and LPBs shifted to the centerline. Case L2D02 is based on the plates with fanning shifted to the centerline. Both cases in Series L2D have essentially the same reactivity, although the case without fanning is slightly larger, with  $k_s = 0.64061$ .

In Series L2E, the effect of water density is considered. In Series L2A through L2D, the maximum water density of  $1.0 \text{ g/cm}^3$  is modeled within the package cavity. The most reactive Case L2D02 is modeled with uniformly reduced water densities within the package cavity to demonstrate that the system is most reactive with full density water.

In Series L2A through L2E, all eight LPBs are modeled with the same number of plates per LPB. It is demonstrated that modeling 31 plates per LPB is the most reactive condition. During a loading or unloading operation, the total number of fuel plates in the basket may vary between one (i.e., one plate in one LPB) to 248 (i.e., 31 plates in eight LPBs). Based on the results in Series L2A through L2E, it may be inferred that reactivity increases as each fuel plate is added to the basket, reaching the maximum reactivity for a fully loaded basket (i.e., 248 fuel plates). Transporting less than 248 fuel plates is less reactive and acceptable. While it is not practical to evaluate every scenario between one and 248 plates, in Series L2F, the number of plates in the basket is varied from 217 to 248 plates by loading seven LPBs with 31 plates and one LPB with

a reduced number of plates. For simplicity, Case L2A04 is used as the base case, in which the fuel plates are centered in the LPBs and spaced uniformly within the compartment. The LPB with the reduced number of plates is an inner LPB, as indicated in Figure 6.4-7, to maximize the reactivity changes. Results are provided in Table 6.4-10. As expected, the reactivity decreases as plates are removed from the LPB. Therefore, the criticality analysis bounds the loading and unloading operations of 10 CFR 71.55(b).

The maximum reactivity occurs for Case L2D01, with  $k_s = 0.64061$ . This case features 31 plates arranged in a non-uniform pitch (25 plates in an expanded pitch), and the LPBs and fuel plates shifted to the radial centerline. This value is significantly below the USL of 0.9209.

Conclusions from the LPB analysis are:

- Limit on U-Florida plates:  $\leq 31$  plates per LPB
- Limit on U-Mass(AI) plates:  $\leq 31$  plates per LPB
- Limit on Purdue plates:  $\leq 31$  plates per LPB
- The system with 31 plates is undermoderated but has the highest fissile mass. For this system, 31 undermoderated plates are more reactive than fewer plates with greater moderation. Optimal moderation is achieved with  $\sim 7$  plates, although the reactivity of the optimally moderated system is low due to the low fissile mass.
- Due to geometrical constraints, it is not possible to transport 31 U-Florida plates in an LPB. As noted above, transporting fewer than 31 plates is less reactive and therefore acceptable.
- The LPB criticality analysis bounds the requirements of 71.55(b) for loading and unloading operations because 31 plates are more reactive than a lesser number plates that could be present during loading/unloading operations.

#### SFB Plate Fuel

Seven intact plate-fuel types may be transported in the SFB. To determine the most reactive element type, each element is modeled in its nominal condition, flooded with water, and centered in the SFB compartment openings. All fuel designs with the exception of U-Florida feature structural side combs along the entire length of the fuel element. These side combs are conservatively ignored in the MCNP models. Results for the SFB plate-fuel-element payloads are provided in Table 6.4-11 in Series PF2A. The maximum  $k_s$  of all of the plate fuel payloads is 0.69500 and corresponds to the RINSC fuel payload. RINSC fuel also has the largest U-235 loading of the seven fuel designs. Therefore, RINSC bounds all SFB plate fuel types that remain intact under HAC.

The fuel elements are free to move laterally within a fuel compartment. This effect is exaggerated in the MCNP models because the aluminum combs are not modeled, which allows more space for lateral shifting. In Series PF2B, several different radial locations of the RINSC fuel element are investigated. The outer six and inner two fuel elements are allowed to shift independently of one another. The radial offset is measured from the centerline of the fuel element to the centerline of the package (positive offset is toward the centerline and negative offset is away from the centerline). Two different examples of the radial offset models are illustrated in Figure 6.4-8, Cases PF2B4 and PF2B9. Case PF2B4 is the most reactive, with the outer fuel elements shifted as close as possible to the package centerline and the inner fuel elements shifted near the centerline of the package. The reactivity of this case is  $k_s = 0.74099$ .

While RINSC bounds all plate fuels that remain intact under HAC, it is postulated that U-Florida fuel may be damaged in an accident. Therefore, an analysis of U-Florida fuel is performed with postulated fuel damage. However, it is demonstrated that a damaged U-Florida fuel element is bounded by the RINSC fuel element.

U-Florida fuel elements are significantly smaller than RINSC fuel elements, resulting in significant void space within the compartments. If the plate pitch is allowed to expand into the free space, the reactivity increases. Results for the U-Florida analysis are provided in Table 6.4-12. The effect of both uniform and non-uniform pitch expansion for U-Florida fuel is investigated in Series PF2C. To mitigate the effects of potential fuel damage due to pitch expansion, U-Florida fuel elements are transported using aluminum dunnage in each compartment. This dunnage has nominal dimensions of 27-in long, 3-in wide, and 0.8-in thick. It is modeled with a thickness of 0.8-in, although the length and width are modeled to match the plate fuel dimensions for convenience. The width of the compartment is 3.4-in, so the space available for pitch expansion is  $3.4\text{-in} - 0.8\text{-in} = 2.6\text{-in}$  (6.604 cm). Based on the allowable space and 14 fuel plates, the maximum regular pitch is limited to 0.50 cm. Several different increased pitches are investigated with the fuel element centered in the compartment (Cases PF2C01 through PF2C03), and reactivity is maximized for the maximum pitch. In these initial cases, the aluminum spacer block is not explicitly modeled.

In Case PF2C04, the 0.8-in thick aluminum spacer block is modeled explicitly, see Figure 6.4-9. The reactivity is essentially the same when the aluminum spacer is added to the model. As the spacer is required to be present, it is modeled explicitly in subsequent cases.

In Cases PF2C05 through PF2C08, the effect of a non-uniform pitch is investigated. While non-uniform pitches may form an infinite number of combinations, the approach is to model some plates in close-contact so that the pitch for the remaining plates may continue to expand. This approach conserves the fissile mass while allowing greater moderation for most of the plates. Various non-uniform pitch configurations are illustrated in Figure 6.4-10. Case PF2C06 is the most reactive, with 12 plates at the maximum uniform pitch. However, the  $k_s$  of this case ( $k_s = 0.61869$ ) is only slightly larger than the  $k_s$  of the maximum case with a uniform pitch (Case PF2C04,  $k_s = 0.61454$ ), indicating there is not a large increase in reactivity for non-uniform pitches.

In Series PF2D, horizontal fanning of the fuel plates is investigated, similar to the approach used in the LPB analysis. Non-uniform pitch Case PF2C06 is used as the base case. In the horizontal fanning models, the fuel element is centered in the compartment while the plates are alternately shifted in the x-direction, see Figure 6.4-11. Fanning the fuel plates in this manner increases the moderation. Three different fanning configurations are investigated (0.39 cm, 0.78 cm, and 1.17 cm), and reactivity is maximized for the maximum fanning (Case PF2D03,  $k_s = 0.64312$ ). Vertical fanning is neglected because the amount of space for vertical fanning is negligible compared to the length of the fuel plates.

In Series PF2E, radial placement of the fuel elements within the SFB is investigated, similar to the RINSC analysis. Non-uniform pitch Case PF2C06 is used as the base case. Horizontal fanning is not included in the radial placement models because the fuel cannot be shifted radially for maximum fanning (i.e., maximum fanning fills the entire compartment). The outer six and inner two fuel elements are allowed to shift independently of one another. The radial offset is measured from the centerline of the fuel element to the centerline of the package (positive offset

is toward the centerline and negative offset is away from the centerline). Two different examples of the radial offset models are illustrated in Figure 6.4-12, Cases PF2E04 and PF2E08. Case PF2E04 is the most reactive, with the outer fuel elements shifted as close as possible to the package centerline and the inner fuel elements shifted near the centerline of the package. The reactivity of this case is  $k_s = 0.66094$ . Note that this case is more reactive than the case with maximum fanning due to the more compact arrangement of the eight fuel elements.

The relative location of the aluminum spacer in each compartment is random in the actual loading configuration and is not required to follow the pattern shown in Figure 6.4-9. In Series PF2F, two additional orientations of the aluminum spacers are investigated, as illustrated in Figure 6.4-13. The reactivity of Case PF2F01 increases slightly to  $k_s = 0.66336$ . While many other orientations are possible, the effect on the reactivity would be low and the overall system reactivity for U-Florida is bounded by RINSC fuel. Therefore, sufficient configurations of U-Florida fuel have been investigated.

In Case PF203, most reactive Case PF201 is run with a wide aluminum spacer that spans the 3.4-in width of the cavity, bounding the nominal spacer width of 3-in. In the previous models, the spacer is modeled to match the width of the fuel for convenience, or 2.47-in (see Figure 6.4-9). Reactivity decreases slightly for Case PF203, indicating that modeling the spacer with a width  $< 3$ -in is acceptable.

Comparing the SFB plate fuels, RINSC is bounding, with  $k_s = 0.74099$  (Case PF2B4). The reactivity of RINSC also bounds damaged U-Florida fuel by a large margin, as  $k_s = 0.66336$  for the most reactive U-Florida configuration.

#### Combinations of SFB Contents

The most reactive SFB contents are:

- $k_s = 0.81215$  for PULSTAR
- $k_s = 0.64061$  for the LPB, and
- $k_s = 0.74099$  for plate fuels (RINSC)

Therefore, the reactivity for any combination of SFB contents will not exceed the reactivity of the PULSTAR payload.

## **6.4.2 Results**

Following are the tabulated results for the single package cases. The most reactive configuration within each series is listed in boldface.

**Table 6.4-1 – NCT Single Package Results, MURR, MITR-II, ATR**

Case ID	Filename	$k_{eff}$	$\sigma$	$k_s$ ( $k+2\sigma$ )
<b>MURR</b>				
A1	NS_MURR	0.08167	0.00023	0.08213
A2	NS_MURR_IN	0.08152	0.00022	0.08196
<b>A3</b>	<b>NS_MURR_INUP</b>	<b>0.08499</b>	<b>0.00023</b>	<b>0.08545</b>
<b>MITR-II</b>				
A10	NS_MIT2	0.05655	0.00015	0.05685
A11	NS_MIT2_IN	0.05709	0.00016	0.05741
<b>A12</b>	<b>NS_MIT2_INUP</b>	<b>0.05808</b>	<b>0.00014</b>	<b>0.05836</b>
A13	NS_MIT2_OUTUP	0.05762	0.00016	0.05794
<b>ATR</b>				
A20	NS_ATR	0.08689	0.00024	0.08737
A21	NS_ATR_IN	0.08759	0.00025	0.08809
<b>A22</b>	<b>NS_ATR_INUP</b>	<b>0.08797</b>	<b>0.00026</b>	<b>0.08849</b>

**Table 6.4-2 – NCT Single Package Results, TRIGA**

Case ID	Filename	$k_{eff}$	$\sigma$	$k_s$ ( $k+2\sigma$ )
<b>Type 109</b>				
A30	NS_TRIGA	0.39557	0.00089	0.39735
A31	NS_TRIGA_IN	0.40299	0.00092	0.40483
A32	NS_TRIGA_INOUT	0.40078	0.00092	0.40262
<b>A33</b>	<b>NS_TRIGA_INUP</b>	<b>0.41493</b>	<b>0.00089</b>	<b>0.41671</b>
<b>Type 119</b>				
TL1A1	TR_NCT_SGL_A_01	0.38203	0.00034	0.38271



**Table 6.4-3 – NCT Single Package Results, Square Fuel Basket**

Case ID	Filename	$k_{\text{eff}}$	$\sigma$	$k_s$ ( $k+2\sigma$ )
<b>PULSTAR</b>				
P1A1	NS_PULSTAR	0.14653	0.00015	0.14683
<b>Loose Plate Box</b>				
L1A1	NS_LOOSE_EXP25SH	0.05196	0.00009	0.05214
<b>Plate Fuels (RINSC)</b>				
PF1A1	NS_RINSC_SH3A	0.03633	0.00007	0.03647

**Table 6.4-4 – HAC Single Package Results, MURR, MITR-II, ATR**

Case ID	Filename	Water Density (g/cm <sup>3</sup> )	$k_{\text{eff}}$	$\sigma$	$k_s$ ( $k+2\sigma$ )
<b>MURR</b>					
B1	HS_MURR	1.0	0.75395	0.00115	0.75625
B2	HS_MURR_IN	1.0	0.75287	0.00123	0.75533
B3	HS_MURR_INUP	1.0	0.75898	0.00113	0.76124
B4	HS_MURR_C080INUP	0.8	0.69306	0.00108	0.69522
B5	HS_MURR_C090INUP	0.9	0.72871	0.00118	0.73107
<b>B6</b>	<b>HS_MURR_INUPC</b>	<b>1.0</b>	<b>0.78186</b>	<b>0.00123</b>	<b>0.78432</b>
<b>MITR-II</b>					
B20	HS_MIT2_W100	1.0	0.50737	0.00107	0.50951
B21	HS_MIT2_W100IN	1.0	0.52143	0.00111	0.52365
B22	HS_MIT2_W100INUP	1.0	0.52284	0.00103	0.52490
B23	HS_MIT2_W100OUTUP	1.0	0.49263	0.00103	0.49469
B24	HS_MIT2_W100INUP_R11	1.0	0.48905	0.00107	0.49119
B25	HS_MIT2_W100INUP_R11P5	1.0	0.49907	0.00095	0.50097
B26	HS_MIT2_W080INUP	0.8	0.48751	0.00096	0.48943
B27	HS_MIT2_W090INUP	0.9	0.50573	0.00102	0.50777
<b>B28</b>	<b>HS_MIT2_W100INUPC</b>	<b>1.0</b>	<b>0.57166</b>	<b>0.00108</b>	<b>0.57382</b>
<b>ATR</b>					
B40	HS_ATR	1.0	0.67992	0.00113	0.68218
B41	HS_ATR_IN	1.0	0.68013	0.00110	0.68233
B42	HS_ATR_INUP	1.0	0.68279	0.00123	0.68525
B43	HS_ATR_C080INUP	0.8	0.64718	0.00105	0.64928
B44	HS_ATR_C090INUP	0.9	0.66179	0.00106	0.66391
<b>B45</b>	<b>HS_ATR_INUPC</b>	<b>1.0</b>	<b>0.70183</b>	<b>0.00113</b>	<b>0.70409</b>

**Table 6.4-5 – HAC Single Package Results, TRIGA**

Case ID	Filename	Water Density (g/cm <sup>3</sup> )	k <sub>eff</sub>	σ	k <sub>s</sub> (k+2σ)
<b>Type 109</b>					
B60	HS_TRIGA_W100	1.0	0.66788	0.00108	0.67004
B61	HS_TRIGA_W100IN	1.0	0.69115	0.00097	0.69309
B62	HS_TRIGA_W100INOUT	1.0	0.67398	0.00098	0.67594
B63	HS_TRIGA_W100UP	1.0	0.66998	0.00112	0.67222
B64	HS_TRIGA_W100INUP	1.0	0.69348	0.00106	0.69560
B65	HS_TRIGA_W040INUP	0.4	0.67497	0.00119	0.67735
B66	HS_TRIGA_W050INUP	0.5	0.69534	0.00124	0.69782
B67	HS_TRIGA_W060INUP	0.6	0.70552	0.00104	0.70760
<b>B68</b>	<b>HS_TRIGA_W070INUP</b>	<b>0.7</b>	<b>0.70661</b>	<b>0.00104</b>	<b>0.70869</b>
B69	HS_TRIGA_W080INUP	0.8	0.70510	0.00099	0.70708
B70	HS_TRIGA_W090INUP	0.9	0.70164	0.00106	0.70376
<b>Type 119</b>					
TL2A1	TR_HAC_SGL_A_01	0.4	0.66703	0.00049	0.66801
TL2A2	TR_HAC_SGL_A_02	0.5	0.68848	0.00048	0.68944
TL2A3	TR_HAC_SGL_A_03	0.6	0.70051	0.00049	0.70149
TL2A4	TR_HAC_SGL_A_04	0.7	0.70596	0.00043	0.70682
<b>TL2A5</b>	<b>TR_HAC_SGL_A_05</b>	<b>0.8</b>	<b>0.70605</b>	<b>0.00049</b>	<b>0.70703</b>
TL2A6	TR_HAC_SGL_A_06	0.9	0.70302	0.00046	0.70394

Table 6.4-6 – HAC Single Package Results, PULSTAR

Case ID	Filename	Water Density (g/cm <sup>3</sup> )	R1 (cm)	R2 (cm)	k <sub>eff</sub>	σ	k <sub>s</sub> (k+2σ)
<b>P2A, Water Density</b>							
P2A01	PS_SNGL_HAC_2A_01	0.5	4.59	12.93	0.68160	0.00106	0.68372
P2A02	PS_SNGL_HAC_2A_02	0.6	4.59	12.93	0.71530	0.00097	0.71724
P2A03	PS_SNGL_HAC_2A_03	0.7	4.59	12.93	0.73743	0.00101	0.73945
P2A04	PS_SNGL_HAC_2A_04	0.8	4.59	12.93	0.75614	0.00099	0.75812
P2A05	PS_SNGL_HAC_2A_05	0.9	4.59	12.93	0.76771	0.00101	0.76973
<b>P2A06</b>	<b>PS_SNGL_HAC_2A_06</b>	<b>1.0</b>	<b>4.59</b>	<b>12.93</b>	<b>0.77708</b>	<b>0.00109</b>	<b>0.77926</b>
<b>P2B, Outer Horizontal Compartments, Horizontal Element Placement</b>							
<b>P2A06</b>	<b>PS_SNGL_HAC_2A_06</b>	<b>1.0</b>	<b>4.59</b>	<b>12.93</b>	<b>0.77708</b>	<b>0.00109</b>	<b>0.77926</b>
P2B01	PS_SNGL_HAC_2B_01	1.0	4.59	13.35	0.77768	0.00115	0.77998
P2B02	PS_SNGL_HAC_2B_02	1.0	4.59	13.76	0.77754	0.00101	0.77956
P2B03	PS_SNGL_HAC_2B_03	1.0	4.59	14.18	0.77600	0.00106	0.77812
P2B04	PS_SNGL_HAC_2B_04	1.0	4.59	14.59	0.77034	0.00113	0.77260
<b>P2C, Inner Horizontal Compartments, Horizontal Element Placement</b>							
P2C01	PS_SNGL_HAC_2C_01	1.0	3.76	12.93	0.78011	0.00049	0.78109
P2C02	PS_SNGL_HAC_2C_02	1.0	3.96	12.93	0.78075	0.00047	0.78169
<b>P2C03</b>	<b>PS_SNGL_HAC_2C_03</b>	<b>1.0</b>	<b>4.17</b>	<b>12.93</b>	<b>0.78182</b>	<b>0.00046</b>	<b>0.78274</b>
P2C04	PS_SNGL_HAC_2C_04	1.0	4.38	12.93	0.78018	0.00046	0.78110
<b>P2A06</b>	<b>PS_SNGL_HAC_2A_06</b>	<b>1.0</b>	<b>4.59</b>	<b>12.93</b>	<b>0.77710</b>	<b>0.00112</b>	<b>0.77934</b>
P2C05	PS_SNGL_HAC_2C_05	1.0	4.79	12.93	0.77471	0.00047	0.77565
P2C06	PS_SNGL_HAC_2C_06	1.0	5.00	12.93	0.77096	0.00049	0.77194
P2C07	PS_SNGL_HAC_2C_07	1.0	5.21	12.93	0.76548	0.00044	0.76636
P2C08	PS_SNGL_HAC_2C_08	1.0	5.42	12.93	0.75993	0.00044	0.76081
<b>P2D, Rod Pitch Maximized in Element Box</b>							
<b>P2D01</b>	<b>PS_SINGLE_HAC_2D_01</b>	<b>1.0</b>	<b>4.17</b>	<b>12.93</b>	<b>0.81125</b>	<b>0.00045</b>	<b>0.81215</b>

**Table 6.4-7 – HAC Single Package Results, Loose Plate Box, Uniform Pitch Study**

Case ID	Filename	Number of Plates in LPB	Uniform Pitch (cm)	$k_{eff}$	$\sigma$	$k_s$ ( $k+2\sigma$ )
<b>L2A, Uniform Pitch</b>						
L2A01	HS_LOOSE_P06	31	0.1200	0.45998	0.00030	0.46058
L2A02	HS_LOOSE_P08	31	0.1600	0.52275	0.00034	0.52343
L2A03	HS_LOOSE_P10	31	0.2000	0.58386	0.00034	0.58454
L2A04	HS_LOOSE_P1046	31	0.2092	0.59814	0.00033	<b>0.59880</b>
L2A05	HS_LOOSE_N29	29	0.2240	0.59503	0.00033	0.59569
L2A06	HS_LOOSE_N27	27	0.2414	0.59062	0.00032	0.59126
L2A07	HS_LOOSE_N25	25	0.2614	0.58505	0.00032	0.58569
L2A08	HS_LOOSE_N23	23	0.2852	0.57812	0.00033	0.57878
L2A09	HS_LOOSE_N21	21	0.3136	0.56841	0.00033	0.56907
L2A10	HS_LOOSE_N19	19	0.3486	0.55708	0.00030	0.55768
L2A11	HS_LOOSE_N17	17	0.3922	0.54219	0.00030	0.54279
L2A12	HS_LOOSE_N15	15	0.4482	0.52419	0.00030	0.52479
L2A13	HS_LOOSE_N13	13	0.5228	0.50018	0.00028	0.50074
L2A14	HS_LOOSE_N11	11	0.6274	0.46927	0.00026	0.46979
L2A15	HS_LOOSE_N9	9	0.7842	0.42976	0.00025	0.43026
L2A16	HS_LOOSE_N7	7	1.0456	0.37615	0.00023	0.37661

**Table 6.4-8 – HAC Single Package Results, Loose Plate Box, Non-Uniform Pitch Study**

Case ID	Filename	Number of Plates in LPB	Number of Plates with Expanded Pitch	Expanded Pitch (cm)	$k_{eff}$	$\sigma$	$k_s$ ( $k+2\sigma$ )
<b>L2B, Non-Uniform Pitch, 31 plates per LPB</b>							
L2B01	HS_LOOSE_EXP30	31	30	0.2138	0.60221	0.00032	0.60285
L2B02	HS_LOOSE_EXP29	31	29	0.2186	0.60525	0.00032	0.60589
L2B03	HS_LOOSE_EXP28	31	28	0.2238	0.60766	0.00034	0.60834
L2B04	HS_LOOSE_EXP27	31	27	0.2296	0.60852	0.00032	0.60916
L2B05	HS_LOOSE_EXP26	31	26	0.2358	0.60919	0.00033	0.60985
L2B06	HS_LOOSE_EXP25	31	25	0.2424	0.60984	0.00032	<b>0.61048</b>
L2B07	HS_LOOSE_EXP24	31	24	0.2496	0.60974	0.00032	0.61038
L2B08	HS_LOOSE_EXP23	31	23	0.2574	0.60885	0.00032	0.60949
L2B09	HS_LOOSE_EXP22	31	22	0.2660	0.60756	0.00034	0.60824
L2B10	HS_LOOSE_EXP21	31	21	0.2756	0.60647	0.00033	0.60713
L2B11	HS_LOOSE_EXP20	31	20	0.2860	0.60473	0.00033	0.60539
<b>L2B, Non-Uniform Pitch, 25 plates per LPB</b>							
L2B21	HS_N25_E24	25	24	0.2694	0.58946	0.00032	0.59010
L2B22	HS_N25_E23	25	23	0.2782	0.59255	0.00032	0.59319
L2B23	HS_N25_E22	25	22	0.2878	0.59433	0.00033	0.59499
L2B24	HS_N25_E21	25	21	0.2984	0.59428	0.00033	0.59494
L2B25	HS_N25_E20	25	20	0.3102	0.59442	0.00030	<b>0.59502</b>
L2B26	HS_N25_E19	25	19	0.3232	0.59292	0.00031	0.59354
L2B27	HS_N25_E18	25	18	0.3376	0.59151	0.00032	0.59215
L2B28	HS_N25_E17	25	17	0.3540	0.58910	0.00033	0.58976
L2B29	HS_N25_E16	25	16	0.3726	0.58632	0.00031	0.58694
L2B30	HS_N25_E15	25	15	0.3938	0.58186	0.00031	0.58248
L2B31	HS_N25_E14	25	14	0.4182	0.57752	0.00031	0.57814

(1/2)

Table 6.4-8 – HAC Single Package Results, Loose Plate Box, Non-Uniform Pitch Study

Case ID	Filename	Number of Plates in LPB	Number of Plates with Expanded Pitch	Expanded Pitch (cm)	$k_{eff}$	$\sigma$	$k_s$ ( $k+2\sigma$ )
L2B, Non-Uniform Pitch, 19 plates per LPB							
L2B41	HS_N19_E18	19	18	0.3646	0.56133	0.00031	0.56195
L2B42	HS_N19_E17	19	17	0.3826	0.56356	0.00030	<b>0.56416</b>
L2B43	HS_N19_E16	19	16	0.4030	0.56291	0.00031	0.56353
L2B44	HS_N19_E15	19	15	0.4264	0.56147	0.00030	0.56207
L2B45	HS_N19_E14	19	14	0.4532	0.55848	0.00031	0.55910
L2B46	HS_N19_E13	19	13	0.4848	0.55491	0.00030	0.55551
L2B47	HS_N19_E12	19	12	0.5218	0.54916	0.00029	0.54974
L2B48	HS_N19_E11	19	11	0.5664	0.54289	0.00030	0.54349
L2B49	HS_N19_E10	19	10	0.6208	0.53426	0.00029	0.53484
L2B50	HS_N19_E9	19	9	0.6890	0.52443	0.00029	0.52501
L2B51	HS_N19_E8	19	8	0.7766	0.51260	0.00028	0.51316
L2B52	HS_N19_E7	19	7	0.8932	0.49927	0.00028	0.49983

(2/2)

**Table 6.4-9 – HAC Single Package Results, Loose Plate Box, Additional Cases**

Case ID	Filename	Horizontal Fanning (cm)	Water Density (g/cm <sup>3</sup> )	k <sub>eff</sub>	σ	k <sub>s</sub> (k+2σ)
<b>L2C, Horizontal Fanning</b>						
L2C01	HS_LOOSE_EXP25H1	0.3285	1.0	0.61655	0.00032	0.61719
L2C02	HS_LOOSE_EXP25H2	0.6470	1.0	0.63063	0.00034	0.63131
<b>L2D, Radial Shifting of LPB to Centerline</b>						
L2D01	HS_LOOSE_EXP25SH	0.0000	1.0	0.64001	0.00030	<b>0.64061</b>
L2D02	HS_LOOSE_EXP25H2SH	0.6470	1.0	0.63936	0.00031	0.63998
<b>L2E, Reduced Moderator Density</b>						
L2E01	HS_LOOSE_EXP25SH_W090	0.0000	0.9	0.62555	0.00032	0.62619
L2E02	HS_LOOSE_EXP25SH_W080	0.0000	0.8	0.60948	0.00032	0.61012
L2E03	HS_LOOSE_EXP25SH_W070	0.0000	0.7	0.59170	0.00032	0.59234
L2E04	HS_LOOSE_EXP25SH_W060	0.0000	0.6	0.56848	0.00032	0.56912
L2E05	HS_LOOSE_EXP25SH_W050	0.0000	0.5	0.53896	0.00030	0.53956

Note: All cases in this table feature 31 plates in a non-uniform lattice, with 25 plates in an expanded pitch of 0.2424 cm.

**Table 6.4-10 – HAC Single Package Results, Loose Plate Box, Loading/Unloading**

Case ID	Filename	Number of Plates per LPB, 7 LPBs	Number of Plates in Inner LPB	Total Number of Plates in Basket	$k_{eff}$	$\sigma$	$k_s$ ( $k+2\sigma$ )
<b>L2F, 7 LPBs with 31 plates per LPB, one inner LPB with a reduced number of plates</b>							
L2A04	HS_LOOSE_P1046	31	31	248	0.59814	0.00033	<b>0.59880</b>
L2F01	HS_LOOSE_P1046_IP29	31	29	246	0.59765	0.00031	0.59827
L2F02	HS_LOOSE_P1046_IP27	31	27	244	0.59720	0.00033	0.59786
L2F03	HS_LOOSE_P1046_IP25	31	25	242	0.59584	0.00033	0.59650
L2F04	HS_LOOSE_P1046_IP23	31	23	240	0.59495	0.00032	0.59559
L2F05	HS_LOOSE_P1046_IP21	31	21	238	0.59289	0.00032	0.59353
L2F06	HS_LOOSE_P1046_IP19	31	19	236	0.58972	0.00032	0.59036
L2F07	HS_LOOSE_P1046_IP17	31	17	234	0.58702	0.00032	0.58766
L2F08	HS_LOOSE_P1046_IP15	31	15	232	0.58382	0.00032	0.58446
L2F09	HS_LOOSE_P1046_IP13	31	13	230	0.57860	0.00032	0.57924
L2F10	HS_LOOSE_P1046_IP11	31	11	228	0.57260	0.00031	0.57322
L2F11	HS_LOOSE_P1046_IP09	31	9	226	0.56535	0.00031	0.56597
L2F12	HS_LOOSE_P1046_IP07	31	7	224	0.55781	0.00032	0.55845
L2F13	HS_LOOSE_P1046_IP0	31	0	217	0.52322	0.00031	0.52384



**Table 6.4-11 – HAC Single Package Results, SFB Plate Fuel**

Case ID	Filename	Element	Inner Offset (cm)①	Outer Offset (cm)①	$k_{eff}$	$\sigma$	$k_s (k+2\sigma)$
<b>PF2A, Determination of Bounding Plate Fuel Type</b>							
PF2A1	PF_SINGLE_HAC_2A_01	U-Florida	0	0	0.55832	0.00046	0.55924
PF2A2	PF_SINGLE_HAC_2A_02	OSU	0	0	0.61832	0.00046	0.61924
PF2A3	PF_SINGLE_HAC_2A_03	U-Mass (Si)	0	0	0.61116	0.00041	0.61198
PF2A4	PF_SINGLE_HAC_2A_04	Missouri S&T	0	0	0.68039	0.00045	0.68129
PF2A5	PF_SINGLE_HAC_2A_05	RINSC	0	0	0.69400	0.00050	<b>0.69500</b>
PF2A6	PF_SINGLE_HAC_2A_06	Purdue	0	0	0.55388	0.00037	0.55462
PF2A7	PF_SINGLE_HAC_2A_07	U-Mass (Al)	0	0	0.58884	0.00041	0.58966
<b>PF2B, Location Study for RINSC</b>							
PF2B1	HS_RINSC_SH1	RINSC	0.39	0.39	0.70976	0.00077	0.71130
PF2B2	HS_RINSC_SH2	RINSC	0.78	0.78	0.72122	0.00080	0.72282
PF2B3	HS_RINSC_SH3	RINSC	1.17	1.17	0.73677	0.00070	0.73817
PF2B4	HS_RINSC_SH3A	RINSC	0.78	1.17	0.73961	0.00069	<b>0.74099</b>
PF2B5	HS_RINSC_SH3B	RINSC	0.39	1.17	0.73875	0.00079	0.74033
PF2B6	HS_RINSC_SH3C	RINSC	0	1.17	0.73575	0.00076	0.73727
PF2B7	HS_RINSC_SH3D	RINSC	-0.39	1.17	0.72848	0.00076	0.73000
PF2B8	HS_RINSC_SH3E	RINSC	-0.78	1.17	0.71899	0.00074	0.72047
PF2B9	HS_RINSC_SH3F	RINSC	-1.17	1.17	0.71142	0.00075	0.71292

①Offset is measured radially from the center of the fuel element to the centerline of the package. “Inner” refers to the two inner fuel elements, and “outer” refers to the outer six fuel elements.

Table 6.4-12 – HAC Single Package Results, U-Florida

Case ID	Filename	Pitch (cm)	Plates at Expanded Pitch	Horizontal Fanning (cm)	Inner Offset (cm)①	Outer Offset (cm)①	$k_{eff}$	$\sigma$	$k_s (k+2\sigma)$
<b>PF2C, Pitch Variation</b>									
PF2C01	HS_FLORIDA_P20	0.4000	14	0	0	0	0.57413	0.00032	0.57477
PF2C02	HS_FLORIDA_P22	0.4400	14	0	0	0	0.59002	0.00032	0.59066
PF2C03	HS_FLORIDA_P25	0.5021	14	0	0	0	0.61349	0.00031	0.61411
PF2C04	HS_FLORIDA_AL_14EXP	0.5021	14	0	0	0	0.61396	0.00029	0.61454
PF2C05	HS_FLORIDA_AL_13EXP	0.5376	13	0	0	0	0.61731	0.00030	0.61791
PF2C06	HS_FLORIDA_AL_12EXP	0.5796	12	0	0	0	0.61809	0.00030	<b>0.61869</b>
PF2C07	HS_FLORIDA_AL_11EXP	0.6299	11	0	0	0	0.61556	0.00029	0.61614
PF2C08	HS_FLORIDA_AL_10EXP	0.6914	10	0	0	0	0.60880	0.00030	0.60940
<b>PF2D, Horizontal Plate Fanning</b>									
PF2D01	HS_FLORIDA_AL_12EXP_H1	0.5796	12	0.39	0	0	0.62317	0.00030	0.62377
PF2D02	HS_FLORIDA_AL_12EXP_H2	0.5796	12	0.78	0	0	0.63293	0.00028	0.63349
PF2D03	HS_FLORIDA_AL_12EXP_H3	0.5796	12	1.17	0	0	0.64252	0.00030	<b>0.64312</b>
<b>PF2E, Location Study</b>									
PF2E01	HS_FLORIDA_AL_12EXP_SH1	0.5796	12	0	0.39	0.39	0.63321	0.00028	0.63377
PF2E02	HS_FLORIDA_AL_12EXP_SH2	0.5796	12	0	0.78	0.78	0.64695	0.00028	0.64751
PF2E03	HS_FLORIDA_AL_12EXP_SH3	0.5796	12	0	1.17	1.17	0.65836	0.00029	0.65894
PF2E04	HS_FLORIDA_AL_12EXP_SH3A	0.5796	12	0	0.78	1.17	0.66032	0.00031	<b>0.66094</b>
PF2E05	HS_FLORIDA_AL_12EXP_SH3B	0.5796	12	0	0.39	1.17	0.65881	0.00030	0.65941
PF2E06	HS_FLORIDA_AL_12EXP_SH3C	0.5796	12	0	0.00	1.17	0.65474	0.00029	0.65532
PF2E07	HS_FLORIDA_AL_12EXP_SH3D	0.5796	12	0	-0.39	1.17	0.64867	0.00029	0.64925
PF2E08	HS_FLORIDA_AL_12EXP_SH3E	0.5796	12	0	-0.78	1.17	0.64175	0.00029	0.64233
PF2E09	HS_FLORIDA_AL_12EXP_SH3F	0.5796	12	0	-1.17	1.17	0.63367	0.00029	0.63425

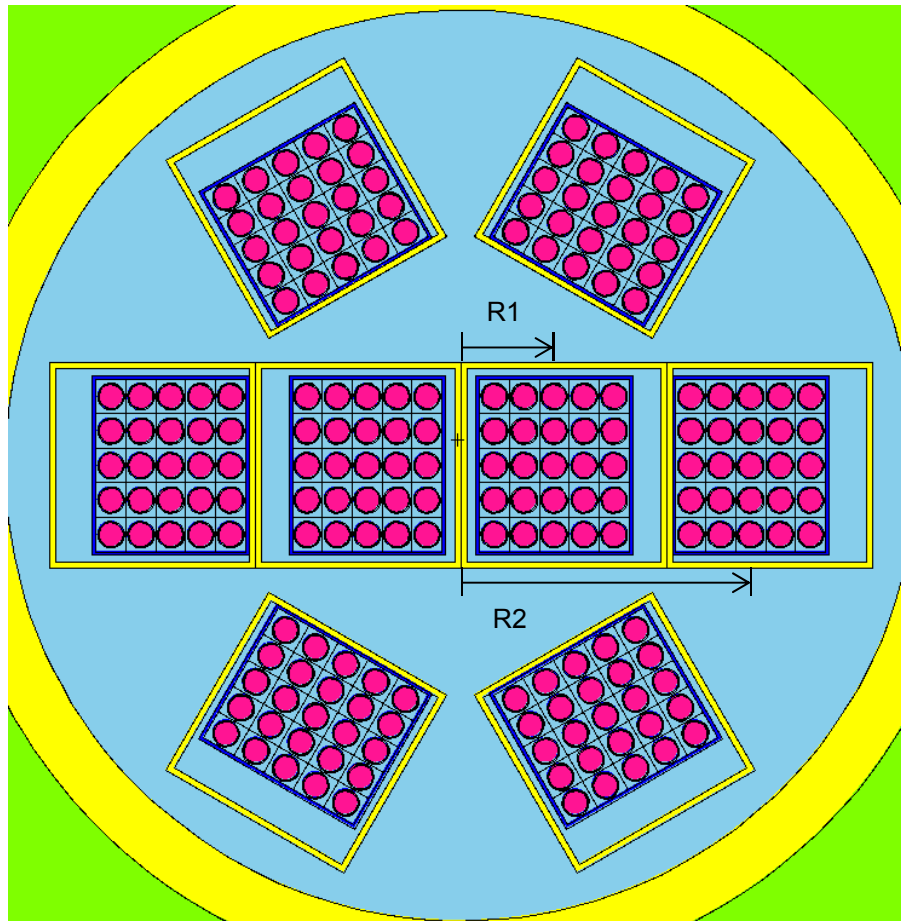
①Offset is measured radially from the center of the fuel element to the centerline of the package. “Inner” refers to the two inner fuel elements, and “outer” refers to the outer six fuel elements.

(continued)

Table 6.4-12 – HAC Single Package Results, U-Florida (concluded)

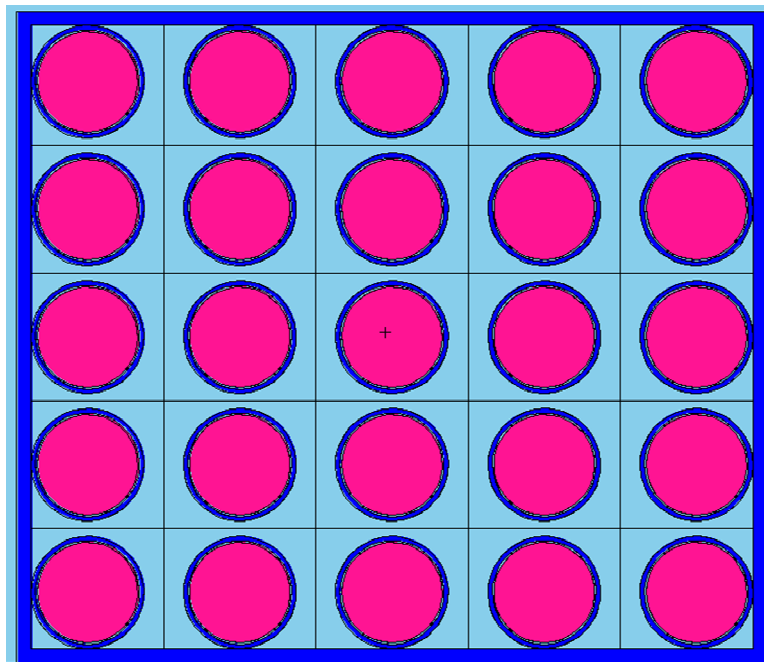
Case ID	Filename	Pitch (cm)	Plates at Expanded Pitch	Horizontal Fanning (cm)	Inner Offset (cm)①	Outer Offset (cm)①	$k_{eff}$	$\sigma$	$k_s (k+2\sigma)$
<b>PF2F, Alternate Configurations of Aluminum Spacer</b>									
PF2F01	HS_FLORIDA_AL2_12EXP_SH3A	0.5796	12	0	0.78	1.17	0.66276	0.0003	<b>0.66336</b>
PF2F02	HS_FLORIDA_AL3_12EXP_SH3A	0.5796	12	0	0.78	1.17	0.66007	0.0003	0.66067
PF2F03	HS_FLORIDA_AL4_12EXP_SH3A	0.5796	12	0	0.78	1.17	0.65973	0.0003	0.66033

①Offset is measured radially from the center of the fuel element to the centerline of the package. “Inner” refers to the two inner fuel elements, and “outer” refers to the outer six fuel elements.

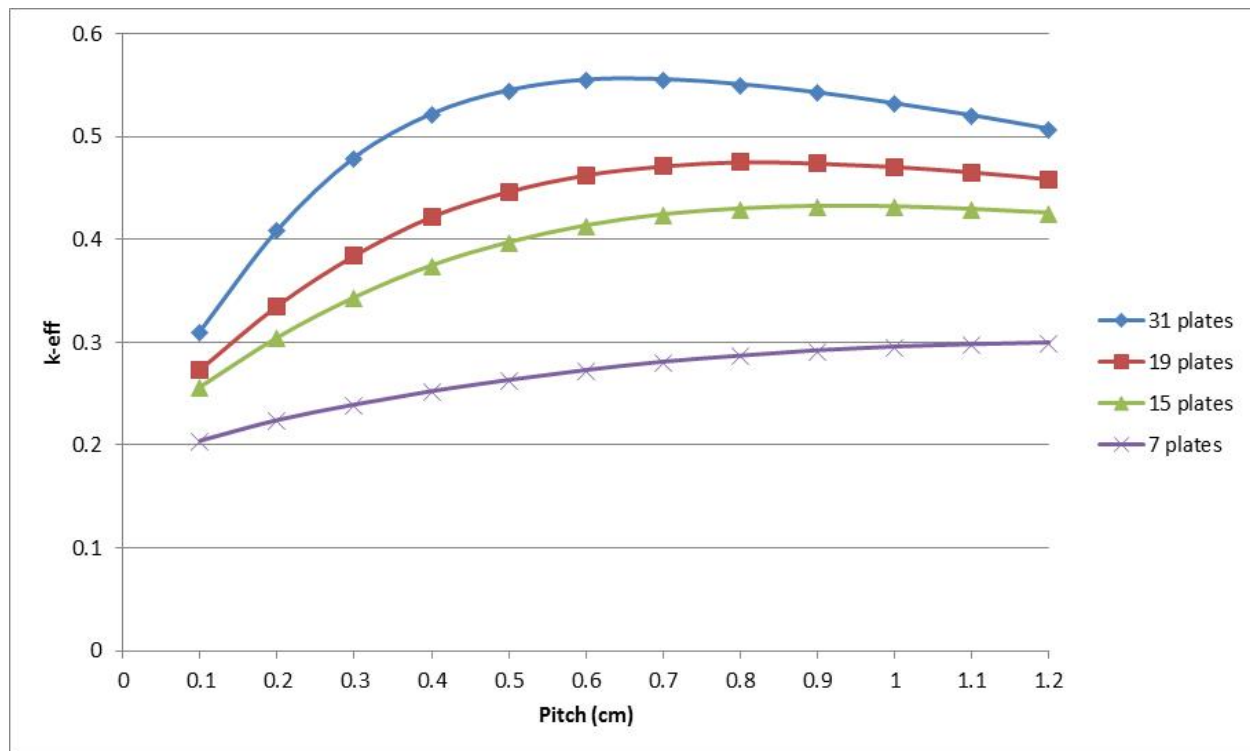


Orientation shown is for Case P2C03 ( $R1 = 4.17$  cm,  $R2 = 12.93$  cm)

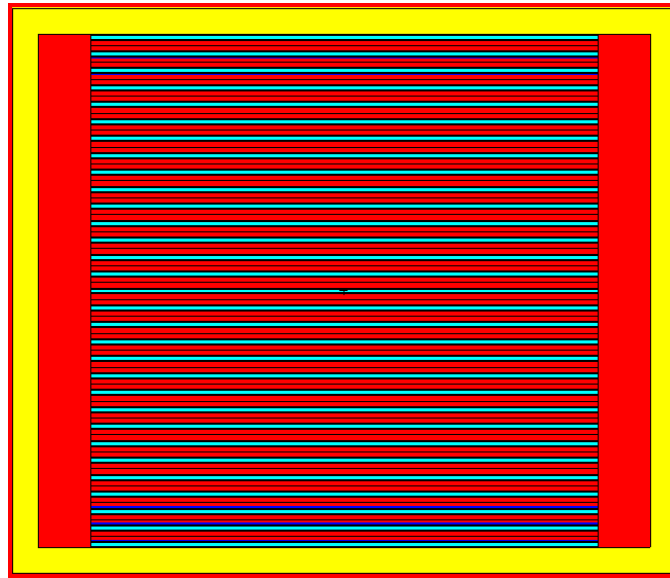
**Figure 6.4-1 – PULSTAR Element Positions**



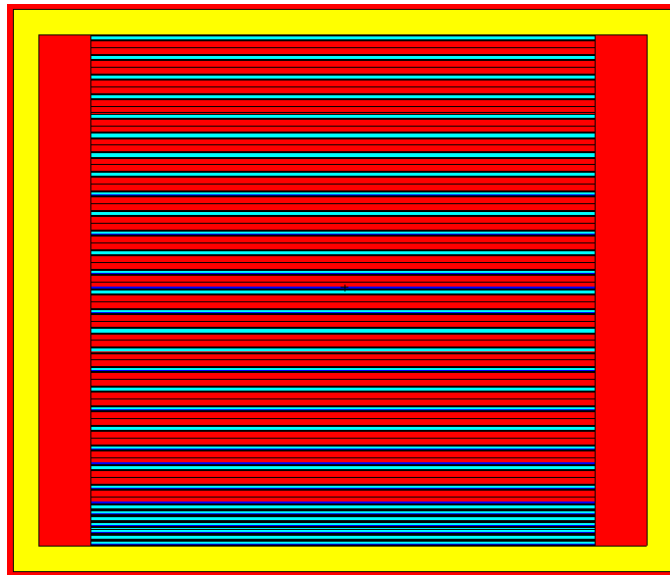
**Figure 6.4-2 – PULSTAR Damaged Fuel Element Model**



**Figure 6.4-3 – Plate Optimization Study**



31 plates with uniform pitch (Case L2A04)



31 plates with non-uniform pitch (25 expanded) (Case L2B06)

**Figure 6.4-4 – LPB Pitch Configurations**



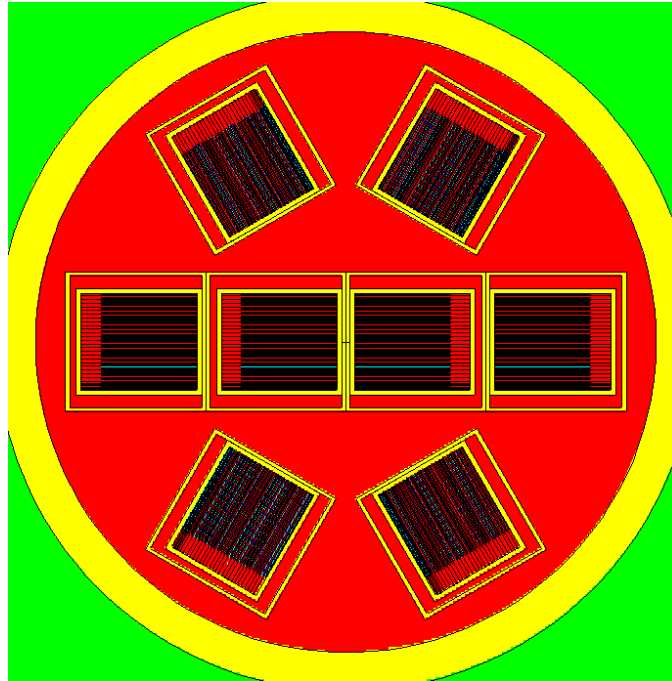
Horizontal Fanning (0.3285 cm) (Case L2C01)



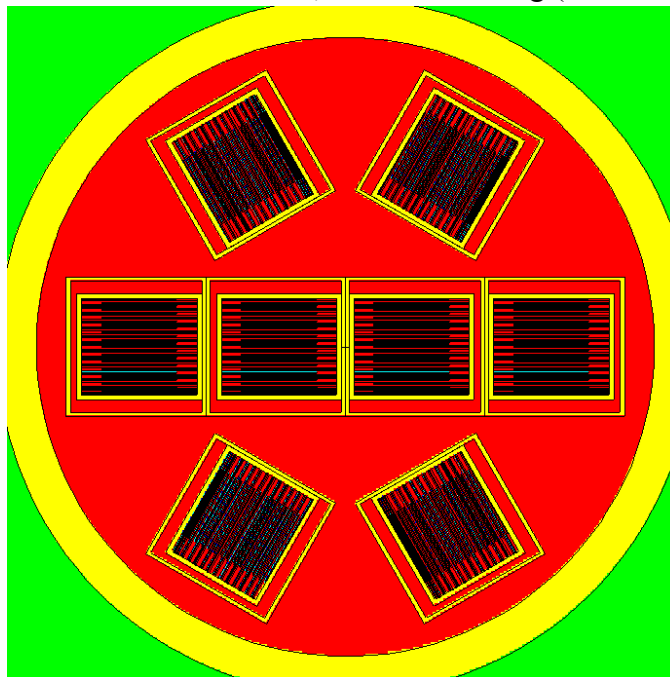
Horizontal Fanning (0.6470 cm) (Case L2C02)

**Figure 6.4-5 – LPB Horizontal Fanning Configurations**



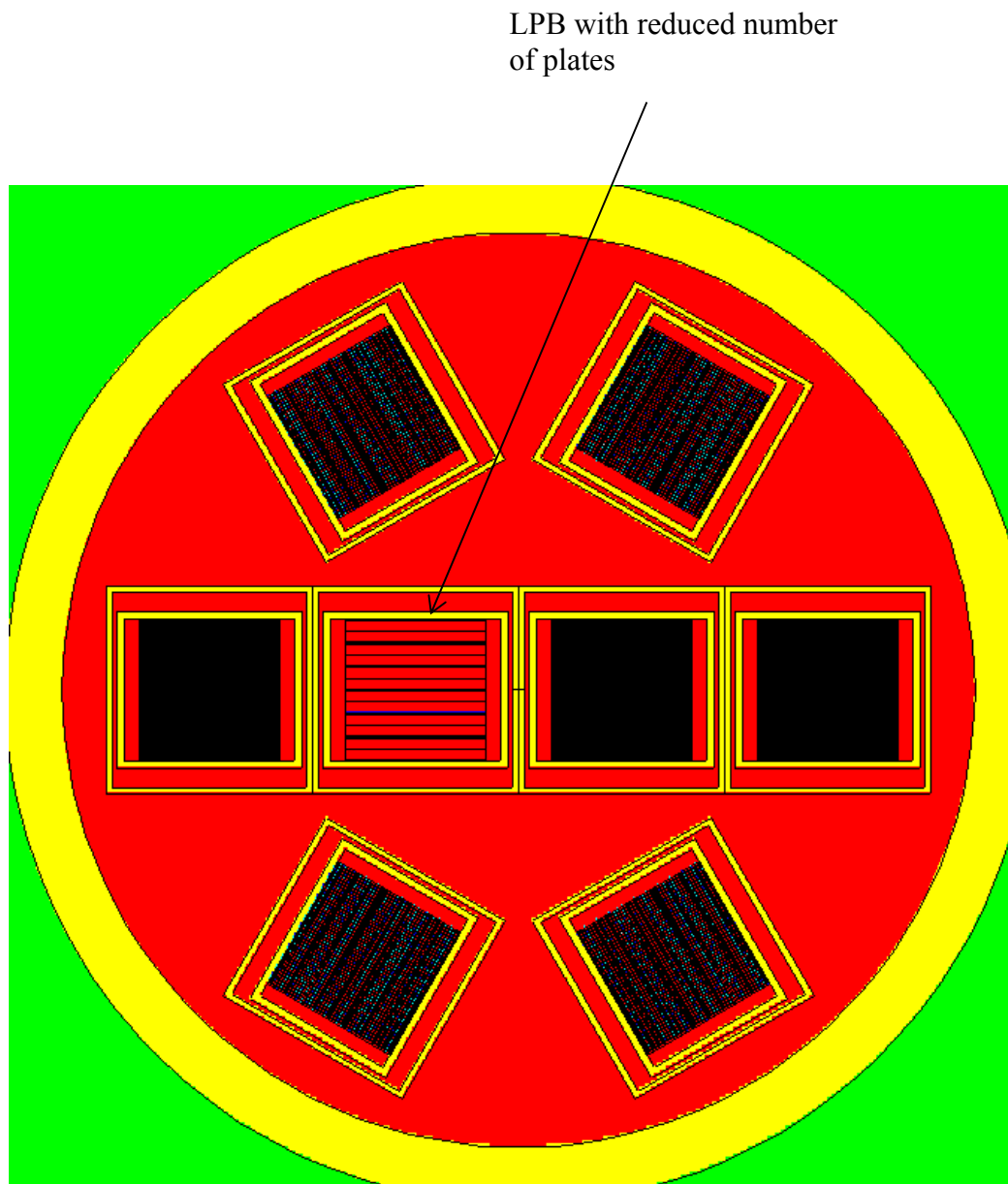


LPBs Shifted to Centerline, Without Fanning (Case L2D01)

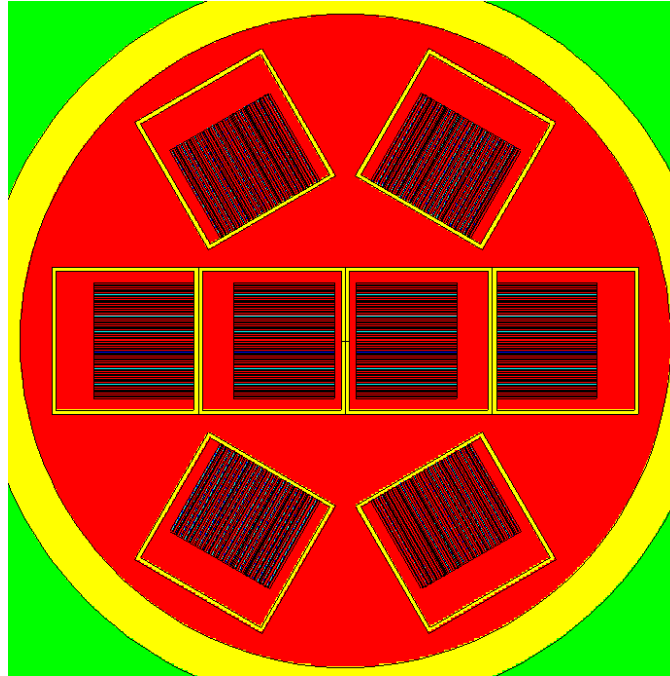


LPBs Shifted to Centerline, With Fanning (Case L2D02)

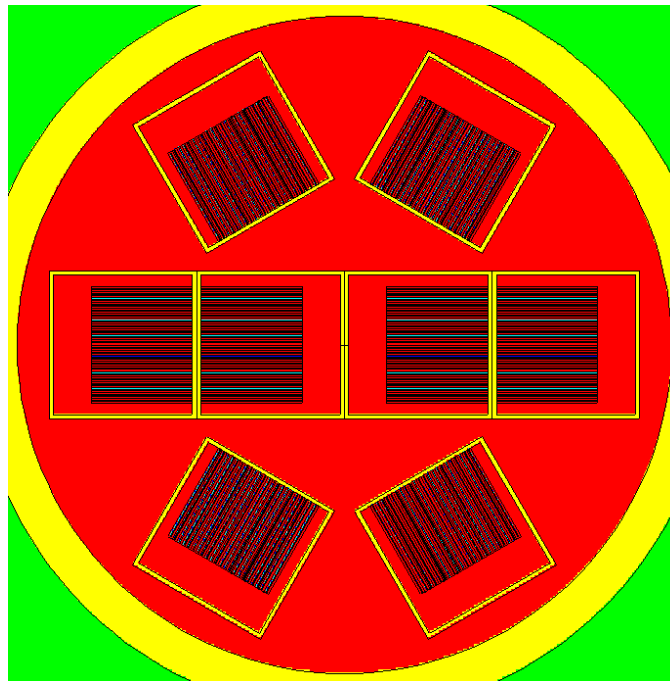
**Figure 6.4-6 – LPB Radial Arrangement**



**Figure 6.4-7 – LPB Loading/Unloading**

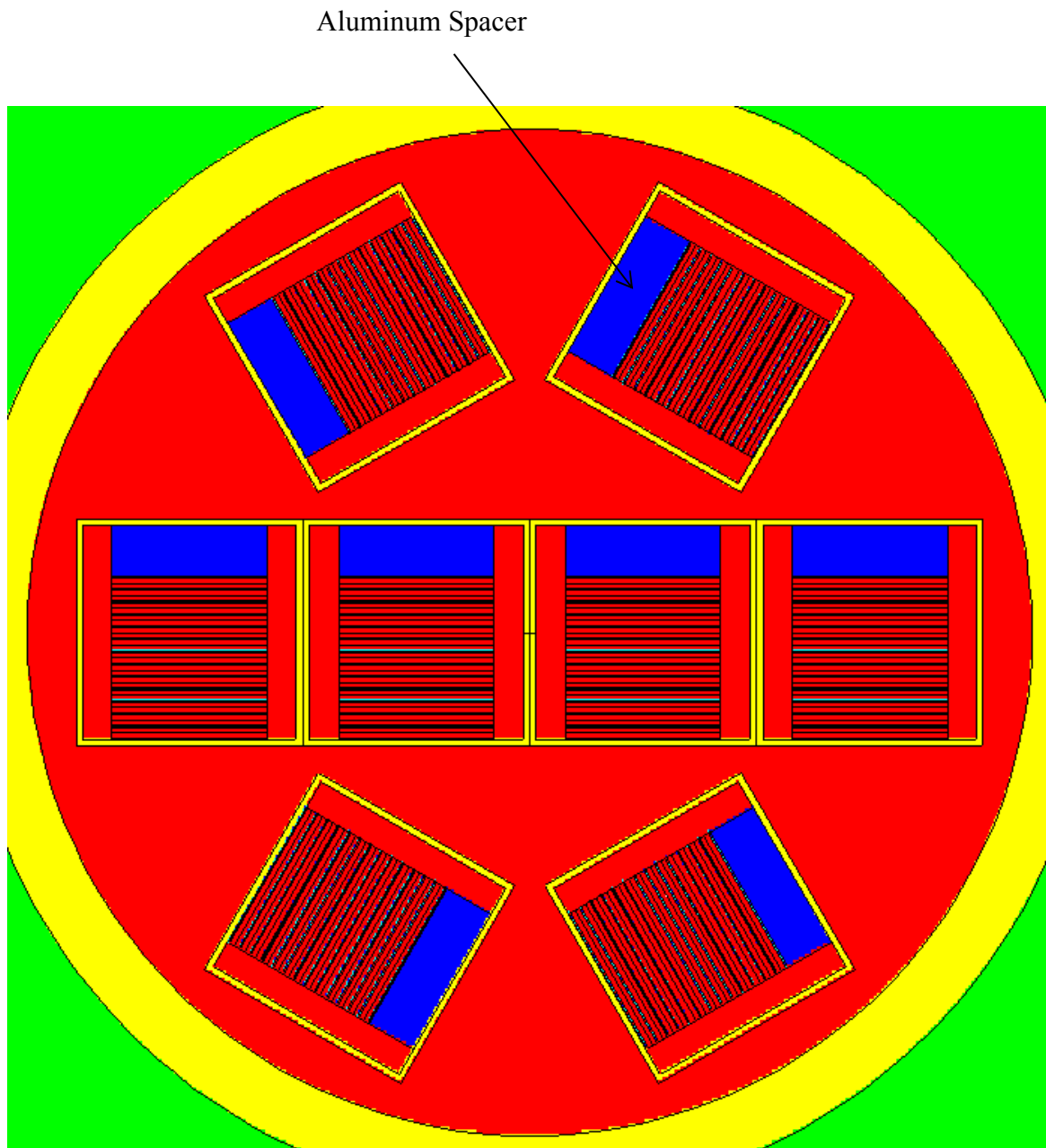


Inner offset = 0.78 cm, Outer offset = 1.17 cm (Case PF2B4)

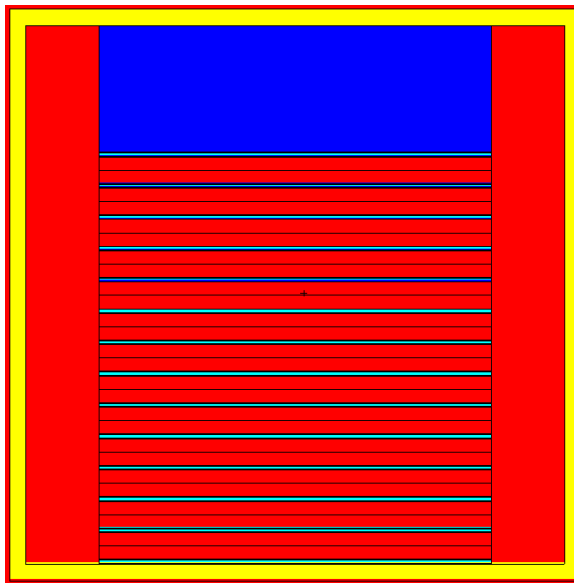


Inner offset = -1.17 cm, Outer offset = 1.17 cm (Case PF2B9)

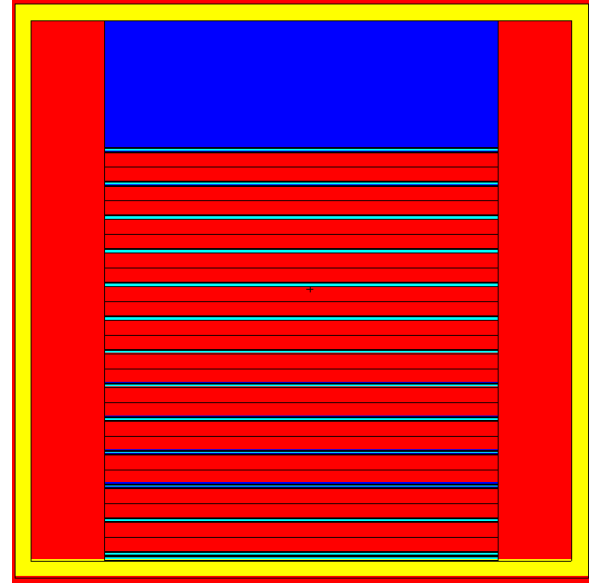
**Figure 6.4-8 – RINSC Radial Arrangement**



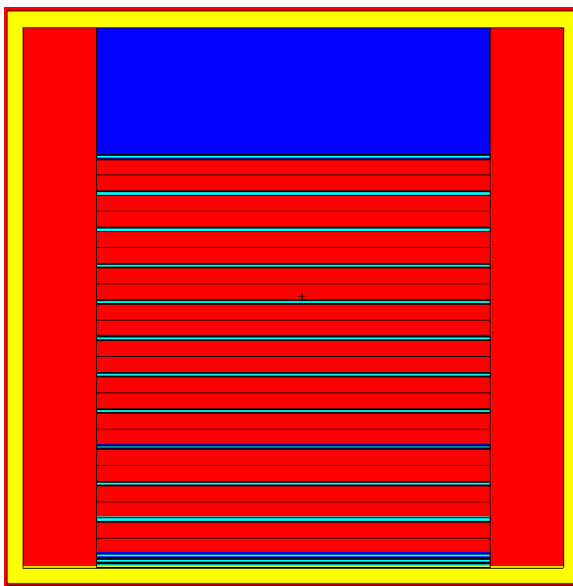
**Figure 6.4-9** – Damaged U-Florida Element with Aluminum Spacer



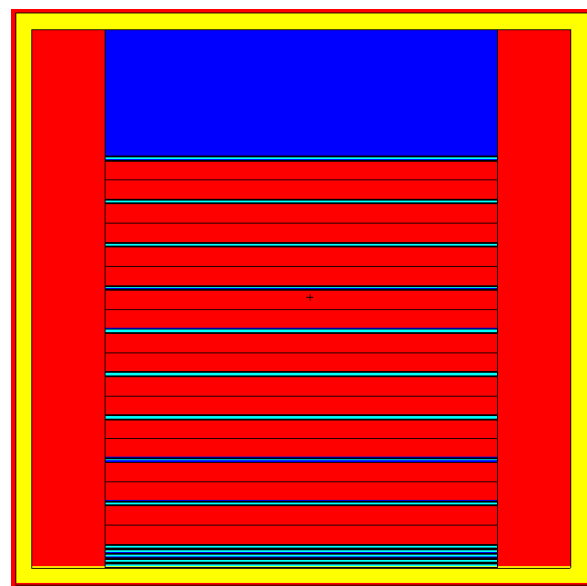
14 plates expanded pitch (Case PF2C04)



13 plates expanded pitch (Case PF2C05)



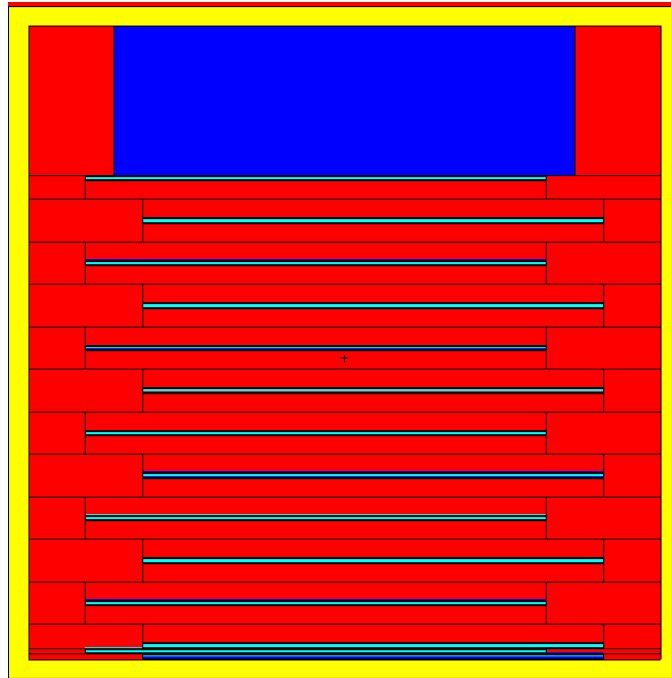
12 plates expanded pitch (Case PF2C06)



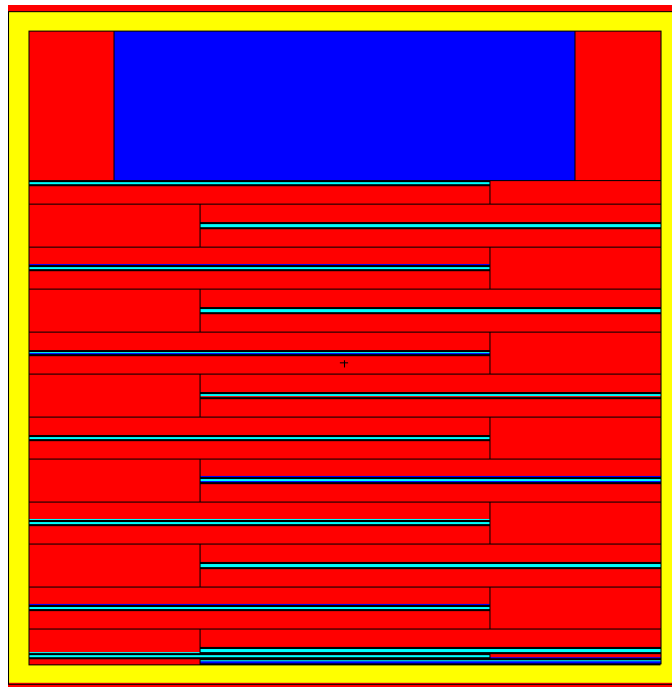
10 plates expanded pitch (Case PF2C08)

Note: All configurations feature 14 fuel plates.

**Figure 6.4-10 – Damaged U-Florida Element, Pitch Configurations**

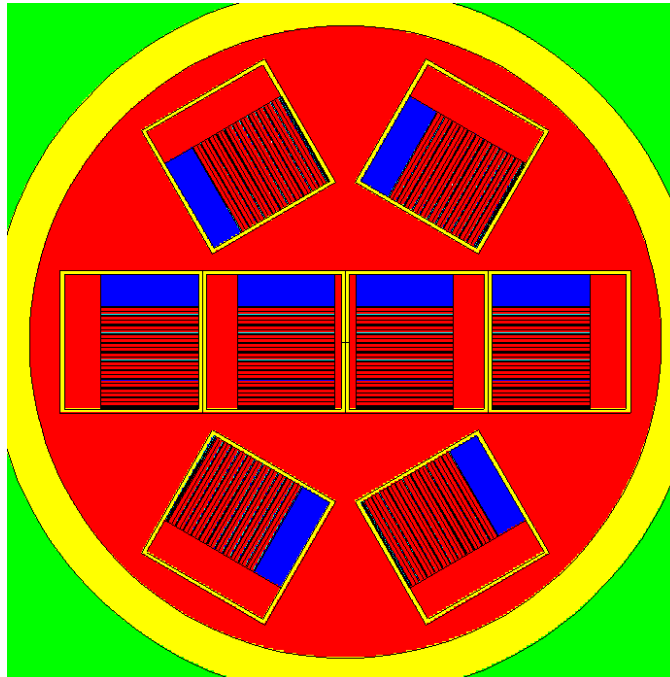


Horizontal Fanning 0.39 cm (Case PF2D01)

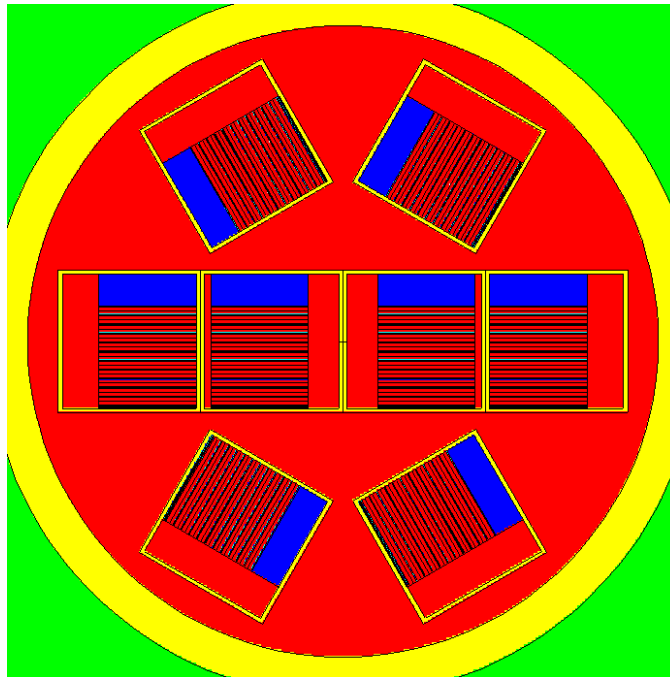


Horizontal Fanning 1.17 cm (Case PF2D03)

**Figure 6.4-11 – Damaged U-Florida Element, Fanning Configurations**

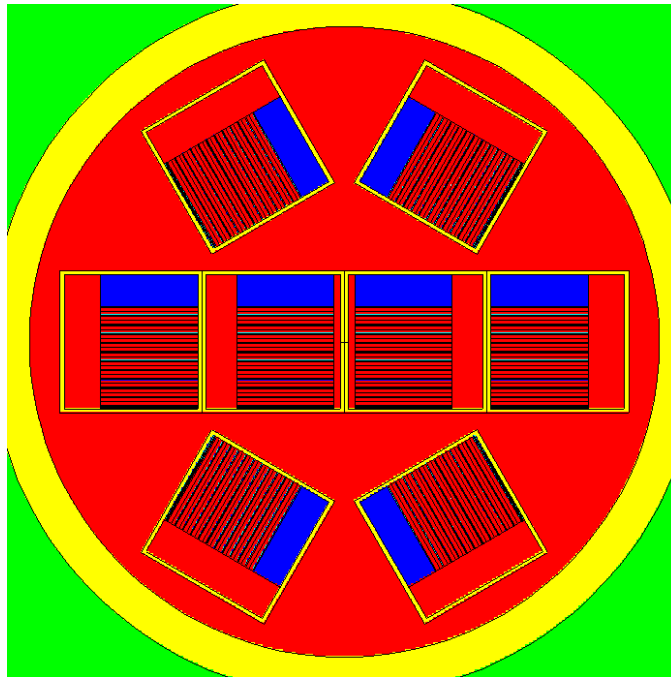


Case PF2E04 (inner offset = 0.78 cm, outer offset = 1.17 cm)

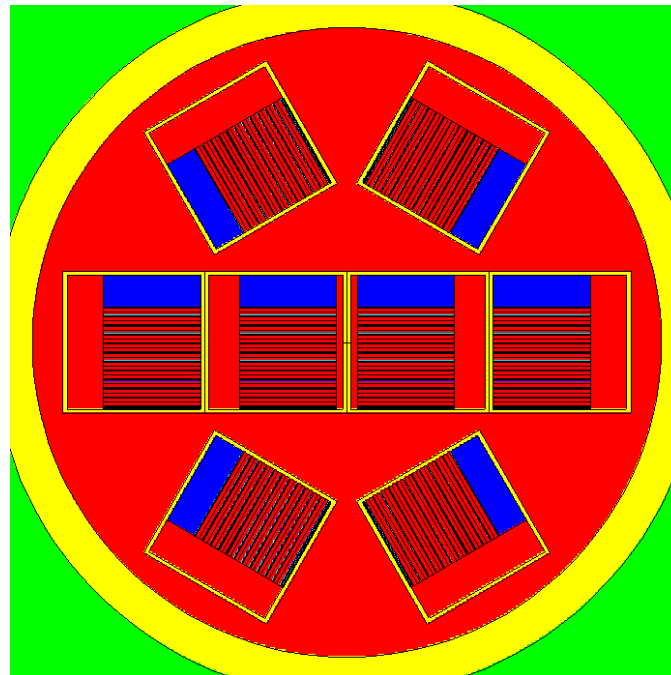


Case PF2E08 (inner offset = -0.78 cm, outer offset = 1.17 cm)

**Figure 6.4-12 – Damaged U-Florida Element, Radial Arrangement**



Alternate Configuration 1 (Case PF2F01)



Alternate Configuration 2 (Case PF2F02)

**Figure 6.4-13** – Damaged U-Florida Element, Alternate Configurations



## 6.5 Evaluation of Package Arrays under Normal Conditions of Transport

### 6.5.1 Configuration

In the NCT array configurations, the most reactive NCT single package configuration for each fuel type determined in Section 6.4.1.1, *NCT Single Package Configuration*, is utilized. A hexagonal reflective surface is added around the package, as shown in Figure 6.5-1. The SFB model is not shown in this figure but the boundary conditions are the same. This simulates a close-packed infinite hexagonal array of packages. The reflective boundary is also present on the top and bottom surfaces.

Five cases are run for MURR, MITR-II, ATR, and TRIGA. The initial case is simply the most reactive NCT single package case with reflective boundary conditions and no water between the packages. In the remaining four cases, the water density between the packages is varied between 0.25 and 1.0 g/cm<sup>3</sup>. In each case, the reactivity is maximized with no water between the packages. This conclusion is applied to the subsequent SFB models. Also, each SFB payload is evaluated in a nominal configuration and centered in the SFB compartment.

MURR, MITR-II, and ATR results are summarized in Table 6.5-1. Cases C1 through C5 are for MURR, Cases C10 through C14 are for MITR-II, and Cases C20 through C24 are for ATR. TRIGA results are summarized in Table 6.5-2. Cases C30 through C34 are for TRIGA Type 109 and Case TL3A1 is for TRIGA Type 119. The SFB payload results are provided in Table 6.5-3.

TRIGA fuel Case C30 with no water between the packages is the most reactive, with  $k_s = 0.53939$ . Consistent with the single package results, TRIGA Type 109 bounds Type 119. TRIGA fuel is significantly more reactive than the other fuels because hydrogen is present in the fuel matrix and the package cavity is modeled as dry for NCT.

### 6.5.2 Results

The results for the NCT array cases are provided in Table 6.5-1 through Table 6.5-3. The most reactive configuration for each fuel type is listed in boldface.

**Table 6.5-1 – NCT Array Results, MURR, MITR-II, ATR**

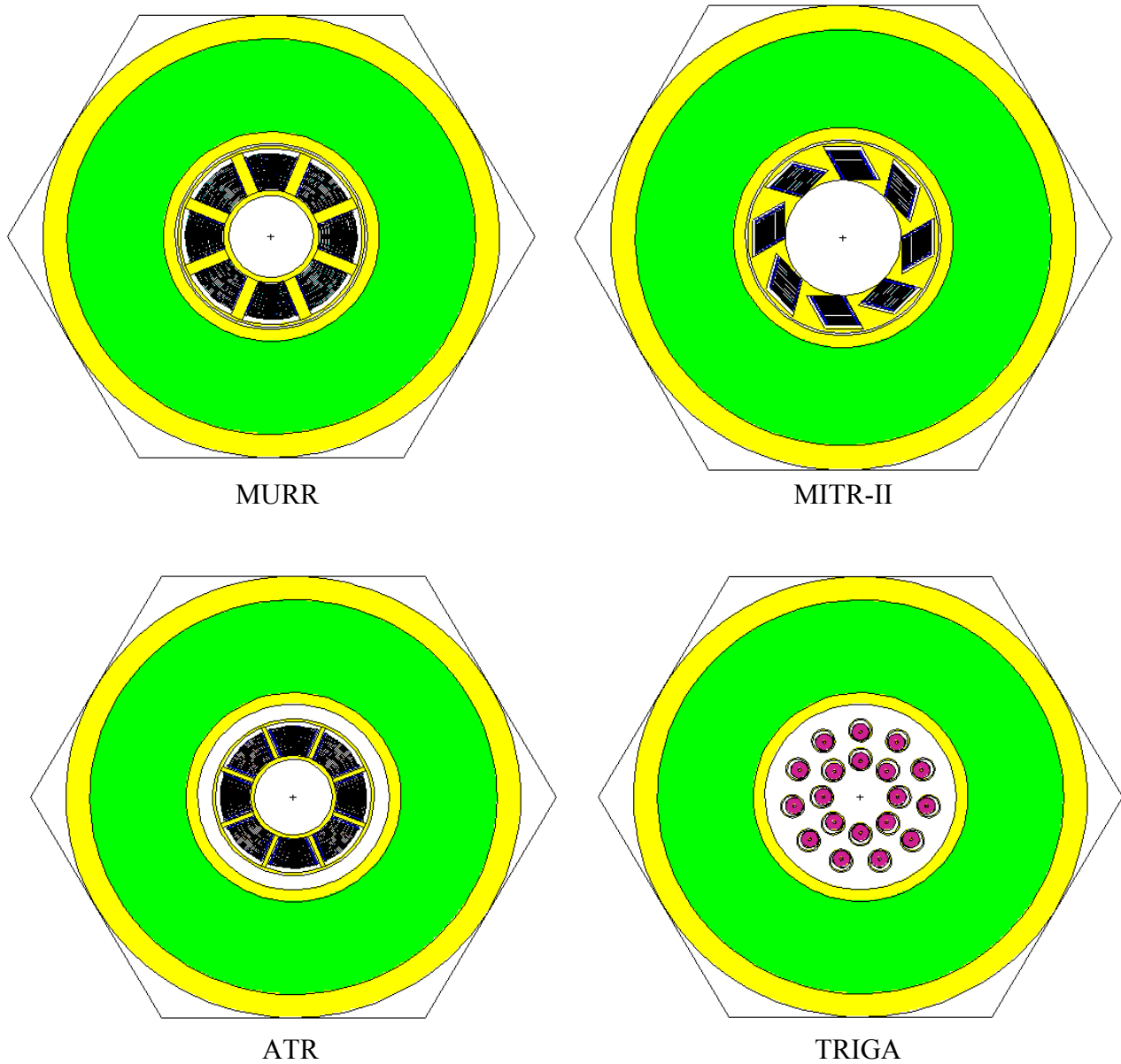
<b>Case ID</b>	<b>Filename</b>	<b>External Water Density (g/cm<sup>3</sup>)</b>	<b>k<sub>eff</sub></b>	<b>σ</b>	<b>k<sub>s</sub> (k+2σ)</b>
<b>MURR</b>					
<b>C1</b>	<b>NA_MURR_INUP</b>	<b>0</b>	<b>0.19604</b>	<b>0.00037</b>	<b>0.19678</b>
C2	NA_MURR_W025INUP	0.25	0.12467	0.00031	0.12529
C3	NA_MURR_W050INUP	0.50	0.11327	0.00029	0.11385
C4	NA_MURR_W075INUP	0.75	0.10858	0.00026	0.10910
C5	NA_MURR_W100INUP	1.0	0.10606	0.00027	0.10660
<b>MITR-II</b>					
<b>C10</b>	<b>NA_MIT2_W000</b>	<b>0</b>	<b>0.14305</b>	<b>0.00028</b>	<b>0.14361</b>
C11	NA_MIT2_W025	0.25	0.09091	0.00027	0.09145
C12	NA_MIT2_W050	0.50	0.08283	0.00021	0.08325
C13	NA_MIT2_W075	0.75	0.07970	0.00022	0.08014
C14	NA_MIT2_W100	1.0	0.07704	0.00021	0.07746
<b>ATR</b>					
<b>C20</b>	<b>NA_ATR_INUP</b>	<b>0</b>	<b>0.23274</b>	<b>0.00041</b>	<b>0.23356</b>
C21	NA_ATR_W025INUP	0.25	0.13567	0.00032	0.13631
C22	NA_ATR_W050INUP	0.50	0.12103	0.00031	0.12165
C23	NA_ATR_W075INUP	0.75	0.11473	0.00029	0.11531
C24	NA_ATR_W100INUP	1.0	0.11116	0.00028	0.11172

**Table 6.5-2 – NCT Array Results, TRIGA**

Case ID	Filename	External Water Density (g/cm <sup>3</sup> )	k <sub>eff</sub>	σ	k <sub>s</sub> (k+2σ)
<b>Type 109</b>					
C30	NA_TRIGA_INUP	0	0.53733	0.00103	0.53939
C31	NA_TRIGA_W025INUP	0.25	0.46130	0.00099	0.46328
C32	NA_TRIGA_W050INUP	0.50	0.44977	0.00096	0.45169
C33	NA_TRIGA_W075INUP	0.75	0.44506	0.00096	0.44698
C34	NA_TRIGA_W100INUP	1.0	0.43997	0.00094	0.44185
<b>Type 119</b>					
TL3A1	TR_NCT_ARY_A_01	0	0.49222	0.00038	0.49298

**Table 6.5-3 – NCT Array Results, Square Fuel Basket**

Case ID	Filename	External Water Density (g/cm <sup>3</sup> )	k <sub>eff</sub>	σ	k <sub>s</sub> (k+2σ)
<b>PULSTAR</b>					
P3A1	NA_PULSTAR	0.0	0.22802	0.00048	0.22898
<b>Loose Plate Box</b>					
L3A1	NA_LOOSE_EXP25SH	0.0	0.12015	0.00018	0.12051
<b>Plate Fuels (RINSC)</b>					
PF3A1	NA_RINSC_SH3A	0.0	0.09325	0.00032	0.09389



**Figure 6.5-1 – NCT Array Geometry**

## 6.6 Package Arrays under Hypothetical Accident Conditions

### 6.6.1 Configuration

In the HAC array configuration, an infinite hexagonal array of packages is modeled in the same manner as the NCT array. Various internal moderation conditions are examined, as well as various moderation conditions between packages.

#### MURR

The MURR results are reported in Table 6.6-1 as Cases D1 through D8. In Cases D1 through D7, the cladding thickness and channel spacing are modeled consistent with the NCT analysis. In Case D1, the fuel elements are moved radially inward and shifted to the top of the package, which was determined to be the most reactive single package orientation. The package cavity is flooded with full-density water, and void is modeled between the packages.

In Cases D2 and D3, the configuration of Case D1 is modified so that all water inside the cavity is treated as variable density (0.8 and 0.9 g/cm<sup>3</sup>, respectively). Because the water density between the fuel plates is reduced in this configuration, moderation is decreased and the reactivity decreases.

In Cases D4 through D7, the most reactive case (Case D1) is run with variable water density between the packages. The reactivity decreases when water is added to this region.

In Case D8, Case D1 is rerun using the minimum cladding thickness of 0.008-in and channel spacing of 0.094-in. Case D8 is the most reactive, with  $k_s = 0.82681$ . Note that this is also the most reactive case of all fuel types examined.

#### MITR-II

The MITR-II results are reported in Table 6.6-2 as Cases D20 through D27. In Cases D20 through D27, the cladding thickness and channel spacing are modeled consistent with the NCT analysis. In Case D20, the fuel elements are pushed radially inward and shifted to the top of the package, which was determined to be the most reactive single package orientation. The package cavity is flooded with full-density water, and void is modeled between the packages.

In Cases D21 and D22, the configuration of Case D20 is modified so that all water inside the cavity is treated as variable density (0.8 and 0.9 g/cm<sup>3</sup>, respectively). Because the water density between the fuel plates is reduced in this configuration, moderation is decreased and the reactivity decreases.

In Cases D23 through D26, the most reactive case (Case D20) is run with variable water density between the packages. The reactivity decreases when water is added to this region.

In Case D27, Case D20 is rerun using the minimum cladding thickness of 0.008-in and channel spacing of 0.116-in. Case D27 is the most reactive, with  $k_s = 0.60948$ .

#### ATR

The ATR results are reported in Table 6.6-3 as Cases D40 through D47. In Cases D40 through D46, the cladding thickness and channel spacing are modeled consistent with the NCT analysis. In Case D40, the fuel elements are moved radially inward and shifted to the top of the package,

## BRR Package Safety Analysis Report

which was determined to be the most reactive single package orientation. The package cavity is flooded with full-density water, and void is modeled between the packages.

In Cases D41 and D42, the configuration of Case D40 is modified so that all water inside the cavity is treated as variable density (0.8 and 0.9 g/cm<sup>3</sup>, respectively). Because the water density between the fuel plates is reduced in this configuration, moderation is decreased and the reactivity decreases.

In Cases D43 through D46, the most reactive case (Case D40) is run with variable water density between the packages. The reactivity decreases when water is added to this region.

In Case D47, Case D40 is rerun using a cladding thickness of 0.018-in for plates 1 and 19, and 0.008-in for plates 2 through 18. The resulting channel spacing is 0.097-in between plates 1 and 2, 0.107-in between plates 18 and 19, and 0.092-in between the remaining plates. Therefore, Case D47 is the most reactive, with  $k_s = 0.72066$ .

### TRIGA

The TRIGA results are reported in Table 6.6-4. Type 109 results are provided in Cases D60 to D71, and Type 119 results are provided in Cases TL4A1 through TL4A6. In all models, the fuel elements are moved radially inward and axially shifted to the top of the cask, which was determined to be the most reactive single package orientation. It is expected that the most reactive condition will occur at a reduced internal water density, consistent with the single package TRIGA results.

In Cases D60 through D67, the cavity water density is varied from 0.3 to 1.0 g/cm<sup>3</sup>, while void is modeled external to the package. The maximum reactivity occurs for Case D63, which has a water density of 0.6 g/cm<sup>3</sup>. In Cases D68 through D71, the internal water density is modeled at 0.6 g/cm<sup>3</sup> (Case D63 configuration) while the external water density is varied between 0.25 and 1.0 g/cm<sup>3</sup>. The reactivity decreases when water is modeled between the packages. Therefore, Case D63 is the most reactive, with  $k_s = 0.72039$ .

Because of the difference in composition between rod Types 109 and 119, the effect of moderator density is reevaluated for Type 119. External water (between packages in the array) is demonstrated to reduce reactivity in Type 109 cases D68-D71. This finding is applicable to the Type 119 payload and therefore these cases are evaluated with void between adjacent packages in the array. The highest  $k_s$  observed for the Type 119 payload is 0.71738 and occurs with a moderator density of 0.7 g/cm<sup>3</sup>. The Type 119 rods are therefore slightly less reactive than the HEU bearing Type 109 rods. Peak reactivity for the Type 119 rods occurs at a somewhat higher moderator density (0.7 g/cm<sup>3</sup> vs. 0.6 g/cm<sup>3</sup>), which is attributable to the reduced enrichment and the corresponding increased role of U-238.

### Square Fuel Basket

It is observed from the results for MURR, MITR-II, and ATR that reactivity in an infinite array is maximized with full moderation within the cavity and void between adjacent packages. Therefore, only this moderation condition is considered in the SFB HAC array cases. The most reactive SFB single package cases from Section 6.4, *Single Package Evaluation*, are modified to change the boundary condition to a close-packed reflective hexagonal array, which represents an infinite array of packages. Results are provided in Table 6.6-5. The HAC array results are:

- $k_s = 0.82202$  for PULSTAR

- $k_s = 0.64661$  for the LPB, and
- $k_s = 0.74629$  for plate fuels (RINSC)

All results are significantly below the USL of 0.9209. The reactivity for any combination of authorized SFB contents will not exceed the reactivity of the PULSTAR payload.

### **6.6.2 Results**

Following are the tabulated results for the HAC array cases. The most reactive configuration in each series is listed in boldface.

**Table 6.6-1 – HAC Array Results, MURR**

Case ID	Filename	Internal Water Density (g/cm <sup>3</sup> )	External Water Density (g/cm <sup>3</sup> )	k <sub>eff</sub>	σ	k <sub>s</sub> (k+2σ)
D1	HA_MURR	1.0	0	0.80428	0.00115	0.80658
D2	HA_MURR_C080	0.8	0	0.74913	0.00111	0.75135
D3	HA_MURR_C090	0.9	0	0.77692	0.00116	0.77924
D4	HA_MURR_W025	1.0	0.25	0.77495	0.00125	0.77745
D5	HA_MURR_W050	1.0	0.50	0.77403	0.00106	0.77615
D6	HA_MURR_W075	1.0	0.75	0.77030	0.00115	0.77260
D7	HA_MURR_W100	1.0	1.0	0.76810	0.00131	0.77072
<b>D8</b>	<b>HA_MURRC</b>	<b>1.0</b>	<b>0</b>	<b>0.82441</b>	<b>0.00120</b>	<b>0.82681</b>

**Table 6.6-2 – HAC Array Results, MITR-II**

Case ID	Filename	Internal Water Density (g/cm <sup>3</sup> )	External Water Density (g/cm <sup>3</sup> )	k <sub>eff</sub>	σ	k <sub>s</sub> (k+2σ)
D20	HA_MIT2	1.0	0	0.56103	0.00102	0.56307
D21	HA_MIT2_C080	0.8	0	0.53082	0.00099	0.53280
D22	HA_MIT2_C090	0.9	0	0.54724	0.00106	0.54936
D23	HA_MIT2_W025	1.0	0.25	0.54199	0.00096	0.54391
D24	HA_MIT2_W050	1.0	0.50	0.53616	0.00096	0.53808
D25	HA_MIT2_W075	1.0	0.75	0.53278	0.00111	0.53500
D26	HA_MIT2_W100	1.0	1.0	0.53347	0.00105	0.53557
<b>D27</b>	<b>HA_MIT2C</b>	<b>1.0</b>	<b>0</b>	<b>0.60736</b>	<b>0.00106</b>	<b>0.60948</b>

**Table 6.6-3 – HAC Array Results, ATR**

Case ID	Filename	Internal Water Density (g/cm <sup>3</sup> )	External Water Density (g/cm <sup>3</sup> )	k <sub>eff</sub>	σ	k <sub>s</sub> (k+2σ)
D40	HA_ATR	1.0	0	0.69505	0.00117	0.69739
D41	HA_ATR_C080	0.8	0	0.66976	0.00104	0.67184
D42	HA_ATR_C090	0.9	0	0.68206	0.00109	0.68424
D43	HA_ATR_W025	1.0	0.25	0.68753	0.00115	0.68983
D44	HA_ATR_W050	1.0	0.50	0.68575	0.00111	0.68797
D45	HA_ATR_W075	1.0	0.75	0.68528	0.00106	0.68740
D46	HA_ATR_W100	1.0	1.0	0.68342	0.00110	0.68562
<b>D47</b>	<b>HA_ATRC</b>	<b>1.0</b>	<b>0</b>	<b>0.71864</b>	<b>0.00101</b>	<b>0.72066</b>



**Table 6.6-4 – HAC Array Results, TRIGA**

Case ID	Filename	Internal Water Density (g/cm <sup>3</sup> )	External Water Density (g/cm <sup>3</sup> )	k <sub>eff</sub>	σ	k <sub>s</sub> (k+2σ)
<b>Type 109</b>						
D60	HA_TRIGA_W0C030	0.3	0	0.68281	0.00107	0.68495
D61	HA_TRIGA_W0C040	0.4	0	0.70304	0.00102	0.70508
D62	HA_TRIGA_W0C050	0.5	0	0.71234	0.00113	0.71460
<b>D63</b>	<b>HA_TRIGA_W0C060</b>	<b>0.6</b>	<b>0</b>	<b>0.71827</b>	<b>0.00106</b>	<b>0.72039</b>
D64	HA_TRIGA_W0C070	0.7	0	0.71592	0.00107	0.71806
D65	HA_TRIGA_W0C080	0.8	0	0.71130	0.00109	0.71348
D66	HA_TRIGA_W0C090	0.9	0	0.70455	0.00107	0.70669
D67	HA_TRIGA_W0C100	1.0	0	0.69737	0.00112	0.69961
D68	HA_TRIGA_W025C060	0.6	0.25	0.70793	0.00125	0.71043
D69	HA_TRIGA_W050C060	0.6	0.50	0.70781	0.00097	0.70975
D70	HA_TRIGA_W075C060	0.6	0.75	0.70655	0.00110	0.70875
D71	HA_TRIGA_W100C060	0.6	1.0	0.70660	0.00105	0.70870
<b>Type 119</b>						
TL4A1	TR_HAC_ARY_A_01	0.4	0	0.69599	0.00040	0.69679
TL4A2	TR_HAC_ARY_A_02	0.5	0	0.70854	0.00045	0.70944
TL4A3	TR_HAC_ARY_A_03	0.6	0	0.71531	0.00046	0.71623
<b>TL4A4</b>	<b>TR_HAC_ARY_A_04</b>	<b>0.7</b>	<b>0</b>	<b>0.71646</b>	<b>0.00046</b>	<b>0.71738</b>
TL4A5	TR_HAC_ARY_A_05	0.8	0	0.71293	0.00047	0.71387
TL4A6	TR_HAC_ARY_A_06	0.9	0	0.70827	0.00050	0.70927

**Table 6.6-5 – HAC Array Results, Square Fuel Basket**

Case ID	Filename	Internal Water Density (g/cm <sup>3</sup> )	External Water Density (g/cm <sup>3</sup> )	k <sub>eff</sub>	σ	k <sub>s</sub> (k+2σ)
<b>PULSTAR</b>						
P4A1	PS_ARRAY_HAC_4B_01	1.0	0	0.82114	0.00044	0.82202
<b>Loose Plate Box</b>						
L4A1	HA_LOOSE_EXP25SH	1.0	0	0.64597	0.00032	0.64661
<b>Plate Fuels (RINSC)</b>						
PF4A1	HA_RINSC_SH3A	1.0	0	0.74471	0.00079	0.74629

## **6.7 Fissile Material Packages for Air Transport**

This section is not applicable, because air transport is not claimed.

## 6.8 Benchmark Evaluations

The Monte Carlo computer program MCNP5 v1.30 is utilized for this benchmark analysis [1]. MCNP has been used extensively in criticality evaluations for several decades and is considered a standard in the industry.

The ORNL USLSTATS code [2] is used to establish a USL for the analysis. USLSTATS provides a simple means of evaluating and combining the statistical error of the calculation, code biases, and benchmark uncertainties. The USLSTATS calculation uses the combined uncertainties and data to provide a linear trend and an overall uncertainty. Computed multiplication factors,  $k_{\text{eff}}$ , for the package are deemed to be adequately subcritical if the computed value of  $k_s$  is less than or equal to the USL as follows:

$$k_s = k_{\text{eff}} + 2\sigma \leq \text{USL}$$

The USL includes the combined effects of code bias, uncertainty in the benchmark experiments, uncertainty in the computational evaluation of the benchmark experiments, and an administrative margin. This methodology has accepted precedence in establishing criticality safety limits for transportation packages complying with 10 CFR 71.

### 6.8.1 Applicability of Benchmark Experiments

The fuel types analyzed fall into four distinct categories (1) high-enriched aluminum plate fuel, which includes MURR, MITR-II, and ATR, and (2) low-enriched plate fuel with an aluminide or silicide fuel matrix, which includes all of the Square plate fuels, (3)  $\text{UO}_2$  rods of the PULSTAR fuel, and (4) zirconium hydride (TRIGA) fuel. An explicit benchmark analysis is performed for categories (1) and (4) and applied to all four fuel categories. The critical experiment benchmarks are selected from the *International Handbook of Evaluated Criticality Safety Benchmark Experiments* [3] based upon their similarity to the packaging and contents.

#### 6.8.1.1 HEU Plate Fuel

The important selection parameters are high-enriched uranium plate-type fuel with a thermal spectrum. Thirty-five (35) benchmarks that meet these criteria are selected from the *Handbook*. The titles for all utilized experiments are listed in Table 6.8-1. Note that the benchmark from experiment set HEU-MET-THERM-022 is for the Advanced Test Reactor itself, so the fuel configuration in this benchmark is essentially the same as the ATR fuel modeled in the packaging analysis.

Ideally, benchmarks would be limited to those with a fuel matrix of  $\text{UAl}_x$  and aluminum, aluminum cladding, and no absorbers, consistent with the aluminum plate fuel criticality models. Experiment set HEU-COMP-THERM-022 consists of 11 benchmark experiments that utilize  $\text{UO}_2$  powder sintered with stainless steel, and stainless steel cladding. Experiments 1 through 5 (Cases BA1 through BA5) do not utilize control rods, while experiments 6 through 11 (Cases BA6 through BA11) utilize boron control rods. Experiment set HEU-MET-THERM-006 consists of 23 benchmark experiments. The first 16 experiments are directly applicable (Cases BA12 through BA27), although experiments 17 and 18 (Cases BA28 and BA29) utilize thin cadmium sheets, and experiments 19 through 23 (Cases BA30 through BA34) utilize uranium in solution in addition to the fuel plates. HEU-MET-THERM-022 (Case BA35) is a detailed model of the ATR core using explicit ATR fuel elements very similar to the ATR fuel element model

utilized in the criticality analysis. However, this full-core model necessarily contains absorber materials. Despite the presence of absorbers, because this benchmark utilizes ATR fuel, it is considered directly applicable to the plate fuel criticality analysis.

Therefore, of these 35 benchmarks, 17 benchmarks are directly applicable, while 18 benchmarks are applicable to a lesser degree. To compensate for the benchmarks that are not directly applicable, trending will be performed both on all 35 benchmark experiments and on the subset of 17 directly applicable benchmark experiments. The USL selected is the minimum of both benchmark sets.

#### 6.8.1.2 LEU Plate Fuel

The results of the HEU aluminum plate fuel benchmarks are applied to the LEU aluminide and silicide, Square plate fuels. The benchmarks are deemed applicable due to similarity of the fuel types, which essentially only differ in their U-235 enrichment. While the impact of additional U-238 in the system, and the corresponding increase in resonance interactions, may introduce some bias and hence, conceivably changes to the USL, the impact would not be significant for payloads with relatively low reactivity, such as those carried in the BRR Package. The USL for LEU plate fuel carried in the SFB will therefore be based on the most restrictive USL for HEU plate fuel.

#### 6.8.1.3 PULSTAR UO<sub>2</sub> Fuel

Undermoderated UO<sub>2</sub> systems are the basis of essentially all civil nuclear power production. The use of MCNP and its datasets to determine reactivity for such systems is therefore very well established. Supported by the combination of extensive simulation experience and relatively low reactivity of the PULSTAR fuel (even under HAC conditions), benchmarks for the UO<sub>2</sub> fuel are deemed unnecessary. The USL for PULSTAR fuel will therefore be based on the most restrictive USL determined for the other fuel types.

#### 6.8.1.4 TRIGA Fuel

The important selection parameters are uranium enrichment (20% and 70% U-235/U), zirconium hydride fuel, and a thermal spectrum. No directly applicable HEU benchmark experiments are available in the *Handbook*, although the *Handbook* does contain two intermediate-enriched (20%) TRIGA benchmarks. The available TRIGA benchmarks are for an entire Mark II core and hence contain absorber materials as well as a graphite reflector. While the BRR package TRIGA criticality analysis does not contain absorbers, these experiments are utilized because they represent the most similar available benchmarks.

Because a sample set of two benchmarks is not of sufficient size to obtain a statistical distribution, additional benchmarks are selected to supplement the two available TRIGA benchmarks. As zirconium hydride fuel contains moderator embedded in the fuel matrix, 10 high-enriched (93%) and 9 low-enriched (10%) uranium solution benchmarks are also utilized to simulate fuel intimately mixed with moderator. Therefore, a total of 21 benchmarks are utilized for benchmarking of TRIGA fuel. These 21 benchmarks are divided into three groups for trending: (1) all 21 benchmarks, (2) a subset of the 10 HEU benchmarks and two TRIGA benchmarks, and (3) a subset of the 9 LEU benchmarks and two TRIGA benchmarks. The USL selected is the minimum of all three benchmark sets.

## 6.8.2 Bias Determination

The USL is calculated by application of the USLSTATS computer program [2]. USLSTATS receives as input the  $k_{\text{eff}}$  as calculated by MCNP, the total 1- $\sigma$  uncertainty (combined benchmark and MCNP uncertainties), and a trending parameter.

The uncertainty value,  $\sigma_{\text{total}}$ , assigned to each case is a combination of the benchmark uncertainty for each experiment,  $\sigma_{\text{bench}}$ , and the Monte Carlo uncertainty associated with the particular computational evaluation of the case,  $\sigma_{\text{MCNP}}$ , or:

$$\sigma_{\text{total}} = (\sigma_{\text{bench}}^2 + \sigma_{\text{MCNP}}^2)^{1/2}$$

These values are input into the USLSTATS program in addition to the following parameters, which are the values recommended by the USLSTATS user's manual [2]:

- P, proportion of population falling above lower tolerance level = 0.995 (note that this parameter is required input but is not utilized in the calculation of USL Method 1)
- $1-\gamma$ , confidence on fit = 0.95
- $\alpha$ , confidence on proportion P = 0.95 (note that this parameter is required input but is not utilized in the calculation of USL Method 1)
- $\Delta k_m$ , administrative margin used to ensure subcriticality = 0.05.

These data are followed by triplets of trending parameter value, computed  $k_{\text{eff}}$ , and uncertainty for each case. A confidence band analysis is performed on the data for each trending parameter using USL Method 1.

### 6.8.2.1 HEU Plate Fuel

Five trending parameters are selected for the HEU plate fuel: (1) Energy of the Average neutron Lethargy causing Fission (EALF), (2) U-235 number density, (3) channel spacing, (4) ratio of the number of hydrogen atoms in a unit cell to the number of U-235 atoms in a unit cell (H/U-235), and (5) plate pitch.

The USL generated for each of the trending parameters utilized is provided in Table 6.8-2. All benchmark data used as input to USLSTATS are reported in Table 6.8-4.

#### Energy of the Average neutron Lethargy causing Fission (EALF)

The EALF is used as the first trending parameter for the benchmark cases. The EALF comparison provides a means to observe neutron spectral dependencies or trends. Over the range of applicability, the minimum USL is 0.9254 for the full benchmark set, and 0.9212 for the subset of directly applicable benchmarks.

The HAC ATR cases that are moderated with full-density water fall within the range of applicability. For reduced water density ATR cases, the EALF sometimes exceeds the range of applicability, although the reactivity drops for these cases. None of the HAC MURR or MITR-II cases fall within the range of applicability, even with full-density water, although the most reactive MURR case is only slightly outside the range of applicability (1.62E-07 MeV for Case D8 versus 1.59E-07 MeV upper range). Because the margin to the USL is large, and the EALF is only slightly outside the range of applicability, this behavior is considered to be acceptable. All of the NCT models for MURR, MITR-II, and ATR fall outside the range of applicability for

## **BRR Package Safety Analysis Report**

this parameter. This behavior is expected, because the NCT cases are unmoderated and the EALF is relatively large for these cases. Also, the NCT cases have very low reactivity and are not a concern. Therefore, this parameter is judged to be acceptable for the MURR, MITR-II, and ATR fuels.

### U-235 Number Density

The U-235 number density is used as the second trending parameter for the benchmark cases. Over the range of applicability, the minimum USL is 0.9240 for the full benchmark set, and 0.9209 for the subset of directly applicable benchmarks.

The U-235 number densities for the three plate fuels are as follows:

- MURR: 3.65E-03 atom/b-cm
- MITR-II: 3.68E-03 atom/b-cm
- ATR: variable, see Table 6.2-6

This parameter is within the range of applicability for both MURR and MITR-II fuel. For the ATR fuel element model, the U-235 number densities for plates 1 through 4 and 16 through 19 fall within the range of applicability, while the number densities for plates 5 through 15 exceed the range of applicability (maximum value = 4.22E-03 atom/b-cm). The maximum range of applicability is 3.92E-03 atom/b-cm, so range is exceeded only slightly. Also, the average U-235 number density for the fuel element is 3.73E-03 atom/b-cm, which is within the allowable range. Therefore, application of this USL to the ATR criticality models is considered acceptable.

### Channel Spacing

The channel spacing is used as the third trending parameter for the benchmark cases. Over the range of applicability, the minimum USL is 0.9225 for the full benchmark set, and 0.9209 for the subset of directly applicable benchmarks.

The maximum modeled channel spacing for the three plate fuels are as follows:

- MURR: 0.094-in
- MITR-II: 0.116-in
- ATR: 0.092-in (excluding plates 1 and 19)

The channel spacing for all three plate type fuels exceeds the maximum channel spacing of 0.078-in of the benchmark experiments. However, this parameter is only slightly larger than the maximum benchmark experiment channel spacing, and was maximized in order to maximize model reactivity. Extrapolation of the USL equation ( $0.9218 - 1.1029E-02 \cdot X$ ) to the maximum channel spacing of 0.116-in yields a USL of 0.9205, which is essentially identical to the non-extrapolated value of 0.9209. Therefore, application of the non-extrapolated USL (0.9209) to the criticality models is considered acceptable.

### H/U-235 Atom Ratio

The H/U-235 atom ratio is used as the fourth trending parameter for the benchmark cases. The H/U-235 atom ratio is defined here as the ratio of hydrogen atoms to U-235 atoms in a unit cell. This parameter is computed by the following equation:

$$NH \cdot C / (NU_{235} \cdot M)$$

where,

NH is the hydrogen number density

C is the channel spacing

NU235 is the U-235 number density

M is the fuel meat width

Over the range of applicability, the minimum USL is 0.9257 for the full benchmark set, and 0.9209 for the subset of directly applicable benchmarks.

- MURR: The H/U-235 value may be computed as:

$$6.687\text{E-}02 * 0.094 / (3.6519\text{E-}03 * 0.02) = 86.1$$

Therefore, H/U-235 of the most reactive MURR models is acceptably within the range of applicability of the benchmarks.

- MITR-II: The H/U-235 atom ratio may be computed as:

$$6.687\text{E-}02 * 0.116 / (3.6835\text{E-}03 * 0.03) = 70.2$$

Therefore, H/U-235 of the most reactive MITR-II models is acceptably within the range of applicability of the benchmarks.

- ATR: Using the maximum ATR plate U-235 number density, the H/U-235 value may be computed as:

$$6.687\text{E-}02 * 0.092 / (4.224\text{E-}03 * 0.02) = 72.8$$

Therefore, H/U-235 of the most reactive ATR models is acceptably within the range of applicability of the benchmarks.

### Pitch

The fuel plate pitch is used as the fifth trending parameter for the benchmark cases. Over the range of applicability, the minimum USL is 0.9225 for the full benchmark set, and 0.9209 for the subset of directly applicable benchmarks.

- MURR: The fuel plate pitch is fixed at 0.13-in for all fuel element models. This pitch falls within the range of the benchmark experiments.
- MITR-II: The fuel plate pitch is fixed at 0.16-in for all fuel element models. The maximum pitch of the benchmark models is 0.128-in, so the pitch in the models exceeds the range of the benchmarks. However, the pitch is directly related to system moderation, and the acceptability of the EALF indicator demonstrates that MCNP is performing acceptably for thermal conditions. Therefore, this parameter is considered to be acceptable.
- ATR: The fuel plate pitch is fixed at 0.128-in for all ATR models (excluding the pitch for plates 1 and 19, which is slightly bigger because these plates are thicker). This pitch falls within the range of the benchmark experiments.

### Recommended USL

For the full benchmark set, the minimum USL is 0.9225, while for the subset of directly applicable benchmarks, the USL is 0.9209. Therefore, the USL is trending lower for the subset of directly applicable benchmarks. Note, however, that the average  $k_{\text{eff}} = 0.992$  for both the full benchmark set and directly applicable subset. The USL could likely be improved by development of additional benchmark models, but given the large margins to the most reactive case, the lower value (0.9209) is conservatively selected as the USL for this analysis.

#### **6.8.2.2 LEU Plate Fuel**

The HEU plate fuel USL of 0.9209 is applied to the LEU plate fuels in the SFB.

#### **6.8.2.3 PULSTAR UO<sub>2</sub> Fuel**

The HEU plate fuel USL of 0.9209 is applied to PULSTAR fuel.

#### **6.8.2.4 TRIGA Fuel**

Three trending parameters are selected for the TRIGA fuel: (1) Energy of the Average neutron Lethargy causing Fission (EALF), (2) U-235 number density, and (3) ratio of the number of hydrogen atoms to U-235 atoms in the fuel matrix (H/U-235).

The USL generated for each of the trending parameters utilized is provided in Table 6.8-3. All benchmark data used as input to USLSTATS are reported in Table 6.8-5.

##### Energy of the Average neutron Lethargy causing Fission (EALF)

The EALF is used as the first trending parameter for the benchmark cases. The EALF comparison provides a means to observe neutron spectral dependencies or trends. Over the range of applicability, the minimum USL is 0.9301 for the subset consisting of 10 HEU solution benchmarks and 2 TRIGA benchmarks.

All HAC TRIGA models fall within the range of applicability for this parameter, including the most reactive TRIGA case (Case D63). None of the NCT TRIGA models fall within the range of applicability, although this behavior is expected, because the NCT cases are unmoderated (except for the hydrogen in the fuel matrix). Also, because the NCT cases are much lower in reactivity than the HAC cases, this parameter is considered to be acceptable.

##### U-235 Number Density

The U-235 number density is used as the second trending parameter for the benchmark cases. Over the range of applicability, the minimum USL is 0.9306 for the subset consisting of 10 HEU solution benchmarks and 2 TRIGA benchmarks.

The U-235 number density in the BRR TRIGA models is 9.0406E-04 atom/b-cm, which is only slightly outside the maximum range of applicability of the benchmark models (EALF = 8.5392E-04 atom/b-cm). Therefore, this parameter is considered acceptable.

##### H/U-235 Atom Ratio

The H/U-235 atom ratio is used as the third trending parameter for the benchmark cases. Over the range of applicability, the minimum USL is 0.9318 for the subset consisting of 10 HEU solution benchmarks and 2 TRIGA benchmarks. The H/U-235 atom ratio is 62.0, which is only



slightly outside the minimum range of applicability of the benchmark models ( $H/U-235 = 68.2$ ). Therefore, this parameter is considered acceptable.

#### Recommended USL

The minimum USL of 0.9301 occurs for the EALF parameter over the subset of HEU solution and TRIGA benchmarks. Because the USL for the HEU plate fuel is lower (0.9209), and only two TRIGA benchmarks are available, the USL of 0.9209 is recommended for use in the TRIGA analysis to add additional margin.

**Table 6.8-1 – Benchmark Experiments Utilized**

Series	Title
<b>HEU Plate Fuel (MURR, MITR-II, ATR)</b>	
HEU-COMP-THERM-022	SPERT III Stainless-Steel-Clad Plate-Type Fuel in Water
HEU-MET-THERM-006	SPERT-D Aluminum-Clad Plate-Type Fuel in Water, Dilute Uranyl Nitrate, or Borated Uranyl Nitrate
HEU-MET-THERM-022	Advanced Test Reactor: Serpentine Arrangement of Highly Enriched Water-Moderated Uranium-Aluminide Fuel Plates Reflected by Beryllium
<b>TRIGA Fuel</b>	
IEU-COMP-THERM-003	TRIGA Mark II Reactor: U(20) – Zirconium Hydride Fuel Rods in Water with Graphite Reflector
HEU-SOL-THERM-001	Minimally Reflected Cylinders of Highly Enriched Solutions of Uranyl Nitrate
LEU-SOL-THERM-003	Full and Truncated Bare Spheres of 10% Enriched Uranyl Nitrate Water Solutions

**Table 6.8-2 – USL Results for HEU Plate Fuel**

<b>Trending Parameter (X)</b>	<b>Minimum USL Over Range of Applicability</b>	<b>Range of Applicability</b>
<b>35 Experiment Set</b>		
EALF (MeV)	0.9254	$5.22210\text{E-}08 \leq X \leq 1.58510\text{E-}07$
U-235 Number Density (atom/b-cm)	0.9240	$1.84900\text{E-}03 \leq X \leq 3.92600\text{E-}03$
Channel spacing (in)	0.9225	$6.45700\text{E-}02 \leq X \leq 7.80000\text{E-}02$
H/U-235	0.9257	$65.100 \leq X \leq 116.50$
Pitch (in)	0.9225	$0.12457 \leq X \leq 0.12800$
<b>17 Experiment Set</b>		
EALF (MeV)	0.9212	$5.22210\text{E-}08 \leq X \leq 1.58510\text{E-}07$
U-235 Number Density (atom/b-cm)	0.9209	$1.84900\text{E-}03 \leq X \leq 3.92600\text{E-}03$
Channel spacing (in)	0.9209	$6.45700\text{E-}02 \leq X \leq 7.80000\text{E-}02$
H/U-235	0.9209	$66.0 \leq X \leq 116.50$
Pitch (in)	0.9209	$0.12457 \leq X \leq 0.12800$

**Table 6.8-3 – USL Results for TRIGA Fuel**

<b>Trending Parameter (X)</b>	<b>Minimum USL Over Range of Applicability</b>	<b>Range of Applicability</b>
<b>21 Experiment Set</b>		
EALF (MeV)	0.9320	$3.42760\text{E-}08 \leq X \leq 2.95740\text{E-}07$
U-235 Number Density (atom/b-cm)	0.9331	$4.33640\text{E-}05 \leq X \leq 8.53920\text{E-}04$
H/U-235	0.9350	$68.200 \leq X \leq 1437.5$
<b>12 Experiment Set (HEU solution + TRIGA)</b>		
EALF (MeV)	0.9301	$4.29310\text{E-}08 \leq X \leq 2.95740\text{E-}07$
U-235 Number Density (atom/b-cm)	0.9306	$1.31030\text{E-}04 \leq X \leq 8.53920\text{E-}04$
H/U-235	0.9318	$68.200 \leq X \leq 499.40$
<b>11 Experiment Set (LEU solution + TRIGA)</b>		
EALF (MeV)	0.9338	$3.42760\text{E-}08 \leq X \leq 8.71200\text{E-}08$
U-235 Number Density (atom/b-cm)	0.9339	$4.33640\text{E-}05 \leq X \leq 3.68010\text{E-}04$
H/U-235	0.9340	$150.10 \leq X \leq 1437.5$

**Table 6.8-4 – Benchmark Experiment Data for HEU Plate Fuel**

Case ID	Filename	k	$\sigma_{mcnp}$	$\sigma_{bench}$	$\sigma_{total}$	EALF (MeV)	U-235 (atom/b-cm)	Chanel Width (in)	H/U-235	Pitch (in)
BA1	HCT022_C01	0.98895	0.00060	0.0081	0.0081	9.528E-08	3.3155E-03	0.06457	65.1	0.12457
BA2	HCT022_C02	0.98980	0.00061	0.0081	0.0081	9.665E-08	3.3155E-03	0.06457	65.1	0.12457
BA3	HCT022_C03	0.98985	0.00063	0.0081	0.0081	9.809E-08	3.3155E-03	0.06457	65.1	0.12457
BA4	HCT022_C04	0.98856	0.00060	0.0081	0.0081	9.917E-08	3.3155E-03	0.06457	65.1	0.12457
BA5	HCT022_C05	0.98909	0.00063	0.0081	0.0081	9.587E-08	3.3155E-03	0.06457	65.1	0.12457
BA6	HCT022_C06	0.98902	0.00059	0.0081	0.0081	9.840E-08	3.3155E-03	0.06457	65.1	0.12457
BA7	HCT022_C07	0.98963	0.00056	0.0081	0.0081	9.890E-08	3.3155E-03	0.06457	65.1	0.12457
BA8	HCT022_C08	0.98908	0.00057	0.0081	0.0081	9.951E-08	3.3155E-03	0.06457	65.1	0.12457
BA9	HCT022_C09	0.98840	0.00056	0.0081	0.0081	9.589E-08	3.3155E-03	0.06457	65.1	0.12457
BA10	HCT022_C10	0.98845	0.00060	0.0081	0.0081	9.963E-08	3.3155E-03	0.06457	65.1	0.12457
BA11	HCT022_C11	0.98930	0.00060	0.0081	0.0081	1.001E-07	3.3155E-03	0.06457	65.1	0.12457
BA12	HMT006_C01	0.99240	0.00082	0.0044	0.0045	8.481E-08	1.8490E-03	0.06457	116.5	0.12457
BA13	HMT006_C02	0.99331	0.00088	0.0040	0.0041	7.044E-08	1.8490E-03	0.06457	116.5	0.12457
BA14	HMT006_C03	0.99740	0.00072	0.0040	0.0041	6.338E-08	1.8490E-03	0.06457	116.5	0.12457
BA15	HMT006_C04	0.99282	0.00081	0.0040	0.0041	6.185E-08	1.8490E-03	0.06457	116.5	0.12457
BA16	HMT006_C05	0.99230	0.00079	0.0040	0.0041	5.852E-08	1.8490E-03	0.06457	116.5	0.12457
BA17	HMT006_C06	0.99010	0.00071	0.0040	0.0041	5.615E-08	1.8490E-03	0.06457	116.5	0.12457
BA18	HMT006_C07	0.98783	0.00073	0.0040	0.0041	5.432E-08	1.8490E-03	0.06457	116.5	0.12457
BA19	HMT006_C08	0.98428	0.00076	0.0040	0.0041	5.245E-08	1.8490E-03	0.06457	116.5	0.12457
BA20	HMT006_C09	0.98657	0.00072	0.0040	0.0041	5.222E-08	1.8490E-03	0.06457	116.5	0.12457
BA21	HMT006_C10	0.99885	0.00085	0.0040	0.0041	8.220E-08	1.8490E-03	0.06457	116.5	0.12457
BA22	HMT006_C11	0.98965	0.00081	0.0040	0.0041	6.236E-08	1.8490E-03	0.06457	116.5	0.12457
BA23	HMT006_C12	0.99403	0.00070	0.0040	0.0041	5.415E-08	1.8490E-03	0.06457	116.5	0.12457

(continued)

Table 6.8-4 – Benchmark Experiment Data for HEU Plate Fuel (concluded)

Case ID	Filename	k	$\sigma_{mcnp}$	$\sigma_{bench}$	$\sigma_{total}$	EALF (MeV)	U-235 (atom/b-cm)	Chanel Width (in)	H/U-235	Pitch (in)
BA24	HMT006_C13	1.01283	0.00086	0.0040	0.0041	8.231E-08	1.8490E-03	0.06457	116.5	0.12457
BA25	HMT006_C14	0.98495	0.00071	0.0061	0.0061	5.715E-08	1.8490E-03	0.06457	116.5	0.12457
BA26	HMT006_C15	0.98128	0.00077	0.0040	0.0041	5.654E-08	1.8490E-03	0.06457	116.5	0.12457
BA27	HMT006_C16	0.99241	0.00078	0.0040	0.0041	6.330E-08	1.8490E-03	0.06457	116.5	0.12457
BA28	HMT006_C17	0.98934	0.00082	0.0040	0.0041	7.405E-08	1.8490E-03	0.06457	116.5	0.12457
BA29	HMT006_C18	0.99282	0.00087	0.0040	0.0041	8.003E-08	1.8490E-03	0.06457	116.5	0.12457
BA30	HMT006_C19	0.99360	0.00068	0.0040	0.0041	5.243E-08	1.8490E-03	0.06457	113.9	0.12457
BA31	HMT006_C20	0.99275	0.00076	0.0040	0.0041	6.471E-08	1.8490E-03	0.06457	113.7	0.12457
BA32	HMT006_C21	0.99469	0.00077	0.0040	0.0041	6.917E-08	1.8490E-03	0.06457	113.7	0.12457
BA33	HMT006_C22	0.99670	0.00080	0.0040	0.0041	7.407E-08	1.8490E-03	0.06457	113.6	0.12457
BA34	HMT006_C23	1.00132	0.00080	0.0040	0.0041	7.670E-08	1.8490E-03	0.06457	113.5	0.12457
BA35	HMT022_C01	0.99179	0.00013	0.0035	0.0035	1.585E-07	3.9260E-03	0.078	66.0	0.12800

**Table 6.8-5 – Benchmark Experiment Data for TRIGA Fuel**

Case ID	Filename	k	$\sigma_{mcnp}$	$\sigma_{bench}$	$\sigma_{total}$	EALF (MeV)	U-235 (atom/b-cm)	H/U-235
BT1	HST001_C01	0.99686	0.00068	0.0060	0.0060	8.147E-08	3.4777E-04	181.8
BT2	HST001_C02	0.99418	0.00072	0.0072	0.0072	2.763E-07	8.2771E-04	70.6
BT3	HST001_C03	1.00015	0.00067	0.0035	0.0036	8.014E-08	3.4118E-04	185.7
BT4	HST001_C04	0.99470	0.00069	0.0053	0.0053	2.957E-07	8.5392E-04	68.2
BT5	HST001_C05	0.99727	0.00059	0.0049	0.0049	4.293E-08	1.3103E-04	499.4
BT6	HST001_C06	1.00351	0.00057	0.0046	0.0046	4.450E-08	1.4240E-04	458.8
BT7	HST001_C07	0.99609	0.00071	0.0040	0.0041	7.710E-08	3.2800E-04	193.3
BT8	HST001_C08	0.99648	0.00067	0.0038	0.0039	8.174E-08	3.4777E-04	181.8
BT9	HST001_C09	0.99068	0.00068	0.0054	0.0054	2.954E-07	8.5392E-04	68.2
BT10	HST001_C10	0.99130	0.00055	0.0054	0.0054	4.609E-08	1.5266E-04	427.4
BT11	ICT003_C01	0.99699	0.00052	0.0056	0.0056	8.712E-08	3.6801E-04	150.1
BT12	ICT003_C02	1.00145	0.00052	0.0056	0.0056	8.678E-08	3.6801E-04	150.1
BT13	LST003_C01	0.99485	0.00044	0.0039	0.0039	4.098E-08	7.6403E-05	770.3
BT14	LST003_C02	0.99401	0.00042	0.0042	0.0042	3.921E-08	6.8143E-05	877.6
BT15	LST003_C03	0.99902	0.00041	0.0042	0.0042	3.886E-08	6.7111E-05	897.0
BT16	LST003_C04	0.99249	0.00039	0.0042	0.0042	3.875E-08	6.5820E-05	913.2
BT17	LST003_C05	0.99573	0.00035	0.0048	0.0048	3.593E-08	5.2398E-05	1173.4
BT18	LST003_C06	0.99694	0.00031	0.0049	0.0049	3.564E-08	5.0849E-05	1213.1
BT19	LST003_C07	0.99602	0.00031	0.0049	0.0049	3.554E-08	4.9817E-05	1239.8
BT20	LST003_C08	0.99930	0.00028	0.0052	0.0052	3.447E-08	4.4138E-05	1411.6
BT21	LST003_C09	0.99606	0.00027	0.0052	0.0052	3.428E-08	4.3364E-05	1437.5

## 6.9 Appendices

### 6.9.1 References

1. MCNP5, “MCNP – A General Monte Carlo N-Particle Transport Code, Version 5; Volume II: User’s Guide,” LA-CP-03-0245, Los Alamos National Laboratory, April 2003. MCNP5 is distributed by the Radiation Safety Information Computational Center (www-rsicc.ornl.gov), Release C00710MNYCP02 (Windows PC).
2. USLSTATS, “USLSTATS: A Utility To Calculate Upper Subcritical Limits For Criticality Safety Applications,” Version 1.4.2, Oak Ridge National Laboratory, April 23, 2003. Note: USLSTATS is described in Appendix C, *User’s Manual for USLSTATS V1.0*, in NUREG/CR-6361 *Criticality Benchmark Guide for Light-Water-Reactor Fuel in Transportation and Storage Packages*, March 1997. No new user’s manual has been developed for later updates to the program.
3. *International Handbook of Evaluated Criticality Safety Benchmark Experiments*, Nuclear Energy Agency, NEA/NSC/DOC(95)03, September 2006.
4. *Standard Composition Library*, ORNL/TM-2005/39, Version 5, Vol. III, Section M8, April 2005.

### 6.9.2 Parametric Evaluations to Determine the Most Reactive Fuel Geometries

#### 6.9.2.1 ATR Fuel Parametric Evaluation

A parametric analysis is performed to determine the impacts of various fuel element tolerances on the reactivity. This parametric analysis considers the effects of a number of parameters, such as fuel meat arc length, fuel meat thickness, channel spacing, and active fuel length.

Because the ATR fuel element is complex, with 19 unique fuel plates and 19 unique fuel material descriptions, performing this parametric study on the actual fuel element geometry would be cumbersome. Rather, the approach utilized is to perform the parametric study on a system of 19 identical flat plates. This geometry mimics the ATR fuel element to determine trends in the data. Note that the reactivity of the 19 flat plate model is not identical to the reactivity of an actual ATR fuel element due to geometrical and material differences, although the trends are the same. The most reactive model variations are then incorporated into the ATR fuel element model.

In the parametric models, 1200 g U-235 is equally distributed between 19 identical flat plates. The base configuration consists of plates with a fuel meat width of 6.7355 cm (the average meat arc length for an ATR fuel element), active fuel height of 48-in, fuel meat thickness of 0.02-in, fuel cladding thickness of 0.015-in (total plate thickness of 0.050-in), and fuel channel spacing of 0.078-in. A total of 12 parametric models are developed, as summarized below.

Case ID	ATR Parametric Study Case Description
P1	Base case
P2	Increase width of fuel meat by 0.1-in
P3	Decrease width of fuel meat by 0.1-in
P4	Increase thickness of fuel meat by 0.002-in
P5	Decrease thickness of fuel meat by 0.002-in
P6	Increase thickness of fuel meat by 0.002-in but decrease the cladding thickness to maintain a nominal plate thickness
P7	Decrease thickness of fuel meat by 0.002-in but increase the cladding thickness to maintain a nominal plate thickness
P8	Increase water channel spacing to 0.085-in
P9	Increase water channel spacing to 0.085-in by reducing the cladding thickness
P10	Decrease active fuel length to 47.0-in
P11	Reduce cladding thickness to the minimum value of 0.008-in
P12	Combine cases P2 and P9

The geometry of Case P1 is shown in Figure 6.9-1. The fuel element is reflected by approximately 12-in of water.

In Cases P2 through P12, each case is identical to the base case P1 with the exception of the changes identified in the table above. The pitch, which is the sum of the plate thickness and channel spacing, is treated as a dependant variable and is allowed to vary as the independent parameters are changed. For example, in Case P5, decreasing the thickness of the fuel meat decreases the pitch, although the channel spacing remains constant. The detailed model description of the parametric cases is summarized in Table 6.9-1.

The results of the parametric analysis are summarized in Table 6.9-2. Because the uncertainty in the calculation is  $\sim 0.001$ , a difference of at least 0.002 (2 milli-k, abbreviated mk) between the various cases is required in order to distinguish a real effect from statistical fluctuation. The results indicate a reactivity increase of 4.3 mk for Case P2, when the width of the fuel meat is increased, and a decrease of 5.4 mk for Case P3, when the width of the fuel meat is decreased. Therefore, reactivity increases when the width of the fuel meat is maximized.

The nominal thickness of the fuel meat is 0.02-in. No tolerance on the fuel meat is provided on the fuel fabrication drawings because the fuel plates are fabricated using a rolling process. A thickness tolerance of 0.002-in ( $\pm 10\%$ ) is assumed for computational purposes. In Cases P4 and P5, the fuel meat thickness is adjusted for constant channel spacing and variable pitch, while for Cases P6 and P7 the fuel meat thickness is adjusted for constant plate thickness and nominal pitch. The reactivity fluctuations are within 2 mk in all four cases, and it is concluded that a nominal fuel meat thickness of 0.02-in is acceptable for modeling purposes.

In Case P8, the water channel spacing is increased to 0.085-in (increase in pitch), while in Case P9 the water channel spacing is increased by artificially reducing the cladding thickness



(nominal pitch). Both cases P8 and P9 show large reactivity gains of 9.6 and 12.9 mk, respectively, indicating that reactivity is maximized when the water channel spacing is maximized.

In Case P10, the active fuel length is reduced to a lower bound value of 47.0-in. The reactivity increase is within statistical fluctuation. It may be inferred that increasing the active fuel length would also result in a reactivity effect within statistical fluctuation.

In Case P11, the cladding thickness is reduced to the minimum value of 0.008-in, and the reactivity increases by 5.5 mk. This reactivity gain is likely due to the more compact geometry, as the pitch reduces considerably. This scenario is not directly applicable to an ATR fuel element because the pitch is fixed by the side plates and such a configuration is not possible.

The only cases that show a statistically significant increase are P2, P8, P9, and P11. In Case P12, the increased fuel meat width of Case P2 and increased channel spacing of Case P9 are combined. This model geometry bounds Case P8, and Case P11 is incorporated in an approximate manner because the cladding thickness has been reduced to accommodate the larger channel. The reactivity of Case P12 represents an increase of 19.5 mk over base Case P1.

Based on the parametric evaluation, an optimized fuel model is developed with both increased channel spacing and increased meat arc length. In this model, a nominal pitch is utilized (i.e., the centerline radial locations of the 19 plates are the same in each model, as indicated in Table 6.2-4), and the channel spacing is increased by removing cladding. This approach is highly conservative, because it is unlikely (if not impossible) to maximize the channel spacing between each plate. In an actual fuel element, maximizing the channel spacing between two plates would likely minimize the channel spacing between the next two plates, as the overall plate thickness is held to a rather tight tolerance. In the most reactive HAC models, large channel spacings are utilized, as indicated in Section 6.2.3.

### **6.9.2.2 MURR Fuel Parametric Evaluation**

A parametric analysis is performed to determine the impacts of various fuel element tolerances on the reactivity. In the parametric analysis for ATR fuel, it is determined that reactivity is maximized by maximizing the arc length of the fuel meat and the channel spacing. Because ATR and MURR are both plate-type and utilize similar enrichments, it is expected that MURR fuel will also experience maximum reactivity with these parameters maximized. Therefore, the parametric analysis considers the effects of only the following parameters: fuel meat arc length/width, channel spacing, and active fuel length.

The base configuration for MURR consists of plates with a nominal meat arc length/width, nominal active fuel length, and nominal channel spacing. In each parametric case, the indicated parameter is modified in comparison with the base case. The minimum, nominal, and maximum meat arc lengths are provided in Table 6.9-3. The minimum meat arc lengths are obtained directly from Figure 6.2-2 (see dimension B). The maximum meat arc lengths are computed by subtracting twice the fuel-free width ( $2 \times 0.115$ -in) from the maximized plate width (dimension C of Figure 6.2-2 + 0.010-in). The nominal value is computed as the average of the minimum and maximum values. The detailed model description of the parametric cases is summarized in Table 6.9-4. A total of 7 parametric models are developed, as summarized below.

Case ID	MURR Parametric Study Case Description
PM1	Base MURR case
PM2	Decrease active fuel length to minimum value
PM3	Increase active fuel length to maximum value
PM4	Increase channel spacing to 0.088-in
PM5	Decrease width of fuel meat to minimum value
PM6	Increase width of fuel meat to maximum value
PM7	Combine cases PM4 and PM6

The geometry of base MURR parametric Case PM1 is shown in Figure 6.9-1. The fuel element is reflected with approximately 12-in of water. Note that, unlike the ATR parametric model, the MURR parametric model is an explicit geometrical representation of the MURR fuel element. Although the ATR and MURR fuel elements appear to be rather similar, because all MURR plates utilize the same fuel number densities and fuel meat to side structure distance, performing the parametric study on the actual geometry for MURR fuel is relatively straightforward.

The results of the parametric analysis are summarized in Table 6.9-5. Because the uncertainty in the calculation is  $\sim 0.001$ , a difference of at least 0.002 (2 milli-k, abbreviated mk) between the various cases is required in order to distinguish a real effect from statistical fluctuation. The variation of the active fuel length has a negligible effect on the results. Also, the fuel shows a positive reactivity increase of 23.8 mk when the fuel meat is widened and the channel spacing is increased (compare Case PM7 with Case PM1). This result is consistent with the results obtained in the ATR fuel parametric analysis. Therefore, in all MURR fuel models, the fuel is modeled with nominal active fuel length, maximum fuel width, and maximum channel spacing. The maximum channel spacing is achieved by artificially reducing the cladding thickness. In the most reactive HAC models, a large channel spacing is utilized, as indicated in Section 6.2.1.

### 6.9.2.3 MITR-II Fuel Parametric Evaluation

A parametric analysis is performed to determine the impacts of various fuel element tolerances on the reactivity. In the parametric analysis for ATR and MURR fuel, it is determined that reactivity is maximized by maximizing the arc length of the fuel meat and the channel spacing. Because ATR, MURR, and MITR-II are all plate-type and utilize similar enrichments, it is expected that MITR-II fuel will also experience maximum reactivity with these parameters maximized. Therefore, the parametric analysis considers the effects of only the following parameters: fuel meat arc length/width, channel spacing, and active fuel length.

The base configuration for MITR-II consists of plates with a nominal meat arc length/width, nominal active fuel length, and nominal channel spacing. In each parametric case, the indicated parameter is modified in comparison with the base case. The detailed model description of the parametric cases is summarized in Table 6.9-6. A total of 7 parametric models are developed, as summarized below.

Case ID	MITR-II Parametric Study Case Description
PN1	Base MITR-II case
PN2	Decrease active fuel length to minimum value
PN3	Increase active fuel length to maximum value
PN4	Increase channel spacing to 0.094-in
PN5	Decrease width of fuel meat to minimum value
PN6	Increase width of fuel meat to maximum value
PN7	Combine cases PN4 and PN6

The geometry of base MITR-II parametric Case PN1 is shown in Figure 6.9-1. The fuel element is reflected with approximately 12-in of water. Note that, like the MURR parametric model, the MITR-II parametric model is an explicit geometrical representation of the MITR-II fuel element.

The results of the parametric analysis are summarized in Table 6.9-7. Because the uncertainty in the calculation is  $\sim 0.001$ , a difference of at least 0.002 (2 milli-k, abbreviated mk) between the various cases is required in order to distinguish a real effect from statistical fluctuation. The variation of the active fuel length has a negligible effect on the results. Although Case PN2 shows a positive reactivity increase when the active fuel height is reduced, because the increase is less than 2 mk, it is concluded that the increase is simply statistical fluctuation. Also, the fuel shows a positive reactivity increase of 11.0 mk when the fuel meat is widened and the channel spacing is increased (compare Case PN7 with Case PN1). This result is consistent with the results obtained in the ATR and MURR fuel parametric analyses. Therefore, in all MITR-II fuel models, the fuel is modeled with nominal active fuel length, maximum fuel width, and maximum channel spacing. The maximum channel spacing is achieved by artificially reducing the cladding thickness. In the most reactive HAC models, a large channel spacing is utilized, as indicated in Section 6.2.2.

Table 6.9-1 – ATR Parametric Analysis Input Data

Parameter	P1	P2	P3	P4	P5	P6
Fuel Arc (cm)	6.7355	6.9895	6.4815	6.7355	6.7355	6.7355
Meat thickness (in)	0.02	0.02	0.02	0.022	0.018	0.022
Active fuel height (in)	48	48	48	48	48	48
Channel (in)	0.078	0.078	0.078	0.078	0.078	0.078
Cladding (in)	0.015	0.015	0.015	0.015	0.015	0.014
Total plate (in)	0.050	0.050	0.050	0.052	0.048	0.050
Pitch (in)	0.128	0.128	0.128	0.130	0.126	0.128
Volume (cm <sup>3</sup> )	41.7164	43.2895	40.1432	45.8880	37.5447	45.8880
U-235 (g)	63.2	63.2	63.2	63.2	63.2	63.2
U-235 density (g/cm <sup>3</sup> )	1.51	1.46	1.57	1.38	1.68	1.38
UAlx+Al density (g/cm <sup>3</sup> )	3.86	3.81	3.91	3.74	4.00	3.74
N U-234	2.4865E-05	2.3962E-05	2.5840E-05	2.2605E-05	2.7628E-05	2.2605E-05
N U-235	3.8789E-03	3.7380E-03	4.0309E-03	3.5263E-03	4.3099E-03	3.5263E-03
N U-236	1.4382E-05	1.3859E-05	1.4945E-05	1.3074E-05	1.5980E-05	1.3074E-05
N U-238	2.0576E-04	1.9828E-04	2.1382E-04	1.8705E-04	2.2862E-04	1.8705E-04
N U-Al	5.0157E-02	5.0391E-02	4.9905E-02	5.0742E-02	4.9442E-02	5.0742E-02
Total	5.4281E-02	5.4365E-02	5.4190E-02	5.4491E-02	5.4024E-02	5.4491E-02

Parameter	P7	P8	P9	P10	P11	P12
Fuel Arc (cm)	6.7355	6.7355	6.7355	6.7355	6.7355	6.9895
Meat thickness (in)	0.018	0.02	0.02	0.02	0.02	0.02
Active fuel height (in)	48	48	48	47	48	48
Channel (in)	0.078	0.085	0.085	0.078	0.078	0.085
Cladding (in)	0.016	0.015	0.0115	0.015	0.008	0.0115
Total plate (in)	0.050	0.050	0.0430	0.050	0.036	0.0430
Pitch (in)	0.128	0.135	0.128	0.128	0.114	0.128
Volume (cm <sup>3</sup> )	37.5447	41.7164	41.7164	40.8473	41.7164	43.2895
U-235 (g)	63.2	63.2	63.2	63.2	63.2	63.2
U-235 density (g/cm <sup>3</sup> )	1.68	1.51	1.51	1.55	1.51	1.46
UAlx+Al density (g/cm <sup>3</sup> )	4.00	3.86	3.86	3.89	3.86	3.81
N U-234	2.7628E-05	2.4865E-05	2.4865E-05	2.5394E-05	2.4865E-05	2.3962E-05
N U-235	4.3099E-03	3.8789E-03	3.8789E-03	3.9615E-03	3.8789E-03	3.7380E-03
N U-236	1.5980E-05	1.4382E-05	1.4382E-05	1.4688E-05	1.4382E-05	1.3859E-05
N U-238	2.2862E-04	2.0576E-04	2.0576E-04	2.1014E-04	2.0576E-04	1.9828E-04
N U-Al	4.9442E-02	5.0157E-02	5.0157E-02	5.0020E-02	5.0157E-02	5.0391E-02
Total	5.4024E-02	5.4281E-02	5.4281E-02	5.4232E-02	5.4281E-02	5.4365E-02

**Table 6.9-2 – ATR Parametric Analysis Results**

<b>Case ID</b>	<b>Filename</b>	<b><math>k_{\text{eff}}</math></b>	<b><math>\sigma</math></b>	<b><math>k_s</math> (<math>k+2\sigma</math>)</b>	<b><math>\Delta</math> from P1 (mk)</b>
P1	HS_ATR_P1	0.46601	0.00096	0.46793	--
P2	HS_ATR_P2	0.47015	0.00102	0.47219	4.3
P3	HS_ATR_P3	0.46045	0.00102	0.46249	-5.4
P4	HS_ATR_P4	0.46403	0.00101	0.46605	-1.9
P5	HS_ATR_P5	0.46442	0.00111	0.46664	-1.3
P6	HS_ATR_P6	0.46753	0.00105	0.46963	1.7
P7	HS_ATR_P7	0.46683	0.00101	0.46885	0.9
P8	HS_ATR_P8	0.47528	0.00112	0.47752	9.6
P9	HS_ATR_P9	0.47879	0.00100	0.48079	12.9
P10	HS_ATR_P10	0.46704	0.00106	0.46916	1.2
P11	HS_ATR_P11	0.47123	0.00108	0.47339	5.5
<b>P12</b>	<b>HS_ATR_P12</b>	<b>0.48534</b>	<b>0.00104</b>	<b>0.48742</b>	<b>19.5</b>

**Table 6.9-3 – MURR Meat Arc Lengths**

<b>Plate</b>	<b>Minimum (in)</b>	<b>Nominal (in)</b>	<b>Maximum (in)</b>
1	1.643	1.708	1.773
2	1.745	1.810	1.875
3	1.847	1.912	1.977
4	1.950	2.015	2.080
5	2.052	2.117	2.182
6	2.154	2.219	2.284
7	2.256	2.321	2.386
8	2.358	2.423	2.488
9	2.460	2.525	2.590
10	2.562	2.627	2.692
11	2.664	2.729	2.794
12	2.766	2.831	2.896
13	2.868	2.933	2.998
14	2.971	3.036	3.101
15	3.073	3.138	3.203
16	3.175	3.240	3.305
17	3.277	3.342	3.407
18	3.379	3.444	3.509
19	3.481	3.546	3.611
20	3.583	3.648	3.713
21	3.685	3.750	3.815
22	3.787	3.852	3.917
23	3.889	3.954	4.019
24	3.992	4.057	4.122

**Table 6.9-4 – MURR Parametric Analysis Input Data**

Parameter	PM1/PM4	PM2	PM3	PM5	PM6/PM7
Fuel width (in)	nominal	nominal	nominal	nominal-0.065	nominal+0.065
Meat thickness (in)	0.02	0.02	0.02	0.02	0.02
Active fuel height (in)	24	23.25	24.75	24	24
Channel (in)	0.08/0.088	0.08	0.08	0.08	0.08/0.088
Cladding (in)	0.015/0.011	0.015	0.015	0.015	0.015/0.011
Total plate (in)	0.050/0.042	0.050	0.050	0.050	0.050/0.042
Pitch (in)	0.13	0.13	0.13	0.13	0.13
Meat volume (cm <sup>3</sup> )	544.13	527.13	561.14	531.86	556.40
U-235 mass (g)	785	785	785	785	785
U-235 den (g/cm <sup>3</sup> )	1.44	1.49	1.40	1.48	1.41
UAlx+Al den (g/cm <sup>3</sup> )	3.80	3.84	3.76	3.82	3.77
N-234 (atom/b-cm)	2.3694E-05	2.4458E-05	2.2976E-05	2.4241E-05	2.3171E-05
N-235 (atom/b-cm)	3.6962E-03	3.8154E-03	3.5842E-03	3.7815E-03	3.6147E-03
N-236 (atom/b-cm)	1.3704E-05	1.4146E-05	1.3289E-05	1.4020E-05	1.3402E-05
N-238 (atom/b-cm)	1.9607E-04	2.0239E-04	1.9012E-04	2.0059E-04	1.9174E-04
N-Al (atom/b-cm)	5.0460E-02	5.0262E-02	5.0646E-02	5.0319E-02	5.0596E-02
Total (atom/b-cm)	5.4390E-02	5.4319E-02	5.4457E-02	5.4339E-02	5.4439E-02

**Table 6.9-5 – MURR Parametric Analysis Results**

Case ID	Filename	k <sub>eff</sub>	σ	k <sub>s</sub> (k+2σ)	Δ from PM1 (mk)
PM1	HS_MURR3_P1	0.50645	0.00110	0.50865	--
PM2	HS_MURR3_P2	0.50715	0.00099	0.50913	0.5
PM3	HS_MURR3_P3	0.50612	0.00109	0.50830	-0.3
PM4	HS_MURR3_P4	0.52638	0.00103	0.52844	19.8
PM5	HS_MURR3_P5	0.50314	0.00099	0.50512	-3.5
PM6	HS_MURR3_P6	0.50980	0.00106	0.51192	3.3
PM7	HS_MURR3_P7	0.53021	0.00114	0.53249	23.8

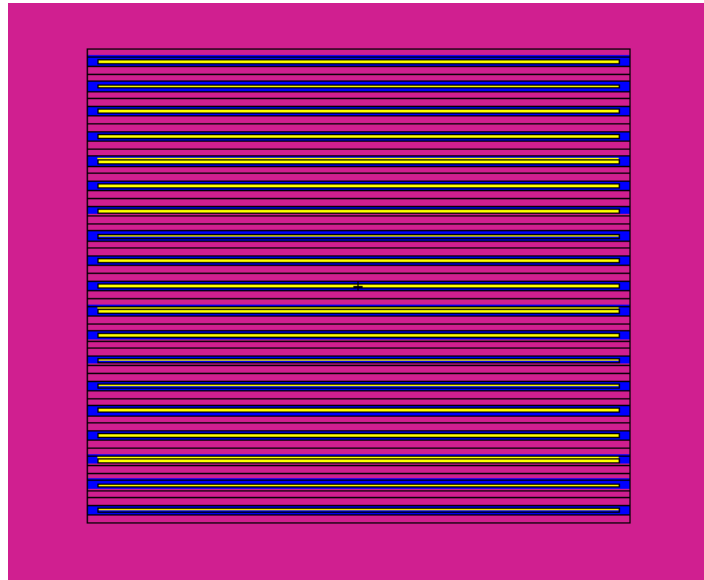
**Table 6.9-6 – MITR-II Parametric Analysis Input Data**

Parameter	PN1/PN4	PN2	PN3	PN5	PN6/PN7
Fuel width (in)	2.076	2.076	2.076	1.981	2.171
Meat thickness (in)	0.03	0.03	0.03	0.03	0.03
Active fuel height (in)	22.375	21.99	22.76	22.375	22.375
Channel (in)	0.090/0.094	0.090	0.090	0.090	0.090/0.094
Cladding (in)	0.019/0.017	0.019	0.019	0.019	0.019/0.017
Total plate (in)	0.068/0.064	0.068	0.068	0.068	0.068/0.064
Pitch (in)	0.158	0.158	0.158	0.158	0.158
Meat volume (cm <sup>3</sup> )	342.53	336.64	348.43	326.86	358.21
U-235 mass (g)	515	515	515	515	515
U-235 den (g/cm3)	1.503	1.530	1.478	1.576	1.438
UAlx+Al den (g/cm3)	3.85	3.87	3.83	3.91	3.79
N-234 (atom/b-cm)	2.4693E-05	2.5125E-05	2.4275E-05	2.5877E-05	2.3613E-05
N-235 (atom/b-cm)	3.8521E-03	3.9195E-03	3.7869E-03	4.0368E-03	3.6835E-03
N-236 (atom/b-cm)	1.4282E-05	1.4532E-05	1.4040E-05	1.4967E-05	1.3657E-05
N-238 (atom/b-cm)	2.0433E-04	2.0791E-04	2.0088E-04	2.1413E-04	1.9539E-04
N-Al (atom/b-cm)	5.0202E-02	5.0090E-02	5.0310E-02	4.9895E-02	5.0481E-02
Total (atom/b-cm)	5.4297E-02	5.4257E-02	5.4336E-02	5.4187E-02	5.4398E-02

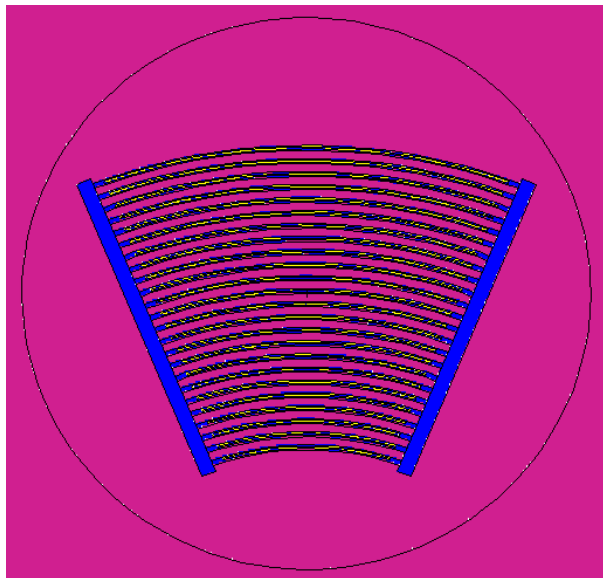
**Table 6.9-7 – MITR-II Parametric Analysis Results**

Case ID	Filename	k <sub>eff</sub>	σ	k <sub>s</sub> (k+2σ)	Δ from PN1 (mk)
PN1	HS_MIT2_P1	0.39975	0.00089	0.40153	
PN2	HS_MIT2_P2	0.40082	0.00093	0.40268	1.1
PN3	HS_MIT2_P3	0.39965	0.00088	0.40141	-0.1
PN4	HS_MIT2_P4	0.40562	0.00105	0.40772	6.2
PN5	HS_MIT2_P5	0.39724	0.00096	0.39916	-2.4
PN6	HS_MIT2_P6	0.40496	0.00087	0.40670	5.2
PN7	HS_MIT2_P7	<b>0.41052</b>	<b>0.00098</b>	<b>0.41248</b>	<b>11.0</b>

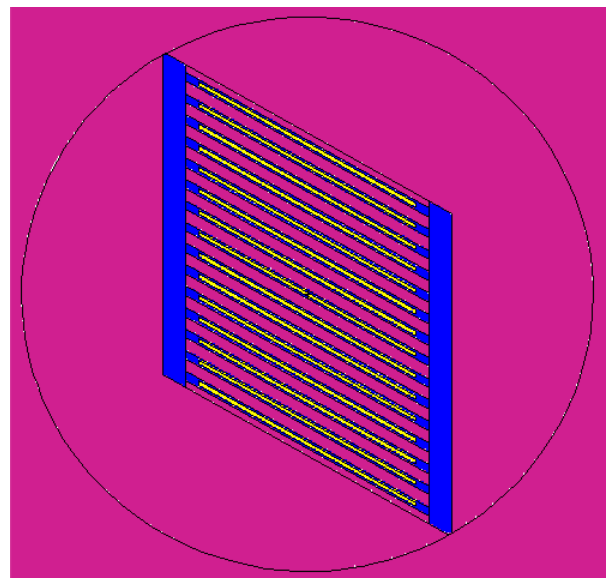




ATR



MURR



MITR-II

**Figure 6.9-1 – ATR, MURR, and MITR-II Base Parametric Models**

### 6.9.3 Sample Input Files

A sample input file is provided for the most reactive case for each of the fuel types.

#### MURR Case D8 (HA\_MURRC)

```

MURR
c
c      Basket
c
300    0      -400 424 -410 fill=6      imp:n=1 $ cavity
c
c      Cask
c
310    4 -7.94      (-424:410:400) 423 -411 -401 imp:n=1 $ inner steel
311    5 -11.35     (-423:411:401) 422 -412 -402 imp:n=1 $ lead
312    4 -7.94      (-422:412:402) 421 -413 -403 imp:n=1 $ outer steel
313    0      (-421:413:403) -405      imp:n=1 $ between
c
999    0      405      imp:n=0
c
c      Universe 1: MURR Fuel Element (infinitely long)
c
2      3 -2.7      -6 8 9 -10      u=1 imp:n=1 $ left Al piece
4      3 -2.7      -5 7 9 -10      u=1 imp:n=1 $ right Al piece
6      10 5.4439E-02 52 -53 -16 -15      u=1 imp:n=1 $ plate 1
8      3 -2.7      51 -54 -7 -8      #6 u=1 imp:n=1
10     2 -1.0      54 -55 -7 -8      u=1 imp:n=1
12     10 5.4439E-02 56 -57 -16 -15      u=1 imp:n=1 $ plate 2
14     3 -2.7      55 -58 -7 -8      #12 u=1 imp:n=1
16     2 -1.0      58 -59 -7 -8      u=1 imp:n=1
18     10 5.4439E-02 60 -61 -16 -15      u=1 imp:n=1 $ plate 3
20     3 -2.7      59 -62 -7 -8      #18 u=1 imp:n=1
22     2 -1.0      62 -63 -7 -8      u=1 imp:n=1
24     10 5.4439E-02 64 -65 -16 -15      u=1 imp:n=1 $ plate 4
26     3 -2.7      63 -66 -7 -8      #24 u=1 imp:n=1
28     2 -1.0      66 -67 -7 -8      u=1 imp:n=1
30     10 5.4439E-02 68 -69 -16 -15      u=1 imp:n=1 $ plate 5
32     3 -2.7      67 -70 -7 -8      #30 u=1 imp:n=1
34     2 -1.0      70 -71 -7 -8      u=1 imp:n=1
36     10 5.4439E-02 72 -73 -16 -15      u=1 imp:n=1 $ plate 6
38     3 -2.7      71 -74 -7 -8      #36 u=1 imp:n=1
40     2 -1.0      74 -75 -7 -8      u=1 imp:n=1
42     10 5.4439E-02 76 -77 -16 -15      u=1 imp:n=1 $ plate 7
44     3 -2.7      75 -78 -7 -8      #42 u=1 imp:n=1
46     2 -1.0      78 -79 -7 -8      u=1 imp:n=1
48     10 5.4439E-02 80 -81 -16 -15      u=1 imp:n=1 $ plate 8
50     3 -2.7      79 -82 -7 -8      #48 u=1 imp:n=1
52     2 -1.0      82 -83 -7 -8      u=1 imp:n=1
54     10 5.4439E-02 84 -85 -16 -15      u=1 imp:n=1 $ plate 9
56     3 -2.7      83 -86 -7 -8      #54 u=1 imp:n=1
58     2 -1.0      86 -87 -7 -8      u=1 imp:n=1
60     10 5.4439E-02 88 -89 -16 -15      u=1 imp:n=1 $ plate 10
62     3 -2.7      87 -90 -7 -8      #60 u=1 imp:n=1
64     2 -1.0      90 -91 -7 -8      u=1 imp:n=1
66     10 5.4439E-02 92 -93 -16 -15      u=1 imp:n=1 $ plate 11
68     3 -2.7      91 -94 -7 -8      #66 u=1 imp:n=1

```

# BRR Package Safety Analysis Report

Docket No. 71-9341  
Rev. 9, January 2016

```

70      2 -1.0      94 -95   -7 -8      u=1 imp:n=1
72      10 5.4439E-02 96 -97 -16 -15      u=1 imp:n=1 $ plate 12
74      3 -2.7      95 -98   -7 -8      #72 u=1 imp:n=1
76      2 -1.0      98 -99   -7 -8      u=1 imp:n=1
78      10 5.4439E-02 100 -101 -16 -15      u=1 imp:n=1 $ plate 13
80      3 -2.7      99 -102   -7 -8      #78 u=1 imp:n=1
82      2 -1.0      102 -103   -7 -8      u=1 imp:n=1
84      10 5.4439E-02 104 -105 -16 -15      u=1 imp:n=1 $ plate 14
86      3 -2.7      103 -106   -7 -8      #84 u=1 imp:n=1
88      2 -1.0      106 -107   -7 -8      u=1 imp:n=1
90      10 5.4439E-02 108 -109 -16 -15      u=1 imp:n=1 $ plate 15
92      3 -2.7      107 -110   -7 -8      #90 u=1 imp:n=1
94      2 -1.0      110 -111   -7 -8      u=1 imp:n=1
96      10 5.4439E-02 112 -113 -16 -15      u=1 imp:n=1 $ plate 16
98      3 -2.7      111 -114   -7 -8      #96 u=1 imp:n=1
100     2 -1.0      114 -115   -7 -8      u=1 imp:n=1
102     10 5.4439E-02 116 -117 -16 -15      u=1 imp:n=1 $ plate 17
104     3 -2.7      115 -118   -7 -8      #102 u=1 imp:n=1
106     2 -1.0      118 -119   -7 -8      u=1 imp:n=1
108     10 5.4439E-02 120 -121 -16 -15      u=1 imp:n=1 $ plate 18
110     3 -2.7      119 -122   -7 -8      #108 u=1 imp:n=1
112     2 -1.0      122 -123   -7 -8      u=1 imp:n=1
114     10 5.4439E-02 124 -125 -16 -15      u=1 imp:n=1 $ plate 19
116     3 -2.7      123 -126   -7 -8      #114 u=1 imp:n=1
118     2 -1.0      126 -127   -7 -8      u=1 imp:n=1
120     10 5.4439E-02 128 -129 -16 -15      u=1 imp:n=1 $ plate 20
122     3 -2.7      127 -130   -7 -8      #120 u=1 imp:n=1
124     2 -1.0      130 -131   -7 -8      u=1 imp:n=1
126     10 5.4439E-02 132 -133 -16 -15      u=1 imp:n=1 $ plate 21
128     3 -2.7      131 -134   -7 -8      #126 u=1 imp:n=1
130     2 -1.0      134 -135   -7 -8      u=1 imp:n=1
132     10 5.4439E-02 136 -137 -16 -15      u=1 imp:n=1 $ plate 22
134     3 -2.7      135 -138   -7 -8      #132 u=1 imp:n=1
136     2 -1.0      138 -139   -7 -8      u=1 imp:n=1
138     10 5.4439E-02 140 -141 -16 -15      u=1 imp:n=1 $ plate 23
140     3 -2.7      139 -142   -7 -8      #138 u=1 imp:n=1
142     2 -1.0      142 -143   -7 -8      u=1 imp:n=1
144     10 5.4439E-02 144 -145 -16 -15      u=1 imp:n=1 $ plate 24
146     3 -2.7      143 -146   -7 -8      #144 u=1 imp:n=1
150     2 -1.0      6:5:-9:10:9 -51 -8 -7:146 -10 -8 -7 u=1 imp:n=1
c
c      Universe 6: Basket
c
600     4 -7.94      600 -601 -620      u=6 imp:n=1 $ bottom
601     4 -7.94      600 -604 620 -621 u=6 imp:n=1 $ bottom
602     4 -7.94      604 -605 620      u=6 imp:n=1 $ shelf
603     4 -7.94      602 -604 622 -623 u=6 imp:n=1 $ shelf
604     4 -7.94      602 -603 623      u=6 imp:n=1 $ inner ring
610     2 -1.0      -600 -621      u=6 imp:n=1 $ bottom air
611     2 -1.0      601 -620 -605      u=6 imp:n=1 $ bottom air corner
612     2 -1.0      605      u=6 imp:n=1 $ side and top air
613     2 -1.0      -604 621 -622      u=6 imp:n=1 $ inner air
614     2 -1.0      -602 622      u=6 imp:n=1 $ inner air
615     0      603 -604 623      637 -630 fill=20 u=6 imp:n=1 $ basket
loc 1 (top)
616     0      603 -604 623      631 -634 fill=20(2) u=6 imp:n=1 $ basket
loc 2

```

**BRR Package Safety Analysis Report**

```

617      0          603 -604 623      635  633 fill=20(3) u=6 imp:n=1 $ basket
loc 3
618      0          603 -604 623      637 -632 fill=20(4) u=6 imp:n=1 $ basket
loc 4
619      0          603 -604 623      631 -636 fill=20(5) u=6 imp:n=1 $ basket
loc 5
620      0          603 -604 623      -630  635 fill=20(6) u=6 imp:n=1 $ basket
loc 6
621      0          603 -604 623      -632 -634 fill=20(7) u=6 imp:n=1 $ basket
loc 7
622      0          603 -604 623      633 -636 fill=20(8) u=6 imp:n=1 $ basket
loc 8
630      4  -7.94    603 -604 630 -631 623      u=6 imp:n=1 $ web
631      4  -7.94    603 -604 632 -633 623      u=6 imp:n=1 $ web
632      4  -7.94    603 -604 634 -635 623      u=6 imp:n=1 $ web
633      4  -7.94    603 -604 636 -637 623      u=6 imp:n=1 $ web
c
c      Universe 20: MURR fuel element moved +y
c
200      0          -203 24 -25      fill=1(11) u=20 imp:n=1 $ MURR
201      2 -1.0      203:-24:25      u=20 imp:n=1 $ water

5        p  2.4142136 -1 0 -0.13275  $ right Al outer
6        p -2.4142136 -1 0 -0.13275  $ left Al outer
7        p  2.4142136 -1 0 -1.09516  $ right Al inner
8        p -2.4142136 -1 0 -1.09516  $ left Al inner
9        cz 6.858      $ Al boundary
10       cz 14.884     $ Al boundary
c
15       p  2.4142136 -1 0 -1.39997  $ plate meat boundary
16       p -2.4142136 -1 0 -1.39997  $ plate meat boundary
c
24       pz  76.1821   $ bottom of fuel
25       pz  137.1421  $ top of fuel (24")
c
51 cz 7.0536
52 cz 7.0739
53 cz 7.1247
54 cz 7.1450
c
55 cz 7.3838
56 cz 7.4041
57 cz 7.4549
58 cz 7.4752
c
59 cz 7.7140
60 cz 7.7343
61 cz 7.7851
62 cz 7.8054
c
63 cz 8.0442
64 cz 8.0645
65 cz 8.1153
66 cz 8.1356
c
67 cz 8.3744
68 cz 8.3947

```

**BRR Package Safety Analysis Report**

---

69 cz 8.4455  
70 cz 8.4658  
c  
71 cz 8.7046  
72 cz 8.7249  
73 cz 8.7757  
74 cz 8.7960  
c  
75 cz 9.0348  
76 cz 9.0551  
77 cz 9.1059  
78 cz 9.1262  
c  
79 cz 9.3650  
80 cz 9.3853  
81 cz 9.4361  
82 cz 9.4564  
c  
83 cz 9.6952  
84 cz 9.7155  
85 cz 9.7663  
86 cz 9.7866  
c  
87 cz 10.0254  
88 cz 10.0457  
89 cz 10.0965  
90 cz 10.1168  
c  
91 cz 10.3556  
92 cz 10.3759  
93 cz 10.4267  
94 cz 10.4470  
c  
95 cz 10.6858  
96 cz 10.7061  
97 cz 10.7569  
98 cz 10.7772  
c  
99 cz 11.0160  
100 cz 11.0363  
101 cz 11.0871  
102 cz 11.1074  
c  
103 cz 11.3462  
104 cz 11.3665  
105 cz 11.4173  
106 cz 11.4376  
c  
107 cz 11.6764  
108 cz 11.6967  
109 cz 11.7475  
110 cz 11.7678  
c  
111 cz 12.0066  
112 cz 12.0269  
113 cz 12.0777  
114 cz 12.0980

**BRR Package Safety Analysis Report**

---

c  
115 cz 12.3368  
116 cz 12.3571  
117 cz 12.4079  
118 cz 12.4282  
c  
119 cz 12.6670  
120 cz 12.6873  
121 cz 12.7381  
122 cz 12.7584  
c  
123 cz 12.9972  
124 cz 13.0175  
125 cz 13.0683  
126 cz 13.0886  
c  
127 cz 13.3274  
128 cz 13.3477  
129 cz 13.3985  
130 cz 13.4188  
c  
131 cz 13.6576  
132 cz 13.6779  
133 cz 13.7287  
134 cz 13.7490  
c  
135 cz 13.9878  
136 cz 14.0081  
137 cz 14.0589  
138 cz 14.0792  
c  
139 cz 14.3180  
140 cz 14.3383  
141 cz 14.3891  
142 cz 14.4094  
c  
143 cz 14.6482  
144 cz 14.6685  
145 cz 14.7193  
146 cz 14.7396  
c  
203 cz 100 \$ dummy  
c  
400 cz 20.32 \$ IR cask  
401 cz 22.86 \$ IR lead  
402 cz 43.18 \$ OR lead  
403 cz 48.26 \$ OR cask  
404 cz 78.74 \$ 1 foot water reflector  
\*405 hex 0 0 -25.25 0 0 190.5355 0 48.27 0  
c  
410 pz 137.1422 \$ bottom of lid  
411 pz 139.6822 \$ steel  
412 pz 164.0154 \$ lead  
413 pz 165.2854 \$ steel  
414 pz 195.7654 \$ 1 foot water reflector  
c  
420 pz -55.72 \$ 1 foot water reflector

# BRR Package Safety Analysis Report

```

421      pz -25.24    $ bottom of cask
422      pz -22.7     $ steel
423      pz -3.0912   $ lead
424      pz 0         $ steel
c
c      basket surfaces
c
600      cz 15.4432
601      cz 16.3957
602      cz 8.89
603      cz 10.0813
604      cz 19.177
605      cz 19.812
620      pz 5.715
621      pz 6.6675
622      pz 50.9778
623      pz 51.9303
630 12   px -1.27
631 12   px  1.27
632 12   py -1.27
633 12   py  1.27
634 13   px -1.27
635 13   px  1.27
636 13   py -1.27
637 13   py  1.27

m2      1001.62c  2          $ water
        8016.62c  1
mt2     lwtr.60t
m3      13027.62c 1          $ Al
m4      6000.66c  -0.08     $ SS-304
        14000.60c  -1.0
        15031.66c  -0.045
        24000.50c  -19.0
        25055.62c  -2.0
        26000.55c  -68.375
        28000.50c  -9.5
m5      82000.50c 1          $ Pb
m10     92234.69c 2.3171E-05 $ fuel.
        92235.69c 3.6147E-03
        92236.69c 1.3402E-05
        92238.69c 1.9174E-04
        13027.62c 5.0596E-02
c
c      total 5.4439E-02
c
*tr2    0 0 0 45 135 90 45 45 90          $ loc 2
*tr3    0 0 0 90 180 90 0 90 90          $ loc 3
*tr4    0 0 0 135 225 90 45 135 90        $ loc 4
*tr5    0 0 0 180 90 90 90 180 90        $ loc 5
*tr6    0 0 0 135 45 90 225 135 90        $ loc 6
*tr7    0 0 0 90 0 90 180 90 90          $ loc 7
*tr8    0 0 0  45 45 90 135 45 90        $ loc 8
*tr11   0 3.4 0                          $ u=20
*tr12   0 0 0 22.5 112.5 90 67.5 22.5 90  $ rotate 22.5 deg
*tr13   0 0 0 67.5 157.5 90 22.5 67.5 90  $ rotate 67.5 deg
c
mode    n

```

```

kcode 2500 1.0 50 250
sdef rad=d1 ext=d2 axs=0 0 1
si1 10 18.5
si2 76 137

```

**MITR-II Case D27 (HA\_MIT2C)**

```

MIT
c
c      Basket
c
300      0 630 -631 633 -632 680 -410 fill=5          imp:n=1 $ basket
location 1
301      like 300 but trcl=2          imp:n=1 $ basket
location 2
302      like 300 but trcl=3          imp:n=1 $ basket
location 3
303      like 300 but trcl=4          imp:n=1 $ basket
location 4
304      like 300 but trcl=5          imp:n=1 $ basket
location 5
305      like 300 but trcl=6          imp:n=1 $ basket
location 6
306      like 300 but trcl=7          imp:n=1 $ basket
location 7
307      like 300 but trcl=8          imp:n=1 $ basket
location 8
320      4 -7.94          680 -410 687 -683 #300 #301 #302 #303
          #304 #305 #306 #307          imp:n=1 $ inside
basket
c 330      2 -1.0          410 -410 -400          imp:n=1 $ above
basket
331      4 -7.94          682 -680 -683          imp:n=1 $ support
plate
332      4 -7.94          684 -685 -682 424          imp:n=1 $ basket
bottom
333      2 -1.0          -684 -682 424          imp:n=1
334      2 -1.0          682 -680 683 -400          imp:n=1
335      2 -1.0          685 -682 424 -400          imp:n=1
336      2 -1.0          680 -410 -687          imp:n=1 $ inner air
337      2 -1.0          680 -410 683 -400          imp:n=1 $ annular
air
c
c      Cask
c
410      4 -7.94          (-424:410:400) 423 -411 -401 imp:n=1 $ inner steel
411      5 -11.35          (-423:411:401) 422 -412 -402 imp:n=1 $ lead
412      4 -7.94          (-422:412:402) 421 -413 -403 imp:n=1 $ outer steel
413      0          (-421:413:403) -405          imp:n=1 $ between
c
999      0          405          imp:n=0
c
c      Universe 1: MIT Fuel Element (infinitely long)
c
10      3 -2.7          10 -11 18 -19          u=1 imp:n=1 $ right Al piece
11      3 -2.7          13 -12 18 -19          u=1 imp:n=1 $ left Al piece
12      2 -1.0          12 -10 18 -50          u=1 imp:n=1

```



```

20      10 5.4398E-02 40 -41 70 -90      u=1 imp:n=1 $ plate 1
21      3 -2.7      12 -10 50 -110 #20    u=1 imp:n=1
22      2 -1.0      12 -10 110 -51      u=1 imp:n=1
30      10 5.4398E-02 40 -41 71 -91      u=1 imp:n=1 $ plate 2
31      3 -2.7      12 -10 51 -111 #30    u=1 imp:n=1
32      2 -1.0      12 -10 111 -52      u=1 imp:n=1
40      10 5.4398E-02 40 -41 72 -92      u=1 imp:n=1 $ plate 3
41      3 -2.7      12 -10 52 -112 #40    u=1 imp:n=1
42      2 -1.0      12 -10 112 -53      u=1 imp:n=1
50      10 5.4398E-02 40 -41 73 -93      u=1 imp:n=1 $ plate 4
51      3 -2.7      12 -10 53 -113 #50    u=1 imp:n=1
52      2 -1.0      12 -10 113 -54      u=1 imp:n=1
60      10 5.4398E-02 40 -41 74 -94      u=1 imp:n=1 $ plate 5
61      3 -2.7      12 -10 54 -114 #60    u=1 imp:n=1
62      2 -1.0      12 -10 114 -55      u=1 imp:n=1
70      10 5.4398E-02 40 -41 75 -95      u=1 imp:n=1 $ plate 6
71      3 -2.7      12 -10 55 -115 #70    u=1 imp:n=1
72      2 -1.0      12 -10 115 -56      u=1 imp:n=1
80      10 5.4398E-02 40 -41 76 -96      u=1 imp:n=1 $ plate 7
81      3 -2.7      12 -10 56 -116 #80    u=1 imp:n=1
82      2 -1.0      12 -10 116 -57      u=1 imp:n=1
90      10 5.4398E-02 40 -41 77 -97      u=1 imp:n=1 $ plate 8
91      3 -2.7      12 -10 57 -117 #90    u=1 imp:n=1
92      2 -1.0      12 -10 117 -58      u=1 imp:n=1
100     10 5.4398E-02 40 -41 78 -98      u=1 imp:n=1 $ plate 9
101     3 -2.7      12 -10 58 -118 #100    u=1 imp:n=1
102     2 -1.0      12 -10 118 -59      u=1 imp:n=1
110     10 5.4398E-02 40 -41 79 -99      u=1 imp:n=1 $ plate 10
111     3 -2.7      12 -10 59 -119 #110    u=1 imp:n=1
112     2 -1.0      12 -10 119 -60      u=1 imp:n=1
120     10 5.4398E-02 40 -41 80 -100     u=1 imp:n=1 $ plate 11
121     3 -2.7      12 -10 60 -120 #120    u=1 imp:n=1
122     2 -1.0      12 -10 120 -61      u=1 imp:n=1
130     10 5.4398E-02 40 -41 81 -101     u=1 imp:n=1 $ plate 12
131     3 -2.7      12 -10 61 -121 #130    u=1 imp:n=1
132     2 -1.0      12 -10 121 -62      u=1 imp:n=1
140     10 5.4398E-02 40 -41 82 -102     u=1 imp:n=1 $ plate 13
141     3 -2.7      12 -10 62 -122 #140    u=1 imp:n=1
142     2 -1.0      12 -10 122 -63      u=1 imp:n=1
150     10 5.4398E-02 40 -41 83 -103     u=1 imp:n=1 $ plate 14
151     3 -2.7      12 -10 63 -123 #150    u=1 imp:n=1
152     2 -1.0      12 -10 123 -64      u=1 imp:n=1
160     10 5.4398E-02 40 -41 84 -104     u=1 imp:n=1 $ plate 15
161     3 -2.7      12 -10 64 -124 #160    u=1 imp:n=1
162     2 -1.0      12 -10 124 -19      u=1 imp:n=1
170     2 -1.0      -13:11:-18:19      u=1 imp:n=1 $ water in pipe
c
c      Universe 5: Element rotated 30 degrees CCW and moved to wedge 1
location outer
c
500     0      -700 24 fill=1(12)      u=5 imp:n=1
501     2 -1.0      -700 -24      u=5 imp:n=1
c 502     2 -1.0      -700 25      u=5 imp:n=1

10      px 2.5451      $ Al side
11      px 3.0226      $ Al side
12      px -2.5451     $ Al side

```

**BRR Package Safety Analysis Report**

---

```
13      px -3.0226   $ Al side
18 10   py -3.02768  $ Al bottom
19 10   py 3.02768   $ Al top
c
24      pz 80.3097   $ bottom of fuel
c 25    pz 130.7439  $ top of fuel (22.375")
c
40      px -2.3878  $ meat width (w/2*cos(30))
41      px 2.3878   $ meat width
c
50 10   py -2.86258  $ cladding bottom
51 10   py -2.46126
52 10   py -2.05994
53 10   py -1.65862
54 10   py -1.25730
55 10   py -0.85598
56 10   py -0.45466
57 10   py -0.05334
58 10   py 0.34798
59 10   py 0.74930
60 10   py 1.15062
61 10   py 1.55194
62 10   py 1.95326
63 10   py 2.35458
64 10   py 2.75590
c
70 10   py -2.84734  $ meat bottom
71 10   py -2.44602
72 10   py -2.04470
73 10   py -1.64338
74 10   py -1.24206
75 10   py -0.84074
76 10   py -0.43942
77 10   py -0.03810
78 10   py 0.36322
79 10   py 0.76454
80 10   py 1.16586
81 10   py 1.56718
82 10   py 1.96850
83 10   py 2.36982
84 10   py 2.77114
c
90 10   py -2.77114  $ meat top
91 10   py -2.36982
92 10   py -1.96850
93 10   py -1.56718
94 10   py -1.16586
95 10   py -0.76454
96 10   py -0.36322
97 10   py 0.03810
98 10   py 0.43942
99 10   py 0.84074
100 10  py 1.24206
101 10  py 1.64338
102 10  py 2.04470
103 10  py 2.44602
104 10  py 2.84734
```

# BRR Package Safety Analysis Report

```

c
110 10    py -2.75590 $ cladding top
111 10    py -2.35458
112 10    py -1.95326
113 10    py -1.55194
114 10    py -1.15062
115 10    py -0.74930
116 10    py -0.34798
117 10    py 0.05334
118 10    py 0.45466
119 10    py 0.85598
120 10    py 1.25730
121 10    py 1.65862
122 10    py 2.05994
123 10    py 2.46126
124 10    py 2.86258
c
400      cz 20.32 $ IR cask
401      cz 22.86 $ IR lead
402      cz 43.18 $ OR lead
403      cz 48.26 $ OR cask
404      cz 78.74 $ 1 foot water reflector
*405     hex 0 0 -25.25 0 0 190.5355 0 48.27 0
c
410      pz 137.1422 $ bottom of lid
411      pz 139.6822 $ steel
412      pz 164.0154 $ lead
413      pz 165.2854 $ steel
414      pz 195.7654 $ 1 foot water reflector
c
420      pz -55.72   $ 1 foot water reflector
421      pz -25.24   $ bottom of cask
422      pz -22.7    $ steel
423      pz -3.0912  $ lead
424      pz 0        $ steel
c
c      basket surfaces
c
630      1    py -3.3909
631      1    py  3.3909
632      1    p  -1.7321 -1 0   6.7818 $ left basket inner bound
633      1    p  -1.7321 -1 0  -6.7818 $ right basket inner bound
c
680      pz  67.4878 $ top of plate
682      pz  66.2178 $ bottom of plate
683      cz  19.8501 $ OR of basket
684      cz  17.145
685      cz  17.78
687      cz  12      $ IR of basket
700      cz  1000    $ dummy

m2      1001.62c  2          $ water
        8016.62c  1
mt2     lwtr.60t
m3      13027.62c 1          $ Al
m4      6000.66c  -0.08     $ SS-304
        14000.60c -1.0

```

```

15031.66c -0.045
24000.50c -19.0
25055.62c -2.0
26000.55c -68.375
28000.50c -9.5
m5      82000.50c 1          $ Pb
m10     92234.69c 2.3613E-05 $ fuel
        92235.69c 3.6835E-03
        92236.69c 1.3657E-05
        92238.69c 1.9539E-04
        13027.62c 5.0481E-02
c        total 5.4398E-02
c
*tr1    1.7413 15.5236 0          $ wedge 1
*tr2    0 0 0          45 135 90 45 45 90 $ wedge 2 (8)
*tr3    0 0 0          90 180 90 0 90 90 $ wedge 3 (7)
*tr4    0 0 0          135 225 90 45 135 90 $ wedge 4 (6)
*tr5    0 0 0          180 90 90 90 180 90 $ wedge 5
*tr6    0 0 0          135 45 90 225 135 90 $ wedge 6
*tr7    0 0 0          90 0 90 180 90 90 $ wedge 7
*tr8    0 0 0          45 45 90 135 45 90 $ wedge 8
*tr10   0 0 0          30 120 90 60 30 90 $ rotate fuel surfaces 30 deg
CW
*tr12   1.7413 15.15 0 30 60 90 120 30 90 $ rotate 30 CCW
c
mode    n
kcode   2500 1.0 50 250
sdef    rad=d1 ext=d2 axs=0 0 1
si1     12 20
si2     80 137

```

**ATR Case D47 (HA\_ATRC)**

```

ATR
300      0          -400 424 -410 fill=6      imp:n=1 $ cavity
c
c        Cask
c
310      4 -7.94      (-424:410:400) 423 -411 -401 imp:n=1 $ inner steel
311      5 -11.35     (-423:411:401) 422 -412 -402 imp:n=1 $ lead
312      4 -7.94      (-422:412:402) 421 -413 -403 imp:n=1 $ outer steel
313      0            (-421:413:403) -405      imp:n=1 $ between
c
999      0            405                  imp:n=0
c
c        Universe 1: ATR Fuel Element (infinitely long)
c
2         3 -2.7          -6 8 9 -10          u=1 imp:n=1 $ left Al piece
4         3 -2.7          -5 7 9 -10          u=1 imp:n=1 $ right Al piece
6         10 5.5010E-02   52 -53 -14 -13      u=1 imp:n=1 $ plate 1
8         3 -2.7          51 -54 -7 -8        #6 u=1 imp:n=1
10        2 -1.0          54 -55 -7 -8        u=1 imp:n=1
12        11 5.4998E-02   56 -57 -16 -15      u=1 imp:n=1 $ plate 2
14        3 -2.7          55 -58 -7 -8        #12 u=1 imp:n=1
16        2 -1.0          58 -59 -7 -8        u=1 imp:n=1
18        12 5.4574E-02   60 -61 -16 -15      u=1 imp:n=1 $ plate 3
20        3 -2.7          59 -62 -7 -8        #18 u=1 imp:n=1

```

22	2 -1.0	62 -63 -7 -8	u=1 imp:n=1
24	13 5.4583E-02	64 -65 -16 -15	u=1 imp:n=1 \$ plate 4
26	3 -2.7	63 -66 -7 -8	#24 u=1 imp:n=1
28	2 -1.0	66 -67 -7 -8	u=1 imp:n=1
30	14 5.4115E-02	68 -69 -16 -15	u=1 imp:n=1 \$ plate 5
32	3 -2.7	67 -70 -7 -8	#30 u=1 imp:n=1
34	2 -1.0	70 -71 -7 -8	u=1 imp:n=1
36	15 5.4106E-02	72 -73 -16 -15	u=1 imp:n=1 \$ plate 6
38	3 -2.7	71 -74 -7 -8	#36 u=1 imp:n=1
40	2 -1.0	74 -75 -7 -8	u=1 imp:n=1
42	16 5.4102E-02	76 -77 -16 -15	u=1 imp:n=1 \$ plate 7
44	3 -2.7	75 -78 -7 -8	#42 u=1 imp:n=1
46	2 -1.0	78 -79 -7 -8	u=1 imp:n=1
48	17 5.4098E-02	80 -81 -16 -15	u=1 imp:n=1 \$ plate 8
50	3 -2.7	79 -82 -7 -8	#48 u=1 imp:n=1
52	2 -1.0	82 -83 -7 -8	u=1 imp:n=1
54	18 5.4095E-02	84 -85 -16 -15	u=1 imp:n=1 \$ plate 9
56	3 -2.7	83 -86 -7 -8	#54 u=1 imp:n=1
58	2 -1.0	86 -87 -7 -8	u=1 imp:n=1
60	19 5.4092E-02	88 -89 -16 -15	u=1 imp:n=1 \$ plate 10
62	3 -2.7	87 -90 -7 -8	#60 u=1 imp:n=1
64	2 -1.0	90 -91 -7 -8	u=1 imp:n=1
66	20 5.4089E-02	92 -93 -16 -15	u=1 imp:n=1 \$ plate 11
68	3 -2.7	91 -94 -7 -8	#66 u=1 imp:n=1
70	2 -1.0	94 -95 -7 -8	u=1 imp:n=1
72	21 5.4086E-02	96 -97 -16 -15	u=1 imp:n=1 \$ plate 12
74	3 -2.7	95 -98 -7 -8	#72 u=1 imp:n=1
76	2 -1.0	98 -99 -7 -8	u=1 imp:n=1
78	22 5.4083E-02	100 -101 -16 -15	u=1 imp:n=1 \$ plate 13
80	3 -2.7	99 -102 -7 -8	#78 u=1 imp:n=1
82	2 -1.0	102 -103 -7 -8	u=1 imp:n=1
84	23 5.4081E-02	104 -105 -16 -15	u=1 imp:n=1 \$ plate 14
86	3 -2.7	103 -106 -7 -8	#84 u=1 imp:n=1
88	2 -1.0	106 -107 -7 -8	u=1 imp:n=1
90	24 5.4075E-02	108 -109 -16 -15	u=1 imp:n=1 \$ plate 15
92	3 -2.7	107 -110 -7 -8	#90 u=1 imp:n=1
94	2 -1.0	110 -111 -7 -8	u=1 imp:n=1
96	25 5.4544E-02	112 -113 -16 -15	u=1 imp:n=1 \$ plate 16
98	3 -2.7	111 -114 -7 -8	#96 u=1 imp:n=1
100	2 -1.0	114 -115 -7 -8	u=1 imp:n=1
102	26 5.4544E-02	116 -117 -16 -15	u=1 imp:n=1 \$ plate 17
104	3 -2.7	115 -118 -7 -8	#102 u=1 imp:n=1
106	2 -1.0	118 -119 -7 -8	u=1 imp:n=1
108	27 5.4949E-02	120 -121 -18 -17	u=1 imp:n=1 \$ plate 18
110	3 -2.7	119 -122 -7 -8	#108 u=1 imp:n=1
112	2 -1.0	122 -123 -7 -8	u=1 imp:n=1
114	28 5.4967E-02	124 -125 -14 -13	u=1 imp:n=1 \$ plate 19
116	3 -2.7	123 -126 -7 -8	#114 u=1 imp:n=1
122	2 -1.0	6:5:-9:10:9 -51 -8 -7:126 -10 -8 -7	u=1 imp:n=1
c			
c	Universe 6: Basket		
c			
600	4 -7.94	602 -603 623	u=6 imp:n=1 \$ inner ring
601	4 -7.94	602 -604 622 -623	u=6 imp:n=1 \$ bottom plate
602	4 -7.94	604 -605	u=6 imp:n=1 \$ outer ring
603	2 -1.0	-604 -622	u=6 imp:n=1 \$ bottom void
604	2 -1.0	-602 622	u=6 imp:n=1 \$ inner void

```

605      2 -1.0      605                                u=6 imp:n=1 $ inf. water
614      0          603 -604 623      637 -630 fill=20      u=6 imp:n=1 $ basket
loc 1 (top)
615      0          603 -604 623      631 -634 fill=20(2) u=6 imp:n=1 $ basket
loc 2
616      0          603 -604 623      635 633 fill=20(3) u=6 imp:n=1 $ basket
loc 3
617      0          603 -604 623      637 -632 fill=20(4) u=6 imp:n=1 $ basket
loc 4
618      0          603 -604 623      631 -636 fill=20(5) u=6 imp:n=1 $ basket
loc 5
619      0          603 -604 623      -630 635 fill=20(6) u=6 imp:n=1 $ basket
loc 6
620      0          603 -604 623      -632 -634 fill=20(7) u=6 imp:n=1 $ basket
loc 7
621      0          603 -604 623      633 -636 fill=20(8) u=6 imp:n=1 $ basket
loc 8
630      4 -7.94      603 -604 630 -631 623      u=6 imp:n=1 $ web
631      4 -7.94      603 -604 632 -633 623      u=6 imp:n=1 $ web
632      4 -7.94      603 -604 634 -635 623      u=6 imp:n=1 $ web
633      4 -7.94      603 -604 636 -637 623      u=6 imp:n=1 $ web
c
c      Universe 20: ATR fuel element moved +y
c
200      0          -203 24 -25      fill=1(11) u=20 imp:n=1
201      2 -1.0      203:-24:25      u=20 imp:n=1 $ water

5      p 2.4142136 -1 0 -0.2665911 $ right Al outer
6      p -2.4142136 -1 0 -0.2665911 $ left Al outer
7      p 2.4142136 -1 0 -1.474587 $ right Al inner
8      p -2.4142136 -1 0 -1.474587 $ left Al inner
9      cz 7.52856 $ Al boundary
10     cz 14.015466 $ Al boundary
c
13     p 2.4142136 -1 0 -2.4370013 $ plate 1 & 19 meat
14     p -2.4142136 -1 0 -2.4370013 $ plate 1 & 19 meat
15     p 2.4142136 -1 0 -1.7732672 $ plate 2-17 meat
16     p -2.4142136 -1 0 -1.7732672 $ plate 2-17 meat
17     p 2.4142136 -1 0 -1.9060140 $ plate 18 meat
18     p -2.4142136 -1 0 -1.9060140 $ plate 18 meat
c
24     pz 15.2221 $ bottom of fuel
25     pz 137.1421 $ top of fuel (48")
c
51     cz 7.68858
52     cz 7.73430
53     cz 7.78510
54     cz 7.83082
c
55     cz 8.07720
56     cz 8.09752
57     cz 8.14832
58     cz 8.16864
c
59     cz 8.40232
60     cz 8.42264
61     cz 8.47344

```

**BRR Package Safety Analysis Report**

---

62            CZ 8.49376  
C  
63            CZ 8.72744  
64            CZ 8.74776  
65            CZ 8.79856  
66            CZ 8.81888  
C  
67            CZ 9.05256  
68            CZ 9.07288  
69            CZ 9.12368  
70            CZ 9.14401  
C  
71            CZ 9.37768  
72            CZ 9.39800  
73            CZ 9.44880  
74            CZ 9.46912  
C  
75            CZ 9.70280  
76            CZ 9.72312  
77            CZ 9.77392  
78            CZ 9.79424  
C  
79            CZ 10.02792  
80            CZ 10.04824  
81            CZ 10.09904  
82            CZ 10.11936  
C  
83            CZ 10.35304  
84            CZ 10.37336  
85            CZ 10.42416  
86            CZ 10.44448  
C  
87            CZ 10.67816  
88            CZ 10.69848  
89            CZ 10.74928  
90            CZ 10.76960  
C  
91            CZ 11.00328  
92            CZ 11.02360  
93            CZ 11.07440  
94            CZ 11.09472  
C  
95            CZ 11.32840  
96            CZ 11.34872  
97            CZ 11.39952  
98            CZ 11.41984  
C  
99            CZ 11.65352  
100           CZ 11.67384  
101           CZ 11.72464  
102           CZ 11.74496  
C  
103           CZ 11.97864  
104           CZ 11.99896  
105           CZ 12.04976  
106           CZ 12.07008  
C

# **BRR Package Safety Analysis Report**

```

107      cz 12.30376
108      cz 12.32408
109      cz 12.37488
110      cz 12.39520
c
111      cz 12.62888
112      cz 12.64920
113      cz 12.70000
114      cz 12.72032
c
115      cz 12.95400
116      cz 12.97432
117      cz 13.02512
118      cz 13.04544
c
119      cz 13.27912
120      cz 13.29944
121      cz 13.35024
122      cz 13.37056
c
123      cz 13.64234
124      cz 13.68806
125      cz 13.73886
126      cz 13.78458
c
203      cz 100      $ dummy
c
400      cz 20.32      $ IR cask
401      cz 22.86      $ IR lead
402      cz 43.18      $ OR lead
403      cz 48.26      $ OR cask
404      cz 78.74      $ 1 foot water reflector
*405     hex 0 0 -25.25 0 0 190.5355 0 48.27 0
c
410      pz 137.1422 $ bottom of lid
411      pz 139.6822 $ steel
412      pz 164.0154 $ lead
413      pz 165.2854 $ steel
414      pz 195.7654 $ 1 foot water reflector
c
420      pz -55.72      $ 1 foot water reflector
421      pz -25.24      $ bottom of cask
422      pz -22.7       $ steel
423      pz -3.0912     $ lead
424      pz 0           $ steel
c
c      basket surfaces
c
602      cz 8.255
603      cz 9.144
604      cz 16.51
605      cz 17.145
622      pz 4.0132
623      pz 5.2832
c 624      pz 135.763
630 12    px -0.47625
631 12    px 0.47625

```



# **BRR Package Safety Analysis Report**

```

632 12  py -0.47625
633 12  py  0.47625
634 13  px -0.47625
635 13  px  0.47625
636 13  py -0.47625
637 13  py  0.47625

m2      1001.62c  2          $ water
        8016.62c  1
mt2     lwtr.60t
m3      13027.62c 1          $ Al
m4      6000.66c -0.08      $ SS-304
        14000.60c -1.0
        15031.66c -0.045
        24000.50c -19.0
        25055.62c -2.0
        26000.55c -68.375
        28000.50c -9.5
m5      82000.50c 1          $ Pb
m10     92234.69c 1.7026E-05 $ fuel plate 1
        92235.69c 2.6560E-03
        92236.69c 9.8475E-06
        92238.69c 1.4089E-04
        13027.62c 5.2187E-02
c       total      5.5010E-02
m11     92234.69c 1.7156E-05 $ fuel plate 2
        92235.69c 2.6763E-03
        92236.69c 9.9226E-06
        92238.69c 1.4196E-04
        13027.62c 5.2153E-02
c       total      5.4998E-02
m12     92234.69c 2.1711E-05 $ fuel plate 3
        92235.69c 3.3869E-03
        92236.69c 1.2557E-05
        92238.69c 1.7966E-04
        13027.62c 5.0974E-02
c       total      5.4574E-02
m13     92234.69c 2.1618E-05 $ fuel plate 4
        92235.69c 3.3724E-03
        92236.69c 1.2503E-05
        92238.69c 1.7889E-04
        13027.62c 5.0998E-02
c       total      5.4583E-02
m14     92234.69c 2.6648E-05 $ fuel plate 5
        92235.69c 4.1571E-03
        92236.69c 1.5413E-05
        92238.69c 2.2051E-04
        13027.62c 4.9696E-02
c       total      5.4115E-02
m15     92234.69c 2.6746E-05 $ fuel plate 6
        92235.69c 4.1724E-03
        92236.69c 1.5470E-05
        92238.69c 2.2132E-04
        13027.62c 4.9670E-02
c       total      5.4106E-02
m16     92234.69c 2.6790E-05 $ fuel plate 7
        92235.69c 4.1791E-03

```

**BRR Package Safety Analysis Report**

	92236.69c	1.5495E-05	
	92238.69c	2.2168E-04	
	13027.62c	4.9659E-02	
c	total	5.4102E-02	
m17	92234.69c	2.6830E-05	\$ fuel plate 8
	92235.69c	4.1854E-03	
	92236.69c	1.5518E-05	
	92238.69c	2.2201E-04	
	13027.62c	4.9649E-02	
c	total	5.4098E-02	
m18	92234.69c	2.6867E-05	\$ fuel plate 9
	92235.69c	4.1911E-03	
	92236.69c	1.5539E-05	
	92238.69c	2.2232E-04	
	13027.62c	4.9639E-02	
c	total	5.4095E-02	
m19	92234.69c	2.6901E-05	\$ fuel plate 10
	92235.69c	4.1965E-03	
	92236.69c	1.5559E-05	
	92238.69c	2.2260E-04	
	13027.62c	4.9630E-02	
c	total	5.4092E-02	
m20	92234.69c	2.6933E-05	\$ fuel plate 11
	92235.69c	4.2015E-03	
	92236.69c	1.5577E-05	
	92238.69c	2.2287E-04	
	13027.62c	4.9622E-02	
c	total	5.4089E-02	
m21	92234.69c	2.6963E-05	\$ fuel plate 12
	92235.69c	4.2061E-03	
	92236.69c	1.5595E-05	
	92238.69c	2.2311E-04	
	13027.62c	4.9614E-02	
c	total	5.4086E-02	
m22	92234.69c	2.6990E-05	\$ fuel plate 13
	92235.69c	4.2105E-03	
	92236.69c	1.5611E-05	
	92238.69c	2.2334E-04	
	13027.62c	4.9607E-02	
c	total	5.4083E-02	
m23	92234.69c	2.7017E-05	\$ fuel plate 14
	92235.69c	4.2145E-03	
	92236.69c	1.5626E-05	
	92238.69c	2.2356E-04	
	13027.62c	4.9600E-02	
c	total	5.4081E-02	
m24	92234.69c	2.7077E-05	\$ fuel plate 15
	92235.69c	4.2239E-03	
	92236.69c	1.5661E-05	
	92238.69c	2.2406E-04	
	13027.62c	4.9585E-02	
c	total	5.4075E-02	
m25	92234.69c	2.2037E-05	\$ fuel plate 16
	92235.69c	3.4377E-03	
	92236.69c	1.2746E-05	
	92238.69c	1.8235E-04	
	13027.62c	5.0889E-02	

```

c      total      5.4544E-02
m26    92234.69c  2.2037E-05 $ fuel plate 17
        92235.69c  3.4377E-03
        92236.69c  1.2745E-05
        92238.69c  1.8235E-04
        13027.62c  5.0889E-02
c      total      5.4544E-02
m27    92234.69c  1.7683E-05 $ fuel plate 18
        92235.69c  2.7586E-03
        92236.69c  1.0228E-05
        92238.69c  1.4633E-04
        13027.62c  5.2016E-02
c      total      5.4949E-02
m28    92234.69c  1.7487E-05 $ fuel plate 19
        92235.69c  2.7279E-03
        92236.69c  1.0114E-05
        92238.69c  1.4470E-04
        13027.62c  5.2067E-02
c      total      5.4967E-02
c
*tr2    0 0 0 45 135 90 45 45 90      $ loc 2
*tr3    0 0 0 90 180 90 0 90 90      $ loc 3
*tr4    0 0 0 135 225 90 45 135 90    $ loc 4
*tr5    0 0 0 180 90 90 90 180 90    $ loc 5
*tr6    0 0 0 135 45 90 225 135 90    $ loc 6
*tr7    0 0 0 90 0 90 180 90 90      $ loc 7
*tr8    0 0 0 45 45 90 135 45 90      $ loc 8
*tr11   0 1.7 0                      $ u=20
*tr12   0 0 0 22.5 112.5 90 67.5 22.5 90 $ rotate 22.5 deg
*tr13   0 0 0 67.5 157.5 90 22.5 67.5 90 $ rotate 67.5 deg
c
mode    n
kcode   2500 1.0 50 250
sdef    rad=d1 ext=d2 axs=0 0 1
si1     9.5 16
si2     15 137

```

**TRIGA Case D63 (HA\_TRIGA\_W0C060)**

```

TRIGA
300      0          -400 424 -410  fill=1      imp:n=1 $ cavity
c
c      Cask
c
310      4 -7.94      (-424:410:400) 423 -411 -401 imp:n=1 $ inner steel
311      5 -11.35     (-423:411:401) 422 -412 -402 imp:n=1 $ lead
312      4 -7.94      (-422:412:402) 421 -413 -403 imp:n=1 $ outer steel
313      0            (-421:413:403) -405          imp:n=1 $ between
c
999      0            405              imp:n=0
c
c      Universe 1: Basket
c
601      0            601 -611  trcl=1 fill=2      u=1 imp:n=1
602      like 601 but trcl=2              u=1 imp:n=1
603      like 601 but trcl=3              u=1 imp:n=1
604      like 601 but trcl=4              u=1 imp:n=1

```

**BRR Package Safety Analysis Report****Docket No. 71-9341****Rev. 9, January 2016**

```
605      like 601 but trcl=5          u=1 imp:n=1
606      like 601 but trcl=6          u=1 imp:n=1
607      like 601 but trcl=7          u=1 imp:n=1
608      like 601 but trcl=8          u=1 imp:n=1
610      like 601 but trcl=9          u=1 imp:n=1
611      like 601 but trcl=10         u=1 imp:n=1
612      like 601 but trcl=11         u=1 imp:n=1
613      like 601 but trcl=12         u=1 imp:n=1
614      like 601 but trcl=13         u=1 imp:n=1
615      like 601 but trcl=14         u=1 imp:n=1
616      like 601 but trcl=15         u=1 imp:n=1
617      like 601 but trcl=16         u=1 imp:n=1
618      like 601 but trcl=17         u=1 imp:n=1
619      like 601 but trcl=18         u=1 imp:n=1
620      like 601 but trcl=19         u=1 imp:n=1
625      2 -0.6          601 #601 #602 #603 #604 #605 #606 #607 #608
                        #610 #611 #612 #613 #614 #615 #616 #617
                        #618 #619 #620          u=1 imp:n=1
c 630      0          -600          u=1 imp:n=1 $ below
basket
631      4 -7.94          600 -601 -602          u=1 imp:n=1 $ basket plate
632      2 -0.6          600 -601 602          u=1 imp:n=1
633      4 -7.94          603 -604 -600          u=1 imp:n=1 $ bottom
support
634      2 -0.6          604 -600          u=1 imp:n=1
635      2 -0.6          -603 -600          u=1 imp:n=1
c
c      Universe 2: Fuel in tube
c
650      0          -610 fill=3(0 -0.38 111.488) u=2 imp:n=1 $ inside tube
651      4 -7.94          610          u=2 imp:n=1 $ tube
c
c      Universe 3: Fuel
c
200      7 -6.5          31 -32 -10 imp:n=1 u=3 $ zirc rod
201      2 -0.6          31 -32 10 -11 imp:n=1 u=3 $ gap
202      1 9.2354E-02 31 -32 11 -20 imp:n=1 u=3 $ fuel
203      6 -1.6          30 -31 -20 imp:n=1 u=3 $ bottom graphite
204      6 -1.6          32 -33 -20 imp:n=1 u=3 $ top graphite
205      4 -7.94          30 -33 20 -22 imp:n=1 u=3 $ cladding
206      2 -0.6          -30:33:22 imp:n=1 u=3 $ inf. water

10      cz 0.28575 $ zirc OR
11      cz 0.3175 $ fuel IR
20      cz 1.8288 $ fuel OR
22      cz 1.8796 $ cladding OR
c
30      pz -28.448 $ bottom graphite
31      pz -19.05 $ bottom fuel
32      pz 19.05 $ top fuel
33      pz 25.654 $ top graphite
c
400     cz 20.32 $ IR cask
401     cz 22.86 $ IR lead
402     cz 43.18 $ OR lead
403     cz 48.26 $ OR cask
404     cz 78.74 $ 1 foot water reflector
```

**BRR Package Safety Analysis Report**

```

*405      hex 0 0 -25.25 0 0 190.5355 0 48.27 0
c
410      pz 137.1422 $ bottom of lid
411      pz 139.6822 $ steel
412      pz 164.0154 $ lead
413      pz 165.2854 $ steel
414      pz 195.7654 $ 1 foot water reflector
c
420      pz -55.72   $ 1 foot water reflector
421      pz -25.24   $ bottom of cask
422      pz -22.7    $ steel
423      pz -3.0912  $ lead
424      pz 0        $ steel
c
c      basket surfaces
c
600      pz 18.5928   $ bottom of basket support plate
601      pz 19.2278   $ top of basket support plate
602      cz 20.0025   $ bottom plate
603      cz 15.875    $ IR bottom
604      cz 16.51     $ OR bottom
610      cz 2.2606    $ IR inner tube
611      cz 2.54      $ OR inner tube

m1      1001.62c  5.6041E-02 $ fuel
        40000.66c 3.5025E-02
        92235.69c 9.0406E-04
        92238.69c 3.8442E-04
c      Total      9.2354E-02
mt1     h/zr.60t
        zr/h.60t
m2      1001.62c  2          $ water
        8016.62c  1
mt2     lwtr.60t
m4      6000.66c  -0.08     $ SS-304
        14000.60c -1.0
        15031.66c -0.045
        24000.50c -19.0
        25055.62c -2.0
        26000.55c -68.375
        28000.50c -9.5
m5      82000.50c 1          $ Pb
m6      6000.66c  1          $ graphite
mt6     grph.60t
m7      40000.66c 1          $ Zr
c
*tr1    0 -8.255 0  j j j j j j j j j -1
*tr2    0 -8.255 0  45 135 90 45 45 90 j j j -1
*tr3    0 -8.255 0  90 180 90 0 90 90 j j j -1
*tr4    0 -8.255 0  135 225 90 45 135 90 j j j -1
*tr5    0 -8.255 0  180 270 90 90 180 90 j j j -1
*tr6    0 -8.255 0  135 45 90 225 135 90 j j j -1
*tr7    0 -8.255 0  90 0 90 180 90 90 j j j -1
*tr8    0 -8.255 0  45 45 90 135 45 90 j j j -1
c
*tr9    0 -14.605 0  j j j j j j j j j -1
*tr10   0 -14.605 0  32.7 122.7 90 57.3 32.7 90 j j j -1

```

**BRR Package Safety Analysis Report****Rev. 9, January 2016**

```

*tr11      0 -14.605 0 65.5 155.5 90 24.5 65.5 90 j j j -1
*tr12      0 -14.605 0 98.1 188.1 90 8.1 98.1 90 j j j -1
*tr13      0 -14.605 0 130.8 220.8 90 40.8 130.8 90 j j j -1
*tr14      0 -14.605 0 163.5 253.5 90 73.5 163.5 90 j j j -1
*tr15      0 -14.605 0 163.5 73.5 90 253.5 163.5 90 j j j -1
*tr16      0 -14.605 0 130.8 40.8 90 220.8 130.8 90 j j j -1
*tr17      0 -14.605 0 98.1 8.1 90 188.1 98.1 90 j j j -1
*tr18      0 -14.605 0 65.5 24.5 90 155.5 65.5 90 j j j -1
*tr19      0 -14.605 0 32.7 57.3 90 122.7 32.7 90 j j j -1

```

```

c
mode      n
kcode     2500 1.0 50 250
sdef      rad=d1 ext=d2 axs=0 0 1
sil       5.5 16.2
si2       92 130

```

**PULSTAR Case P4A1 (PS\_ARRAY\_HAC\_4B\_01)**

Pulstar Series P4B

```

c
c
c Simple Fills
1      2 -1.0 -1:1          u=1  imp:n=1 $ fuel element voids fill
2      2 -1.0 -1:1          u=2  imp:n=1 $ basket voids fill
c
c Basket
c
200      0          -600 fill=72(1) u=21 imp:n=1 $ assembly opening
201      4 -7.9 600 -601          u=21 imp:n=1 $ square SS304 tube
202      0          -602 fill=72(2) u=21 imp:n=1 $ assembly opening
203      4 -7.9 602 -603          u=21 imp:n=1 $ square SS304 tube
204      0          -604 fill=72(3) u=21 imp:n=1 $ assembly opening
205      4 -7.9 604 -605          u=21 imp:n=1 $ square SS304 tube
206      0          -606 fill=72(4) u=21 imp:n=1 $ assembly opening
207      4 -7.9 606 -607          u=21 imp:n=1 $ square SS304 tube
208      0          -608 fill=72(5) u=21 imp:n=1 $ assembly opening
209      4 -7.9 608 -609          u=21 imp:n=1 $ square SS304 tube
210      0          -610 fill=72(6) u=21 imp:n=1 $ assembly opening
211      4 -7.9 610 -611          u=21 imp:n=1 $ square SS304 tube
212      0          -612 fill=72(7) u=21 imp:n=1 $ assembly opening
213      4 -7.9 612 -613          u=21 imp:n=1 $ square SS304 tube
214      0          -614 fill=72(8) u=21 imp:n=1 $ assembly opening
215      4 -7.9 614 -615          u=21 imp:n=1 $ square SS304 tube
c
299      0          #200 #201 #202 #203 #204
                #205 #206 #207 #208
                #209 #210 #211 #212
                #213 #214 #215 fill=2 u=21 imp:n=1
c
c      Cask
c
300      0          -400 424 -410          fill=21  imp:n=1 $ cavity
310      4 -7.94    (-424:410:400) 423 -411 -401 imp:n=1 $ inner steel
311      5 -11.35   (-423:411:401) 422 -412 -402 imp:n=1 $ lead
312      4 -7.94    (-422:412:402) 421 -413 -403 imp:n=1 $ outer steel
313      0          (-421:413:403) -405          imp:n=1 $ between

```

```

c
999      0              405              imp:n=0
c
c fuel element
c
c
700  10 -10.494      -706              u=70 imp:n=1      $ fuel
column
701   0   706 -707              fill=1  u=70 imp:n=1      $ gap
702  11  -6.5   707 -708              u=70 imp:n=1      $ clad
703   0   708              fill=1  u=70 imp:n=1      $ outside
clad
704   0              702 -703 704 -705  lat=1 fill=70 u=71 imp:n=1      $ pin unit
cell
705   0      -700              fill=71 u=72 imp:n=1      $ element
lattice inside box
706  11  -6.5   700 -701              u=72 imp:n=1      $ wall of
element box
707   0   701              fill=1  u=72 imp:n=1      $ outside
element box

c
c pulsar fuel
c
700 rpp -3.85445 3.85445 -3.33375 3.33375 -30.607 30.607      $ element shell
inner
701 rpp -4.00685 4.00685 -3.48615 3.48615 -30.607 30.607      $ element shell
outer
702 px  -0.8131175 $ fuel pin unit cell x-
703 px   0.8131175 $ fuel pin unit cell x+
704 py  -0.6829425 $ fuel pin unit cell y-
705 py   0.6829425 $ fuel pin unit cell y+
706 cz   0.53721 $ fuel column
707 cz   0.55499 $ gap
708 cz   0.60198 $ fuel clad
c
c Ambiguity
c
1 px 0
c
c cask surfaces
c
400      cz 20.32      $ IR cask
401      cz 22.86      $ IR lead
402      cz 43.18      $ OR lead
403      cz 48.26      $ OR cask
404      cz 78.74      $ 1 foot water reflector
*405     hex 0 0 -25.25 0 0 190.5355 0 48.27 0
c
410      pz 137.1422 $ bottom of lid
411      pz 139.6822 $ steel
412      pz 164.0154 $ lead
413      pz 165.2854 $ steel
414      pz 195.7654 $ 1 foot water reflector
c
420      pz -55.72     $ 1 foot water reflector
421      pz -25.24     $ bottom of cask

```

# BRR Package Safety Analysis Report

Docket No. 71-9341  
Rev. 9, January 2016

```

422      pz -22.7      $ steel
423      pz -3.0912    $ lead
424      pz 0          $ steel
c
c basket surfaces
c
600  11  rpp -4.318  4.318  -4.318  4.318  -1000 1000 $ assembly opening
601  11  rpp -4.5857 4.5857 -4.5857 4.5857 -1000 1000 $ 304 stainless tube
602  12  rpp -4.318  4.318  -4.318  4.318  -1000 1000 $ assembly opening
603  12  rpp -4.5857 4.5857 -4.5857 4.5857 -1000 1000 $ 304 stainless tube
604  13  rpp -4.318  4.318  -4.318  4.318  -1000 1000 $ assembly opening
605  13  rpp -4.5857 4.5857 -4.5857 4.5857 -1000 1000 $ 304 stainless tube
606  14  rpp -4.318  4.318  -4.318  4.318  -1000 1000 $ assembly opening
607  14  rpp -4.5857 4.5857 -4.5857 4.5857 -1000 1000 $ 304 stainless tube
608  15  rpp -4.318  4.318  -4.318  4.318  -1000 1000 $ assembly opening
609  15  rpp -4.5857 4.5857 -4.5857 4.5857 -1000 1000 $ 304 stainless tube
610  16  rpp -4.318  4.318  -4.318  4.318  -1000 1000 $ assembly opening
611  16  rpp -4.5857 4.5857 -4.5857 4.5857 -1000 1000 $ 304 stainless tube
612  17  rpp -4.318  4.318  -4.318  4.318  -1000 1000 $ assembly opening
613  17  rpp -4.5857 4.5857 -4.5857 4.5857 -1000 1000 $ 304 stainless tube
614  18  rpp -4.318  4.318  -4.318  4.318  -1000 1000 $ assembly opening
615  18  rpp -4.5857 4.5857 -4.5857 4.5857 -1000 1000 $ 304 stainless tube

*tr1    0      -12.93  -106.5    90 0 90 180 90 90 90 90 0 -1
*tr2    0      -4.1706 -106.5    90 0 90 180 90 90 90 90 0 -1
*tr3    0       4.1706 -106.5    90 0 90 180 90 90 90 90 0 -1
*tr4    0      12.93  -106.5    90 0 90 180 90 90 90 90 0 -1
*tr5    0     -12.925  -106.5    30 120 90 60 30 90 3j -1
*tr6    0     12.925  -106.5    30 120 90 60 30 90 3j -1
*tr7    0     -12.925  -106.5    30 60 90 120 30 90 3j -1
*tr8    0     12.925  -106.5    30 60 90 120 30 90 3j -1
*tr11   13.7573  0      -106.5    9j -1
*tr12   4.5858  0      -106.5    9j -1
*tr13  -4.5858  0      -106.5    9j -1
*tr14 -13.7573  0      -106.5    9j -1
*tr15    0     -13.7573 -106.5    30 120 90 60 30 90 3j -1
*tr16    0     13.7573 -106.5    30 120 90 60 30 90 3j -1
*tr17    0     -13.7573 -106.5    30 60 90 120 30 90 3j -1
*tr18    0     13.7573 -106.5    30 60 90 120 30 90 3j -1
m2      1001.62c  2      $ water
      8016.62c  1
mt2     lwtr.60t
m3      13027.62c  1      $ Al
m4      6000.66c -0.08    $ SS-304
      14000.60c -1.0
      15031.66c -0.045
      24000.50c -19.0
      25055.62c -2.0
      26000.55c -68.375
      28000.50c -9.5
m5      82000.50c  1      $ Pb
m10     8016.62c -1.244    $ fuel.
      92235.69c -0.555
      92238.69c -8.694
m11     40000.66c  1
mode    n
kcode   15000 1.0 25 200

```



```
sdef    rad=d1 ext=d2 axs=0 0 1
si1     0 19
si2     76 137
```

## 7.0 PACKAGE OPERATIONS

### 7.1 Procedures for Loading the Package

This section delineates the procedures for loading a payload from the BRR packaging. Hereafter, reference to specific BRR packaging components may be found in Appendix 1.3.3, *Packaging General Arrangement Drawings*.

#### 7.1.1 Preparation for Loading

1. Remove the BRR package tie-down cover from the upper impact limiter.
2. Optionally, remove the cask and transport pallet from the transport trailer using the fork pockets in the pallet. Before lifting the pallet from the trailer, secure the tie-down cover to the pallet using the chains provided. Remove the tiedown cover and chains when pallet movement is complete.
3. Attach rigging to the upper impact limiter using the three (3) 1/2–13 UNC threaded holes marked as impact limiter lift points.
4. Remove the (8) eight Ø1-inch ball lock pins from each upper impact limiter attachment.
5. Using an overhead crane (or equivalent), lift and remove the upper impact limiter from the cask body.
6. Secure the lift adaptor to the cask body using the four (4) 1–8UNC bolts. If rigging is used, secure the swivel hoist rings in place using swivel hoist ring 1-8UNC fasteners. Tighten the bolts/fasteners to 220 ±20 ft-lb torque.
7. Remove the (8) eight Ø1-inch ball lock pins from each lower impact limiter attachment.
8. Lift the cask body from the lower impact limiter, and place it on the facility transport equipment or in the desired staging location.
9. Secure the cask body to the facility transport equipment or in the staging location, and remove the rigging from the lift adaptor.

#### 7.1.2 Loading of Contents

The BRR package is designed to be loaded either in a pool of water (wet) or in a hot cell (dry), as delineated in the following sections.

##### 7.1.2.1 Wet Loading

1. Remove the twelve (12) 1–8UNC socket head cap screws (SHCSs) that retain the closure lid.
2. Install three (3) hoist rings (or equivalent) into the three (3) 1/2–13 UNC threaded holes in the closure lid.
3. Lift and remove the closure lid from the cask body. Store the closure lid in a manner to minimize potential damage to the O-ring seals and sealing surfaces.
4. Install and secure the sealing surface protector to the cask body.

5. Using the center 1/2-13 UNC threaded hole in the shield plug as a lift point, remove the shield plug from the cask body.
6. If not previously installed, install the appropriate fuel basket into the cask body cavity. Verify that spacer pedestals are installed if required, as specified by Table 7.1-1 for Square fuels and Table 7.1-2 for TRIGA fuels. (Note: spacer pedestals are not used with the MURR, MITR-II, or ATR baskets.)
7. Remove the drain port dust cover and then the drain port plug. Install an appropriate drain fitting to the drain port.
8. Using an overhead crane (or equivalent), and attached to the lift adaptor, lift the cask body with the fuel basket from the facility transport equipment or staging location and position over the spent fuel pool staging area.
9. Slowly lower the cask body into the pool until the cavity is flooded, and the cask body is properly positioned and secured for fuel loading.
10. Verify that fuel to be loaded is intact and undamaged. ATR fuel end boxes may be trimmed.
11. Load fuel elements into the designated fuel basket.
  - a. Up to eight (8) fuel elements may be loaded into the MURR, MITR-II, ATR, or Square fuel baskets. Mixing of element types in the Square fuel basket is permitted.
  - b. When loading fuel elements from the University of Florida reactor, place an aluminum spacer plate,  $27 \pm \frac{1}{4}$  inches long,  $3 \pm \frac{1}{4}$  inches wide, and 0.8, -0.0/+0.03 inches thick, into the Square fuel basket opening beside the fuel element, oriented parallel to the fuel plates. The spacer plate is shown on the left side of the drawing in Figure 7.1-1.
  - c. Up to nineteen (19) fuel elements may be loaded into the TRIGA basket. Mixing of TRIGA element types in the same basket is permitted.
12. If shipping loose plates:
  - a. Load loose plates into the loose plate box. This may be performed before or after placing the loose plate box into the Square fuel basket.
  - b. Using aluminum dunnage sheets as necessary, reduce the free space between the flat face of the loose plates and the box opening to a value of  $\frac{1}{4}$  inches or less. The dunnage sheets shall be  $25\frac{1}{2} \pm \frac{1}{4}$  inches long,  $2\frac{1}{2} \pm \frac{1}{4}$  inches wide, and a minimum of  $\frac{1}{16}$  inches thick. A dunnage sheet is shown on the right side of the drawing in Figure 7.1-1.
  - c. Up to eight (8) loose plate boxes may be loaded into the Square fuel basket, each box containing up to thirty-one (31) loose plates of the types shown in Table 7.1-1. Mixing of loose plate boxes and elements in the Square fuel basket is permitted.
13. Using the center 1/2-13 UNC threaded hole as a lift point, lower the shield plug into the cask body cavity. Visually verify that the shield plug is properly seated, and reposition if necessary.
14. If required, install the shield plug restraint, or optionally, install the shield plug restraint once the cask body has been raised to the working level.

15. Lift the loaded cask body from the spent fuel pool while rinsing exposed portions with clean demineralized water. Perform a radiological survey of the cask body as it is raised out of the pool.
16. Open the drain fitting to drain the pool water from the cavity. Continue draining the cavity until no appreciable water is noted. Close the drain fitting. Optionally, the cavity may be drained after securing the cask body in the facility work area.
17. Lift the loaded cask body out of the spent fuel pool area and secure it in the facility work area.
18. Connect drain tubing to the drain fitting, and route the drain tubing to an appropriate container. Open the drain fitting.
19. Remove the sealing surface protector and, if installed, the shield plug restraint from the shield plug and cask body.
20. Remove and discard both main O-ring seals (if present), and clean and inspect the sealing surfaces in the closure lid and the mating surfaces on the cask body. If damage is present which is sufficient to impair containment integrity (scratches or dents, etc.), repair the damaged surfaces per Section 8.2.3.2, *Sealing Area Routine Inspection and Repair*.
21. Install two new (unused) O-rings in the appropriate grooves in the closure lid. As an option, sparingly apply vacuum grease to the O-ring seals and/or sealing surfaces.
22. Install the closure lid on the cask body, using the alignment pin to guide the closure lid into position.
23. Visually inspect the closure SHCSs for wear or damage that could impair their function and, if necessary, replace or repair per the requirements of the drawings in Appendix 1.3.3, *Packaging General Arrangement Drawings*.
24. Install the twelve (12) 1-8UNC SHCSs to secure the closure lid to the cask body. Using a star pattern, tighten the closure SHCSs to  $220 \pm 20$  ft-lb torque (lubricated).
25. Remove the vent port dust cover, vent port plug, test port dust cover, and test port plug.
26. Install a vent port tool into the vent port, and connect a source of dry pressurized air to the vent port tool.
27. Open the air supply flow control valve to permit dry pressurized air flowing through the cavity, ensuring that the air pressure does not exceed 25 psig. Continue the air supply flow until all apparent free standing water has been removed from the cavity.
28. Remove the drain port fitting and tubing from the drain port.
29. Remove and discard the vent, test, and drain port sealing washers from their respective port plugs (if present), and clean and inspect each sealing surface. If damage is present that is sufficient to impair containment integrity (scratches or dent, etc.), repair the damaged surfaces per Section 8.2.3.2, *Sealing Area Routine Inspection and Repair*.
30. Install the drain port plug and a new (unused) sealing washer in the drain port. Tighten the drain port plug to  $20 \pm 2$  ft-lb torque.
31. Using the vent port tool, install the vent port plug with a new (unused) sealing washer. Ensure that the vent port plug is sufficiently loose to allow airflow through the vent port.

32. Install the test port plug and a new (unused) sealing washer in the closure lid approximately finger-tight.
33. Connect a vacuum pump and a shutoff valve to the vent port tool and evacuate the cavity until the internal pressure is 1 – 2 torr. Isolate the vacuum pump from the cask body cavity by closing the shutoff valve and shutting off the vacuum pump, closing the shutoff valve and venting the suction line to atmosphere, or other appropriate means that does not maintain a vacuum on the outlet of the shutoff valve.
34. Monitor the cavity pressure for a minimum of 30 minutes. If the cavity pressure does not exceed 3 torr at the end of the time period, proceed to Step 36. If it appears that cavity pressure will exceed 3 torr, it is not necessary to wait 30 minutes before proceeding to step 35. As an option, repeat Steps 33 and 34 without first performing Step 35.
35. Open the port tool to re-pressurize the cask body cavity to atmospheric pressure and repeat Steps 33 and 34. The cask may be re-pressurized with air, nitrogen, or helium.
36. Disconnect the vacuum pump from the vent port tool and connect a source of helium gas.
37. Provide a helium atmosphere inside the cask payload cavity by backfilling with helium gas to a pressure of slightly greater than atmospheric pressure, i.e., +1, -0 psig.
38. Disconnect the helium gas source from the vent port tool.
39. Using the vent port tool, tighten the vent port plug to  $9 \pm 1$  ft-lb torque.
40. Perform leakage rate testing on the containment O-ring seal and the drain and vent port sealing washers per Section 8.2.2.2, *Helium leakage Rate Testing the Main Containment O-ring Seal*, Section 8.2.2.3, *Helium Leakage Rate Testing the Drain Port Sealing Washer*, and Section 8.2.2.4, *Helium Leakage Rate Testing the Vent Port Sealing Washer*.
41. At the conclusion of all leakage rate testing, install the drain port dust cover, the test port dust cover, and vent port dust cover.

### 7.1.2.2 Dry Loading

Steps 1 – 6 may be performed either inside or outside of the hot cell. A transfer cask may be used in place of the hot cell for this procedure. The cask must remain upright at all times.

1. Remove the twelve (12) 1-8UNC socket head cap screws (SHCSs) that retain the closure lid.
2. Install three (3) hoist rings (or equivalent) into the three (3) 1/2-13 UNC threaded holes in the closure lid.
3. Lift and remove the closure lid from the cask body. Store the closure lid in a manner to minimize potential damage to the O-ring seals and sealing surfaces.
4. Install and secure the sealing surface protector to the cask body.
5. Using the center 1/2-13 UNC threaded hole in the shield plug as a lift point, remove the shield plug from the cask body.
6. If not previously installed, install the appropriate fuel basket into the cask body cavity. Verify that spacer pedestals are installed if required, as specified by Table 7.1-1 for Square fuels and Table 7.1-2 for TRIGA fuels. (Note: spacer pedestals are not used with the MURR, MITR-II, or ATR baskets.)

7. If steps 1 – 6 were performed outside of the hot cell, reinstall shield plug in cask.
8. Mate the cask opening with the hot cell. If necessary, place the cask body inside the hot cell.
9. If required, remove the shield plug.
10. Verify that fuel to be loaded is intact and undamaged. ATR fuel end boxes may be trimmed.
11. Load fuel elements into the designated fuel basket.
  - a. Up to eight (8) fuel elements may be loaded into the MURR, MITR-II, ATR, or Square fuel baskets. Mixing of element types in the square fuel basket is permitted.
  - b. When loading fuel elements from the University of Florida reactor, place an aluminum spacer plate,  $27 \pm \frac{1}{4}$  inches long,  $3 \pm \frac{1}{4}$  inches wide, and 0.8,  $-0.0/+0.03$  inches thick, into the Square fuel basket opening beside the fuel element, oriented parallel to the fuel plates. The spacer plate is shown on the left side of the drawing in Figure 7.1-1.
  - c. Up to nineteen (19) fuel elements may be loaded into the TRIGA basket. Mixing of TRIGA element types in the same basket is permitted.
12. If shipping loose plates:
  - a. Load loose plates into the loose plate box. This may be performed before or after placing the loose plate box into the Square fuel basket.
  - b. Using aluminum dunnage sheets as necessary, reduce the free space between the flat face of the loose plates and the box opening to a value of  $\frac{1}{4}$  inches or less. The dunnage sheets shall be  $25\frac{1}{2} \pm \frac{1}{4}$  inches long,  $2\frac{1}{2} \pm \frac{1}{4}$  inches wide, and a minimum of  $\frac{1}{16}$  inches thick. A dunnage sheet is shown on the right side of the drawing in Figure 7.1-1.
  - c. Up to eight (8) loose plate boxes may be loaded into the Square fuel basket, each box containing up to thirty-one (31) loose plates of the types shown in Table 7.1-1. Mixing of loose plate boxes and elements in the Square fuel basket is permitted.
13. Using the center 1/2–13 UNC threaded hole as a lift point and a remote lift adapter, lower the shield plug into the cask body cavity. Visually verify that the shield plug is properly seated, and reposition if necessary.
14. Optionally, install the shield plug restraint.
15. If the cask was placed within the hot cell remove the loaded cask body from the hot cell. Perform a radiological survey of the cask body as it is removed.
16. If the cask was mated to the hot cell, disconnect the cask from the hot cell. Perform a radiological survey of the cask body as it is removed.
17. Remove the sealing surface protector and, if installed, the shield plug restraint from the shield plug and cask body.
18. Remove and discard both main O-ring seals (if present), and clean and inspect the sealing surfaces in the closure lid and the mating surfaces on the cask body. If damage is present which is sufficient to impair containment integrity (scratches or dents, etc.), repair the damaged surfaces per Section 8.2.3.2, *Sealing Area Routine Inspection and Repair*.

19. Install two new (unused) O-rings in the appropriate grooves in the closure lid. As an option, sparingly apply vacuum grease to the O-ring seals and/or sealing surfaces.
20. Install the closure lid on the cask body, using the alignment pin to guide the closure lid into position.
21. Visually inspect the closure SHCSs for wear or damage that could impair their function and, if necessary, replace or repair per the requirements of the drawings in Appendix 1.3.3, *Packaging General Arrangement Drawings*.
22. Install the twelve (12) 1-8UNC SHCSs to secure the closure lid to the cask body. Using a star pattern, tighten the closure SHCSs to  $220 \pm 20$  ft-lb torque (lubricated).
23. Remove the vent port dust cover, vent port plug, test port dust cover, and test port plug.
24. Remove the drain port dust cover and drain port plug.
25. Remove and discard the vent, test, and drain port sealing washers from their respective port plugs (if present), and clean and inspect each sealing surface. If damage is present that is sufficient to impair containment integrity (scratches or dent, etc.), repair the damaged surfaces per Section 8.2.3.2, *Sealing Area Routine Inspection and Repair*.
26. Install the drain port plug and a new (unused) sealing washer in the drain port. Tighten the drain port plug to  $20 \pm 2$  ft-lb torque.
27. Using the vent port tool, install the vent port plug with a new (unused) sealing washer. Ensure that the vent port plug is loose enough to allow airflow through the vent port.
28. Install the test port plug and a new (unused) sealing washer in the closure lid approximately finger-tight.
29. Connect a vacuum pump and a shutoff valve to the vent port tool and evacuate the cavity until the internal pressure is 1 – 2 torr. Isolate the vacuum pump from the cask body cavity by closing the shutoff valve and shutting off the vacuum pump, closing the shutoff valve and venting the suction line to atmosphere, or other appropriate means that does not maintain a vacuum on the outlet of the shutoff valve.
30. Monitor the cavity pressure for a minimum of 30 minutes. If the cavity pressure does not exceed 3 torr at the end of the time period, proceed to Step 32. If it appears that cavity pressure will exceed 3 torr, it is not necessary to wait 30 minutes before proceeding to step 31. As an option, repeat Steps 29 and 30 without first performing Step 31.
31. Open the port tool to re-pressurize the cask body cavity to atmospheric pressure and repeat Steps 29 and 30. The cask may be re-pressurized with air, nitrogen, or helium.
32. Disconnect the vacuum pump from the vent port tool and connect a source of helium gas.
33. Provide a helium atmosphere inside the cask payload cavity by backfilling with helium gas to a pressure of slightly greater than atmospheric pressure, i.e., +1, -0 psig.
34. Disconnect the helium gas source from the vent port tool.
35. Using the vent port tool, tighten the vent port plug to  $9 \pm 1$  ft-lb torque.
36. Perform leakage rate testing on the containment O-ring seal and the drain and vent port sealing washers per Section 8.2.2.2, *Helium leakage Rate Testing the Main Containment O-ring Seal*,

Section 8.2.2.3, *Helium Leakage Rate Testing the Drain Port Sealing Washer*, and Section 8.2.2.4, *Helium Leakage Rate Testing the Vent Port Sealing Washer*.

37. At the conclusion of all leakage rate testing, install the drain port dust cover, the test port dust cover, and vent port dust cover.

### **7.1.3 Preparation for Transport**

1. Utilizing the lift adaptor, or optional rigging, lift and lower the cask body into the lower impact limiter that is located on the transport pallet. Ensure that the cask body is aligned with the impact limiter alignment stripe for correct circumferential location.
2. Install the (8) eight Ø1–inch ball lock pins into each lower impact limiter attachment.
3. Remove the (4) four 1 – 8 UNC bolts that attach the lift adaptor to the cask body. Remove the lift adaptor or rigging hardware. The lifting holes may be optionally plugged.
4. Lift and lower the upper impact limiter onto the cask body. Ensure that the upper impact limiter is aligned with the cask body stripe for correct circumferential location.
5. Install the (8) eight Ø1–inch ball lock pins into each upper impact limiter attachment.
6. Install the tamper–indicating device (security seal) in the appropriate upper impact limiter attachment location.
7. Remove the rigging from the upper impact limiter lift points. The lifting holes may be optionally plugged.
8. Place the BRR package tie–down cover over the upper impact limiter.
9. If the transport pallet was removed from the transport trailer, secure the tie–down cover to the pallet using the chains provided. Using the fork pockets in the pallet, place the pallet on the transport trailer and attach to the trailer. Then, remove the chains between the tie–down cover and pallet.
10. Secure the tie–down cover to the transport trailer using the tie–down attachments. Optionally, install a weather seal on the bottom impact limiter.
11. Monitor external radiation for each loaded BRR package per the requirements of 49 CFR §173.441.
12. Determine that surface contamination levels for each loaded BRR package is per the requirements of 10 CFR §71.87(i) and 49 CFR §173.443.
13. Determine the transport index for each loaded BRR package per the requirements of 49 CFR §173.403.
14. Complete all necessary shipping papers in accordance with Subpart C of 49 CFR 172 [3].
15. BRR package marking shall be in accordance with 10 CFR §71.85(c) and Subpart D of 49 CFR 172. Package labeling shall be in accordance with Subpart E of 49 CFR 172. Package placarding shall be in accordance with Subpart F of 49 CFR 172.



**Table 7.1-1 – Spacer Pedestal Requirements for Square Fuels**

<b>Fuel Payload Type</b>	<b>Spacer Pedestal Height, inches<sup>②</sup></b>
RINSC <sup>①</sup>	None used
U-Mass (aluminide)	None used
U-Mass (silicide)	None used
Ohio State	4.44
Missouri S&T	5.19
Purdue	7.20
PULSTAR	1.46
U-Florida	12.31
Loose plates from: •U-Mass (aluminide) •U-Florida •Purdue	Loose Plate Box <sup>②</sup>

Notes:

1. Rhode Island Nuclear Science Center.
2. Spacer pedestals and the Loose Plate Box are shown on drawing 1910-01-03-SAR.

**Table 7.1-2 – Spacer Pedestal Requirements for TRIGA Fuels**

<b>TRIGA Fuel Catalog No.</b>	<b>Spacer Length, in<sup>①</sup></b>	<b>Spacer Description</b>
101	19.01	Adjustable, 4 <sup>th</sup> position
201	18.48	Adjustable, 3 <sup>rd</sup> position
103, 105, 109	18.48	Adjustable, 3 <sup>rd</sup> position
117, 119	17.70	Adjustable, 2 <sup>nd</sup> position
107	17.25	Adjustable, 1 <sup>st</sup> position
403, 405, 417, 419	17.25	Adjustable, 1 <sup>st</sup> position
217, 219	7.28	Fixed, long
303, 305, 317, 319	3.63	Fixed, medium
203, 205, 207, 503, 505, 517, 519	2.13	Fixed, short

Notes:

1. Spacer pedestals are shown on drawing 1910-01-03-SAR.

**Security-Related Information Figure  
Withheld Under 10 CFR 2.390.**

**Figure 7.1-1 - Drawing of U-Florida Spacer Plate and Loose Plate  
Dunnage Sheet**

## 7.2 Procedures for Unloading the Package

This section delineates the procedures for unloading a payload from the BRR packaging. Hereafter, reference to specific BRR packaging components may be found in Appendix 1.3.3, *Packaging General Arrangement Drawings*.

### 7.2.1 Receipt of Package from Carrier

1. Remove the BRR package tie-down cover from the upper impact limiter.
2. Verify that the tamper-indicating device (security seal) has not been tampered with or removed.
3. Attach rigging to the upper impact limiter using the three (3) 1/2-13 UNC threaded holes marked as impact limiter lift points.
4. Remove the tamper-indicating device (security seal) and the (8) eight Ø1-inch ball lock pins from each upper impact limiter attachment.
5. Using an overhead crane (or equivalent), lift and remove the upper impact limiter from the cask body.
6. Secure the lift adaptor to the cask body using the (4) four 1-8UNC bolts. If rigging is used, secure the swivel hoist rings in place using swivel hoist ring 1-8UNC fasteners. Tighten the bolts to 220 ±20 ft-lb.
7. Remove the (8) eight Ø1-inch ball lock pins from each lower impact limiter attachment.
8. Lift the loaded cask body from the lower impact limiter, and place it on the facility transport equipment.
9. Secure the cask body to the facility transport equipment, and remove the rigging from the lift adaptor.

### 7.2.2 Removal of Contents

The BRR package is designed to be unloaded either in a pool of water (wet) or in a hot cell (dry), as delineated in the following sections. The unloading procedures may require removal of the lift adapter to facilitate gas sampling or other testing. If the lift adapter is removed for this purpose, reinstall per Paragraph 7.2.1, step 6 upon completion of sampling or testing.

#### 7.2.2.1 Wet Unloading

1. Remove the vent port dust cover and connect a vent port tool to the vent port. Connect a gas sampling device to the vent port tool.
2. Loosen and remove the vent port plug using the vent port tool so that a gas sample may be extracted from the cavity.
3. Following verification of no contamination in the gas sample, vent the cavity to atmosphere to equalize cavity pressure.
4. Install three (3) hoist rings (or equivalent) into the three (3) 1/2-13 UNC threaded holes in the closure lid.
5. Remove the twelve (12) 1-8UNC socket head cap screws (SHCSs) that secure the closure lid.

6. Lift and remove the closure lid from the cask body. Store the closure lid in a manner to minimize potential damage to the O-ring seals and sealing surfaces.
7. Install and secure the sealing surface protector to the cask body.
8. Optionally, install the shield plug restraint over the shield plug in the cask body.
9. Remove the drain port dust cover and then the drain port plug. Install an appropriate fitting to the drain port.
10. Using appropriate rigging and an overhead crane (or equivalent) attached to the lift adaptor, lift the loaded cask body from the facility transport equipment and position over the spent fuel pool staging area.
11. If installed, remove the shield plug restraint, or optionally, remove the restraint after the cask body is secured in the facility fuel unloading station.
12. Slowly lower the cask body into the pool until the cavity is flooded, and secure the loaded cask body in the facility fuel unloading station.
13. Using the center 1/2-13 UNC threaded hole in the shield plug as a lift point, remove the shield plug from the cask body.
14. Remove the fuel elements or loose plate box from the basket and place in the facility's receiving station.
15. Using the center 1/2-13 UNC threaded hole as a lift point, lower the shield plug into the cask body cavity. Visually verify that the shield plug is properly seated, and reposition if necessary.
16. Optionally, install the shield plug restraint. The shield plug restraint may be installed once the cask body has been raised to the working level.
17. Lift the cask body from the spent fuel pool while spraying exposed portions with clean demineralized water. Perform a radiological survey of the cask body as it is raised out of the pool.
18. Open the drain fitting to drain the pool water from the cavity. Continue draining the cavity until no appreciable water is noted. Optionally, the cavity may be drained after securing the cask body in the facility work area.
19. Close the drain fitting, and remove the connecting plumbing from the drain fitting.
20. Lift the cask body out of the spent fuel pool area and secure it in the facility work area.
21. Remove the sealing surface protector and, if installed, the shield plug restraint from the shield plug and cask body.
22. Install the closure lid on the cask body, using the alignment pin to guide the closure lid into position.
23. Install the twelve (12) 1-8UNC SHCSs to secure the closure to the cask body. Using a star pattern, tighten the closure SHCSs to  $220 \pm 20$  ft-lb torque (lubricated).
24. Install the vent port plug and tighten to  $9 \pm 1$  ft-lb torque. Install the vent port dust cover.
25. Install the drain port plug and tighten to  $20 \pm 2$  ft-lb torque. Install the drain port dust cover.

26. Assemble the impact limiters onto the package and secure the package to the transport trailer as described in Section 7.1.3, *Preparation for Transport*. A tamper-indicating device is not required.

#### **7.2.2.2 Dry Unloading**

Steps 1 – 9 may be performed either inside or outside of the hot cell. A transfer cask may be used in place of the hot cell for this procedure. The cask must remain upright at all times

1. Remove the vent port dust cover and connect a vent port tool to the vent port. Connect a gas sampling device to the vent port tool.
2. Loosen and remove the vent port plug using the vent port tool so that a gas sample may be extracted from the cavity.
3. Following verification of no contamination in the gas sample, vent the cavity to atmosphere to equalize cavity pressure.
4. Install three (3) hoist rings (or equivalent) into the three (3) 1/2-13 UNC threaded holes in the closure lid.
5. Remove the twelve (12) 1-8UNC socket head cap screws (SHCSs) that retain the closure lid.
6. Lift and remove the closure lid from the cask body. Store the closure lid in a manner to minimize potential damage to the O-ring seals and sealing surfaces.
7. Install and secure the sealing surface protector to the cask body.
8. Optionally, install the shield plug restraint over the shield plug in the cask body.
9. Install a remote lift adaptor in the center 1/2-13 UNC threaded hole of the shield plug.
10. Mate the cask opening with the hot cell. If required, place the loaded cask body into the hot cell.
11. Remove the shield plug restraint (if installed) and lift the shield plug from the cask body.
12. Remove the fuel elements or loose plate box from the basket and place in the facility's receiving station.
13. Replace the shield plug into the cask body cavity. Optionally, install the shield plug restraint.
14. Remove or disconnect the unloaded cask body from the hot cell.
15. Remove the remote lift adaptor from the shield plug.
16. Remove the shield plug restraint (if installed) and remove the sealing surface protector.
17. Install the closure lid on the cask body, using the alignment pin to guide the closure lid into position.
18. Install the twelve (12) 1-8UNC SHCSs to secure the closure to the cask body. Using a star pattern, tighten the closure SHCSs to 220 ±20 ft-lb torque (lubricated).
19. Install the vent port plug and tighten to 9 ±1 ft-lb torque. Install the vent port dust cover.
20. If used, install the drain port plug and tighten to 20 ±2 ft-lb torque. Install the drain port dust cover.
21. Assemble the impact limiters onto the package and secure the package to the transport trailer as described in Section 7.1.3, *Preparation for Transport*. A tamper-indicating device is not required.

### **7.3 Preparation of an Empty Package for Transport**

Previously used and empty BRR packagings shall be prepared and transported per the requirements of 49 CFR §173.428.

## **7.4 Appendix**

### **7.4.1 References**

1. Title 10, Code of Federal Regulations, Part 71 (10 CFR 71), *Packaging and Transportation of Radioactive Material*, 01–01–08 Edition.
2. Title 49, Code of Federal Regulations, Part 173 (49 CFR 173), *Shippers–General Requirements for Shipments and Packagings*, 10–01–08 Edition
3. Title 49, Code of Federal Regulations, Part 172 (49 CFR 172), *Hazardous Materials Tables and Hazardous Communications Regulations*, 10–01–08 Edition.

## 8.0 ACCEPTANCE TESTS AND MAINTENANCE PROGRAM

This section describes the acceptance tests and the maintenance program that shall be used on the BRR package in compliance with Subpart G of 10 CFR 71 [1].

### 8.1 Acceptance Tests

Per the requirements of 10 CFR §71.85, this section discusses the inspections and tests to be performed prior to first use of the BRR packaging. Acceptance criteria for all inspections and tests are found either on the drawings in Appendix 1.3.3, *Packaging General Arrangement Drawings*, or in the sections that follow. Deviations from requirements will be recorded and dispositioned in accordance with the cognizant quality assurance program.

#### 8.1.1 Visual Inspection and Measurements

Each BRR packaging will be visually inspected and measured to ensure that all of the requirements delineated on the drawings in Appendix 1.3.3, *Packaging General Arrangement Drawings*, are satisfied. This includes but is not limited to such items as materials, physical arrangement of components, quantities, dimensions, welds, and measurements.

#### 8.1.2 Weld Examinations

The locations, types, and sizes of all welds will be identified and recorded to ensure compliance with the drawings in Appendix 1.3.3, *Packaging General Arrangement Drawings*. All welds are subject to visual examination per AWS D1.6 [2]. The welds between the inner containment shell and either end structure, the welds between the outer shell and either end structure, and the longitudinal weld(s) in the outer shell, if any, are examined by ultrasonic inspection in accordance with the ASME Code, Subsection NB, Article NB-5000, and Section V, Article 4 [4]. Optionally, the weld between the inner containment shell and the lower end structure may be examined by radiographic inspection in accordance with the ASME Code, Subsection NB, Article NB-5000, and Section V, Article 2 [3]. All welds on the BRR package, except seal welds, are liquid penetrant inspected on the final pass in accordance with the ASME Code, Subsection Nx, Article Nx-5000, and Section V, Article 6 [5]. The appropriate Subsection for the containment welds and outer shell welds is NB; for other cask body welds and the impact limiter shells, NF; and for the fuel baskets, NG.

#### 8.1.3 Structural and Pressure Tests

##### 8.1.3.1 Lifting Device Load Testing

The BRR package does not contain any lifting devices that require load testing.

##### 8.1.3.2 Containment Boundary Pressure Testing

The BRR package containment boundary shall be pressure tested to the greater of 125% of the design pressure per the requirements of ASME Code, Subsection NB, Article NB-6220 [6], or 150% of the maximum normal operating pressure (MNOP), per 10 CFR §71.85(b). Since the MNOP of the BRR package is 10 psig, and the design pressure is 25 psig, the test pressure shall be a minimum of  $1.25 \times 25 = 31.25$  psig.



Following pressure testing of the containment boundary, welds directly related to the pressure testing and accessible base material adjacent to the welds shall be visually inspected for plastic deformation or cracking in accordance with AWS D1.6, and liquid penetrant inspected per ASME Code, Subsection NB, Article NB–5000, and Section V, Article 6, as delineated on the drawings in Appendix 1.3.3, *Packaging General Arrangement Drawings*. Indications of cracking or distortion shall be recorded and evaluated in accordance with the cognizant quality assurance program.

Except for the leakage rate testing of the containment body structure prior to lead pour, leakage rate testing per Section 8.1.4, *Fabrication Leakage Rate Tests*, shall be performed after completion of pressure testing to verify package configuration and performance to design criteria.

#### **8.1.4 Fabrication Leakage Rate Tests**

This section provides the generalized procedure for fabrication leakage rate testing of the containment vessel boundaries and penetrations during and following the completion of fabrication. Fabrication leakage rate testing shall follow the guidelines of Section 7.3, *Fabrication Leakage Rate Test*, of ANSI N14.5 [7].

Prior to leakage rate testing, internal components that are not permanently affixed to the containment boundary, such as shield plug and spent fuel baskets, shall be removed. For ease of leakage rate testing, the interior surfaces of the containment boundary should be thoroughly cleaned.

Fabrication leakage rate testing shall be performed on the containment boundary. Four separate tests comprise the series. Each test shall meet the acceptance criteria delineated in Section 8.1.4.1, *Fabrication Leakage Rate Test Acceptance Criteria*.

##### **8.1.4.1 Fabrication Leakage Rate Test Acceptance Criteria**

1. To be acceptable, each leakage rate test shall demonstrate a “leaktight” leakage rate of  $1 \times 10^{-7}$  reference cubic centimeters per second (ref-cm<sup>3</sup>/s), air, or less, per Section 6.3, *Application of Reference Air Leakage Rate ( $L_R$ )*, of ANSI N14.5.
2. In order to demonstrate the leaktight leakage rate, the sensitivity of the leakage rate test procedure shall be  $5 \times 10^{-8}$  cm<sup>3</sup>/s, air, or less, per Section 8.4, *Sensitivity*, of ANSI N14.5.
3. Failure to meet the stated leakage rate shall be recorded and evaluated in accordance with the cognizant quality assurance program.

##### **8.1.4.2 Helium Leakage Rate Testing the Containment Structure Integrity**

Fabrication leakage rate testing of the containment structure integrity is performed in two stages: prior to lead pour, and following lead pour. These two stages are necessitated by the in-situ lead shielding surrounding the cylindrical containment shell between the upper and lower end structures, which would prevent helium gas from reaching the surface of the steel.

###### **8.1.4.2.1 Containment Body Structure (Prior to Lead Pour)**

This leakage rate test verifies the leak tightness of the upper and lower end forgings/castings, and the inner shell that comprise the primary metallic containment boundary of the BRR packaging.

1. The fabrication leakage rate test shall be performed following the guidelines of Section A.5.3, *Gas Filled Envelope – Gas Detector*, of ANSI N14.5.

**BRR Package Safety Analysis Report**

---

2. The BRR packaging shall be assembled with a test lid and seal in place of the closure lid onto the partially fabricated cask, consisting of the upper and lower end structures, inner containment shell, and outer structural shell.
3. Connect a port tool to the drain port in the lower end forging.
4. Install a helium mass spectrometer leak detector (MSLD) to the port tool. Evacuate through the drain port until the vacuum is sufficient to operate the MSLD.
5. Surround the outer surface of the containment body with an envelope filled with helium gas (99% purity or better) to a minimum concentration of 50%, and to a pressure slightly greater than atmospheric pressure. The final leakage rate shall be adjusted for the helium concentration in the envelope.
6. Perform the helium leakage rate test to the requirements of Section 8.1.4.1, *Fabrication Leakage Rate Test Acceptance Criteria*. If, after repeated attempts, the containment structure fails to pass the leakage rate test, isolate the leak path and, prior to repairing the leak path and repeating the leakage rate test, record on a nonconformance report and disposition prior to final acceptance in accordance with the cognizant quality assurance program.
7. Disconnect the port tool from the drain port in the lower end forging.

**8.1.4.2.2 Containment Body Structure (Following Lead Pour)**

This leakage rate test verifies the leak tightness of the closure lid, and the final machined configuration of the upper end structure that comprise the balance of the metallic containment boundary of the BRR packaging.

1. The fabrication leakage rate test shall be performed following the guidelines of Section A.5.3, *Gas Filled Envelope – Gas Detector*, of ANSI N14.5.
2. The BRR packaging shall be assembled with the two O-ring seals installed in the closure lid, and the vent and seal test port plugs installed with their associated sealing washers. If not previously tightened, tighten the closure lid bolts to 200 – 240 ft-lb torque (lubricated). Assembly is as shown in Appendix 1.3.3, *Packaging General Arrangement Drawings*.
3. Connect a port tool to the drain port in the lower end of the packaging.
4. Install a helium mass spectrometer leak detector (MSLD) to the port tool. Evacuate through the drain port until the vacuum is sufficient to operate the MSLD.
5. Surround the outer surface of the closure lid and upper end structure with an envelope filled with helium gas (99% purity or better) to a minimum concentration of 50%, and to a pressure slightly greater than atmospheric pressure. The final leakage rate shall be adjusted for the helium concentration in the envelope.
6. Perform the helium leakage rate test to the requirements of Section 8.1.4.1, *Fabrication Leakage Rate Test Acceptance Criteria*. If, after repeated attempts, the containment structure fails to pass the leakage rate test, isolate the leak path and, prior to repairing the leak path and repeating the leakage rate test, record on a nonconformance report and disposition prior to final acceptance in accordance with the cognizant quality assurance program.
7. Remove the port tool and re-install the drain port plug. Tighten to 18 – 22 ft-lb torque.

**8.1.4.3 Helium Leakage Rate Testing the Main Containment O-ring Seal**

1. The fabrication leakage rate test of the BRR package containment O-ring seal integrity shall be performed following the guidelines of Section A.5.4, *Evacuated Envelope – Gas Detector*, of ANSI N14.5.
2. Assemble the BRR package with the two O-ring seals installed in the closure lid. Ensure the vent and seal test ports are installed with their associated sealing washers. Assembly is as shown in Appendix 1.3.3, *Packaging General Arrangement Drawings*.
3. Utilizing a port tool, attach a vacuum pump and a source of helium gas, in parallel, to the vent port.
4. Close the valve to the source of helium gas and open the valve to the vacuum pump.
5. Utilizing a port tool, rotate the vent port plug to the open position.
6. Evacuate the system to a 90% vacuum or better ( $\leq 10\%$  ambient atmospheric pressure). Isolate the vacuum pump from the system.
7. Provide a helium atmosphere inside the evacuated cavity by backfilling with helium gas (99% purity or better) to ambient atmospheric pressure (+1 psi, -0 psi).
8. Utilizing the port tool, rotate the vent port plug to the closed position, and remove the helium-contaminated port tool from the vent port.
9. Install a clean (helium-free) port tool into the seal test port.
10. Utilizing appropriate fittings, attach a helium MSLD to the port tool.
11. Utilizing the port tool, rotate the seal test port plug to the open position.
12. Evacuate the cavity between the containment O-ring seal and the test O-ring seal until the vacuum is sufficient to operate the leak detector per the manufacturer's recommendations.
13. Perform the helium leakage rate test to the requirements of Section 8.1.4.1, *Fabrication Leakage Rate Test Acceptance Criteria*. If, after repeated attempts, the BRR package containment O-ring seal fails to pass the leakage rate test, isolate the leak path and, prior to repairing the leak path and repeating the leak test, record on a nonconformance report and disposition prior to final acceptance in accordance with the cognizant quality assurance program.

**8.1.4.4 Helium Leakage Rate Testing the Drain Port Sealing Washer**

1. The fabrication leakage rate test of the drain port plug containment sealing washer integrity shall be performed following the guidelines of Section A.5.4, *Evacuated Envelope – Gas Detector*, of ANSI N14.5.
2. The BRR package shall be assembled with the two O-ring seals installed on the closure lid. Ensure the vent and seal test port plugs are installed with their associated sealing washers. Assembly is as shown in Appendix 1.3.3, *Packaging General Arrangement Drawings*.
3. Verify the presence of a helium atmosphere below the vent port plug containment sealing washer, as specified above in Steps 3 – 8 of Section 8.1.4.3, *Helium Leakage Rate Testing the Main Containment O-ring Seal*.
4. Install a port tool into the drain port.
5. Utilizing appropriate fittings, attach a helium MSLD to the port tool.

**BRR Package Safety Analysis Report**

6. Evacuate the cavity above the drain port plug containment sealing washer until the vacuum is sufficient to operate the leak detector per the manufacturer’s recommendations.
7. Perform the helium leakage rate test to the requirements of Section 8.1.4.1, *Fabrication Leakage Rate Test Acceptance Criteria*. If, after repeated attempts, the drain port plug containment sealing washer fails to pass the leakage rate test, isolate the leak path and, prior to repairing the leak path and repeating the leak test, record on a nonconformance report and disposition prior to final acceptance in accordance with the cognizant quality assurance program.

**8.1.4.5 Helium Leakage Rate Testing the Vent Port Sealing Washer**

The fabrication leakage rate test of the vent port sealing washer may also be performed during the leakage rate testing of the metallic containment boundary following lead pour per Section 8.1.4.2.2, *Containment Body Structure (Following Lead Pour)*.

1. The fabrication leakage rate test of the vent port plug containment sealing washer integrity shall be performed following the guidelines of Section A.5.4, *Evacuated Envelope – Gas Detector*, of ANSI N14.5.
2. The BRR package shall be assembled with the two O–ring seals installed on the closure lid. Ensure the vent and seal test port plugs are installed with their associated sealing washers. Assembly is as shown in Appendix 1.3.3, *Packaging General Arrangement Drawings*.
3. Verify the presence of a helium atmosphere below the vent port plug containment sealing washer, as specified above in Steps 3 – 8 of Section 8.1.4.3, *Helium Leakage Rate Testing the Main Containment O–ring Seal*.
4. Install a port tool into the vent port.
5. Utilizing appropriate fittings, attach a helium MSLD to the port tool.
6. Evacuate the cavity above the vent port plug containment sealing washer until the vacuum is sufficient to operate the leak detector per the manufacturer’s recommendations.
7. Perform the helium leakage rate test to the requirements of Section 8.1.4.1, *Fabrication Leakage Rate Test Acceptance Criteria*. If, after repeated attempts, the vent port plug containment sealing washer fails to pass the leakage rate test, isolate the leak path and, prior to repairing the leak path and repeating the leak test, record on a nonconformance report and disposition prior to final acceptance in accordance with the cognizant quality assurance program.

**8.1.5 Component and Material Tests****8.1.5.1 Polyurethane Foam**

This section establishes the requirements and acceptance criteria for installation, inspection, and testing of the rigid, closed–cell, polyurethane foam utilized within the BRR packaging impact limiters.

**8.1.5.1.1 Introduction and General Requirements**

The polyurethane foam used within the BRR packaging is comprised of a specific “formulation” of foam constituents that, when properly apportioned, mixed, and reacted, produce a polyurethane foam material with physical characteristics consistent with the requirements given in Section 8.1.5.1.2, *Physical Characteristics*. In practice, the chemical constituents are batched into multiple parts (e.g.,

parts A and B) for later mixing in accordance with a formulation. Therefore, a foam “batch” is considered to be a specific grouping and apportionment of chemical constituents into separate and controlled vats or bins for each foam formulation part. Portions from each batch part are combined in accordance with the foam formulation requirements to produce the liquid foam material for pouring into a component or box. Thus, a foam “pour” is defined as apportioning and mixing the batch parts into a desired quantity for subsequent installation (pouring). Finally, all contiguous pours into a single mold are termed a “bun”.

The following sections describe the general requirements for constituent storage, and foam pour and test data records.

#### **8.1.5.1.1.1 Polyurethane Foam Constituent Storage**

The foam supplier shall certify that the polyurethane foam constituents have been properly stored prior to use, and that the polyurethane foam constituents have been used within their shelf life.

#### **8.1.5.1.1.2 Impact Limiter Shell Preparation**

Prior to installing foam into the impact limiter shells, the interior surfaces of the shells shall be treated with an antibonding agent, such as a paste wax.

#### **8.1.5.1.1.3 Polyurethane Foam Installation**

The foam shall be installed while the longitudinal axis of the impact limiter shell is vertical. The walls of the shell where the liquid foam material is to be installed shall be between 55 °F and 95 °F prior to foam installation. Measure and record the shell temperature to an accuracy of  $\pm 2$  °F prior to foam installation.

In the case of multiple pours into a single impact limiter, the cured level of each pour shall be measured and recorded to an accuracy of  $\pm 1$  inch.

Measure and record the weight of liquid foam material installed during each pour to an accuracy of  $\pm 10$  pounds.

All test samples shall be poured into disposable containers at the same time as the actual pour it represents, clearly marking the test sample container with the pour date and a unique pour identification number. All test samples shall be cut from a larger block to obtain freshly cut faces. Prior to physical testing, each test sample shall be cleaned of superfluous foam dust.

#### **8.1.5.1.1.4 Polyurethane Foam Pour and Test Data Records**

A production pour and testing record shall be compiled by the foam supplier during the foam pouring operation and subsequent physical testing. Upon completion of production and testing, the foam supplier shall issue a certification referencing the production record data and test data pertaining to each foamed component. At a minimum, relevant pour and test data shall include:

- formulation, batch, and pour numbers, with foam material traceability, and pour date,
- instrumentation description, serial number, and calibration due date,
- pour and test data (e.g., date, temperature, dimensional, and/or weight measurements, compressive stress, etc., as applicable), and
- technician and Quality Assurance/Quality Control (QA/QC) sign-off.

### 8.1.5.1.2 Physical Characteristics

The following subsections define the required physical characteristics of the polyurethane foam material.

Testing for the various polyurethane foam physical characteristics is based on a “formulation”, “batch”, or “pour”, as appropriate, as defined in Section 8.1.5.1.1, *Introduction and General Requirements*. The physical characteristics determined for a specific foam formulation are relatively insensitive to small variations in chemical constituents and/or environmental conditions, and therefore include physical testing only for leachable chlorides, thermal conductivity, and specific heat. Similarly, the physical characteristics determined for a batch are only slightly sensitive to small changes in formulation and/or environmental conditions during batch mixing, and therefore include physical testing only for flame retardancy. Finally, the physical characteristics determined for a pour are also only slightly sensitive to small changes in formulation and slightly more sensitive to variations in environmental conditions during pour mixing, and therefore include physical testing for density and compressive stress.

#### 8.1.5.1.2.1 Physical Characteristics Determined for a Foam Formulation

##### 8.1.5.1.2.1.1 Leachable Chlorides

The leachable chloride physical characteristic shall be determined once for a particular foam formulation. If multiple components are to utilize a specific foam formulation, then additional physical testing, as defined below, need not be performed.

1. The leachable chlorides test shall be performed using an ion chromatograph (IC) apparatus. The IC measures inorganic anions of interest (i.e., chlorides) in water. Description of a typical IC is provided in EPA Method 300.0 [8]. The IC shall be calibrated against a traceable reference specimen per the IC manufacturer’s operating instructions.
2. One test sample shall be taken from a pour for each foam formulation. The test sample shall be a cube with dimensions of  $2.00 \pm 0.06$  in.
3. Place the test sample in a room (ambient) temperature environment (i.e., 68 °F to 86 °F) for sufficient time to thermally stabilize the test sample. Measure and record the room temperature to an accuracy of  $\pm 2$  °F.
4. Obtain a minimum of 550 mL of distilled or de-ionized water for testing. The test water shall be from a single source to ensure consistent anionic properties for testing control.
5. Obtain a 400 mL, or larger, contaminant free container that is capable of being sealed. Fill the container with  $250 \pm 3$  mL of test water. Fully immerse the test sample inside the container for a duration of  $72 \pm 3$  hours. If necessary, use an inert standoff to ensure the test sample is completely immersed for the full test duration. Seal the container prior to the 72-hour duration.
6. Obtain a second, identical container to use as a “control”. Fill the control container with  $250 \pm 3$  mL of the same test water. Seal the control container prior to the 72-hour duration.
7. At the end of the test period, measure and record the leachable chlorides in the test water per the IC manufacturer’s operating instructions. The leachable chlorides in the test water shall not exceed one part per million (1 ppm).

**BRR Package Safety Analysis Report**

8. Should leachable chlorides in the test water exceed 1 ppm, measure and record the leachable chlorides in the test water from the “control” container. The difference in leachable chlorides from the test water and “control” water sample shall not exceed 1 ppm.

**8.1.5.1.2.1.2 Thermal Conductivity**

1. The thermal conductivity test shall be performed using a heat flow meter (HFM) apparatus. The HFM establishes steady state unidirectional heat flux through a test specimen between two parallel plates at constant but different temperatures. By measurement of the plate temperatures and plate separation, Fourier’s law of heat conduction is used by the HFM to automatically calculate thermal conductivity. Description of a typical HFM test method is provided in ASTM C518 [9]. The HFM shall be calibrated against a traceable reference specimen per the HFM manufacturer’s operating instructions.
2. Three test samples shall be taken from the sample pour. Each test sample shall be of sufficient size to enable testing per the HFM manufacturer’s operating instructions.
3. Place the test samples in a room (ambient) temperature environment (i.e., 68 °F to 86 °F) for sufficient time to thermally stabilize the test samples.
4. Measure and record the necessary test sample parameters as input data to the HFM apparatus per the HFM manufacturer’s operating instructions.
5. Perform thermal conductivity testing and record the measured thermal conductivity for each test sample following the HFM manufacturer’s operating instructions.
6. Determine and record the average thermal conductivity of the three test samples. The numerically averaged thermal conductivity of the three test samples shall be within the range between 0.17 and 0.25 (BTU-in)/(hr-ft<sup>2</sup>-°F).

**8.1.5.1.2.1.3 Specific Heat**

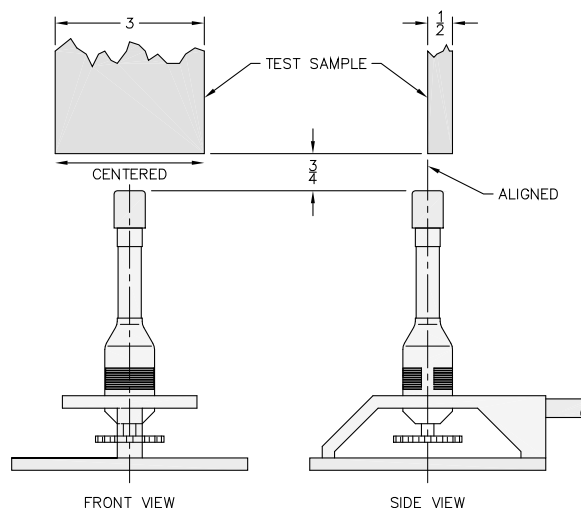
1. The specific heat test shall be performed using a differential scanning calorimeter (DSC) apparatus. The DSC establishes a constant heating rate and measures the differential heat flow into both a test specimen and a reference specimen. Description of a typical DSC is provided in ASTM E1269 [10]. The DSC shall be calibrated against a traceable reference specimen per the DSC manufacturer’s operating instructions.
2. Three test samples shall be taken from the sample pour. Each test sample shall be of sufficient size to enable testing per the DSC manufacturer’s operating instructions.
3. Place the test samples in a room (ambient) temperature environment (i.e., 68 °F to 86 °F) for sufficient time to thermally stabilize the test samples.
4. Measure and record the necessary test sample parameters as input data to the DSC per the DSC manufacturer’s operating instructions.
5. Perform specific heat testing and record the measured specific heat for each test sample following the DSC manufacturer’s operating instructions.
6. Determine and record the average specific heat of the three test specimens. The numerically averaged specific heat of the three test samples shall be within the range between 0.28 and 0.42 Btu/lb<sub>m</sub>-°F.

#### 8.1.5.1.2.2 Physical Characteristics Determined for a Foam Batch

Polyurethane foam material physical characteristics for flame retardancy shall be determined once for a particular foam batch based on the batch definition in Section 8.1.5.1.1, *Introduction and General Requirements*. If single or multiple components are to utilize a single foam batch, then additional flame retardancy testing, as defined below, need not be performed for each foam pour.

Polyurethane foam shall be tested for flame retardancy as follows:

1. Three test samples shall be taken from a pour from each foam batch. Each test sample shall be a rectangular prism with nominal dimensions of 0.5 inches thick, 3.0 inches wide, and a minimum length of 7.0 inches. In addition, individual sample lengths must not be less than the total burn length observed for the sample when tested.
2. Place the test samples in a room (ambient) temperature environment (i.e., 68 °F to 86 °F) for sufficient time to thermally stabilize the test samples. Measure and record the room temperature to an accuracy of  $\pm 2$  °F.
3. Measure and record the length of each test sample to an accuracy of  $\pm 0.15$  in.
4. Install an approximately 3/8-inch, or larger, Bunsen or Tirrill burner inside an enclosure of sufficient size to perform flame retardancy testing. Adjust the burner flame height to  $1\frac{1}{2} \pm \frac{1}{4}$  inch. Verify that the burner flame temperature is 1,550 °F, minimum.
5. Support the test sample with the long axis oriented vertically within the enclosure such that the test sample's bottom edge will be  $\frac{3}{4} \pm \frac{1}{8}$  inch (see adjacent figure) above the top edge of the burner.
6. Move the burner flame under the test sample for an elapsed time of  $60 \pm 2$  seconds. As illustrated, align the burner flame with the front edge of the test sample thickness and the center of the test sample width.
7. Immediately after removal of the test sample from the burner flame, measure and record the following data:
  - a. Measure and record, to the nearest second, the elapsed time until flames from the test sample extinguish.
  - b. Measure and record, to the nearest second, the elapsed time from the occurrence of drips, if any, until drips from the test sample extinguish.
  - c. Measure and record, to the nearest 0.15 inch, the burn length following cessation of all visible burning and smoking.
8. Flame retardancy testing acceptance is based on the following criteria:





- a. The numerically averaged flame extinguishment time of the three test samples shall not exceed fifteen seconds.
- b. The numerically averaged flame extinguishment time of drips from the three test samples shall not exceed three seconds.
- c. The numerically averaged burn length of the three test samples shall not exceed 6.0 in.

#### 8.1.5.1.2.3 Physical Characteristics Determined for a Foam Pour

##### 8.1.5.1.2.3.1 Density

Polyurethane foam material physical characteristic for density shall be determined for each foam pour based on the pour definition in Section 8.1.5.1.1, *Introduction and General Requirements*.

1. Three test samples shall be taken from the foam pour. Each test sample shall be a rectangular prism with minimum nominal dimensions of 1.0 inch thick (T) × 2.0 inch wide (W) × 2.0 inch long (L).
2. Place the test samples in a room (ambient) temperature environment (i.e., 68 °F to 86 °F) for sufficient time to thermally stabilize the test samples. Measure and record the room temperature to an accuracy of ±2 °F.
3. Measure and record the weight of each test sample to an accuracy of ±1 gram.
4. Measure and record the thickness, width, and length of each test sample to an accuracy of ±0.03 in.
5. Determine and record the room temperature density of each test sample utilizing the following formula:

$$\rho_{foam} = \frac{\text{Weight, g}}{453.6 \text{ g/lb}_m} \times \frac{1,728 \text{ in}^3/\text{ft}^3}{T \times W \times L, \text{ in}^3}, \text{ lb}_m/\text{ft}^3$$

6. Determine and record the average density of the three test samples. The numerically averaged density of the three test samples shall be within ±15% of the specified nominal foam density, i.e., within the range of 7.7 to 10.4 lb<sub>m</sub>/ft<sup>3</sup> for a nominal 9 lb<sub>m</sub>/ft<sup>3</sup> foam.

##### 8.1.5.1.2.3.2 Compressive Stress

1. Three test samples shall be taken from each foam pour. Each test sample shall be a rectangular prism with minimum nominal dimensions of 1.0 inch thick (T) × 2.0 inch wide (W) × 2.0 inch long (L). The thickness dimension shall be the parallel-to-rise direction (for the perpendicular-to-rise direction, see below).
2. Place the test samples in a room (ambient) temperature environment (i.e., 68 °F to 86 °F) for sufficient time to thermally stabilize the test samples. Measure and record the room temperature to an accuracy of ±2 °F.
3. Measure and record the thickness, width, and length of each test sample to an accuracy of ±0.03 inch.
4. Compute and record the surface area of each test sample by multiplying the width by the length (i.e., W × L).

5. Place a test sample in a Universal Testing Machine. Lower the machine's crosshead until it touches the test sample. Set the machine's parameters for the thickness of the test sample.
6. Determine and record the average parallel-to-rise compressive stress of the three test samples from each batch pour for each foam density. As shown in Table 8.1-1, the average parallel-to-rise compressive stress for each foam pour shall be the nominal compressive stress  $\pm 15\%$  at strains of 20%, 40%, and 70%.
7. Determine and record the average parallel-to-rise compressive stress of all test samples from each foamed component. As shown in Table 8.1-1, the average parallel-to-rise compressive stress for all foam pours used in a single bun shall be the nominal compressive stress  $\pm 10\%$  at strains of 20%, 40%, and 70%.
8. Data for compressive stress in the perpendicular-to-rise direction shall be obtained in an identical manner, using three additional test samples, except that the thickness dimension of the test samples shall be perpendicular to the foam rise direction. As shown in Table 8.1-2, the average perpendicular-to-rise compressive stress for each foam pour shall be the nominal compressive stress  $\pm 15\%$  at strains of 20%, 40%, and 70%. As further shown in Table 8.1-2, the average perpendicular-to-rise compressive stress for all foam pours used in a single bun shall be the nominal compressive stress  $\pm 10\%$  at strains of 20%, 40%, and 70%.

#### **8.1.5.2 Butyl Rubber O-rings**

Physical characteristics of the butyl rubber containment O-ring seals and sealing washers for the following parameters shall be determined for each lot based on the following acceptance tests. All material shall conform to the following ASTM D2000 [11] designation:

M4AA710 A13 B13 F17 F48 Z Trace Element.

##### **8.1.5.2.1 Durometer**

The durometer of each lot of the butyl rubber material shall be determined in accordance with ASTM D2240 [12]. Each lot of butyl rubber material shall have a hardness of  $70 \pm 5$  Shore A durometer (i.e., within the range of 65 to 75 Shore A durometer).

##### **8.1.5.2.2 Tensile Strength and Elongation**

The tensile strength of each lot of the butyl rubber material shall be determined in accordance with ASTM D412 [13]. Each lot of butyl rubber material shall have a minimum tensile strength of 10 MPa and a minimum elongation of 250%.

##### **8.1.5.2.3 Heat Resistance**

The heat resistance of each lot of the butyl rubber material shall be determined in accordance with ASTM D573 [14]. Each lot of butyl rubber material shall experience a maximum 10 Shore A durometer hardness increase, a maximum reduction in tensile strength of 25%, and a maximum reduction in ultimate elongation of 25%, when tested at 70 °C.

#### **8.1.5.2.4 Compression Set**

The compression set of each lot of the butyl rubber material shall be determined in accordance with Method B of ASTM D395 [15]. After 22 hours at 70 °C, each lot of butyl rubber material shall have a maximum compression set of 25%.

#### **8.1.5.2.5 Cold Temperature Resistance**

The cold temperature resistance of each lot of the butyl rubber material shall be determined in accordance with Method A, 9.3.2 of ASTM D2137 [16]. After 3 minutes at -40 °C, each lot of butyl rubber material shall be non-brittle.

#### **8.1.5.2.6 Cold Temperature Resiliency**

The cold temperature resiliency of each lot of the butyl rubber material shall be determined in accordance with the TR-10 test of ASTM D1329 [17]. Each lot of butyl rubber material shall be resilient at a test temperature of -50 °C or less.

### **8.1.6 Shielding Integrity Tests**

#### **8.1.6.1 In-Situ Lead Shielding**

In-situ or poured lead shielding integrity shall be confirmed via gamma scanning. Two gamma scan techniques are utilized. The primary difference is in the method used to determine acceptance criteria. Both gamma scan techniques are exactly the same in all other respects and are conducted as discussed below.

A gamma probe is used to scan the outer cask surface while a Cobalt-60 or similar gamma source of sufficient strength is positioned within a collimator or guide tube along the centerline of the cask cavity. The cask outer surface is marked with a grid and a chart is made to reflect the gridded surface. The source is first placed on the bottom of the cask cavity while the surface is scanned around its circumference. The source is then moved up the predetermined distance to the next gridline and the circumference scanned again. This sequence is repeated until the entire cask outer surface is scanned. Dose rates are recorded from each grid square by scanning every point in the grid and recording the maximum dose rates in the corresponding grid on the chart. This data then serves as the raw gamma scan results.

The dose rates are evaluated by comparing them to predetermined dose rate values for nominal lead thickness and nominal-less-10% lead thickness. The two methods utilized to determine acceptance criteria for this data are as follows:

The first method, the *Laboratory Calibration Method*, utilizes test blocks of the cask wall made up of lead and steel plates. The test blocks simulate nominal and nominal-less-10% lead thicknesses. The source is placed behind the nominal test block assembly at a distance equal to the inside radius of the cask. The probe is then placed on the outside of the test block assembly and the dose rate recorded. This test sequence is repeated on the nominal-less-10% test block assembly. The resultant dose rate values are then utilized as acceptance criteria for the actual cask gamma scan. Additionally, the expected dose rate values for nominal and reduced (nominal-less-10%) thickness shielding are calculated utilizing attenuation values for steel and lead as correlation verification.

**BRR Package Safety Analysis Report**

The second, the *Field Calibration Method*, utilizes a specially fabricated test lid that incorporates a holder for various lead and steel plate thicknesses. The fixture is installed onto the cask with the test lid set up to simulate the nominal lead thickness. The source is placed below the test lid, inside the cask, at a distance equal to the inside radius of the cask, along the centerline of the cask body. The dose rate is then measured and recorded. The test lid is adjusted to establish the nominal-less-10% lead thickness configuration. The source is again placed below the test lid at a distance equal to the inside radius of the cask, and the dose rate is again measured and recorded. The value for nominal-less-10% lead thickness is utilized as the maximum acceptable dose rate value for the BRR packaging.

**8.1.6.2 Plate or Sheet Lead Shielding**

Plate or sheet lead is utilized in the bottom end of the cask body and in the removable shield plug. Ultrasonic examination of each plate or sheet is performed prior to installation to ensure that no voids exist in excess of 10% of the lead plate or sheet thickness.

**8.1.7 Thermal Tests**

Tests to demonstrate the heat transfer capability of the packaging are not required because the thermal evaluations presented in Chapter 3, *Thermal Evaluation*, are based on well established heat transfer properties and methodologies and demonstrate relatively large thermal margins for all components. As such, the uncertainties in the predicted temperature levels are small. Further, since the thermal modeling incorporates several conservative assumptions, it is expected that the peak temperatures achieved will be less than predicted. See Chapter 3, *Thermal Evaluation*, for further discussions.

**Table 8.1-1 – Compressive Strength (psi) Parallel-to-Foam Rise at 65°F to 85°F**

Strain	Minimum		Nominal	Maximum	
	Nom. -15%	Nom. -10%		Nom. +10%	Nom. +15%
20%	234	248	275	303	316
40%	252	267	297	327	342
70%	644	682	758	834	872

**Table 8.1-2 – Compressive Strength (psi) Perpendicular-to-Foam Rise at 65°F to 85°F**

Strain	Minimum		Nominal	Maximum	
	Nom. -15%	Nom. -10%		Nom. +10%	Nom. +15%
20%	225	239	265	292	305
40%	250	265	294	323	338
70%	652	690	767	844	882

## 8.2 Maintenance Program

This section describes the maintenance program used to ensure continued performance of the BRR packaging.

### 8.2.1 Structural and Pressure Tests

No structural or pressure tests are necessary to ensure continued performance of the packaging.

### 8.2.2 Maintenance/Periodic Leakage Rate Tests

This section provides the generalized procedure for maintenance/periodic leakage rate testing of the containment boundary penetrations during routine maintenance, or at the time of seal replacement or sealing area repair. Maintenance leakage rate testing shall follow the guidelines of Section 7.4, *Maintenance Leakage Rate Test*, and Section 7.5, *Periodic Leakage Rate Test*, of ANSI N14.5.

Maintenance/periodic leakage rate testing shall be performed on the main O-ring seal, the vent port sealing washer, and the drain port sealing washer for the containment boundary in accordance with Section 8.2.2.2, *Helium Leakage Rate Testing the Main Containment O-ring Seal*, 8.2.2.3, *Helium Leakage Rate Testing the Drain Port Sealing Washer*, and 8.2.2.4, *Helium Leakage Rate Testing the Vent Port Sealing Washer*. Each leakage rate test shall meet the acceptance criteria delineated in Section 8.2.2.1, *Maintenance/Periodic Leakage Rate Test Acceptance Criteria*.

#### 8.2.2.1 Maintenance/Periodic Leakage Rate Test Acceptance Criteria

Maintenance/periodic leakage rate test acceptance criteria are identical to the criteria delineated in Section 8.1.4.1, *Fabrication Leakage Rate Test Acceptance Criteria*.

#### 8.2.2.2 Helium Leakage Rate Testing the Main Containment O-ring Seal

1. The maintenance/periodic leakage rate test of the BRR package containment O-ring seal integrity shall be performed following the guidelines of Section A.5.4, *Evacuated Envelope – Gas Detector*, of ANSI N14.5.
2. The BRR package shall be assembled with the two O-ring seals installed in the closure lid, and the vent and seal test ports are installed with their associated sealing washers. If not previously tightened, tighten the closure lid bolts to 200 – 240 ft-lb torque. Assembly is as shown in Appendix 1.3.3, *Packaging General Arrangement Drawings*.
3. Utilizing a port tool, attach a vacuum pump and a source of helium gas, in parallel, to the vent port.
4. Close the valve to the source of helium gas and open the valve to the vacuum pump.
5. Utilizing a port tool, rotate the vent port plug to the open position.
6. Evacuate the system to a 90% vacuum or better ( $\leq 10\%$  ambient atmospheric pressure). Isolate the vacuum pump from the system.
7. Provide a helium atmosphere inside the evacuated cavity by backfilling with helium gas (99% purity or better) to ambient atmospheric pressure (+1 psi, -0 psi).
8. Utilizing the port tool, rotate the vent port plug to the closed position, and remove the helium-contaminated port tool from the vent port.

**BRR Package Safety Analysis Report**

9. Install a clean (helium-free) port tool into the seal test port.
10. Utilizing appropriate fittings, attach a helium MSLD to the port tool.
11. Utilizing the port tool, rotate the seal test port plug to the open position.
12. Evacuate the cavity between the containment O-ring seal and the test O-ring seal until the vacuum is sufficient to operate the leak detector per the manufacturer's recommendations.
13. Perform the helium leakage rate test to the requirements of Section 8.2.2.1, *Maintenance/Periodic Leakage Rate Test Acceptance Criteria*. If, after repeated attempts, the BRR package containment O-ring seal fails to pass the leakage rate test, isolate the leak path and, prior to repairing the leak path and repeating the leak test, record on a nonconformance report and disposition prior to final acceptance in accordance with the cognizant quality assurance program.

**8.2.2.3 Helium Leakage Rate Testing the Drain Port Sealing Washer**

1. The maintenance/periodic leakage rate test of the drain port plug containment sealing washer integrity shall be performed following the guidelines of Section A.5.4, *Evacuated Envelope – Gas Detector*, of ANSI N14.5.
2. The BRR package shall be assembled with the two O-ring seals installed on the closure lid. Ensure the vent and seal test port plugs are installed with their associated sealing washers. Assembly is as shown in Appendix 1.3.3, *Packaging General Arrangement Drawings*.
3. Verify the presence of a helium atmosphere below the vent port plug containment sealing washer, as specified above in Steps 3 – 8 of Section 8.2.2.2, *Helium Leakage Rate Testing the Main Containment O-ring Seal*.
4. Install a port tool into the drain port.
5. Utilizing appropriate fittings, attach a helium MSLD to the port tool.
6. Evacuate the cavity above the drain port plug containment sealing washer until the vacuum is sufficient to operate the leak detector per the manufacturer's recommendations.
7. Perform the helium leakage rate test to the requirements of Section 8.2.2.1, *Maintenance/Periodic Leakage Rate Test Acceptance Criteria*. If, after repeated attempts, the drain port plug containment sealing washer fails to pass the leakage rate test, isolate the leak path and, prior to repairing the leak path and repeating the leak test, record on a nonconformance report and disposition prior to final acceptance in accordance with the cognizant quality assurance program.

**8.2.2.4 Helium Leakage Rate Testing the Vent Port Sealing Washer**

1. The maintenance/periodic leakage rate test of the vent port plug containment sealing washer integrity shall be performed following the guidelines of Section A.5.4, *Evacuated Envelope – Gas Detector*, of ANSI N14.5.
2. The BRR package shall be assembled with the two O-ring seals installed on the closure lid. Ensure the vent and seal test port plugs are installed with their associated sealing washers. Assembly is as shown in Appendix 1.3.3, *Packaging General Arrangement Drawings*.

## BRR Package Safety Analysis Report

3. Verify the presence of a helium atmosphere below the vent port plug containment sealing washer, as specified above in Steps 3 – 8 of Section 8.2.2.2, *Helium Leakage Rate Testing the Main Containment O–ring Seal*.
4. Install a port tool into the vent port.
5. Utilizing appropriate fittings, attach a helium MSLD to the port tool.
6. Evacuate the cavity above the vent port plug containment sealing washer until the vacuum is sufficient to operate the leak detector per the manufacturer’s recommendations.
7. Perform the helium leakage rate test to the requirements of Section 8.2.2.1, *Maintenance/Periodic Leakage Rate Test Acceptance Criteria*. If, after repeated attempts, the vent port plug containment sealing washer fails to pass the leakage rate test, isolate the leak path and, prior to repairing the leak path and repeating the leak test, record on a nonconformance report and disposition prior to final acceptance in accordance with the cognizant quality assurance program.

### 8.2.3 Component and Material Tests

#### 8.2.3.1 Fasteners

All threaded components shall be visually inspected before installation for deformed or stripped threads. Damaged threaded components shall be repaired or replaced prior to further use. The threaded components to be visually inspected include the closure lid bolts, vent port plug, and drain port plug.

#### 8.2.3.2 Sealing Area Routine Inspection and Repair

Before each use and at the time of seal replacement, containment sealing surfaces shall be visually inspected for damage that could impair the sealing capabilities of the packaging. Perform surface finish inspections for the closure lid O–ring grooves, the mating sealing area on the cask body, and the surfaces that mate with the sealing washer in the vent port and drain port. Damage shall be repaired prior to further use (e.g., using emery cloth or other surface finishing techniques) to restore the sealing surfaces to the value specified on the drawings in Appendix 1.3.3, *Packaging General Arrangement Drawings*.

Upon completion of any surface finish repairs, perform a leakage rate test per Section 8.2.2, *Maintenance/Periodic Leakage Rate Tests*.

#### 8.2.3.3 Impact Limiters

Before each use, the impact limiters shall be inspected for tears or perforations in the stainless steel sheets, and for the presence of the fire–consumable plastic plugs. The ball–lock pins that retain the impact limiters shall be visually inspected for any damage that could reduce their effectiveness. Any damage shall be repaired prior to further use.

#### 8.2.3.4 Seals

The containment boundary O–ring seal, the vent port sealing washer, and the drain port sealing washer shall be replaced within the 12–month period prior to shipment or when damaged (whichever is sooner), per the size and material requirements delineated on the drawings in Appendix 1.3.3, *Packaging General Arrangement Drawings*. Following seal replacement and

prior to a loaded shipment, the new seals shall be leakage rate tested to the requirements of Section 8.2.2, *Maintenance/Periodic Leakage Rate Tests*.

#### **8.2.4 Thermal Tests**

No thermal tests are necessary to ensure continued performance of the BRR packaging.



## 8.3 Appendix

### 8.3.1 References

1. Title 10, Code of Federal Regulations, Part 71 (10 CFR 71), Packaging and Transportation of Radioactive Material, 01–01–08 Edition.
2. ANSI/AWS D1.6/D.6M:2007, *Structural Welding Code–Stainless Steel*, American Welding Society (AWS).
3. American Society of Mechanical Engineers (ASME) Boiler and Pressure Vessel Code, Section III, *Rules for Construction of Nuclear Facility Components*, Division 1 – Subsection NB, *Class 1 Components*, and Section V, *Nondestructive Examination*, Article 2, *Radiographic Examination*, 2007 Edition.
4. American Society of Mechanical Engineers (ASME) Boiler and Pressure Vessel Code, Section III, *Rules for Construction of Nuclear Facility Components*, Division 1 – Subsection NB, *Class 1 Components*, and Section V, *Nondestructive Examination*, Article 4, *Ultrasonic Examination Methods for Welds*, 2007 Edition.
5. American Society of Mechanical Engineers (ASME) Boiler and Pressure Vessel Code, Section III, *Rules for Construction of Nuclear Facility Components*, Division 1 – Subsection NB, *Class 1 Components*, and Section V, *Nondestructive Examination*, Article 6, *Liquid Penetrant Examination*, 2007 Edition.
6. American Society of Mechanical Engineers (ASME) Boiler and Pressure Vessel Code, Section III, *Rules for Construction of Nuclear Facility Components*, Division 1 – Subsection NB, *Class 1 Components*, Article NB–6220, 2007 Edition.
7. ANSI N14.5–1997, *American National Standard for Radioactive Materials – Leakage Tests on Packages for Shipment*, American National Standards Institute (ANSI), Inc.
8. EPA Method 300.0, Revision 2.2 (October 1999), *Determination of Inorganic Anions by Ion Chromatography*, U.S. Environmental Protection Agency.
9. ASTM C518–04, *Standard Test Method for Steady–State Thermal Transmission Properties by Means of the Heat Flow Meter Apparatus*, American Society for Testing and Materials (ASTM).
10. ASTM E1269, *Standard Test Method for Determining Specific Heat Capacity by Differential Scanning Calorimetry*, American Society for Testing and Materials (ASTM).
11. ASTM D2000–05, *Standard Classification System for Rubber Products in Automotive Applications*, American Society for Testing and Materials (ASTM).
12. ASTM D2240–05, *Standard Test Method for Rubber Property – Durometer Hardness*, American Society for Testing and Materials (ASTM).
13. ASTM D412–98a(2002)e1, *Standard Test Methods for Vulcanized Rubber and Thermoplastic Rubbers and Thermoplastic Elastomers – Tension*, American Society for Testing and Materials (ASTM).
14. ASTM D573–04, *Standard Test Method for Rubber – Deterioration in an Air Oven*, American Society for Testing and Materials (ASTM).

15. ASTM D395–03, *Standard Test Methods for Rubber Property – Compression Set*, American Society for Testing and Materials (ASTM).
16. ASTM D2137–94(2000), *Standard Test Methods for Rubber Property – Brittleness Point of Flexible Polymers and Coated Fabrics*, American Society for Testing and Materials (ASTM).
17. ASTM D1329–02, *Standard Test Method for Evaluating Rubber Property – Retraction at Lower Temperatures (TR Test)*, American Society for Testing and Materials (ASTM).